

Reactivity of Carbanions Generated via Reductive Radical-Polar Crossover and Regio-, Diastereo- and Enantioselectivity in their Generation

Dissertation

Zur Erlangung des Doktorgrades der Naturwissenschaften

(Dr. rer. nat)

an der Fakultät für Chemie und Pharmazie

der Universität Regensburg



vorgelegt von

Sascha Grotjahn

aus Eggenfelden

Regensburg – 2024

The experimental work has been carried out between May 2020 and March 2024 under the supervision of Prof. Dr. Burkhard König at the University of Regensburg, Institute of Organic Chemistry. Parts of the experimental work have been carried out during short research stays in the groups of Prof. Dr. Jana Roithová at Radboud University, Nijmegen, the Netherlands (March 2024) and in the group of Prof. Dr. Magnus Rueping at King Abdullah University of Science and Technology, Thuwal, Saudi-Arabia (January until March 2024).

Date of submission: 25.09.2024

Date of colloquium: 09.12.2024

Board of examiners:

PD Dr. Jonathan O. Bauer (chair)

Prof. Dr. Burkhard König (1st referee)

Prof. Dr. Oliver Reiser (2nd referee)

Prof. Dr. Patrick Nürnberger (examiner)

“I am among those who think that science has great beauty. A scientist in his laboratory is not a mere technician; he is also a child placed before natural phenomena which impress him like a fairy tale”

- *Marie Skłodowska Curie*

TABLE OF CONTENTS

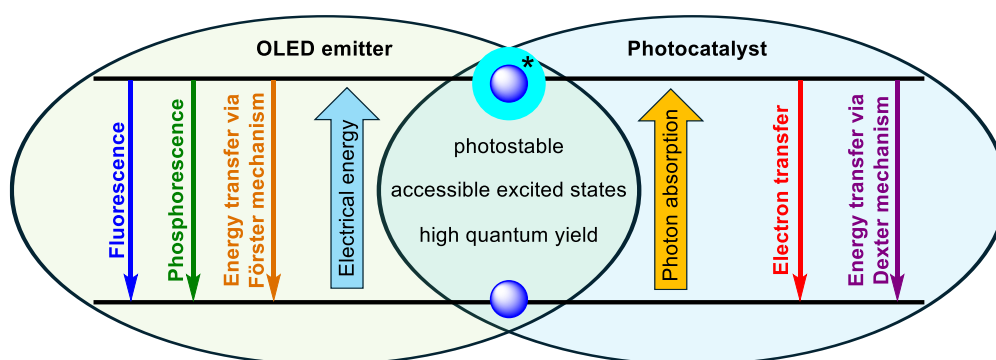
1	Common Ground and Divergence: OLED Emitters as Photocatalysts.....	1
1.1	Introduction.....	3
1.2	The connection between OLED emitters and photocatalysts	4
1.3	First generation OLEDs	5
1.4	Second generation OLEDs	6
1.5	Third generation OLEDs	7
1.6	Fourth generation OLEDs	8
1.7	Importance of TADF emitters as photocatalysts.....	11
1.8	Conclusion	13
1.9	References.....	14
2	Photosubstitution in Dicyanobenzene-based Photocatalysts	19
2.1	Introduction.....	21
2.2	Results and discussion	22
2.3	Conclusion	26
2.4	Experimental part.....	27
2.4.1	General information.....	27
2.4.2	Photoreactor setups.....	28
2.4.3	Effect of water and solvent on photosubstitution in 4CzIPN	29
2.4.4	Synthetic procedures.....	30
2.4.4.1	<i>General procedure 2-A: Synthesis of carbazole(9-yl)-dicyanobenzenes</i>	<i>30</i>
2.4.4.2	<i>Synthesis of chiral BINOL containing carbazole(9-yl)-dicyanobenzenes.....</i>	<i>31</i>
2.4.4.3	<i>General procedure 2-B: Photosubstitution in dicyanobenzene photocatalysts</i>	<i>33</i>
2.4.4.4	<i>Scale-up to 1 mmol.....</i>	<i>45</i>
2.4.4.5	<i>Photosubstitution by solvent fragments.....</i>	<i>46</i>
2.4.5	Comparison of the catalytic activity of 4CzIPN, 2CzPN and their photosubstitution products	49
2.4.6	Comparison of solubilities in MeCN.....	52
2.5	References.....	53
3	Reactivity of Superbasic Carbanions Generated via Reductive Radical-Polar Crossover in the Context of Photoredox Catalysis	55
3.1	Introduction.....	57

3.2 Results and discussion	58
3.2.1 Evidence for free carbanions in solution	58
3.2.2 Comparison with gas-phase reactivity of isolated carbanions.....	61
3.2.3 Isotopic fractionation and kinetic isotope effects	63
3.2.4 Excited state dynamics of the photocatalyst.....	64
3.2.5 Importance for reactions involving photocatalytically generated carbanions	66
3.3 Conclusion	71
3.4 Experimental part.....	73
3.4.1 General information.....	73
3.4.2 Photoreactor setup	75
3.4.3 Synthetic procedures.....	76
3.4.3.1 <i>Synthesis of photocatalysts</i>	76
3.4.3.2 <i>Synthesis of benzyl trifluoroborates</i>	78
3.4.3.3 <i>Synthesis of Ω-phenylalkylcarboxylic acid esters</i>	81
3.4.3.4 <i>Synthesis of benzyltriphenylphosphonium bromides</i>	84
3.4.3.5 <i>Synthesis of deuterated substrates</i>	85
3.4.4 Generation of carbanions	87
3.5.1 Comparison of the catalytic activity of 4CzIPN and its photosubstitution products....	89
3.4.6 Gas-phase reactivity of carbanions.....	91
3.4.6.1 <i>Qualitative gas-phase reactivity</i>	92
3.4.6.2 <i>Determination of kinetic isotope effects of benzylic carbanions reacting with acetonitrile-d_0/d_3</i>	99
3.4.7 Isotopic labelling of substrates and solvents	105
3.4.7.1 <i>Deuteration of photocatalytically generated carbanions by solvents</i>	108
3.4.7.2 <i>Deuterium labelling of acetonitrile and ethyl acetate</i>	110
3.4.8 Kinetic isotope effects and isotopic fractionation	112
3.4.8.1 <i>Kinetic isotope effects of carbanion protonation</i>	112
3.4.8.2 <i>Kinetic isotope effect of benzylic C-H activation</i>	118
3.4.8.3 <i>Isotopic fractionation with carbanions generated via C-H activation</i>	120
3.4.9 Spectroscopy.....	122
3.4.10 Carbanion generation from benzyltriphenylphosphonium bromides	128
3.4.11 DFT calculations.....	131
3.4.11.1 <i>Kinetic isotope effects for hydrogen atom abstraction</i>	131
3.4.11.2 <i>Kinetic isotope effect for carbanion protonation</i>	133
3.4.11.3 <i>Cyclization of phenylvaleric and phenylhexanoic acid esters</i>	134
3.5 References.....	136

4	Regio-, Diastereo- and Enantioselectivity in the Photocatalytic Generation of Carbanions via Hydrogen Atom Transfer and Reductive Radical-Polar Crossover	141
4.1	Introduction.....	143
4.2	Results and discussion	146
4.2.1	Identification of reactive benzylic C-H bonds.....	146
4.2.2	Epimerization via diastereoselective hydrogen atom abstraction.....	148
4.2.3	Deracemization via enantioselective hydrogen atom abstraction.....	151
4.3	Conclusion	154
4.4	Experimental part.....	155
4.4.1	General information.....	155
4.4.2	Photoreactor setups.....	157
4.4.3	Synthetic procedures.....	160
4.4.3.1	<i>Synthesis of photocatalysts</i>	<i>160</i>
4.4.3.2	<i>Synthesis of substrates for C-H activation</i>	<i>160</i>
4.4.3.3	<i>Synthesis of chiral silane thiols.....</i>	<i>170</i>
4.4.4	Deuteration via benzylic C-H activation	184
4.4.4.1	<i>Extended substrate scope of benzylic deuteration</i>	<i>185</i>
4.4.4.2	<i>Computational investigations</i>	<i>187</i>
4.4.4.3	<i>Isolated deuterated compounds</i>	<i>191</i>
4.4.5	Application of benzofuran isomerization via a photocatalytic HAT/RRPCO/protonation sequence	196
4.4.5.1	<i>Photocatalytic synthesis of 1,2-diarylethanol derivatives.....</i>	<i>197</i>
4.4.5.2	<i>Synthesis of dihydrobenzofurans.....</i>	<i>205</i>
4.4.6	Kinetic studies for dihydrobenzofuran <i>cis/trans</i> isomerization and deuteration.....	208
4.4.7	Deracemization via enantioselective HAT with chiral silane thiols	226
4.4.7.1	<i>TADDOL-derived silane thiols as HAT reagents and their stability.....</i>	<i>226</i>
4.4.7.2	<i>Deracemization with chiral HAT-reagents.....</i>	<i>227</i>
4.4.7.3	<i>Unsuccessful substrates.....</i>	<i>232</i>
4.4.8	In situ generation of the active photocatalyst by photocyclization of 3DPA2FBN....	233
4.5	References.....	235
5	Summary.....	242
6	Zusammenfassung	246
7	Appendix.....	250

7.1 Abbreviations	250
7.2 Appendix chapter 2.....	252
7.2.1 Cyclic voltammetry	252
7.2.2 UV/Vis spectra, emission spectra, and fluorescence lifetime.....	260
7.2.3 NMR spectra.....	271
7.3 Appendix chapter 3.....	309
7.3.1 Cyclic voltammetry	309
7.3.2 DFT calculations (optimized structures)	312
5.2.2.1 <i>Kinetic isotope effects for hydrogen atom abstraction.....</i>	<i>312</i>
7.3.2.2 <i>Kinetic isotope effects for carbanion protonation</i>	<i>324</i>
7.3.2.3 <i>Cyclization of phenylvaleric and phenylhexanoic acid esters</i>	<i>329</i>
7.3.3 NMR spectra.....	337
7.4 Appendix chapter 4.....	362
7.4.1 DFT calculations (optimized structures)	362
7.4.2 Single-Crystal X-Ray Diffraction Analysis	386
7.4.3 NMR spectra.....	389
7.4.3.1 <i>NMR spectra of crude reaction mixtures for determination of deuteration degrees</i>	<i>389</i>
7.4.3.2 <i>NMR spectra of isolated deuterated compounds</i>	<i>411</i>
7.4.3.3 <i>NMR spectra of other isolated compounds.....</i>	<i>421</i>
7.5 Curriculum Vitae	488
8 Acknowledgements	490

1 Common Ground and Divergence: OLED Emitters as Photocatalysts



This chapter has been submitted in a slightly modified version as a feature article and is under peer-review at the time of submission of this thesis.

Abstract

Many photocatalysts were initially developed or used as emitters for light emitting diodes (OLEDs). This feature article summarizes the different generations of OLED emitters and connects the photophysical processes with those relevant for photocatalysis. The focus is on the general properties OLED emitters and photocatalysts are designed for and how photocatalysis has benefitted from OLED research. Sometimes, optimization of an OLED emitter leads to a better photocatalyst while some properties are optimized into opposite directions. To discover new classes of photocatalysts in the future it is important to consider what good OLED emitters and good photocatalyst have in common and where they diverge. Within recent years, fully organic thermally activated delayed fluorescence (TADF) emitters had the most significant impact in both fields and thus are discussed with specific focus.

1.1 Introduction

A catalyst is defined as “a substance that increases the rate of a reaction without modifying the overall standard Gibbs energy change in the reaction.”¹ Traditional organic synthesis uses thermal energy to overcome reaction barriers and thus a catalyst lowers the activation energy to increase the reaction rate. Photocatalysis utilizes a different concept to overcome reaction barriers. A photocatalyst is a molecule or material that, upon absorption of a photon, is transferred to an electronically excited state from which it triggers a chemical reaction either by photoinduced electron transfer (PET) or photoinduced energy transfer (PEnT). Many currently used photocatalysts were initially developed in organic light emitting diode (OLED) research and each milestone led to new or improved photocatalytic transformations. Some photocatalysts initially used or developed in OLED research are depicted in Figure 1.1. Most organic molecules capable of light emission in the visible range are fluorescent molecules. Thus, it is not surprising that first generation OLED emitters are based on fluorescent emitters such as anthracene² and its derivatives (**1**).^{3,4} Second generation OLEDs are phosphorescence emitters and a variety of phosphorescent ruthenium and iridium complexes were developed for this purpose.⁵ Since the photophysical characterization of Ru(bpy)₃Cl₂ (**2**),⁶ and the use of *fac*-Ir(ppy)₃ (**3**) as OLED emitter^{7,8} these phosphorescent precious metal complexes became prototypical photocatalysts and part of a standard catalyst repertoire of organic chemists.⁹ A breakthrough in OLED development was reached with the design of the third generation fully organic thermally activated delayed fluorescence (TADF) emitter 4CzIPN (**4**)¹⁰ which also turned out to be an efficient photocatalyst.¹¹

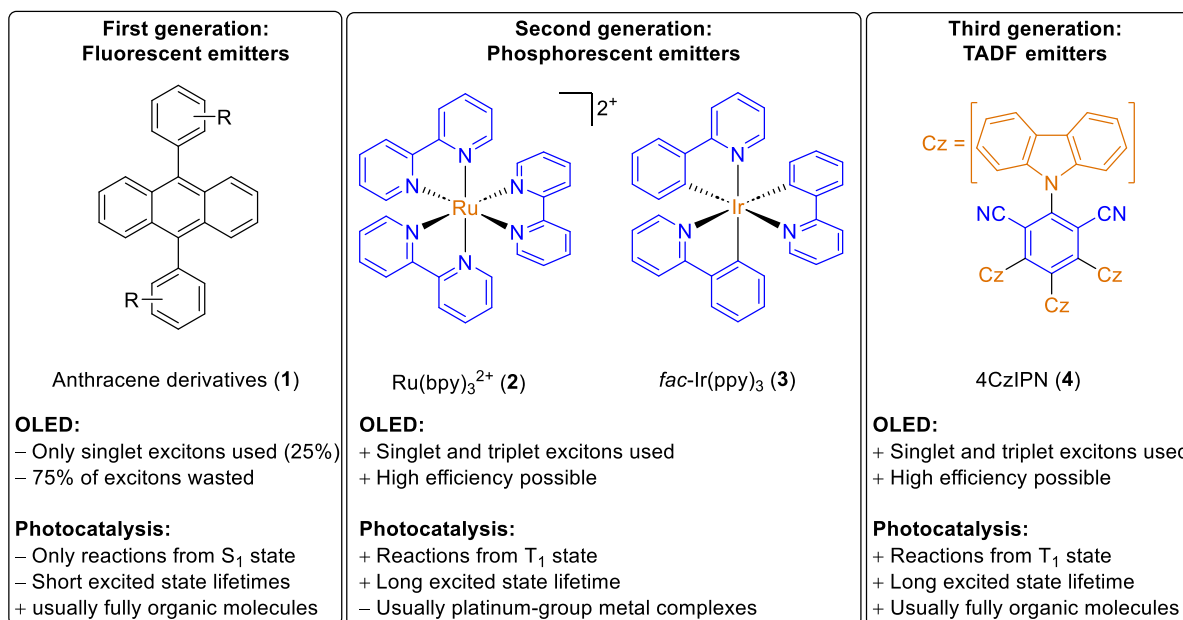


Figure 1.1. Photocatalysts based on anthracene, Ru(bpy)₃Cl₂, *fac*-Ir(ppy)₃, and 4CzIPN were initially used as emitters in organic light emitting diodes before they found widespread use in photocatalysis.

1.2 The connection between OLED emitters and photocatalysts

The fact that many OLED emitters are also good photocatalysts is not a coincidence but a consequence of the photophysical requirements for both applications. While OLEDs convert electrical energy into light, photocatalysts convert light into chemical energy. Both processes proceed through an excited state of the respective molecule which should not lose its energy as heat but utilize it for light emission (in OLEDs) or for chemical reactions (in photocatalysis). Although light emission is an unproductive pathway for a photocatalyst, a high luminescence quantum yield demonstrates that other deactivation pathways are not competing to notable extent. Thus, compounds for both applications are designed for having low rates of non-radiative transitions to the ground state and being chemically stable in their electronically excited states. A schematic representation of an OLED is depicted in Figure 1.2 together with a Jabłoński diagram for the photophysical processes occurring within the emissive layer (EML). Some materials unite properties of multiple layers and the introduction of additional layers can be beneficial depending on the application.^{12,13} The simultaneous presence of electrons and holes in the EML generates excitons. In OLEDs, these excitons are either excited state emitter molecules or electron/hole pairs within the host material which then transfer their energy to generate excited state emitter molecules.

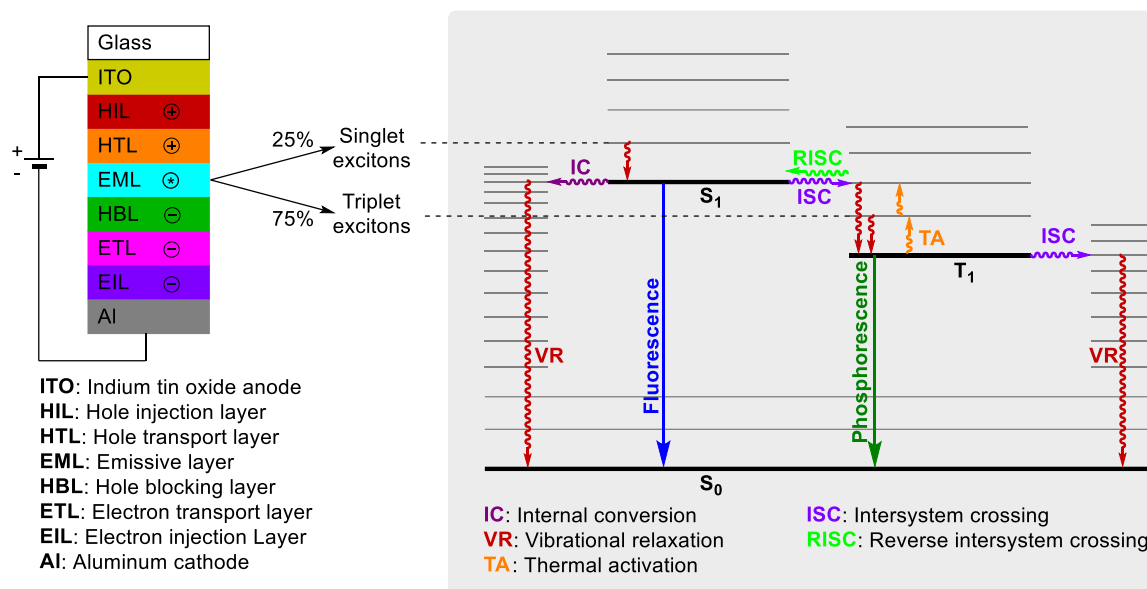


Figure 1.2. Schematic construction of an OLED and the corresponding Jabłoński diagram for the photophysical processes in the emissive layer. Wavy arrows represent non-radiative transitions and straight arrows represent radiative transitions. Thin horizontal lines represent vibrational levels of the respective electronically excited state (S_1 and T_1) or ground state (S_0). Depending on the specific system different processes dominate. The most important aspects of OLED emitters are discussed in more detail in the following sections.

1.3 First generation OLEDs

Due to spin statistics, excitons are generated in a 3:1 ratio of triplet and singlet states in the emissive layer.¹⁴ First generation OLEDs are based on fluorescence emitters. As phosphorescence is not observed in these emitters at room temperature only singlet excitons (25%) are used for light emission. Triplet excitons (75%) lose their energy to thermal motion and only contribute to heating of the device. Thus, fluorescent OLEDs have a maximum internal quantum efficiency (IQE) of 25% and are inherently limited in their efficiency. The IQE can be increased by triplet-triplet annihilation to obtain a maximum exciton utilization of 62.5%. This has been utilized for OLED applications¹⁵ but reports in photocatalysis are scarce¹⁶ and will not be discussed in further detail in this chapter. For use of fluorescence emitters as photocatalysts the limitations of fluorescent OLED emitters caused by triplet excitons do not apply because excitation from singlet ground states by photon absorption leads to singlet excited states while excitation from the singlet ground state to triplet states or intersystem crossing (ISC) from the S_1 to the T_1 state are spin-forbidden. Additionally, photocatalysis can also occur from triplet states. Although not among the most efficient fluorescent emitters, 9,10-diphenylanthracene (DPA) was identified as one of the first fully organic emitters for blue OLEDs⁴ and later found to be an efficient photoredox catalyst. In its S_1 state DPA is a strong oxidant and a strong reductant and thus can undergo oxidative¹⁷ as well as reductive quenching¹⁸ as depicted in Figure 1.3.

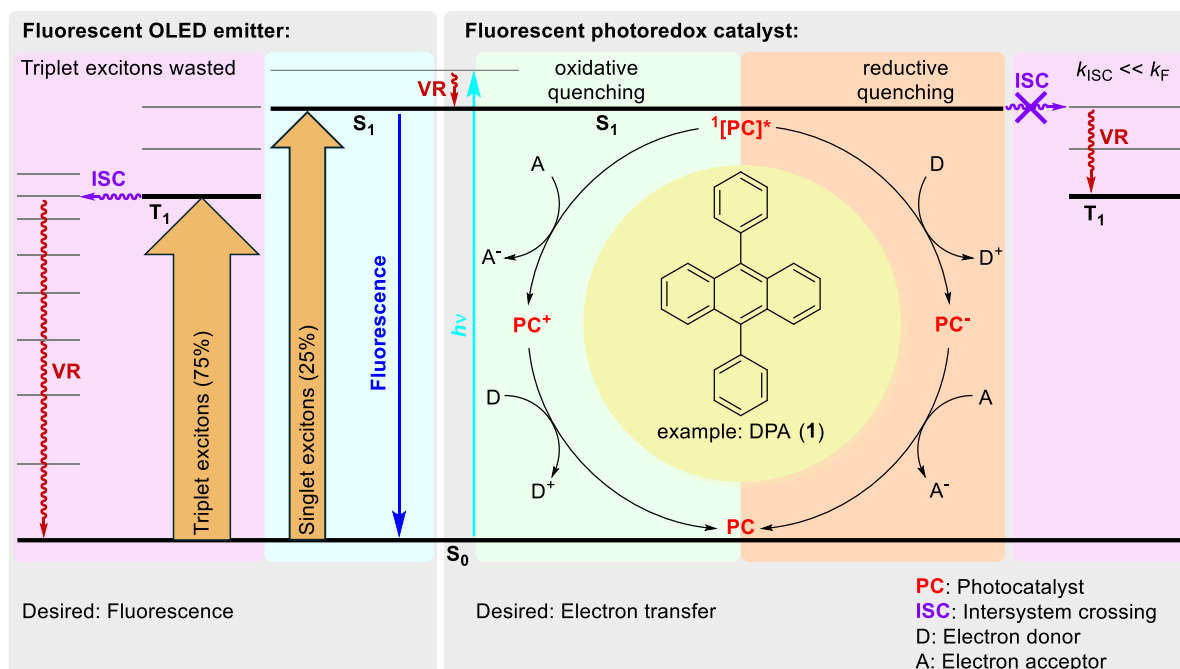


Figure 1.3. 9,10-Diphenylanthracene (DPA, **1**) is a first-generation OLED emitter and photoredox catalyst.

1.4 Second generation OLEDs

OLEDs of the second generation utilize phosphorescent emitters. Phosphorescence, as a spin-forbidden process, is usually slow and at room temperature cannot compete with radiationless deactivation pathways in most organic molecules. However, strong spin-orbit coupling in complexes of heavy metals such as platinum, ruthenium, and iridium makes these transitions weakly allowed. This is known as the heavy atom effect.^{19,20} Consequently, a fast ISC from the S_1 state to the T_1 state becomes possible and the radiative transition from T_1 to S_0 can compete with non-radiative relaxation pathways so that singlet and triplet excitons can be utilized by emission of phosphorescence.²¹ The use of triplet excitons for light emission is known as triplet harvesting and can give IQEs of up to 100%. However, platinum-group metals are among the least abundant metals on earth and, thus, they are rather expensive, and their use is hardly sustainable. Despite these issues, ruthenium- and iridium-based complexes remain widely used in OLED applications and are currently among the most widely used photocatalysts. Although the phosphorescence rate is increased in phosphorescent OLED emitters, the T_1 lifetime is still well above the lifetime of >1 ns needed for bimolecular reactions to be competitive with emission.²² $\text{Ru}(\text{bpy})_3^{2+}$ (**2**) and $\text{fac-Ir}(\text{ppy})_3$ (**3**), for example, have lifetimes from hundreds of nanoseconds up to a few microseconds, depending on the solvent.^{7,9,23} In the T_1 state these complexes are stronger oxidants and stronger reductants than in the ground state. While in OLED applications electron transfer can lead to degradation of the emitter,²⁴ in photoredox catalysis electron transfer is the desired pathway. The excited state photocatalyst undergoes either oxidative quenching or reductive quenching by an electron acceptor or donor, respectively. To close the catalytic cycle an electron transfer in the opposite direction must occur at a later stage as depicted in Figure 1.4. While the catalytic cycle is similar to that with fluorescence emitters (Figure 1.3) the T_1 state of phosphorescent emitters is substantially longer-lived than the S_1 state of fluorescent emitters and usually the excited state from which reactions occur.

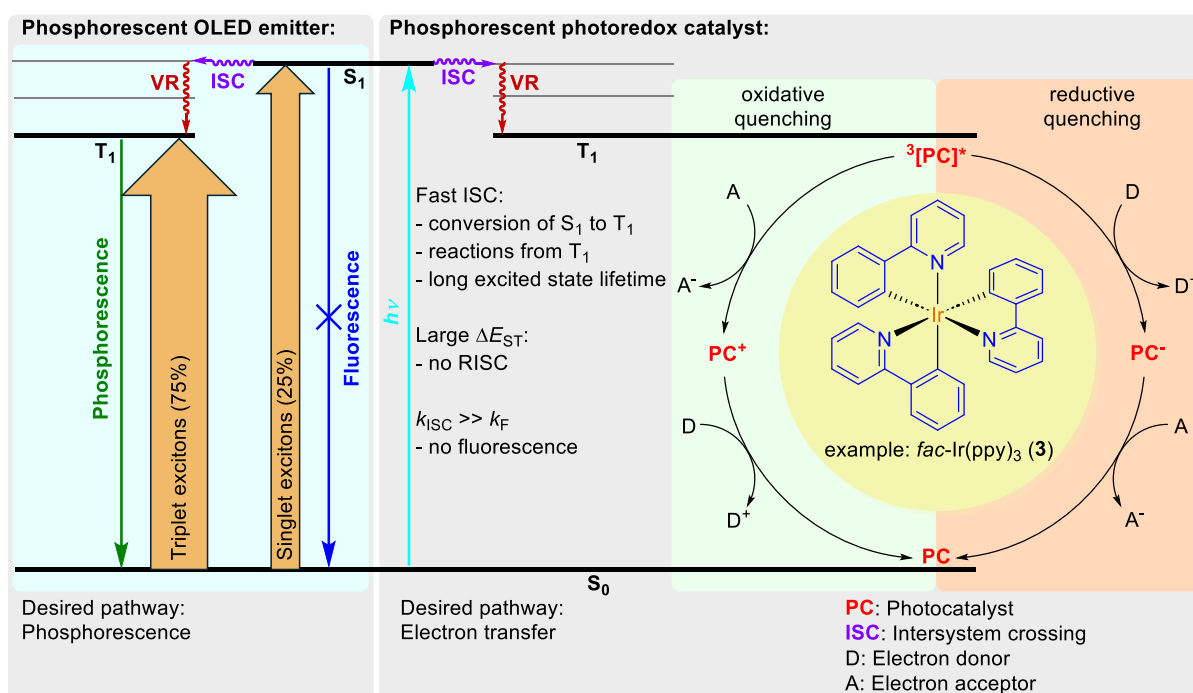


Figure 1.4. Second generation OLED emitters such as $\text{fac-Ir}(\text{ppy})_3$ (**3**) are among the most widely used catalysts in photoredox catalysis.

1.5 Third generation OLEDs

Third generation OLEDs employ a strategy for triplet-harvesting called thermally activated delayed fluorescence (TADF). In a TADF emitter the energy difference between S_1 and T_1 state (ΔE_{ST}) is small enough to repopulate the S_1 state from the T_1 state in a Boltzmann equilibrium at room temperature. If fluorescence from the S_1 state and reverse intersystem crossing (RISC) from the T_1 state to the S_1 state are fast, while the lifetime of the T_1 state is long, all excitons can be channeled into fluorescence. Thus, TADF emitters have internal quantum efficiencies of up to 100%. TADF has initially been observed in eosin Y²⁵ and more efficiently in transition metal complexes, especially copper-based.^{26,27} Today, purely organic TADF emitters of the donor-acceptor type are more widely used in OLED research and photocatalysis.²⁸ For photocatalysis, there are three main reasons why TADF emitters are perfect candidates for photocatalysts. First, as most excited state molecules reside in the T_1 state the excited state lifetime is generally long. In acetonitrile the prototypical TADF emitter 4CzIPN has a lifetime for the delayed fluorescence of 1390 ns,²⁹ similar to platinum-group based emitters. The second reason for their success as photocatalysts arises from the small ΔE_{ST} . While both, phosphorescent and TADF emitters, lose this energy upon transition into the T_1 state, ΔE_{ST} is intrinsically small in TADF emitters, thus, less energy is lost to vibrational relaxation after ISC, and more energy is available for chemical reactions from the T_1 state. Additionally, RISC constantly provides excited state molecules for reactions from the energetically higher S_1 state. The third reason for the success of TADF photocatalysts is their relatively easy synthesis and structural modification, providing access to a variety of photocatalysts with different redox potentials as will be discussed later.

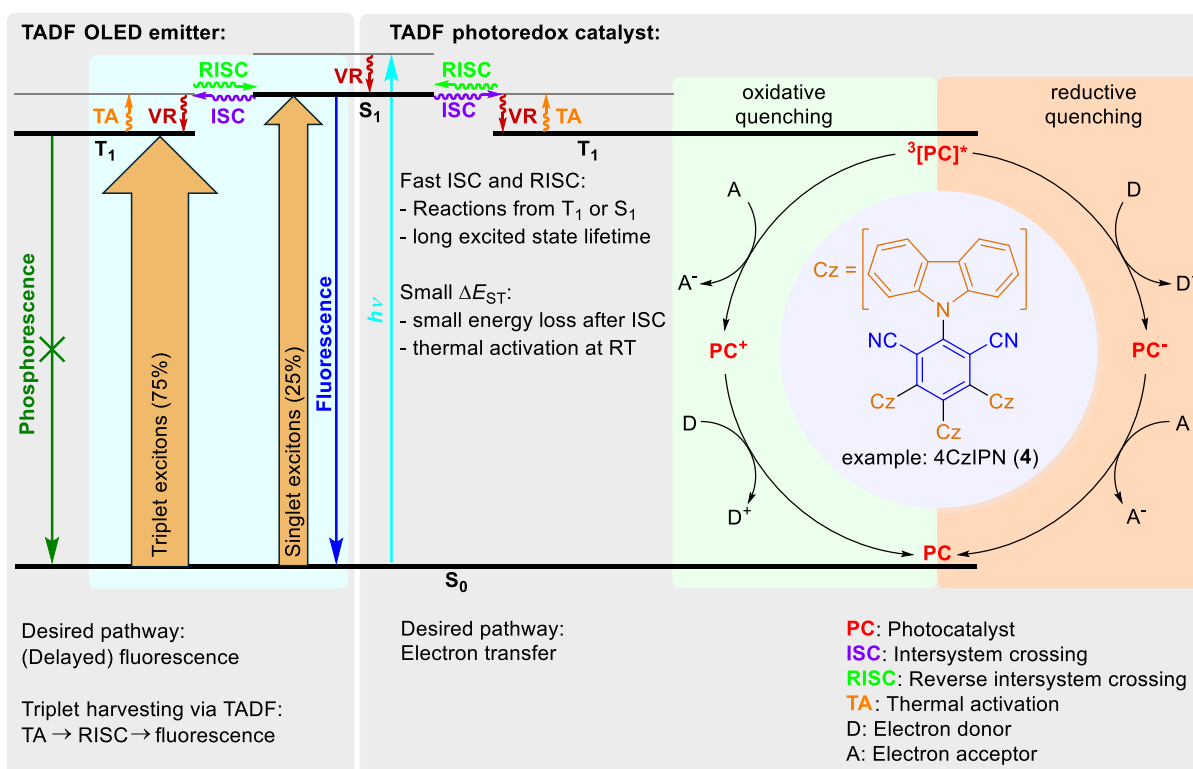


Figure 1.5. Third generation OLEDs use TADF emitters. Triplet harvesting is achieved via thermal activation (TA) and RISC to the S_1 state. Photocatalysis mainly occurs from the long-lived T_1 state but the S_1 state can also participate in reactions.

1.6 Fourth generation OLEDs

Fourth generation OLED emitters utilize a sequence termed hyperfluorescence. A TADF dye collects singlet and triplet excitons generated in the emissive layer and transfers their energy via Förster resonance energy transfer (FRET)³⁰ from the TADF dye's S_1 state to a fluorescent emitter. Triplet excitons are first upconverted via TADF and the energy transferred from the singlet state of the donor (TADF dye) to the fluorescent dye as terminal emitter. Thus, hyperfluorescent OLEDs also have an IQE of up to 100%. The benefit over third generation OLED emitters utilizing the TADF dye directly as emitter are high color purity and improved performance at high current densities. High color purity is especially desirable for display applications and is improved in hyperfluorescent OLEDs due to the narrow emission of the fluorescent emitter compared to the broad emission of TADF emitters. The drop in efficiency upon increased current density is known as efficiency roll-off.³¹ There are multiple mechanisms for efficiency roll-off, of which some are caused by bimolecular reactions between two excitons or between excitons and polarons.³² The efficiency roll-off due to exciton-exciton annihilation such as triplet-triplet,³³ singlet-singlet,³⁴ and singlet-triplet annihilation³⁵ as well as exciton-polaron annihilation³⁶ is reduced by shorter lifetimes. In addition to reduction in efficiency these processes also lead to device degradation.³⁶⁻³⁸ The fluorescent terminal emitter with a high fluorescence rate quenches the long-lived excited TADF sensitizer and thus reduces the buildup of excitons.

FRET proceeds through long-range dipole-dipole coupling and only occurs if there is spectral overlap between the emission of the donor and the absorption of the acceptor, and transitions within both molecules follow the selection rules for absorption and emission. FRET usually refers to FRET_{S-S} in which the singlet state of the donor transfers its energy to the acceptor in its S_0 state which is excited to its S_1 state. With elaborate design of donor and acceptor FRET_{T-S} can also occur by transfer of triplet energy to an acceptor which is excited to its S_1 state.³⁹ However, due to the spin-forbidden nature of the $T_1 \rightarrow S_0$ transition in the donor FRET_{T-S} is a slow process and thus less practical for OLED emitters. FRET in general is also rarely used in photocatalysis because it only gives excited singlet states also accessible by direct excitation, but it is widely used for analytical purposes due to its distance dependence of $1/r^6$, and thus high sensitivity for changes in molecular geometry and assembly.⁴⁰ A general Jabłoński diagram for FRET_{S-S} and FRET_{T-S} is depicted in Figure 1.6.

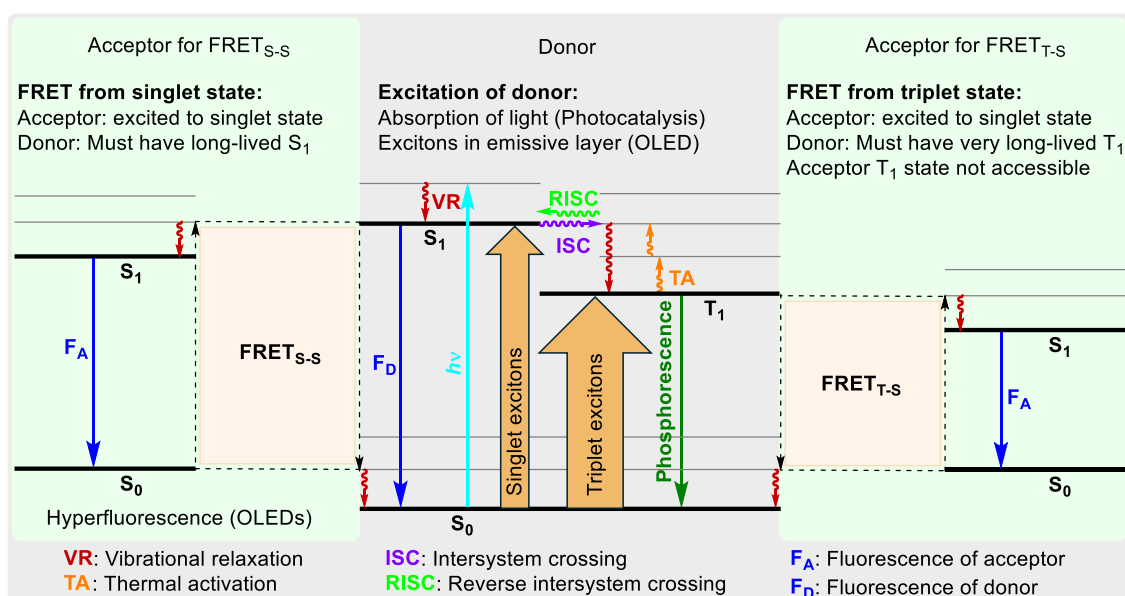


Figure 1.6. Jablonski diagram for FRET from an excited sensitizer (donor) to an acceptor. Wavy arrows represent non-radiative transitions and straight arrows represent radiative transitions. FRET usually refers to the more common FRET_{S-S} but in some cases FRET_{T-S} is also possible.

Besides FRET, energy can also be transferred via a Dexter mechanism (DET).⁴¹ While FRET cannot change the multiplicity of the acceptor, DET is limited only by that the overall multiplicity of the system must be retained. Thus, DET between the T₁ state of the donor and the S₀ state of the acceptor generally yields the T₁ state of the acceptor while the donor is converted back to its S₀ ground state. This is due to DET proceeding via electron exchange between donor and acceptor as schematically depicted in Figure 1.7. In hyperfluorescent OLEDs Dexter energy transfer must be suppressed as it can generate non-emissive triplet states of the terminal fluorescent emitter and contributes to device degradation.^{38,42} In energy transfer (EnT) photocatalysis however, DET is the desired pathway as it can generate reactive triplet states of the acceptor inaccessible by direct excitation or FRET.⁴³

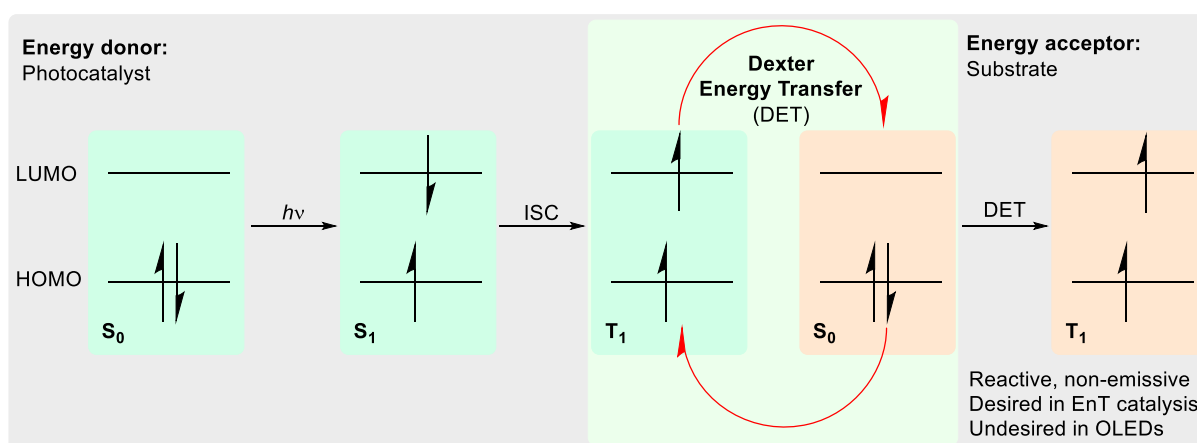
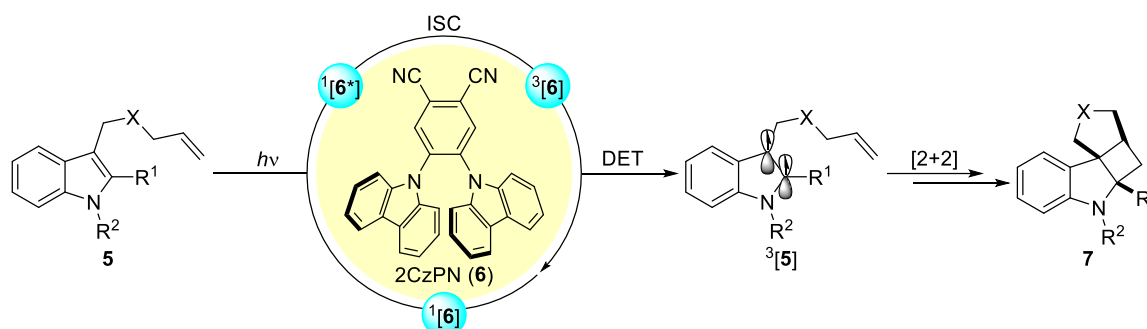


Figure 1.7. Energy transfer via Dexter mechanism can generate triplet excited states of the acceptor inaccessible via direct excitation or FRET.

Triplet states of organic molecules undergo reactions such as [2+2] cycloadditions,^{44–47} *E/Z*-isomerizations,^{48,49} and σ -bond cleavage.^{50–52} Indole derivative **5** depicted in Scheme 1.1 does not absorb light in the visible range, but its

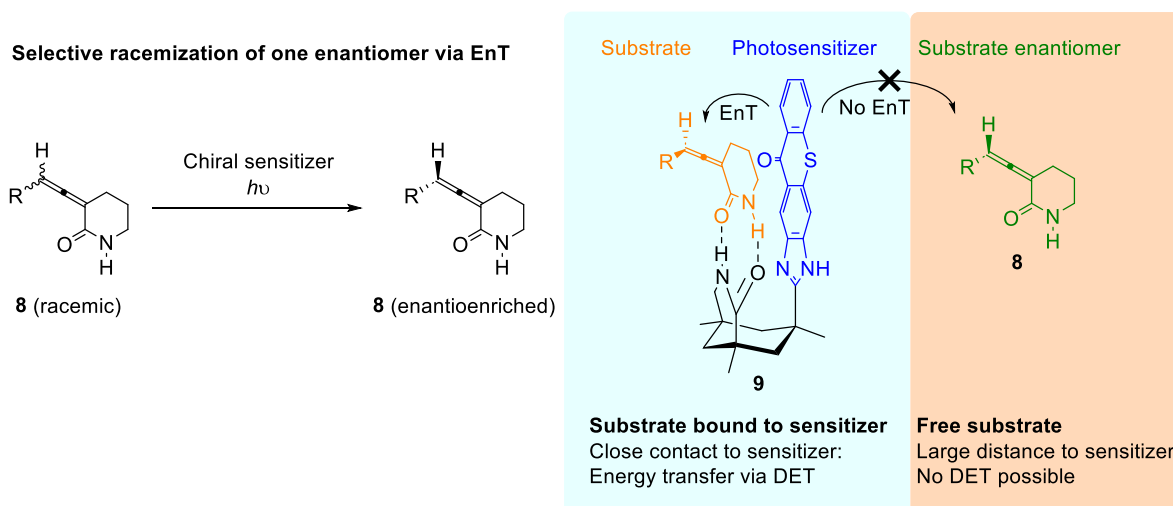
triplet energy is sufficiently low for sensitization by photocatalysts absorbing light in the visible range. By using triplet sensitizers such as phosphorescent Ir-complexes^{45,46} or TADF emitters with sufficient triplet energy⁴⁴ a [2+2] cycloaddition is induced as depicted in Scheme 1.1.



Scheme 1.1. Triplet sensitization induced [2+2] cycloaddition. Initially developed with iridium-based phosphorescent emitters,⁴⁶ fully organic TADF emitters such as 2CzPN are also effective photocatalysts for the reaction.⁴⁴

While FRET can occur over long distances of up to 10 nm, DET is limited to direct contact between substrate and sensitizer (usually below 1 nm) because sufficient orbital overlap is needed to facilitate the electron exchange.⁴¹ The addition of steric hindrance into the sensitizer was shown to improve the efficiency of hyperfluorescent OLEDs by suppressing the generation of non-emissive emitter triplet states,⁴² while a triplet sensitizer for photocatalysis must be accessible by the substrate. Although the short range of DET makes it less efficient over long distances, it is beneficial for enantioselective triplet sensitizations by chiral sensitizers as the substrate must be in close proximity to the chiral information for the sensitization to occur. This was utilized for a [2+2] cycloaddition by chiral phosphoric acid catalysts bearing TADF emitting moieties⁵³ and for deracemization of allenes⁵⁴ and alkenes⁵⁵ by a chiral thioxanthone sensitizer. The substrate-catalyst assembly responsible for the enantioselectivity in the deracemization is depicted in Scheme 1.2. Two reasons for the selectivity were found: First, one enantiomer has a higher affinity to the chiral photosensitizer and thus is preferentially sensitized. This only explains part of the experimentally observed enantiomeric ratio. Another reason is that within the substrate-catalyst complex the substrate enantiomer with the R-group facing away from the thioxanthone photosensitizer moiety places the double bond to be sensitized closer to the thioxanthone moiety and thus makes DET within the substrate-catalyst complex more efficient. The non-stereoselective background reaction between unbound substrate and photosensitizer is suppressed by the strong distance dependence of DET.

As an efficient triplet sensitizer, thioxanthone is a good example for where OLED research and photocatalysis have fundamentally different requirements. The high rate of ISC with low rate of RISC prevents thioxanthone to be a candidate for (hyper)fluorescent OLEDs and due to the low phosphorescent yield at room temperature from the long-lived T_1 state it cannot give efficient phosphorescent OLEDs either. However, high rate of ISC and long triplet lifetime are exactly the properties needed for a triplet sensitizer. This does not generally exclude thioxanthone-based molecules from being used as OLED emitters, but optimization for OLED applications led to molecules with reduced triplet lifetime by increasing the rate of RISC and thus in opposite directions as for EnT photocatalysis.⁵⁶



Scheme 1.2. Deracemization of chiral allenes via triplet sensitization utilizes the distance dependence of DET. Free substrate is at a larger distance compared to bound substrate and thus the racemic background reaction leading to racemization is substantially slower.

1.7 Importance of TADF emitters as photocatalysts

Fully organic TADF emitters are especially desirable photocatalysts, not only due to their low cost of production but also due to their easily tunable redox properties. The prototypical TADF emitter 4CzIPN (**4**) was disclosed in 2012.¹⁰ In 2016, the photocatalytic potential of such donor-acceptor TADF emitters was demonstrated on the example of a photoredox/nickel dual catalytic C-C cross coupling¹¹ and in 2018 a rational approach to construct photocatalysts based on such donor-acceptor TADF molecules was published.⁵⁷ Since then, 4CzIPN and similar TADF molecules became some of the most widely used photocatalysts. The basic design principle for such photocatalysts is based on the spatial separation of HOMO and LUMO. This is only a crude approximation and usually not sufficient for the design of efficient TADF emitters with a small ΔE_{ST} , large k_{RISC} , and large k_F , where locally excited states need to be considered.⁵⁸ However approximation of HOMO and LUMO as donor and acceptor centered orbitals suffices for a rather independent tuning of oxidation and reduction potentials in the context of photocatalysis as exemplarily depicted in Figure 1.8.⁵⁷

Although high oxidation and high reduction potentials in a single photocatalyst are often desirable, a large redox window necessitates a large excited state energy and thus a blueshift of the absorption. For visible light photoredox catalysis 4CzIPN stands out as a rather general photocatalyst due to its balanced redox potentials and good absorption of light in the blue range of the visible spectrum.

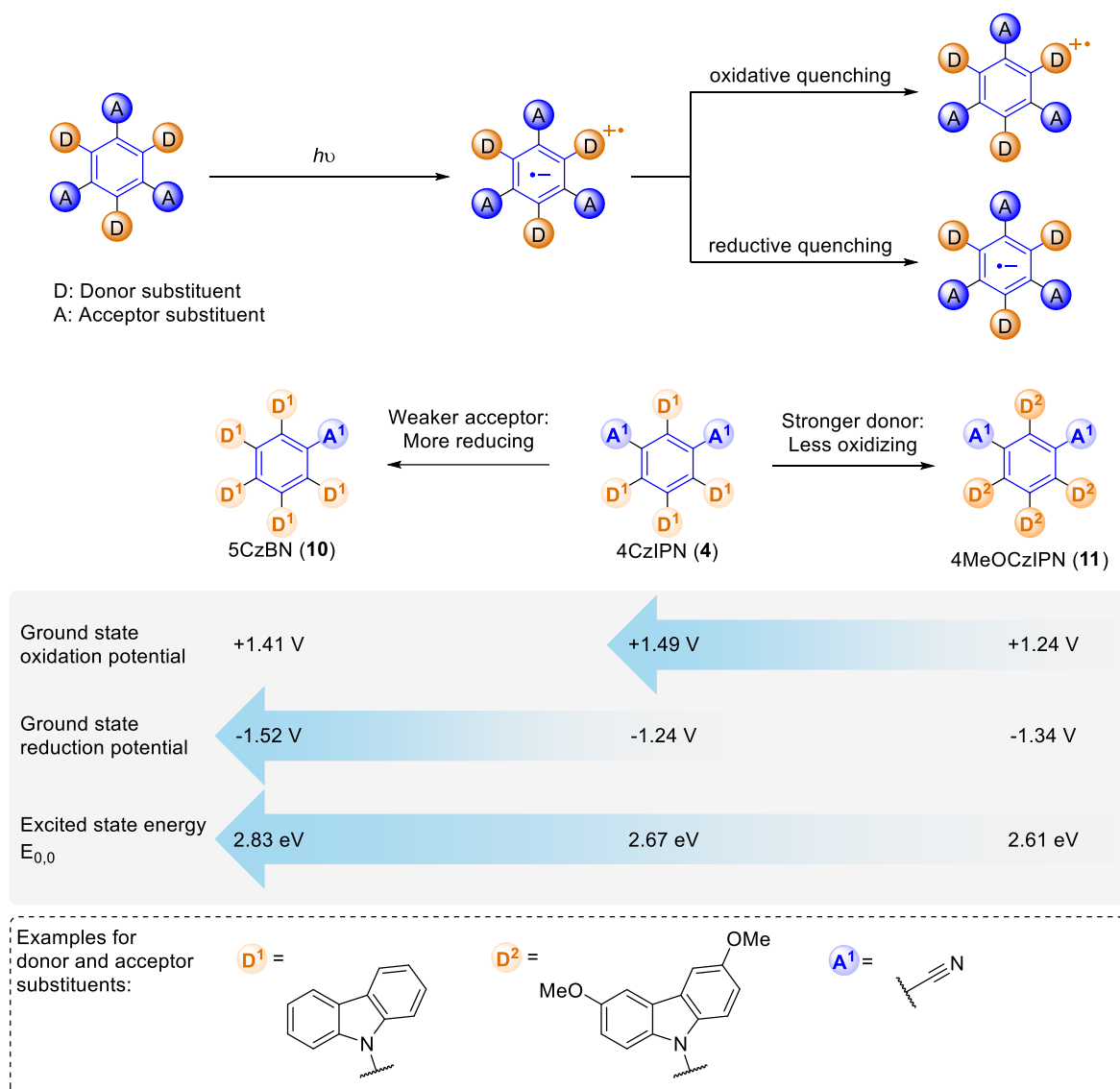
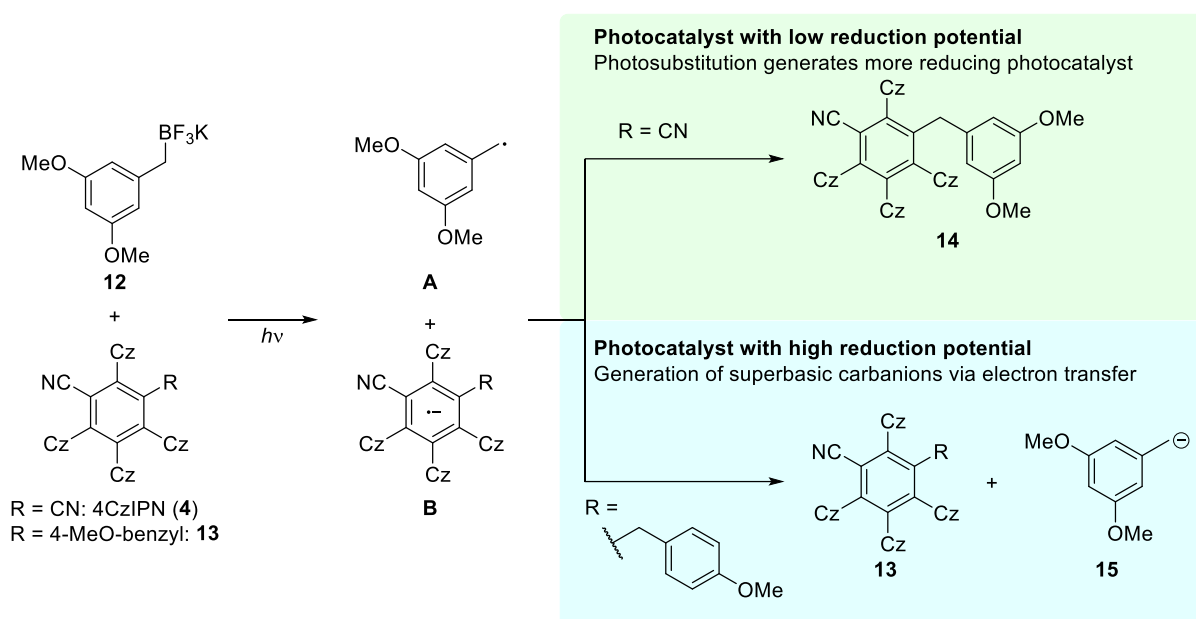


Figure 1.8. The most widely used organic donor-acceptor TADF emitters consist of a cyanoarene acceptor core with carbazole or diphenylamine donor substituents. The core structure has the largest influence on the reductive properties and the donor substituents have the largest influence on the oxidative properties. Redox potentials vs. SCE in MeCN (**10** and **4**) or MeCN/DCM 5:1 v:v (**11**).⁵⁷

Under certain reaction conditions 4CzIPN is not photostable. However, this can be beneficial due to formation of a more reducing photocatalyst. If reduction of an intermediate radical is too slow, photosubstitution of a cyano group substitutes an acceptor group by a neutral or weak donor group and thus in situ generates a photocatalyst with increased reduction potential as depicted in Scheme 1.3.⁵⁹

In redox-neutral reactions generating reactive carbanions via reductive radical-polar crossover (RRPCO)^{60–67} donor-acceptor TADF emitters and their photosubstitution products stand out as particularly effective and often surpass the previous benchmark photocatalysts based on platinum-group metals. Besides a large redox window, the excited state lifetime and stability of the photocatalyst radical anion is important for both, photosubstitution and RRPCO to provide sufficient time for the bimolecular reactions to occur. Transient absorption spectroscopy as described in Chapter 3 showed that the reductive quenching of the excited state of photocatalyst **13** as an example for a catalytically active photosubstitution product of 4CzIPN proceeds on the timescale of a few microseconds and the RRPCO step on the time scale of hundreds of microseconds.⁶⁴ The required excited state lifetime and radical anion stability are reached

in many TADF emitters. Radical anions of cyanoarene-based TADF emitters have been found to be rather stable in solution^{64,68} and the radical anion of structurally similar dicyanoanthracene has been characterized in the solid state.⁶⁹



Scheme 1.3. Dicyanobenzene-based donor-acceptor TADF emitters such as 4CzIPN undergo photosubstitution, exchanging one of the cyano groups by an alkyl or benzyl group.⁵⁹ The molecules generated upon photosubstitution are chemically more stable under the reaction conditions, more reducing and often the actual catalytically active species if superbasic carbanions are generated in the reaction. This is discussed in more detail in Chapters 2 and 3.

1.8 Conclusion

In conclusion, researchers working in photocatalysis acquired a significant part of their catalyst repertoire from OLED research. This is understandable, considering that both applications are based on excited state molecules and many of the processes occurring within the emissive layer of an OLED also occur in a photoreactor. Both applications need photostable molecules with excitation energies usually within or close to the visible range of the electromagnetic spectrum. Depending on the type of OLED, singlet or triplet excited states are utilized for emission or energy transfer to a terminal emitter and often the same excited states can trigger photocatalytic reactions. However, some properties are optimized in opposite directions for each application. The most critical differences are the desired excited state lifetime, efficiency of energy transfer via Förster and Dexter mechanism (FRET and DET), and efficiency of electron transfer. Long excited state lifetimes are desired for photocatalysts to allow bimolecular reactions, while short excited state lifetimes are desired for OLED applications to prevent efficiency roll off and device degradation. Energy transfer via FRET is desired for hyperfluorescent OLEDs while it has little use in photocatalysis. Energy transfer via DET is the main mechanism in energy transfer photocatalysis as it generates reactive triplet states of organic molecules not accessible via direct excitation, but in OLEDs it generates non-emissive triplet states and leads to device degradation. The same holds true for photoredox catalysis where electron transfer from the excited state catalyst is the desired pathway while this reduces the efficiency and lifetime of an OLED. However, often there is substantial overlap between what is still acceptable for an OLED emitter and what is necessary for a photocatalyst. An excited state lifetime of 1 μ s for example, is considered short for a phosphorescent or TADF OLED emitter, while this is a long

excited state lifetime for a photocatalyst. Thus, new classes of OLED emitters are generally good candidates for future photocatalysts, but to select the best candidates it is important to consider the different requirements for each application and that the perfect photocatalyst is not necessarily among the best OLED emitters.

1.9 References

- (1) Braslavsky, S. E. Glossary of terms used in photochemistry, 3rd edition (IUPAC Recommendations 2006). *Pure and Applied Chemistry* **2007**, *79*, 293–465.
- (2) Pope, M.; Kallmann, H. P.; Magnante, P. Electroluminescence in Organic Crystals. *J. Chem. Phys.* **1963**, *38*, 2042–2043.
- (3) Shi, J.; Tang, C. W. Anthracene derivatives for stable blue-emitting organic electroluminescence devices. *Appl. Phys. Lett.* **2002**, *80*, 3201–3203.
- (4) Adachi, C.; Tsutsui, T.; Saito, S. Blue light-emitting organic electroluminescent devices. *Appl. Phys. Lett.* **1990**, *56*, 799–801.
- (5) Li, T.-Y.; Wu, J.; Wu, Z.-G.; Zheng, Y.-X.; Zuo, J.-L.; Pan, Y. Rational design of phosphorescent iridium(III) complexes for emission color tunability and their applications in OLEDs. *Coord. Chem. Rev.* **2018**, *374*, 55–92.
- (6) Paris, J. P.; Brandt, W. W. CHARGE TRANSFER LUMINESCENCE OF A RUTHENIUM(II) CHELATE. *J. Am. Chem. Soc.* **1959**, *81*, 5001–5002.
- (7) Baldo, M. A.; Lamansky, S.; Burrows, P. E.; Thompson, M. E.; Forrest, S. R. Very high-efficiency green organic light-emitting devices based on electrophosphorescence. *Appl. Phys. Lett.* **1999**, *75*, 4–6.
- (8) Adachi, C.; Baldo, M. A.; Forrest, S. R.; Thompson, M. E. High-efficiency organic electrophosphorescent devices with tris(2-phenylpyridine)iridium doped into electron-transporting materials. *Appl. Phys. Lett.* **2000**, *77*, 904–906.
- (9) Day, J. I.; Teegardin, K.; Weaver, J.; Chan, J. Advances in Photocatalysis: A Microreview of Visible Light Mediated Ruthenium and Iridium Catalyzed Organic Transformations. *Organic process research & development* **2016**, *20*, 1156–1163.
- (10) Uoyama, H.; Goushi, K.; Shizu, K.; Nomura, H.; Adachi, C. Highly efficient organic light-emitting diodes from delayed fluorescence. *Nature* **2012**, *492*, 234–238.
- (11) Luo, J.; Zhang, J. Donor–Acceptor Fluorophores for Visible-Light-Promoted Organic Synthesis: Photoredox/Ni Dual Catalytic C(sp³)–C(sp²) Cross-Coupling. *ACS Catal.* **2016**, *6*, 873–877.
- (12) Geffroy, B.; Le Roy, P.; Prat, C. Organic light-emitting diode (OLED) technology: materials, devices and display technologies. *Polym. Int.* **2006**, *55*, 572–582.
- (13) Bae, H. W.; Son, Y. H.; Kang, B. Y.; Lee, J. M.; Nam, H.; Kwon, J. H. Luminance uniformity study of OLED lighting panels depending on OLED device structures. *Opt. Express* **2015**, *23*, 30701–30708.
- (14) Baldo, M. A.; O'Brien, D. F.; Thompson, M. E.; Forrest, S. R. Excitonic singlet-triplet ratio in a semiconducting organic thin film. *Phys. Rev. B* **1999**, *60*, 14422–14428.
- (15) Jiang, H.; Tao, P.; Wong, W.-Y. Recent Advances in Triplet–Triplet Annihilation-Based Materials and Their Applications in Electroluminescence. *ACS Materials Lett.* **2023**, *5*, 822–845.
- (16) Jin, J.; Yu, T.; Chen, J.; Hu, R.; Yang, G.; Zeng, Y.; Li, Y. Recent advances of triplet–triplet annihilation upconversion in photochemical transformations. *Curr. Opin. Green Sustain. Chem.* **2023**, *43*, 100841.
- (17) Hu, A.; Chen, Y.; Guo, J.-J.; Yu, N.; An, Q.; Zuo, Z. Cerium-Catalyzed Formal Cycloaddition of Cycloalkanols with Alkenes through Dual Photoexcitation. *J. Am. Chem. Soc.* **2018**, *140*, 13580–13585.
- (18) Neumeier, M.; Chakraborty, U.; Schaarschmidt, D.; La Pena O'Shea, V. de; Perez-Ruiz, R.; Jacobi von Wangelin, A. Combined Photoredox and Iron Catalysis for the Cyclotrimerization of Alkynes. *Angew. Chem., Int. Ed.* **2020**, *59*, 13473–13478.
- (19) McClure, D. S. Triplet-Singlet Transitions in Organic Molecules. Lifetime Measurements of the Triplet State. *J. Chem. Phys.* **1949**, *17*, 905–913.
- (20) Koziar, J. C.; Cowan, D. O. Photochemical heavy-atom effects. *Acc. Chem. Res.* **1978**, *11*, 334–341.
- (21) Baldo, M. A.; O'Brien, D. F.; You, Y.; Shoustikov, A.; Sibley, S.; Thompson, M. E.; Forrest, S. R. Highly efficient phosphorescent emission from organic electroluminescent devices. *Nature* **1998**, *395*, 151–154.
- (22) Romero, N. A.; Nicewicz, D. A. Organic Photoredox Catalysis. *Chem. Rev.* **2016**, *116*, 10075–10166.

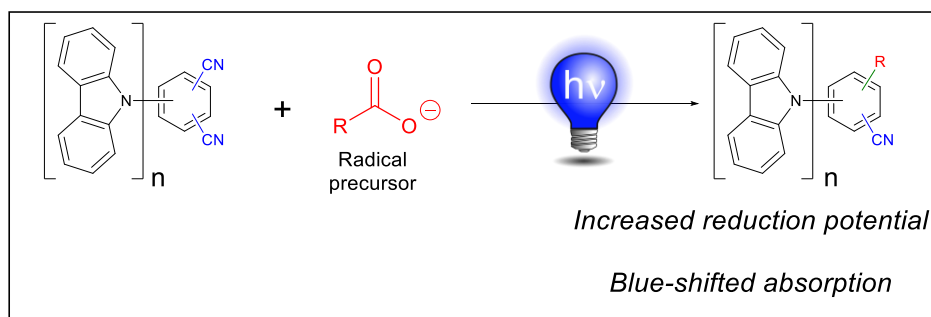
- (23) Caspar, J. V.; Meyer, T. J. Photochemistry of tris(2,2'-bipyridine)ruthenium(2+) ion (Ru(bpy)₃²⁺). Solvent effects. *J. Am. Chem. Soc.* **1983**, *105*, 5583–5590.
- (24) Moon, Y. K.; Jang, H. J.; Hwang, S.; Kang, S.; Kim, S.; Oh, J.; Lee, S.; Kim, D.; Lee, J. Y.; You, Y. Modeling Electron-Transfer Degradation of Organic Light-Emitting Devices. *Adv. Mater.* **2021**, *33*, e2003832.
- (25) Parker, C. A.; Hatchard, C. G. Triplet-singlet emission in fluid solutions. Phosphorescence of eosin. *Trans. Faraday Soc.* **1961**, *57*, 1894.
- (26) Blasse, G.; McMillin, D. R. On the luminescence of bis (triphenylphosphine) phenanthroline copper (I). *Chem. Phys. Lett.* **1980**, *70*, 1–3.
- (27) Ferraro, V.; Bizzarri, C.; Bräse, S. Thermally Activated Delayed Fluorescence (TADF) Materials Based on Earth-Abundant Transition Metal Complexes: Synthesis, Design and Applications. *Adv. Sci.* **2024**, e2404866.
- (28) Bryden, M. A.; Zysman-Colman, E. Organic thermally activated delayed fluorescence (TADF) compounds used in photocatalysis. *Chem. Soc. Rev.* **2021**, *50*, 7587–7680.
- (29) Ishimatsu, R.; Matsunami, S.; Shizu, K.; Adachi, C.; Nakano, K.; Imato, T. Solvent effect on thermally activated delayed fluorescence by 1,2,3,5-tetrakis(carbazol-9-yl)-4,6-dicyanobenzene. *J. Phys. Chem. A* **2013**, *117*, 5607–5612.
- (30) Förster, T. Zwischenmolekulare Energiewanderung und Fluoreszenz. *Ann. Phys.* **1948**, *437*, 55–75.
- (31) Murawski, C.; Leo, K.; Gather, M. C. Efficiency roll-off in organic light-emitting diodes. *Adv. Mater.* **2013**, *25*, 6801–6827.
- (32) Reineke, S.; Walzer, K.; Leo, K. Triplet-exciton quenching in organic phosphorescent light-emitting diodes with Ir-based emitters. *Phys. Rev. B* **2007**, *75*.
- (33) Baldo, M. A.; Adachi, C.; Forrest, S. R. Transient analysis of organic electrophosphorescence. II. Transient analysis of triplet-triplet annihilation. *Phys. Rev. B* **2000**, *62*, 10967–10977.
- (34) Sokolik, I.; Priestley, R.; Walser, A. D.; Dorsinville, R.; Tang, C. W. Bimolecular reactions of singlet excitons in tris (8-hydroxyquinoline) aluminum. *Appl. Phys. Lett.* **1996**, *69*, 4168–4170.
- (35) Zhang, Y.; Whited, M.; Thompson, M. E.; Forrest, S. R. Singlet–triplet quenching in high intensity fluorescent organic light emitting diodes. *Chem. Phys. Lett.* **2010**, *495*, 161–165.
- (36) Hasan, M.; Saggarr, S.; Shukla, A.; Bencheikh, F.; Sobus, J.; McGregor, S. K. M.; Adachi, C.; Lo, S.-C.; Namdas, E. B. Probing polaron-induced exciton quenching in TADF based organic light-emitting diodes. *Nat. Commun.* **2022**, *13*, 254.
- (37) Hasan, M.; Shukla, A.; Ahmad, V.; Sobus, J.; Bencheikh, F.; McGregor, S. K. M.; Mamada, M.; Adachi, C.; Lo, S.-C.; Namdas, E. B. Exciton–Exciton Annihilation in Thermally Activated Delayed Fluorescence Emitter. *Adv. Funct. Mater.* **2020**, *30*.
- (38) Sandanayaka, A. S. D.; Matsushima, T.; Adachi, C. Degradation Mechanisms of Organic Light-Emitting Diodes Based on Thermally Activated Delayed Fluorescence Molecules. *J. Phys. Chem. C* **2015**, *119*, 23845–23851.
- (39) Sk, B.; Tsuru, R.; Hayashi, K.; Hirata, S. Selective Triplet–Singlet Förster-Resonance Energy Transfer for Bright Red Afterglow Emission. *Adv. Funct. Mater.* **2022**, *33*.
- (40) Wu, L.; Huang, C.; Emery, B. P.; Sedgwick, A. C.; Bull, S. D.; He, X.-P.; Tian, H.; Yoon, J.; Sessler, J. L.; James, T. D. Förster resonance energy transfer (FRET)-based small-molecule sensors and imaging agents. *Chem. Soc. Rev.* **2020**, *49*, 5110–5139.
- (41) Dexter, D. L. A Theory of Sensitized Luminescence in Solids. *J. Chem. Phys.* **1953**, *21*, 836–850.
- (42) Cho, H.-H.; Congrave, D. G.; Gillett, A. J.; Montanaro, S.; Francis, H. E.; Riesgo-Gonzalez, V.; Ye, J.; Chowdury, R.; Zeng, W.; Etherington, M. K.; Royackers, J.; Millington, O.; Bond, A. D.; Plasser, F.; Frost, J. M.; Grey, C. P.; Rao, A.; Friend, R. H.; Greenham, N. C.; Bronstein, H. Suppression of Dexter transfer by covalent encapsulation for efficient matrix-free narrowband deep blue hyperfluorescent OLEDs. *Nat. Mater.* **2024**, *23*, 519–526.
- (43) Dutta, S.; Erchinger, J. E.; Strieth-Kalthoff, F.; Kleinmans, R.; Glorius, F. Energy transfer photocatalysis: exciting modes of reactivity. *Chem. Soc. Rev.* **2024**, *53*, 1068–1089.
- (44) Rolka, A. B.; Koenig, B. Dearomative Cycloadditions Utilizing an Organic Photosensitizer: An Alternative to Iridium Catalysis. *Org. Lett.* **2020**, *22*, 5035–5040.
- (45) James, M. J.; Schwarz, J. L.; Strieth-Kalthoff, F.; Wibbeling, B.; Glorius, F. Dearomative Cascade Photocatalysis: Divergent Synthesis through Catalyst Selective Energy Transfer. *J. Am. Chem. Soc.* **2018**, *140*, 8624–8628.

- (46) Zhu, M.; Zheng, C.; Zhang, X.; You, S.-L. Synthesis of Cyclobutane-Fused Angular Tetracyclic Spiroindolines via Visible-Light-Promoted Intramolecular Dearomatization of Indole Derivatives. *J. Am. Chem. Soc.* **2019**, *141*, 2636–2644.
- (47) Sicignano, M.; Rodríguez, R. I.; Alemán, J. Recent Visible Light and Metal Free Strategies in [2+2] and [4+2] Photocycloadditions. *Eur. J. Org. Chem.* **2021**, *2021*, 3303–3321.
- (48) Singh, K.; Staig, S. J.; Weaver, J. D. Facile synthesis of Z-alkenes via uphill catalysis. *J. Am. Chem. Soc.* **2014**, *136*, 5275–5278.
- (49) Nevesely, T.; Molloy, J. J.; McLaughlin, C.; Brüss, L.; Daniliuc, C. G.; Gilmour, R. Leveraging the $n \rightarrow \pi^*$ Interaction in Alkene Isomerization by Selective Energy Transfer Catalysis. *Angew. Chem., Int. Ed.* **2022**, *61*, e202113600.
- (50) Da Lee, S.; Soni, V. K.; Cho, E. J. N-O Bond Activation by Energy Transfer Photocatalysis. *Acc. Chem. Res.* **2022**, *55*, 2526–2541.
- (51) Tan, G.; Das, M.; Kleinmans, R.; Katzenburg, F.; Daniliuc, C.; Glorius, F. Energy transfer-enabled unsymmetrical diamination using bifunctional nitrogen-radical precursors. *Nat. Catal.* **2022**, *5*, 1120–1130.
- (52) Patra, T.; Mukherjee, S.; Ma, J.; Strieth-Kalthoff, F.; Glorius, F. Visible-Light-Photosensitized Aryl and Alkyl Decarboxylative Functionalization Reactions. *Angew. Chem., Int. Ed.* **2019**, *58*, 10514–10520.
- (53) Rolka, A. B.; Archipowa, N.; Kutta, R. J.; König, B.; Toste, F. D. Hybrid Catalysts for Enantioselective Photo-Phosphoric Acid Catalysis. *J. Org. Chem.* **2023**, *88*, 6509–6522.
- (54) Hölzl-Hobmeier, A.; Bauer, A.; Silva, A. V.; Huber, S. M.; Bannwarth, C.; Bach, T. Catalytic deracemization of chiral allenes by sensitized excitation with visible light. *Nature* **2018**, *564*, 240–243.
- (55) Kratz, T.; Steinbach, P.; Breitenlechner, S.; Storch, G.; Bannwarth, C.; Bach, T. Photochemical Deracemization of Chiral Alkenes via Triplet Energy Transfer. *J. Am. Chem. Soc.* **2022**, *144*, 10133–10138.
- (56) Li, Z.; Wei, X.; Yi, Y.; Wang, P.; Wang, Y. Stable organic light-emitting diodes based on thioxanthone derivative with shortened photoluminescence delayed lifetime. *Org. Electron.* **2022**, *104*, 106490.
- (57) Speckmeier, E.; Fischer, T. G.; Zeitler, K. A Toolbox Approach To Construct Broadly Applicable Metal-Free Catalysts for Photoredox Chemistry: Deliberate Tuning of Redox Potentials and Importance of Halogens in Donor-Acceptor Cyanoarenes. *J. Am. Chem. Soc.* **2018**, *140*, 15353–15365.
- (58) Silva, P. de; Kim, C. A.; Zhu, T.; van Voorhis, T. Extracting Design Principles for Efficient Thermally Activated Delayed Fluorescence (TADF) from a Simple Four-State Model. *Chem. Mater.* **2019**, *31*, 6995–7006.
- (59) Grotjahn, S.; König, B. Photosubstitution in Dicyanobenzene-based Photocatalysts. *Org. Lett.* **2021**, *23*, 3146–3150.
- (60) Pitzer, L.; Schwarz, J. L.; Glorius, F. Reductive radical-polar crossover: traditional electrophiles in modern radical reactions. *Chem. Sci.* **2019**, *10*, 8285–8291.
- (61) Donabauer, K.; König, B. Strategies for the Photocatalytic Generation of Carbanion Equivalents for Reductant-Free C-C Bond Formations. *Acc. Chem. Res.* **2021**, *54*, 242–252.
- (62) Phelan, J. P.; Lang, S. B.; Compton, J. S.; Kelly, C. B.; Dykstra, R.; Gutierrez, O.; Molander, G. A. Redox-Neutral Photocatalytic Cyclopropanation via Radical/Polar Crossover. *J. Am. Chem. Soc.* **2018**, *140*, 8037–8047.
- (63) Abrams, R.; Clayden, J. Photocatalytic Difunctionalization of Vinyl Ureas by Radical Addition Polar Truce-Smiles Rearrangement Cascades. *Angew. Chem., Int. Ed.* **2020**, *59*, 11600–11606.
- (64) Grotjahn, S.; Graf, C.; Zelenka, J.; Pattanaik, A.; Müller, L.; Kutta, R. J.; Rehbein, J.; Roithová, J.; Gschwind, R. M.; Nuernberger, P.; König, B. Reactivity of Superbasic Carbanions Generated via Reductive Radical-Polar Crossover in the Context of Photoredox Catalysis. *Angew. Chem., Int. Ed.* **2024**, e202400815.
- (65) Berger, A. L.; Donabauer, K.; König, B. Photocatalytic carbanion generation from C-H bonds - reductant free Barbier/Grignard-type reactions. *Chem. Sci.* **2019**, *10*, 10991–10996.
- (66) Donabauer, K.; Maity, M.; Berger, A. L.; Huff, G. S.; Crespi, S.; König, B. Photocatalytic carbanion generation - benzylation of aliphatic aldehydes to secondary alcohols. *Chem. Sci.* **2019**, *10*, 5162–5166.
- (67) Meng, Q.-Y.; Schirmer, T. E.; Berger, A. L.; Donabauer, K.; König, B. Photocarboxylation of Benzylic C-H Bonds. *J. Am. Chem. Soc.* **2019**, *141*, 11393–11397.
- (68) Kwon, Y.; Lee, J.; Noh, Y.; Kim, D.; Lee, Y.; Yu, C.; Roldao, J. C.; Feng, S.; Gierschner, J.; Wannemacher, R.; Kwon, M. S. Formation and degradation of strongly reducing cyanoarene-based radical anions towards efficient radical anion-mediated photoredox catalysis. *Nat. Commun.* **2023**, *14*, 92.

(69) Horsewill, S. J.; Hierlmeier, G.; Farasat, Z.; Barham, J. P.; Scott, D. J. Shining Fresh Light on Complex Photoredox Mechanisms through Isolation of Intermediate Radical Anions. *ACS Catal.* **2023**, *13*, 9392–9403.



2 Photosubstitution in Dicyanobenzene-based Photocatalysts



Major parts of this chapter have been published. For reference see: S. Grotjahn and B. König *Org. Lett.* **2021**, 23, 8, 3146–3150.

Adapted with permission. Copyright 2021 American Chemical Society.

Author contributions: Sascha Grotjahn conducted all experiments. Burkhard König supervised the project. Cyclic voltammetry was conducted by Regina Hoheisel.

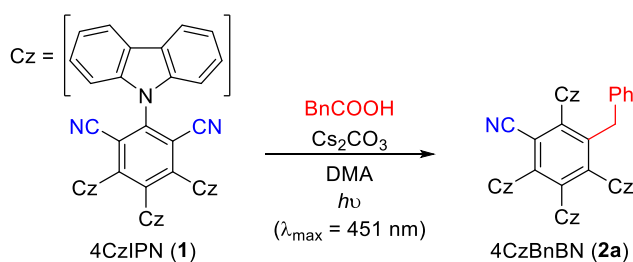
Compounds **2o**, **2p**, and **4d** were synthesized after publication. Compound **2p** was synthesized during a research stay in the group of Prof. Dr. Magnus Rueping at King Abdullah University of Science and Technology (KAUST), Thuwal, Saudi-Arabia. A manuscript including compound **2p** is currently under preparation.

Abstract

A photosubstitution of one cyano group in dicyanobenzene based photocatalysts and TADF emitters is reported. The reaction is a general degradation pathway for some widely used organic photocatalysts such as 4CzIPN and suggests that the active photocatalyst in many reactions is likely different from the photocatalyst initially added to the reaction. On the other hand, the photosubstitution is a facile route to diverse highly reducing photocatalysts and TADF emitters.

2.1 Introduction

The organic dye 4CzIPN (**1**) was developed in 2012 by Adachi and co-workers as a highly efficient thermally activated delayed fluorescence (TADF) emitter.¹ In 2016, Zhang and co-workers used 4CzIPN and analogous TADF emitting organic dyes in photoredox/Ni dual catalysis.² Only 2 years, later Zeitler and co-workers reported a rational design to tune redox potentials of 4CzIPN and similar cyanobenzene derived photocatalysts, thus, providing access to organic dyes for a wide range of redox potentials.³ Application of 4CzIPN as an organic photocatalyst has been reviewed in 2019.⁴ In general, 4CzIPN and closely related organic dyes perform similar to classical ruthenium and iridium based photocatalysts. In reactions including a reductive radical-polar crossover (RRPCO)⁵ 4CzIPN is often superior to transition metal based photocatalysts. In recent years, the concept has gained increasing attention with the development of methods for photocatalytic cyclopropanations,^{6,7} carboxylations using CO₂⁸⁻¹⁰ and the Truce-Smith rearrangement.¹¹ In previous work employing the concept of RRPCO 4CzIPN enabled the generation of benzylic carbanions from phenylacetic acids.¹² However, it was noticed that 4CzIPN is not the active catalyst. Instead, an exchange of one of the cyano groups by a benzyl group was observed converting 4CzIPN to 4CzBnBN within the first minutes of the reaction according to Scheme 2.1.

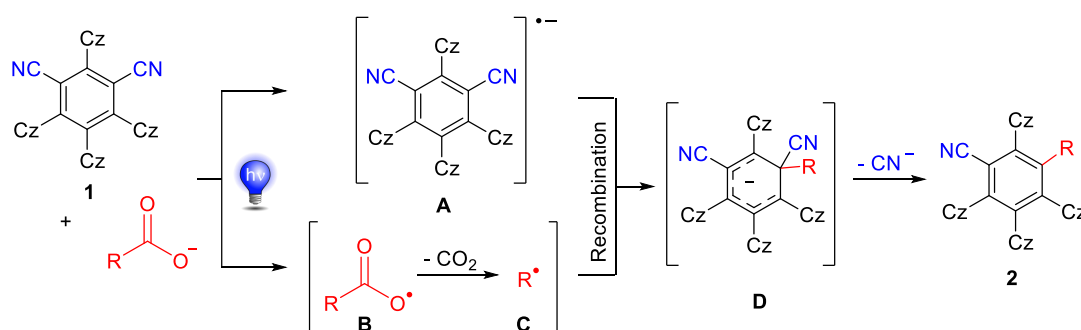


Scheme 2.1. Previously reported in situ photosubstitution of 4CzIPN (**1**) to 4CzBnBN (**2a**).

Photosubstitution in unsubstituted dicyanobenzenes using group 14 organometallic reagents¹³ or aliphatic carboxylic acids¹⁴ has been reported previously. However, only 1,2- and 1,4-dicyanobenzenes gave corresponding products in moderate to good yields while 1,3-dicyanobenzenes gave no photosubstitution product or poor yield and unselective reaction.

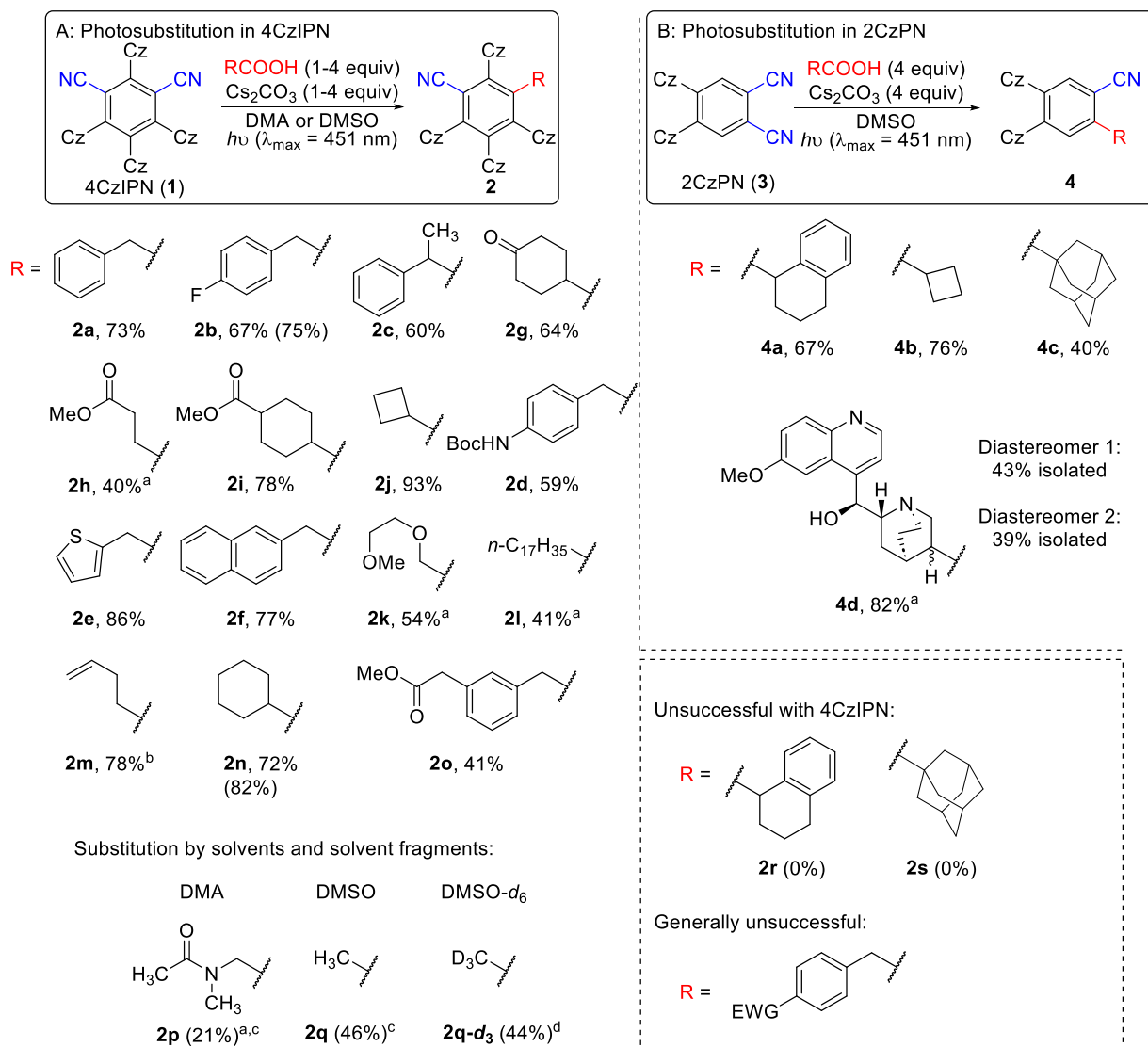
2.2 Results and discussion

This chapter provides deeper insights into this photosubstitution, focusing on the importance for photocatalysis where dicyanobenzene based photocatalysts are widely used. First, the influence of solvent and water on photosubstitution of 4CzIPN with 4-fluorophenylacetic acid (see experimental part 2.4.3 for details) was tested. The reaction performs similarly well in different polar solvents (DMA, DMF, DMSO, MeCN) and is slower in EtOAc and THF. The long reaction time in EtOAc and THF can be attributed to the low solubility of 4CzIPN. In DCM and ⁱPrOH no conversion was observed. The presence of 0 – 20 equivalents of water does not influence the reaction. Thus, it can be concluded that photosubstitution does occur via radical recombination of intermediates A and C with subsequent cyanide elimination from anionic intermediate D and not in an S_NAr-type reaction via a carbanion. This is important to note as it implies that many reactions using 4CzIPN to generate carbanions via RRPCO exclusively form a photosubstitution product of 4CzIPN before carbanions are generated and 4CzIPN itself does not at all participate in the RRPCO step. A proposed mechanism is depicted in Scheme 2.2 in agreement with the reported mechanism for photosubstitution in unsubstituted dicyanobenzenes.¹⁴ In contrast to unsubstituted 1,3-dicyano benzene, 4CzIPN yields the corresponding photosubstitution products cleanly. A likely rationale is steric hindrance by the carbazole units allowing radical recombination only at the positions of the CN-groups. However, a trend towards increased stability of 4CzIPN in comparison to 1,2 and 1,4 dicyanobenzene based photocatalysts has already been observed earlier by Zhang and co-workers.² These observations suggest that in the case of 4CzIPN in the presence of good radical trapping reagents other reaction pathways dominate over photosubstitution.



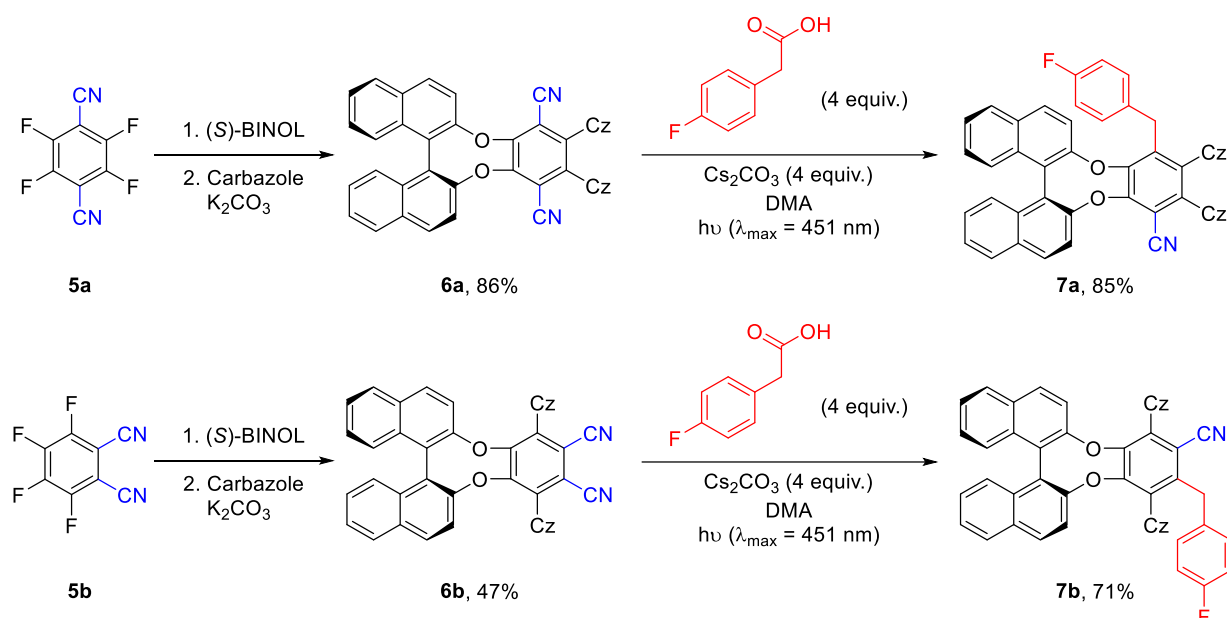
Scheme 2.2. Mechanistic proposal for the photosubstitution of 4CzIPN.

Photosubstitution in 4CzIPN and 2CzPN takes place with a variety of carboxylic acids as depicted in Scheme 2.3. The reaction is not limited to phenylacetic acids, but also proceeds with aliphatic carboxylic acids which give non-stabilized or stabilized alkyl radicals upon oxidation. However, the synthesis of **2h** and **2l** proceeds via non-stabilized primary alkyl radical intermediates, which lead to side reactions and reduced yield. The reaction mixture turned dark orange or brown in these cases. If secondary alkyl radicals are formed as intermediates the reaction proceeds without, or with only small amounts of side products and the solution remains transparent. Reaction completion can be determined by the fading of the yellow/green fluorescence of 4CzIPN. The reaction fails when electron withdrawing groups are present or steric hindrance prohibits the radical recombination. A noteworthy substrate that gave poor conversion and selectivity is tetrahydronaphthoic acid leading to product **2r**. The radical recombination step is likely inhibited by steric hindrance. Tetrahydronaphthoic acid reacts cleanly with the sterically more accessible 2CzPN to give photosubstitution product **4a**. Even the sterically highly demanding adamantane carboxylic acid cleanly reacted to photosubstitution product **4c** while photosubstitution was not observed with 4CzIPN. The moderate isolated yield is attributed to difficulties in workup. Under some reaction conditions photosubstitution occurs with solvent fragments. In presence of DABCO in DMA as solvent one cyano group was substituted by DMA to give photosubstitution product **2p** and in presence of DIPEA and oxygen a methyl group from DMSO substituted one cyano group providing 4CzMeBN (**2q**). These products are also observed in trace amounts in absence of DABCO and DIPEA, respectively.



Scheme 2.3. Substrate scope for photosubstitution in 4CzIPN and 2CzPN. All yields are isolated yields; products were purified by recrystallization of the crude product unless otherwise noted; yields in parentheses are from upscaling to 1 mmol; ^apurified via column chromatography; ^bcyclopropylacetic acid was used as radical precursor; ^cDABCO was added instead of carboxylic acid; ^dDIPEA was added instead of carboxylic acid and the reaction performed under air.

The method was also successfully applied to the synthesis of chiral BINOL-derivative **7a** from the corresponding literature known TADF emitter for circularly polarized light **6a**.¹⁵ Chiral BINOL derivative **7b** was synthesized from the isomer **6b**.¹⁶ Both gave the corresponding photosubstitution product in good yield as depicted in Scheme 1.3. However, it should be mentioned that the analogous reaction with cyclobutane carboxylic acid gave a complex mixture of products despite a clean reaction occurred with 4CzIPN and 2CzPN to products **2j** and **4b**, respectively.



Scheme 2.4. Synthesis of chiral carbazolyl dicyanobenzenes and their photosubstitution. ^aSynthesized one-pot; ^bsynthesized in two steps with isolation of intermediate **9** (see experimental part 2.4.4.2 for details).

Substitution of a cyano group in and 2CzPN 4CzIPN and its isomers 4CzPN and 4CzTPN has been proposed as a degradation pathway of these photocatalysts in the first report of 4CzIPN's use in photocatalysis.² The activity of each catalyst was correlated with its stability and it was concluded that 4CzIPN was among the most active catalysts due to its higher stability. Under the reaction conditions used by Zhang et al. this conclusion was correct. However, the findings presented in this work indicate that this is not due to lack of catalytic activity of the degradation products but due to a blue-shifted absorption. The 2CzPN derived molecules (**4**) do not absorb light above 380 nm, as depicted in Figure 2.1.

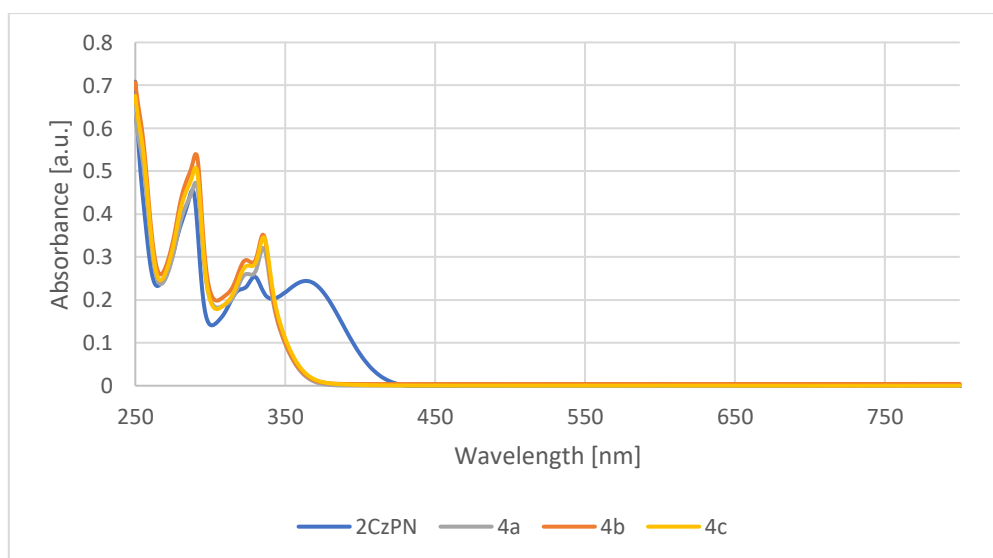


Figure 2.1. Absorption spectra of 2CzPN and photosubstitution products; 20 μ M in MeCN.

Photosubstitution products of 4CzIPN, however, start to absorb below 430 nm, as depicted in Figure 2.2. Thus, standard blue LEDs with an emission maximum near 450 nm do still excite photosubstitution products of 4CzIPN, although less efficiently. Photosubstitution products of 2CzPN need UV light for excitation.

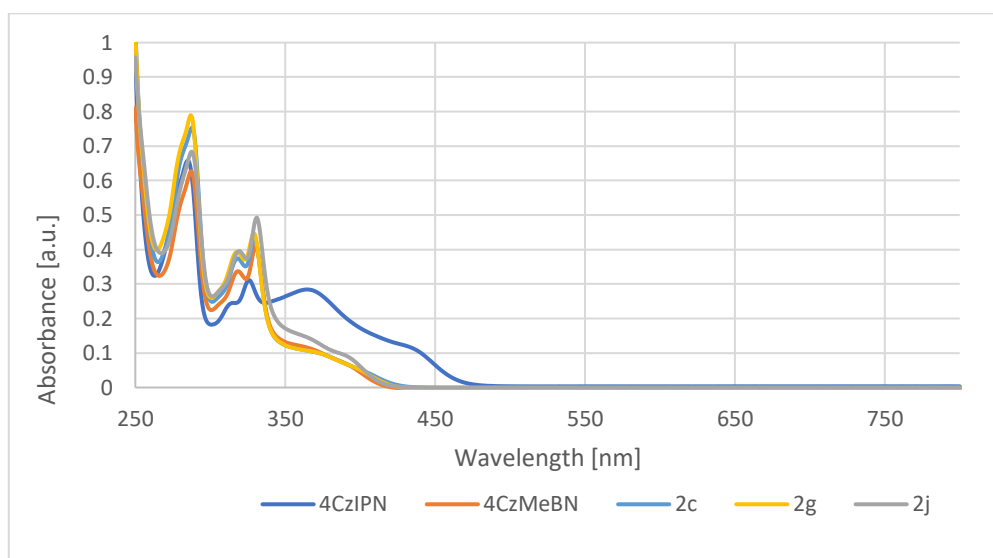
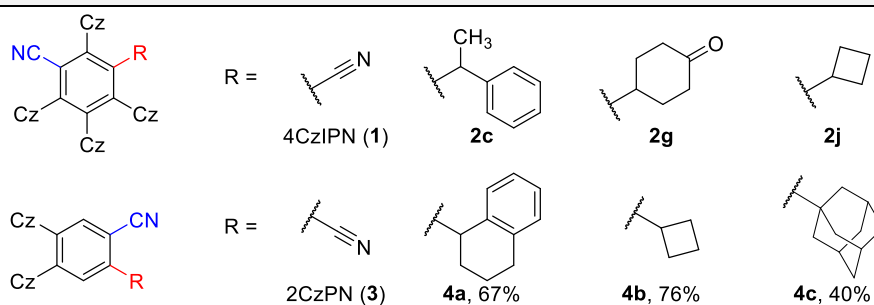


Figure 2.2. Absorption spectra of 4CzIPN and photosubstitution products; 20 μ M in MeCN.

The blue LEDs and CFL used by Zhang and co-workers have only little emission in the range where the photosubstitution products of 4CzIPN absorb and almost no emission in the range where the photosubstitution products of 2CzPN absorb. Thus, it is not surprising that photosubstitution of the catalyst shuts down the reaction and as a direct consequence conversion and yield are depending on the catalyst stability. However, if irradiation is shifted to the blue edge of the visible spectrum the photosubstitution products absorb some of the light. Previous reports on photocatalytic carbanion generation¹² and isotopic labeling¹⁷ demonstrate that photosubstitution of the initial catalyst is necessary for these reactions to occur. Comparison of the cyclic voltammograms of 4CzIPN and 2CzPN with some of their photosubstitution products show a strong increase in ground state reduction potentials while only minor decrease in ground state oxidation potentials is observed (Table 2.1). This is in line with the observations presented by Zeitler and co-workers for rational design of organic photocatalysts that HOMO and LUMO can be tuned rather independently by substitution of the acceptor and donor part, respectively.³ The increased reduction potential upon photosubstitution also explains why 4CzIPN can be used in reactions that are not expected to occur based on 4CzIPN's reduction potential. Benzyl radicals for example, are reported to require a reduction potential of about -1.4 V vs. SCE to be reduced to the corresponding anion,¹⁸ which is less than 4CzIPN's reduction potential of -1.2 V,³ but its photosubstitution products with a reduction potential of approximately -1.7 V vs. SCE are reducing enough. For 2CzPN photosubstitution products $E_{1/2}(\text{PC}/\text{PC}^-)$ is increased by 0.6 V, up to -2.1 V vs. SCE. This is especially noteworthy as 4CzIPN is among the most effective photocatalysts for reactions including an RRPCO step. The increased reductive power of 2CzPN derived catalysts suggest that the scope of these reactions might be expanded to substrates with reduction potentials out of reach for 4CzIPN's photosubstitution products. A comparison of the catalytic activity of 2CzPN, 4CzIPN and their photosubstitution products can be found in the experimental part 2.4.5. In summary, the results show that 2CzPN's photosubstitution products are indeed ineffective if a 451 nm LED is used but perform well when changing the light source to a 400 nm LED. In reactions where 2CzPN is used for energy transfer¹⁹ instead of electron transfer blue light is sufficient because 2CzPN itself still absorbs in the visible range and photosubstitution does not occur under these conditions. Although some organic photocatalysts such as anthrolates²⁰ and *N*-phenylphenothiazines²¹ are known to have more reductive power, these are only poorly oxidizing. Photosubstitution products of 4CzIPN and 2CzPN come with sufficient oxidation potentials to generate radicals from common precursors such as alkylcarboxylic acids, alkyltrifluoroborates, and alkylsilicates.²²

Table 2.1. Ground state potentials and estimated excited state potentials of 4CzIPN, 2CzPN and some photosubstitution products.

Entry	Molecule	$E_{1/2}(\text{PC}/\text{PC}^{\cdot-})^{\text{a}}$	$E_{1/2}(\text{PC}^{\cdot+}/\text{PC})^{\text{a}}$	$E_{1/2}(\text{PC}/\text{PC}^{\cdot-})^{\text{b}}$	$E_{1/2}(\text{PC}^*/\text{PC}^{\cdot-})^{\text{a,b}}$	E_{0-0} [V]	τ [ns] ^c
1	1	-1.44	1.49	-1.37	1.42	2.86	8.5
2	4a	-2.05	1.30	-2.03	1.28	3.33	11.0
3	4b	-2.06	1.37	-1.95	1.26	3.32	10.7
4	4c	-2.06	1.34	-1.98	1.26	3.32	10.4
5	3	-1.23	1.53	-1.14	1.44	2.67	12.7
6	2c	-1.63	1.47	-1.43	1.27	2.90	18.1 ^d
7	2g	-1.63	1.43	-1.47	1.27	2.90	18.9
8	2j	-1.70	1.47	-1.50	1.28	2.97	18.4



^aHalf wave potentials from cyclic voltammetry in MeCN vs SCE; ^bexcited state potentials were estimated from the ground state potentials and the crossing point of the normalized absorption and emission spectra; ^cexcited state lifetime measured in air-saturated MeCN; ^dfor excited state lifetime in deoxygenated MeCN see appendix, Figure 2.32.

Other aspects to note are that yields are generally lower if 4CzIPN is used as a catalyst precursor instead of a photosubstitution product due to 1 equivalent of the radical precursor being consumed upon formation of the active catalyst. Some substrates do not or not cleanly form such highly reducing catalysts in situ and solubility of the photosubstitution products is usually lower than for their dicyanobenzene precursor (see experimental part 2.4.6). However, the method reported herein allows the introduction of different functional groups to tune physical properties such as solubility, if necessary.

2.3 Conclusion

In summary, dicyanobenzene based photocatalysts such as 4CzIPN react with oxidatively generated radicals under substitution of a cyano group. The photosubstitution products should not be mistaken as degradation products but themselves are highly reducing photocatalysts and likely the active catalyst in many reactions previously thought to be catalyzed by 4CzIPN and similar dicyanobenzene-based photocatalysts. 2CzPN derived catalysts were found to have ground state reduction potentials of up to -2.06 V vs. SCE and thus are more reducing than currently used cyanobenzene based photocatalysts and their photosubstitution products while oxidation potentials are only little affected. Absorption- and emission spectra are blue shifted by up to 50 nm, which is important for choosing a suitable irradiation wavelength for reactions where the photocatalyst is first converted to the active catalyst. The procedure described herein allows for an easy synthesis of these photosubstitution products to be used as photocatalysts. Described catalysts are TADF emitting in the blue range which offers an easy method to obtain blue shifted emitters from currently known dicyanobenzene based TADF emitters and thus may also contribute to the development of organic LEDs.

2.4 Experimental part

2.4.1 General information

All reactions were conducted in dried and deoxygenated solvents unless otherwise stated. Solvents for column chromatography were distilled prior to use. Commercially available starting materials were used as received.

NMR Analysis

NMR spectra were recorded using a Bruker Avance 400 (400 MHz for ^1H , 101 MHz for ^{13}C , 376 MHz for ^{19}F) except for compound **2p** which was measured on a Bruker DRX-500 (500 MHz for ^1H , 126 MHz for ^{13}C). Chemical shifts are reported in ppm on the δ scale with the solvent residual signal as internal standard (CDCl_3 : 7.26 ppm for ^1H and 77.00 ppm for ^{13}C ; CD_2Cl_2 : 5.32 ppm for ^1H , 53.84 Hz for ^{13}C). As abbreviations for the multiplicity were used: s = singlet, d = doublet, t = triplet, q = quartet, m = multiplet. Spectra were analyzed using Topspin 4.0.6.

Thin Layer Chromatography

Thin layer chromatography was done on with silica gel pre-coated aluminum sheets (Machery-Nagel, silica gel 60 G/UV254, 0.2 mm) and for visualization UV-light (254 nm and 365 nm) and potassium permanganate stain.

Cyclic Voltammetry

CV measurements were performed by Regina Hoheisel with the three-electrode potentiostat galvanostat PGSTAT302N from Metrohm Autolab using a glassy carbon working electrode, a platinum wire counter electrode, a silver wire as a reference electrode and tetrabutylammonium tetrafluoroborate (TBATFB) (0.1 M) as supporting electrolyte. Potentials vs. Saturated Calomel Electrode with ferrocene added as internal standard with $E_{1/2}(\text{Fc}/\text{Fc}^+) = 0.380 \text{ V vs SCE}$.

UV/Vis

UV/Vis spectra were measured on a Cary 4000 UV/Vis at room temperature in air-saturated MeCN.

Fluorescence emission

Fluorescence emission spectra were measured on a Horiba FluoroMax-4 spectrometer at room temperature in air-saturated MeCN at a concentration of 20 μM with an excitation wavelength of 350 nm.

Fluorescence lifetime

Fluorescence lifetime was measured on a Horiba DeltaFlex system with Horiba DeltaDiode DD-370 (370 nm) at room temperature in air-saturated MeCN unless otherwise stated.

High resolution mass spectrometry

HRMS were measured at the Central Analytical Laboratory of the University of Regensburg on an Agilent Q-TOF 6540 UHD instrument and compound **2p** at King Abdullah University of Science and Technology (Thuwal, Saudi Arabia) on a Thermo LTQ Velos Orbitrap mass spectrometer equipped with an ESI source.

Melting Points

Melting points were determined using an SRS MPA100 OptiMelt Automated Melting Point System.

2.4.2 Photoreactor setups

Photoreactions were performed in the reactor depicted in Figure 2.3. Reagents were put into 6 mL crimp-capped vials. The vials fit into a cooling block kept at 25 °C by a thermostat. The vials were irradiated from below via OSRAM Osolon SSL 80 LT-1960 royal-blue LEDs ($\lambda_{\text{max}} = 451 \text{ nm}$). Short wavelength irradiation was done with Edison EDEV-SLC1-03 LEDs ($\lambda_{\text{max}} = 400 \text{ nm}$). Stirring was achieved via a magnetic stirrer placed below the reactor.

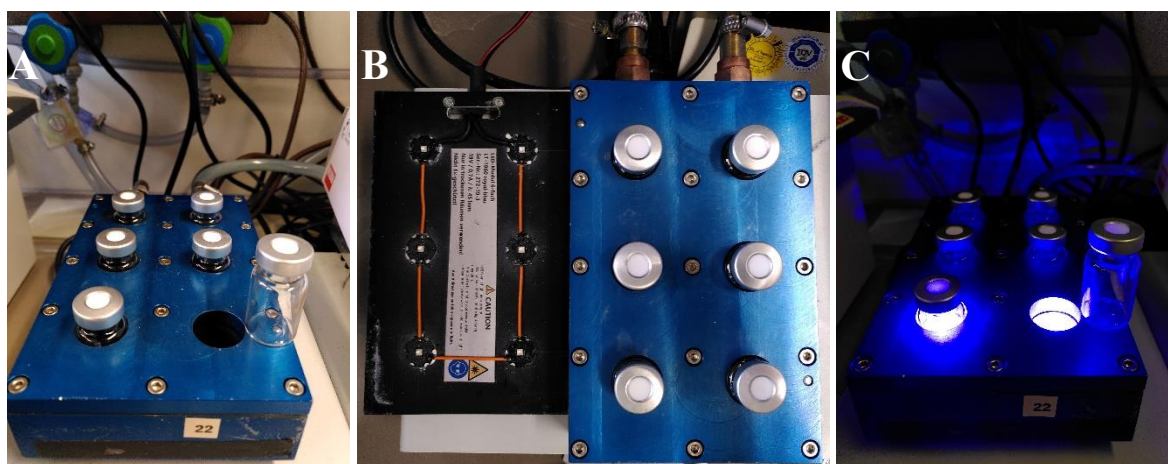


Figure 2.3. Photoreactor setup for small scale reaction. A: Cooling block front view; B: Cooling block and LED module top view; C: Photoreactor setup in operation.

The reactions at 1 mmol scale were performed in a crimp-capped vial placed into the reactor depicted in Figure 2.4. Stirring was achieved via a magnetic stirrer placed below the reactor. The reaction mixture was irradiated by 36 blue LEDs.

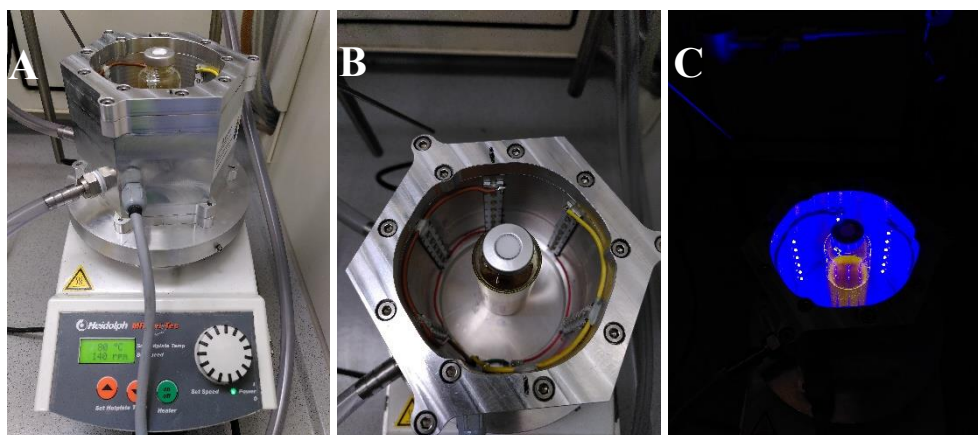
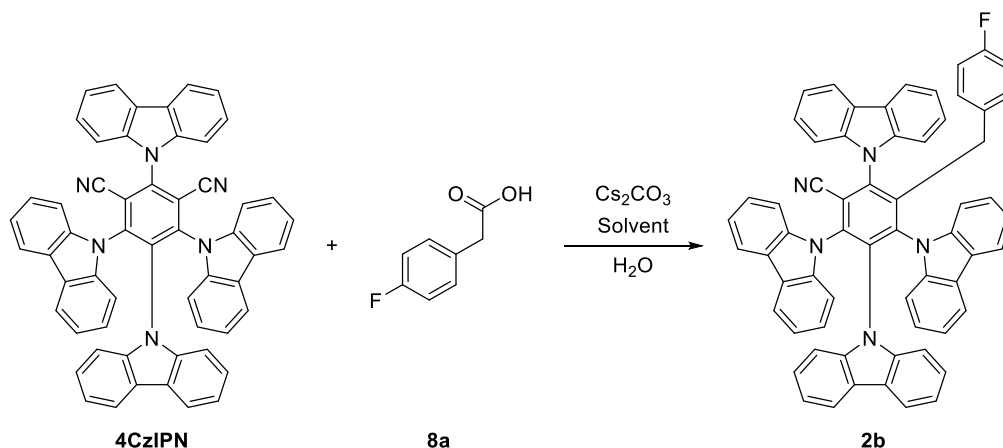


Figure 2.4. Reactor for large scale reactions. A: Front view; B: Top view; C: Photoreactor in operation.

2.4.3 Effect of water and solvent on photosubstitution in 4CzIPN

To investigate the mechanism of the photosubstitution and to estimate in which solvents it occurs, the photosubstitution reaction between 4CzIPN and 4-fluorophenylacetic acid (**8a**) was performed under different conditions.

Table 2.2. Screening of solvents, carboxylic acid equivalents and water tolerance.



Entry	Solvent	Carboxylic acid (8) (equiv.)	Water (equiv.)	Reaction time	Conversion
1	DMF	4	0	5-10 min	Full
2	MeCN	4	0	10-30 min	Full
3	DMSO	4	0	5-10 min	Full
4	EtOAc	4	0	16 h	Moderate
5	DCM	4	0	16 h	None
6	THF	4	0	16 h	Full
7	ⁱ PrOH	4	0	16 h	None
8	DMA, air	4	0	10-30 min	Full
9	DMA	4	0	2-5 min	Full
10	DMA	4	4	2-5 min	Full
11	DMA	4	8	2-5 min	Full
12	DMA	4	12	2-5 min	Full
13	DMA	4	16	2-5 min	Full
14	DMA	4	20	2-5 min	Full
15	DMA	1	0	10 min	Almost full
16	DMA	1.5	0	2-5 min	Full
17	DMA	2	0	2-5 min	Full
18	DMA	2.5	0	2-5 min	Full
19	DMA	3	0	2-5 min	Full
29	DMA	3.5	0	2-5 min	Full

General reaction conditions: Inside crimp-capped vial with 2 mL solvent (15 mM). All solid compounds added before closing the vial. Solvent and water added through septum after flushing vial with N₂. Degassed by 3 cycles of freeze-pump-thaw except for entry 8 which was not degassed. Reaction end was determined by fading of 4CzIPN's green-yellow fluorescence.

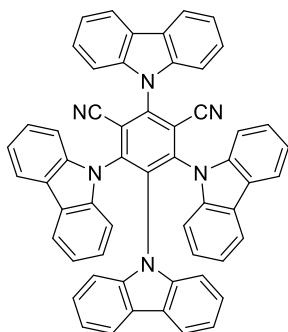
2.4.4 Synthetic procedures

2.4.4.1 General procedure 2-A: Synthesis of carbazole(9-yl)-dicyanobenzenes

Derived from literature procedure.²³

Carbazole (1.1 equiv. per substituted fluorine) is dissolved in anhydrous THF (0.14 M based on fluorinated benzonitrile derivative). A solution of NaHMDS (2M in THF) is added via cannula while cooling in an ice bath. The solution is stirred at room temperature for 30 min. Fluorinated benzonitrile derivative is dissolved in a few mL THF and added dropwise. The reaction mixture is stirred for 24 h at 60 °C in an oil bath. The solvent is removed under reduced pressure and the residue suspended in diethyl ether. The solid is filtered and washed with diethyl ether (40 mL per mmol product). The solid is extracted with chloroform until the extract is almost colorless (roughly 70 mL per mmol product). The solvent is removed under reduced pressure and washed with a 9:1 mixture of hexane/acetone (vol:vol, 5 mL per mmol product) and hexane (5 mL per mmol product). The product is dried under high vacuum.

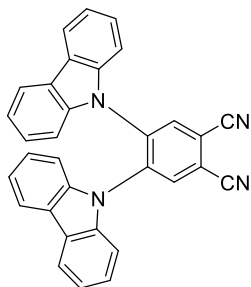
2,4,5,6-Tetrakis(9*H*-carbazol-9-yl)-4,6-dicyanobenzene (4CzIPN, 1)



Synthesized according to general procedure 2-A on 5 mmol scale. The product was obtained as a bright yellow powder (3.20 g, 4.06 mmol, 81%). The ¹H-NMR spectrum is in accordance with literature.²³

¹H NMR (400 MHz, CDCl₃): δ [ppm] = 8.23 (d, *J* = 7.72 Hz, 2H), 7.76 – 7.66 (m, 8H), 7.53 – 7.46 (m, 2H), 7.33 (d, *J* = 7.60, 2H), 7.25 – 7.20 (m, 4H), 7.13 – 7.04 (m, 8H), 6.87 – 6.79 (m, 4H), 6.67 – 6.60 (m, 2H).

4,5-Di(9*H*-carbazol-9-yl)phthalonitrile (2CzPN, 3)



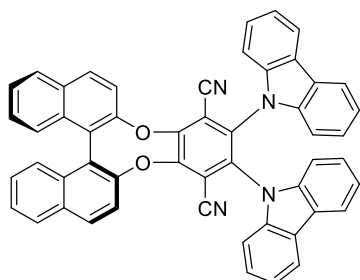
Synthesized according to general procedure 2-A on 2.5 mmol scale. The product was obtained as greenish-yellow needles (750 mg, 1.64 mmol, 65%). The ¹H-NMR spectrum is in accordance with the previously reported spectrum.¹⁹

¹H NMR (400 MHz, CDCl₃): δ [ppm] = 8.32 (s, 2H), 7.80 (d, *J* = 7.49 Hz, 4H), 7.15 – 7.04 (m, 12H).

2.4.4.2 Synthesis of chiral BINOL containing carbazole(9-yl)-dicyanobenzenes

The procedure for synthesis of BINOL containing dicyanobenzenes was derived from literature procedure.¹⁵

2,3-Di(9*H*-carbazol-9-yl)benzo[*b*]dinaphtho[2,1-*e*:1',2'-*g*][1,4]dioxocine-1,4-dicarbonitrile (**6a**)

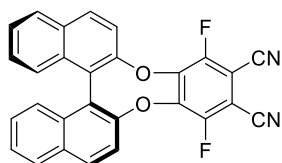


Literature known compound **6a** was synthesized according to the procedure reported in literature.¹⁵

Tetrafluoro terephthalonitrile (100 mg, 500 μmol , 1 equiv.) was dissolved in dry DMF (2.5 mL). Potassium carbonate (138 mg, 1 mmol, 2.0 equiv.) and (*S*)-(-)-1,1'-bi(2-naphthol) (143 mg, 500 μmol , 1 equiv.) were added and the reaction mixture was stirred over night at room temperature under nitrogen. Potassium carbonate (2.5 mmol, 346 mg, 5 equiv.) and carbazole (1.1 mmol, 184 mg, 2.2 equiv.) were added. The reaction mixture was stirred for 2.5 h at room temperature under nitrogen. The reaction mixture was diluted with water (2 mL) and DCM (5 mL), and the organic phase was washed with water (3 x 5 mL) and brine (1 x 5 mL). The organic phase was dried over Na_2SO_4 , and the solvent was removed under reduced pressure. The resulting yellow solid was purified via column chromatography (25% EA in PE) to give the desired product as yellow solid (319 mg, 431 μmol , 86 %).

TLC: $R_f = 0.38$ (20% EA in PE). **^1H NMR (400 MHz, CDCl_3):** δ [ppm] = 8.16 (d, $J = 8.84$ Hz, 2H), 8.06 (d, $J = 8.20$ Hz, 2H), 7.82 – 7.73 (m, 4H), 7.67 – 7.57 (m, 6H), 7.52 – 7.45 (m, 2H), 7.28 – 7.16 (m, 6H), 6.99 – 6.93 (m, 2H), 6.82 – 6.69 (m, 4H) **$^{13}\text{C}\{^1\text{H}\}$ NMR (101 MHz, CDCl_3):** $\delta = 151.1, 149.3, 138.9, 138.3, 135.0, 132.4, 132.0, 131.8, 128.6, 127.6, 126.7, 126.6, 125.8, 125.1, 124.9, 124.1, 123.9, 121.3, 121.0, 120.6, 120.3, 119.9, 114.4, 111.7, 109.7, 109.6$.

1,4-Difluorobenzo[*b*]dinaphtho[2,1-*e*:1',2'-*g*][1,4]dioxocine-2,3-dicarbonitrile (**9**)

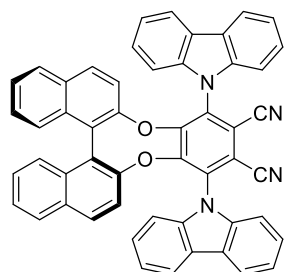


Tetrafluoro phtalonitrile (200 mg, 1 mmol, 1 equiv.) was dissolved in dry DMF (5 mL). Potassium Carbonate (276 mg, 2 mmol, 2.0 equiv.) and (*S*)-(-)-1,1'-bi(2-naphthol) (286 mg, 1 mmol, 1 equiv.) were added and the reaction mixture was stirred over night at room temperature under nitrogen. The solution was diluted with dichloromethane, washed with water (3 x 5 mL) and brine (5 mL) and dried over Na_2SO_4 . The solvent was removed under reduced pressure. The product was purified via column chromatography (25% EA in PE) to give the desired product as a yellow solid. (242 mg, 542 μmol , 54%).

Regioselectivity of the substitution was determined via NMR. ^1H , ^{19}F and ^{13}C spectra are in accordance with a C_2 -symmetric molecule and literature.¹⁶

TLC: $R_f = 0.45$ (20% EA in PE). **$^1\text{H NMR}$ (400 MHz, CDCl_3):** δ [ppm] = 8.06 (d, $J = 8.88$ Hz, 2H), 8.01 (d, $J = 8.24$ Hz, 2H), 7.61 – 7.54 (m, 2H), 7.50 – 7.44 (m, 2H), 7.44 – 7.36 (m, 4H). **$^{13}\text{C}\{^1\text{H}\}$ NMR (101 MHz, CDCl_3):** $\delta = 153.4$ (dd, $J = 262.75, 3.30$ Hz), 148.7, 143.8 (dd, $J = 11.04, 5.00$ Hz), 132.1, 131.8, 131.7, 128.4, 127.6, 126.5, 126.4, 124.6, 120.0, 109.5, 99.0 (dd, $J = 14.43, 6.34$ Hz). **$^{19}\text{F NMR}$ (376 MHz, CDCl_3):** $\delta = -122.86$ (s). **HRMS (FD+) m/z :** $[\text{M}]^+$ Calcd for $\text{C}_{28}\text{H}_{12}\text{N}_2\text{O}_2\text{F}_2$ 446.0861; Found: 446.0865.

1,4-Di(9H-carbazol-9-yl)benzo[*b*]dinaphtho[2,1-*e*:1',2'-*g*][1,4]dioxocine-2,3-dicarbonitrile (6b)



A 10 mL Flask was loaded with difluorinated precursor **S2** (200 mg, 432 μmol , 1 equiv.) and dry DMF (5 mL). Potassium carbonate (298 mg, 2.16 mmol, 5 equiv.) and carbazole (159 mg, 951 μmol , 2.2 equiv.) were added. The reaction mixture was stirred for 2.5 h at room temperature under nitrogen. After completion of the reaction, the mixture was diluted with water (2 mL) and dichloromethane (5 mL), the organic phase washed with water (3 x 5 mL) and brine (1 x 5 mL). The organic phase was dried over Na_2SO_4 and the solvent removed under reduced pressure. The solid was purified via column chromatography (25% EA in PE) and recrystallized from Et_2O to give the desired product as colourless solid (279 mg, 376 μmol , 87 %).

TLC: $R_f = 0.25$ (20% EA in PE). **$^1\text{H NMR}$ (400 MHz, CDCl_3):** δ [ppm] = 8.26 (d, $J = 7.72$ Hz, 2H), 8.13 (d, $J = 7.40$ Hz, 2H), 7.86 (d, $J = 8.28$ Hz, 2H), 7.79 (d, $J = 8.92$ Hz, 2H), 7.74 – 7.68 (m, 2H), 7.52 (t, $J = 7.36$ Hz, 2H), 7.49 – 7.42 (m, 4H), 7.29 – 7.16 (m, 8H), 6.83 (d, $J = 8.08$ Hz, 2H), 6.60 (d, $J = 9.00$ Hz, 2H). **$^{13}\text{C}\{^1\text{H}\}$ NMR (101 MHz, CDCl_3):** $\delta = 152.9, 148.9, 140.6, 140.4, 135.3, 131.9, 131.6, 131.5, 128.3, 127.1, 126.8, 126.7, 126.6, 126.2, 124.6, 124.5, 124.1, 121.8, 121.3, 121.2, 120.6, 119.7, 114.3, 112.0, 109.9, 109.3$. **HRMS (FD+) m/z :** $[\text{M}]^+$ Calcd for $\text{C}_{52}\text{H}_{28}\text{N}_4\text{O}_2$ 740.2207; Found 740.220.

2.4.4.3 General procedure 2-B: Photosubstitution in dicyanobenzene photocatalysts

Dicyanobenzene derivative (90 μmol), carboxylic acid (1.5 – 4 equiv.) and Cs_2CO_3 (same equivalents as carboxylic acid) are added to a 9 mL crimp vial. The vial is capped, evacuated via cannula and backfilled with nitrogen. Via syringe 6 mL of DMSO is added. The reaction mixture is degassed by 3 cycles of freeze-pump-thaw. The solution is irradiated with blue light ($451 \pm 20 \text{ nm}$) for 5 – 30. min. If 4CzIPN is used as substrate completion of the reaction can be seen by the fading of 4CzIPN's characteristic yellow/green fluorescence (see Figure 2.5). The content of the vials is diluted with DCM or EtOAc, washed with water and brine. The organic phase is dried over Na_2SO_4 , and the solvent evaporated under reduced pressure. Most products can be crystallized by dissolving the residue in an appropriate amount of DCM, addition of approximately the same amount of EtOAc and evaporation of the DCM either under reduced pressure or under ambient conditions, if higher quality crystals are needed. The crystals are filtered, washed with EtOAc and Et_2O and dried under vacuum. Additional product can be obtained from the remaining solution by repeating the procedure or column chromatography. However, column chromatography with EtOAc/PE mixtures is not recommended, as products tend to precipitate on the column. For some photosubstitution products DCM/PE mixtures were later found to be suited solvent mixtures for column chromatography.

Reactions with phenylacetic acid derivatives can be performed in DMSO, DMA, DMF and MeCN if the phenylacetic acid derivative is at least moderately soluble. Reactions with alkyl substituted carboxylic acids give best yields in DMSO and poor to no yield of desired product in DMA, DMF and MeCN. DMSO turned out to be the most reliable solvent.

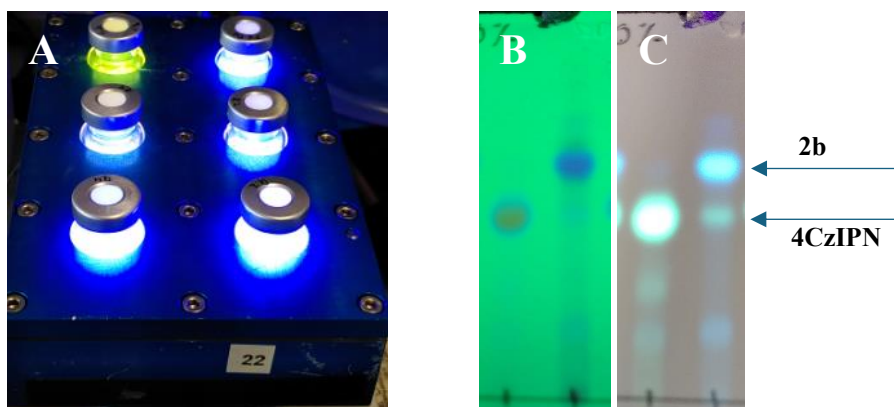
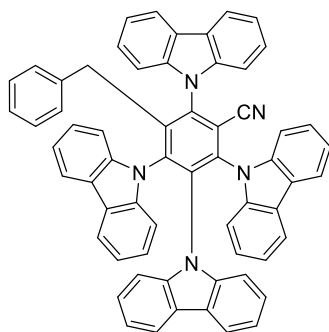
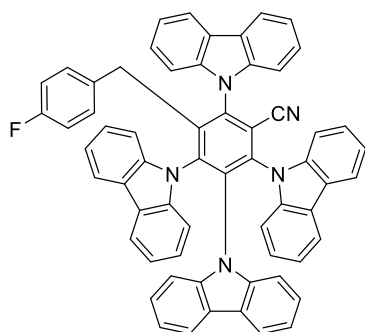


Figure 2.5. A: Photosubstitution reactions in the photoreactor. Fading of the yellow/green fluorescence indicates full conversion of 4CzIPN; B: TLC of photosubstitution in 4CzIPN with 4-fluorophenylacetic acid under 254 nm light; C: TLC under 365 nm light.

3-Benzyl-2,4,5,6-tetra(9*H*-carbazol-9-yl)benzonitrile (4CzBnBN, 2a)

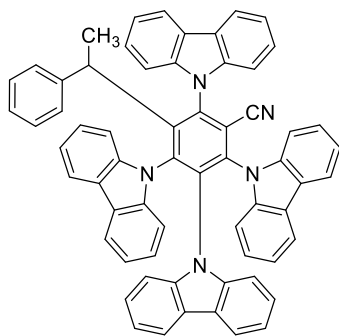
Literature known compound.¹² Synthesized according to general procedure 2-B from 4CzIPN and phenylacetic acid on 540 μmol scale (6 x 90 μmol) in DMA. The product was obtained as yellow, crystalline solid together with one equivalent of ethyl acetate in the crystal (375 mg, 398 μmol , 74%). Experimental spectra are in accordance with those previously reported. Reported literature yield was 55%, likely due to poor solubility in EtOAc/PE mixtures used for column chromatography.

TLC: $R_f = 0.35$ (20% EA in PE). **$^1\text{H NMR}$ (400 MHz, CDCl_3):** δ [ppm] = 8.19 (d, $J = 7.7$ Hz, 2H), 7.71 – 7.59 (m, 6H), 7.47 – 7.38 (m, 4H), 7.27 (t, $J = 7.8$ Hz, 4H), 7.10 – 6.99 (m, 10H), 6.92 (d, $J = 8.08$ Hz, 2H), 6.76 (t, $J = 7.4$ Hz, 2H), 6.62 (t, $J = 7.5$ Hz, 2H), 6.53 (t, $J = 7.24$ Hz, 1H), 6.46 (t, $J = 7.42$ Hz, 2H), 5.95 (d, $J = 7.16$ Hz, 2H), 4.13 (q, $J = 7.15$ Hz, 2H), 3.80 (s, 2H), 2.05 (s, 3H), 1.26 (t, $J = 7.16$ Hz, 3H). **$^{13}\text{C}\{^1\text{H}\}$ NMR (101 MHz, CDCl_3):** $\delta = 171.1, 145.4, 142.0, 140.9, 140.1, 139.9, 138.8, 138.6, 137.8, 136.1, 127.7, 127.3, 126.7, 125.9, 125.42, 125.35, 124.2, 124.14, 124.06, 123.7, 123.5, 121.2, 121.1, 121.0, 120.6, 120.2, 120.1, 119.3, 117.6, 112.5, 110.1, 110.0, 109.8, 109.0, 60.4, 35.0, 21.0, 14.2$.

2,3,4,6-Tetra(9*H*-carbazol-9-yl)-5-(4-fluorobenzyl)benzonitrile (2b)

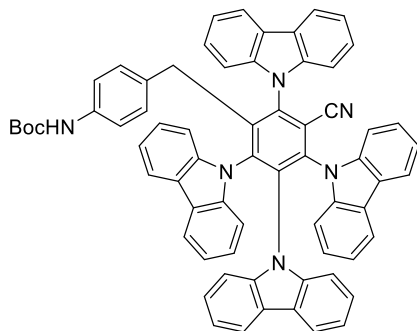
Synthesized according to general procedure 2-B from 4-fluorophenylacetic acid on 270 μmol scale (6 x 45 μmol) in DMA. The product was obtained as a yellow, crystalline solid (158 mg, 181 μmol , 67%).

TLC: $R_f = 0.38$ (20% EA in PE). **$^1\text{H NMR}$ (400 MHz, CDCl_3):** δ [ppm] = 8.21 (d, $J = 7.68$ Hz, 2H), 7.72 – 7.63 (m, 6H), 7.49 – 7.41 (m, 4H), 7.28 (t, $J = 7.44$ Hz, 4H), 7.14 – 7.00 (m, 10H), 6.94 (d, $J = 8.24$ Hz, 2H), 6.77 (t, $J = 7.32$ Hz, 2H), 6.69 – 6.61 (m, 2H), 6.22 – 6.12 (m, 2H), 5.94 – 5.85 (m, 2H), 3.77 (s, 2H). **$^{13}\text{C}\{^1\text{H}\}$ NMR (101 MHz, CDCl_3):** $\delta = 161.0$ (d, $J = 245.03$ Hz), 145.0, 141.9, 140.7, 140.1, 140.0, 138.8, 138.5, 137.8, 136.3, 132.3, 132.25, 128.9, 128.8, 126.8, 125.4, 124.2, 124.12, 124.07, 123.7, 123.5, 121.4, 121.1, 121.1, 120.8, 120.22, 120.18, 120.17, 119.4, 117.7, 114.6, 114.4, 112.5, 110.0, 109.9, 109.7, 107.0, 34.1. **$^{19}\text{F NMR}$ (377 MHz, CDCl_3):** δ [ppm] = -117.32 – -117.42 (m). **HRMS (+ESI) m/z:** $[\text{M} + \text{H}]^+$ Calcd for $\text{C}_{62}\text{H}_{39}\text{N}_5\text{F}$ 872.3184; Found 872.3182.

2,3,4,6-Tetra(9*H*-carbazol-9-yl)-5-(1-phenylethyl)benzonitrile (4CzPEBN, 2c)

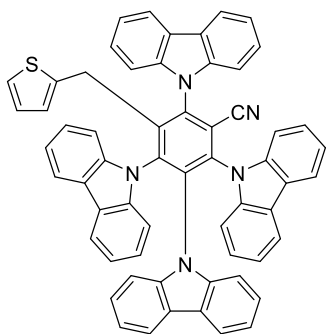
Literature known compound.⁸ Synthesized according to general procedure 2-B from 4CzIPN and 2-phenylpropionic acid on 360 μmol scale (4 x 90 μmol) in DMA. The product was obtained as a yellow, crystalline solid (188 mg, 217 μmol , 60%). NMR spectra are in agreement with those previously reported.

TLC: $R_f = 0.29$ (20% EA in PE). **¹H NMR (400 MHz, CDCl₃):** δ [ppm] = 8.19 (d, $J = 7.69$ Hz, 1H), 8.05 (d, $J = 7.53$ Hz, 1H), 7.74 (d, $J = 7.69$ Hz, 1H), 7.70 – 7.62 (m, 3H), 7.54 (t, $J = 8.21$ Hz, 2H), 7.48 – 7.40 (m, 2H), 7.37 (t, $J = 7.67$ Hz, 1H), 7.29 – 7.08 (m, 9H+2 from residual solvent peak), 7.02 (d, $J = 8.25$ Hz, 1H), 6.99 – 6.90 (m, 3H), 6.90 – 6.82 (m, 2H), 6.79 – 6.69 (m, 4H), 6.69–6.59 (m, 4H), 6.47 – 6.39 (m, 3H), 4.26 (q, $J = 7.39$ Hz, 1H), 1.52 (d, $J = 7.53$ Hz, 3H). **¹³C{¹H} NMR (101 MHz, CDCl₃):** $\delta = 152.5, 142.5, 142.3, 142.2, 142.1, 140.6, 140.3, 140.1, 139.4, 139.1, 138.5, 138.1, 138.02, 138.00, 127.8, 127.3, 126.4, 126.4, 126.0, 125.7, 125.4, 125.0, 124.8, 124.5, 124.1, 124.0, 123.9, 123.8, 123.6, 123.5, 123.5, 123.4, 121.1, 121.03, 121.01, 120.8, 120.7, 120.6, 120.4, 120.31, 120.29, 120.2, 120.1, 120.0, 119.7, 119.2, 119.2, 111.5, 110.7, 110.6, 110.5, 110.31, 110.28, 110.2, 109.9, 108.9, 38.8, 18.6.$

***tert*-Butyl (4-(2,3,4,6-tetra(9*H*-carbazol-9-yl)-5-cyanobenzyl)phenyl)carbamate (2d)**

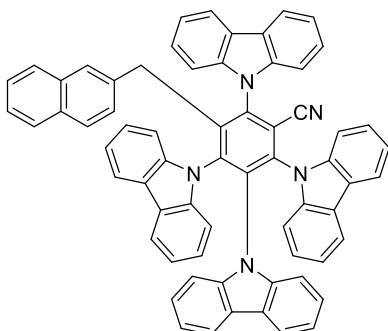
Synthesized according to general procedure 2-B on 360 μmol scale (4 x 90 μmol) in DMA. The product was obtained as a yellow, crystalline solid. Isolated yield: 206 mg, 213 μmol , 59%.

TLC: $R_f = 0.23$ (20% EA in PE). **¹H NMR (400 MHz, CDCl₃):** δ [ppm] = 8.19 (d, $J = 7.65$ Hz, 2H), 7.72 – 7.64 (m, 4H), 7.64 – 7.57 (m, 2H), 7.44 – 7.36 (m, 4H), 7.30 – 7.22 (m, 4H, overlapping with CHCl₃ signal), 7.12 – 6.98 (m, 10H), 6.90 (d, $J = 8.25$ Hz, 2H), 6.76 (t, $J = 7.33$ Hz, 2H), 6.66 – 6.59 (m, 2H), 6.45 (d, $J = 8.25$ Hz, 2H), 5.92 (s, 1H), 5.84 (d, $J = 8.41$ Hz, 2H), 3.71 (s, 2H), 1.46 (s, 9H). **¹³C{¹H} NMR (101 MHz, CDCl₃):** $\delta = 152.4, 145.7, 141.9, 140.8, 140.1, 139.9, 138.9, 138.7, 137.8, 136.3, 136.2, 131.3, 128.1, 126.7, 125.5, 124.2, 124.1, 124.0, 123.7, 123.5, 121.2, 121.03, 121.01, 120.6, 120.14, 120.13, 120.1, 119.3, 117.7, 117.6, 112.5, 110.1, 110.0, 109.8, 109.1, 80.3, 34.3, 30.91, 28.3.$ **HRMS (+ESI) m/z:** $[M + Na]^+$ Calcd for C₆₇H₄₈N₆O₂Na 969.3912; Found 969.3904.

2,3,4,6-Tetra(9*H*-carbazol-9-yl)-5-(thiophen-2-ylmethyl)benzonitrile (2e)

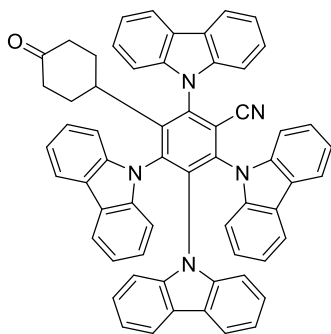
Synthesized according to general procedure 2-B from 4CzIPN and 2-thiopheneacetic acid on 360 μmol scale (4 x 90 μmol) in DMA. The product was obtained as a yellow, crystalline solid (266 mg, 309 μmol , 86%).

TLC: R_f = 0.31 (20% EA in PE). **$^1\text{H NMR}$ (400 MHz, CDCl_3):** δ [ppm] = 8.21 (d, J = 7.68 Hz, 2H), 7.72 – 7.62 (m, 6H), 7.51 (d, J = 8.12 Hz, 2H), 7.46 – 7.40 (m, 2H), 7.30 – 7.25 (m, 4H + 1H from CHCl_3 signal), 7.11 – 7.01 (m, 10H), 6.92 (d, J = 8.16 Hz, 2H), 6.79 – 6.74 (m, 2H), 6.66 – 6.61 (m, 2H), 6.52 (dd, J = 5.12, 1.12 Hz, 1H), 6.00 (dd, J = 5.12, 3.48 Hz, 1H), 5.37 (dd, J = 3.40, 0.84 Hz, 1H), 4.02 (s, 2H). **$^{13}\text{C}\{^1\text{H}\}$ NMR (101 MHz, CDCl_3):** δ = 144.6, 141.9, 140.7, 140.3, 140.2, 138.8, 138.7, 138.6, 137.8, 136.2, 126.7, 126.0, 125.44, 125.36, 125.1, 124.21, 124.17, 124.1, 123.7, 123.6, 123.5, 121.3, 120.7, 120.18, 120.16, 120.1, 119.3, 117.6, 112.5, 110.0, 109.9, 109.8, 109.1, 29.3. **HRMS (+ESI) m/z :** $[\text{M} + \text{H}]^+$ Calcd for $\text{C}_{60}\text{H}_{38}\text{N}_5\text{S}$ 860.2842; Found 860.2840.

2,3,4,6-Tetra(9*H*-carbazol-9-yl)-5-(naphthalen-2-ylmethyl)benzonitrile (2f)

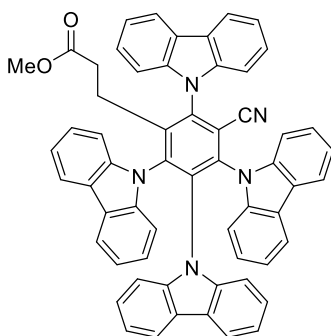
Synthesized according to general procedure 2-B from 4CzIPN and 2-naphthaleneacetic acid on 30 μmol scale in DMA. The product was obtained as a yellow, crystalline solid (23 mg, 23 μmol , 77%).

TLC: R_f = 0.35 (20% EA in PE). **$^1\text{H NMR}$ (400 MHz, CDCl_3):** δ [ppm] = 8.16 (d, J = 7.69 Hz, 2H), 7.70-7.61 (m, 4H), 7.55 (t, J = 7.03 Hz, 2H), 7.44 (d, J = 8.13 Hz, 2H), 7.35 (t, J = 7.29 Hz, 3H), 7.31 – 7.22 (m, 4H), 7.20 – 7.13 (m, 2H), 7.10 – 6.95 (m, 11H), 6.95 – 6.87 (m, 3H), 6.75 (t, J = 7.35 Hz, 2H), 6.62 (t, J = 7.25 Hz, 2H), 6.22 (dd, J = 8.39, 1.50 Hz, 1H), 6.03 (s, 1H), 4.13 (q, J = 7.14 Hz, 2H), 3.95 (s, 2H), 2.05 (s, 3H), 1.27 (t, J = 7.17 Hz, 3H). **$^{13}\text{C}\{^1\text{H}\}$ NMR (101 MHz, CDCl_3):** δ = 171.1, 145.2, 142.0, 140.8, 140.1, 140.0, 138.8, 138.7, 137.8, 136.2, 133.5, 132.5, 131.6, 127.7, 127.0, 126.9, 126.7, 126.6, 125.6, 125.4, 125.3, 125.0, 124.17, 124.16, 124.1, 123.7, 123.5, 121.3, 121.01, 120.96, 120.7, 120.2, 120.1, 120.0, 119.3, 117.7, 112.5, 110.1, 109.9, 109.8, 109.0, 60.4, 35.2, 21.0, 14.2. **HRMS (+ESI) m/z :** $[\text{M} + \text{H}]^+$ Calcd for $\text{C}_{66}\text{H}_{42}\text{N}_5$ 904.3435; Found 904.3429.

2,3,4,6-Tetra(9*H*-carbazol-9-yl)-5-(4-oxocyclohexyl)benzonitrile (2g)

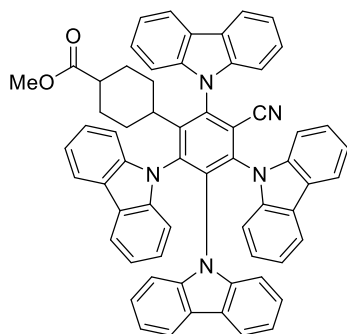
Synthesized according to general procedure 2-B from 4CzIPN and 4-oxocyclohexanecarboxylic acid on 180 μmol scale (2 x 90 μmol) in DMSO. The product was obtained as a yellow, crystalline solid (89 mg, 103 μmol , 64%).

Melting point: 386 – 390 °C. **TLC:** $R_f = 0.15$ (20% EA in PE). **$^1\text{H NMR}$ (400 MHz, CDCl_3):** δ [ppm] = 8.22 (d, $J = 7.68$ Hz, 2H), 7.75 (d, $J = 7.32$ Hz, 2H), 7.69 – 7.60 (m, 4H), 7.47 – 7.37 (m, 4H), 7.30 (d, $J = 7.32$ Hz, 2H), 7.20 (d, $J = 7.72$ Hz, 2H), 7.18 – 7.12 (m, 4H), 7.12 – 7.06 (m, 2H), 7.04 – 6.98 (m, 4H), 6.94 (d, $J = 8.28$ Hz, 2H), 6.81 – 6.74 (m, 2H), 6.70 – 6.62 (m, 2H), 2.87 – 2.74 (m, 1H), 1.98 – 1.86 (m, 2H), 1.86 – 1.77 (m, 2H), 1.66 – 1.49 (m, 2H + 1H residual water), 1.38 – 1.25 (m, 2H). **$^{13}\text{C}\{^1\text{H}\}$ NMR (101 MHz, CDCl_3):** $\delta = 208.5, 150.2, 142.9, 142.5, 141.5, 140.8, 140.0, 138.7, 138.3, 138.1, 126.9, 125.7, 125.4, 124.5, 124.1, 124.1, 123.6, 123.5, 121.6, 121.5, 121.1, 121.0, 120.5, 120.2, 120.1, 119.8, 119.4, 111.5, 110.3, 110.0, 109.7, 41.4, 40.0, 31.8$. **HRMS (+ESI) m/z:** $[\text{M} + \text{Na}]^+$ Calcd for $\text{C}_{61}\text{H}_{41}\text{N}_5\text{ONa}$ 882.3203; Found 882.3203.

Methyl 3-(2,3,4,6-tetra(9*H*-carbazol-9-yl)-5-cyanophenyl)propanoate (2h)

Synthesized according to general procedure 2-B from 4CzIPN and succinic acid monomethylester on 240 μmol scale (4 x 60 μmol) in DMSO. The crude product was purified via column chromatography (5 \rightarrow 20% EA in PE) and the product obtained as a yellow, crystalline solid, crystallized with 0.75 equivalents ethyl acetate (90 mg, 96 μmol , 40%).

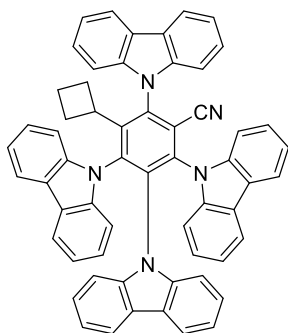
TLC: $R_f = 0.23$ (20% EA in PE). **$^1\text{H NMR}$ (400 MHz, CDCl_3):** δ [ppm] = 8.22 (d, $J = 7.69$ Hz, 2H), 7.73 – 7.63 (m, 6H), 7.60 (d, $J = 8.05$ Hz, 2H), 7.44 (t, $J = 7.45$ Hz, 2H), 7.26 (t, $J = 8.63$ Hz, 4H), 7.14 (d, $J = 7.89$ Hz, 2H), 7.18 – 6.99 (m, 8H), 6.90 (d, $J = 8.05$ Hz, 2H), 6.74 (t, $J = 7.39$ Hz, 2H), 6.61 (t, $J = 7.61$ Hz, 2H), 2.97 (s, 3H), 2.87 (t, $J = 7.33$ Hz, 2H), 1.72 (t, $J = 7.35$ Hz, 2H). **$^{13}\text{C}\{^1\text{H}\}$ NMR (101 MHz, CDCl_3):** $\delta = 171.2, 144.4, 142.2, 140.9, 140.4, 140.2, 138.7, 137.8, 136.3, 126.9, 125.51, 125.4, 124.2, 124.1, 124.0, 123.7, 123.4, 121.4, 121.2, 121.0, 120.8, 120.2, 120.12, 120.11, 119.3, 117.5, 112.4, 110.1, 109.97, 109.95, 109.3, 51.2, 32.8, 24.5$. **HRMS (+ESI) m/z:** $[\text{M} + \text{H}]^+$ Calcd for $\text{C}_{59}\text{H}_{40}\text{N}_5\text{O}_2$ 850.3177; Found 850.3172.

Methyl 4-(2,3,4,6-tetra(9*H*-carbazol-9-yl)-5-cyanophenyl)cyclohexane-1-carboxylate (2i)

Synthesized according to general procedure 2-B from 4CzIPN and 4-(methoxycarbonyl)cyclohexanecarboxylic acid on 240 μmol scale (4 x 60 μmol) in DMSO. The product was obtained as a yellow, crystalline solid (169 mg, 187 μmol , 78%).

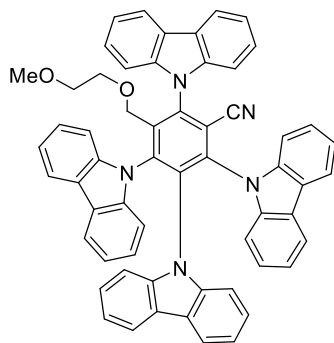
TLC: R_f = 0.18 (20% EA in PE). **$^1\text{H NMR}$ (400 MHz, CDCl_3):** δ [ppm] = 8.24 (d, J = 7.32 Hz, 2H), 7.75 – 7.65 (m, 4H), 7.65 – 7.59 (m, 2H), 7.45 (t, J = 7.34 Hz, 4H), 7.27 (d, J = 8.04 Hz, 2H), 7.18 – 6.96 (m, 12H), 6.91 (d, J = 8.08 Hz, 2H), 6.75 (t, J = 7.32 Hz, 2H), 6.68 – 6.61 (m, 2H), 3.36 (s, 3H), 2.52 – 2.42 (m, 1H), 1.74 (d, J = 11.56 Hz, 2H), 1.55 – 1.42 (m, 3H), 1.33 – 1.18 (m, 2H). **$^{13}\text{C}\{^1\text{H}\}$ NMR (101 MHz, CDCl_3):** δ = 175.2, 151.8, 142.8, 142.7, 141.4, 140.4, 139.9, 138.8, 138.1, 138.0, 126.8, 125.4, 125.3, 124.4, 124.00, 123.98, 123.5, 123.4, 121.3, 121.2, 121.0, 120.7, 120.3, 120.0, 120.0, 119.6, 119.3, 111.6, 110.3, 110.00, 109.98, 109.7, 51.3, 41.7, 41.0, 31.8, 29.2.

HRMS (+ESI) m/z : $[\text{M} + \text{H}]^+$ Calcd for $\text{C}_{63}\text{H}_{46}\text{N}_5\text{O}_2$ 904.3652; Found 904.3642.

2,3,4,6-Tetra(9*H*-carbazol-9-yl)-5-cyclobutylbenzonitrile (2j)

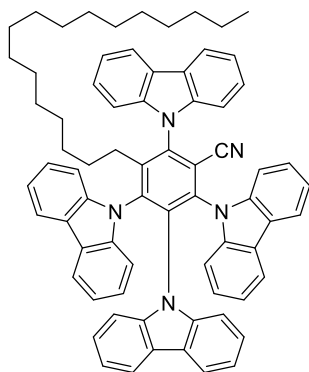
Synthesized according to general procedure 2-B from 4CzIPN and cyclobutanecarboxylic acid on 360 μmol scale (4 x 90 μmol) in DMSO. The product was obtained as a yellow, crystalline solid (273 mg, 343 μmol , 93%).

Melting point: 376 – 380 $^\circ\text{C}$. **TLC:** R_f = 0.34 (20% EA in PE). **$^1\text{H NMR}$ (400 MHz, CDCl_3):** δ [ppm] = 8.22 (d, J = 7.68 Hz, 2H), 7.80 – 7.64 (m, 8H), 7.46 (t, J = 7.34 Hz, 2H), 7.29 (t, J = 7.01 Hz, 4H), 7.18 – 7.01 (m, 10H), 6.88 (d, J = 8.24 Hz, 2H), 6.77 (t, J = 7.34 Hz, 2H), 6.61 (t, J = 7.46 Hz, 2H), 3.59 – 3.45 (m, 1H), 1.39 – 1.23 (m, 2H), 1.06 – 0.83 (m, 2H), 0.50 – 0.35 (m, 2H). **$^{13}\text{C}\{^1\text{H}\}$ NMR (101 MHz, CDCl_3):** δ = 147.7, 140.4, 140.3, 139.3, 139.2, 139.0, 138.9, 137.9, 135.5, 126.7, 125.42, 125.41, 124.2, 124.4, 124.0, 123.5, 123.5, 121.3, 121.1, 120.9, 120.6, 120.2, 120.14, 120.07, 119.3, 117.2, 112.8, 110.0, 109.9, 109.7, 109.4, 37.7, 29.7, 17.8. **HRMS (+ESI) m/z :** $[\text{M} + \text{H}]^+$ Calcd for $\text{C}_{59}\text{H}_{40}\text{N}_5$ 818.3278; Found 818.3282.

2,3,4,6-Tetra(9*H*-carbazol-9-yl)-5-((2-methoxyethoxy)methyl)benzonitrile (2k)

Synthesized according to general procedure 2-B from 4CzIPN and 2-(2-methoxyethoxy)acetic acid on 270 μmol scale (3 x 90 μmol) in DMSO. The product was obtained as a yellow, crystalline solid (125 mg, 147 μmol , 54%).

TLC: R_f = 0.18 (20% EA in PE). **^1H NMR (400 MHz, CDCl_3):** δ [ppm] = 8.21 (d, J = 7.73 Hz, 2H), 7.74 – 7.64 (m, 6H), 7.59 (d, J = 8.09 Hz, 2H), 7.43 (t, J = 7.35 Hz, 2H), 7.53 (d, J = 5.26 Hz, 2H), 7.25 – 7.21 (m, 2H), 7.19 – 7.13 (m, 2H), 7.11 – 7.01 (m, 8H), 6.89 (d, J = 8.25 Hz, 2H), 6.77 (t, J = 4.23 Hz, 2H), 6.63 (t, J = 7.71 Hz, 2H), 4.15 (s, 2H), 2.72 (s, 3H), 2.48 (t, J = 4.76 Hz, 2H), 2.31 (t, J = 4.86 Hz, 2H). **$^{13}\text{C}\{^1\text{H}\}$ NMR (101 MHz, CDCl_3):** δ = 142.3, 141.8, 141.2, 141.0, 140.9, 139.4, 138.8, 137.8, 136.0, 126.7, 125.5, 125.5, 124.3, 124.1, 124.1, 123.7, 123.6, 121.2, 121.1, 121.0, 120.8, 120.2, 120.2, 120.0, 119.3, 117.6, 112.5, 110.0, 109.9, 109.5, 70.5, 69.8, 66.1, 58.3. **HRMS (+ESI) m/z :** $[\text{M} + \text{H}]^+$ Calcd for $\text{C}_{59}\text{H}_{42}\text{N}_5\text{O}_2$ 851.3255; Found: 851.3255.

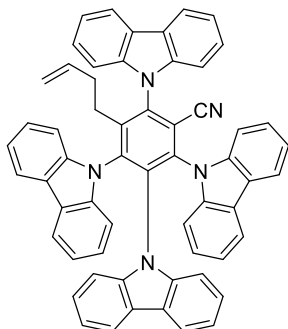
2,3,4,6-Tetra(9*H*-carbazol-9-yl)-5-heptadecylbenzonitrile (2l)

Synthesized according to general procedure 2-B from 4CzIPN and stearic acid on 240 μmol scale (4 x 60 μmol) in DMSO. The crude product was purified via column chromatography (5 \rightarrow 10% EA in PE) to give the product as a yellow/orange, amorphous solid (98 mg, 98 μmol , 41%). In contrast to 4CzIPN and most other photosubstitution products the compound is well soluble in toluene.

TLC: R_f = 0.55 (20% EA in PE). **^1H NMR (400 MHz, CDCl_3):** δ [ppm] = 8.24 (d, J = 7.68 Hz, 2H), 7.74 – 7.66 (m, 6H), 7.57 (d, J = 8.08 Hz, 2H), 7.48 – 7.42 (m, 2H), 7.31 – 7.25 (m, 4H), 7.14 – 7.01 (m, 10H), 6.92 (d, J = 8.08 Hz, 2H), 6.77 (t, J = 7.16 Hz, 2H), 6.68 – 6.60 (m, 2H), 2.44 (t, J = 7.80 Hz, 2H), 1.33 – 1.14 (m, 16H+1H impurity), 1.12 – 1.02 (m, 2H), 0.95 – 0.87 (m, 5H), 0.87 – 0.77 (m, 2H), 0.77 – 0.66 (m, 2H), 0.54 – 0.39 (m, 4H), 0.30 – 0.19 (m, 2H). **$^{13}\text{C}\{^1\text{H}\}$ NMR (101 MHz, CDCl_3):** δ = 147.5, 142.1, 140.7, 140.6, 139.5, 138.9, 137.9, 136.5, 126.8, 125.4, 125.4, 124.1, 124.1, 124.0, 123.6, 123.5, 121.3, 121.2, 121.0, 120.6, 120.2, 120.1, 119.3, 117.7, 112.6, 110.1, 110.0,

109.9, 109.2, 31.9, 30.2, 29.7, 29.7, 29.7, 29.6, 29.6, 29.4, 29.3, 29.2, 29.1, 28.8, 28.5, 27.9, 22.7, 14.1. **HRMS (+ESI) m/z:** $[M + H]^+$ Calcd for $C_{72}H_{68}N_5$ 1002.5469; Found: 1002.5445.

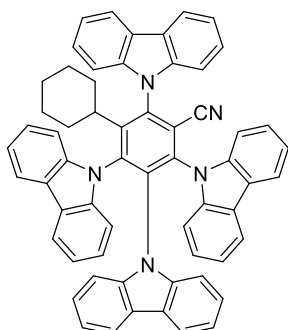
3-(But-3-en-1-yl)-2,4,5,6-tetra(9*H*-carbazol-9-yl)benzonitrile (2m)



Synthesized according to general procedure 2-B from 4CzIPN and cyclopropylacetic acid (ring opening of the intermediate cyclopropylmethyl radical) on 180 μ mol scale (2 x 90 μ mol) in DMSO. The product was obtained as a yellow, crystalline solid (115 mg, 141 μ mol, 78%).

TLC: R_f = 0.33 (20% EA in PE). **1H NMR (400 MHz, $CDCl_3$):** δ [ppm] = 8.25 (d, J = 7.22 Hz, 2H), 7.77 – 7.65 (m, 6H), 7.60 (d, J = 8.24 Hz, 2H), 7.46 (t, J = 7.34 Hz, 2H), 7.33 – 7.23 (m, 4H, overlapping with $CHCl_3$ signal), 7.17 – 7.00 (m, 10H), 6.89 (d, J = 8.08 Hz, 2H), 6.77 (t, J = 3.42 Hz, 2H), 6.67 – 6.60 (m, 2H), 4.95 – 4.80 (m, 1H), 4.56 – 4.46 (m, 1H), 4.32 – 4.19 (m, 1H), 2.63 (t, J = 7.42 Hz, 2H), 1.58 (q, J = 7.28 Hz, 2H). **$^{13}C\{^1H\}$ NMR (101 MHz, $CDCl_3$):** δ = 145.9, 142.2, 140.8, 140.5, 139.8, 138.9, 138.8, 137.8, 136.4, 136.2, 126.8, 125.4, 125.4, 124.2, 124.2, 124.0, 123.7, 123.5, 121.4, 121.2, 121.0, 120.7, 120.2, 120.1, 120.1, 119.3, 117.5, 116.1, 112.5, 110.0, 109.9, 109.3, 34.0, 29.2. **HRMS (+ESI) m/z:** $[M + H]^+$ Calcd for $C_{59}H_{40}N_5$ 818.3278; Found 818.3267.

2,3,4,6-Tetra(9*H*-carbazol-9-yl)-5-cyclohexylbenzonitrile (2n)

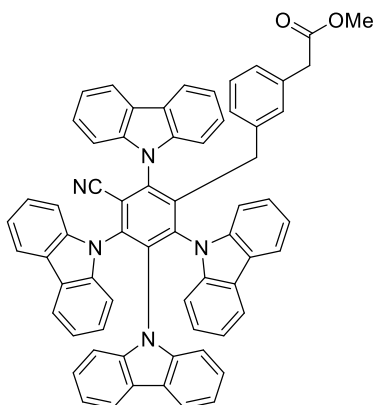


Synthesized according to general procedure 2-B from 4CzIPN and cyclohexanecarboxylic acid on 90 μ mol scale in DMSO. The product was obtained as a yellow, crystalline solid (55 mg, 65 μ mol, 72%).

TLC: R_f = 0.34 (20% EA in PE). **1H NMR (400 MHz, $CDCl_3$):** δ [ppm] = 8.25 – 8.20 (m, 2H), 7.72 (d, J = 7.43 Hz, 2H), 7.69 – 7.60 (m, 4H), 7.46 – 7.41 (m, 4H), 7.27 (d, J = 7.72, 2H), 7.19 – 7.09 (m, 6H), 7.08 – 7.03 (m, 2H), 7.03 – 6.95 (m, 4H), 6.91 (d, J = 8.15 Hz, 2H), 6.78 – 6.71 (m, 2H), 6.68 – 6.59 (m, 2H), 2.48 – 2.36 (m, 1H), 1.62 (d, J = 11.41 Hz, 1H), 1.22 – 0.99 (m, 5H). **$^{13}C\{^1H\}$ NMR (101 MHz, $CDCl_3$):** δ = 152.9, 142.8, 142.7, 141.5, 140.1, 140.0, 138.9, 138.2, 137.9, 126.7, 125.4, 125.3, 124.4, 124.00, 123.96, 123.5, 123.4, 121.11, 121.08, 120.9, 120.5,

120.1, 119.993, 119.986, 119.6, 119.2, 111.7, 110.4, 110.2, 110.1, 110.0, 42.1, 33.0, 26.9, 25.0. **HRMS (+ESI):** $[M + H]^+$ Calcd for $C_{61}H_{44}N_5$ 846.3591; Found: 846.3584.

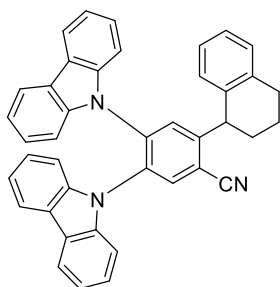
Methyl 2-(3-(2,3,4,6-tetra(9*H*-carbazol-9-yl)-5-cyanobenzyl)phenyl)acetate (2o)



Synthesized according to general procedure 2-B from 4CzIPN and *m*-phenylenediacetic acid (1.3 equiv.) on 720 μ mol scale (8 x 90 μ mol) in DMSO. The product was obtained as a yellow, crystalline solid, crystallized with 1 equiv. EtOAc (301 mg, 297 μ mol, 41%).

1H NMR (400 MHz, $CDCl_3$): δ [ppm] = 8.18 (d, $J = 7.7$ Hz, 2H), 7.72 – 7.64 (m, 4H), 7.61 (t, $J = 7.6$ Hz, 2H), 7.48 (d, $J = 8.1$ Hz, 2H), 7.40 (t, $J = 7.44$, 2H), 7.31 (d, $J = 7.7$ Hz, 2H), 7.28 (d, $J = 7.6$ Hz, 2H), 7.11 – 6.97 (m, 12H), 6.76 (t, $J = 7.4$ Hz, 2H), 6.63 (t, $J = 7.5$ Hz, 2H), 6.47 – 6.36 (m, 2H), 5.95 (s, 1H), 5.87 (d, $J = 7.3$ Hz, 1H), 4.13 (q, $J = 7.1$ Hz, 2H, EtOAc), 7.36 (s, 2H), 3.65 (s, 3H), 2.96 (s, 2H), 2.05 (s, 3H, EtOAc), 1.27 (t, $J = 7.2$, 3H, EtOAc). **$^{13}C\{^1H\}$ NMR (101 MHz, $CDCl_3$):** δ = 171.7, 171.1 (EtOAc), 145.6, 142.0, 140.8, 140.1, 140.0, 138.9, 138.7, 137.9, 137.0, 136.2, 133.1, 128.8, 127.9, 126.7, 126.1, 125.4, 124.2, 124.1, 124.0, 123.6, 123.5, 121.2, 121.0, 120.9, 120.6, 120.14, 120.11, 120.0, 119.3, 117.6, 112.6, 110.2, 110.0, 109.8, 109.1, 60.4 (EtOAc), 51.8, 40.1, 34.8, 21.0 (EtOAc), 14.2 (EtOAc). **HRMS (+ESI) m/z:** $[M + H]^+$ Calcd for $C_{65}H_{44}N_5O_2$ 926.3500; Found: 926.3490.

4,5-Di(9*H*-carbazol-9-yl)-2-(1,2,3,4-tetrahydronaphthalen-1-yl)benzonitrile (4a)

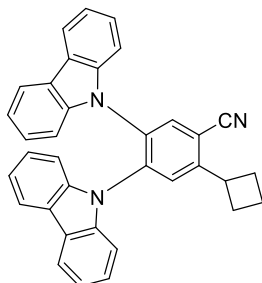


Synthesized according to general procedure 2-B from 2CzPN and tetrahydronaphthoic acid on 360 μ mol scale (4 x 90 μ mol) in DMSO. The product was obtained as a colorless, solid (136 mg, 238 μ mol, 66%).

TLC: $R_f = 0.30$ (10% EA in PE). **1H NMR (400 MHz, $CDCl_3$):** δ [ppm] = 8.15 (s, 1H), 7.83 (d, $J = 7.36$ Hz, 1H), 7.76 (d, $J = 7.68$ Hz, 2H), 7.70 (d, $J = 7.64$ Hz, 1H), 7.43 (s, 1H), 7.31 – 6.85 (m, 16H+1H overlapping $CHCl_3$ solvent peak), 4.85 (t, $J = 6.60$ Hz, 1H), 2.90 (t, $J = 6.32$ Hz, 2H), 2.55 – 2.44 (m, 1H), 2.17 – 2.04 (m, 1H), 2.04 – 1.87 (m,

2H). $^{13}\text{C}\{^1\text{H}\}$ NMR (101 MHz, CDCl_3): δ = 152.0, 139.3, 139.00, 138.98, 138.7, 137.9, 137.8, 136.6, 134.5, 132.4, 131.9, 129.9, 129.8, 127.0, 126.6, 125.8, 125.7, 125.5, 125.4, 123.8, 123.8, 123.0, 123.5, 120.7, 120.6, 120.5, 120.4, 120.2, 120.0, 119.9, 119.9, 116.9, 112.0, 109.4, 109.3, 109.3, 109.2, 43.6, 32.2, 29.4, 20.6. HRMS (+ESI) m/z : $[\text{M} + \text{Na}]^+$ Calcd for $\text{C}_{41}\text{H}_{29}\text{N}_3\text{Na}$ 586.2254; Found: 586.2249.

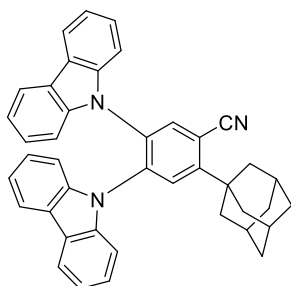
4,5-Di(9*H*-carbazol-9-yl)-2-cyclobutylbenzonitrile (4b)



Synthesized according to general procedure 2-B from 2CzPN and cyclobutanecarboxylic acid on 360 μmol scale (4 x 90 μmol) in DMSO. The product was obtained as a colorless, crystalline solid (133 mg, 273 μmol , 76%).

Melting point: 265 – 267 °C. **TLC:** R_f = 0.35 (10% EA in PE). ^1H NMR (400 MHz, CDCl_3): δ [ppm] = 8.07 (s, 1H), 7.92 (s, 1H), 7.83 – 7.77 (m, 4H), 7.18 – 7.04 (m, 12H), 4.11 (p, J = 8.71 Hz, 1H), 2.70 – 2.60 (m, 2H), 2.41 – 2.28 (m, 2H), 2.27 – 2.13 (m, 1H), 2.03 – 1.92 (m, 1H). $^{13}\text{C}\{^1\text{H}\}$ NMR (101 MHz, CDCl_3): δ = 150.0, 139.3, 139.1, 138.4, 134.7, 132.4, 128.8, 125.72, 125.65, 123.8, 123.6, 120.6, 120.4, 120.09, 120.06, 116.9, 111.1, 109.4, 109.2, 38.6, 29.3, 18.2. HRMS (+ESI) m/z : $[\text{M} + \text{Na}]^+$ Calcd for $\text{C}_{35}\text{H}_{25}\text{N}_3\text{Na}$ 510.1941; Found 510.1941.

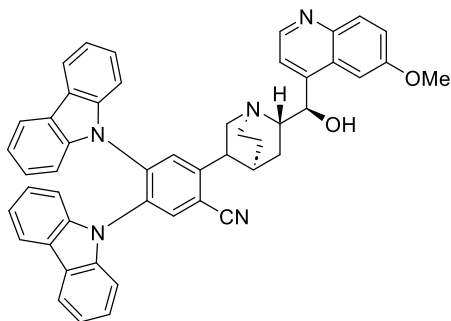
2-((1*s*,3*s*)-Adamantan-1-yl)-4,5-di(9*H*-carbazol-9-yl)benzonitrile (4c)



Synthesized according to general procedure 2-B from 2CzPN and 1-adamantanecarboxylic acid on 240 μmol scale (4 x 60 μmol) in DMSO. The product was obtained as a colorless solid (55 mg, 97 μmol , 40%).

Melting point: 286 – 290 °C. **TLC:** R_f = 0.53 (10% EA in PE). ^1H NMR (400 MHz, CDCl_3): δ [ppm] = 8.16 (s, 1H), 7.91 (s, 1H), 7.84 – 7.76 (m, 4H), 7.17 – 7.02 (m, 12H), 2.38 – 2.28 (m, 6H), 2.24 (broad s, 3H), 1.94 – 1.82 (m, 6H). $^{13}\text{C}\{^1\text{H}\}$ NMR (101 MHz, CDCl_3): δ = 153.98, 139.21, 139.10, 137.88, 137.25, 131.86, 128.68, 125.73, 125.66, 123.81, 123.66, 120.57, 120.44, 120.08, 120.05, 118.97, 110.10, 109.45, 109.30, 41.26, 37.83, 36.28, 28.77. HRMS (+ESI) m/z : $[\text{M} + \text{H}]^+$ Calcd for $\text{C}_{41}\text{H}_{34}\text{N}_3$ 568.2747; Found 568.2746.

4,5-Di(9*H*-carbazol-9-yl)-2-((1*S*,4*S*,6*S*)-6-((*R*)-hydroxy(6-methoxyquinolin-4-yl)methyl)quinuclidin-3-yl)benzotrile (4d)



Synthesized according to general procedure 2-B from 2CzPN (4 x 60 μmol) and quitenine²⁴ (3 equiv.) in DMSO. An additional washing step of the organic phase with concentrated aqueous KOH was added to the procedure to remove excess quitenine. Purified via column chromatography (5% MeOH in DCM). The diastereomers were separable.

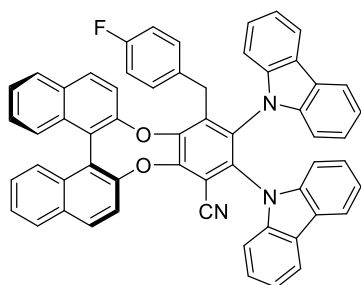
Diastereomer 1: Colorless solid (76 mg, 104 μmol , 43%)

¹H NMR (400 MHz, CDCl₃): δ [ppm] = 8.62 (d, *J* = 4.5 Hz, 1H), 8.06 (s, 1H), 7.98 – 7.86 (m, 2H), 7.84 – 7.67 (m, 4H), 7.54 (d, *J* = 4.4 Hz, 1H), 7.30 – 7.19 (m, 2H, overlap with solvent residual signal), 7.19 – 6.91 (m, 12H), 5.73 (s, 1H), 3.87 (s, 3H), 3.72 (s, 1H), 3.65 – 3.48 (m, 2H), 3.49 – 3.35 (m, 1H), 3.22 – 3.04 (s, 1H), 2.93 – 2.75 (s, 1H), 2.26 (s, 1H), 2.17 (t, *J* = 10.0 Hz, 1H), 1.85 – 1.59 (m, 3H). **¹³C{¹H} NMR (101 MHz, CDCl₃):** δ = 157.8, 147.4, 144.1, 139.1, 139.00, 128.97, 138.89, 138.0, 135.4, 132.8, 131.4, 128.6, 126.4, 125.9, 125.72, 125.67, 125.60, 123.9, 123.8, 123.7, 123.6, 121.6, 120.8, 120.7, 120.6, 120.5, 120.2, 120.14, 120.12, 120.0, 118.4, 116.7, 113.2, 109.20, 109.16, 109.12, 101.2, 59.6, 55.8, 54.7, 43.7, 39.2, 29.4, 20.5.

Diastereomer 2: Colorless solid (68 mg, 93 μmol , 39%)

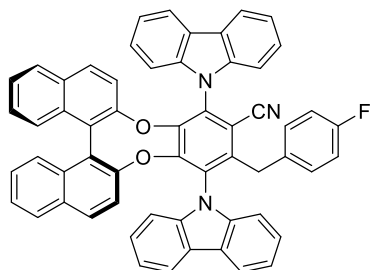
¹H NMR (400 MHz, CDCl₃): δ [ppm] = 8.57 (d, *J* = 4.8 Hz, 1H), 8.10 (s, 1H), 7.88 – 7.76 (m, 2H), 7.76 – 7.66 (m, 4H), 7.46 (d, *J* = 4.4 Hz, 1H), 7.17 – 7.05 (m, 5H), 7.02 – 6.79 (m, 8H), 6.58 (s, 1H), 5.68 (s, 1H), 3.81 – 3.48 (m, 6H), 3.34 – 3.23 (m, 1H), 3.23 – 3.11 (m, 1H), 2.99 – 2.81 (m, 1H), 2.37 (s, 1H), 2.17 – 1.85 (m, 3H), 1.61 (t, *J* = 11.3 Hz, 1H). **¹³C{¹H} NMR (101 MHz, CDCl₃):** δ = 157.8, 147.2, 144.0, 139.1, 138.83, 138.81, 138.6, 138.0, 135.4, 132.7, 131.4, 128.2, 126.2, 125.8, 125.62, 125.566, 125.53, 123.82, 123.78, 123.71, 123.5, 121.5, 120.9, 120.73, 120.66, 120.50, 120.2, 120.1, 120.0, 118.4, 116.8, 112.9, 109.1, 109.0, 108.5, 100.8, 60.5, 55.6, 43.4, 39.7, 28.9, 27.6, 21.2.

HRMS (+ESI) *m/z*: [*M* + *H*]⁺ Calcd for C₄₉H₄₀N₅O₂ 730.3177; Found 730.3185 and 730.3182.

2,3-Di(9*H*-carbazol-9-yl)-4-(4-fluorobenzyl)benzo[*b*]dinaphtho[2,1-*e*:1',2'-*g*][1,4]dioxocine-1-carbonitrile (7a)

Synthesized according to general procedure 2-B from chiral dicyanobenzene derivative **6a** and 4-fluorophenylacetic acid on 240 μmol scale (4 x 60 μmol) in DMA. The crude product was purified via column chromatography (10 \rightarrow 20% EtOAc in PE) and the product was obtained as a colorless solid (168 mg, 204 μmol , 85%).

TLC: R_f = 0.30 (20% EtOAc in PE). **^1H NMR (400 MHz, CDCl_3):** δ [ppm] = 8.16 (d, J = 8.85 Hz, 1H), 8.08 (d, J = 8.17 Hz, 1H), 8.02 – 7.95 (m, 2H), 7.79 (d, J = 8.81 Hz, 1H), 7.73 – 7.52 (m, 8H), 7.52 – 7.41 (m, 2H), 7.24 – 7.15 (m, 2H), 7.15 – 7.03 (m, 3H), 6.94 – 6.86 (m, 2H), 6.86 – 6.75 (m, 4H), 6.73 (d, J = 8.81 Hz, 1H), 6.66 (d, J = 8.09 Hz, 1H), 6.56 (d, J = 7.01 Hz, 4H), 4.25 (d, J = 14.89 Hz, 1H), 4.16 (d, J = 15.09 Hz, 1H). **$^{13}\text{C}\{^1\text{H}\}$ NMR (101 MHz, CDCl_3):** δ = 162.5, 160.1, 151.4, 150.1, 149.8, 148.5, 141.7, 139.8, 139.2, 139.1, 138.7, 135.5, 133.80, 133.77, 132.6, 132.3, 132.1, 132.0, 131.4, 131.2, 129.7, 129.6, 128.6, 128.4, 127.3, 126.8, 126.7, 126.23, 126.18, 125.5, 125.5, 125.4, 125.3, 124.8, 124.7, 123.7, 123.6, 123.4, 123.1, 121.0, 120.6, 120.4, 120.3, 120.2, 120.0, 119.6, 115.1, 114.9, 112.6, 110.2, 109.94, 109.92, 109.7, 109.3, 32.1. **^{19}F NMR (377 MHz, CDCl_3):** δ [ppm] = -116.94 – -117.05 (m). **HRMS (+ESI) m/z :** $[\text{M} + \text{H}]^+$ Calcd for $\text{C}_{58}\text{H}_{35}\text{FN}_3\text{O}_2$ 824.2708; Found 824.2708.

1,4-Di(9*H*-carbazol-9-yl)-3-(4-fluorobenzyl)benzo[*b*]dinaphtho[2,1-*e*:1',2'-*g*][1,4]dioxocine-2-carbonitrile (7b)

Synthesized according to general procedure 2-B from chiral dicyanobenzene derivative **6b** and 4-fluorophenylacetic acid on 180 μmol scale (3 x 60 μmol) in DMA. The crude product was purified via column chromatography (10 \rightarrow 20% EtOAc in PE) and the product was obtained as a colorless solid. Isolated yield: 106 mg, 129 μmol , 71%.

TLC: R_f = 0.30 (20% EtOAc in PE). **^1H NMR (400 MHz, CDCl_3):** δ [ppm] = 8.32 – 8.24 (m, 2H), 8.19 – 8.12 (m, 1H), 8.08 (d, J = 7.68 Hz, 1H), 8.08 (t, J = 7.68 Hz, 2H), 7.76 – 7.66 (m, 3H), 7.63 (t, J = 7.70 Hz, 1H), 7.55 – 7.45 (m, 2H), 7.45 – 7.34 (m, 3H), 7.29 – 7.11 (m, 8H), 7.06 – 7.00 (m, 1H), 7.00 – 6.93 (m, 1H), 6.61 – 6.47 (m, 6H), 6.45 (d, J = 8.08 Hz, 1H), 4.17 (d, J = 14.72 Hz, 1H), 3.95 (d, J = 14.76 Hz, 1H). **$^{13}\text{C}\{^1\text{H}\}$ NMR (101 MHz, CDCl_3):** δ = 162.7, 160.2, 153.5, 149.6, 149.5, 147.5, 143.6, 141.0, 140.9, 140.8, 140.2, 134.5, 132.8, 132.7, 131.74, 131.68, 131.66, 131.6, 131.1, 130.9, 130.5, 129.64, 129.56, 128.1, 126.8, 126.7, 126.6, 126.4, 126.2, 125.80, 125.76, 124.90, 124.85, 124.3, 123.9, 123.8, 123.0, 121.2, 121.1, 121.0, 120.7, 120.5, 120.3, 120.2, 120.1, 115.1, 114.9, 114.8, 111.0,

110.1, 109.6, 109.4, 109.3, 36.2. ^{19}F NMR (377 MHz, CDCl_3): δ [ppm] = -116.68 – -116.83 (m). HRMS (FD+) m/z : $[\text{M}]^+$ Calcd for $\text{C}_{58}\text{H}_{34}\text{N}_3\text{O}_2\text{F}$ 823.2630; Found 823.2644.

2.4.4.4 Scale-up to 1 mmol

Synthesis of photosubstitution products **2b** and **2n** was repeated at 1 mmol scale. Carboxylic acid equivalents were lowered to 1.5 while still reaching full conversion. Concentration of starting material was doubled to decrease solvent use.

4CzIPN (789 mg, 1 mmol), carboxylic acid (1.5 mmol, 1.5 equiv.) and Cs_2CO_3 (489 mg, 1.5 mmol, 1.5 equiv.) were dissolved in 33 mL DMSO inside a crimp-capped vial. The vial was irradiated in the reactor depicted in Figure 2.4 for 1 h while stirring. The reaction might be completed earlier. However, due to the reactor design consumption of 4CzIPN cannot be determined by the change in fluorescence without removing an aliquot. The reaction mixture was diluted with 100 mL EtOAc and washed with water (3 x 100 mL) and brine (1 x 100 mL). The organic layer was dried over Na_2SO_4 , and the solvent removed under reduced pressure. The residue was dissolved in 7 mL DCM and 7 mL EtOAc were added. The DCM was slowly removed under reduced pressure (400 mbar, 50 °C). The solution was cooled to 4 °C to increase crystallization. The product was filtered, the solution evaporated to half its volume and cooled to 4 °C to afford additional product. Both, **2b** and **2n** were obtained in higher yields than on smaller scale. This can be attributed to smaller losses during the recrystallization step if conducted on larger scale.

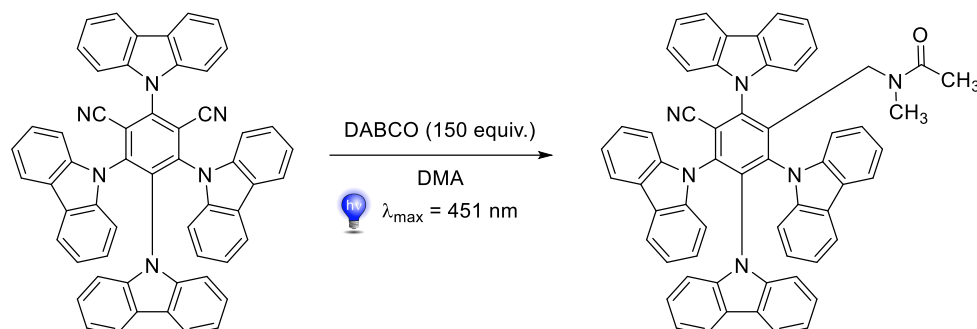
Total yield of **2b**: 658 mg, 755 μmol , 75%. The product was obtained as a yellow, crystalline solid.

Total yield of **2n**: 695 mg, 821 μmol , 82%. The product was obtained as a yellow, crystalline solid.

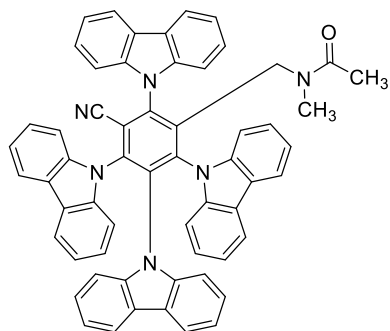
2.4.4.5 Photosubstitution by solvent fragments

Photosubstitution by DMA

In presence of DABCO in DMA a product was observed with one cyano group substituted by DMA. The reaction might proceed via abstraction of a hydrogen atom from DMA by a DABCO radical cation.



Scheme 2.5. Photosubstitution of a cyano group in 4CzIPN by DMA.

N-Methyl-*N*-(2,3,4,6-tetra(9*H*-carbazol-9-yl)-5-cyanobenzyl)acetamide (**2p**)

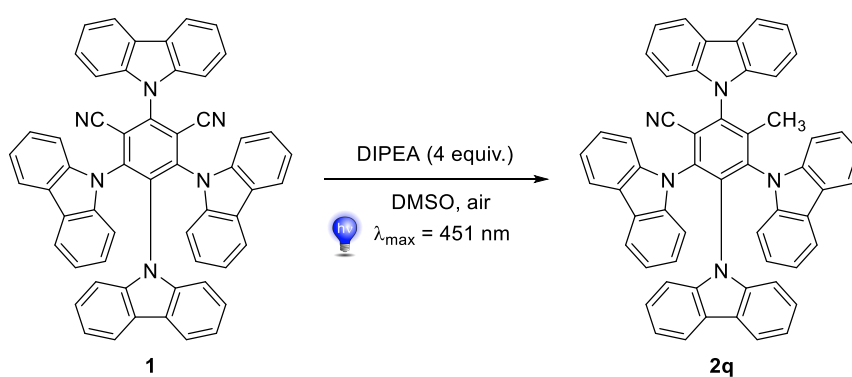
Synthesized according to general procedure 2-B with only 4CzIPN (4 x 30 μ mol) and DABCO (4 x 6 mmol, 150 equiv.) in 2 mL DMA per vial. Irradiated at 445 nm for 4 days. At this scale the reaction was not completed. No side products were observed. The reaction mixture was diluted with EtOAc, washed with water and brine, dried over Na_2SO_4 , and the solvent evaporated under reduced pressure. A recrystallization of the crude mixture from DCM/EtOAc was unsuccessful due to the large amount of unreacted 4CzIPN which could not be removed by recrystallization. The product was purified via column chromatography (Hexane/DCM 1:1) until all 4CzIPN eluted, then switched to 100% DCM to elute the product. Hexane/EtOAc mixtures were not suited for chromatography of the compound due to very low solubility in this solvent mixture. Only moderately clean product was obtained after column. Recrystallization from DCM/EtOAc yielded clean product as a yellow crystalline solid (21.0 mg, 24.7 μ mol, 21%).

^1H NMR (500 MHz, CD_2Cl_2): δ [ppm] = 8.27 (d, J = 4.57 Hz, 2H), 7.76 (d, J = 6.70 Hz, 6H), 7.66 (d, J = 7.95 Hz, 2H), 7.49 (t, J = 7.20 Hz, 2H), 7.34 (dd, J = 18.15, 7.70 Hz, 4H), 7.22 (d, J = 7.95 Hz, 2H), 7.17 – 7.05 (m, 8H), 7.02 (d, J = 8.05 Hz, 2H), 6.81 (t, J = 7.15 Hz, 2H), 6.70 (t, J = 7.53 Hz, 2H), 4.16 (s, 2H), 1.56 (s, 3H, overlap with H_2O).
 $^{13}\text{C}\{^1\text{H}\}$ NMR (126 MHz, CDCl_3): δ = 170.8, 142.9, 141.9, 140.69, 140.67, 140.48, 139.35, 139.33, 128.5, 136.6, 127.4, 126.1, 126.0, 124.8, 124.5, 124.2, 124.0, 123.7, 121.8, 121.5, 121.4, 121.1, 120.6, 120.51, 120.45, 119.6, 117.7, 113.1, 110.8, 110.6, 110.5, 109.9, 48.3, 37.0, 21.3. **HRMS (+ESI) m/z :** $[\text{M} + \text{Na}]^+$ Calcd for $\text{C}_{59}\text{H}_{40}\text{N}_6\text{ONa}^+$ 871.3156; Found 871.3196.

Photosubstitution by methyl groups from DMSO

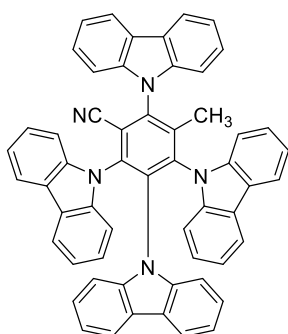
Upon irradiation of solutions containing 4CzIPN and an electron donor in DMSO a photosubstitution reaction was observed, exchanging one of the cyano groups by a methyl group from DMSO, although the reaction needed multiple hours instead of a few minutes compared to the photosubstitution reactions with carboxylates.

This might be explained by 4CzIPN reducing traces of molecular oxygen leaking through the septum to superoxide, reacting with DMSO to form methyl radicals.²⁵ Recombination with a 4CzIPN radical anion and cyanide elimination yields 4CzMeBN. To test whether the reaction is caused by oxygen we compared the time for reaction completion under air and in degassed DMSO (3 cycles of freeze-pump-thaw) on a 30 μmol scale. Indeed, under air the reaction is completed within 10 minutes while under degassed conditions only traces of product are obtained after 10 min and the reaction took 16 hours for almost full conversion. Without DIPEA photosubstitution to the same product occurs, but the reaction is slower and does not reach completion within 24 h.



Scheme 2.6. Photosubstitution by a methyl group from DMSO.

2,3,4,6-Tetra(9*H*-carbazol-9-yl)-5-methylbenzonitrile (4CzMeBN, 2q)

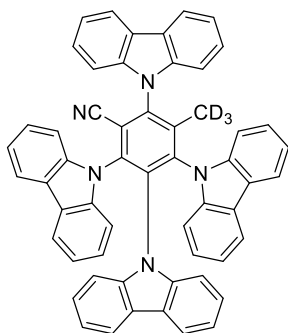


Synthesized according to general procedure 2-B from only 4CzIPN and DIPEA (4 equiv.) on 360 μmol scale in DMSO (4 x 90 μmol in 4 mL DMSO). The solution was not degassed and irradiated for 2 h under air. The product was obtained as a yellow solid (191 mg, 246 μmol , 68%).

The same reaction at 90 μmol scale under nitrogen atmosphere took 16 h for almost full completion and gave an isolated yield of only 46%. The product crystallized with 1 equivalent EtOAc which could not be removed under high vacuum. By dissolving in a small amount of chloroform and removal under reduced pressure twice the EtOAc could be removed.

TLC: $R_f = 0.35$ (20% EtOAc in PE). **^1H NMR (400 MHz, CDCl_3):** δ [ppm] = 8.24 (d, $J = 7.72$ Hz, 2H), 7.76 – 7.65 (m, 6H), 7.53 (d, $J = 8.08$ Hz, 2H), 7.45 (t, $J = 7.52$ Hz, 2H), 7.33 – 7.25 (m, 4H), 7.15 – 7.01 (m, 10H), 6.96 (d, $J = 8.04$ Hz, 2H), 6.78 (t, $J = 7.42$ Hz, 2H), 6.65 (t, $J = 7.62$ Hz, 2H), 4.13 (q, $J = 7.15$ Hz (q, EtOAc), 2.05 (s, EtOAc), 1.78 (s, 3H), 1.27 (t, $J = 7.14$ Hz, EtOAc). **$^{13}\text{C}\{^1\text{H}\}$ NMR (101 MHz, CDCl_3):** $\delta = 142.1, 141.6, 140.8, 140.1, 139.1, 138.9, 138.6, 138.0, 136.0, 126.8, 125.5, 125.4, 124.3, 124.1, 124.0, 123.6, 123.5, 121.3, 121.2, 121.0, 120.7, 120.3, 120.20, 120.17, 119.4, 117.0, 112.7, 110.1, 109.93, 109.90, 109.2, 15.0$. **HRMS (+ESI) m/z :** $[\text{M} + \text{H}]^+$ Calcd for $\text{C}_{56}\text{H}_{36}\text{N}_5$ 778.2965; Found 778.2961.

2,3,4,6-Tetra(9*H*-carbazol-9-yl)-5-(methyl- d_3)benzonitrile (2q- d_3)



Synthesized according to general procedure 2-B from only 4CzIPN and DIPEA (4 equiv.) on 158 μmol scale in DMSO-d_6 (2 x 90 μmol and 2 x 0.5 mL removed for NMR analysis before and after irradiation). The solution was not degassed and irradiated for 2 h under air. The product was obtained as a yellow solid (78 mg, 100 μmol , 63%)

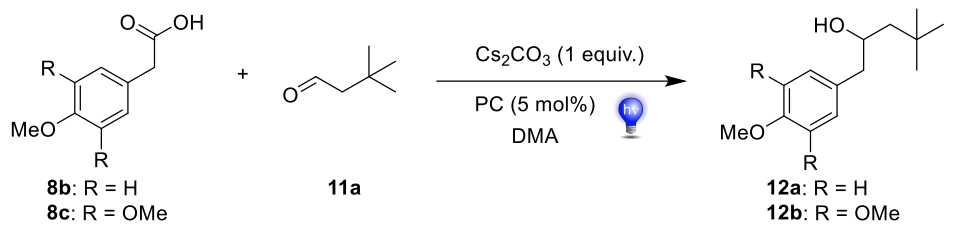
The same reaction at 90 μmol scale under nitrogen atmosphere took 16 h for almost full completion and gave an isolated yield of only 31 mg, 40 μmol , 44%. The product crystallized with 1 equivalent EtOAc which could not be removed under high vacuum. By dissolving in a small amount of chloroform and removal under reduced pressure twice the EtOAc could be removed. NMR spectra fit to non-deuterated 4CzMeBN except for the missing methyl signals. The expected septet in the ^{13}C NMR is not visible due to the low signal intensity.

TLC: $R_f = 0.35$ (20% EtOAc in PE). **^1H NMR (400 MHz, CDCl_3):** δ [ppm] = 8.24 (d, $J = 7.72$ Hz, 2H), 7.76 – 7.65 (m, 6H), 7.53 (d, $J = 8.08$ Hz, 2H), 7.45 (t, $J = 7.52$ Hz, 2H), 7.33 – 7.25 (m, 4H), 7.15 – 7.01 (m, 10H), 6.96 (d, $J = 8.04$ Hz, 2H), 6.78 (t, $J = 7.42$ Hz, 2H), 6.65 (t, $J = 7.62$ Hz, 2H). **$^{13}\text{C}\{^1\text{H}\}$ NMR (101 MHz, CDCl_3):** $\delta = 142.2, 141.5, 140.7, 140.1, 139.1, 138.9, 138.6, 138.0, 136.0, 126.8, 125.5, 125.4, 124.3, 124.1, 124.0, 123.6, 123.5, 121.3, 121.2, 121.0, 120.7, 120.3, 120.20, 120.17, 119.4, 116.9, 112.7, 110.1, 109.93, 109.89, 109.1$. **HRMS (+ESI) m/z :** $[\text{M} + \text{H}]^+$ Calcd for $\text{C}_{58}\text{H}_{31}\text{D}_3\text{N}_5$ 781.3154; Found 781.3179.

2.4.5 Comparison of the catalytic activity of 4CzIPN, 2CzPN and their photosubstitution products

Reduction of electron rich benzylic radicals to the corresponding carbanions

Table 2.3. Dependence of decarboxylative benzylation on irradiation wavelength and choice of catalyst.



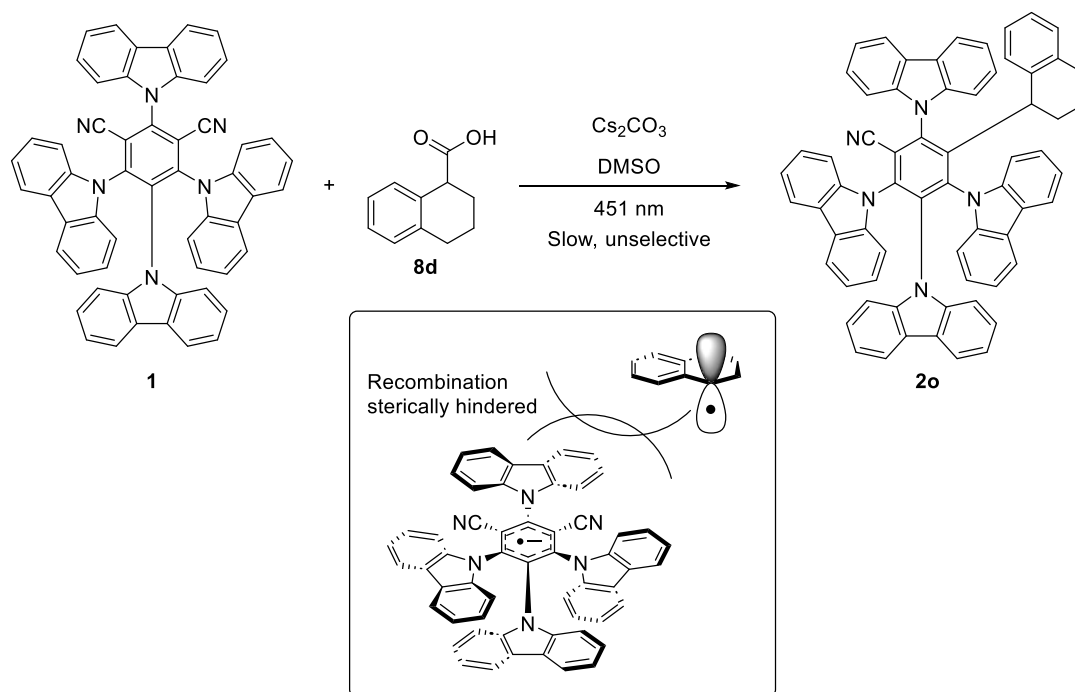
Entry	Substrate	Product	Catalyst	Wavelength	NMR yield
1	8b	12a	2CzPN	451 nm	0%
2	8b	12a	4CzIPN	451 nm	32%
3	8b	12a	2CzPN	400 nm	73%
4	8c	12b	2CzPN	400 nm	56%
5	8c	12b	4CzIPN	400 nm	78%

2CzPN is ineffective if 451 nm LEDs are used for irradiation. In entries 1, 3, and 4 Table 2.3 the yellow color of 2CzPN faded within seconds of irradiation and a colorless solution was obtained. No product **12a** was obtained after irradiation for 16 h at 451 nm (entry 1). This is expected as the photosubstitution products of 2CzPN do not absorb within the emission range of the LEDs. 4CzIPN's photosubstitution products, however, absorb some of the light and moderate yield of 32% was obtained (entry 2). When switching to lower wavelength 2CzPN's photosubstitution products become effective. Irradiation with 400 nm LEDs gave 73% yield (entry 3). This was also observed with 3,4,5-trimethoxyphenylacetic acid as carbanion precursor (entry 4), although 4CzIPN's photosubstitution products gave higher yield (entry 5).

These experiments do not allow a general comment on whether one of the catalysts is superior to others. However, it is important to note that 2CzPN's photosubstitution products are active and stable photocatalysts if the blue shifted absorption in comparison to 2CzPN is considered. The increased redox window and reduction potentials (see Table 2.1) put these catalysts among the most reductive carbazoyl cyanobenzene photocatalysts, exceeding reduction potentials reached by previously reported derivatives.³

Substrate where in situ photosubstitution is impeded

Tetrahydronaphthoic acid (**8d**) reacts sluggishly with 4CzIPN. A likely rationale is steric hindrance by the carbazole units. Radical recombination can only occur with the benzonitrile core of the 4CzIPN radical anion and the ring system of the tetrahydronaphthyl radical parallel to each other. The carbazole units are tilted, thus limit the space above the benzonitrile core of 4CzIPN. The observation that the sterically more accessible 2CzPN cleanly reacts with tetrahydronaphthoic acid **8d** to product **4a** is further evidence for this explanation.



Scheme 2.7. Tetrahydronaphthoic acid (**8d**) reacts sluggishly with 4CzIPN under color change to dark green/brown.

Reacting 4CzIPN with tetrahydronaphthoic acid (**8d**) according to general procedure B leads to a color change to dark green/brown within seconds of irradiation. After irradiation for 16 h moderate conversion and a mixture of products is observed while other carboxylic acids usually react within minutes and give a clear yellow/orange solution.

To test whether this affects reactions where 4CzIPN is a pre-catalyst and acid **8d** is a substrate we reacted **8a** with pentanal under our previously reported conditions for photocatalytic decarboxylative benzylation.¹² The reaction with 4CzIPN turned dark within seconds of irradiation while the reaction with photosubstitution product **2j** showed no color change. After 1 h the dark color in the reaction with 4CzIPN began to cease and the solution was almost colorless after 3 h. While the reaction with catalyst **2j** was close to completion after 1 h the reaction with 4CzIPN showed only small amounts of product. However, after 3 h both reactions were completed and did not show substantial increase in yield upon irradiation for additional 13 h. If 4CzIPN is used as catalyst yields stay slightly below those for catalyst **2j**. This is expected as 1 equivalent of substrate with respect to 4CzIPN is needed for photosubstitution to convert 4CzIPN into the active catalyst.

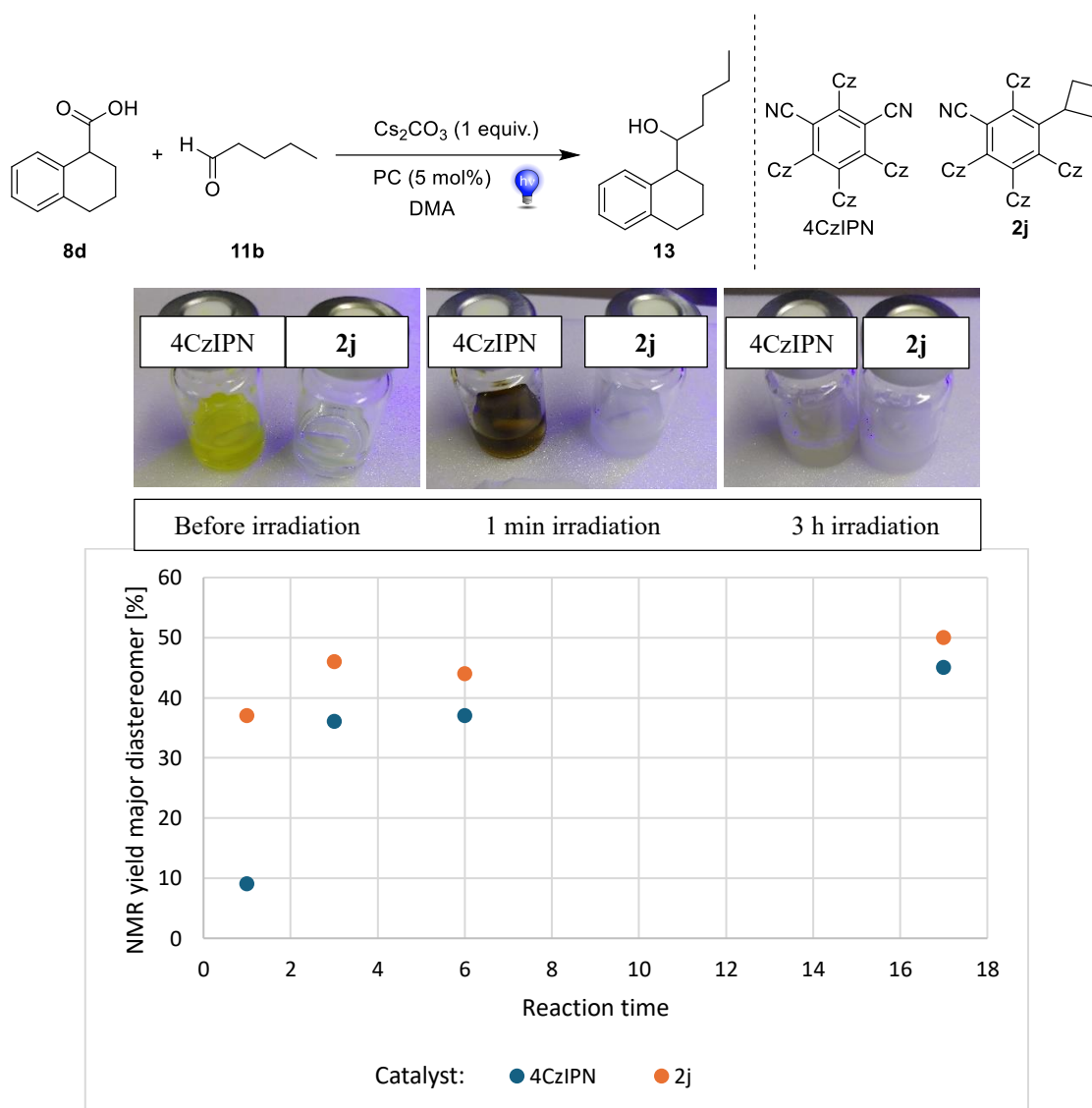


Figure 2.6. NMR yield of the major diastereomer of product **13** with 4CzIPN and photosubstitution product **2j** as catalyst. Two diastereomers are formed in approximately 1.3:1 ratio. Only the major diastereomer was used for comparison of the yield due to overlapping signals of the minor diastereomer. Total yield is by a factor of approximately 1.7 higher.

2.4.6 Comparison of solubilities in MeCN

Solubilities were estimated by preparation of a saturated solution of the substance in approximately 1 mL MeCN, filtration through a PTFE HPLC filter (Chromafil® O-20/15 MS, pore size 0.2 μM), dilution to approximately 20 μM and measurement of the UV/Vis absorbance. Additionally, a 20 μM solution of each compound was prepared as reference. Concentrations of the diluted solutions were then calculated using Beer-Lambert's law and solubility was obtained by correction by the dilution factor.

Solubility of photosubstitution products was found to be substantially smaller than solubility of their dicyanobenzene precursor 4CzIPN or 2CzPN, respectively.

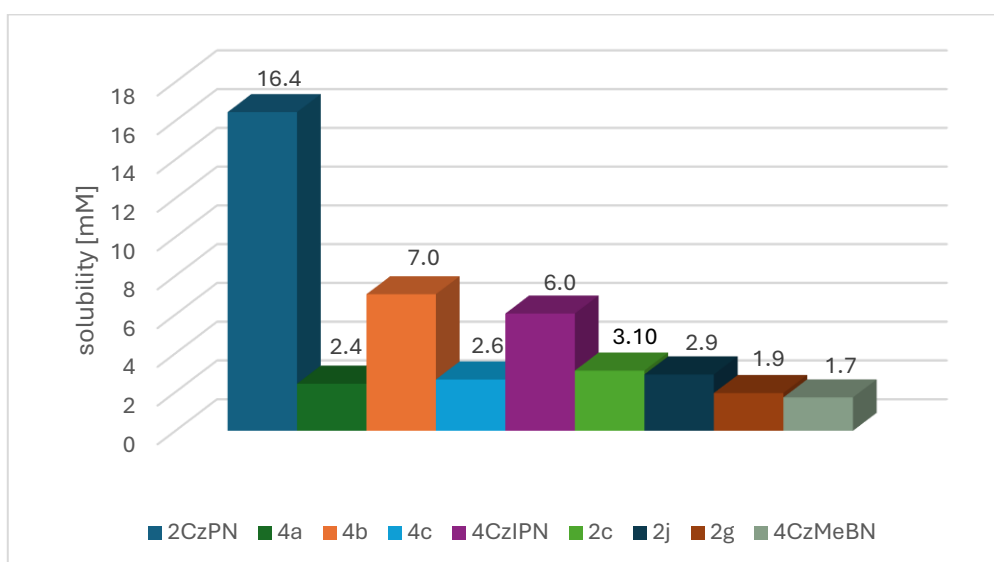


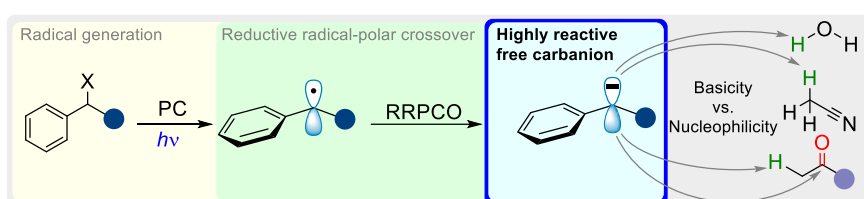
Figure 2.7. Solubility of 2CzPN, 4CzIPN and photosubstitution products in MeCN.

2.5 References

- (1) Uoyama, H.; Goushi, K.; Shizu, K.; Nomura, H.; Adachi, C. Highly efficient organic light-emitting diodes from delayed fluorescence. *Nature* **2012**, *492*, 234–238.
- (2) Luo, J.; Zhang, J. Donor–Acceptor Fluorophores for Visible-Light-Promoted Organic Synthesis: Photoredox/Ni Dual Catalytic C(sp³)–C(sp²) Cross-Coupling. *ACS Catal.* **2016**, *6*, 873–877.
- (3) Speckmeier, E.; Fischer, T. G.; Zeitler, K. A Toolbox Approach To Construct Broadly Applicable Metal-Free Catalysts for Photoredox Chemistry: Deliberate Tuning of Redox Potentials and Importance of Halogens in Donor–Acceptor Cyanoarenes. *J. Am. Chem. Soc.* **2018**, *140*, 15353–15365.
- (4) Shang, T.-Y.; Lu, L.-H.; Cao, Z.; Liu, Y.; He, W.-M.; Yu, B. Recent advances of 1,2,3,5-tetrakis(carbazol-9-yl)-4,6-dicyanobenzene (4CzIPN) in photocatalytic transformations. *Chem. Commun.* **2019**, *55*, 5408–5419.
- (5) Pitzer, L.; Schwarz, J. L.; Glorius, F. Reductive radical-polar crossover: traditional electrophiles in modern radical reactions. *Chem. Sci.* **2019**, *10*, 8285–8291.
- (6) Shu, C.; Mega, R. S.; Andreassen, B. J.; Noble, A.; Aggarwal, V. K. Synthesis of Functionalized Cyclopropanes from Carboxylic Acids by a Radical Addition-Polar Cyclization Cascade. *Angew. Chem., Int. Ed.* **2018**, *57*, 15430–15434.
- (7) Phelan, J. P.; Lang, S. B.; Compton, J. S.; Kelly, C. B.; Dykstra, R.; Gutierrez, O.; Molander, G. A. Redox-Neutral Photocatalytic Cyclopropanation via Radical/Polar Crossover. *J. Am. Chem. Soc.* **2018**, *140*, 8037–8047.
- (8) Meng, Q.-Y.; Schirmer, T. E.; Berger, A. L.; Donabauer, K.; König, B. Photocarboxylation of Benzylic C-H Bonds. *J. Am. Chem. Soc.* **2019**, *141*, 11393–11397.
- (9) Zhang, B.; Yi, Y.; Wu, Z.-Q.; Chen, C.; Xi, C. Photoredox-catalyzed dicarbofunctionalization of styrenes with amines and CO₂: a convenient access to γ -amino acids. *Green Chem.* **2020**, *22*, 5961–5965.
- (10) Ju, T.; Fu, Q.; Ye, J.-H.; Zhang, Z.; Liao, L.-L.; Yan, S.-S.; Tian, X.-Y.; Luo, S.-P.; Li, J.; Yu, D.-G. Selective and Catalytic Hydrocarboxylation of Enamides and Imines with CO₂ to Generate α,α -Disubstituted α -Amino Acids. *Angew. Chem., Int. Ed.* **2018**, *57*, 13897–13901.
- (11) Abrams, R.; Clayden, J. Photocatalytic Difunctionalization of Vinyl Ureas by Radical Addition Polar Truce-Smiles Rearrangement Cascades. *Angew. Chem., Int. Ed.* **2020**, *59*, 11600–11606.
- (12) Donabauer, K.; Maity, M.; Berger, A. L.; Huff, G. S.; Crespi, S.; König, B. Photocatalytic carbanion generation - benzylation of aliphatic aldehydes to secondary alcohols. *Chem. Sci.* **2019**, *10*, 5162–5166.
- (13) Mizuno, K.; Nakanishi, K.; Otsuji, Y. Photosubstitution of Dicyanobenzenes by Group 14 Organometallic Compounds via Photoinduced Electron-Transfer. Additive and Medium Effects on Photoinduced Electron Transfer Reaction. *Chem. Lett.* **1988**, *17*, 1833–1836.
- (14) Itou, T.; Yoshimi, Y.; Morita, T.; Tokunaga, Y.; Hatanaka, M. Decarboxylative photosubstitution of dicyanobenzenes with aliphatic carboxylate ions. *Tetrahedron* **2009**, *65*, 263–269.
- (15) Feuillastre, S.; Pauton, M.; Gao, L.; Desmarchelier, A.; Riives, A. J.; Prim, D.; Tondelier, D.; Geffroy, B.; Muller, G.; Clavier, G.; Pieters, G. Design and Synthesis of New Circularly Polarized Thermally Activated Delayed Fluorescence Emitters. *J. Am. Chem. Soc.* **2016**, *138*, 3990–3993.
- (16) Frédéric, L.; Desmarchelier, A.; Plais, R.; Lavnevich, L.; Muller, G.; Villafuerte, C.; Clavier, G.; Quesnel, E.; Racine, B.; Meunier-Della-Gatta, S.; Dognon, J. P.; Thuéry, P.; Crassous, J.; Favereau, L.; Pieters, G. Maximizing Chiral Perturbation on Thermally Activated Delayed Fluorescence Emitters and Elaboration of the First Top-Emission Circularly Polarized OLED. *Adv. Funct. Mater.* **2020**, *30*.
- (17) Kong, D.; Munch, M.; Qiqige, Q.; Cooze, C. J. C.; Rotstein, B. H.; Lundgren, R. J. Fast Carbon Isotope Exchange of Carboxylic Acids Enabled by Organic Photoredox Catalysis. *J. Am. Chem. Soc.* **2021**, *143*, 2200–2206.
- (18) Wayner, D. D. M.; McPhee, D. J.; Griller, D. Oxidation and reduction potentials of transient free radicals. *J. Am. Chem. Soc.* **1988**, *110*, 132–137.
- (19) Rolka, A. B.; Koenig, B. Dearomatic Cycloadditions Utilizing an Organic Photosensitizer: An Alternative to Iridium Catalysis. *Org. Lett.* **2020**, *22*, 5035–5040.
- (20) Schmalzbauer, M.; Svejstrup, T. D.; Fricke, F.; Brandt, P.; Johansson, M. J.; Bergonzini, G.; König, B. Redox-Neutral Photocatalytic C–H Carboxylation of Arenes and Styrenes with CO₂. *Chem* **2020**, *6*, 2658–2672.
- (21) Speck, F.; Rombach, D.; Wagenknecht, H.-A. N-Arylphenothiazines as strong donors for photoredox catalysis - pushing the frontiers of nucleophilic addition of alcohols to alkenes. *Beilstein J. Org. Chem.* **2019**, *15*, 52–59.

- (22) Matsui, J. K.; Lang, S. B.; Heitz, D. R.; Molander, G. A. Photoredox-Mediated Routes to Radicals: The Value of Catalytic Radical Generation in Synthetic Methods Development. *ACS Catal.* **2017**, *7*, 2563–2575.
- (23) Engle, S.; Takisha R. Kirkner; Christopher B. Kelly. Preparation of 2,4,5,6-Tetra(9H-carbazol-9-yl)isophthalonitrile. *Org. Synth.* **2019**, *96*, 455–473.
- (24) Uccello-Barretta, G.; Vanni, L.; Berni, M. G.; Balzano, F. NMR enantiodiscrimination by pentafluorophenylcarbamoyl derivatives of quinine: C10 versus C9 derivatization. *Chirality* **2011**, *23*, 417–423.
- (25) Herscu-Kluska, R.; Masarwa, A.; Saphier, M.; Cohen, H.; Meyerstein, D. Mechanism of the reaction of radicals with peroxides and dimethyl sulfoxide in aqueous solution. *Chemistry* **2008**, *14*, 5880–5889.

3 Reactivity of Superbasic Carbanions Generated via Reductive Radical-Polar Crossover in the Context of Photoredox Catalysis



This chapter has been published in a slightly modified version. For reference see: S. Grotjahn; C. Graf; J. Zelenka; A. Pattanaik; L. Müller; R. J. Kutta; J. Rehbein; J. Roithová; R. M. Gschwind; P. Nuernberger; B. König *Angew. Chem. Int. Ed.* **2024**, e202400815. Copyright © 1999-2024 John Wiley & Sons, Inc

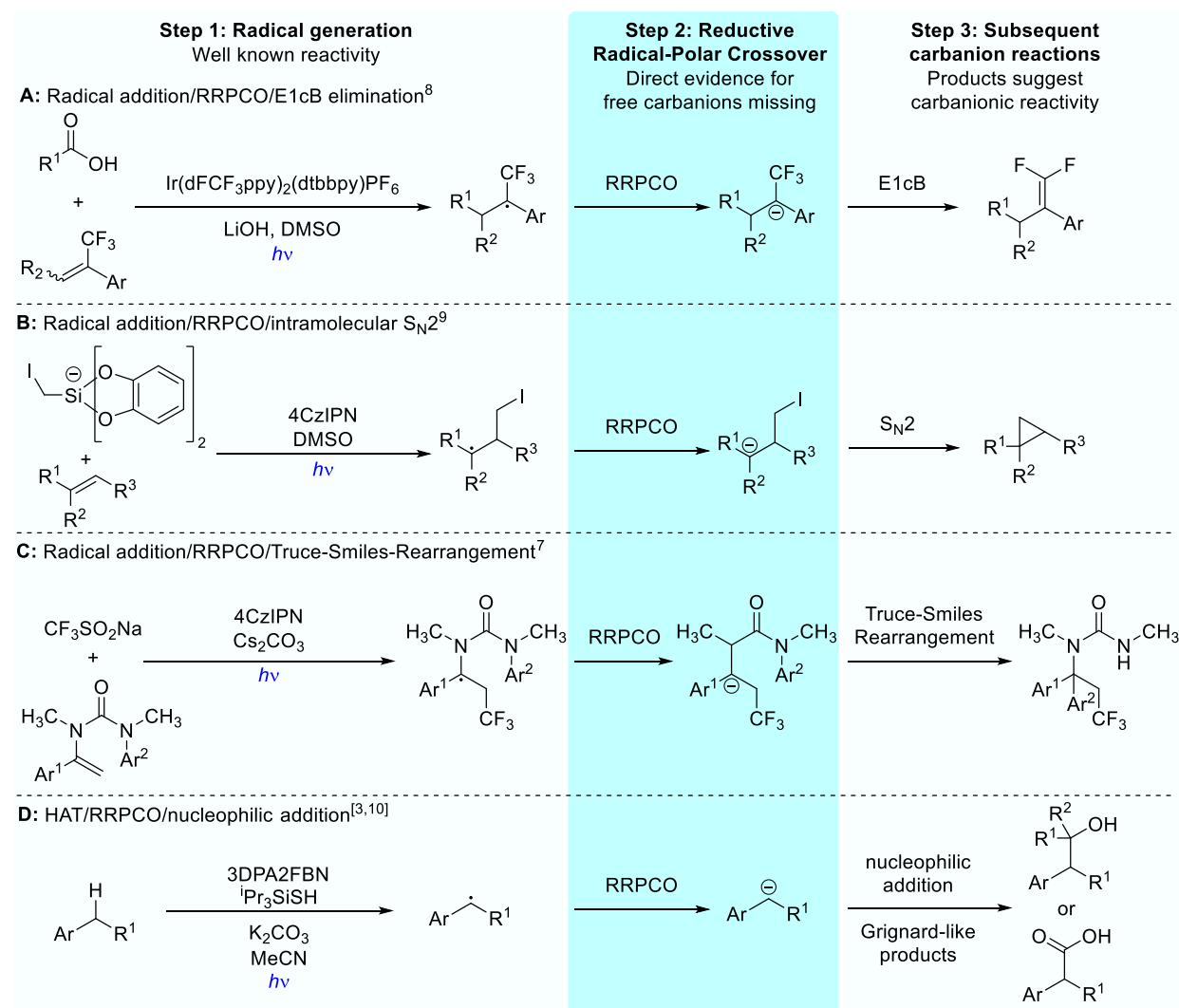
Author contributions: Sascha Grotjahn coordinated the project, synthesized all compounds, performed in solution KIE experiments and photoreactions under supervision of Burkhard König. Sascha Grotjahn and Jan Zelenka performed initial gas-phase KIE experiments and gas-phase deprotonations and Jan Zelenka conducted all detailed gas-phase experiments under supervision of Jana Roithová. Chrisina Graf and Roger-Jan Kutta performed transient absorption measurements under supervision of Patrick Nuernberger. Aryaman Pattanaik performed DFT calculations under supervision of Julia Rehbein. Lea Müller measured ^2H NMR spectra under supervision of Ruth M. Gschwind.

Abstract

Photocatalytic reactions involving a reductive radical-polar crossover (RRPCO) generate intermediates with carbanionic reactivity. Many of these proposed intermediates resemble highly reactive organometallic compounds. However, conditions of their formation are generally not tolerated by their isolated organometallic versions and often a different reactivity is observed. Our investigations on their nature and reactivity under commonly used photocatalytic conditions demonstrate that these intermediates are indeed best described as free, superbasic carbanions capable of deprotonating common polar solvents usually assumed to be inert such as acetonitrile, dimethylformamide, and dimethylsulfoxide. Their basicity not only towards solvents but also towards electrophiles, such as aldehydes, ketones, and esters, is comparable to the reactivity of isolated carbanions in the gas-phase. Previously unsuccessful transformations thought to result from a lack of reactivity are explained by their high reactivity towards the solvent and weakly acidic protons of reaction partners. An intuitive explanation for the mode of action of photocatalytically generated carbanions is provided, which enables methods to verify reaction mechanisms proposed to involve an RRPCO step and to identify the reasons for the limitations of current methods.

3.1 Introduction

Within the last years, photocatalytic reactions involving a reductive radical-polar crossover (RRPCO)^{1,2} step were reported by multiple groups. In an RRPCO a radical intermediate is converted to an anionic species, thus bringing the catalytic cycle back into the singlet spin-state while retaining reactivity for subsequent reaction steps. This allows the diversification of scaffolds obtainable by a single photocatalytic reaction. C-C bond formation through radical addition can be subsequently coupled to nucleophilic addition to carbonyl groups,³⁻⁶ rearrangements,⁷ E1cB-type eliminations,⁸ and intramolecular S_N2 reactions⁹ as depicted in Scheme 3.1.



Scheme 3.1. Selection of reactions proposed to involve a short-lived carbanionic intermediate.

Recently, reactions have been developed that focus especially on the generation of carbanions from easily accessible precursors such as decarboxylative carbanion generation⁴ and C-H activation,^{3,5,10-12} as well as carbanion generation from C-N¹³ and C-O bonds,¹⁴ to allow Grignard-like reactions, carboxylations, and isotopic labeling with up to 100% atom economy. As RRPCO is a common step to close photocatalytic cycles, Scheme 3.1 provides only some selected examples. Other reactions proposed to proceed via an RRPCO step include photocatalytic dearomatizations,¹⁵⁻¹⁸ Giese-type reactions,¹⁹⁻²¹ and electrochemical cross-electrophile coupling.²² Often, the carbanionic intermediate is

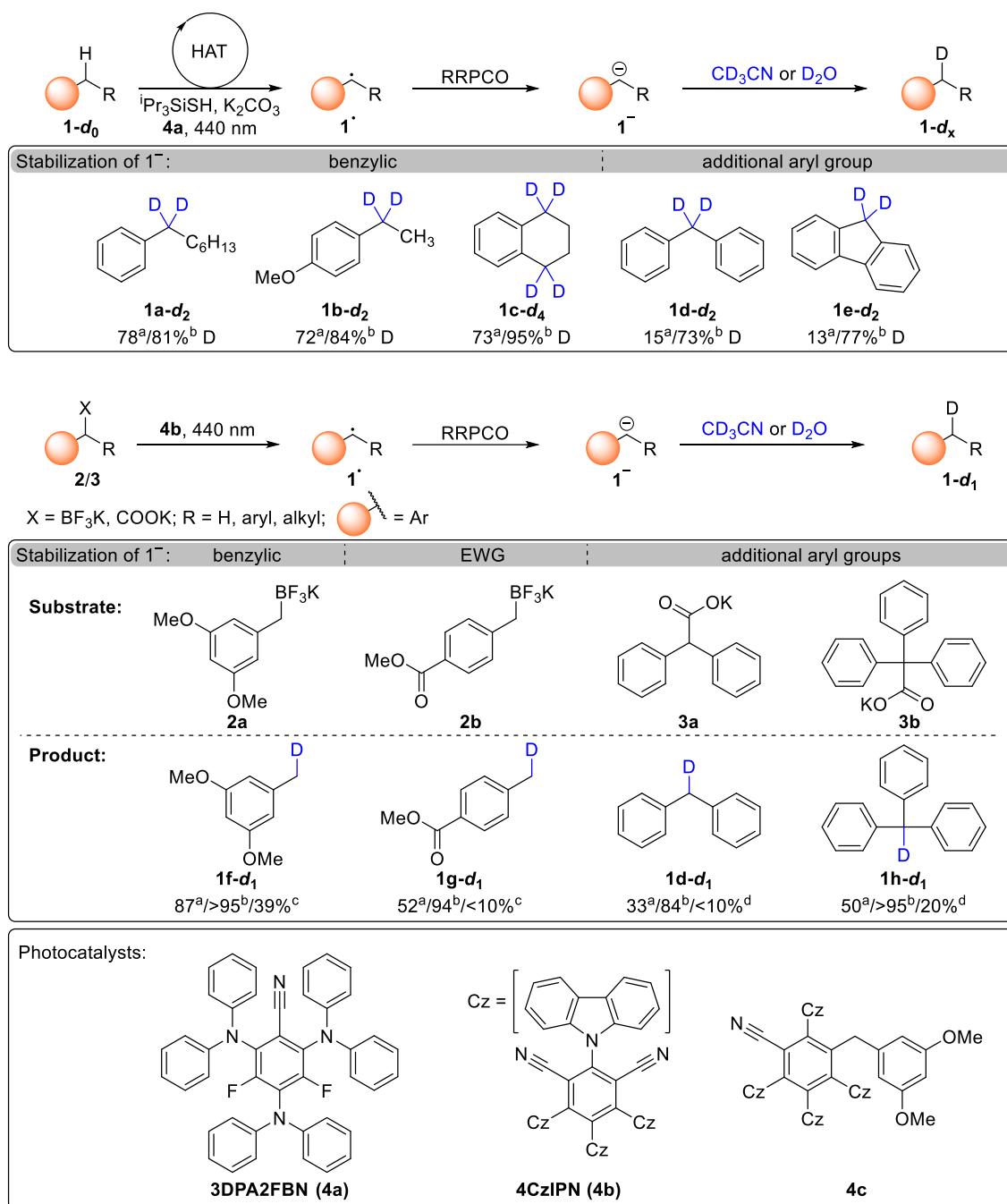
not explicitly mentioned if a catalytic cycle is closed by reduction of a radical species to a carbanion with subsequent protonation. These steps are then combined into a single reaction step described as electron-transfer, proton-transfer (ETPT) or as a stepwise proton-coupled electron transfer (PCET). Despite the vast number of reactions achieved with classic organometallic carbanions such as Grignard²³ or organolithium reagents,²⁴ intermolecular C-C bond-forming reactions of photocatalytically generated carbanions seem to be restricted to carbon dioxide, aldehydes, and ketones with already noticeable drop in reaction yield from aldehydes to ketones.^{3-5,10,11,21,25-27} Approaches to react carbanions generated under previously reported conditions in intermolecular S_N2 reactions or Grignard-type reactions with esters or similarly reactive electrophiles were generally unsuccessful. Here, we explore the nature of photocatalytically generated carbanions in more detail to give a rationale for the difference in reactivity compared to their organometallic analogs.

3.2 Results and discussion

3.2.1 Evidence for free carbanions in solution

The reports on reactions involving photocatalytically generated carbanions depicted in Scheme 3.1 provide clear evidence for carbanionic reactivity. The usual control reaction for distinguishing between a radical pathway and carbanionic reactivity is the addition of D₂O to the reaction mixture, quenching the carbanion and incorporating deuterium at the respective position. Although this experiment provides evidence for carbanionic reactivity and generally excludes a direct radical pathway, it does not provide information about whether the carbanion is truly a free carbanion or stabilized by some kind of interaction with a species present in the reaction mixture. Even classical organometallic reagents show a pronounced difference in reactivity for different alkali and alkaline earth metal compounds due to aggregation and ion pairing.²⁸ However, a direct comparison of the reactivity in the same environment with organometallic reagents is not possible due to the incompatibility of highly reactive organometallic compounds with solvents generally used in photocatalytic reactions generating carbanions. This incompatibility of classic organometallic reagents with high polarity solvents raised the question why photocatalytic reactions proposed to involve a carbanion were possible under these conditions.

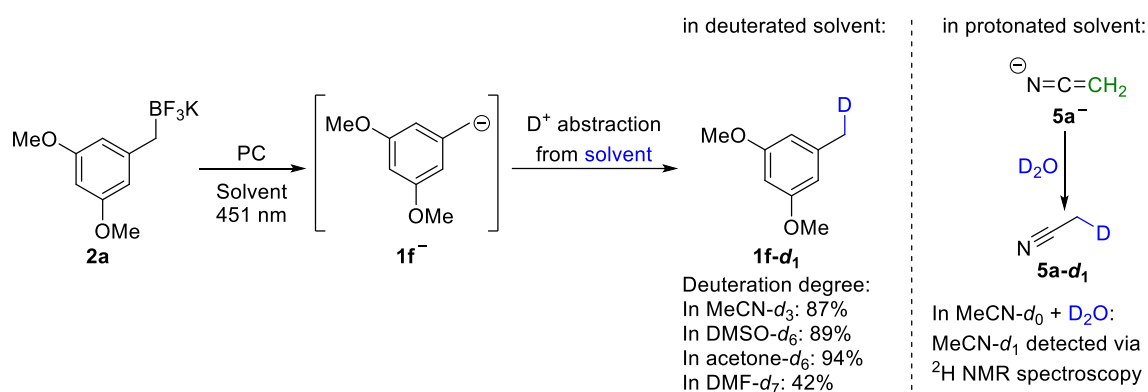
In this work, it was found that under absence of a suitable coupling partner for carbanions the corresponding protonated species is formed as the major product. When using CD₃CN as solvent a high degree of deuteration at the benzylic position can be obtained, depending on the electronic properties of the carbanion formed, thus demonstrating that the solvent indeed cannot be assumed to be inert. The addition of H₂O suppresses this deuteration while addition of D₂O leads to high deuteration even in non-deuterated solvents. The degrees of deuteration for a selection of electronically different substrates is depicted in Scheme 3.2. d_x describes the number of deuterium atoms in the molecule, with the non-deuterated molecule labelled with d_0 . A more detailed description on the determination of deuteration degrees can be found in the experimental part 3.4.7.



Scheme 3.2. Deuterium incorporation into the benzylic position. Deuteration degrees are determined by ¹H NMR spectroscopy and based on the theoretically possible equivalents of deuterium that can be incorporated based on the mechanism (1 D per benzylic hydrogen of the substrate in C-H activation, 1 D per molecule in carbanion generation from trifluoroborates and carboxylates); photocatalyst **4c** is formed in situ from 4CzIPN (**4b**) and trifluoroborate **2a** (see chapter 2 for details);²⁹ ^adeuteration without D₂O; ^bdeuteration with 10 equiv. D₂O; ^c0.5 equiv. of H₂O added to provide 1 equiv. of protons; ^dcarboxylic acid with 1 equiv. Cs₂CO₃ used instead of potassium salt, no D₂O was added.

The deprotonation of the only slightly acidic acetonitrile C-H bonds (or C-D bonds) with a pK_a of approximately 31 (dissolved in DMSO)³⁰ by non-stabilized benzylic carbanions **1a⁻**, **1b⁻**, **1c⁻**, and **1f⁻** demonstrates that photocatalytically generated carbanions can be highly basic. It was expected that compounds with higher C-H acidity would generate less basic carbanions upon C-H activation. Indeed, benzylic C-H activation of diphenylmethane (**1d**) and fluorene (**1e**) to the corresponding carbanions **1d⁻** and **1e⁻**, respectively, was achieved under standard reaction

conditions but only low D-incorporation was observed in dry CD₃CN, while deuteration was high in the presence of 10 equivalents D₂O. Carbanions generated from carboxylates and trifluoroborate salts follow the same trend with high incorporation of deuterium into non-stabilized benzylic carbanion **1f⁻** and decreasing D-incorporation with better stabilization of the negative charge, while D-incorporation remains high in all examples in the presence of D₂O. For less reactive carbanions stabilized by electron withdrawing groups (**1g⁻**) or an additional aryl group (**1d⁻**, **1e⁻**, **1h⁻**) under proton free conditions there is still moderate deuterium incorporation into the product. However, the lack of abstractable protons likely leads to regeneration of the starting material by reaction of the carbanion with the formed CO₂ or BF₃ which can then re-enter the photocatalytic cycle until either a deuterium is abstracted from CD₃CN or a proton from another source (e.g., residual moisture). The reaction of carbanions generated under similar conditions with CO₂ was reported previously¹⁰ and is also observed in the gas phase (see experimental part, Figure 3.15). More comparable results are obtained if one equivalent of abstractable protons is still present in the reaction mixture. For carbanion generation from carboxylates this is achieved by using the carboxylic acid and a mild base instead of a carboxylate salt, which resembles a previously described procedure for photocatalytic Grignard-type reactions.⁴ For trifluoroborates (**2**), 0.5 equivalents of water were added to provide 1 equivalent of protons. If carbanions are generated from C-H bonds the abstracted hydrogen atoms remain in solution as hydrogen carbonate and silane thiol, thus a small amount of acidic protons is always present under these conditions. Proton (or deuterium) abstraction from the solvent by stabilized carbanions **1g⁻**, **1d⁻**, and **1h⁻** is mostly suppressed if acidic protons are present, while non-stabilized carbanions are less selective and abstract protons (or deuterons) from the solvent even in presence of substantially more acidic protons. The difference in reactivity of non-stabilized and stabilized carbanions towards moderately acidic protons has important synthetic implications for isotopic labelling, especially for tritium labelling where it is desirable to quantitatively incorporate tritium from stoichiometric amounts of the tritium source into a target molecule to minimize radioactive waste.³¹ Deprotonation of the solvent also occurs in DMSO, DMF and acetone. Potassium trifluoroborate salt **2a** was used as carbanion precursor because trifluoroborates generate carbanions more reliably under different reaction conditions, while carbanion generation from carboxylates is more sensitive to the reaction conditions. In DMSO-*d*₆ as well as in acetone-*d*₆ the corresponding 3,5-dimethoxytoluene (**1f-d₁**) was produced with high degree of mono-deuteration, similar to the outcome in acetonitrile-*d*₃ (Scheme 3) and in DMF-*d*₇ a moderate deuteration degree of 42% was observed. In acetone the corresponding tertiary alcohol **7b** was obtained in similar amounts as the toluene derivative **1f-d₁**, (Scheme 3.8). Deprotonation of the solvent generates the corresponding solvent anion **5⁻**. We could indirectly detect this species formed from acetonitrile-*d*₀ in the presence of 1 equivalent D₂O. Under these reaction conditions the deprotonated solvent was deuterated by D₂O to form acetonitrile-*d*₁ which was detected in the ²H NMR spectrum (see experimental part, Figure 3.33).



Scheme 3.3. Photocatalytically generated non-stabilized benzylic carbanion **1f⁻** is able to abstract a deuteron from acetonitrile- d_3 , DMSO- d_6 , DMF- d_7 , and acetone- d_6 . MeCN- d_1 was detected by deuterium NMR spectroscopy when the reaction was performed in acetonitrile- d_0 in the presence of D₂O. PC – photocatalyst **4c** is generated in situ from 4CzIPN as described in chapter 2.²⁹

3.2.2 Comparison with gas-phase reactivity of isolated carbanions

Next, the reactivity of isolated/non-solvated carbanions generated via collision-induced dissociation (CID) was tested in the gas phase (Figure 3.1, see experimental part section 3.4.6 for details). In agreement with the results obtained under photocatalytic conditions in solution, non-stabilized benzylic carbanions readily deprotonate α -positions of carbonyl and nitrile groups. Carbanions with additional stabilization by an electron withdrawing ester group (**1g⁻**) on the aryl group or additional phenyl groups (**1d⁻**, **1e⁻**, **1h⁻**) at the benzylic position did not deprotonate acetonitrile in the gas phase. A strong drop in reactivity under the photocatalytic conditions used to generate carbanions in solution was also observed for all carbanions with conjugated acids with a pK_a close to or below that of acetonitrile. Thus, basicity of carbanions generated under photocatalytic conditions relative to acetonitrile is similar to isolated carbanions in the gas phase.

REACTIVITY OF SUPERBASIC CARBANIONS GENERATED VIA REDUCTIVE RADICAL-POLAR CROSSOVER IN THE CONTEXT OF PHOTOREDOX CATALYSIS

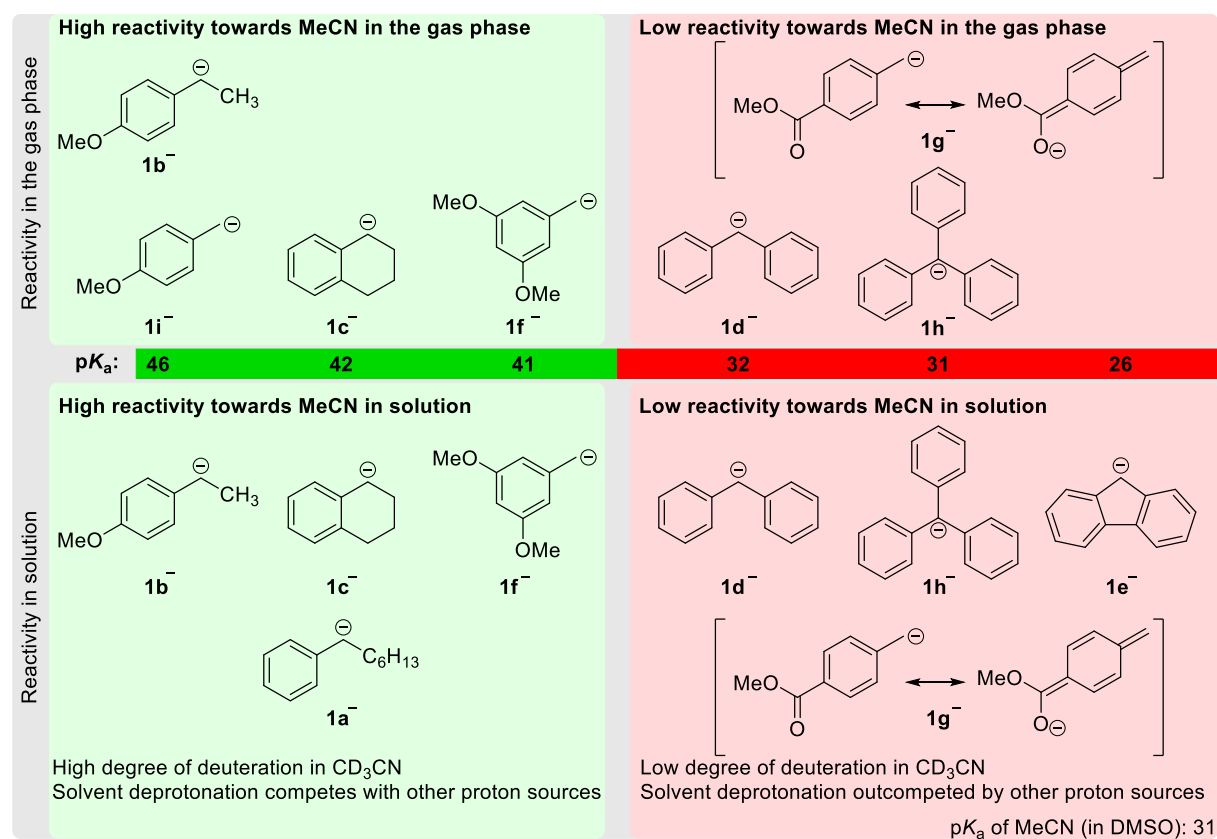


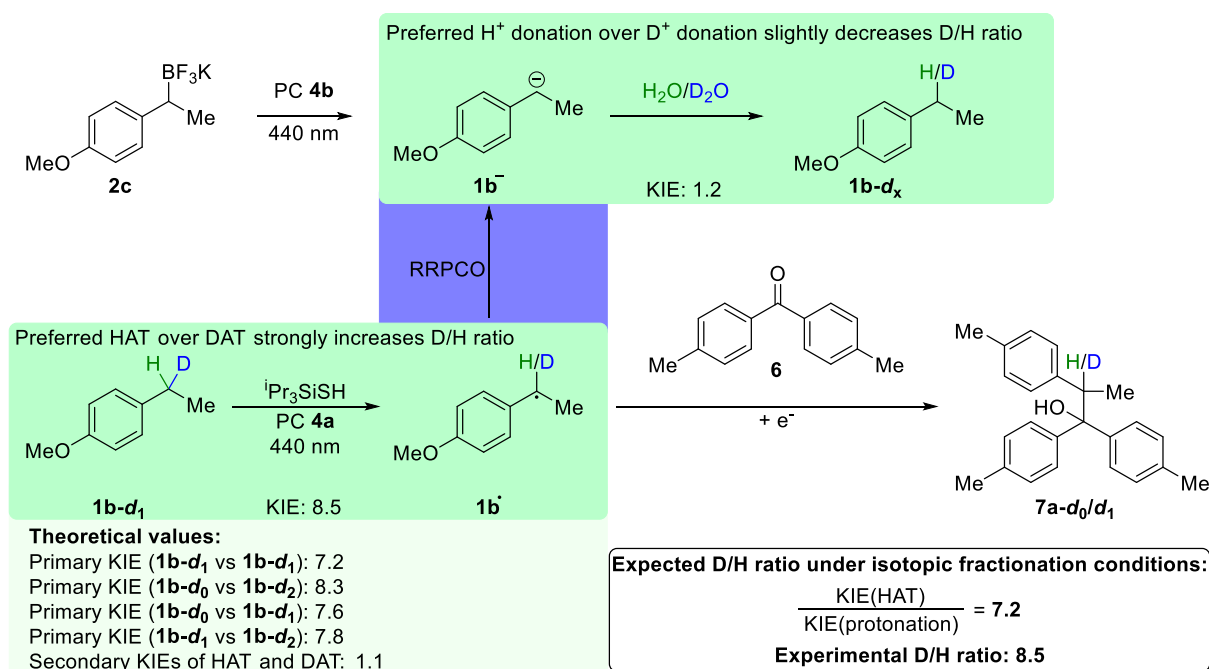
Figure 3.1. Gas phase reactivity between carbanions generated via collision-induced dissociation (CID) and acetonitrile and comparison with solution reactivity. Molecules are grouped into high reactivity towards deprotonation of MeCN and low or no reactivity towards MeCN. Molecules are placed at the approximate pK_a values of the respective conjugate acid, where values of the respective compound or closely related compounds in DMSO are accessible.^{30,32,33}

In addition to qualitatively separating carbanions into high and low reactivity towards deprotonation of acetonitrile, the deprotonation in the gas phase showed a pronounced kinetic isotope effect (KIE). Following KIEs for reactions with acetonitrile-*d*₀/*d*₃ were found: for anion **1f**⁻ 6.5±0.5, for **1b**⁻ 3.2±0.5, for **1i**⁻ 3.0±1.0 and for **1c**⁻ 4.0±0.5, in agreement with their relative pK_a difference to acetonitrile.³⁴ The same experiment with photocatalytically generated carbanion **1f**⁻ in solution with varying mixtures of acetonitrile-*d*₀/*d*₃ resulted in a KIE of 9.0. The theoretical KIE calculated at the B97D3/Def2TZVP level of theory is 6.8 and, thus, in line with the experimental values of 6.5 in the gas-phase and 9.0 in solution. Although exact pK_a values cannot be derived solely from KIE data and vice versa, the experimental results of gas phase and solution KIEs are in the range expected according to the Bell-Goodall curve revised by Bordwell and Boyle.³⁴ Extensive studies on proton transfer KIEs with photocatalytically generated carbanions are outside the scope of this work, but the results suggest that the obtained KIEs are suitable for experimental estimation of the basicity of carbanionic intermediates, which are too basic to be stable in the respective solvent.

3.2.3 Isotopic fractionation and kinetic isotope effects

Recently, an isotopic fractionation method was described for determining the sequence of elementary steps in hydrogen isotope exchange (HIE) reactions based on the observation that hydrogen atom abstraction usually has a larger KIE than deprotonation.³⁵ If an HIE reaction proceeds via a reversible hydrogen atom transfer (HAT), the H-atom abstraction and donation proceed via the same transition state and, thus, have the same KIE. As the KIEs of both steps influence the equilibrium D/H fraction in opposing directions the D/H fraction is solely dependent on the equilibrium D/H fraction of the HAT reagent, which usually does not show a strong isotope effect. Therefore, a direct linear correlation between the equilibrium D/H ratio and the D/H ratio of a D/H reservoir is expected. A slope substantially deviating from 1 indicates that H-atom abstraction and donation proceed via distinct transition states.

We applied this concept to the carbanion generation from benzylic C-H bonds on the example of ethyl anisole (**1b**), in which the reaction does not reach its equilibrium state. Correlating the product D/H ratio with the isotopic fractionation from partially deuterated starting material resulted in a slope of ca. 8.5, which is in agreement with the value of 7.2 expected from the individual steps as determined according to Scheme 3.4. Indeed, a slightly higher experimental D/H ratio than calculated from the individual steps is expected due to secondary KIEs. Abstraction of an H-atom from **1b-d₀** is favored over abstraction of an H-atom from **1b-d₁**, while abstraction of a D-atom from **1b-d₁** is favored over abstraction of a D-atom from **1b-d₂**, thus, shifting the equilibrium D/H ratio further to the side of deuterium. Moreover, the result of an H/D ratio clearly above 1.5 is in agreement with the proposed mechanism of an HAT followed by an ETPT sequence. This demonstrates that the isotopic fractionation method is not only applicable to reactions reaching equilibrium, but also enables approximate values for lower catalyst turnovers.



Scheme 3.4. Kinetic isotope effects for HAT and protonation measured independently. If carbanions are generated via C-H activation both steps are connected via a RRPCO step. PC – Photocatalyst **4b** was used as pre-catalyst. The active catalyst was formed in situ via photosubstitution as described in chapter 2.²⁹

The KIE of the HAT-step was determined from the coupling between ethyl anisole mono-deuterated at the benzylic position (**1b-d₁**) and benzophenone **6** as coupling partner because **6** can react in a radical-radical recombination with

benzylic radical **1b**^o generated via HAT but can also react with carbanion **1b**⁻ formed upon reduction of the radical **1b**^o.³⁶ Since the reduction potentials for both, radical **1b**^o and benzophenone **6** are -1.8 V vs. SCE,^{32,37} they can be reduced to the corresponding carbanion and radical anion, respectively, by the photocatalyst 3DPA2FBN with a reduction potential of -1.9 V vs. SCE.³⁸ Trapping carbanions by aldehydes or ketones with α -C-H bonds could give misleading results due to deprotonation in α -position (Schemes 3.8 and 3.9) of the carbonyl reaction partner. Additionally, protons from the solvent and residual water can be incorporated into the substrate, if carbanions are generated preferentially, potentially leading to scrambling of the deuterium between substrate molecules and D-H exchange between substrate and solvent, which should be minimized to reduce the experimental error.

3.2.4 Excited state dynamics of the photocatalyst

Transient absorption (TA) spectroscopy was used to observe short-lived intermediates. Although carbanion **1f**⁻ generated under photocatalytic conditions could not be directly observed, the timescales of the individual processes were estimated by following the transient species of photocatalyst **4d**. Recording the transient absorption of photocatalyst **4d** excited at 355 nm under ambient conditions (ca. 23 °C) in acetonitrile, a broad positive absorption of the triplet state ³[**4d**] ranging from ca. 300 to 750 nm is observed within the temporal width of the excitation pulse, intersected by a strong negative emission from the first excited singlet state ¹[**4d**^{*}] peaking at 500 nm and a negative ground state bleach (GSB) peaking at ca. 375 nm (experimental part, Figure 3.43). While the short emission signal decays within the temporal width of the excitation pulse, the triplet absorption and GSB signals exhibit a decay on a 1 μ s time scale indicative of reverse intersystem crossing (RISC) into the ground-state species without formation of further intermediates and photoproducts, rendering **4d** as a photostable compound, which is also evident from the steady-state absorption prior and post the TA recording (Figure 3.44). Time-resolved emission studies of ¹[**4d**^{*}] disclose an excited-state lifetime of 18 ns (Figure 3.45a) that is not resolved in the TA data. The ³[**4d**] spectrum (Figure 3.46a) decays under non-degassed conditions with a lifetime of 453 ns, in agreement with thermally activated delayed fluorescence (TADF) decaying on the order of 400 ns (Figure 3.45a).

After removing molecular oxygen from the solution, the lifetime of ¹[**4d**^{*}] is prolonged to 28 ns (Figure 3.45b). In the TA data, identical spectral features are observed, but the triplet lifetime is prolonged to 19.7 μ s, demonstrating that the triplet ³[**4d**] undergoes a diffusion-controlled reaction ³ with molecular oxygen via energy transfer. Considering a concentration of molecular oxygen of $c(\text{O}_2) = 2.42 \text{ mM}$,³⁹ the bimolecular rate constant is given to $k_{\text{O}_2} = \frac{k_{\text{T1}} - k_{\text{T1}}^{-\text{O}_2}}{c(\text{O}_2)} = 8.91 \cdot 10^8 \text{ M}^{-1}\text{s}^{-1}$ (k_{T1} and $k_{\text{T1}}^{-\text{O}_2}$ are the rate constants in the presence and absence of O₂, respectively), which is close to the diffusion limit.

In the presence of the substrate **2a** (10 mM, which is close to the solubility limit) under non-degassed conditions, no further spectra of species other than the triplet state become obvious. However, the triplet state lifetime is quenched to 397 ns indicating an additional reaction with a yield of $1 - k_{\text{T1}}/k_{\text{T1}}^{2\text{a}} = 12.6\%$ (k_{T1} and $k_{\text{T1}}^{2\text{a}}$ are the rate constants in the presence and absence of **2a**, respectively). Thus, the formed reaction products either do not absorb in the experimental spectral detection window or molecular oxygen reacts faster with these intermediates forming new species which also do not absorb significantly in the accessible spectral range. Comparing the steady-state absorption spectra before and after the TA recordings, a new absorption contribution is evident, which confirms photoproduct formation (experimental part, Figure 3.44).

In the presence of **2a** (10 mM) but in the absence of O₂ the intrinsic lifetime of ³[**4d**] is quenched from 19.7 μs to 5.0 μs and the decay of the triplet spectrum is accompanied by the rise of new spectral contributions that persist on a time scale longer than 1 ms (Figure 3.2). As the persisting difference spectrum is in striking agreement with the difference spectrum of the electrochemically formed radical anion of **4d**^{•-} and its ground-state absorption (Figure 3.47), the newly formed species arises from a diffusion-controlled electron transfer from **2a** to the triplet ³[**4d**], which in the absence of molecular oxygen becomes highly efficient with $1 - k_{T1}^{-O_2} / k_{T1}^{2a, -O_2} = 74.6\%$ ($k_{T1}^{-O_2}$ and $k_{T1}^{2a, -O_2}$ are the rate constants in the presence and absence of **2a** under degassed conditions, respectively) of the ³[**4d**] molecules being quenched in this way. With a maximum **2a** concentration of $c(\mathbf{2a}) = 10$ mM, the bimolecular rate constant is given to $k_{2a} = \frac{k_{T1}^{2a, -O_2} - k_{T1}^{-O_2}}{c(\mathbf{2a})} = 1.49 \cdot 10^7 \text{ M}^{-1} \text{ s}^{-1}$ (k_{T1} and $k_{T1}^{-O_2}$ are the rate constants in the presence and absence of O₂, respectively). Since on this time scale the reaction with residual O₂ is negligible, **4d**^{•-} can accumulate under these conditions. The decay of **4d**^{•-} can be well described by a bi-exponential ansatz with lifetimes of 231 μs and >>1 ms (Figure 3.2). As the **4d**^{•-} formation is accompanied by **2a**[•] and subsequent **1f**[•] formation to the identical amount the first phase of the **4d**^{•-} decay may be attributed to RRPCO forming the carbanion **1f**⁻ and partially the initial **4d** (Scheme 3.5) while residual radicals **1f**[•] undergo dimerization to bibenzyl **8a**, leaving some **4d**^{•-} after consumption of all benzyl radicals. Since all reactive intermediates **1f**[•] have either dimerized or undergone electron transfer within 500 μs, the second phase of the **4d**^{•-} decay may result from reaction with residual O₂ forming a new photoproduct.

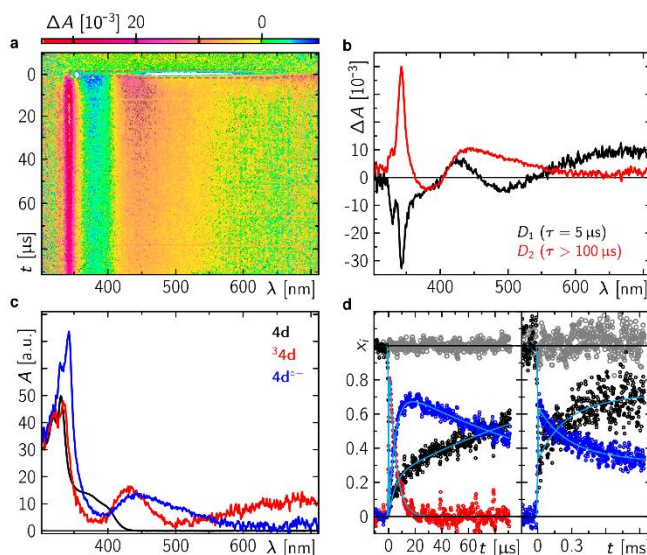
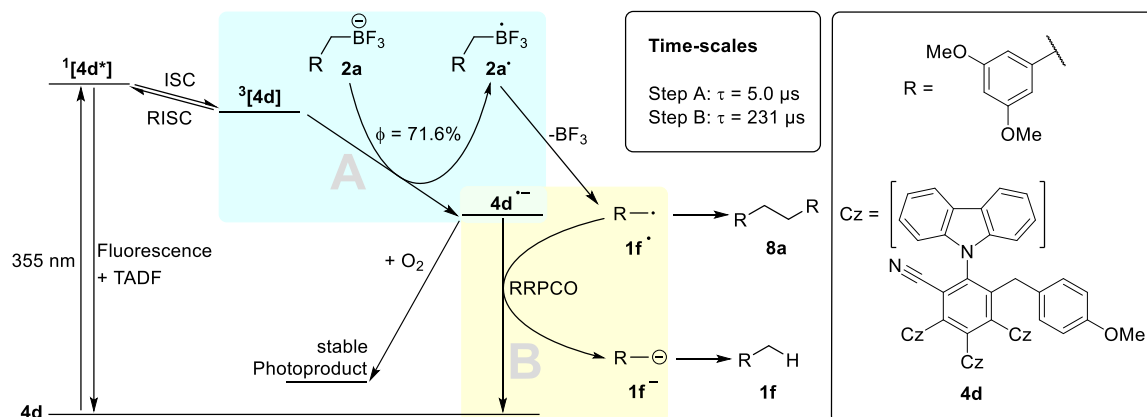


Figure 3.2. Time-resolved absorption data of photocatalyst **4d** in the presence of trifluoroborate **2a** (10 mM) and absence of O₂ following excitation at 355 nm. (a) Time-resolved spectra. The dashed rectangles indicate data ranges that were excluded from the global analysis as described elsewhere.⁴⁰ (b) decay associated difference spectra as a result from a global bi-exponential fit to the data in (a). (c) Species associated spectra (SAS) contributing to the data in (a) as indicated. (d) Mole fraction-time profiles of the SAS (open circles) contributing to the data in (a) and to data recorded in a 1 ms time window (Figure 3.43). The corresponding global fits are shown as cyan lines.

As the steady-state absorption spectra after the TA recording of the degassed samples in the presence and absence of **2a** differ (Figure 3.44), it is tempting that the latter scenario plays a significant role. Since neither spectral features of **1f**[•] nor of **1f**⁻ are observed, their lifetimes may only be estimated based on the dynamics of the accompanying counter radical **4d**^{•-}. As the **4d**^{•-} dynamics is biphasic, dimerization and RRPCO compete on the time scale of the first phase of the **4d**^{•-} decay. Since nucleophilic additions to aliphatic aldehydes⁴ could be detected in a preparative ansatz, only

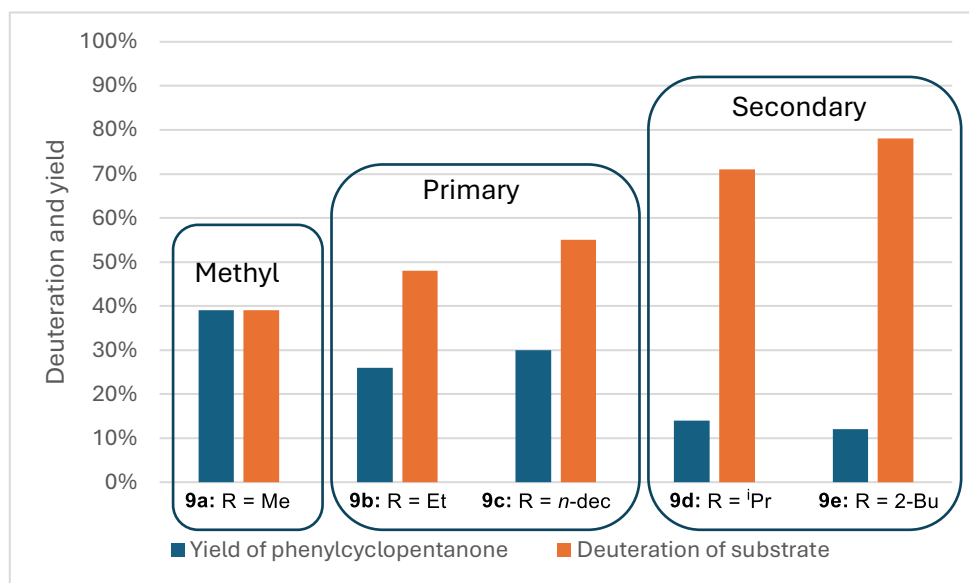
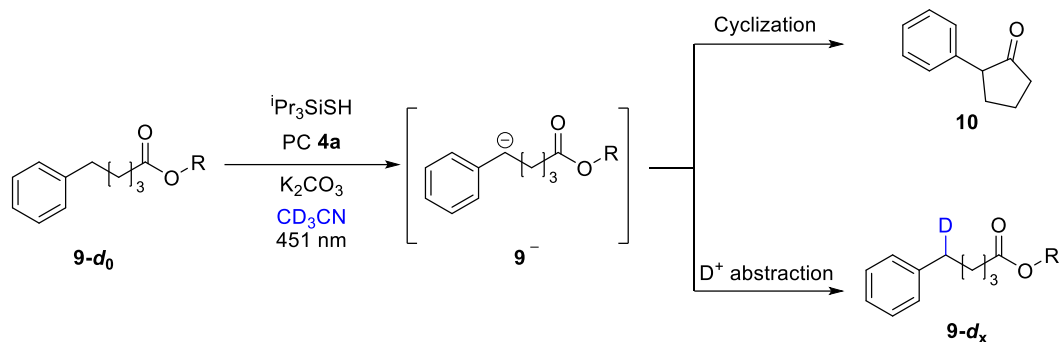
accessible via bimolecular reactions, this requires a lifetime of the carbanion on the diffusion time scale of ns at substrate concentrations in the mM range in solvents with similar viscosities as acetonitrile.



Scheme 3.5. Proposed photocatalytic cycle for dimerization and carbanion formation of $1f^-$ mediated by triplet $^3[4d]$ in MeCN. $4d$ is excited into the singlet state $^1[4d^*]$, which then either fluoresces or undergoes intersystem crossing (ISC) and reaches the triplet state $^3[4d]$. Reverse intersystem crossing (RISC) partially occurs, leading to thermally activated delayed fluorescence (TADF). Initial electron transfer from $2a$ to $^3[4d]$ forms a radical pair $^3[4d^{\bullet-}]$, $1f^\bullet$ that partially proceeds via RRPCO regenerating the $4d$ and forming the carbanion $1f^-$, which deprotonates MeCN. Dimerization of $1f^\bullet$ significantly reduces carbanion formation, so that $4d^\bullet$ partly reacts with residual oxygen. Both products could be identified by mass analysis (Figures 3.48 and 3.49).

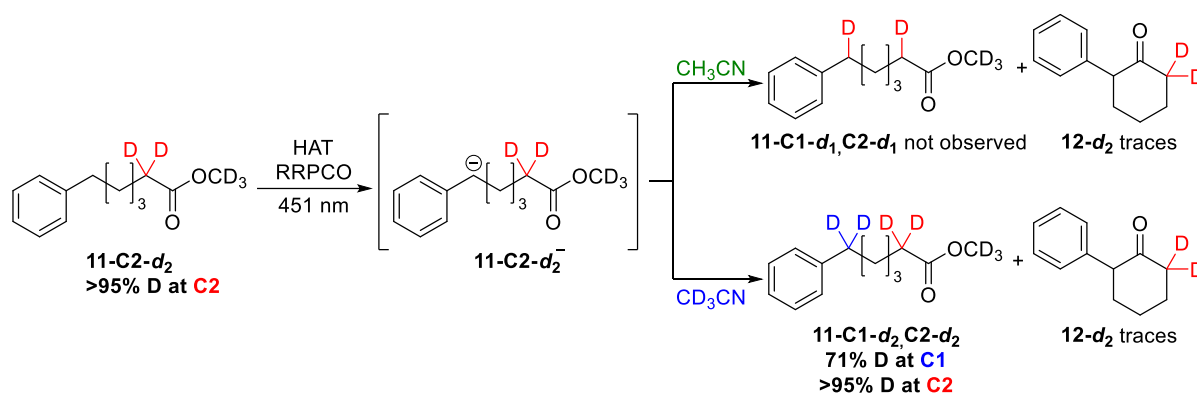
3.2.5 Importance for reactions involving photocatalytically generated carbanions

The high basicity of photocatalytically generated carbanions poses important consequences and limitations for their utilization in organic synthesis. Standard solvents used in photoredox catalysis such as MeCN and DMSO possess weakly acidic protons that can be abstracted by highly basic carbanions formed under photocatalytic RRPCO conditions. Intermolecular C-C bond-forming reactions usually cannot compete with a fast deprotonation of the surrounding bulk solvent unless the reaction partner is sufficiently electrophilic. An intramolecular example is the photocatalytic C-H activation of phenylvaleric acid ethyl esters to the corresponding carbanions³ where solvent reactivity is expected to be the limiting parameter. When such cyclizations are conducted in acetonitrile- d_3 the recovered starting material has a high degree of deuteration at the benzylic position. In agreement with a direct competition between intramolecular Grignard reaction and solvent deprotonation, the increase in steric bulk on the ester leads to a decrease in yield of cyclization product, while the degree of deuteration at the benzylic position increases (Scheme 3.6). These findings demonstrate that formation of cyclization product 2-phenylcyclopentanone (**10**) is primarily limited by the rate constant of carbanion protonation relative to cyclization.



Scheme 3.6. 5-Phenylvaleric acid esters **9a-e** cyclize to 2-phenylcyclopentanone (**10**). Solvent deprotonation competes with Grignard-type cyclization. Yield and degree of deuteration determined by ^1H NMR spectroscopy.

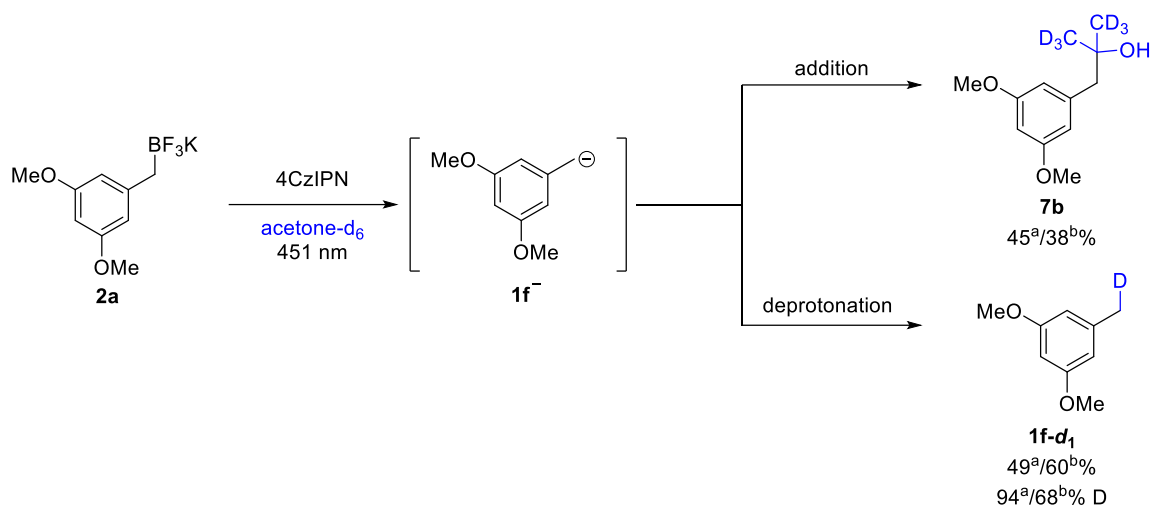
In contrast to phenylvaleric acid ethyl ester (**9b**), the homolog which is shorter by one methylene group, phenylbutyric acid ethyl ester, did not cyclize to the corresponding 2-cyclobutanone and the longer phenylhexanoic acid ethyl ester did only give traces of the corresponding 2-phenylcyclohexanone (**12**).³ While a four-membered ring is expected to be thermodynamically unfavorable, formation of 2-phenylcyclohexanone (**12**) from 6-phenylhexanoic acid ester **11** should be energetically more favorable compared to cyclization of the corresponding phenylvaleric acid ester **9a** to phenylcyclopentanone **10**. Subjecting deuterated phenylhexanoic acid ester **11-C2-d₂** to the conditions for benzylic carbanion generation according to Scheme 3.7, no shift of deuterium from the α -position of the ester to the benzylic position was observed and the deuteration degree of the starting material at C2 remained unchanged which excludes an intramolecular deprotonation. Conducting the reaction in CD_3CN gave additional 71% deuteration at the benzylic position. The analogous reaction with deuterated phenylvaleric acid ester **9a-C2-d₂** confirmed no intramolecular deuterium transfer also for the shorter homolog. This is in agreement with literature reports corroborating that activation barriers for proton transfer reactions increase with deviation from a linear transition state.⁴¹



Scheme 3.7. Carbanion generation at the benzylic position of 6-phenylhexanoic acid ester **11-C2-d₂** results only in traces of the corresponding 2-phenylcyclohexanone (**12-d₂**) and no intramolecular deuterium-shift. A high degree of deuteration at the benzylic position if CD_3CN is used as solvent confirms benzylic C-H activation to the corresponding carbanion under the reaction conditions.

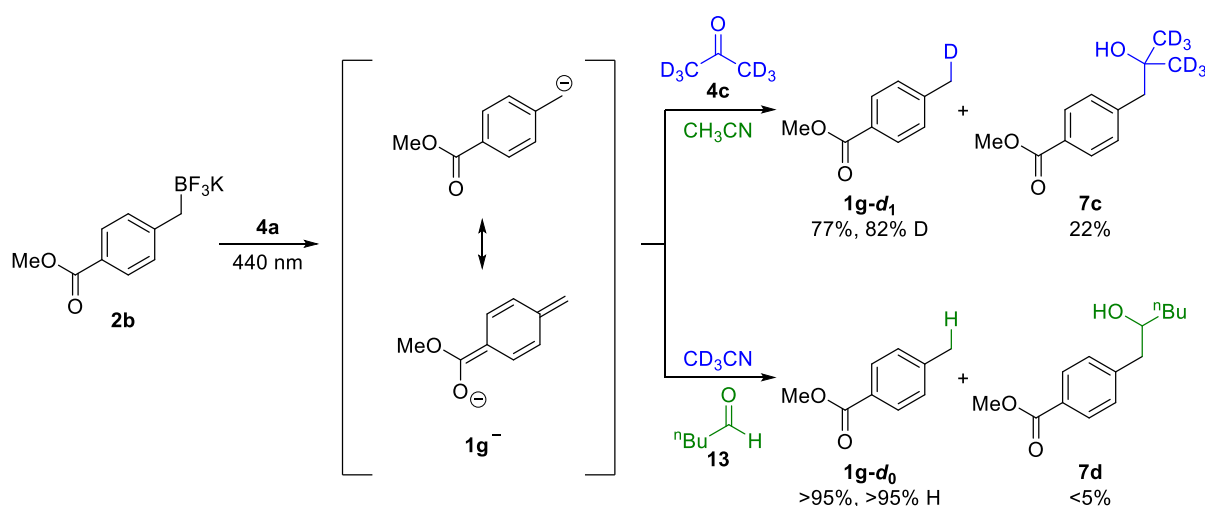
The barriers for cyclization of the carbanions derived from phenylvaleric acid methyl ester (**9a**) and phenylhexanoic acid methyl ester (**11**) calculated at the M06-2X/6-31G(d) level of theory for optimization and frequency analysis and at the wb97XD/Def2TZVP level of theory for single point are 5.9 kcal/mol and 2.1 kcal/mol, respectively, and thus are contrary to the experimental trend. This suggests the relative rates of cyclization are primarily influenced by diffusional motion between the reacting moieties. While the rate for carbanion protonation by the solvent is expected to be independent of the alkyl chain length, cyclization will proceed faster for shorter chains due to significantly shorter average distances between the benzylic position and the carbonyl group as well as due to less sampled configurational space during diffusion.

The strong basicity of photocatalytically generated benzylic carbanions is not only relevant with respect to the solvent but also towards reaction partners with weakly acidic protons such as acetone, a common reaction partner for Grignard-type reactions, having mildly acidic α -protons and being readily available in its deuterated form. Indeed, when generating carbanion **1f⁻** in acetone-*d*₆ according to Scheme 3.8, the corresponding mono-deuterated toluene derivative **1f-d₁** and the addition product **7b** were obtained in a 1:1 ratio in near quantitative combined yield. The toluene derivative had a high degree of mono-deuteration (94%) demonstrating that the yield of tertiary alcohol is limited by the competing reactivity of the carbanion acting as base instead of nucleophile while factors such as residual moisture or radical side reactions are negligible.



Scheme 3.8. Benzylic carbanion **1f⁻** reacts with acetone in a Grignard-type addition and in a deprotonation. ^aIn acetone-*d*₆ as solvent; ^bin 1:1 mixture acetone-*d*₆/acetonitrile-*d*₀; ¹Pr₃SiSH was used as HAT-reagent, 4CzIPN was used as pre-catalyst. The active catalyst was formed in situ via photosubstitution as described in chapter 2.²⁹

When electron withdrawing groups (EWG) stabilize the carbanion, its nucleophilic reactivity is decreased and lower yield for addition to aldehydes and ketones is observed (Scheme 3.9). However, basicity of the carbanion **1g⁻** is still high enough to deprotonate the α -position of acetone resulting in protonation of the carbanion as the major reaction pathway. On the other side, when using the less electrophilic reaction partner ethyl acetate as solvent in combination with trifluoroborate **2a**, giving more reactive carbanion **1f⁻**, no addition product is observed while deprotonation is still the predominant reaction pathway, which was indirectly observed in the ²H NMR spectrum in the presence of D₂O, showing a signal for mono-deuterated ethyl acetate (see experimental part Figure 3.34). This again demonstrates that reactivity of photocatalytically generated carbanions is predominantly limited by their high basicity.

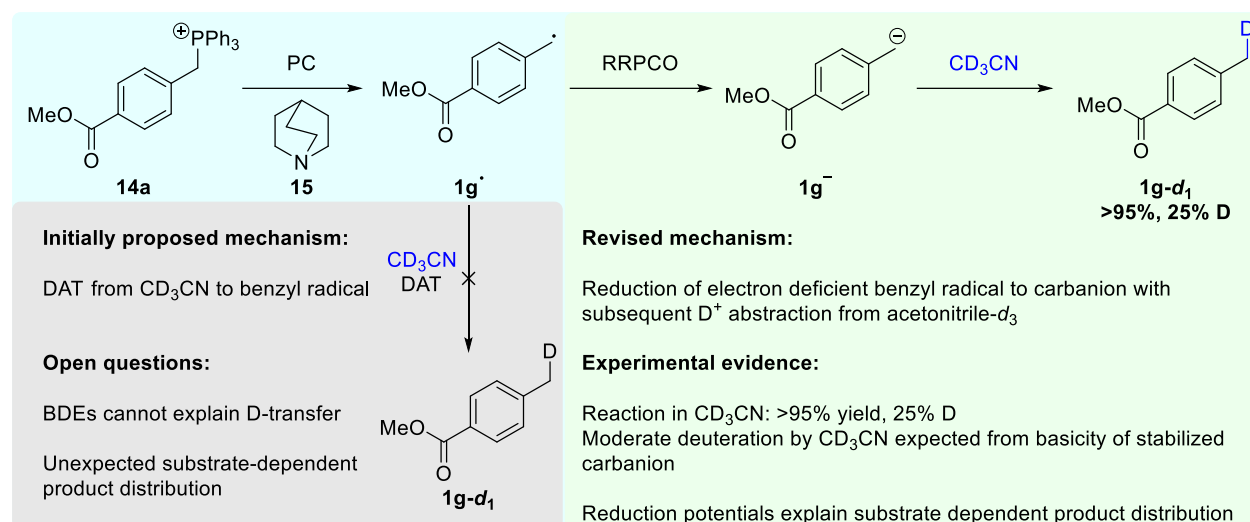


Scheme 3.9. Stabilization of benzylic carbanions by electron withdrawing groups reduces their nucleophilicity. Despite reduced basicity deprotonation of aldehydes and ketones is still possible, thus giving the corresponding toluene derivative as the major product. Yields and deuteration determined by ¹H NMR spectroscopy.

To note, 4CzIPN itself acts as a photocatalyst only if substrates are substituted with electron withdrawing groups or sterically hindered substrates are used, while primary benzylic radicals substituted with electron donating groups first

react in a photosubstitution reaction substituting one of the CN-groups to form the active catalyst as described in chapter 2.²⁹ Accordingly, the reduction of electron poor benzyl radicals is favored over radical recombination with the 4CzIPN radical anion while neutral and electron rich benzyl radicals are difficult to reduce by the 4CzIPN radical anion and rather trigger photosubstitution of 4CzIPN forming a more stable and stronger reducing photocatalyst. The observation that electron withdrawing groups lead to favoring RRPCO over other reaction pathways even for only moderately reducing photocatalysts explains previous reports.⁴² For instance, the reactivity of benzyltriphenylphosphonium salts (**14**) under reductive photocatalytic conditions strongly depends on the electronic nature of substituents on the aromatic ring. While electron-rich benzyl radicals dimerize to the corresponding bibenzyls, benzyltriphenylphosphonium salts bearing electron withdrawing groups such as **14a** exclusively form the corresponding toluene derivative (substrate **14a** gives toluene derivative **1g**). Due to deuteration of the benzylic position when CD₃CN was used as solvent a HAT from the solvent acetonitrile or, depending on the electron donor, from an amine radical cation to the benzyl radical was proposed to occur with electron deficient benzyl radicals, while dimerization to the bibenzyl derivative was proposed to be disfavored due to a polarity mismatch. However, this could not explain, for instance, a difference in the product distribution if started from a benzyl bromide instead of a benzyltriphenylphosphonium salt. Furthermore, the proposed HAT is energetically not plausible, since the bond dissociation energy (BDE) of toluenes (88 kcal/mol for unsubstituted toluene)⁴³ is below that of acetonitrile (96 kcal/mol).⁴⁴

Based on the results presented in this work, we suggest revising the mechanism for electron-withdrawing group substituted benzyltriphenylphosphonium salts according to Scheme 3.10. The iridium-based photocatalyst [Ir(dtbbpy)(ppy)₂]⁺PF₆⁻ used is slightly more reducing compared to 4CzIPN (-1.51 V⁴⁵ and -1.24 V³⁸ vs. SCE). For electron rich benzyl radicals reduction to carbanions is slow or not feasible (-1.43 V vs. SCE for unsubstituted benzyl radical in MeCN)³² so that benzyl radical build-up leads to dimerization as proposed. In contrast, electron-deficient benzyl radicals such as **1g**[•] are faster reduced to the corresponding carbanions than a critical benzyl radical concentration for dimerization will build up. The carbanion is not able to form bibenzyl, but it is sufficiently basic to deprotonate either the amine radical cation (if DIPEA is used as sacrificial electron donor) or just basic enough to deprotonate the solvent acetonitrile (see Scheme 3.2) in the absence of more acidic protons. The different product distribution for benzyl bromide substrates is also easily explained by that mechanism: Since electron deficient benzyl bromides are more easily reduced to generate the corresponding radical (-1.29 V vs. SCE in MeCN), benzyl bromides will mainly form benzyl radicals while radicals are first reduced to carbanions when triphenylphosphonium salts are used as radical precursor, changing from radical to carbanionic reactivity depending on the radical source.

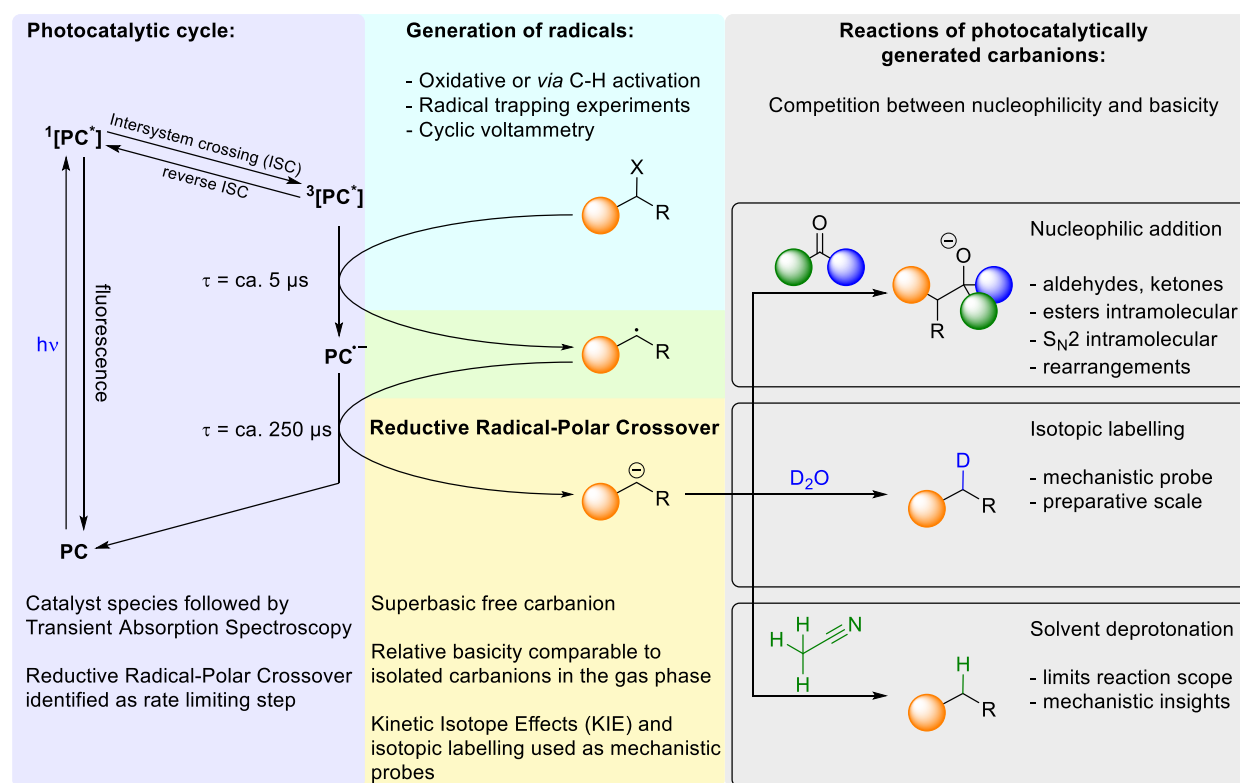


Scheme 3.10. Electron-withdrawing group substituted benzyltriphenylphosphonium salts undergo reduction to the corresponding toluene derivative, while electron-donating group substituted benzyltriphenylphosphonium salts form bibenzyls under reductive photocatalytic conditions. The initially proposed mechanism via HAT or DAT from acetonitrile is unlikely and instead an RRPCO with subsequent protonation is more plausible as supported by data presented in this work. PC – photocatalyst = [Ir(dtbbpy)(ppy)₂]⁺PF₆⁻.

3.3 Conclusion

In conclusion, it was demonstrated that carbanions generated via a photocatalytic RRPCO step are superbasic intermediates capable of deprotonating common polar solvents such as acetonitrile, DMSO, and DMF. Their reactivity is comparable to the gas-phase reactivity of isolated carbanions so that these are best described as monomeric, free carbanions, answering the fundamental question about the nature of these often-proposed intermediates. The general mechanism and methods used to analyze the individual steps are summarized in Scheme 3.11. Moreover, it was demonstrated that previously unsuccessful nucleophilic addition and substitution reactions were not limited by the nucleophilicity of the carbanions but by their high basicity towards solvents and abstractable protons commonly present in electrophiles. The time-scale of the individual steps was determined by time-resolved spectroscopy and identified the RRPCO step as rate-limiting with a lifetime of 231 μs for the photocatalyst radical anion reducing a benzyl radical to the carbanion. Kinetic isotope effects and selectivity for deprotonations by photocatalytically generated carbanions can act as mechanistic probe to indirectly detect carbanionic intermediates by their specific reactivity. This was demonstrated for carbanion generation from benzylic C-H bonds, supporting the initially proposed mechanism. Further a substrate dependent change in the mechanism for photoreduction of benzyltriphenylphosphonium salts was detected. Overall, the results provide an intuitive qualitative estimation of the limits for reactions involving photocatalytically generated carbanions as reactive intermediates and will help to rationally develop solutions to overcome these limitations.

REACTIVITY OF SUPERBASIC CARBANIONS GENERATED VIA REDUCTIVE RADICAL-POLAR CROSSOVER IN THE CONTEXT OF PHOTOREDOX CATALYSIS



Scheme 3.11. Summary of the mechanistic cycle for generation of carbanions via photocatalytic reductive radical-polar crossover (RRPCO) and methods used to elucidate the mechanism. Transient species of the photocatalyst (PC) **4d** were followed via transient absorption (TA) spectroscopy with trifluoroborate **2a** as substrate. Decay times should only give an estimate as the bimolecular rate constants are expected to vary depending on the specific substrate, photocatalyst, and concentration. The presence of benzyl radicals was demonstrated in previous work by radical trapping.¹⁰ The reactivity of photocatalytically generated carbanions was investigated with the focus on competing nucleophilicity and basicity. Tandem mass spectrometry was used to compare the basicity in solution to the basicity of isolated carbanions in the gas phase.

3.4 Experimental part

3.4.1 General information

All reactions were conducted in dried and deoxygenated solvents unless otherwise stated. Solvents for column chromatography and recrystallization were distilled prior to use. Commercially available starting materials were used as received.

NMR Analysis

NMR spectra were recorded using a Bruker Avance 400 (400 MHz for ^1H , 101 MHz for ^{13}C , 376 MHz for ^{19}F , 128 MHz for ^{11}B) and a Bruker Avance III HD 600 (600 MHz for ^1H , 92 MHz for ^2H). Chemical shifts are reported in ppm on the δ scale with residual CHCl_3 as internal standard (7.26 ppm for ^1H and 77.16 ppm for ^{13}C). Abbreviations for the multiplicity: s = singlet, d = doublet, t = triplet, q = quartet, quint = quintet, sept = septet, m = multiplet. Spectra were analyzed using Topspin 4.0.6 and 4.3.0. The degree of mono-deuteration of slightly overlapping signals was determined via deconvolution using the mldcon -pp function of Topspin 4.3.0.

Thin Layer Chromatography

With silica gel pre-coated aluminum sheets (Machery-Nagel, silica gel 60 G/UV254, 0.2 mm) were used for thin layer chromatography. Visualization of the separated compounds was achieved by UV-light (254 nm and 365 nm) and by staining with potassium permanganate.

Cyclic Voltammetry

The CV was performed by Regina Hoheisel with the three-electrode potentiostat galvanostat PGSTAT302N from Metrohm Autolab using a glassy carbon working electrode, a platinum wire counter electrode, a silver wire as a reference electrode, and tetrabutylammonium tetrafluoroborate (TBATFB; 0.1 M) as supporting electrolyte. Potentials vs. saturated calomel electrode were recorded with ferrocene added as internal standard with $E_{1/2}(\text{Fc}/\text{Fc}^+) = 0.380$ V vs. SCE. Half-wave potentials for irreversible peaks were estimated from the first derivative of the cyclic voltammogram.⁴⁶

High resolution mass spectrometry

HRMS were measured at the Central Analytical Laboratory of the University of Regensburg on an Agilent Q-TOF 6540 UHD and a Jeol AccuTOF GCX instrument.

Gas-phase reactions

Gas-phase reactions were recorded using a TSQ-7000 quadrupole-octopole-quadrupole tandem mass spectrometer, equipped with an mks Baratron[®] pressure meter. The exact gas-phase ratios of acetonitrile- d_0/d_3 present in the collision cell during the experiments were determined through adduct formation with a mass-selected $[\text{Au}(\text{PPh}_3)]^+$.^{47,48} To compensate for secondary collisions, a quadratic equation^{49,50} in a whole pressure range and separately in a range between 15 and 70 μTorr was fitted to the intensity data of the product ions with the constrained to converge towards zero at zero pressure (ax^2+bx+c , where a is an arbitrary constant to compensate for secondary-collision events, $c = 0$,

and b determines the slope at the zero pressure). The KIE values were determined from the slopes ratio of the fitted curves at zero pressure. Experimental details can be found in section 3.4.6.

3.4.2 Photoreactor setup

Photoreactions were performed in the reactor depicted in Figure 3.3. Reagents were placed in 6 mL crimp-capped vials. The vials fit into a cooling block kept at 20 °C by a thermostat. The vials were irradiated from below via OSRAM Osolon SSL 80 LT-1960 royal-blue LEDs ($\lambda_{\text{max}} = 440 \text{ nm}$). Stirring was achieved via a magnetic stirrer placed below the reactor. Although the emission maximum is reported at 451 nm by the supplier it was determined to be at 440 nm with a range of approximately 400 – 500 nm.

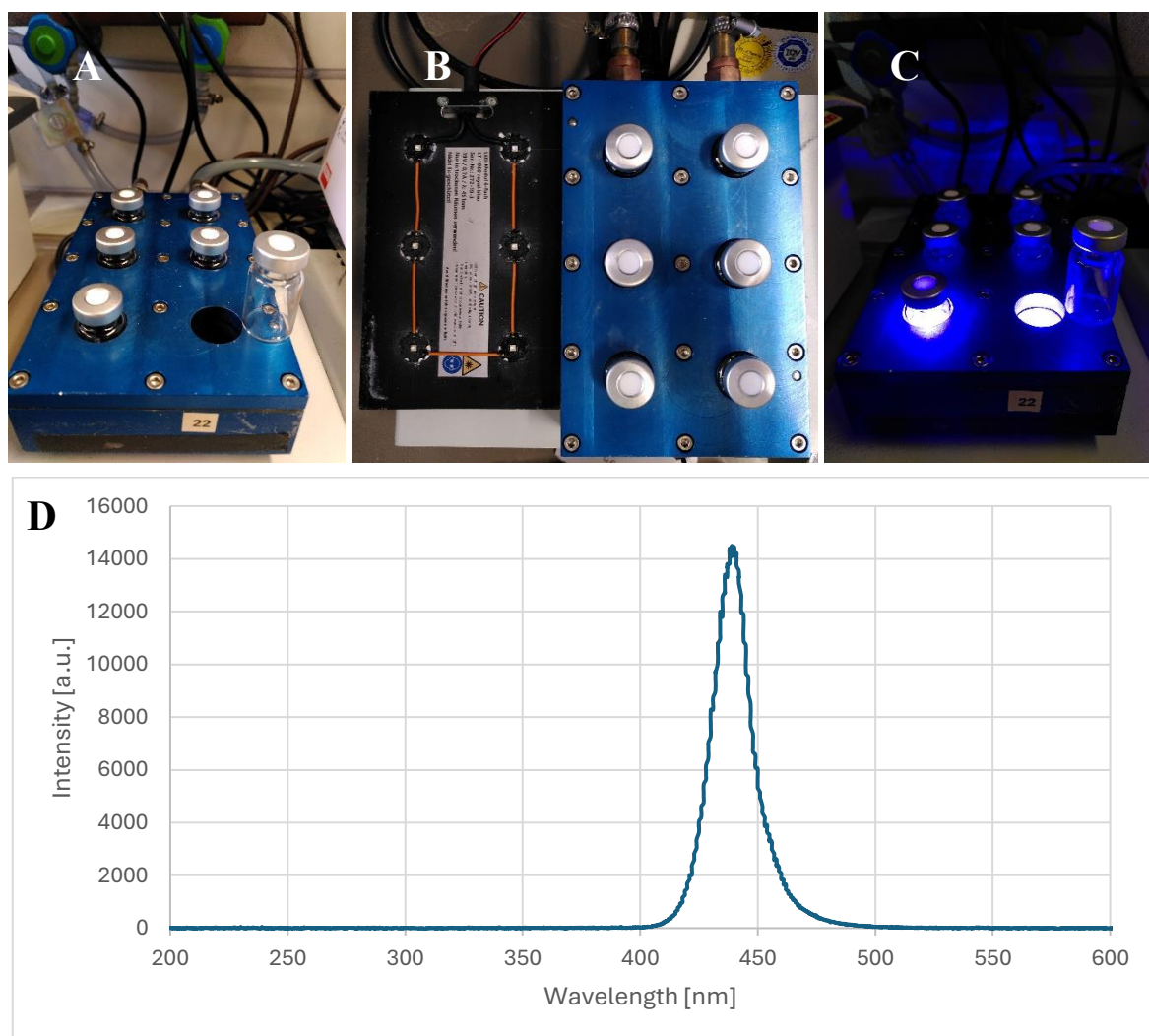


Figure 3.3. Photoreactor setup for small scale reactions. A: Cooling block front view; B: Cooling block and LED module top view; C: Photoreactor setup in operation; D: Emission spectrum of the LEDs.

3.4.3 Synthetic procedures

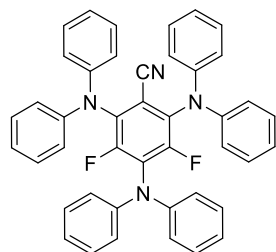
3.4.3.1 Synthesis of photocatalysts

General procedure 3-A: Synthesis of literature known cyanobenzene-based photocatalysts

Derived from literature procedure.⁵¹

Carbazole or diphenylamine (1.1 equiv. per substituted fluorine) is dissolved in anhydrous THF (0.14 M based on the fluorinated benzonitrile derivative). A solution of sodium bis(trimethylsilyl)amide (NaHMDS; 2M in THF) is added via cannula while cooling in an ice bath. The solution is stirred at room temperature for 30 min. The fluorinated benzonitrile derivative is dissolved in a few mL THF and added dropwise. The reaction mixture is stirred for 24 h at 60 °C (synthesis of 4CzIPN) or 3 h at 50 °C and 18 h at room temperature (synthesis of 3DPA2FBN). The solvent is removed under reduced pressure and the residue suspended in diethyl ether. The solid is filtered and washed with diethyl ether (40 mL per mmol product). The solid is extracted with chloroform until the extract is almost colorless (roughly 70 mL per mmol product). The solvent is removed under reduced pressure and washed with a 9:1 mixture of hexane/acetone (v:v 5 mL per mmol product) and hexane (5 mL per mmol product). The product is dried under high vacuum. Photocatalysts 4CzIPN (**4b**) used in this work was synthesized in the same batch as used for chapter 2 and analytical data can be found there.

2,4,6-Tris(diphenylamino)-3,5-difluorobenzonitrile (3DPA2FBN, **4a**)



Synthesized according to general procedure 3-A on 5 mmol scale from pentafluorobenzonitrile (5 mmol, 965 mg) and diphenylamine (2.79 g, 16.5 mmol, 3.3 equiv.). The product was obtained as a bright yellow powder (800 mg, 1.25 mmol, 25%). The ¹H- and ¹⁹F-NMR spectra are in accordance with literature.³⁸

¹H-NMR (400 MHz, CDCl₃): δ [ppm] = 7.27 – 7.22 (m, 12+1 H, overlapping with residual CHCl₃), 7.06 – 6.94 (m, 18H). ¹⁹F-NMR (377 MHz, CDCl₃): δ [ppm] = -120.73 (s).

General procedure 3-B: Photosubstitution in dicyanobenzene photocatalysts

Photosubstitution of 4CzIPN for synthesis of the active catalysts was done according to the procedure reported in chapter 2.

4CzIPN (90 μmol), carboxylic acid (2 equiv.) and Cs₂CO₃ (2 equiv.) are placed in a 9 mL crimp vial. The vial is capped, evacuated via cannula and backfilled with nitrogen. Via syringe 6 mL of DMSO are added. The reaction mixture is degassed by 3 cycles of freeze-pump-thaw. The solution is irradiated with blue LEDs (λ_{max} = 440 nm) for 0.5 – 2 h until the fading of CzIPN's characteristic yellow/green fluorescence (see Figure 3.4) indicates full conversion. Usually, the reaction is finished within 5-30 min. However, longer reaction times have no detrimental effect and unreacted 4CzIPN is sometimes difficult to remove. The content of the vials is diluted with DCM, washed

with water and brine. The organic phase is dried over Na_2SO_4 and the solvent evaporated under reduced pressure. The crude products are recrystallized by dissolving in a minimum amount of DCM, approximately the same amount of EtOAc is added and the DCM evaporated either under reduced pressure or under ambient conditions. The crystals are filtered, washed with EtOAc and dried under vacuum.

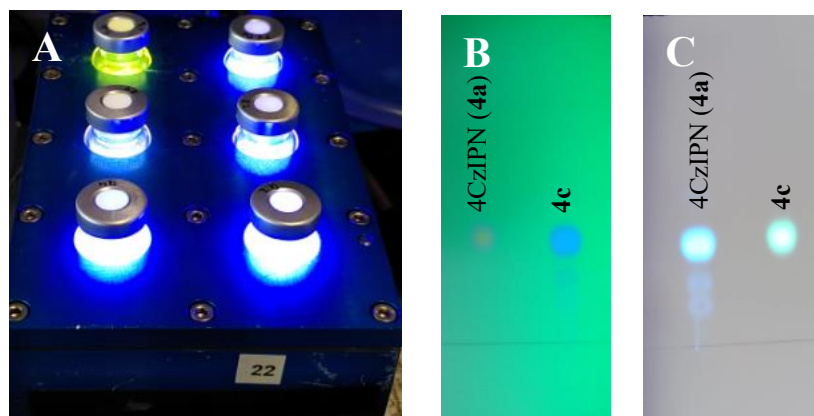
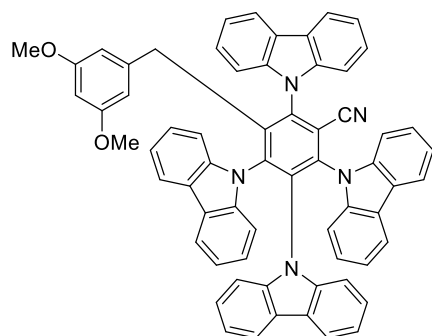


Figure 3.4. A: Photosubstitution reactions in the photoreactor. Fading of the yellow/green fluorescence indicates full conversion of 4CzIPN; TLC of photosubstitution in 4CzIPN with 3,5-dimethoxyphenylacetic acid to photosubstitution product **4c**; B: TLC illuminated at 254 nm; C: TLC illuminated at 365 nm.

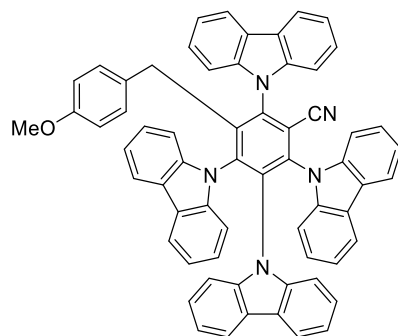
2,3,4,6-Tetra(9*H*-carbazol-9-yl)-5-(3,5-dimethoxybenzyl)benzotrile (**4c**)



Synthesized according to general procedure 3-B from 4CzIPN (**4a**) and 3,5-dimethoxyphenylacetic acid on 240 μmol scale in DMSO (4 x 60 μmol). The product was obtained as yellow, crystalline solid with 0.9 equivalents of DMSO which could not be separated by recrystallization (177 mg, 178 μmol , 74%). A tendency for similar compounds to crystallize with 1 equivalent of solvents was also observed in previous reports.^{4,29}

^1H NMR (400 MHz, CDCl_3): δ [ppm] = 8.18 (d, J = 7.7 Hz, 2H), 7.72 – 7.60 (m, 6H), 7.48 (d, J = 8.1 Hz, 2H), 7.41 (t, J = 7.4 Hz, 2H), 7.27 (t, J = 7.4 Hz, 4H), 7.11 – 7.00 (m, 10H), 6.92 (d, J = 8.3 Hz, 2H), 6.76 (t, J = 7.4 Hz, 2H), 6.63 (t, J = 7.6 Hz, 2H), 5.57 (s, 1H), 5.10 (d, J = 2.0 Hz, 2H), 3.71 (s, 2H), 3.20 (s, 6H), 2.59 (s, 5.5H, 0.9 equiv. DMSO). **$^{13}\text{C}\{^1\text{H}\}$ NMR (101 MHz, CDCl_3):** δ = 159.9, 145.3, 142.1, 140.9, 140.3, 140.1, 139.0, 138.8, 138.7, 137.9, 136.3, 126.8, 125.6, 125.5, 124.4, 124.3, 124.2, 123.8, 123.6, 121.4, 121.2, 121.1, 120.8, 120.34, 120.31, 120.2, 119.5, 117.8, 112.7, 110.2, 110.1, 109.9, 109.2, 105.7, 98.4, 54.8, 41.1 (DMSO), 35.4. **HRMS (+ESI) m/z :** $[\text{M} + \text{H}]^+$ Calcd for $\text{C}_{64}\text{H}_{44}\text{N}_5\text{O}_2$ 914.3490; Found 914.3487.

2,3,4,6-Tetra(9*H*-carbazol-9-yl)-5-(4-methoxybenzyl)benzonitrile (4d)

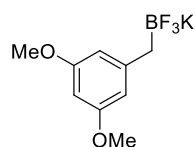


Synthesized according to general procedure 2-B from 4CzIPN and 4-methoxyphenylacetic acid on 180 μmol scale (2 x 90 μmol) in DMSO. The product was obtained as yellow, crystalline solid (130 mg, 147 μmol , 82%). Due to its low solubility only very weak signals in the ^{13}C NMR spectrum could be obtained.

^1H NMR (400 MHz, CDCl_3): δ [ppm] = 8.19 (d, J = 7.68 Hz, 2H), 7.72 – 7.59 (m, 6H), 7.46 – 7.38 (m, 4H), 7.31 – 7.21 (m, 4H), 7.11 – 6.98 (m, 10H), 6.91 (d, J = 8.1 Hz, 2H), 6.76 (t, J = 7.4 Hz, 2H), 6.62 (t, J = 7.6 Hz, 1H), 5.98 (d, J = 8.4 Hz, 2H), 5.81 (d, J = 8.6 Hz, 2H), 3.71 (s, 2H), 3.40 (s, 3H). **HRMS (+ESI) m/z :** $[\text{M} + \text{Na}]^+$ $\text{C}_{63}\text{H}_{41}\text{N}_5\text{ONa}^+$ 906.3203; Found 906.3203.

3.4.3.2 Synthesis of benzyl trifluoroborates

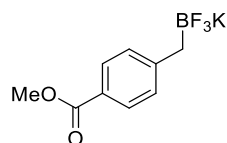
Potassium trifluoro(3,5-dimethoxybenzyl)borate (2a)



According to literature procedure:⁵²

Bis(pinacolato)diboron (2.29 g, 9 mmol, 1.5 equiv.), triphenylphosphine (205 mg, 780 μmol , 13 mol%), copper(I) iodide (114 mg, 600 μmol , 10 mol%), and lithium methoxide (466 mg, 12 mmol, 2 equiv.) were dissolved in DMF (10 mL). 3,5-dimethoxybenzyl bromide (1.38 g, 6 mmol, 1 equiv.) was added and the solution stirred overnight (16 h) at room temperature. Water was added and the mixture extracted with EtOAc. The organic phase was washed with water and brine, dried over Na_2SO_4 , and the solvent evaporated under reduced pressure. Methanol (50 mL) and KHF_2 (3.75 g, 48 mmol, 8 equiv.) dissolved in water at 0 $^\circ\text{C}$ was added to the residue. The mixture was stirred at room temperature for 1 h, concentrated under reduced pressure and azeotroped with EtOH three times to remove most of the water and pinacol. The residue was extracted with boiling acetone, the solvent removed under reduced pressure, and the crude product washed with DCM and then hexane to yield the product as colorless, fine needles (1.35 g, 5.23 mmol, 87%). The ^1H NMR spectrum is in accordance with literature.

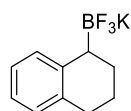
^1H NMR (400 MHz, CD_3CN): δ [ppm] = 6.27 (d, J = 2.2 Hz, 2H), 6.10 (t, J = 2.3 Hz, 1H), 3.71 (s, 6H), 1.62 – 1.44 (m, 2H).

Potassium trifluoro(4-(methoxycarbonyl)benzyl)borate (2b)

According to literature procedure:⁵³

Methyl 4-(bromomethyl)benzoate (1.15 g, 5 mmol, 1 equiv.), Pd₂dba₃ (92 mg, 100 μmol, 2 mol%), *p*-tol₃P (91 mg, 300 μmol, 6 mol%), potassium acetate (736 mg, 7.5 mmol, 1.5 equiv.), and bis(pinacolato)diboron (1.4 g, 5.5 mmol, 1.1 equiv.) were suspended in toluene (30 mL) and stirred for 24 h at 50 °C. The mixture was filtered through a plug of silica and eluted with EtOAc. The solvent was removed under reduced pressure and the residue dissolved in a mixture of EtOAc (20 mL) and MeOH (30 mL). A solution of KHF₂ (2.43 g, 30 mmol, 6 equiv.) in 7 mL H₂O was added at 0 °C and the mixture stirred at room temperature for 1 h. The solvent was removed under reduced pressure, the residue azeotroped three times with EtOH and dried under high vacuum for 2 h. The product was extracted with boiling acetone and the filtrate concentrated under reduced pressure. The crude product was recrystallized from acetone/Et₂O to yield the final product as colorless, fine needles (530 mg, 2.07 mmol, 41%). The ¹H NMR spectrum is in accordance with literature.

¹H NMR (400 MHz, DMSO-*d*₆): δ [ppm] = 7.67 (d, *J* = 8.26 Hz, 2H), 7.09 (d, *J* = 8.15 Hz, 2H), 3.79 (s, 3H), 1.66 – 1.48 (m, 2H). ¹⁹F NMR (376 MHz, DMSO-*d*₆): δ = 135.9 – 136.8 (m). ¹¹B NMR (128 MHz, DMSO-*d*₆): δ = 5.48 – 2.43 (m).

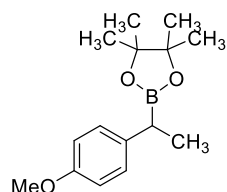
Potassium trifluoro(1,2,3,4-tetrahydronaphthalen-1-yl)borate (2c)

According to literature procedure:⁵⁴

1,2-Dihydronaphthalene (976 mg, 7.5 mmol, 1 equiv.) in 2 mL THF was added dropwise to a solution of BH₃•THF (15 mL, 20 mmol, 2 equiv., 1 M solution in THF) at 0 °C and stirred for 2 h at room temperature. Water (1 mL) was added, and the mixture stirred for another 3 h at room temperature. The solvent was evaporated under reduced pressure, the residue dissolved in EtOAc, washed with saturated aqueous NaHCO₃ solution and brine, dried over Na₂SO₄, the solution concentrated under reduced pressure to a volume of approximately 4 mL, and petroleum ether was added to precipitate the boronic acid. The boronic acid was then dissolved in MeOH (12 mL), and KHF₂ (2.39 g, 37.5 mmol, 5 equiv.) in H₂O (2.5 mL) was added at 0 °C. The suspension was stirred for 2 h and the solvent evaporated under reduced pressure. The residue was extracted with boiling acetone and the solvent removed under reduced pressure to a volume of approximately 5 mL. The product was precipitated by addition of diethyl ether as a colorless solid (1.39 g, 5.84 mmol, 78 %). The ¹H NMR spectrum is in accordance with literature.

¹H NMR (400 MHz, DMSO-*d*₆): δ [ppm] = 7.18 (d, *J* = 7.49, 1H), 6.90 – 6.73 (m, 3H), 2.57 (t, *J* = 6.4 Hz, 2H), 1.96 – 1.82 (m, 1H), 1.78 – 1.51 (m, 3H), 1.51 – 1.38 (m, 1H). ¹⁹F NMR (376 MHz, DMSO-*d*₆): δ = -138.6 – -139.6. ¹³C{¹H} NMR (101 MHz, CDCl₃): δ = 145.2, 135.8, 129.50, 129.49, 127.8, 124.0, 121.9, 30.3, 25.7, 25.67, 25.66, 22.

2-(1-(4-Methoxyphenyl)ethyl)-4,4,5,5-tetramethyl-1,3,2-dioxaborolane (17)



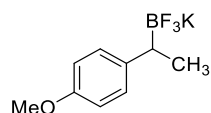
According to literature procedure:⁵⁵

1,3-Bis(diphenylphosphino)-propane nickel(II) chloride (271 mg, 500 μ mol, 5 mol%) and potassium acetate (1.96 g, 20 mmol, 2 equiv.) were stirred in a mixture of toluene (60 mL) and MeOH (20 mL) for 5 min at room temperature. Bis(pinacolato)diboron (5.08 g, 20 mmol, 2 equiv.) and *p*-methoxy styrene were added and stirred overnight at room temperature. The reaction mixture was diluted with water (50 mL), extracted with EtOAc, and dried over Na₂SO₄. The solvent was removed under reduced pressure and the crude product purified by column chromatography (5 \rightarrow 20% EtOAc in PE). The product was obtained as a colorless liquid (1.52 g, 5.8 mmol, 58%).

In the original procedure NiCl₂(dppe) is used instead of NiCl₂(dppp), which is reported to result in higher yields. Here, NiCl₂(dppp) was only used as an available alternative.

¹H NMR (400 MHz, CDCl₃): δ [ppm] = 7.13 (d, *J* = 8.6 Hz, 2H), 6.81 (d, *J* = 8.6 Hz, 2H), 3.77 (s, 2H), 2.38 (q, *J* = 7.5 Hz, 1H), 1.29 (d, *J* = 7.5 Hz, 3H), 1.21 + 1.20 (2s, 12H).

Potassium trifluoro(1-(4-methoxyphenyl)ethyl)borate (2d)



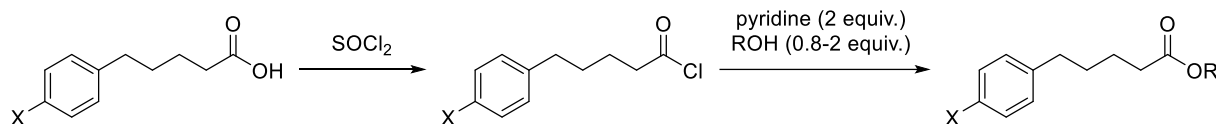
Pinacolborane **17** (1 g, 3.81 mmol, 1 equiv.) was dissolved in 12 mL MeOH. KHF₂ (1.34 g, 17.12 mmol, 4.5 equiv.) dissolved in 6 mL H₂O was added at 0 °C. The reaction mixture was stirred at room temperature for 3 h, then the solvent was removed under reduced pressure and the residue azeotroped four times with EtOH to remove most of the pinacol. The residue was extracted with boiling acetone and the solvent evaporated. The crude residue was dissolved in DCM (2 mL) and the product crystallized overnight as a colorless solid (437 mg, 1.81 mmol, 47%).

The ¹H NMR spectrum is in accordance with literature.⁵⁶

¹H NMR (400 MHz, CDCl₃): δ [ppm] = 7.09 – 7.02 (m, 2H), 6.75 – 6.69 (m, 2H), 3.72 (s, 3H), 1.62 (broad s, 1H), 1.08 (d, *J* = 7.4 Hz, 3H).

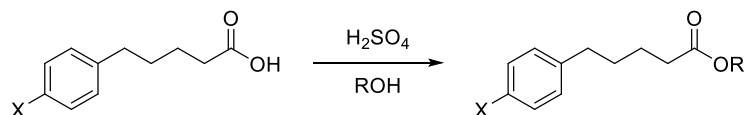
3.4.3.3 Synthesis of Ω -phenylalkylcarboxylic acid esters

General procedure 3-C: Esterification of carboxylic acids via the acyl chloride



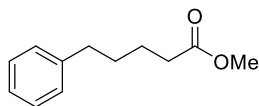
Carboxylic acid (2.5 mmol) is refluxed in SOCl_2 (1.5 – 2.5 equiv.) for 2 h. Excess thionyl chloride is removed under reduced pressure and the residue dissolved in 2 mL DCM. The alcohol (usually 2 equiv.) and pyridine (403 μL , 5 mmol, 2 equiv.) are added and the mixture stirred for 3 h at room temperature. The equivalents of alcohol in the following reactions were chosen depending on whether the carboxylic acid or the alcohol is more readily available. If not stated otherwise, 2 equivalents of alcohol were used. Depending on the alcohol, the reaction time might be reduced. After completion of the reaction the suspension is diluted with EtOAc, washed with water, diluted HCl (1 M), saturated aqueous K_2CO_3 , and brine. The organic layer is dried over Na_2SO_4 and the solvent evaporated under reduced pressure. The crude product is purified via column chromatography (0 \rightarrow 5% ethyl acetate in petrol ether).

General procedure 3-D: Acid catalyzed esterification of carboxylic acids



Carboxylic acid is dissolved in the alcohol used for esterification (2.1 mL per mmol carboxylic acid). Sulfuric acid (2 equiv.) is added and the reaction mixture stirred for 1 h at room temperature. The reaction mixture is quenched with water, extracted with EtOAc, washed with saturated aqueous K_2CO_3 and brine, dried with Na_2SO_4 , and the solvent removed under reduced pressure. Products were obtained in sufficient purity and used without further purification.

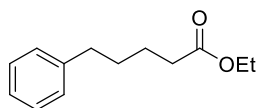
Methyl 5-phenylpentanoate (9a)



Literature known compound.⁵⁷ Synthesized according to general procedure 3-D on 2.5 mmol scale. The compound was obtained as a colorless liquid (407 mg, 2.12 mmol, 85%). The NMR spectra are in accordance with literature.

^1H NMR (400 MHz, CDCl_3): δ [ppm] = 7.34 – 7.27 (m, 2H), 7.24 – 7.17 (m, 3H), 3.68 (s, 3H), 2.71 – 2.61 (m, 2H), 2.41 – 2.31 (m, 2H), 1.76 – 1.64 (m, 4H). $^{13}\text{C}\{^1\text{H}\}$ NMR (101 MHz, CDCl_3): δ [ppm] = 173.9, 142.0, 128.25, 128.19, 125.6, 51.3, 35.4, 33.8, 30.8, 24.5.

Ethyl 5-phenylpentanoate (9b)



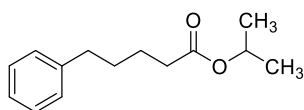
Literature known compound.³ Synthesized according to general procedure 3-C on 10 mmol scale and according to general procedure 3-D on 5 mmol scale. NMR spectra are in accordance with literature.

Procedure 1: The product was obtained as colorless liquid (1.77 g, 8.58 mmol, 86%).

Procedure 2: The product was obtained as a colorless liquid (920 mg, 4.46 mmol, 89%).

¹H NMR (400 MHz, CDCl₃): δ [ppm] = 7.33 – 7.25 (m, 2H), 7.25 – 7.12 (m, 3H), 4.14 (q, J = 7.2 Hz, 2H), 2.70 – 2.61 (m, 2H), 2.38 – 2.29 (m, 2H), 1.75 – 1.63 (m, 4H), 1.27 (t, J = 7.1 Hz, 3H). **¹³C{¹H} NMR (101 MHz, CDCl₃):** δ [ppm] = 173.51, 142.07, 128.29, 128.22, 125.67, 60.11, 35.49, 34.10, 30.82, 24.52, 14.16.

Isopropyl 5-phenylpentanoate (9d)

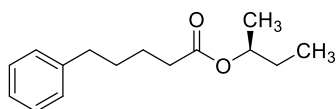


Literature known compound.⁵⁸ Synthesized according to general procedure 3-C on 2.5 mmol scale. The compound was obtained as a colorless liquid (477 mg, 2.17 mmol, 87%).

The NMR spectra are in accordance with literature.

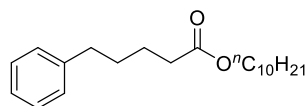
¹H NMR (400 MHz, CDCl₃): δ [ppm] = 7.31 – 7.24 (m, 2H), 7.21 – 7.14 (m, 3H), 5.01 (sept, J = 6.3 Hz, 1H), 2.68 – 2.60 (m, 2H), 2.33 – 2.26 (m, 2H), 1.72 – 1.63 (m, 4H), 1.23 (d, J = 6.2 Hz, 6H). **¹³C{¹H} NMR (101 MHz, CDCl₃):** δ [ppm] = 173.3, 142.3, 128.5, 128.4, 125.9, 67.6, 35.7, 34.7, 31.0, 24.8, 22.0.

(S)-sec-Butyl 5-phenylpentanoate (9e)



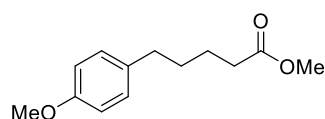
Synthesized according to general procedure 3-C on 2.5 mmol scale with 1 equiv. (*S*)-sec-butanol. The compound was obtained as a colorless liquid (510 mg, 2.18 mmol, 87%).

¹H NMR (400 MHz, CDCl₃): δ [ppm] = 7.32 – 7.23 (m, 2H), 7.22 – 7.14 (m, 3H), 7.91 – 4.77 (m, 1H), 2.70 – 2.58 (m, 2H), 2.36 – 2.28 (m, 2H), 1.75 – 1.47 (m, 6H), 1.29 (d, J = 6.3 Hz, 3H), 0.90 (t, J = 7.5 Hz, 3H). **¹³C{¹H} NMR (101 MHz, CDCl₃):** δ [ppm] = 173.3, 142.2, 128.33, 128.25, 125.69, 35.55, 34.48, 30.87, 28.77, 24.68, 19.45, 9.65. **HRMS (EI+) m/z:** [M]⁺ Calcd for C₁₅H₂₂O₂ 234.1614; Found: 234.1614.

Decyl 5-phenylpentanoate (9c)

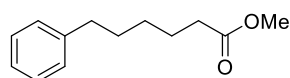
Synthesized according to general procedure 3-C on 2.5 mmol scale with 2 equiv. *n*-decanol. The compound was obtained as a colorless liquid (705 mg, 2.21 mmol, 89%).

¹H NMR (400 MHz, CDCl₃): δ [ppm] = 7.38 – 7.32 (m, 2H), 7.29 – 7.21 (m, 3H), 4.14 (t, *J* = 6.8 Hz, 2H), 7.80 – 2.64 (m, 2H), 2.48 – 2.33 (m, 2H), 1.82 – 1.62 (m, 6H), 1.46 – 1.31 (m, 14H + 1H impurities), 0.97 (t, *J* = 6.9 Hz, 3H) **¹³C{¹H} NMR (101 MHz, CDCl₃):** δ [ppm] = 173.8, 142.3, 128.48, 128.41, 125.9, 64.6, 35.7, 34.3, 32.0, 31.0, 29.648, 29.643, 29.42, 29.37, 28.8, 26.1, 24.8, 22.8, 14.2 **HRMS (EI+) m/z:** [M]⁺ Calcd for C₂₁H₃₄O₂ 318.2553, found: 318.2551.

Methyl 5-(4-methoxyphenyl)pentanoate (9f)

Literature known compound.⁵⁹ Synthesized according to general procedure 3-D on 1.2 mmol scale. The compound was obtained as a colorless liquid (262 mg, 1.18 mmol, 98%). NMR spectra are in accordance with literature.

¹H NMR (400 MHz, CDCl₃): δ [ppm] = 7.09 (d, *J* = 8.7 Hz, 2H), 6.82 (d, *J* = 8.5 Hz, 2H), 3.78 (s, 3H), 3.66 (s, 3H), 2.57 (t, *J* = 7.2 Hz, 2H), 2.33 (t, *J* = 7.0 Hz, 3H), 1.73 – 1.54 (m, 4H). **¹³C{¹H} NMR (101 MHz, CDCl₃):** δ [ppm] = 174.1, 157.7, 134.2, 129.2, 113.7, 55.2, 51.4, 34.6, 33.9, 31.1, 24.5.

Methyl 6-phenylhexanoate (11)

Literature known compound.⁶⁰ Synthesized according to general procedure 3-D on 3 mmol scale. The compound was obtained as a colorless liquid (614 mg, 2.98 mmol, 99%). The ¹H NMR spectrum is in accordance with literature.

¹H NMR (400 MHz, CDCl₃): δ [ppm] = 7.32 – 7.23 (m, 2H), 7.22 – 7.13 (m, 3H), 3.67 (s, 3H), 2.61 (t, *J* = 7.7 Hz, 2H), 2.31 (t, *J* = 7.5 Hz, 2H), 1.75 – 1.56 (m, 4H), 1.44 – 1.31 (m, 2H).

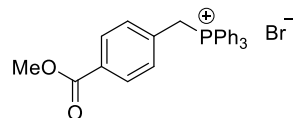
3.4.3.4 Synthesis of benzyltriphenylphosphonium bromides

General procedure 3-E:

Benzyltriphenylphosphonium bromides were synthesized according to literature procedure.⁴²

Triphenylphosphine (2.85 mmol, 1 equiv.) and substituted benzyl bromide (3.14 mmol, 1.1 equiv.) were refluxed in toluene (10 mL) for 3 h. After cooling to room temperature, the product was filtered, washed with toluene and *n*-hexane, and dried under vacuum.

[4-(Methoxycarbonyl)benzyl]triphenylphosphonium bromide (14a)

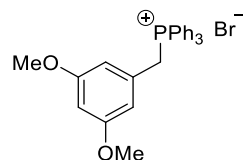


Synthesized according to general procedure 3-E. The product was obtained as colorless powder (1.30 g, 2.65 mmol, 92%).

The ¹H NMR spectrum is in accordance with literature.⁶¹

¹H NMR (400 MHz, CD₃CN): δ [ppm] = 7.92 – 7.82 (m, 3H), 7.81 – 7.74 (m, 2H), 7.72 – 7.61 (m, 12H), 7.18 – 7.10 (m, 2H), 5.10 (d, *J* = 15.5 Hz, 2H), 3.83 (s, 3H).

(3,5-Dimethoxybenzyl)triphenylphosphonium bromide (14b)

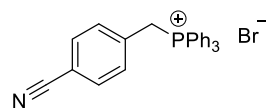


Synthesized according to general procedure 3-E. The product was obtained as colorless powder (1.39 g, 2.82 mmol, 99%).

The ¹H NMR spectrum is in accordance with literature.⁶²

¹H NMR (400 MHz, CD₃CN): δ [ppm] = 7.91 – 7.82 (m, 3H), 7.73 – 7.58 (m, 12H), 6.40 (q, *J* = 2.25 Hz, 1H), 6.17 (t, *J* = 2.38 Hz, 2H), 4.81 (d, *J* = 14.68 Hz, 2H), 3.52 (s, 6H).

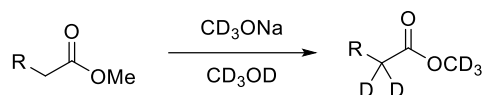
[4-Cyanobenzyl]triphenylphosphonium bromide (14c)



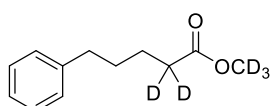
Synthesized according to general procedure 3-E. The product was obtained as colorless powder (1.25 g, 2.73 mmol, 96%).

¹H NMR (400 MHz, CD₃CN): δ [ppm] = 7.92 – 7.85 (m, 3H), 7.73 – 7.59 (m, 12H), 7.55 (d, *J* = 7.9 Hz, 2H), 7.16 (dd, *J* = 8.4, 2.3 Hz, 2H), 4.96 (d, *J* = 15.5 Hz, 2H).

3.4.3.5 Synthesis of deuterated substrates

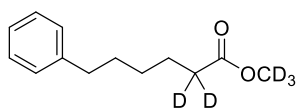
General procedure 3-F: Deuteration in α -position to ester groups

Sodium (2 equiv.) is added to CD_3OD (3 mL/mmol ester) and stirred until all sodium has reacted. After addition of the ester (1 equiv.) the solution is stirred overnight. The reaction is quenched with D_2O (100 μL /mmol), diluted with EtOAc, washed with water and brine, dried with Na_2SO_4 , and the solvent removed under reduced pressure to yield the product without further purification.

Methyl- d_3 5-phenylpentanoate-2,2- d_2 (**9a-C2- d_2**)

Synthesized according to general procedure 3-F on 1 mmol scale. The product was obtained as colorless liquid (154 mg, 781 μmol , 78%) with 87% deuteration at the α -position. NMR spectra match those of the respective non-deuterated compound **9a** except for the deuterated positions.

^1H NMR (400 MHz, CD_3OD): δ [ppm] = 7.28 – 7.20 (m, 2H), 7.20 – 7.11 (m, 3H), 2.68 – 2.54 (m, 2H), 2.37 – 2.27 (m, 0.27H, incomplete deuteration), 1.69 – 1.56 (m, 4H) $^{13}\text{C}\{^1\text{H}\}$ NMR (101 MHz, CD_3OD): δ [ppm] = 175.9, 143.4, 129.4, 129.3, 126.8, 51.2 (t, J = 22.3 Hz), 36.5, 34.5 – 33.8 (overlapping deuterated and partially deuterated α -Cs) HRMS (EI+) m/z : $[M]^+$ Calcd for $\text{C}_{12}\text{H}_{11}\text{D}_5\text{O}_2$ 197.1459; Found 197.1462.

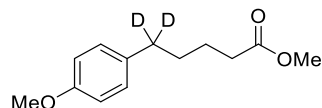
Methyl- d_3 5-phenylhexanoate-2,2- d_2 (**11-C2- d_2**)

Synthesized according to general procedure 3-F on 2.5 mmol scale in 5 mL CD_3OD . The procedure was repeated twice to improve the deuteration degree. The product was obtained as colorless liquid (402 mg, 1.92 mmol, 76%) with >99% deuteration in α -position. NMR spectra match those of the respective non-deuterated compound **11** except for the deuterated positions.

^1H NMR (400 MHz, CDCl_3): δ [ppm] = 7.32 – 7.26 (m, 2H), 7.23 – 7.15 (m, 3H), 2.63 (t, J = 7.7 Hz, 2H), 2.34 – 2.27 (m, 0.017H, residual H in α -position), 1.72 – 1.59 (m, 4H), 1.44 – 1.33 (m, 2H). $^{13}\text{C}\{^1\text{H}\}$ NMR (101 MHz, CDCl_3): δ [ppm] = 174.3, 142.6, 128.5, 128.4, 125.8, 50.8 (sept, J = 22.4 Hz, peak at 50.11 ppm likely lost in the noise), 35.8, 33.5 (quint, J = 19.6), 31.2, 28.8, 24.8. HRMS (EI+) m/z : $[M]^+$ Calcd for $\text{C}_{13}\text{H}_{13}\text{D}_5\text{O}_2$ 211.1615; Found 211.1611.

Synthesis of other deuterated substrates

Methyl 5-(4-methoxyphenyl)pentanoate-5,5-*d*₂ (**9f-d**₂)



Synthesized according to general procedure 3-G on 400 μ mol scale.

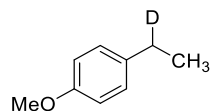
The product was purified via column chromatography (10% EtOAc in PE) and obtained as colorless liquid (73 mg, 325 μ mol, 81%) with 83% deuteration at the benzylic position.

NMR spectra match those for non-deuterated compound **9f** except for the deuterated position. Signals from the monodeuterated compound show small chemical shift differences in the ¹³C NMR spectrum and are marked with *d*₁.

¹H NMR (400 MHz, CDCl₃): δ [ppm] = 7.13 – 7.04 (m, 2H), 6.87 – 6.78 (m, 2H), 3.78 (s, 3H), 3.66 (s, 3H), 2.61 – 2.51 (m, 0.333H, 83% D), 2.33 (t, *J* = 7.1 Hz, 2H), 1.72 – 1.54 (m, 4H) ¹³C{¹H} NMR (101 MHz, CDCl₃): δ [ppm] = 174.2, 157.9, 134.29 (*d*₁), 134.26, 129.4, 113.9, 55.4, 51.6, 34.8 – 33.8 (m), 34.08, 31.2 (*d*₁), 31.1, 24.61 (*d*₁), 24.59

HRMS (EI+): [M]⁺ Calcd for C₁₃H₁₆D₂O₃ 224.1376; Found 224.1376.

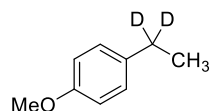
1-(Ethyl-1-*d*)-4-methoxybenzene (**1b-d**₁)



Synthesized according to general procedure 3-H from trifluoroborate **2d** with 10 equiv. D₂O as deuterium source. Purified via column chromatography (100% *n*-pentane). The product was obtained as colorless liquid (28 mg, 204 μ mol, 68%) in moderate purity with >95% mono-deuteration. NMR spectra are in accordance with literature and non-deuterated **1b** except for the deuterated position.⁶³

¹H NMR (400 MHz, CDCl₃): δ [ppm] = 7.15 – 7.08 (m, 2H), 6.86 – 6.80 (m, 2H), 3.79 (s, 3H), 2.58 (qt, *J* = 7.6, 2.07 Hz, 1H), 1.23 – 1.18 (m, 3H) ¹³C{¹H} NMR (101 MHz, CDCl₃): δ [ppm] = 157.8, 136.5, 128.8, 113.9, 55.4, 27.8 (t, *J* = 19.3 Hz, benzylic C), 15.9.

1-(Ethyl-1,1-*d*₂)-4-methoxybenzene (**1b-d**₂)



Synthesized according to literature.⁶⁴

AlCl₃ (1.42 g, 10.62 mmol, 1.77 equiv.) and LiAlD₄ (252 mg, 6 mmol, 1 equiv.) were suspended in 20 mL Et₂O. 4-Methoxyacetophenone (901 mg, 6 mmol, 1 equiv.) was added dropwise. The mixture was stirred for 1 h at room temperature, then 20 mL H₂O were added dropwise. After the H₂ evolution stopped the mixture was extracted with *n*-pentane (3 x 20 mL), the organic phase washed with water and brine, dried over Na₂SO₄, the solvent removed under reduced pressure (120 mbar, 40 °C to avoid evaporation of product), and the crude product purified via column chromatography (100% *n*-pentane). The compound was obtained as a colorless liquid (692 mg, 5.01 mmol, 83%) with a deuteration degree of >99%. NMR spectra are in accordance with literature and ethyl anisole-*d*₀.

¹H NMR (400 MHz, CDCl₃): δ [ppm] = 7.16 – 7.10 (m, 2H), 6.88 – 6.81 (m, 2H), 3.80 (s, 3H), 1.21 (s, 3H)
¹³C{¹H} NMR (101 MHz, CDCl₃): δ [ppm] = 157.8, 136.5, 128.8, 113.9, 55.4, 27.4 (quint, J = 19.3 Hz, benzylic position), 15.8.

3.4.4 Generation of carbanions

General Procedure 3-G: Carbanion generation from benzylic C-H bonds

Carbanion generation from benzylic C-H bonds was done as previously reported on benzylic C-H activation:³ Benzylic substrate (1 equiv., 100 μ mol per mL solvent), K₂CO₃ (10 mol%) and photocatalyst 3DPA2FBN (**4b**, 3 mol%) are placed in a 6 mL crimp-capped vial with a stirring bar and closed. The vial is evacuated and backfilled with nitrogen 3 times via cannula. HAT-catalyst ⁱPr₃SiSH (10 mol%) and solvent (MeCN or MeCN/acetone 1:1) are added via syringe. Solid reaction partners are added before closing the vial and liquids via syringe after closing the vial. The reaction mixture is degassed by 3 cycles of freeze-pump-thaw and irradiated by blue light (LEDs; λ_{max} = 440 nm) overnight.

Addition of molecular sieves as previously reported³ can slightly increase the yield by binding residual water. However, the heterogeneity of this system was detrimental to analysis and reproducibility. Thus, molecular sieves were not used in this work to improve reproducibility. As the focus was on mechanistic investigations, maximizing yields was not required.

For isolation of tertiary alcohol products, the reaction mixture is diluted with water, extracted with EtOAc, and dried over Na₂SO₄. After solvent removal under reduced pressure the crude product is purified via column chromatography with appropriate EtOAc/PE mixtures.

For isolation of alkyl benzyl compounds the reaction mixture is diluted with water, extracted with *n*-pentane, and dried over Na₂SO₄. The solvent is removed under reduced pressure. Where necessary, column chromatography with appropriate mixtures of EtOAc/PE can be used for purification. Most compounds in this work were obtained in sufficient purity without further purification.

General procedure 3-H: Carbanion generation from carboxylic acids, carboxylates and trifluoroborates

Carbanion generation from carboxylic acids and benzyl trifluoroborate salts was done as previously reported:⁴ Carbanion precursor (1 equiv. 100 μ mol per mL solvent) and photocatalyst (5 mol%) are placed in a 6 mL crimp-capped vial. If the carbanion precursor is a carboxylic acid, additional Cs₂CO₃ (1 equiv.) is added. The vial is evacuated and backfilled with nitrogen 3 times via cannula. Solvent (MeCN for trifluoroborates and DMA for carboxylates, if not stated otherwise) and reaction partners (acetone, H₂O, D₂O) are added, the reaction mixture degassed by 3 cycles of freeze-pump-thaw and irradiated by blue light (LEDs; λ_{max} = 440 nm) for 3 – 16 h. Exact reaction times depend on the substrate and conditions. Trifluoroborates usually give full conversion within 1 – 4 hours, carboxylates within 3 – 10 h. If not stated otherwise, reactions with trifluoroborates were run for 4 h, with carboxylates and carboxylic acids overnight (16 h) to ensure maximum conversion.

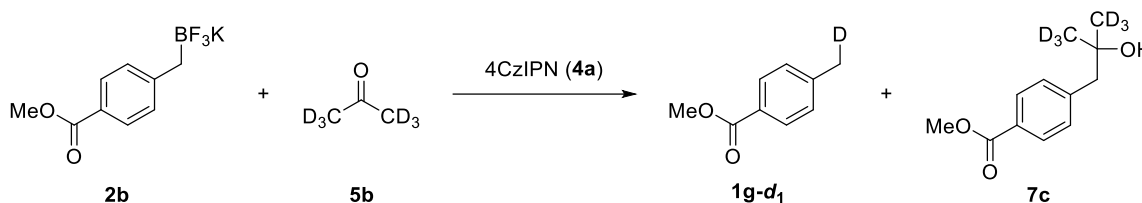
If products are isolated, the same isolation procedure as for carbanion generation via benzylic C-H activation is followed. To note, in this work the focus is on the reactivity of the carbanions and not on maximizing yields. Thus, to

give comparable data, conditions for some reactions were chosen to closely resemble other reactions, often not being optimal for achieving maximum yield of the specific compound.

As photocatalyst, 4CzIPN can be used as pre-catalyst or the photosubstitution products can be used directly. A more detailed explanation and comparison can be found in section 3.4.5.

Methyl 4-(methyl-*d*)benzoate (**1g-d₁**)

and methyl 4-(2-hydroxy-2-(methyl-*d*₃)propyl-3,3,3-*d*₃)benzoate (**7c**)



The reaction was conducted according to general procedure 3-H in 2 mL of a 1:1 mixture acetone-*d*₆/CH₃CN on 100 μmol scale. Concentration was half of the general procedure due to the low solubility of the substrate.

Methyl 4-(methyl-*d*)benzoate

Methyl 4-(methyl-*d*)benzoate was obtained as a colorless liquid with 86% mono-deuteration at the benzylic position (11.3 mg, 75 μmol, 75%).

¹H NMR (400 MHz, CDCl₃): δ [ppm] = 7.97 – 7.89 (m, 2H), 7.26 – 7.21 (m, 2H), 3.90 (s, 3H), 2.41 (s, benzylic CH₃ of non-deuterated product), 2.39 (t, *J* = 2.1 Hz, CH₂D, 2.25 H together with non-deuterated product). **¹³C{¹H} NMR (101 MHz, CDCl₃):** δ [ppm] = 167.4, 143.7, 129.7, 129.2, 127.6, 52.1, 21.79 (benzylic C of **1g-d₀**), 21.5 (t, *J* = 19.45 Hz, benzylic C of **1g-d₁**). **HRMS (+APCI) m/z:** Calc. for C₉H₁₀DO₂ 152.0816; Found 152.0816.

Methyl 4-(2-hydroxy-2-(methyl-*d*₃)propyl-3,3,3-*d*₃)benzoate (**7c**)

Obtained as a colorless, viscous liquid (4.3 mg, 20 μmol, 20%).

¹H NMR (400 MHz, CDCl₃): δ [ppm] = 8.01 – 7.96 (m, 2H), 7.33 – 7.28 (m, 2H), 3.91 (s, 3H), 2.82 (s, 2H). **HRMS (+APCI) m/z:** [M + H]⁺ Calcd for C₁₂H₁₁D₆O₃ 215.1549; Found 215.1551 and [M + NH₄]⁺ Calcd for C₁₂H₁₄D₆NO₃ 232.1814; Found 232.11815 (mass for [M + NH₄]⁺ shows that [M + H]⁺ is indeed [M + H]⁺ and not [M⁺] of **7c-d₅**).

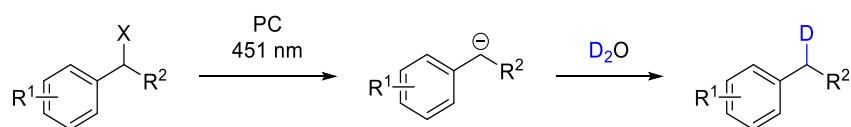
3.5.1 Comparison of the catalytic activity of 4CzIPN and its photosubstitution products

Photosubstitution of one of the cyano groups in 4CzIPN proceeds rapidly with sterically unhindered carboxylates and trifluoroborates unless electron withdrawing groups are present on the aryl group. Sterically hindered substrates such as carboxylates **3a** and **3c** do not undergo photosubstitution with 4CzIPN. Electron deficient, neutral and electron rich benzyl trifluoroborates and diphenylcarboxylates are oxidized by 4CzIPN to generate the corresponding radicals. Electron poor and diphenylmethyl radicals are subsequently reduced to the corresponding carbanions. Electron rich benzyl radicals are not reduced by 4CzIPN and instead undergo photosubstitution reaction so far steric hindrance permits it. The addition of water does not influence the photosubstitution reaction and if equimolar ratios of 4CzIPN and Molander borate **2a** are irradiated only traces (<10%) of the corresponding toluene derivative are formed and 4CzIPN is quantitatively converted to its photosubstitution product **4c**. This demonstrates that carbanion generation does not start before most of the 4CzIPN has converted to its photosubstitution product.

The yield of carbanions (measured as its toluene derivative after quenching with D₂O) generated either from Molander borate **2a** or **2b** is similar. Only 1 equivalent of substrate relative to the pre-catalyst 4CzIPN is required to generate the active catalyst. Sterically hindered, electron rich carboxylate **3c** forms the corresponding *p*-isopropylanisole in only moderate yield, but without substantial difference when either using 4CzIPN or its photosubstitution product **4c**. Thus, for most substrates no pre-synthesized photocatalyst is required, which is adapted to the structure of the substrate. 4CzIPN can be used to either directly catalyze carbanion generation or in situ generates a photocatalyst capable of catalyzing carbanion generation, depending on the substrate as explained in chapter 2.

However, there are cases where 4CzIPN is superior to its photosubstitution products (4CzRBN). Potassium diphenyl acetate gives diphenylmethane in poor yield of 13% if photosubstitution product **3c** is used as photocatalyst while the reaction is quantitative when 4CzIPN is used under otherwise identical reaction conditions. This may be attributed to the slightly decreased oxidation potential of photosubstituted 4CzIPN derivatives compared to 4CzIPN.

For investigations by optical spectroscopy photosubstitution product **4d** was used to observe the reductive radical-polar crossover.



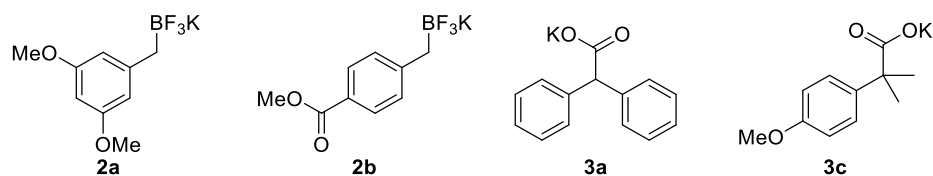
Scheme 3.12. Phenylacetates and benzyltrifluoroborates generate carbanions under redox-neutral photocatalytic conditions. Deuteration at the benzylic position by D₂O was used as model reaction to compare the efficiency of carbanion generation by 4CzIPN and its photosubstitution products **4c** and **4d**.

REACTIVITY OF SUPERBASIC CARBANIONS GENERATED VIA REDUCTIVE RADICAL-POLAR
CROSSOVER IN THE CONTEXT OF PHOTOREDOX CATALYSIS

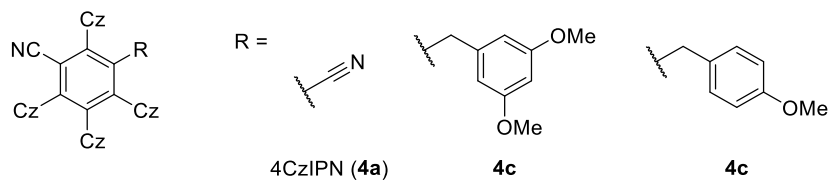
Table 3.1. Photocatalyst comparison for different carboxylic acids and trifluoroborates. Reaction conditions according to general procedure 3-H on 100 μ mol scale.

Entry	Substrate	Photocatalyst	Photosubstitution	NMR-yield	Deuteration
1	2b	4CzIPN	No	>95%	93%
2	2b	4c	No	>95%	92%
3	3a	4CzIPN	No	>95%	79%
4	3a	4c	No	12%	75%
5	2a	4CzIPN	Yes	70%	87%
6	2a	4c	No	87%	88%
7	2a	4d	No	>95%	88%
8	3c	4CzIPN	No	53%	69%
9	3c	4c	No	56%	71%

Substrate:

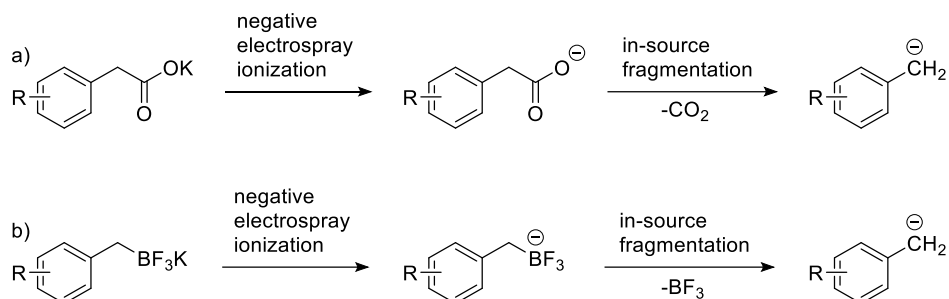


Photocatalyst:



3.4.6 Gas-phase reactivity of carbanions

For assessing the involvement of isolated benzyl carbanions in solution, their gas-phase reactivity was explored on a molecular level and compared to the corresponding in-solution reactivity. The carbanions proposed as intermediates were generated from their precursors (benzyltrifluoroborates and carboxylates) by in-source fragmentation during electrospray ionization mass spectrometry measurements (Scheme 3.13).^{65–68}



Scheme 3.13. Generation of carbanions by in-source fragmentation during the electrospray ionization.

A TSQ-7000 quadrupole-octopole-quadrupole tandem mass spectrometer, equipped with an mks Baratron[®] pressure meter was used as follows (Figure 3.5): Benzyl anions were generated in an electrospray ionization source and mass-selected by the first quadrupole. The selected ions subsequently reacted in the octopole collision cell with a gaseous substrate. The reaction products were analyzed by the second quadrupole.

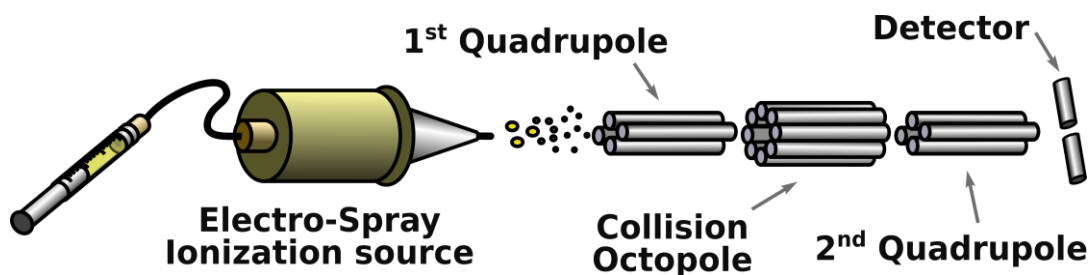


Figure 3.5. Simplified scheme of the TSQ-7000 mass spectrometer.

The kinetic energy of the ions and thus collision energy was changed by setting the DC potential of the octopole.⁶⁹ Zero kinetic energy of ions (E_{kin}) was determined by stopping-potential analysis (Figure 3.6) before each measurement.⁶⁹

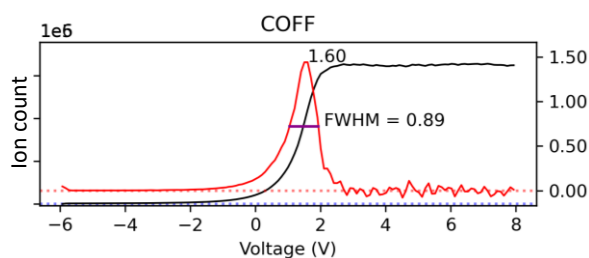
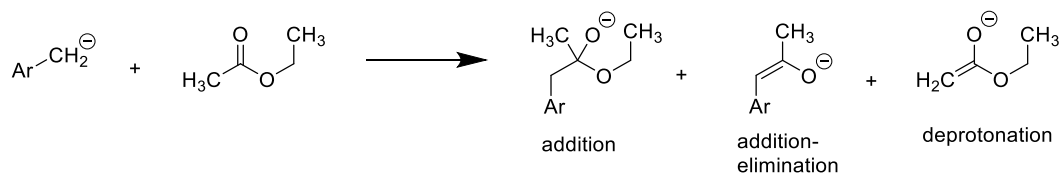


Figure 3.6. Stopping-potential analysis of E_{kin} distribution of carbanion **1f**⁻. The black curve describes the dependency of the ion current on the DC potential of the octopole collision cell. The lowest average translational energy of the ions is in this case observed at a collision cell DC potential of 1.6 V, as illustrated by the derivative of the ion current (red curve). The shape of the derivative illustrates the energy distribution in the ion beam at the octopole entrance.

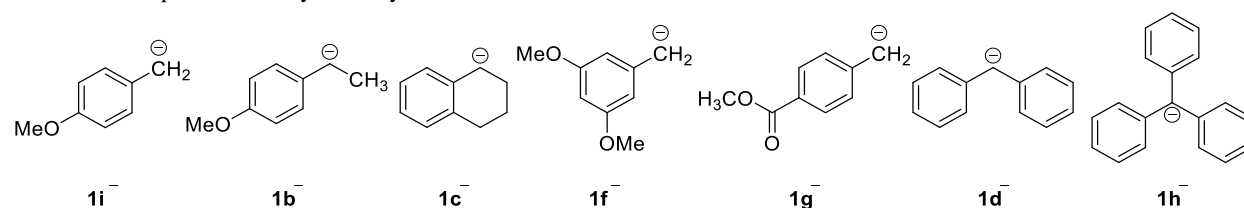
3.4.6.1 Qualitative gas-phase reactivity

We tested the reactivity of benzyl anions with a different degree of charge stabilization. We observed the products of three types of reactions: addition, addition-elimination, and deprotonation (Scheme 3.14). Table 3.2 summarizes the gas-phase reactivity of all tested compounds.



Scheme 3.14. Observed gas-phase reaction pathways illustrated on the products of the reaction between benzyl anion and ethyl acetate.

Table 3.2. Gas-phase reactivity of benzyl anions.



Substrate	1i ⁻	1b ⁻	1c ⁻	1f ⁻	1g ⁻	1d ⁻	1h ⁻
	deprotonation, addition- elimination	-	addition- elimination	deprotonation, addition- elimination	no reaction	no reaction	no reaction
	-	-	-	addition- elimination	addition- elimination	addition	-
	-	-	-	addition- elimination	-	-	-
	deprotonation	-	deprotonation	deprotonation	no reaction	no reaction	-
	deprotonation	deprotonation	deprotonation	deprotonation	no reaction	no reaction	no reaction
	deprotonation (KIE 3.2)	deprotonation (KIE 3.0)	deprotonation (KIE 4.0)	deprotonation (KIE 6.5)	no reaction	no reaction	no reaction
CO ₂	-	-	-	addition	-	-	-

(-) ... not tested

Gas-phase reactivity with acetone

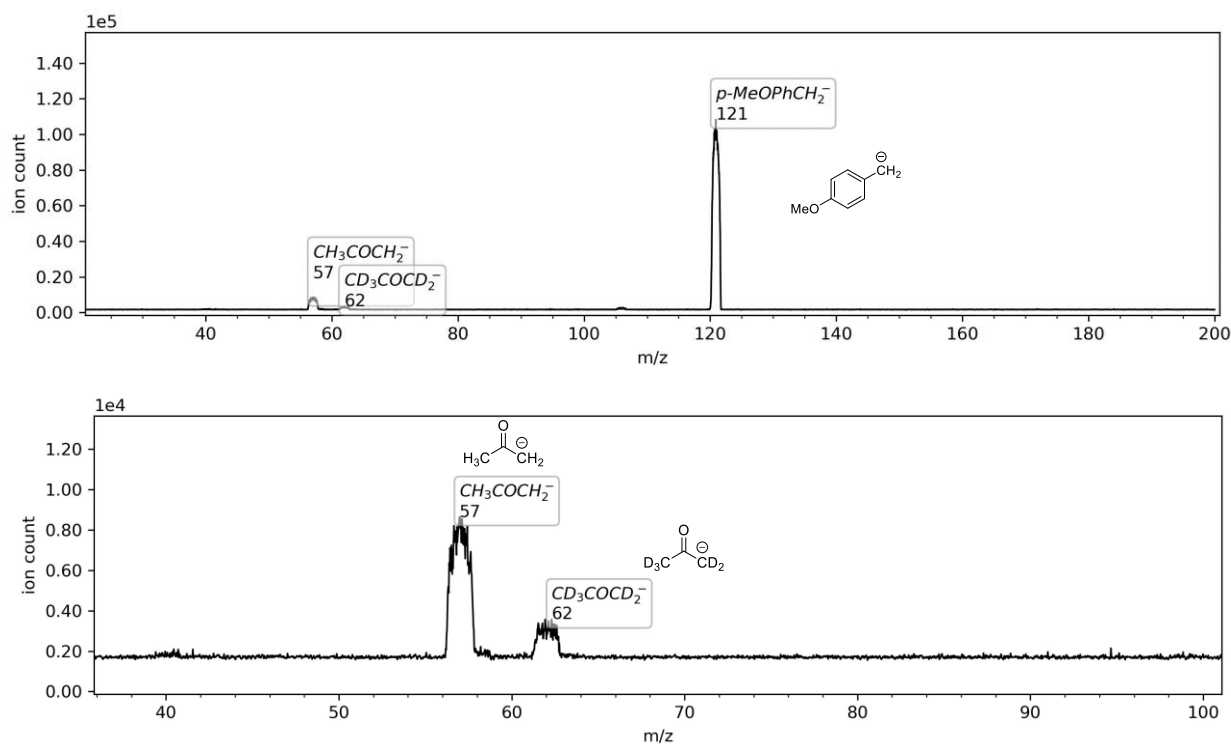


Figure 3.7. ESI-MS/MS spectrum of the gas-phase reactivity of carbanion $1i^-$ (parent, m/z 121) with acetone- d_0/d_6 (roughly 1:1 $d_0:d_6$ ratio), $p(\text{acetone-}d_0/d_6) = 0.26$ mTorr (nom.), $E_{\text{kin}} = 0$ eV.

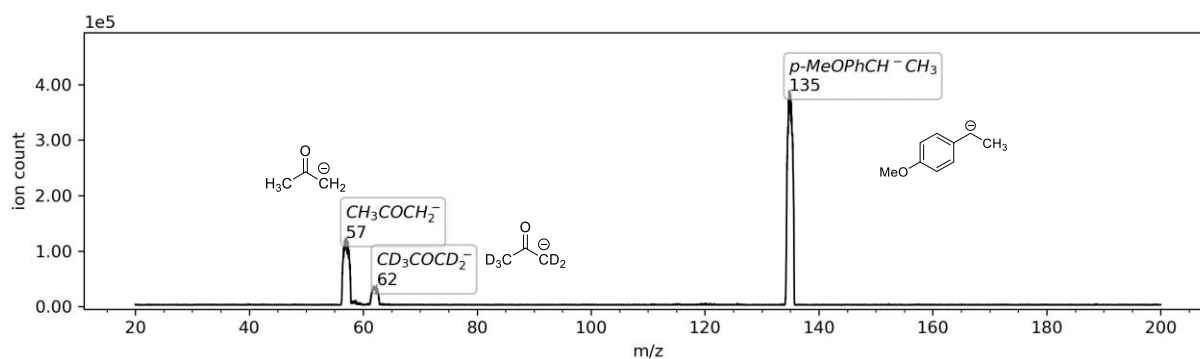


Figure 3.8. ESI-MS/MS spectrum of the gas-phase reactivity of carbanion $1b^-$ (parent, m/z 135) with acetone- d_0/d_6 (roughly 1:1 $d_0:d_6$ ratio), $p(\text{acetone-}d_0/d_6) = 0.31$ mTorr (nom.), $E_{\text{kin}} = 0$ eV.

REACTIVITY OF SUPERBASIC CARBANIONS GENERATED VIA REDUCTIVE RADICAL-POLAR
CROSSOVER IN THE CONTEXT OF PHOTOREDOX CATALYSIS

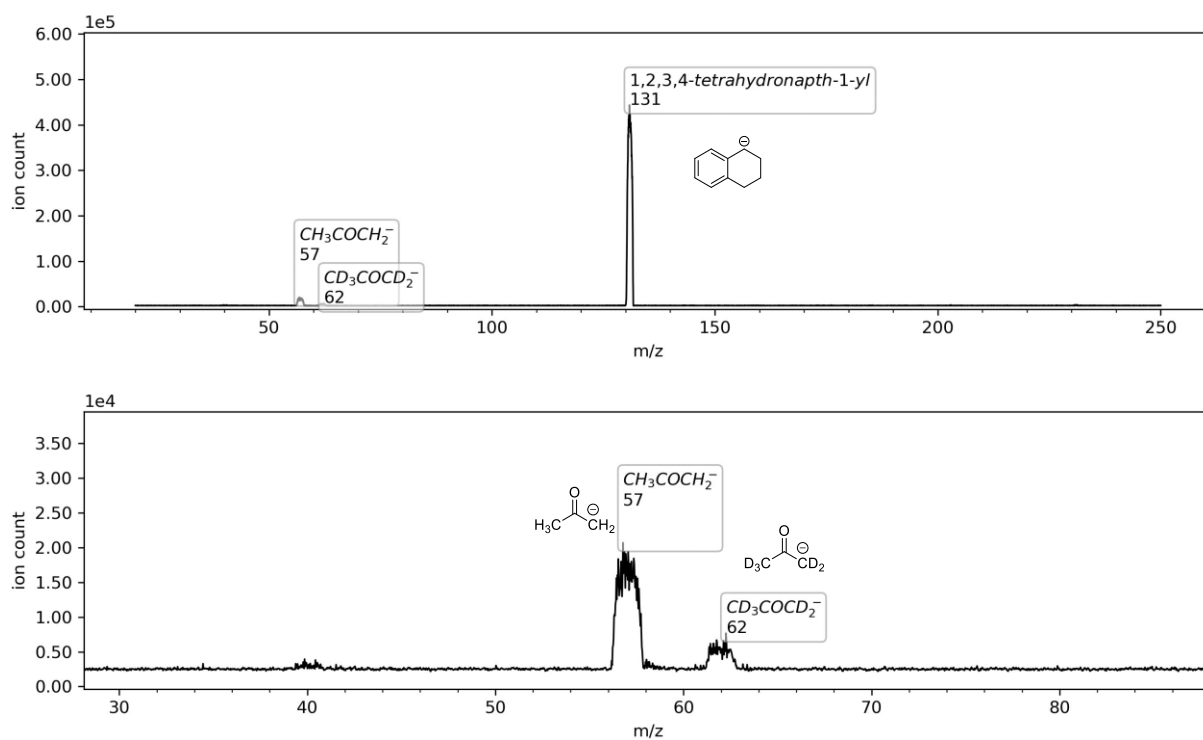


Figure 3.9. ESI-MS/MS spectrum of the gas-phase reactivity of carbanion $1c^-$ (parent, m/z 131) with acetone- d_0/d_6 (roughly 1:1 $d_0:d_6$ ratio), $p(\text{acetone-}d_0/d_6) = 0.28$ mTorr (nom.), $E_{\text{kin}} = 0$ eV.

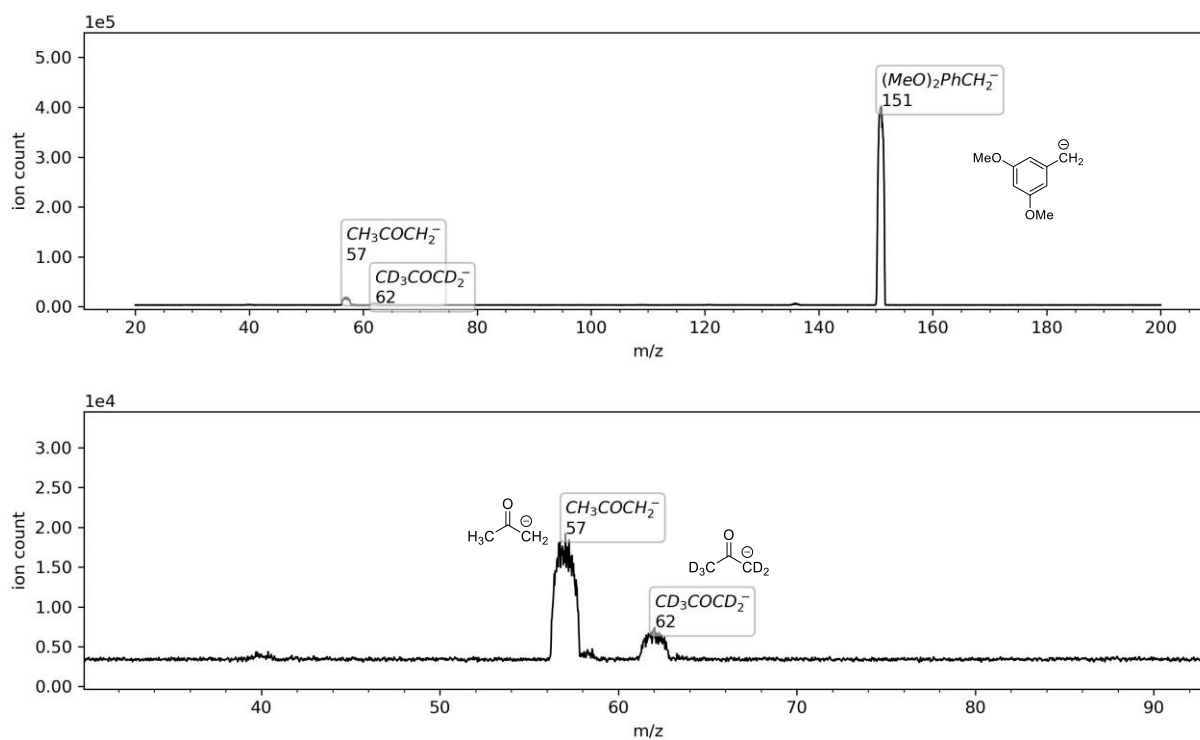


Figure 3.10. ESI-MS/MS spectrum of the gas-phase reactivity of carbanion $1\mathbf{f}^-$ (parent, m/z 151) with acetone- d_0/d_6 (roughly 1:1 $d_0:d_6$ ratio), $p(\text{acetone-}d_0/d_6) = 0.53$ mTorr (nom.), $E_{\text{kin}} = 0$ eV.

Gas-phase reactivity with acetonitrile

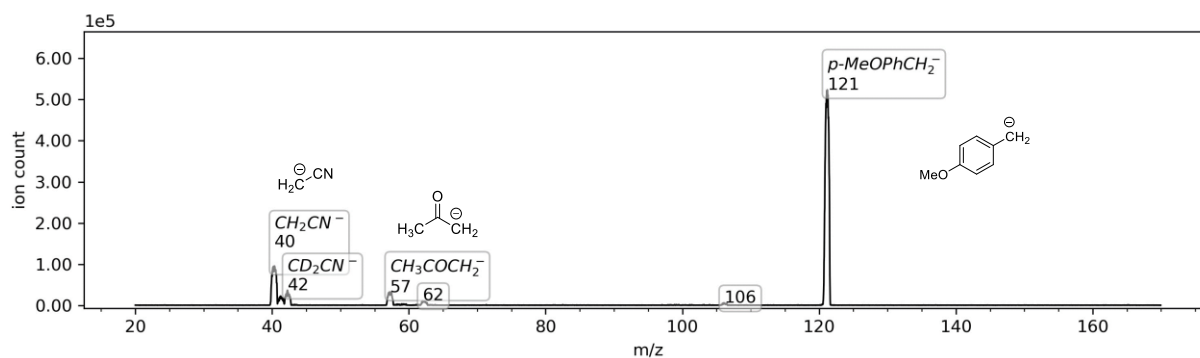


Figure 3.11. ESI-MS/MS spectrum of the gas-phase reactivity of carbanion **1i**⁻ (parent, *m/z* 121) with acetonitrile-*d*₀/*d*₃ (roughly 1:1 *d*₀:*d*₃ ratio), *p*(acetonitrile-*d*₀/*d*₃) = 0.20 mTorr (nom.), *E*_{kin} = 0 eV. Peaks of *m/z* 57 and 62 belong to acetone-*d*₀/*d*₆ which was present in the collision cell from previous experiments.

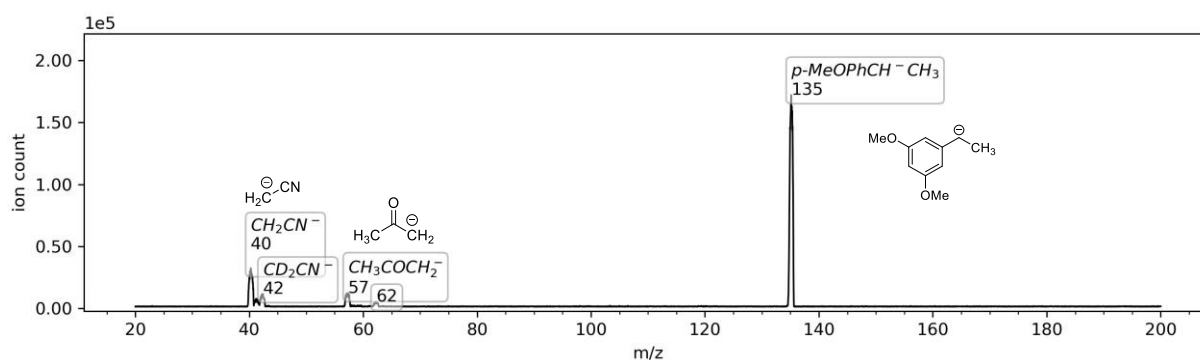


Figure 3.12. ESI-MS/MS spectrum of the gas-phase reactivity of carbanion **1b**⁻ (parent, *m/z* 135) with acetonitrile-*d*₀/*d*₃ (roughly 1:1 *d*₀:*d*₃ ratio), *p*(acetonitrile-*d*₀/*d*₃) = 0.20 mTorr (nom.), *E*_{kin} = 0 eV. Peaks of *m/z* 57 and 62 belong to acetone-*d*₀/*d*₆ which was present in the collision cell from previous experiments.

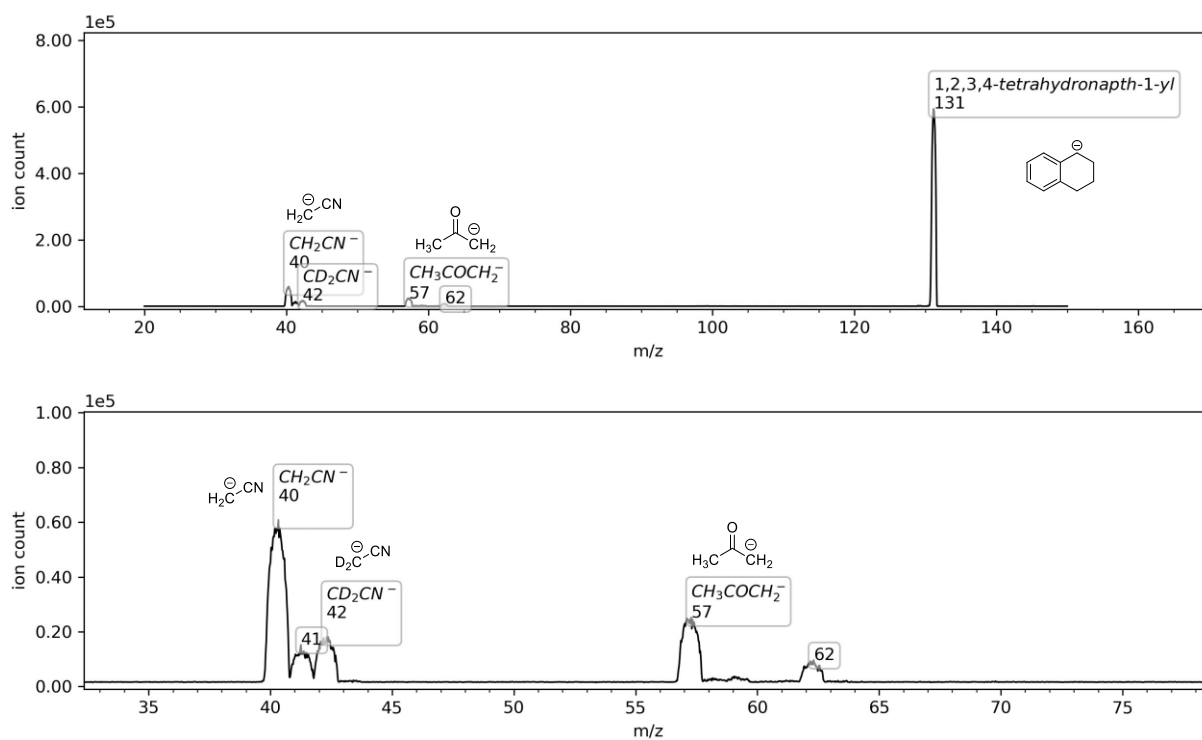


Figure 3.13. ESI-MS/MS spectrum of the gas-phase reactivity of carbanion $1c^-$ (parent, m/z 131) with acetonitrile- d_0/d_3 (roughly 1:1 $d_0:d_3$ ratio), $p(\text{acetonitrile-}d_0/d_3) = 0.20$ mTorr (nom.), $E_{\text{kin}} = 0$ eV. Peaks of m/z 57 and 62 belong to acetone- d_0/d_6 which was present in the collision cell from previous experiments. The peak of m/z 41 which fits to CHDCN^- is presumed to be formed by hydrogen exchange between acetonitrile- d_0/d_3 and acetonitrile- d_0/d_2 anion.

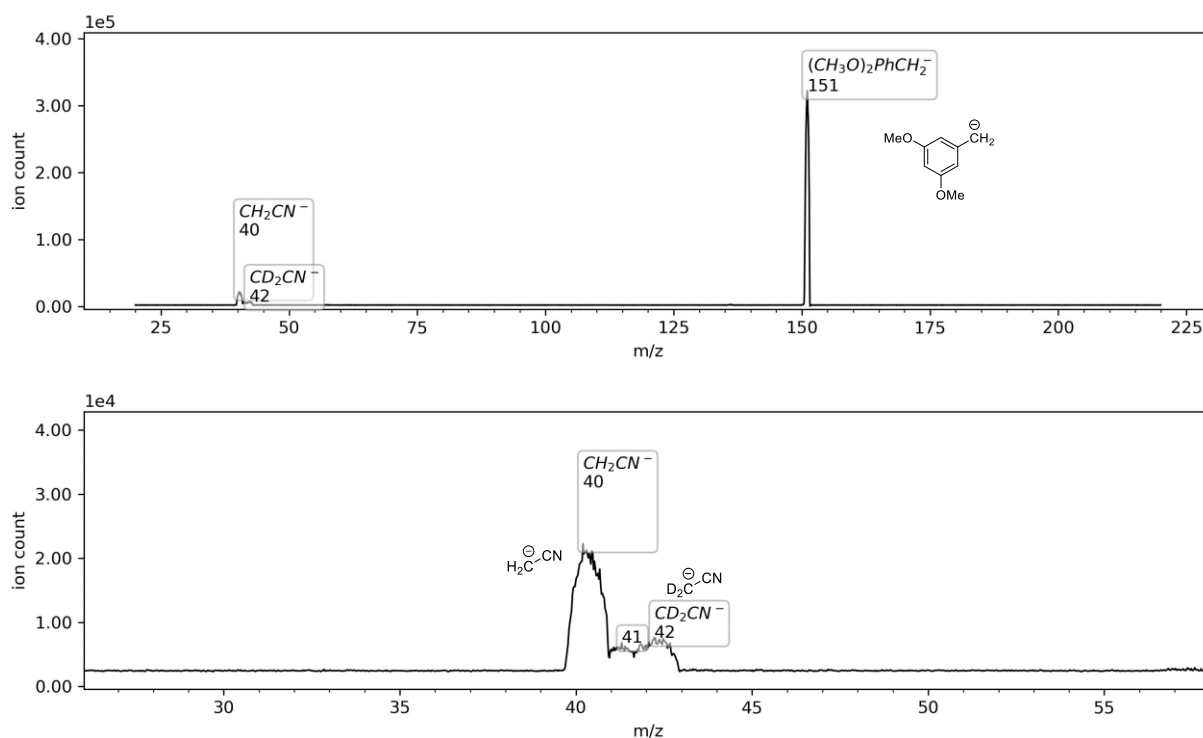


Figure 3.14. ESI-MS/MS spectrum of the gas-phase reactivity of carbanion **1f⁻** (parent, *m/z* 151) with acetonitrile-*d*₀/*d*₃ (roughly 1:1 *d*₀:*d*₃ ratio), *p*(acetonitrile-*d*₀/*d*₃) = 0.30 mTorr (nom.), *E*_{kin} = 0 eV. The peak of *m/z* 41 which fits to CHDCN⁻ is presumed to be formed by hydrogen exchange between acetonitrile-*d*₀/*d*₃ and acetonitrile-*d*₀/*d*₂ anion.

Gas-phase reactivity of carbanion **1f⁻** with CO₂

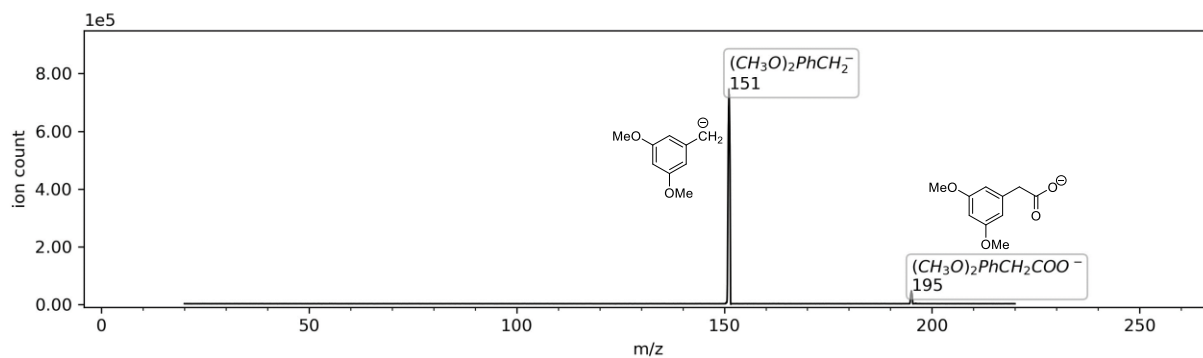


Figure 3.15. ESI-MS/MS spectrum of the gas-phase reactivity of carbanion **1f⁻** (parent, *m/z* 151) with CO₂, *p*(CO₂) = 0.10 mTorr (nom.), *E*_{kin} = 0 eV. The peak of *m/z* 195 corresponds to CO₂ addition to the benzyl anion.

3.4.6.2 Determination of kinetic isotope effects of benzylic carbanions reacting with acetonitrile- d_0/d_3

KIEs in the gas-phase reactions of carbanions with acetonitrile- d_0/d_3 were determined for the following carbanions: *p*-methoxybenzyl anion (**1i**⁻, KIE = 3.0±1.0), 3,5-dimethoxybenzyl anion (**1f**⁻, KIE = 6.5±0.5), 1,2,3,4-tetrahydronaphthalen-1-yl anion (**1c**⁻, KIE = 4.0±0.5) and *p*-methoxy- α -methylbenzyl anion (**1b**⁻, KIE = 3.2±0.5). The diphenylmethyl anion (**1d**⁻), triphenylmethyl anion (**1h**⁻), and *p*-methoxycarbonylbenzyl anion (**1g**⁻) did not react with acetonitrile. Reactivities were recorded at zero collision energy.

Acetonitrile- $[\text{Au}(\text{PPh}_3)]^+$ adducts formations

Figure 3.16 shows the relative intensities of the product ions ($[\text{Au}(\text{PPh}_3)(\text{CH}_3\text{CN})]^+$ - green, $[\text{Au}(\text{PPh}_3)(\text{CD}_3\text{CN})]^+$ - red, $[\text{Au}(\text{PPh}_3)(\text{CH}_3\text{CH}_2\text{SH})]^+$ - blue) and the parent ion ($[\text{Au}(\text{PPh}_3)]^+$ - black) in the reaction between $[\text{Au}(\text{PPh}_3)]^+$ and acetonitrile- d_0/d_3 . The majority of the data points was recorded under multiple-collision conditions. For instance, at the pressure of 50 μTorr , only about 40% of the parent ions did not react. The rest of the ions collided with the neutrals present in the trap, forming the product ions. If we assume that 60% of the ions collided at least once, then roughly 36% of the ions collided multiple times.⁴⁷

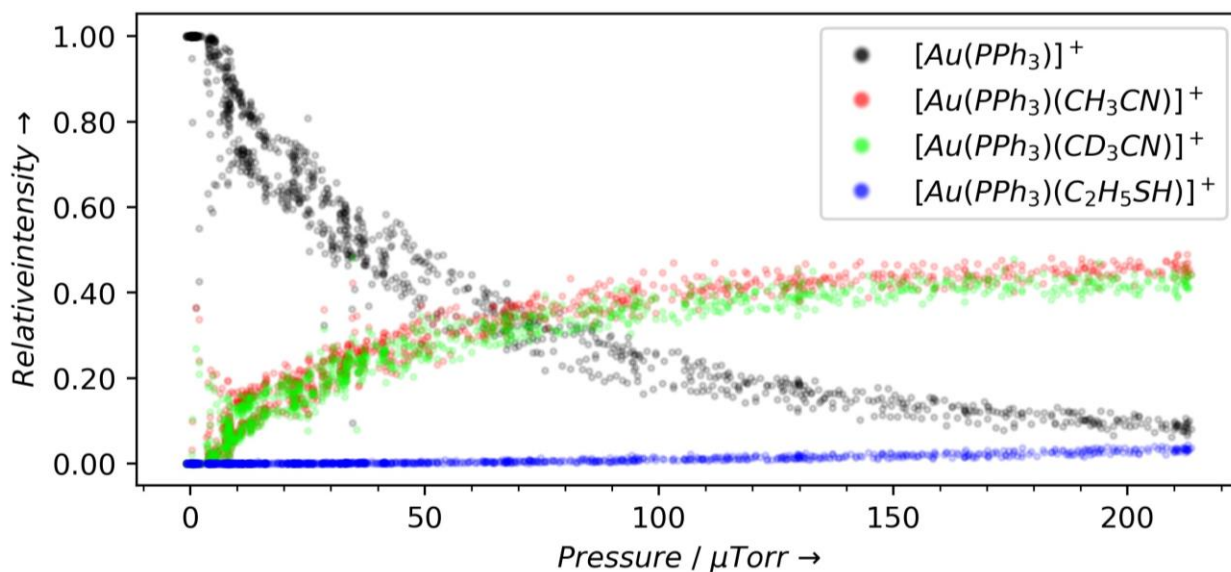


Figure 3.16. Pressure dependence of the formation of the adducts between $[\text{Au}(\text{PPh}_3)]^+$ and molecules of the gas mixture (mainly acetonitrile- d_0/d_3) present in the collision cell.

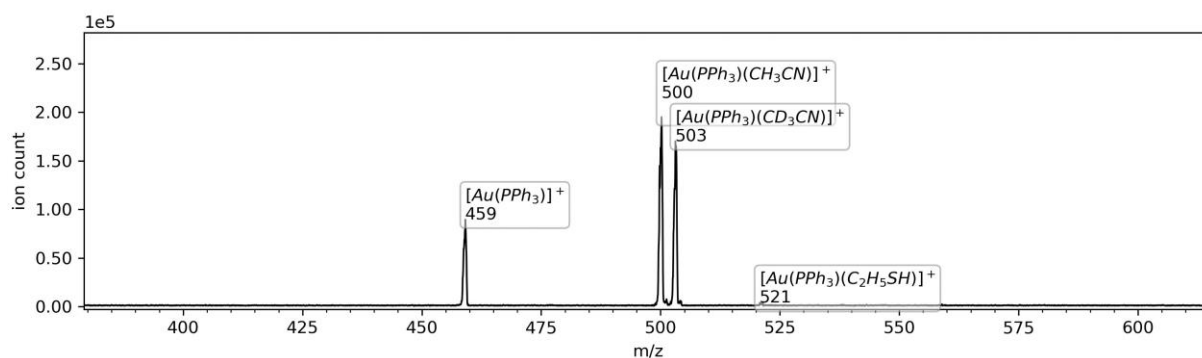


Figure 3.17. Mass spectrum after $[\text{Au}(\text{PPh}_3)]^+$ has passed the gas-mixture present in the collision cell. Spectrum shows that the only compounds present in the collision cell were: acetonitrile- d_0 , acetonitrile- d_3 , and minor traces of probably ethanethiol from recent experiments with this compound on the same instrument.

Pressure-dependent reactivity of the carbanions with acetonitrile

The gas-phase KIEs were determined for a series of gas-phase reactions with the mixture of approximately 1:1 acetonitrile- d_0 :acetonitrile- d_3 . The precise ratio of acetonitrile- d_0/d_3 was determined from adducts formed with $[\text{Au}(\text{PPh}_3)]^+$. A quadratic equation function was fitted to the experimental intensity data of the acetonitrile anions. As one may expect the impact of the depletion of the parent ion and also a substantial contribution of higher-order collisions at higher pressures, the fit was performed in the full data range and separately in a range between 15 and 70 μTorr .⁴⁷ Values of the apparent KIEs were determined from the ratio of slopes of these fits at zero pressure. Values were then compensated for the precise acetonitrile- d_0/d_3 ratio. The KIE was determined as an average of three individually measured data sets, and the error was arbitrarily defined to be either ± 0.5 or ± 1 based on the difference between the data sets, evaluations (fits to the restricted and full-range), and the apparent quality of the underlying data (signal-to-noise, spread). The error range was set arbitrarily as the statistically calculated error of the average may be misleading in this case due to a substantial overestimation of the quality of the underlying data.

Pressure-dependent reactivity of 3,5-dimethoxybenzyl anion (**1f**) with acetonitrile

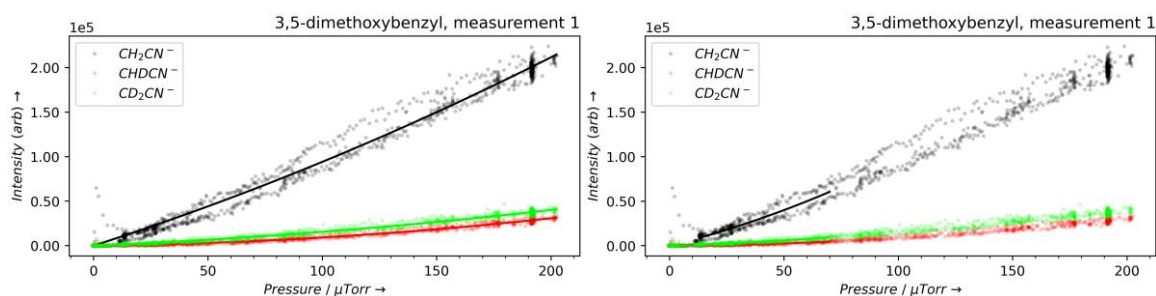


Figure 3.18. Pressure dependence of the selected ions intensities in the gas-phase reaction of carbanion **1f** with acetonitrile- d_0/d_3 (1:1), measurement 1. Uncorrected KIE ratio: 7.49 (7.28 for fitting between 15 and 70 μTorr). The ratio corrected for the precise acetonitrile concentration was 6.56 (6.37 for the smaller fitting region).

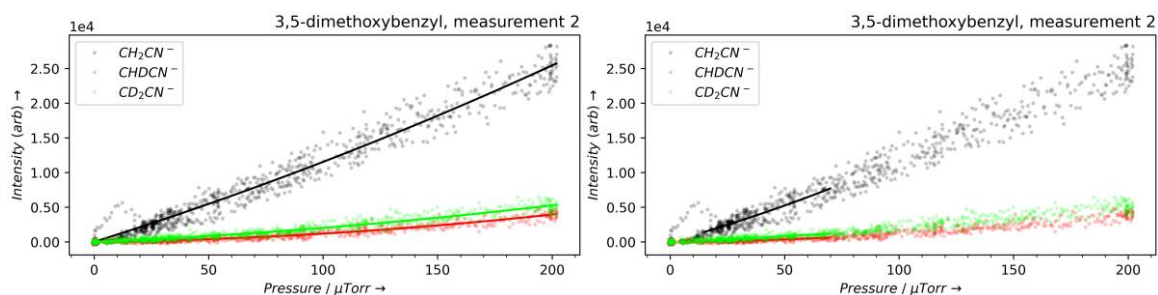


Figure 3.19. Pressure dependence of the selected ion intensities in the gas-phase reaction of carbanion **1f**⁻ with acetonitrile-*d*₀/*d*₃ (1:1), measurement 2. Uncorrected KIE ratio: 7.36 (6.59 for fitting between 15 and 70 μTorr). The ratio corrected for the precise acetonitrile concentration was 6.71 (6.00 for the smaller fitting region).

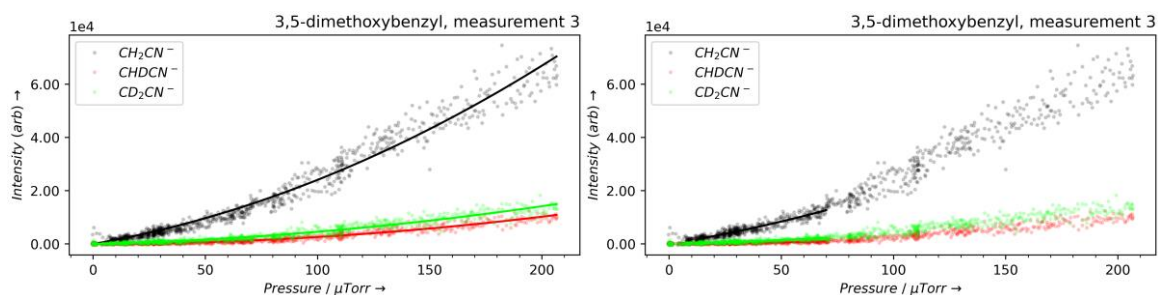


Figure 3.20. Pressure dependence of the selected ion intensities in the gas-phase reaction of carbanion **1f**⁻ with acetonitrile-*d*₀/*d*₃ (1:1), measurement 3. Uncorrected KIE ratio: 7.06 (6.79 for fitting between 15 and 70 μTorr). The ratio corrected for the precise acetonitrile concentration was 6.76 (6.50 for the smaller fitting region).

Based on three independently recorded datasets, the experimental KIE observed in the gas-phase reaction of carbanion **1f**⁻ with acetonitrile is 6.5 ± 0.5 .

Pressure-dependent reactivity of *p*-methoxybenzyl anion (**1i**⁻) with acetonitrile

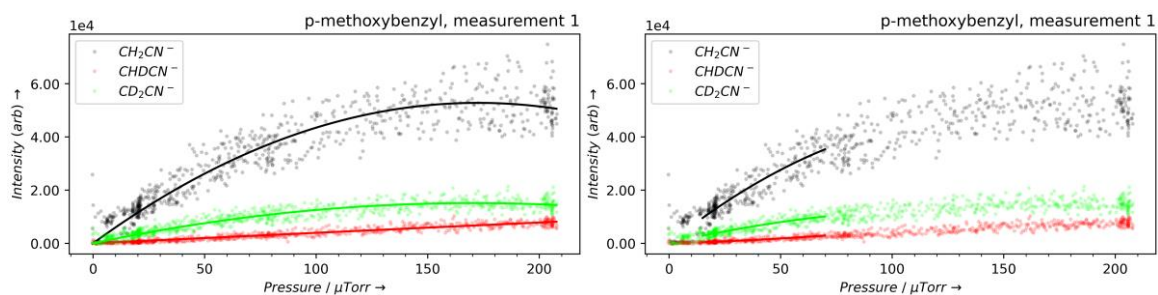


Figure 3.21. Pressure dependence of the selected ion intensities in the gas-phase reaction of carbanion **1i**⁻ with acetonitrile-*d*₀/*d*₃ (1:1), measurement 1. Uncorrected KIE ratio: 3.46 (3.39 for fitting between 15 and 70 μTorr). The ratio corrected for the precise acetonitrile concentration was 3.15 (3.09 for the smaller fitting region).

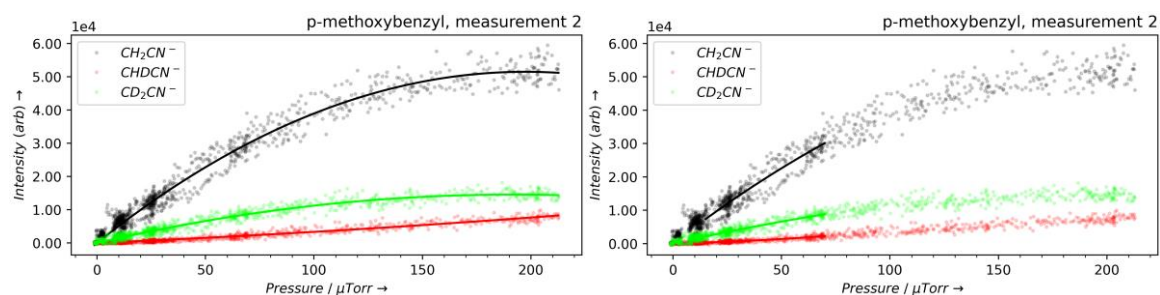


Figure 3.22. Pressure dependence of the selected ion intensities in the gas-phase reaction of carbanion **1i**⁻ with acetonitrile-*d*₀/*d*₃ (1:1), measurement 2. Uncorrected KIE ratio: 3.44 (3.44 for fitting between 15 and 70 μTorr). The ratio corrected for the precise acetonitrile concentration was 3.13 (3.13 for the smaller fitting region).

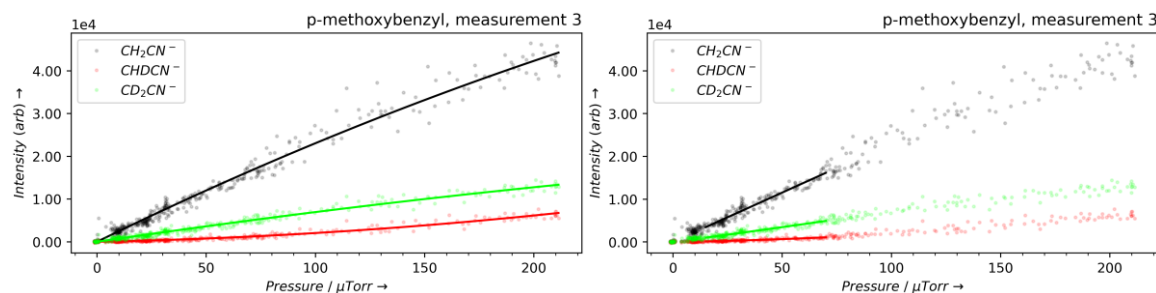


Figure 3.23. Pressure dependence of the selected ion intensities in the gas-phase reaction of carbanion **1i**⁻ with acetonitrile-*d*₀/*d*₃ (1:1), measurement 3. Uncorrected KIE ratio: 3.32 (3.45 for fitting between 15 and 70 μTorr). The ratio corrected for the precise acetonitrile concentration was 3.18 (3.30 for the smaller fitting region).

Based on three independently recorded datasets, the experimental KIE observed in the gas-phase reaction of carbanion **1c**⁻ with acetonitrile is 3.2 ± 0.5 .

Pressure-dependent reactivity of *p*-methoxy- α -methylbenzyl anion (**1b**⁻) with acetonitrile

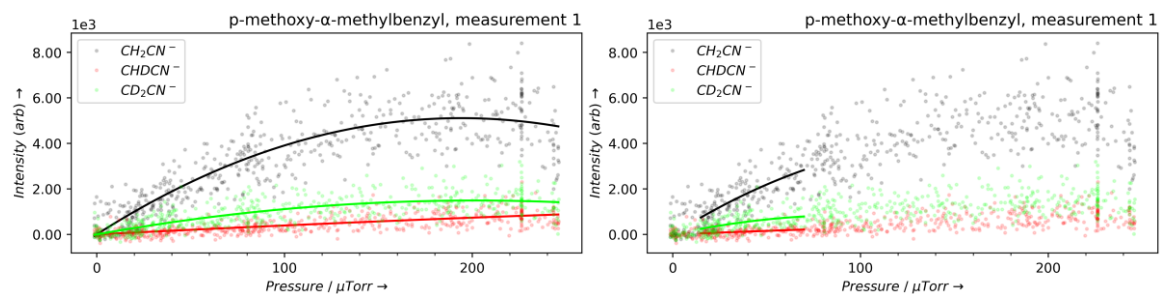


Figure 3.24. Pressure dependence of the selected ion intensities in the gas-phase reaction of carbanion **1b**⁻ with acetonitrile-*d*₀/*d*₃ (1:1), measurement 1. Uncorrected KIE ratio: 3.56 (2.92 for fitting between 15 and 70 μTorr). The ratio corrected for the precise acetonitrile concentration was 3.25 (2.67 for the smaller fitting region).

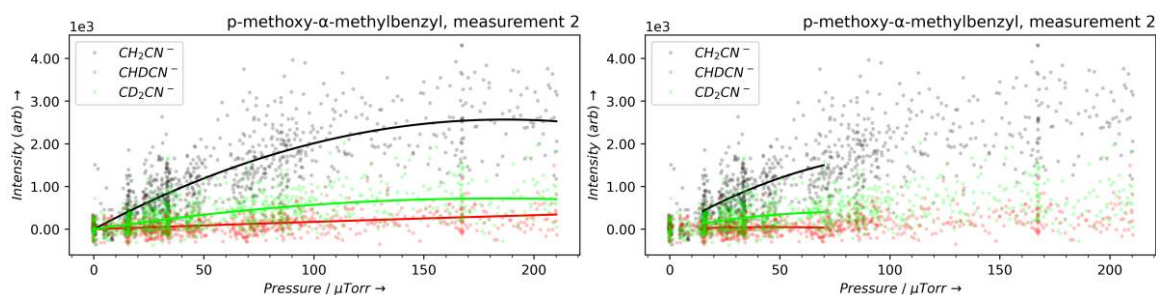


Figure 3.25. Pressure dependence of the selected ion intensities in the gas-phase reaction of carbanion **1b**⁻ with acetonitrile-*d*₀/*d*₃ (1:1), measurement 2. Uncorrected KIE ratio: 3.49 (3.01 for fitting between 15 and 70 μTorr). The ratio corrected for the precise acetonitrile concentration was 3.18 (2.74 for the smaller fitting region).

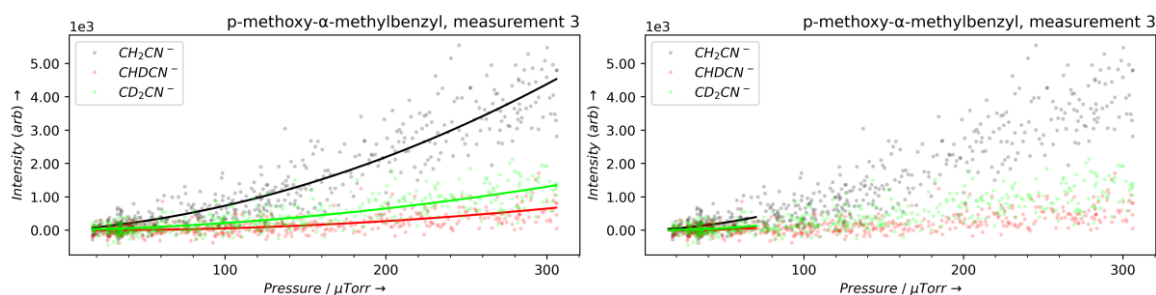


Figure 3.26. Pressure dependence of the selected ion intensities in the gas-phase reaction of carbanion **1b**⁻ with acetonitrile-*d*₀/*d*₃ (1:1), measurement 3. Uncorrected KIE ratio: 3.45 (-3.86 for fitting between 15 and 70 μTorr). Ratio corrected for the precise acetonitrile concentration was 3.30 (-3.70 for the smaller fitting region).

Based on three independently recorded datasets, the experimental KIE observed in the gas-phase reaction of *p*-methoxy- α -methylbenzyl anion with acetonitrile is 3.0 ± 1.0 (the evaluation of the third dataset in the smaller fitting region was omitted from averaging).

Pressure-dependent reactivity of 1,2,3,4-tetrahydronaphthyl anion (**1c**⁻) with acetonitrile

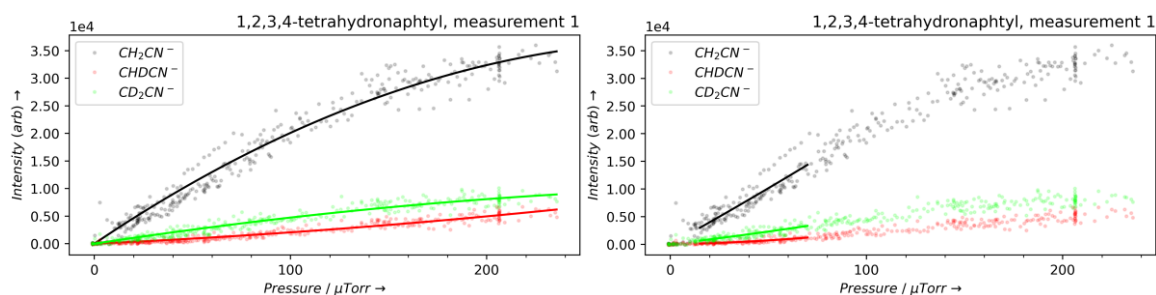


Figure 3.27. Pressure dependence of the selected ion intensities in the gas-phase reaction of carbanion **1c**⁻ with acetonitrile-*d*₀/*d*₃ (1:1), measurement 1. Uncorrected KIE ratio: 4.42 (4.59 for fitting between 15 and 70 μTorr). The ratio corrected for the precise acetonitrile concentration was 3.86 (4.02 for the smaller fitting region).

REACTIVITY OF SUPERBASIC CARBANIONS GENERATED VIA REDUCTIVE RADICAL-POLAR CROSSOVER IN THE CONTEXT OF PHOTOREDOX CATALYSIS

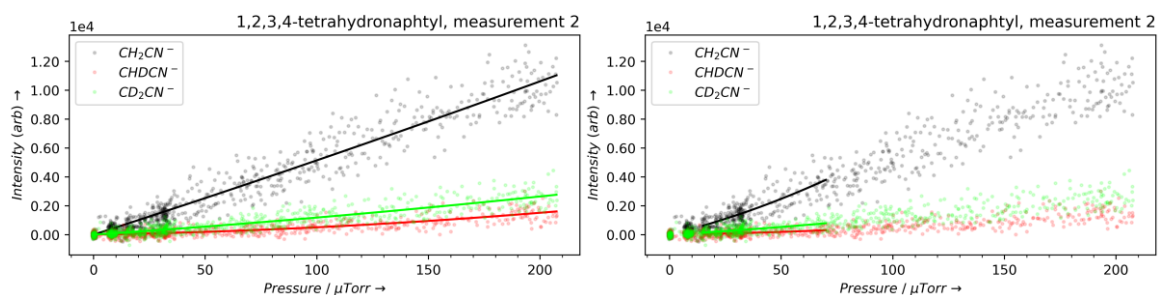


Figure 3.28. Pressure dependence of the selected ion intensities in the gas-phase reaction of carbanion **1c⁻** with acetonitrile-*d*₀/*d*₃ (1:1), measurement 2. Uncorrected KIE ratio: 4.77 (4.18 for fitting between 15 and 70 μTorr). The ratio corrected for the precise acetonitrile concentration was 4.35 (3.80 for the smaller fitting region).

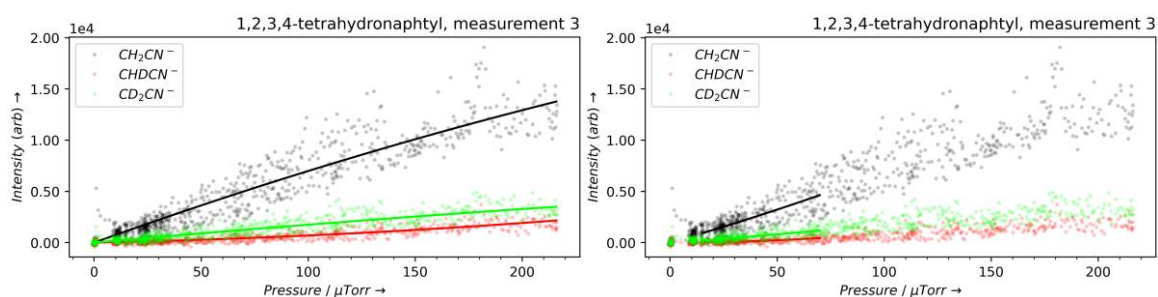


Figure 3.29. Pressure dependence of the selected ion intensities in the gas-phase reaction of carbanion **1c⁻** with acetonitrile-*d*₀/*d*₃ (1:1), measurement 3. Uncorrected KIE ratio: 4.04 (4.39 for fitting between 15 and 70 μTorr). The ratio corrected for the precise acetonitrile concentration was 3.87 (4.20 for the smaller fitting region).

Based on three independently recorded datasets, the experimental KIE observed in the gas-phase reaction of carbanion **1c⁻** with acetonitrile is 4.0 ± 0.5 .

3.4.7 Isotopic labelling of substrates and solvents

Isotopic labelling of benzylic C-H bonds was conducted according to general procedures 3-G and 3-H for carbanion generation. Unless otherwise noted, deuteration degrees were determined via ^1H NMR spectroscopy. In isotopic fractionation experiments deuteration degrees were determined via mass spectrometry. Depending on whether deuteration occurred via C-H activation (general procedure 3-G) or from carboxylates or trifluoroborates (general procedure 3-H) different approaches for the determination of the deuteration degree via ^1H NMR spectroscopy were used.

Chemical shifts of benzylic protons differ slightly for non-deuterated compounds compared to mono-deuterated compounds. Thus, where only mono-deuteration was observed the degree of deuteration was determined by the ratio of the integrals of benzylic protons corrected by the number of benzylic protons of the respective molecule. Due to partly overlapping signals, the mldcon -pp function of TopSpin 4.3.0 was used to deconvolute the signals. This is exemplarily shown in Figure 3.30 for toluene derivative **1f**. **1f-d₀** has a singlet at 2.27 ppm and **1f-d₁** a triplet at 2.25 ppm with $J = 2.2$ Hz.

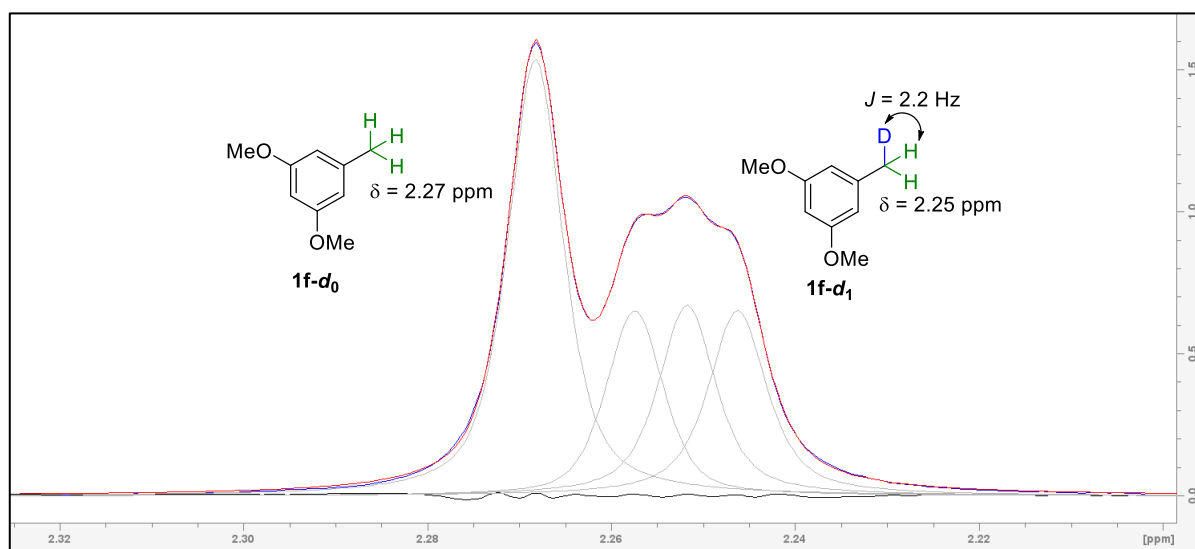


Figure 3.30. Section of the ^1H NMR spectrum showing the signals for the benzylic protons of toluene derivative **1f** with a deuteration degree of 67% (Scheme 3.15, entry 1, 0.5 h). blue: original spectrum; green: individual singlets obtained for each peak by deconvolution; red: sum of singlets from deconvolution; black: residuals.

The deuteration degree of **1f** from Figure 3.30 was determined as follows:

$$\%D = \frac{\frac{\text{integrals}(\mathbf{1f-d}_1)}{\text{benzylic H } \mathbf{1f-d}_1}}{\frac{\text{integral}(\mathbf{1f-d}_0)}{\text{benzylic H } \mathbf{1f-d}_0} + \frac{\text{integrals}(\mathbf{1f-d}_1)}{\text{benzylic H } \mathbf{1f-d}_1}} * 100\% = \frac{\frac{8023886}{2}}{\frac{5983259}{3} + \frac{8023886}{2}} * 100\% = 67\%$$

Integral for **1f-d₀**: 5983259

Integrals for **1f-d₁**: 2707330 + 2629666 + 2686890 = 8023886

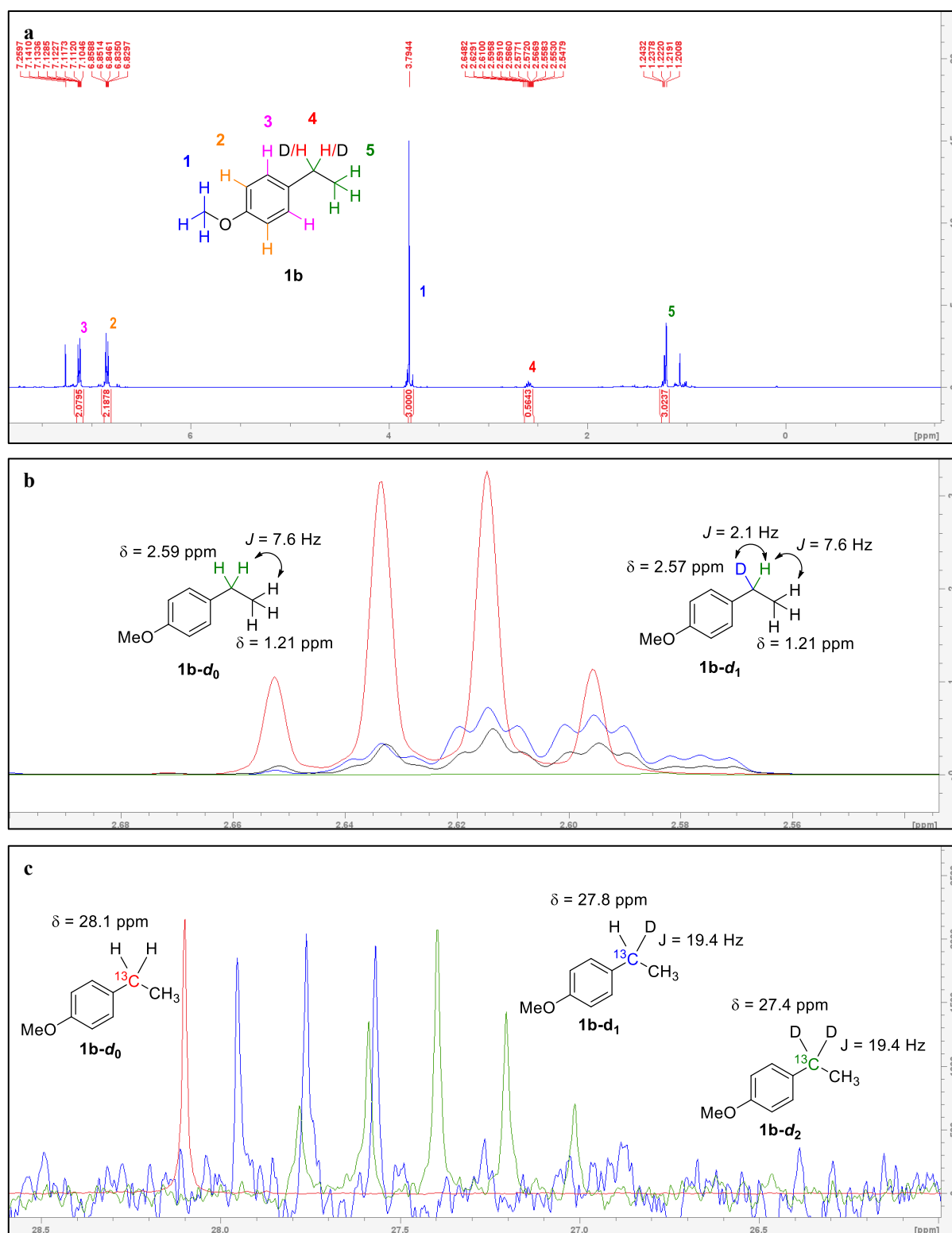


Figure 3.31. a: Mixture of **1b-d₁**, **1b-d₂**, and traces of **1b-d₀** obtained under C-H deuteration conditions according to general procedure 3-G in acetonitrile-*d*₃. b: Section of the ¹H NMR spectra showing the signals for the benzylic protons of ethyl anisole (**1b**) with different deuteration pattern. Red: non-deuterated compound **1b-d₀**; blue: **1b-d₁** with >95% mono-deuteration; black: section of the ¹H NMR showing the benzylic protons of a mixture of **1b-d₀**, **1b-d₁**, and **1b-d₂** depicted in a; green: double-deuterated compound **1b-d₂**; The spectra are scaled to represent the relative intensities at same concentrations. c: section of the ¹³C NMR spectra showing the signal for the benzylic carbon. Red: non-deuterated compound **1b-d₀**; blue: mono-deuterated compound **1b-d₁**; green: double deuterated compound **1b-d₂**. Intensities of the ¹³C signals do not represent the relative intensities.

Deuteration degrees of compounds where additional coupling to neighboring protons is present, multiple hydrogen atoms can be exchanged by C-H activation, or only a single C-H bond is present could not be analyzed by comparing the integrals of non-deuterated compound to deuterated compound. Instead, the deuteration degree was determined from the decrease in the integral upon deuteration. However, the need for non-overlapping reference integrals makes this method more prone to errors from other molecules present in the reaction mixture (catalysts and traces of side products).

Figure 3.31a shows the ^1H spectrum of ethyl anisole (**1b**) as a mixture of **1b-d₀**, **1b-d₁**, and **1b-d₂** as obtained under C-H deuteration conditions according to general procedure 3-G in acetonitrile- d_3 . The section for the benzylic protons at different deuteration degrees and deuterium distribution is depicted in Figure 3.31b. **1b-d₀** gives a quartet at 2.59 ppm with $J = 7.6$ Hz, **1b-d₁** gives a quartet of triplets at 2.57 Hz with $J = 7.6$ Hz and $J = 2.1$ Hz, and **1b-d₂** has no benzylic hydrogen atoms and thus does not give a signal in the depicted range of the ^1H NMR spectrum. Thus, the difference between the blue line (**1b-d₁**) and the black line (mixture of **1b-d₁** and **1b-d₂**) corresponds to the relative concentration of **1b-d₂**.

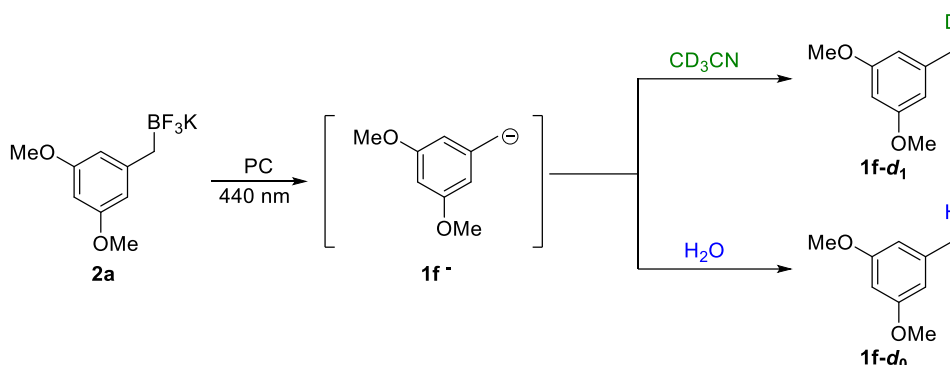
The deuteration degree of **1b** from Figure 3.31a was determined as follows:

$$\%D = \left(1 - \frac{\text{integral}(\mathbf{1b})}{\text{number of benzylic H in } \mathbf{1b-d_0}} \right) * 100\% = \left(1 - \frac{0.5643}{2} \right) * 100\% = 72\%$$

The integral for the methoxy group was used as reference and set to 3.0000.

3.4.7.1 Deuteration of photocatalytically generated carbanions by solvents

Influence of reaction time and residual moisture



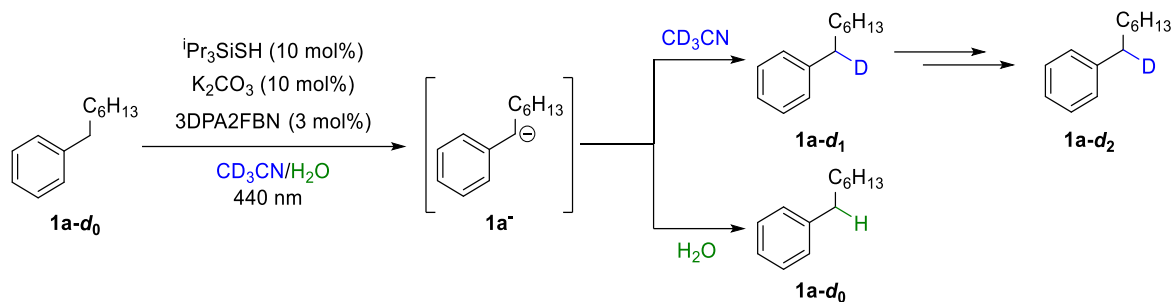
Reaction time:	Entry	0.5 h	1 h	2 h	3 h	4 h	24 h
Dry solvent, dry vial	1	67%	86%	86%	79%		
	2	81%	88%	90%	90%	92%	
	3	80%	87%		90%	90%	
Non-dried solvent	4	67%		74%		76%	78%
Non-dried vial	5	64%		74%		75%	74%

Scheme 3.15. Deuteration of carbanion $1f^-$ competes with protonation by residual moisture. If solvent or reaction vial are not dried the degree of deuteration is lower. PC – photocatalyst 4CzIPN was used as pre-catalyst. The active photocatalyst **4c** was formed in situ.

The degree of deuteration is lower in the beginning of the reaction, which may be attributed to residual protons in the system which are more reactive than acetonitrile, as evidenced by a slightly lower degree of deuteration, in case solvents or reaction vials are not dried properly. After full conversion of the substrate (after 1 – 2 h) the degree of deuteration does not change with prolonged reaction time. Thus, reaction times of at least 2 h guarantee maximal deuteration.

Influence of water on solvent deprotonation

The interfering influence of water on deuterium abstraction by photocatalytically generated carbanions from acetonitrile was investigated following the general procedure 3-G in presence of different concentrations of water. At low H_2O concentrations deuterium incorporation was constantly high. Only at 1 equivalent H_2O the deuterium incorporation started to drop noticeably and linearly with the ratio of $H_2O:CD_3CN$. Therefore, the carbanions have a high reactivity abstracting deuterons from CD_3CN even in the presence of moderate amounts of water.



equiv. H ₂ O	0.00	0.10	0.20	0.25	0.50	1.00	2.50	5.00
H ₂ O/CD ₃ CN	0.00	1.91×10^{-5}	3.83×10^{-5}	4.79×10^{-5}	9.57×10^{-5}	1.91×10^{-4}	4.79×10^{-4}	9.57×10^{-4}
H/D product	0.28	0.32	0.26	0.20	0.39	0.84	3.50	7.47

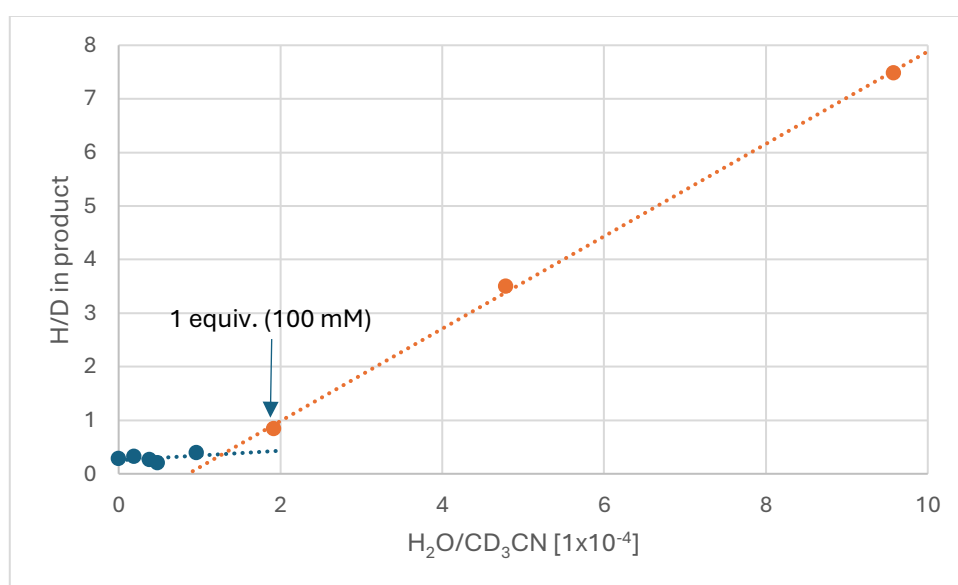
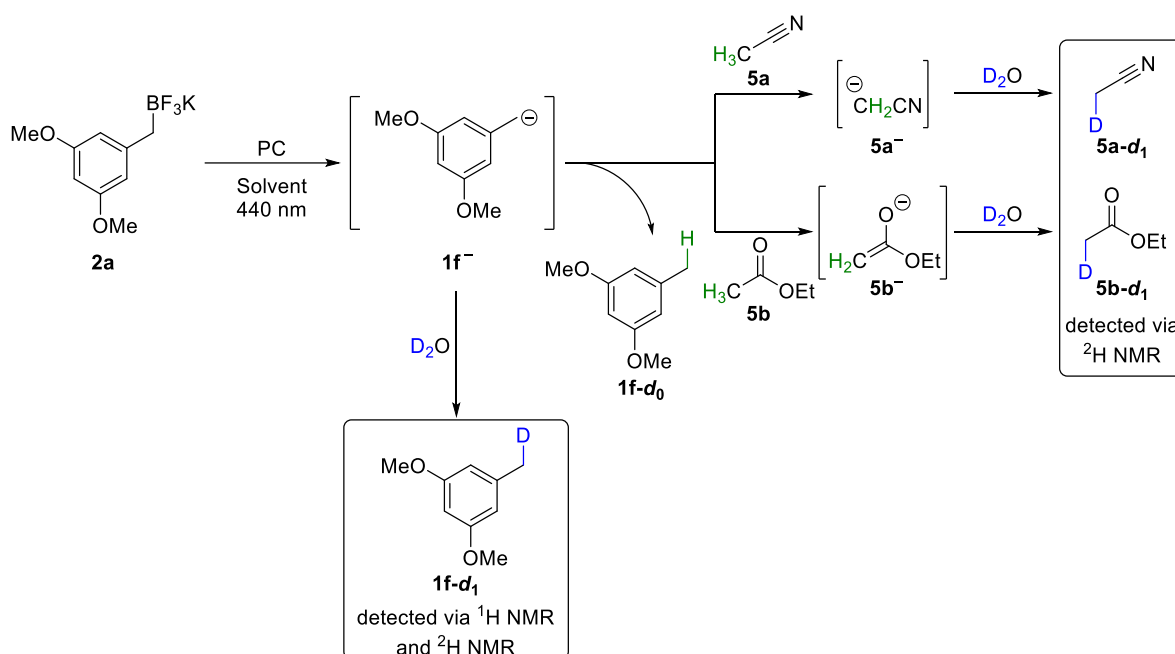


Figure 3.32. At low H₂O concentrations deuterium incorporation via D⁺ abstraction by **1a⁻** from the solvent CD₃CN is high. At H₂O concentrations higher than 100 mM the ratio between protons and deuterium at the benzylic position increases linearly with increasing ratio H₂O/CD₃CN.

3.4.7.2 Deuterium labelling of acetonitrile and ethyl acetate

Abstraction of a proton or deuteron from the solvent generates a solvent anion. While this is the species directly observed in our gas-phase reactions (section 3.4.6), its high basicity makes a direct observation in solution difficult. Its indirect observation can be achieved by adding D₂O to the reaction depicted in Scheme 3.16 in CH₃CN and ethyl acetate, respectively, and recording the corresponding ²H NMR spectra. 1 equivalent of D₂O with respect to the formed carbanions was used to have solvent deprotonation as a major carbanion quenching pathway, while offering enough D⁺ to deuterate all solvent anions that might form under these conditions. In acetonitrile as well as in ethyl acetate the mono-deuterated solvent **5a-d₁** and **5b-d₁**, respectively, and mono-deuterated toluene derivative as the major deuterium containing products could be observed. To note, deuteration of ethyl acetate under these conditions explains why intermolecular addition to esters is not observed.



Scheme 3.16. Photocatalytically generated carbanions can deprotonate acetonitrile and ethyl acetate. Deprotonated solvents are deuterated by D₂O to indirectly prove their formation. Reactions were performed according to general procedure 3-H in acetonitrile and ethyl acetate, respectively. PC – 4CzIPN was used as a pre-catalyst to generate the active photocatalyst via photosubstitution in situ as described in chapter 2.

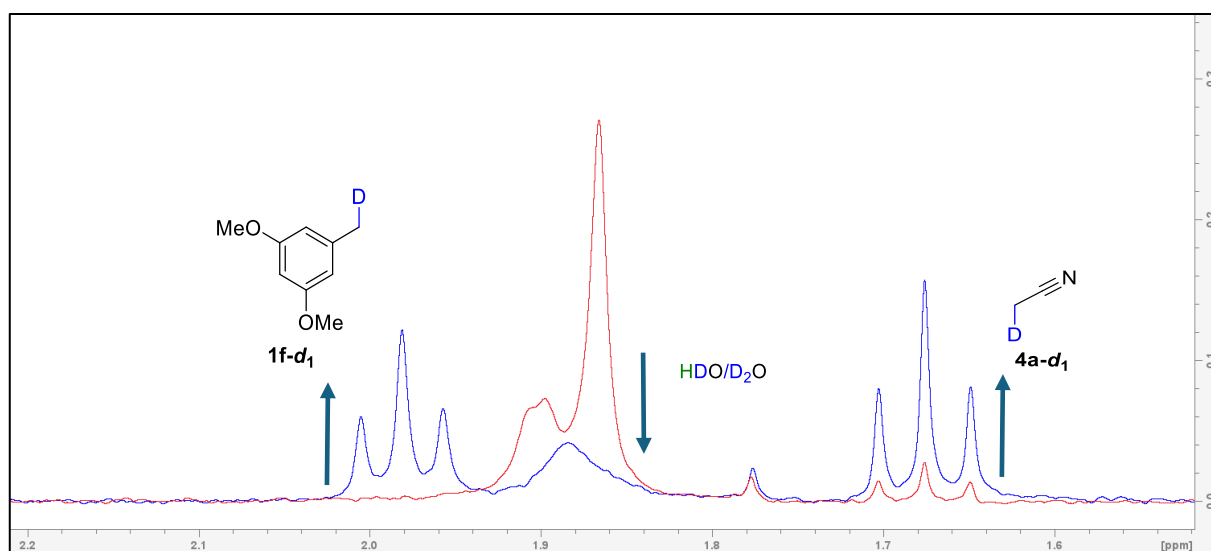


Figure 3.33. When generating carbanion **1f⁻** in CH₃CN in presence of 1 equiv. D₂O with respect to the formed carbanions the corresponding toluene derivative **1f-d₁** and mono-deuterated MeCN (**4a-d₁**) are formed as evident by the ²H NMR spectra before (red) and after irradiation (blue) in presence of D₂O. Arrows indicate emerging (up) and decreasing (down) signals.

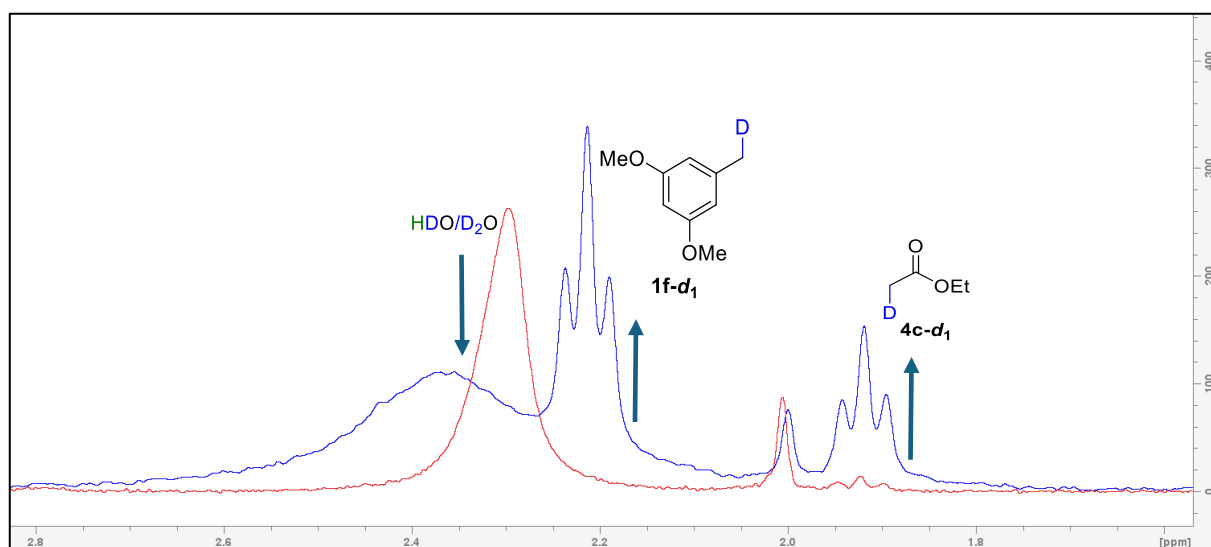


Figure 3.34. When generating carbanion **1f⁻** in ethyl acetate in presence of 1 equiv. D₂O with respect to the formed carbanions the corresponding toluene derivative **1f-d₁** and mono-deuterated ethyl acetate (**4a-d₁**) are formed as evident by the ²H NMR spectra before (red) and after irradiation (blue) in presence of D₂O. Arrows indicate emerging (up) and decreasing (down) signals.

3.4.8 Kinetic isotope effects and isotopic fractionation

Kinetic isotope effects (KIEs) provide valuable mechanistic information about bond-forming and bond-cleaving elementary steps. In classical catalysis, KIEs can tell whether the isotopically labelled bond is involved in the rate-determining step. In photocatalysis, these steps often occur from high energy intermediates after an electron transfer from or to the excited photocatalyst and are not rate limiting. Additionally, other factors such as poorly dissolving solid components (in our case K_2CO_3), photobleaching, photosubstitution of the photocatalyst and fluctuating light intensity can strongly influence rate constants.

Thus, only competitive KIEs were determined, which are not limited to rate determining steps and insensitive to reaction parameters such as light intensity or incompletely dissolved solid K_2CO_3 .

3.4.8.1 Kinetic isotope effects of carbanion protonation

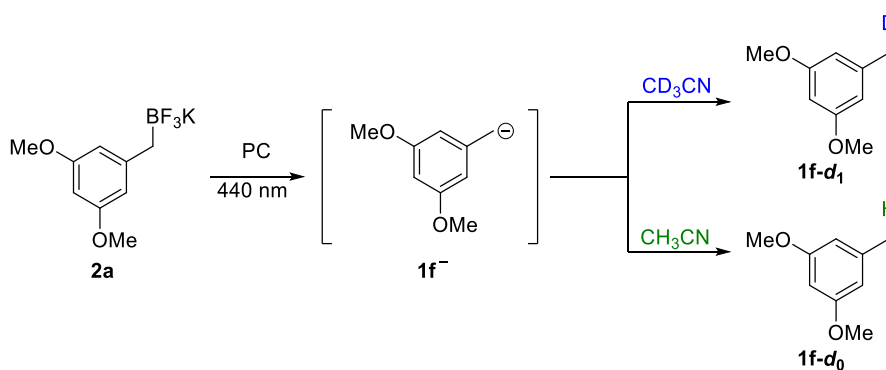
Reactions for measuring KIEs of carbanion protonation were set up on 100 μ mol scale in 1 mL solvent. All solvents were dried over molecular sieves.

Potassium trifluoro(3,5-dimethoxybenzyl)borate (**2a**, 25.8 mg, 100 μ mol) and 4CzIPN (**4a**, 3.9 mg, 5 μ mol, 5 mol%) were placed in a 6 mL crimp-capped vial and sealed. The vial was evacuated and backfilled with nitrogen 3 times via cannula. Solvent (1 mL) and the additional proton/deuterium source were added. Solvent mixtures of non-deuterated and deuterated solvents were used without an additional proton/deuterium source if the KIE of solvent deprotonation was measured. For determining the KIE in the protonation by water the reaction was performed in CH_3CN and 50 μ L mixtures of H_2O/D_2O were added. Reactions were irradiated at 451 nm for at least 2 h in acetonitrile and at least 4 h in other solvents. Solvents were then removed under reduced pressure (reactions in MeCN and acetone). The minimum pressure was set to 120 mbar at 40 °C heating to avoid evaporation of the product. Full removal of the solvent was not necessary as only the ratio of protonated to deuterated product was determined. The degree of deuteration was determined via 1H NMR spectroscopy in $CDCl_3$ or via mass spectrometry, as specified. H/D-ratios of the products were plotted against the H/D-ratios of the H/D-reservoir (solvent or added H_2O/D_2O) and the KIE determined from the slope.

Calculated H/D ratios are based on the single H/D-atom that is incorporated during the reaction. Deuterated product contains a CH_2D group and non-deuterated product contains a CH_3 group. This differs from the isotopic fractionation method in section 3.4.8.3 where 2 benzylic protons are exchanged.

Benzyltrifluoroborate **2a** was used as model substrate for various reasons: The methoxy groups act as a reference point in the NMR spectrum, an up-field shift of the aromatic protons reduce overlap with aromatic protons of the photocatalyst or the $CDCl_3$ residual peak, and volatility of the corresponding toluene derivative is sufficiently reduced to allow easy removal of the solvent after the reaction without evaporating too much of the compound.

Kinetic isotope effect determination for deprotonation of acetonitrile



Scheme 3.17. Carbanion **1f⁻** generated from trifluoroborate **2a** deprotonates acetonitrile. The KIE for the deprotonation was determined from the H/D ratio in toluene derivative **1f** in a mixture of acetonitrile-*d*₀/*d*₃. PC – Photocatalyst 4CzIPN was used as pre-catalyst to generate the active photocatalyst **4c** in situ upon photosubstitution as described in chapter 2.

Values were determined via mass spectrometry and corrected for background protonation from traces of additional protons. Values are corrected by subtraction of the protonated product at 100% deuterated solvent (17% H) from the other values.

$\text{CH}_3\text{CN}/\text{CD}_3\text{CN}$	3.00	1.00	0.33	0.05	0.00
H/D product	26.06	11.88	4.22	0.61	0.00

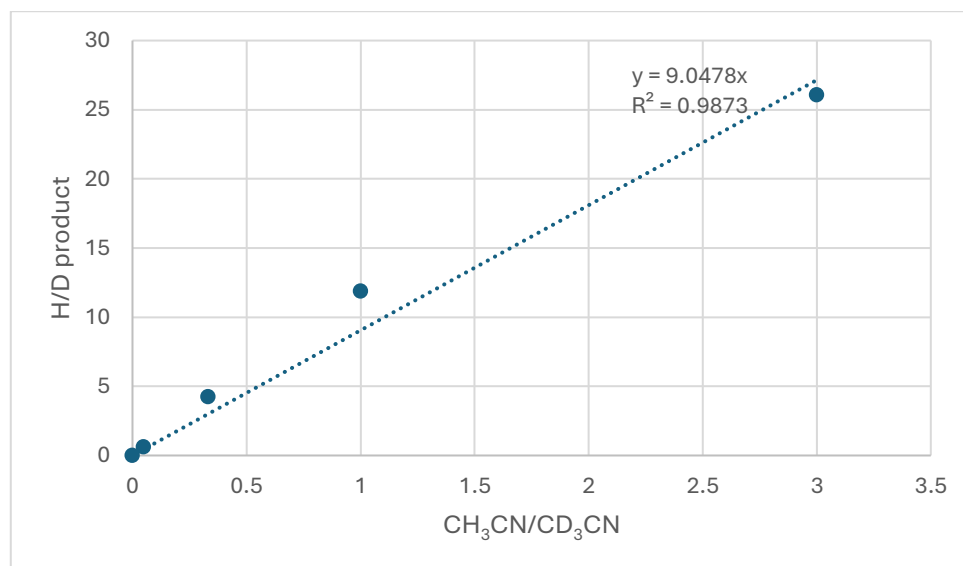
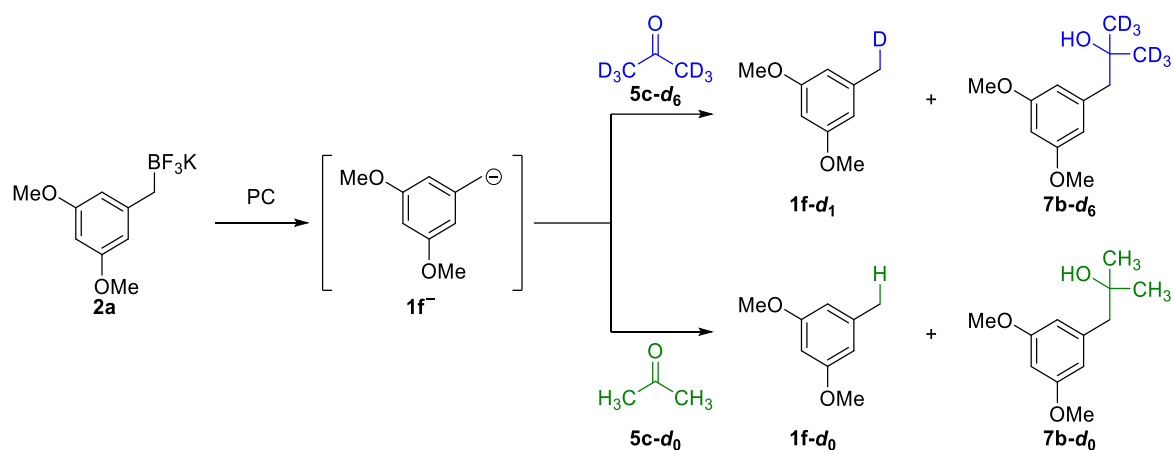


Figure 3.35. Determination of the KIE for deprotonation of acetonitrile by carbanion **1f⁻**.

Kinetic isotope effect determination for deprotonation of acetone



Scheme 3.18. Carbanion **1f⁻** reacts with acetone via nucleophilic addition to the carbonyl group or via deprotonation in the α -position. PC – Photocatalyst 4CzIPN was used as pre-catalyst to generate the active photocatalyst **4c** in situ upon photosubstitution as described in chapter 2.

Reactions were performed analogously as in the case of acetonitrile as solvent. Beside deprotonation also nucleophilic addition to the carbonyl group occurred. Values were determined via mass spectrometry and corrected for background protonation from traces of additional protons. Values are corrected by subtraction of the protonated product at 100% deuterated solvent (9% H) from the other values.

For deprotonation, a moderate KIE of 1.4 is observed.

Acetone- d_0/d_6	3.00	2.00	1.00	0.33	0.10	0.00
H/D product	4.35	2.32	1.40	0.47	0.01	0.00

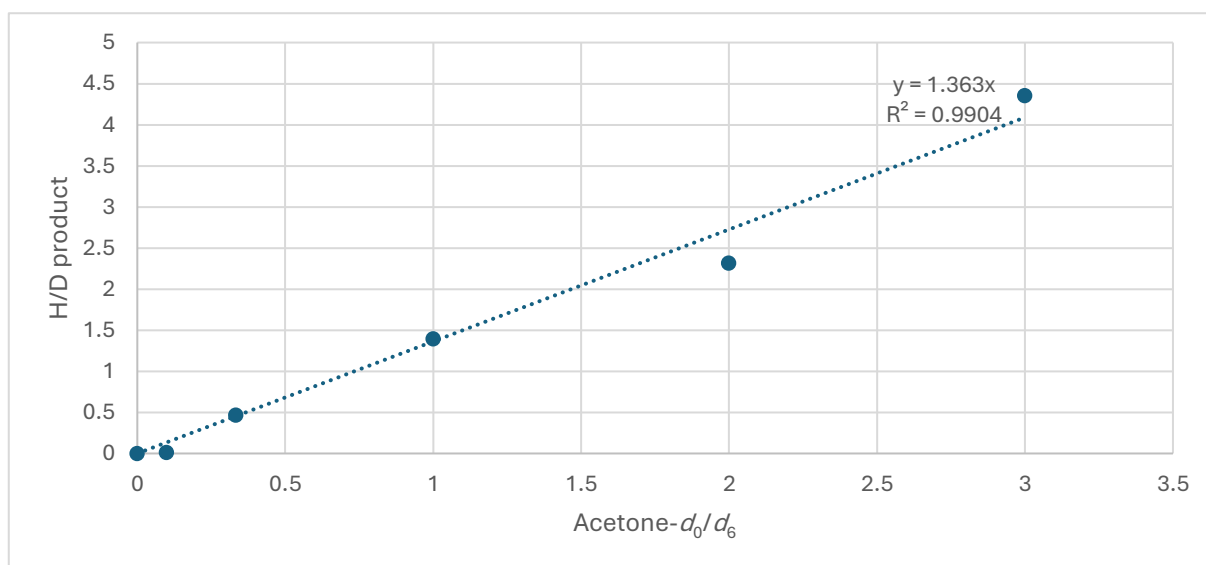


Figure 3.36. Determination of the KIE for deprotonation of acetone by carbanion **1f⁻**.

For nucleophilic addition of carbanion **1f**⁻ to acetone no KIE (1.0) is observed. The datapoint for nucleophilic addition at acetone- d_0/d_3 ratio of 3 is deviating from an expected linear correlation and thus may represent an outlier. Excluding this point from the KIE evaluation gives a value of 1.2. Due to slightly different GC-retention times and fragmentation pattern for the isotopomers these results give only a crude estimate. Result of no or only small KIEs is within expectations for a secondary kinetic isotope effect.

Products with intermediate deuteration degrees between d_0 and d_6 were not observed to notable extent under the reaction conditions. Thus, scrambling of deuterium and hydrogen between acetone- d_0 and acetone- d_6 likely does not have a considerable effect on the obtained KIE values.

Acetone d_0/d_6	3.00	2.00	1.00	0.33	0.10	0.00
H/D product	2.62	2.40	1.20	0.42	0.17	0.00

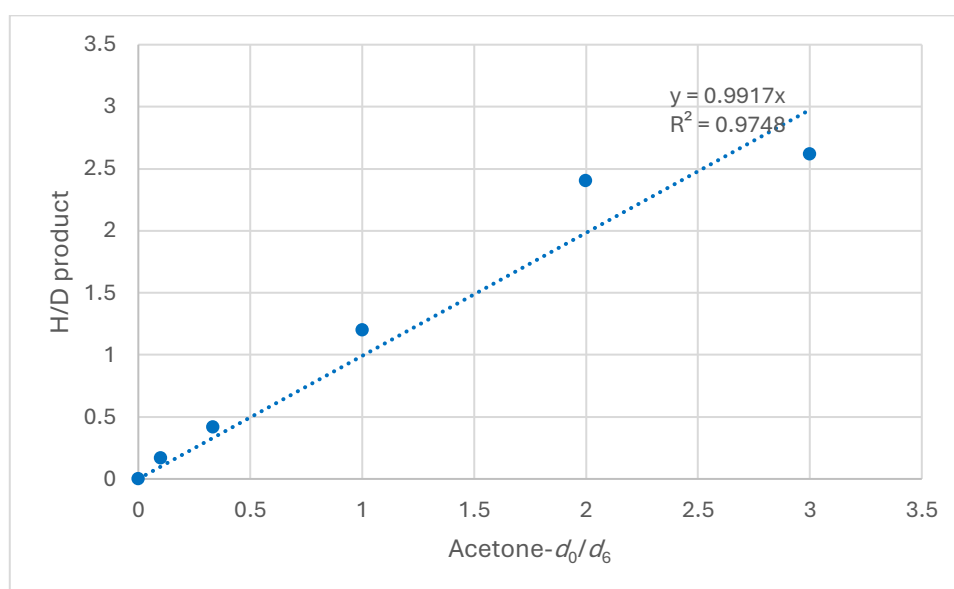
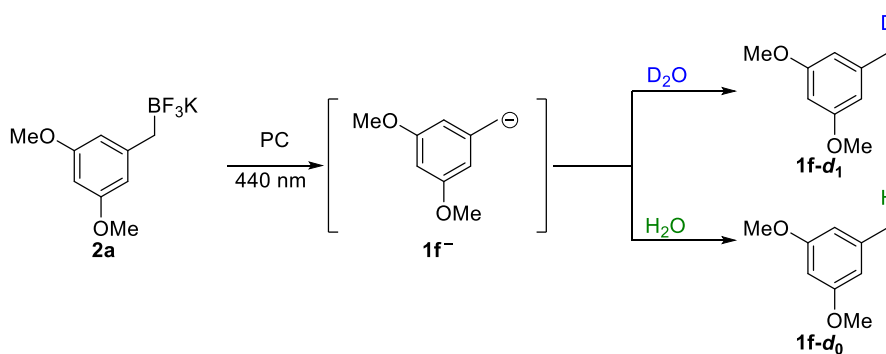


Figure 3.37. Determination of the KIE for addition of carbanion **1f**⁻ to acetone.

Kinetic isotope effect determination for deprotonation of water



Scheme 3.19. Carbanion $1f^-$ generated from trifluoroborate $2a$ deprotonates water. The KIE for the deprotonation was determined from the H/D ratio of toluene derivative $1f$ in a mixture of H_2O/D_2O . PC – Photocatalyst 4CzIPN was used as pre-catalyst to generate the active photocatalyst $4c$ in situ upon photosubstitution as described in chapter 2.

H_2O/D_2O	3.00	1.00	1.00	0.33	0.00
H/D product	4.34	1.47	1.48	0.50	0.00

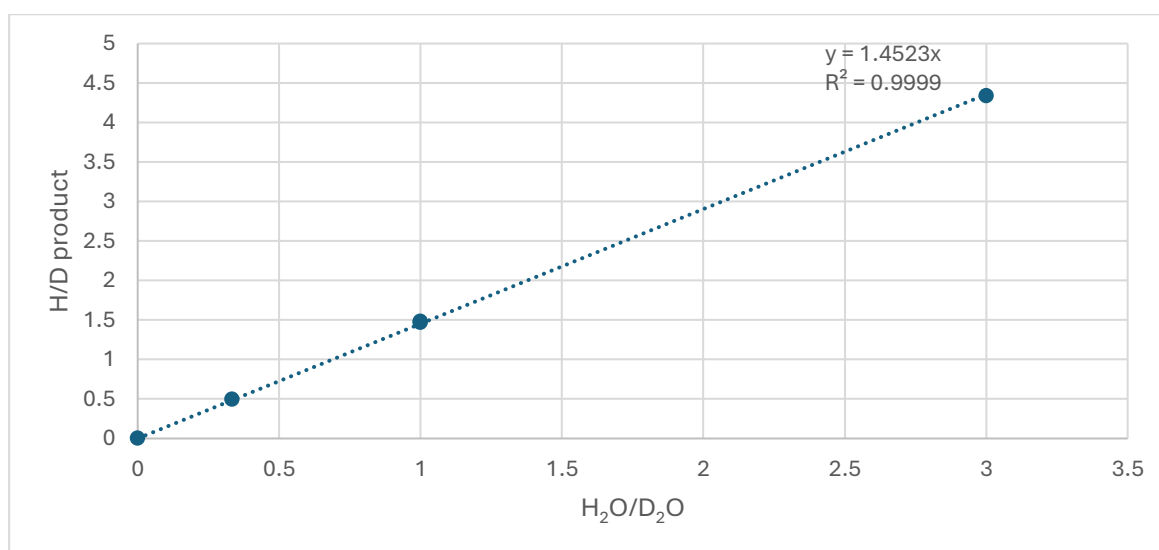
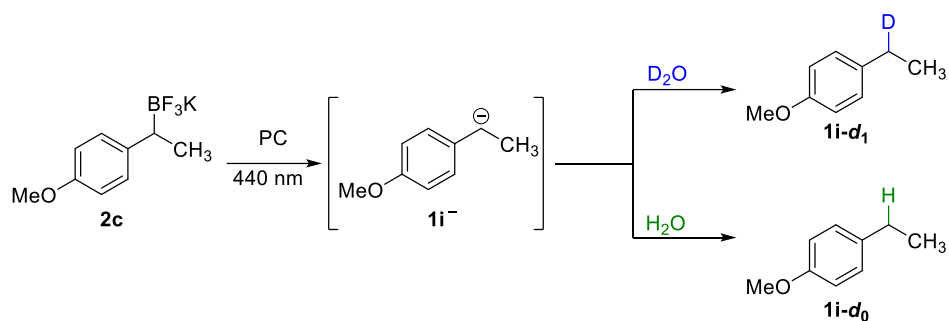


Figure 3.38. Determination of the KIE for deprotonation of water by carbanion $1f^-$.

Values were determined via mass spectrometry and corrected for background protonation from traces of additional protons. Values were corrected by subtraction of the protonated product at 100% deuterated solvent (6% H) from the other values. The reaction with 1:1 mixture of H_2O/D_2O was conducted twice to check the reproducibility.



Scheme 3.20. Carbanion $1c^-$ generated from trifluoroborate $2c$ deprotonates water. The KIE for the deprotonation was determined from the H/D ratio in toluene derivative $1i$ in a mixture of acetonitrile- d_0/d_3 . PC – Photocatalyst 4CzIPN was used as pre-catalyst to generate the active photocatalyst in situ upon photosubstitution as described in chapter 2.

H ₂ O/D ₂ O	3.00	2.00	1.00	0.50	0.33	0.00
H/D product	3.36	2.66	1.22	0.62	0.48	0.00

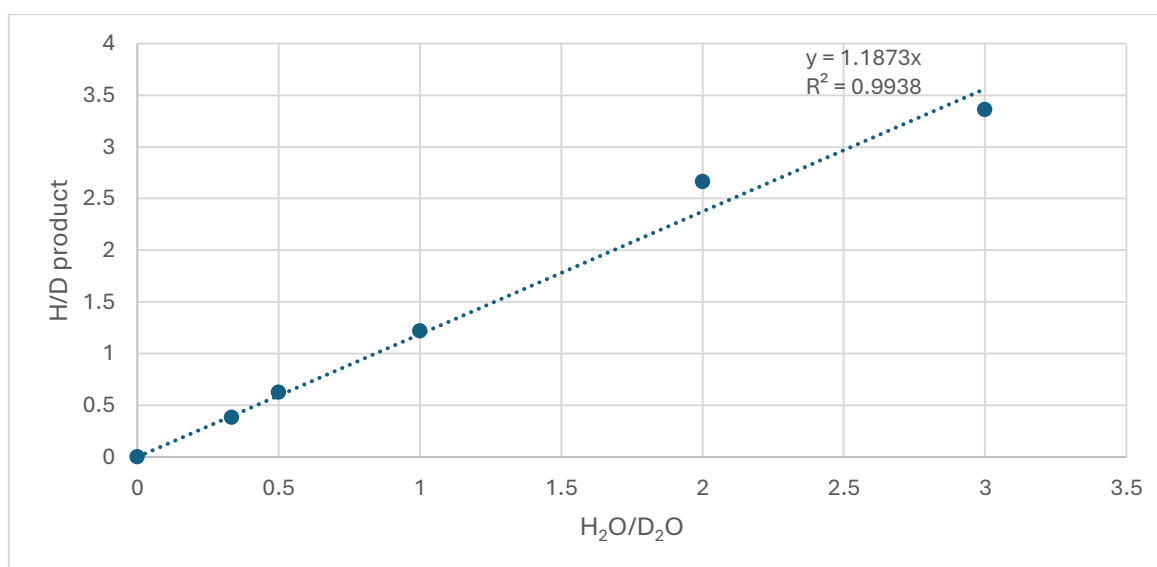
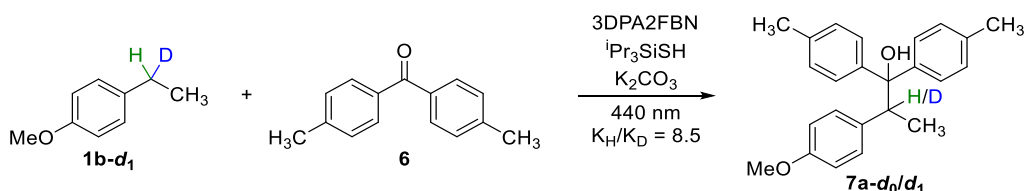


Figure 3.39. Determination of the KIE for deprotonation of water by carbanion $1i^-$.

Values were determined via mass spectrometry and corrected for background protonation from traces of additional protons. Values were corrected by subtraction of the protonated product at 100% deuterated solvent (20% H) from the other values. In contrast to the analogous reaction with primary trifluoroborate $2c$ the 1H NMR spectrum of the crude reaction mixture contains substantial amounts of side products. However, these side reactions are not expected to influence the H/D ratio of the protonated carbanion.

3.4.8.2 Kinetic isotope effect of benzylic C-H activation

The KIE for C-H activation was determined by trapping the corresponding radical **1b[•]** and carbanion **1b⁻** by benzophenone **6**. Reactions were conducted according to general procedure 3-G with 10 equiv. 4,4'-dimethylbenzophenone on 200 μmol scale in 2 mL CD₃CN. The reaction mixture was irradiated for 3 h at 451 nm. The reaction was stopped at incomplete conversion to avoid product decomposition which might influence the deuteration degree.

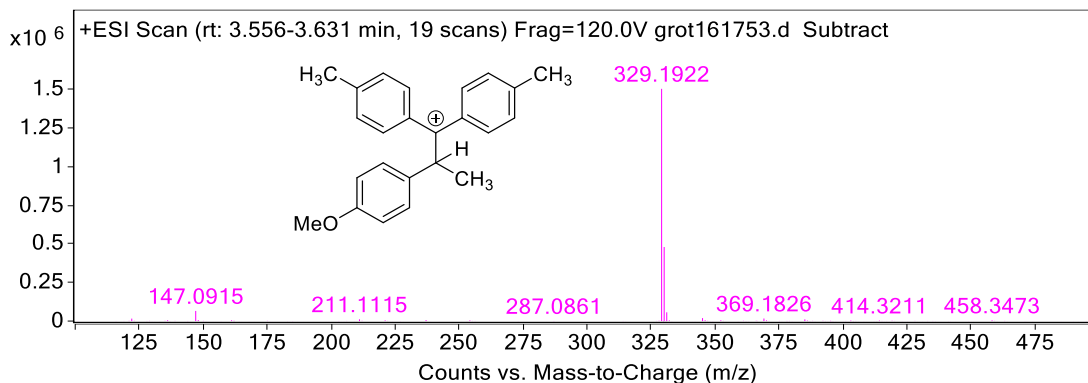


Scheme 3.21. Tertiary alcohol **7a** is formed upon radical generation from ethyl anisole (**1b**) in presence of benzophenone derivative **6**. The KIE of the C-H abstraction was determined from the H/D-ratio in the product when monodeuterated substrate **1b-d₁** is used.

Remaining ethyl anisole still contained 1 D per molecule which confirms the product's deuteration degree is indicative of the KIE for C-H abstraction and deuteration of the substrate does not occur to notable extent.

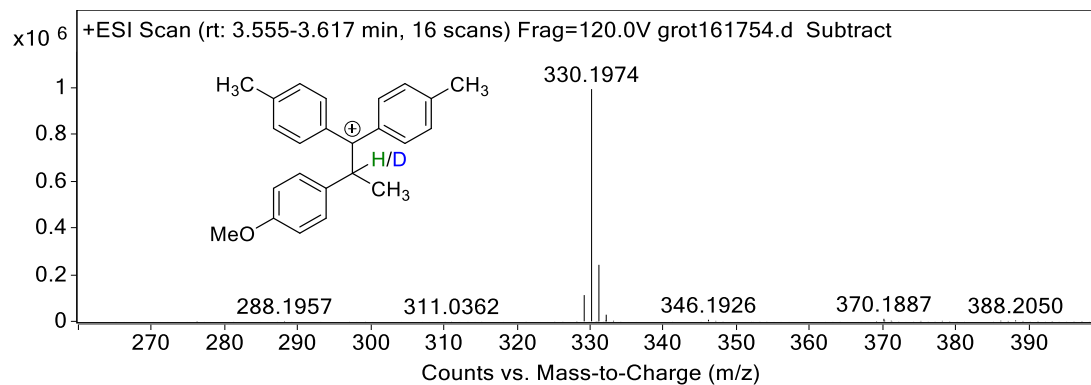
In the positive electrospray ionization (+ESI) the compound fragments almost exclusively to [M - OH]⁺ for both, deuterated and non-deuterated compound. A KIE of 8.53 was obtained.

With **1b-d₀**



Peak List

m/z	z	Abund	m/z	z	Abund
122.0964	1	15945.93	332.1997	1	4491.84
136.1117	1	5318.6	345.1849	1	19268.29
147.0915	1	65600.74	346.1884	1	5481.75
148.0952	1	6183.82	352.3393	1	4735.35
161.1071	1	4968.75	369.1826	1	16575.76
211.1115	1	11355.28	385.174	1	11051.53
237.1277	1	6195.99	539.2714	2	5323.05
329.1922	1	1503206.88	539.773	2	4545.44
330.1938	1	479220.72	715.3759	1	18062.95
331.197	1	56743.22	716.3793	1	9942.29

With **1b-d₁**

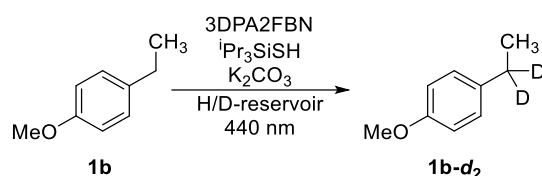
Peak List

m/z	z	Abund	m/z	z	Abund
122.0964	1	4810.97	371.1924	1	2732.27
136.1118	1	1881.9	375.2505	1	1905.86
147.0916	1	14806.37	378.1813	1	2129.5
148.0948	1	2177.6	386.1828		2959.28
163.1118	1	7205.05	387.1953		1757.7
254.2481	1	104665.65	388.205	1	4155.79
255.2513	1	18795.71	389.2095	1	1800.48
288.1957	1	1569.96	404.1266	1	2478.96
329.1905	2	112429.45	414.3214	1	3958.12
330.1974	1	994303.25	419.2767	1	2790.03
331.2	1	242002.19	458.3474	1	3668.43
332.1748	2	4257.95	463.3031	1	1666.56
332.203	1	28499.43	502.3735	1	2339.26
333.2052	1	2515.34	546.4	1	1650.55
346.1926	1	6880.61	716.3835		1953.96
347.1948	1	2104.6	717.3883	1	7946.8
370.1887	1	10963.72	718.3917	1	4078.29
370.2949	1	3316.65			

3.4.8.3 Isotopic fractionation with carbanions generated via C-H activation

Isotopic fractionation was conducted according to the procedure described previously³⁵ using the reaction conditions described in general procedure 3-G. Ethyl anisole was used as model substrate. D/H ratios of the products were plotted against D/H ratios of the H/D-reservoir. The influence of water, methanol and acetonitrile as different H/D reservoirs were tested. Reactions with water and methanol were conducted in 1 mL solvent mixtures with 9:1 acetonitrile:water and acetonitrile:methanol, respectively.

The slopes differed substantially, with the same trend as the KIE values for carbanion protonation. In acetonitrile, less deuterium was incorporated than with water or methanol of the same degree of deuteration as expected due to the large preference of benzyl carbanions to abstract a proton over a deuteron from acetonitrile, while deprotonation of water is rather unselective.



	D/H reservoir	0.00	0.33	0.50	1.00	2.00	3.00
D/H product	water	0.04	0.25	0.35	0.63		1.46
	methanol	0.03	0.20		0.55		0.74
	acetonitrile	0.06	0.18	0.21		0.48	0.65

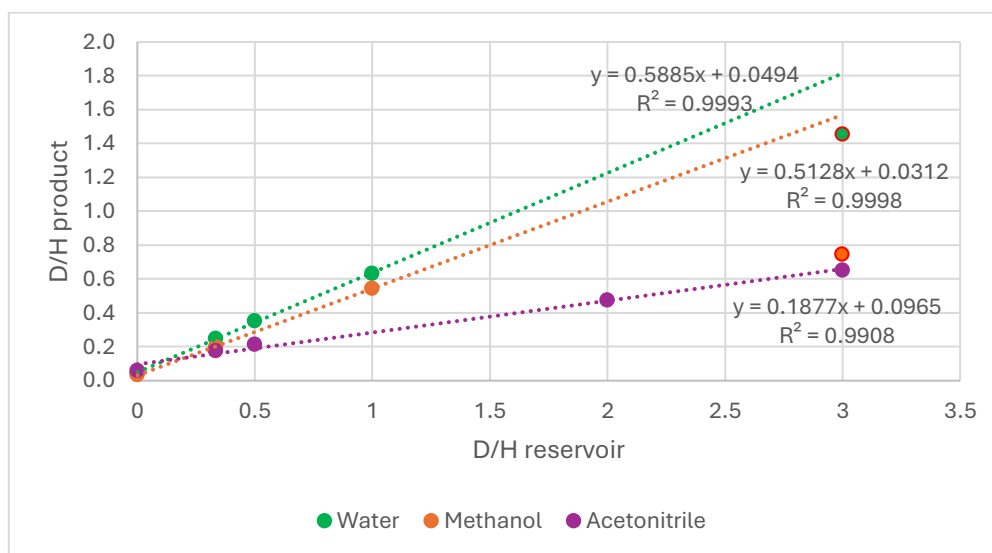


Figure 3.40. Isotopic fractionation with ethyl anisole under the used conditions for photocatalytic carbanion generation via C-H activation. At the highest D/H ratio (3:1) the reactions with water and methanol are substantially smaller than expected from the other values and were not used for calculating the slope (red points).

When submitting a partially deuterated substrate to the reaction conditions the deuteration degree increased instead of converging to the same value as when using a non-deuterated substrate. Accordingly, under the initial conditions the system is far from equilibrium and, thus, the KIE for the protonation step dominates. Starting from a 3:1 mixture of ethyl anisole- d_2/d_0 the reactions with higher than 2:1 ratio of H₂O:D₂O showed a strong increase in deuteration degree.

Thus, the minimum value for the slope at equilibrium is 5.7 while the highest value would give a slope of 11.4. Therefore, the slope of 8.5 when taking all data points into account is likely only a very crude estimate. However, the real value is certainly larger than 1.5, in accordance with a HAT/ETPT sequence.

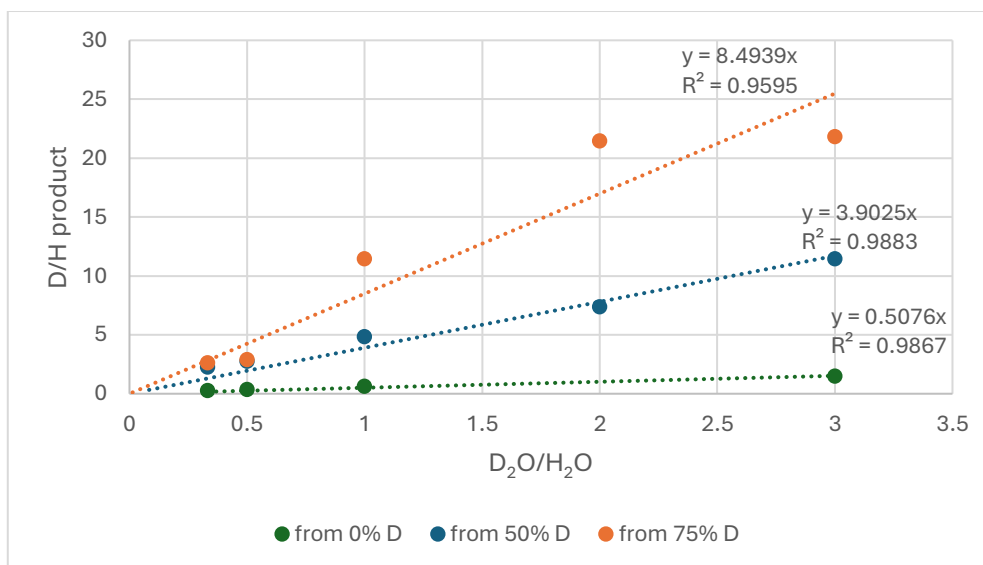


Figure 3.41. Isotopic fractionation with partially deuterated **1b** (mixtures of **1b-d₂** and **1b-d₀**).

3.4.9 Spectroscopy

The previously described in house built transient absorption spectrometer using a streak camera-based detection system was used.^{40,70,71} The obtained transient absorption data were analyzed by a global fit using an exponential ansatz, which is adequate for the description of the photophysics of a single chromophore in solution and a single chromophore in the presence of a reaction partner at much higher concentrations fulfilling pseudo-first order conditions. The global fits were performed using an in-house written program described previously.^{40,71-74}

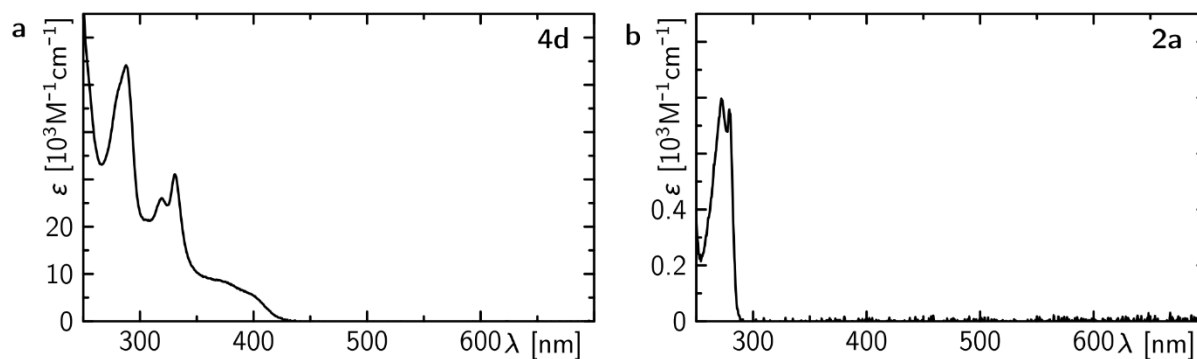


Figure 3.42. Steady state absorption spectra of the photocatalyst **4d** (a) and trifluoroborate **2a** (b) in ACN.

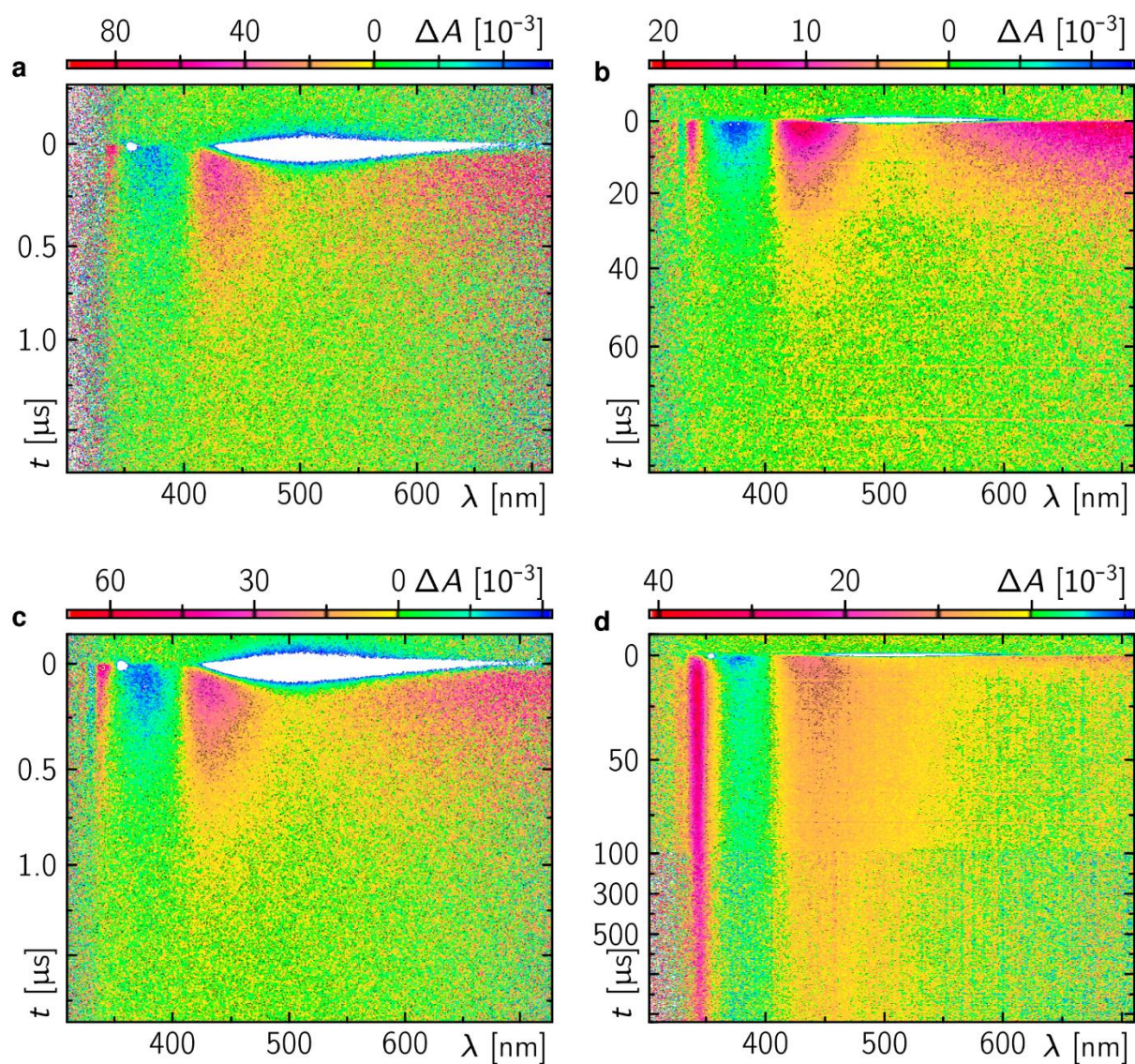


Figure 3.43. Time-resolved absorption data of **4d** in ACN in dependence on O_2 and **2a** following excitation at 355 nm. (a) in the absence of **2a** and presence of O_2 . (b) in the absence of **2a** and O_2 . (c) in the presence of **2a** (10 mM) and O_2 . (d) in the presence of **2a** (10 mM) and absence O_2 . To note the data shown in (d) are fused data from two different experimental time windows, i.e., 100 μs and 1 ms.

REACTIVITY OF SUPERBASIC CARBANIONS GENERATED VIA REDUCTIVE RADICAL-POLAR CROSSOVER IN THE CONTEXT OF PHOTOREDOX CATALYSIS

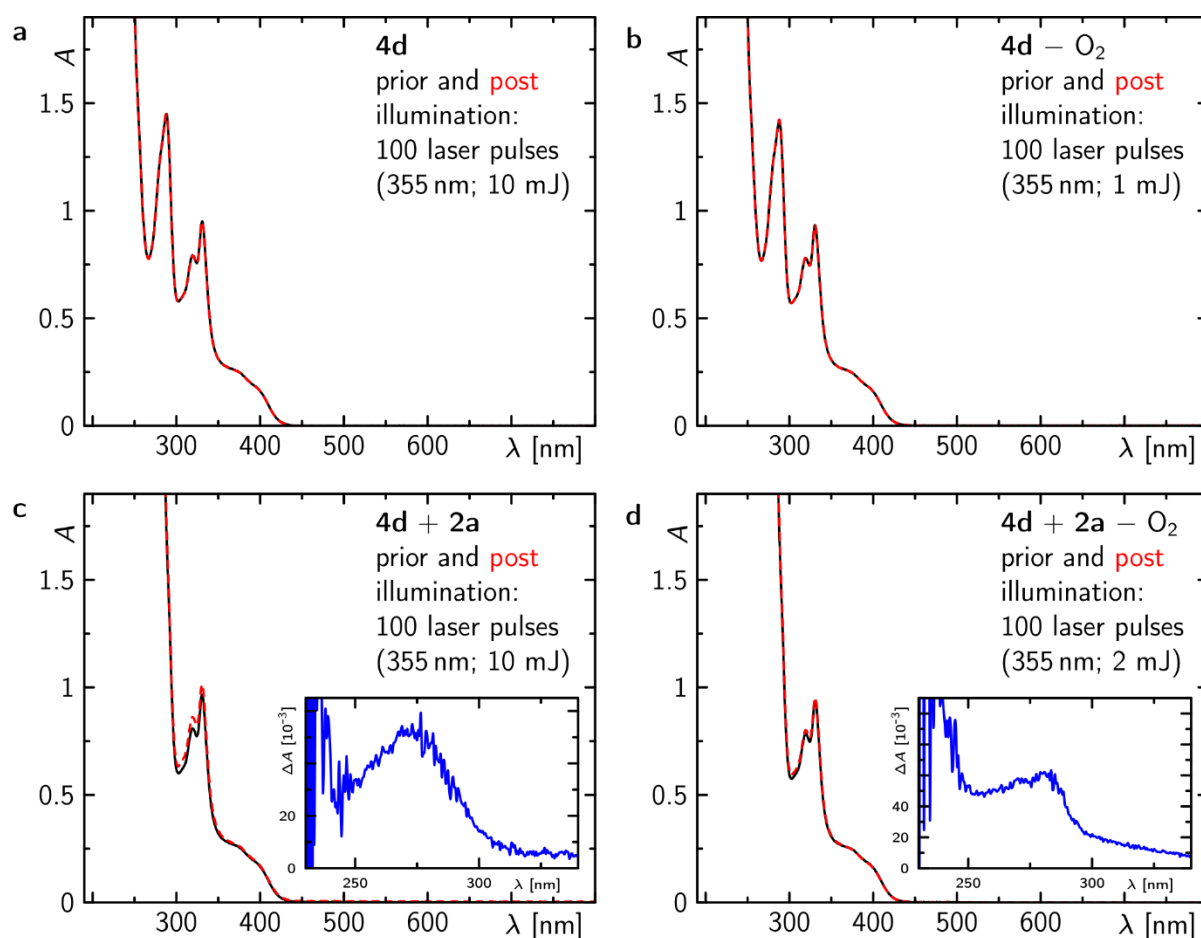


Figure 3.44. Electronic absorption spectra of **4d** in MeCN in dependence on O_2 and **2a** prior and post illumination at 355 nm, used to measure TA (100 laser pulses at pulse energies as indicated). (a) in the absence of **2a** and presence of O_2 . (b) in the absence of **2a** and O_2 . (c) in the presence of **2a** (10 mM) and O_2 . (d) in the presence of **2a** (10 mM) and absence of O_2 . The insets in c and d show the corresponding difference spectra.

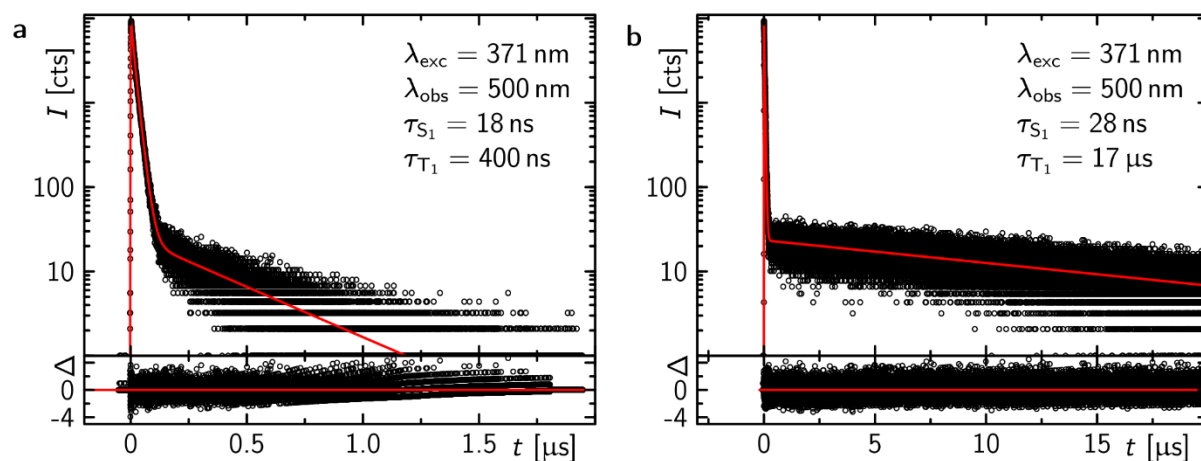


Figure 3.45. Time-resolved emission of **4d** in ACN in presence (a) and absence (b) of O_2 . The red line corresponds to a bi-exponential fit to the data. The Poissonian-weighted (weighted by $1/\sqrt{N}$ where N is the number of counted photons in each channel) residuals are shown in the lower panels.

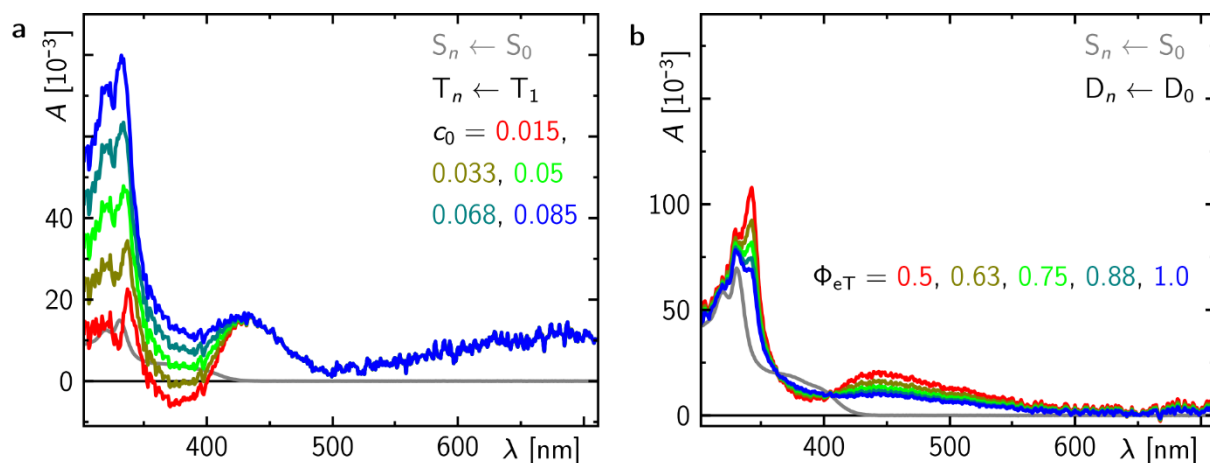


Figure 3.46. SAS of **4d** in ACN (a) in the T_1 state, $T_n \leftarrow T_1$ transitions, and (b) in the D_0 state, $D_n \leftarrow D_0$ transitions. The contribution of the ground state spectrum, c_0 , was varied between 0.015 (red) and 0.085 (blue). Below $c_0 = 0.033$ the T_1 spectrum becomes negative and above 0.05 the contributions of the S_0 spectrum arise. The electron transfer (eT) yield, Φ_{eT} , was varied between 0.25 (red) and 1.0 (blue). The optimal and experimentally determined value is given to $\Phi_{eT} = 1 - k_{T_1}^{-O_2} / k_{T_1}^{2a, -O_2} = 74.6\%$ ($k_{T_1}^{-O_2}$ and $k_{T_1}^{2a, -O_2}$ are the rate constants in the presence and absence of **2a** under degassed conditions, respectively).

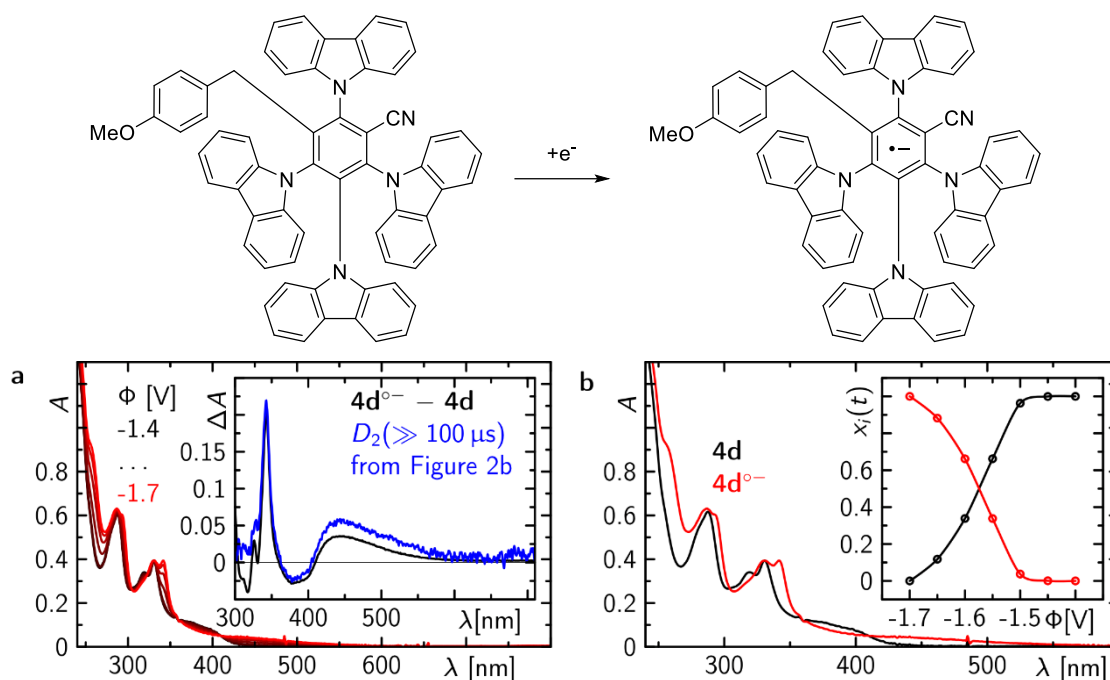


Figure 3.47. (a) Electrochemical reduction of **4d** to **4d^{•-}** followed by steady-state absorption spectra in the UV/Vis spectral range. In the inset, the difference spectrum post and prior reduction is shown in comparison to the second decay associated difference spectrum from the global analysis on the transient absorption data (see Figure 3.2b). (b) The pure spectra of **4d** and **4d^{•-}** and the corresponding mole fraction as a function of the applied voltage in the inset. The reduction starts from a voltage < -1.5 V.

REACTIVITY OF SUPERBASIC CARBANIONS GENERATED VIA REDUCTIVE RADICAL-POLAR
CROSSOVER IN THE CONTEXT OF PHOTOREDOX CATALYSIS

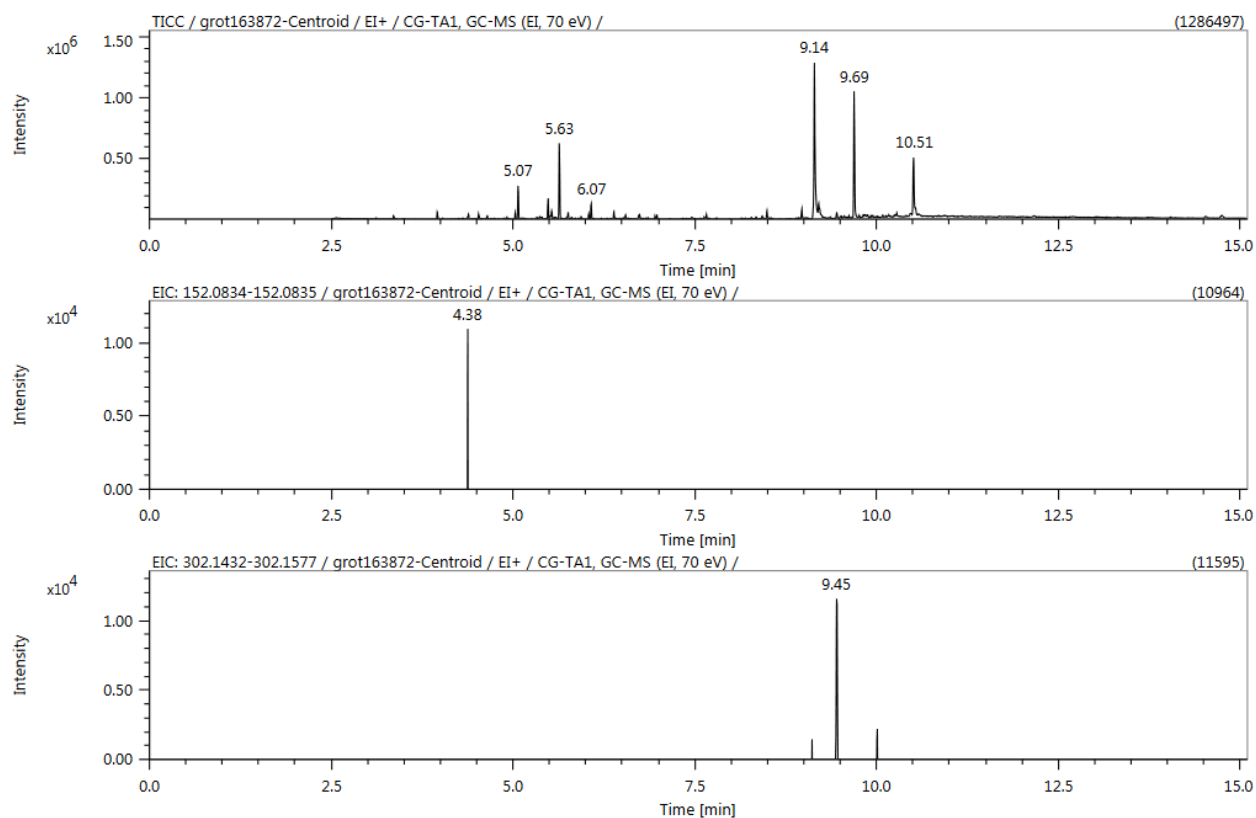


Figure 3.48. Gas chromatogram of the solution after the transient absorption measurement. The toluene derivative **1f** (4.38 min) resulting from protonation of carbanion **1f⁻** and bibenzyl **8a** (9.45 min) resulting from dimerization of radical **1f[•]** were detectable.

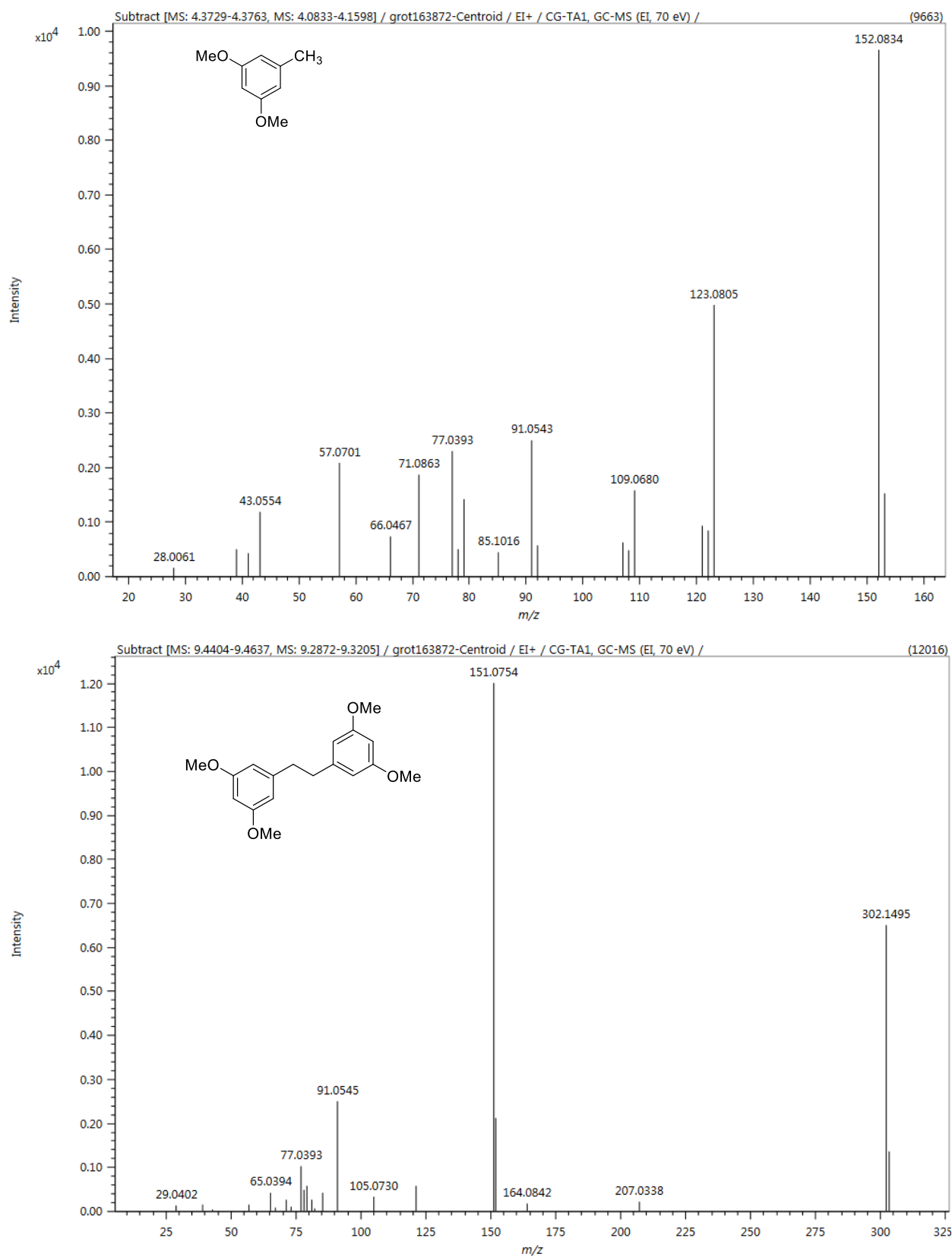
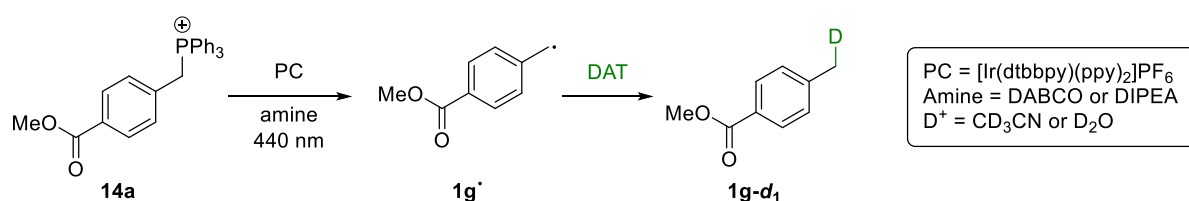


Figure 3.49. The mass spectra are in accordance with toluene **1f** (top) and bibenzyl **8a** (bottom).

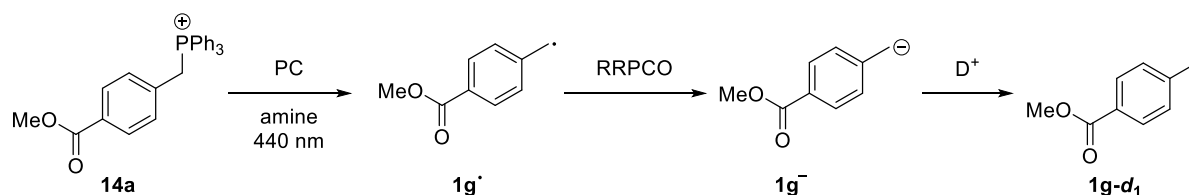
3.4.10 Carbanion generation from benzyltriphenylphosphonium bromides

Benzyltriphenylphosphonium salts substituted with electron withdrawing groups have been reported to react to the corresponding toluene derivative under reductive photocatalytic conditions.⁴² A HAT from the solvent MeCN was proposed. However, results presented in this work support an ionic mechanism via the corresponding carbanion. Deuteration in CD₃CN is moderate, in agreement with the reactivity of the same carbanion generated under redox-neutral photocatalytic conditions from the corresponding trifluoroborate **2b**. Although addition of D₂O gives a high degree of mono-deuteration, some di-deuteration is observed, likely due to proton-deuteron exchange via the corresponding phosphorus ylide under basic conditions. Moreover, in presence of D₂O alkaline hydrolysis of benzyltriphenylphosphonium salts generates the corresponding toluene derivative without irradiation.⁷⁵ Thus, addition of D₂O cannot be used as mechanistic probe for the photocatalytic reaction. If *N,N*-diisopropylethylamine (DIPEA) is used as sacrificial electron donor no deuteration is observed in CD₃CN. Whether this is due to HAT from the DIPEA radical cation to the benzyl radical or proton abstraction from the DIPEA radical cation by the benzyl carbanion cannot be determined from the experimental results.

Initially proposed mechanism:



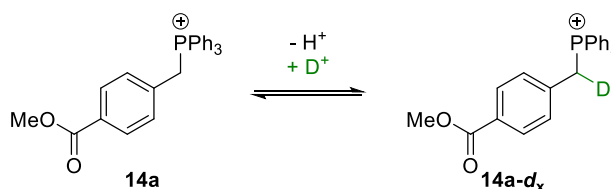
Revised mechanism:



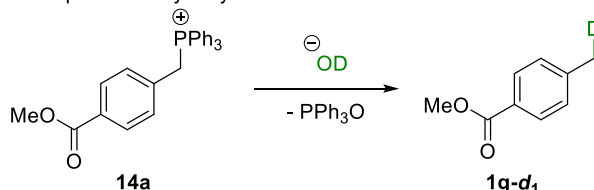
Entry	Amine	Additive	Light	Deuteration
1	DIPEA	-	yes	0%
2	DABCO	-	yes	25%
3	DABCO	D ₂ O	yes	126%
4	DABCO	D ₂ O	no	114%

Background reactions in presence of D₂O

Deuteration via P-ylide

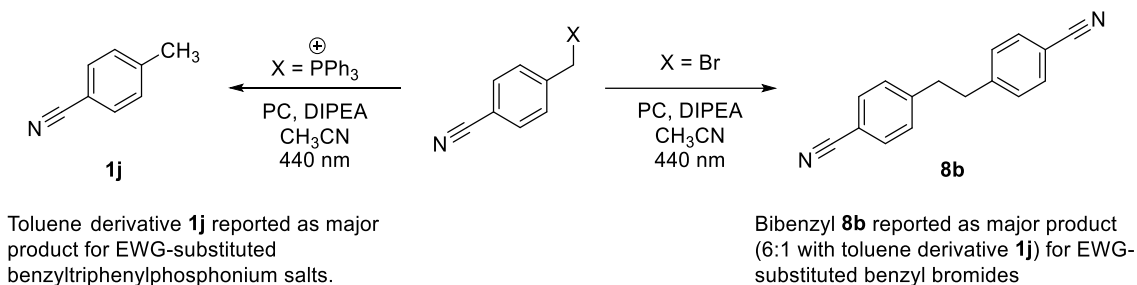


Base-promoted hydrolysis



Scheme 3.22. Toluene derivative **1g** generated under reductive photocatalytic conditions has a moderate degree of deuteration in CD₃CN. In presence of D₂O non-photocatalytic processes can also lead to deuterated **1g**.

A difference in product distribution was described for benzyltriphenylphosphonium salts compared to benzyl bromides. As the initially generated radical is identical, this difference in reactivity cannot be explained by the polarity of the benzyl radical. It was mentioned that a change in mechanism might occur depending on the substrate, but no specific mechanism was proposed.



Scheme 3.23. Benzyltriphenylphosphonium bromides preferentially react to the corresponding toluene derivative while benzyl bromides give the corresponding bibenzyl as major product.⁴²

The revised mechanism via carbanion generation explains the change in product distribution. CN-substituted triphenylphosphonium salt **14c** has a half-wave reduction potential of $E_{1/2} = -1.58$ V vs. SCE, similar to the reduction potential of the photocatalyst ($E_{1/2} = -1.51$ V vs. SCE).⁴⁵ The corresponding benzyl bromide **17** can be reduced more easily by 0.29 V ($E_{1/2} = -1.29$ V vs. SCE). 4-Cyanobenzyl radical (**1j'**) is easily reduced to the carbanion ($E_{1/2} = -0.77$ V vs. SCE)⁷⁶ and thus the ratio of bibenzyl **8b** (resulting from radical dimerization) and toluene **1j** (resulting from deprotonation of the solvent MeCN) is expected to shift towards toluene for difficult to reduce substrates and more towards bibenzyl for more easily reduced substrates as a direct consequence of competition between carbanion generation via reduction of radicals already present and generation of more benzyl radicals which can then undergo dimerization.

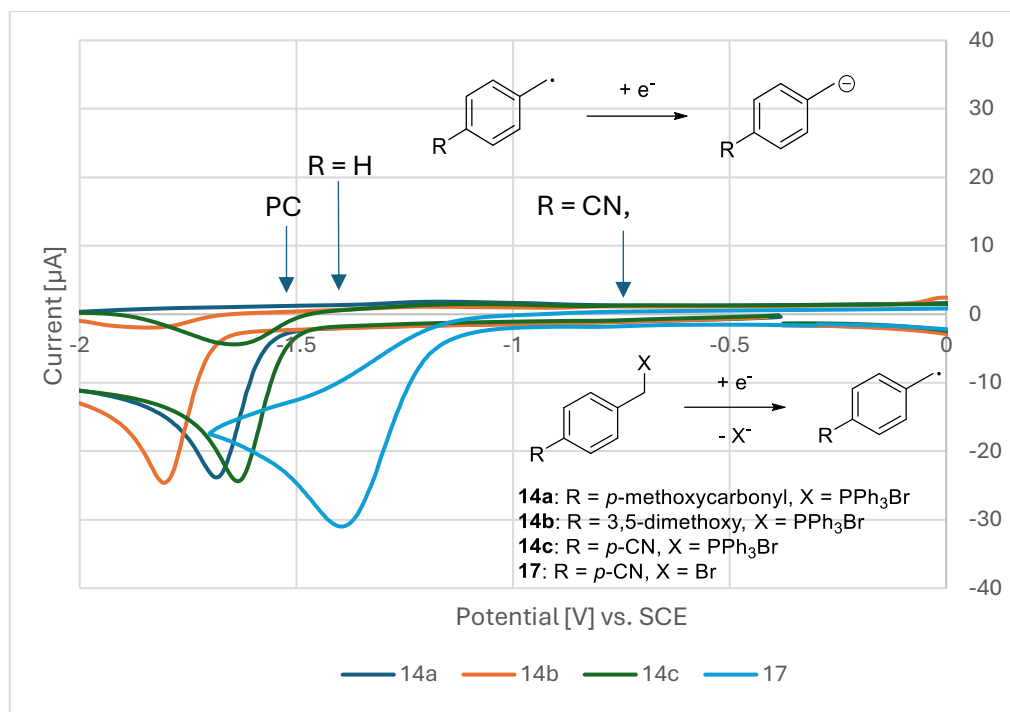


Figure 3.50. Reductive part of the cyclic voltammograms of benzyltriphenylphosphonium bromides **14a-c** and 4-cyanobenzyl bromide (**17**). Approximate half-wave potentials for reduction of the corresponding benzyl radicals and the photocatalyst are marked with arrows.

3.4.11 DFT calculations

3.4.11.1 Kinetic isotope effects for hydrogen atom abstraction

Kinetic isotope effects (KIE) arise from the fact that bonds to different isotopes have different zero-point energies (ZPE). The heavier an isotope the lower is the ZPE. Therefore, the dissociation barriers differ for different isotopically labeled molecules. To calculate the KIE, the deuterated species and non-deuterated species were fully optimized along with their respective transition states. All the optimization and frequency analysis of the transition state and the substrates were done using the B97D3/Def2TZVP level of theory using Gaussian 16 C.01 software package.⁷⁷⁻⁸¹ Stationary points were characterized by a frequency analysis with a single imaginary frequency indicating a saddle point of first order and zero imaginary frequencies a minimum energy structure. The reported enthalpies and Gibbs free energies remained unscaled and have been calculated assuming standard conditions. Cartesian coordinates of the optimized structures can be found in the appendix.

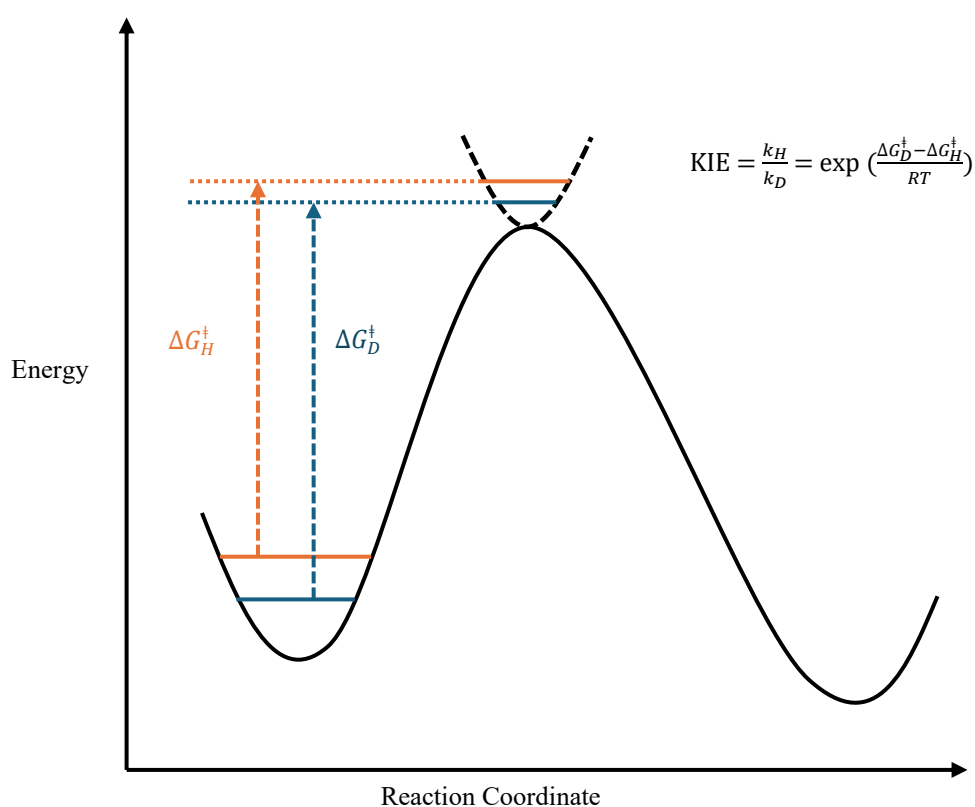


Figure 3.51. Schematic ground state potential surface for a proton and deuteron abstraction and the definition of the kinetic isotope effect.

The absolute difference between the free energies of reactants, substrate-catalyst assembly, and the transition states (TS) were considered in the calculations. The underlying principle for calculation of KIE is schematically described in Figure 3.51. Table 3.3 summarizes all free Gibbs energies of all calculated structures (all in kcal/mol).

REACTIVITY OF SUPERBASIC CARBANIONS GENERATED VIA REDUCTIVE RADICAL-POLAR
CROSSOVER IN THE CONTEXT OF PHOTOREDOX CATALYSIS

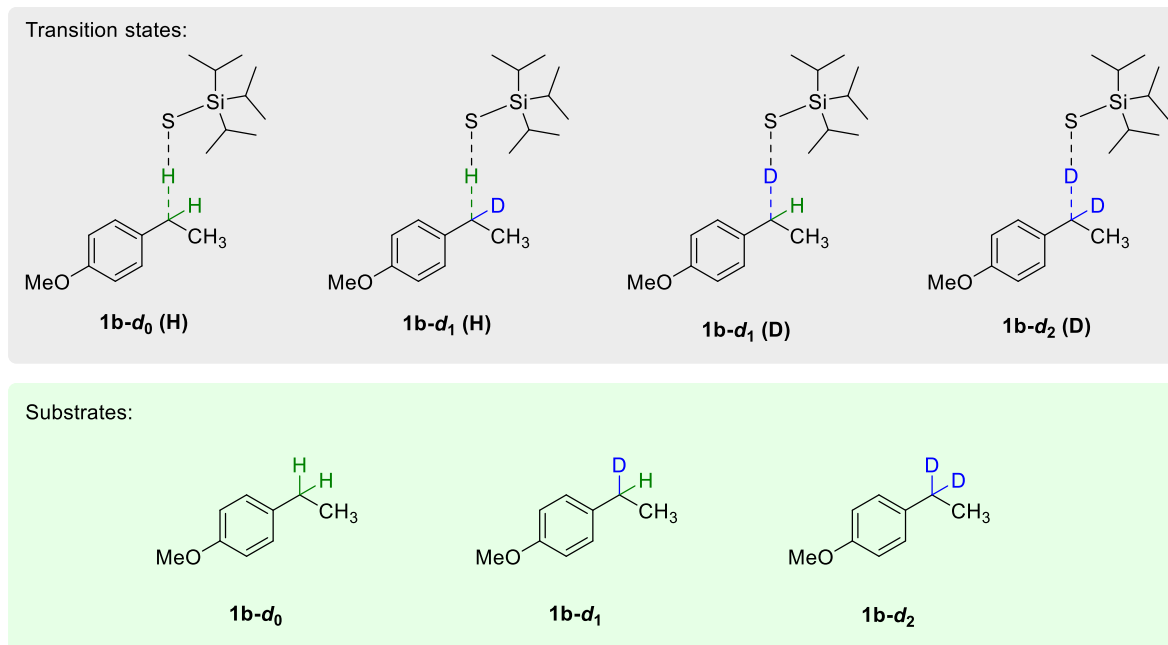


Figure 3.52. Transition states considered for calculation of kinetic isotope effects. (D/H) after the molecule number indicates whether D or H is abstracted.

The reaction activation energy barriers were calculated by taking the difference between the transition state free energy and the sum of free energies of the reactants. The KIEs calculated by this method are tabulated in table 3.3.

Table 3.3. Free Gibbs energies of all calculated structures (in kcal/mol) based on the difference between the transition state free energy and the sum of free energies of the reactants.

	ΔG_1^\ddagger	ΔG_2^\ddagger	$\Delta G_2^\ddagger - \Delta G_1^\ddagger$	KIE
1b-d₀ (H) vs 1b-d₁ (D)	7.445287	8.64956	1.204172	7.632463
1b-d₀ (H) vs 1b-d₂ (D)	7.445287	8.69715	1.251862	8.272213
1b-d₁ (H) vs 1b-d₁ (D)	7.483565	8.64946	1.165890	7.154958
1b-d₁ (H) vs 1b-d₂ (D)	7.483565	8.69715	1.213585	7.754684
1b-d₀ (H) vs 1b-d₁ (H)	7.445287	7.483565	0.038277	1.066738
1b-d₁ (D) vs 1b-d₂ (D)	8.64946	8.69715	0.047690	1.083820

Another way of calculating the reaction barriers is by optimizing the pre-TS complex of the reactants and take its difference of free energy or from that of the TS. The KIEs from these calculations are summarized in Table 3.4.

Table 3.4. Free Gibbs energies of all calculated structures (in kcal/mol) based on the energy difference between pre-TS.

	ΔG_1^\ddagger	ΔG_2^\ddagger	$\Delta G_2^\ddagger - \Delta G_1^\ddagger$	KIE
1b-d₀ (H) vs 1b-d₁ (D)	4.738253	5.948072	1.20982	7.705562
1b-d₀ (H) vs 1b-d₂ (D)	4.738253	5.82069	1.082437	6.214874
1b-d₁ (H) vs 1b-d₁ (D)	4.604595	5.948072	1.343477	9.655527
1b-d₁ (H) vs 1b-d₂ (D)	4.604595	5.82069	1.216095	7.787605
1b-d₀ (H) vs 1b-d₁ (H)	4.738253	4.604595	-0.13366	0.798047
1b-d₁ (D) vs 1b-d₂ (D)	5.948072	5.82069	-0.12738	0.806544

3.4.11.2 Kinetic isotope effect for carbanion protonation

Similar KIE calculations were performed for acetonitrile deprotonation by benzylic carbanion **1f**. The transition state was optimized using the B97D3/Def2TZVP level of theory in Gaussian 16 C.01 software package.⁷⁷⁻⁸¹

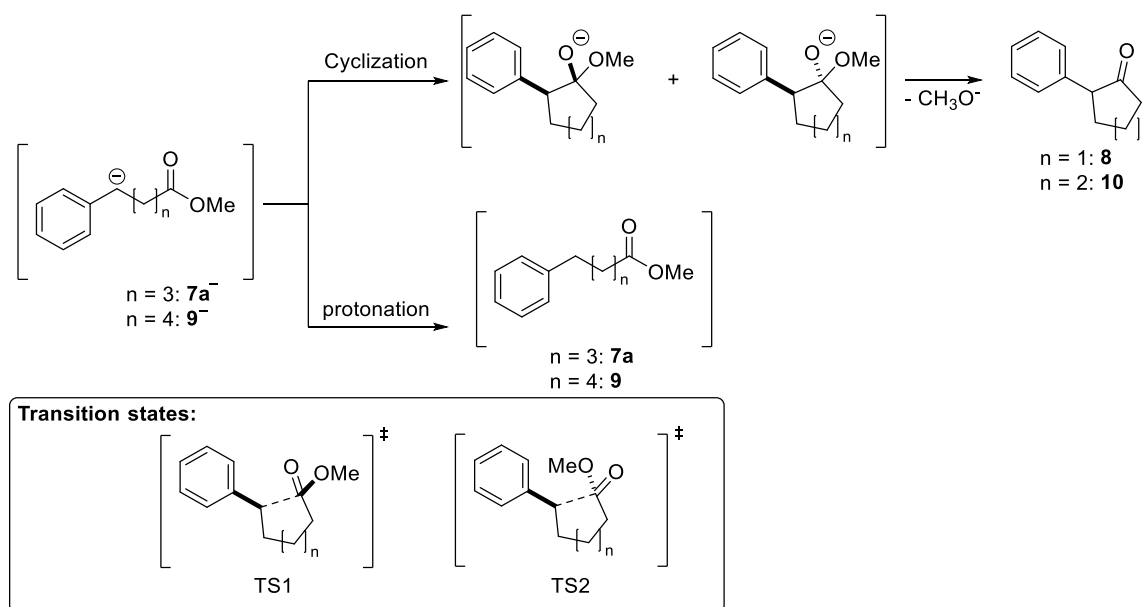
Since deprotonation is a very fast reaction, the difference in energy of substrates and the transition states are considered for the computation of the KIE. Barriers were calculated for the proton and the deuterium isotopomers and the relative activation barrier used for calculating the relative rate constants, i.e. the KIE.

Table 3.5. Relative free Gibbs energies in kcal/mol for proton and deuterium abstraction from acetonitrile-*d*₀/*d*₃ and the corresponding theoretical kinetic isotope effect. The calculated KIE is in accordance with the experimentally determined KIE in the gas phase.

	$\Delta G_{\text{Substrates}}$	ΔG_{TSs}	$\Delta G_{\text{TS}}^\ddagger - \Delta G_{\text{Substrates}}^\ddagger$	KIE	Exp
ACN - ACN-<i>d</i>₃	6.2	5.1	1.1	6.8	6.5

3.4.11.3 Cyclization of phenylvaleric and phenylhexanoic acid esters

All geometry optimization and frequency analysis was done using the M06-2X/6-31G(d)⁸²⁻⁹¹ level of theory and the electronic energy was improved by performing single point energy calculation at the optimized geometries using the wB97XD/Def2TZVP^{77,78,92} level of theory. The energies of an open and a folded (attack-conformer) conformer of the carbanion were optimized along with two diastereotopic transition states. The closed conformer was obtained from the internal reaction coordinates (IRC) of the transition state. The energies (all energies in kcal/mol) for ring closure can be found in Tables 3.6 and 3.7. TS1 was the low-lying transition state for the 5-membered ring and TS2 for the 6-membered ring, hence these were considered for comparison.



Scheme 3.24. Cyclization of carbanions **7a⁻** and **9⁻** to cyclic ketones **8** and **10**.

Table 3.6. Free Gibbs energies of carbanions **7a⁻** and **9⁻** and transition state energies for their cyclization.

Substrate	Method	$\Delta G_{\text{Open}-\text{Close}}$	$\Delta G_{\text{TS2}-\text{Close}}^\ddagger$	$\Delta G_{\text{TS1}-\text{Open}}^\ddagger$	$\Delta G_{\text{TS1}-\text{Close}}^\ddagger$	$\Delta G_{\text{TS2}-\text{Close}}^\ddagger$	$\Delta \Delta G_{\text{TSs}}$
7a⁻	M062X/6-31G(d)	1.519178	5.341907	12.43768	3.82273	10.9185	7.095770
	Combination	3.308180	9.919915	14.57432	5.89097	11.26614	5.375165
9⁻	M062X/6-31G(d)	-3.426150	-1.00275	-2.35689	2.423405	1.06926	-1.35415
	Combination	0.822025	3.397913	2.926032	2.575888	2.104007	-0.47188

Table 3.7. Absolute energies of substrates, products, and transition states. All energies are given in in Hartree.

Substrate	M062X/6-31G(d)	Free Energy Contribution	wB97XD/Def2TZVP
5-membered open	-616.268023	0.199450	-616.784644
5-membered close	-616.265602	0.205860	-616.785782
5-membered TS1	-616.259510	0.206962	-616.777496
5-membered TS2	-616.248202	0.205322	-616.767290
6-membered open	-655.533420	0.225882	-656.100023
6-membered close	-655.538880	0.234504	-656.107335
6-membered TS1	-655.535018	0.234628	-656.103354
6-membered TS2	-655.537176	0.235613	-656.105091

3.5 References

- (1) Donabauer, K.; König, B. Strategies for the Photocatalytic Generation of Carbanion Equivalents for Reductant-Free C-C Bond Formations. *Acc. Chem. Res.* **2021**, *54*, 242–252.
- (2) Pitzer, L.; Schwarz, J. L.; Glorius, F. Reductive radical-polar crossover: traditional electrophiles in modern radical reactions. *Chem. Sci.* **2019**, *10*, 8285–8291.
- (3) Berger, A. L.; Donabauer, K.; König, B. Photocatalytic carbanion generation from C-H bonds - reductant free Barbier/Grignard-type reactions. *Chem. Sci.* **2019**, *10*, 10991–10996.
- (4) Donabauer, K.; Maity, M.; Berger, A. L.; Huff, G. S.; Crespi, S.; König, B. Photocatalytic carbanion generation - benzylation of aliphatic aldehydes to secondary alcohols. *Chem. Sci.* **2019**, *10*, 5162–5166.
- (5) Donabauer, K.; Murugesan, K.; Rozman, U.; Crespi, S.; König, B. Photocatalytic Reductive Radical-Polar Crossover for a Base-Free Corey-Seebach Reaction. *Chemistry* **2020**, *26*, 12945–12950.
- (6) Babin, V.; Talbot, A.; Labiche, A.; Destro, G.; Del Vecchio, A.; Elmore, C. S.; Taran, F.; Sallustrau, A.; Audisio, D. Photochemical Strategy for Carbon Isotope Exchange with CO₂. *ACS Catal.* **2021**, *11*, 2968–2976.
- (7) Abrams, R.; Clayden, J. Photocatalytic Difunctionalization of Vinyl Ureas by Radical Addition Polar Truce-Smiles Rearrangement Cascades. *Angew. Chem., Int. Ed.* **2020**, *59*, 11600–11606.
- (8) Xiao, T.; Li, L.; Zhou, L. Synthesis of Functionalized gem-Difluoroalkenes via a Photocatalytic Decarboxylative/Defluorinative Reaction. *J. Org. Chem.* **2016**, *81*, 7908–7916.
- (9) Phelan, J. P.; Lang, S. B.; Compton, J. S.; Kelly, C. B.; Dykstra, R.; Gutierrez, O.; Molander, G. A. Redox-Neutral Photocatalytic Cyclopropanation via Radical/Polar Crossover. *J. Am. Chem. Soc.* **2018**, *140*, 8037–8047.
- (10) Meng, Q.-Y.; Schirmer, T. E.; Berger, A. L.; Donabauer, K.; König, B. Photocarboxylation of Benzylic C-H Bonds. *J. Am. Chem. Soc.* **2019**, *141*, 11393–11397.
- (11) Murugesan, K.; Donabauer, K.; Narobe, R.; Derdau, V.; Bauer, A.; König, B. Photoredox-Catalyzed Site-Selective Generation of Carbanions from C(sp³)-H Bonds in Amines. *ACS Catal.* **2022**, *12*, 3974–3984.
- (12) Schmalzbauer, M.; Svejstrup, T. D.; Fricke, F.; Brandt, P.; Johansson, M. J.; Bergonzini, G.; König, B. Redox-Neutral Photocatalytic C-H Carboxylation of Arenes and Styrenes with CO₂. *Chem* **2020**, *6*, 2658–2672.
- (13) Liao, L.-L.; Cao, G.-M.; Ye, J.-H.; Sun, G.-Q.; Zhou, W.-J.; Gui, Y.-Y.; Yan, S.-S.; Shen, G.; Yu, D.-G. Visible-Light-Driven External-Reductant-Free Cross-Electrophile Couplings of Tetraalkyl Ammonium Salts. *J. Am. Chem. Soc.* **2018**, *140*, 17338–17342.
- (14) Ran, C.-K.; Niu, Y.-N.; Song, L.; Wei, M.-K.; Cao, Y.-F.; Luo, S.-P.; Yu, Y.-M.; Liao, L.-L.; Yu, D.-G. Visible-Light Photoredox-Catalyzed Carboxylation of Activated C(sp³)-O Bonds with CO₂. *ACS Catal.* **2022**, *12*, 18–24.
- (15) Day, J. I.; Grotjahn, S.; Senaweera, S.; Koenig, B.; Weaver III, J. D. Defluorodearomatization: A Photocatalytic Birch-Like Reduction That Enables C-C Bond Formation and Provides Access to Unnatural Cannabinoids. *J. Org. Chem.* **2021**, *86*, 7928–7945.
- (16) Flynn, A. R.; McDaniel, K. A.; Hughes, M. E.; Vogt, D. B.; Jui, N. T. Hydroarylation of Arenes via Reductive Radical-Polar Crossover. *J. Am. Chem. Soc.* **2020**, *142*, 9163–9168.
- (17) McAttee, R. C.; Noten, E. A.; Stephenson, C. R. J. Arene dearomatization through a catalytic N-centered radical cascade reaction. *Nat. Commun.* **2020**, *11*, 2528.
- (18) Cole, J. P.; Chen, D.-F.; Kudisch, M.; Pearson, R. M.; Lim, C.-H.; Miyake, G. M. Organocatalyzed Birch Reduction Driven by Visible Light. *J. Am. Chem. Soc.* **2020**, *142*, 13573–13581.
- (19) El-Hage, F.; Schöll, C.; Pospech, J. Photo-Mediated Decarboxylative Giese-Type Reaction Using Organic Pyrimidopteridine Photoredox Catalysts. *J. Org. Chem.* **2020**, *85*, 13853–13867.
- (20) Kleinmans, R.; Will, L. E.; Schwarz, J. L.; Glorius, F. Photoredox-enabled 1,2-dialkylation of α -substituted acrylates via Ireland-Claisen rearrangement. *Chem. Sci.* **2021**, *12*, 2816–2822.
- (21) Yatham, V. R.; Shen, Y.; Martin, R. Catalytic Intermolecular Dicarbofunctionalization of Styrenes with CO₂ and Radical Precursors. *Angew. Chem. Int. ed.* **2017**, *56*, 10915–10919.
- (22) Zhang, W.; Lu, L.; Zhang, W.; Wang, Y.; Ware, S. D.; Mondragon, J.; Rein, J.; Strotman, N.; Lehnher, D.; See, K. A.; Lin, S. Electrochemically driven cross-electrophile coupling of alkyl halides. *Nature* **2022**, *604*, 292–297.
- (23) Seyferth, D. The Grignard Reagents. *Organometallics* **2009**, *28*, 1598–1605.
- (24) Reich, H. J. Role of organolithium aggregates and mixed aggregates in organolithium mechanisms. *Chem. Rev.* **2013**, *113*, 7130–7178.

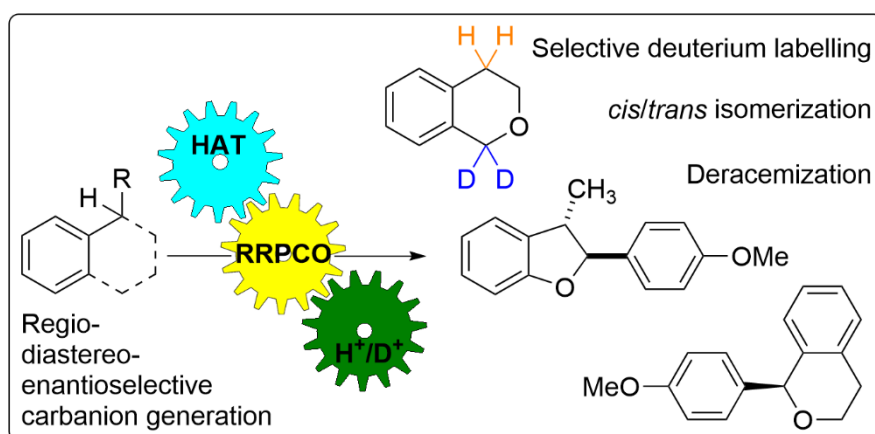
- (25) Kong, D.; Munch, M.; Qiqige, Q.; Cooze, C. J. C.; Rotstein, B. H.; Lundgren, R. J. Fast Carbon Isotope Exchange of Carboxylic Acids Enabled by Organic Photoredox Catalysis. *J. Am. Chem. Soc.* **2021**, *143*, 2200–2206.
- (26) Zhang, B.; Yi, Y.; Wu, Z.-Q.; Chen, C.; Xi, C. Photoredox-catalyzed dicarbofunctionalization of styrenes with amines and CO₂: a convenient access to γ -amino acids. *Green Chem.* **2020**, *22*, 5961–5965.
- (27) Benedetti Vega, K.; Campos Delgado, J. A.; Pungal, L. V. B. L.; König, B.; Menezes Correia, J. T.; Weber Paixão, M. Divergent Functionalization of Styrenes via Radical/Polar Crossover with CO₂ and Sodium Sulfinates. *Chemistry* **2022**, e202203625.
- (28) GILMAN, H.; YOUNG, R. V. RELATIVE REACTIVITIES OF ORGANOMETALLIC COMPOUNDS. XV. ORGANOALKALI COMPOUNDS. *J. Org. Chem.* **1936**, *01*, 315–331.
- (29) Grotjahn, S.; König, B. Photosubstitution in Dicyanobenzene-based Photocatalysts. *Org. Lett.* **2021**, *23*, 3146–3150.
- (30) Matthews, W. S.; Bares, J. E.; Bartmess, J. E.; Bordwell, F. G.; Cornforth, F. J.; Drucker, G. E.; Margolin, Z.; McCallum, R. J.; McCollum, G. J.; Vanier, N. R. Equilibrium acidities of carbon acids. VI. Establishment of an absolute scale of acidities in dimethyl sulfoxide solution. *J. Am. Chem. Soc.* **1975**, *97*, 7006–7014.
- (31) Kopf, S.; Bourriquen, F.; Li, W.; Neumann, H.; Junge, K.; Beller, M. Recent Developments for the Deuterium and Tritium Labeling of Organic Molecules. *Chem. Rev.* **2022**, *122*, 6634–6718.
- (32) Sim, B. A.; Griller, D.; Wayner, D. D. M. Reduction potentials for substituted benzyl radicals: pK_a values for the corresponding toluenes. *J. Am. Chem. Soc.* **1989**, *111*, 754–755.
- (33) Zhang, X. M.; Bordwell, F. G.; van der Puy, M.; Fried, H. E. Equilibrium acidities and homolytic bond dissociation energies of the acidic carbon-hydrogen bonds in N-substituted trimethylammonium and pyridinium cations. *J. Org. Chem.* **1993**, *58*, 3060–3066.
- (34) Bordwell, F. G.; Boyle, W. J. Kinetic isotope effects as guides to transition-state structures in deprotonation reactions. *J. Am. Chem. Soc.* **1971**, *93*, 512–514.
- (35) Qiu, G.; Ni, C.-L.; Knowles, R. R. Isotopic Fractionation as a Mechanistic Probe in Light-Driven C-H Bond Exchange Reactions. *J. Am. Chem. Soc.* **2023**, *145*, 11537–11543.
- (36) Berger, A. L.; Donabauer, K.; König, B. Photocatalytic Barbier reaction - visible-light induced allylation and benzylation of aldehydes and ketones. *Chem. Sci.* **2018**, *9*, 7230–7235.
- (37) Curphey, T. J.; Trivedi, L. D.; Layloff, T. Electrochemical reductive acylation of benzophenone. *J. Org. Chem.* **1974**, *39*, 3831–3834.
- (38) Speckmeier, E.; Fischer, T. G.; Zeitler, K. A Toolbox Approach To Construct Broadly Applicable Metal-Free Catalysts for Photoredox Chemistry: Deliberate Tuning of Redox Potentials and Importance of Halogens in Donor-Acceptor Cyanoarenes. *J. Am. Chem. Soc.* **2018**, *140*, 15353–15365.
- (39) Franco, C.; Olmsted, J. Photochemical determination of the solubility of oxygen in various media. *Talanta* **1990**, *37*, 905–909.
- (40) Kutta, R.-J.; Langenbacher, T.; Kensy, U.; Dick, B. Setup and performance of a streak camera apparatus for transient absorption measurements in the ns to ms range. *Appl. Phys. B* **2013**, *111*, 203–216.
- (41) Duan, X.; Scheiner, S. Energetics, proton transfer rates, and kinetic isotope effects in bent hydrogen bonds. *J. Am. Chem. Soc.* **1992**, *114*, 5849–5856.
- (42) Boldt, A. M.; Dickinson, S. I.; Ramirez, J. R.; Benz-Weeden, A. M.; Wilson, D. S.; Stevenson, S. M. Reactions of benzyltriphenylphosphonium salts under photoredox catalysis. *Org. Biomol. Chem.* **2021**, *19*, 7810–7815.
- (43) Khursan, S. L.; Mikhailov, D. A.; Yanborisov, V. M.; Borisov, D. I. AM1 calculations of bond dissociation energies. Allylic and benzylic C-H bonds. *React. Kinet. Catal. Lett.* **1997**, *61*, 91–95.
- (44) Luo, Y.-R. *Handbook of bond dissociation energies in organic compounds*; CRC Press: Boca Raton, Fla., 2003.
- (45) Lowry, M. S.; Goldsmith, J. I.; Slinker, J. D.; Rohl, R.; Pascal, R. A.; Malliaras, G. G.; Bernhard, S. Single-Layer Electroluminescent Devices and Photoinduced Hydrogen Production from an Ionic Iridium(III) Complex. *Chem. Mater.* **2005**, *17*, 5712–5719.
- (46) Espinoza, E. M.; Clark, J. A.; Soliman, J.; Derr, J. B.; Morales, M.; Vullev, V. I. Practical Aspects of Cyclic Voltammetry: How to Estimate Reduction Potentials When Irreversibility Prevails. *J. Electrochem. Soc.* **2019**, *166*, H3175-H3187.
- (47) Jašíková, L.; Roithová, J. Interaction of the Gold(I) Cation Au(PMe₃)⁺ with Unsaturated Hydrocarbons. *Organometallics* **2012**, *31*, 1935–1942.

- (48) Kler, N. R. M. de; Roithová, J. Copper aryl nitrene intermediates: formation, structure and reactivity. *Chem. Commun.* **2020**, 56, 12721–12724.
- (49) Armentrout, P. Kinetic energy dependence of ion–molecule reactions: guided ion beams and threshold measurements. *Int. J. Mass spectrom.* **2000**, 200, 219–241.
- (50) Armentrout, P. B. Mass spectrometry--not just a structural tool: the use of guided ion beam tandem mass spectrometry to determine thermochemistry. *J. Am. Soc. Mass. Spectrom.* **2002**, 13, 419–434.
- (51) Engle, S.; Takisha R. Kirkner; Christopher B. Kelly. Preparation of 2,4,5,6-Tetra(9*H*-carbazol-9-yl)isophthalonitrile. *Org. Synth.* **2019**, 96, 455–473.
- (52) Luo, J.; Hu, B.; Wu, W.; Hu, M.; Liu, T. L. Nickel-Catalyzed Electrochemical C(sp³)-C(sp²) Cross-Coupling Reactions of Benzyl Trifluoroborate and Organic Halides. *Angew. Chem. Int. ed.* **2021**, 60, 6107–6116.
- (53) Stache, E. E.; Rovis, T.; Doyle, A. G. Dual Nickel- and Photoredox-Catalyzed Enantioselective Desymmetrization of Cyclic meso-Anhydrides. *Angew. Chem. Int. ed.* **2017**, 56, 3679–3683.
- (54) Weng, W.-Z.; Liang, H.; Zhang, B. Visible-Light-Mediated Aerobic Oxidation of Organoboron Compounds Using in Situ Generated Hydrogen Peroxide. *Org. Lett.* **2018**, 20, 4979–4983.
- (55) Hashimoto, T.; Ishimaru, T.; Shiota, K.; Yamaguchi, Y. Bottleable NiCl₂(dppf) as a catalyst for the Markovnikov-selective hydroboration of styrenes with bis(pinacolato)diboron. *Chem. Commun.* **2020**, 56, 11701–11704.
- (56) Greenwood, J. W.; Boyle, B. T.; McNally, A. Pyridylphosphonium salts as alternatives to cyanopyridines in radical-radical coupling reactions. *Chem. Sci.* **2021**, 12, 10538–10543.
- (57) Bertrand, X.; Pucheault, M.; Chabaud, L.; Paquin, J.-F. Synthesis of Tertiary Fluorides through an Acid-Mediated Deoxyfluorination of Tertiary Alcohols. *J. Org. Chem.* **2023**, 88, 14527–14539.
- (58) Deng, Z.; Han, S.; Ke, M.; Ning, Y.; Chen, F.-E. Ligand-enabled palladium-catalyzed hydroesterification of vinyl arenes with high linear selectivity to access 3-arylpropanoate esters. *Chem. Commun.* **2022**, 58, 3921–3924.
- (59) Yan, X.-B.; Li, C.-L.; Jin, W.-J.; Guo, P.; Shu, X.-Z. Reductive coupling of benzyl oxalates with highly functionalized alkyl bromides by nickel catalysis. *Chem. Sci.* **2018**, 9, 4529–4534.
- (60) Wakayama, F.; Ito, R.; Park, K.; Ishida, M.; Yamada, Y.; Ichihara, S.; Takada, H.; Nakamura, S.; Kato, A.; Yamada, T.; Sajiki, H.; Monguchi, Y. Esterification or Thioesterification of Carboxylic Acids with Alcohols or Thiols Using Amphipathic Monolith-SO₃ H Resin. *Bull. Chem. Soc. Jpn.* **2021**, 94, 2702–2710.
- (61) Motoshima, K.; Ishikawa, M.; Hashimoto, Y.; Sugita, K. Peroxisome proliferator-activated receptor agonists with phenethylphenylphthalimide skeleton derived from thalidomide-related liver X receptor antagonists: relationship between absolute configuration and subtype selectivity. *Bioorg. Med. Chem.* **2011**, 19, 3156–3172.
- (62) Nomura, S.; Endo-Umeda, K.; Aoyama, A.; Makishima, M.; Hashimoto, Y.; Ishikawa, M. Styrylphenylphthalimides as Novel Transrepression-Selective Liver X Receptor (LXR) Modulators. *ACS Med. Chem. Lett.* **2015**, 6, 902–907.
- (63) Espinal-Viguri, M.; Neale, S. E.; Coles, N. T.; Macgregor, S. A.; Webster, R. L. Room Temperature Iron-Catalyzed Transfer Hydrogenation and Regioselective Deuteration of Carbon-Carbon Double Bonds. *J. Am. Chem. Soc.* **2019**, 141, 572–582.
- (64) Sahoo, P. K.; Zhang, Y.; Qin, Y.; Ren, P.; Cauwenbergh, R.; Siva Raman, G.; Das, S. Robust late-stage benzylic C(sp³)-H aminations by using transition metal-free photoredox catalysis. *J. Catal.* **2023**, 425, 80–88.
- (65) Marquet, P.; Venisse, N.; Lacassie, É.; Lachâtre, G. In-source CID mass spectral libraries for the “general unknown” screening of drugs and toxicants. *Analisis* **2000**, 28, 925–934.
- (66) Crellin, K. C.; Sible, E.; van Antwerp, J. Quantification and confirmation of identity of analytes in various matrices with in-source collision-induced dissociation on a single quadrupole mass spectrometer. *Int. J. Mass spectrom.* **2003**, 222, 281–311.
- (67) Andris, E.; Jašík, J.; Gómez, L.; Costas, M.; Roithová, J. Spectroscopic Characterization and Reactivity of Triplet and Quintet Iron(IV) Oxo Complexes in the Gas Phase. *Angew. Chem. Int. ed.* **2016**, 55, 3637–3641.
- (68) Parcher, J. F.; Wang, M.; Chittiboyina, A. G.; Khan, I. A. In-source collision-induced dissociation (IS-CID): Applications, issues and structure elucidation with single-stage mass analyzers. *Drug Test Anal.* **2018**, 10, 28–36.
- (69) Teloy, E.; Gerlich, D. Integral cross sections for ion—molecule reactions. I. The guided beam technique. *Chem. Phys.* **1974**, 4, 417–427.
- (70) Kutta, R. J. Blitzlichtphotolyse - Untersuchung Zu LOV-Domänen Und Photochromen Systemen. PhD Thesis, University of Regensburg, Regensburg, 2012.

- (71) Dick, B.; Kensy, U.; Kutta, R. J. 17. Transient absorption with a streak camera. In *Chemical Photocatalysis*, 2nd edition; König, B., Ed.; De Gruyter: Berlin, Boston, 2020; pp 415–442.
- (72) Kutta, R. J.; Archipowa, N.; Scrutton, N. S. The sacrificial inactivation of the blue-light photosensor cryptochrome from *Drosophila melanogaster*. *Phys. Chem. Chem. Phys.* **2018**, *20*, 28767–28776.
- (73) Hartman, T.; Reisnerová, M.; Chudoba, J.; Svobodová, E.; Archipowa, N.; Kutta, R. J.; Cibulka, R. Photocatalytic Oxidative 2+2 Cycloelimination Reactions with Flavinium Salts: Mechanistic Study and Influence of the Catalyst Structure. *ChemPlusChem* **2021**, *86*, 373–386.
- (74) Archipowa, N.; Kutta, R. J.; Heyes, D. J.; Scrutton, N. S. Stepwise Hydride Transfer in a Biological System: Insights into the Reaction Mechanism of the Light-Dependent Protochlorophyllide Oxidoreductase. *Angew. Chem. Int. ed.* **2018**, *57*, 2682–2686.
- (75) Siegel, B. Mechanism of base-promoted phosphonium salt hydrolyses. Kinetics and multiple substituent effects for a nucleophilic attack at phosphorus. *J. Am. Chem. Soc.* **1979**, *101*, 2265–2268.
- (76) Wayner, D. D. M.; McPhee, D. J.; Griller, D. Oxidation and reduction potentials of transient free radicals. *J. Am. Chem. Soc.* **1988**, *110*, 132–137.
- (77) Weigend, F. Accurate Coulomb-fitting basis sets for H to Rn. *Phys. Chem. Chem. Phys.* **2006**, *8*, 1057–1065.
- (78) Weigend, F.; Ahlrichs, R. Balanced basis sets of split valence, triple zeta valence and quadruple zeta valence quality for H to Rn: Design and assessment of accuracy. *Phys. Chem. Chem. Phys.* **2005**, *7*, 3297–3305.
- (79) Grimme, S. Semiempirical GGA-type density functional constructed with a long-range dispersion correction. *J. Comput. Chem.* **2006**, *27*, 1787–1799.
- (80) Grimme, S.; Ehrlich, S.; Goerigk, L. Effect of the damping function in dispersion corrected density functional theory. *J. Comput. Chem.* **2011**, *32*, 1456–1465.
- (81) Frisch, M. J.; Trucks, G. W.; Schlegel, H. B.; Scuseria, G. E.; Robb, M. A.; Cheeseman, J. R.; Scalmani, G.; Barone, V.; Petersson, G. A.; Nakatsuji, H.; Li, X.; Caricato, M.; Marenich, A. V.; Bloino, J.; Janesko, B. G.; Gomperts, R.; Mennucci, B.; Hratchian, H. P.; Ortiz, J. V.; Izmaylov, A. F.; Sonnenberg, J. L.; Williams-Young, D.; Ding, F.; Lipparini, F.; Egidi, F.; Goings, J.; Peng, B.; Petrone, A.; Henderson, T.; Ranasinghe, D.; Zakrzewski, V. G.; Gao, J.; Rega, N.; Zheng, G.; Liang, W.; Hada, M.; Ehara, M.; Toyota, K.; Fukuda, R.; Hasegawa, J.; Ishida, M.; Nakajima, T.; Honda, Y.; Kitao, O.; Nakai, H.; Vreven, T.; Throssell, K.; Montgomery, J. A.; Peralta, J. E.; Ogliaro, F.; Bearpark, M. J.; Heyd, J. J.; Brothers, E. N.; Kudin, K. N.; Staroverov, V. N.; Keith, T. A.; Kobayashi, R.; Normand, J.; Raghavachari, K.; Rendell, A. P.; Burant, J. C.; Iyengar, S. S.; Tomasi, J.; Cossi, M.; Millam, J. M.; Klene, M.; Adamo, C.; Cammi, R.; Ochterski, J. W.; Martin, R. L.; Morokuma, K.; Farkas, O.; Foresman, J. B.; Fox, D. J. *Gaussian 16, Revision C.01*; Gaussian, Inc.: Wallingford CT, 2019.
- (82) Rassolov, V. A.; Ratner, M. A.; Pople, J. A.; Redfern, P. C.; Curtiss, L. A. 6-31G* basis set for third-row atoms. *J. Comput. Chem.* **2001**, *22*, 976–984.
- (83) Rassolov, V. A.; Pople, J. A.; Ratner, M. A.; Windus, T. L. 6-31G* basis set for atoms K through Zn. *J. Chem. Phys.* **1998**, *109*, 1223–1229.
- (84) Blaudeau, J.-P.; McGrath, M. P.; Curtiss, L. A.; Radom, L. Extension of Gaussian-2 (G2) theory to molecules containing third-row atoms K and Ca. *J. Chem. Phys.* **1997**, *107*, 5016–5021.
- (85) Petersson, G. A.; Al-Laham, M. A. A complete basis set model chemistry. II. Open-shell systems and the total energies of the first-row atoms. *J. Chem. Phys.* **1991**, *94*, 6081–6090.
- (86) Binning, R. C.; Curtiss, L. A. Compact contracted basis sets for third-row atoms: Ga–Kr. *J. Comput. Chem.* **1990**, *11*, 1206–1216.
- (87) Francl, M. M.; Pietro, W. J.; Hehre, W. J.; Binkley, J. S.; Gordon, M. S.; DeFrees, D. J.; Pople, J. A. Self-consistent molecular orbital methods. XXIII. A polarization-type basis set for second-row elements. *J. Chem. Phys.* **1982**, *77*, 3654–3665.
- (88) Gordon, M. S. The isomers of silacyclop propane. *Chem. Phys. Lett.* **1980**, *76*, 163–168.
- (89) Hariharan, P. C.; Pople, J. A. The influence of polarization functions on molecular orbital hydrogenation energies. *Theoret. Chim. Acta* **1973**, *28*, 213–222.
- (90) Hehre, W. J.; Lathan, W. A. Self-Consistent Molecular Orbital Methods. XIV. An Extended Gaussian-Type Basis for Molecular Orbital Studies of Organic Molecules. Inclusion of Second Row Elements. *J. Chem. Phys.* **1972**, *56*, 5255–5257.
- (91) Ditchfield, R.; Hehre, W. J.; Pople, J. A. Self-Consistent Molecular-Orbital Methods. IX. An Extended Gaussian-Type Basis for Molecular-Orbital Studies of Organic Molecules. *The Journal of Chemical Physics* **1971**, *54*, 724–728.

(92) Chai, J.-D.; Head-Gordon, M. Long-range corrected hybrid density functionals with damped atom-atom dispersion corrections. *Phys. Chem. Chem. Phys.* **2008**, *10*, 6615–6620.

4 Regio-, Diastereo- and Enantioselectivity in the Photocatalytic Generation of Carbanions via Hydrogen Atom Transfer and Reductive Radical-Polar Crossover



This chapter has been published. For reference see: S. Grotjahn, L. Müller, A. Pattanaik, A. Falk, G. Barison, J. O. Bauer, J. Rehbein, R. M. Gschwind and Burkhard König, *Org. Chem. Front.*, 2024, Accepted Manuscript. DOI: 10.1039/D4QO01219D

Adapted with permission from the Royal Society of Chemistry.

Author contributions: Sascha Grotjahn conceived the idea and coordinated the collaborations. Sascha Grotjahn and Giorgia Barison (under supervision of Sascha Grotjahn) synthesized compounds for C-H activation and performed the substrate screening under supervision of Burkhard König. Sascha Grotjahn measured preliminary kinetics, Lea Müller conducted detailed kinetic studies and synthesized compounds **4i**, **18h**, **18d**, **35** and *cis*-**4c** under supervision of Burkhard König and Ruth M. Gschwind. Sascha Grotjahn developed the synthesis of TADDOL-based chiral silane thiols under supervision of Burkhard König. Alexander Falk developed the synthesis of menthol-based silane thiol **11** and silicon-chiral silane thiols under supervision of Jonathan O. Bauer. Sascha Grotjahn performed deracemization reactions under supervision of Burkhard König. Aryaman Pattanaik performed DFT calculations under supervision of Julia Rehbein. Sascha Grotjahn wrote the manuscript with the input of all other authors.

Abstract

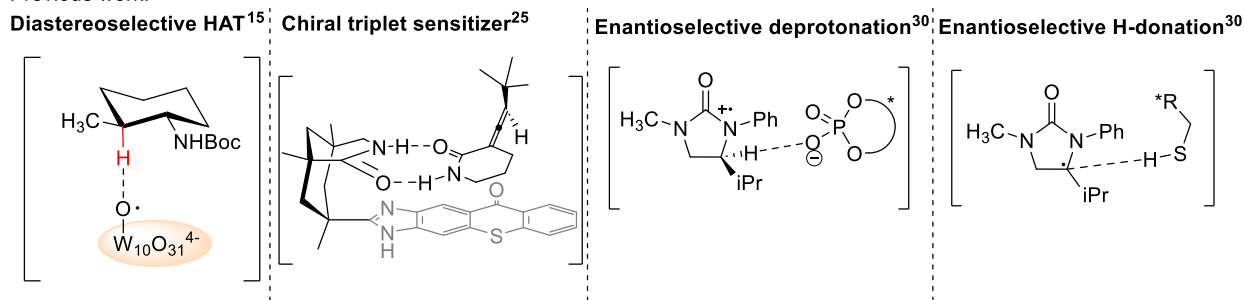
A sequence consisting of photocatalytic hydrogen atom abstraction (HAT), reductive radical-polar crossover (RRPCO), and protonation/deuteration for stereochemical editing at benzylic positions is described. A systematic screening of substrates with benzylic C-H bonds provides trends in reactivity for C-H activation by silane thiols. A *cis/trans* isomerization of dihydrobenzofurans proceeding under kinetic control in the HAT step is presented and the concept transferred to a deracemization by chiral silane thiols as HAT reagents in a proof-of-concept study.

4.1 Introduction

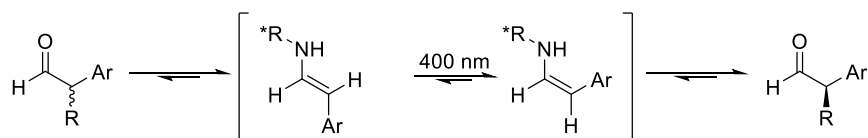
The C-H bond is the most prevalent functional group in organic compounds and the cleavage of this bond is one of the most atom- and step-economic ways to activate organic molecules.^{1,2} However, the low polarity and high bond strength often necessitate the use of reactive hydrogen atom abstraction reagents or strong bases. While deprotonation of acidic C-H bonds, for example in α -position to carbonyl groups, is a standard method in organic chemistry, less acidic C-H bonds are more difficult to activate. In recent years, various photocatalytic methods emerged to enable the activation of rather inert C-H bonds to the corresponding radicals. Despite the progress in C-H activation, selectivity in the C-H abstraction and diastereo- or enantioselective reactions with the generated reactive intermediates are still challenging. An especially appealing type of reactions conceivable with the utilization of photocatalytic C-H activation are stereochemical editing methods and in particular deracemizations in which the product and substrate only differ in the configuration at a single carbon atom. Although with $\Delta G = 0.40$ kcal/mol between a racemic mixture and an enantiomerically pure compound the energy that must be provided is small in absolute terms, microscopic reversibility inevitably causes racemization in a thermodynamic equilibrium.³⁻⁵ To enable deracemization via cleavage and formation of a C-H bond, both steps must proceed via distinct transition states. In classical catalysis, this cannot be achieved without the use of sacrificial reagents, although one-pot procedures using oxidation/reduction sequences⁶⁻⁹ and biocatalytic methods have been reported.¹⁰⁻¹² In photocatalysis, however, at least one reaction step proceeds from an excited state energetically out of reach for the back reaction. Thus, limitations caused by microscopic reversibility in traditional catalysis can be avoided, making deracemizations and contra thermodynamic stereochemical editing in general possible without the need of sacrificial reagents.¹³ The same concept can be used in stereochemical editing techniques in which one diastereomer is converted to another. Although both diastereomers are usually of different energy, the diastereomeric ratio in hydrogen exchange reactions under photocatalytic conditions is not limited by the relative thermodynamic stability of the diastereomers. This has been previously demonstrated on the examples of selective epimerization for the synthesis of rare sugar isomers¹⁴ and in the epimerization of tertiary stereocenters.¹⁵ Both proceed under kinetic control via two distinct hydrogen atom transfer steps (HAT/HAT). Photocatalytic epimerization reactions governed by thermodynamic control are also known,¹⁶⁻²⁰ but the mechanistic concept is fundamentally different from stereochemical editing under kinetic control. The first photocatalytic deracemization using a chiral catalyst was reported in 1965 using energy transfer from a chiral photosensitizer, albeit only low enantiomeric excesses were achieved.²¹ Similar reactions and mechanistic investigations were published in the following years²²⁻²⁴ but only recently more broadly applicable methods with good enantiomeric excess (*ee*) were reported. Such methods utilize energy transfer from a chiral photosensitizer,²⁵⁻²⁸ photochemical E/Z isomerization,²⁹ an electron transfer/proton transfer/HAT sequence,³⁰ photoredox deprotonation/protonation,^{31,32} and photoinduced ring opening/closure by an Al-salen complex³³ or BINOL-phosphate Ti-complex.³⁴ The proposed transition states and steps responsible for the diastereo- and enantioselectivity of a selection of stereochemical editing and deracemization reactions are depicted in Scheme 4.1. A more detailed overview and additional examples of photocatalytic deracemization can be found in recent reviews.^{35,36}

REGIO-, DIASTEREO- AND ENANTIOSELECTIVITY IN THE PHOTOCATALYTIC GENERATION OF CARBANIONS VIA HYDROGEN ATOM ABSTRACTION AND REDUCTIVE RADICAL-POLAR CROSSOVER

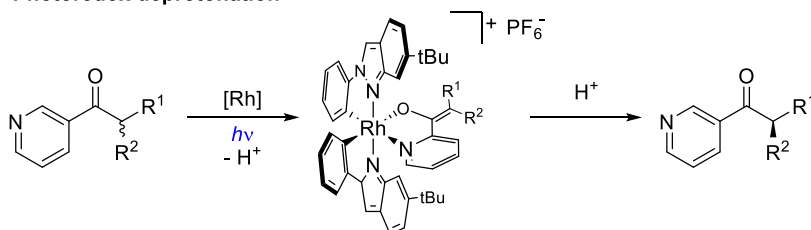
Previous work:



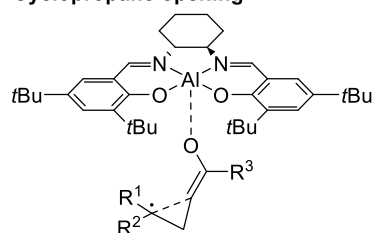
Deracemization via photochemical *E/Z* isomerization of enamines²⁹



Photoredox deprotonation³¹

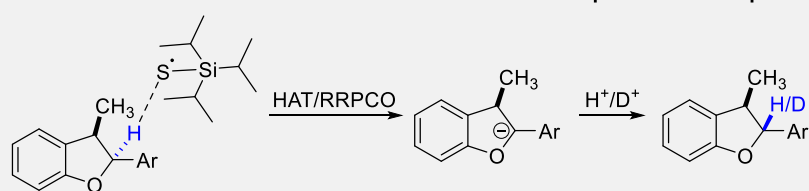


Cyclopropane opening³³

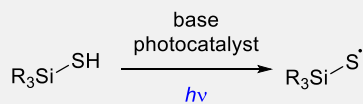


This work:

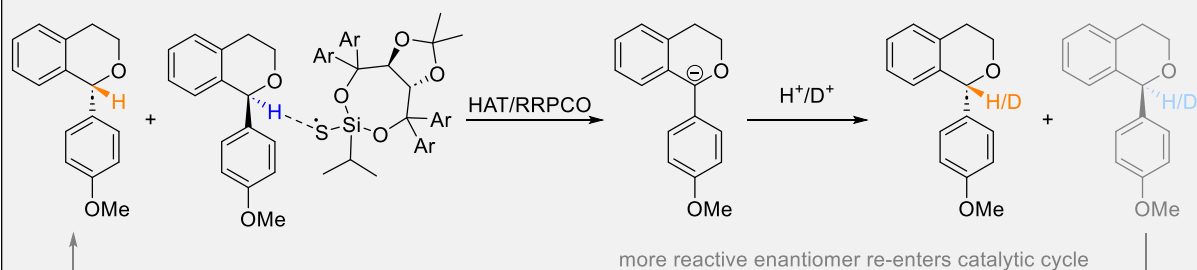
cis/trans-isomerization via diastereoselective HAT/RRPCO/protonation sequence



Photocatalytic activation of HAT-reagent



Deracemization via enantioselective HAT/RRPCO/protonation sequence



Scheme 4.1. Selection of known methods for photocatalytic stereochemical editing including epimerization via a diastereoselective HAT/HAT sequence,¹⁵ deracemization via energy transfer from a chiral photosensitizer,²⁵ enantioselective PCET with chiral phosphates,³⁰ enantioselective H-atom donation,³⁰ photochemical *E/Z*-isomerization of chiral enamines,²⁹ photoredox deprotonation/enantioselective protonation^{31,32} and photoinduced cyclopropane opening/closure by an Al-salen complex.³³ This work: *cis/trans*-isomerization of dihydrobenzofurans and proof of concept for deracemization via a HAT/RRPCO/protonation sequence.

In this work, we demonstrate that the same logic can be applied to a sequence consisting of a hydrogen atom transfer, reductive radical-polar crossover, followed by protonation (HAT/RRPCO/protonation) in which the bond breaking step proceeds via hydrogen atom abstraction and the bond forming step via protonation of a highly basic carbanion.

In this sequence the RRPCO³⁷ connects the radical pathway to erase stereoinformation via HAT to a polar reaction resetting the stereocenter via protonation. This sequence was applied to *cis/trans*-epimerization by an achiral HAT reagent and subsequently transferred to a photocatalytic deracemization by chiral silane thiol HAT reagents. A general overview of the concept of deracemization via a HAT/RRPCO/protonation sequence is depicted in Figure 4.1.

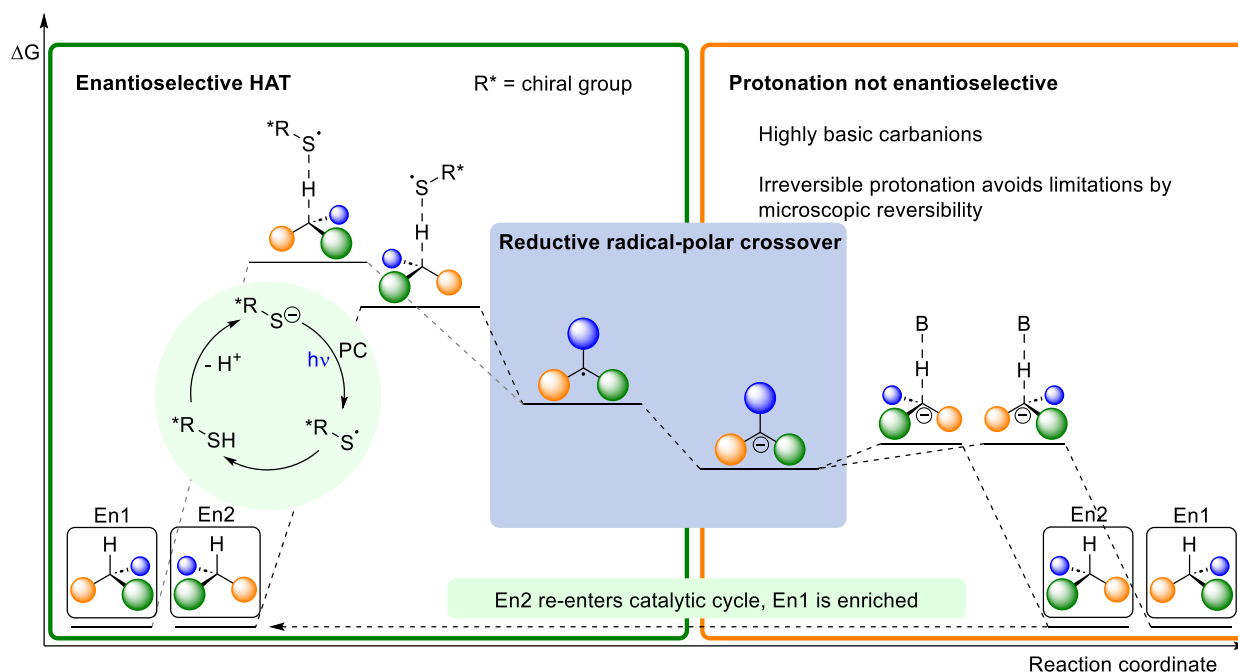


Figure 4.1. Simplified energy diagram for photocatalytic deracemization via a HAT/RRPCO/protonation sequence. Activation of the HAT catalyst by an excited photocatalyst starts the reaction sequence. RRPCO followed by protonation converts the C-centered radical back to the substrate. The barrier for the back reaction is too high and thus limitations caused by microscopic reversibility under non-photocatalytic conditions are avoided. If the barrier for C-H activation of enantiomer En2 is lower than for En1, En2 is preferentially racemized and En1 is enriched.

4.2 Results and discussion

4.2.1 Identification of reactive benzylic C-H bonds

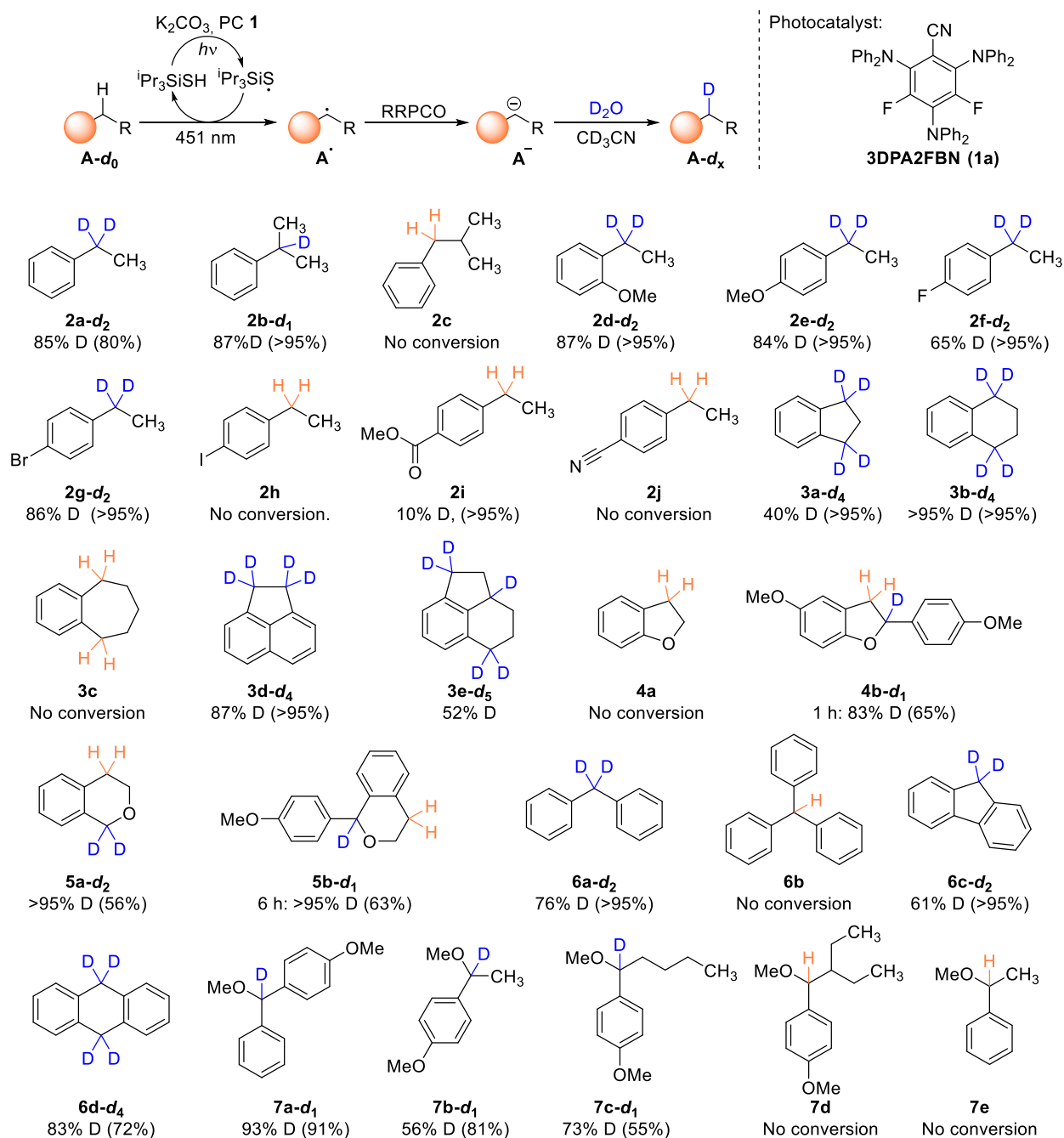
C-H activation of benzylic C-H bonds via a HAT/RRPCO sequence has been reported previously.³⁸ However, the focus was on the development of a photocatalytic version of the Grignard-reaction and the selectivity of the C-H activation step was not included. The first step in the development of a diastereo- and enantioselective HAT/RRPCO sequence, is a systematic screening of compounds with benzylic C-H bonds to understand the selectivity and to rationally predict which C-H bonds can be activated. Deuteration by D₂O was chosen as model reaction to efficiently convert carbanions back to stable molecules with minimal steric interference and to keep the model system close to later deracemization approaches as product and substrate only differ in the hydrogen isotope at the benzylic position. In this work, deuteration serves primarily as a tool to investigate the activation to the corresponding carbanions under HAT/RRPCO conditions. However, it is synthetically useful in the development of deuterated molecules for example in drug discovery.³⁹

C-H bonds in alkyl benzenes are activated to give the corresponding benzyl carbanions unless electron withdrawing groups or bulky substituents in the α -position are present. While **2a** and **2b** give high degrees of deuteration at the benzylic position, **2c** with a sterically hindering isopropyl group next to the benzylic C-H bond does not give any conversion. The same trend in reactivity is observed when comparing unhindered benzyl ethers **7a**, **7b**, and **7c** to sterically demanding benzyl ether **7d**, and when comparing diphenylbenzene (**6a**) to triphenylbenzene (**6b**). This last example is particularly interesting because the trityl radical is known to be a rather stable radical⁴⁰ and in chapter 3 on the reactivity of photocatalytically generated carbanions the corresponding trityl anion formed cleanly from triphenylacetic acid. This demonstrates that hydrogen atom abstraction from triphenylmethane does not occur while the subsequent reductive radical-polar crossover step proceeds under similar reaction conditions.

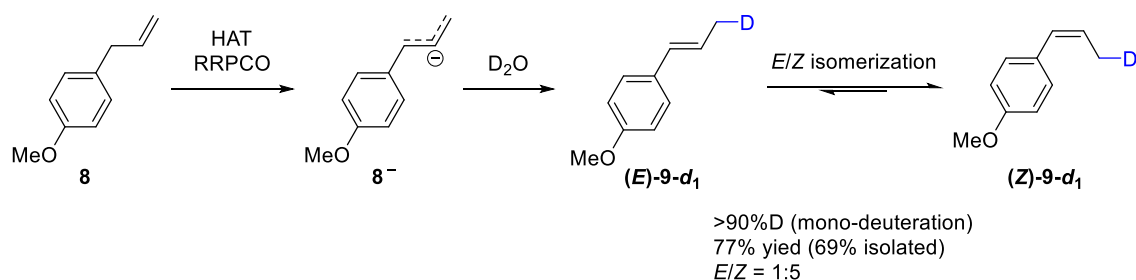
Benzylic C-H bonds in 5-membered (**3a**, **3d**, **3e**, **6c**) and 6-membered carbocycles (**3b**, **3e**, **6d**) are similarly or more easily activated compared to their acyclic analogs while the benzylic C-H bonds in the 7-membered ring of **3c** are inert towards C-H abstraction by silanethiol radicals. Benzylic positions adjacent to oxygen atoms can be activated if part of an isochromane ring (**5a**), while similar acyclic benzylic positions are inert (**7e**) but can be deuterated if additional activation by a methoxy group in the para position (**7b**, **7c**) or another adjacent aryl ring (**7a**) is present.

In general, the reactivity of benzylic C-H bonds towards C-H abstraction under the respective reaction conditions is only partially dictated by the bond dissociation energies (BDEs). While high BDEs do limit the reactivity, some substrates with particularly low BDEs are unreactive. This is affirmed by the calculated BDEs for a selection of reacting and inert substrates discussed in more detail in the experimental part section 4.4.4.1.

In the presence of a double bond adjacent to the benzylic position, isomerization to the corresponding styrene was observed upon protonation of the corresponding carbanion. Subjecting 4-methoxyallyl benzene (**8**) to the deuteration conditions of Scheme 4.2 gave *cis*-anethole ((**Z**)-**9-d₁**) with a high degree of deuteration at the terminal methyl group as depicted in Scheme 4.3. Control reactions suggest that *E/Z* isomerization occurs via photosensitization of *trans*-anethole ((**E**)-**9-d₁**) by the photocatalyst while no deuteration of (**E**)-**9** is observed under otherwise identical reaction conditions. This is in agreement with literature reports.⁴¹ Whether an *E/Z* selectivity is present in the deuteration step is not derivable from the results. Without the addition of photocatalyst, (**E**)-**9** is configurationally stable under irradiation with blue light.



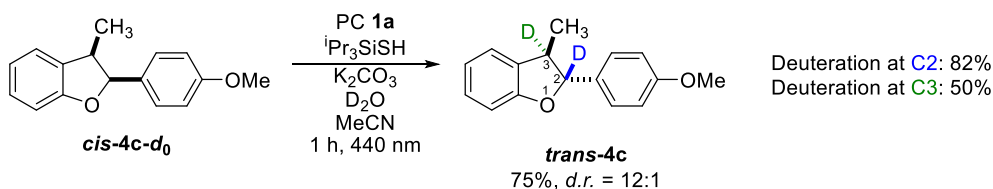
Scheme 4.2. Benzylic deuteration via C-H activation to the corresponding carbanions A^- and subsequent deuteration by D_2O . Positions marked in blue were efficiently labelled, positions marked in orange did not undergo deuteration to notable extent. Reaction time: 16-18 h, unless otherwise noted. Experimental details and an expanded substrate scope can be found in the supporting information section 4.1. 3DPA2FBN (**1a**) likely is not the active catalyst but rather converts to a catalytically active species under irradiation, similar to previous reports.^{42,43} For details see supporting information section 8.

Allylbenzenes: Double bond migration via HAT/RRPCO/protonation and *E/Z* isomerization via sensitization


Scheme 4.3. Double bond migration via HAT/RRPCO/protonation sequence under reaction conditions identical to scheme 4.2.

4.2.2 Epimerization via diastereoselective hydrogen atom abstraction

In the next step, diastereoselectivity was investigated using dihydrobenzofuran *cis-4c-d₀* as an example. Under conditions for hydrogen isotope exchange via a HAT/RRPCO/deuteration sequence epimerization to *trans-4c-d₀* is observed with a diastereomeric ratio (*d.r.*) of 12:1 within 1 h of irradiation (Scheme 4.4). With longer reaction time a *trans/cis* ratio of >20:1 is obtained, albeit at the cost of diminished yield.

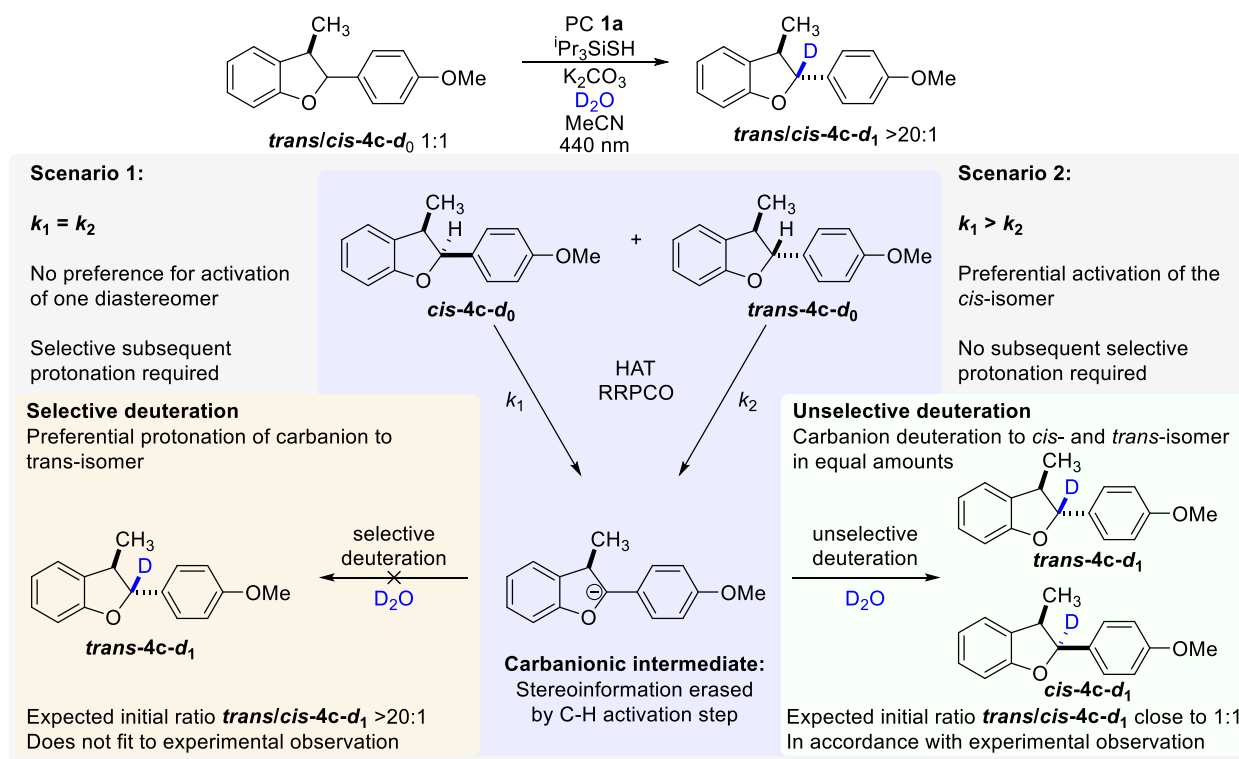


Scheme 4.4. A HAT/RRPCO/deuteration sequence isomerizes *cis-4c* to *trans-4c* with good diastereomeric ratio of 12:1 and high degree of deuteration in the 2-position and additional moderate deuteration in the 3-position within 1 hour. The diastereomeric ratio (*d.r.*) is further increased with prolonged reaction time (see below). Yield, *d.r.* and deuteration degrees were determined via ¹H NMR spectroscopy of the reaction mixture.

Two conceptually distinct scenarios to explain the *trans*-selectivity are conceivable: Preferential protonation/deuteration of carbanion **4c⁻** to *trans-4c* over *cis-4c* (Scheme 4.5, scenario 1) would selectively set the stereocenter in the protonation/deuteration step, analogously to known thermodynamically driven stereochemical editing methods.^{16,18–20} In the other scenario, a faster C-H activation of *cis-4c* compared to *trans-4c* preferentially epimerizes *cis-4c* with no selectivity for the subsequent protonation/deuteration step (Scheme 4.5, scenario 2), analogously to previously reported HAT/HAT sequences.^{14,15} Kinetic control was also observed to diminish the diastereoselectivity under non-optimized reaction conditions in a HAT/HAT sequence for epimerization to the thermodynamic product.¹⁸

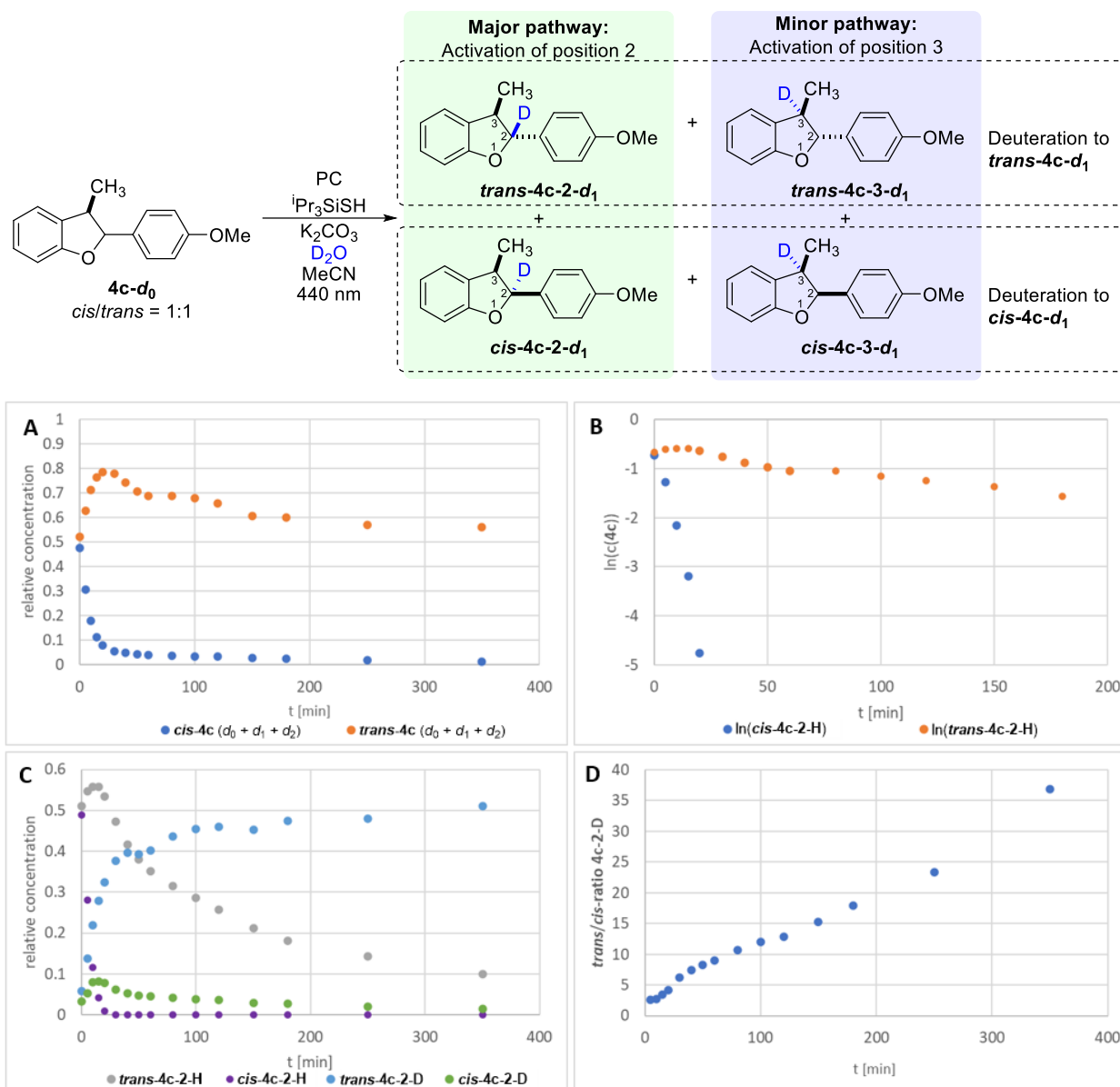
To differentiate between these scenarios in a HAT/RRPCO/protonation sequence, deuterium labelling was used as mechanistic probe. When subjecting a 1:1 mixture of *cis-4c* and *trans-4c* to the conditions for benzylic deuteration by D₂O, substrates *cis-4c-d₀* and *trans-4c-d₀* are distinguished from the products *cis-4c-d₁* and *trans-4c-d₁* by the hydrogen isotope in the benzylic position. Although both mechanistic scenarios can lead to the same *trans/cis* ratio in a dynamic equilibrium, the intermediate *trans/cis* ratios are different. If C-H activation is unselective (scenario 1), both, *trans-4c-d₀* and *cis-4c-d₀* would be converted with the same rate constant while the products *trans-4c-d₁* and *cis-4c-d₁* are generated with a constantly high *trans/cis* ratio. On the other hand, if scenario 2 is responsible for the

trans-selectivity, *cis-4c-d₀* would be converted with a larger rate constant compared to *trans-4c-d₀* while the *trans/cis* ratio of the product is initially close to 1 and rises with the reaction progress. If both scenarios complement each other, a faster conversion of *cis-4c-d₀* would be observed while the product *trans/cis* ratio starts at a moderate level and further increases with the reaction progress. The competitive deuteration experiment depicted in Scheme 4.5 confirmed that mainly scenario 2 is responsible for the observed *trans*-selectivity by favoring the epimerization of *cis-4c* with only low *trans*-selectivity of <3:1 in the protonation/deuteration step.



Scheme 4.5. Competitive deuteration experiment. C-H activation of a diastereomeric mixture of *cis-4c-d₀* and *trans-4c-d₀* to the corresponding carbanion followed by RRPCO and protonation yields *trans-4c-d₁* and *cis-4c-d₁* with high *d.r.* in favor of the *trans*-isomer. The change in the ratio between *cis-4c-d₀* and *trans-4c-d₀* was used as mechanistic probe to distinguish between scenario 1 and scenario 2. Deuteration in the 3-position is also observed, but to a lower extent (see Scheme 4.4)

A fast decrease in signal intensity for the proton in the 2-position of *cis-4c* (*cis-4c-2-H*) with a rate constant of $2.0 \cdot 10^{-1} \text{ min}^{-1}$ is observed while the proton in the 2-position of *trans-4c* (*trans-4c-2-H*) even shows a slight initial increase (Schemes 4.6B and 4.6C, for a more detailed analysis of the observed behavior see experimental part, Figure 4.28). Only after almost full conversion of *cis-4c-2-H*, the signal intensity of *trans-4c-2-H* starts to decrease slowly with a rate constant of $1.1 \cdot 10^{-2} \text{ min}^{-1}$ as depicted in Scheme 4.6B. The rate constants measured for the diastereomerically pure compounds are $1.6 \cdot 10^{-1} \text{ min}^{-1}$ for *cis-4c* and $1.7 \cdot 10^{-2} \text{ min}^{-1}$ for *trans-4c* (experimental part, Figures 4.19 and 4.23) and thus in agreement with the rate constants obtained in the competitive deuteration experiment. Deuteration also occurs in the 3-position of **4c**, contributing to the isomerization, albeit to lower extent. For clarity, deuteration in the 3-position is not depicted in Scheme 4.6 and **4c-2-H** only refers to the respective proton in the 2-position, irrespective of deuteration in the 3-position.



Scheme 4.6. Competitive deuteration of a 1:1 mixture of trans-4c-d_0 and cis-4c-d_0 . For experimental details see experimental part 4.4.6. $\text{cis}/\text{trans-4c-2-H} = \text{cis}/\text{trans-4c-d}_0 + \text{cis}/\text{trans-4c-3-d}_1$; $\text{cis}/\text{trans-4c-2-D} = \text{cis}/\text{trans-4c-2-d}_1 + \text{cis}/\text{trans-4c-d}_2$. **A:** Relative concentrations of cis-4c (cis-4c-d_0 , cis-4c-d_1 , cis-4c-d_2) and trans-4c (trans-4c-d_0 , trans-4c-d_1 , trans-4c-d_2). Concentrations were determined via ^1H NMR spectroscopy in CD_3CN at a substrate concentration of 100 mM. **B:** At low degrees of deuteration, consumption of cis-4c-d_0 and trans-4c-d_0 can be approximated by a first order kinetic with rate constants of $2.0 \cdot 10^{-1} \text{ min}^{-1}$ and $1.1 \cdot 10^{-2} \text{ min}^{-1}$, respectively. For determination of the rate constant for trans-4c-d_0 data points before 20 min and after 60 min were excluded due to competition with $\text{cis-4c-d}_{0/1/2}$ and $\text{trans-4c-d}_{1/2}$, respectively, which cause deviation from a first-order reaction. **C:** Concentrations of deuterated products were determined by ^1H NMR spectroscopy by comparison of benzylic hydrogens at C2 with the methyl groups at C3. Both benzylic positions are activated by HAT catalyst $i\text{Pr}_3\text{SiSH}$ with a preference for the 2-position. For clarity, only deuteration in the 2-position is depicted. **D:** The initial trans/cis -ratio is low and increases with the reaction progress. This demonstrates that deuteration of carbanion 4c^- by D_2O is only weakly stereoselective and selectivity is mostly determined by the C-H activation step.

The trans/cis ratio is initially low and increases with reaction progress. A low trans selectivity of 1.5 in the protonation step is obtained from extrapolation of the trans/cis ratio according to Scheme 6D. Due to low concentrations of products in the initial minutes of the reaction trans/cis -ratios could not be obtained before 5 minutes. However, even the trans/cis ratios at 5 min and 10 min are only 2.6 and 2.8, respectively, while a trans/cis ratio of 18:1 is obtained

after 3 h of irradiation and >40:1 when starting from a 10:1 mixture *trans/cis-4c-d₀*. This demonstrates that the deuteration step cannot explain the high *trans*-selectivity, but that the overall selectivity in the epimerization reaction mainly occurs in the C-H activation step while only low selectivity is observed in the deuteration step. This is particularly intriguing for the fact that unstabilized benzyl carbanions are short lived intermediates which are difficult to be integrated into stereoselective reactions. The results demonstrate that shifting the focus from the unselective bond-forming step to the bond-breaking step enables stereocontrol. The epimerization presented is not only useful for mechanistic investigations, but late-stage stereochemical editing also allows different synthetic routes which initially lead to the wrong isomer or isomeric mixtures, providing more general access to the desired products.¹³ An example of the synthesis of dihydrobenzofurans utilizing a photocatalytic C-C bond-forming reaction with subsequent *cis/trans*-isomerization can be found in the experimental part 4.4.5.

4.2.3 Deracemization via enantioselective hydrogen atom abstraction

Based on the results from the diastereoselective C-H activation from the previous section, the stereoinformation was subsequently transferred from substrate control to reagent control. As the selectivity in our approach is in the bond-breaking step rather than the bond-forming step, an enantioselective reaction must be designed as a deracemization or desymmetrization. To introduce enantioselectivity in the photocatalytic generation of carbanions from benzylic C-H bonds, the stereoinformation needs to be on the HAT reagent. This sequence of enantioselective HAT/RRPCO/protonation is yet unprecedented. During the development of a photocatalytic alternative to the Grignard reaction via HAT/RRPCO, silane thiols were the only HAT reagents effectively catalyzing the reaction.³⁸ In this work triphenylgermanium thiol was found to also catalyze the reaction. However, it was less efficient than triphenylsilane thiol and trisopropylsilane thiol. Thus, chiral silane thiols were targeted as HAT reagents. Chiral silane thiols can be separated into two groups. Molecules with the silicon atom surrounded by chiral groups (Figure 4.2, group 1) and molecules with the silicon as stereocenter (Figure 4.2, group 2). The limited reports on chiral silicon compounds and silane thiols, even as achiral derivatives, limit the current accessibility of chiral silane thiols.

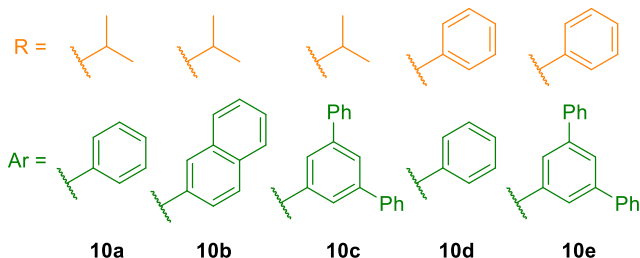
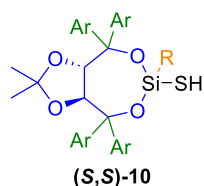
Chiral silane thiols:

Group 1: Silicon bound to chiral alcohols

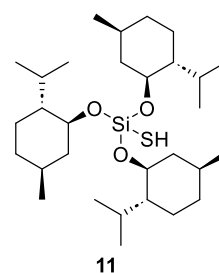
Derived from tartaric acid

-Both enantiomers available

-Modular synthesis



Derived from menthol



Group 2: Silicon-chiral silane thiols

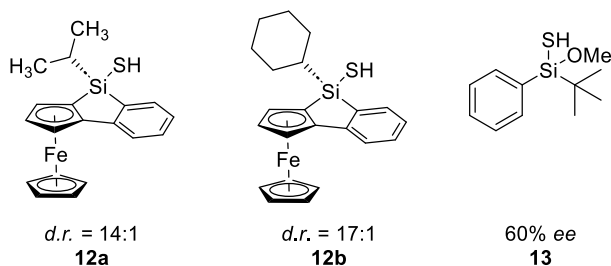
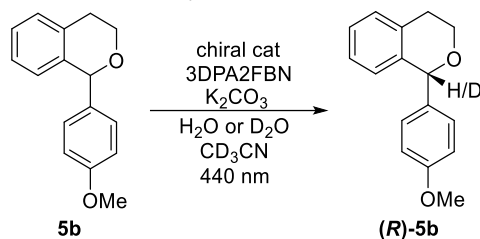


Figure 4.2. Chiral silane thiols designed as HAT catalysts. Absolute configurations of catalysts of group 1 were set by the configuration of the chiral alcohols. Absolute configuration of the major diastereomer of silicon-chiral silane thiols **12a** and **12b** was determined by single crystal X-ray diffraction analysis. Synthesis of silicon-chiral silane thiol **13** was published elsewhere⁴⁴ and the absolute configuration of the major enantiomer was not determined.

Tartaric acid derived TADDOL and monoterpene menthol were successfully incorporated into silane thiols. Additionally, three silane thiols with silicon as chirality center were synthesized. However, partial racemization occurred during the synthesis of silicon-chiral silane thiol **13** to give only moderate *ee* of 60%. Silane thiols **12a** and **12b** were obtained in diastereomeric ratios of 14:1 and 17:1, respectively. The yet unprecedented class of tartaric acid based TADDOL silane thiols **10** was especially appealing due to the possibility of systematic modification and accessibility of both enantiomers of tartaric acid.

Table 4.1. Deracemization of isochromane derivative **5b** by chiral silane thiols.

Entry	HAT catalyst	T	H ⁺ /D ⁺	time [h]	ee
1	(<i>R,R</i>)- 10a	rt	H ₂ O	6 h	4% (<i>R</i>)
2	(<i>R,R</i>)- 10a	-17 °C	CD ₃ OD	6 h	6% (<i>R</i>)
3	(<i>R,R</i>)- 10a	-17 °C	-	6 h	7% (<i>R</i>)
4	(<i>R,R</i>)- 10b	-17 °C	D ₂ O	6 h	3% (<i>R</i>)
5	(<i>R,R</i>)- 10b	-17 °C	H ₂ O	6 h	2% (<i>R</i>)
6	(<i>R,R</i>)- 10c	-17 °C	D ₂ O	6 h	-19% (<i>S</i>)
7	(<i>R,R</i>)- 10c	-17 °C	H ₂ O	6 h	-13% (<i>S</i>)
8	(<i>R,R</i>)- 10a	-17 °C	D ₂ O	16 h	7% (<i>R</i>)
9	(<i>R,R</i>)- 10c	-17 °C	D ₂ O	16 h	-32% (<i>S</i>)
10	(<i>R,R</i>)- 10c	-17 °C	-	16 h	-25% (<i>S</i>)
11	(<i>R,R</i>)- 10d	-17 °C	D ₂ O	16 h	13% (<i>S</i>)
12	(<i>S,S</i>)- 10d	-17 °C	D ₂ O	16 h	-11% (<i>R</i>)
13	(<i>S,S</i>)- 10e	-17 °C	D ₂ O	16 h	14% (<i>S</i>)
14	(<i>S,S</i>)- 10c	-17 °C	D ₂ O	16 h	32% (<i>R</i>)
15	(<i>S,S</i>)- 10c	-17 °C	D ₂ O	24 h	33% (<i>R</i>)
16	(<i>S,S</i>)- 10c	-17 °C	D ₂ O, acetone	16 h	37% (<i>R</i>)
17	13	-17 °C	-	16 h	10% (<i>R</i>)
18	13	-17 °C	D ₂ O	16 h	12% (<i>R</i>)
19	11	-17 °C	D ₂ O	16 h	1% (<i>R</i>)
20	12a	-17 °C	D ₂ O	16 h	-

Reaction conditions: 100 mM substrate in CD₃CN, 10 mol% chiral silane thiol, 10 mol% K₂CO₃, 3 mol% photocatalyst and 10 equiv. H⁺/D⁺ source. If no H⁺/D⁺ source is added, protons/deuterons are abstracted from the solvent acetonitrile as described in chapter 3. The absolute configuration of the major enantiomer in parentheses was determined by chiral HPLC analysis and comparison with reported data.⁷

Under standard reaction conditions for benzylic C-H activation to carbanions, TADDOL-derived silane thiols **10**, trimenthoxysilane thiol (**11**), and silicon-chiral silane thiol **13** were effective HAT-catalysts. Ferrocene-based chiral silane thiols **12a** and **12b** underwent decomposition under the reaction conditions within minutes of irradiation, likely due to the ferrocene unit itself being redox active. Consequently, no deuteration of substrate was observed, indicating that this structural motif cannot be used for HAT reagents under the reaction conditions. Table 4.1 summarizes the results for deracemization of isochromane derivative **5b** with various HAT catalysts and reaction conditions. An initial screening of chiral benzyl ethers with silane thiols **10a-c** gave mostly racemic mixtures, except for isochromane **5b** which was obtained with low enantiomeric excess of 4% with HAT-catalyst (*R,R*)-**10a** (entry 1) and up to 13% ee in

favor of (**S**)-**5b** when the aryl groups were changed to sterically demanding terphenyl groups ((**R,R**)-**10c**, entry 7) and the temperature lowered to -17 °C (entry 2). Addition of D₂O to the reaction mixture instead of H₂O slightly increased the enantiomeric excess to 19% and additionally the benzylic deuteration could be used to confirm that C-H abstraction is occurring. With prolonged reaction time of 16 h the enantiomeric excess was increased to 32% (entry 9) and no significant further increase was observed at 24 h (33% *ee*, entry 15). The (*S,S*)-enantiomer of the most selective HAT-catalyst (**R,R**)-**10c** gave an inverted enantiomeric excess of 32% in favor of the (*R*)-enantiomer (entry 14). A slight further increase to 37% *ee* was achieved by using acetone as co-solvent (entry 16). However, more side-reactions were observed, likely due to aldol condensation under the basic reaction conditions and nucleophilic addition of the intermediate carbanion to acetone. Silicon-chiral silane thiol **13** gave a lower but measurable enantiomeric excess of up to 12% (entry 18). Considering the only moderate enantiomeric purity of catalyst **13**, this class of catalysts appears promising. However, the synthesis of the corresponding naphthyl analog was so far unsuccessful. The observed partial racemization during the synthesis of silicon-chiral silane thiols necessitates the development of improved synthetic methods to access silane thiol-based chiral HAT-catalysts.

4.3 Conclusion

In conclusion, it was demonstrated that silane thiol-based hydrogen atom transfer catalysts can be used to selectively activate specific benzylic C-H bonds to the corresponding carbanions based on general and predictable steric and electronic conditions. Abstraction of diastereomeric hydrogen atoms can be highly selective and, coupled with non-stereoselective protonation of the intermediate carbanion, enabling stereochemical editing without the need for selective bond formation. The concept was then transferred to deracemization of tertiary benzylic positions by chiral silane thiol HAT-catalysts. The utilization of a photocatalytic HAT/RRPCO/protonation sequence avoids limitations of non-photocatalytic reactions due to microscopic reversibility by enabling only the forward reaction. Although the enantiomeric excess of up to 37% is low and limited with regards to the substrate, it provides proof of concept for the yet unprecedented redox neutral, fully catalytic deracemization sequence of enantioselective HAT/RRPCO/protonation. The applicability is currently limited by the lack of easily accessible chiral hydrogen atom abstractors capable of catalysing C-H activation to the corresponding carbanions and improvements are expected from future development of new classes of chiral silane thiols and chiral HAT-reagents in general.

4.4 Experimental part

4.4.1 General information

All reactions were conducted in dried and deoxygenated solvents unless otherwise stated. Ethyl acetate (EtOAc) and petroleum ether (PE) for column chromatography and recrystallization were distilled prior to use. Commercially available starting materials were used as received.

NMR Analysis

NMR spectra were recorded using a Bruker Avance 400 or Bruker Avance III HD 400 (400 MHz for ^1H , 101 MHz for ^{13}C , 376 MHz for ^{19}F , 79 MHz for ^{29}Si) at a temperature of 298 K. Chemical shifts are reported in ppm on the δ scale with the solvent residual signal as internal standard wherever possible. Abbreviations for the multiplicity: s = singlet, d = doublet, t = triplet, q = quartet, quint = quintet, m = multiplet. Spectra were analyzed using Topspin 4.3.0. The degree of mono-deuteration of slightly overlapping signals was determined via deconvolution using the mldcon -pp function of Topspin 4.3.0.

Thin Layer Chromatography

With silica gel pre-coated aluminum sheets (Machery-Nagel, silica gel 60 G/UV254, 0.2 mm) were used for thin layer chromatography. Visualization of the separated compounds was achieved by UV-light (254 nm and 365 nm) and by staining with potassium permanganate.

High Resolution Mass Spectrometry

HRMS were measured at the Central Analytical Laboratory of the University of Regensburg on an Agilent Q-TOF 6540 UHD and a Jeol AccuTOF GCX instrument.

Elemental Analysis

Elemental analyses were performed on a Vario MICRO cube apparatus.

Single-Crystal X-Ray Diffraction Analysis

The crystals were selected and measured on a SuperNova Dualflex diffractometer equipped with a TitanS2 detector. Data collection and reduction were performed with CrysAlisPro {Version 1.171.43.36a}.⁴⁵ An analytical numeric absorption correction using a multifaceted crystal model, based on expressions derived by Clark and Reid⁴⁶ and a numerical absorption correction based on Gaussian integration over a multifaceted crystal model, and an empirical absorption correction using spherical harmonics, implemented in SCALE3 ABSPACK scaling algorithm was applied. Using Olex2,⁴⁷ the structures were solved with ShelXT⁴⁸ and a least-square refinement on F^2 was carried out with ShelXL.⁴⁹ All non-hydrogen atoms were refined anisotropically. Hydrogen atoms at the carbon atoms were located in idealized positions and refined isotropically according to the riding model. Hydrogen atoms on sulfur atoms were located from the difference Fourier map and refined without restraints. The figures were created with Olex2.⁴⁷

Chiral HPLC analysis

Chiral HPLC analysis was performed using a CHIRALPAK[®] AD-3 column (250 x 4.6 mm, 3 μ m) and CHIRALCEL[®] OD-H column (250 x 4.6 mm, 5 μ m) on an Agilent 1260 Infinity II system with photodiode array detector. Enantiomeric excess of benzochromane derivative **5b** was determined at a wavelength of 220 nm. Additionally, absorption at 200 nm, 250 nm and 280 nm was measured to verify the results.

Graphical representation of stereochemical configuration

Stereochemistry in molecular structures is represented according to IUPAC recommendations.⁵⁰

No stereochemistry specified: The structure or name refers to a mixture of all possible diastereomers in a racemic mixture or is meant as a general comment true for any possible stereoisomer. If relevant, the diastereomeric ratio is explicitly mentioned.

Straight bold or hashed lines: The structure refers to a specific diastereomer as a racemate.

Wedge-shaped lines: The structure refers to a specific enantiomer. Bold wedged bonds point from the stereocenter to above the plain and hashed wedged bonds point from the stereocenter to below the plain. The directionality is from the narrow end representing the atom in plain for both, the bold and the hashed bond.

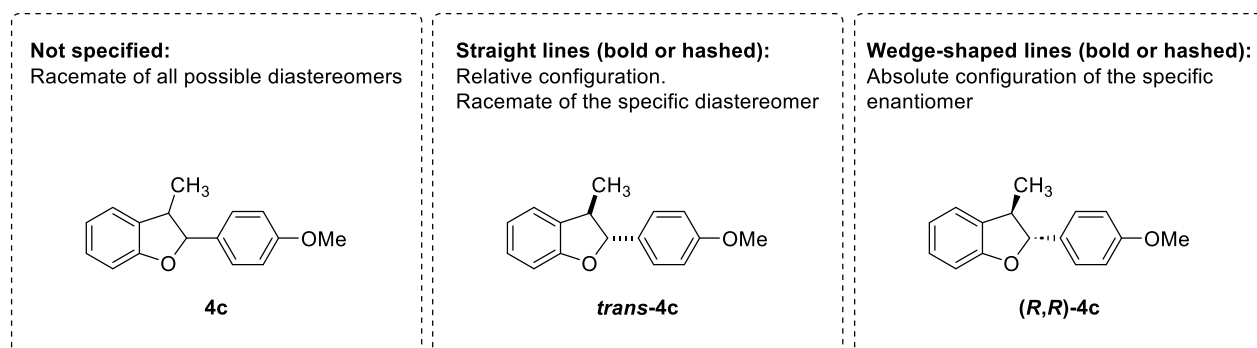


Figure 4.3. Graphical representation of stereochemistry as used in this work.

4.4.2 Photoreactor setups

Small scale room temperature photoreactions

Room temperature photoreactions were performed in the reactor depicted in Figure 4.4. Reagents were placed in 6 mL crimp-capped vials. The vials fit into a cooling block kept at 20 °C by a thermostat. The vials were irradiated from below via OSRAM Oslon SSL 80 LT-1960 royal-blue LEDs ($\lambda_{\text{max}} = 440 \text{ nm}$). Stirring was achieved via a magnetic stirrer placed below the reactor. Although the emission maximum is reported at 451 nm by the supplier, it was determined to be at 440 nm with a range of approximately 400 – 500 nm.

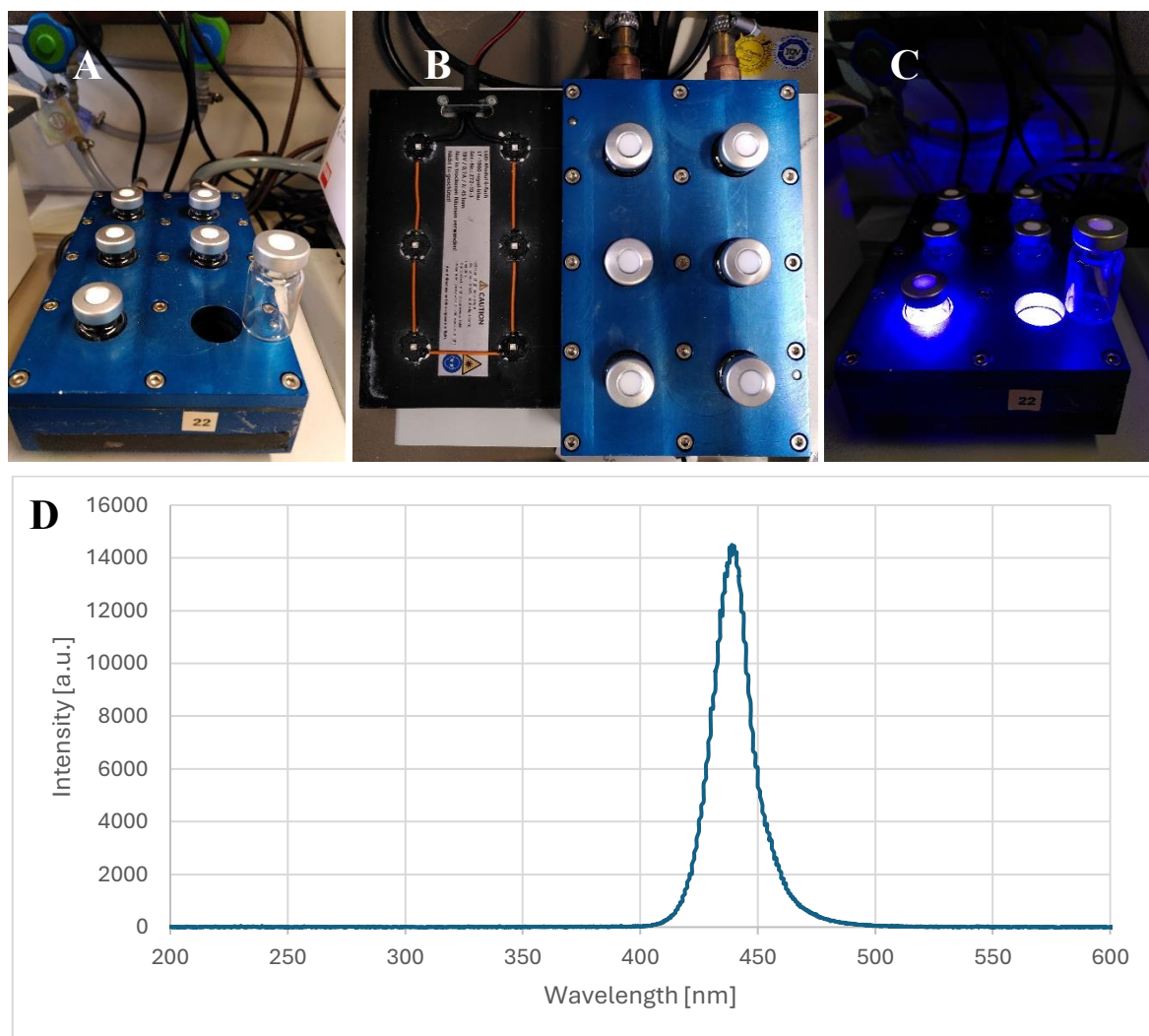


Figure 4.4. Photoreactor setup for small scale reactions. A: Cooling block front view; B: Cooling block and LED module top view; C: Photoreactor setup in operation; D: Emission spectrum of the LEDs.

Large scale room temperature photoreactions

Large scale room temperature photoreactions were performed in the reactor depicted in Figure 4.5. All reagents and the solvent were put into the reaction flask together with a stirring bar. Reaction mixtures were degassed by purging with nitrogen gas via a cannula for 20 minutes. Reactions were irradiated by 24 LEDs ($\lambda_{\text{max}} = 455 \text{ nm}$). The temperature was controlled via a cold finger connected to a thermostat.

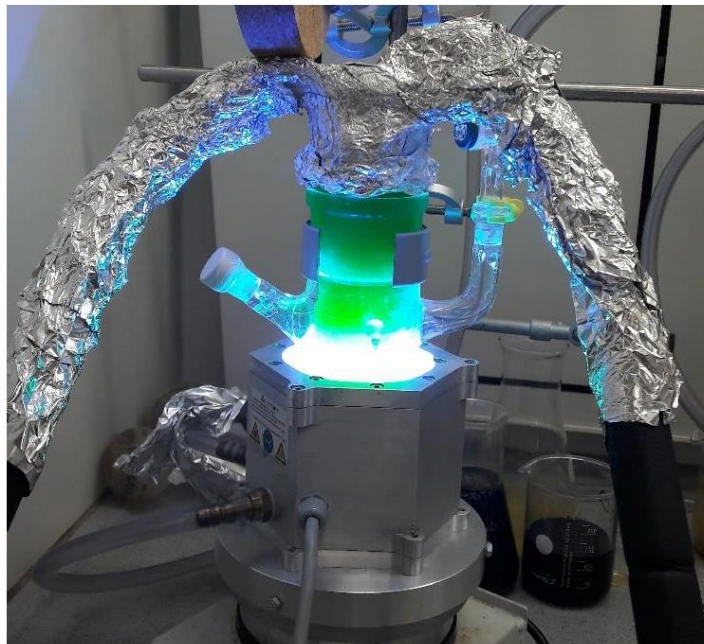


Figure 4.5. Large scale reactor. The green cooling liquid (ethylene glycol/H₂O 1:1) can be seen inside the cold finger.

Low temperature photoreactions

Low temperature photoreactions were performed in a TAK120 LC photoreactor from HK-Testsysteme GmbH. Temperature was measured via a sensor inside the reaction vials and thus corresponds to the actual reaction temperature. Reactions were irradiated by blue LEDs with an emission maximum at 441 nm at an optical power of 2.5 W/vial.

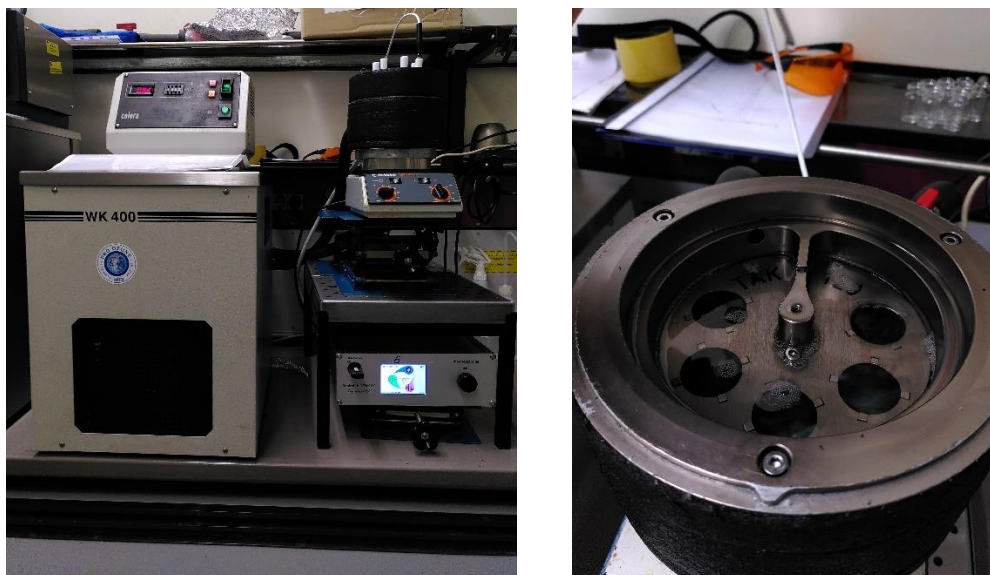


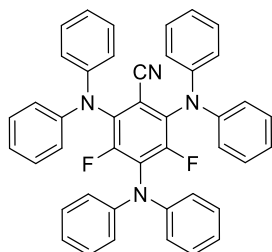
Figure 4.6. Low temperature photoreactor setup. A: complete setup with cryostat, photoreactor and control unit; B: Liquid cooled reactor compartment.

4.4.3 Synthetic procedures

4.4.3.1 Synthesis of photocatalysts

Photocatalysts 3DPA2FBN (**1a**) and 4CzIPN (**1b**) have been synthesized according to general procedure 3-A of chapter 3. 4CzIPN was used from the previous batch synthesized for chapter 2. Characterization data can be found there. 3DPA2FBN (**1a**) was previously synthesized in chapter 3 but new 3DPA2FBN was synthesized for this project.

3DPA2FBN (**1a**)



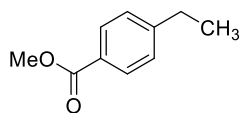
Synthesized according to general procedure 3-A (see chapter 3) on 1.5 mmol scale from pentafluorobenzonitrile (290 mg, 1.5 mmol) and diphenylamine (838 mg, 4.95 mmol, 3.3 equiv.). The product was obtained as a bright yellow powder (731 mg, 1.24 mmol, 76%). The ^1H and ^{19}F NMR spectra are in accordance with literature.⁵¹

$^1\text{H-NMR}$ (400 MHz, CDCl_3): δ [ppm] = 7.28 – 7.21 (m, 12+1 H, overlapping with solvent residual signal), 7.07 – 6.93 (m, 18H). $^{19}\text{F-NMR}$ (377 MHz, CDCl_3): δ [ppm] = -120.73 (s).

4.4.3.2 Synthesis of substrates for C-H activation

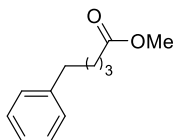
Note: Synthesis of dihydrobenzofuran derivatives, including the corresponding intermediate carboxylic acids and secondary alcohols, is described in section 4.4.5. Other substrates for C-H activation not mentioned in this section were used as received from commercial suppliers.

Methyl 4-ethylbenzoate (**2i**)

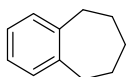


4-Ethylbenzoic acid (1.5 g, 10 mmol) was dissolved in 10 mL methanol. Concentrated sulfuric acid (1.07 mL, 20 mmol, 2 equiv.) was added dropwise and the solution stirred at room temperature for 2 h. The solution was diluted with 50 mL EtOAc, washed with water, saturated aqueous K_2CO_3 solution, and brine. The solvent was removed under reduced pressure to yield clean product without further purification (1.61 g, 9.89 mmol, 98%). The NMR spectra are in accordance with literature.⁵²

$^1\text{H NMR}$ (400 MHz, CDCl_3): δ [ppm] = 8.02 – 7.92 (m, 2H), 7.31 – 7.23 (m, 2H), 3.92 (s, 3H), 2.72 (q, J = 7.6 Hz, 2H), 1.27 (t, J = 7.61 Hz, 3H). $^{13}\text{C}\{^1\text{H}\}$ NMR (101 MHz, CDCl_3): δ [ppm] = 167.3, 149.8, 129.8, 128.0, 127.7, 52.0, 29.0, 15.3.

Methyl 5-phenylpentanoate (2s)

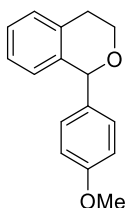
Ester **2s** was synthesized for chapter 3. The same batch was used in this work.

6,7,8,9-Tetrahydro-5H-benzo[7]annulene (3c)

Synthesized according to literature procedure.⁵³

6,7,8,9-Tetrahydro-5H-benzo[7]annulene-5-one (985 mg, 6.16 mmol, 1 equiv.) was dissolved in 10 mL trifluoroacetic acid. Triethylsilane (1.88 mL, 9.24 mmol, 1.5 equiv.) was added dropwise and the solution stirred at 60 °C overnight. Most of the trifluoroacetic acid was removed under reduced pressure, the residue poured onto ice, extracted with EtOAc, the organic phase washed with water and brine, dried over Na₂SO₄, the solvent removed under reduced pressure, and the crude product purified via column chromatography (PE) to give the product as a colorless liquid. The yield was not determined. The ¹H NMR spectrum is in accordance with literature.⁵³

¹H NMR (400 MHz, CDCl₃): δ [ppm] = 7.12 – 7.06 (m, 4H), 2.83 – 2.75 (m, 4H), 1.88 – 1.79 (m, 2H), 1.70 – 1.59 (m, 4H).

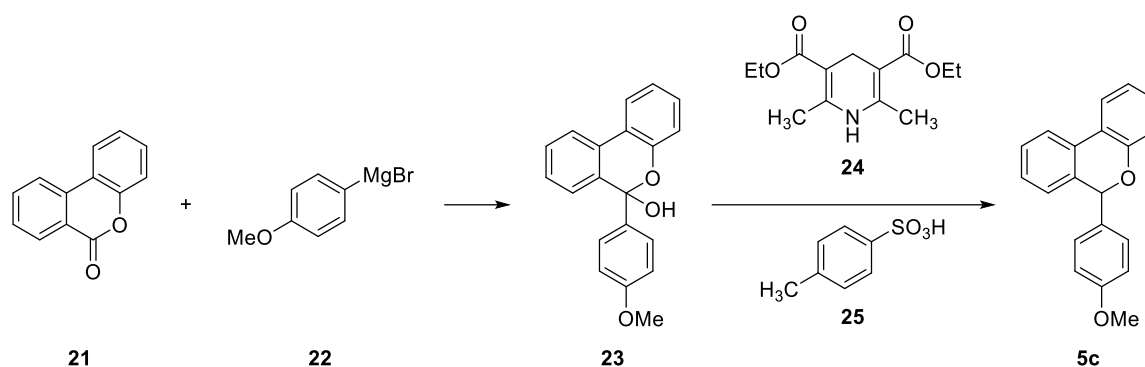
1-(4-Methoxyphenyl)isochromane (5b)

Synthesized according to literature procedure.⁵⁴

Isochromane (2.0 mL, 15.9 mmol, 1 equiv.) and anisole (10 mL, 95.4 mmol, 6 equiv.) were mixed. 2,3-Dichloro-5,6-dicyano-1,4-benzoquinone (DDQ, 3.97 g, 17.49 mmol, 1.1 equiv.) and CuCl₂ (214 mg, 9.5 mmol, 10 mol%) were added and the suspension stirred for 36 h at 100 °C. The solution was filtered, and the product purified via column chromatography (0→10% EtOAc in PE). Recrystallization from EtOAc/*n*-hexane yielded the product as colorless needles (2.39 g, 63%).

The ¹H NMR spectrum is in accordance with literature.⁵⁴

¹H NMR (400 MHz, CDCl₃): δ [ppm] = 7.25 – 7.19 (m, 2H), 7.19 – 7.14 (m, 2H), 7.12 – 7.05 (m, 1H), 6.90 – 6.85 (m, 2H), 6.76 (d, *J* = 7.7 Hz, 1H), 5.70 (s, 1H), 4.18 (ddd, *J* = 11.3, 5.5, 3.9 Hz, 1H), 3.92 (ddd, *J* = 11.4, 9.4, 4.0 Hz, 1H), 3.81 (s, 3H), 3.19 – 3.06 (m, 1H), 2.81 (dt, *J* = 16.3, 3.9 Hz, 1H).

6-(4-Methoxyphenyl)-6*H*-benzo[*c*]chromen-6-ol (5c)


Synthesized according to literature procedure.⁵⁵

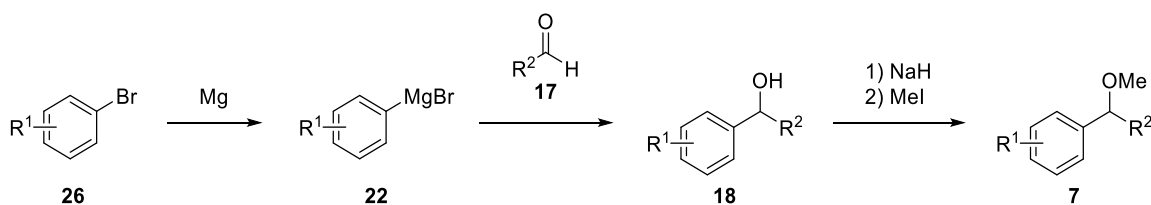
Step 1: A Grignard-solution was prepared from 4-bromoanisole (608 mg, 3.25 mmol, 1.3 equiv.) and activated magnesium turnings (91 mg, 3.75 mmol, 1.3 equiv.) in 3.25 mL THF. 6*H*-Benzo[*c*]chromen-6-one (**21**, 491 mg, 2.5 mmol, 1.0 equiv.) was dissolved in 5 mL THF and the solution cooled to -78 °C. The Grignard solution was added dropwise, and the cooling bath removed. The solution was stirred for 2 h at room temperature, quenched with saturated aqueous NH₄Cl solution, extracted with EtOAc, the organic phase washed with brine, dried over Na₂SO₄, the solvent removed under reduced pressure, and the crude product purified via column chromatography (10→20% EtOAc in PE) to yield the intermediate **23** as a slightly yellow solid (614 mg, 2.02 mmol, 81%).

Step 2: 6-(4-Methoxyphenyl)-6*H*-benzo[*c*]chromen-6-ol (**23**, 380 mg, 1.25 mmol, 1 equiv.), Hantz's chiral ester (**24**, 380 mg, 1.5 mmol, 1.2 equiv.) and *p*-toluenesulfonic acid (**25**, 43 mg, 250 μmol, 20 mol%) were dissolved in 5 mL DCM and the solution stirred at room temperature for 1 h. The solution was then diluted with EtOAc (50 mL), washed with saturated aqueous K₂CO₃ solution and brine, dried over Na₂SO₄, the solvent removed under reduced pressure and the crude product purified via column chromatography (0→20% EtOAc in PE) to yield the product as slightly yellow solid (350 mg, 1.21 mmol, 97%).

The NMR spectra are in accordance with literature.⁵⁵

¹H NMR (400 MHz, CDCl₃): δ [ppm] = 7.82 – 7.72 (m, 2H), 7.44 – 7.37 (m, 1H), 7.33 – 7.27 (m, 2H), 7.25 – 7.17 (m, 2H), 7.04 (td, *J* = 7.5, 1.1 Hz, 1H), 6.98 (dd, *J* = 8.1, 1.0 Hz, 1H), 6.92 – 6.85 (m, 3H), 6.14 (s, 1H), 3.80 (s, 3H).
¹³C{¹H} NMR (101 MHz, CDCl₃): δ [ppm] = 159.8, 153.8, 134.3, 131.9, 130.2, 129.71, 129.66, 128.5, 127.7, 126.4, 123.2, 122.9, 122.20, 122.16, 118.1, 114.0, 79.5, 55.4.

Synthesis of benzyl alcohol methyl ethers



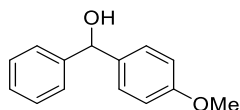
General procedure 4-A: Synthesis of benzyl alcohols

A 1 M or 1.5 M (specified in the specific reaction procedures) solution of the respective aryl bromide (**26**, 1 equiv.) in THF is prepared. A small portion of the solution is added to activated magnesium turnings (1.1 equiv.) to just cover the magnesium. A grain of iodine is added, and the solution heated with a heat gun until boiling without stirring. The start of the reaction is evident by fading of the color. The heating is stopped, and the remaining solution added dropwise while stirring to keep the reaction gently refluxing. After addition of all aryl bromide stirring is continued until the solution has cooled to room temperature. The respective aldehyde (**17**, 1.2 equiv.) is dissolved in a small amount of THF (solid aldehydes) or added directly to the Grignard solution (liquid aldehydes) at room temperature. The solution is stirred at room temperature for 2 h, quenched with saturated aqueous NH_4Cl solution, extracted with EtOAc, the organic phase washed with 1 M HCl, water and brine, dried over Na_2SO_4 , and the solvent removed under reduced pressure. The crude alcohol is purified via column chromatography with appropriate mixtures of EtOAc/PE. The products were then methylated according to general procedure 4-B.

General procedure 4-B: Synthesis of benzyl alcohol methyl ethers

Sodium hydride (2 equiv.) is suspended in THF. A solution of secondary alcohol (obtained according to general procedure 2-B or if available from a commercial supplier) in THF is added slowly while stirring and cooling in an ice bath. The suspension is then stirred at room temperature until the hydrogen evolution stops (1 – 2 h). Methyl iodide (1.5 equiv.) is added, and the reaction mixture stirred at room temperature for 2 h. Saturated aqueous NH_4Cl solution is then added, the mixture extracted with EtOAc, the organic phase washed with water and brine, dried over Na_2SO_4 and the solvent evaporated under reduced pressure. The crude product is purified via column chromatography with appropriate mixtures of EtOAc/PE.

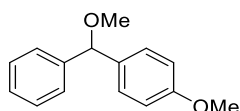
(4-Methoxyphenyl)(phenyl)methanol (**18m**)



Synthesized according to general procedure 4-A from 4-bromoanisole (16.5 mmol scale) and benzaldehyde. The Grignard solution was prepared as a stock solution on 150 mmol scale (1.5 M) and 11 mL (16.5 mmol) were used for this reaction. The product was obtained as a colorless solid (2.64 g, 12.32 mmol, 75%). The NMR spectra are in accordance with literature.⁵⁶

^1H NMR (400 MHz, CDCl_3): δ [ppm] = 7.40 – 7.24 (m, 7H), 6.90 – 6.84 (m, 2H), 5.80 (s, 1H), 3.79 (s, 3H), 2.25 (s, 1H). $^{13}\text{C}\{^1\text{H}\}$ NMR (101 MHz, CDCl_3): δ [ppm] = 159.2, 144.1, 136.3, 128.6, 128.0, 127.5, 126.5, 114.0, 75.9, 55.4.

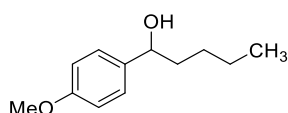
1-Methoxy-4-(methoxy(phenyl)methyl)benzene (7a)



Synthesized according to general procedure 4-B from alcohol **18m** (536 mg, 2.5 mmol). The product was obtained as colorless liquid (454 mg, 1.99 mmol, 80%). The NMR spectra are in accordance with literature.⁵⁷

¹H NMR (400 MHz, CDCl₃): δ [ppm] = 7.37 – 7.30 (m, 4H), 7.29 – 7.12 (m, 3H), 6.89 – 6.84 (m, 2H), 5.21 (s, 1H), 3.78 (s, 3H), 3.37 (s, 3H). **¹³C{¹H} NMR (101 MHz, CDCl₃):** δ [ppm] = 159.1, 142.5, 134.4, 128.5, 128.4, 127.5, 126.9, 113.9, 85.1, 57.0, 55.4.

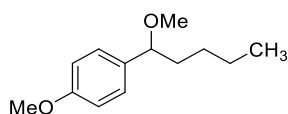
1-(4-Methoxyphenyl)pentan-1-ol (18n)



Synthesized according to general procedure 4-A from 4-bromoanisole (16.5 mmol scale) and *n*-pentanal. The Grignard solution was prepared as a stock solution on 150 mmol scale (1.5 M) and 11 mL (16.5 mmol) were used for this reaction. The product was obtained as a colorless solid (2.64 g, 12.32 mmol, 75%). The NMR spectra are in accordance with literature.⁵⁸

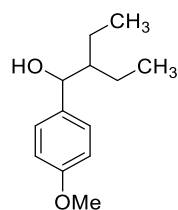
¹H NMR (400 MHz, CDCl₃): δ [ppm] = 7.31 – 7.22 (m, 2H), 6.91 – 6.84 (m, 2H), 4.60 (t, *J* = 6.8 Hz, 1H), 3.80 (s, 3H), 1.89 – 1.75 (m, 2H), 1.74 – 1.62 (m, 1H), 1.42 – 1.28 (m, 3H), 1.28 – 1.14 (m, 1H), 0.88 (t, *J* = 7.1 Hz, 3H). **¹³C{¹H} NMR (101 MHz, CDCl₃):** δ [ppm] = 159.1, 137.2, 127.3, 113.9, 55.4, 38.8, 28.2, 22.7, 14.1.

1-Methoxy-4-(1-methoxypentyl)benzene (7c)



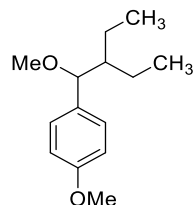
Synthesized according to general procedure 4-B from alcohol **18n** (2.5 mmol). The product was obtained as colorless liquid (450 mg, 2.16 mmol, 86%). The NMR spectra are in accordance with literature.⁵⁹

¹H NMR (400 MHz, CDCl₃): δ [ppm] = 7.24 – 7.16 (m, 2H), 6.93 (m, 2H), 4.02 (t, *J* = 6.7 Hz, 1H), 3.81 (s, 3H), 3.17 (s, 3H), 1.87 – 1.74 (m, 1H), 1.66 – 1.54 (m, 1H), 1.40 – 1.24 (m, 3H), 1.24 – 1.13 (m, 1H), 0.86 (t, *J* = 7.1 Hz, 3H). **¹³C{¹H} NMR (101 MHz, CDCl₃):** δ [ppm] = 159.1, 134.7, 128.0, 113.8, 83.8, 56.5, 55.4, 37.9, 28.2, 22.8, 14.1.

2-Ethyl-1-(4-methoxyphenyl)butan-1-ol (18o)

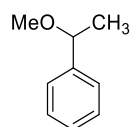
Synthesized according to general procedure 4-A from 4-bromoanisole (33.0 mmol) and 2-ethyl butanal. The Grignard solution was prepared as a stock solution on 150 mmol scale (1.5 M) and 22 mL (16.5 mmol) were used for this reaction. The product was obtained as a colorless liquid (4.10 g, 19.68 mmol, 60%). The NMR spectra are in accordance with literature.⁶⁰

¹H NMR (400 MHz, CDCl₃): δ [ppm] = 7.27 – 7.20 (m, 2H), 6.90 – 6.84 (m, 2H), 4.55 (d, J = 6.6 Hz, 1H), 3.80 (s, 3H), 1.79 (s, 1H), 1.60 – 1.38 (m, 3H), 1.33 – 1.21 (m, 1H), 1.20 – 1.07 (m, 1H), 0.90 (t, J = 7.3 Hz, 3H), 0.82 (t, J = 7.4 Hz, 3H). **¹³C{¹H} NMR (101 MHz, CDCl₃):** δ [ppm] = 158.9, 136.3, 127.8, 113.7, 75.7, 55.3, 47.8, 21.7, 20.8, 11.3, 10.9.

1-(2-Ethyl-1-methoxybutyl)-4-methoxybenzene (7d)

Synthesized according to general procedure 4-B from alcohol **18o** (2.5 mmol). The product was obtained as a colorless liquid (400 mg, 1.80 mmol, 74%).

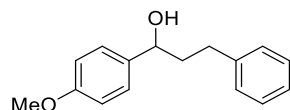
TLC: R_f = 0.41 (hexanes/EtOAc 20:1). **¹H NMR (400 MHz, CDCl₃):** δ [ppm] = 7.22 – 7.13 (m, 2H), 6.92 – 6.83 (m, 2H), 3.93 (d, J = 6.9 Hz, 1H), 3.81 (s, 3H), 3.16 (s, 3H), 1.59 – 1.39 (m, 3H), 1.31 – 1.18 (m, 1H), 1.13 – 0.99 (m, 1H), 0.88 (t, J = 7.2 Hz, 3H), 0.78 (t, J = 7.4 Hz, 3H). **¹³C{¹H} NMR (101 MHz, CDCl₃):** δ [ppm] = 159.0, 133.5, 128.7, 113.6, 85.5, 56.8, 55.3, 47.3, 21.6, 21.1, 11.2, 10.9. **HRMS (EI⁺) m/z:** [M]⁺ Calcd for C₁₄H₂₂O₂ 222.16143; Found 222.16178.

(1-Methoxyethyl)benzene (7e)

Synthesized according to general procedure 4-B from commercially available 1-phenylethanol (12.28 mmol). The product was obtained as colorless liquid. The yield was not determined. The ¹H NMR spectrum is in accordance with literature.⁶¹

¹H NMR (400 MHz, CDCl₃): δ [ppm] = 7.38 – 7.25 (m, 5H), 4.30 (q, J = 6.5 Hz, 1H), 3.23 (s, 3H), 1.44 (d, J = 6.5 Hz, 3H).

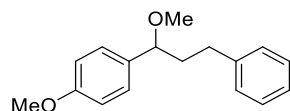
1-(4-Methoxyphenyl)-2-phenylpropan-1-ol (**18p**)



Synthesized according to general procedure 4-A from 4-bromoanisole (33.0 mmol scale) and 2-phenylethanal. The Grignard solution was prepared as a stock solution on 150 mmol scale (1.5 M) and 22 mL (16.5 mmol) were used for this reaction. The product was obtained as a colorless liquid (3.80 g, 15.68 mmol, 48%). The NMR spectra are in accordance with literature.⁶²

TLC: R_f = 0.38 (PE/EtOAc 5:1). **¹H NMR (400 MHz, CDCl₃):** δ [ppm] = 7.32 – 7.26 (m, 4H), 7.23 – 7.17 (m, 3H), 6.02 – 6.87 (m, 2H), 4.64 (t, J = 6.6 Hz, 1H), 3.82 (s, 3H), 2.79 – 2.60 (m, 2H), 2.21 – 2.08 (m, 1H), 2.08 – 1.95 (m, 1H), 1.89 (s, 1H). **¹³C{¹H} NMR (101 MHz, CDCl₃):** δ [ppm] = 159.2, 142.0, 136.8, 128.6, 128.5, 127.3, 125.9, 114.0, 73.6, 55.4, 40.5, 32.2.

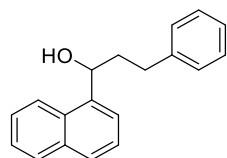
1-Methoxy-4-(1-methoxy-3-phenylpropyl)benzene (**7k**)



Synthesized according to general procedure 4-B from alcohol **18p** (606 mg, 2.5 mmol). The product was obtained as a colorless liquid (480 mg, 1.87 mmol, 75%).

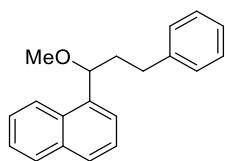
TLC: R_f = 0.28 (PE/EtOAc 20:1). **¹H NMR (400 MHz, CDCl₃):** δ [ppm] = 7.37 – 7.31 (m, 2H), 7.30 – 7.20 (m, 5H), 6.98 – 6.92 (m, 2H), 4.10 (dd, J = 7.6, 5.8 Hz, 1H), 3.87 (s, 3H), 3.25 (s, 3H), 2.82 – 2.63 (m, 2H), 2.27 – 2.13 (m, 1H), 2.04 – 1.91 (m, 1H). **¹³C{¹H} NMR (101 MHz, CDCl₃):** δ [ppm] = 159.2, 142.1, 134.2, 128.6, 128.4, 128.1, 125.9, 113.9, 82.7, 56.5, 55.4, 39.7, 32.2. **HRMS (EI+)** m/z : [M]⁺ Calcd for C₁₇H₂₀O₂ 256.14578; Found 256.14529.

1-(Naphthalen-1-yl)-3-phenylpropan-1-ol (**18q**)



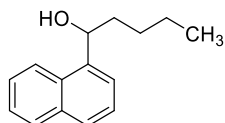
Synthesized according to general procedure 4-A from 1-bromonaphthalene (49.0 mmol scale) and 2-phenylethanal. The Grignard solution was prepared as a stock solution on 150 mmol scale (1 M) and 49.0 mL (49.0 mmol) were used for this reaction. The product was obtained as a colorless liquid (4.2 g, 16.01 mmol, 33%). The NMR spectra are in accordance with literature.⁶³

TLC: R_f = 0.49 (PE/EtOAc 5:1). **¹H NMR (400 MHz, CDCl₃):** δ [ppm] = 7.96 – 7.85 (m, 2H), 7.79 (d, J = 8.2 Hz, 1H), 7.68 (d, J = 7.1 Hz, 1H), 7.55 – 7.43 (m, 3H), 7.36 – 7.28 (m, 2H), 7.28 – 7.20 (m, 2H), 5.47 (dd, J = 7.4, 5.1 Hz, 1H), 2.96 – 2.79 (m, 2H), 2.33 – 2.18 (m, 2H), 2.05 (s, 1H). **¹³C{¹H} NMR (101 MHz, CDCl₃):** δ [ppm] = 141.9, 140.4, 133.9, 130.4, 129.0, 128.7, 128.1, 126.1, 126.0, 125.7, 125.6, 123.2, 122.9, 70.5, 39.8, 32.5.

1-(1-Methoxy-3-phenylpropyl)naphthalene (7h)

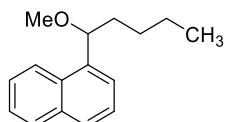
Synthesized according to general procedure 4-B from alcohol **18q** (656 mg, 2.5 mmol). The product was obtained as a slightly yellow liquid (314 mg, 1.14 mmol, 45%).

TLC: $R_f = 0.40$ (PE/EtOAc 20:1). **$^1\text{H NMR}$ (400 MHz, CDCl_3):** δ [ppm] = 7.96 (d, $J = 8.0$ Hz, 1H), 7.90 – 7.85 (m, 1H), 7.78 (d, $J = 8.1$ Hz, 1H), 7.56 (d, $J = 6.4$ Hz, 1H), 7.51 – 7.41 (m, 3H), 7.33 – 7.27 (m, 2H), 7.25 – 7.17 (m, 3H), 4.84 (dd, $J = 8.4, 4.3$ Hz, 1H), 3.31 (s, 3H), 2.92 – 2.73 (m, 2H), 2.32 – 2.11 (m, 2H). **$^{13}\text{C}\{^1\text{H}\}$ NMR (101 MHz, CDCl_3):** δ [ppm] = 142.0, 137.9, 134.1, 131.2, 129.0, 128.8, 128.5, 128.0, 125.98, 125.96, 125.6, 124.0, 123.4, 80.7, 57.0, 39.3, 32.5. **HRMS (EI+) m/z :** $[\text{M}]^+$ Calcd for $\text{C}_{20}\text{H}_{20}\text{O}$ 267.15087; Found 267.15078.

1-(Naphthalen-1-yl)pentan-1-ol (18r)

Synthesized according to general procedure 4-A from 1-bromonaphthalene (49.0 mmol scale) and pentanal. The Grignard solution was prepared as a stock solution on 150 mmol scale (1 M) and 49.0 mL (49.0 mmol) were used for this reaction. The product was obtained as a colorless liquid (6.00 g, 28.00 mmol, 57%). The NMR spectra are in accordance with literature.⁶⁴

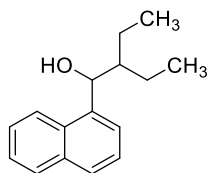
TLC: $R_f = 0.56$ (PE/EtOAc 5:1). **$^1\text{H NMR}$ (400 MHz, CDCl_3):** δ [ppm] = 8.16 – 8.09 (m, 1H), 7.91 – 7.84 (m, 1H), 7.78 (d, $J = 8.20$ Hz, 1H), 7.65 (d, $J = 6.9$ Hz, 1H), 7.56 – 7.44 (m, 3H), 5.47 (dd, $J = 7.7, 4.8$ Hz, 1H), 2.03 – 1.86 (m, 3H), 1.62 – 1.29 (m, 4H), 0.92 (t, $J = 7.2$ Hz, 3H). **$^{13}\text{C}\{^1\text{H}\}$ NMR (101 MHz, CDCl_3):** δ [ppm] = 140.8, 134.0, 130.6, 129.0, 128.0, 126.1, 125.63, 125.59, 123.3, 122.9, 71.5, 38.2, 28.6, 22.8, 14.2.

1-(1-Methoxypentyl)naphthalene (7i)

Synthesized according to general procedure 4-B from alcohol **18r** (536 mg, 2.5 mmol). The product was obtained as a slightly yellow liquid (430 mg, 1.88 mmol, 75%) in low purity.

TLC: $R_f = 0.48$ (PE/EtOAc 20:1). **$^1\text{H NMR}$ (400 MHz, CDCl_3):** δ [ppm] = 8.26 – 8.15 (m, 1H), 7.92 – 7.87 (m, 1H), 7.79 (d, $J = 7.7$ Hz, 1H), 7.58 – 7.45 (m, 4H), 4.87 (dd, $J = 7.5, 5.4$ Hz, 1H), 3.29 (s, 3H), 2.01 – 1.83 (m, 2H), 1.43 – 1.27 (m, 4H), 0.89 (t, $J = 7.1$ Hz, 3H). **$^{13}\text{C}\{^1\text{H}\}$ NMR (101 MHz, CDCl_3):** δ [ppm] = 138.2, 134.1, 131.3, 129.0, 127.9, 125.9, 125.55, 125.53, 123.6, 82.1, 57.0, 37.6, 28.7, 22.8, 14.2. **HRMS (EI+) m/z :** $[\text{M}]^+$ Calcd for $\text{C}_{16}\text{H}_{20}\text{O}$ 228.15087; Found 228.15082.

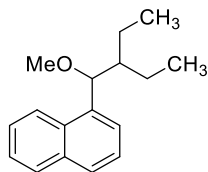
2-Ethyl-1-(naphthalen-1-yl)butan-1-ol (18s)



Synthesized according to general procedure 4-A from 1-bromonaphthalene (49.0 mmol scale) and 2-ethylbutanal. The Grignard solution was prepared as a stock solution on 150 mmol scale (1 M) and 49.0 mL (49.0 mmol) were used for this reaction. The product was obtained as a colorless liquid (4.20 g, 18.39 mmol, 54%). The NMR spectra are in accordance with literature.⁶⁵

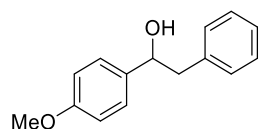
TLC: R_f = 0.63 (PE/EtOAc 5:1). **¹H NMR (400 MHz, CDCl₃):** δ [ppm] = 8.15 – 8.08 (m, 1H), 7.92 – 7.86 (m, 1H), 7.28 (d, J = 8.2 Hz, 1H), 7.64 (d, J = 7.1 Hz, 1H), 7.55 – 7.44 (m, 3H), 5.49 (d, J = 5.7 Hz, 1H), 1.89 (s, 1H), 1.87 – 1.79 (m, 1H), 1.66 – 1.29 (m, 4H), 0.99 (t, J = 7.4 Hz, 3H), 0.83 (t, J = 7.5 Hz, 3H). **¹³C{¹H} NMR (101 MHz, CDCl₃):** δ [ppm] = 139.9, 134.0, 130.8, 129.1, 127.8, 125.9, 125.5, 125.4, 124.2, 123.5, 72.5, 46.7, 22.9, 20.5, 11.8, 11.2.

1-(2-Ethyl-1-methoxybutyl)naphthalene (7j)



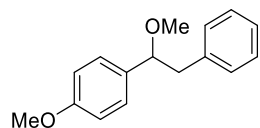
Synthesized according to general procedure 4-B from alcohol **18s** (571 mg, 2.5 mmol). The product was obtained as a slightly yellow liquid (494 mg, 2.04 mmol, 82%) in moderate purity.

TLC: R_f = 0.53 (PE/EtOAc 20:1). **¹H NMR (400 MHz, CDCl₃):** δ [ppm] = 8.24 – 8.13 (m, 1H), 7.93 – 7.83 (m, 1H), 7.79 (d, J = 7.9 Hz, 1H), 7.57 – 7.42 (m, 4H), 4.82 (d, J = 6.2 Hz, 1H), 3.24 (s, 3H), 1.87 – 1.74 (m, 1H), 1.62 – 1.45 (m, 2H), 1.41 – 1.20 (m, 2H), 0.90 (t, J = 7.5 Hz, 3H), 0.82 (t, J = 7.5 Hz, 3H). **¹³C{¹H} NMR (101 MHz, CDCl₃):** δ [ppm] = 137.1, 134.1, 131.8, 129.0, 127.8, 125.7, 125.4, 125.3, 123.8, 83.4, 57.4, 46.6, 22.6, 21.0, 11.7, 11.0. **HRMS (EI+) m/z:** [M]⁺ Calcd for C₁₇H₂₂O 242.16652; Found 242.16596.

1-(4-Methoxyphenyl)-2-phenylethan-1-ol (18t)

Synthesized according to general procedure 4-A from anisaldehyde (1.22 mL, 10 mmol, 1 equiv.) and benzylmagnesium bromide (7.5 mL, 2 M in THF, 15 mmol, 1.5 equiv.). The product was obtained as a colorless solid (1.72 g, 7.5 mmol, 75%). The NMR spectra are in accordance with literature.⁶⁶

¹H NMR (400 MHz, CDCl₃): δ [ppm] = 7.34 – 7.23 (m, 5H), 7.22 – 7.17 (m, 2H), 6.92 – 6.86 (m, 2H), 4.89 – 4.80 (m, 1H), 3.82 (s, 3H), 3.02 (d, J = 6.8 Hz, 2H), 2.05 (d, J = 2.6 Hz, 1H). **¹³C{¹H} NMR (101 MHz, CDCl₃):** δ [ppm] = 159.1, 138.3, 136.1, 129.6, 128.5, 127.3, 126.6, 113.9, 75.1, 55.4, 46.1.

1-Methoxy-4-(1-methoxy-2-phenylethyl)benzene (7f)

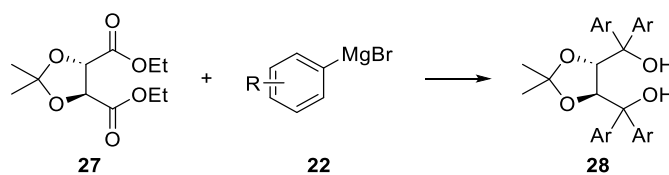
Synthesized according to general procedure 4-B from alcohol **18t** (571 mg, 2.5 mmol). The product was obtained as a slightly yellow liquid (628 mg, 2.75 mmol, 79%). The ¹H NMR spectrum is in accordance with literature.⁶⁷

¹H NMR (400 MHz, CDCl₃): δ [ppm] = 7.39 – 7.24 (m, 5H), 7.24 – 7.19 (m, 2H), 7.01 – 6.95 (m, 2H), 4.40 (t, J = 6.7 Hz, 1H), 3.93 (s, 3H), 3.29 (s, 3H), 3.25 (dd, J = 13.7, 7.4 Hz, 1H), 3.00 (dd, J = 13.7, 6.1 Hz, 1H).

4.4.3.3 Synthesis of chiral silane thiols

Synthesis of tartaric acid based chiral silane thiols

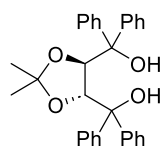
General procedure 4-C: Synthesis of TADDOL derivatives



A Grignard reagent is prepared by dropwise addition of a 1 M solution of the corresponding aryl bromide (6 equiv. with respect to ester **27**) in THF to activated magnesium turnings. First, enough of the solution is added to cover the magnesium. A small grain of iodine is added, and the solution heated without stirring until it starts boiling. The heating is stopped and checked if the reaction started, visible from immediate fading of the iodine color. If not, the heating procedure is repeated until reaction is observed. Once the reaction has started, the remaining aryl bromide solution is added dropwise under stirring to keep the reaction gently boiling. After complete addition, the mixture is further stirred until it has reached room temperature.

Diethyl 2,2-dimethyl-1,3-dioxolane-4,5-dicarboxylate (**27**) is dissolved in a few milliliters THF (the exact amount does not influence the reaction) and added dropwise to the Grignard reagent (strongly exothermic reaction). The reaction mixture is stirred at room temperature for at least 2 h, usually overnight. The reaction is quenched by addition of at least twice the volume of saturated aqueous NH_4Cl solution, extracted with ethyl acetate, washed with water and brine, dried over Na_2SO_4 , and the solvent removed under reduced pressure. The crude product is purified by dissolving it in a small amount of DCM and addition of *n*-hexane until the solution starts to become cloudy. Cooling at $-18\text{ }^\circ\text{C}$ overnight completes the crystallization. If the product contains some sticky residues after the first crystallization an additional recrystallization yields the clean product.

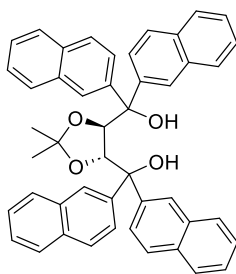
((*4R,5R*)-2,2-Dimethyl-1,3-dioxolane-4,5-diyl)bis(diphenylmethanol) ((*R,R*)-**28a**)



Synthesized according to general procedure 4-C on 6 mmol scale.

The compound was obtained as colorless crystalline solid (2.39 g, 5.12 mmol, 85%). The enantiomer (*S,S*)-**28a** was also synthesized on 6 mmol scale and obtained as a colorless crystalline solid (2.19 g, 4.69 mmol, 78%). The ^1H NMR spectra are in accordance with literature.⁶⁸

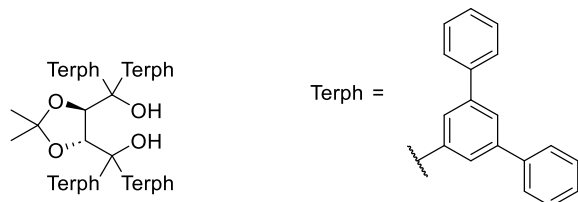
^1H NMR (400 MHz, CDCl_3): δ [ppm] = 7.56 – 7.50 (m, 4H), 7.37 – 7.22 (m, 16H+2H solvent residual signal), 4.61 (s, 2H), 3.85 (s, 2H), 1.04 (s, 6H).

((4*R*,5*R*)-2,2-Dimethyl-1,3-dioxolane-4,5-diyl)bis(di(naphthalen-2-yl)methanol) ((*R,R*)-28b)

Synthesized according to general procedure 4-C on 6.09 mmol scale.

The compound was obtained as colorless crystalline solid (2.70 g, 4.05 mmol, 66%). The ^1H NMR spectrum is in accordance with literature.⁶⁹

^1H NMR (400 MHz, CDCl_3): δ [ppm] = 8.20 (s, 2H), 7.94 (d, J = 1.2 Hz, 2H), 7.92 – 7.84 (m, 4H), 7.80 (d, J = 8.6 Hz, 2H), 7.76 – 7.64 (m, 6H), 7.56 – 7.47 (m, 6H), 7.47 – 7.38 (m, 4H), 7.28 – 7.22 (m, 2H), 4.99 (s, 2H), 4.31 (s, 2H), 1.19 (s, 6H).

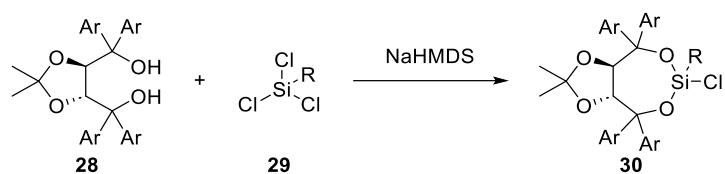
((4*R*,5*R*)-2,2-Dimethyl-1,3-dioxolane-4,5-diyl)bis(di([1,1':3',1''-terphenyl]-5'-yl)methanol) ((*R,R*)-28c)

Synthesized according to general procedure 4-C on 934 μmol scale. **28c** is literature known as an intermediate but no NMR spectra were reported.⁷⁰⁻⁷²

The compound was obtained as colorless crystalline solid (629 mg, 585 μmol , 64%). The enantiomer (***S,S***-**28c**) was synthesized on 6 mmol scale and obtained as colorless crystalline solid (4.78 g, 4.45 mmol, 74%).

^1H NMR (400 MHz, CDCl_3): δ [ppm] = 7.94 (d, J = 1.6 Hz, 4H), 7.80 (t, J = 1.6 Hz, 2H), 7.73 (d, J = 1.6 Hz, 4H), 7.69 – 7.64 (m, 10H), 7.53 – 7.49 (m, 8H), 7.44 – 7.29 (m, 24H), 5.08 (s, 2H), 4.20 (broad s, 2H), 1.10 (s, 6H). **$^{13}\text{C}\{^1\text{H}\}$ NMR (101 MHz, CDCl_3):** δ [ppm] = 146.8, 143.9, 141.7, 141.3, 141.2, 141.0, 128.94, 128.89, 127.52, 127.50, 127.4, 126.5, 125.9, 125.58, 125.55, 110.22, 81.8, 78.7, 27.5.

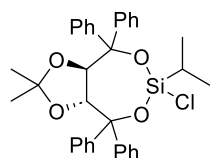
General procedure 4-D: Synthesis of TADDOL-silyl chlorides (30)



TADDOL-silyl chlorides (**30**) were synthesized by a modified literature procedure.⁷³

The TADDOL derivative (**28**) is dissolved in toluene (0.2 M) and NaHMDS (2 M in THF, 2.1 equiv.) is added slowly at 0 °C. The solution is stirred for 1 h at 0 °C and trichlorosilane derivative (**29**) is added at 0 °C. The solution is stirred at room temperature for at least 1 h, usually overnight. Longer stirring (tested up to 4 d) does not influence the reaction outcome. Within seconds after addition of the trichlorosilane the reaction mixture turns into a gel. The solvent is removed under reduced pressure, the residue extracted with boiling *n*-hexane and filtered. The solvent is removed under reduced pressure and the crude product purified via recrystallization from *n*-hexane. The formation of a gel is not reported in the literature procedure. Also, the literature procedure states that sodium chloride should precipitate and can be filtered off. However, this did not happen in any of the reactions attempted. Still, the reactions proceed quantitatively with losses in yield attributed only to the workup. No side products containing the TADDOL part are observed in the crude NMR. In the literature report the crude product was used without further purification. It is also not required for synthesis of the corresponding silane thiols. However, as purification of silane thiols **10** synthesized in the last step is difficult it is recommended to recrystallize silyl chlorides before use.

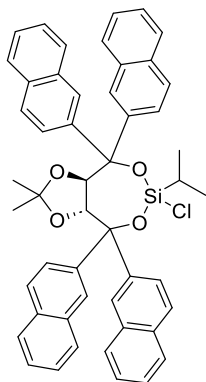
(3*aR*,8*aR*)-6-Chloro-6-isopropyl-2,2-dimethyl-4,4,8,8-tetraphenyltetrahydro-[1,3]dioxolo[4,5-*e*][1,3,2]dioxasilpine ((*R,R*)-30a**)**



Synthesized according to general procedure 4-D from TADDOL (2.5 g, 5.36 mmol) and *i*PrSiCl₃. The product was obtained as colorless, crystalline solid (2.6 g, 4.55 mmol, 85%). The enantiomer (*S,S*)-**30a** was synthesized from (*S,S*)-TADDOL (1.10 g, 2.36 mmol) and obtained as a colorless, crystalline solid (1.03g, 1.80 mmol, 76%). The NMR spectra are in accordance with literature.⁷³

¹H NMR (400 MHz, CDCl₃): δ [ppm] = 7.62 – 7.49 (m, 4H), 7.41 – 7.14 (m, 16H), 5.17 (d, *J* = 7.3 Hz, 1H), 5.11 (d, *J* = 7.2 Hz, 1H), 1.16 – 1.02 (m, 1H), 1.02 – 0.90 (m, 6H), 0.56 (s, 3H), 0.52 (s, 3H). ¹³C{¹H} NMR (101 MHz, CDCl₃): δ [ppm] = 147.0, 145.9, 142.1, 142.0, 129.6, 129.0, 128.2, 128.0, 127.7, 127.6, 127.29, 127.25, 127.18, 127.1, 114.2, 85.1, 83.0, 80.96, 80.91, 27.2, 16.3, 16.2. HRMS (EI+) *m/z*: [*M*]⁺ Calcd for C₃₄H₃₅ClO₄Si 570.19877; Found 570.19773.

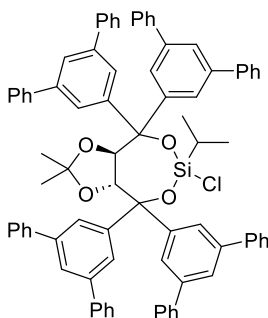
(3*aR*,8*aR*)-6-Chloro-6-isopropyl-2,2-dimethyl-4,4,8,8-tetra(naphthalen-2-yl)tetrahydro-[1,3]dioxolo[4,5-*e*][1,3,2]dioxasilepine ((*R,R*)-30b)



Synthesized according to general procedure 4-D from TADDOL derivative (**(*R,R*)-28b**) (1.33 g, 2.0 mmol) and isopropyltrichlorosilane. The product was obtained as a colorless, crystalline solid (1.40 g, 1.81 mmol, 91%).

¹H NMR (400 MHz, CDCl₃): δ [ppm] = 8.30 – 8.22 (m, 3H), 8.09 (s, 1H), 8.00 – 7.94 (m, 2H), 7.94 – 7.74 (m, 8H), 7.68 (dd, *J* = 8.7, 4.3 Hz, 2H), 7.63 – 7.47 (m, 10H), 7.43 (dt, *J* = 8.7, 1.9 Hz, 2H), 5.55 (d, *J* = 7.3 Hz, 1H), 5.49 (d, *J* = 7.2 Hz, 1H), 1.34 – 1.22 (m, 1H + 1H overlap with traces of hexane), 1.13 (t, *J* = 7.81 Hz, 6H), 0.68 (s, 3H), 0.61 (s, 3H). **¹³C{¹H} NMR (101 MHz, CDCl₃):** δ [ppm] = 144.1, 143.0, 139.6, 139.4, 132.98, 132.95, 132.94, 132.70, 132.67, 132.61, 131.1, 128.96, 128.95, 128.91, 128.73, 128.80, 128.24, 128.14, 128.03, 128.01, 127.7, 127.6, 127.5, 127.3, 126.42, 126.39, 126.36, 126.27, 126.25, 126.23, 126.22, 126.17, 126.04, 125.99, 125.89, 125.2, 124.9, 114.4, 85.5, 83.2, 81.5, 81.4, 27.5, 27.4, 16.5, 16.4, 16.3. **HRMS (FD⁺) m/z:** [M]⁺ Calcd for C₅₀H₄₃ClO₄Si 770.26137; Found 770.26037.

(3*aR*,8*aR*)-4,4,8,8-Tetra([1,1':3',1''-terphenyl]-5'-yl)-6-chloro-6-isopropyl-2,2-dimethyltetrahydro-[1,3]dioxolo[4,5-*e*][1,3,2]dioxasilepine ((*R,R*)-30c)

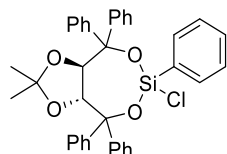


Synthesized according to general procedure 4-D from TADDOL derivative (**(*R,R*)-28c**) (538 mg, 500 μmol) and isopropyltrichlorosilane. The product was obtained as a colorless, crystalline solid (480 mg, 407 μmol, 81%). The enantiomer (**(*S,S*)-30d**) was synthesized from TADDOL derivative (**(*S,S*)-28c**) (1.04 g, 870 μmol) and obtained as a colorless, crystalline solid (622 mg, 527 μmol, 54%).

¹H NMR (400 MHz, CDCl₃): δ [ppm] = 7.98 (s, 4H), 7.89 – 7.74 (m, 9H), 7.72 – 7.62 (m, 17H), 7.50 – 7.33 (m, 27H), 5.69 (d, *J* = 7.2 Hz, 1H), 5.63 (d, *J* = 7.2 Hz, 1H), 1.40 – 1.30 (m, 1H + 2H overlap with residual n-hexane), 1.17 (t, *J* = 8.1 Hz, 6H), 0.77 (s, 3H), 0.68 (s, 3H). **¹³C{¹H} NMR (101 MHz, CDCl₃):** δ [ppm] = 147.8, 146.6, 143.0, 142.9, 141.7, 141.6, 141.54, 141.46, 141.35, 141.26, 141.25, 140.7, 140.5, 129.01, 128.97, 128.92, 127.59, 127.52,

127.46, 127.43, 127.40, 127.31, 127.27, 126.9, 126.1, 126.0, 125.6, 125.4, 125.2, 114.6, 85.6, 83.4, 81.1, 81.0, 27.5, 27.3, 22.8, 16.42, 16.37, 16.32. **HRMS (FD+)** m/z : $[M]^+$ Calcd for $C_{82}H_{67}ClO_4Si^+$ 1178.44917; Found 1178.44611.

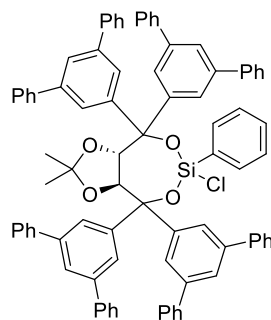
(3aR,8aR)-6-Chloro-2,2-dimethyl-4,4,6,8,8-pentaphenyltetrahydro-[1,3]dioxolo[4,5-*e*][1,3,2]dioxasilepine ((R,R)-30d)



Synthesized according to general procedure 4-D from **(R,R)-28a** (1.63 g, 3.5 mmol) and phenyltrichlorosilane. The product was obtained as a colorless, crystalline solid (1.95 g, 3.22 mmol, 92%). The enantiomer **(S,S)-30d** was synthesized from **(S,S)-28a** (467 mg, 1.00 mmol) and obtained as a colorless, crystalline solid (498 mg, 823 μ mol, 82%).

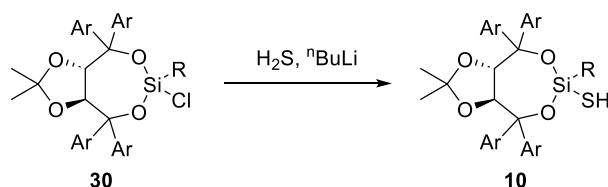
1H NMR (400 MHz, $CDCl_3$): δ [ppm] = 7.70 – 7.63 (m, 2H), 7.62 – 7.52 (m, 4H), 7.52 – 7.21 (m, 19H), 5.33 (d, J = 7.2 Hz, 1H), 5.23 (d, J = 7.2 Hz, 1H), 0.67 (s, 3H), 0.58 (s, 3H). **$^{13}C\{^1H\}$ NMR (101 MHz, $CDCl_3$):** δ [ppm] = 146.4, 145.7, 141.82, 141.79, 134.0, 131.3, 131.2, 129.6, 129.1, 128.13, 128.05, 127.75, 127.72, 127.39, 127.36, 127.34, 127.19, 127.16, 114.2, 85.7, 83.8, 81.2, 81.0, 27.2, 27.1.

(3aS,8aS)-4,4,8,8-Tetra([1,1':3',1''-terphenyl]-5'-yl)-6-chloro-2,2-dimethyl-6-phenyltetrahydro-[1,3]dioxolo[4,5-*e*][1,3,2]dioxasilepine ((S,S)-30e)



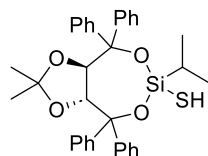
Synthesized according to general procedure 4-D from TADDOL derivative **(S,S)-28c**, (500 mg, 465 μ mol) and phenyltrichlorosilane. The product was obtained as a colorless, solid (320 mg, 264 μ mol, 57%).

1H NMR (400 MHz, $CDCl_3$): δ [ppm] = 8.07 – 8.00 (m, 2H), 7.95 – 7.89 (m, 4H), 7.87 – 7.83 (m, 2H), 7.81 – 7.73 (m, 6H), 7.72 – 7.66 (m, 8H), 7.62 – 7.57 (m, 4H), 7.53 – 7.48 (m, 4H), 7.48 – 7.29 (m, 30H), 5.81 (d, J = 7.3 Hz, 1H), 5.69 (d, J = 7.3 Hz, 1H), 0.79 (s, 3H), 0.73 (s, 3H). **$^{13}C\{^1H\}$ NMR (101 MHz, $CDCl_3$):** δ [ppm] = 147.0, 146.4, 142.5, 141.7, 141.6, 141.5, 141.30, 141.27, 141.2, 140.7, 140.6, 134.0, 131.5, 131.0, 128.98, 128.93, 128.89, 128.2, 127.54, 127.48, 127.4, 127.3, 127.2, 127.0, 126.2, 126.0, 125.5, 125.43, 125.39, 125.3, 114.7, 85.9, 84.4, 81.6, 81.2, 27.4, 27.4. **HRMS (FD+):** $[M]^+$ Calcd for $C_{85}H_{65}ClO_4Si$ 1212.4335; Found 1212.4443.

General Procedure 4-E: Synthesis of TADDOL-silane thiols (10)

A septum capped Schlenk flask connected to a hydrogen sulfide gas cylinder is charged with THF (20 mL per mmol chlorosilane). A second inlet for nitrogen is connected to avoid negative pressure in the apparatus and to remove excess H₂S after the reaction. A subsequent gas-washing bottle with aqueous NaOH solution is used for binding excess hydrogen sulfide. The reaction flask is cooled in liquid nitrogen until the THF has frozen. A slow flow of H₂S is started until an excess of H₂S has condensed into the flask. The liquid nitrogen is exchanged by a -78 °C cooling bath to melt the THF and H₂S. At -78 °C *n*-BuLi (4 equiv., 2 M in THF) is added dropwise and the solution warmed to 0 °C within 1 h. The solution is cooled to -78 °C again and the chlorosilane **30**, dissolved in a few milliliters of THF, is added. The solution is warmed to room temperature within 1 – 2 h. The reaction flask is purged with nitrogen for a few hours (or overnight) to remove most of the hydrogen sulfide (this step is not necessary but reduced the amount of H₂S released). The solvent is then removed under reduced pressure and the residue extracted with boiling *n*-hexane. The solvent is removed under reduced pressure to yield the product in sufficient purity.

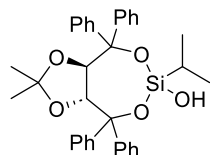
If necessary, column chromatography (10% EtOAc in PE) can be used. However, slow hydrolysis to the corresponding silanol is observed on silica which causes some product loss.

(3*aR*,8*aR*)-6-Isopropyl-2,2-dimethyl-4,4,8,8-tetraphenyltetrahydro-[1,3]dioxolo[4,5-*e*][1,3,2]dioxasilpine-6-thiol ((*R,R*)-10a)

Synthesized according to general procedure 4-E from chlorosilane (***R,R*-30a**) (1.20 g, 2.10 mmol). The product was obtained as a colorless foam (1.09 g, 1.92 mmol, 91%).

¹H NMR (400 MHz, CDCl₃): δ [ppm] = 7.61 – 7.54 (m, 4H), 7.42 – 7.17 (m, 16H), 5.27 (d, *J* = 7.3 Hz, 1H), 5.12 (d, *J* = 7.3 Hz, 1H), 1.06 – 0.88 (m, 7H), 0.59 (s, 3H), 0.48 (s, 3H), -0.20 (s, 1H). **¹³C{¹H} NMR (101 MHz, CDCl₃):** δ [ppm] = 147.3, 146.4, 142.53, 142.46, 129.6, 129.1, 128.3, 128.1, 127.7, 127.6, 127.4, 127.25, 127.22, 127.20, 127.1, 114.1, 84.8, 82.6, 81.1, 81.0, 27.2, 27.1, 17.7, 16.5, 16.4. **HRMS (FD+) *m/z*:** [*M*]⁺ Calcd for C₃₄H₃₆O₄SSi 568.20981; Found 568.20892.

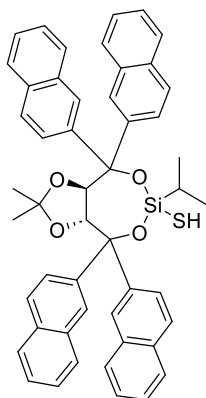
(3*aR*,8*aR*)-6-Isopropyl-2,2-dimethyl-4,4,8,8-tetraphenyltetrahydro-[1,3]dioxolo[4,5-*e*][1,3,2]dioxasilepin-6-ol ((*R,R*)-31a)



Obtained as side product in the synthesis of (*R,R*)-10a in trace amounts.

¹H NMR (400 MHz, CDCl₃): δ [ppm] = 7.68 – 7.57 (m, 4H) 7.45 – 7.18 (m, 16H), 5.12 + 5.10 (d, *J* = 7.6 Hz + d, *J* = 7.6 Hz, 2H), 1.86 (s, 1H), 1.01 – 0.88 (m, 7H), 0.65 (s, 3H), 0.49 (s, 3H). **¹³C{¹H} NMR (101 MHz, CDCl₃):** δ [ppm] = 147.63, 147.56, 142.8, 142.5, 129.4, 129.0, 128.5, 128.0, 127.7, 127.4, 127.3, 127.13, 127.10, 127.04, 126.99, 126.8, 113.7, 83.1, 81.4, 81.4, 81.1, 27.3, 26.9, 16.6, 12.3. **HRMS (FD+) m/z:** [M]⁺ Calcd for C₃₄H₃₆O₅Si 552.23265; Found 552.23170.

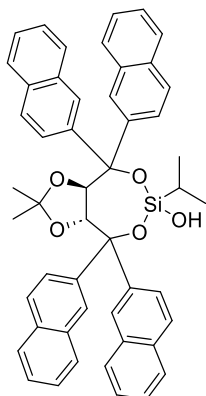
(3*aR*,8*aR*)-6-Isopropyl-2,2-dimethyl-4,4,8,8-tetra(naphthalen-2-yl)tetrahydro-[1,3]dioxolo[4,5-*e*][1,3,2]dioxasilepine-6-thiol ((*R,R*)-10b)



Synthesized according to general procedure 4-E from (*R,R*)-30b (154 mg, 200 μmol). The product was obtained as a colorless foam (98.0 mg, 127 μmol, 64%).

¹H NMR (400 MHz, CDCl₃): δ [ppm] = 8.34 (d, *J* = 1.2 Hz, 1H), 8.32 (d, *J* = 1.08 Hz, 1H), 8.30 (d, *J* = 0.96, 1H), 8.17 (d, *J* = 1.0 Hz, 1H), 8.04 – 7.98 (m, 2H), 7.98 – 7.93 (m, 1H), 7.93 – 7.82 (m, 7H), 7.73 (d, *J* = 8.7 Hz, 2H), 7.67 – 7.61 (m, 2H), 7.61 – 7.46 (m, 10H), 5.70 (d, *J* = 7.3 Hz, 1H), 5.55 (d, *J* = 7.3 Hz, 1H), 1.25 – 1.19 (m, 1H), 1.17 (d, *J* = 6.4 Hz, 3H), 1.13 (d, *J* = 6.6 Hz, 3H), 0.75 (s, 3H), 0.61 (s, 3H), -0.02 (s, 1H). **¹³C{¹H} NMR (101 MHz, CDCl₃):** δ [ppm] = 144.3, 143.4, 139.93, 139.92, 133.04, 132.96, 132.92, 132.70, 132.65, 132.63, 131.0, 128.97, 128.91, 128.84, 128.75, 128.69, 128.29, 128.01, 127.99, 127.75, 127.70, 127.58, 127.51, 127.3, 126.5, 126.4, 126.33, 126.27, 126.21, 126.16, 125.95, 125.87, 125.5, 124.9, 114.3, 85.2, 82.8, 81.6, 81.5, 27.5, 27.4, 17.8, 16.7, 16.5. **HRMS (FD+) m/z:** [M]⁺ Calcd for C₅₀H₄₄O₄SSi⁺ 768.27241; Found 768.27431.

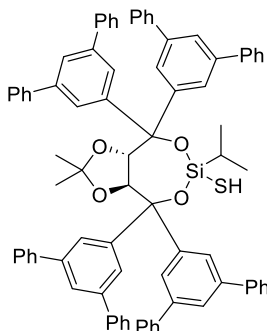
(3*aR*,8*aR*)-6-Isopropyl-2,2-dimethyl-4,4,8,8-tetra(naphthalen-2-yl)tetrahydro-[1,3]dioxolo[4,5-*e*][1,3,2]dioxasilepin-6-ol ((*R,R*)-31b)



Obtained as side product in the synthesis of (*R,R*)-10b as a colorless foam (14 mg, 18.6 μ mol, 9%).

^1H NMR (400 MHz, CDCl_3): δ [ppm] = 8.23 (d, J = 1.2 Hz, 1H), 8.21 (d, J = 1.1 Hz, 1H), 8.19 (d, J = 1.0 Hz, 1H), 8.08 (d, J = 1.1 Hz, 1H), 7.97 – 7.89 (m, 2H), 7.88 – 7.73 (m, 8H), 7.66 – 7.56 (m, 4H), 7.55 – 7.36 (m, 10H), 5.42 (s, 2H), 1.94 (s, 1H), 1.10 – 0.99 (m, 7H), 0.68 (s, 3H), 0.50 (s, 3H). **$^{13}\text{C}\{^1\text{H}\}$ NMR (101 MHz, CDCl_3):** δ [ppm] = 143.70, 143.67, 139.3, 139.0, 132.1, 131.97, 131.94, 131.87, 131.71, 131.67, 131.63, 127.96, 127.93, 127.8, 127.7, 127.5, 127.3, 126.9, 126.80, 126.75, 126.70, 126.6, 126.5, 126.3, 125.6, 125.4, 125.33, 125.28, 125.2, 125.1, 125.0, 124.9, 124.8, 124.7, 123.9, 123.8, 113.0, 82.5, 80.8, 80.7, 80.6, 26.6, 26.2, 16.0, 15.9, 11.4. **HRMS (FD+) m/z :** $[\text{M}]^+$ Calcd for $\text{C}_{50}\text{H}_{44}\text{O}_5\text{Si}$ 752.29548; Found 752.29673.

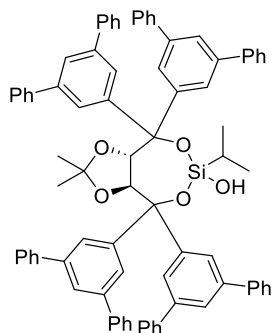
(3*aS*,8*aS*)-4,4,8,8-Tetra([1,1':3',1''-terphenyl]-5'-yl)-6-isopropyl-2,2-dimethyltetrahydro-[1,3]dioxolo[4,5-*e*][1,3,2]dioxasilepine-6-thiol ((*S,S*)-10c)



Synthesized according to general procedure 4-E from (*S,S*)-30c (472 mg, 400 μ mol). The product was obtained as a colorless foam (183 mg, 155 μ mol, 39%). The enantiomer (*R,R*)-10c was synthesized from (*R,R*)-30c (354 mg, 300 μ mol) and obtained as a colorless foam (249 mg, 211 μ mol, 70%).

^1H NMR (400 MHz, CDCl_3): δ [ppm] = 7.99 (d, J = 1.6 Hz, 2H), 7.97 (d, J = 1.6 Hz, 2H), 7.89 (d, J = 1.5 Hz, 2H), 7.87 – 7.83 (m, 3H), 7.81 – 7.76 (m, 3H), 7.74 – 7.62 (m, 16H), 7.49 – 7.33 (m, 25+1H), 5.82 (d, J = 7.3 Hz, 1H), 5.61 (d, J = 7.2 Hz, 1H), 1.18 – 1.13 (m, 6H), 1.02 – 0.92 (m, 1H), 0.03 (s, 1H). **$^{13}\text{C}\{^1\text{H}\}$ NMR (101 MHz, CDCl_3):** δ [ppm] = 148.1, 147.2, 143.4, 143.3, 141.8, 141.5, 141.41, 141.36, 141.33, 141.30, 140.63, 140.56, 128.99, 128.97, 127.53, 127.51, 127.49, 127.45, 127.41, 127.35, 127.28, 127.0, 126.1, 125.9, 125.5, 125.30, 125.25, 114.5, 85.3, 83.0, 81.3, 81.2, 27.6, 27.2, 17.9, 16.6, 16.5. **HRMS (FD+) m/z :** $[\text{M}]^+$ Calcd for $\text{C}_{37}\text{H}_{34}\text{O}_4\text{SSi}$ 1176.4602; Found 1176.4630.

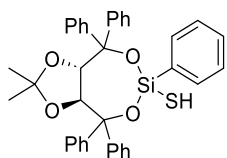
(3*aS*,8*aS*)-4,4,8,8-Tetra([1,1':3',1''-terphenyl]-5'-yl)-6-isopropyl-2,2-dimethyltetrahydro-[1,3]dioxolo[4,5-*e*][1,3,2]dioxasilepin-6-ol ((*S,S*)-31c)



Obtained as side product in the synthesis of (*S,S*)-10c as a colorless foam (38 mg, 32.7 μ mol, 8%).

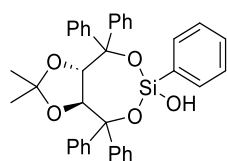
^1H NMR (400 MHz, CDCl_3): δ [ppm] = 7.97 (d, J = 1.6 Hz, 2H), 7.93 (d, J = 1.6 Hz, 2H), 7.83 – 7.76 (m, 4H), 7.74 – 7.70 (m, 4H), 7.66 – 7.56 (m, 16H), 7.44 – 7.27 (m, 24H), 5.57 (d, J = 7.4 Hz, 1H), 5.50 (d, J = 7.4 Hz, 1H), 1.22 (s, 1H), 1.12 – 1.04 (m, 7H), 0.74 (s, 3H), 0.57 (m, 3H). **$^{13}\text{C}\{^1\text{H}\}$ NMR (101 MHz, CDCl_3):** δ [ppm] = 148.5, 148.4, 143.7, 143.4, 141.9, 141.49, 141.47, 141.45, 141.2, 140.6, 140.5, 129.00, 128.99, 128.96, 128.92, 127.6, 127.47, 127.43, 127.36, 127.28, 126.99, 125.96, 125.7, 125.4, 125.3, 124.8, 114.2, 83.5, 81.9, 81.42, 81.39, 27.6, 27.1, 17.0, 16.9, 12.4. **HRMS (FD⁺) m/z:** [M]⁺ Calcd for $\text{C}_{82}\text{H}_{68}\text{O}_5\text{Si}$ 1160.4836; Found 1160.48628.

(3*aS*,8*aS*)-2,2-Dimethyl-4,4,6,8,8-pentaphenyltetrahydro-[1,3]dioxolo[4,5-*e*][1,3,2]dioxasilepine-6-thiol ((*S,S*)-10d)



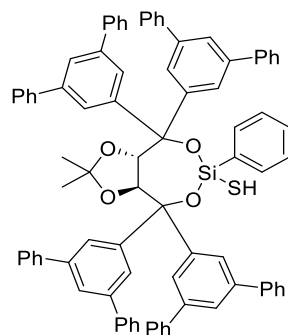
Synthesized according to general procedure 4-E from chlorosilane (*S,S*)-30d (60.5 mg, 100 μ mol). The product was purified via column chromatography (0 \rightarrow 10% EtOAc in PE) and obtained as a colorless foam (39.0 mg, 64.7 μ mol, 65%). The enantiomer (*R,R*)-10d was synthesized from (*R,R*)-30d (454 mg, 750 μ mol) and obtained as a colorless foam (365 mg, 605 μ mol, 81%).

^1H NMR (400 MHz, CDCl_3): δ [ppm] = 7.68 – 7.63 (m, 2H), 7.57 – 7.51 (m, 4H), 7.51 – 7.46 (m, 2H), 7.42 – 7.36 (m, 3H), 7.36 – 7.18 (m, 14H), 5.38 (d, J = 7.3 Hz, 1H), 5.21 (d, J = 7.3 Hz, 1H), 0.67 (s, 3H), 0.50 (s, 3H), 0.10 (s, 1H). **$^{13}\text{C}\{^1\text{H}\}$ NMR (101 MHz, CDCl_3):** δ [ppm] = 146.6, 146.2, 142.4, 142.1, 134.1, 134.0, 130.9, 129.6, 129.2, 128.4, 128.0, 127.92, 127.85, 127.60, 127.52, 127.42, 127.31, 127.27, 127.19, 127.14, 114.1, 85.3, 83.3, 81.3, 81.2, 27.3, 27.0. **HRMS (FD⁺) m/z:** [M]⁺ Calcd for $\text{C}_{37}\text{H}_{34}\text{O}_4\text{SSi}$ 602.19416; Found 602.19556.

(3a*S*,8a*S*)-2,2-dimethyl-4,4,6,8,8-pentaphenyltetrahydro-[1,3]dioxolo[4,5-*e*][1,3,2]dioxasilepin-6-ol ((*S,S*)-31d)

Obtained as side product in the synthesis of (***S,S***)-**10d** as a colorless foam (9 mg, 15.3 μmol , 15%) in low purity.

$^1\text{H NMR}$ (400 MHz, CDCl_3): δ [ppm] = 7.71 – 7.66 (m, 2H), 7.57 – 7.51 (m, 4H), 7.50 – 7.45 (m, 2H), 7.42 – 7.36 (m, 3H), 7.35 – 7.18 (m, 14H + 11H overlap with solvent residual signal), 5.23 (d, $J = 7.44$ Hz, 1H), 5.18 (d, $J = 7.4$ Hz, 1H), 0.69 (s, 3H), 0.50 (s, 3H). The O-H proton is not visible, potentially due to overlap/exchange with residual H_2O . **HRMS (FD+)** m/z : $[\text{M}]^+$ Calcd for $\text{C}_{37}\text{H}_{34}\text{O}_5\text{Si}$ 586.21700; Found 586.21567.

(3a*S*,8a*S*)-4,4,8,8-Tetra([1,1':3',1''-terphenyl]-5'-yl)-2,2-dimethyl-6-phenyltetrahydro-[1,3]dioxolo[4,5-*e*][1,3,2]dioxasilepine-6-thiol ((*S,S*)-10e)

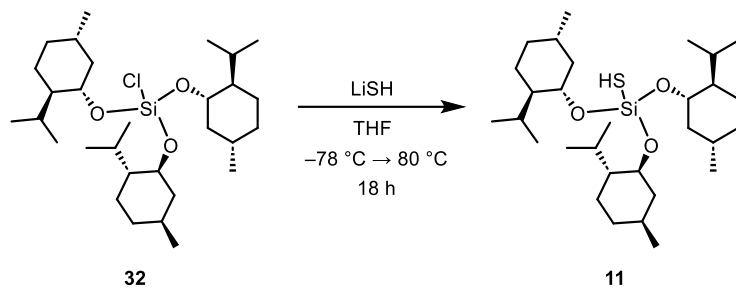
Synthesized according to general procedure 4-E from chlorosilane (***S,S***)-**30e** (243 mg, 200 μmol). The product was obtained as a colorless foam (138 mg, 114 μmol , 57%). The compound could not be fully separated from the corresponding silanol and was used as a mixture.

Silane thiol (***S,S***)-**10e**: **HRMS (FD+)**: exact mass calcd for $\text{C}_{85}\text{H}_{66}\text{O}_4\text{SSi}^+$ $[\text{M}]^+$: $m/z = 1210.4446$, found: 1210.4271.

Silanol (***S,S***)-**31e**: **HRMS (FD+)**: $[\text{M}]^+$ Calcd for $\text{C}_{85}\text{H}_{66}\text{O}_5\text{Si}$ 1194.4674; Found: 1194.4474.

Synthesis of menthol-based silane thiol **11**

Tris((1*S*,2*R*,5*S*)-menthoxy)silane thiol (**11**)



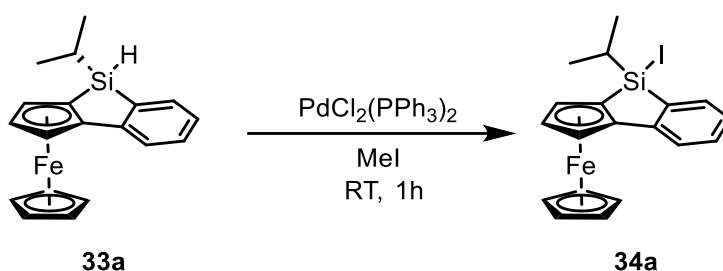
First, H₂S (52.07 mL of a 1 M solution in THF, 52.07 mmol, 1.2 equiv.) was diluted in 100 mL of THF and cooled to -78 °C. Then *n*-Butyllithium (18.23 mL, 2.5 M in hexane, 45.57 mmol, 1.05 equiv.) was added dropwise. The reaction mixture was stirred in the cooling bath until it reached a temperature of 0 °C, then it was cooled to -78 °C again. Next, trimenthoxy(chloro)silane⁷⁴ (**32**, 22.97 g, 43.40 mmol, 1 equiv.) was added. The reaction was allowed to stir for 18 h at room temperature and then 18 h at 80 °C. The reaction mixture was then checked by NMR analysis, and since no complete conversion was observed another portion of LiSH (26.4 mmol, 1.6 equiv.) in situ prepared in the aforementioned manner was added. The reaction mixture was then stirred for 72 h at room temperature. Afterwards all volatiles were removed in vacuo and the oily suspension extracted with 50 mL of hot toluene. The cloudy suspension was filtered using a P3-Frit with added celite and silica. After removal of all volatiles in vacuo silane thiol **11** was obtained as a slightly yellow oil (20.8 g, 39.5 mmol, 91%).

¹H NMR (400 MHz, C₆D₆): δ [ppm] = 4.10 – 3.83 (m, 3H), 2.69 – 2.23 (m, 6H), 1.66 – 1.45 (m, 6H), 1.44 – 1.19 (m, 9H), 1.12 – 0.65 (m, 33H), 0.19 (s, 1H, SH). ¹³C{¹H} NMR (101 MHz, CDCl₃): δ [ppm] = 74.4 (s, CH), 50.2 (s, CH), 45.3 (s, CH₂), 34.7 (s, CH₂), 31.9 (s, CH), 25.8 (s, CH), 23.1 (s, CH₂), 22.4 (s, CH₃), 21.5 (s, CH₃), 16.3 (s, CH₃). ²⁹Si{¹H} NMR (79 MHz, C₆D₆): δ [ppm] = -59.2 (Si–SH). CHN Analysis: Calcd for C₃₀H₅₈O₃SSi: C, 68.38; H, 11.10. Found: C, 68.69; H, 10.72.

Synthesis of silicon-chiral silane thiols

Reactions were performed in an inert atmosphere of purified nitrogen by using standard Schlenk techniques or an MBraun Unilab 1200/780 glovebox. Glassware was heated at 600 °C prior to use. DCM, *n*-hexane, *n*-pentane, THF, and toluene were dried and degassed with an MBraun SP800 solvent purification system. (^RSi, *S_P*)-8,8 isopropyl(hydrido)benzosilolo[2,3-*a*]ferrocene and (^RSi, *S_P*)-8,8-cyclohexyl(hydrido)benzosilolo[2,3-*a*]ferrocene were prepared according to literature procedures.⁷⁵ A stock solution of hydrogen sulfide in THF was prepared by saturating THF with gaseous hydrogen sulfide and checking the concentration by NMR with 1,3,5-trimethoxybenzene as internal standard. C₆D₆ and CD₂Cl₂ used for NMR spectroscopy were dried over 3 Å molecular sieves and degassed by a standard freeze-pump-thaw procedure.

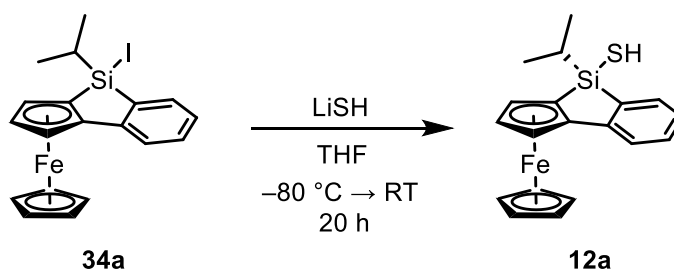
8,8-Isopropyl(iodo)benzosilolo[2,3-*a*]ferrocene (**34a**)



Prepared according to a modified literature procedure.⁷⁶

First (^RSi, *S_P*)-8,8-isopropyl(hydrido)benzosilolo[2,3-*a*]ferrocene⁷⁵ (150 mg, 0.45 mmol, 1 equiv.) was combined with bis(triphenylphosphine)palladium(II) dichloride (15.84 mg, 0.022 mmol, 0.05 equiv.) in a flame dried Schlenk flask. The mixture was then dissolved in methyl iodide (0.5 mL, 8.13 mmol, 18 equiv.) and stirred for 1 h at room temperature. Afterwards all volatiles were removed in vacuo. The remaining red solid was immediately used in the next reaction step without further purification.

12a

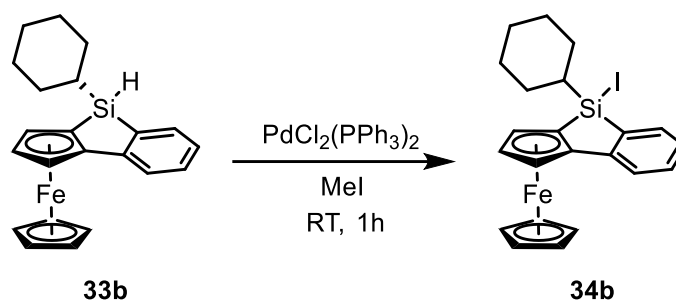


First H₂S (8.99 mL, 0.5 M in THF, 4.5 mmol, 10 equiv.) was cooled to -80 °C and then *n*-butyllithium (0.9 mL, 2.5 M in hexane, 2.25 mmol, 5 equiv.) was added, and the mixture stirred for 20 min. In a separate Schlenk flask 8,8-isopropyl(iodo)benzosilolo[2,3-*a*]ferrocene⁷⁵ (**34a**, 206 mg, 0.445 mmol, 1 equiv.) was dissolved in 10 mL of THF and added to the cooled mixture. The reaction mixture was allowed to slowly warm up in the cooling bath, and then stirred for 20 h at room temperature. Next all volatiles were removed in vacuo and the black-green residue suspended with 5 mL of hot hexane and filtered using a teflon cannula. The filtrate was concentrated in vacuo and purified by thin-layer chromatography (hexane, *R_f* = 0.4). Silane thiol **12a** was obtained as a red powder (53.0 mg, 145 μmol,

32%, *d.r.* = 14:1). Crystals of the major diastereomer suitable for single-crystal X-ray diffraction analysis were obtained from a concentrated *n*-pentane solution at -30°C. The absolute configuration was determined as (^SSi, *S*_P).

¹H NMR (400 MHz, C₆D₆): δ [ppm] = 7.51 (d, *J* = 7.17 Hz, 1H), 7.23 – 7.12 (m, 2H, overlapping with solvent residual signal), 7.03 (td, *J* = 7.1, 1.5 Hz, 1H), 4.59 – 4.56 (m, 1H), 4.35 (t, *J* = 2.28 Hz, 1H), 4.30 – 4.27 (m, 1H), 3.83 (s, 5H), 1.57 – 1.46 (m, 1H, overlap with minor diastereomer), 1.37 (d, *J* = 7.1 Hz, 3H), 1.35 (d, *J* = 7.3 Hz, 3H), -0.19 (s, 1H). ¹³C{¹H} NMR (101 MHz, C₆D₆): δ [ppm] = 147.8, 140.0, 133.7, 130.7, 126.3, 121.4, 96.3, 74.4, 71.2, 71.0, 70.5 (probably diastereomer), 70.4, 64.9, 17.8, 17.7, 16.3. ²⁹Si{¹H} NMR (79 MHz, C₆D₆): δ [ppm] = 9.5. CHN Analysis: Calcd for C₁₉H₂₀FeSSi: C, 62.6; H, 5.5. Found: C, 62.92; H, 5.80.

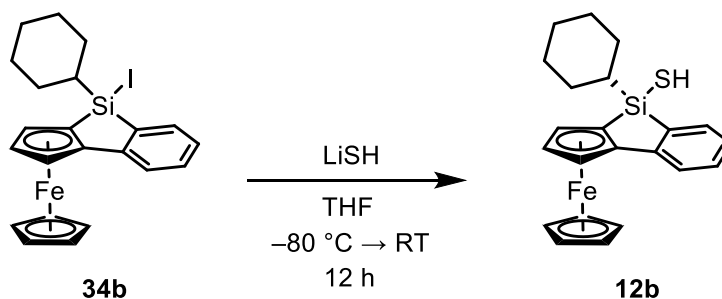
8,8-Cyclohexyl(iodo)benzosilolo[2,3-*a*]ferrocene (**34b**)



Prepared according to a modified literature procedure.⁷⁶

First (^RSi, *S*_P)-8,8-cyclohexyl(hydrido)benzosilolo[2,3-*a*]ferrocene⁷⁵ (**33b**, 140 mg, 375 μmol, 1 equiv.) was combined with bis(triphenylphosphine)palladium(II) dichloride (13.2 mg, 18.0 μmol, 5 mol%) in a flame dried Schlenk flask. The mixture was then dissolved in methyl iodide (0.42 mL, 6.77 mmol, 18 equiv.) and stirred for 1 h at room temperature. Afterwards all volatiles were removed in vacuo. The remaining red solid was immediately used in the next reaction step without further purification.

12b



First, H₂S (11.24 mL of a 0.5 M solution in THF, 5.62 mmol, 20 equiv.) was cooled to -80 °C and then *n*-butyllithium (1.12 mL of a 2.5 M solution in *n*-hexane, 2.81 mmol, 10 equiv.) was added and the mixture stirred for 20 min. In a separate Schlenk flask 8,8-cyclohexyl(iodo)benzosilolo[2,3-*a*]ferrocene (**34b**, 140 mg, 280 μmol, 1 equiv.) was dissolved in 10 mL of THF and added to the cooled mixture. The reaction mixture was allowed to slowly warm up to room temperature in the cooling bath, and then stirred for 12 h at room temperature. Next, all volatiles were removed in vacuo, the residue suspended with 5 mL of hot *n*-hexane, and filtered using a teflon cannula. Crystals suitable for

single-crystal X-ray diffraction analysis were obtained from the filtrate at -30°C . The product was isolated via filtration and dried in vacuo to yield the product as an orange, crystalline solid (83 mg, 205 μmol , 73%, *d.r.* = 17:1). Crystals of the major diastereomer suitable for single-crystal X-ray diffraction analysis were obtained from a concentrated *n*-pentane solution at -30°C . The absolute configuration was determined as ($^{\text{S}}\text{Si}$, S_{P}).

^1H NMR (400 MHz, C_6D_6): δ [ppm] = 7.53 – 7.49 (m, 1H), 7.23 – 7.18 (m, 1H), 7.04 (td, $J = 7.2, 1.4$ Hz, 1H), 4.58 (dd, $J = 2.3, 0.7$ Hz, 1H), 4.26 (t, $J = 2.3$ Hz, 1H), 4.31 (dd, $J = 2.2, 0.6$ Hz, 1H), 3.87 (s, 5H), 2.25 – 2.11 (m, 2H), 1.84 – 1.62 (m, 5H), 1.51 – 1.41 (m, 1H), 1.33 – 1.22 (m, 3H), -0.13 (s, 1H). **$^{13}\text{C}\{^1\text{H}\}$ NMR (101 MHz, C_6D_6):** δ [ppm] = 147.8, 140.1, 133.9, 130.7, 126.3, 121.5, 96.4, 74.3, 71.3, 71.2, 40.4, 70.1 (probably diastereomer), 64.8, 28.1, 28.00, 27.98, 27.87, 27.6, 26.9. **$^{29}\text{Si}\{^1\text{H}\}$ NMR (79 MHz, C_6D_6):** δ [ppm] = 6.0 (s, Si-SH). **CHN Analysis:** Calcd for $\text{C}_{22}\text{H}_{24}\text{FeSSi}$: C, 65.34; H, 5.98. Found: C, 65.81; H, 6.35.

4.4.4 Deuteration via benzylic C-H activation

General procedure 4-F: Benzylic deuteration

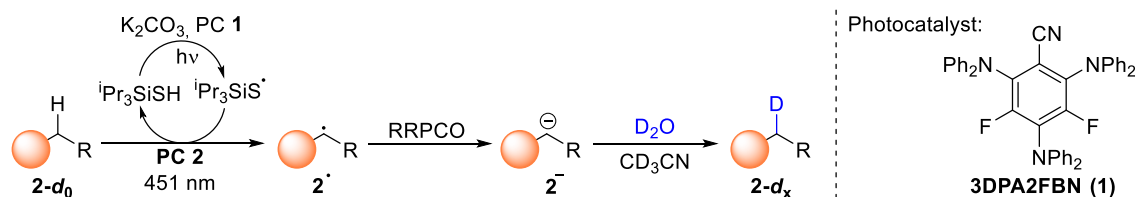
Carbanion generation from benzylic C-H bonds was done according to a slightly modified previous report on benzylic C-H activation:³⁸

Benzylic substrate (1 equiv., 100 μmol per mL solvent), K_2CO_3 (10 mol%) and photocatalyst 3DPA2FBN (**1a**, 3 mol%) are placed in a 6 mL crimp capped vial with a stirring bar and closed. The vial is evacuated and backfilled with nitrogen 3 times via cannula. HAT-catalyst ($^i\text{Pr}_3\text{SiSH}$ unless otherwise noted, 10 mol%), D_2O (10 equiv.), and solvent (CH_3CN or CD_3CN) are added via syringe. Solid reaction partners are added before closing the vial and liquids via syringe after closing the vial. The reaction mixture is degassed by 3 cycles of freeze-pump-thaw and irradiated by blue light (LEDs; $\lambda_{\text{max}} = 440 \text{ nm}$) for the time specified. Reactions were generally irradiated overnight (16 h) to ensure maximum deuterium incorporation unless otherwise noted. However, for synthetic applications the optimal reaction time is expected to vary depending on the substrate and higher yields are expected at shorter reaction times. The optimal compromise between yield and degree of deuteration also depends on the specific application.

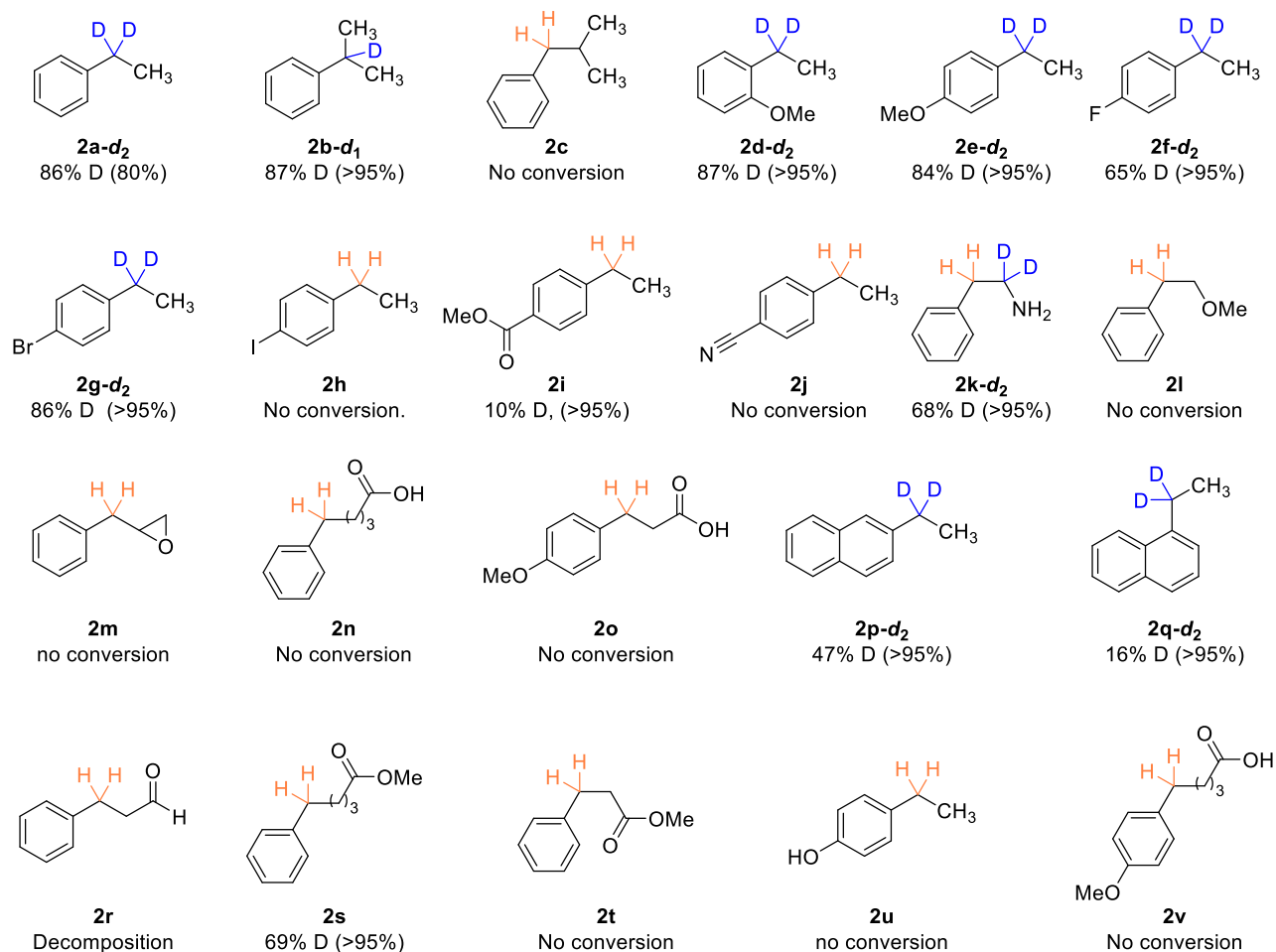
For isolation the reaction mixture is diluted with water, extracted with *n*-pentane, and dried over Na_2SO_4 . The solvent is removed under reduced pressure. Crude compounds are purified via column chromatography with appropriate mixtures of EtOAc/PE.

For determination of deuteration degrees the reactions were conducted on 100 μmol scale in 1 mL CD_3CN . 1,1,2,2-Tetrachloroethane was added as NMR standard after the reaction to estimate the yield. For reactions where aliquots were taken at different time points the residual solvent signal was used as internal standard. To note, benzylic carbanions generated in this work are highly basic and most of them are expected to or have been shown to deprotonate acetonitrile which can potentially influence the residual solvent signal. However, it has been demonstrated in chapter 3 that in the presence of at least 5 equivalents of $\text{H}_2\text{O}/\text{D}_2\text{O}$ solvent deprotonation is outcompeted and the residual solvent remains constant.⁷⁷

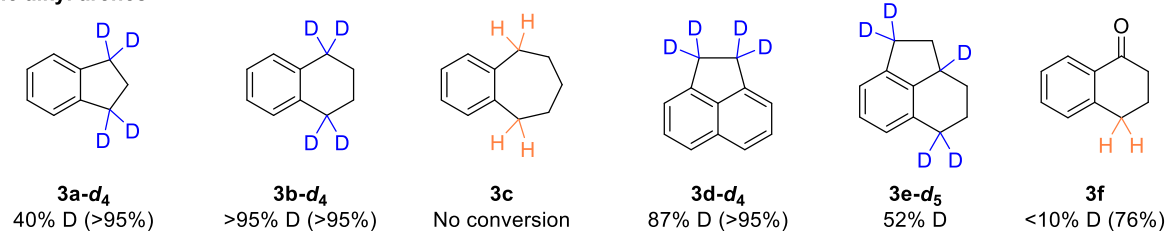
4.4.4.1 Extended substrate scope of benzylic deuteration



Acyclic alkyl arenes

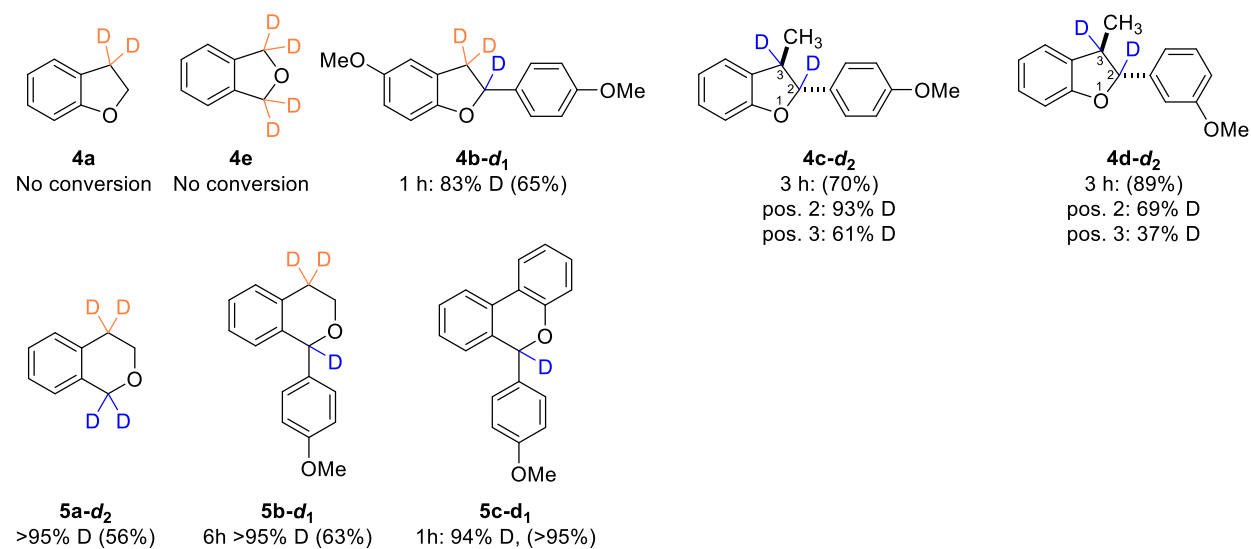


Cyclic alkyl arenes

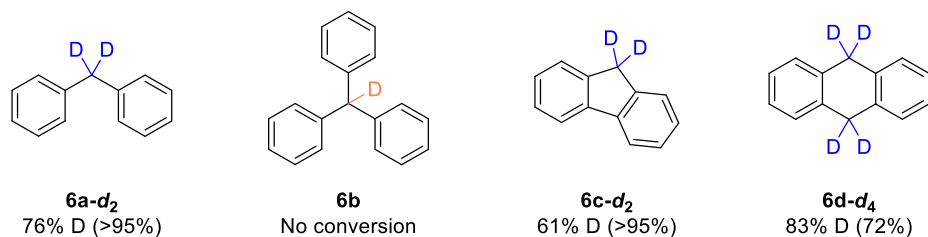


REGIO-, DIASTEREO- AND ENANTIOSELECTIVITY IN THE PHOTOCATALYTIC GENERATION OF CARBANIONS VIA HYDROGEN ATOM ABSTRACTION AND REDUCTIVE RADICAL-POLAR CROSSOVER

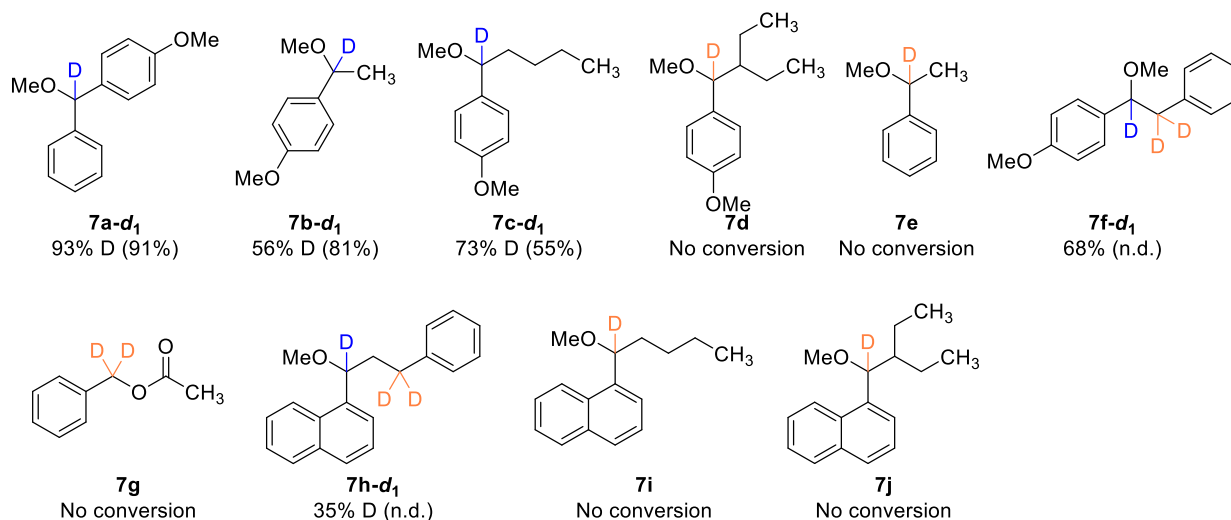
Benzofurans and isochromanones



Hydrocarbons with doubly or triply benzylic positions



Benzyl ethers



Scheme 4.7. Extended substrate scope for benzylic deuteration via a HAT/RRPCO/deuteration sequence. Reaction conditions according to general procedure 4-F. Positions deuterated to notable extent are marked in blue, positions not deuterated to notable extent are marked in orange. NMR yield in parentheses. Photocatalyst **1a** is not stable under irradiation and a photocyclization product is likely the active catalyst. For details see section 4.4.8.

4.4.4.2 Computational investigations

The trends in reactivity according to Scheme 4.7 follow C-H bond dissociation energies (BDEs) only to some extent. For a more quantitative overview and to separate steric and electronic effects, density functional theory (DFT) calculations were performed. All the optimization and frequency calculations were performed on the r²SCAN-3c⁷⁸⁻⁸² level of theory as implemented in the quantum chemical software ORCA version 5.0.4.⁸³⁻⁸⁶ Fully optimized structures were characterized to be either local minima or saddle points of first order, i.e. transition state structures by the number of imaginary frequencies. Minimum energy structures feature zero imaginary frequencies, whereas transition states have exactly one. The correct minimum energy pathways associated with the respective imaginary frequency of a given transition state structure was traced by an IRC calculation in the back- and forward direction. Energy values were derived from frequency analysis using the harmonic oscillator approach and include zero-point energy (ZPE) correction. Values of enthalpy (*H*) and Gibb's free energy (*G*) are unscaled and are report for standard conditions if not stated otherwise.

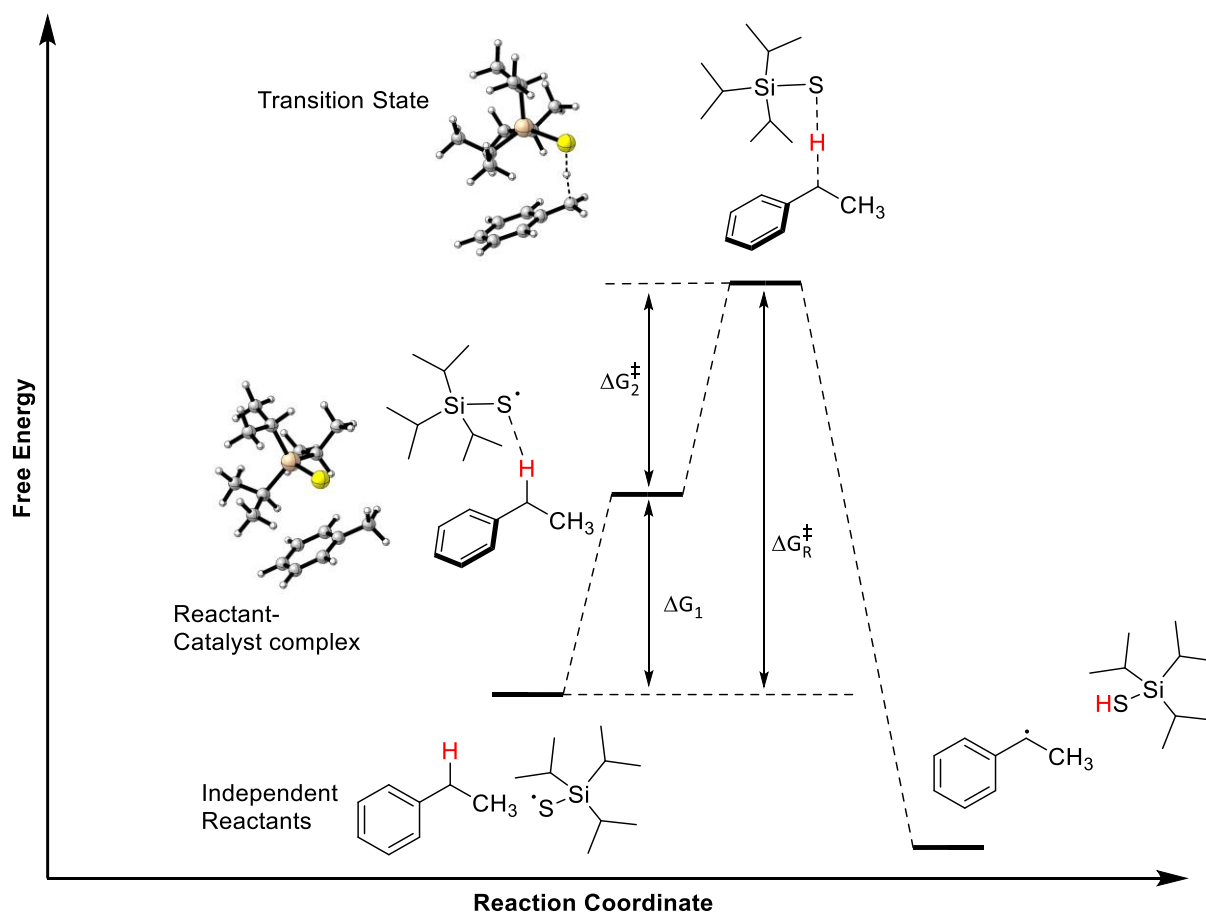


Figure 4.7. Reaction free energy profile.

To establish a trend for benzylic C-H activation, the hydrogen atom transfer (HAT) reaction barriers were calculated for a selection of substrates. To obtain the optimized reactant-catalyst pre-TS complex, the appropriate IRC end point was optimized, and the local minima were confirmed by all positive frequencies.

For a HAT process to be thermodynamically favored, the C-H bond dissociation energy (BDE) of the substrate must be lower than that of the X-H bond (S-H, in this case) of the catalyst. The BDEs were calculated by taking the

difference of free energy of dissociated species (radical and hydrogen atom) and the substrate. The free energies according to Figure 4.7 and BDEs are tabulated in Table 4.2.

Table 4.2. Free energies of reactant-catalyst-complexes and transition states for the HAT-step relative to the substrates and BDEs of the respective benzylic C-H bonds.

Substrates	ΔG_1 (kcal/mol)	ΔG_2^\ddagger (kcal/mol)	ΔG_R^\ddagger (kcal/mol)	BDE (kcal/mol)	Reactive
ⁱ Pr ₃ SiSH				84.56	Catalyst
toluene	5.51	6.71	12.22	83.81	No
2a	5.78	2.90	8.68	79.62	Yes
2b				79.63	Yes
2c	5.91	4.34	10.25	82.30	No
2e	6.66	1.82	8.48	80.29	Yes
2i	8.09	2.66	10.75	78.93	No
3b	5.19	2.59	7.78	79.09	Yes
3c	5.67	2.51	8.19	80.78	No
6b	7.37	-0.05	7.32	71.07	No
7b	6.30	0.31	6.61	76.67	Yes
7e	6.38	1.08	7.45	75.98	No

It is evident that the trends in BDEs only reflect the reactivity of the substrates to some extent. Toluene, **2c**, and **3c** have the highest BDEs and are unreactive towards HAT. However, triphenylmethane (**6b**) and benzyl ether **7e** have the lowest BDE of all substrates calculated but are also unreactive. The transition state energy reflects the trend in BDEs for the substrates with high BDEs and in addition identified ester substituted substrate **2i** as kinetically unfavored for HAT despite its rather low BDE. A possible explanation will be discussed later.

Substrates **2a** and **2b** are reactive towards benzylic HAT while **2c** with an isopropyl group adjacent to the benzylic position did not give any conversion. The low reactivity of **2c** is reflected in the high BDE and transition state energy. The high BDE suggests that the steric bulk of the isopropyl group interferes with stabilization of the radical due to steric hindrance in the preferred orientation for stabilization of the unpaired electron by the π -system.

The role of steric effects is further highlighted by the non-reactivity of triphenylmethane (**6b**) despite having the lowest BDE. The free-energy difference between the reactant-catalyst complex and that of independent reactants (ΔG_1) is the second highest calculated after the also unreactive ester substituted substrate **2i**. This suggests that destabilization of the substrate-catalyst-complex can prevent HAT even if the abstraction step itself is thermodynamically feasible. The optimized structures for substrate-catalyst-complexes and transition states suggest the preferred orientation of the triisopropylsilyl moiety is face-to-face above the aromatic system for all substrates with no substituents or electron donating substituents on the arene while this orientation is unfavored for electron poor substrate **2i**. Thus, dispersion interactions between electron rich π -systems and the triisopropylsilyl group might be necessary for HAT to be feasible. These interactions are prevented by electron withdrawing groups or by steric hindrance in the case of triphenylmethane (**6b**) where the tilted phenyl groups block access to the π -system. Optimized structures of substrate-catalyst-complexes and transition states for a representative selection of substrates is depicted in Figure 4.8. Electronically similar substrates prefer similar orientation compared to the examples depicted in Figure 4.8.

Substrate-catalyst complex

Transition state for C-H activation

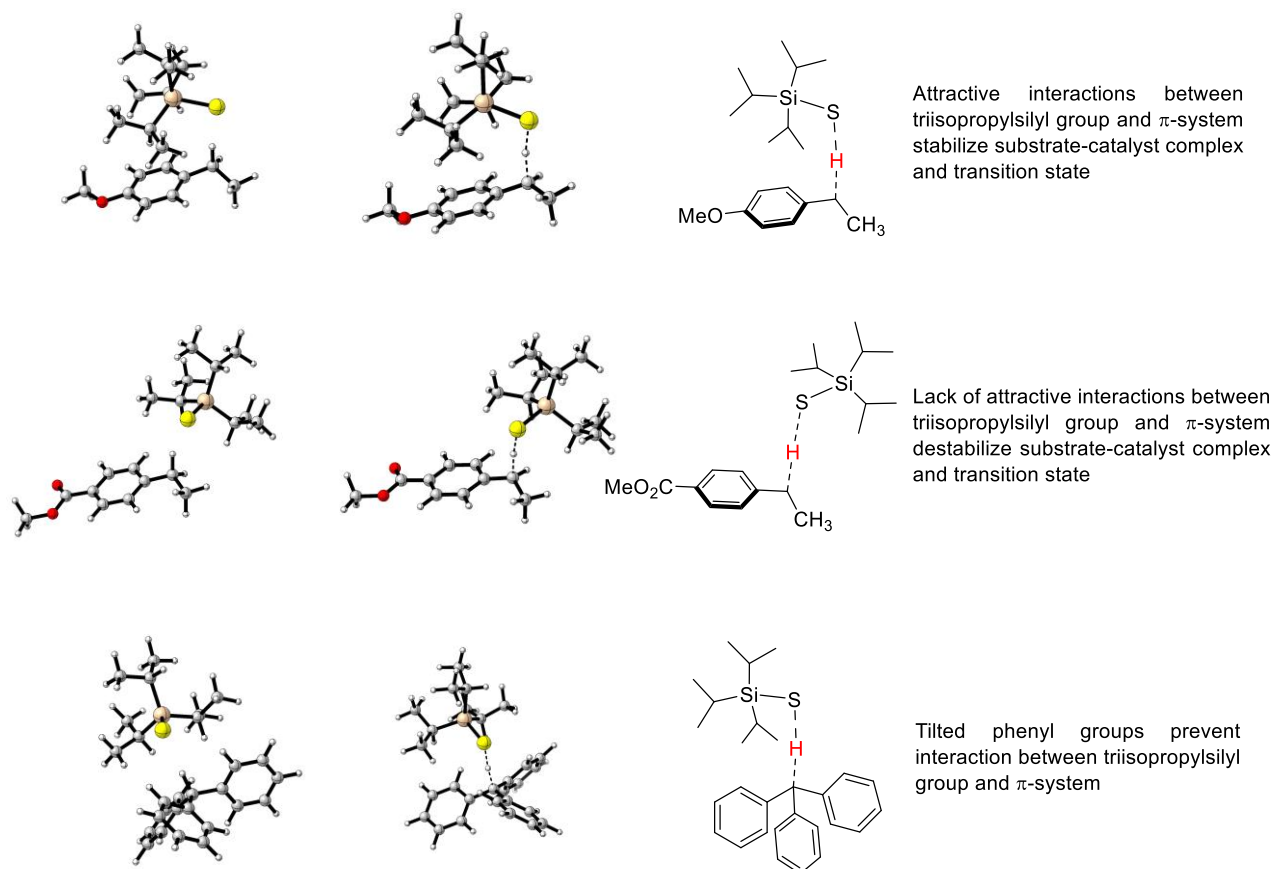


Figure 4.8. Substrate-catalyst-complexes and transition states for a selection of substrates.

Another interesting observation is the effect of ring sizes. While the six-membered substrate **3b** undergoes efficient deuteration in the benzylic positions, benzylic positions in the seven-membered ring system of **3c** do not. The reason for this anomaly might be attributed to the steric hindrance offered by the 1,4-H interaction in the benzylic position (Figure 4.9). The calculated BDE of **3c** is also slightly higher compared to **3b** (80.78 vs. 79.09 kcal/mol) which suggests less stabilization of the unpaired electron in the seven-membered ring compared to the 6-membered ring.

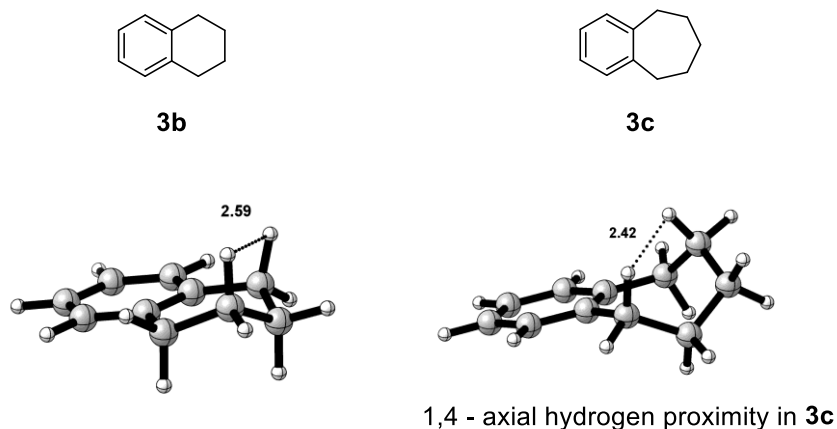
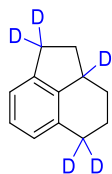


Figure 4.9. Inherent steric interactions in **3b** and **3c**.

Considering all these factors, it is concluded that the BDEs are not the only determining factor in the initial HAT process and steric and electronic effects stabilizing or destabilizing the reactant complex play a definitive role in the reactivity of substrates towards C-H abstraction.

4.4.4.3 Isolated deuterated compounds

1,2,2a,3,4,5-Hexahydroacenaphthylene-1,1,2a,5,5-*d*₅ (**3e-d₅**)

Synthesized according to general procedure 4-F from hexahydroacenaphthylene (190 mg, 6 x 200 μ mol) in CH_3CN . The product was obtained as a colorless liquid (86.8 mg, 538 μ mol, 45%).

NMR spectra are in accordance with the non-deuterated compound. Most signals in the $^{13}\text{C}\{^1\text{H}\}$ NMR are doubled and multiple multiplets from coupling to deuterium are visible. Due to the presence of different diastereomers and compounds with different degree of deuteration no assignment to the individual benzylic positions was made. According to the $^{13}\text{C}\{^1\text{H}\}$ NMR the benzylic methine C-H is almost fully deuterated while the methylene C-H bonds are moderately deuterated.

^1H NMR (400 MHz, CDCl_3): δ [ppm] = 7.19 – 7.05 (m, 2H), 6.97 (d, J = 6.9 Hz, 1H), 2.99 – 2.66 (m, 2.39H, corresponds to 52% deuteration), 2.42 – 2.30 (m, 1H), 2.24 – 2.06 (m, 2H), 1.90 – 1.75 (m, 1H), 1.66 – 1.54 (m, 1H), 1.28 (t, J = 12.6 Hz, 1H).

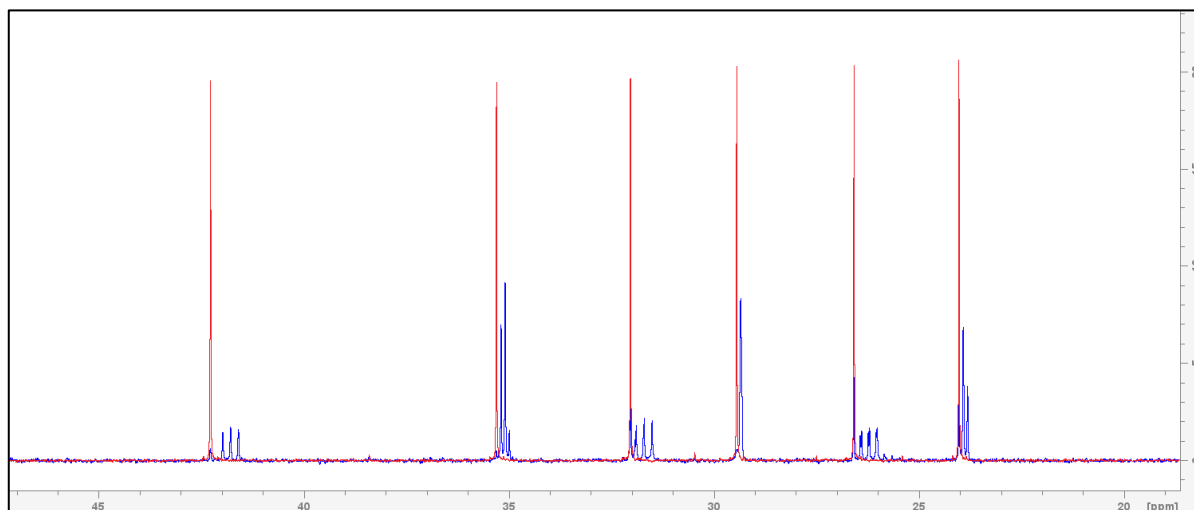
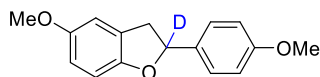


Figure 4.10. Superimposed aliphatic region of the $^{13}\text{C}\{^1\text{H}\}$ NMR spectra of deuterated **3e** (blue) and **3e-d₀** (red). The full NMR spectrum can be found in the appendix.

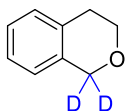
5-Methoxy-2-(4-methoxyphenyl)-2,3-dihydrobenzofuran-2-*d* (Corsifuran A-*d*₁, **4b-d₁**)

Synthesized according to general procedure 4-F from Corsifuran A (51.3 mg, 200 μ mol) in 2 mL CD_3CN and 500 μ L aliquots were removed for NMR analysis before irradiation and after 1 h of irradiation. The remaining solution after 1 h of irradiation was treated according to general procedure 4-F for isolation. The product was obtained as a colorless solid (15.0 mg, 58.3 μ mol, 58%).

The NMR spectra are in accordance with the non-deuterated compound **4b** with differences only in the benzylic position and adjacent positions as expected.

¹H NMR (400 MHz, CDCl₃): δ [ppm] = 7.37 – 7.31 (m, 2H), 6.93 – 6.88 (m, 2H), 6.79 (d, *J* = 2.44 Hz, 1H), 6.75 (d, *J* = 8.60 Hz, 1H), 6.70 (dd, *J* = 8.64, 2.60 Hz, 1H), 5.69 (t, *J* = 8.80 Hz, 0.11H, corresponds to 89% deuteration), 3.81 (s, 3H), 3.77 (s, 3H), 3.54 (d, *J* = 15.73 Hz, 1H), 3.19 (d, *J* = 15.69 Hz, 1H). **¹³C{¹H} NMR (101 MHz, CDCl₃):** δ [ppm] = 159.6, 154.4, 153.9, 134.0, 127.8, 127.4, 144.1, 133.1, 111.3, 109.3, 84.3 (residual **4b-d₀**) 83.9 (t, *J*_{C,D} = 23.0 Hz), 56.4, 55.4, 38.7. **HRMS (EI+) m/z:** [M]⁺ Calcd for C₁₆H₁₅O₃D 257.11567; Found 257.11565.

Isochromane-1,1-*d*₂ (**5a-d₂**)

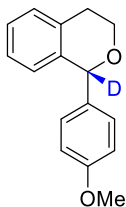


Synthesized according to general procedure 4-F from isochromane (53.7 mg, 2 x 200 μmol) in CH₃CN. The product was obtained as a colorless liquid (26.0 mg, 191 μmol, 48%). Due to its volatility the compound was not dried under high vacuum and some petrol ether remained in the product.

NMR spectra are in accordance with literature⁸⁷ and the NMR spectra of the non-deuterated compound **5a** with differences only in the benzylic position as expected.

¹H NMR (400 MHz, CDCl₃): δ [ppm] = 7.20 – 7.09 (m, 3H), 7.02 – 6.94 (m, 1H), 4.76 (s, 0.05H, corresponds to 98% deuteration), 3.98 (t, *J* = 5.7 Hz, 2H), 2.87 (t, *J* = 5.7 Hz, 2H). **¹³C{¹H} NMR (101 MHz, CDCl₃):** δ [ppm] = 134.9, 133.4, 129.0, 126.5, 126.1, 124.6, 67.4 (quint, *J*_{C,D} = 21.9 Hz, almost lost in the noise), 65.5, 28.5. **HRMS (EI+) m/z:** [M]⁺ Calcd for C₉H₈OD₂ 136.08517F Found 136.08471.

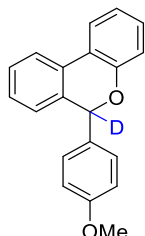
(*R*)-1-(4-Methoxyphenyl)isochromane-1-*d* (**5b-d₁**)



Synthesized according to general procedure 4-F from isochromane derivative **5b** (48.06 mg, 200 μmol) in CD₃CN with chiral HAT-catalyst (*S,S*)-**10c**. 500 μL of the solution were removed before irradiation for NMR analysis. The remaining solution (150 μmol substrate in 1.5 mL CD₃CN) was irradiated for 16 h at -17 °C and the product isolated according to general procedure G. The product was obtained as a colorless liquid (29.71 mg, 123 μmol, 82%, 32% *ee*). The enantiomeric excess was determined by chiral HPLC on a CHIRALPAK® AD-3 column (iPrOH/*n*-hexane 10:1, flow rate 0.8 mL/min). *t*_{minor} = 7.284 min, *t*_{major} = 8.365 min. The absolute configuration of the (*S*)-enantiomer was determined by chiral HPLC on a CHIRALCEL® OD-H column. Racemic **5b-d₁** was synthesized using triisopropylsilane thiol as HAT catalyst but not isolated. The NMR spectra are in accordance with those of the non-deuterated compound **5b** with differences only in the benzylic position as expected. Compound **5b-d₁** is mentioned in the literature but was not characterized.⁸⁸

^1H NMR (400 MHz, CDCl_3): δ [ppm] = 7.25 – 7.20 (m, 2H), 7.19 – 7.14 (m, 2H), 7.11 – 7.05 (m, 1H), 6.91 – 6.85 (m, 2H), 6.76 (d, J = 7.7 Hz, 1H), 5.70 (s, 0.12H, corresponds to 88% deuteration), 4.22 – 4.13 (m, 1H), 3.97 – 3.87 (m, 1H), 3.81 (s, 3H), 3.19 – 3.06 (m, 1H), 2.81 (dt, J = 16.3, 3.6 Hz, 1H). **$^{13}\text{C}\{^1\text{H}\}$ NMR (101 MHz, CDCl_3):** δ [ppm] = 159.6, 137.7, 134.6, 124.1, 130.3, 128.8, 127.1, 126.7, 126.0, 113.9, 78.8 (t, $J_{\text{C,D}}$ = 21.4 Hz), 63.8, 55.4, 29.0.

6-(4-Methoxyphenyl)-6H-benzo[*c*]chromene-6-*d* (5c-*d*₁)

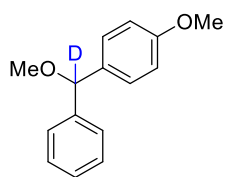


Synthesized according to general procedure 4-F from isochromane derivative **5c** (57.7 mg, 200 μmol) in CD_3CN . The product was obtained as a colorless solid (49.1 mg, 170 μmol , 85%).

The NMR spectra are in accordance with those of the non-deuterated compound **5c** with differences only in the benzylic position as expected.

^1H NMR (400 MHz, CDCl_3): δ [ppm] = 7.83 – 7.73 (m, 2H), 7.41 (td, J = 7.6, 1.17 Hz, 1H), 7.35 – 7.19 (m, 4H), 7.05 (dt, J = 7.5, 1.0 Hz, 1H), 7.00 (dd, J = 8.1, 1.0 Hz, 1H), 6.93 – 6.86 (m, 3H), 6.15 (s, 0.06H, corresponds to 96% deuteration). **$^{13}\text{C}\{^1\text{H}\}$ NMR (101 MHz, CDCl_3):** δ [ppm] = 159.8, 159.7, 134.3, 134.2, 131.9, 131.8, 130.2, 129.7, 129.6, 128.5, 127.7, 126.4, 123.2, 122.9, 122.2, 122.1, 118.0, 114.0, 79.0 (t, $J_{\text{C,D}}$ = 22.38 Hz), 55.4.

1-Methoxy-4-(methoxy(phenyl)methyl-*d*)benzene (7a-*d*₁)

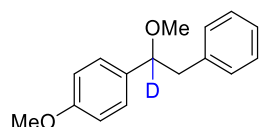


Synthesized according to general procedure 4-F from benzyl ether **7a** (22.8 mg, 100 μmol) with chiral HAT-catalyst (**S,S**)-**10c** in 1 mL CD_3CN . The product was obtained as a colorless liquid (19.0 mg, 82.9 μmol , 83%).

The NMR spectra are in accordance with those of the non-deuterated compound **7a** with differences only in the benzylic position as expected.

^1H NMR (400 MHz, CDCl_3): δ [ppm] = 7.38 – 7.31 (m, 4H), 7.29 – 7.23 (m, 3H), 6.89 – 6.84 (m, 2H), 5.21 (s, 0.04H, corresponds to 96% deuteration), 3.78 (s, 3H), 3.37 (s, 3H). **$^{13}\text{C}\{^1\text{H}\}$ NMR (101 MHz, CDCl_3):** δ [ppm] = 159.1, 142.4, 134.4, 128.5, 128.4, 127.5, 127.0, 113.9, 85.1 (residual **5c-d**₀), 84.6 (t, $J_{\text{C,D}}$ = 21.5 Hz), 57.0, 55.4.

1-Methoxy-4-(1-methoxy-2-phenylethyl-1-*d*)benzene (7f-*d*₁)

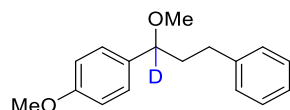


Synthesized according to general procedure 4-F from benzyl ether **7f** (24.2 mg, 100 μmol) with chiral HAT-catalyst (**S,S**)-**10c** in 1 mL CD₃CN. The product was obtained as a colorless liquid (18.1 mg, 74.4 μmol, 74%).

NMR spectra are in accordance with those of the non-deuterated compound **7f** with differences only in the benzylic position and adjacent positions as expected.

¹H NMR (400 MHz, CDCl₃): δ [ppm] = 7.25 – 7.12 (m, 5H), 7.12 – 7.07 (m, 2H), 6.88 – 6.83 (m, 2H), 4.28 (t, *J* = 6.7 Hz, 0.12H, corresponds to 88% deuteration), 3.81 (s, 3H), 3.17 (s, 3H), 3.12 (d, *J* = 13.7 Hz, 1H), 2.87 (d, *J* = 13.7 Hz, 1H). ¹³C{¹H} NMR (101 MHz, CDCl₃): δ [ppm] = 159.2, 138.7, 133.7, 129.6, 128.2, 128.1, 126.2, 113.8, 84.6 (**7f-d₀**), 84.3 (t, *J* = 21.7 Hz), 56.6, 55.4, 44.8.

1-Methoxy-4-(1-methoxy-3-phenylpropyl-1-*d*)benzene (7k-*d*₁)

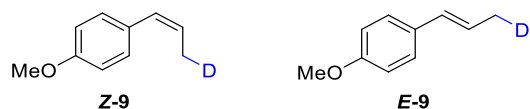


Synthesized according to general procedure 4-F from benzyl ether **7k** (25.6 mg, 100 μmol) with chiral HAT-catalyst (**S,S**)-**10c** in 1 mL CD₃CN. The product was obtained as a colorless liquid (21.0 mg, 81.6 μmol, 81%).

NMR spectra are in accordance with those of the non-deuterated compound **7k** with differences only in the benzylic position and adjacent position as expected and some small shifts for some of the signals in the ¹³C NMR. Due to the only moderate deuteration degree signals for both, the deuterated and non-deuterated compound are visible with similar intensity.

¹H NMR (400 MHz, CDCl₃): δ [ppm] = 7.31 – 7.24 (m, 2H + 1H solvent residual signal), 7.24 – 7.15 (m, 5H), 6.92 – 6.87 (m, 2H), 4.03 (dd, *J* = 7.7, 5.7 Hz, 0.52H, corresponds to 48% deuteration), 3.82 (s, 3H), 3.19 (s, 3H), 2.76 – 2.55 (m, 2H), 2.19 – 2.07 (m, 1H), 1.97 – 1.86 (m, 1H). ¹³C{¹H} NMR (101 MHz, CDCl₃): δ [ppm] = 159.2, 142.1, 134.23 (**7k-d₀**), 134.17, 128.6, 128.5, 128.1, 125.9, 113.9, 82.7 (**7f-d₀**), 82.2 (t, *J*_{C,D} = 21.7 Hz), 56.8, 56.5 (**7k-d₀**), 56.4, 55.4, 39.7 (**7k-d₀**), 39.6, 32.18 (residual **7k-d₀**), 32.15.

1-Methoxy-4-(prop-1-en-1-yl-3-*d*)benzene (9-*d*₁, mixture of (*E*)- and (*Z*) isomer)



Synthesized according to general procedure 4-F from 1-allyl-4-methoxybenzene (**8**, 59.3 mg, 400 μmol) in 4 mL CD₃CN. The product was obtained as a colorless liquid (41.0 mg, 275 μmol, 69%, *Z/E* = 3:1, >90% mono-deuteration). The crude product had a *Z/E* ratio of 4:1. The crude product in the mechanistic investigations had a *Z/E* ratio of 5:1 which indicates that the *Z*-selectivity is established in a separate energy transfer reaction after double bond migration.

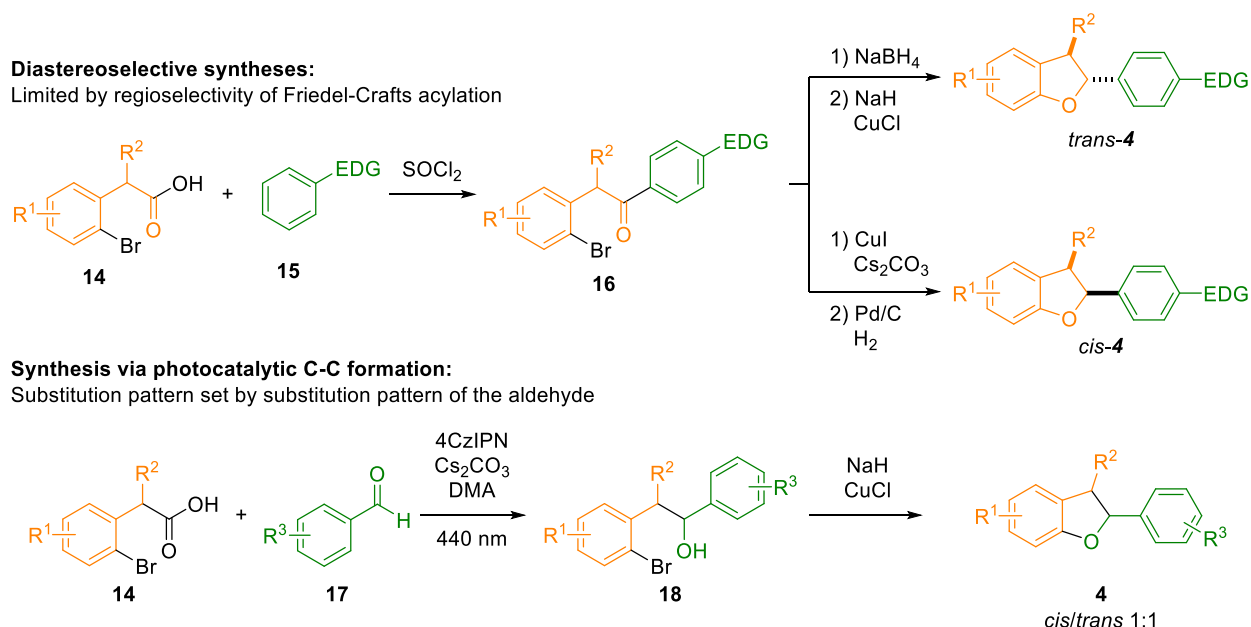
The NMR spectra of (*Z*)-**9** are in accordance with literature reports of the non-deuterated compound with differences only in the allylic position and adjacent vinylic position as expected.⁸⁹ (*E*)-**9-d**₁ was compared to commercially available (*E*)-**9-d**₀ and the NMR spectra also match except for differences in the allylic position and adjacent vinylic position as expected. Following NMR-data refers to the (*Z*)-isomer.

¹H NMR (400 MHz, CDCl₃): δ [ppm] = 7.19 – 7.14 (m, 2H, overlap with (*E*)-**9**), 6.84 – 6.78 (m, 2H), 6.33 – 6.27 (m, 1H), overlap with (*E*)-**9**, 5.68 – 5.56 (m, 1H), 3.74 (s, 3H), 1.84 – 1.71 (m, 2.47H, overlap with (*E*)-**9**, corresponds to >90% mono-deuteration). **¹³C{¹H} NMR (101 MHz, CDCl₃):** δ [ppm] = 158.2, 130.5, 130.1, 129.4, 125.2, 113.7, 55.4, 14.5 (t, $J_{C,D}$ = 19.4 Hz).

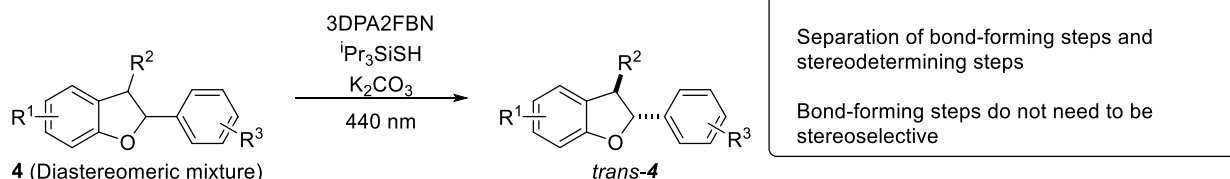
4.4.5 Application of benzofuran isomerization via a photocatalytic

HAT/RRPCO/protonation sequence

The dihydrobenzofuran scaffold is a common motif in natural products and different synthetic methods have been reported for their synthesis.⁹⁰ A straightforward synthesis of 2,3-dihydrobenzofurans (**4**) starts from phenylacetic acid derivatives and electron rich benzenes. After Friedel-Crafts acylation a divergent synthesis gives the *cis*- or the *trans*-dihydrobenzofurans. However, the substitution pattern on the pendent aryl group is limited by the directing effect of the substituents. Based on previous reports on photocatalytic Barbier and Grignard-like reactions a method for a synthesis of 2,3-dihydrobenzofurans by decarboxylative C-C coupling between bromophenylacetic acids and aromatic aldehydes was developed.



Stereochemical editing:
Enabling other synthetic routes

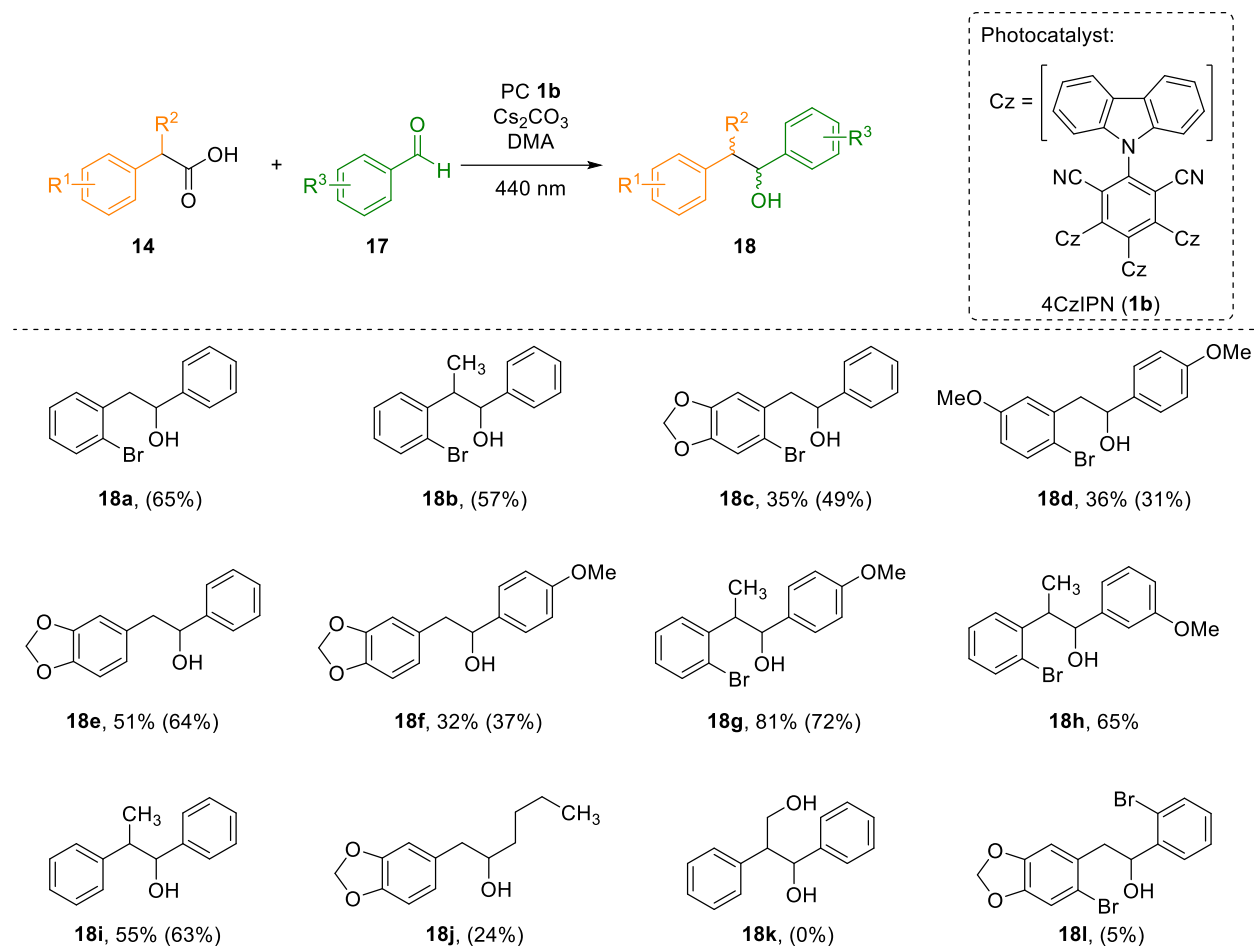


Scheme 4.8. Synthetic routes to dihydrobenzofurans.

In contrast to the non-photocatalytic pathways, the photocatalytic C-C coupling lacks diastereoselectivity. The dihydrobenzofurans are obtained in a 1:1 diastereomeric mixture if a methyl group is present in the 3-position. Other substituents at this position have not been tested but it is expected that diastereoselectivity is also low. By subjecting the mixture of diastereomers to reaction conditions for isomerization via a HAT/RRPCO/protonation sequence the *trans*-isomer is obtained selectively. In total, the sequence based on non-diastereoselective photocatalytic C-C coupling and late stage stereochemical editing is short, provides the *trans*-2,3-dihydrobenzofurans with high atom economy and access to substitution patterns not obtainable by Friedel-Crafts acylation. This is demonstrated on the example of a diastereomeric mixture of meta-substituted dihydrobenzofuran **4d** synthesized in this section which is converted to pure *trans*-**4d** in section 4.4.6.

4.4.5.1 Photocatalytic synthesis of 1,2-diarylethanol derivatives

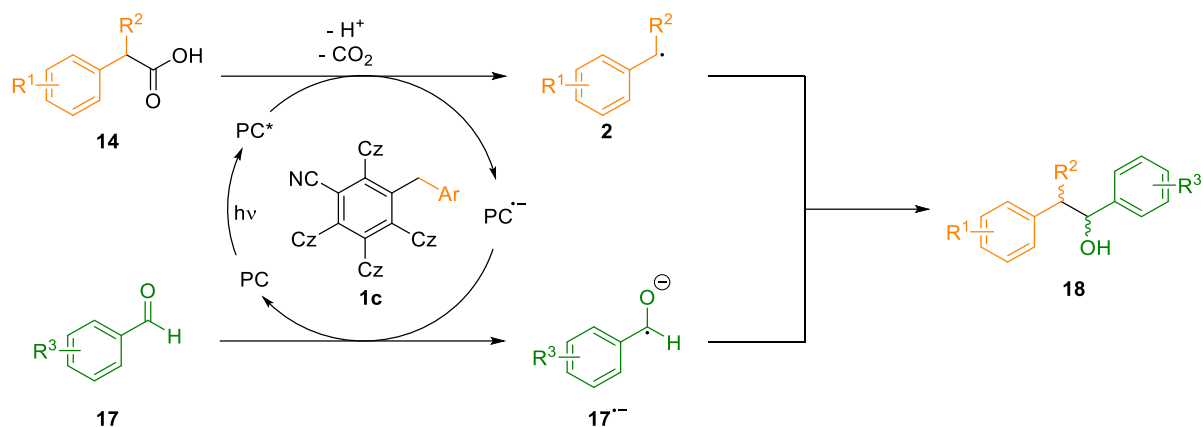
1,2-Diarylethanol derivatives were synthesized according to general procedure 4-G via a previously published method⁹¹ and obtained in moderate yields. However, no optimization of the reaction conditions for the specific substrates was conducted. 4CzIPN acts only as precursor of the active catalyst which is generated in situ via a photosubstitution with the respective carboxylic acid substrate as described in chapter 2. Thus, the active catalyst is different for each substrate.



Scheme 4.9. Photocatalytic synthesis of 1,2-diarylethanol (**18**). Isolated yields where isolated, NMR yields in parentheses, determined via ¹H NMR spectroscopy with 1,4-dicyanobenzene (0.25 equiv.) as internal standard for a separate reaction (150 μmol scale in 2 mL MeCN). Compounds **18b**, **18g**, **18h** and **18i** were formed as diastereomeric mixtures (*d.r.* = 1:1). Isolated diastereomeric ratios vary slightly mostly due to moderate separation of diastereomers during column chromatography.

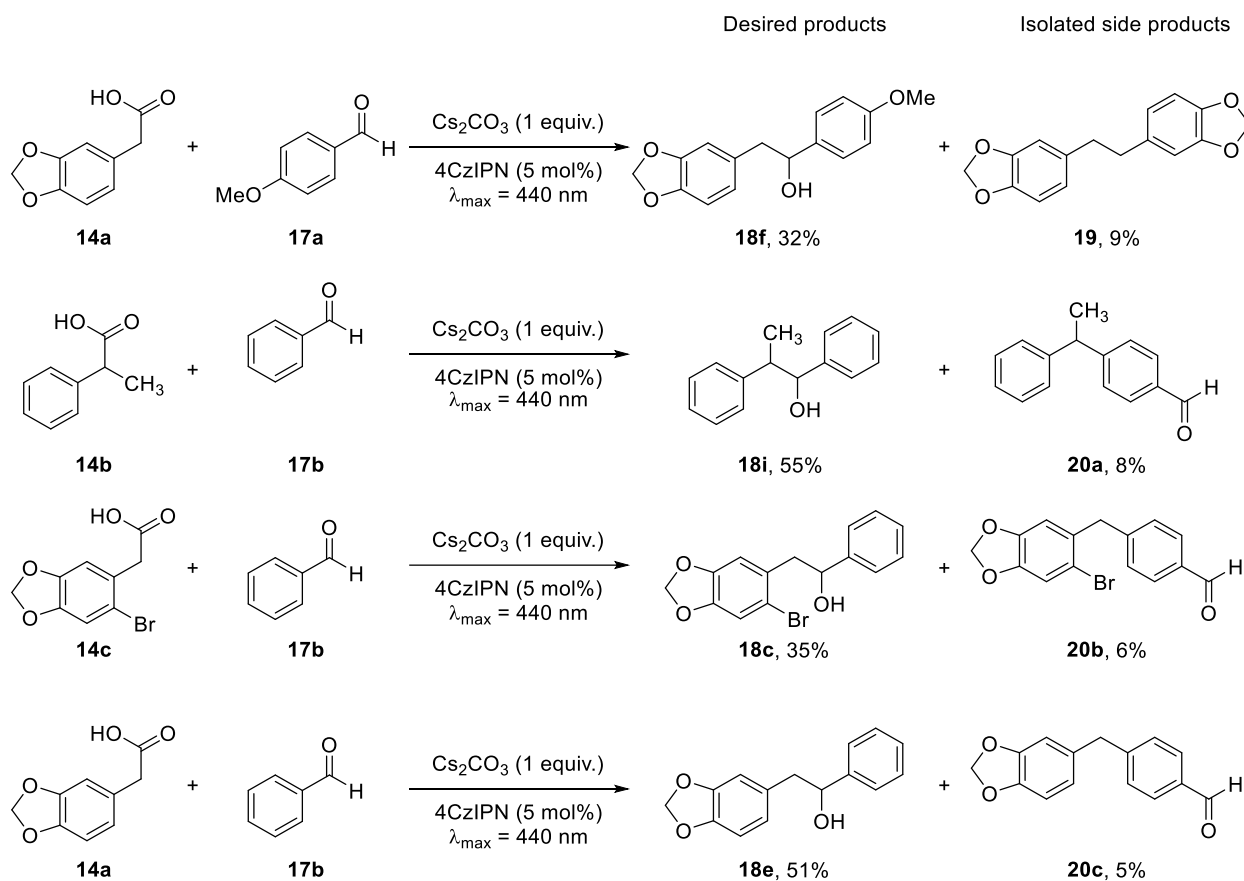
With aromatic aldehydes the reaction likely proceeds via radical-radical coupling according to Scheme 4.10 as has been proposed previously.⁹¹

REGIO-, DIASTEREO- AND ENANTIOSELECTIVITY IN THE PHOTOCATALYTIC GENERATION OF CARBANIONS VIA HYDROGEN ATOM ABSTRACTION AND REDUCTIVE RADICAL-POLAR CROSSOVER

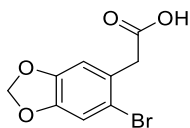


Scheme 4.10. Proposed reaction mechanism for coupling of phenylacetic acids with aromatic aldehydes. The active photocatalyst **1c** is formed in situ via a photosubstitution reaction between 4CzIPN (**1b**) and the corresponding carboxylic acid as described in chapter 2.

The proposed mechanism is supported by the observation that the reaction is insensitive to addition of water and by the observed side products **19** and **20**. Dimerization of the benzyl radicals to bibenzyl **19** and benzyl substitution in the 4-position of the aromatic aldehydes are observed in low but notable yield. Isolated products and side products are summarized in Scheme 4.11.



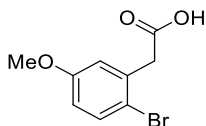
Scheme 4.11. Reactions scaled up for isolation of products where side products were isolated. All yields are isolated yields.

Synthesis of carboxylic acids (14)**2-(6-Bromobenzo[d][1,3]dioxol-5-yl)acetic acid (14c)**

Synthesized according to literature procedure.⁹²

Carboxylic acid **14a** (1.80 g, 10 mmol, 1 equiv.) was dissolved in 10 mL CHCl_3 . Bromine (615 μL , 12 mmol, 1.2 equiv.) was added dropwise and the solution stirred for 2 h at room temperature. The reaction was quenched with saturated aqueous sodium thiosulfate solution, the organic phase extracted with 3 M aqueous NaOH solution (3 x 10 mL) and the combined aqueous phases washed with Et_2O . The aqueous phase was then acidified with concentrated HCl to a pH of approximately 2. The suspension was extracted with Et_2O (3 x 20 mL), the organic phase washed with water and brine, dried over Na_2SO_4 , and the solvent removed under reduced pressure to yield the product as colorless solid (1.80 g, 6.95 mmol, 69%). The ^1H NMR is in accordance with literature.⁹²

^1H NMR (400 MHz, CDCl_3): δ [ppm] = 7.03 (s, 1H), 6.78 (s, 1H), 5.98 (s, 2H), 3.75 (s, 2H).

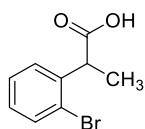
2-(2-Bromo-5-methoxyphenyl)acetic acid (14d)

Synthesized according to literature procedure.⁹²

3-Methoxyphenylacetic acid (1.16 g, 7.0 mmol, 1 equiv.) was dissolved in 10 mL CHCl_3 . Bromine (430 μL , 8.4 mmol, 1.2 equiv.) was added dropwise and the solution stirred for 2 h at room temperature. The reaction was quenched with saturated aqueous sodium thiosulfate solution, the organic phase extracted with 3 M aqueous NaOH solution (3 x 10 mL) and the combined aqueous phases washed with Et_2O . The aqueous phase was then acidified with concentrated HCl to a pH of approximately 2. The suspension was extracted with Et_2O (3 x 20 mL), the organic phase washed with water and brine, dried over Na_2SO_4 , and the solvent removed under reduced pressure to yield the product as colorless solid (1.55 g, 6.32 mmol, 90%). The ^1H NMR is in accordance with literature.⁹³

^1H NMR (400 MHz, CDCl_3): δ [ppm] = 7.46 (d, J = 8.8 Hz, 1H), 6.85 (d, J = 3.0 Hz, 1H), 6.73 (dd, J = 8.8, 3.0 Hz, 1H), 3.80 (s, 2H), 3.78 (s, 3H).

2-(2-Bromophenyl)propanoic acid (**14e**)



Synthesized according to literature procedure.⁹⁴

Diisopropylamine (1.49 mL, 10.45 mmol, 2.1 equiv.) was dissolved in 5 mL THF. *n*-BuLi (1.6 M in *n*-hexane, 6.59 mL, 10.54 mmol, 2.1 equiv.) was added at -78 °C and the solution stirred for 30 min at -78 °C. Bromophenylacetic acid (5.02 mmol, 1.08 mmol, 1 equiv.) dissolved in 2 mL THF was added at -78 °C, the solution warmed to 0 °C and stirred for 60 min. Iodomethane (331 μL, 5.32 mmol, 1.06 equiv.) was added and the solution stirred at room temperature overnight. The reaction was quenched with H₂O (0.2 mL) and concentrated under reduced pressure. The residue was dissolved in 10 mL H₂O, acidified to pH 1 and extracted with Et₂O. The solvent was removed under reduced pressure and the crude product recrystallized from EtOAc to yield the product as a colorless, crystalline solid (538 mg, 2.35 mmol, 47%). The ¹H NMR is in accordance with literature.⁹⁴

¹H NMR (400 MHz, CDCl₃): δ [ppm] = 7.58 (dd, *J* = 8.0, 1.1 Hz, 1H), 7.35 (dt, *J* = 7.3, 1.8 Hz, 1H), 7.31 (td, *J* = 7.4, 1.0 Hz, 1H), 7.17 – 7.09 (m, 1H), 4.29 (q, *J* = 7.2 Hz, 1H), 1.52 (d, *J* = 7.3 Hz, 3H).

General procedure 4-G: Benzylation of aromatic aldehydes to secondary alcohols

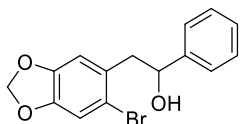
According to previously reported procedure.⁹¹ Phenylacetic acid derivative (**14**, 75 μmol per mL solvent, 1 equiv.), aldehyde (3 equiv.), cesium carbonate (1 equiv.) and 4CzIPN (**1b**, 5 mol%) are added to a crimp-capped vial with septum. DMA (1 mL per 75 μmol of carboxylic acid) is added via syringe. The vials are degassed by three cycles of freeze-pump-thaw and irradiated with blue LEDs ($\lambda_{\text{max}} = 440 \text{ nm}$) overnight at room temperature.

For isolation:

Multiple reactions on 300 μmol scale are combined, diluted with ethyl acetate, washed with water and brine, dried over Na₂SO₄, and the solvent removed under reduced pressure. The crude product is purified via column chromatography (0 → 25% EtOAc in PE).

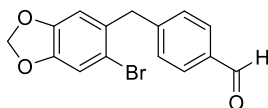
General procedure 4-H: Large scale benzylation of aromatic aldehydes to secondary alcohols

Carboxylic acid (**14**, 4.5 mmol), cesium carbonate (1.47 g, 4.5 mmol, 1 equiv.), and 4CzIPN (**1b**, 177.5 mg, 225 μmol, 5 mol%) are added to a reaction flask under nitrogen atmosphere. Dry DMA (60 mL) and aldehyde (**17**, 13.5 mmol, 3 equiv.) are added, and the solution degassed by purging with nitrogen for 20 min. The solution is irradiated in the reactor depicted in Figure 4.5 for 5 h at room temperature. Isolation according to general procedure 4-G.

2-(6-bromobenzo[*d*][1,3]dioxol-5-yl)-1-phenylethan-1-ol (18c)

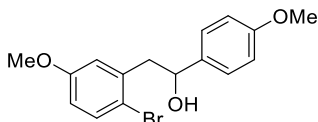
Secondary alcohol **18c** was synthesized according to general procedure 4-G from 2-(6-bromobenzo[*d*][1,3]dioxol-5-yl)acetic acid and benzaldehyde on 2.4 mmol scale (8 x 300 μ mol). The product was obtained as a colorless solid (273 mg, 850 μ mol, 35%).

Melting point: $T_m = 98$ °C. **TLC:** $R_f = 0.50$ (20% EA in PE). **^1H NMR (400 MHz, CDCl_3):** δ [ppm] = 7.43 – 7.33 (m, 4H), 7.33 – 7.27 (m, 1H), 2.03 (m, 1H), 6.70 (s, 1H), 5.95 (d, $J = 1.4$ Hz, 1H), 5.94 (d, $J = 1.4$ Hz, 1H), 4.97 (dd, $J = 8.8, 4.3$ Hz, 1H), 3.11 (dd, $J = 13.9, 4.3$ Hz, 1H), 2.98 (dd, $J = 13.9, 8.9$ Hz, 1H), 1.83 (s, 1H). **$^{13}\text{C}\{^1\text{H}\}$ NMR (101 MHz, CDCl_3):** δ [ppm] = 147.4, 144.0, 130.8, 128.6, 127.8, 125.8, 115.1, 112.9, 111.7, 101.8, 73.9, 46.1. **HRMS (EI+) m/z:** $[\text{M}]^+$ Calcd for $\text{C}_{15}\text{H}_{13}\text{BrO}_3$ 320.00426; Found 320.00415.

4-((6-Bromobenzo[*d*][1,3]dioxol-5-yl)methyl)benzaldehyde (20b)

Compound **20b** was obtained as a side product of secondary alcohol **18c** and obtained as a yellow liquid in low purity (42 mg, 132 μ mol, 6%).

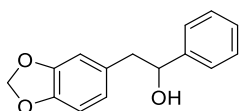
TLC: $R_f = 0.53$ (20% EA in PE). **^1H NMR (400 MHz, CDCl_3):** δ [ppm] = 9.97 (s, 1H), 7.83 – 7.78 (m, 2H), 7.36 – 7.31 (m, 2H), 7.04 (s, 1H), 6.64 (s, 1H), 5.96 (s, 2H), 4.10 (s, 2H). **$^{13}\text{C}\{^1\text{H}\}$ NMR (101 MHz, CDCl_3):** δ [ppm] = 191.9, 147.6, 147.3, 147.1, 134.8, 132.0, 130.0, 129.4, 115.0, 112.9, 110.7, 101.8, 41.8. **HRMS (EI+) m/z:** $[\text{M}]^+$ Calcd for $\text{C}_{15}\text{H}_{11}\text{BrO}_3$ 317.98861; Found 317.98791.

2-(2-Bromo-5-methoxyphenyl)-1-(4-methoxyphenyl)ethan-1-ol (18d)

Secondary alcohol **18d** was synthesized according to general procedure 4-H from carboxylic acid (**14d**) and aldehyde **17a** at 4.5 mmol scale. The product was obtained as a slightly yellow colored solid as a 1:1 mixture of diastereomers (545 mg, 1.62 mmol, 36%). The cooling system failed during the reaction which might be responsible for the low yield. The ^1H and ^{13}C NMR spectra are in accordance with literature.⁹³

Melting point: $T_m = 72$ °C **TLC:** $R_f = 0.53$ (20% EtOAc in PE). **^1H NMR (400 MHz, CDCl_3):** δ [ppm] = 7.44 (d, $J = 8.7$ Hz, 1H), 7.35 – 7.28 (m, 2H), 6.92 – 6.85 (m, 2H), 6.72 (d, $J = 3.0$ Hz, 1H), 6.66 (dd, $J = 8.9, 3.2$ Hz, 1H), 4.96 (dd, $J = 8.6, 4.6$ Hz, 1H), 3.81 (s, 3H), 3.72 (s, 3H), 3.13 (dd, $J = 13.7, 4.78$ Hz, 1H), 3.04 (dd, $J = 13.7, 8.6$ Hz, 1H) 2.03 (s, 1H). **$^{13}\text{C}\{^1\text{H}\}$ NMR (101 MHz, CDCl_3):** δ [ppm] = 159.2, 158.8, 138.8, 136.1, 133.4, 127.1, 117.5, 115.3, 114.3, 113.9, 73.1, 55.5, 55.4, 46.4. **HRMS (EI+) m/z:** $[\text{M} + \text{Na}]^+$ Calcd for $\text{C}_{16}\text{H}_{17}\text{BrNaO}_3$ 359.0253; Found 359.0254.

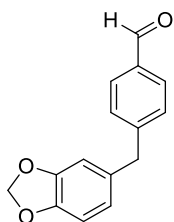
2-(Benzo[d][1,3]dioxol-5-yl)-1-phenylethan-1-ol (18e)



Secondary alcohol **18e** was synthesized according to general procedure 4-G from carboxylic acid **14a** and benzaldehyde (**17b**) on 2.1 mmol scale (7 x 300 μ mol). The product was obtained as a colorless solid (260 mg, 1.07 mmol, 51%). The NMR spectra are in accordance with literature.⁹⁵

Melting point: $T_m = 98$ °C. **TLC:** $R_f = 0.38$ (20% EtOAc in PE). **^1H NMR (400 MHz, CDCl_3):** δ [ppm] = 7.35 (d, $J = 4.3$ Hz, 4H), 7.31 – 7.26 (m, 1H), 6.74 (d, $J = 7.9$ Hz, 1H), 6.79 (d, $J = 1.5$ Hz, 1H), 6.64 (dd, $J = 7.9, 1.5$ Hz, 1H), 5.93 (s, 2H), 4.4 (dd, $J = 8.49, 4.9$ Hz, 1H), 2.96 (dd, $J = 13.8, 4.9$ Hz, 1H), 2.90 (dd, $J = 13.8, 8.4$ Hz, 1H), 1.96 (s, 1H). **$^{13}\text{C}\{^1\text{H}\}$ NMR (101 MHz, CDCl_3):** δ [ppm] = 147.8, 146.4, 143.8, 131.8, 128.6, 127.8, 126.0, 122.6, 109.9, 108.4, 101.0, 75.5, 45.9. **HRMS (EI+) m/z:** $[\text{M}]^+$ Calcd for $\text{C}_{15}\text{H}_{14}\text{O}_3$ 242.09375; Found 242.09360.

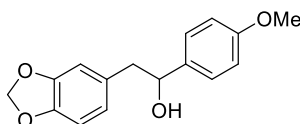
4-(Benzo[d][1,3]dioxol-5-ylmethyl)benzaldehyde (20c)



Compound **20c** was isolated as a side product in the synthesis of secondary alcohol **18e** as a yellow liquid (27 mg, 112 μ mol, 5%).

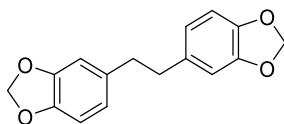
TLC: $R_f = 0.53$ (20% EtOAc in PE). **^1H NMR (400 MHz, CDCl_3):** δ [ppm] = 9.97 (s, 1H), 7.80 (d, $J = 8.1$ Hz, 2H), 7.33 (d, $J = 8.0$ Hz, 2H), 6.75 (d, $J = 7.7$ Hz, 1H), 6.68 – 6.62 (m, 2H), 5.92 (s, 2H), 3.96 (s, 2H). **$^{13}\text{C}\{^1\text{H}\}$ NMR (101 MHz, CDCl_3):** δ [ppm] = 147.4, 144.0, 130.8, 128.6, 127.8, 125.8, 115.1, 112.9, 111.7, 101.8, 73.9, 46.1. **HRMS (EI+) m/z:** $[\text{M}]^+$ Calcd for $\text{C}_{15}\text{H}_{12}\text{O}_3$ 240.07810; Found 240.07816.

2-(Benzo[d][1,3]dioxol-5-yl)-1-(4-methoxyphenyl)ethan-1-ol (18f)



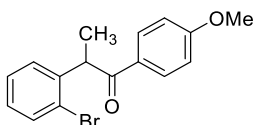
Secondary alcohol **18f** was synthesized according to general procedure 4-G from carboxylic acid **14a** and aldehyde **17a** on 1.2 mmol scale (4 x 300 μ mol). The product was obtained as a colorless solid (104 mg, 382 μ mol, 32%).

Melting point: $T_m = 99$ °C. **TLC:** $R_f = 0.25$ (20% EtOAc in PE). **^1H NMR (400 MHz, CDCl_3):** δ [ppm] = 7.27 (d, $J = 8.5$ Hz, 2H), 6.88 (d, $J = 8.6$ Hz, 2H), 6.73 (d, $J = 7.8$ Hz, 1H), 6.69 (d, $J = 1.0$ Hz, 1H), 6.66 – 6.60 (m, 1H), 5.93 (s, 2H), 4.79 (dd, $J = 7.1, 6.0$ Hz, 1H), 3.81 (s, 3H), 2.97 – 2.85 (m, 2H), 1.93 (s, 1H). **$^{13}\text{C}\{^1\text{H}\}$ NMR (101 MHz, CDCl_3):** δ [ppm] = 159.2, 147.8, 146.4, 136.0, 132.0, 127.3, 122.6, 113.9, 109.9, 108.4, 101.0, 75.1, 55.4, 45.8. **HRMS (EI+):** $[\text{M} + \text{Na}]$ Calcd for $\text{C}_{16}\text{H}_{16}\text{NaO}_4$ 295.0941; Found 295.0945.

1,2-Bis(benzo[d][1,3]dioxol-5-yl)ethane (19)

Bibenzyl **19** was obtained as a side product of secondary alcohol **18f** as colorless needles. The NMR spectra are in accordance with literature.⁹⁶

TLC: $R_f = 0.63$ (20% EtOAc in PE). **¹H NMR (400 MHz, CDCl₃):** δ [ppm] = 6.72 (d, $J = 7.8$ Hz, 2H), 6.66 (d, 1.6 Hz, 2H), 6.60 (dd, $J = 7.9, 1.7$ Hz, 2H), 5.92 (s, 4H), 2.79 (s, 4H). **¹³C{¹H} NMR (101 MHz, CDCl₃):** δ [ppm] = 147.6, 145.8, 135.6, 121.3, 109.1, 108.3, 100.1, 38.3.

2-(2-Bromophenyl)-1-(4-methoxyphenyl)propan-1-one (16a)

2-Bromophenylacetic acid (**14e**) (8.79 g, 38.38 mmol, 1 equiv.) was refluxed in 2.8 mL thionyl chloride for 30 min. The excess SOCl₂ was then evaporated under reduced pressure and the residue redissolved in 70 mL DCM, cooled to 0 °C, and anisole (4.17 mL, 38.38 mmol, 1.0 equiv.) was added. AlCl₃ (5.12 g, 38.38 mmol, 1.0 equiv.) was added in small portions, and stirred for 30 min at room temperature. The reaction mixture was then poured onto ice and extracted with DCM. The organic layer was dried over Na₂SO₄ and the solvent removed under reduced pressure. The crude product was purified via column chromatography (10→50% EtOAc in PE) to give the product as a light orange solid (9.39 g, 29.43 mmol, 86%). The ¹H NMR spectrum is in accordance with Literature.⁹⁷

¹H NMR (400 MHz, CDCl₃): δ [ppm] = 7.96 – 7.87 (m, 2H), 7.59 (dd, $J = 7.9, 1.2$ Hz, 1H), 7.22 – 7.11 (m, 2H), 7.09 – 7.02 (m, 1H), 6.90 – 6.83 (m, 2H), 5.05 (q, $J = 6.8$ Hz, 1H), 3.82 (s, 3H), 1.46 (d, $J = 6.8$ Hz, 3H).

2-(2-Bromophenyl)-1-(4-methoxyphenyl)propan-1-ol (18g)

Diastereomeric mixture:

Secondary alcohol **18g** was synthesized according to general procedure 4-G from carboxylic acid **14b** and aldehyde **17a** on 1.2 mmol scale (4 x 300 μ mol). The product was obtained as a colorless oil as a 1:0.77 mixture of diastereomers not fully separated from aldehyde **17a** (313 mg, 974 μ mol, 81%) and used as a mixture for the synthesis of dihydrobenzofuran **4c**.

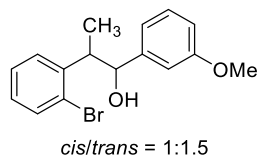
trans-18g

Ketone **16a** (400 mg, 1.25 mmol, 1 equiv.) was dissolved in 4 mL EtOH, NaBH₄ (95.0 mg, 2.50 mmol, 2 equiv.) was added, and the mixture stirred for 2 h at room temperature. The reaction was then quenched by slow addition of 1 M HCl, extracted with EtOAc, the organic phase washed with H₂O and brine, dried over Na₂SO₄, and the crude product

purified via column chromatography (5→20% EtOAc in PE) to give the product as a colorless solid (337 mg, 1.05 mmol, 84%).

¹H NMR (400 MHz, CDCl₃): δ [ppm] = 7.62 – 7.60 (m, 1H), 7.33 – 7.23 (m, 4H), 7.15 – 7.06 (m, 1H), 6.92 – 6.85 (m, 2H), 4.77 (dd, *J* = 8.5, 2.4 Hz, 1H), 3.81 (s, 3H), 1.03 (d, *J* = 7.0 Hz, 3H). **¹³C{¹H} NMR (101 MHz, CDCl₃):** δ [ppm] = 159.5, 143.0, 134.5, 133.2, 128.4, 128.1, 127.9, 113.8, 78.6, 55.4, 17.7.

2-(2-Bromophenyl)-1-(3-methoxyphenyl)propan-1-ol (**18h**)

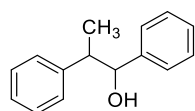


Secondary alcohol **18h** was synthesized according to general procedure 4-G from carboxylic acid **14b** and aldehyde **17c** on 2.1 mmol scale (7 x 300 μmol). The product was obtained as a colorless oil as a mixture of diastereomers (441 mg, 1.37 mmol, 65%, *d.r.* = 1:1.5).

¹H NMR (diastereomeric mixture) (400 MHz, CDCl₃): δ [ppm] = 7.61 – 7.54 (m, 2.8H), 7.38 (dd, *J* = 7.8, 1.7 Hz, 1H), 7.34 – 7.28 (m, 5.2H), 7.25 – 7.22 (m, 1.5H), 7.13 – 7.06 (m, 3H), 7.03 – 6.99 (m, 2H), 6.94 – 6.89 (m, 1.7H), 6.89 – 6.83 (m, 3.6H), 6.82 – 6.77 (m, 1H), 4.97 (d, *J* = 4.0 Hz, 1H), 4.79 (d, *J* = 8.3 Hz, 1.5H), 3.81 + 3.80 (2 x s, 8.1H), 3.76 – 3.63 (m, 3.1H), 1.84 + 1.73 (2 x s, 2.7H), 1.22 (d, *J* = 7.1 Hz, 3H), 1.07 (d, *J* = 7.0 Hz, 4.5H).

¹³C{¹H} NMR (diastereomeric mixture) (101 MHz, CDCl₃): δ [ppm] = 159.7, 159.6, 144.8, 144.0, 143.1, 142.8, 133.2, 133.1, 129.4, 129.3, 129.2, 128.4, 128.2, 127.8, 127.6, 126.1, 125.1, 119.6, 118.5, 113.8, 113.6, 112.9, 112.6, 111.6, 55.4, 45.2, 17.7, 13.1. **HRMS (+APCI) m/z:** [M + NH₄]⁺ Calcd for C₁₆H₂₁BrNO₂ 338.0750; Found 338.0752 and 338.0748.

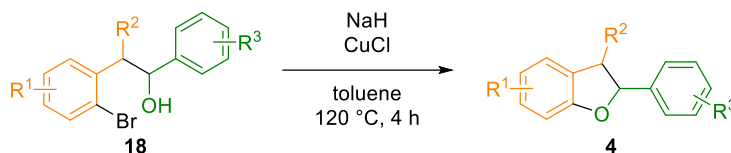
1,2-Diphenylpropan-1-ol (**18i**)



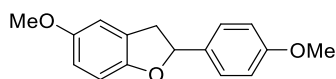
Secondary alcohol **18i** was synthesized according to general procedure 4-H from 2-phenylpropanoic acid and 4-methoxybenzaldehyde (**17a**) on 4.50 mmol scale. The product was obtained as a slightly yellow colored viscous liquid as a 1:1 mixture of diastereomers (561 mg, 2.64 mmol, 59%). The ¹H NMR spectrum is in accordance with literature.⁶⁶ The corresponding *p*-benzylated benzaldehyde was obtained as an additional fraction but was not fully separated from alcohol **18i**. Purification of the side product was not attempted.

TLC: *R_f* = 0.53 (20% EtOAc in PE). **¹H NMR (mixture of diastereomers) (400 MHz, CDCl₃):** δ [ppm] = 7.41 – 7.13 (m, 20H), 4.82 (d, *J* = 5.8 Hz, 1H), 4.67 (d, *J* = 8.7 Hz, 1H), 3.17 – 8.08 (m, 1H), 3.08 – 2.99 (m, 1H), 1.88 (s, 2H), 1.33 (d, *J* = 7.1 Hz, 3H), 1.10 (d, *J* = 7.1 Hz, 3H).

4.4.5.2 Synthesis of dihydrobenzofurans

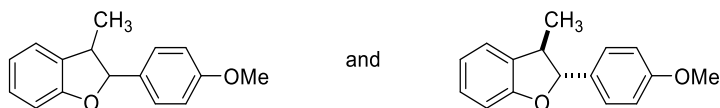
General procedure 4-I: Cyclization of secondary alcohols (**18**) to dihydrobenzofurans (**4**)

According to literature procedure.⁹³ Secondary alcohol (1 equiv.) dissolved in toluene and NaH (60% dispersion in mineral oil; pre-washed with *n*-hexane; 1.25 equiv.) are added to a crimp vial. The solution is stirred for 1 h at room temperature. CuCl (5 mol%), suspended in toluene, and ethyl acetate (1 μ L) are added, and the mixture stirred at 120 $^{\circ}$ C for 4 h. The solution is diluted with ethyl acetate (20 mL), washed with water (3 x 15 mL) and brine (15 mL), dried over Na₂SO₄ and the solvent removed under reduced pressure. The crude product is purified via column chromatography (0 \rightarrow 15% EtOAc in PE).

5-Methoxy-2-(4-methoxyphenyl)-2,3-dihydrobenzofuran (Corsifuran A, **4b**)

Synthesized according to general procedure 4-I with secondary alcohol **18d** (303.5 mg, 900 μ mol). Dihydrobenzofuran **4b** was obtained as colorless, crystalline solid (160 mg, 624.3 μ mol, 69%). The compound is known as natural product Corsifuran A and the NMR spectra are in accordance with literature.⁹³

Melting point: $T_m = 83$ $^{\circ}$ C. **TLC:** $R_f = 0.58$ (20% EA in PE). **¹H NMR (400 MHz, CDCl₃):** δ [ppm] = 7.39 – 7.28 (m, 2H), 6.95 – 6.84 (m, 2H), 6.82 – 6.64 (m, 3H), 5.68 (t, $J = 8.8$ Hz, 1H), 3.81 (s, 3H), 3.77 (s, 3H), 3.55 (dd, $J = 15.79, 9.18$ Hz, 1H), 3.20 (dd, $J = 15.77, 8.44$ Hz, 1H). **¹³C{¹H} NMR (101 MHz, CDCl₃):** δ [ppm] = 159.6, 154.4, 153.9, 134.1, 127.8, 127.4, 114.1, 113.1, 111.3, 109.3, 84.3, 56.2, 55.4, 38.8.

2-(4-Methoxyphenyl)-3-methyl-2,3-dihydrobenzofuran (**4c**)

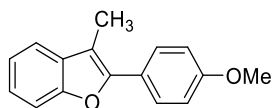
Synthesized according to general procedure 4-I with a diastereomeric mixture of *cis*-**18g** and *trans*-**18g** and in a separate batch with pure *trans*-**18g** obtained in the non-photocatalytic synthesis. The NMR spectra are in accordance with literature.^{98,99}

With a diastereomeric mixture (1:0.71) of secondary alcohol **18g** (161 mg, 500 μ mol). Dihydrobenzofuran **4c** was obtained as yellow liquid (96 mg, 400 μ mol, 80%) as a mixture of both diastereomers (1:0.77).

With *trans*-**18g** (360 mg, 1.12 mmol, *trans/cis* >9:1). *trans*-**4c** was obtained as a yellow liquid (221 mg, 920 μ mol, 82%).

***trans*-4c:** **¹H NMR (400 MHz, CDCl₃):** δ [ppm] = 7.41 – 7.35 (m, 2H), 7.22 – 7.13 (m, 2H), 6.96 – 6.90 (m, 3H), 6.87 (d, $J = 8.0$ Hz, 1H), 5.12 (d, $J = 9.0$ Hz, 1H), 3.83 (s, 3H), 3.45 (quint, $J = 7.3$ Hz, 1H), 1.42 (d, $J = 6.8$ Hz, 3H).

2-(4-Methoxyphenyl)-3-methylbenzofuran (35)

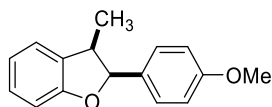


Synthesized according to literature procedure.¹⁰⁰

A mixture of secondary alcohol **18g** (711 mg, 2.23 mmol), Cs₂CO₃ (1.54 g, 4.73 mmol, 2.2 equiv.), and CuI (212 mg, 1.11 mmol, 0.5 equiv.) in dry DMF (10 mL) was stirred at 105 °C for 48 h. After cooling to room temperature, water (50 mL) was added directly to the reaction mixture over 15 minutes and the resulting orange slurry was extracted with EtOAc (3 x 30 mL), the organic phases were combined, dried over MgSO₄, filtered and the solvent evaporated under reduced pressure. The crude product was purified via column chromatography (10% EtOAc in PE) to give benzofuran **35** as yellow oil (481 mg, 2.02 mmol, 68%). The ¹H NMR spectrum is in accordance with literature.¹⁰⁰

¹H-NMR (400 MHz, CDCl₃): δ(ppm) = 7.79 – 7.71 (m, 2H), 7.55 – 7.44 (m, 2H), 7.31 – 7.21 (m, 2H+overlap with solvent residual signal), 7.06 – 6.98 (m, 2H), 3.87 (s, 3H), 2.45 (s, 3H).

***cis*-2-(4-Methoxyphenyl)-3-methyl-2,3-dihydrobenzofuran (*cis*-4c)**



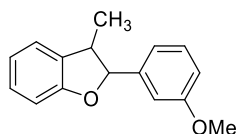
cis-**4c** was synthesized by hydrogenation of the corresponding benzofuran **35**.

Benzofuran **35** (0.57 g, 2.38 mmol, 1 equiv.) was dissolved in a mixture of 5 mL isopropanol and 15 mL ethanol and added to Palladium on activated charcoal (252 mg, 0.24 mmol, 10 mol%) in an autoclave reactor. The setup was charged with 50 bar hydrogen gas and stirred at room temperature for 72 h. The mixture was then filtered through celite, the solvent evaporated, and the product separated from unreacted starting material by column chromatography (toluene/petrol ether, 5:1). The product was obtained as yellow oil (0.21 g, 0.87 mmol, 31%) with a *d.r.* of 6.5:1. The use of a toluene/PE mixture for column chromatography was necessary due to the poor separation of product and starting material with EtOAc/PE mixtures.

The ¹H NMR spectrum is in accordance with literature.⁹⁹

¹H-NMR (300 MHz, CDCl₃): δ(ppm) = 7.25 – 7.20 (m, 2H), 7.19 – 7.12 (m, 2H), 6.94 – 6.85 (m, 4H), 5.77 (d, *J* = 8.8 Hz, 1H), 3.81 (s, 3H), 3.66 (quint, *J* = 7.7 Hz, 1H), 0.83 (d, *J* = 7.1, 3H).

2-(3-methoxyphenyl)-3-methyl-2,3-dihydrobenzofuran (4d)



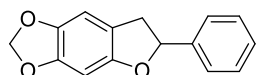
cis/trans = 1:1.5

Synthesized according to general procedure 4-I from **18h** (*cis/trans* = 1:1.5) on 1.37 mmol scale.

The product was obtained as a yellow liquid with the same diastereomeric ratio as the starting material (282 mg, 1.17 mmol, 86%, *cis/trans* = 1:1.5). *cis/trans* isomerization to convert the diastereomeric mixture of **4d** to pure *trans*-**4d** is performed in section 4.4.6.

¹H NMR (diastereomeric mixture) (400 MHz, CDCl₃): δ (ppm) = 7.30 (q, J = 7.9 Hz, 3H), 7.22 – 7.13 (m, 5.4H), 7.04 – 6.98 (m, 2H), 6.96 – 6.83 (m, 10H), 5.79 (d, J = 8.7 Hz, 1H), 5.15 (d, J = 8.7, 1.5H), 3.82 + 3.81 (2 x s, 8.2H), 3.69 (p, J = 7.6 Hz, 1H), 3.45 (p, J = 7.3 Hz, 1.6H), 1.45 (d, J = 6.8, 4.7H), 0.85 (d, J = 7.2 Hz, 3H). **¹³C{¹H} NMR (101 MHz, CDCl₃):** δ (ppm) = 160.0, 159.7, 159.3, 159.2, 142.7, 139.8, 132.9, 132.0, 129.8, 129.4, 128.4, 128.3, 124.5, 123.8, 120.98, 120.92, 118.9, 118.5, 113.9, 113.1, 112.1, 111.6, 109.7, 109.6, 92.4, 87.7, 55.41, 55.36, 45.7, 41.0, 18.3, 17.1. **HRMS (EI+) m/z:** [M]⁺ Calcd for C₁₅H₁₂O₃ 240.11448; Found 240.11475 and 240.11473.

6-Phenyl-6,7-dihydro-[1,3]dioxolo[4,5-f]benzofuran (4e)

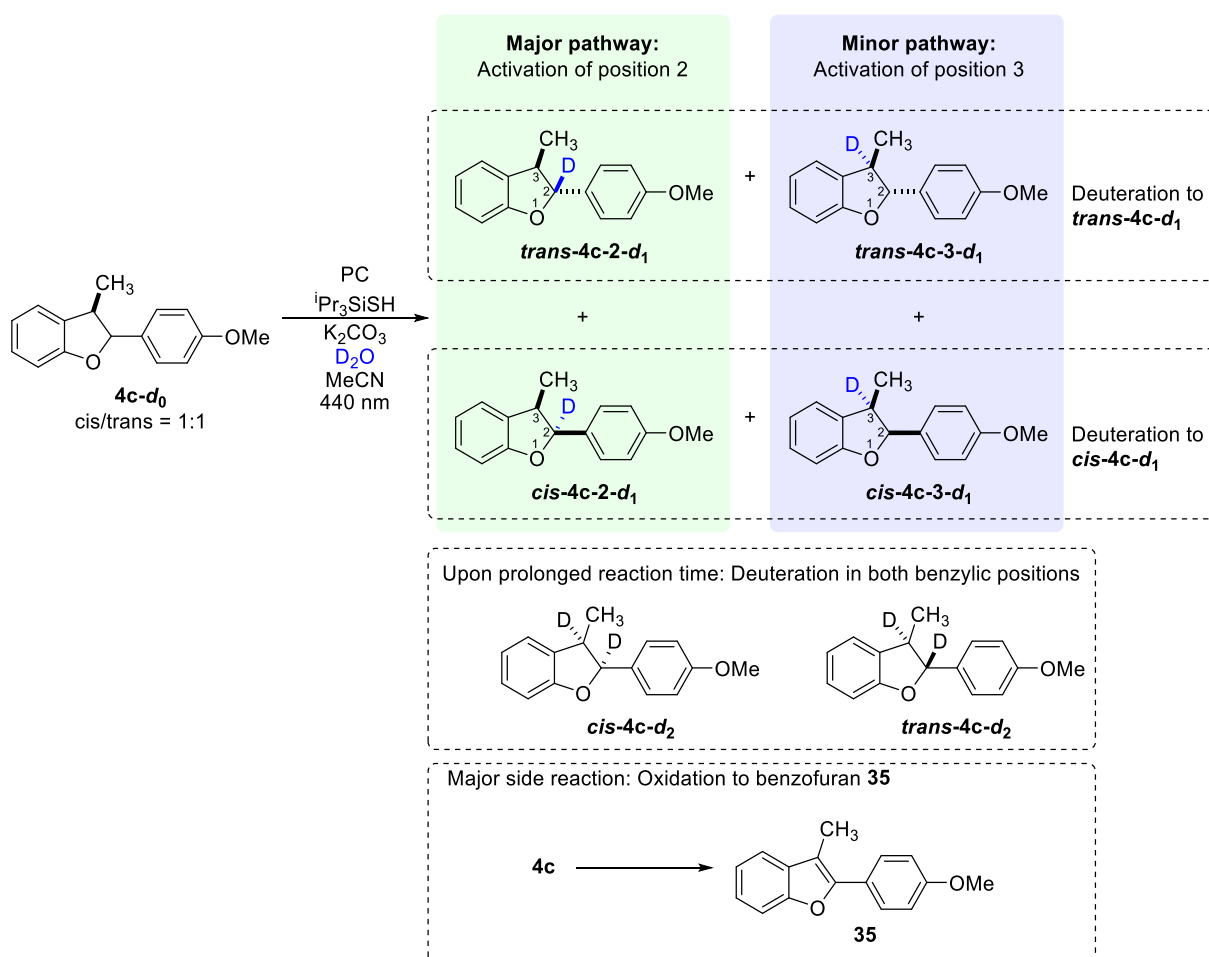


Synthesized according to general procedure 4-I with secondary alcohol **18c** (96.35 mg, 300 μ mol). Dihydrobenzofuran **4e** was obtained as a colorless liquid (55 mg, 229 μ mol, 76%).

TLC: R_f = 0.68 (20% EA in PE). **¹H NMR (400 MHz, CDCl₃):** δ [ppm] = 7.43 – 7.29 (m, 5H), 6.66 (s, 1H), 6.47 (s, 1H), 5.91 (dd, J = 4.0, 1.3 Hz, 2H), 5.75 (t, J = 8.8 Hz, 1H), 3.53 (dd, J = 15.2, 9.5 Hz, 1H), 3.13 (dd, J = 15.1, 8.2 Hz, 1H). **¹³C{¹H} NMR (101 MHz, CDCl₃):** δ [ppm] = 154.3, 147.5, 142.0, 141.8, 128.7, 128.2, 125.9, 117.3, 105.1, 101.2, 93.2, 85.0, 38.6. **HRMS (EI+) m/z:** [M]⁺ Calcd for C₁₅H₁₂O₃ 240.07810; Found 240.07825.

4.4.6 Kinetic studies for dihydrobenzofuran *cis/trans* isomerization and deuteration

Isomerizations and deuterium labelling of dihydrobenzofuran derivatives was conducted according to general procedure 4-F. 50 μL aliquots were removed from the reaction mixtures and diluted with 550 μL CDCl_3 or CD_3CN . Yields were determined via ^1H NMR with 1,1,2,2-tetrachloroethane or the residual solvent signal as standard. The methyl group at the 3-position was used to determine yield and *cis/trans* ratios. Deuteration degrees were determined by comparison of the integrals for the benzylic hydrogens with the integrals for the methyl group in the 3-position. The assignments of the signals and the procedure for determination of deuteration degrees is demonstrated exemplarily for deuteration of a 1:1 mixture of *trans-4c-d₀* and *cis-4c-d₀*.



Scheme 4.12. A 1:1 mixture of *cis-4c-d₀* and *trans-4c-d₀* initially generates monodeuterated products *cis-4c-2-d₁*, *trans-4c-2-d₁*, *cis-4c-3-d₁*, and *trans-4c-3-d₁*. With prolonged reaction time, the doubly deuterated products *cis-4c-d₂* and *trans-4c-d₂* form. Product loss occurs predominantly due to oxidation of dihydrobenzofuran **4c** to the corresponding benzofuran **35**.

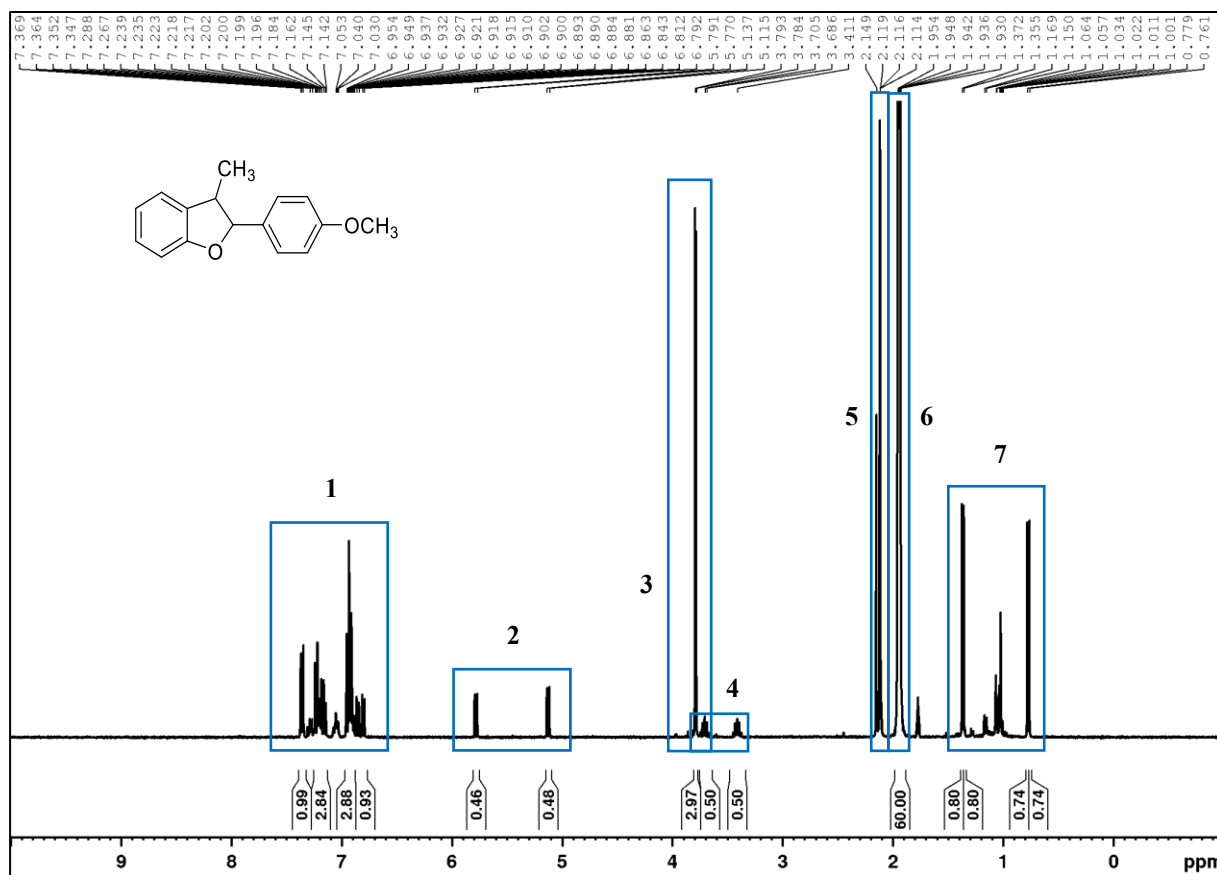


Figure 4.11. 1:1 mixture of *trans*-4c-d₀ and *cis*-4c-d₀. The individual areas relevant for determination of yields and deuteration degrees are depicted individually in Figures 4.12 – 4.15.

Area 1: The aromatic region is crowded and due to overlaps between the diastereomers, photocatalyst, and side products it is less suited for analysis than other areas.

Area 2: This area contains the benzylic hydrogens of position 2. *cis*- and *trans*-isomer are well separated, and the area is free of other signals that might interfere. These signals were used to determine the deuteration degrees in the 2-position by comparison of the respective integral with the integral of the methyl group of the 2-position (area 7). Changes in area 2 during the reaction are depicted in Figure 4.12.

Area 3: Methoxy groups. The signals for both diastereomers are overlapping. Thus, they are less suited for analysis than other areas. The signal for the methoxy group of side product **35** also appears in this area. Changes in area 3 during the reaction are depicted in Figure 4.13.

Area 4: This area contains the benzylic hydrogens in position 3 and was used to determine the deuteration degree in position 3, where possible. The diastereomers are well separated, but in some reactions side products and impurities are interfering, especially when the respective signals are of low intensity due to high degree of deuteration. Deuteration in the 3-position can also be determined from the methyl group in position 3 (area 7). Changes in area 4 during the reaction are depicted in Figure 4.14.

Area 5: Residual H₂O, and HDO. The intensity increases with reaction progress, as abstracted H-atoms end up in the deuterium reservoir (D₂O). As these signals do not belong to the molecules of interest, no information was extracted from this area.

Area 6: The solvent residual signal (residual acetonitrile-d₂) was used as internal standard.

Area 7: Methyl groups in position 3. The signals for both diastereomers are well separated and were used to determine the relative concentration of *cis-4c* and *trans-4c*. Upon H-D exchange in position 3, the doublet changes to a broadened singlet, as expected. Deuteration in position 3 can be estimated from these signals and gives results consistent with those obtained from the integrals for the protons in the 3-position. Changes in area 7 during the reaction are depicted in Figure 4.15.

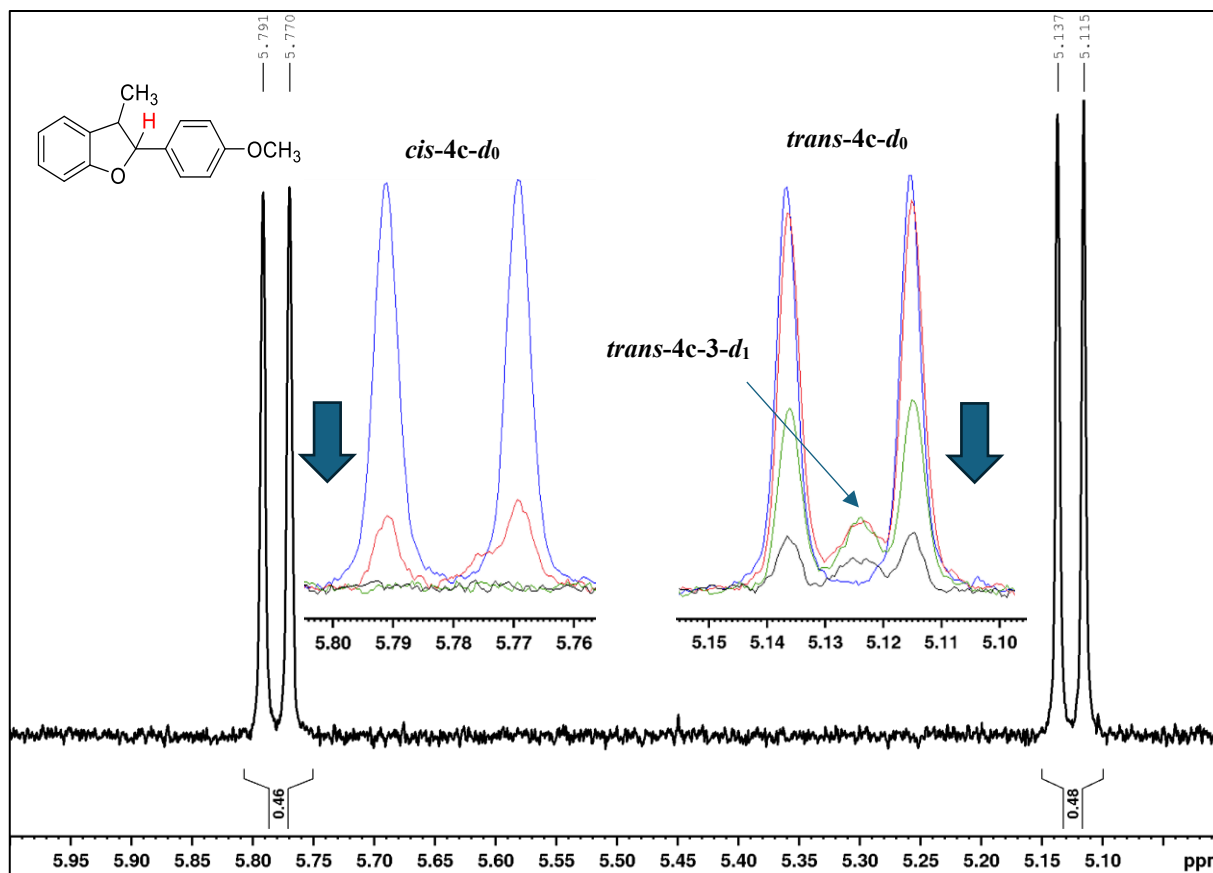


Figure 4.12. Area 2 during the HAT/RRPCO/deuteration reaction, starting with a 1:1 mixture of *cis-4c-d₀* and *trans-4c-d₀*, (Scheme 4.12). The large spectrum shows the ¹H NMR spectrum before irradiation. Inserted superimposed spectra were measured at *t* = 0 min (blue), 10 min (red), 80 min (green), and 350 min (black). The fast consumption of the *cis*-isomer is evident by the strong decrease in signal intensity within the first minutes of irradiation. C-H activation in the 3-position can be seen by the initial appearance of a new singlet for *trans-4c-3-d₁* at 5.124 ppm which later decreased again upon deuteration to *trans-4c-d₂*. As this signal grows substantially slower than the signal for *cis-4c-d₀* decreases, it is evident that C-H activation in the 2-position is faster than C-H activation in the 3-position.

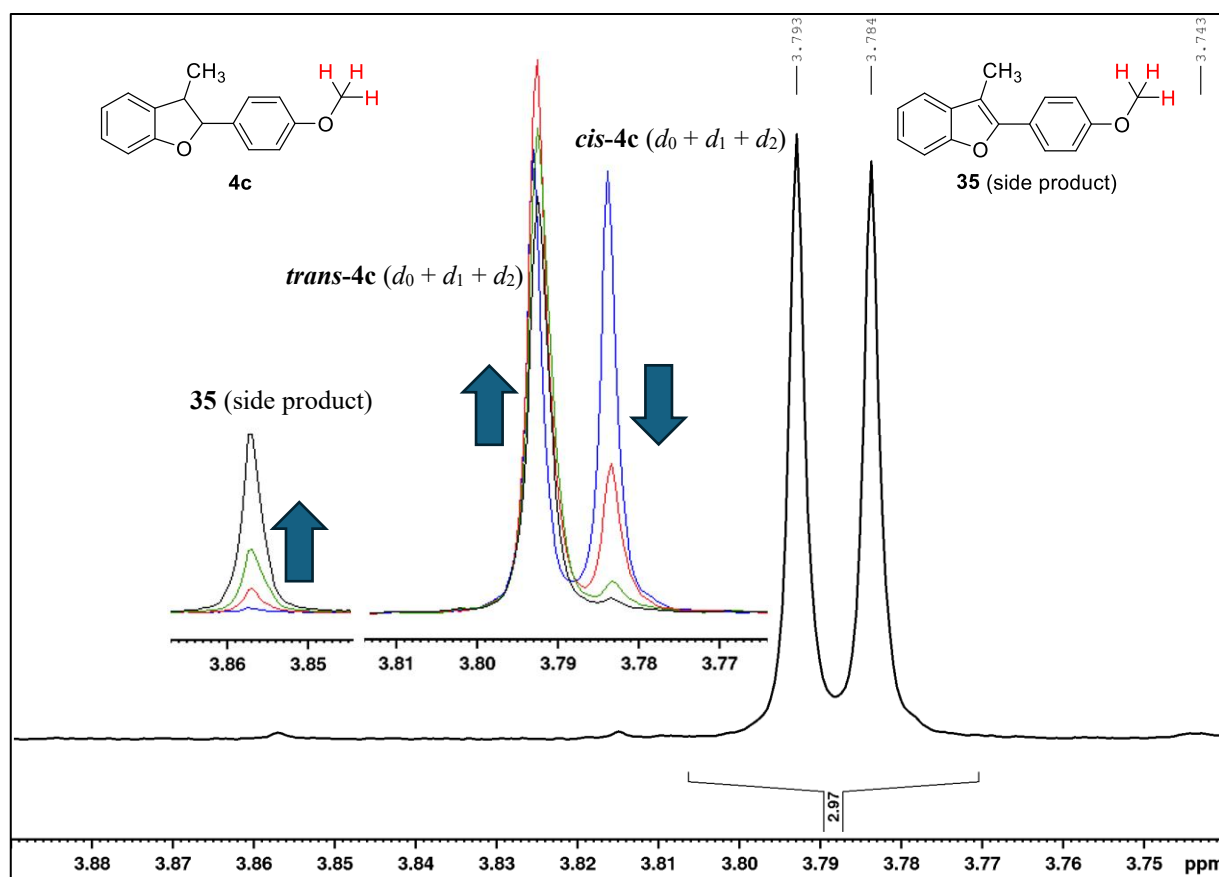


Figure 4.13. Area 3 during the HAT/RRPCO/deuteration reaction, starting with a 1:1 mixture of *cis-4c-d₀* and *trans-4c-d₀*, (Scheme 4.12). The large spectrum shows the ^1H NMR spectrum before irradiation. Inserted superimposed spectra were measured at $t = 0$ min (blue), 10 min (red), 80 min (green), and 350 min (black). The concentration of the *cis* isomer decreases within minutes of irradiation (signal at 3.78 ppm) while the concentration of the *trans* isomer increases (signal at 3.79 ppm). Upon prolonged reaction time, the concentration of *trans-4c* also decreases, mostly due to formation of the oxidation product benzofuran **35**. This is evident by the appearance of a singlet at 3.86 ppm. The corresponding methyl group in position 3 of benzofuran **35** appears at 2.45 ppm. The ^1H NMR spectrum of benzofuran **35** in CD_3CN can be found in section 7.4.3.

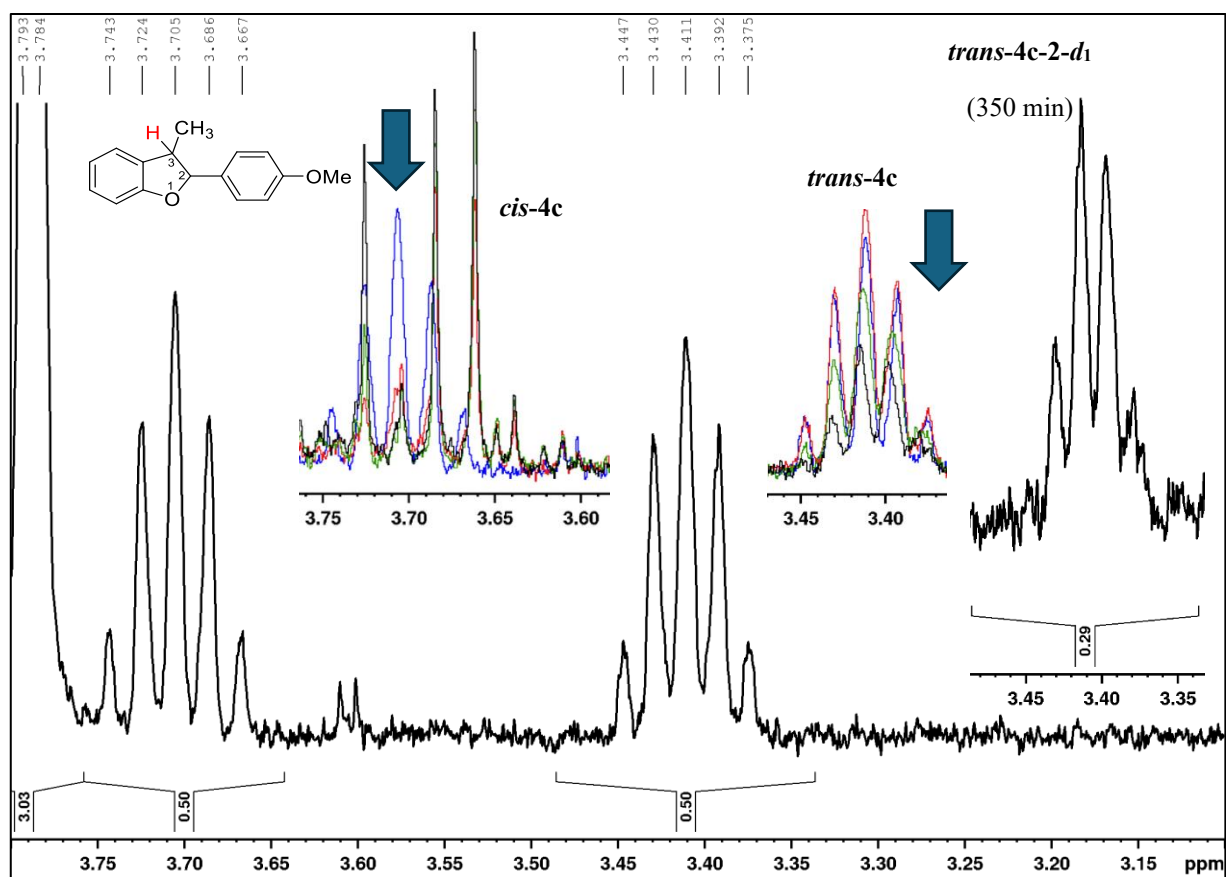


Figure 4.14. Area 4 during the HAT/RRPCO/deuteration reaction, starting with a 1:1 mixture of *cis-4c-d₀* and *trans-4c-d₀*, (Scheme 4.12). The large spectrum shows the ¹H NMR spectrum before irradiation. Inserted superimposed spectra were measured at t = 0 min (blue), 10 min (red), 80 min (green), and 350 min (black). The signal of *cis-4c* decreases within minutes of irradiation, while the signal for *trans-4c* first increases slightly (due to *cis/trans* isomerization) and then decreases slowly, demonstrating an increasing degree of deuteration in the 3-position. The multiplet structure for the *trans*-isomer changes from a quintet to a quartet upon deuteration in the adjacent 2-position (inserted black spectrum, measured at 350 min). Additional signals for side products appear in the range of 3.60 – 3.75 ppm over the course of the reaction and overlap with *cis-4c*, thus, making this signal not suited for determination of the deuteration degree in the 3-position of *cis-4c*. The deuteration degree in the 3-position of *trans-4c* was determined by comparison of the integral for the benzylic hydrogen atom with the methyl group in the 3-position. The integral for the methyl signal of *trans-4c* at 350 min is 1.73. With an integral for the proton in the 3-position of 0.29 a deuteration degree of 50% is obtained. This is in agreement with the deuteration degree as determined solely from the methyl group (48%, see Figure 4.15).

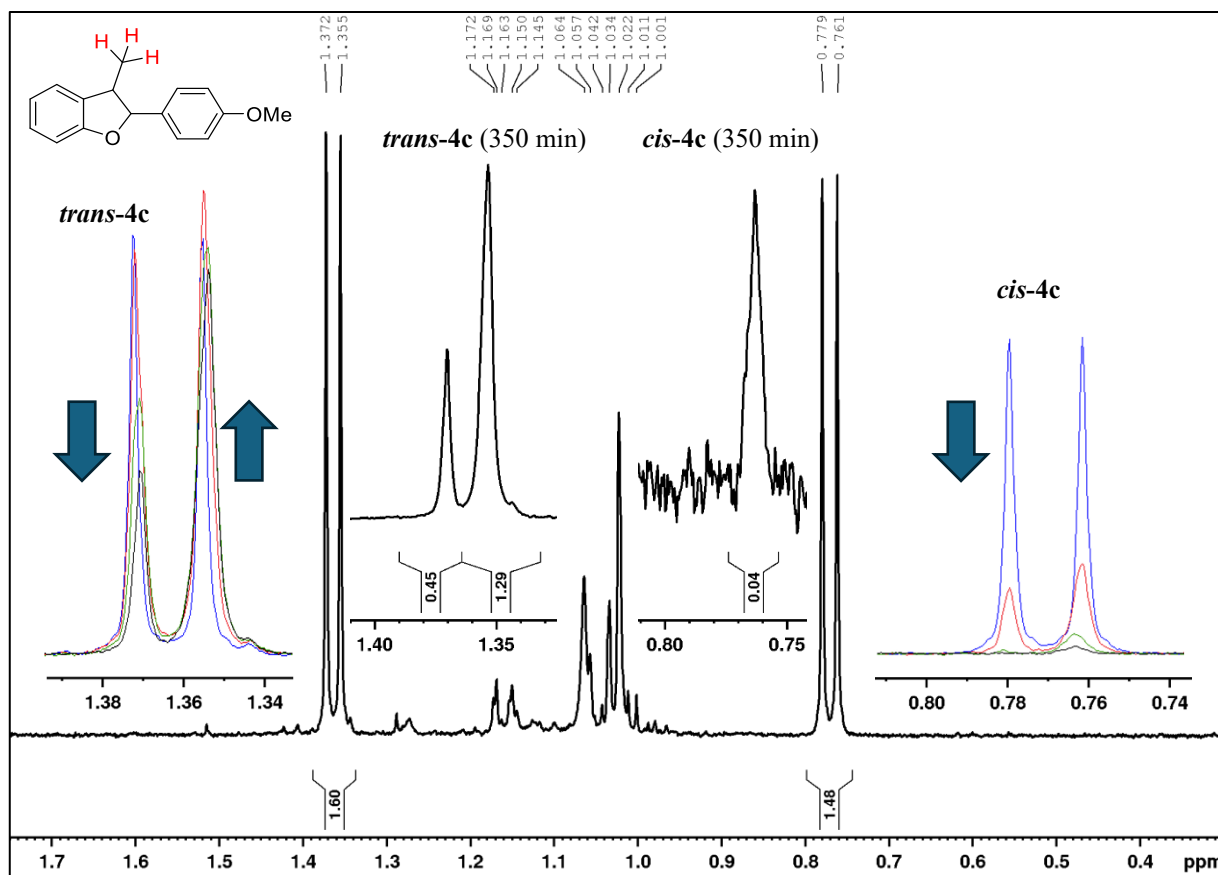
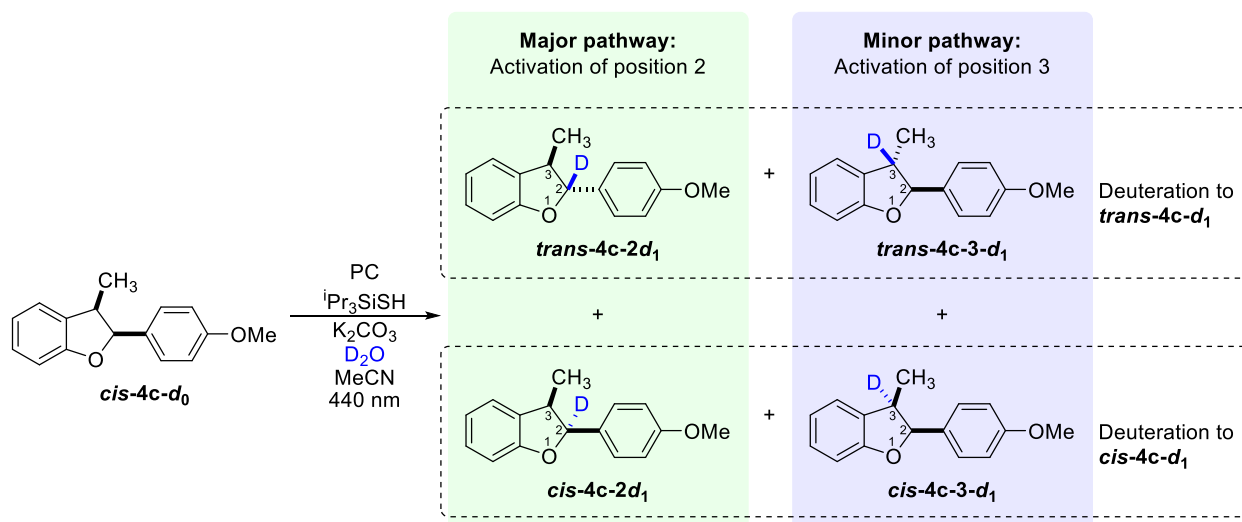


Figure 4.15. Area 7 during the HAT/RRPCO/deuteration reaction, starting with a 1:1 mixture of *cis-4c-d₀* and *trans-4c-d₀*, (Scheme 4.12). The large spectrum shows the ¹H NMR spectrum before irradiation. Inserted superimposed spectra were measured at t = 0 min (blue), 10 min (red), 80 min (green), and 350 min (black). Inserted black spectra show the respective methyl-signal after 350 min of irradiation. The methyl groups of *trans-4c-d₀* and *cis-4c-d₀* give a doublet at 1.36 ppm ($J = 6.8$ Hz, *trans-4c-d₀*) and 0.77 ppm ($J = 7.2$ Hz, *cis-4c-d₀*) which, upon deuteration in the 3-position, change to a singlet at 1.35 ppm (*trans-4c-3-d₁* and *trans-4c-d₂*) and 0.76 ppm (*cis-4c-3-d₁* and *cis-4c-d₂*). The deuteration degree in the 3-position was determined by comparison of the integral for the proton in the 2-position with the integral for the methyl group in the 3-position and additionally from the coupling pattern of the methyl signal to verify the deuteration degrees determined by either method. The deuteration degree in the 3-position at 350 min as determined solely from the methyl signal is $(1.29 - 0.45)/(1.29 + 0.45) = 48\%$. The deuteration degree in the 3-position at 350 min as determined from the signal for the benzylic hydrogen is 50%. Thus, both methods give similar results.

Kinetics with *cis-4c*


Scheme 4.13. Deuteration of *cis-4c-d₀* gives *trans-4c-2-d₁*, *trans-4c-3-d₁*, *cis-4c-2-d₁*, and *cis-4c-3-d₁*. With increasing reaction progress, the corresponding species with deuteration in both benzylic positions (*cis-4c-d₂* and *trans-4c-d₂*) are also formed. Product losses can be attributed predominantly to oxidation of dihydrobenzofuran **4c** to the corresponding benzofuran **35** (Scheme 4.12).

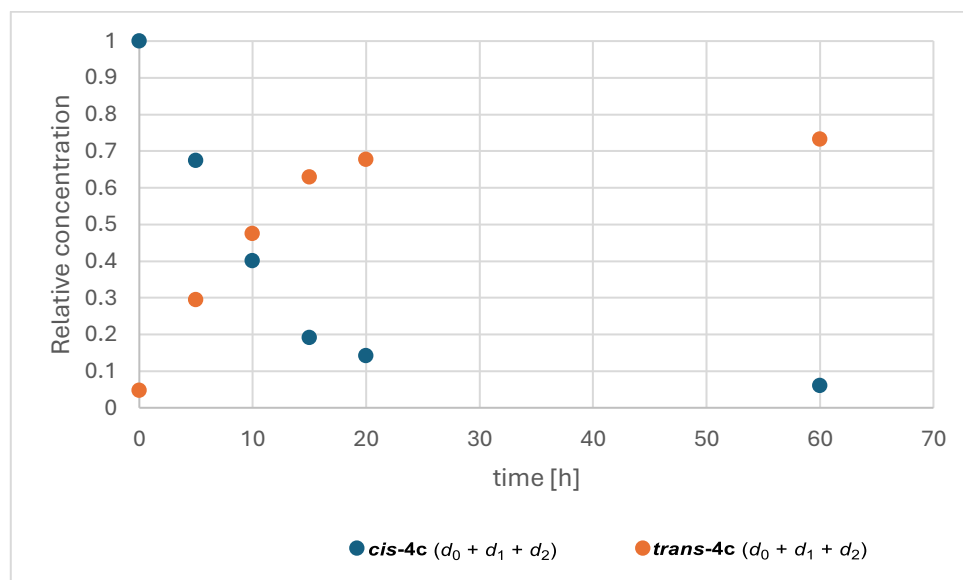


Figure 4.16. Relative concentrations of *cis-4c* (sum of *cis-4c-d₀*, *cis-4c-2-d₁*, *cis-4c-3-d₁*, and *cis-4c-d₂*) and *trans-4c* (sum of *trans-4c-d₀*, *trans-4c-2-d₁*, *trans-4c-3-d₁*, and *trans-4c-d₂*) starting from *cis-4c-d₀*.

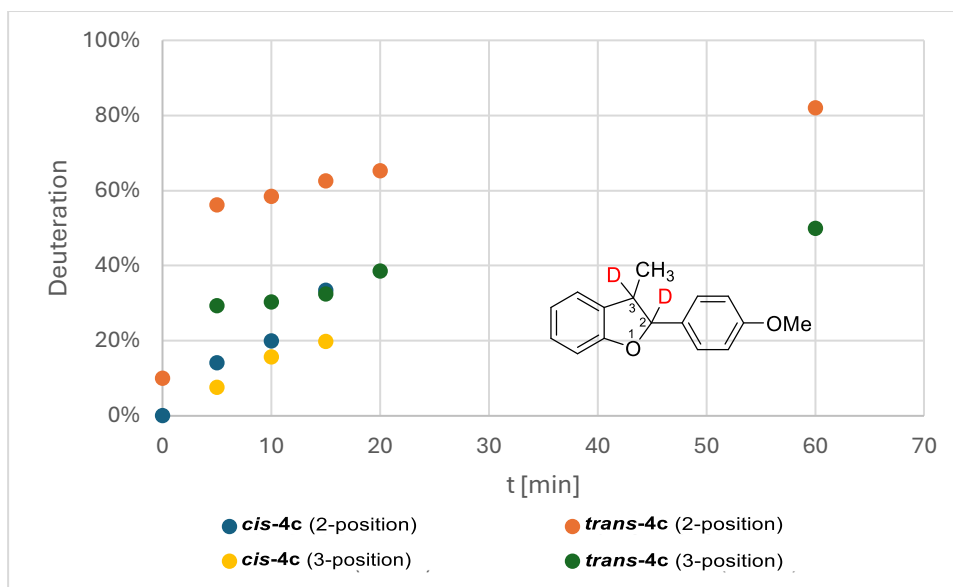


Figure 4.17. Deuteration degrees of *cis-4c* and *trans-4c* in the 2-position and 3-position, starting from *cis-4c-d₀*. Due to the low concentration and fast deuteration of *cis-4c*, deuteration degrees of *cis-4c* could not be determined after 15 min. The deuteration of *trans-4c* in the 2-position during the first minutes of the reaction is almost twice as high as in the 3-position. This demonstrates a 2.0-fold preference for activation of the 2-position over the 3-position in *cis-4c* which is similar to the 2.4-fold preference for activation of the 2-position over the 3-position in *trans-4c* (see Figure 4.22). The values for regioselectivity are under the assumption that protonation of the carbanion in the 2-position and in the 3-position has a similar *cis/trans*-selectivity.

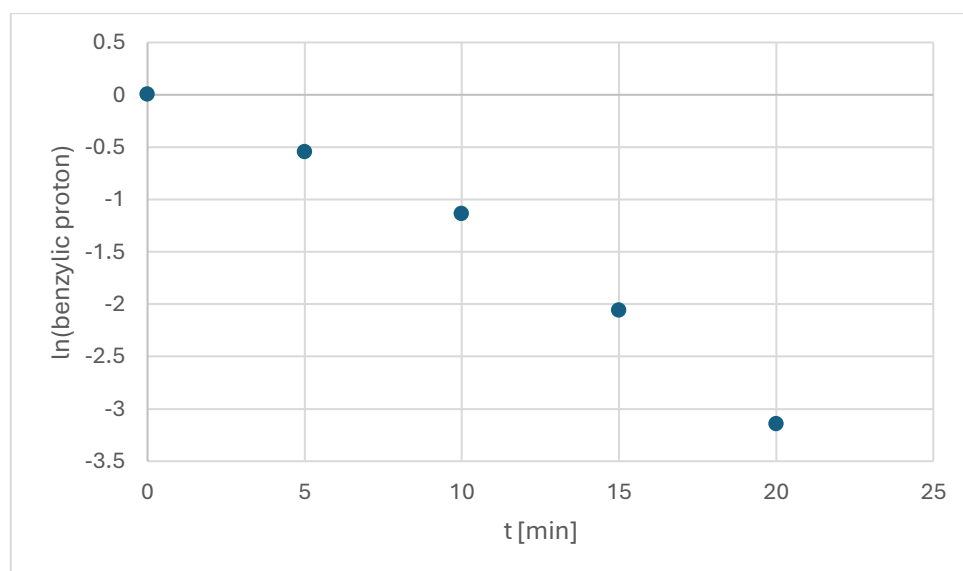


Figure 4.18. Natural logarithm of the integral for the proton in 2-position of *cis-4c*. Deuteration of the substrate can be approximated by a first order kinetic with a rate constant of $1.6 \cdot 10^{-1} \text{ min}^{-1}$. Small deviations from a first order kinetic are expected because *cis-4c-d₁* and *trans-4c-d₁* are also activated under the reaction conditions and constantly regenerate small amounts of *cis-4c-d₀*. Conversion of *cis-4c-d₀* includes the reactions giving *cis-4c-2-d₁*, *trans-4c-2-d₁*, and *trans-4c-3-d₁*.

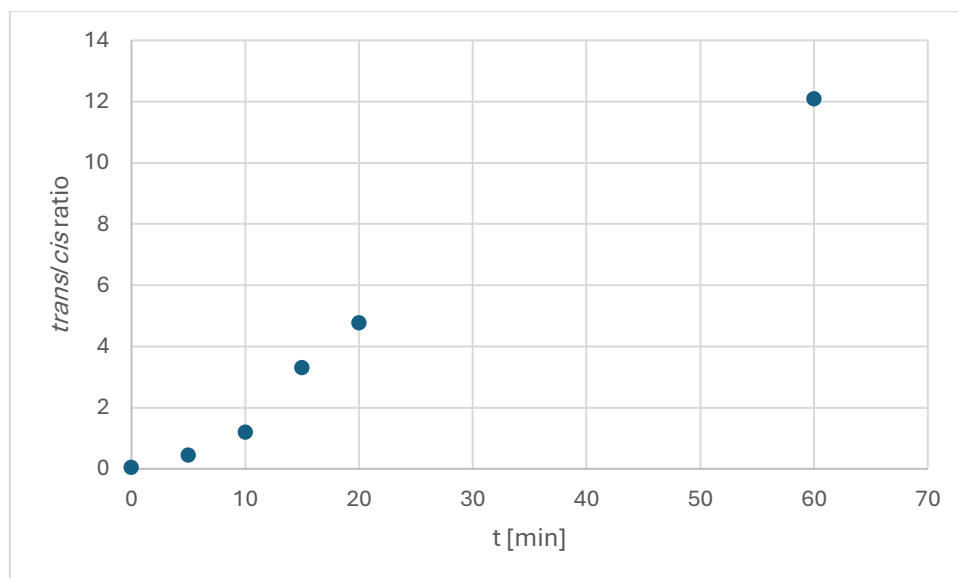
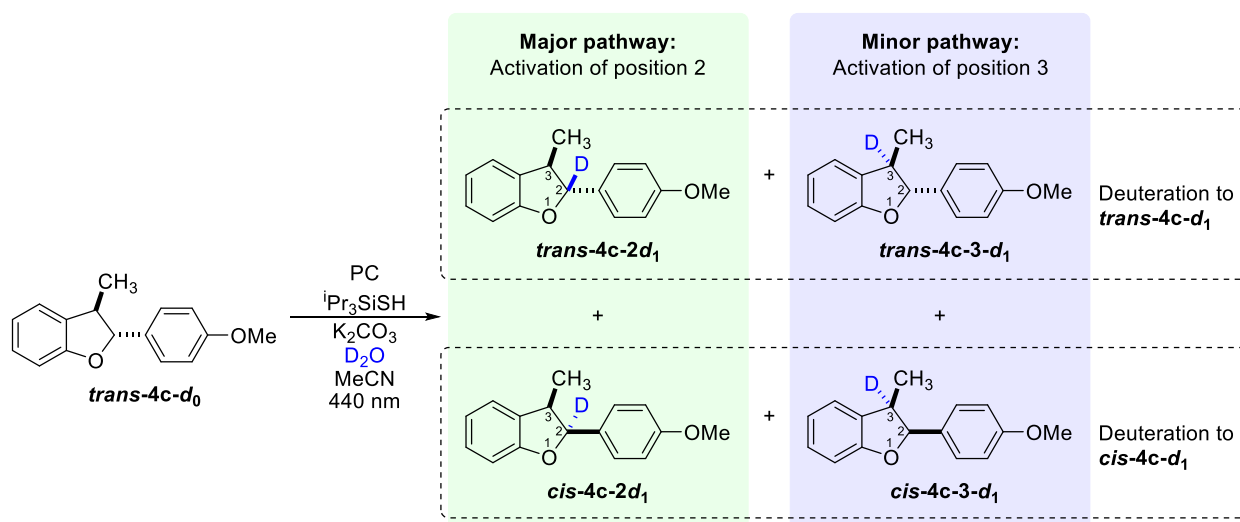


Figure 4.19. Ratio of *trans/cis*-4c during the reaction including all deuterated and non-deuterated species.

Kinetics with *trans-4c*

Scheme 4.14. Deuteration of *trans-4c-d₀* gives *trans-4c-2-d₁*, *trans-4c-3-d₁*, *cis-4c-2-d₁*, and *cis-4c-3-d₁*. With increasing reaction progress, the corresponding species with deuteration in both benzylic positions (*cis-4c-d₂* and *trans-4c-d₂*) are also formed. Product losses can be attributed predominantly to oxidation of dihydrobenzofuran **4c** to the corresponding benzofuran **35** (Scheme 4.12).

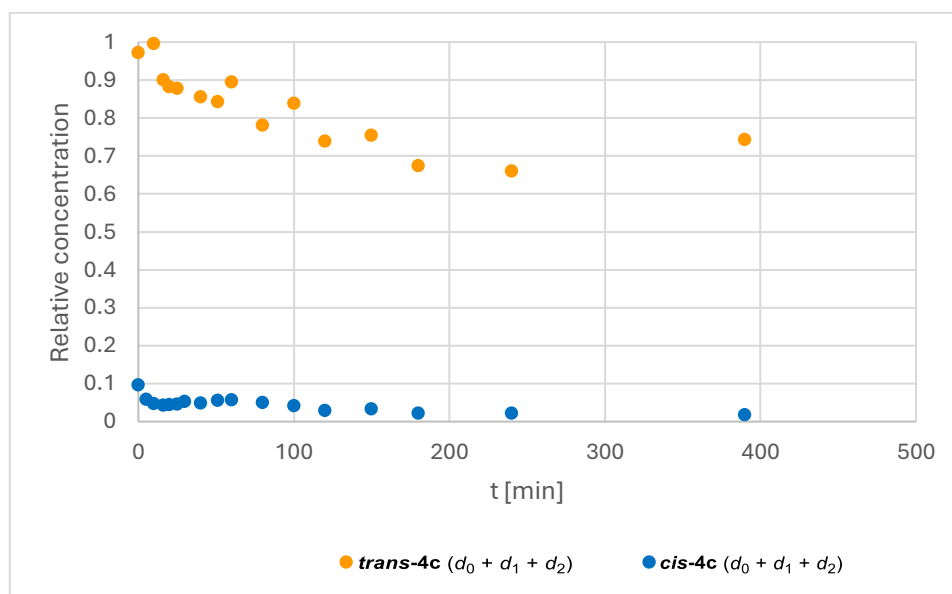


Figure 4.20. Relative concentrations of *cis-4c* (sum of *cis-4c-d₀*, *cis-4c-2-d₁*, *cis-4c-3-d₁*, and *cis-4c-d₂*) and *trans-4c* (sum of *trans-4c-d₀*, *trans-4c-2-d₁*, *trans-4c-3-d₁*, and *trans-4c-d₂*) starting from *trans-4c-d₀* (*d.r.* = 10:1).

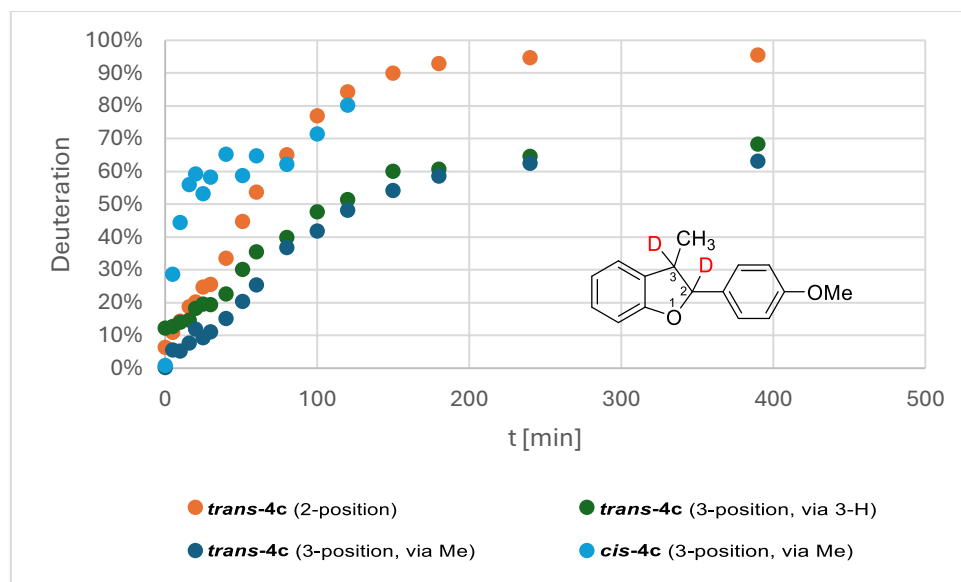


Figure 4.21. Deuteration degrees in the benzylic positions of **4c**, starting from *trans-4c-d₀*. Due to the constantly low concentration of *cis-4c* and fast deuteration, its deuteration degree in the 2-position could not be determined. The deuteration degree of *cis-4c* in the 3-position was determined from the signal for the methyl group in the 3-position until the signal intensity became too low (after 120 min). The deuteration degree of *trans-4c* in the 3-position was determined from the integral for the proton in the 3-position by comparison with the integral for the methyl group in the 3-position (*trans-4c* (3-position, via 3-H)), and additionally, from the signal for the methyl group in the 3-position (*trans-4c* (3-position, via Me)). The initial fast increase in deuteration degree of *cis-4c* in the 3-position is explained by the high reactivity of residual *cis-4c* in both benzylic positions.

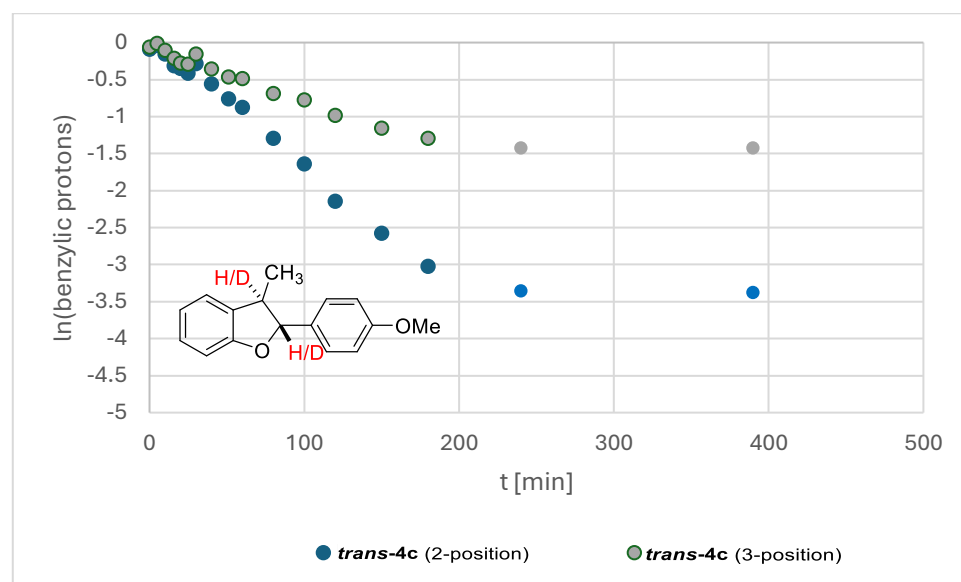


Figure 4.22. Natural logarithm of the signal intensities of the benzylic protons of *trans-4c*. C-H activation of the substrate can be approximated by a first order kinetic with a rate constant of $1.7 \cdot 10^{-2} \text{ min}^{-1}$ for deuteration of the 2-position and a rate constant of $7.2 \cdot 10^{-3} \text{ min}^{-1}$ for deuteration of the 3-position. Small deviations from a first order kinetic are expected because *cis-4c-d₁* and *trans-4c-d₁* are also activated under the reaction conditions and constantly regenerate small amounts of *trans-4c-d₀*. After 180 minutes, almost the final deuteration degrees are reached (Figure 4.21). Thus, data points after 180 min were excluded from approximation of the rate constant.

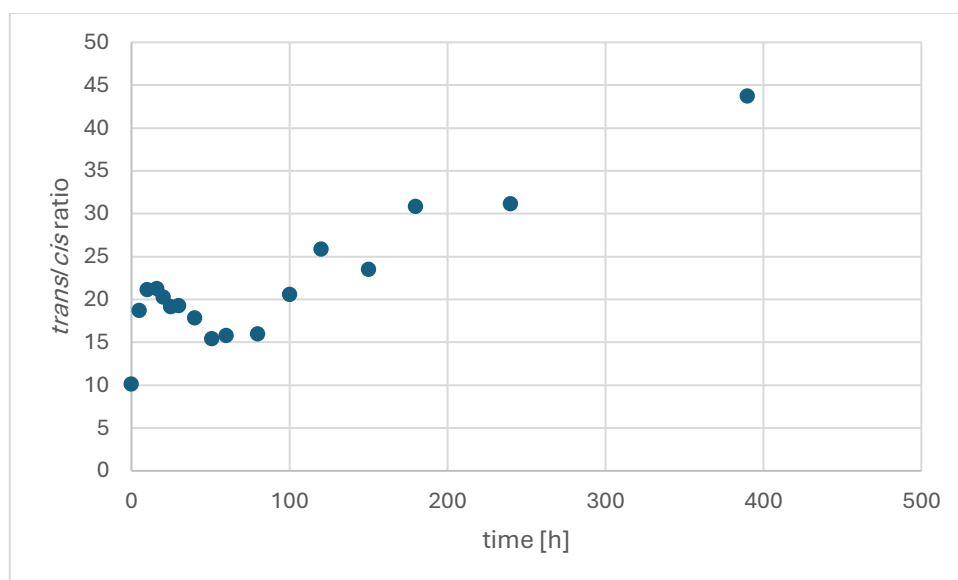
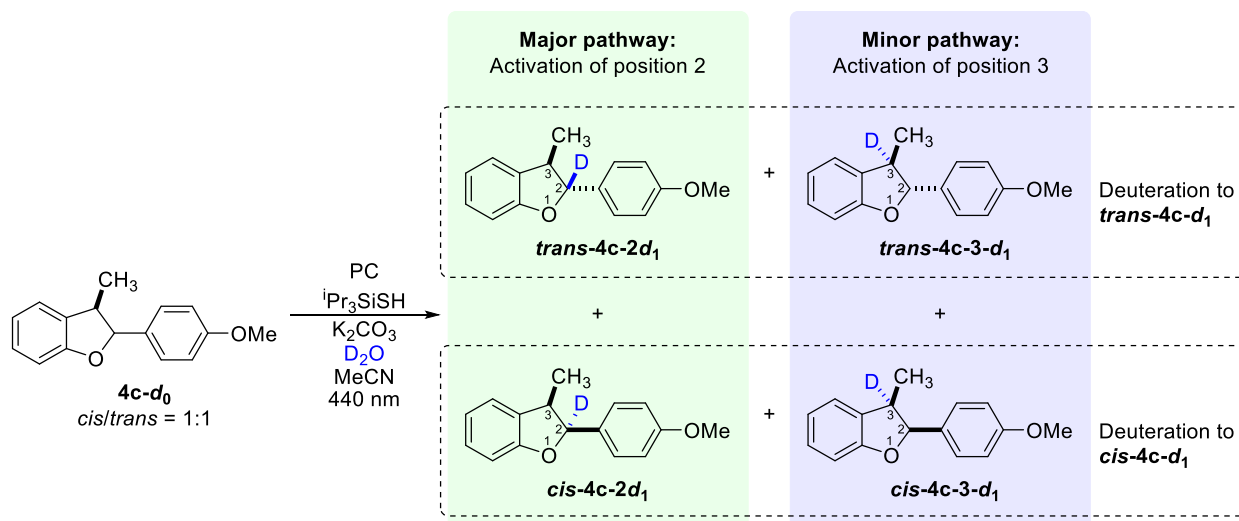


Figure 4.23. Ratio of *trans/cis-4c* during the reaction including all deuterated and non-deuterated species. The initial rapid increase in *trans/cis* ratio followed by a slight decrease is likely due to a kinetic isotope effect leading to faster C-H abstraction compared to C-D abstraction and, thus, a change in relative activation rates upon increasing deuteration degree of *cis-4c*. Kinetic isotope effects under identical reaction conditions have been analyzed in chapter 3 for ethyl anisole.

Kinetics with a diastereomeric mixture of *cis/trans-4c*



Scheme 4.15. Deuteration of a 1:1 mixture of *cis-4c-d₀* and *trans-4c-d₀* gives *trans-4c-2-d₁*, *trans-4c-3-d₁*, *cis-4c-2-d₁*, and *cis-4c-3-d₁*. With increasing reaction progress, the corresponding species with deuteration in both benzylic positions (*cis-4c-d₂* and *trans-4c-d₂*) are also formed. Product losses can be attributed predominantly to oxidation of dihydrobenzofuran **4c** to the corresponding benzofuran **35** (Scheme 4.12).

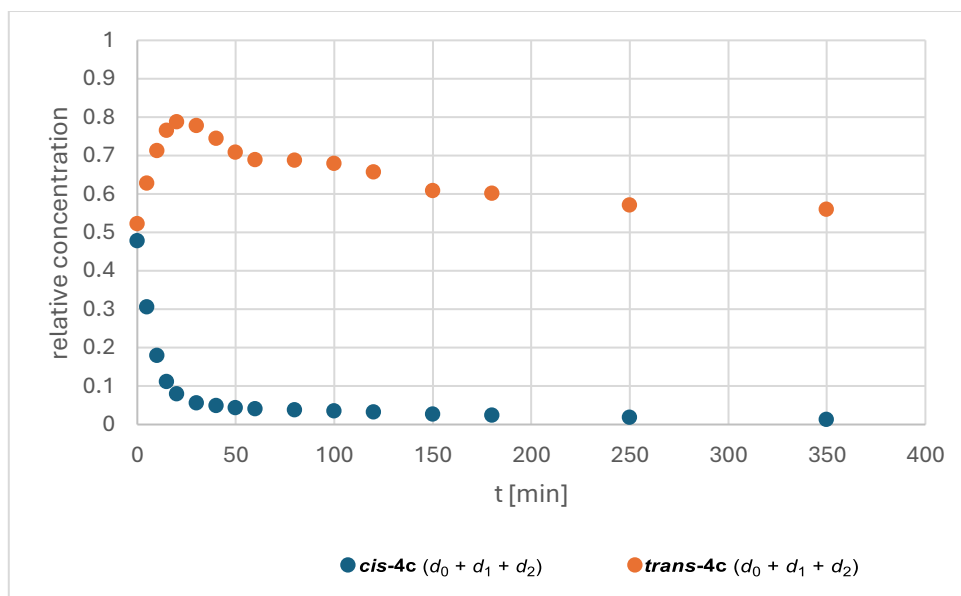


Figure 4.24. Relative concentrations of *cis*-4c (sum of *cis*-4c-*d*₀, *cis*-4c-2-*d*₁, *cis*-4c-3-*d*₁, and *cis*-4c-*d*₂) and *trans*-4c (sum of *trans*-4c-*d*₀, *trans*-4c-2-*d*₁, *trans*-4c-3-*d*₁, and *trans*-4c-*d*₂) starting from a 1:1 mixture of *cis*-4c-*d*₀ and *trans*-4c-*d*₀. Determined from the methyl group in the 3-position.

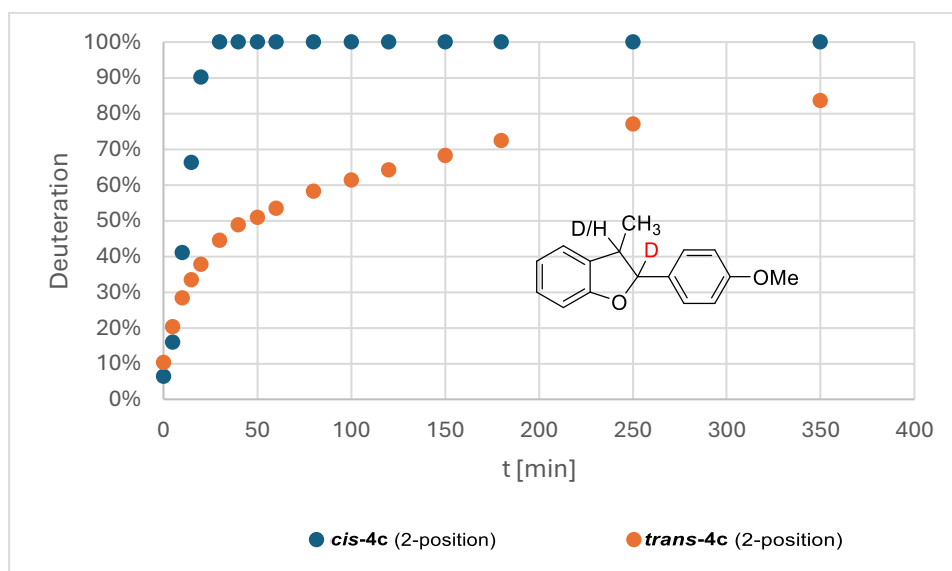


Figure 4.25. Deuterium degrees in the 2-position. After 20 minutes, the signal for *cis*-4c-*d*₀ is not distinguishable from the noise anymore. The actual degree of deuterium is likely between 95 – 100%. The deuterium degree was determined by comparison of the integral for the proton in the 2-position with the integral of the methyl group in the 3-position. Deuterium in the 3-position was also observed and is depicted in Figure 4.26.

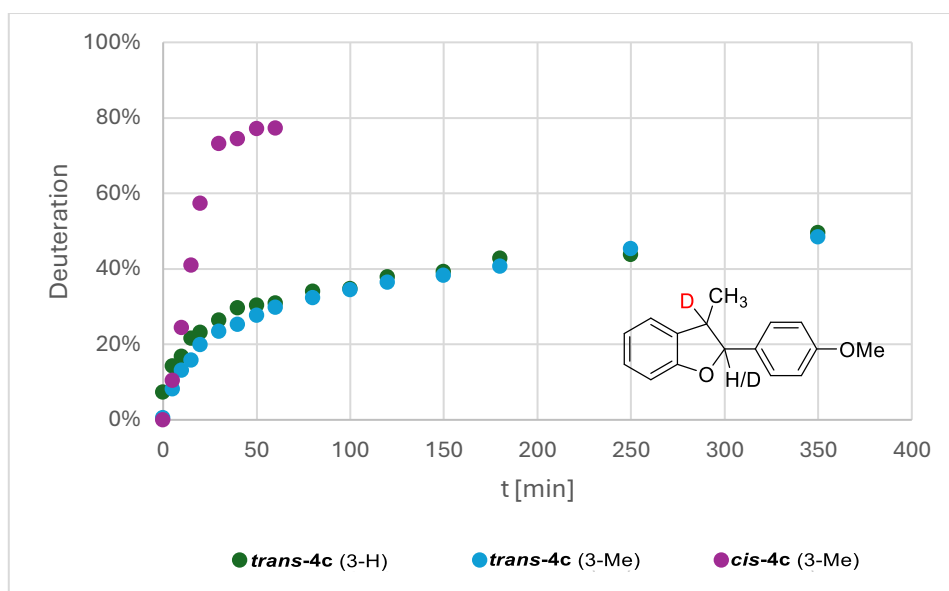


Figure 4.26. Deuteration degrees in the 3-position. After 60 minutes, the signal for *cis-4c-d₀* is not distinguishable from the noise anymore. Deuteration in the 3-position of *cis-4c* was determined from the signal for the methyl group in the 3-position (*cis-4c* (3-Me)). Deuteration in the 3-position of *trans-4c* was additionally determined by comparison of the integral for the proton in the 3-position (*trans-4c* (3-H)). Both methods give similar results.

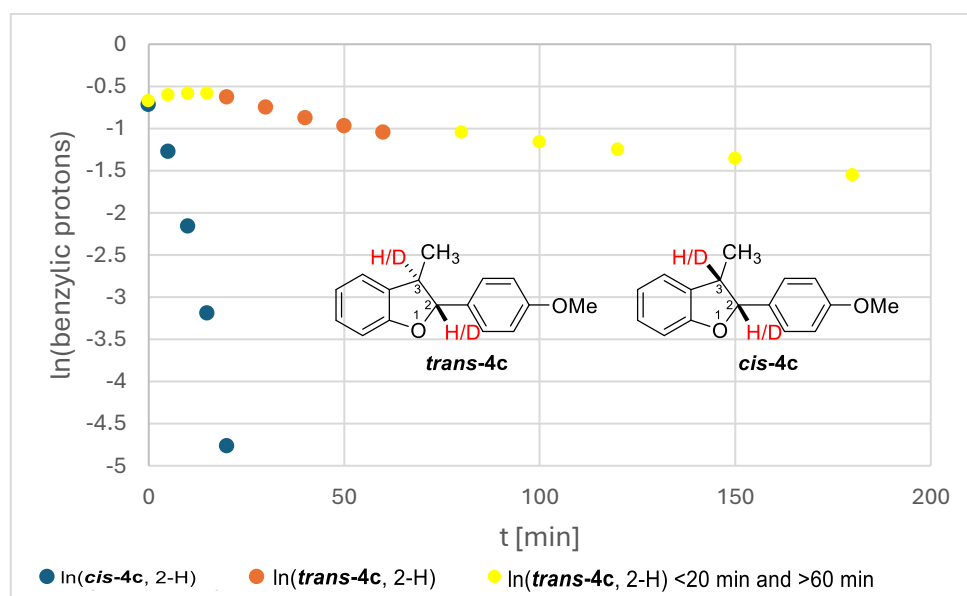


Figure 4.27. Natural logarithm of the integrals for the benzylic protons in the 2-position of *cis-4c* and *trans-4c* (see Figure 4.13, area 2). Deuteration in the 2-position can be approximated by a first order kinetic with rate constants of $2.0 \cdot 10^{-1} \text{ min}^{-1}$ for *cis-4c* and $1.1 \cdot 10^{-2} \text{ min}^{-1}$ for *trans-4c*. Deuteration of *trans-4c* can be separated into 3 parts: <20 min mostly *cis-4c* is activated and isomerized to *trans-4c* due to the higher reactivity of *cis-4c*. The slight initial increase in signal intensity for the proton in 2-position of *trans-4c* is explained by the activation of *cis-4c-d₀* in the 3-position, generating *trans-4c-3-d₁* which still contains a proton in the 2-position. Additionally, the presence of residual protons (residual H₂O, abstracted H-atoms, silane thiol) can protonate a small fraction of the intermediate carbanions in the isomerization of *cis-4-d₀* to give some *trans-4c-d₀*. Between 20 – 60 min, the predominant reaction is deuteration in the 2-position of *trans-4c* (*trans-4c-d₀* and *trans-4c-3-d₁*) (orange) until C-D activation of the 2-position of *trans-4c-2-d₁* and *trans-4c-d₂* becomes more dominant due to high degree of overall deuteration. Thus, the middle part was used for an approximation of the rate constant for C-H activation in the 2-position of *trans-4c* in the mixture.

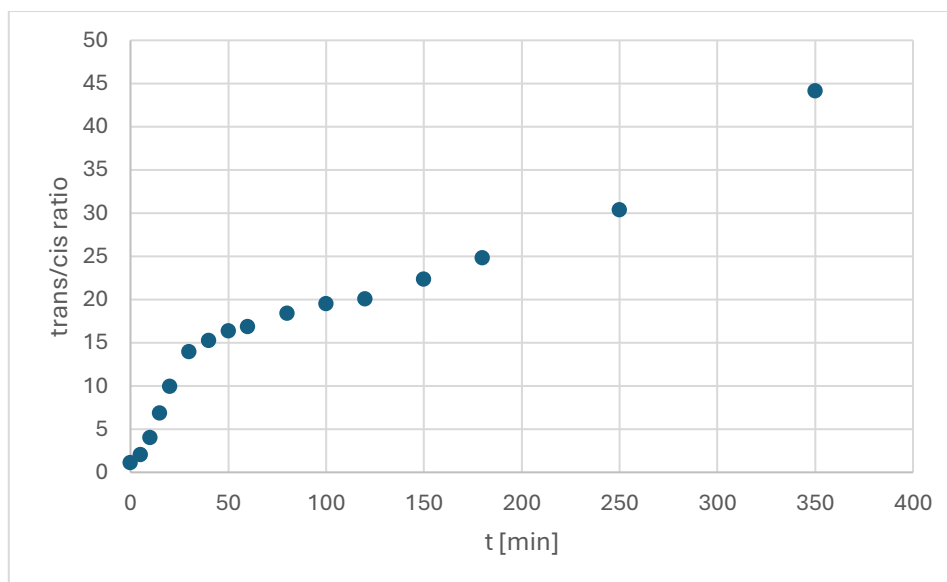


Figure 4.28. Ratio of *trans/cis-4c* during the reaction including all deuterated and non-deuterated species. The *trans/cis* ratio increases quickly until *cis-4c-d₀* is consumed (see Figure 4.24). As C-H activation of *cis-4c-d₀* is likely faster than C-D activation of *cis-4c-d₁* due to a primary kinetic isotope effect the increase in *trans/cis* ratio in the intermediate part of the experiment is slower. With increasing deuteration of *trans-4c* its activation slows down and the relative reaction rate for activation of *cis-4c* over *trans-4c* increases again.

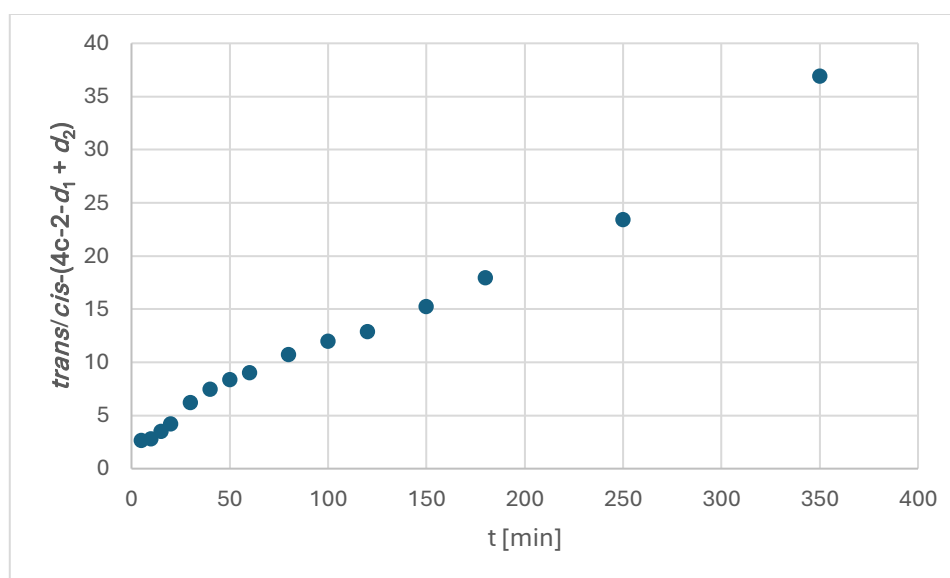
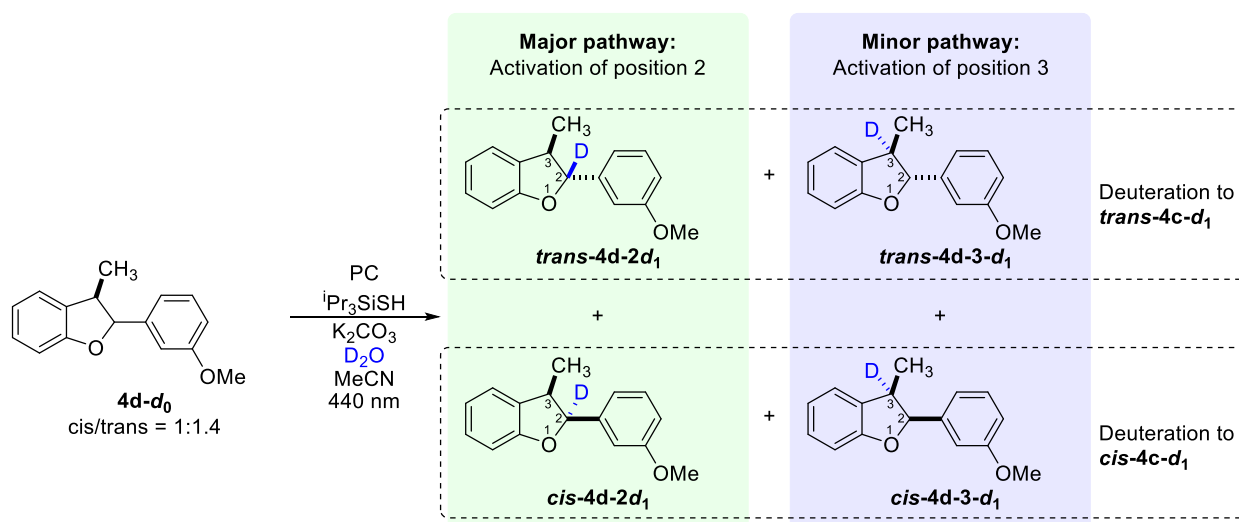


Figure 4.29. Ratio of $(\text{trans-4c-2-d}_1 + \text{trans-4c-d}_2)/(\text{cis-4c-2-d}_1 + \text{cis-4c-d}_2)$ during the reaction. The products deuterated in the 2-position have only a low *trans/cis* ratio of 1:2.6 after 5 minutes of reaction which increases 14-fold over 350 minutes. This demonstrates that the *cis/trans*-isomerization is kinetically driven in the C-H abstraction step and only a small part of the selectivity arises from selective protonation/deuteration.

Kinetics with a diastereomeric mixture of *cis/trans*-4d

Scheme 4.16. Deuteration of a 1:1.4 mixture of *cis*-4d-d₀ and *trans*-4d-d₀ gives *trans*-4d-2-d₁, *trans*-4d-3-d₁, *cis*-4d-2-d₁, and *cis*-4d-3-d₁. With increasing reaction progress, the corresponding species with deuteration in both benzylic positions (*cis*-4d-d₂ and *trans*-4d-d₂) are also formed. Product losses can be attributed predominantly to oxidation of dihydrobenzofuran **4c** to the corresponding benzofuran as observed for substrate **4c** (Scheme 4.12).

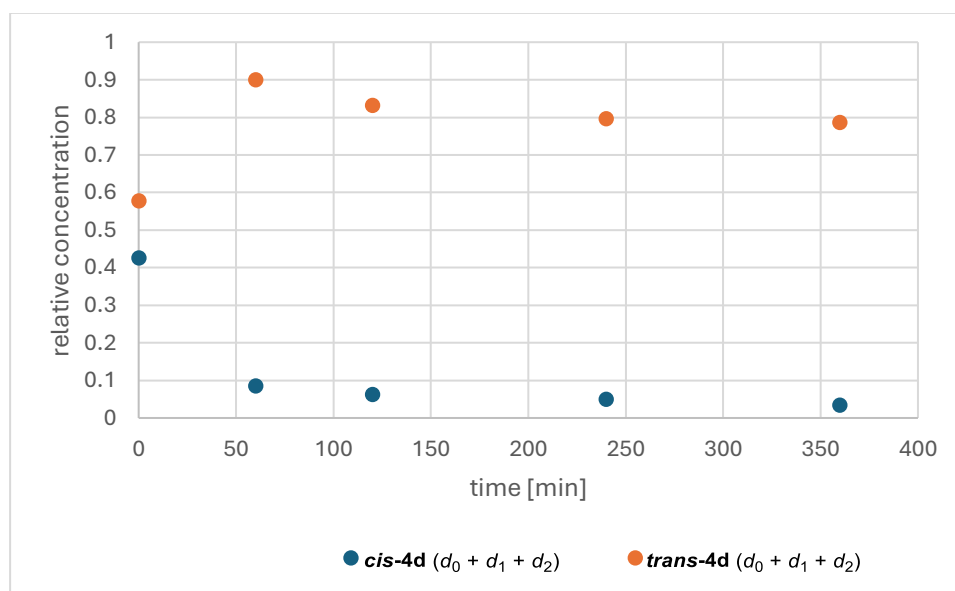


Figure 4.30. Relative concentrations of *cis*-4d (sum of *cis*-4d-d₀, *cis*-4d-2-d₁, *cis*-4d-3-d₁, and *cis*-4d-d₂) and *trans*-4d (sum of *trans*-4d-d₀, *trans*-4d-2-d₁, *trans*-4d-3-d₁, and *trans*-4d-d₂) starting from a 1:1.4 mixture of *cis*-4d-d₀ and *trans*-4d-d₀. Determined from the integral for the methyl group in the 3-position.

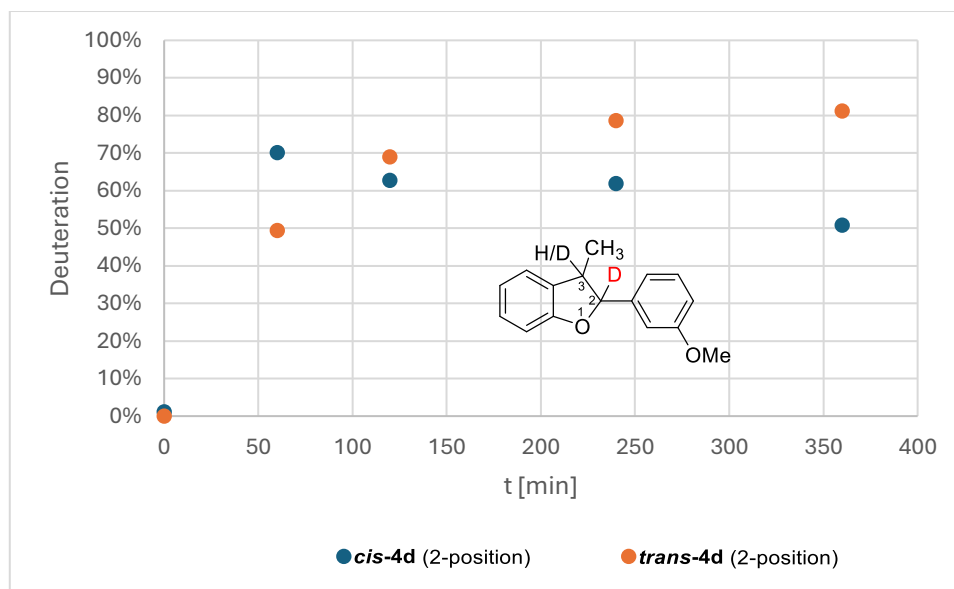


Figure 4.31. Deuteration degrees in the 2-position of **4d**. Determined from comparison of the integral for the proton in the 2-position with the methyl group in the 3-position.

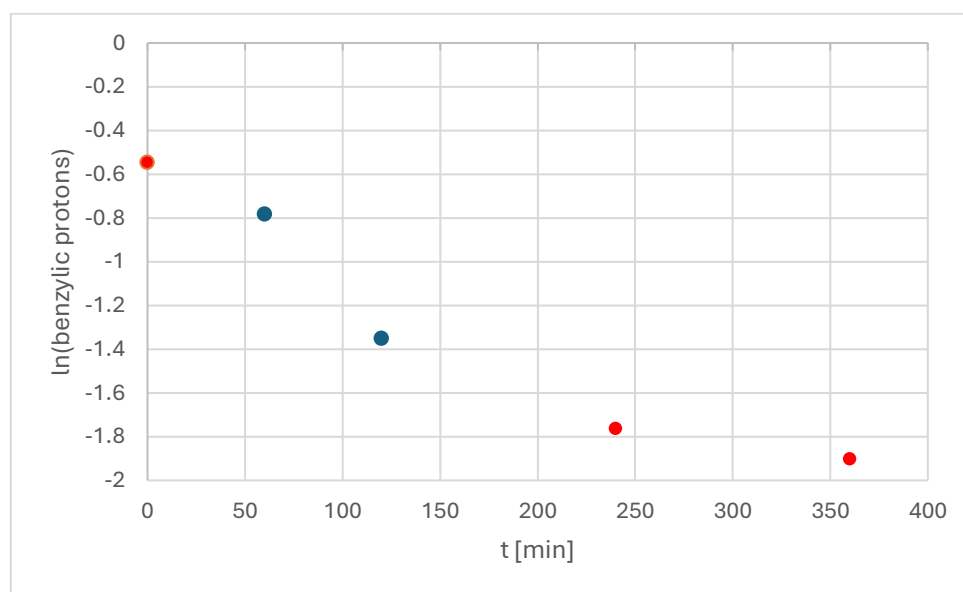


Figure 4.32. Natural logarithm of the integral for the benzylic proton in the 2-position of **trans-4d**. As only few data points have been collected, no exact rate constant can be extracted. Most of the *cis/trans*-isomerization is completed within 60 minutes and high deuteration of **trans-4d** is reached within 120 minutes (see Figures 30 and 31). Thus, the rate constant for C-H activation of the 2-position of **trans-4d** can be roughly approximated by the slope between 60 – 120 min with $1.0 \cdot 10^{-2} \text{ min}^{-1}$ which is close to the 4-substituted derivative **trans-4c-d₀** ($1.1 \cdot 10^{-2}$, see Figure 4.27). Only deuteration in the 2-position was considered.

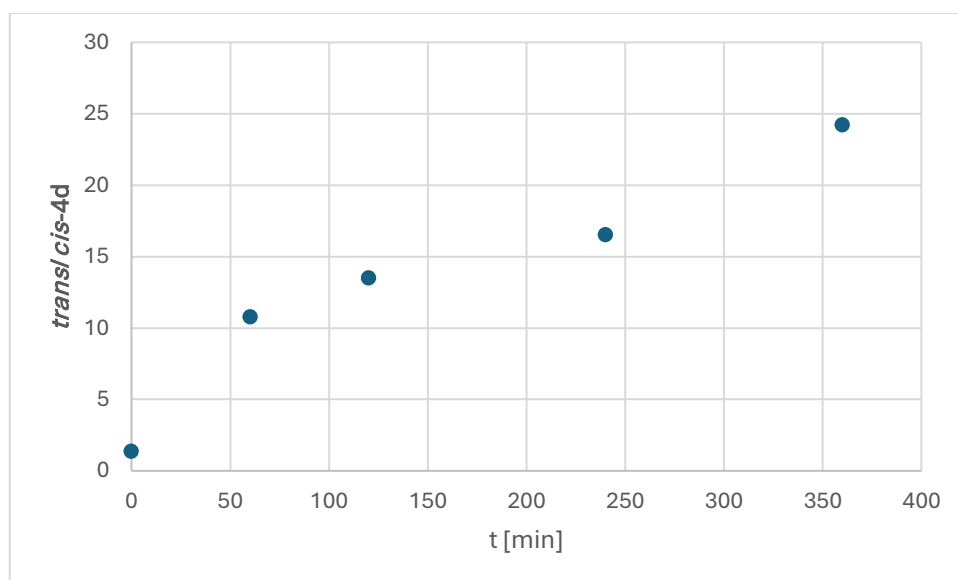


Figure 4.33. Ratio of *trans-4d*/*cis-4d* during the reaction including all deuterated and non-deuterated species.

The influence of the d1 time in the ^1H NMR experiments was tested on the example of compound **4d**. The difference in integrals of the signals for the hydrogen at the 2-position and the methyl group at the 3-position were chosen as reference points and calibrated on 1,1,2,2-tetrachloroethane added as internal standard. As can be seen in Table 4.3 the difference in integrals with longer d1 time is small and the default d1 time of 2 s is sufficient for estimation of yield and deuteration degrees.

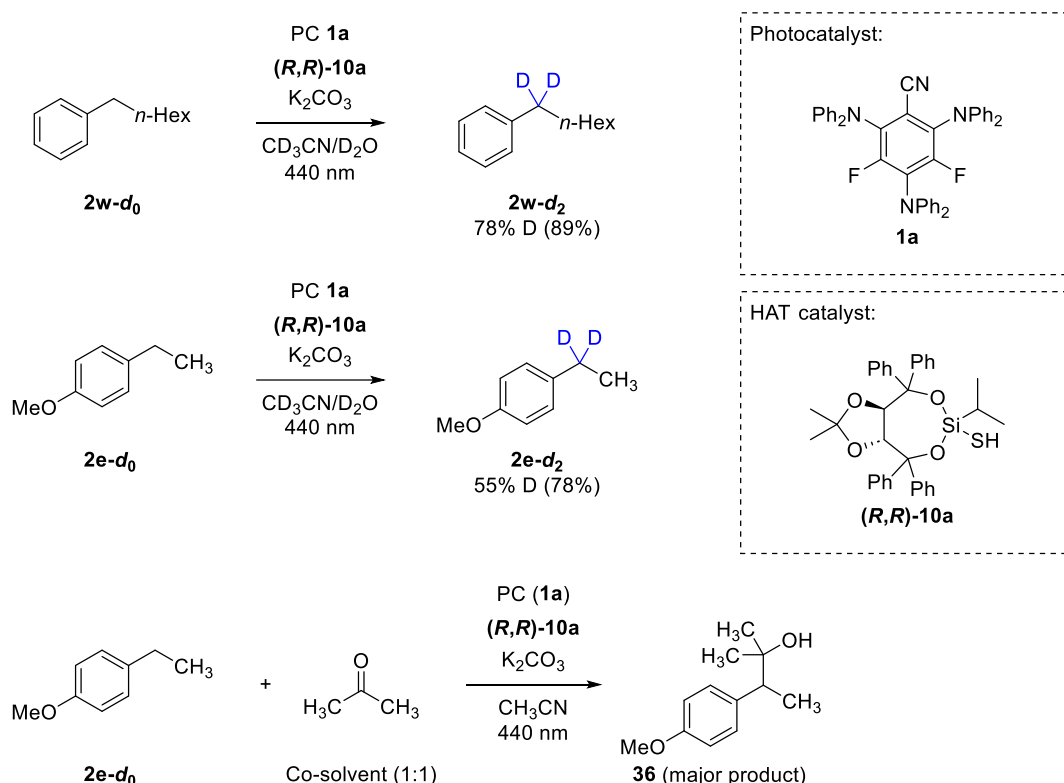
Table 4.3. Difference in integrals in dependence to the d1 time, relative to d1 = 2 s.

d1 [s]	<i>cis</i> -H (0 h)	<i>trans</i> -H (0 h)	<i>trans</i> -Me (0 h)	<i>trans</i> -H (1 h)	<i>trans</i> -Me (1 h)
2	0%	0%	0%	0%	0%
5	6%	-2%	-4%	-6%	-6%
20	2%	-2%	-10%	-5%	-11%

4.4.7 Deracemization via enantioselective HAT with chiral silane thiols

4.4.7.1 TADDOL-derived silane thiols as HAT reagents and their stability

Initial tests to evaluate whether TADDOL-derived chiral silane thiols are capable of catalyzing carbanion generation via a HAT/RRPCO sequence were conducted with heptyl benzene (**2w**) and ethyl anisole (**2e**). Both substrates reacted cleanly with good deuterium incorporation into the benzylic position under the reaction conditions of general procedure 4-F with chiral HAT-catalyst (**(R,R)**-**10a**) as depicted in Scheme 4.17.



Scheme 4.17. Chiral silane thiol (**(R,R)**-**10a**) is an efficient HAT catalyst for photocatalytic generation of benzyl carbanions. Deuteration and nucleophilic addition³⁸ were used as mechanistic probe. NMR yield in parentheses.

The hydrolytic stability of HAT catalyst **10a** is sufficient for use under standard reaction conditions for benzylic deuteration according to general procedure 4-F. After 16 h of irradiation 42% of the initial catalyst are still present in the deuteration of ethyl anisole (**2e**). 53% of the corresponding silanol were detected. In the deuteration of heptyl benzene (**2w**) 24% of the silane thiol remained after 16 h of irradiation together with 42% silanol.

No decomposition of silane thiols **10** was observed during storing at ambient conditions under air for up to 2 years. The corresponding chlorosilanes in solid form can also be stored at ambient conditions without notable decomposition. However, in solution hydrolysis to the silanols occurs within hours in the presence of water. The difference in chemical shifts between both methine protons of the TADDOL backbone is substantially smaller in the silanols compared to the corresponding chlorosilanes and even larger in silane thiols for all TADDOL-based silicon compounds synthesized in this work. The lack of other signals in the range of 5 – 6 ppm makes these protons most suitable for following the fate of these silicon compounds during reactions. A comparison of the signals for the methine protons of chlorosilane **30d**, silane thiol **10d** and silanol **31d** is depicted in Figure 4.34.

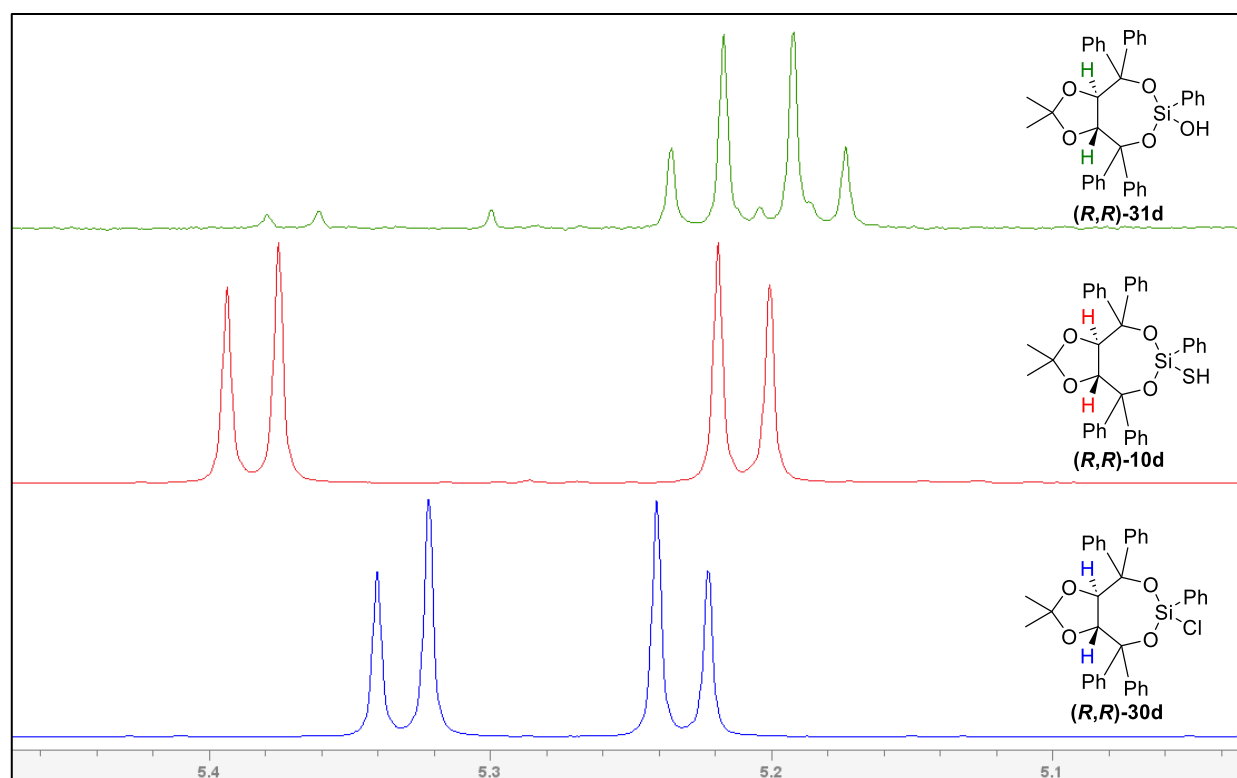


Figure 4.34. Comparison of the methine protons of TADDOL-based silicon compounds **31d**, **10d**, and **30d**. Only the section of the ^1H NMR spectra showing the methine protons of the TADDOL backbone are depicted. The respective compounds have been isolated and characterized in section 4.4.3.3. 400 MHz, CDCl_3 . Chemical shifts in CD_3CN differ only slightly and follow the same trend.

4.4.7.2 Deracemization with chiral HAT-reagents

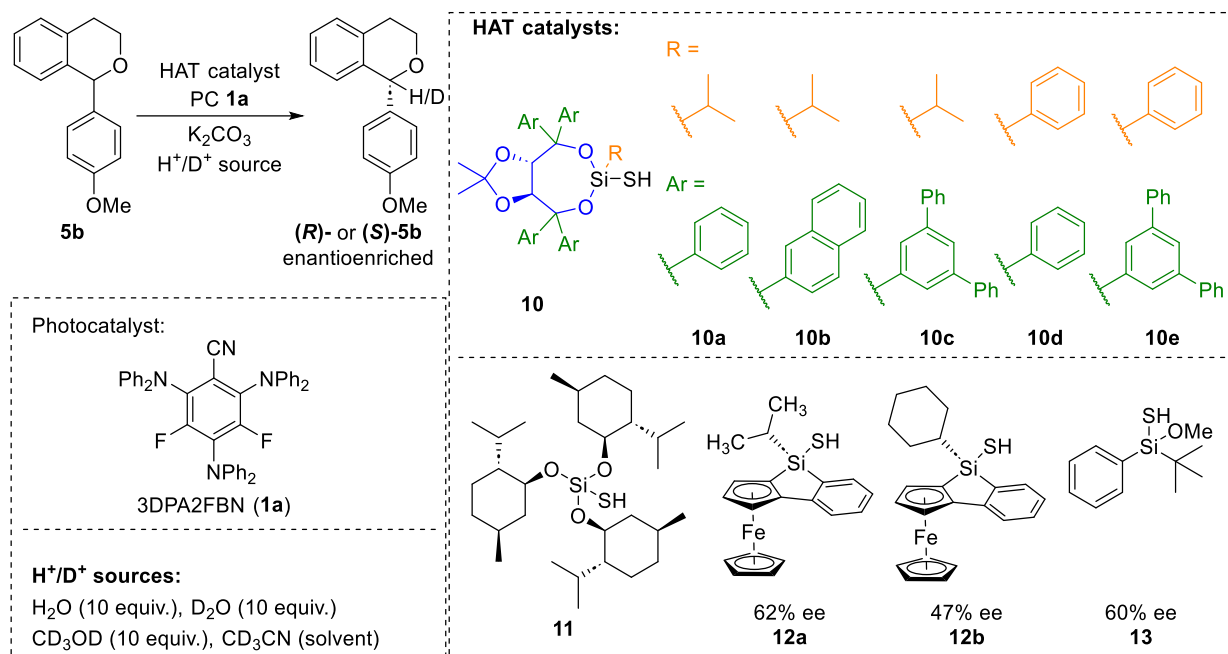
Deracemizations were performed according to general procedure 4-F for benzylic deuteration. Deuteration was used as mechanistic probe to confirm benzylic C-H activation and evaluate the efficiency of the HAT catalysts. For easy determination of NMR yield and deuteration degrees reactions were performed in CD_3CN and the solvent residual signal used as internal standard. Under anhydrous conditions proton/deuteron-abstraction from the solvent by highly basic carbanions and reprotonation can change the deuteration degree of the solvent as reported previously. Solvent deprotonation is outcompeted in the presence of 10 equivalents (corresponds to a concentration of 1 mol/L) $\text{D}_2\text{O}/\text{H}_2\text{O}$ and thus the residual solvent signal can be used as internal standard under the reaction conditions.

To minimize errors in the determination of the enantiomeric excess due to impurities, compounds subjected to chiral HPLC analysis were purified via preparative TLC.

An initial screening of chiral compounds of Scheme 4.7 with TADDOL-based silane thiols **7a**, **7b**, and **7c** gave a notable enantiomeric excess only for isochromane derivative **5b**. The enantiomers of acyclic benzyl ethers (**7a**, **7b**, **7c**) did not fully separate on the chiral HPLC and low selectivity might have been overlooked. However, separation was sufficient to exclude moderate enantioselectivity. Enantiomers of benzochromene derivative **5c** and dihydrobenzofuran derivative **4b** showed good separation on the chiral HPLC but did not give any enantiomeric excess. Thus, isochromane derivative **5b** was chosen as model substrate for the optimization depicted in Table 4.4.

Table 4.4. Deracemization of isochromane derivative **5b** via a HAT/RRPCO/protonation sequence.

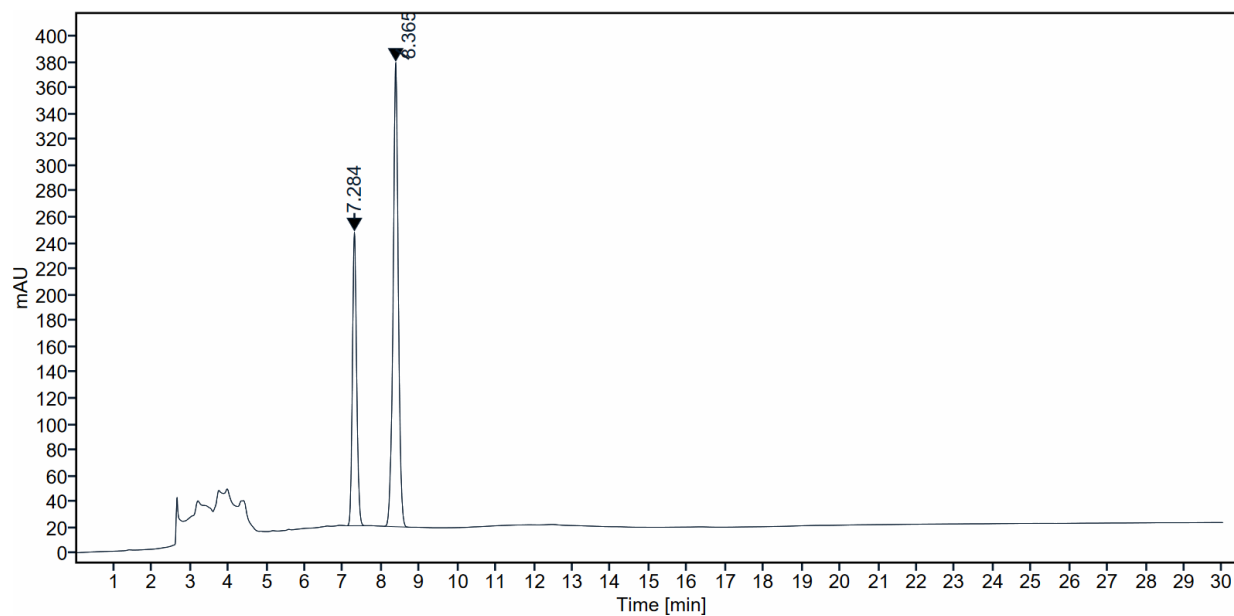
REGIO-, DIASTEREO- AND ENANTIOSELECTIVITY IN THE PHOTOCATALYTIC GENERATION OF CARBANIONS VIA HYDROGEN ATOM ABSTRACTION AND REDUCTIVE RADICAL-POLAR CROSSOVER



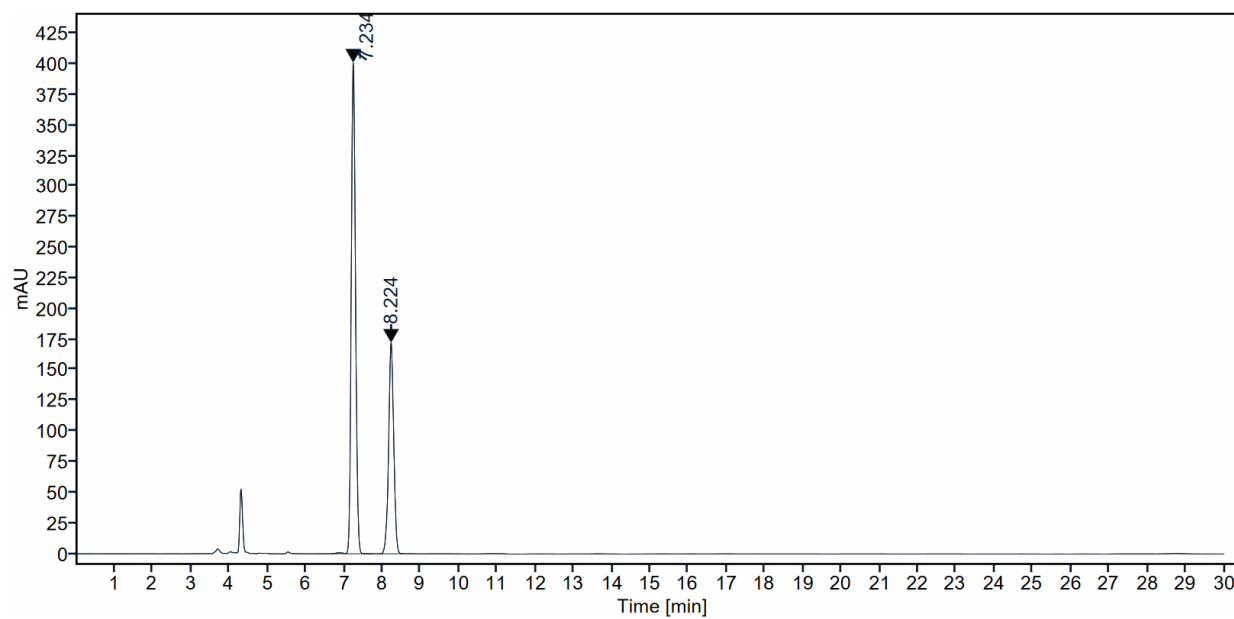
Entry	HAT catalyst	T	H ⁺ /D ⁺	time [h]	ee	Config.	deuteration	yield
1	(<i>R,R</i>)-10a	rt	H ₂ O	6 h	4%	(<i>R</i>)	-	65% ^a
2	(<i>R,R</i>)-10a	-17 °C	CD ₃ OD	6 h	6%	(<i>R</i>)	78%	81% ^a
3	(<i>R,R</i>)-10a	-17 °C	-	6 h	7%	(<i>R</i>)	89%	77% ^a
4	(<i>R,R</i>)-10b	-17 °C	D ₂ O	6 h	3%	(<i>R</i>)	79%	78% ^a /94% ^b
5	(<i>R,R</i>)-10b	-17 °C	H ₂ O	6 h	2%	(<i>R</i>)	-	75% ^a
6	(<i>R,R</i>)-10c	-17 °C	D ₂ O	6 h	-19%	(<i>S</i>)	69%	87% ^a /89% ^b
7	(<i>R,R</i>)-10c	-17 °C	H ₂ O	6 h	-13%	(<i>S</i>)	-	85% ^a
8	(<i>R,R</i>)-10a	-17 °C	D ₂ O	16 h	7%	(<i>R</i>)	93%	n.d.
9	(<i>R,R</i>)-10c	-17 °C	D ₂ O	16 h	-32%	(<i>S</i>)	90	79% ^a
10	(<i>R,R</i>)-10c	-17 °C	-	16 h	-25%	(<i>S</i>)	60%	77% ^a
11	(<i>R,R</i>)-10d	-17 °C	D ₂ O	16 h	13%	(<i>R</i>)	96%	n.d.
12	(<i>S,S</i>)-10d	-17 °C	D ₂ O	16 h	-11%	(<i>S</i>)	93%	87% ^a
13	(<i>S,S</i>)-10e	-17 °C	D ₂ O	16 h	14%	(<i>R</i>)	93%	64% ^a
14	(<i>S,S</i>)-10c	-17 °C	D ₂ O	16 h	32%	(<i>R</i>)	88%	82% ^a / ^{>} 95% ^b
15	(<i>S,S</i>)-10c	-17 °C	D ₂ O	24 h	33%	(<i>R</i>)	92%	n.d.
16	(<i>S,S</i>)-10c	-17 °C	D ₂ O/acetone	16 h	37%	(<i>R</i>)	91%	40% ^a
17	13	-17 °C	-	16 h	10%	(<i>R</i>)	76%	66% ^b
18	13	-17 °C	D ₂ O	16 h	12%	(<i>R</i>)	96%	44% ^b
19	11	-17 °C	D ₂ O	16 h	1%	(<i>R</i>)	91%	82% ^a
20	12a	-17 °C	D ₂ O	16 h	-	-	<5%	No conversion

Reactions were performed according to general procedure 4-F. ^aIsolated yield; ^bNMR yield with solvent residual signal as internal standard. The absolute configuration of the major product was determined via chiral HPLC analysis and comparison with literature data.⁷

Entry 14:

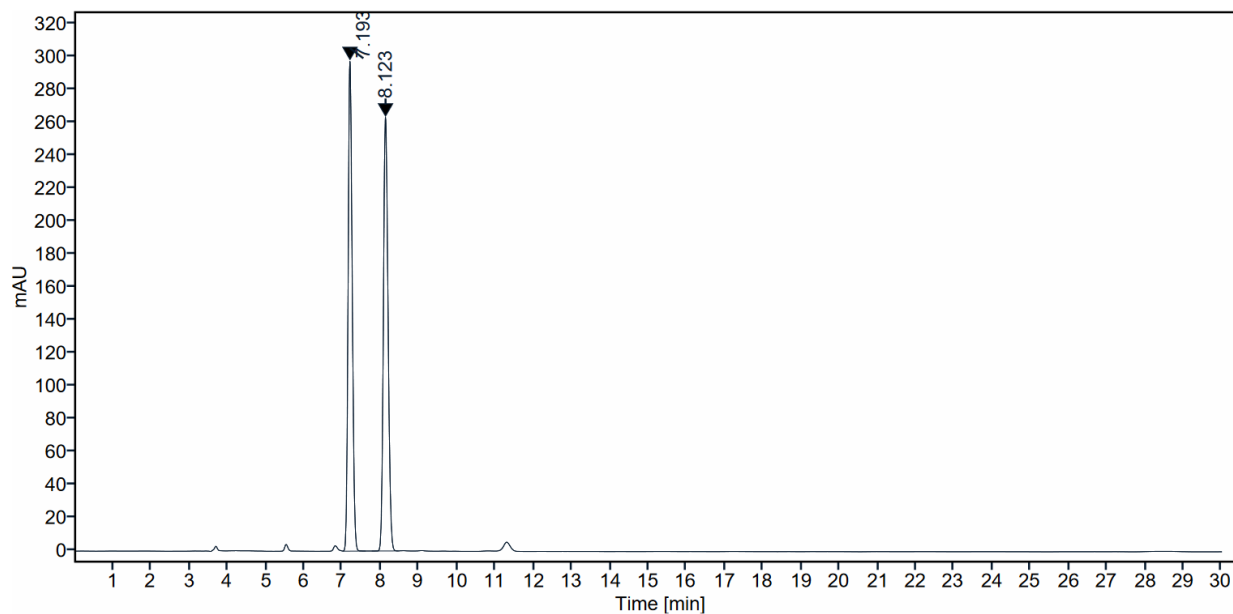


Entry 9:

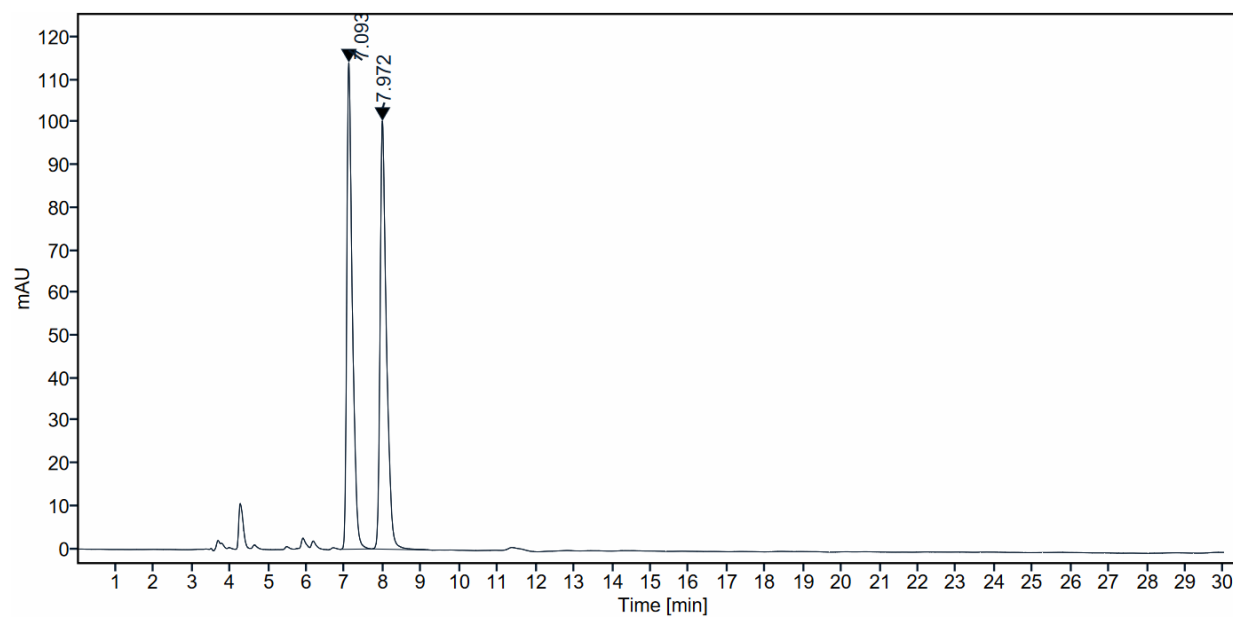


REGIO-, DIASTEREO- AND ENANTIOSELECTIVITY IN THE PHOTOCATALYTIC GENERATION OF CARBANIONS VIA HYDROGEN ATOM ABSTRACTION AND REDUCTIVE RADICAL-POLAR CROSSOVER

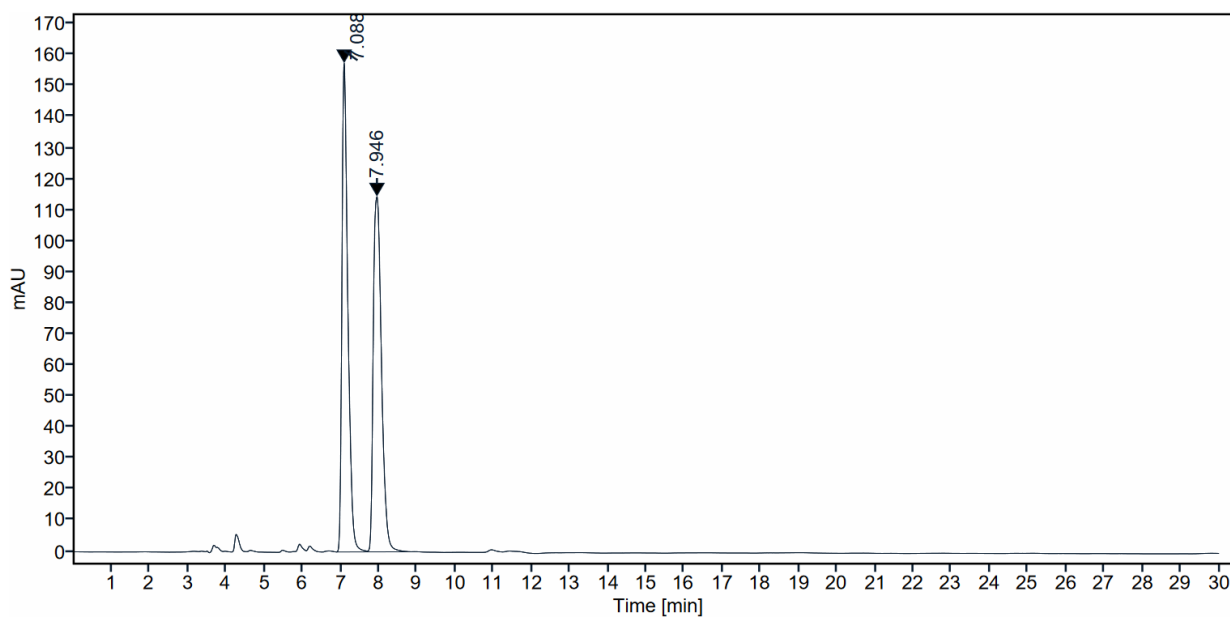
Racemic **5b-d₀**:



Racemic **5b-d₁**:



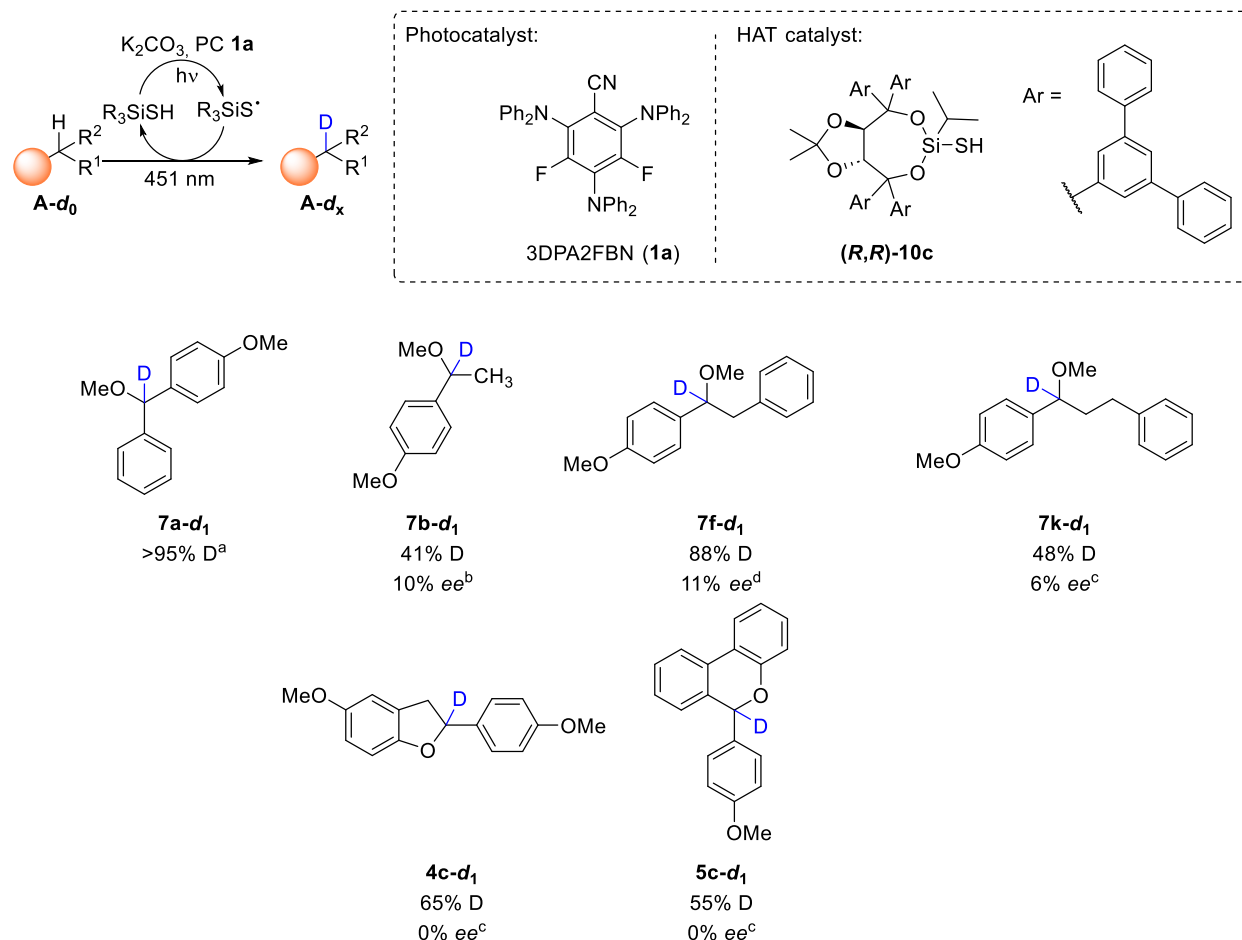
1:1 mixture of racemic **5b-d₀** and **5b-d₁**



It is worth mentioning that (*R*)-**5b-d₀** and (*R*)-**5b-d₁** have slightly different retention times. At moderate deuteration degrees this leads to a slight broadening of the respective signal.

4.4.7.3 Unsuccessful substrates

Substrates depicted in Scheme 4.18 were tested under the optimized reaction conditions (Table 4.4, entry 14). However, only low or no enantiomeric excess was observed, or enantiomers were not sufficiently separable to determine the *ee*.

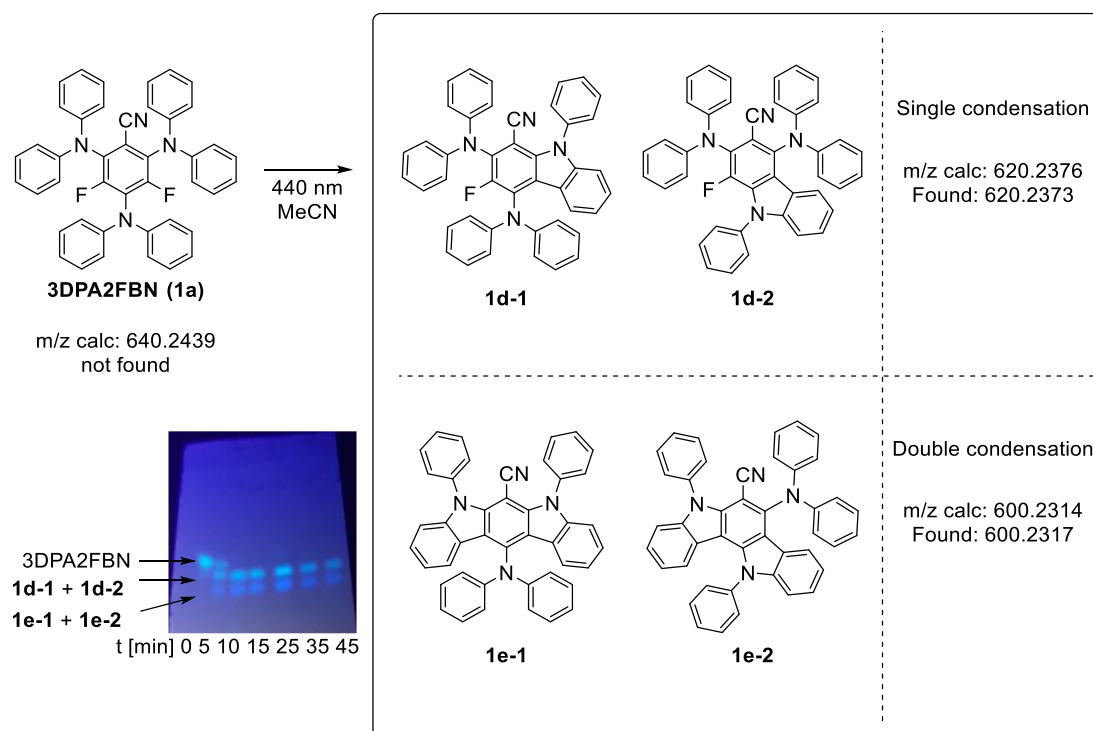


Scheme 4.18. Substrates tested for deracemization where only small or no enantiomeric excess was observed. ^aPoor separation of enantiomers; *ee* could not be determined. ^bModerate separation of enantiomers; *ee* is only a crude estimate. ^cEnantiomers sufficiently separated. ^dImpurity overlapping with major enantiomer; *ee* is only a crude estimate.

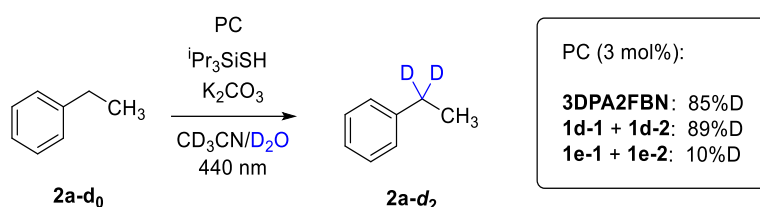
The lower enantiomeric excess of the compounds depicted in Scheme 4.18 compared to isochromane derivative **5b** might be explained by the higher flexibility (**7a**, **7b**, **7f**, **7k**), smaller steric difference between the substituents at the stereocenter and decreased reactivity (**7b**, **7f**, **5c**). However, this is only speculation, and there is not sufficient data to draw such conclusions at the current state.

4.4.8 In situ generation of the active photocatalyst by photocyclization of 3DPA2FBN

The photocatalyst 3DPA2FBN used in this work is not stable under irradiation. Under the reaction conditions for benzylic C-H activation it is converted within minutes. Multiple products were observed but could not be fully separated by column chromatography. These products arise from an intramolecular condensation of one or two of the diphenylamino groups onto the cyanobenzene core as has been reported for a similar photocatalyst.⁴² Two products formed by condensation of one diphenylamino group (**1d-1** and **1d-2**) and two products in which two diphenylamino groups are condensed onto the acceptor part (**1e-1** and **1e-2**) were identified by high resolution mass spectrometry and partially isolated in a separate batch where only 3DPA2FBN was irradiated in MeCN. The isomers were not separable via column chromatography but a fraction containing a mixture of **1d-1** and **1d-2** and a fraction containing a mixture of **1e-1** and **1e-2** were obtained.



Scheme 4.19. Photocatalyst 3DPA2FBN undergoes intramolecular condensation under irradiation.



Scheme 4.20. The mixture of **1d-1** and **1d-2** is similarly active compared to 3DPA2FBN in photocatalytic deuteration of ethylbenzene (**2a**). The mixture of **1e-1** and **1e-2** is almost inactive.

The mixture of **1d-1** and **1d-2** performed similar to pure 3DPA2FBN while the mixture of **1e-1** and **1e-2** was almost inactive. Thus, **1d-1**, **1d-2**, or likely both, are catalytically active and as most of the conversion in the reactions presented in this work occurs long after full photocondensation of 3DPA2FBN, these photocondensation products should not be seen as decomposition products, but they are the actual photocatalysts in the reactions and probably also in most other reactions where 3DPA2FBN is used. When using the mixture of **1d-1** and **1d-2** as photocatalyst, **1e-1** and/or **1e-2** are observed after the reaction. However, even after 16 h of irradiation **1d-1/1d-2** is still present, similar to when 3DPA2FBN is used as catalyst. Thus, 3DPA2FBN can be used as pre-catalyst and the direct use of the photocyclization products is not necessary.

4.5 References

- (1) Dalton, T.; Faber, T.; Glorius, F. C-H Activation: Toward Sustainability and Applications. *ACS Cent. Sci.* **2021**, *7*, 245–261.
- (2) Protti, S.; Fagnoni, M.; Ravelli, D. Photocatalytic C–H Activation by Hydrogen-Atom Transfer in Synthesis. *ChemCatChem* **2015**, *7*, 1516–1523.
- (3) Lewis, G. N. A New Principle of Equilibrium. *Proc. Natl. Acad. Sci. U. S. A.* **1925**, *11*, 179–183.
- (4) Ballard, A.; Narduolo, S.; Ahmed, H. O.; Keymer, N. I.; Asaad, N.; Cosgrove, D. A.; Buurma, N. J.; Leach, A. G. Racemisation in Chemistry and Biology. *Chemistry* **2020**, *26*, 3661–3687.
- (5) Blackmond, D. G. "If pigs could fly" chemistry: a tutorial on the principle of microscopic reversibility. *Angew. Chem., Int. Ed.* **2009**, *48*, 2648–2654.
- (6) Mao, Y.; Wang, Z.; Wang, G.; Zhao, R.; Kan, L.; Pan, X.; Liu, L. Redox Deracemization of Tertiary Stereocenters Adjacent to an Electron-Withdrawing Group. *ACS Catal.* **2020**, *10*, 7785–7791.
- (7) Wan, M.; Sun, S.; Li, Y.; Liu, L. Organocatalytic Redox Deracemization of Cyclic Benzylic Ethers Enabled by An Acetal Pool Strategy. *Angew. Chem., Int. Ed.* **2017**, *56*, 5116–5120.
- (8) Lackner, A. D.; Samant, A. V.; Toste, F. D. Single-operation deracemization of 3*H*-indolines and tetrahydroquinolines enabled by phase separation. *J. Am. Chem. Soc.* **2013**, *135*, 14090–14093.
- (9) Chen, Q.; Zhu, Y.; Shi, X.; Huang, R.; Jiang, C.; Zhang, K.; Liu, G. Light-driven redox deracemization of indolines and tetrahydroquinolines using a photocatalyst coupled with chiral phosphoric acid. *Chem. Sci.* **2023**, *14*, 1715–1723.
- (10) Voss, C. V.; Gruber, C. C.; Kroutil, W. Deracemization of secondary alcohols through a concurrent tandem biocatalytic oxidation and reduction. *Angew. Chem., Int. Ed.* **2008**, *47*, 741–745.
- (11) Gruber, C. C.; Lavandera, I.; Faber, K.; Kroutil, W. From a Racemate to a Single Enantiomer: Deracemization by Stereoinversion. *Adv. Synth. Catal.* **2006**, *348*, 1789–1805.
- (12) Shimizu, S.; Hattori, S.; Hata, H.; Yamada, H. One-Step Microbial Conversion of a Racemic Mixture of Pantoyl Lactone to Optically Active d(-)-Pantoyl Lactone. *Appl. Environ. Microbiol.* **1987**, *53*, 519–522.
- (13) Wang, P.-Z.; Xiao, W.-J.; Chen, J.-R. Light-empowered contra-thermodynamic stereochemical editing. *Nat. Rev. Chem.* **2023**, *7*, 35–50.
- (14) Wang, Y.; Carder, H. M.; Wendlandt, A. E. Synthesis of rare sugar isomers through site-selective epimerization. *Nature* **2020**, *578*, 403–408.
- (15) Zhang, Y.-A.; Palani, V.; Seim, A. E.; Wang, Y.; Wang, K. J.; Wendlandt, A. E. Stereochemical editing logic powered by the epimerization of unactivated tertiary stereocenters. *Science* **2022**, *378*, 383–390.
- (16) Shen, Z.; Walker, M. M.; Chen, S.; Parada, G. A.; Chu, D. M.; Dongbang, S.; Mayer, J. M.; Houk, K. N.; Ellman, J. A. General Light-Mediated, Highly Diastereoselective Piperidine Epimerization: From Most Accessible to Most Stable Stereoisomer. *J. Am. Chem. Soc.* **2021**, *143*, 126–131.
- (17) Oswald, C. J.; MacMillan, D. W. C. Selective Isomerization via Transient Thermodynamic Control: Dynamic Epimerization of trans to cis Diols. *J. Am. Chem. Soc.* **2022**, *144*, 93–98.
- (18) Zhang, Y.-A.; Gu, X.; Wendlandt, A. E. A Change from Kinetic to Thermodynamic Control Enables trans-Selective Stereochemical Editing of Vicinal Diols. *J. Am. Chem. Soc.* **2022**, *144*, 599–605.
- (19) Kazerouni, A. M.; Brandes, D. S.; Davies, C. C.; Cotter, L. F.; Mayer, J. M.; Chen, S.; Ellman, J. A. Visible Light-Mediated, Highly Diastereoselective Epimerization of Lactams from the Most Accessible to the More Stable Stereoisomer. *ACS Catal.* **2022**, *12*, 7798–7803.
- (20) Shen, Z.; Vargas-Rivera, M. A.; Rigby, E. L.; Chen, S.; Ellman, J. A. Visible Light-Mediated, Diastereoselective Epimerization of Morpholines and Piperazines to More Stable Isomers. *ACS Catal.* **2022**, *12*, 12860–12868.
- (21) Hammond, G. S.; Cole, R. S. Asymmetric Induction during Energy Transfer 1. *J. Am. Chem. Soc.* **1965**, *87*, 3256–3257.
- (22) Balavoine, G.; Jugé, S.; Kagan, H. B. Photoactivation optique du methyl p-tolyl sulfoxyde racémique par emploi d'un sensibilisateur chiral. *Tetrahedron Lett.* **1973**, *14*, 4159–4162.
- (23) Inoue, Y.; Kunitomi, Y.; Takamuku, S.; Sakurai, H. Asymmetric *cis*–*trans* photoisomerization of cyclo-octene sensitized by chiral aromatic esters. *J. Chem. Soc., Chem. Commun.* **1978**, 1024–1025.

- (24) Inoue, Y.; Yokoyama, T.; Yamasaki, N.; Tai, A. Temperature switching of product chirality upon photosensitized enantiodifferentiating *cis-trans* isomerization of cyclooctene. *J. Am. Chem. Soc.* **1989**, *111*, 6480–6482.
- (25) Hölzl-Hobmeier, A.; Bauer, A.; Silva, A. V.; Huber, S. M.; Bannwarth, C.; Bach, T. Catalytic deracemization of chiral allenes by sensitized excitation with visible light. *Nature* **2018**, *564*, 240–243.
- (26) Tröster, A.; Bauer, A.; Jandl, C.; Bach, T. Enantioselective Visible-Light-Mediated Formation of 3-Cyclopropylquinolones by Triplet-Sensitized Deracemization. *Angew. Chem., Int. Ed.* **2019**, *58*, 3538–3541.
- (27) Kratz, T.; Steinbach, P.; Breitenlechner, S.; Storch, G.; Bannwarth, C.; Bach, T. Photochemical Deracemization of Chiral Alkenes via Triplet Energy Transfer. *J. Am. Chem. Soc.* **2022**, *144*, 10133–10138.
- (28) Wimberger, L.; Kratz, T.; Bach, T. Photochemical Deracemization of Chiral Sulfoxides Catalyzed by a Hydrogen-Bonding Xanthone Sensitizer. *Synthesis* **2019**, *51*, 4417–4416.
- (29) Huang, M.; Zhang, L.; Pan, T.; Luo, S. Deracemization through photochemical *E/Z* isomerization of enamines. *Science* **2022**, *375*, 869–874.
- (30) Shin, N. Y.; Ryss, J. M.; Zhang, X.; Miller, S. J.; Knowles, R. R. Light-driven deracemization enabled by excited-state electron transfer. *Science* **2019**, *366*, 364–369.
- (31) Zhang, C.; Gao, A. Z.; Nie, X.; Ye, C.-X.; Ivlev, S. I.; Chen, S.; Meggers, E. Catalytic α -Deracemization of Ketones Enabled by Photoredox Deprotonation and Enantioselective Protonation. *J. Am. Chem. Soc.* **2021**, *143*, 13393–13400.
- (32) Gu, Z.; Zhang, L.; Li, H.; Cao, S.; Yin, Y.; Zhao, X.; Ban, X.; Jiang, Z. Deracemization through Sequential Photoredox-Neutral and Chiral Brønsted Acid Catalysis. *Angew. Chem., Int. Ed.* **2022**, *61*, e202211241.
- (33) Onneken, C.; Morack, T.; Soika, J.; Sokolova, O.; Niemeyer, N.; Mück-Lichtenfeld, C.; Daniliuc, C. G.; Neugebauer, J.; Gilmour, R. Light-enabled deracemization of cyclopropanes by Al-salen photocatalysis. *Nature* **2023**, *621*, 753–759.
- (34) Wen, L.; Ding, J.; Duan, L.; Wang, S.; An, Q.; Wang, H.; Zuo, Z. Multiplicative enhancement of stereo-enrichment by a single catalyst for deracemization of alcohols. *Science* **2023**, *382*, 458–464.
- (35) Großkopf, J.; Bach, T. Catalytic Photochemical Deracemization via Short-Lived Intermediates. *Angew. Chem., Int. Ed.* **2023**, *62*, e202308241.
- (36) Wang, J.; Lv, X.; Jiang, Z. Visible-Light-Mediated Photocatalytic Deracemization. *Chemistry* **2023**, *29*, e202204029.
- (37) Pitzer, L.; Schwarz, J. L.; Glorius, F. Reductive radical-polar crossover: traditional electrophiles in modern radical reactions. *Chem. Sci.* **2019**, *10*, 8285–8291.
- (38) Berger, A. L.; Donabauer, K.; König, B. Photocatalytic carbanion generation from C-H bonds - reductant free Barbier/Grignard-type reactions. *Chem. Sci.* **2019**, *10*, 10991–10996.
- (39) Di Martino, R. M. C.; Maxwell, B. D.; Piralì, T. Deuterium in drug discovery: progress, opportunities and challenges. *Nat. Rev. Drug Discov.* **2023**, *22*, 562–584.
- (40) Lankamp, H.; Nauta, W.; MacLean, C. A new interpretation of the monomer-dimer equilibrium of triphenylmethyl- and alkylsubstituted-diphenyl methyl-radicals in solution. *Tetrahedron Lett.* **1968**, *9*, 249–254.
- (41) Singh, K.; Staig, S. J.; Weaver, J. D. Facile synthesis of *Z*-alkenes via uphill catalysis. *J. Am. Chem. Soc.* **2014**, *136*, 5275–5278.
- (42) Pinosa, E.; Bassan, E.; Cetin, S.; Villa, M.; Potenti, S.; Calogero, F.; Gualandi, A.; Fermi, A.; Ceroni, P.; Cozzi, P. G. Light-Induced Access to Carbazole-1,3-dicarbonitrile: A Thermally Activated Delayed Fluorescent (TADF) Photocatalyst for Cobalt-Mediated Allylations. *J. Org. Chem.* **2023**, *88*, 6390–6400.
- (43) Grotjahn, S.; König, B. Photosubstitution in Dicyanobenzene-based Photocatalysts. *Org. Lett.* **2021**, *23*, 3146–3150.
- (44) Kümper, M.; Götz, T.; Espinosa-Jalapa, N. A.; Falk, A.; Rothfelder, R.; Bauer, J. O. Stereochemically Pure Si-Chiral Aminochlorosilanes. *Z. anorg. allg. Chem.* **2023**, *649*, e202300067.
- (45) *ChrysAlisPro Software System*; Rigaku Oxford Diffraction, 2020.
- (46) Clark, R. C.; Reid, J. S. The analytical calculation of absorption in multifaceted crystals. *Acta Crystallogr.* **1995**, *51*, A51, 887–897.
- (47) Dolomanov, O. V.; Bourhis, L. J.; Gildea, R. J.; Howard, J. A. K.; Puschmann, H. OLEX2: a complete structure solution, refinement and analysis program. *J. Appl. Crystallogr.* **2009**, *42*, 339–341.

- (48) Sheldrick, G. M. SHELXT - integrated space-group and crystal-structure determination. *Acta Crystallogr.* **2015**, *71*, A71, 3-8.
- (49) Sheldrick, G. M. Crystal structure refinement with SHELXL. *Acta Crystallogr.* **2015**, *71*, C71, 3-8.
- (50) Brecher, J. Graphical representation of stereochemical configuration (IUPAC Recommendations 2006). *Pure Appl. Chem.* **2006**, *78*, 1897–1970.
- (51) Speckmeier, E.; Fischer, T. G.; Zeitler, K. A Toolbox Approach To Construct Broadly Applicable Metal-Free Catalysts for Photoredox Chemistry: Deliberate Tuning of Redox Potentials and Importance of Halogens in Donor-Acceptor Cyanoarenes. *J. Am. Chem. Soc.* **2018**, *140*, 15353–15365.
- (52) Frank, D. J.; Guet, L.; Käslin, A.; Murphy, E.; Thomas, S. P. Iron-catalysed alkene hydrogenation and reductive cross-coupling using a bench-stable iron(II) pre-catalyst. *RSC Adv.* **2013**, *3*, 25698.
- (53) Wang, Y.; Di, H.; Chen, F.; Xu, Y.; Xiao, Q.; Wang, X.; Wei, H.; Lu, Y.; Zhang, L.; Zhu, J.; Lan, L.; Li, J. Discovery of Benzocycloalkane Derivatives Efficiently Blocking Bacterial Virulence for the Treatment of Methicillin-Resistant *S. aureus* (MRSA) Infections by Targeting Diapophytoene Desaturase (CrtN). *J. Med. Chem.* **2016**, *59*, 4831–4848.
- (54) Park, S. J.; Price, J. R.; Todd, M. H. Oxidative arylation of isochroman. *J. Org. Chem.* **2012**, *77*, 949–955.
- (55) Li, Y.; Wan, M.; Sun, S.; Fu, Z.; Huang, H.; Liu, L. Efficient access to chiral benzo [*c*] chromenes via asymmetric transfer hydrogenation of ketals. *Org. Chem. Front.* **2018**, *5*, 1280–1283.
- (56) Presset, M.; Paul, J.; Cherif, G. N.; Ratnam, N.; Laloi, N.; Léonel, E.; Gosmini, C.; Le Gall, E. CoI -Catalyzed Barbier Reactions of Aromatic Halides with Aromatic Aldehydes and Imines. *Chem. Eur. J.* **2019**, *25*, 4491–4495.
- (57) Muramatsu, W.; Nakano, K.; Li, C.-J. Simple and direct sp³ C-H bond arylation of tetrahydroisoquinolines and isochromans via 2,3-dichloro-5,6-dicyano-1,4-benzoquinone oxidation under mild conditions. *Org. Lett.* **2013**, *15*, 3650–3653.
- (58) Zhong, W.; Wu, Y.; Zhang, X. Efficient chemoselective addition of Grignard reagents to carbonyl compounds in 2-methyltetrahydrofuran. *J. Chem. Res.* **2009**, *2009*, 370–373.
- (59) Huang, P.; Zhang, G.; Wang, Z.; Wu, J. Silver-Catalyzed Synthesis of Benzyl Ethers via Alkoxylation of Benzylic C(sp³)-H Bonds. *Chem. Asian J.* **2023**, *18*, e202300425.
- (60) Garcia, K. J.; Gilbert, M. M.; Weix, D. J. Nickel-Catalyzed Addition of Aryl Bromides to Aldehydes To Form Hindered Secondary Alcohols. *J. Am. Chem. Soc.* **2019**, *141*, 1823–1827.
- (61) Schneider, C.; Jackstell, R.; Maes, B. U. W.; Beller, M. Palladium-Catalyzed Alkoxyacylation of *sec*-Benzylic Ethers. *Eur. J. Org. Chem.* **2020**, *2020*, 932–936.
- (62) Satyanarayana, P.; Reddy, G. M.; Maheswaran, H.; Kantam, M. L. Tris(acetylacetonato)rhodium(III)-Catalyzed α -Alkylation of Ketones, β -Alkylation of Secondary Alcohols and Alkylation of Amines with Primary Alcohols. *Adv. Synth. Catal.* **2013**, *355*, 1859–1867.
- (63) Xu, Q.; Chen, J.; Tian, H.; Yuan, X.; Li, S.; Zhou, C.; Liu, J. Catalyst-free dehydrative α -alkylation of ketones with alcohols: green and selective autocatalyzed synthesis of alcohols and ketones. *Angew. Chem., Int. Ed.* **2014**, *53*, 225–229.
- (64) Bouffard, J.; Itami, K. A nickel catalyst for the addition of organoboronate esters to ketones and aldehydes. *Org. Lett.* **2009**, *11*, 4410–4413.
- (65) Harenberg, J. H.; Weidmann, N.; Wiegand, A. J.; Hofer, C. A.; Annapureddy, R. R.; Knochel, P. (2-Ethylhexyl)sodium: A Hexane-Soluble Reagent for Br/Na-Exchanges and Directed Metalations in Continuous Flow. *Angew. Chem., Int. Ed.* **2021**, *60*, 14296–14301.
- (66) Zhou, C.; Wang, Z. Cadmium-Mediated Carbonyl Benzoylation in Tap Water. *Synthesis* **2005**, 1649–1655.
- (67) Fumagalli, G.; Boyd, S.; Greaney, M. F. Oxyarylation and aminoarylation of styrenes using photoredox catalysis. *Org. Lett.* **2013**, *15*, 4398–4401.
- (68) Zou, L.; Wang, B.; Mu, H.; Zhang, H.; Song, Y.; Qu, J. Development of tartaric acid derived chiral guanidines and their application to catalytic enantioselective α -hydroxylation of β -dicarbonyl compounds. *Org. Lett.* **2013**, *15*, 3106–3109.
- (69) Beck, A. K.; Gysi, P.; La Vecchia, L.; Seebach, D. (4*R*,5*R*)-2,2-DIMETHYL-a,a,a',a'-TETRA(NAPHTH-2-YL)-1,3-DIOXOLANE-4,5-DIMETHANOL FROM DIMETHYL TARTRATE AND 2-NAPHTHYL-MAGNESIUM BROMIDE. *Org. Synth.* **1999**, *76*, 12.
- (70) Wang, Y.-X.; Qi, S.-L.; Luan, Y.-X.; Han, X.-W.; Wang, S.; Chen, H.; Ye, M. Enantioselective Ni-Al Bimetallic Catalyzed exo-Selective C-H Cyclization of Imidazoles with Alkenes. *J. Am. Chem. Soc.* **2018**, *140*, 5360–5364.

- (71) Zhang, T.; Luan, Y.-X.; Zheng, S.-J.; Peng, Q.; Ye, M. Chiral Aluminum Complex Controls Enantioselective Nickel-Catalyzed Synthesis of Indenes: C-CN Bond Activation. *Angew. Chem., Int. Ed.* **2020**, *59*, 7439–7443.
- (72) Liu, Q.-S.; Wang, D.-Y.; Yang, Z.-J.; Luan, Y.-X.; Yang, J.-F.; Li, J.-F.; Pu, Y.-G.; Ye, M. Ni-Al Bimetallic Catalyzed Enantioselective Cycloaddition of Cyclopropyl Carboxamide with Alkyne. *J. Am. Chem. Soc.* **2017**, *139*, 18150–18153.
- (73) Schneider, F.; Samarin, K.; Zanella, S.; Gaich, T. Total synthesis of the complex taxane diterpene canataxpropellane. *Science* **2020**, *367*, 676–681.
- (74) Beckmann, J.; Dakternieks, D.; Tiekink, E. R. Chiral trialkoxysilanols derived from terpene alcohols. *J. Organomet. Chem.* **2002**, *648*, 188–192.
- (75) Ma, W.; Liu, L.-C.; An, K.; He, T.; He, W. Rhodium-Catalyzed Synthesis of Chiral Monohydrosilanes by Intramolecular C-H Functionalization of Dihydrosilanes. *Angew. Chem., Int. Ed.* **2021**, *60*, 4245–4251.
- (76) Kunai, A.; Ohshita, J. Selective synthesis of halosilanes from hydrosilanes and utilization for organic synthesis. *J. Organomet. Chem.* **2003**, *686*, 3–15.
- (77) Grotjahn, S.; Graf, C.; Zelenka, J.; Pattanaik, A.; Müller, L.; Kutta, R. J.; Rehbein, J.; Roithová, J.; Gschwind, R. M.; Nuernberger, P.; König, B. Reactivity of Superbasic Carbanions Generated via Reductive Radical-Polar Crossover in the Context of Photoredox Catalysis. *Angew. Chem., Int. Ed.* **2024**, e202400815.
- (78) Kruse, H.; Grimme, S. A geometrical correction for the inter- and intra-molecular basis set superposition error in Hartree-Fock and density functional theory calculations for large systems. *J. Chem. Phys.* **2012**, *136*, 154101.
- (79) Grimme, S.; Hansen, A.; Ehlert, S.; Mewes, J.-M. r2SCAN-3c: A "Swiss army knife" composite electronic-structure method. *J. Chem. Phys.* **2021**, *154*, 64103.
- (80) Furness, J. W.; Kaplan, A. D.; Ning, J.; Perdew, J. P.; Sun, J. Correction to "Accurate and Numerically Efficient r2SCAN Meta-Generalized Gradient Approximation". *J. Phys. Chem. Lett.* **2020**, *11*, 9248.
- (81) Furness, J. W.; Kaplan, A. D.; Ning, J.; Perdew, J. P.; Sun, J. Accurate and Numerically Efficient r2SCAN Meta-Generalized Gradient Approximation // Accurate and Numerically Efficient r2SCAN Meta-Generalized Gradient Approximation. *J. Phys. Chem. Lett.* **2020**, *11*, 8208–8215.
- (82) Caldeweyher, E.; Bannwarth, C.; Grimme, S. Extension of the D3 dispersion coefficient model. *J. Chem. Phys.* **2017**, *147*, 34112.
- (83) Neese, F.; Wennmohs, F.; Becker, U.; Riplinger, C. The ORCA quantum chemistry program package. *J. Chem. Phys.* **2020**, *152*, 224108.
- (84) Neese, F. Software update: The ORCA program system—Version 5.0. *WIREs Comput. Mol. Sci.* **2022**, *12*.
- (85) Neese, F. Software update: the ORCA program system, version 4.0. *WIREs Comput. Mol. Sci.* **2018**, *8*.
- (86) Neese, F. The ORCA program system. *WIREs Comput. Mol. Sci.* **2012**, *2*, 73–78.
- (87) Finney, L. C.; Mitchell, L. J.; Moody, C. J. Visible light mediated oxidation of benzylic sp³ C–H bonds using catalytic 1,4-hydroquinone, or its biorenewable glucoside, arbutin, as a pre-oxidant. *Green Chem.* **2018**, *20*, 2242–2249.
- (88) Chen, W.; Xie, Z.; Zheng, H.; Lou, H.; Liu, L. Structurally diverse α -substituted benzopyran synthesis through a practical metal-free C(sp³)-H functionalization. *Org. Lett.* **2014**, *16*, 5988–5991.
- (89) Tong, X.; Luo, S.-S.; Shen, H.; Zhang, S.; Cao, T.; Luo, Y.-P.; Huang, L.-L.; Ma, X.-T.; Liu, X.-W. Nickel-catalyzed defluorinative alkylation of C(sp²)-F bonds. *Org. Chem. Front.* **2021**, *8*, 4533–4542.
- (90) Chen, Z.; Pitchakuntla, M.; Jia, Y. Synthetic approaches to natural products containing 2,3-dihydrobenzofuran skeleton. *Nat. Prod. Rep.* **2019**, *36*, 666–690.
- (91) Donabauer, K.; Maity, M.; Berger, A. L.; Huff, G. S.; Crespi, S.; König, B. Photocatalytic carbanion generation - benzylation of aliphatic aldehydes to secondary alcohols. *Chem. Sci.* **2019**, *10*, 5162–5166.
- (92) Hutchings-Goetz, L. S.; Yang, C.; Fyfe, J. W. B.; Snaddon, T. N. Enantioselective Syntheses of Strychnos and Chelidonium Alkaloids through Regio- and Stereocontrolled Cooperative Catalysis. *Angew. Chem., Int. Ed.* **2020**, *59*, 17556–17564.
- (93) Adams, H.; Gilmore, N. J.; Jones, S.; Muldowney, M. P.; Reuss, S. H. von; Vemula, R. Asymmetric synthesis of corsifuran A by an enantioselective oxazaborolidine reduction. *Org. Lett.* **2008**, *10*, 1457–1460.
- (94) Dochnahl, M.; Fu, G. C. Catalytic asymmetric cycloaddition of ketenes and nitroso compounds: enantioselective synthesis of α -hydroxycarboxylic acid derivatives. *Angew. Chem., Int. Ed.* **2009**, *48*, 2391–2393.
- (95) Potrząsaj, A.; Musiejuk, M.; Chaładaj, W.; Giedyk, M.; Gryko, D. Cobalt Catalyst Determines Regioselectivity in Ring Opening of Epoxides with Aryl Halides. *J. Am. Chem. Soc.* **2021**, *143*, 9368–9376.

-
- (96) Sato, K.; Inoue, Y.; Mori, T.; Sakaue, A.; Tarui, A.; Omote, M.; Kumadaki, I.; Ando, A. Csp³-Csp³ homocoupling reaction of benzyl halides catalyzed by rhodium. *Org. Lett.* **2014**, *16*, 3756–3759.
- (97) Melkonyan, F. S.; Kuznetsov, D. E.; Yurovskaya, M. A.; Karchava, A. V. One-pot synthesis of substituted indoles via titanium(IV) alkoxide mediated imine formation – copper-catalyzed N-arylation. *RSC Adv.* **2013**, *3*, 8388.
- (98) Snider, B. B.; Han, L.; Xie, C. Synthesis of 2,3-Dihydrobenzofurans by Mn(OAc)₃ -Based Oxidative Cycloaddition of 2-Cyclohexenones with Alkenes. Synthesis of (±)-Conocarpan. *J. Org. Chem.* **1997**, *62*, 6978–6984.
- (99) Cheung, W.-H.; Zheng, S.-L.; Yu, W.-Y.; Zhou, G.-C.; Che, C.-M. Ruthenium porphyrin catalyzed intramolecular carbenoid C-H insertion. Stereoselective synthesis of *cis*-disubstituted oxygen and nitrogen heterocycles. *Org. Lett.* **2003**, *5*, 2535–2538.
- (100) Chen, C.; Dormer, P. G. Synthesis of benzobfurans via CuI-catalyzed ring closure. *J. Org. Chem.* **2005**, *70*, 6964–6967.



SUMMARY

5 Summary

The concept of reductive radical-polar crossover (RRPCO) gained increasing interest within recent years. In a RRPCO a radical intermediate is reduced to the corresponding anion, thus, changing from radical to polar reactivity. Previously reported reactions utilizing a RRPCO include carbanion generation via decarboxylation or C-H activation, catalyzed by fully organic TADF dyes as photocatalysts and silane thiols as hydrogen atom transfer (HAT) reagents. Reactions of photocatalytically generated carbanions with aldehydes and ketones provide products usually obtained from organometallic reagents such as Grignard- or organolithium reagents. However, their reactivity seemed to be limited to rather reactive electrophiles such as aldehydes or ketones while esters do not provide the products obtained in classical Grignard reactions.

Chapter 1 provides a comparison of organic light emitting diode (OLED) emitters of the different OLED generations and photocatalysts originating thereof with a specific focus on thermally activated delayed fluorescence (TADF) emitters used in third and fourth generation OLEDs. Some properties, such as photostability, excited state in the energy range of visible light, and low rate of radiationless transitions to the ground state are generally desired for both, OLED emitters and photocatalysts. Properties such as the rate of intersystem crossing, lifetimes and energies of singlet and triplet excited states depend on the specific application. Fluorescence and phosphorescence rates, electron transfer and mechanisms of energy transfer are generally designed in opposite directions depending on whether an OLED emitter or photocatalyst is optimized. While light emission is the main goal in OLED emitters it is an unproductive pathway in photocatalysts and high fluorescence or phosphorescence quantum yield is only a sign that other unproductive relaxation pathways are not occurring to notable extent. Electron transfer and energy transfer via Dexter mechanism leads to low efficiency and degradation of OLED devices while they are the desired pathways in photoredox and energy transfer catalysis, respectively. The class of fully organic donor-acceptor type TADF emitters is of particular interest with respect to photocatalytic carbanion generation as many of these organic dyes turned out to catalyze reactions generating radicals, as well as RRPCO to reduce these radicals to the corresponding carbanions. In such reactions TADF dyes are usually superior to classical platinum-group based photocatalysts used in second generation OLEDs. The long excited state lifetime, low cost of production and general design principles for tuning of redox properties in a wide range make donor-acceptor type TADF emitters an attractive class of photocatalysts.

Chapter 2 focuses on the stability of dicyanobenzene-based photocatalysts which are the most widely used class of photocatalysts originating from TADF emitters. It was found that these photocatalysts can undergo photosubstitution reactions under redox-neutral and reductive photocatalytic conditions, substituting one of the cyano groups by an alkyl group. Moreover, under reaction conditions for photocatalytic carbanion generation this photosubstitution occurs quantitatively in the initial phase of the reaction before carbanion generation starts. Thus, photosubstitution must not be seen as a decomposition of the photocatalyst. Especially the photosubstitution products of the most widely used TADF dye 4CzIPN are stable photocatalysts with large redox window and likely the actual photocatalyst in most reactions where 4CzIPN is employed. This also explains why previously published reactions reported to be catalyzed by 4CzIPN were successful despite 4CzIPN not having suitable redox potentials. Photosubstitution in dicyanobenzene-based photocatalysts generally leads to a blue shift in absorption. Thus, the use of an irradiation wavelength not only exciting the pre-catalyst but also the photosubstitution product is necessary to enable photocatalytic reactions. This was demonstrated on the example of 2CzPN which was initially reported as being inferior to 4CzIPN. It turned out that 2CzPN forms photosubstitution products absorbing at wavelengths below those

used in the initial experiments, while switching to slightly lower wavelength enabled photocatalytic reactions in some examples even more efficiently than 4CzIPN and its photosubstitution products.

Chapter 3 focuses on the reactivity of carbanions generated via RRPCO. The seemingly low reactivity observed in previously developed reactions was found to originate from a high basicity. Benzylic carbanions are sufficiently basic to deprotonate many electrophiles such as aldehydes, ketones, and esters but also common organic solvents such as acetonitrile, dimethylsulfoxide, and dimethylformamide. Thus, reactions previously assumed to be unsuccessful due to lack of reactivity of the carbanionic intermediate are actually unsuccessful due to competing deprotonation of reaction partners and solvents. Gas-phase experiments of carbanions, kinetic isotope effect studies, transient absorption spectroscopy, and competitive deuteration experiments further support the conclusion that photocatalytically generated carbanions are superbasic, short-lived, monomeric intermediates with distinct reactivity compared to their organometallic counterparts. For future reactions this knowledge will be helpful for an intuitive estimation of limitations regarding reaction partners and optimization of reaction conditions.

In chapter 4 the focus is shifted towards the selectivity in the C-H activation step. Due to the high reactivity and short lifetime of photocatalytically generated benzylic carbanions, the C-H activation step was identified as the most promising step to introduce diastereo- and enantioselectivity in reactions utilizing a RRPCO step. Deuterium labelling was used as mechanistic probe to identify those benzylic C-H bonds that can be activated to the corresponding carbanion and those that cannot. Bond dissociation energies (BDEs) explain why primary benzylic C-H bonds cannot be activated by silane thiol HAT-reagents, but the general reactivity trends of secondary and tertiary benzylic C-H bonds do not follow BDEs. However, steric hindrance in adjacent positions and electron withdrawing groups on the arene generally explain reduced susceptibility towards benzylic C-H activation while conformational locking in ring systems can render C-H bonds particularly reactive or unreactive, depending on the orientation of the respective C-H bond.

The influence of steric hindrance was then investigated on the epimerization of dihydrobenzofurans. Selective *cis*→*trans* isomerization was observed and kinetic studies and competitive deuteration experiments found the selectivity to originate from kinetic effects in a dynamic equilibrium while the final protonation step setting the stereocenter is unselective. This allows stereochemical editing independent of thermodynamic preferences of the diastereomers. Late stage stereochemical editing such as *cis/trans* isomerization enables new synthesis routes to complex molecules by opening easier non-diastereoselective pathways for bond-forming steps and epimerization to the desired diastereomer at a later stage. This was demonstrated on the example of a dihydrobenzofuran derivative with a substitution pattern not easily accessible by classical approaches.

Based on the observation that the product distribution in hydrogen exchange reactions can be determined by kinetic selectivity in the bond-breaking step the concept was then transferred to photocatalytic deracemization at benzylic stereocenters. Different classes of chiral silane thiols were developed as potential HAT-reagents. Silane thiols based on tartaric acid derived TADDOL were found to be capable of inducing moderate enantioselectivity of up to 37% under hydrogen exchange conditions. Although this enantioselectivity is far from being synthetically useful, it provides proof of concept for the unprecedented deracemization concept of employing a photocatalytic HAT/RRPCO/protonation sequence to separate bond-breaking from bond-forming steps and to enable the reaction only in one direction, thus avoiding limitations caused by microscopic reversibility. Considering that chiral silane thiols were not reported in literature and first examples of this new class of HAT-catalysts already provide moderate

SUMMARY

enantioselectivity it is expected that progress in asymmetric organosilicon chemistry will lead to more selective catalysts for this deracemization approach.

ZUSAMMENFASSUNG

6 Zusammenfassung

Das Konzept des reduktiven Radikal-polaren Übergangs (RRPCO) erhielt innerhalb der letzten Jahre besondere Aufmerksamkeit. In einem RRPCO wird ein radikalisches Intermediat zum entsprechenden Anion reduziert, was einen Wechsel von radikalischer zu polarer Reaktivität bewirkt. Bereits bekannte Reaktionen, die einen RRPCO nutzen, sind unter anderem die Carbanionerzeugung durch Decarboxylierung, oder über C-H Aktivierung, die durch vollständig organische TADF (thermisch aktivierte verzögerte Fluoreszenz) Farbstoffe als Photokatalysatoren und Silanthiolen als Wasserstoffatomtransfer (HAT) Reagenzien katalysiert werden. Reaktionen von photokatalytisch erzeugten Carbanionen mit Aldehyden und Ketonen ergeben Produkte, die für gewöhnlich mit metallorganischen Reagenzien, wie Grignard- oder Organolithiumreagenzien, erhalten werden. Jedoch scheint die Reaktivität dieser unter photokatalytischen Bedingungen erhaltenen Carbanionen auf Aldehyde und Ketone limitiert zu sein, während Ester, die für gewöhnlich bereitwillig mit Grignard-Reagenzien reagieren, im Allgemeinen unreaktiv gegenüber photokatalytisch erzeugten Carbanionen zu sein scheinen.

Kapitel 1 vergleicht Emittter für organische Leuchtdioden (OLED) der verschiedenen Generationen und Photokatalysatoren, die aus der OLED-Forschung hervorgegangen sind. Ein besonderer Fokus liegt dabei auf TADF-Emittern, wie sie in OLEDs der dritten und vierten Generation verwendet werden. Manche Eigenschaften, wie beispielsweise Photostabilität, angeregte Zustände mit Energien im Bereich des sichtbaren Lichts und geringe Raten nicht-radiativer Übergänge zum Grundzustand sind allgemein sowohl für OLED-Emitter, als auch für Photokatalysatoren gewünscht. Eigenschaften wie hohe Interkombinationsraten (ISC) und Lebensdauern und Energien von elektronisch angeregten Singulett- und Triplett-Zuständen sind abhängig von der spezifischen Anwendung. Fluoreszenz- und Phosphoreszenzraten, Effizienz von Elektronentransfer und der Mechanismus für Energieübertragung werden für gewöhnlich in entgegengesetzte Richtungen optimiert, je nachdem, ob OLED-Emitter oder Photokatalysatoren entwickelt werden. Während die Emission von Licht das primäre Ziel von OLED-Emittern ist, stellt dies einen unproduktiven Weg der Relaxation eines Photokatalysators dar, sodass lange Fluoreszenz- oder Phosphoreszenzlebensdauern nur ein Zeichen dafür sind, dass andere unproduktive Wege vom angeregten in den Grundzustand keinen großen Beitrag besitzen. Elektronentransfer im Allgemeinen und Energieübertragung über einen Dexter-Mechanismus führen in OLEDs für gewöhnlich zu Effizienzverlusten und geringer Haltbarkeit, während sie das primäre Ziel in Photoredox- und Energietransferphotokatalyse sind. Vollständig organische Donor-Akzeptor-TADF-Emitter sind für die photokatalytische Erzeugung von Carbanionen besonders interessant, da viele dieser Moleküle sowohl Reaktionen zur Erzeugung von Radikalen katalysieren, als auch ausreichende Reduktionspotentiale für einen RRPCO besitzen. In solchen Reaktionen sind TADF-Photokatalysatoren den klassischen Photokatalysatoren der zweiten Generation von OLED-Emittern, basierend auf Elementen der Platingruppe, für gewöhnlich überlegen. Die langen Lebensdauern der angeregten Zustände, der geringe Preis in der Herstellung und das Verständnis dafür, wie einfache Modifikationen die Redoxpotentiale in einem weiten Bereich beeinflussen, machen TADF-Emitter eine attraktive Klasse von Photokatalysatoren.

Kapitel 2 behandelt die Stabilität von Dicyanobenzol-basierten Photokatalysatoren, welche Teil der am weitesten verbreiteten Photokatalysatoren aus der Gruppe der TADF-Emitter sind. Dabei wurde festgestellt, dass diese Photokatalysatoren unter reduktiven und Redoxneutralen Bedingungen Photosubstitutionsreaktionen eingehen können, wobei eine der Cyanogruppen durch eine Alkylgruppe ersetzt wird. Unter Reaktionsbedingungen zur photokatalytischen Erzeugung von Carbanionen findet diese Photosubstitution in der initialen Phase der Reaktion

statt, bevor die Bildung von Carbanionen einsetzt. Entsprechend darf die Photosubstitution nicht als Zersetzung des Photokatalysators gesehen werden. Vor allem die Photosubstitutionsprodukte des bekannten TADF-Emitters 4CzIPN stellen stabile Photokatalysatoren mit einem großen Redoxfenster dar und sind vermutlich die eigentlichen Photokatalysatoren in vielen Reaktionen, in denen 4CzIPN eingesetzt wird. Dies erklärt auch, warum Reaktionen mit 4CzIPN als Photokatalysator funktionieren, die aufgrund der Redoxpotentiale des 4CzIPNs nicht möglich sein sollten. Photosubstitution in Dicyanobenzol-basierten Photokatalysatoren führt in der Regel zu einer Verschiebung der Absorption zu niedrigeren Wellenlängen. Daher muss die Wellenlänge, mit der photokatalytische Reaktionen belichtet werden, nicht nur auf den initial zugesetzten Vorläufer des Photokatalysators abgestimmt sein, sondern auch geeignet sein, um das Photosubstitutionsprodukt anzuregen. Dies wurde in dieser Arbeit am Beispiel des 2CzPNs gezeigt, das zu Beginn der Anwendung von TADF-Emittern als Photokatalysatoren für wenig aktiv gehalten wurde. Es wurde nun festgestellt, dass 2CzPN Photosubstitutionsprodukte bildet, die erst bei niedrigeren Wellenlängen absorbieren, als in den anfänglichen Experimenten verwendet wurden. Wird eine etwas kürzere Wellenlänge zur Belichtung gewählt, werden die Photosubstitutionsprodukte des 2CzPNs katalytisch aktiv und in sind in machen Reaktionen dem 4CzIPN sogar überlegen.

Kapitel 3 handelt über die Reaktivität von Carbanionen, die über einen RRPCO erzeugt werden. Die scheinbar geringe Reaktivität, die in vorherigen Reaktionen festgestellt wurde, konnte stattdessen auf eine hohe Basizität der Carbanionen zurückgeführt werden. Benzylische Carbanionen sind in der Regel basisch genug, um gängige Elektrophile, wie beispielsweise Aldehyde, Ketone und Ester zu deprotonieren, aber auch klassische polare Lösungsmittel, wie Acetonitril, Dimethylsulfoxid und Dimethylformamid. Daher sind unerfolgreiche Reaktionen, die zuvor auf eine geringe Reaktivität der carbanionischen Intermediate zurückgeführt wurden, eher durch eine konkurrierende Deprotonierung von Reaktionspartnern und Lösungsmitteln zu erklären. Gasphasenexperimente mit Carbanionen, kinetische Isotopeneffekte, transiente Absorptionsspektroskopie und kompetitive Deuterierungsexperimente bekräftigen die Schlussfolgerung, dass die photokatalytisch erzeugten Carbanionen superbasische, kurzlebige, monomere Intermediate sind, mit Reaktivitäten, die sich von den klassischen metallorganischen Analoga unterscheiden. Dieses Wissen ist nützlich für die zukünftige Optimierung von Reaktionen, die einen RRPCO beinhalten und erlaubt ein intuitives Verständnis für die Abschätzung der synthetischen Limitierungen.

In Kapitel 4 liegt der Fokus auf der Selektivität der benzyllischen C-H Aktivierung. Aufgrund der hohen Reaktivität von photokatalytisch erzeugten Carbanionen stellt der vorgelagerte Schritt zur C-H Aktivierung den vielversprechendsten Ansatzpunkt dar, um Diastereo- und Enantioselektivität in Reaktionen mit einem RRPCO-Schritt zu erreichen. Dazu wurde zuerst Isotopenmarkierung mit Deuterium genutzt, um diejenigen benzyllischen Wasserstoffatome zu identifizieren, die eine C-H Aktivierung mit anschließender Reduktion zum entsprechenden Carbanion zulassen. Die Bindungsdissoziationsenergien (BDEs) erklären dabei nur warum primäre benzyllische C-H Bindungen nicht von Silanthiolen als HAT Reagenzien aktiviert werden können, aber die Reaktivität von sekundären und tertiären C-H Bindungen folgt im Allgemeinen nicht den BDEs. Sterisch anspruchsvolle Gruppen in benachbarten Positionen und elektronenziehende Substituenten am aromatischen System führen zu einer Verringerung der Reaktivität, während die Fixierung in einer Konformation die Reaktivität steigern, oder verringern kann, je nach Orientierung der entsprechenden C-H Bindung.

Der Einfluss sterischer Hinderung wurde dann im Hinblick auf die Epimerisierung von Dihydrobenzofuranen untersucht. Die selektive *cis*→*trans* Isomerisierung konnte anhand der Analyse der Reaktionskinetik und kompetitiver

Deuterierungsexperimente auf eine kinetische Selektivität der C-H Aktivierung in einem dynamischen Gleichgewicht zurückgeführt werden, während die finale Protonierung, die die Konfiguration des Stereozentrums setzt, unselektiv ist. Dies erlaubt eine stereochemische Bearbeitung, die nicht durch die thermodynamische Präferenz für eines der Stereoisomere limitiert ist. Stereochemische Bearbeitung in einem späten Schritt einer mehrstufigen Synthese eröffnet neue Synthesewege, indem einfache, aber nicht-stereoselektive Reaktionen für den Aufbau eines Moleküls genutzt werden können und das ungewünschte Diastereomer erst in einem späteren Schritt in das gewünschte Diastereomer umgewandelt wird. Dies wurde in dieser Arbeit anhand eines Dihydrobenzofurans gezeigt, dessen Substitutionsmuster mit klassischen Methoden nur mit höherem Aufwand erhalten wird.

Basierend auf der Beobachtung, dass die Produktverteilung in Wasserstoffatomaustauschreaktionen durch eine kinetische Selektivität im Schritt des Bindungsbruches beeinflusst werden kann, wurde das Konzept auf die photokatalytische Deracemisierung von benzyllischen Stereozentren übertragen. Dazu wurden verschiedene Klassen chiraler Silanthiole als HAT-Katalysatoren entwickelt. Silanthiole basierend auf dem von der Weinsäure abgeleiteten TADDOL-Motiv erreichten dabei einen Enantiomerenüberschuss von bis zu 37%. Zwar ist diese Enantioselektivität zu gering, um synthetisch nützlich zu sein, aber sie zeigt, dass das Konzept einer Deracemisierung, basierend auf einer Sequenz aus HAT, RRPCO und darauffolgender Protonierung möglich ist. Während nicht-photokatalytische Methoden für Deracemisierungen durch mikroskopische Reversibilität limitiert sind, wird dies in der dargestellten Deracemisierung vermieden, indem der RRPCO-Schritt Bindungsbruch und Bindungsbildung voneinander trennt und der Photokatalytische Zyklus den Ablauf der Reaktion nur in eine Richtung erlaubt. Bedenkt man, dass chirale Silanthiole in der Literatur bisher nicht vertreten waren unter den hier entwickelten Silanthiolen bereits moderat enantioselektive HAT-Reagenzien sind, ist zu erwarten, dass Fortschritte im Bereich der Organosiliciumchemie noch selektivere Katalysatoren für diesen Ansatz zur Deracemisierung hervorbringen werden.

APPENDIX

7 Appendix

7.1 Abbreviations

°C	degrees Celsius
λ	wavelength
2-Bu	2-butyl
2CzPN	4,5-di(9 <i>H</i> -carbazol-9-yl)phthalonitrile
3DPA2FBN	2,4,6-tris(diphenylamino)-3,5-difluorobenzonitrile
4CzBnBN	3-benzyl-2,4,5,6-tetra(9 <i>H</i> -carbazol-9-yl)benzonitrile
4CzIPN	2,4,5,6-tetrakis(carbazol-9-yl)-4,6-dicyanobenzene
4CzMeBN	2,3,4,6-tetra(9 <i>H</i> -carbazol-9-yl)-5-methylbenzonitrile
4CzPEBN	2,3,4,6-tetra(9 <i>H</i> -carbazol-9-yl)-5-(1-phenylethyl)benzonitrile
a.u.	arbitrary unit
APCI	Atmospheric-pressure chemical ionization
Ar	aryl
BDE	bond dissociation energy
Bn	benzyl
bpy	2,2'-bipyridine
CID	collision-induced dissociation
CV	cyclic voltammetry
cz	9 <i>H</i> -carbazol-9-yl
dba	dibenzylideneacetone
DCM	dichloromethane
DET	Dexter energy transfer
DFT	density functional theory
DIPEA	<i>N,N</i> -diisopropylethylamine
DMA	<i>N,N</i> -dimethylacetamide
DMF	<i>N,N</i> -dimethylformamide
DMSO	dimethyl sulfoxide
DPA	9,10-diphenylanthracene
dppe	1,2-bis(diphenylphosphino)ethane
dppp	1,2-bis(diphenylphosphino)propane
dtbbpy	4,4'-di- <i>tert</i> -butyl-2,2'-dipyridyl
E1cb	Elimination unimolecular conjugated base
e.g.	for example (lat. <i>exempli gratia</i>)
EI	electron ionization
EML	emissive layer
EnT	energy transfer
equiv.	equivalent
ESI	electrospray ionization
Et	ethyl
et al.	and others (lat. <i>et alii</i>)
EtOAc	ethyl acetate
EtOH	ethanol
ETPT	electron-transfer, proton-transfer
eV	electron volt
Fc	ferrocene
FRET	Förster resonance energy transfer
g	gram
GSB	ground state bleach
h	hour(s)
HAT	hydrogen atom transfer
H(D)AT	hydrogen or deuterium atom transfer
HIE	hydrogen isotope exchange
HOMO	highest occupied molecular orbital
HRMS	high resolution mass spectrometry

<i>hν</i>	incident photon energy
IC	internal conversion
ⁱ Pr	isopropyl
IQE	internal quantum efficiency
ISC	intersystem crossing
K	Kelvin
kcal	kilocalories
L	liter
LED	light emitting diode
LUMO	lowest unoccupied molecular orbital
M	molar (mol/L)
Me	methyl
MeCN	acetonitrile
MeO	methoxy
MeOH	methanol
mg	milligram
min	minute(s)
mL	milliliter
mM	millimolar (mmol/L)
mmol	millimole
MS	mass spectrometry
<i>n</i> -Bu	<i>n</i> -butyl
<i>n</i> -dec	<i>n</i> -decyl
nm	nanometer
NMR	nuclear magnetic resonance
OLED	organic light emitting diode
PC	photocatalyst
PE	petroleum ether
PET	photoinduced electron transfer
Ph	phenyl
p <i>K</i> _a	acid dissociation constant at logarithmic scale
ppy	2-phenylpyridinato
<i>p</i> -tol	4-methylphenyl
R	alkyl, aryl-, or functional group
RISC	reverse intersystem crossing
RRPCO	reductive radical-polar crossover
s	second(s)
SCE	saturated calomel electrode
S _N 2	nucleophilic substitution, second order
S _N Ar	nucleophilic aromatic substitution
SAS	species associated spectra
TADDOL	$\alpha,\alpha,\alpha',\alpha'$ -tetraaryl-2,2-disubstituted 1,3-dioxolane-4,5-dimethanol
TA	thermal activation
TADF	thermally activated delayed fluorescence
THF	tetrahydrofuran
TLC	thin layer chromatography
TS	transition state
UV	ultraviolet light
v:v	volume 1 to volume 2
Vis	visible light
VR	vibrational relaxation
vs.	against (lat. versus)
ZPE	zero-point energy

7.2 Appendix chapter 2

7.2.1 Cyclic voltammetry

4CzIPN (1)

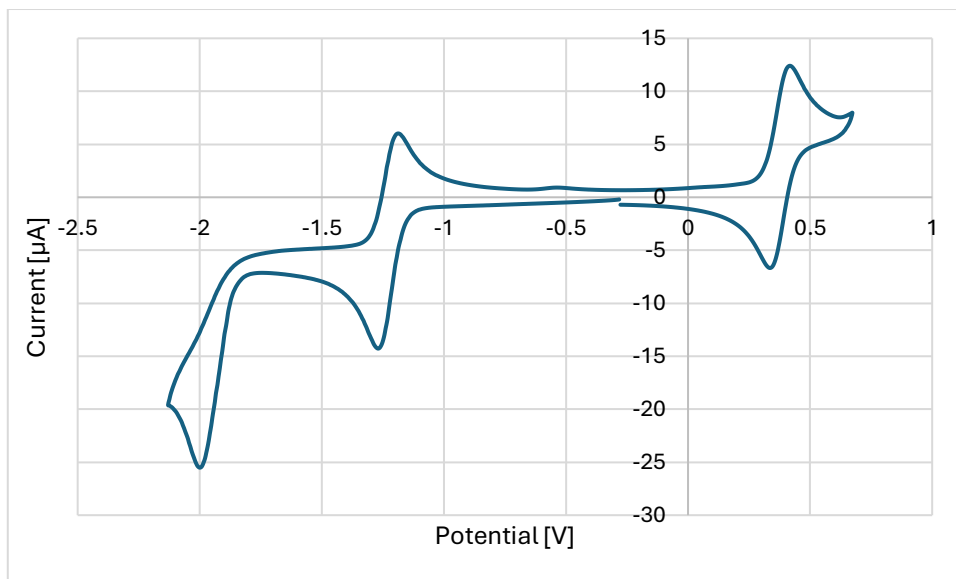


Figure 2.8. Reductive half of the cyclic voltammogram of 4CzIPN with ferrocene as internal standard. $E_{1/2}(\text{X}/\text{X}^{\cdot-}) = -1.23$ V vs. SCE.

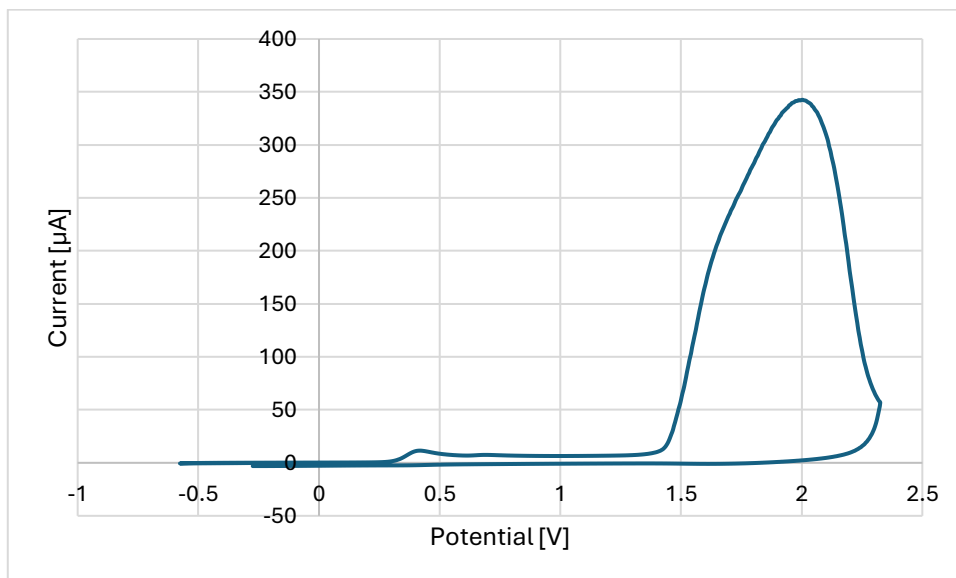


Figure 2.9. Oxidative half of the cyclic voltammogram of 4CzIPN with ferrocene as internal standard. $E_{1/2}(\text{X}^{\cdot+}/\text{X}) = 1.53$ V vs. SCE.

2c

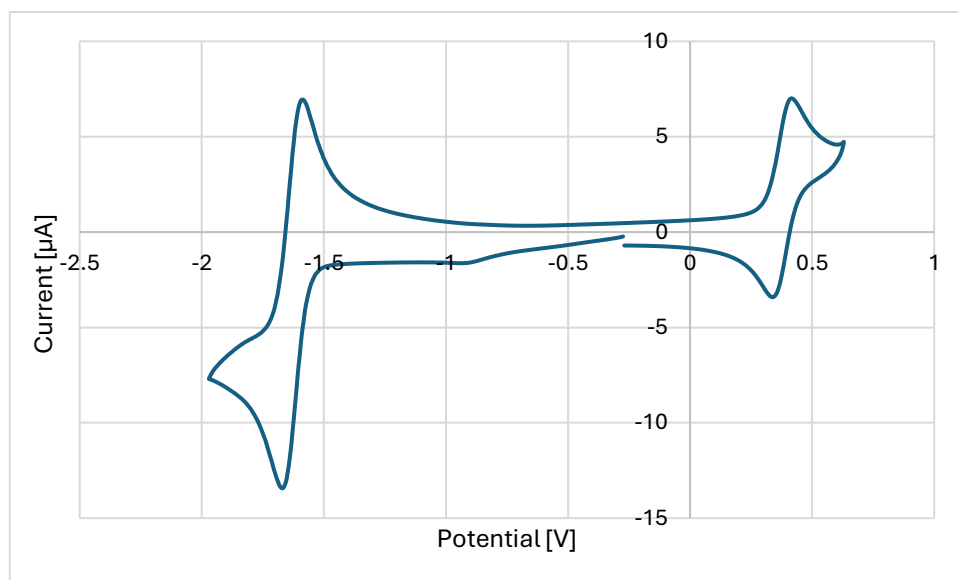


Figure 2.10. Reductive half of the cyclic voltammogram of **2c** with ferrocene as internal standard. $E_{1/2}(X/X^*) = -1.63$ V vs. SCE.

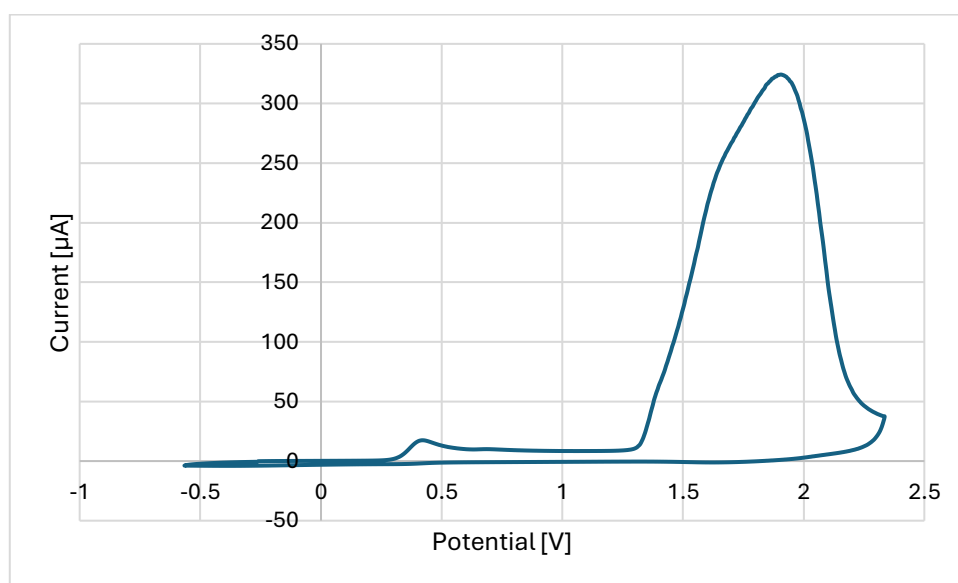


Figure 2.11. Oxidative half of the cyclic voltammogram of **2c** with ferrocene as internal standard. $E_{1/2}(X^{*+}/X) = 1.47$ V vs. SCE.

2g

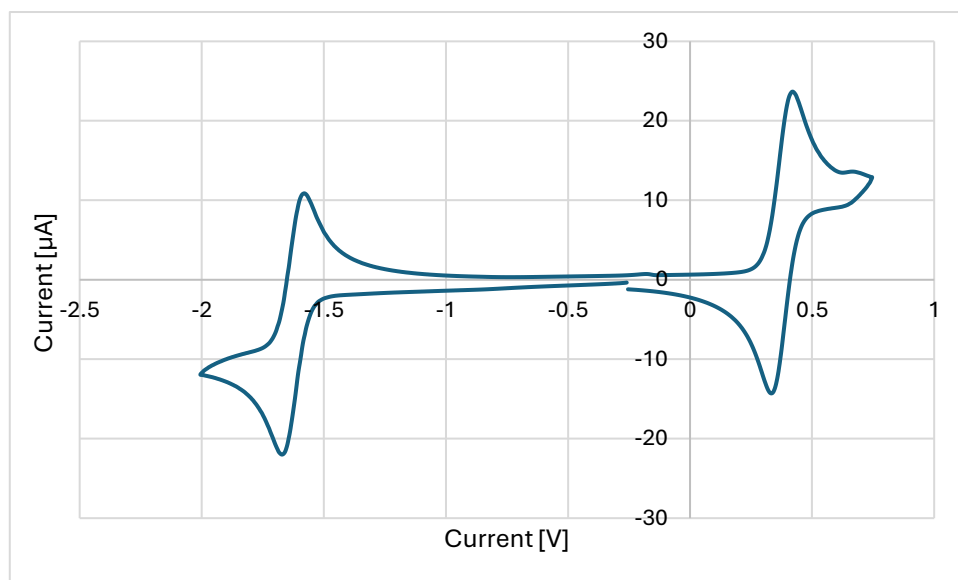


Figure 2.12. Reductive half of the cyclic voltammogram of **2g** with ferrocene as internal standard. $E_{1/2}(X/X^*) = -1.63$ V vs. SCE.

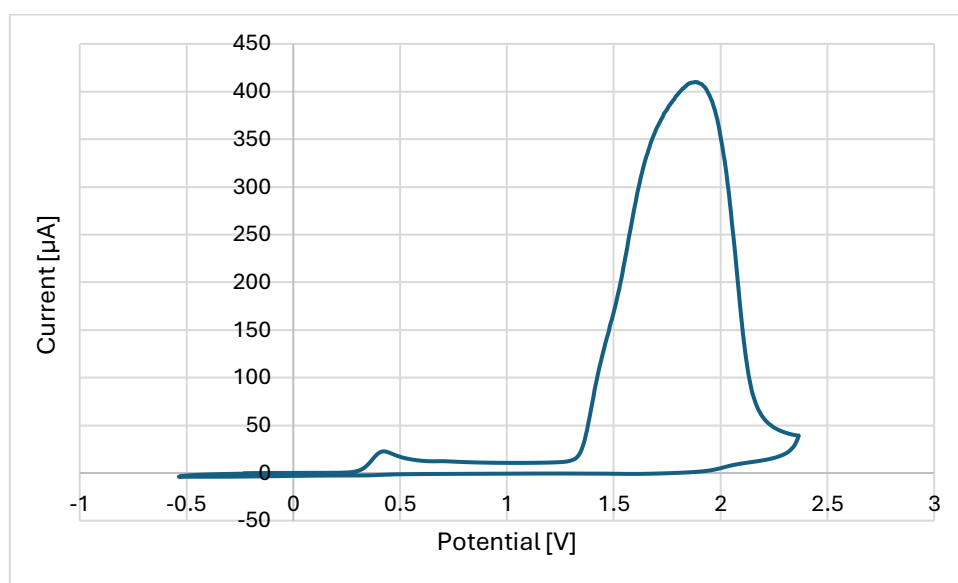


Figure 2.13. Oxidative half of the cyclic voltammogram of **2g** with ferrocene as internal standard. $E_{1/2}(X^{*+}/X) = 1.43$ V vs. SCE.

2j

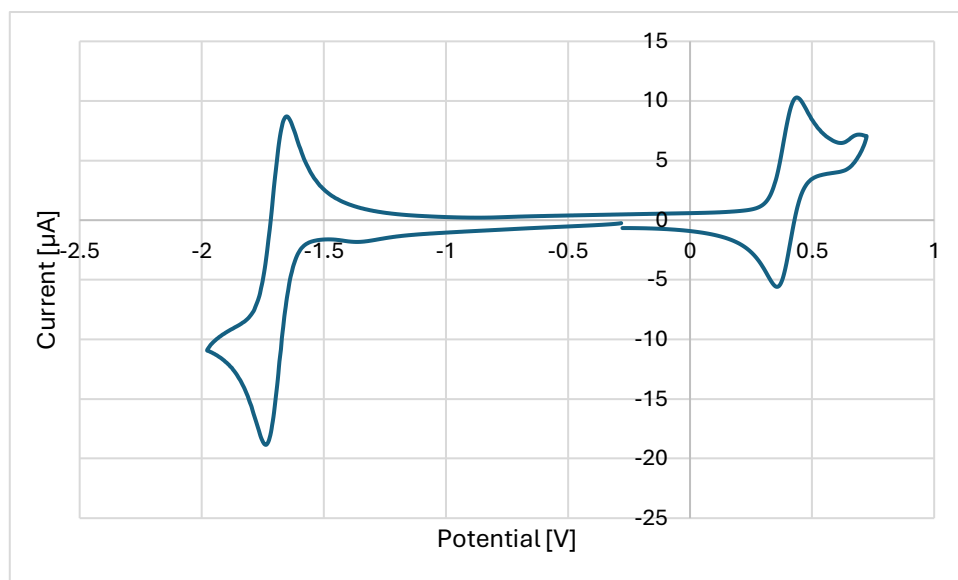


Figure 2.14. Reductive half of the cyclic voltammogram of **2j** with ferrocene as internal standard. $E_{1/2}(\text{X}/\text{X}^-) = -1.69$ V vs. SCE.

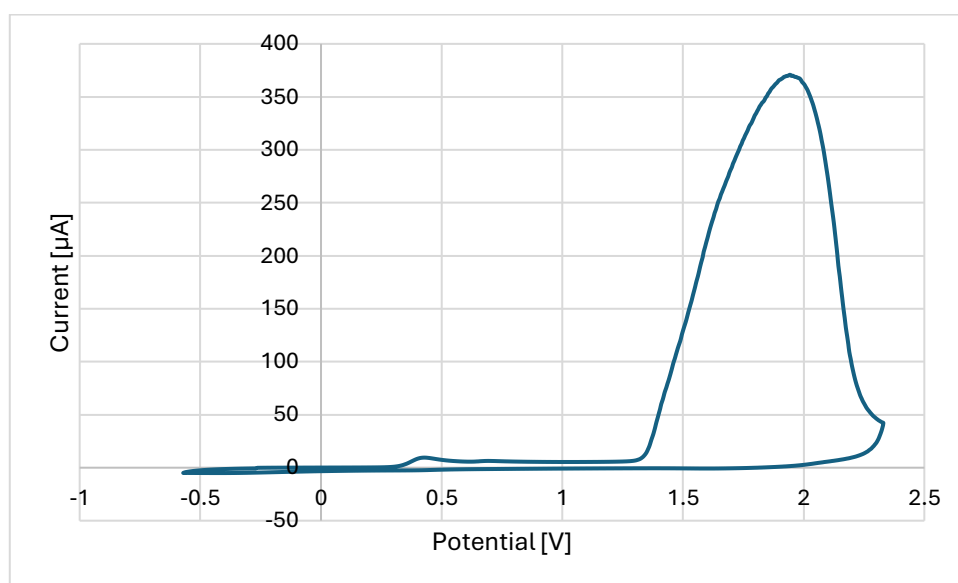


Figure 2.15. Oxidative half of the cyclic voltammogram of **2j** with ferrocene as internal standard. $E_{1/2}(\text{X}^+/\text{X}) = 1.47$ V vs. SCE.

2CzPN (3)

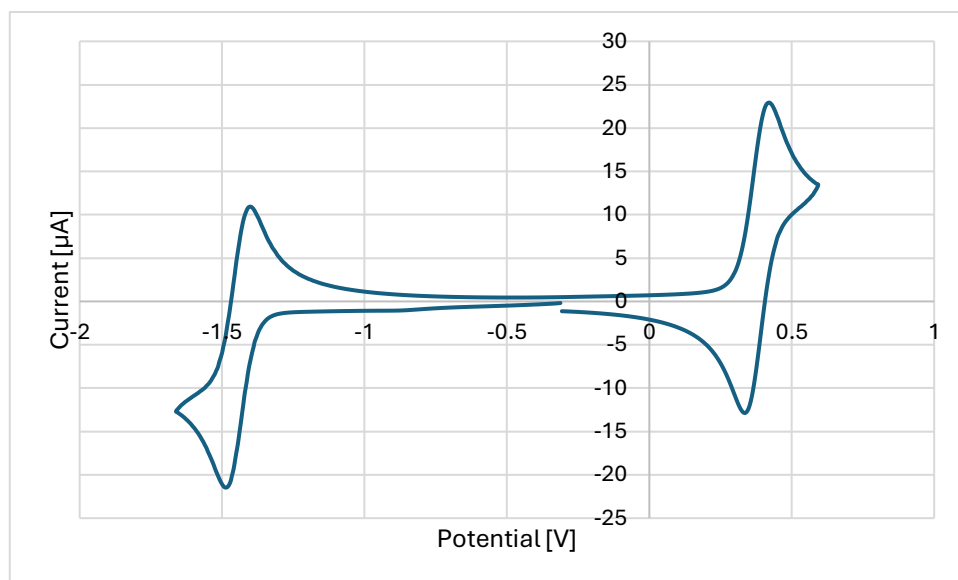


Figure 2.16. Reductive half of the cyclic voltammogram of 2CzPN with ferrocene as internal standard. $E_{1/2}(\text{X}/\text{X}^-) = -1.44$ V vs. SCE.

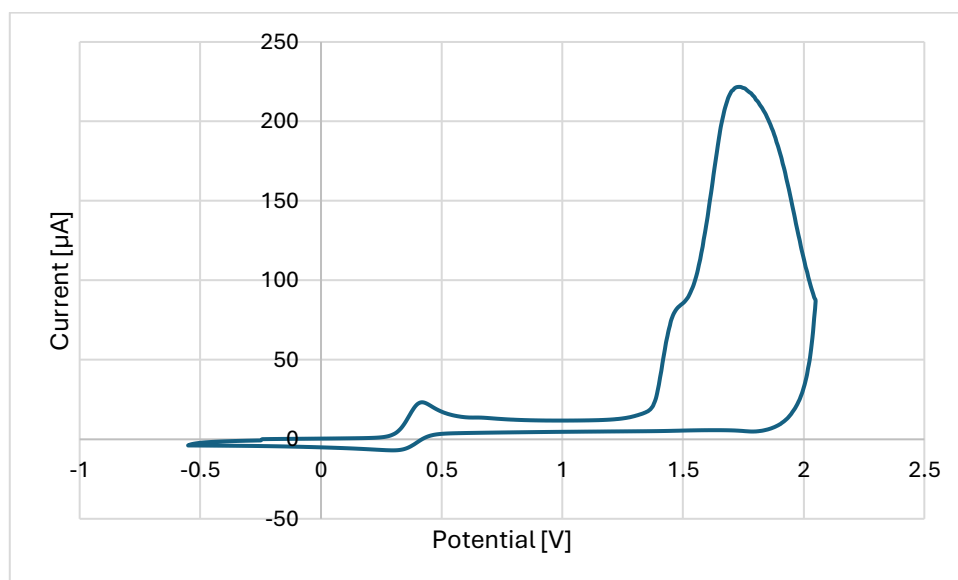


Figure 2.17. Oxidative half of the cyclic voltammogram of 2CzPN with ferrocene as internal standard. $E_{1/2}(\text{X}^+/\text{X}) = 1.49$ V vs. SCE.

4a

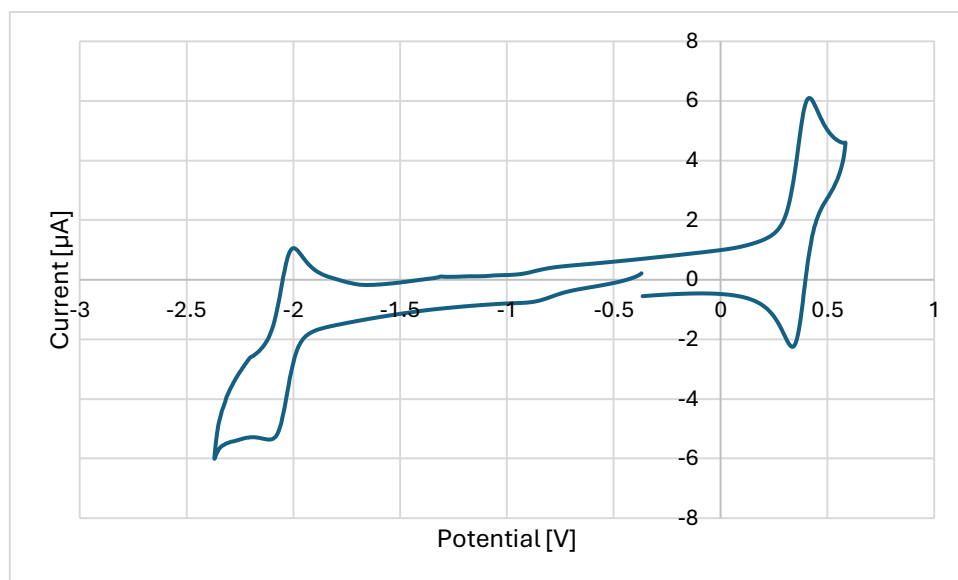


Figure 2.18. Reductive half of the cyclic voltammogram of photosubstitution product **4a** with ferrocene as internal standard. $E_{1/2}(X/X^*) = -2.05$ V vs. SCE.

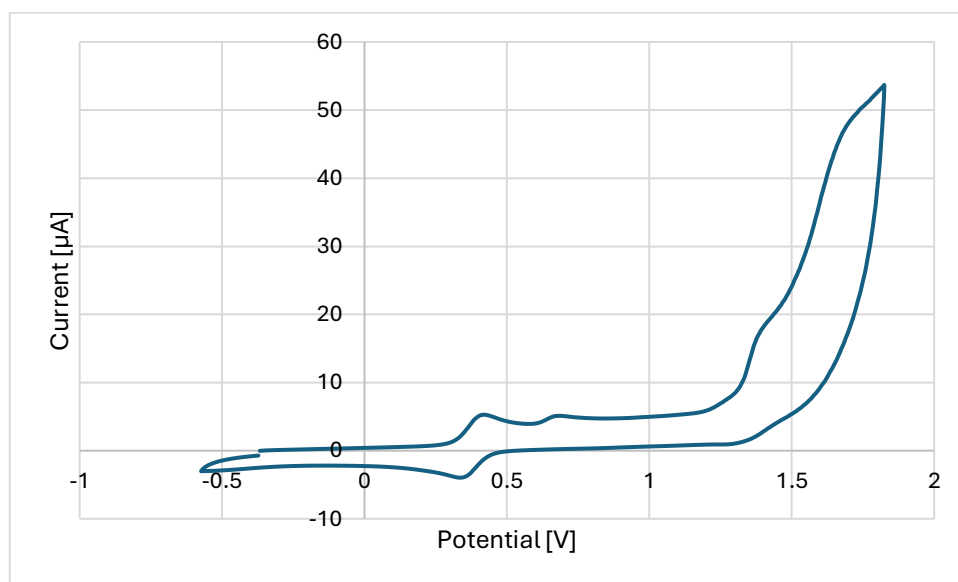


Figure 2.19. Oxidative half of the cyclic voltammogram of **4a** with ferrocene as internal standard. $E_{1/2}(X^{*+}/X) = 1.30$ V vs. SCE.

4b

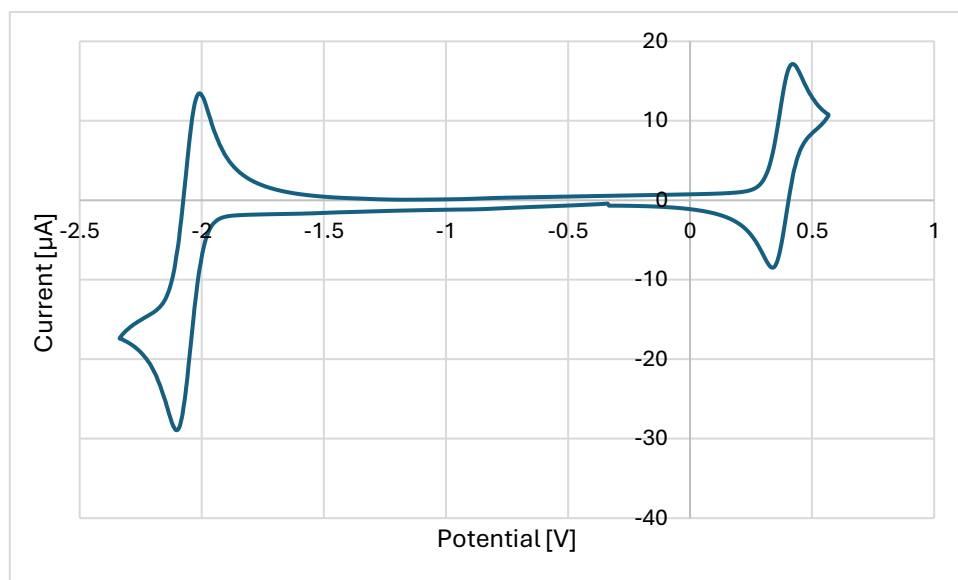


Figure 2.20. Reductive half of the cyclic voltammogram of **4b** with ferrocene as internal standard. $E_{1/2}(X/X^*) = -2.06$ V vs. SCE.

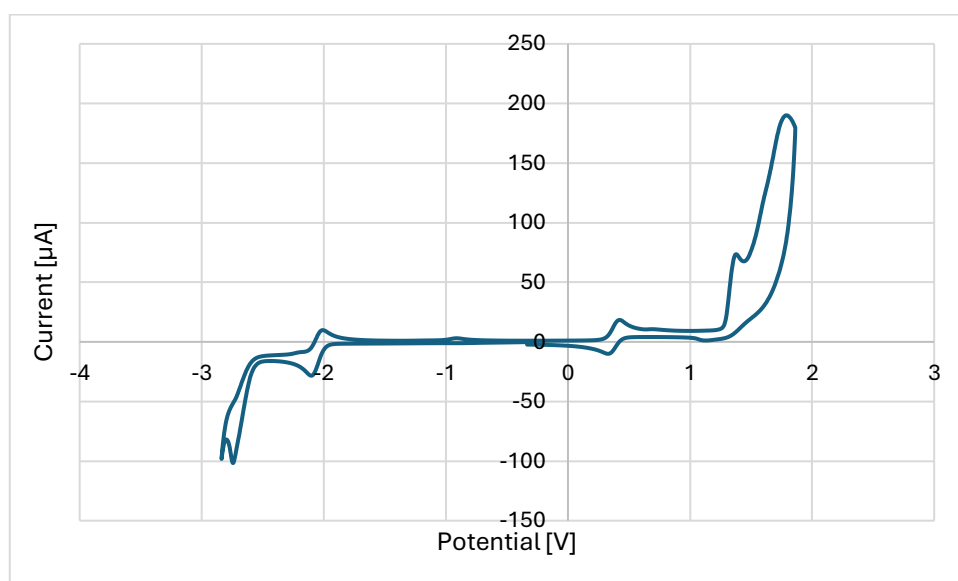


Figure 2.21. Full cyclic voltammogram of **4b** with ferrocene as internal standard. $E_{1/2}(X^+/X) = 1.37$ V vs. SCE.

4c

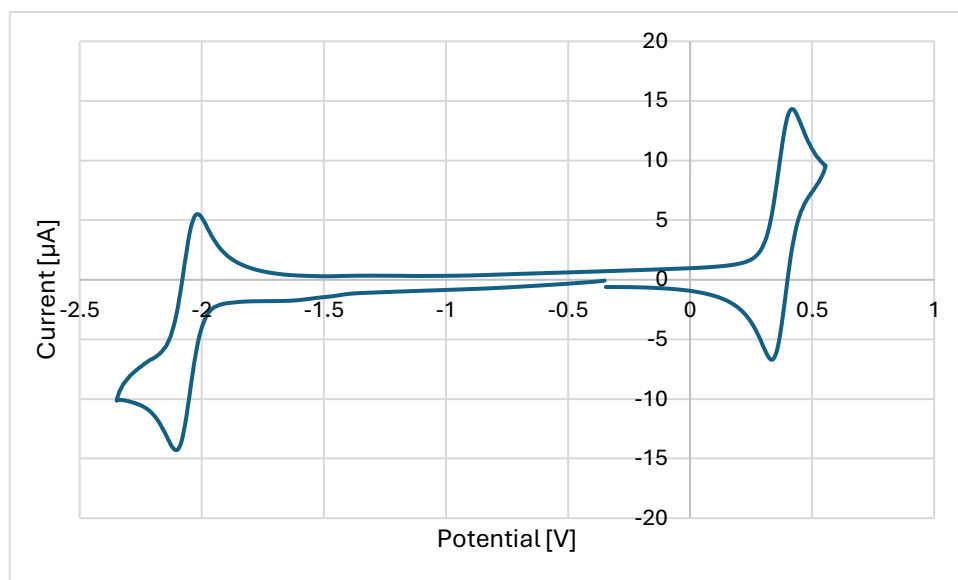


Figure 2.22. Reductive half of the cyclic voltammogram of **4c** with ferrocene as internal standard. $E_{1/2}(X/X^*) = -2.06$ V vs. SCE.

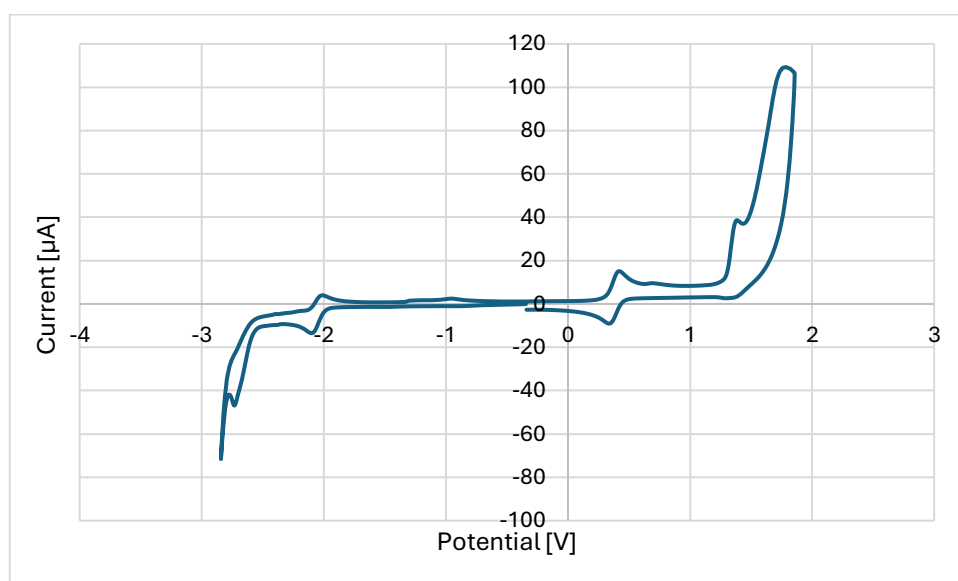


Figure 2.23. Full cyclic voltammogram of **4c** with ferrocene as internal standard. $E_{1/2}(X^+/X) = 1.34$ V vs. SCE.

7.2.2 UV/Vis spectra, emission spectra, and fluorescence lifetime

UV/Vis absorbance and fluorescence emission between different photosubstitution products from the same dicyanobenzene precursor show only minor differences. A superposition of UV/Vis spectra of some examples is depicted in Figures 2.1 and 2.2 under results and discussion. All spectra were recorded at a concentration of 20 μM . The excitation wavelength for recording of fluorescence emission spectra was 350 nm. The signal at 700 nm is a technical artefact and does not arise from the compounds' fluorescence. All emission spectra are normalized with respect to the emission maximum.

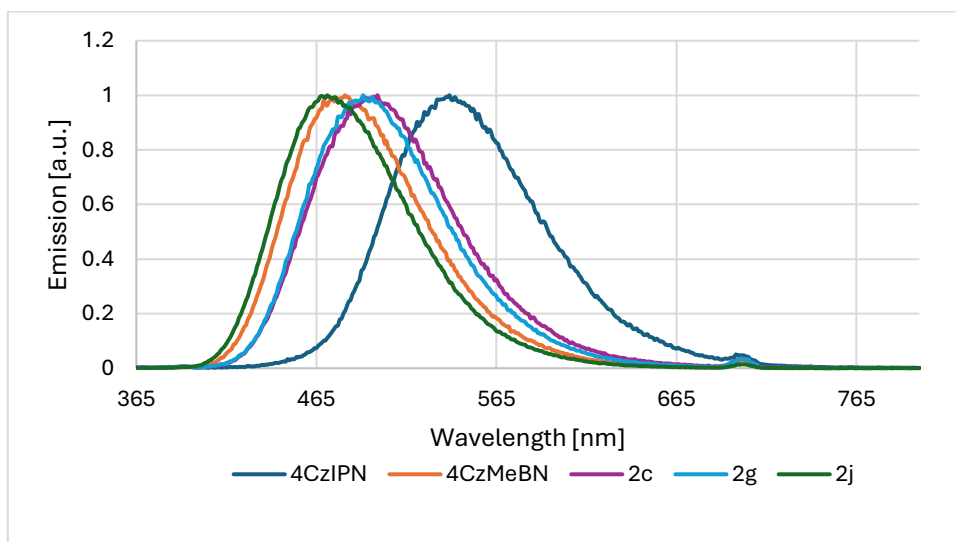


Figure 2.24. Superposition of the fluorescence emission of 4CzIPN and photosubstitution products. 20 μM in MeCN.

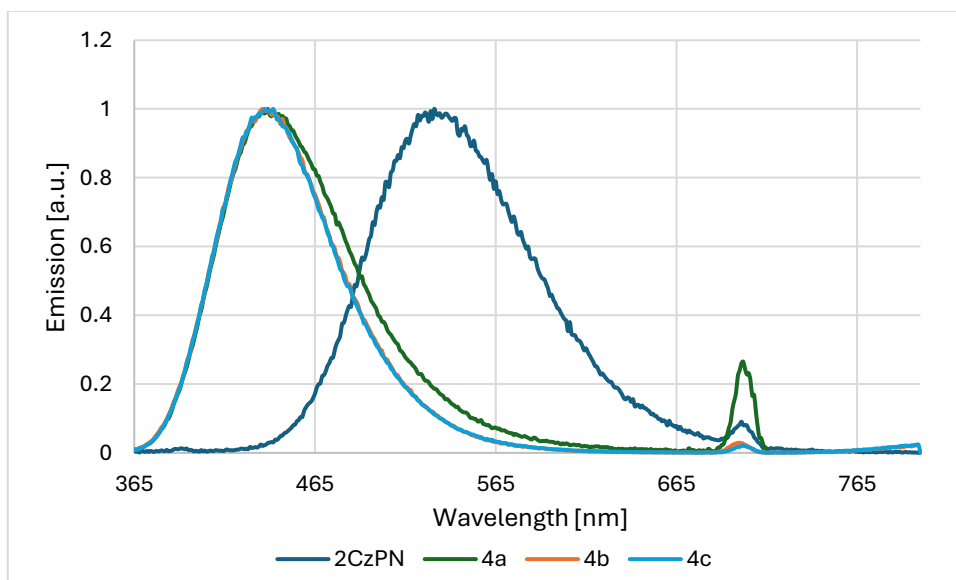


Figure 2.25. Superposition of the fluorescence emission of 2CzPN and photosubstitution products. 20 μM in MeCN.

4CzIPN (1)

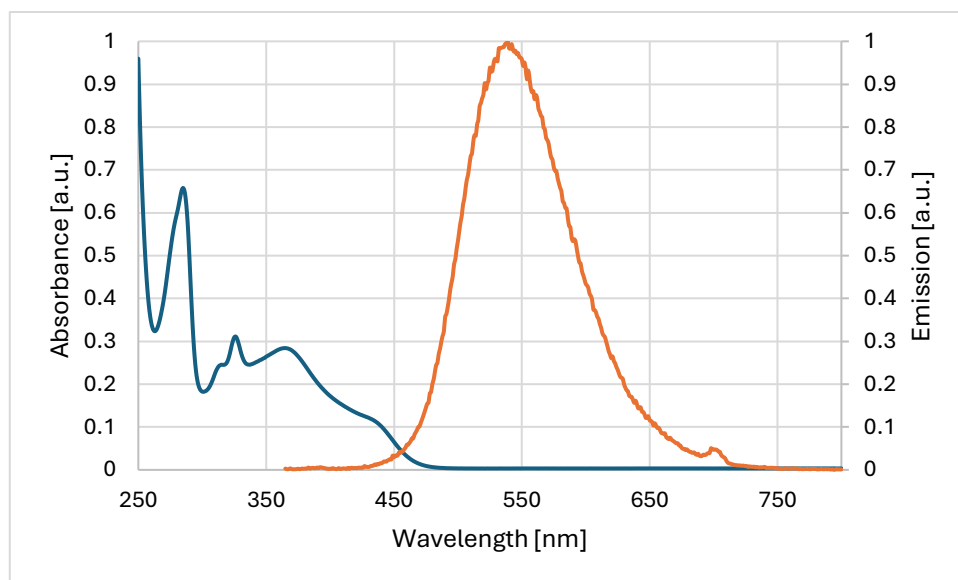


Figure 2.26. UV/Vis absorption and fluorescence emission of 4CzIPN (1). 20 μM in MeCN.

E_{0-0} : 2.67 eV (364 nm)

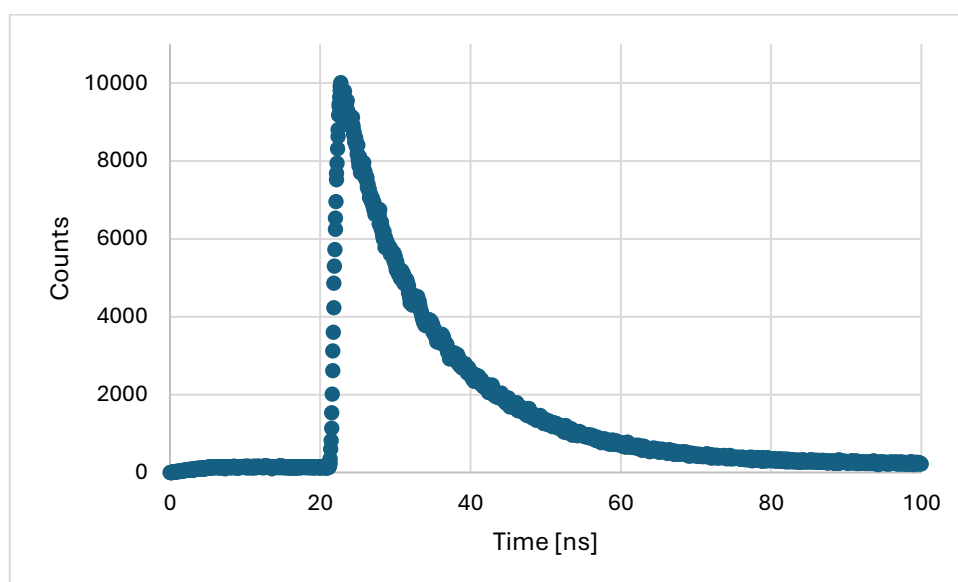


Figure 2.27. Fluorescence decay curve of 4CzIPN. 20 μM in MeCN.

Lifetime τ in MeCN: 12.7 ns

4CzMeBN (10)

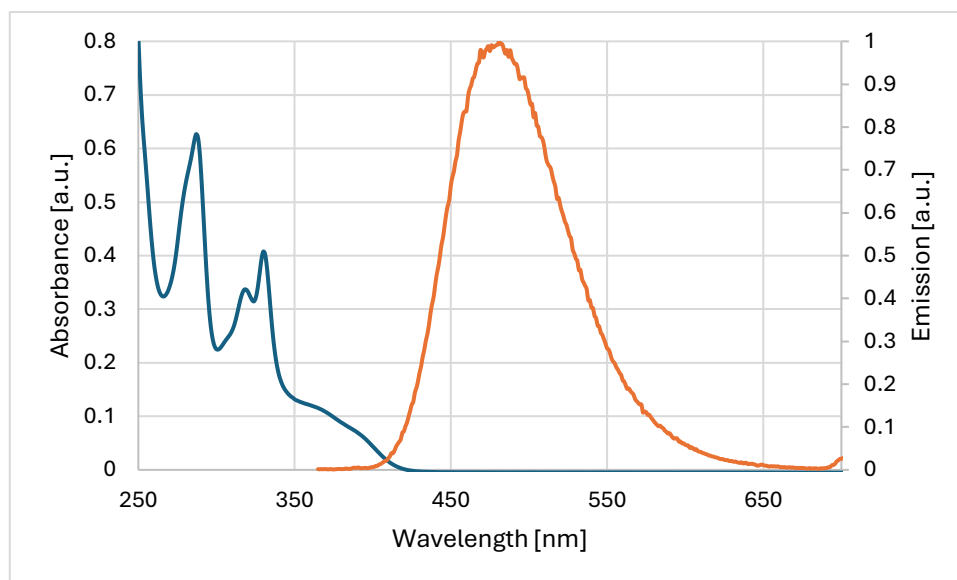


Figure 2.28. UV/Vis absorption and fluorescence emission of photosubstitution product **10**. 20 μM in MeCN.
 E_{0-0} : 2.95 eV (420 nm)

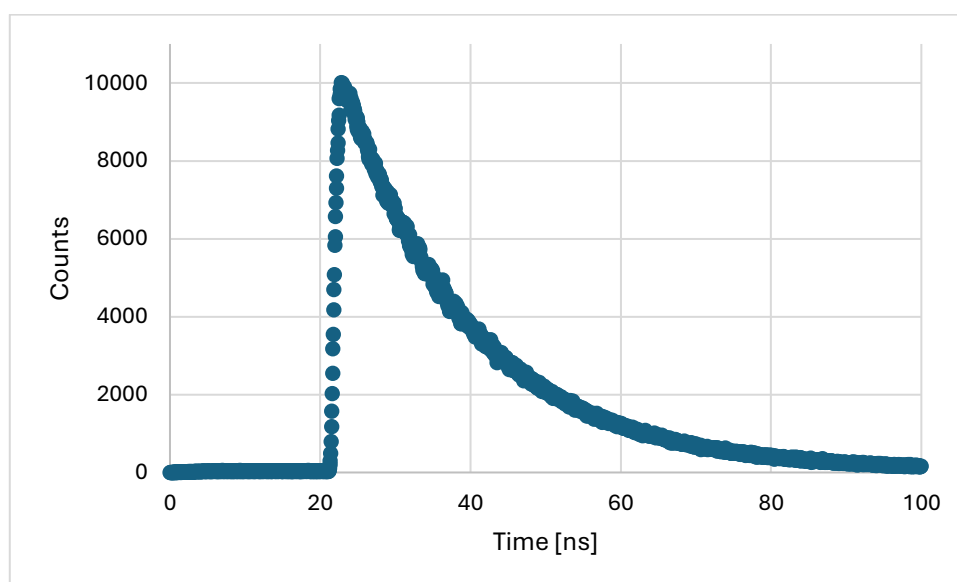


Figure 2.29. Fluorescence decay curve of photosubstitution product **10**. 20 μM in MeCN.
Lifetime τ in MeCN: 17.3 ns

2c

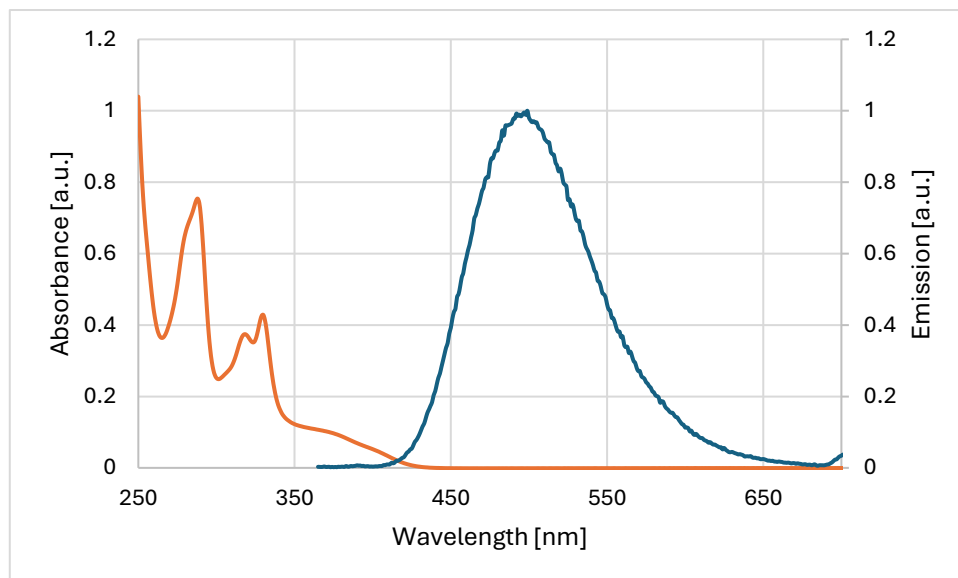


Figure 2.30. UV/Vis absorption and fluorescence emission of photosubstitution product **2c**. 20 μM in MeCN. E_{0-0} : 2.90 eV (428 nm)

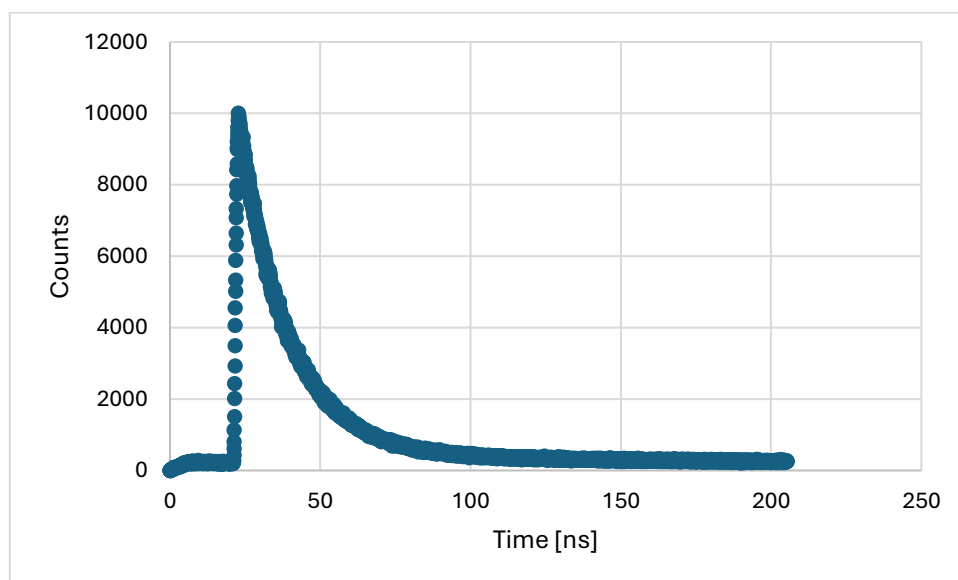


Figure 2.31. Fluorescence decay curve of photosubstitution product **2c**. 20 μM in MeCN. Lifetime τ in MeCN: 18.1 ns

Photosubstitution product **2c** was also measured in nitrogen saturated and oxygen saturated MeCN. In nitrogen saturated solution **2c** shows a prompt fluorescence on the nanosecond scale and a delayed fluorescence on the microsecond scale. The delayed component is most likely based on thermally activated delayed fluorescence (TADF), demonstrating that photosubstitution products of dicyanobenzene based TADF emitters are still TADF emitters.

In oxygen saturated MeCN prompt and delayed fluorescence lifetime are substantially decreased with a 4.7-fold decrease of prompt fluorescence and a 30.1-fold decrease of delayed fluorescence. A similar effect of oxygen was obtained for the fluorescence decay of photocatalyst **4d** in chapter 3 (see Figure 3.45).

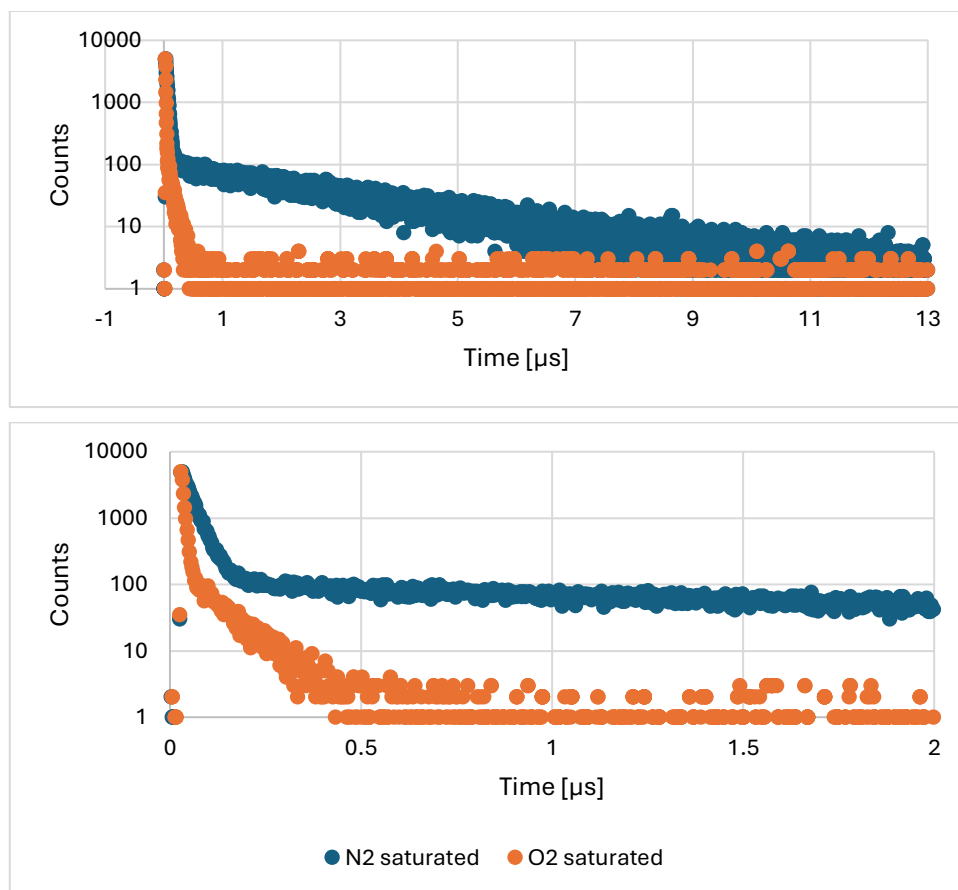


Figure 2.32. Fluorescence decay of photosubstitution product **2c** in nitrogen saturated and oxygen saturated MeCN.

Lifetime τ in N_2 saturated MeCN

Prompt component: 31.0 ns (relative amplitude: 28.05%)

TADF component: 2.8 μ s (relative amplitude: 71.95%)

Lifetime τ in O_2 saturated MeCN

Prompt component: 6.6 ns (relative amplitude: 71.76%)

TADF component: 92.9 ns (relative amplitude: 28.24%)

2g

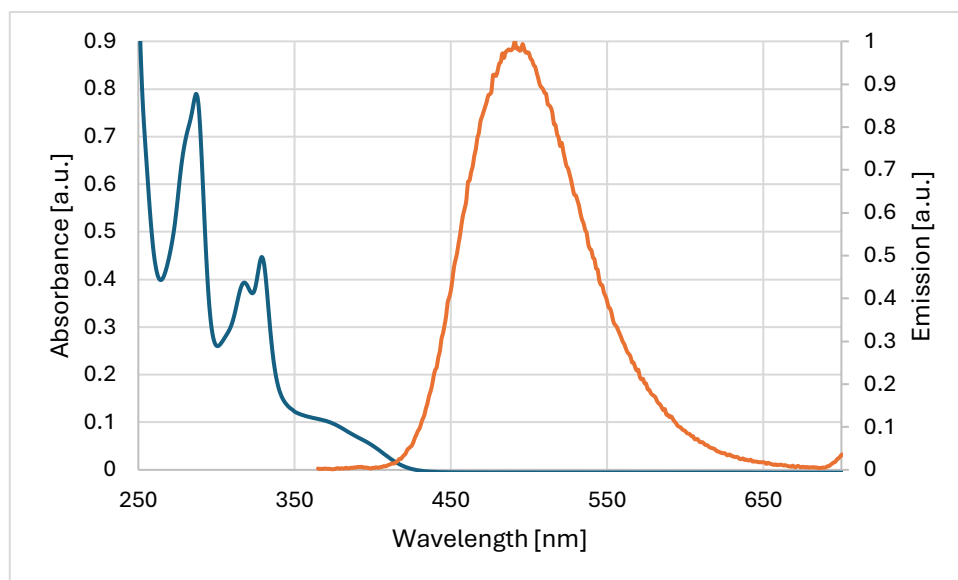


Figure 2.33. UV/Vis absorption and fluorescence emission of photosubstitution product **2g**. 20 μM in MeCN. E_{0-0} : 2.90 eV (428 nm)

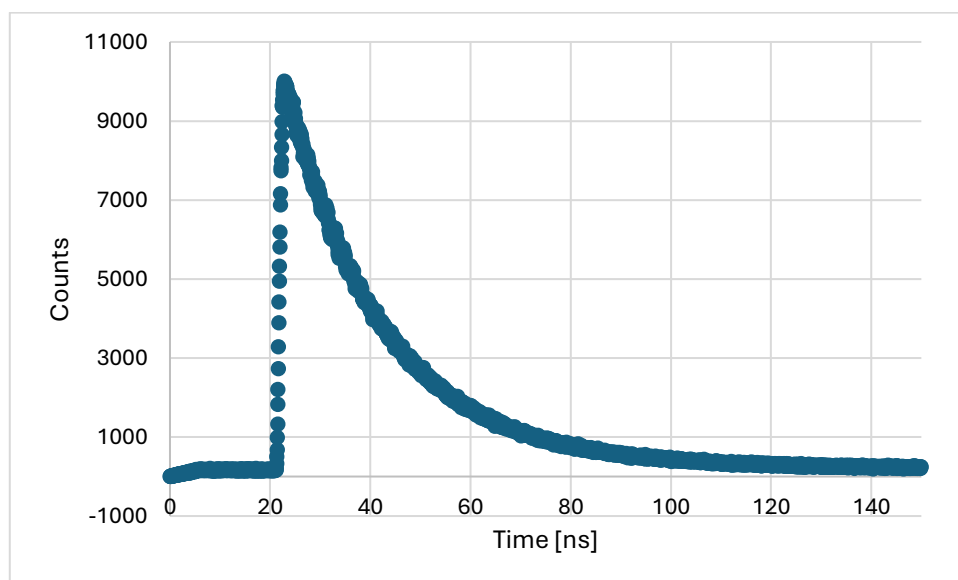


Figure 2.34. Fluorescence decay curve of photosubstitution product **2g**. 20 μM in MeCN. Lifetime τ in MeCN: 18.9 ns

2j

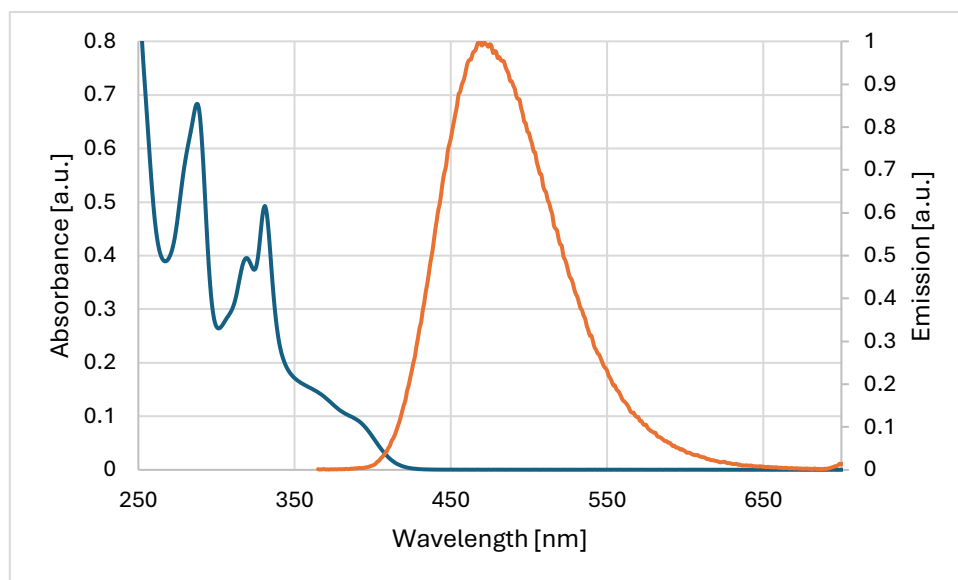


Figure 2.35. UV/Vis absorption and fluorescence emission of photosubstitution product **2j**. 20 μM in MeCN.

E_{0-0} : 2.97 eV (417 nm)

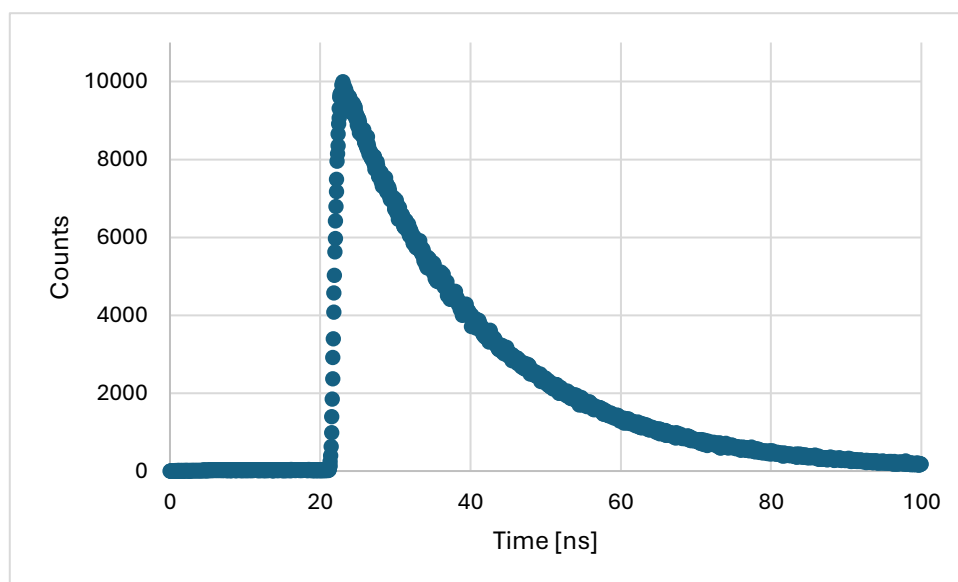


Figure 2.36. Fluorescence decay curve of photosubstitution product **2j**. 20 μM in MeCN.

Lifetime τ in MeCN: 18.4 ns

2CzPN (3)

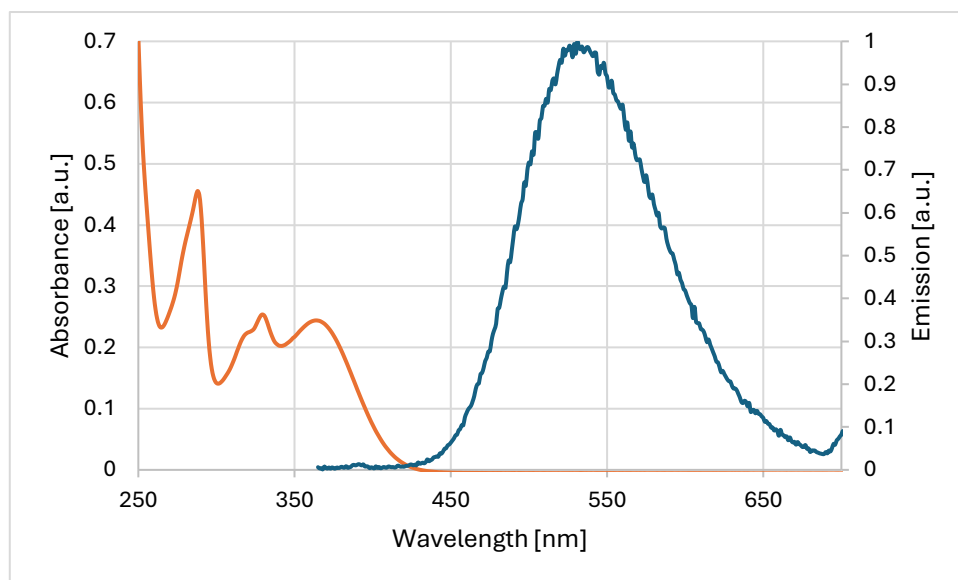


Figure 2.37. UV/Vis absorption and fluorescence emission of 2CzPN. 20 μM in MeCN.

E_{0-0} : 2.86 eV (434 nm)

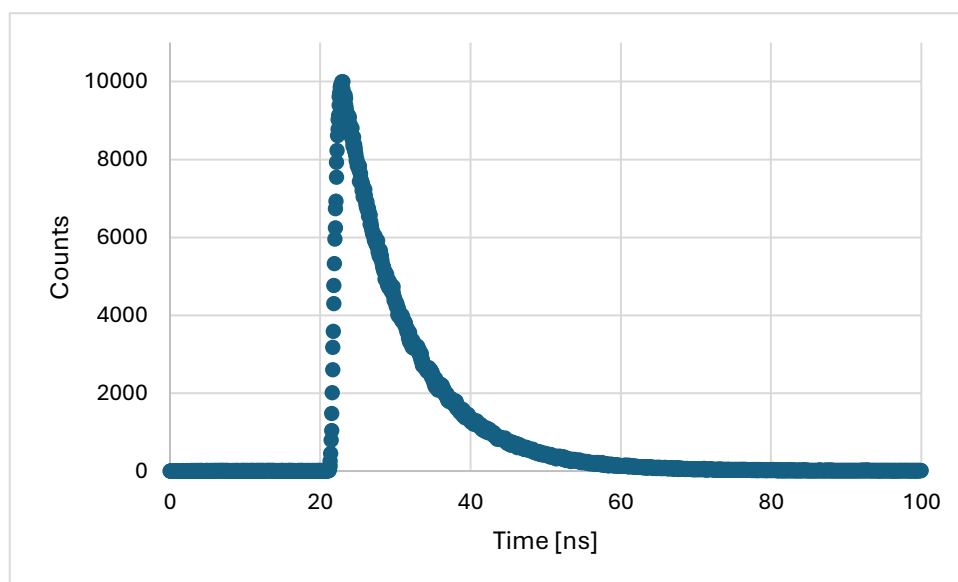


Figure 2.38. Fluorescence decay curve of 2CzPN. 20 μM in MeCN.

Lifetime τ in MeCN: 8.5 ns

4a

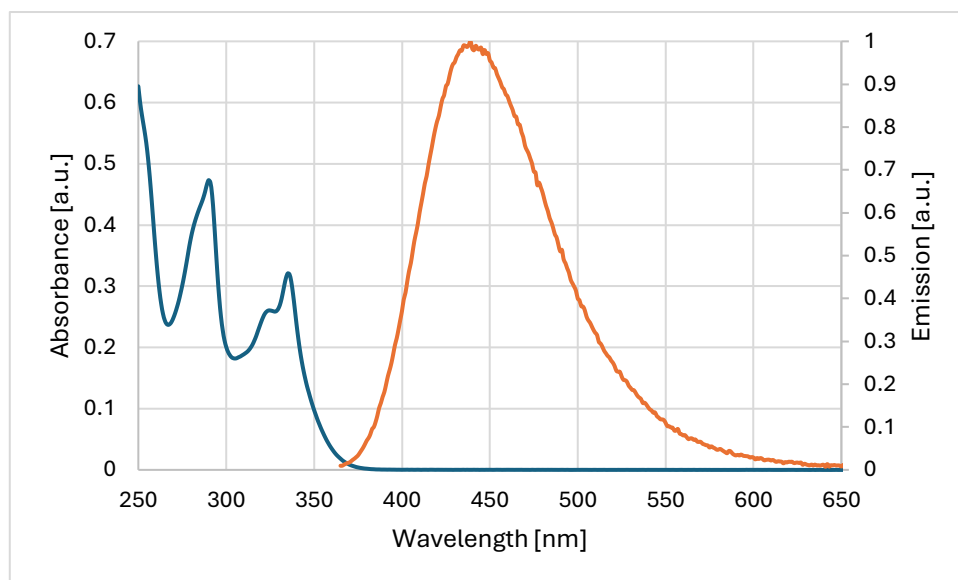


Figure 2.39. UV/Vis absorption and fluorescence emission of photosubstitution product **4a**. 20 μM in MeCN.

E_{0-0} : 3.33 eV (372 nm)

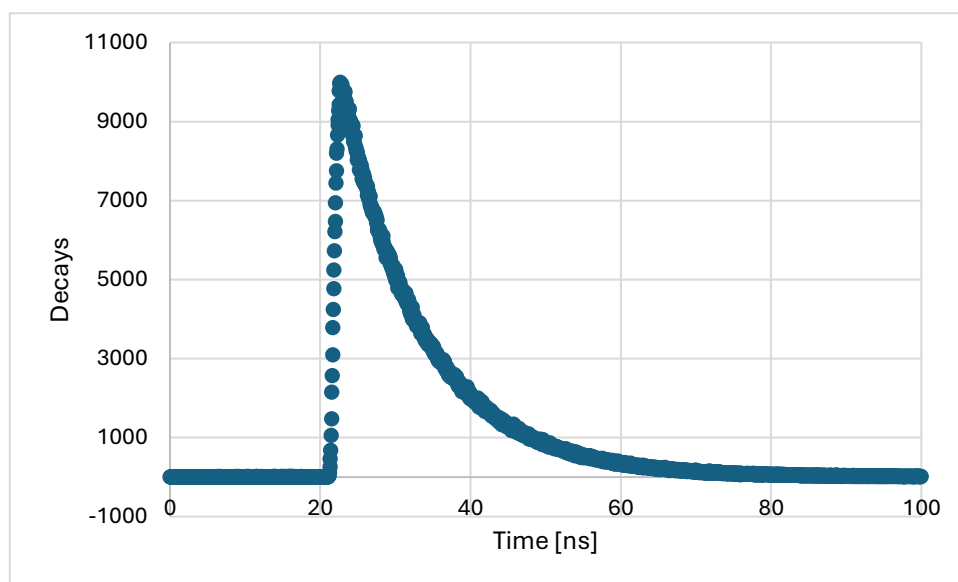


Figure 2.40. Fluorescence decay curve of photosubstitution product **4a**. 20 μM in MeCN.

Lifetime τ in MeCN: 11.0 ns

4b

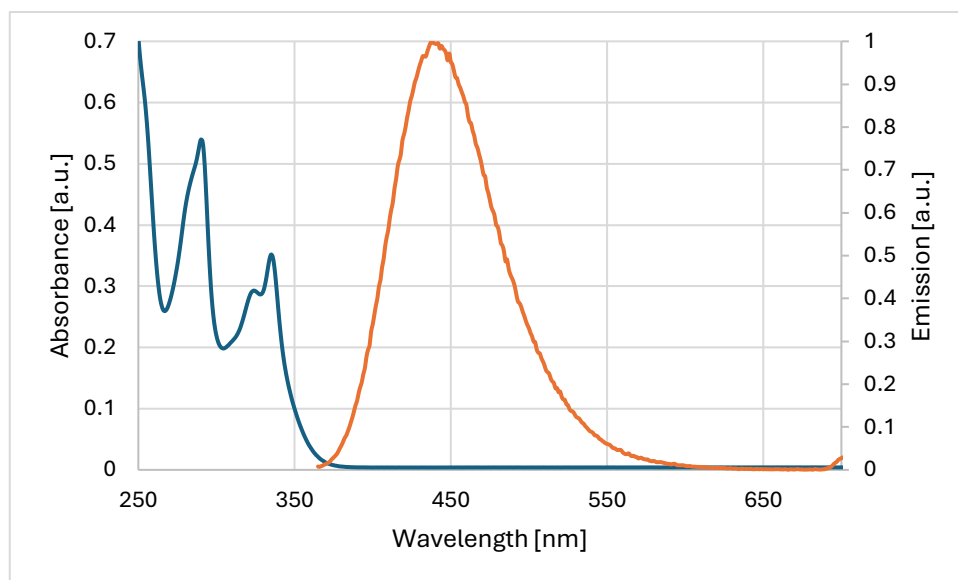


Figure 2.41. UV/Vis absorption and fluorescence emission of photosubstitution product **4b**. 20 μM in MeCN.

E_{0-0} : 3.32 eV (374 nm)

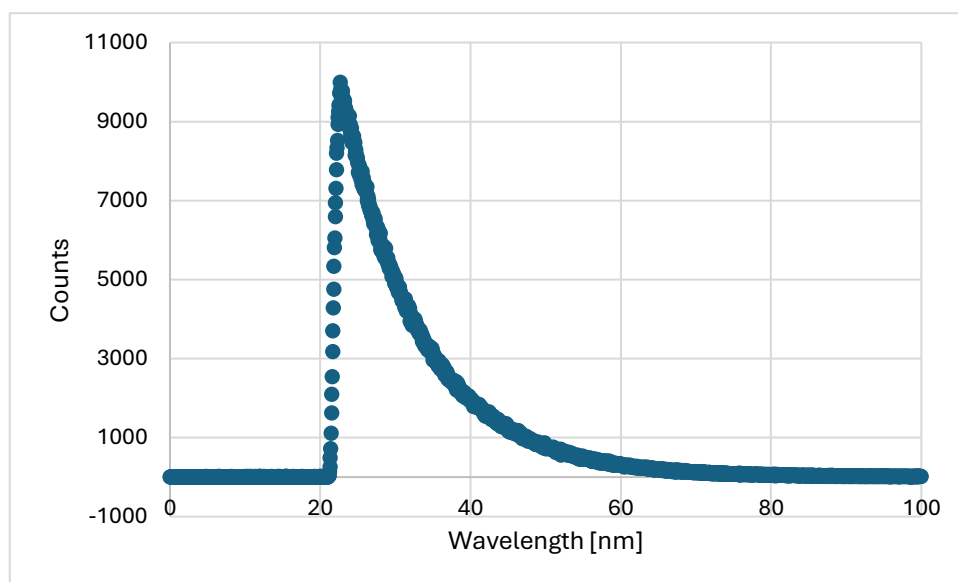


Figure 2.42. Fluorescence decay curve of photosubstitution product **4b**. 20 μM in MeCN.

Lifetime τ in MeCN: 10.7 ns

4c

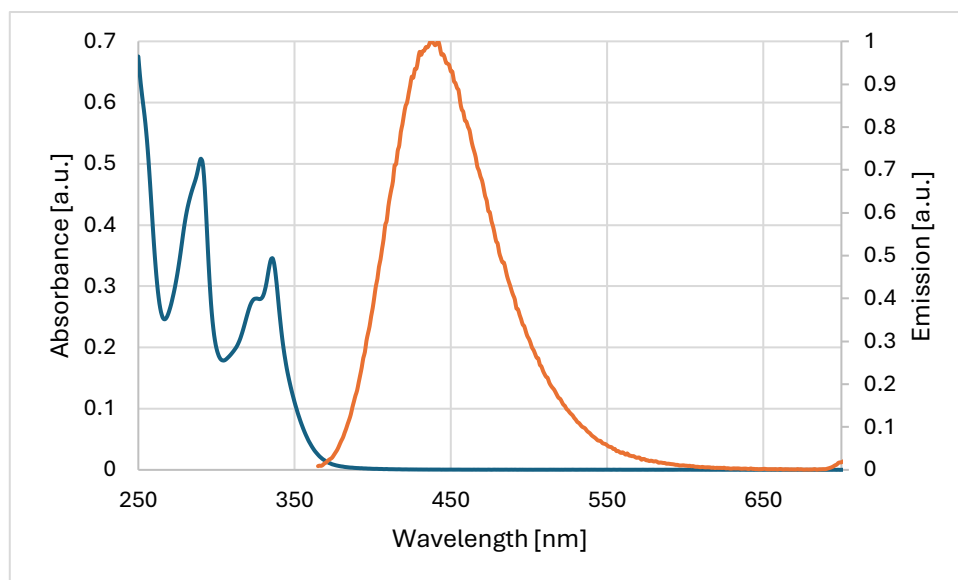


Figure 2.43. UV/Vis absorption and fluorescence emission of photosubstitution product **4c**. 20 μM in MeCN.

E_{0-0} : 3.32 eV (374 nm)

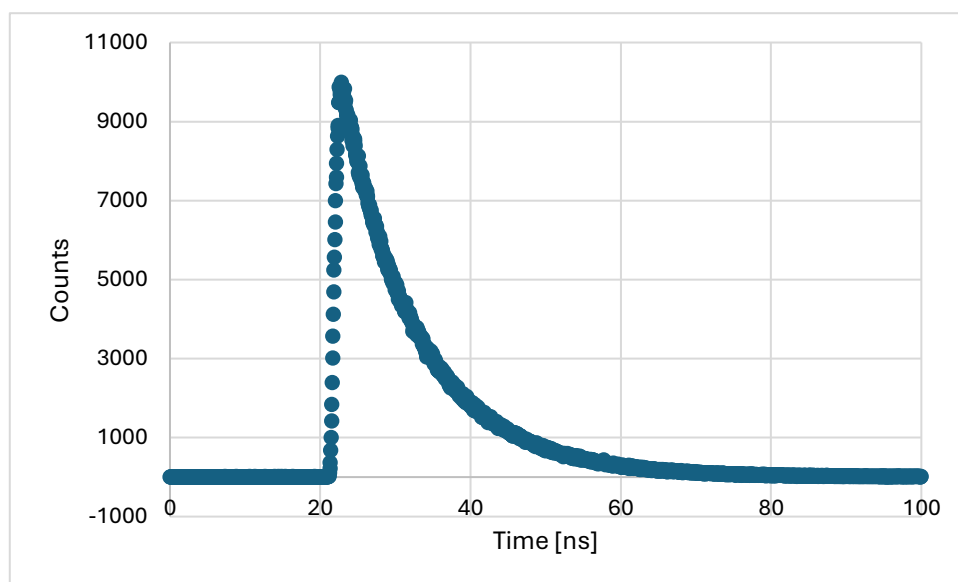
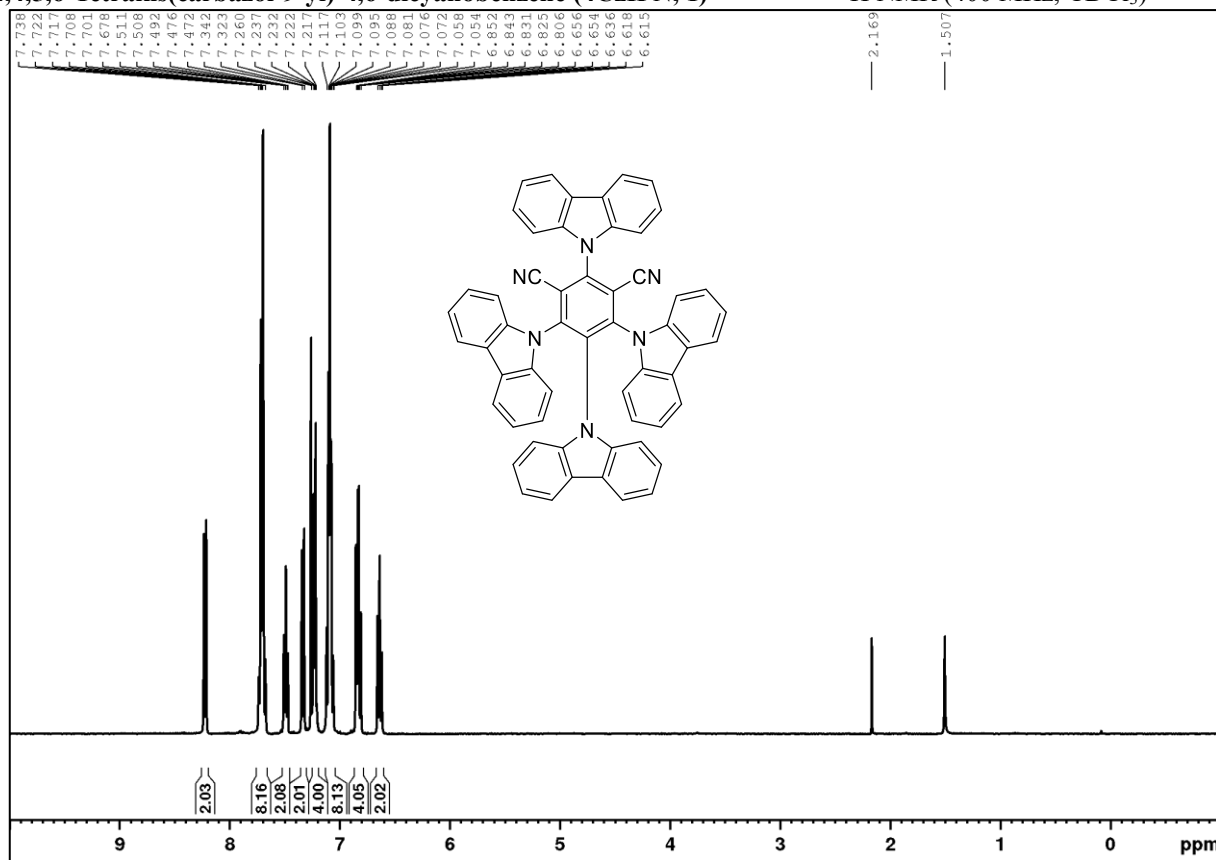


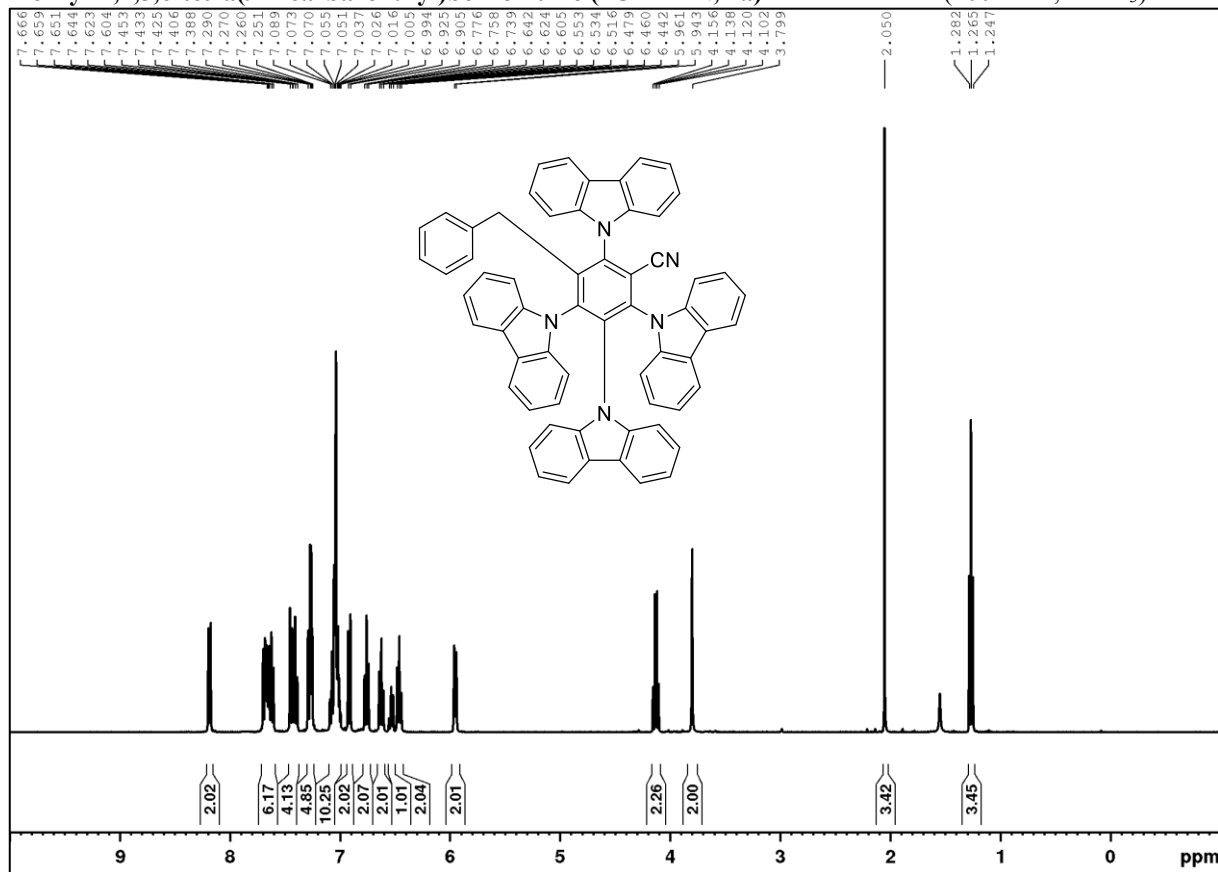
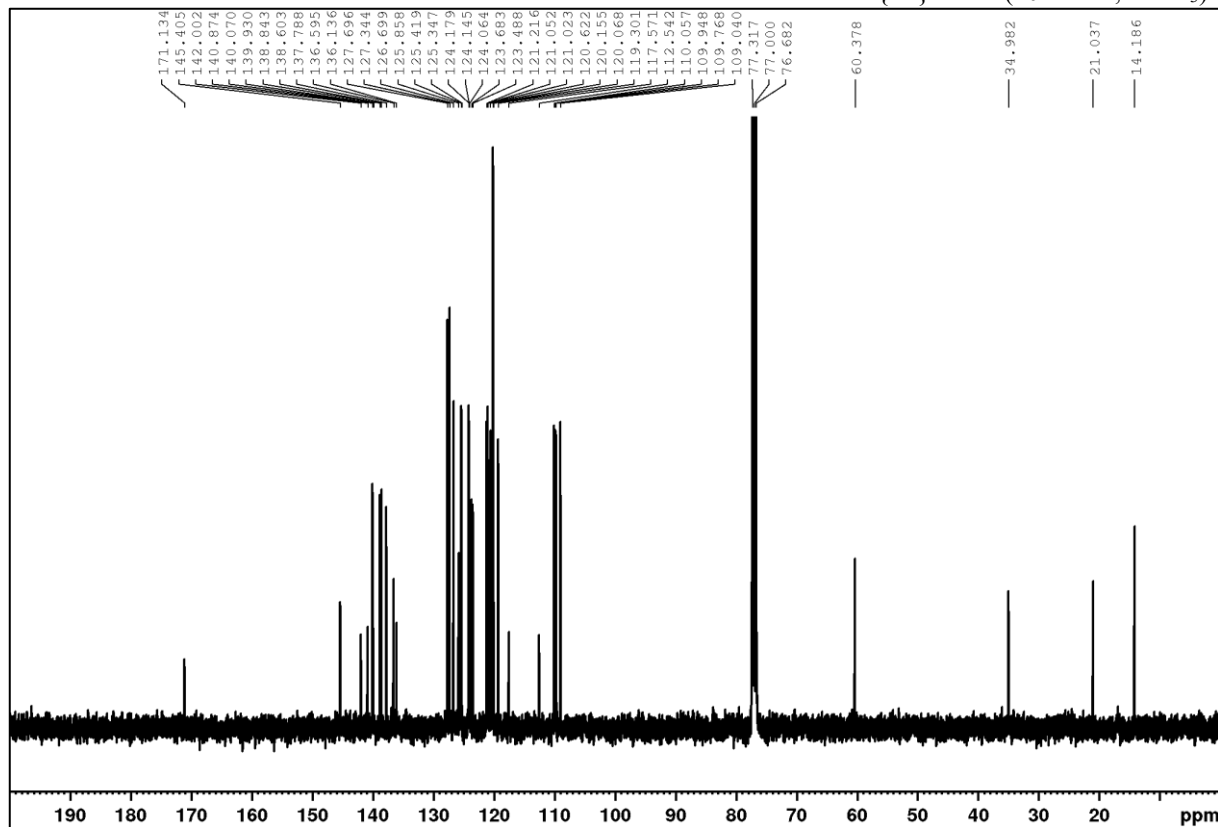
Figure 2.44. Fluorescence decay curve of photosubstitution product **4c**. 20 μM in MeCN.

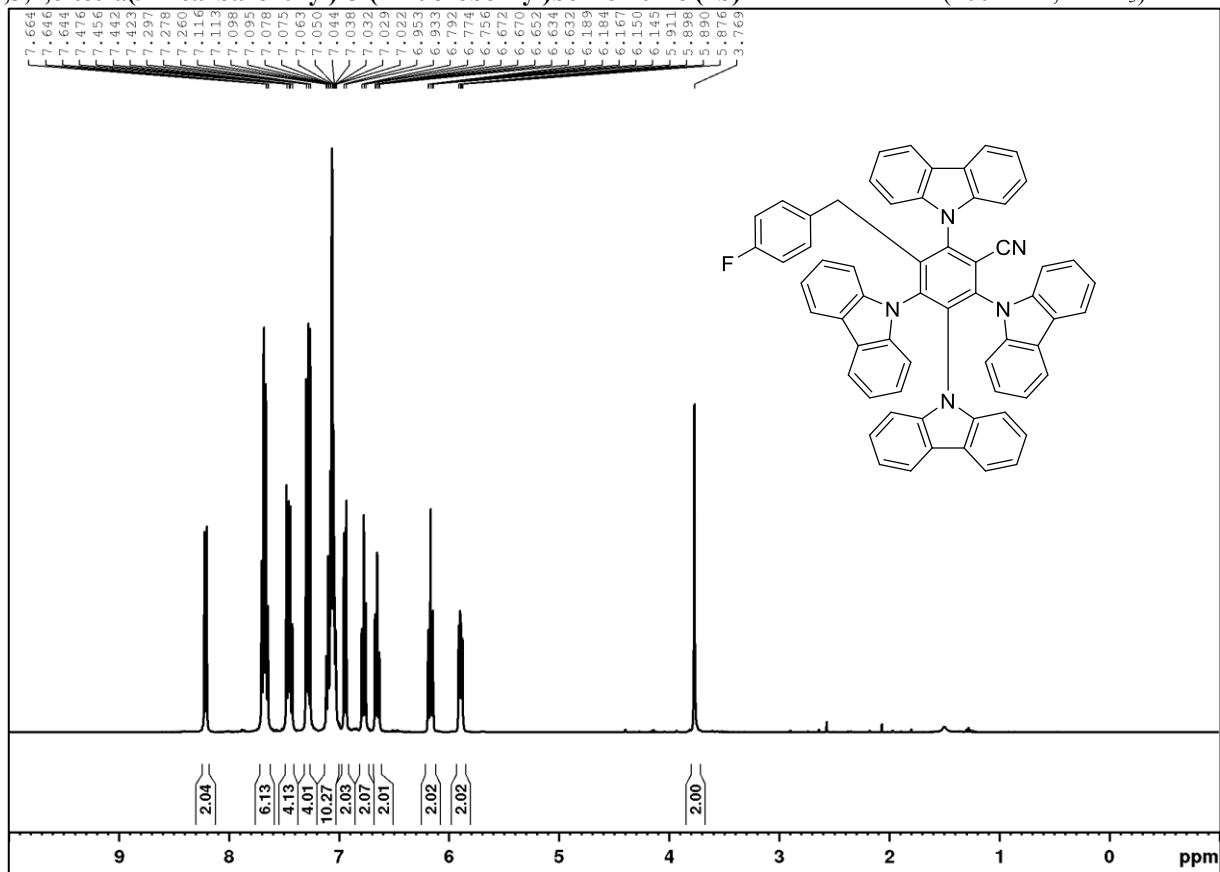
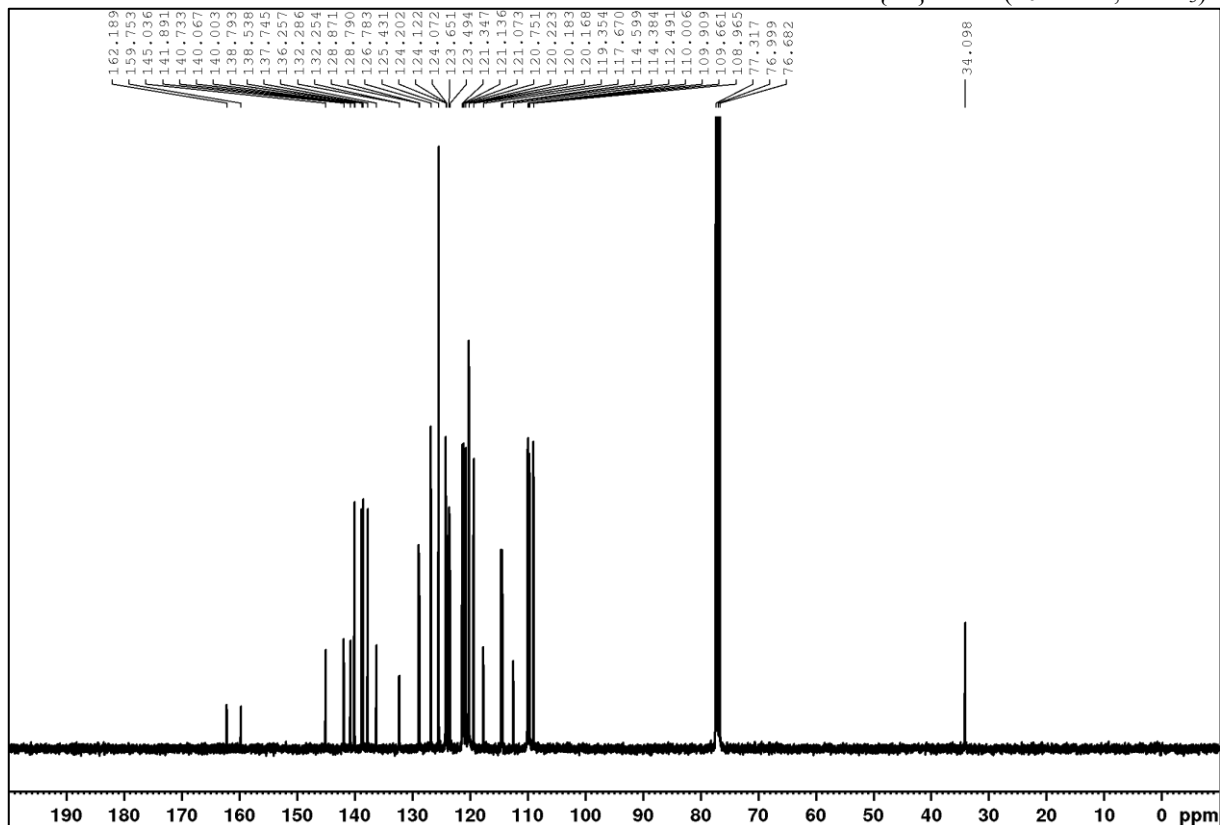
Lifetime τ in MeCN: 10.4 ns

7.2.3 NMR spectra

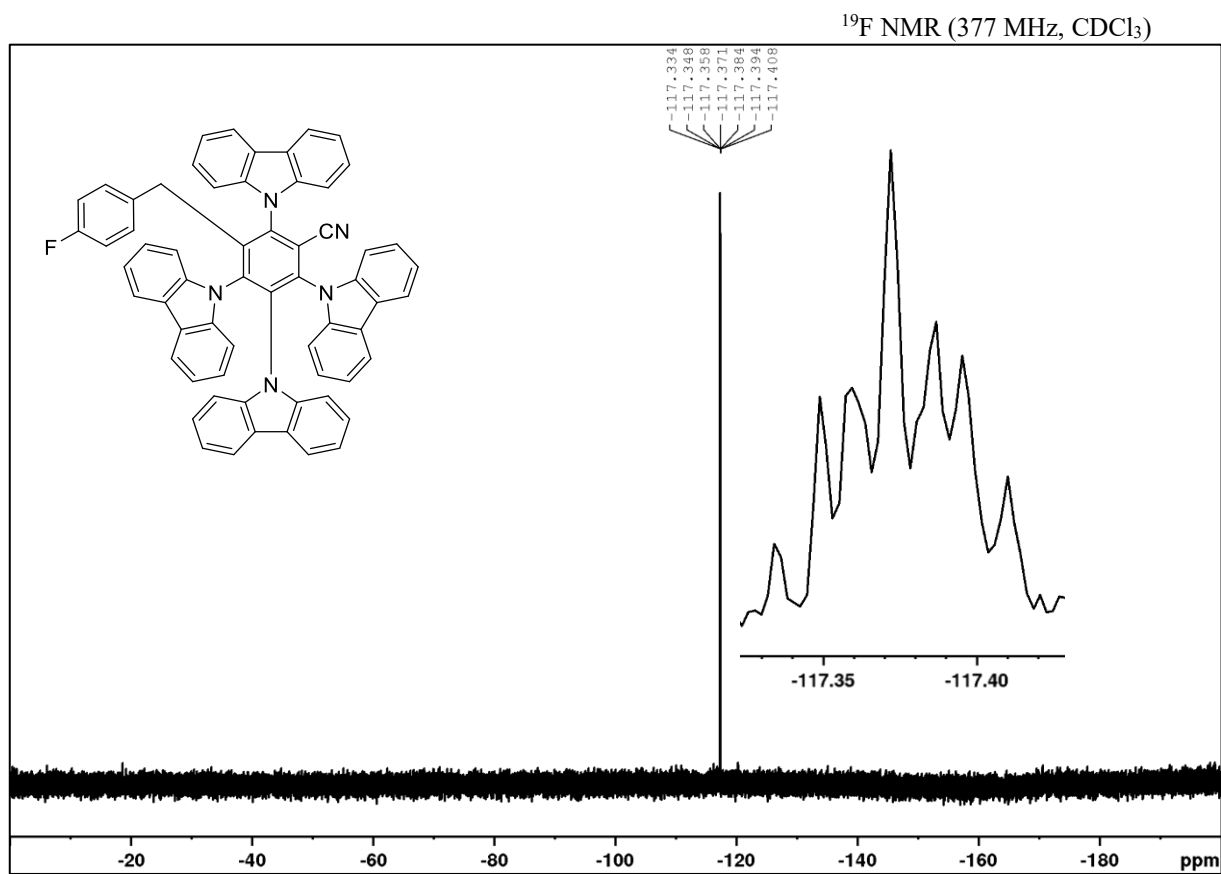
2,4,5,6-Tetrakis(carbazol-9-yl)-4,6-dicyanobenzene (4CzIPN, 1)

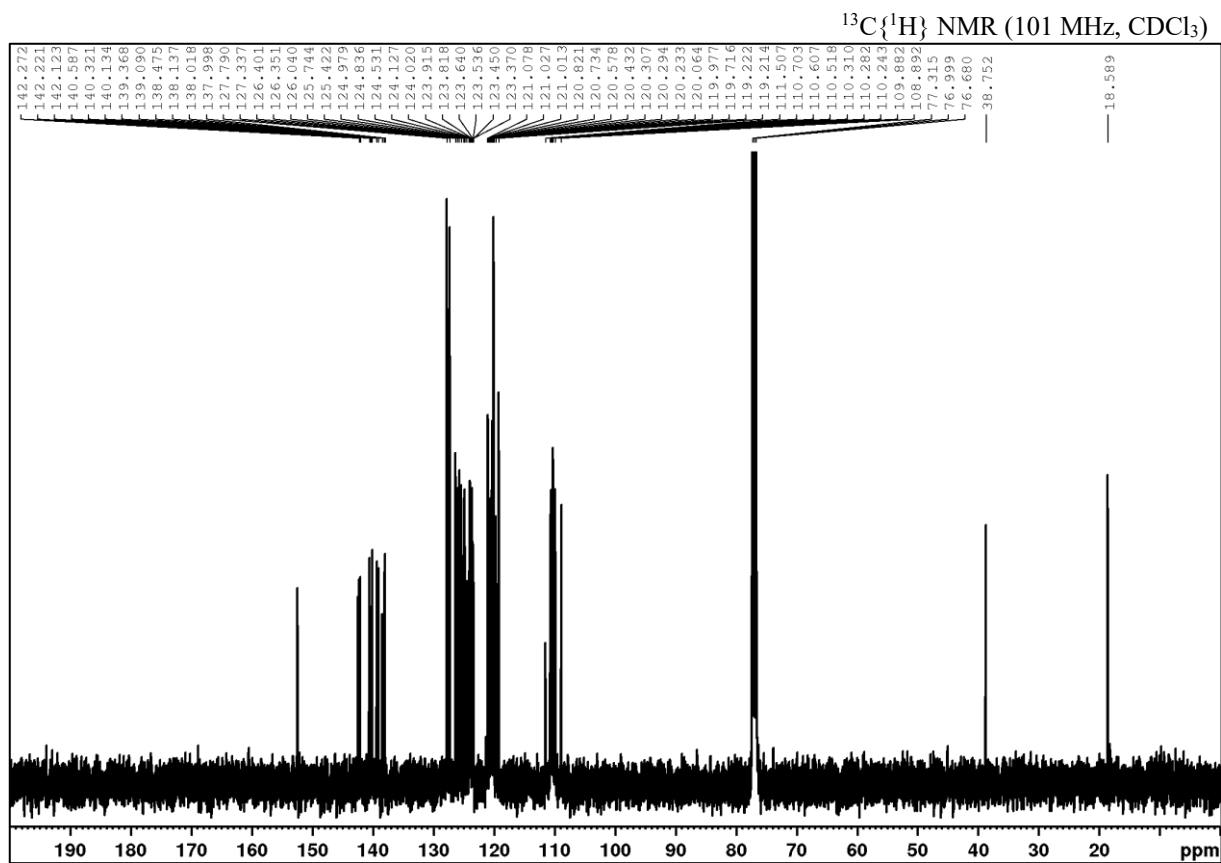
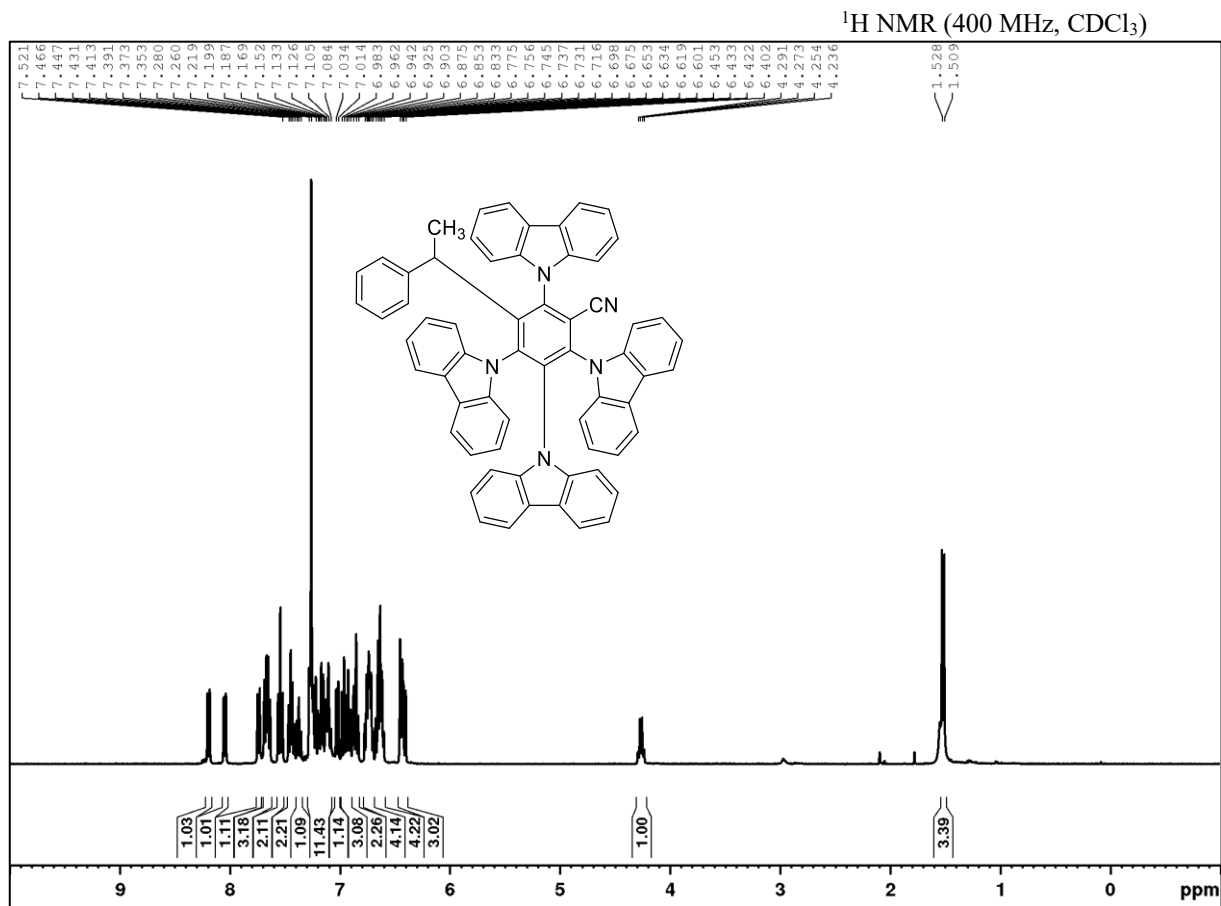
 ^1H NMR (400 MHz, CDCl_3)

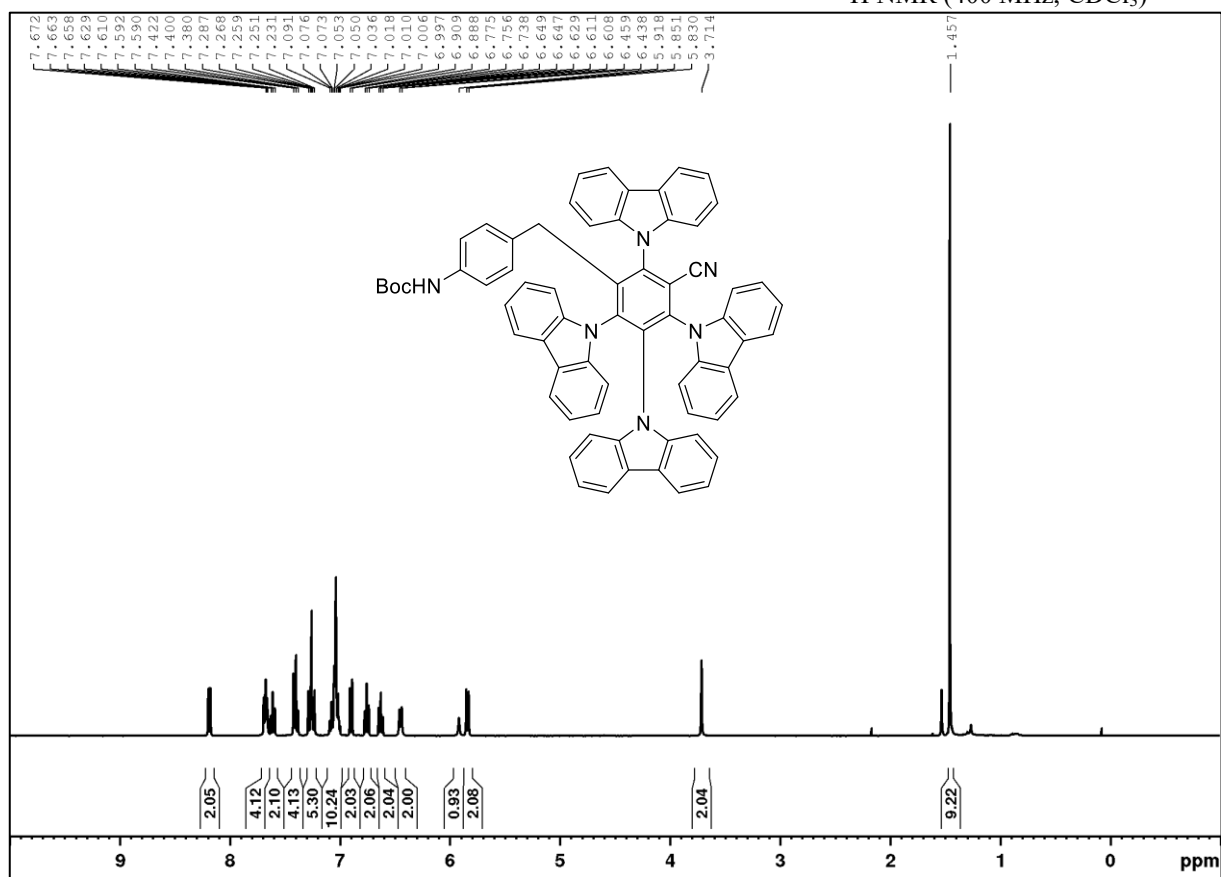
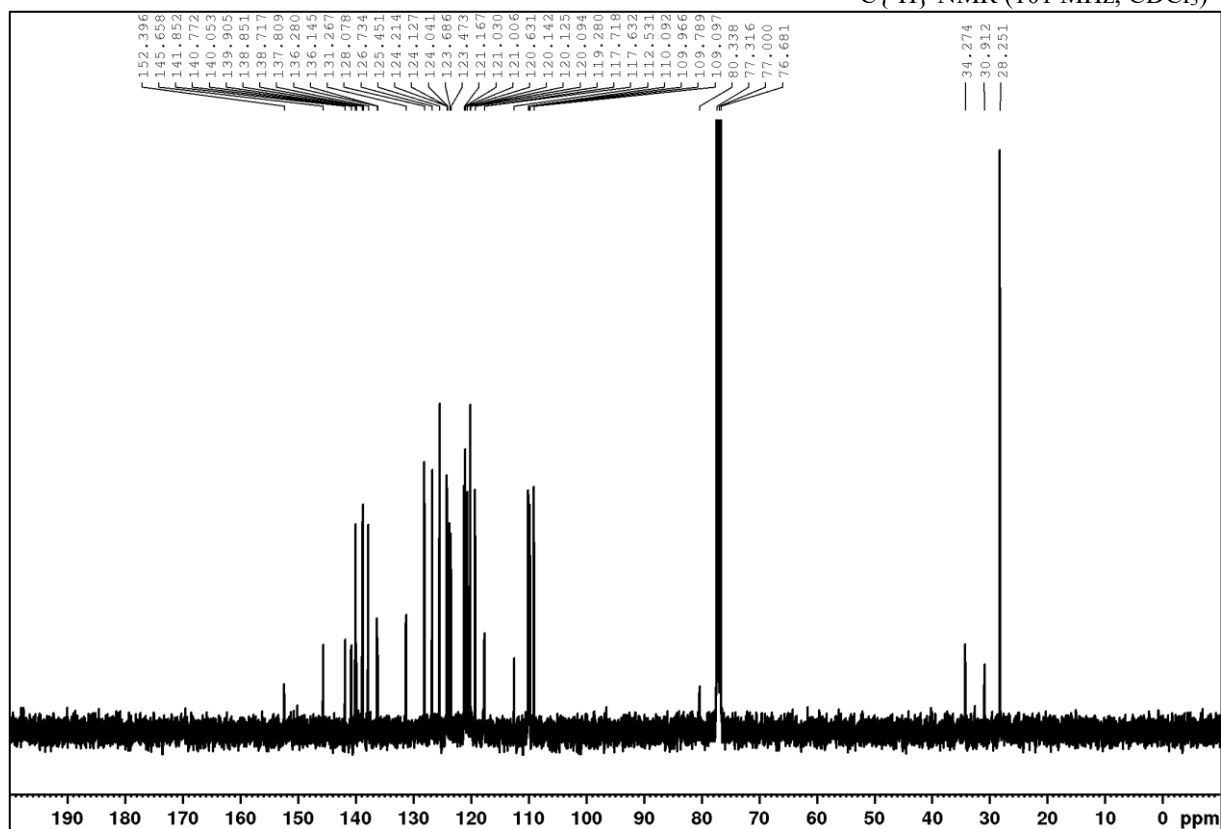
3-Benzyl-2,4,5,6-tetra(9*H*-carbazol-9-yl)benzonitrile (4CzBnBN, 2a)¹H NMR (400 MHz, CDCl₃)¹³C{¹H} NMR (101 MHz, CDCl₃)

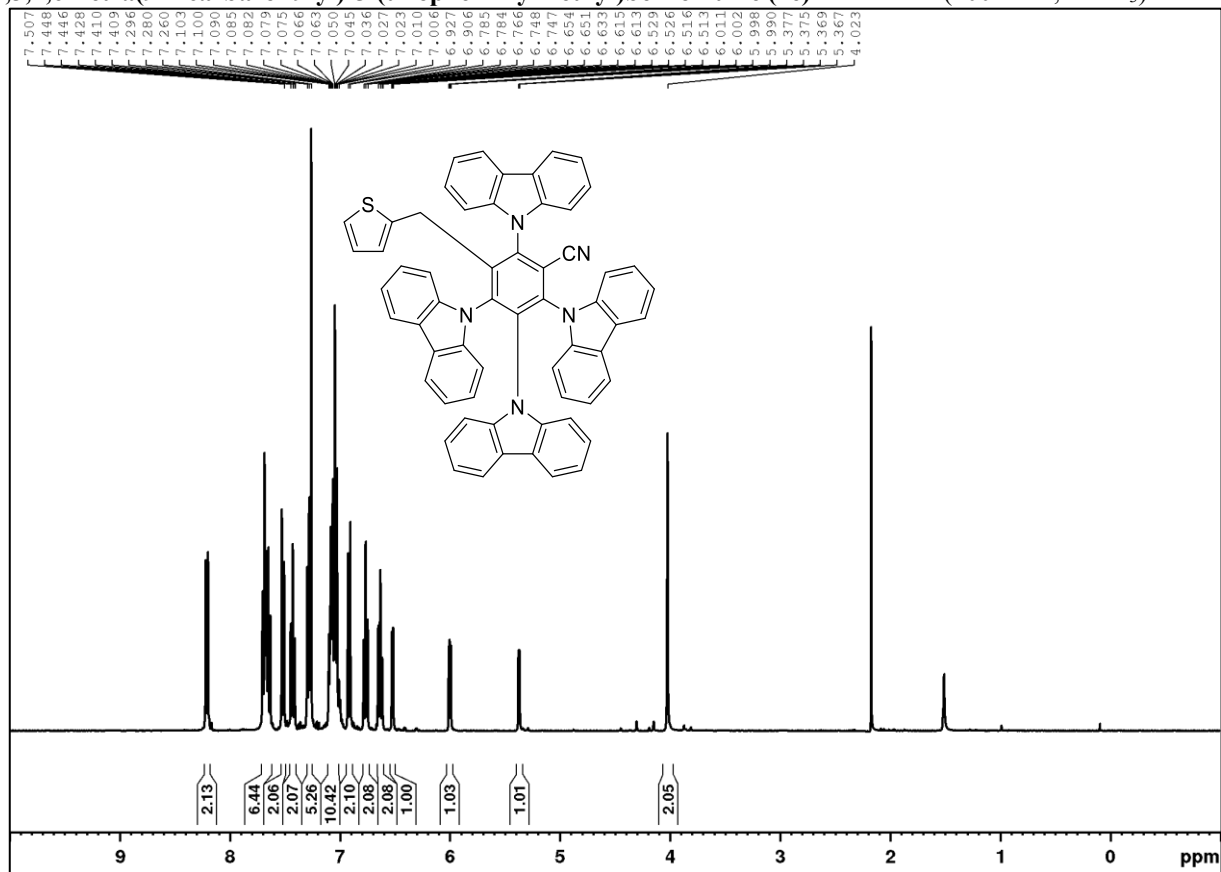
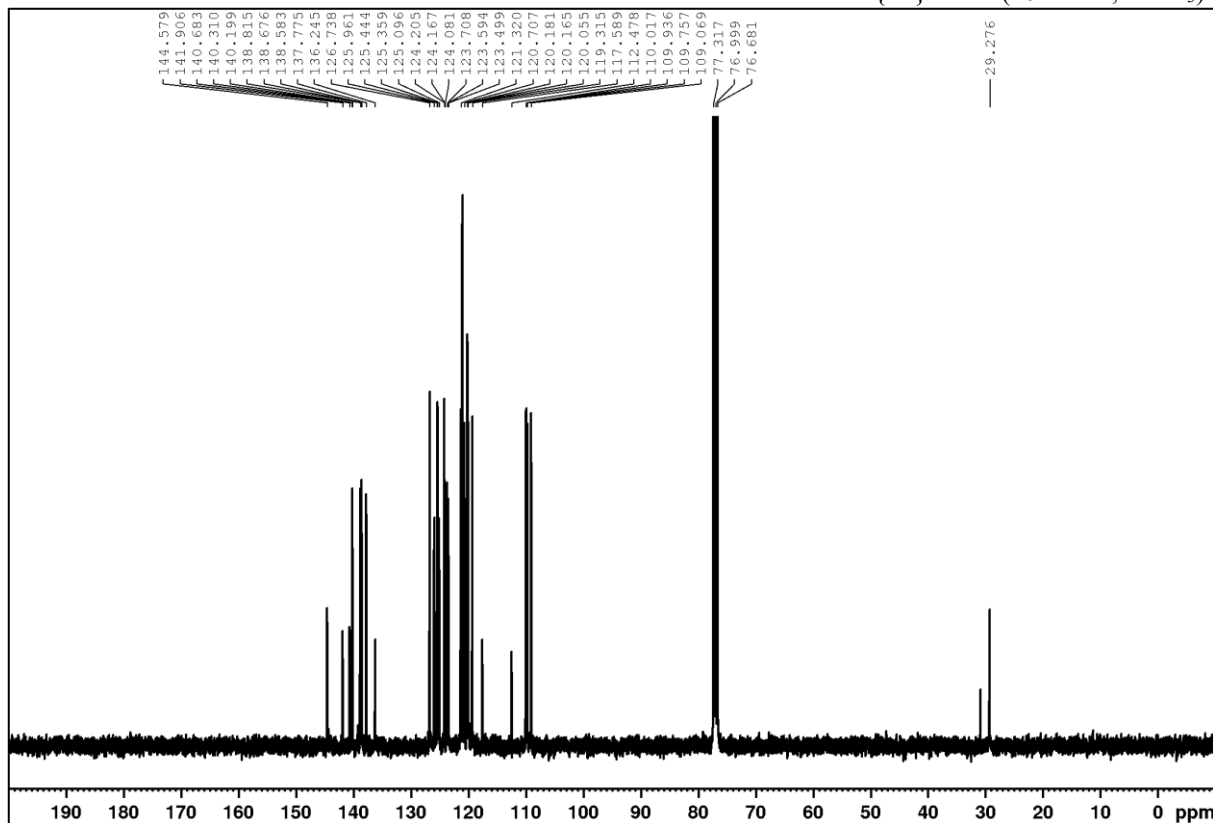
2,3,4,6-tetra(9H-carbazol-9-yl)-5-(4-fluorobenzyl)benzonitrile (2b) ^1H NMR (400 MHz, CDCl_3) $^{13}\text{C}\{^1\text{H}\}$ NMR (101 MHz, CDCl_3)

APPENDIX

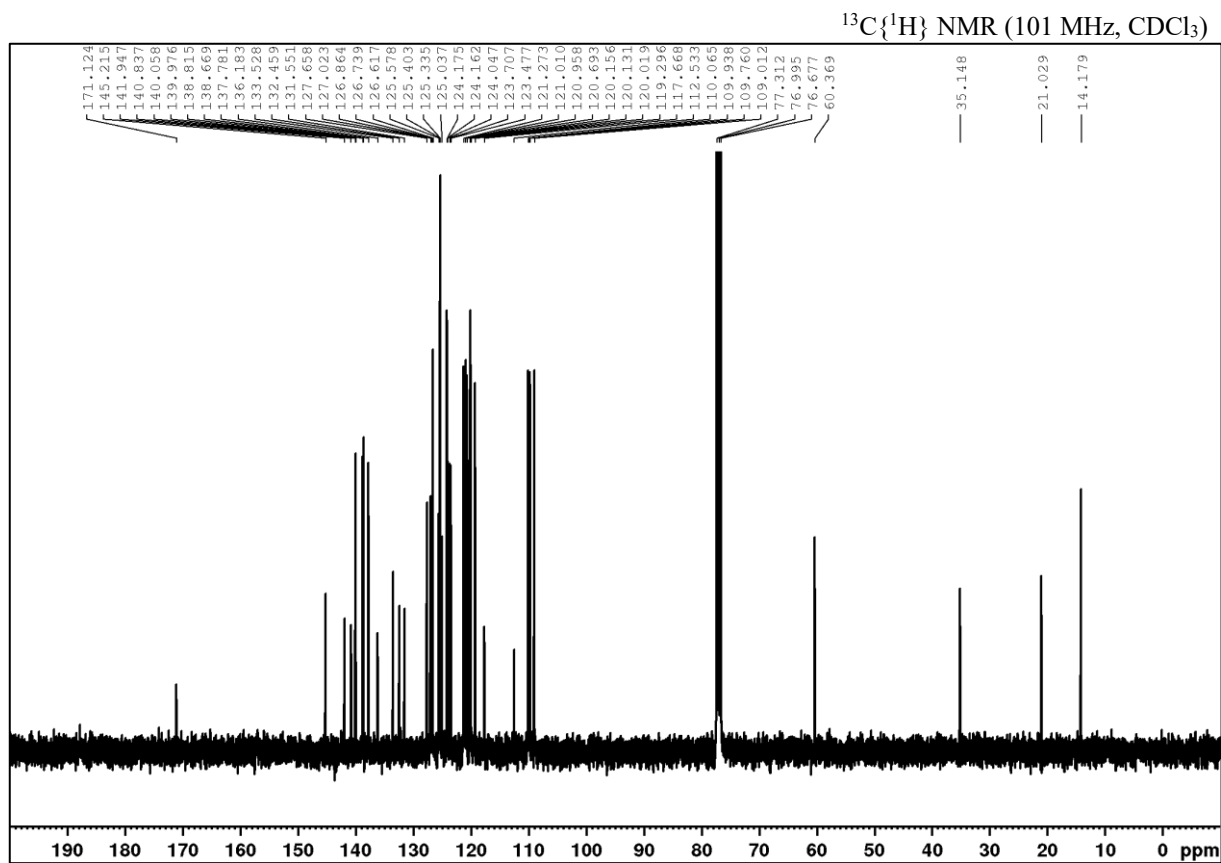
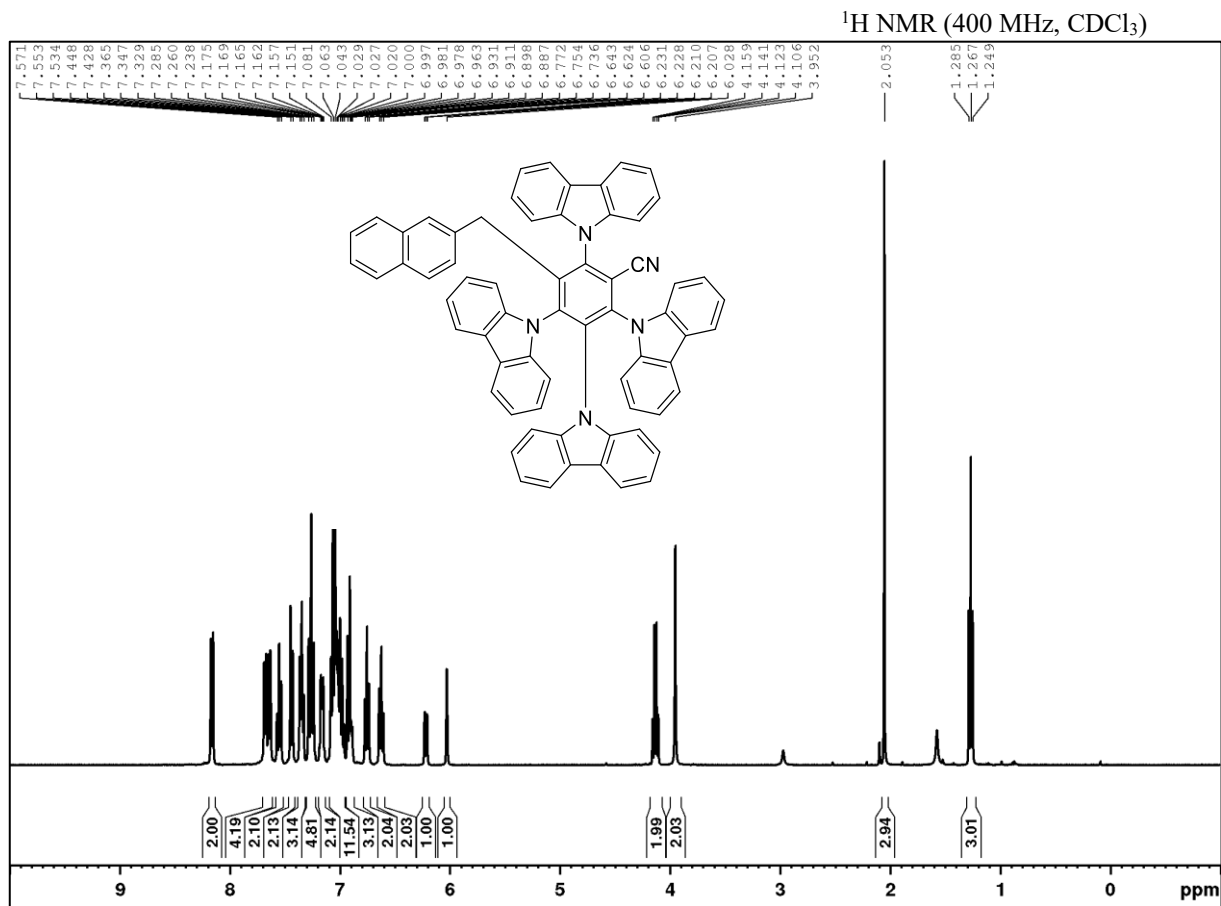


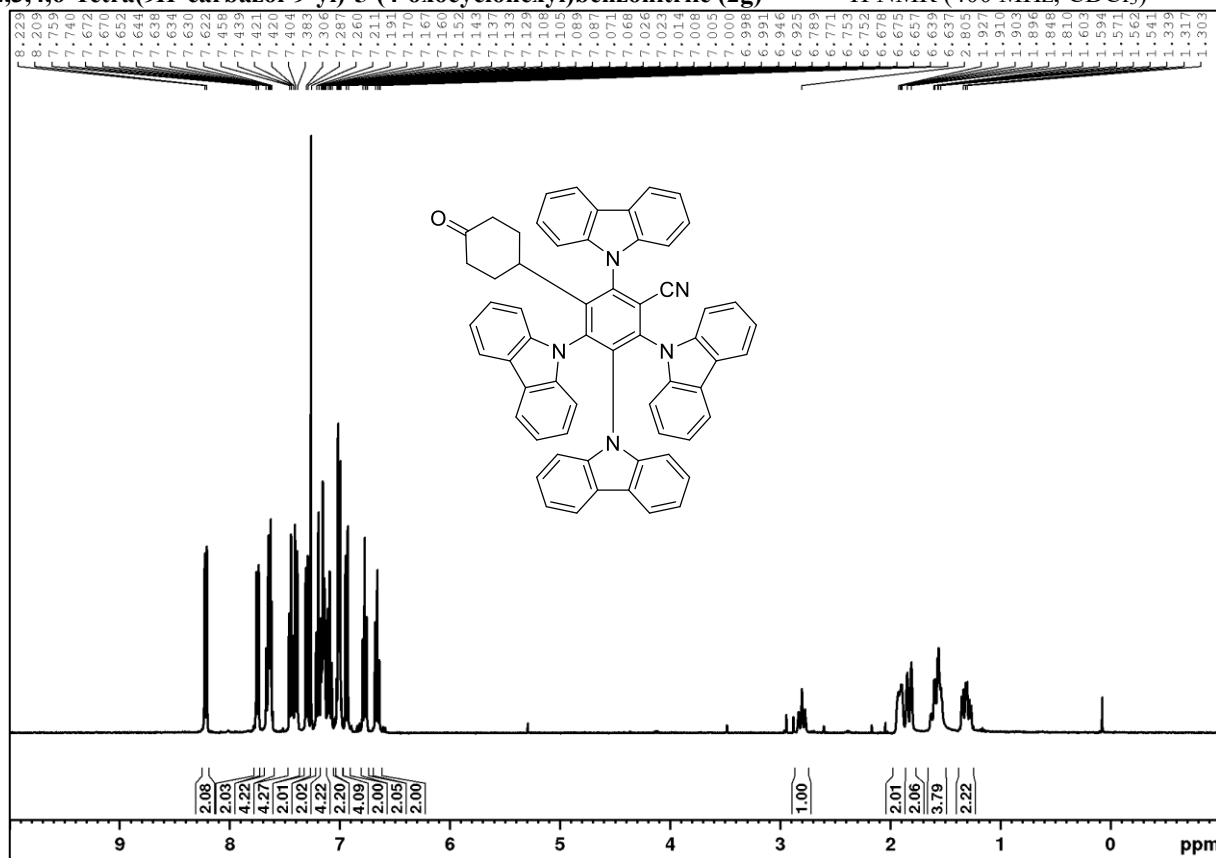
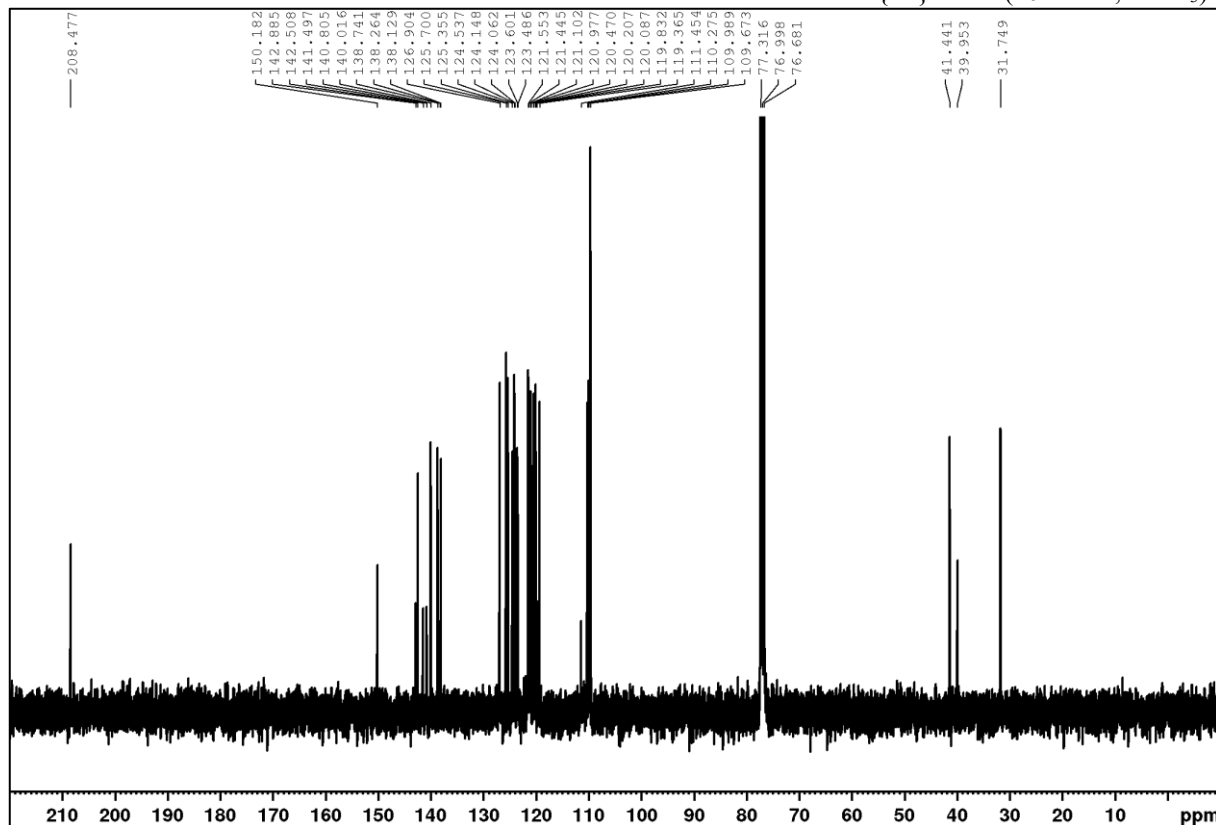
2,3,4,6-tetra(9*H*-carbazol-9-yl)-5-(1-phenylethyl)benzonitrile (4CzPEBN, 2c)

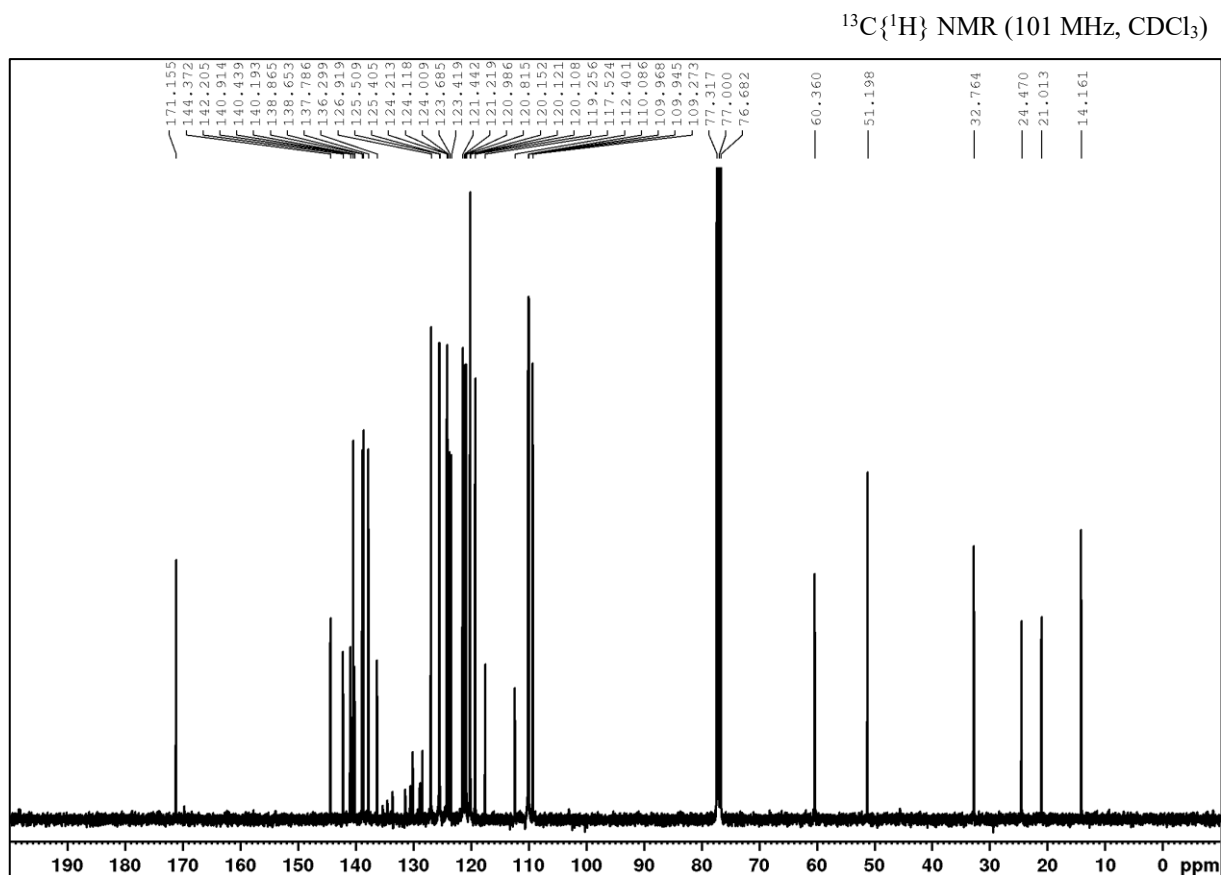
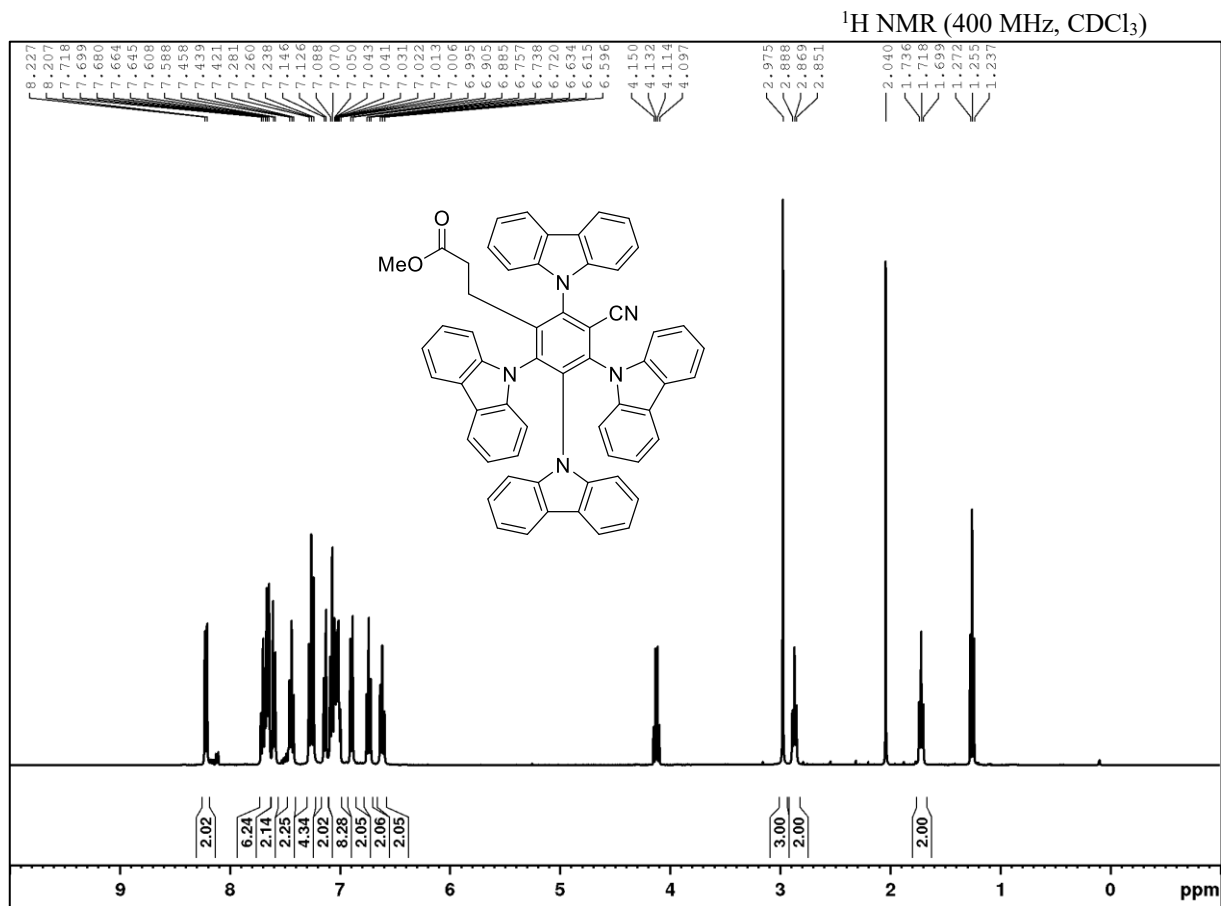
tert-Butyl (4-(2,3,4,6-tetra(9*H*-carbazol-9-yl)-5-cyanobenzyl)phenyl)carbamate (2d)¹H NMR (400 MHz, CDCl₃)¹³C{¹H} NMR (101 MHz, CDCl₃)

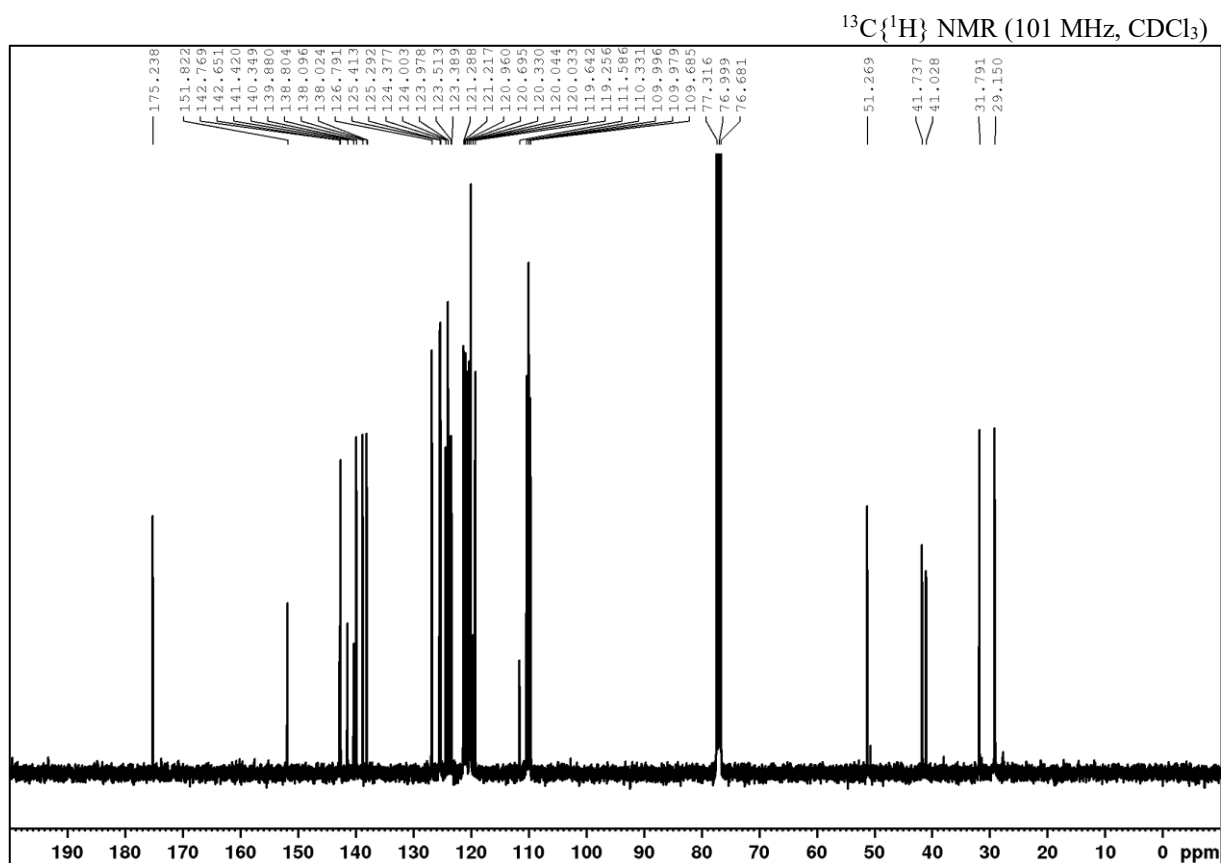
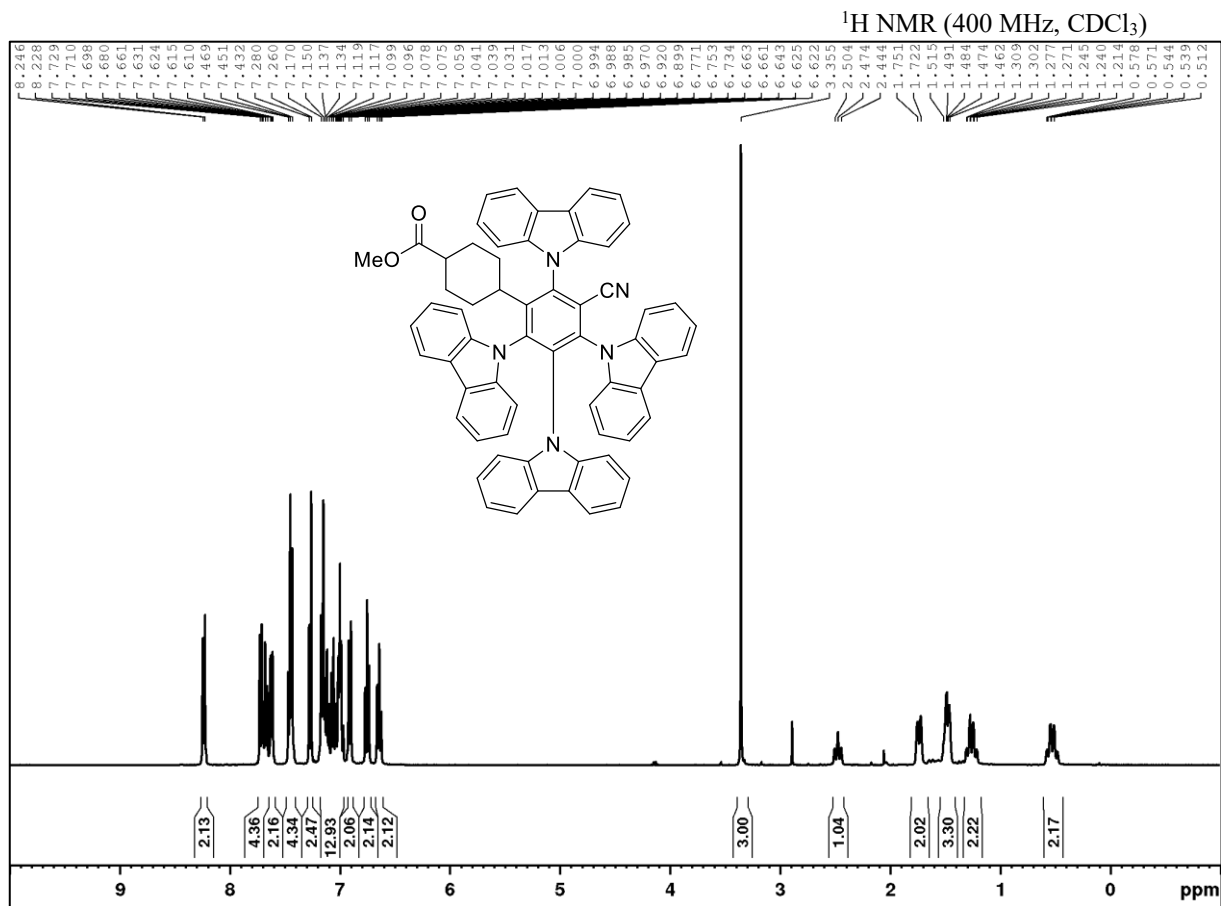
2,3,4,6-Tetra(9H-carbazol-9-yl)-5-(thiophen-2-ylmethyl)benzonitrile (2e) ^1H NMR (400 MHz, CDCl_3) $^{13}\text{C}\{^1\text{H}\}$ NMR (101 MHz, CDCl_3)

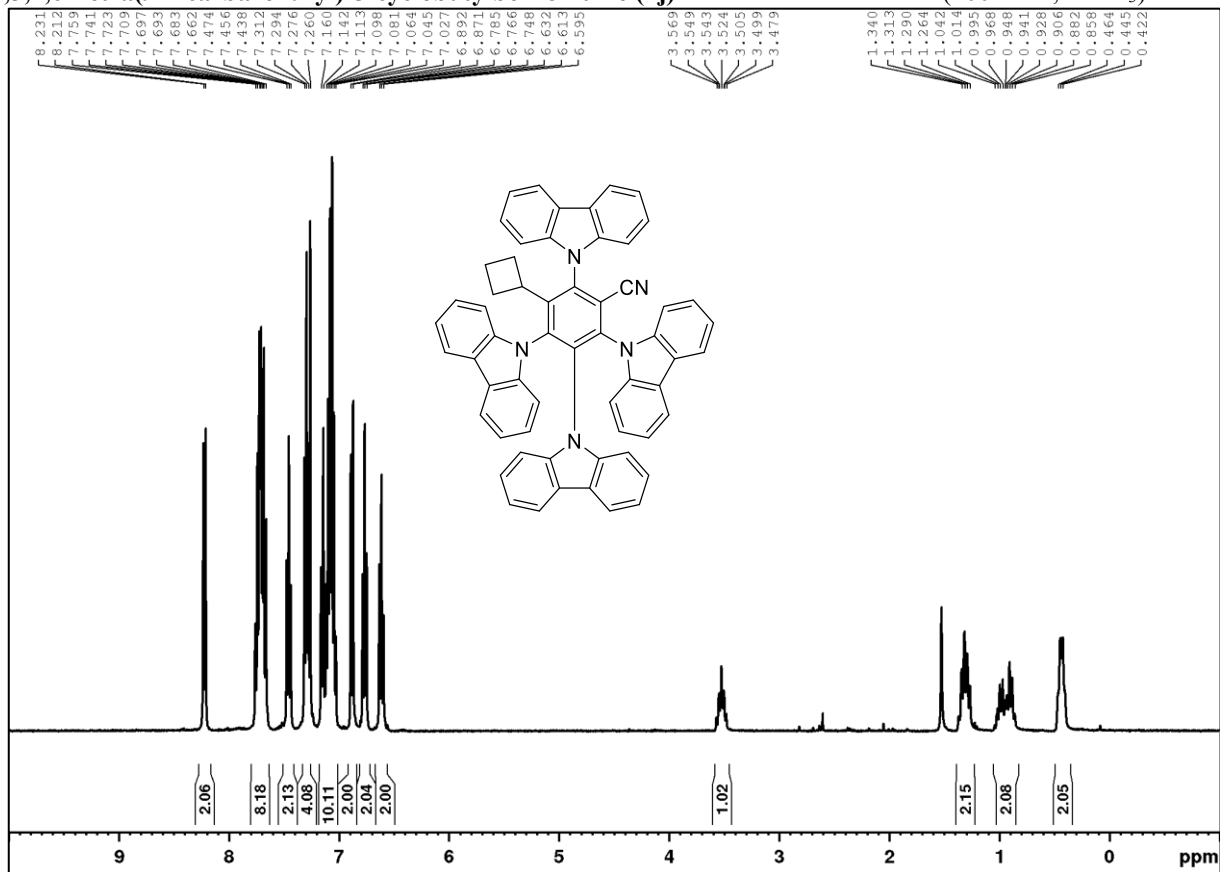
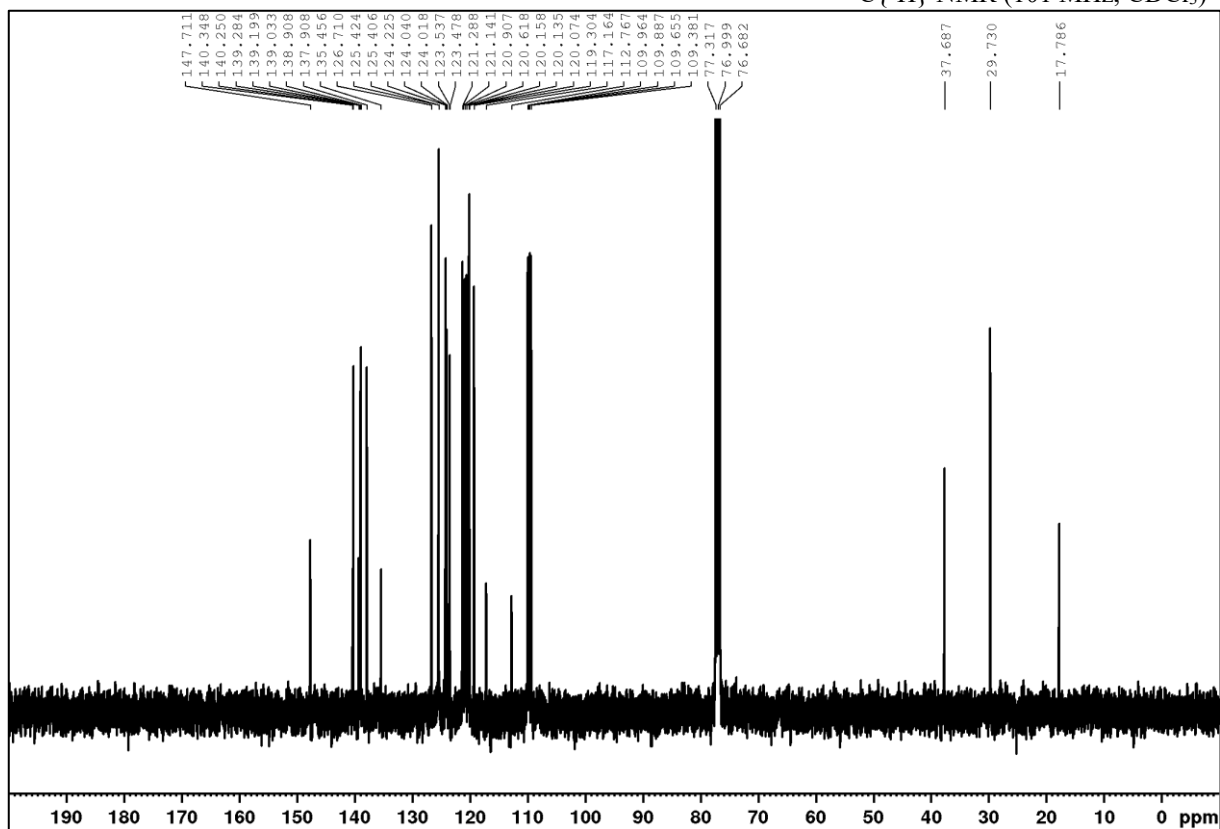
The NMR tube was not sufficiently dried after cleaning and thus a signal for acetone is present.

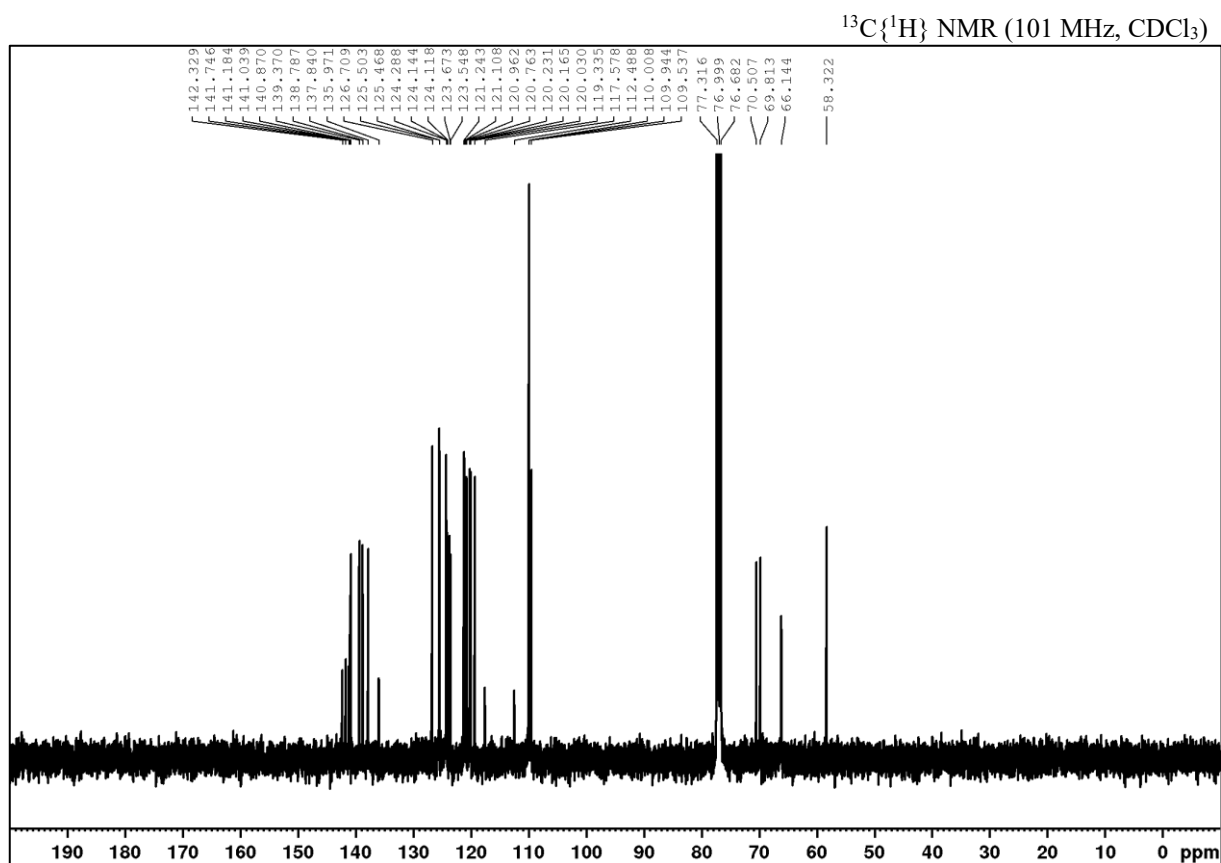
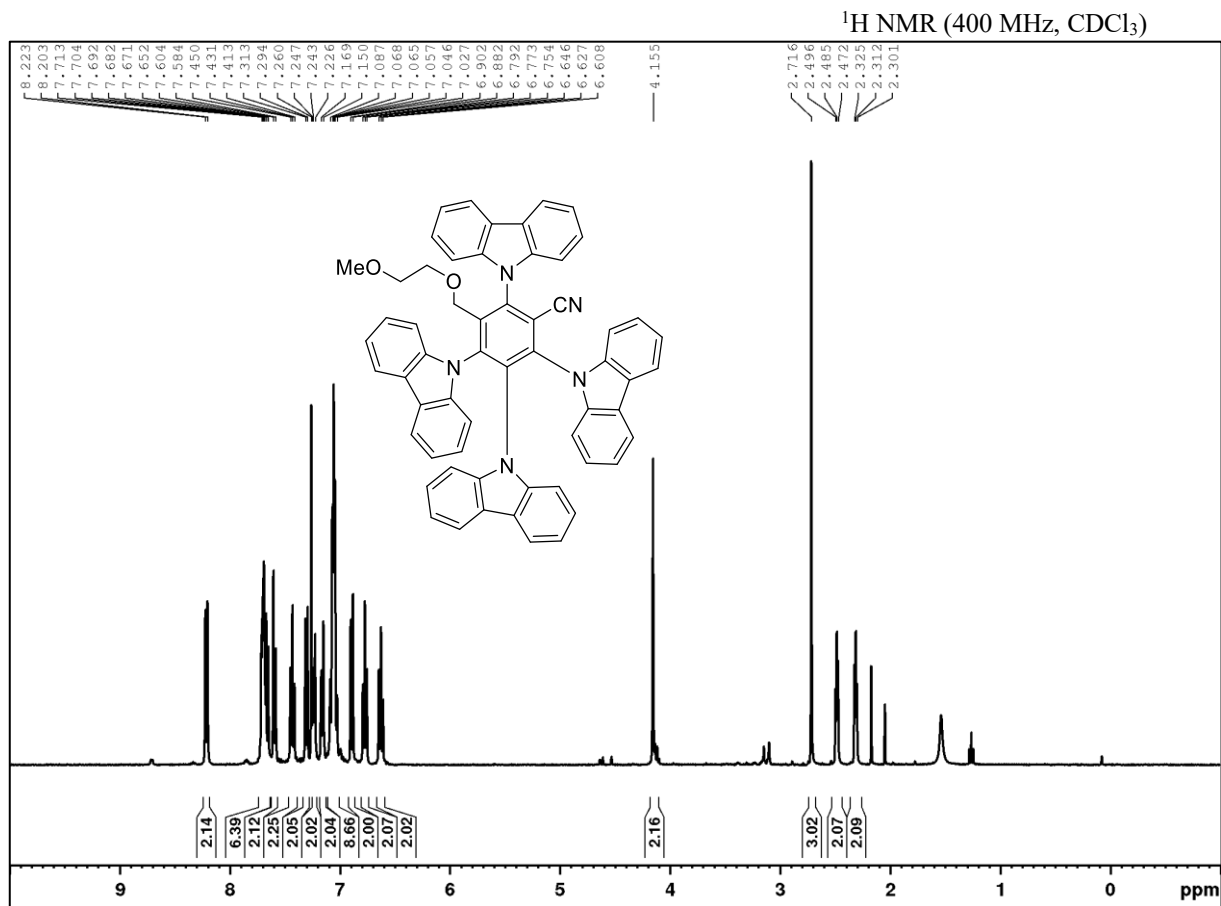
2,3,4,6-Tetra(9*H*-carbazol-9-yl)-5-(naphthalen-2-ylmethyl)benzonitrile (2f)

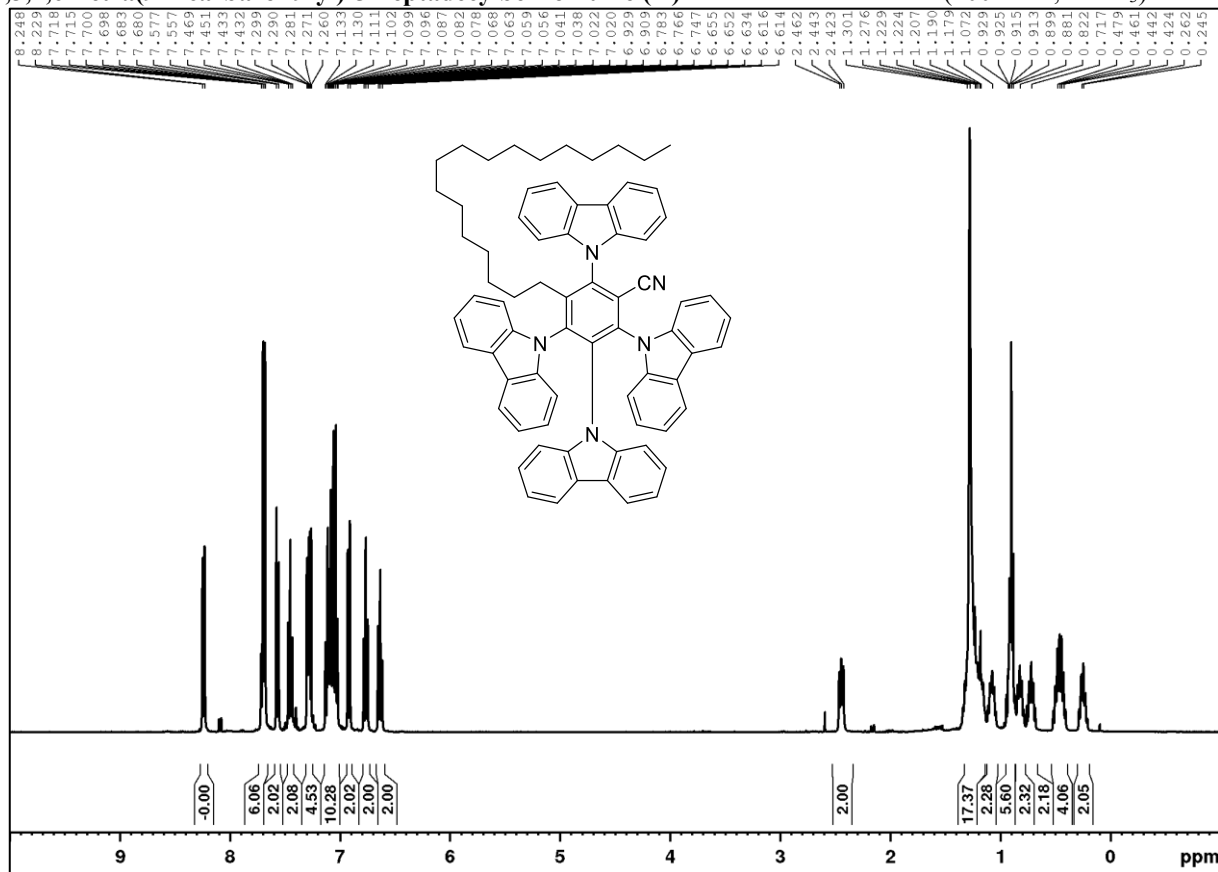
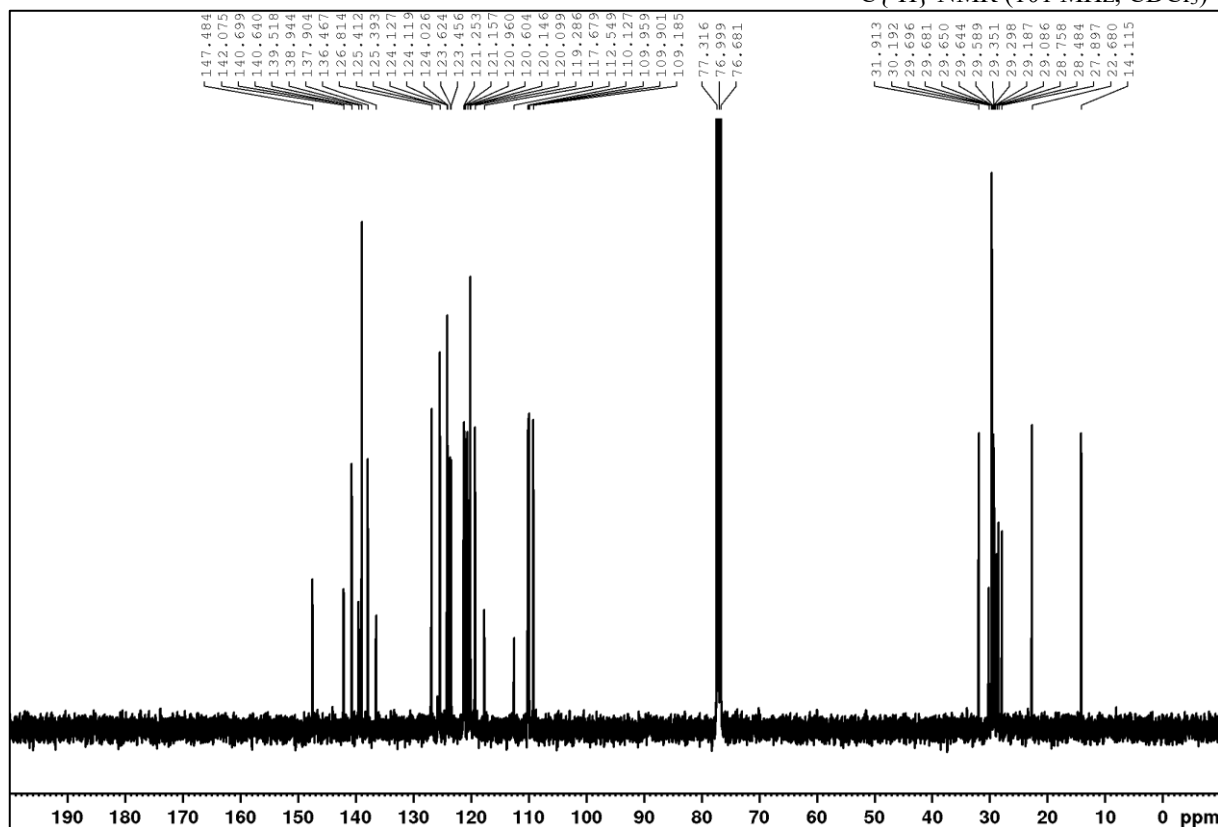
2,3,4,6-Tetra(9H-carbazol-9-yl)-5-(4-oxocyclohexyl)benzonitrile (2g) ^1H NMR (400 MHz, CDCl_3) $^{13}\text{C}\{^1\text{H}\}$ NMR (101 MHz, CDCl_3)

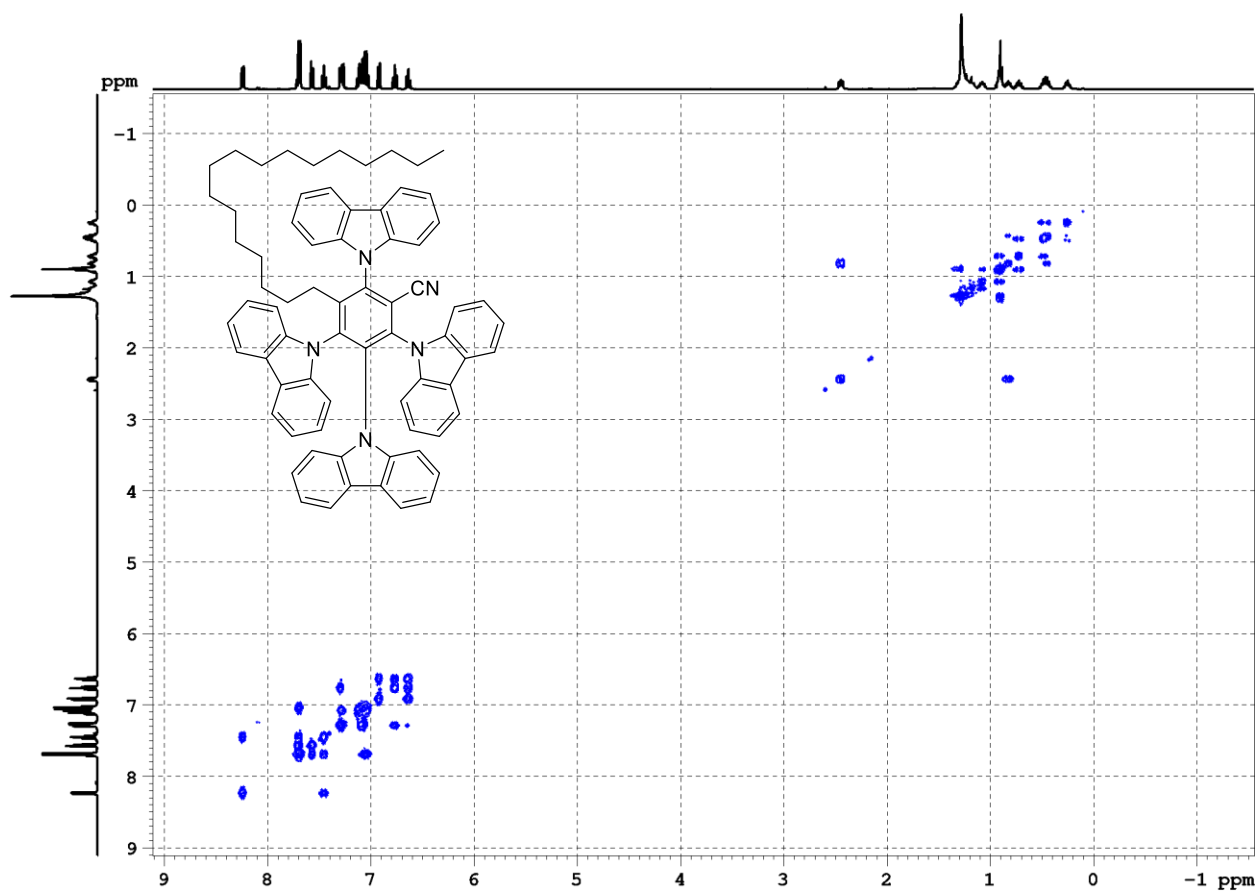
Methyl 3-(2,3,4,6-tetra(9*H*-carbazol-9-yl)-5-cyanophenyl)propanoate (2h)

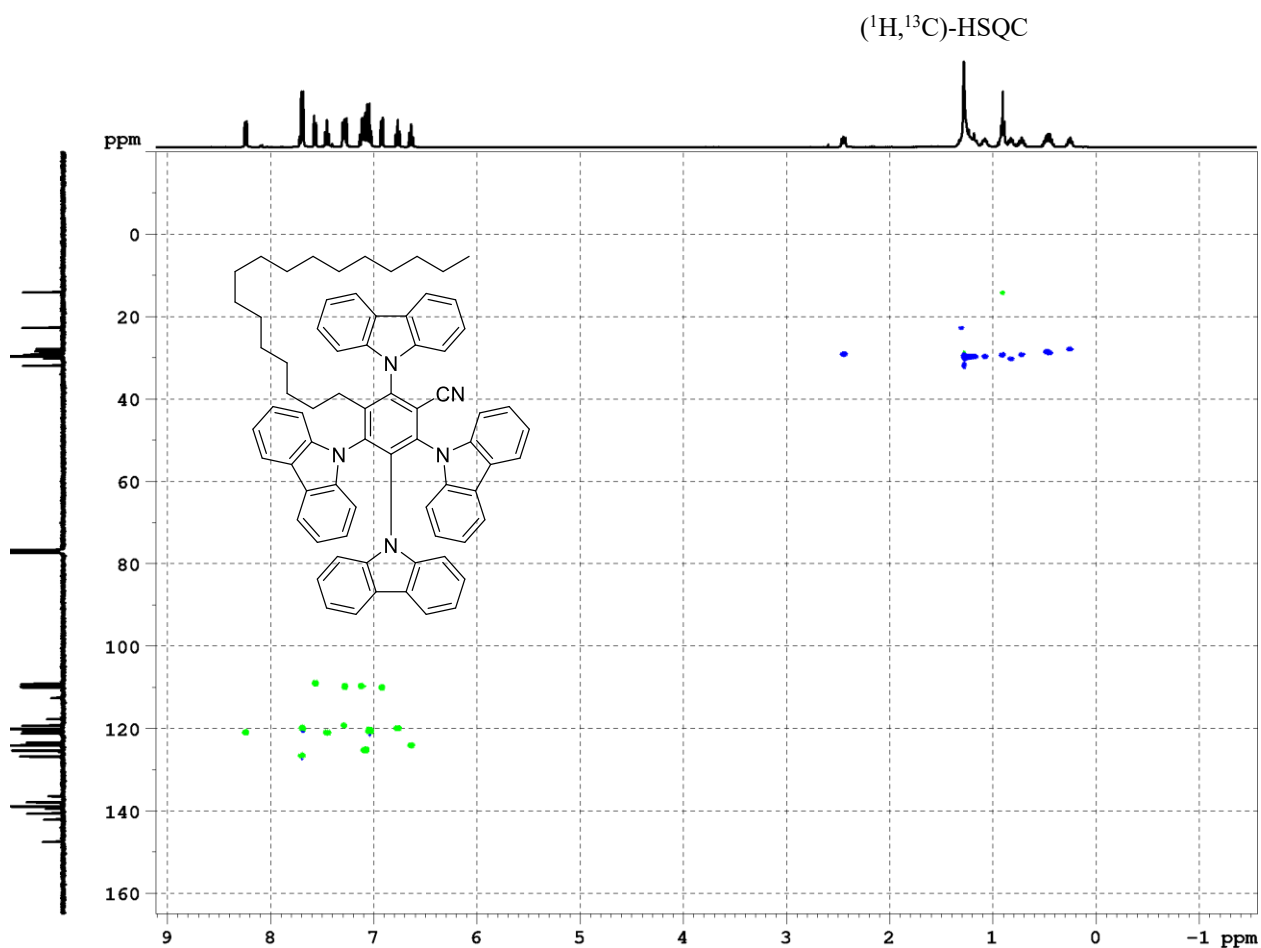
Methyl 4-(2,3,4,6-tetra(9*H*-carbazol-9-yl)-5-cyanophenyl)cyclohexane-1-carboxylate (**2i**)

2,3,4,6-Tetra(9*H*-carbazol-9-yl)-5-cyclobutylbenzonitrile (2j) **^1H NMR (400 MHz, CDCl_3)** **$^{13}\text{C}\{^1\text{H}\}$ NMR (101 MHz, CDCl_3)**

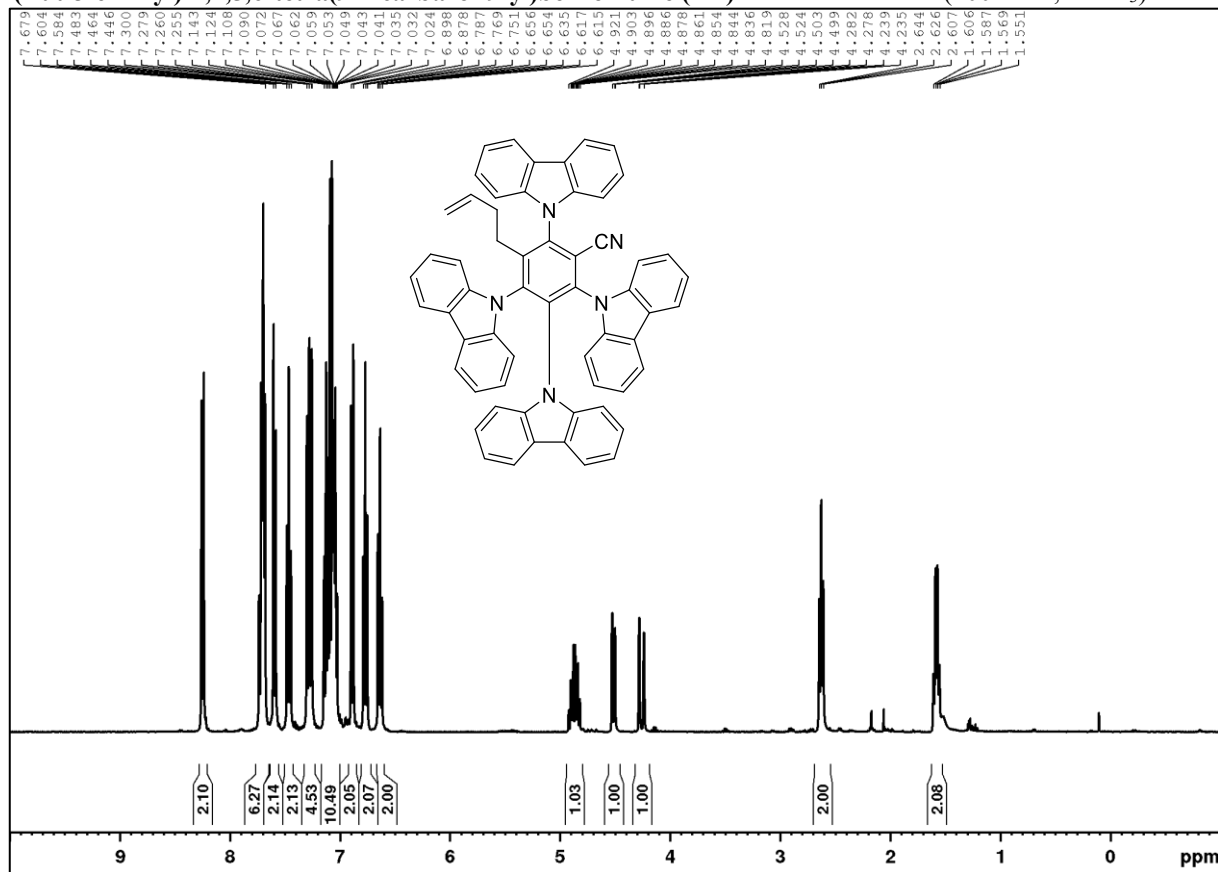
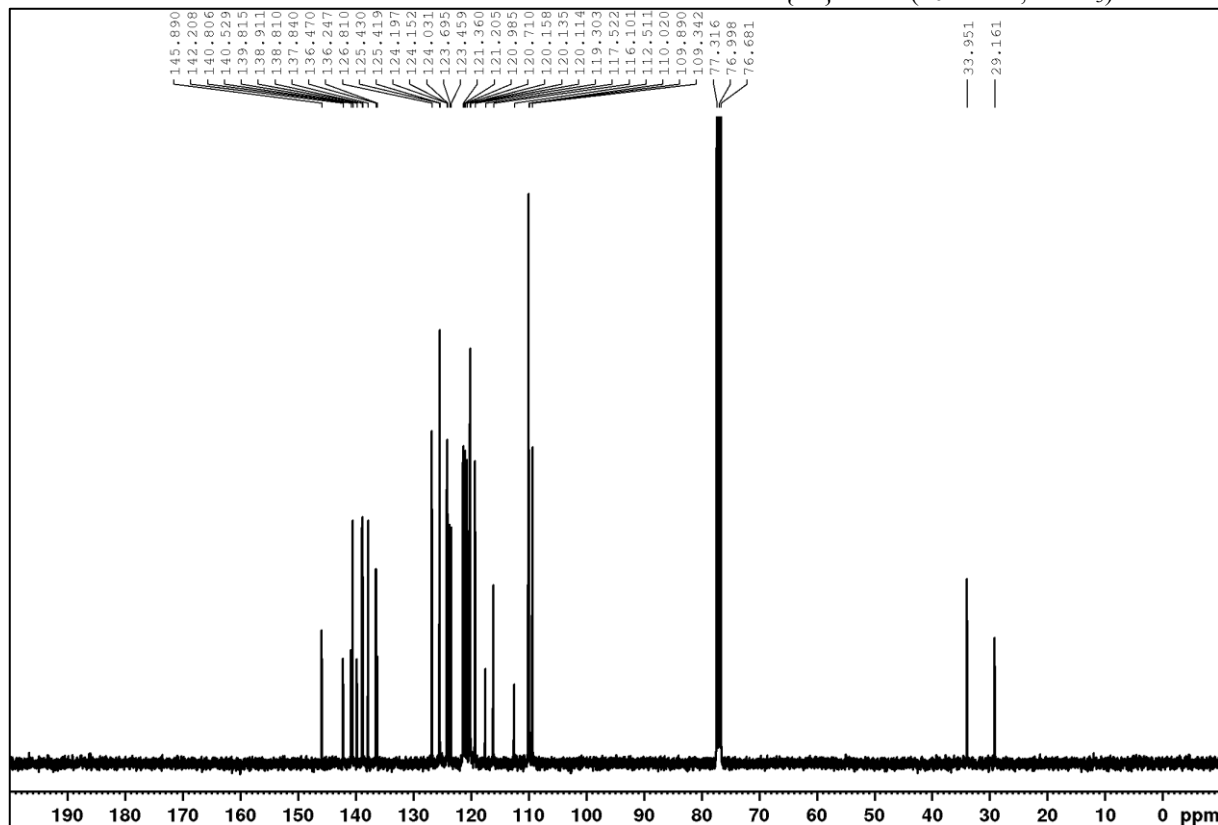
2,3,4,6-Tetra(9H-carbazol-9-yl)-5-((2-methoxyethoxy)methyl)benzonitrile (2k)

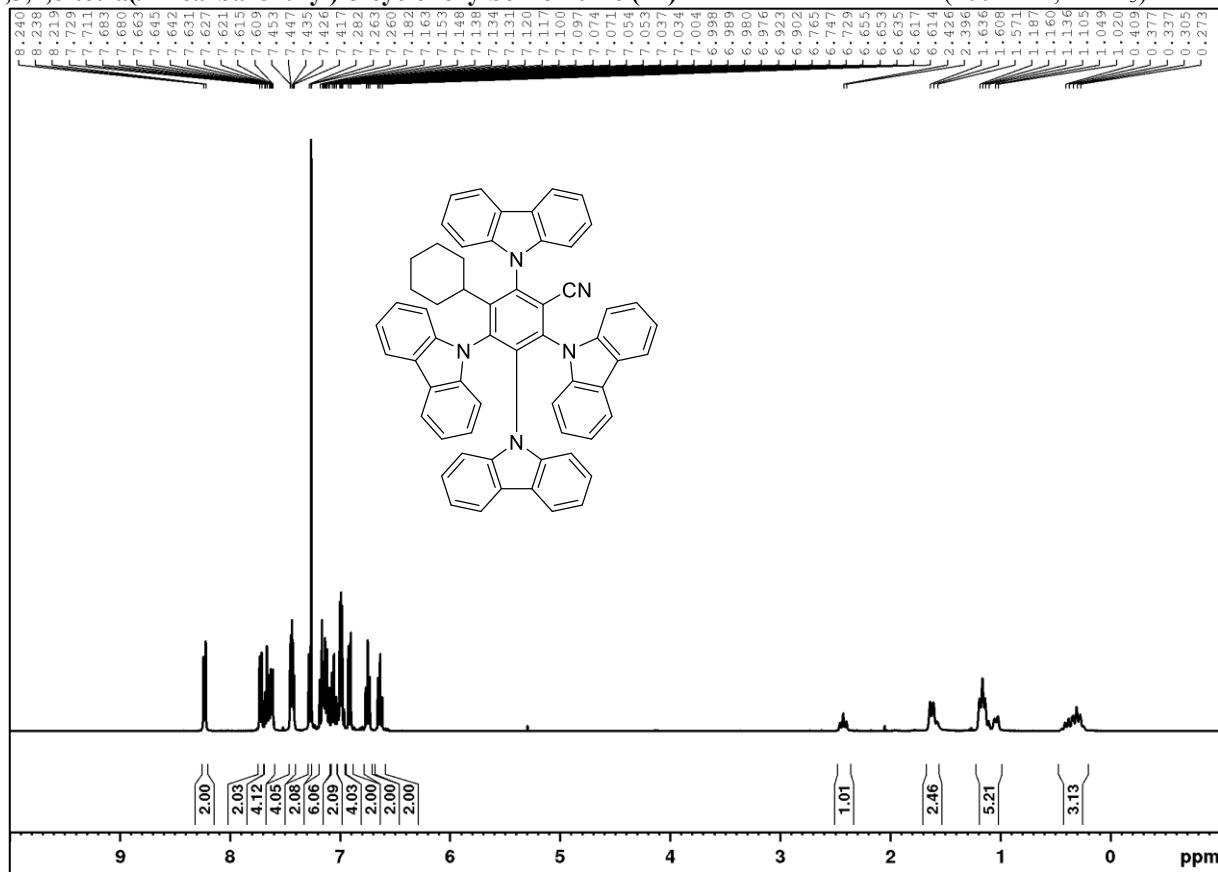
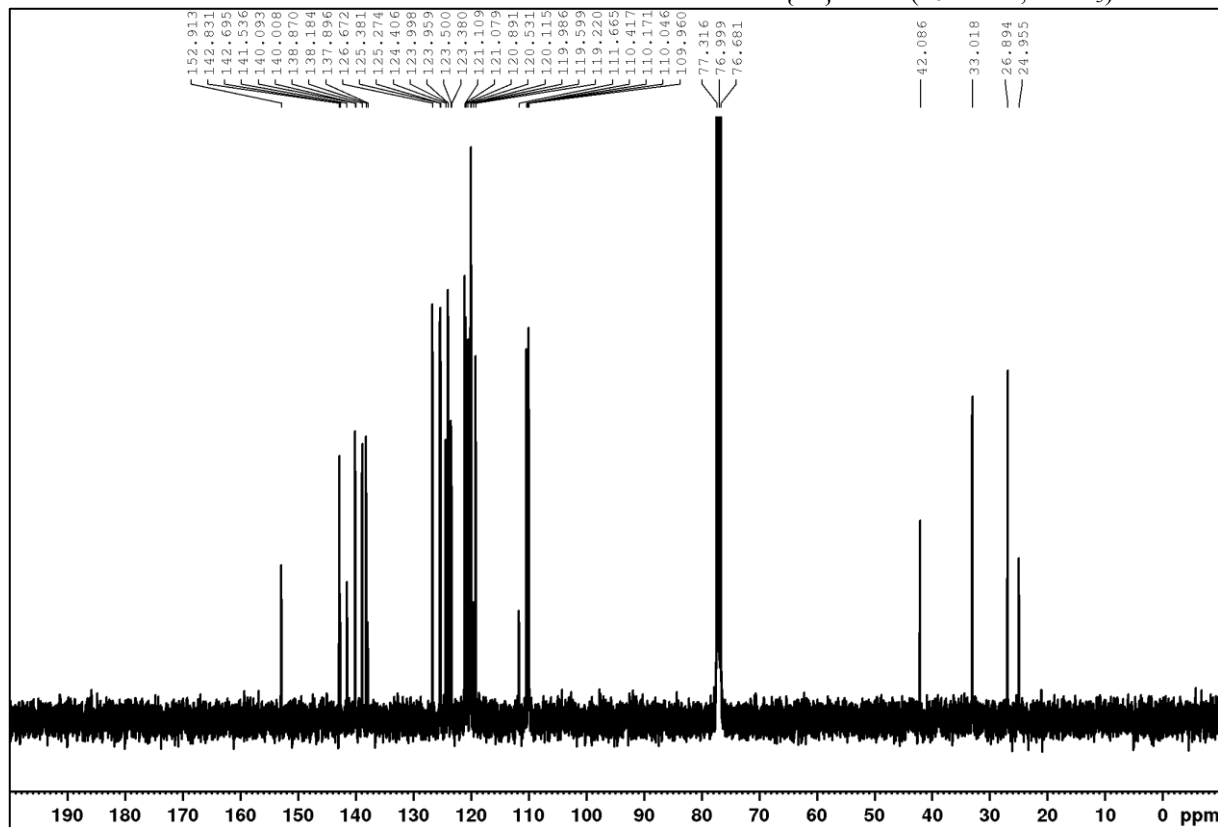
2,3,4,6-Tetra(9*H*-carbazol-9-yl)-5-heptadecylbenzonitrile (21)¹H NMR (400 MHz, CDCl₃)¹³C{¹H} NMR (101 MHz, CDCl₃)

$(^1\text{H}, ^1\text{H})\text{-COSY}$ 

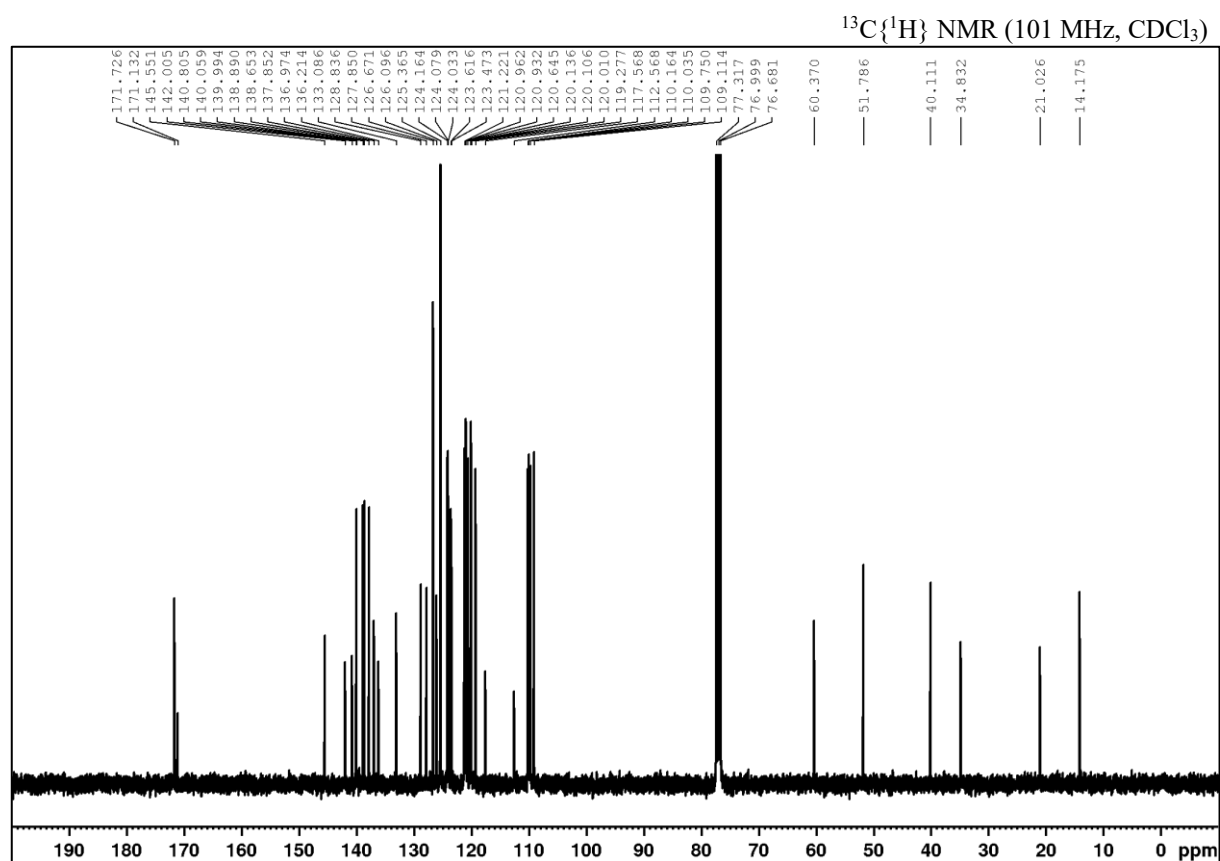
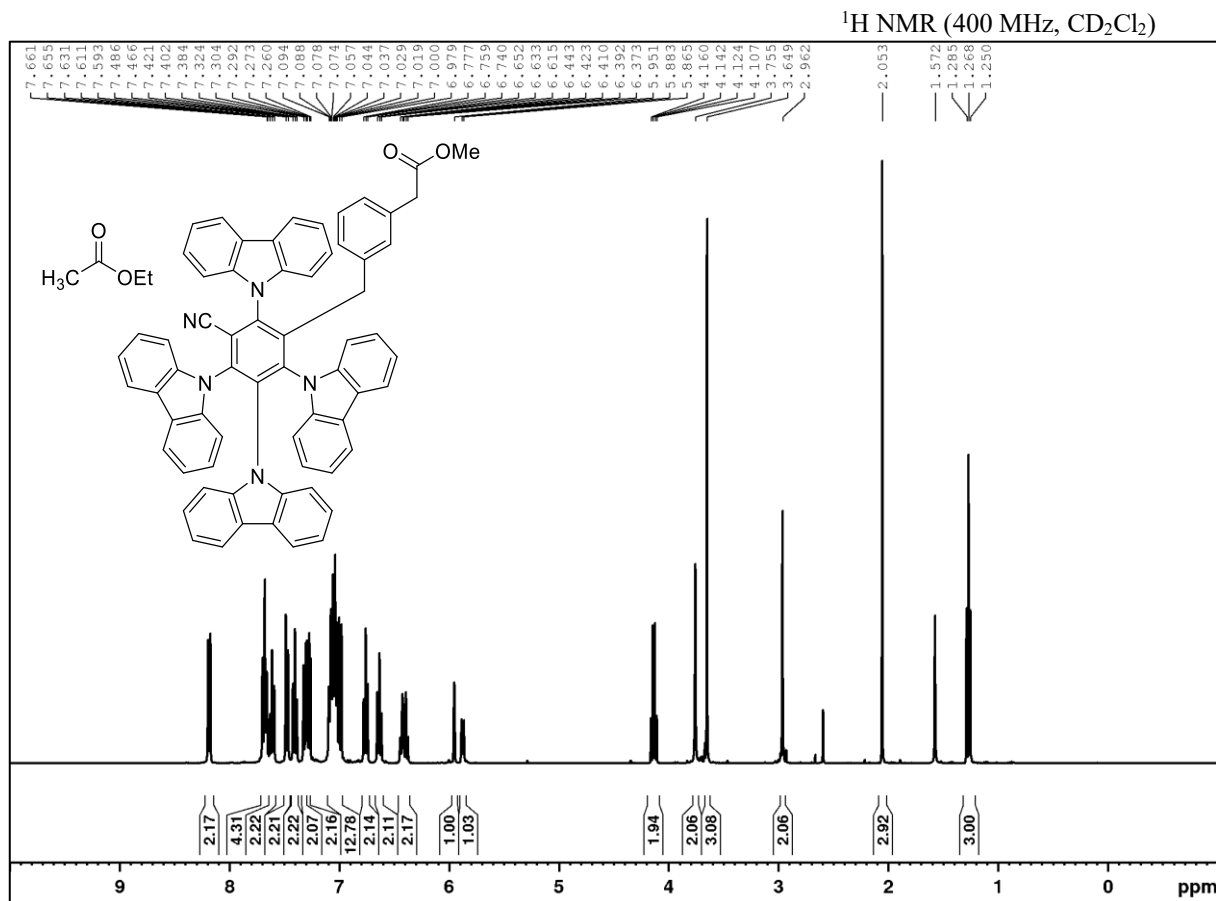


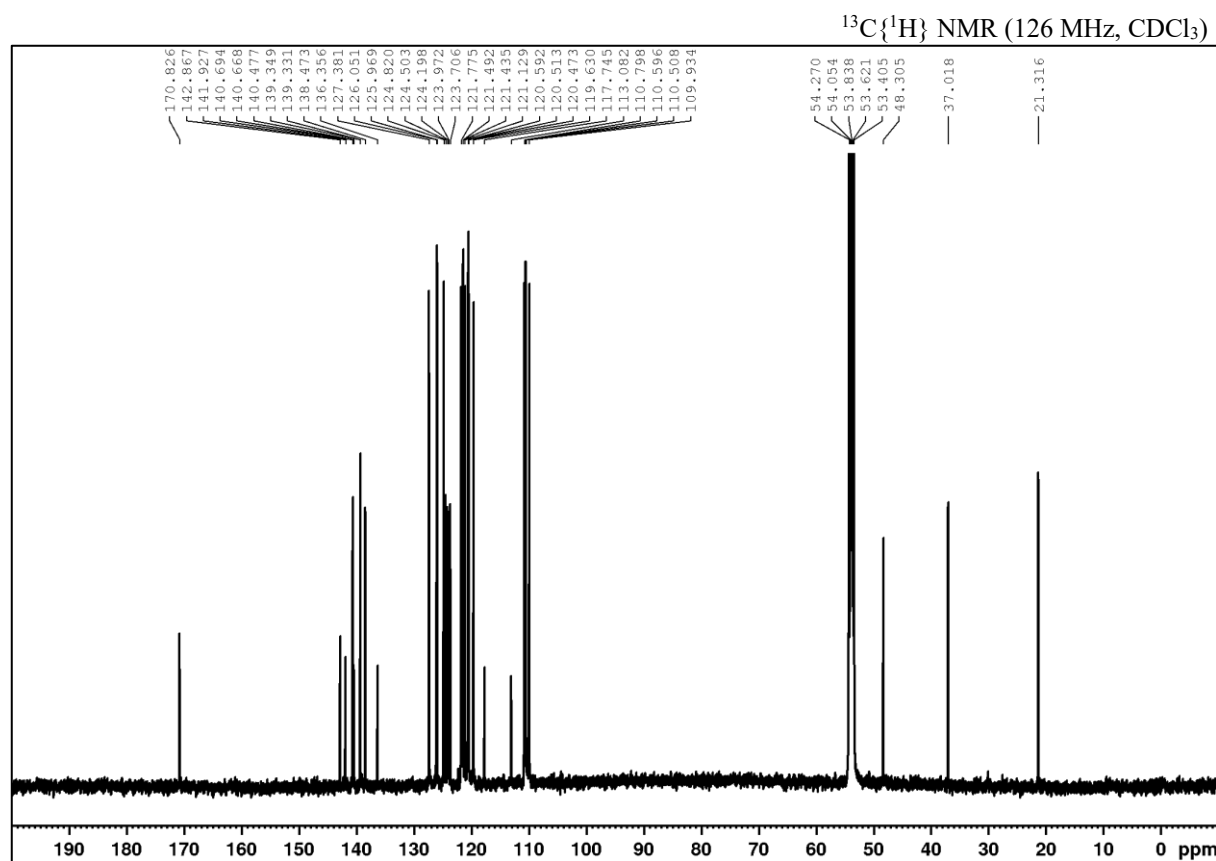
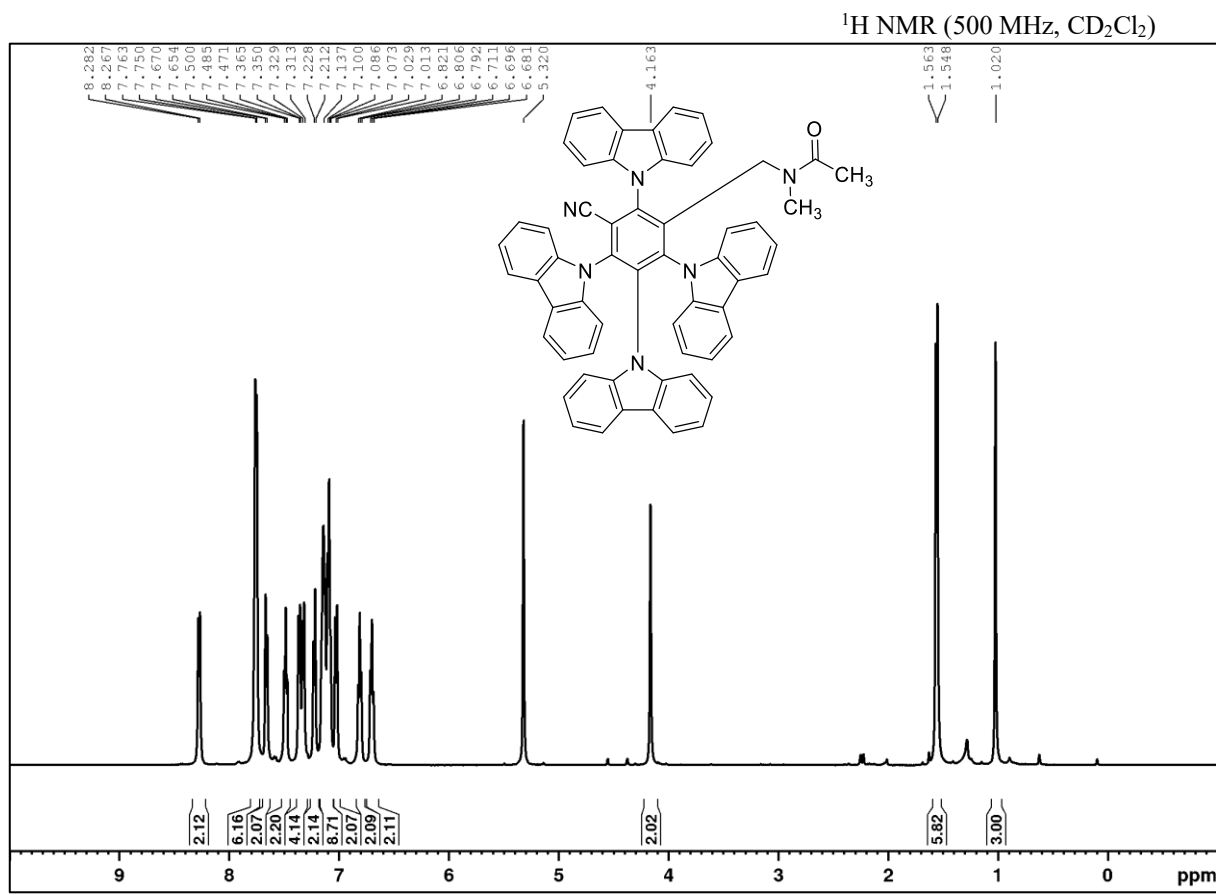
Green: Negative peak (CH, CH₃), Blue: Positive peak (CH₂).

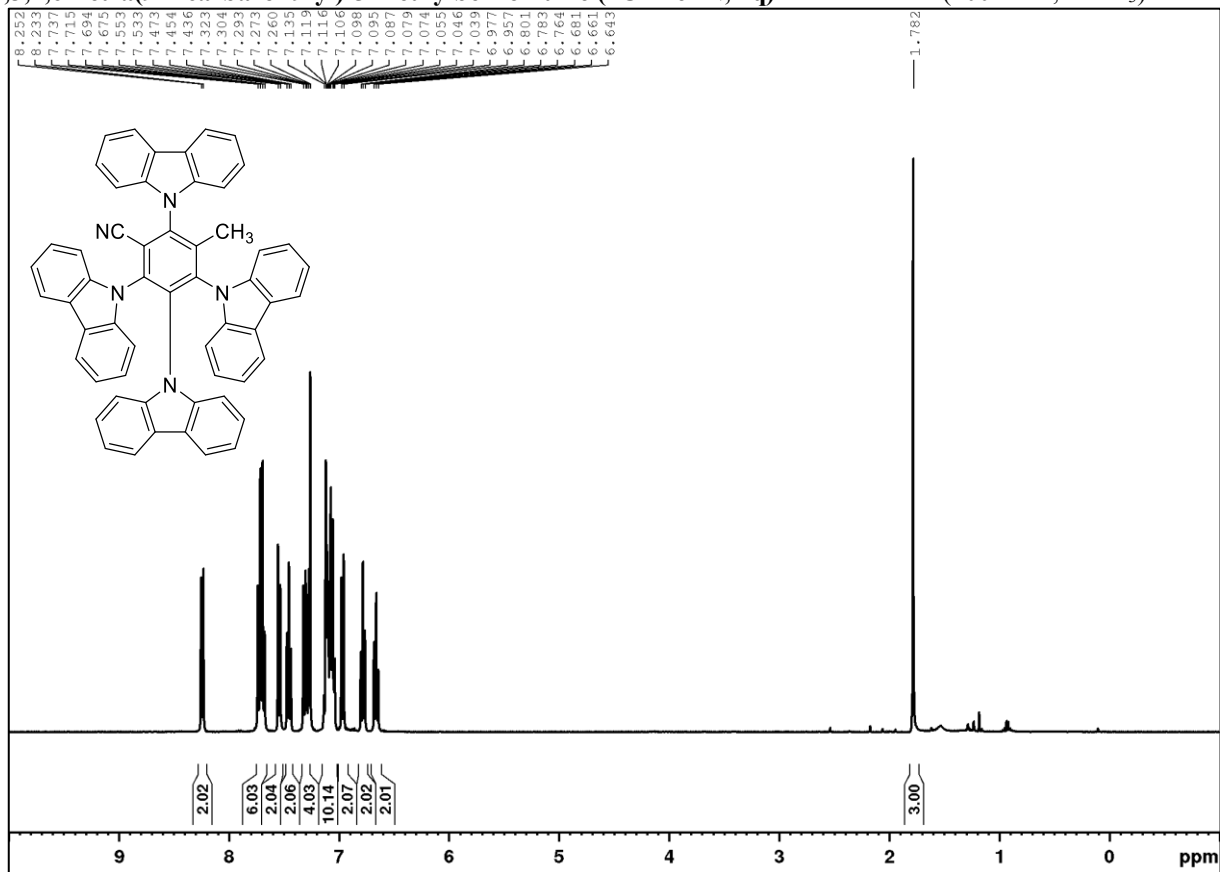
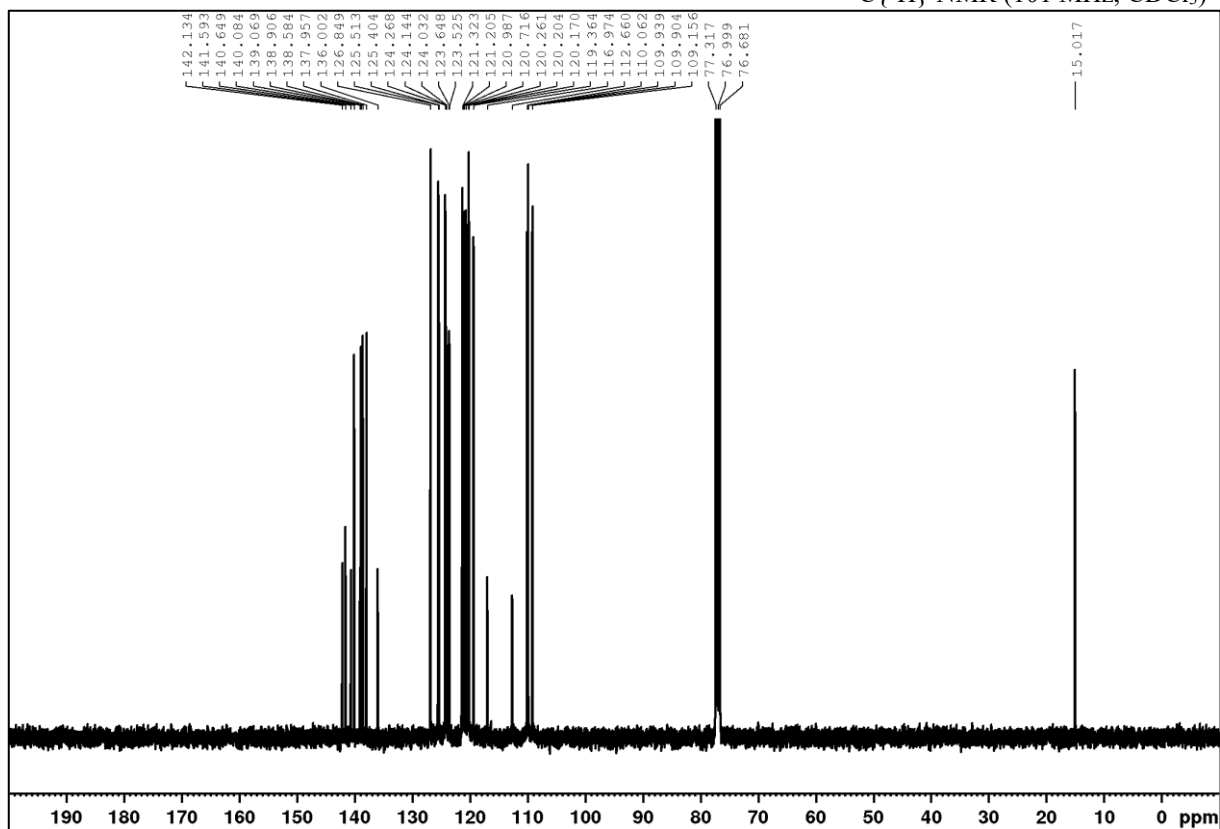
3-(But-3-en-1-yl)-2,4,5,6-tetra(9H-carbazol-9-yl)benzotrile (2m) ^1H NMR (400 MHz, CDCl_3) $^{13}\text{C}\{^1\text{H}\}$ NMR (101 MHz, CDCl_3)

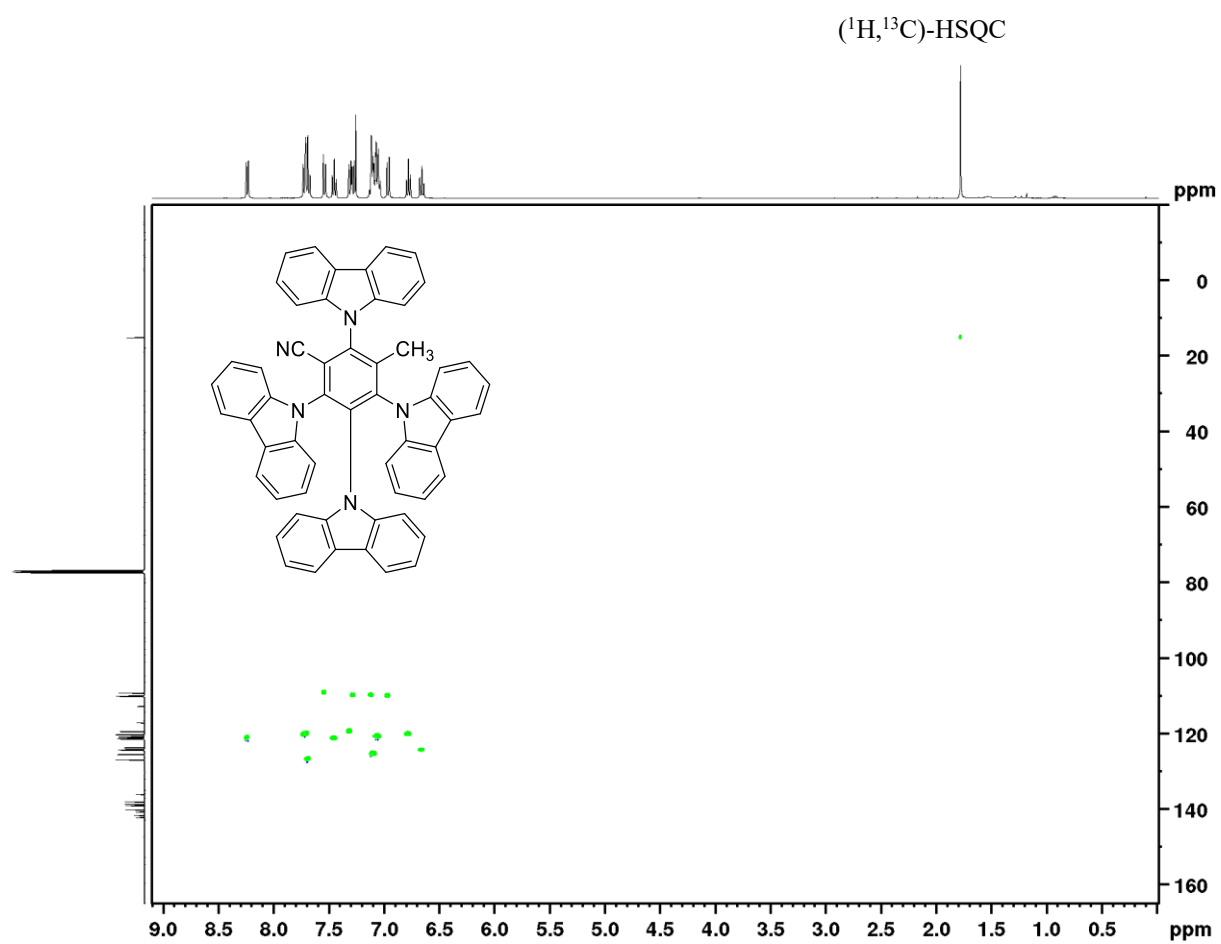
2,3,4,6-tetra(9*H*-carbazol-9-yl)-5-cyclohexylbenzonitrile (**2n**) ^1H NMR (400 MHz, CDCl_3) $^{13}\text{C}\{^1\text{H}\}$ NMR (101 MHz, CDCl_3)

Methyl 2-(3-(2,3,4,6-tetra(9H-carbazol-9-yl)-5-cyanobenzyl)phenyl)acetate (2o)

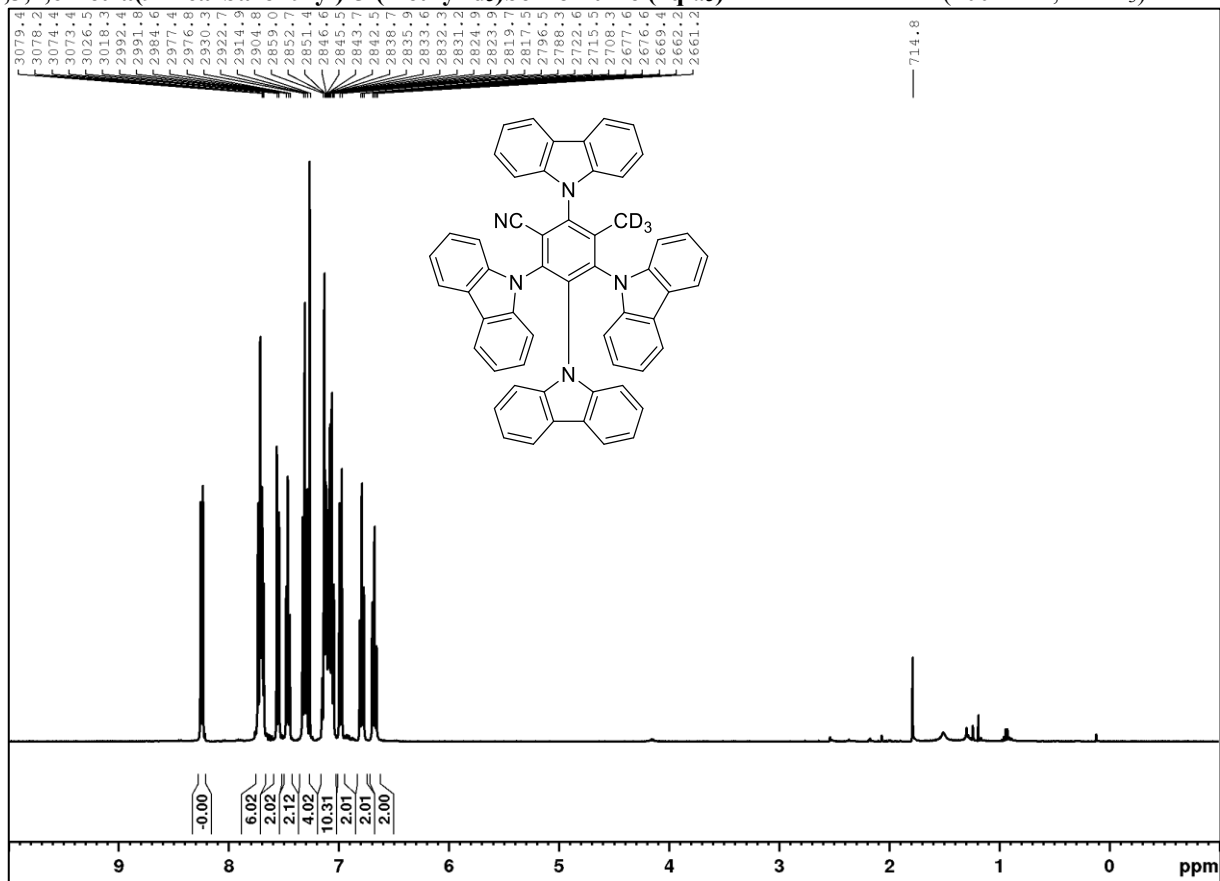
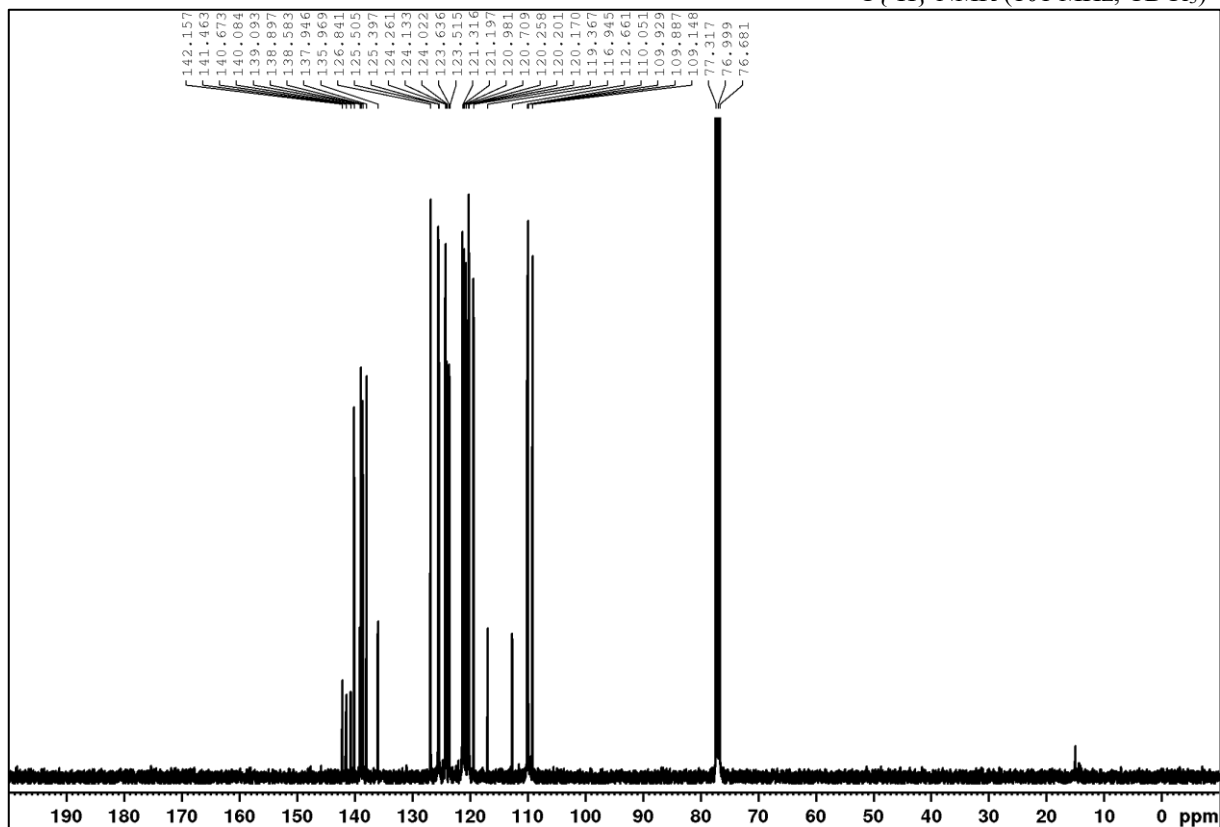


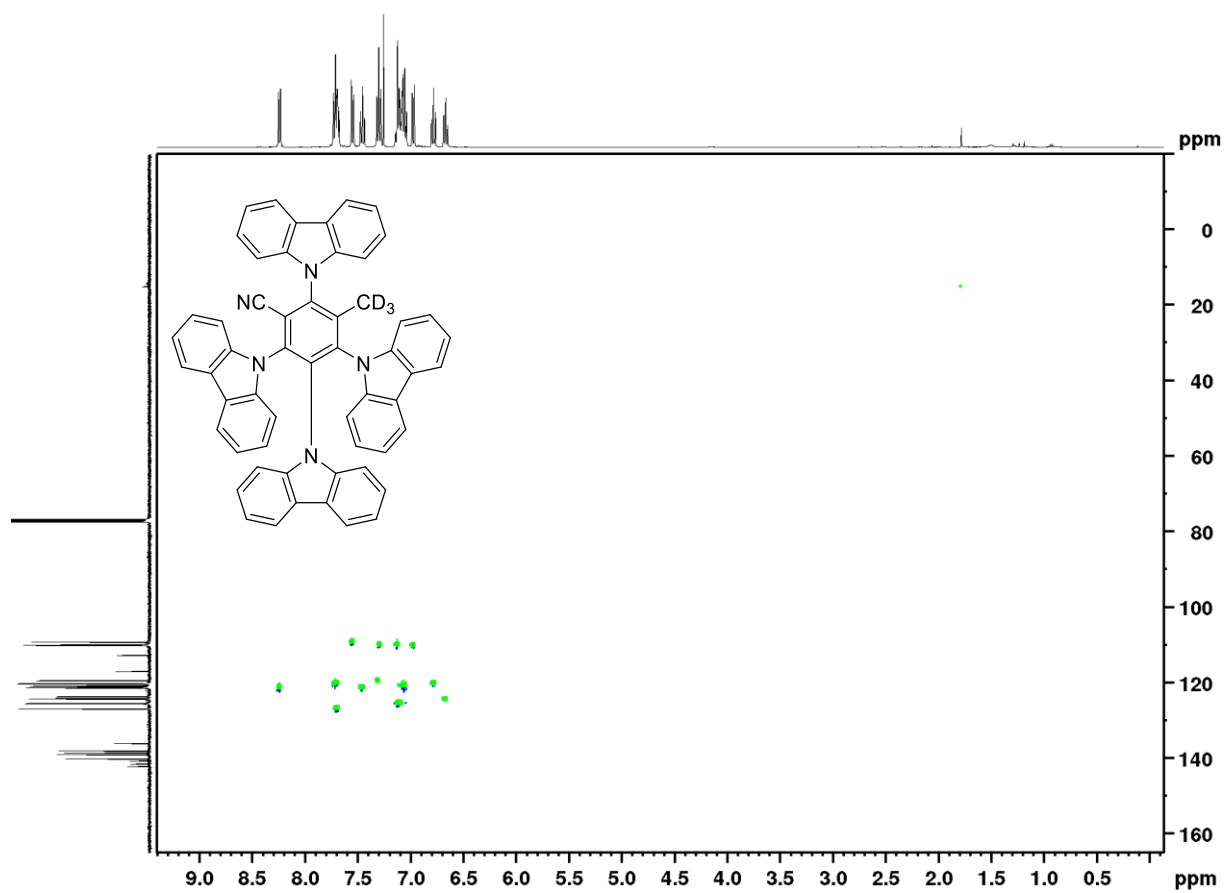
***N*-Methyl-*N*-(2,3,4,6-tetra(9*H*-carbazol-9-yl)-5-cyanobenzyl)acetamide (2p)**

2,3,4,6-Tetra(9H-carbazol-9-yl)-5-methylbenzonitrile (4CzMeBN, 2q) ^1H NMR (400 MHz, CDCl_3) $^{13}\text{C}\{^1\text{H}\}$ NMR (101 MHz, CDCl_3)



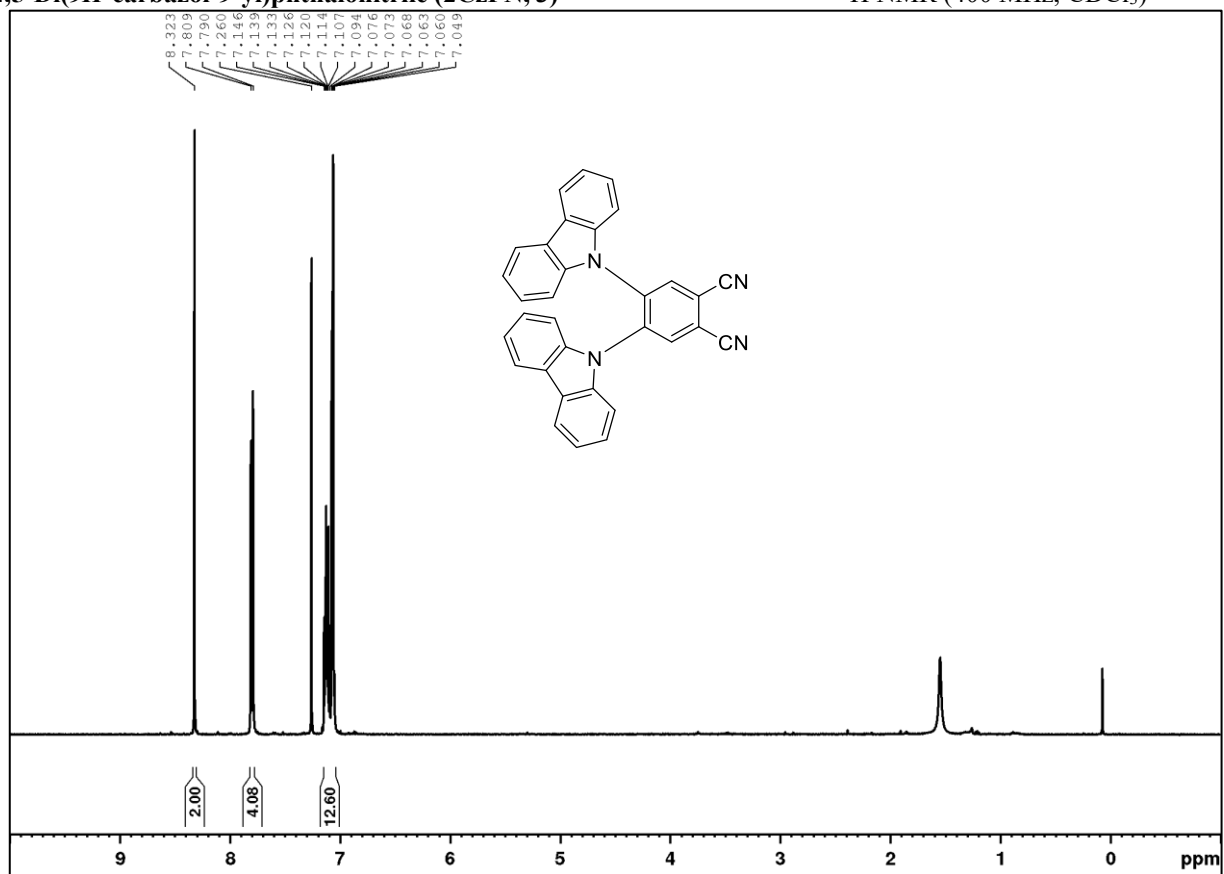
Green: Negative peak (CH, CH₃), Blue: Positive peak (CH₂).

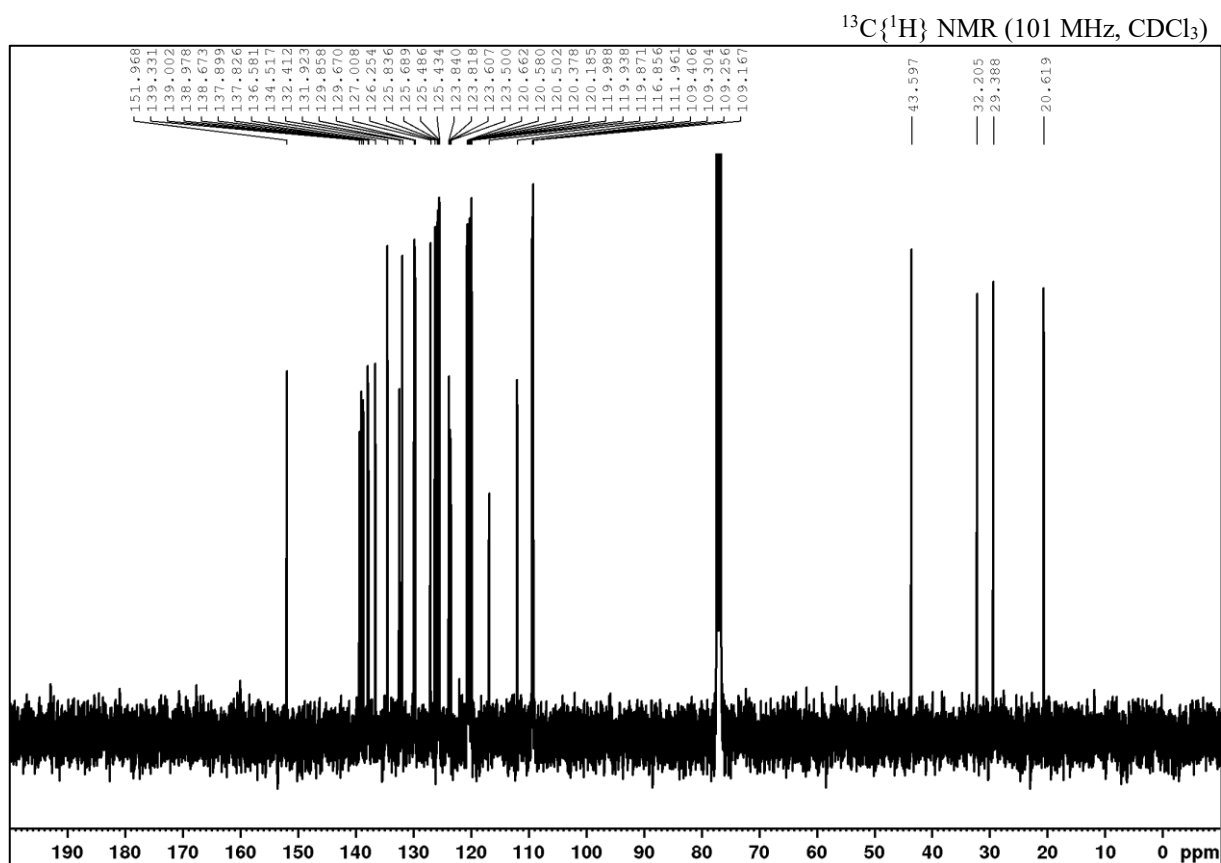
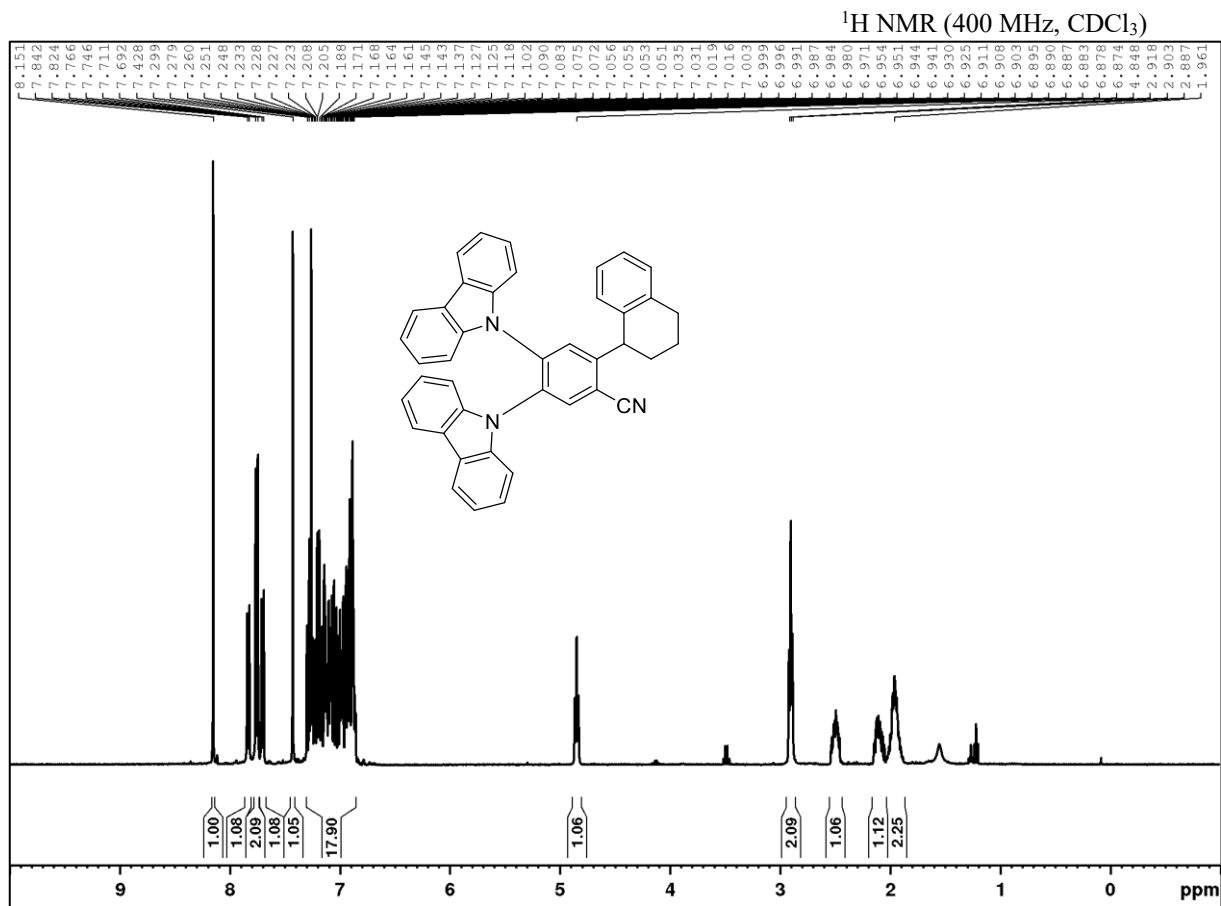
2,3,4,6-Tetra(9H-carbazol-9-yl)-5-(methyl-d₃)benzotrile (2q-d₃)¹H NMR (400 MHz, CDCl₃)¹³C{¹H} NMR (101 MHz, CDCl₃)

$(^1\text{H}, ^{13}\text{C})\text{-HSQC}$ 

Green: Negative peak (CH, CH₃), Blue: Positive peak (CH₂).

4,5-Di(9H-carbazol-9-yl)phthalonitrile (2CzPN, 3)

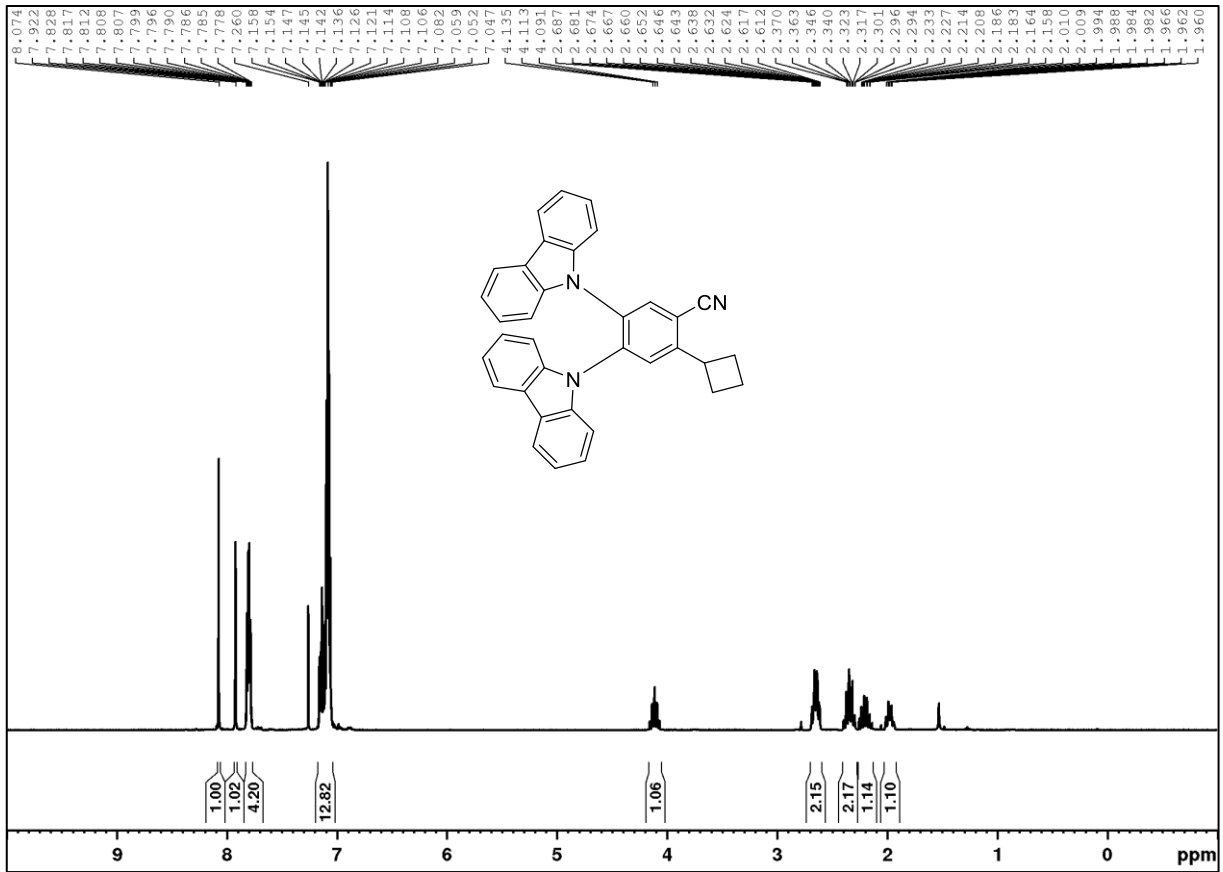
 ^1H NMR (400 MHz, CDCl_3)

4,5-Di(9*H*-carbazol-9-yl)-2-(1,2,3,4-tetrahydronaphthalen-1-yl)benzonitrile (4a)

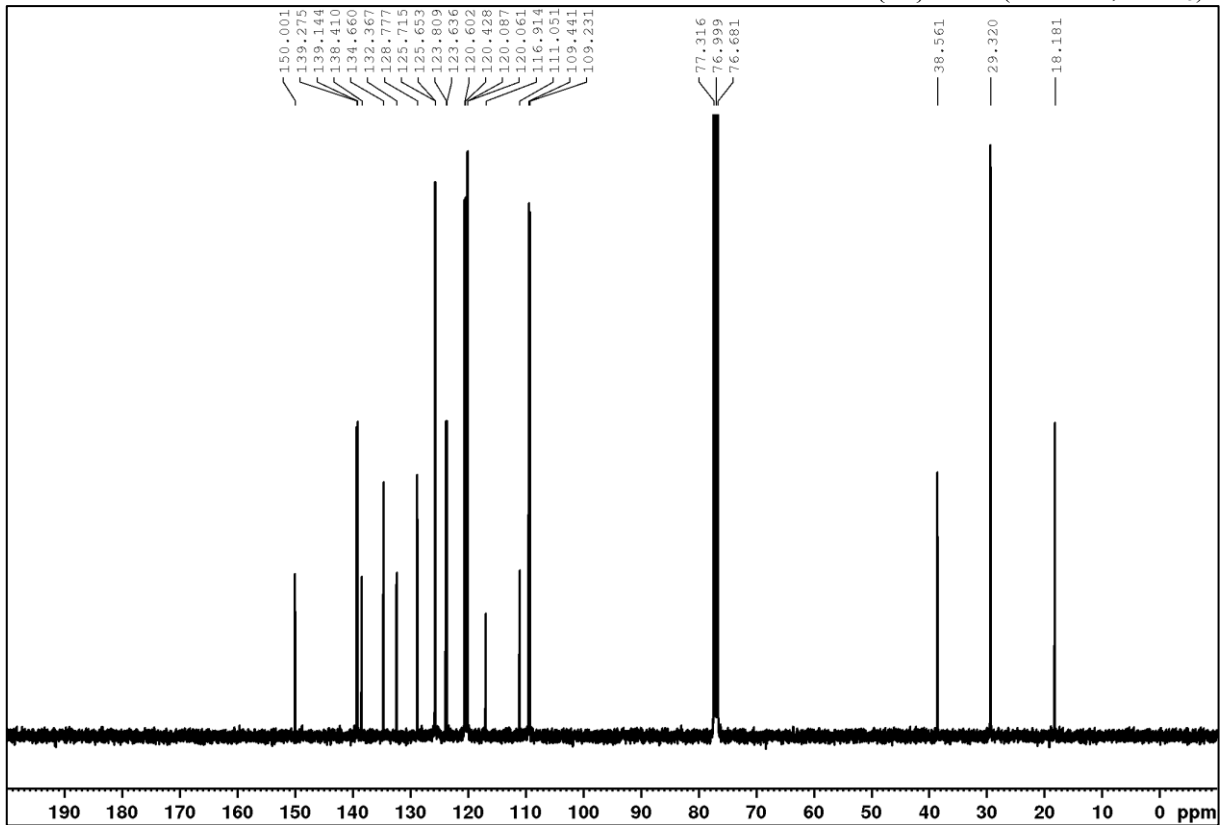
APPENDIX

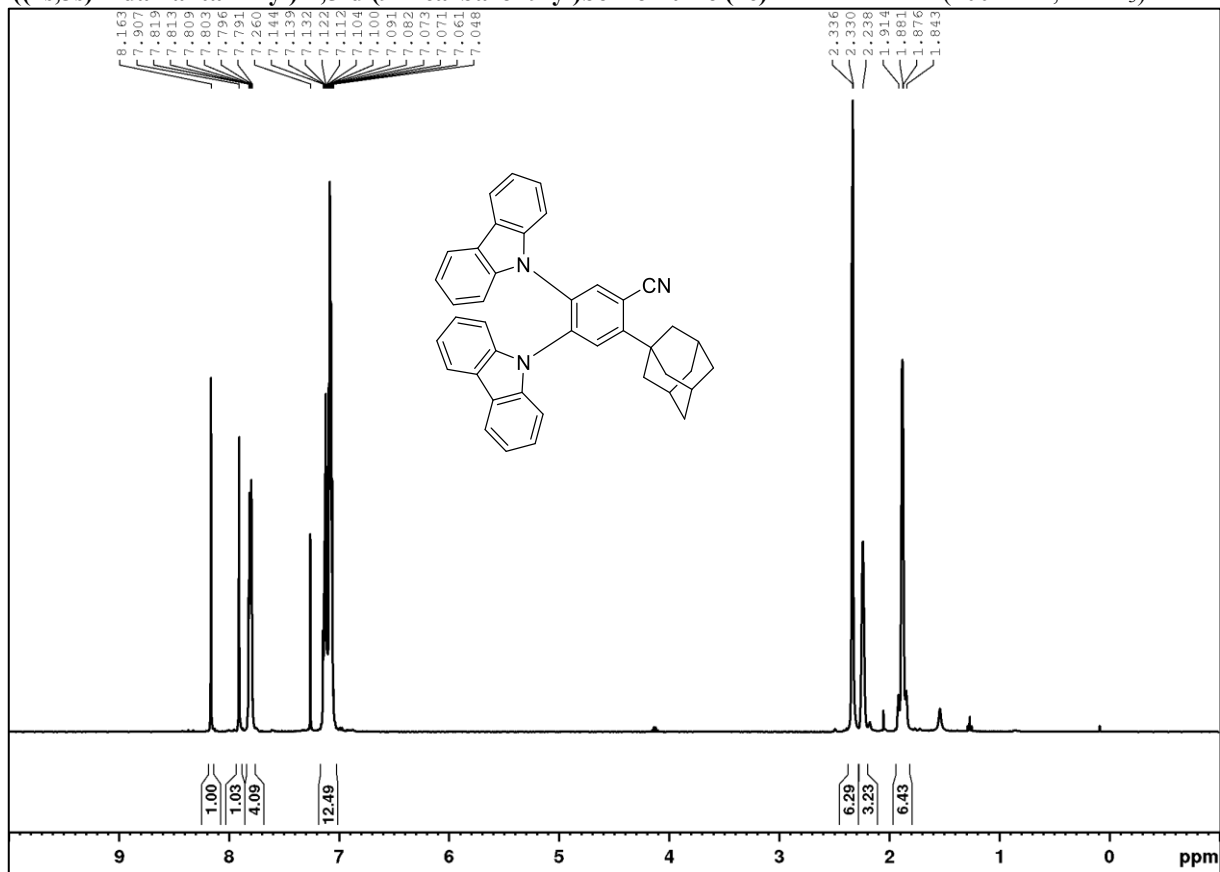
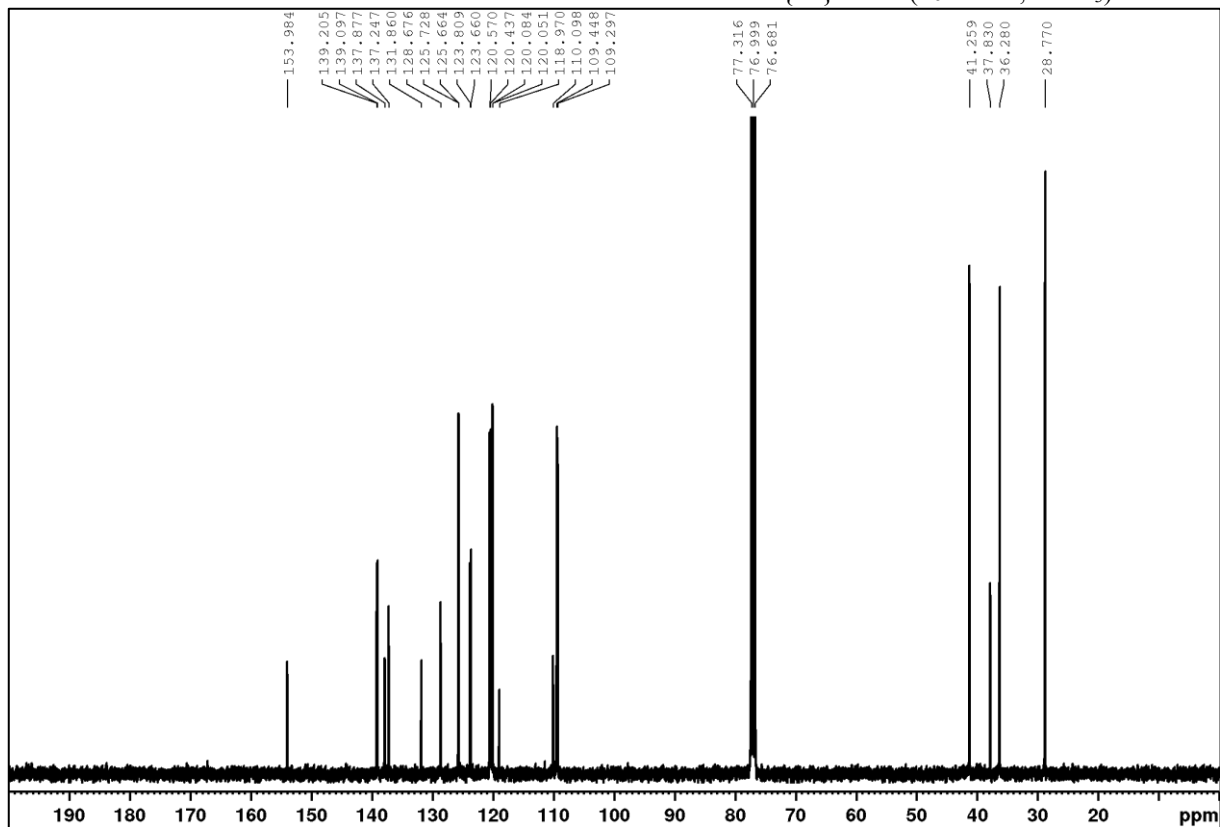
4,5-Di(9*H*-carbazol-9-yl)-2-cyclobutylbenzonitrile (**4b**)

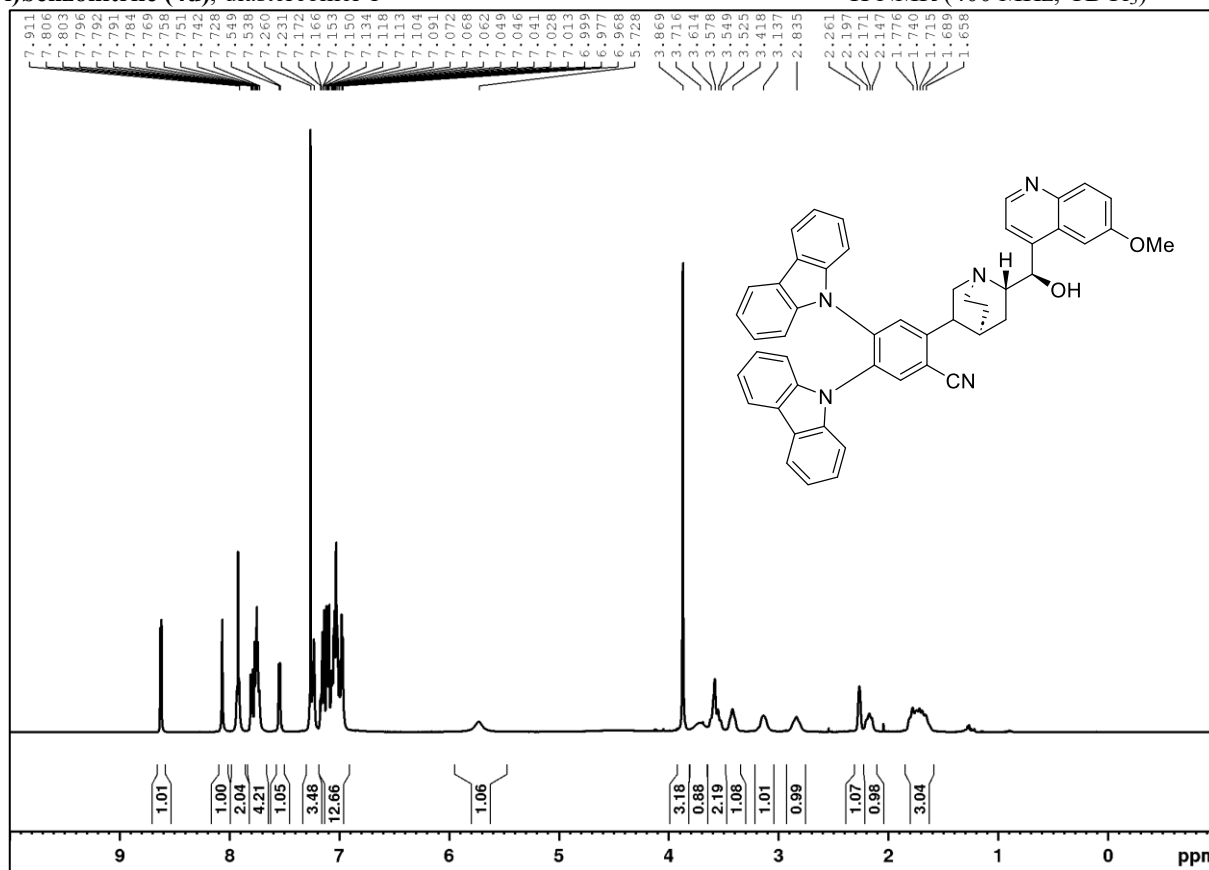
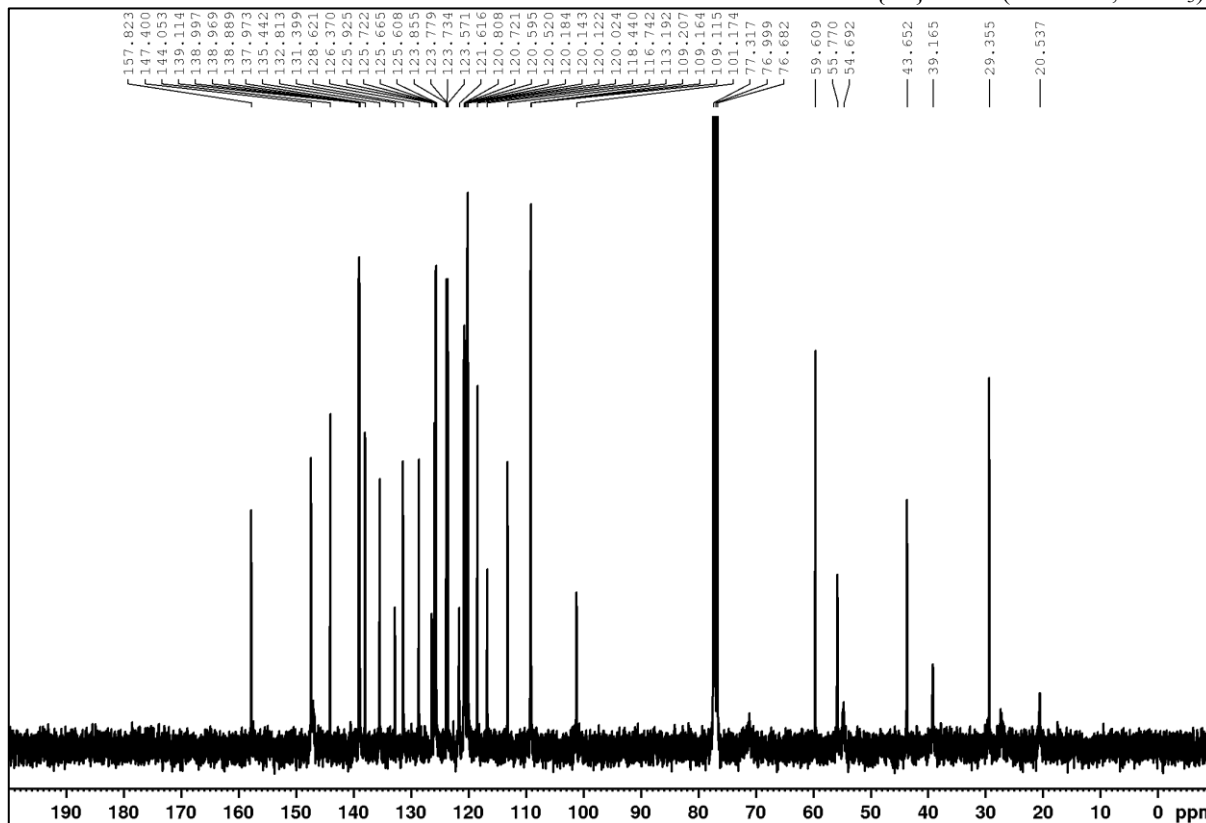
¹H NMR (400 MHz, CDCl₃)



¹³C{¹H} NMR (101 MHz, CDCl₃)



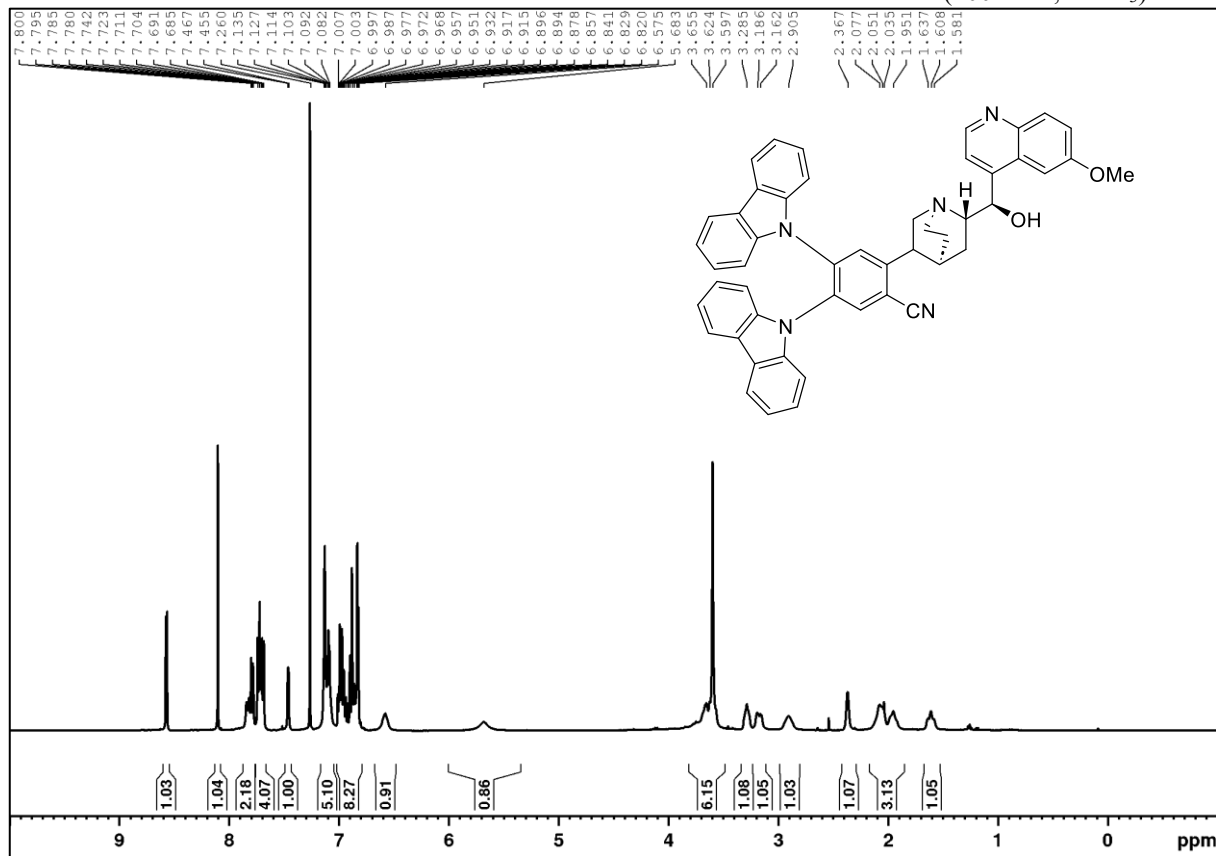
2-((1s,3s)-Adamantan-1-yl)-4,5-di(9H-carbazol-9-yl)benzonitrile (4c) ^1H NMR (400 MHz, CDCl_3) $^{13}\text{C}\{^1\text{H}\}$ NMR (101 MHz, CDCl_3)

4,5-Di(9H-carbazol-9-yl)-2-((1*S*,4*S*,6*S*)-6-((*R*)-hydroxy(6-methoxyquinolin-4-yl)methyl)quinuclidin-3-yl)benzonitrile (4d), diastereomer 1¹H NMR (400 MHz, CDCl₃)¹³C{¹H} NMR (101 MHz, CDCl₃)

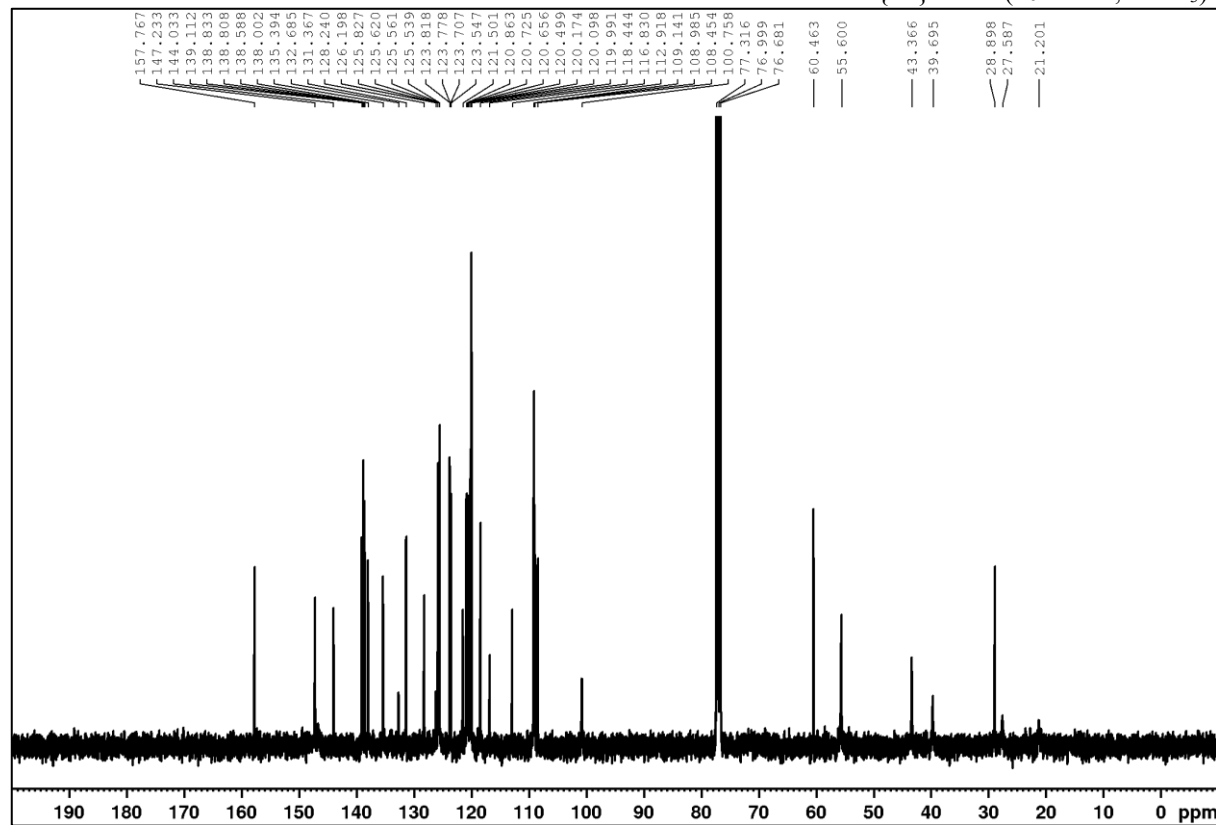
APPENDIX

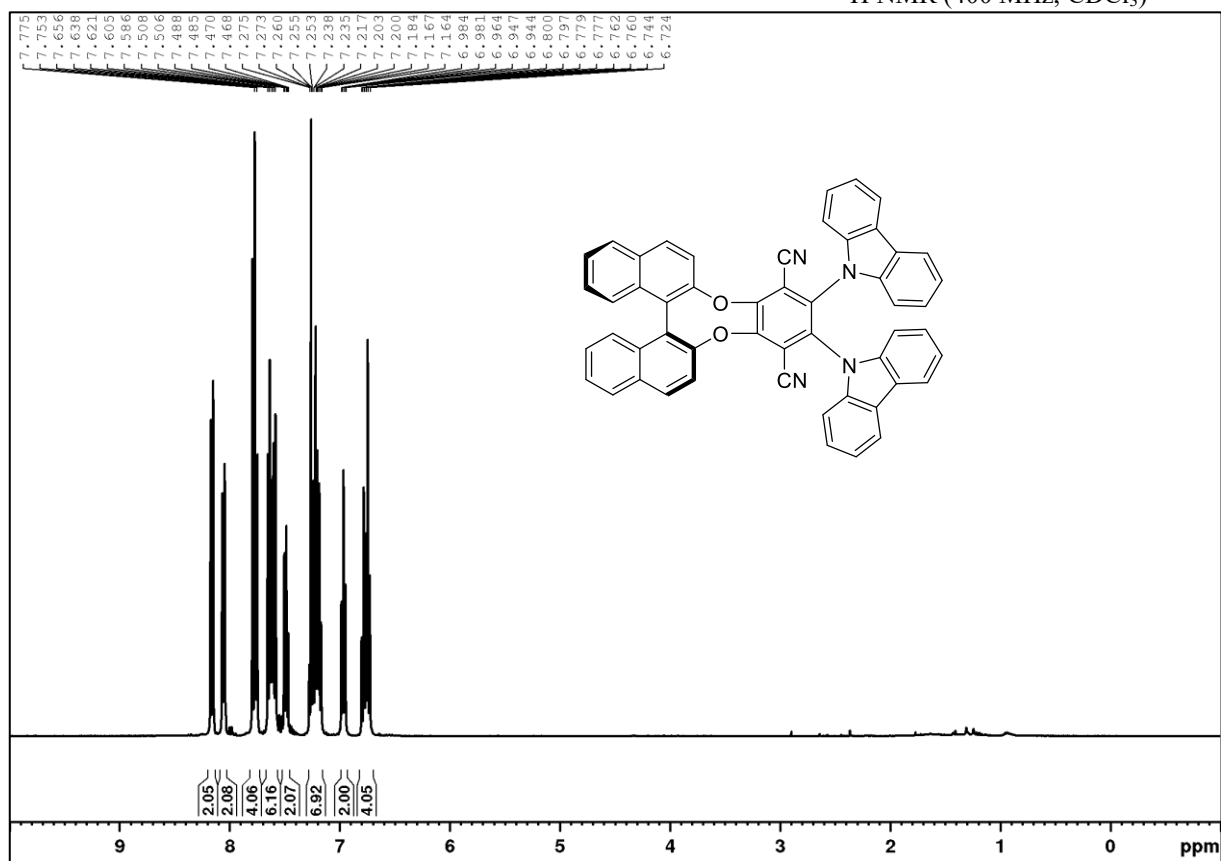
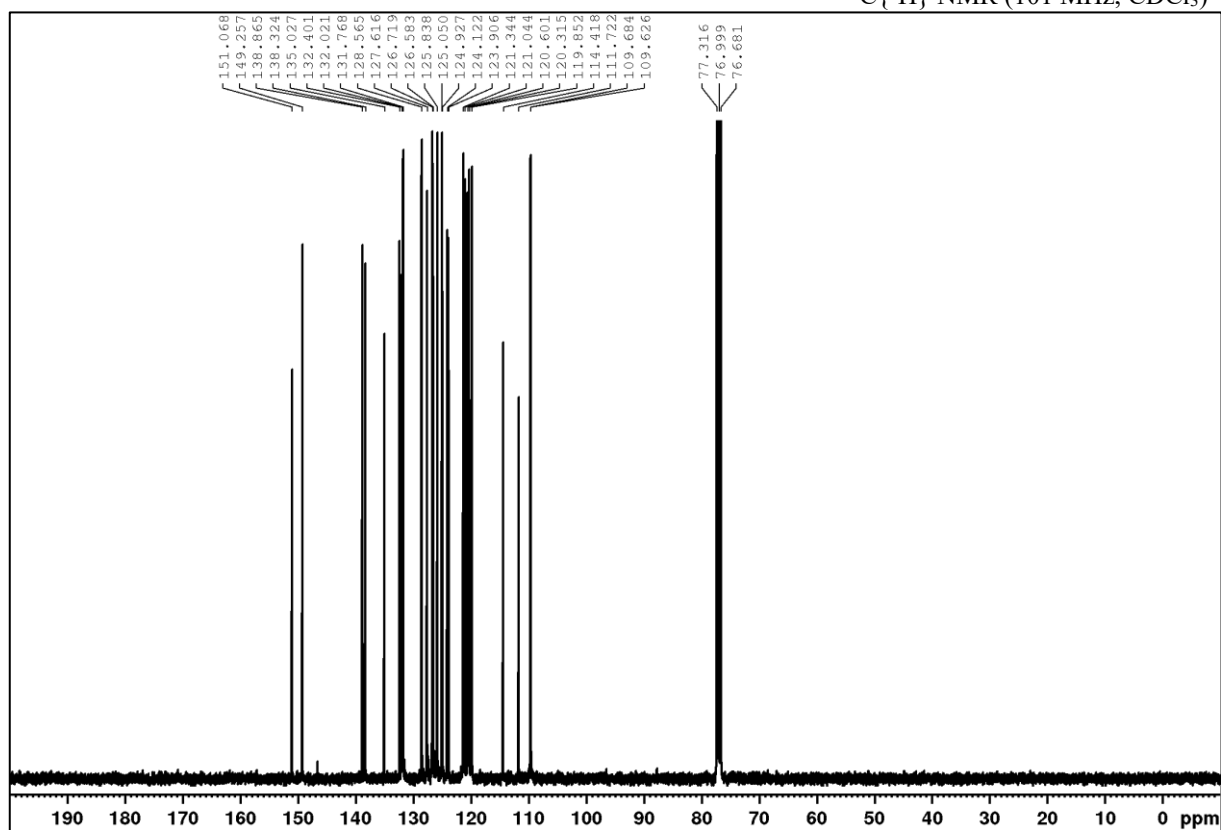
Diastereomer 2

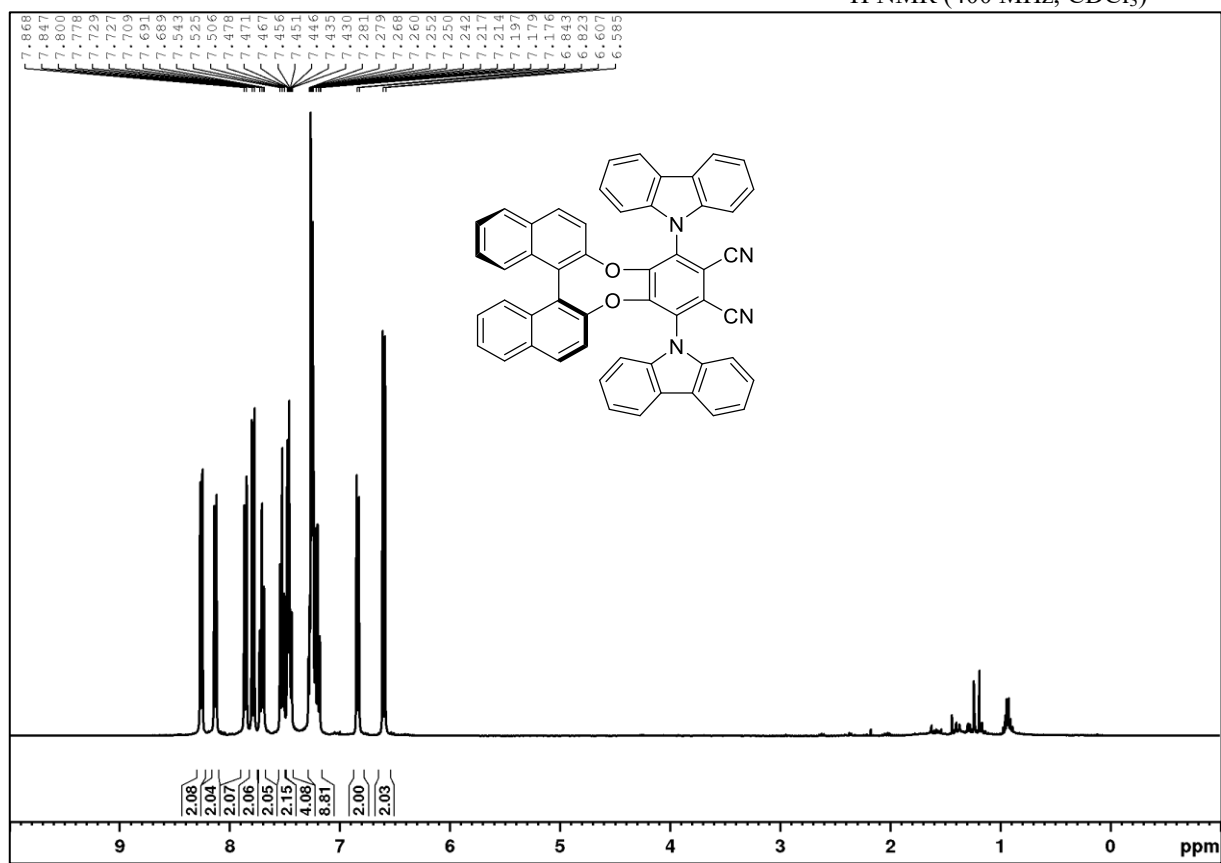
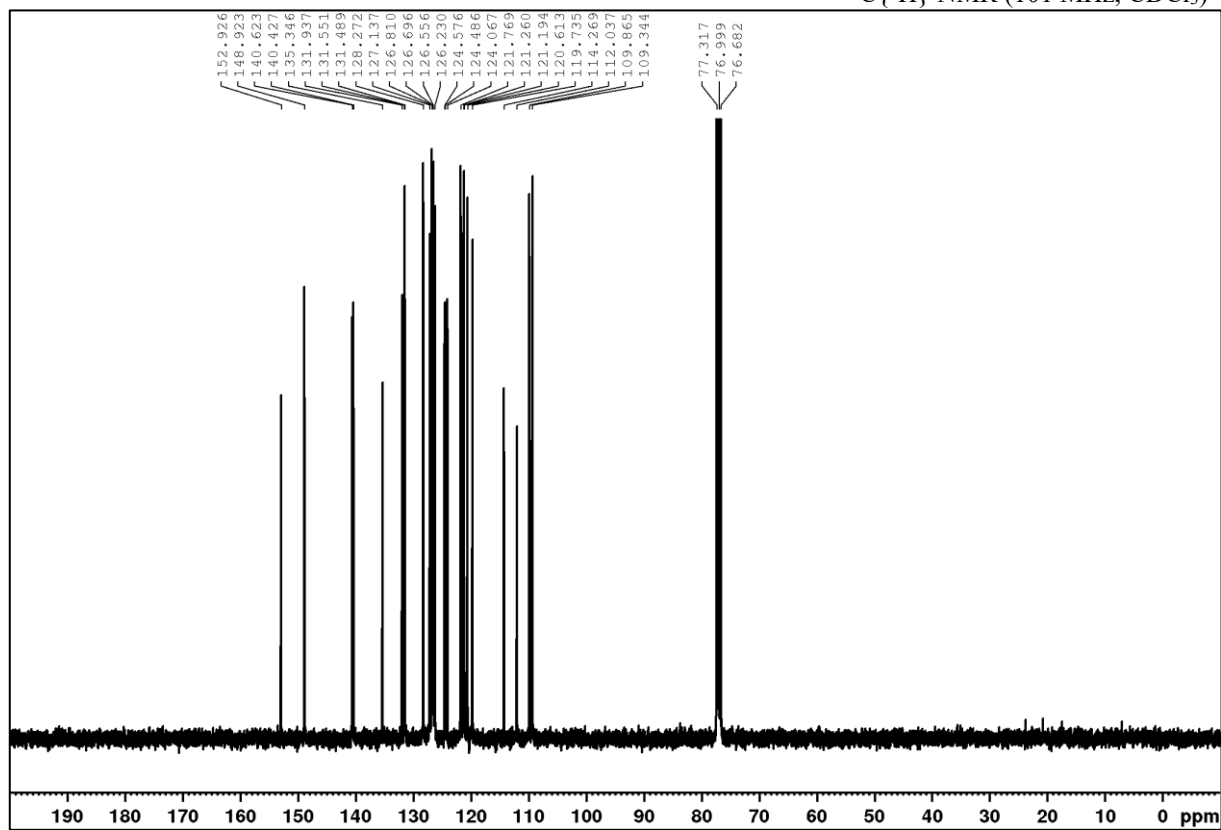
^1H NMR (400 MHz, CDCl_3)

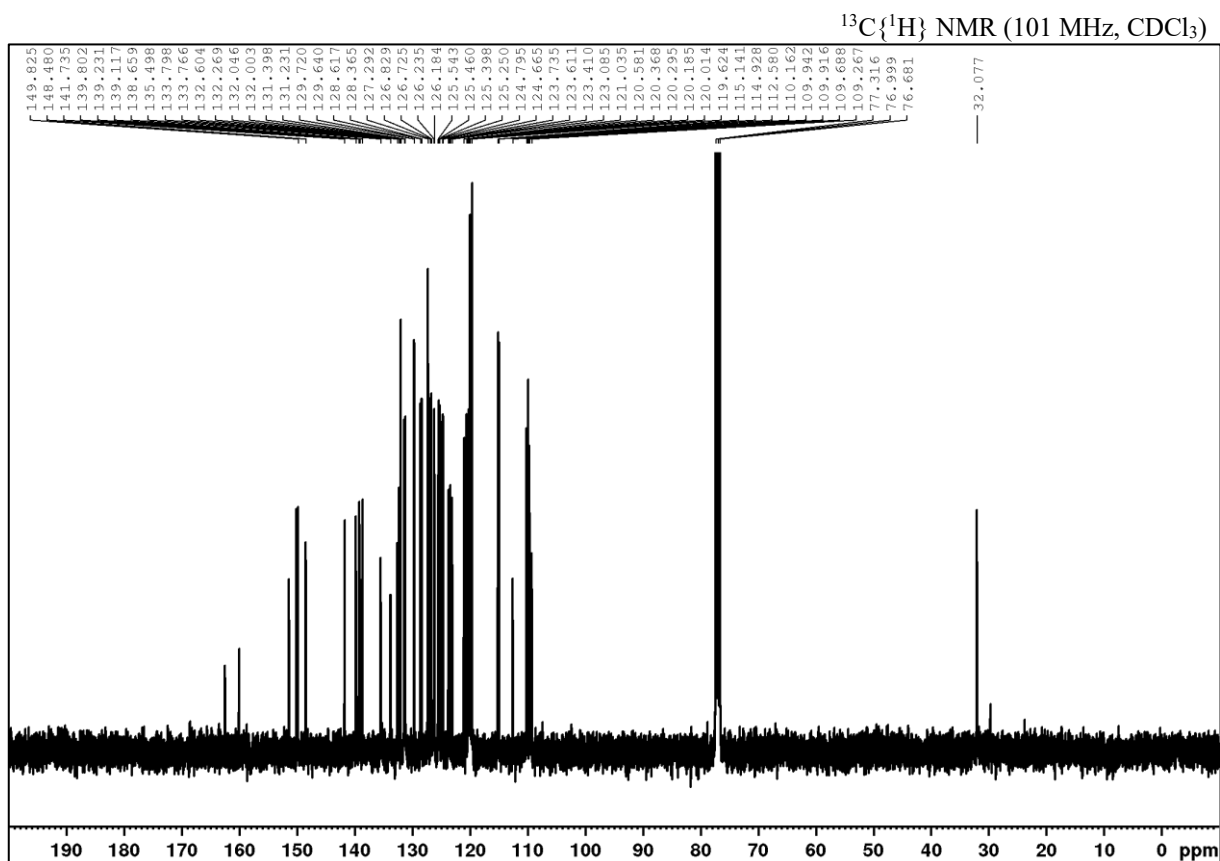
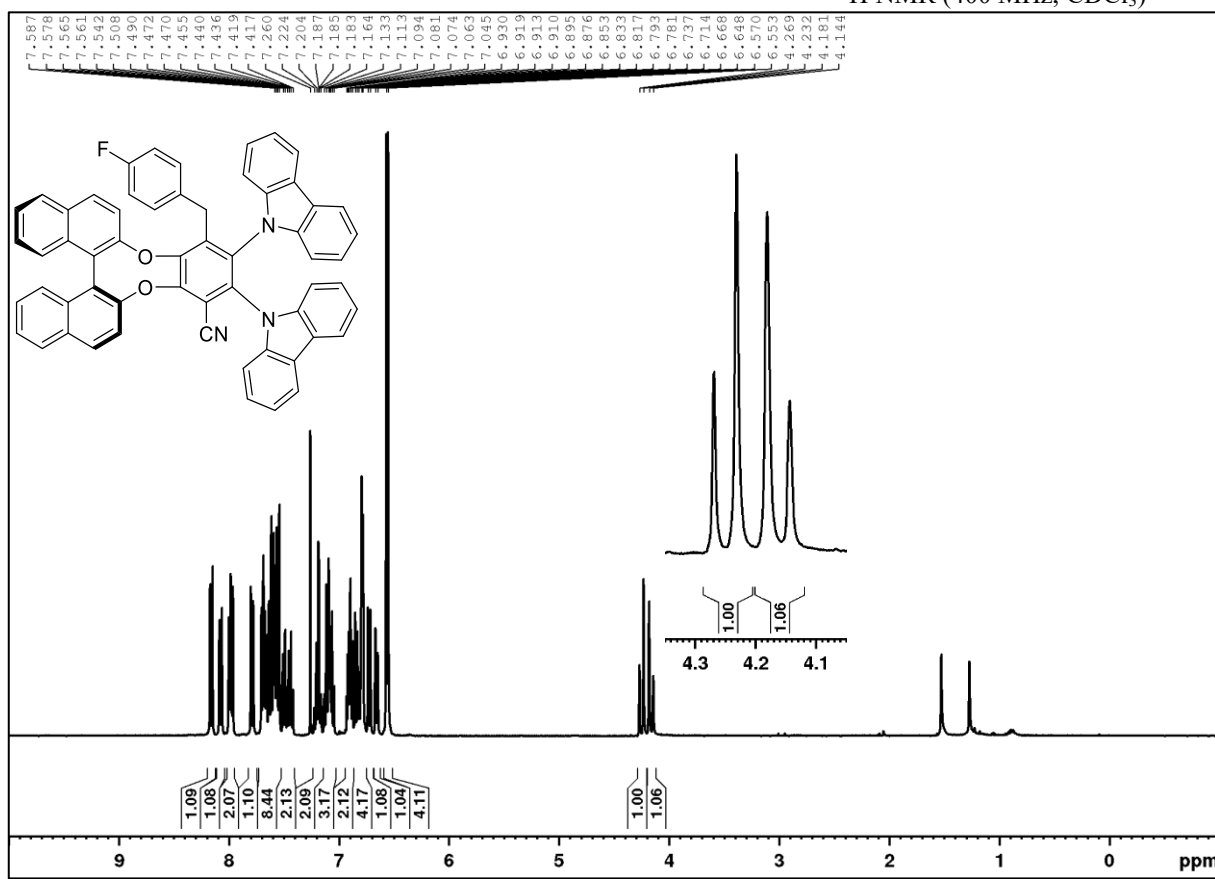


$^{13}\text{C}\{^1\text{H}\}$ NMR (101 MHz, CDCl_3)

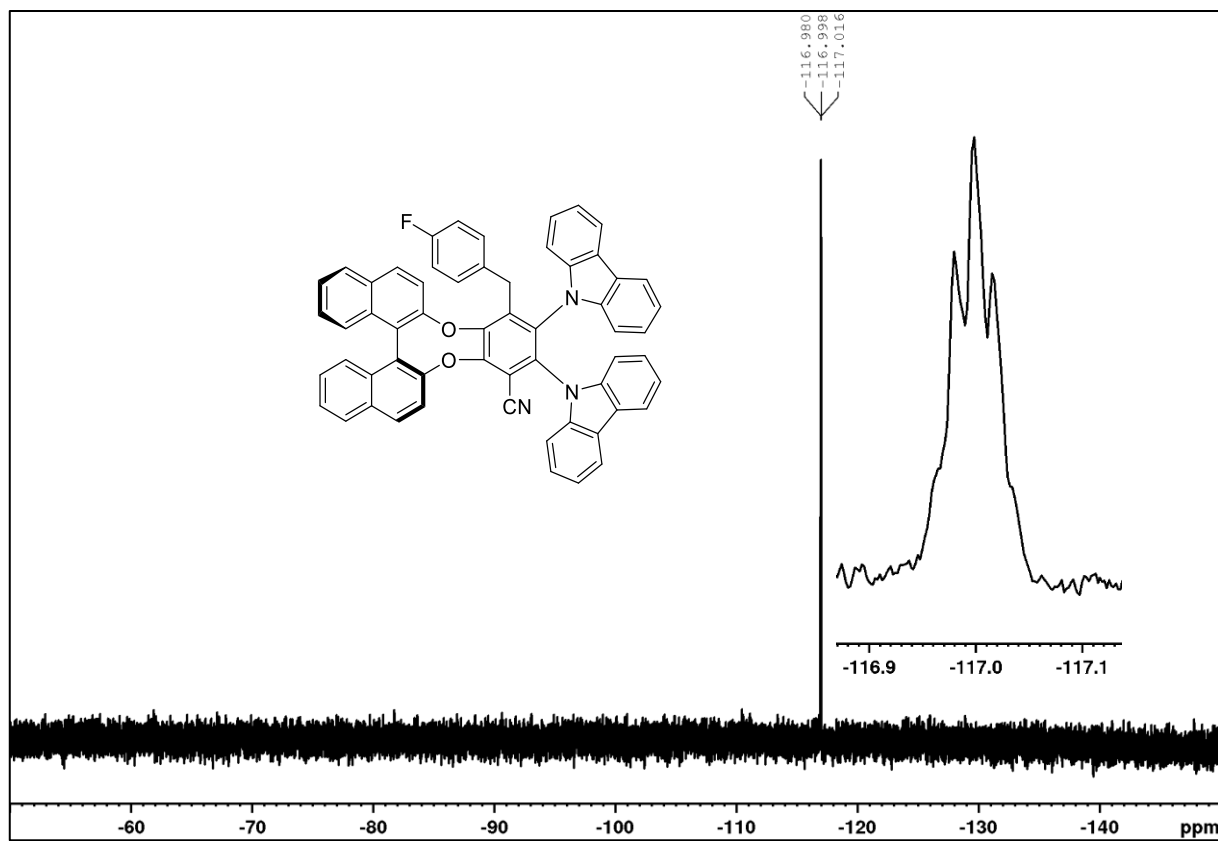


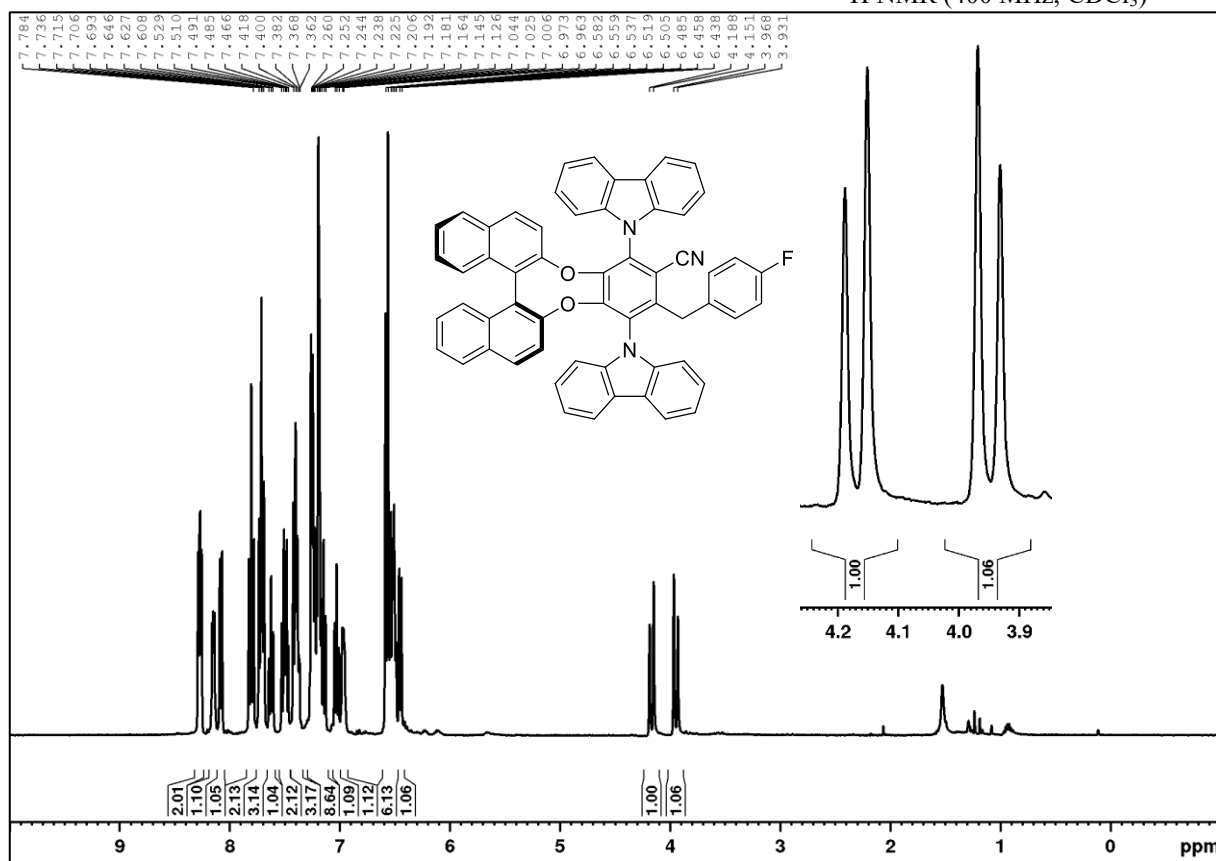
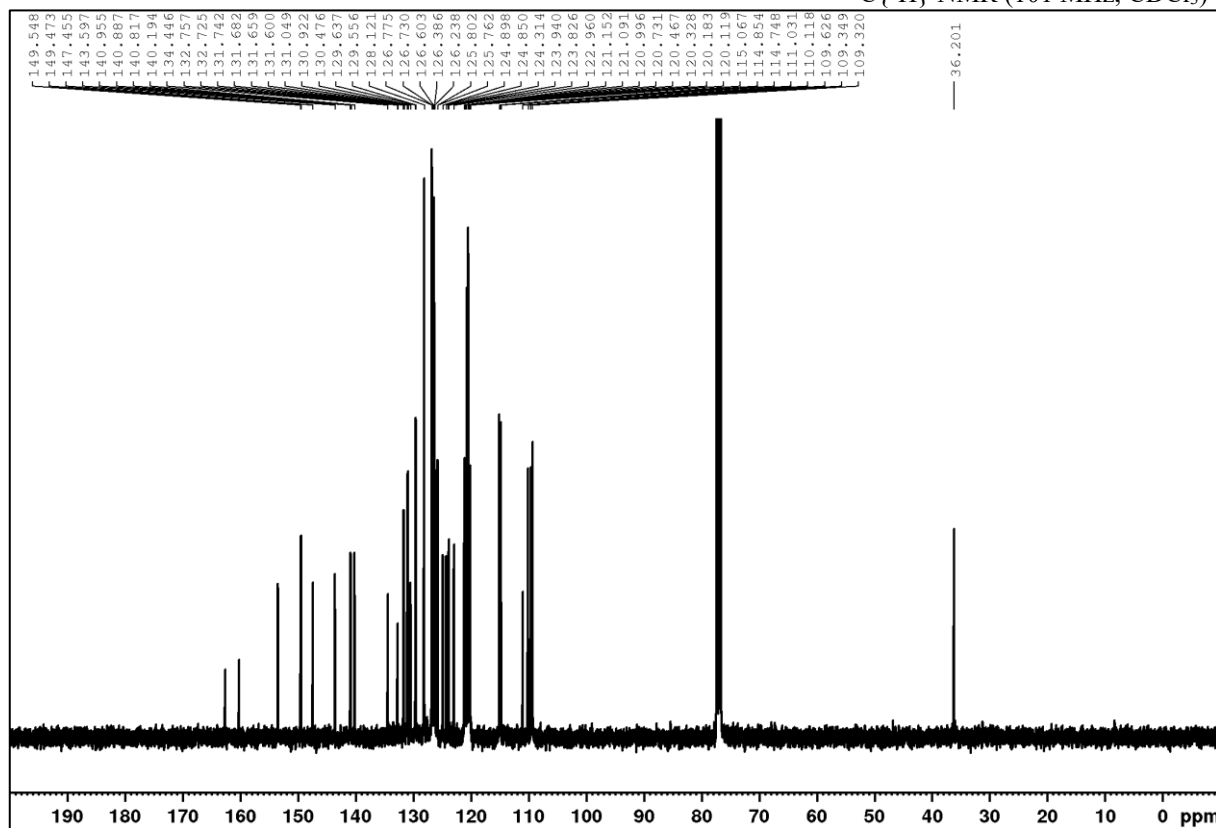
2,3-Di(9*H*-carbazol-9-yl)benzo[*b*]dinaphtho[2,1-*e*:1',2'-*g*][1,4]dioxocine-1,4-dicarbonitrile (6a)¹H NMR (400 MHz, CDCl₃)¹³C{¹H} NMR (101 MHz, CDCl₃)

1,4-Di(9*H*-carbazol-9-yl)benzo[*b*]dinaphtho[2,1-*e*:1',2'-*g*][1,4]dioxocine-2,3-dicarbonitrile (6b)¹H NMR (400 MHz, CDCl₃)¹³C{¹H} NMR (101 MHz, CDCl₃)

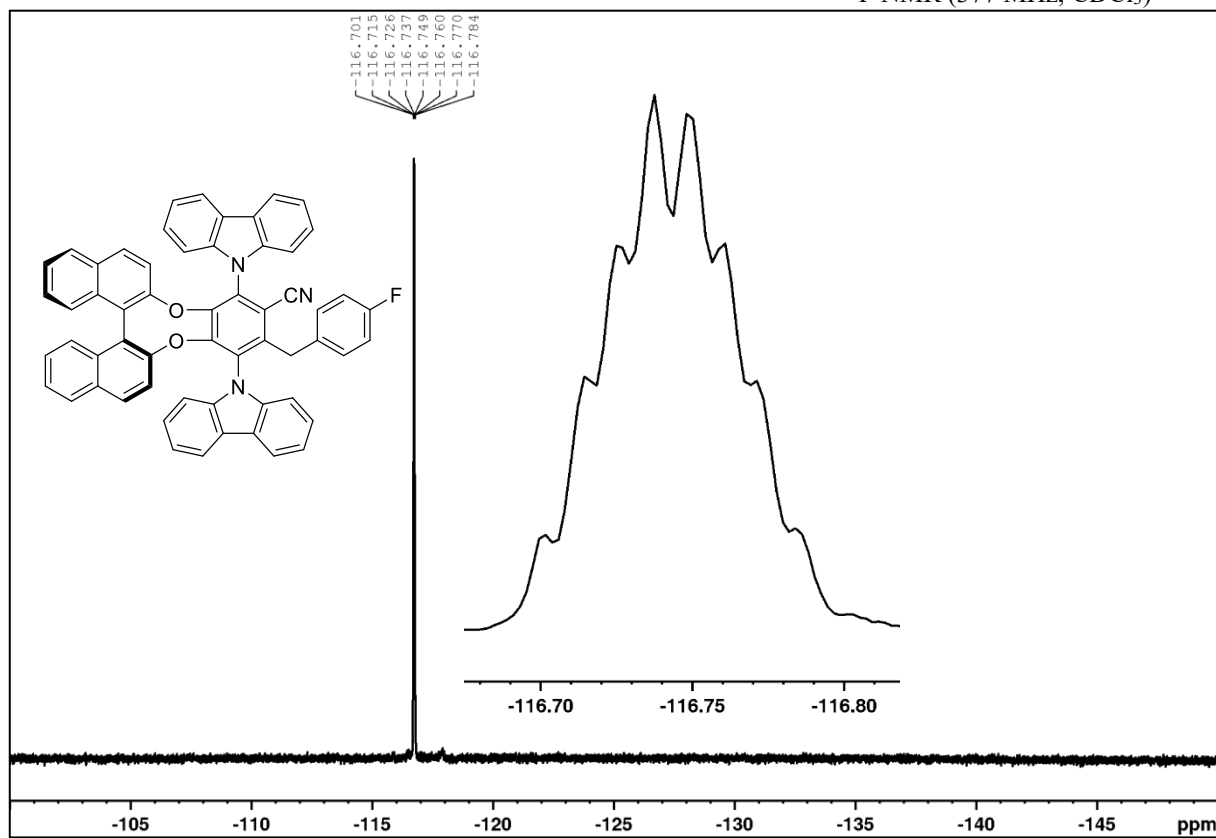
2,3-Di(9H-carbazol-9-yl)-4-(4-fluorobenzyl)benzo[*b*]dinaphtho[2,1-*e*:1',2'-*g*][1,4]dioxocine-1-carbonitrile (7a)
¹H NMR (400 MHz, CDCl₃)

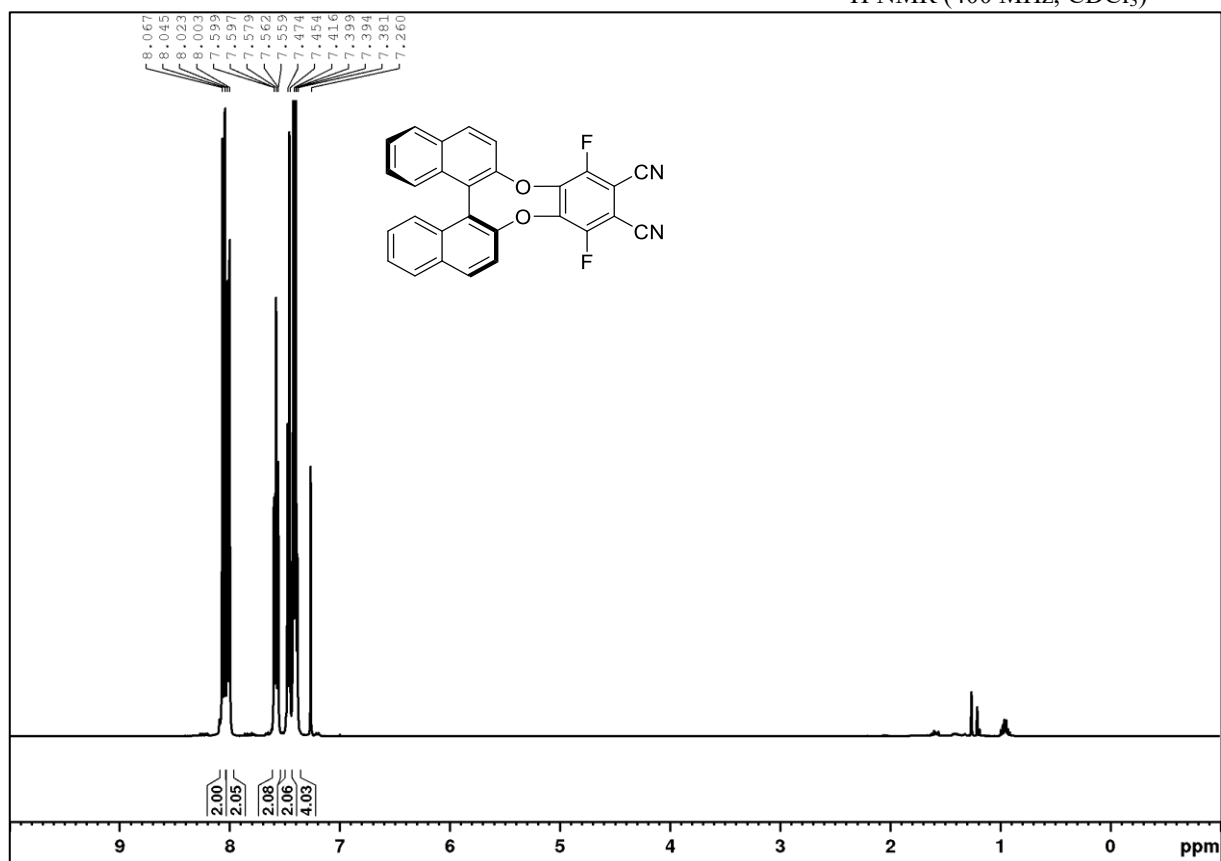
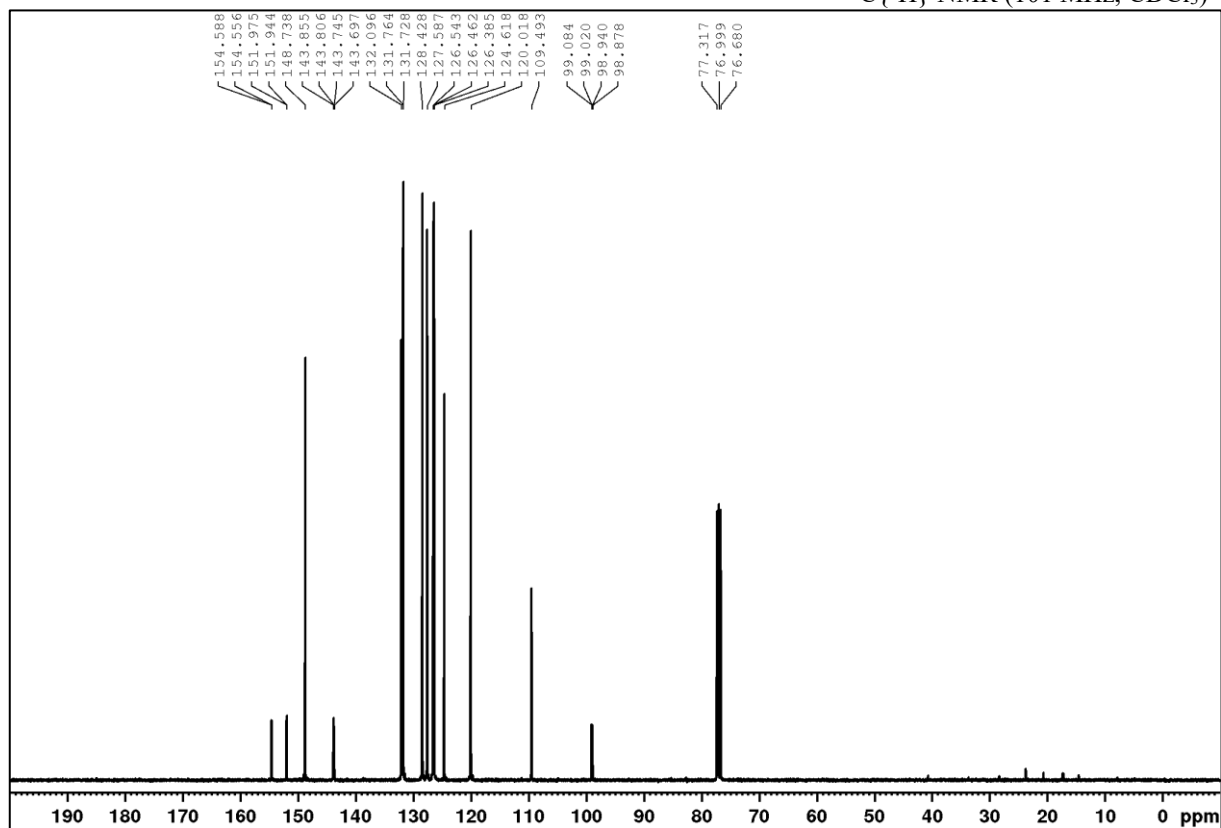
APPENDIX

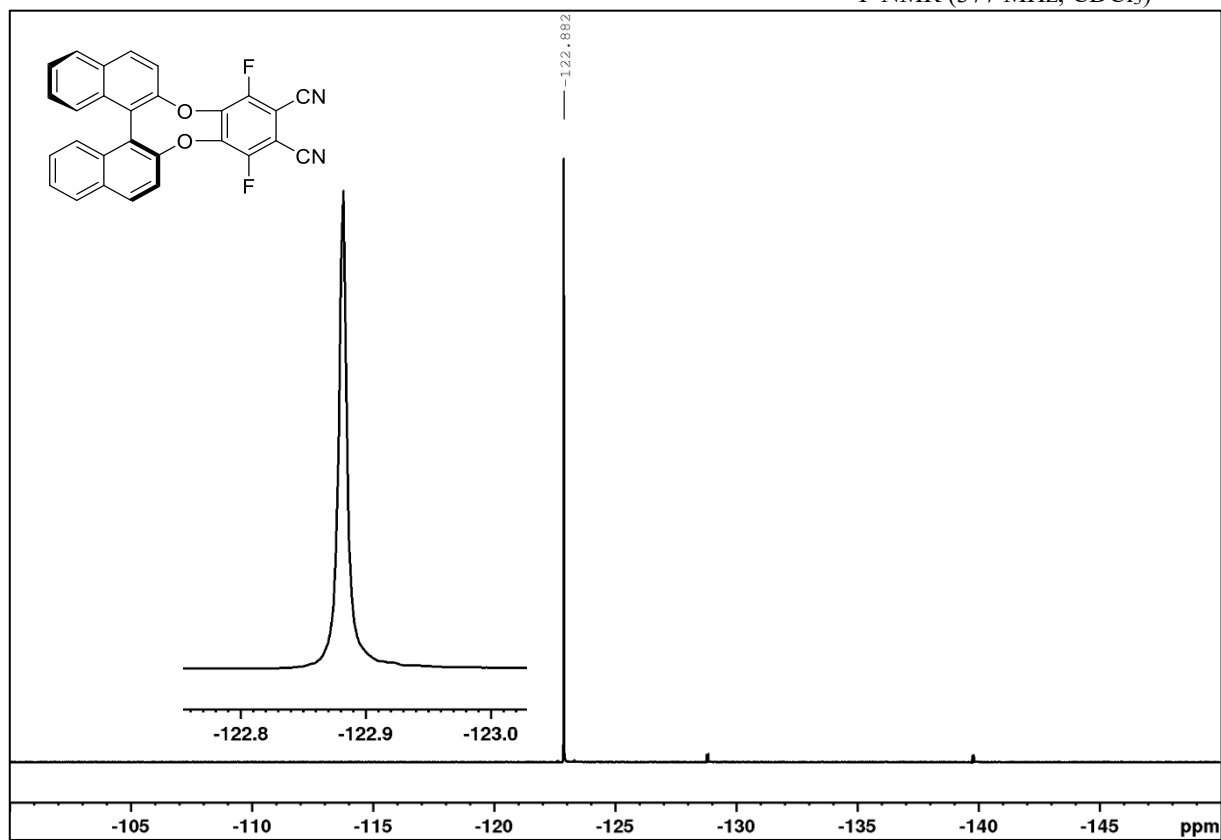
 ^{19}F NMR (377 MHz, CDCl_3)

1,4-Di(9H-carbazol-9-yl)-3-(4-fluorobenzyl)benzo[*b*]dinaphtho[2,1-*e*:1',2'-*g*][1,4]dioxocine-2-carbonitrile (7b)
¹H NMR (400 MHz, CDCl₃)¹³C{¹H} NMR (101 MHz, CDCl₃)

APPENDIX

 ^{19}F NMR (377 MHz, CDCl_3)

1,4-Difluorobenzo[b]dinaphtho[2,1-e:1',2'-g][1,4]dioxocine-2,3-dicarbonitrile (9) ^1H NMR (400 MHz, CDCl_3) $^{13}\text{C}\{^1\text{H}\}$ NMR (101 MHz, CDCl_3)

¹⁹F NMR (377 MHz, CDCl₃)

7.3 Appendix chapter 3

7.3.1 Cyclic voltammetry

[4-(Methoxycarbonyl)benzyl]triphenylphosphonium bromide (**14a**)

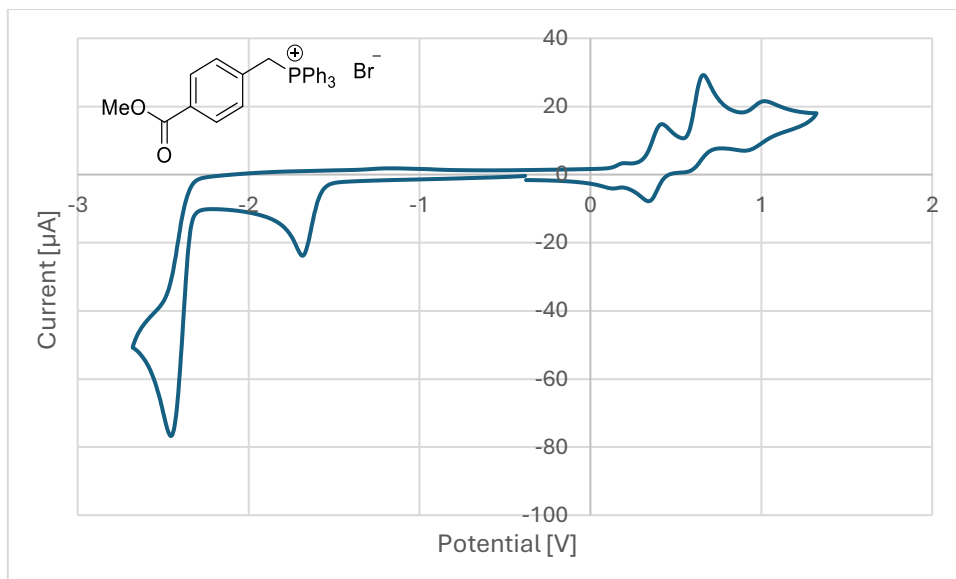


Figure 3.53. Reductive half of the cyclic voltammogram of **14a** with ferrocene as internal standard. $E_{1/2}(X/X^*) = -1.63$ V vs. SCE; peak potential: -1.69 V vs. SCE.

(3,5-Dimethoxybenzyl)triphenylphosphonium bromide (**14b**)

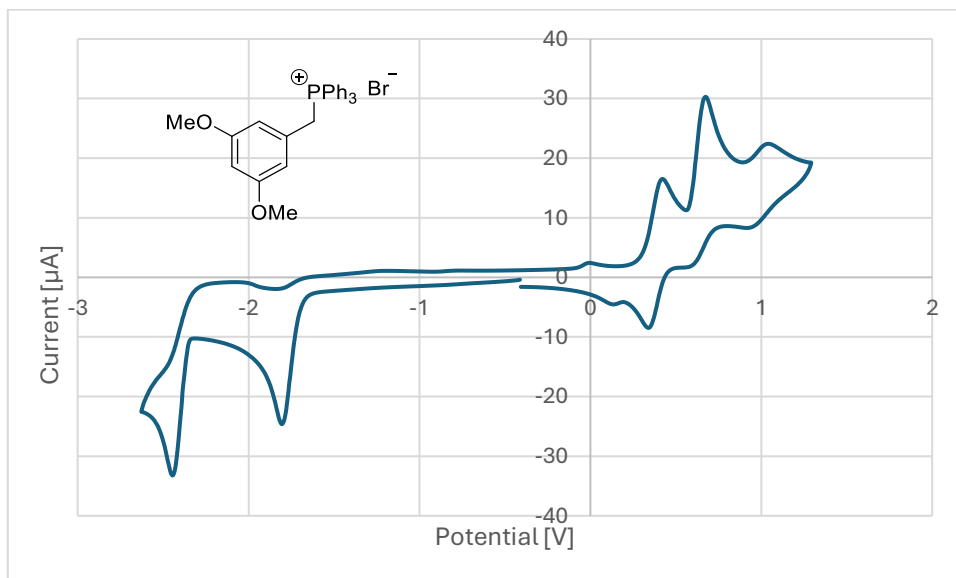


Figure 3.54. Reductive half of the cyclic voltammogram of **14b** with ferrocene as internal standard. $E_{1/2}(X/X^*) = -1.76$ V vs. SCE; peak potential: -2.63 V vs. SCE.

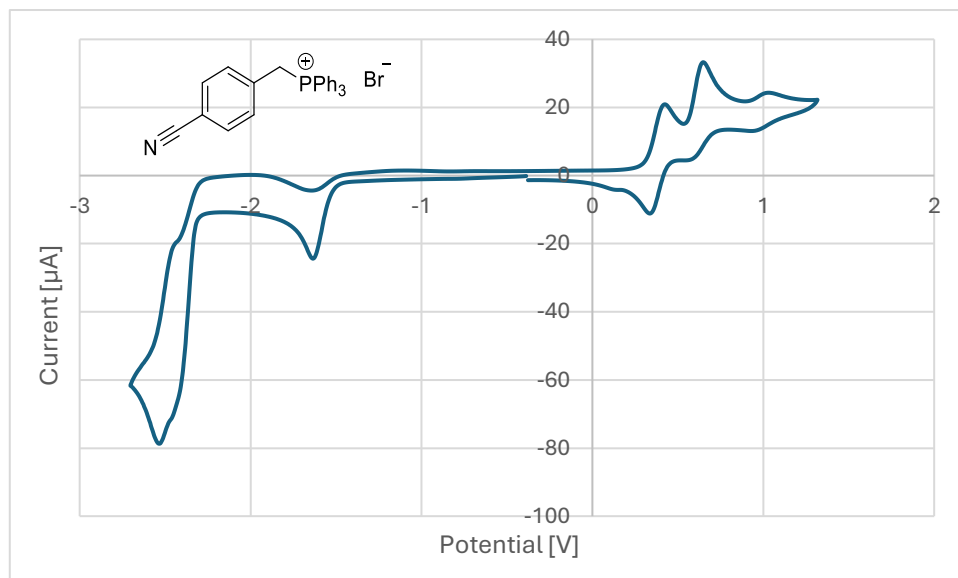
[4-Cyanobenzyl]triphenylphosphonium bromide (14c)

Figure 3.55. Reductive half of the cyclic voltammogram of **14b** with ferrocene as internal standard. $E_{1/2}(\text{X}/\text{X}^{\bullet-}) = -1.58$ V vs. SCE; peak potential: -1.64 V vs. SCE.

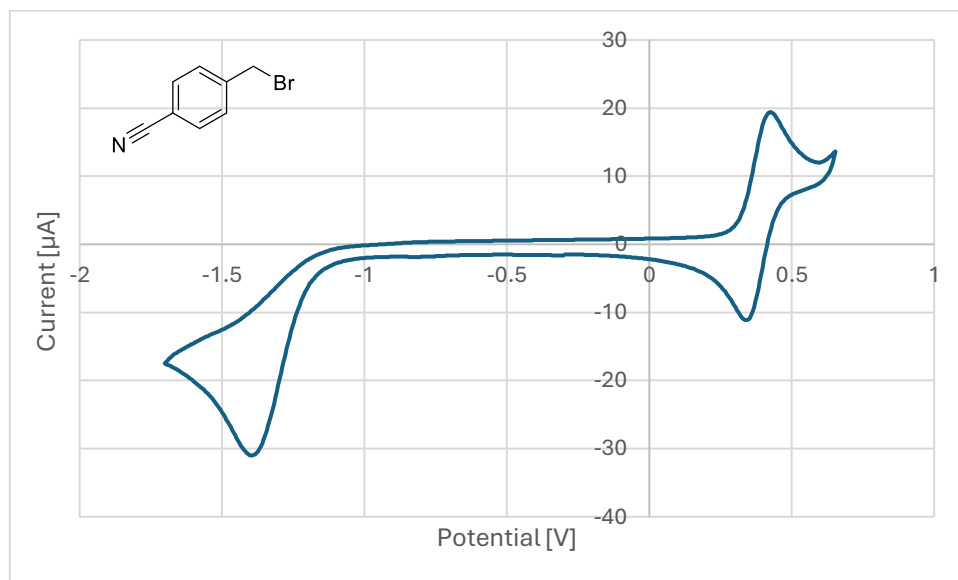
4-(Bromomethyl)benzonitrile (17)

Figure 3.56. Reductive half of the cyclic voltammogram of **17** with ferrocene as internal standard. $E_{1/2}(\text{X}/\text{X}^{\bullet-}) = -1.29$ V vs. SCE; peak potential: -1.39 V vs. SCE.

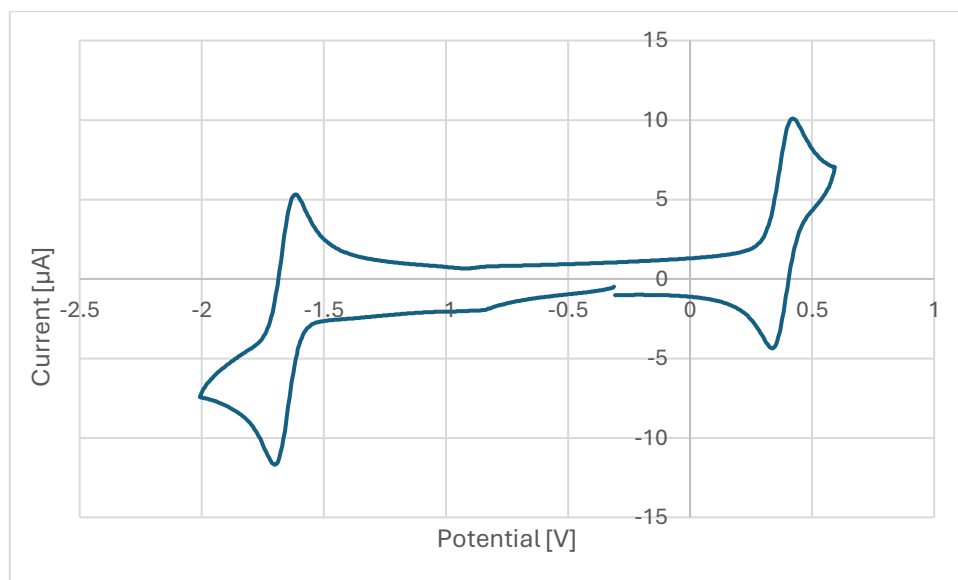
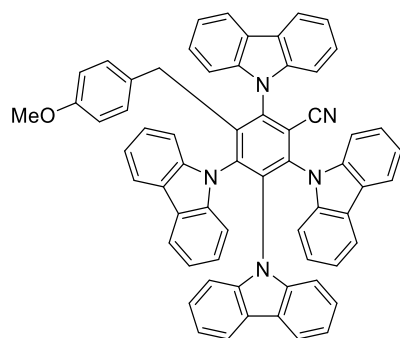
2,3,4,6-Tetra(9*H*-carbazol-9-yl)-5-(4-methoxybenzyl)benzonitrile (4d)

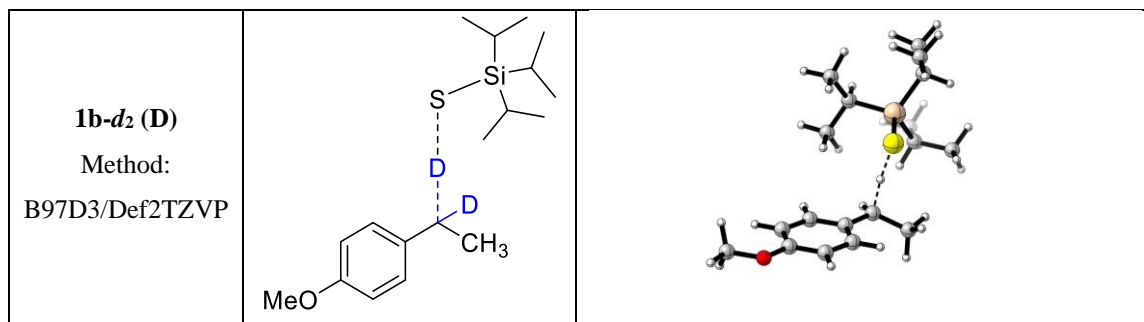
Figure 3.57. Reductive half of the cyclic voltammogram of **4d** with ferrocene as internal standard. $E_{1/2}(X/X^*) = -1.66$ V vs. SCE. The reduction potential matches the value for similar photocatalysts synthesized in chapter 2.

7.3.2 DFT calculations (optimized structures)

5.2.2.1 Kinetic isotope effects for hydrogen atom abstraction

Cartesian coordinates: (All optimized structures)

1b-d₂ (D) (TS):



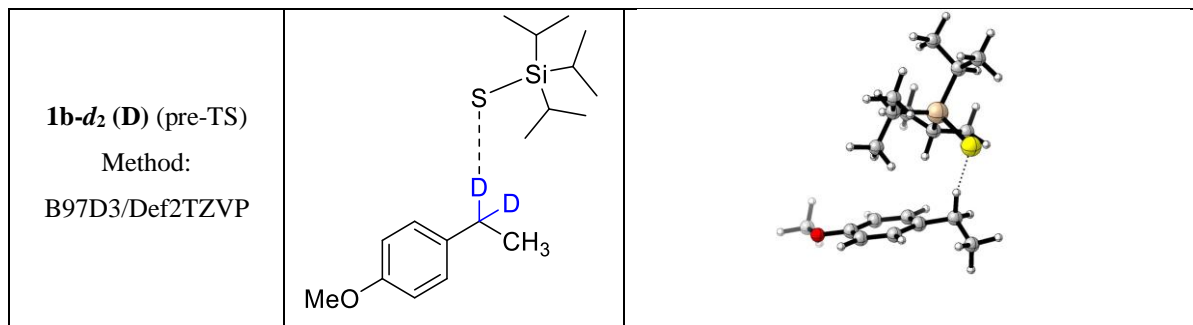
Optimized cartesian coordinates:

Si	2.38357400	-0.20976400	-0.06453600	H	0.93769000	-2.88240800	-0.30762400
C	2.69152200	1.39052300	0.94362100	H	0.92581100	-0.36758100	2.59262800
C	3.14931700	2.55527800	0.05250400	H	-0.11783200	-1.18350600	1.41479500
C	3.63815800	1.21345500	2.14195000	H	0.59005100	-2.09916400	2.75436700
H	1.70088800	1.64974700	1.34508900	S	0.72155400	0.13086300	-1.38409900
H	2.50300300	2.67366000	-0.82353600	H(Iso=2)	-0.22237900	0.90283900	-0.36345600
H	3.14956000	3.50187500	0.61035700	C	-1.08339900	1.70715700	0.38864200
H	4.17207700	2.39334100	-0.30900300	H(Iso=2)	-0.66810200	1.50971400	1.37918800
H	3.31769500	0.40813400	2.81115500	C	-2.38450900	1.09393100	0.17821300
H	4.65863500	0.98565200	1.81350400	C	-3.20513100	1.41440600	-0.92883400
H	3.69055700	2.13722700	2.73469300	C	-2.84836800	0.09146400	1.05450500
C	3.89176300	-0.60825000	-1.17449400	C	-4.41558500	0.77951500	-1.13630800
C	3.56270600	-1.44997600	-2.41809400	H	-2.88007200	2.16997800	-1.63732100
C	5.04733000	-1.23902700	-0.37763100	C	-4.06308800	-0.55442400	0.86008900
H	4.22784400	0.37707700	-1.53031800	H	-2.23842200	-0.18017600	1.91246200
H	2.78992000	-0.97699100	-3.03248700	C	-4.85888700	-0.21344500	-0.24458100
H	4.45891600	-1.58101200	-3.04040100	H	-5.04206000	1.02914400	-1.98781100
H	3.20250300	-2.44822800	-2.14726400	C	-0.77535200	3.08219200	-0.15322100
H	5.34747700	-0.62801200	0.47992500	H	0.25597200	3.36295400	0.07399900
H	4.77506800	-2.23011000	0.00338300	H	-0.89462100	3.12855900	-1.24033800
H	5.93115400	-1.36833300	-1.01733200	H	-1.44318300	3.83413100	0.29065200
C	1.98898200	-1.63707600	1.14043000	H	-4.38106900	-1.31414700	1.56511400
C	1.75330700	-2.97305900	0.41946200	O	-6.06245500	-0.77867100	-0.53680100
C	0.78252400	-1.29665700	2.02902500	C	-6.55121700	-1.80655300	0.32457300
H	2.87375500	-1.74548400	1.78665900	H	-6.70383300	-1.43069500	1.34496200
H	2.64352500	-3.31373300	-0.11830900	H	-7.50883500	-2.11590400	-0.09788000
H	1.47799000	-3.75950300	1.13599300	H	-5.86536400	-2.66352000	0.34853200

Thermodynamic Details:

Imaginary frequency: $\nu_{\text{imaginary}}$: -1047.84 cm^{-1}

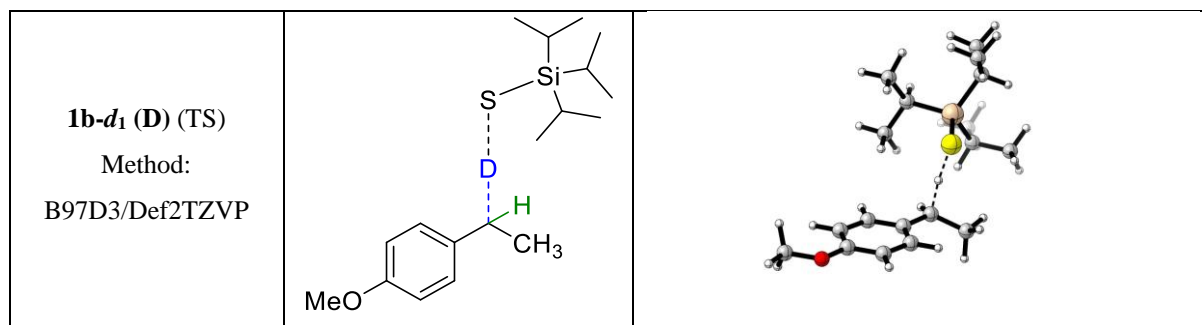
Electronic Energy (EE)	-1468.5523	Hartree
Zero-point Energy Correction	0.453188	Hartree
Thermal Correction to Energy	0.481778	Hartree
Thermal Correction to Enthalpy	0.482722	Hartree
Thermal Correction to Free Energy	0.392659	Hartree
EE + Zero-point Energy	-1468.0992	Hartree
EE + Thermal Energy Correction	-1468.0706	Hartree
EE + Thermal Enthalpy Correction	-1468.0696	Hartree
EE + Thermal Free Energy Correction	-1468.1597	Hartree
E (Thermal)	302.32	kcal/mol
Heat Capacity (Cv)	105.552	cal/mol-kelvin
Entropy (S)	189.554	cal/mol-kelvin

1b-d₂ (D) pre-TS complex**Optimized cartesian coordinates:**

Si	2.09484100	-0.18824900	0.01663300	H	2.34565900	0.02535600	-3.01725100
C	0.92129800	-0.47859200	1.50364700	H	-0.64062500	-1.15356200	-0.90369800
C	1.32705000	0.31191500	2.75373900	H	-0.12889000	0.09862700	-2.03569900
C	0.70678500	-1.96445800	1.83112800	H	-0.34147500	-1.56506600	-2.59907700
H	-0.04065300	-0.08370600	1.15482300	S	1.99891600	1.90088400	-0.45632800
H	1.47118900	1.37396600	2.53261100	H(Iso=2)	-0.10259000	2.17587300	0.20744700
H	0.55773000	0.22469800	3.53402700	C	-1.09823900	2.54757300	0.56809300
H	2.26306000	-0.06963100	3.18004900	H(Iso=2)	-0.98076900	2.63720600	1.65413500
H	0.40256300	-2.54564000	0.95446600	C	-2.12554000	1.50162200	0.26100500
H	1.61573300	-2.42163100	2.23885800	C	-2.64146100	1.32139400	-1.03503000
H	-0.07987700	-2.07643900	2.59055700	C	-2.55385900	0.61178900	1.25362700
C	3.91494600	-0.57577600	0.48937300	C	-3.53573900	0.30347900	-1.32367100
C	4.95945300	0.20178900	-0.32720000	H	-2.32298500	1.98101900	-1.83713100
C	4.20396700	-2.08562600	0.45403200	C	-3.45037900	-0.42243100	0.98536900
H	3.99289000	-0.23638500	1.53301300	H	-2.17290100	0.72541900	2.26636000
H	4.80964500	1.28344400	-0.24365900	C	-3.94570300	-0.58366200	-0.31514500
H	5.97389000	-0.03001000	0.02574000	H	-3.92396300	0.16461100	-2.32851100
H	4.91496700	-0.05725500	-1.39060000	C	-1.31795500	3.92518400	-0.05739000
H	3.50099900	-2.66285100	1.06325600	H	-0.51328900	4.60643600	0.23721900
H	4.15347700	-2.47666200	-0.56856500	H	-1.32169100	3.87755600	-1.15072400
H	5.21566600	-2.29049500	0.83097600	H	-2.27372300	4.35316600	0.26649500
C	1.49189500	-1.23614800	-1.45661700	H	-3.75304800	-1.08617000	1.78734700
C	2.34762700	-1.02906900	-2.71601900	O	-4.81873600	-1.55890800	-0.69851100
C	0.01224500	-0.95225700	-1.75877500	C	-5.24926000	-2.49734700	0.28528900
H	1.58657900	-2.28846400	-1.14664500	H	-5.78721600	-1.99901400	1.10292700
H	3.38904700	-1.33067600	-2.56321200	H	-5.92446900	-3.18121400	-0.23227600
H	1.95217000	-1.61621600	-3.55620200	H	-4.40043700	-3.05996900	0.69670500

Thermodynamic Details:

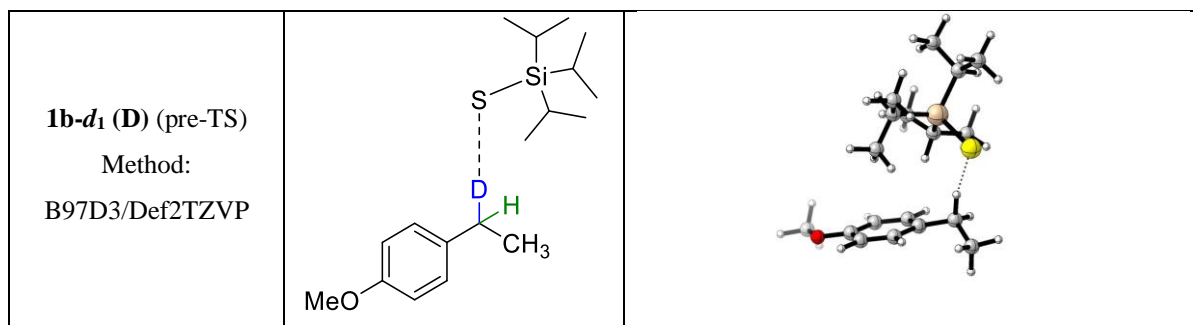
Electronic Energy (EE): -1468.5623 Hartree
 Zero-point Energy Correction: 0.456856 Hartree
 Thermal Correction to Energy: 0.486187 Hartree
 Thermal Correction to Enthalpy: 0.487131 Hartree
 Thermal Correction to Free Energy: 0.393325 Hartree
 EE + Zero-point Energy: -1468.1054 Hartree
 EE + Thermal Energy Correction: -1468.0761 Hartree
 EE + Thermal Enthalpy Correction: -1468.0752 Hartree
 EE + Thermal Free Energy Correction: -1468.169 Hartree
 E (Thermal): 305.087 kcal/mol
 Heat Capacity (Cv): 105.942 cal/mol-kelvin
 Entropy (S): 197.432 cal/mol-kelvin

1b-d₁ (D) (TS)**Optimized cartesian coordinates:**

Si	2.38374400	-0.20972100	-0.06458400	H	0.93771600	-2.88259100	-0.30539300
C	2.69202100	1.39110800	0.94259700	H	0.92750300	-0.36636500	2.59358100
C	3.14915000	2.55548600	0.05064800	H	-0.11679000	-1.18281600	1.41668300
C	3.63940200	1.21472000	2.14043800	H	0.59187600	-2.09788700	2.75623700
H	1.70159100	1.65037700	1.34453700	S	0.72107900	0.13001200	-1.38357100
H	2.50234000	2.67334100	-0.82509700	H(Iso=2)	-0.22263600	0.90230900	-0.36295800
H	3.14956400	3.50235700	0.60803400	C	-1.08355400	1.70665700	0.38918000
H	4.17173600	2.39352100	-0.31134100	H	-0.66833100	1.50892500	1.37969900
H	3.31910800	0.41005200	2.81050900	C	-2.38472500	1.09362000	0.17852400
H	4.65959200	0.98631400	1.81151600	C	-3.20541300	1.41469800	-0.92829400
H	3.69249000	2.13896000	2.73238900	C	-2.84858300	0.09076500	1.05436800
C	3.89148000	-0.60865800	-1.17500800	C	-4.41595200	0.78002000	-1.13594500
C	3.56188300	-1.45067600	-2.41826600	H	-2.88035400	2.17057200	-1.63645700
C	5.04728700	-1.23935800	-0.37842800	C	-4.06338100	-0.55492000	0.85975900
H	4.22754500	0.37653800	-1.53120700	H	-2.23856200	-0.18138100	1.91211200
H	2.78893800	-0.97776400	-3.03251400	C	-4.85928000	-0.21331000	-0.24464600
H	4.45785600	-1.58199600	-3.04085400	H	-5.04248600	1.03013500	-1.98726200
H	3.20164800	-2.44880800	-2.14703000	C	-0.77535100	3.08177600	-0.15236900
H	5.34751700	-0.62841700	0.47915200	H	0.25597400	3.36242700	0.07496700
H	4.77521900	-2.23052100	0.00251200	H	-0.89455700	3.12838200	-1.23948300
H	5.93101000	-1.36846800	-1.01830700	H	-1.44314600	3.83367900	0.29162000
C	1.98988300	-1.63644700	1.14131600	H	-4.38131500	-1.31500400	1.56440800
C	1.75388300	-2.97279500	0.42113000	O	-6.06293400	-0.77830300	-0.53706100
C	0.78391900	-1.29568100	2.03044900	C	-6.55186300	-1.80643700	0.32391900
H	2.87503400	-1.74448200	1.78709200	H	-6.70399800	-1.43106400	1.34455100
H	2.64374900	-3.31357800	-0.11715300	H	-7.50974500	-2.11516200	-0.09838700
H	1.47921800	-3.75895700	1.13822000	H	-5.86635900	-2.66369600	0.34720100

Thermodynamics Details:Imaginary frequency: $\nu_{\text{imaginary}} = -1051.17\text{cm}^{-1}$

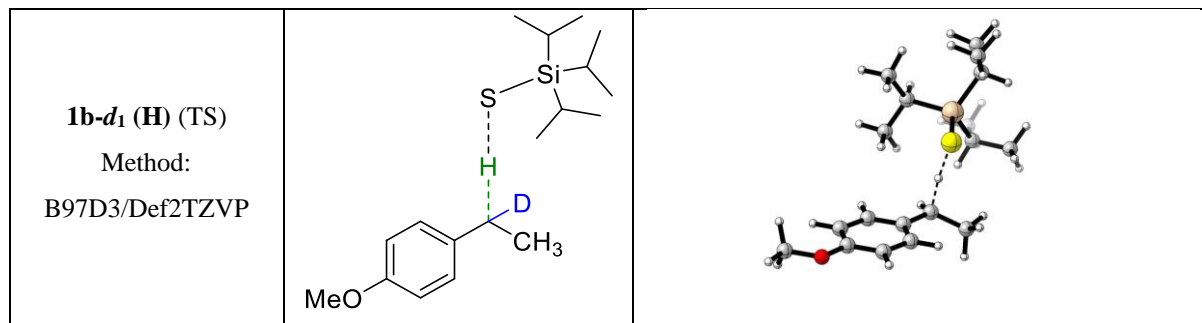
Electronic Energy (EE):	-1468.5523	Hartree
Zero-point Energy Correction:	0.456419	Hartree
Thermal Correction to Energy:	0.484865	Hartree
Thermal Correction to Enthalpy:	0.485809	Hartree
Thermal Correction to Free Energy:	0.395984	Hartree
EE + Zero-point Energy:	-1468.0959	Hartree
EE + Thermal Energy Correction:	-1468.0675	Hartree
EE + Thermal Enthalpy Correction:	-1468.0665	Hartree
EE + Thermal Free Energy Correction:	-1468.1564	Hartree
E (Thermal):	304.257	kcal/mol
Heat Capacity (Cv):	104.821	cal/mol-kelvin
Entropy (S):	189.052	cal/mol-kelvin

1b-d₁ (D) (pre-TS complex)**Optimized cartesian coordinates:**

Si	2.09484100	-0.18824900	0.01663300	H	2.34565900	0.02535600	-3.01725100
C	0.92129800	-0.47859200	1.50364700	H	-0.64062500	-1.15356200	-0.90369800
C	1.32705000	0.31191500	2.75373900	H	-0.12889000	0.09862700	-2.03569900
C	0.70678500	-1.96445800	1.83112800	H	-0.34147500	-1.56506600	-2.59907700
H	-0.04065300	-0.08370600	1.15482300	S	1.99891600	1.90088400	-0.45632800
H	1.47118900	1.37396600	2.53261100	H(Iso=2)	-0.10259000	2.17587300	0.20744700
H	0.55773000	0.22469800	3.53402700	C	-1.09823900	2.54757300	0.56809300
H	2.26306000	-0.06963100	3.18004900	H	-0.98076900	2.63720600	1.65413500
H	0.40256300	-2.54564000	0.95446600	C	-2.12554000	1.50162200	0.26100500
H	1.61573300	-2.42163100	2.23885800	C	-2.64146100	1.32139400	-1.03503000
H	-0.07987700	-2.07643900	2.59055700	C	-2.55385900	0.61178900	1.25362700
C	3.91494600	-0.57577600	0.48937300	C	-3.53573900	0.30347900	-1.32367100
C	4.95945300	0.20178900	-0.32720000	H	-2.32298500	1.98101900	-1.83713100
C	4.20396700	-2.08562600	0.45403200	C	-3.45037900	-0.42243100	0.98536900
H	3.99289000	-0.23638500	1.53301300	H	-2.17290100	0.72541900	2.26636000
H	4.80964500	1.28344400	-0.24365900	C	-3.94570300	-0.58366200	-0.31514500
H	5.97389000	-0.03001000	0.02574000	H	-3.92396300	0.16461100	-2.32851100
H	4.91496700	-0.05725500	-1.39060000	C	-1.31795500	3.92518400	-0.05739000
H	3.50099900	-2.66285100	1.06325600	H	-0.51328900	4.60643600	0.23721900
H	4.15347700	-2.47666200	-0.56856500	H	-1.32169100	3.87755600	-1.15072400
H	5.21566600	-2.29049500	0.83097600	H	-2.27372300	4.35316600	0.26649500
C	1.49189500	-1.23614800	-1.45661700	H	-3.75304800	-1.08617000	1.78734700
C	2.34762700	-1.02906900	-2.71601900	O	-4.81873600	-1.55890800	-0.69851100
C	0.01224500	-0.95225700	-1.75877500	C	-5.24926000	-2.49734700	0.28528900
H	1.58657900	-2.28846400	-1.14664500	H	-5.78721600	-1.99901400	1.10292700
H	3.38904700	-1.33067600	-2.56321200	H	-5.92446900	-3.18121400	-0.23227600
H	1.95217000	-1.61621600	-3.55620200	H	-4.40043700	-3.05996900	0.69670500

Thermodynamic Details:

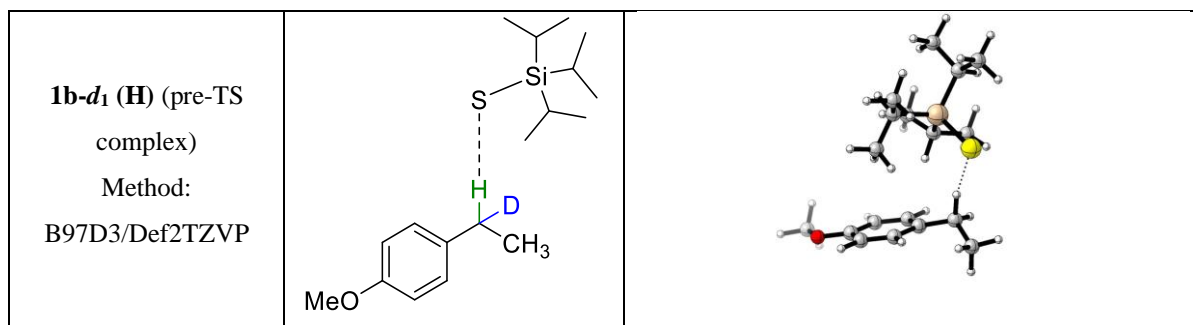
Electronic Energy (EE):	-1468.5623	Hartree
Zero-point Energy Correction:	0.459876	Hartree
Thermal Correction to Energy:	0.489082	Hartree
Thermal Correction to Enthalpy:	0.490026	Hartree
Thermal Correction to Free Energy:	0.396448	Hartree
EE + Zero-point Energy:	-1468.1024	Hartree
EE + Thermal Energy Correction:	-1468.0732	Hartree
EE + Thermal Enthalpy Correction:	-1468.0723	Hartree
EE + Thermal Free Energy Correction:	-1468.1658	Hartree
E (Thermal):	306.904	kcal/mol
Heat Capacity (Cv):	105.261	cal/mol-kelvin
Entropy (S):	196.952	cal/mol-kelvin

1b-d₁ (H) (TS)**Optimized cartesian coordinates:**

Si	2.38373000	-0.20971800	-0.06456800	H	0.93733000	-2.88249500	-0.30540400
C	2.69207100	1.39106300	0.94266600	H	0.92730700	-0.36632000	2.59353800
C	3.14917300	2.55548000	0.05075500	H	-0.11701000	-1.18260500	1.41654400
C	3.63949600	1.21461300	2.14046300	H	0.59149300	-2.09781400	2.75608500
H	1.70165500	1.65031800	1.34465600	S	0.72120700	0.13020600	-1.38368700
H	2.50232300	2.67338500	-0.82495300	H	-0.22255400	0.90241900	-0.36305800
H	3.14962700	3.50232200	0.60819000	C	-1.08351800	1.70669100	0.38912300
H	4.17173800	2.39351900	-0.31129300	H(Iso=2)	-0.66831600	1.50894500	1.37964800
H	3.31925300	0.40987700	2.81047800	C	-2.38466100	1.09359900	0.17842700
H	4.65968300	0.98628000	1.81148600	C	-3.20520100	1.41442000	-0.92857400
H	3.69256500	2.13880600	2.73249100	C	-2.84864000	0.09095600	1.05444900
C	3.89152800	-0.60878000	-1.17485800	C	-4.41573800	0.77973300	-1.13620800
C	3.56196700	-1.45064600	-2.41822800	H	-2.88001600	2.17007900	-1.63690800
C	5.04717100	-1.23970800	-0.37821500	C	-4.06343800	-0.55473600	0.85985800
H	4.22776800	0.37639900	-1.53094300	H	-2.23871800	-0.18102200	1.91231800
H	2.78920800	-0.97754300	-3.03256200	C	-4.85920700	-0.21334700	-0.24470400
H	4.45801100	-1.58209300	-3.04068800	H	-5.04216000	1.02964900	-1.98766700
H	3.20149900	-2.44872800	-2.14711800	C	-0.77536100	3.08185100	-0.15234000
H	5.34697700	-0.62922700	0.47984000	H	0.25608600	3.36234600	0.07463400
H	4.77513500	-2.23114300	0.00203800	H	-0.89500700	3.12865500	-1.23939500
H	5.93115200	-1.36828400	-1.01784300	H	-1.44289100	3.83375800	0.29204400
C	1.98963600	-1.63643200	1.14126800	H	-4.38147300	-1.31465700	1.56464200
C	1.75356200	-2.97274400	0.42104000	O	-6.06288500	-0.77834400	-0.53706200
C	0.78365700	-1.29559000	2.03034900	C	-6.55184600	-1.80626700	0.32414900
H	2.87473800	-1.74456600	1.78709500	H	-6.70363900	-1.43075900	1.34478500
H	2.64337300	-3.31351200	-0.11734500	H	-7.50991100	-2.11481100	-0.09787700
H	1.47895500	-3.75893700	1.13811800	H	-5.86654000	-2.66368900	0.34733900

Thermodynamics Details:Imaginary frequency: $\nu_{\text{imaginary}} = -1397.44\text{cm}^{-1}$

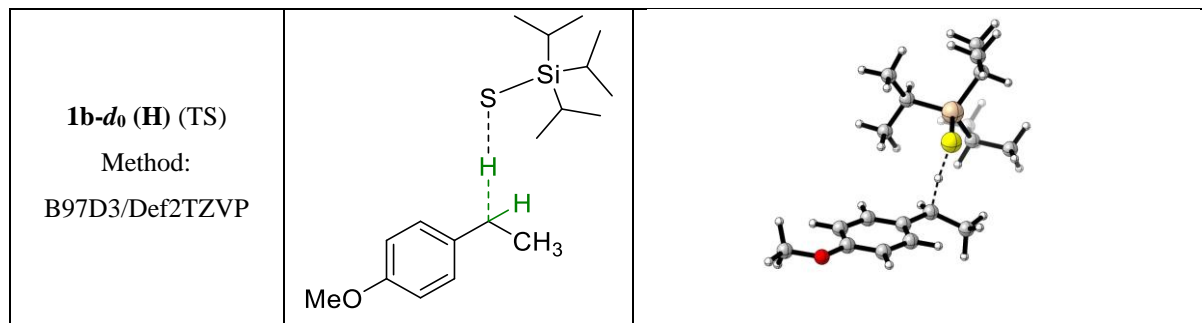
Electronic Energy (EE):	-1468.5523	Hartree
Zero-point Energy Correction:	0.454572	Hartree
Thermal Correction to Energy:	0.483001	Hartree
Thermal Correction to Enthalpy:	0.483945	Hartree
Thermal Correction to Free Energy:	0.394126	Hartree
EE + Zero-point Energy:	-1468.0978	Hartree
EE + Thermal Energy Correction:	-1468.0693	Hartree
EE + Thermal Enthalpy Correction:	-1468.0684	Hartree
EE + Thermal Free Energy Correction:	-1468.1582	Hartree
E (Thermal):	303.088	kcal/mol
Heat Capacity (Cv):	104.679	cal/mol-kelvin
Entropy (S):	189.04	cal/mol-kelvin

1b-d₁ (H) (pre-TS complex)**Optimized cartesian coordinates:**

Si	2.09484100	-0.18824900	0.01663300	H	2.34565900	0.02535600	-3.01725100
C	0.92129800	-0.47859200	1.50364700	H	-0.64062500	-1.15356200	-0.90369800
C	1.32705000	0.31191500	2.75373900	H	-0.12889000	0.09862700	-2.03569900
C	0.70678500	-1.96445800	1.83112800	H	-0.34147500	-1.56506600	-2.59907700
H	-0.04065300	-0.08370600	1.15482300	S	1.99891600	1.90088400	-0.45632800
H	1.47118900	1.37396600	2.53261100	H	-0.10259000	2.17587300	0.20744700
H	0.55773000	0.22469800	3.53402700	C	-1.09823900	2.54757300	0.56809300
H	2.26306000	-0.06963100	3.18004900	H(Iso=2)	-0.98076900	2.63720600	1.65413500
H	0.40256300	-2.54564000	0.95446600	C	-2.12554000	1.50162200	0.26100500
H	1.61573300	-2.42163100	2.23885800	C	-2.64146100	1.32139400	-1.03503000
H	-0.07987700	-2.07643900	2.59055700	C	-2.55385900	0.61178900	1.25362700
C	3.91494600	-0.57577600	0.48937300	C	-3.53573900	0.30347900	-1.32367100
C	4.95945300	0.20178900	-0.32720000	H	-2.32298500	1.98101900	-1.83713100
C	4.20396700	-2.08562600	0.45403200	C	-3.45037900	-0.42243100	0.98536900
H	3.99289000	-0.23638500	1.53301300	H	-2.17290100	0.72541900	2.26636000
H	4.80964500	1.28344400	-0.24365900	C	-3.94570300	-0.58366200	-0.31514500
H	5.97389000	-0.03001000	0.02574000	H	-3.92396300	0.16461100	-2.32851100
H	4.91496700	-0.05725500	-1.39060000	C	-1.31795500	3.92518400	-0.05739000
H	3.50099900	-2.66285100	1.06325600	H	-0.51328900	4.60643600	0.23721900
H	4.15347700	-2.47666200	-0.56856500	H	-1.32169100	3.87755600	-1.15072400
H	5.21566600	-2.29049500	0.83097600	H	-2.27372300	4.35316600	0.26649500
C	1.49189500	-1.23614800	-1.45661700	H	-3.75304800	-1.08617000	1.78734700
C	2.34762700	-1.02906900	-2.71601900	O	-4.81873600	-1.55890800	-0.69851100
C	0.01224500	-0.95225700	-1.75877500	C	-5.24926000	-2.49734700	0.28528900
H	1.58657900	-2.28846400	-1.14664500	H	-5.78721600	-1.99901400	1.10292700
H	3.38904700	-1.33067600	-2.56321200	H	-5.92446900	-3.18121400	-0.23227600
H	1.95217000	-1.61621600	-3.55620200	H	-4.40043700	-3.05996900	0.69670500

Thermodynamic Details:

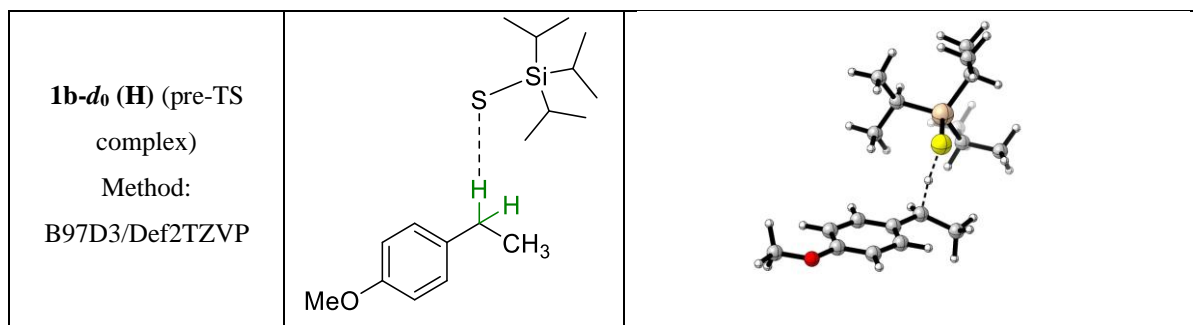
Electronic Energy (EE):	-1468.5623	Hartree
Zero-point Energy Correction:	0.460162	Hartree
Thermal Correction to Energy:	0.489378	Hartree
Thermal Correction to Enthalpy:	0.490322	Hartree
Thermal Correction to Free Energy:	0.396732	Hartree
EE + Zero-point Energy:	-1468.1021	Hartree
EE + Thermal Energy Correction:	-1468.0729	Hartree
EE + Thermal Enthalpy Correction:	-1468.072	Hartree
EE + Thermal Free Energy Correction:	-1468.1656	Hartree
E (Thermal):	307.089	kcal/mol
Heat Capacity (Cv):	105.3	cal/mol-kelvin
Entropy (S):	196.978	cal/mol-kelvin

1b-d₀ (H) (TS)**Optimized cartesian coordinates:**

Si	2.38373000	-0.20971800	-0.06456800	H	0.93733000	-2.88249500	-0.30540400
C	2.69207100	1.39106300	0.94266600	H	0.92730700	-0.36632000	2.59353800
C	3.14917300	2.55548000	0.05075500	H	-0.11701000	-1.18260500	1.41654400
C	3.63949600	1.21461300	2.14046300	H	0.59149300	-2.09781400	2.75608500
H	1.70165500	1.65031800	1.34465600	S	0.72120700	0.13020600	-1.38368700
H	2.50232300	2.67338500	-0.82495300	H	-0.22255400	0.90241900	-0.36305800
H	3.14962700	3.50232200	0.60819000	C	-1.08351800	1.70669100	0.38912300
H	4.17173800	2.39351900	-0.31129300	H	-0.66831600	1.50894500	1.37964800
H	3.31925300	0.40987700	2.81047800	C	-2.38466100	1.09359900	0.17842700
H	4.65968300	0.98628000	1.81148600	C	-3.20520100	1.41442000	-0.92857400
H	3.69256500	2.13880600	2.73249100	C	-2.84864000	0.09095600	1.05444900
C	3.89152800	-0.60878000	-1.17485800	C	-4.41573800	0.77973300	-1.13620800
C	3.56196700	-1.45064600	-2.41822800	H	-2.88001600	2.17007900	-1.63690800
C	5.04717100	-1.23970800	-0.37821500	C	-4.06343800	-0.55473600	0.85985800
H	4.22776800	0.37639900	-1.53094300	H	-2.23871800	-0.18102200	1.91231800
H	2.78920800	-0.97754300	-3.03256200	C	-4.85920700	-0.21334700	-0.24470400
H	4.45801100	-1.58209300	-3.04068800	H	-5.04216000	1.02964900	-1.98766700
H	3.20149900	-2.44872800	-2.14711800	C	-0.77536100	3.08185100	-0.15234000
H	5.34697700	-0.62922700	0.47984000	H	0.25608600	3.36234600	0.07463400
H	4.77513500	-2.23114300	0.00203800	H	-0.89500700	3.12865500	-1.23939500
H	5.93115200	-1.36828400	-1.01784300	H	-1.44289100	3.83375800	0.29204400
C	1.98963600	-1.63643200	1.14126800	H	-4.38147300	-1.31465700	1.56464200
C	1.75356200	-2.97274400	0.42104000	O	-6.06288500	-0.77834400	-0.53706200
C	0.78365700	-1.29559000	2.03034900	C	-6.55184600	-1.80626700	0.32414900
H	2.87473800	-1.74456600	1.78709500	H	-6.70363900	-1.43075900	1.34478500
H	2.64337300	-3.31351200	-0.11734500	H	-7.50991100	-2.11481100	-0.09787700
H	1.47895500	-3.75893700	1.13811800	H	-5.86654000	-2.66368900	0.34733900

Thermodynamic Details:Imaginary frequency: $\nu_{\text{imaginary}}: -1402.76\text{cm}^{-1}$

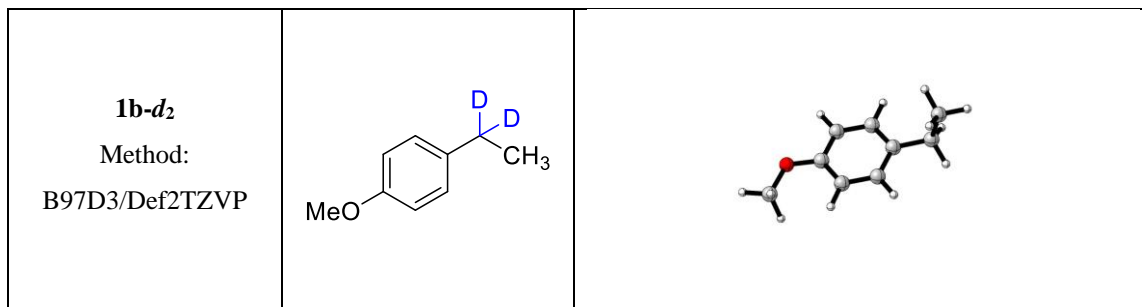
Electronic Energy (EE)	-1468.5523	Hartree
Zero-point Energy Correction	0.457802	Hartree
Thermal Correction to Energy	0.486086	Hartree
Thermal Correction to Enthalpy	0.48703	Hartree
Thermal Correction to Free Energy	0.39745	Hartree
EE + Zero-point Energy	-1468.0945	Hartree
EE + Thermal Energy Correction	-1468.0663	Hartree
EE + Thermal Enthalpy Correction	-1468.0653	Hartree
EE + Thermal Free Energy Correction	-1468.1549	Hartree
E (Thermal)	305.023	kcal/mol
Heat Capacity (Cv)	103.957	cal/mol-kelvin
Entropy (S)	188.536	cal/mol-kelvin

1b-d₀ (H) (pre-TS complex)**Optimized cartesian coordinates:**

Si	2.09484100	-0.18824900	0.01663300	H	2.34565900	0.02535600	-3.01725100
C	0.92129800	-0.47859200	1.50364700	H	-0.64062500	-1.15356200	-0.90369800
C	1.32705000	0.31191500	2.75373900	H	-0.12889000	0.09862700	-2.03569900
C	0.70678500	-1.96445800	1.83112800	H	-0.34147500	-1.56506600	-2.59907700
H	-0.04065300	-0.08370600	1.15482300	S	1.99891600	1.90088400	-0.45632800
H	1.47118900	1.37396600	2.53261100	H	-0.10259000	2.17587300	0.20744700
H	0.55773000	0.22469800	3.53402700	C	-1.09823900	2.54757300	0.56809300
H	2.26306000	-0.06963100	3.18004900	H	-0.98076900	2.63720600	1.65413500
H	0.40256300	-2.54564000	0.95446600	C	-2.12554000	1.50162200	0.26100500
H	1.61573300	-2.42163100	2.23885800	C	-2.64146100	1.32139400	-1.03503000
H	-0.07987700	-2.07643900	2.59055700	C	-2.55385900	0.61178900	1.25362700
C	3.91494600	-0.57577600	0.48937300	C	-3.53573900	0.30347900	-1.32367100
C	4.95945300	0.20178900	-0.32720000	H	-2.32298500	1.98101900	-1.83713100
C	4.20396700	-2.08562600	0.45403200	C	-3.45037900	-0.42243100	0.98536900
H	3.99289000	-0.23638500	1.53301300	H	-2.17290100	0.72541900	2.26636000
H	4.80964500	1.28344400	-0.24365900	C	-3.94570300	-0.58366200	-0.31514500
H	5.97389000	-0.03001000	0.02574000	H	-3.92396300	0.16461100	-2.32851100
H	4.91496700	-0.05725500	-1.39060000	C	-1.31795500	3.92518400	-0.05739000
H	3.50099900	-2.66285100	1.06325600	H	-0.51328900	4.60643600	0.23721900
H	4.15347700	-2.47666200	-0.56856500	H	-1.32169100	3.87755600	-1.15072400
H	5.21566600	-2.29049500	0.83097600	H	-2.27372300	4.35316600	0.26649500
C	1.49189500	-1.23614800	-1.45661700	H	-3.75304800	-1.08617000	1.78734700
C	2.34762700	-1.02906900	-2.71601900	O	-4.81873600	-1.55890800	-0.69851100
C	0.01224500	-0.95225700	-1.75877500	C	-5.24926000	-2.49734700	0.28528900
H	1.58657900	-2.28846400	-1.14664500	H	-5.78721600	-1.99901400	1.10292700
H	3.38904700	-1.33067600	-2.56321200	H	-5.92446900	-3.18121400	-0.23227600
H	1.95217000	-1.61621600	-3.55620200	H	-4.40043700	-3.05996900	0.69670500

Thermodynamic Details:

Electronic Energy (EE):	-1468.5623 Hartree
Zero-point Energy Correction:	0.463162 Hartree
Thermal Correction to Energy:	0.492246 Hartree
Thermal Correction to Enthalpy:	0.49319 Hartree
Thermal Correction to Free Energy:	0.399842 Hartree
EE + Zero-point Energy:	-1468.0991 Hartree
EE + Thermal Energy Correction:	-1468.07 Hartree
EE + Thermal Enthalpy Correction:	-1468.0691 Hartree
EE + Thermal Free Energy Correction:	-1468.1624 Hartree
E (Thermal):	308.889 kcal/mol
Heat Capacity (Cv):	104.633 cal/mol-kelvin
Entropy (S):	196.467 cal/mol-kelvin

1b-d₂**Optimized cartesian coordinates:**

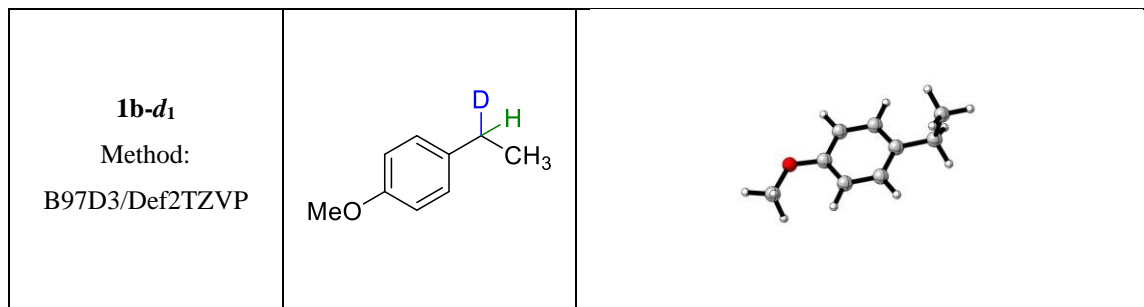
```

H(Iso=2)  3.27508200  0.66338600 -1.08261500
C         2.87065100 -0.17163700 -0.49601800
H(Iso=2)  3.09313300 -1.08687000 -1.05903000
C         1.37545500 -0.01472900 -0.35957600
C         0.79081000  1.25331700 -0.21993100
C         0.52944300 -1.12413600 -0.31462700
C        -0.57810000  1.40722200 -0.04334200
H         1.42297500  2.13895000 -0.25381200
C        -0.85121000 -0.99391600 -0.13768700
H         0.95177600 -2.12175500 -0.42263200
C        -1.41186900  0.28054100  0.00041100
H        -1.02547400  2.39203100  0.05833100
C         3.58285700 -0.22634300  0.86550900
H         4.66674500 -0.33700900  0.74237000
H         3.39434900  0.68861700  1.43846000
H         3.21609900 -1.07099900  1.45969400
H        -1.47020900 -1.88389700 -0.11422500
O        -2.74675100  0.53051400  0.17529000
C        -3.62976300 -0.58492000  0.22411200
H        -3.38599800 -1.25309900  1.06189300
H        -4.62872600 -0.16871800  0.36996300
H        -3.60538900 -1.15714900 -0.71381500
  
```

Thermodynamic Details:

```

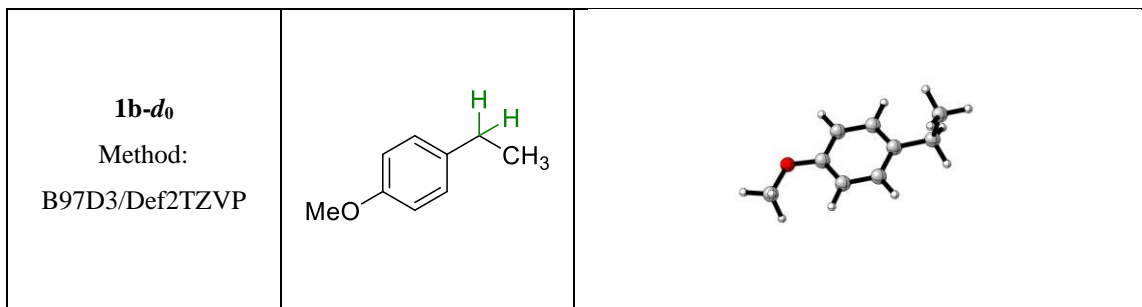
Electronic Energy (EE):  -425.28808  Hartree
Zero-point Energy Correction:  0.178392  Hartree
Thermal Correction to Energy:  0.188703  Hartree
Thermal Correction to Enthalpy:  0.189647  Hartree
Thermal Correction to Free Energy:  0.14231  Hartree
EE + Zero-point Energy:  -425.10969  Hartree
EE + Thermal Energy Correction:  -425.09938  Hartree
EE + Thermal Enthalpy Correction:  -425.09844  Hartree
EE + Thermal Free Energy Correction:  -425.14578  Hartree
E (Thermal):  118.413  kcal/mol
Heat Capacity (Cv):  39.28  cal/mol-kelvin
Entropy (S):  99.63  cal/mol-kelvin
  
```

1b-d₁**Optimized cartesian coordinates:**

H(Iso=2)	3.27506600	0.66333200	-1.08268800
C	2.87065100	-0.17165900	-0.49603400
H	3.09312700	-1.08692500	-1.05899600
C	1.37545600	-0.01475100	-0.35957300
C	0.79081200	1.25329700	-0.21994800
C	0.52944900	-1.12415900	-0.31457700
C	-0.57809600	1.40720100	-0.04334000
H	1.42297500	2.13893000	-0.25385300
C	-0.85120200	-0.99393800	-0.13762500
H	0.95178200	-2.12178200	-0.42254800
C	-1.41186600	0.28052100	0.00042700
H	-1.02546800	2.39201100	0.05832200
C	3.58288200	-0.22628100	0.86548300
H	4.66676900	-0.33694600	0.74233000
H	3.39437800	0.68871100	1.43838400
H	3.21614100	-1.07090400	1.45972400
H	-1.47019400	-1.88391900	-0.11410600
O	-2.74673700	0.53051400	0.17529100
C	-3.62981200	-0.58487300	0.22406200
H	-4.62884600	-0.16857100	0.36910300
H	-3.60486300	-1.15755800	-0.71356600
H	-3.38661200	-1.25263300	1.06231900

Thermodynamic details:

Electronic Energy (EE):	-425.28808	Hartree
Zero-point Energy Correction:	0.181689	Hartree
Thermal Correction to Energy:	0.191889	Hartree
Thermal Correction to Enthalpy:	0.192833	Hartree
Thermal Correction to Free Energy:	0.145711	Hartree
EE + Zero-point Energy:	-425.1064	Hartree
EE + Thermal Energy Correction:	-425.0962	Hartree
EE + Thermal Enthalpy Correction:	-425.09525	Hartree
EE + Thermal Free Energy Correction:	-425.14237	Hartree
E (Thermal):	120.412	kcal/mol
Heat Capacity (Cv):	38.643	cal/mol-kelvin
Entropy (S):	99.176	cal/mol-kelvin

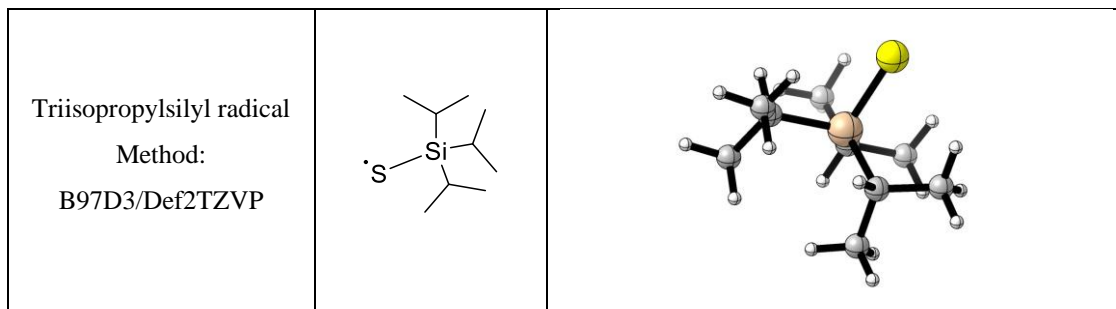
1b-d₀**Optimized cartesian coordinates:**

H	3.27506600	0.66333200	-1.08268800
C	2.87065100	-0.17165900	-0.49603400
H	3.09312700	-1.08692500	-1.05899600
C	1.37545600	-0.01475100	-0.35957300
C	0.79081200	1.25329700	-0.21994800
C	0.52944900	-1.12415900	-0.31457700
C	-0.57809600	1.40720100	-0.04334000
H	1.42297500	2.13893000	-0.25385300
C	-0.85120200	-0.99393800	-0.13762500
H	0.95178200	-2.12178200	-0.42254800
C	-1.41186600	0.28052100	0.00042700
H	-1.02546800	2.39201100	0.05832200
C	3.58288200	-0.22628100	0.86548300
H	4.66676900	-0.33694600	0.74233000
H	3.39437800	0.68871100	1.43838400
H	3.21614100	-1.07090400	1.45972400
H	-1.47019400	-1.88391900	-0.11410600
O	-2.74673700	0.53051400	0.17529100
C	-3.62981200	-0.58487300	0.22406200
H	-4.62884600	-0.16857100	0.36910300
H	-3.60486300	-1.15755800	-0.71356600
H	-3.38661200	-1.25263300	1.06231900

Thermodynamic Details:

Electronic Energy (EE):	-425.28808	Hartree
Zero-point Energy Correction:	0.18496	Hartree
Thermal Correction to Energy:	0.195041	Hartree
Thermal Correction to Enthalpy:	0.195985	Hartree
Thermal Correction to Free Energy:	0.149097	Hartree
EE + Zero-point Energy:	-425.10312	Hartree
EE + Thermal Energy Correction:	-425.09304	Hartree
EE + Thermal Enthalpy Correction:	-425.0921	Hartree
EE + Thermal Free Energy Correction:	-425.13899	Hartree
E (Thermal):	122.39	kcal/mol
Heat Capacity (Cv):	38.015	cal/mol-kelvin
Entropy (S):	98.684	cal/mol-kelvin

Triisopropylsilyl radical

**Optimized cartesian coordinates:**

Si	0.04618800	-0.04632800	0.18984400
C	1.92434200	-0.44236700	0.07231300
C	2.79255100	0.64101700	0.72630100
C	2.38540800	-0.73309700	-1.36579400
H	2.04393100	-1.36711700	0.65540500
H	2.46422300	0.86345000	1.74647700
H	3.84240100	0.32123300	0.76722900
H	2.76113200	1.57430100	0.15099400
H	1.79499200	-1.51990300	-1.84583800
H	2.32391800	0.16240800	-1.99446200
H	3.43488500	-1.05748100	-1.36875600
C	-0.31058700	1.75789500	-0.37968400
C	-1.57208700	2.37965400	0.23976000
C	-0.33552800	1.86295000	-1.91241300
H	0.55597800	2.32235700	-0.00773800
H	-1.51596000	2.39554500	1.33368200
H	-1.69764500	3.41360400	-0.10952700
H	-2.47615700	1.82756900	-0.03667700
H	0.58013500	1.48142500	-2.37521600
H	-1.17941000	1.30912200	-2.33871100
H	-0.44774100	2.91276400	-2.21729600
C	-0.94945800	-1.33860600	-0.79270000
C	-2.46458000	-1.09123300	-0.72955500
C	-0.61597700	-2.76191900	-0.31295900
H	-0.62895200	-1.24434400	-1.84175700
H	-2.74633600	-0.13506200	-1.18202700
H	-3.00898700	-1.88253800	-1.26226100
H	-2.81585600	-1.08762800	0.30911500
H	0.44994700	-2.99581300	-0.40844400
H	-0.89280400	-2.88863700	0.74087900
H	-1.17361500	-3.50869400	-0.89359600
S	-0.46495100	-0.11835900	2.26556800

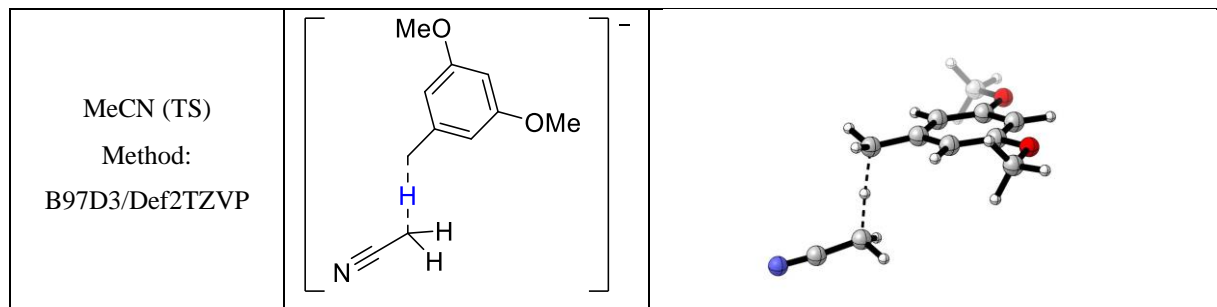
Thermodynamic details:

Electronic Energy (EE):	-1043.2611	Hartree	
Zero-point Energy Correction:		0.277737	Hartree
Thermal Correction to Energy:	0.294759	Hartree	
Thermal Correction to Enthalpy:	0.295703	Hartree	
Thermal Correction to Free Energy:	0.233373	Hartree	
EE + Zero-point Energy:	-1042.9834	Hartree	
EE + Thermal Energy Correction:	-1042.9664	Hartree	
EE + Thermal Enthalpy Correction:	-1042.9654	Hartree	
EE + Thermal Free Energy Correction:	-1043.0278	Hartree	
E (Thermal):	184.964	kcal/mol	
Heat Capacity (Cv):	61.07	cal/mol-kelvin	
Entropy (S):	131.185	cal/mol-kelvin	

7.3.2.2 Kinetic isotope effects for carbanion protonation

Cartesian coordinates: (All optimized structures)

MeCN (TS)



Optimized cartesian coordinates:

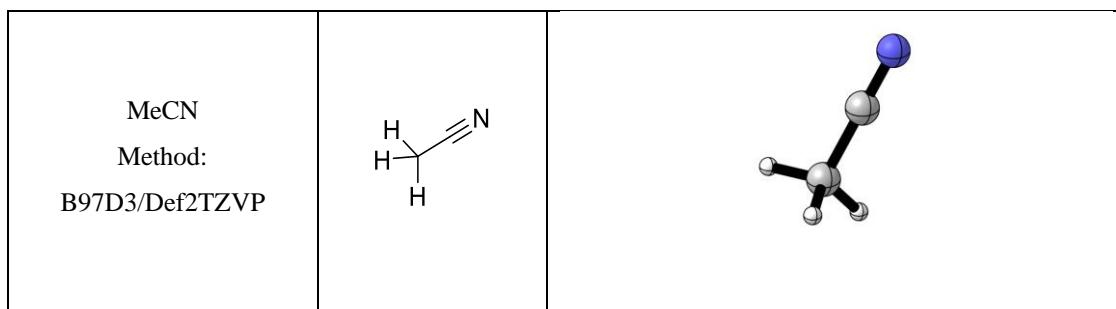
C	-2.34163700	-0.00340700	-0.38987900
C	-1.68863900	-1.20131500	-0.07305500
C	-0.43946000	-1.21389500	0.53974800
C	0.22501500	0.00177700	0.86730200
C	-0.44411200	1.21475800	0.53926900
C	-1.69322200	1.19712400	-0.07357400
H	-3.31548100	-0.00537400	-0.86660000
H	0.05895700	-2.14696000	0.77982000
H	0.05067500	2.14984800	0.77906000
O	-2.38980300	-2.35043300	-0.41397000
O	-2.39874400	2.34340000	-0.41507400
C	-1.78099800	3.58834800	-0.15023900
H	-0.82421000	3.69120100	-0.68396500
H	-2.47822900	4.35460300	-0.50428500
H	-1.59724900	3.73362000	0.92544900
C	-1.76681400	-3.59287800	-0.14952500
H	-2.46118900	-4.36192600	-0.50312900
H	-0.80992600	-3.69184000	-0.68391500
H	-1.58176500	-3.73744600	0.92607200
C	1.56690300	0.00440800	1.39219700
H	2.48978600	0.00506600	0.26653000
H	1.85835400	0.91272400	1.92819500
H	1.86155200	-0.90228900	1.92917800
C	3.34167300	0.00552800	-0.89132600
H	3.04366900	0.90583000	-1.43892400
H	3.04194700	-0.89304100	-1.44083800
C	4.71748200	0.00383800	-0.54765200
N	5.82776300	0.00236200	-0.16569900

Thermodynamic Details:

Imaginary frequency: $\nu_{\text{imaginary}}: -1002.63\text{cm}^{-1}$

Electronic Energy (EE)	-632.60378	Hartree	
Zero-point Energy Correction		0.213878	Hartree
Thermal Correction to Energy	0.229641	Hartree	
Thermal Correction to Enthalpy	0.230585	Hartree	
Thermal Correction to Free Energy	0.167755	Hartree	
EE + Zero-point Energy	-632.3899	Hartree	
EE + Thermal Energy Correction	-632.37414	Hartree	
EE + Thermal Enthalpy Correction	-632.37319	Hartree	
EE + Thermal Free Energy Correction	-632.43602	Hartree	
E (Thermal)	144.102	kcal/mol	
Heat Capacity (Cv)	57.239	cal/mol-kelvin	
Entropy (S)	132.236	cal/mol-kelvin	

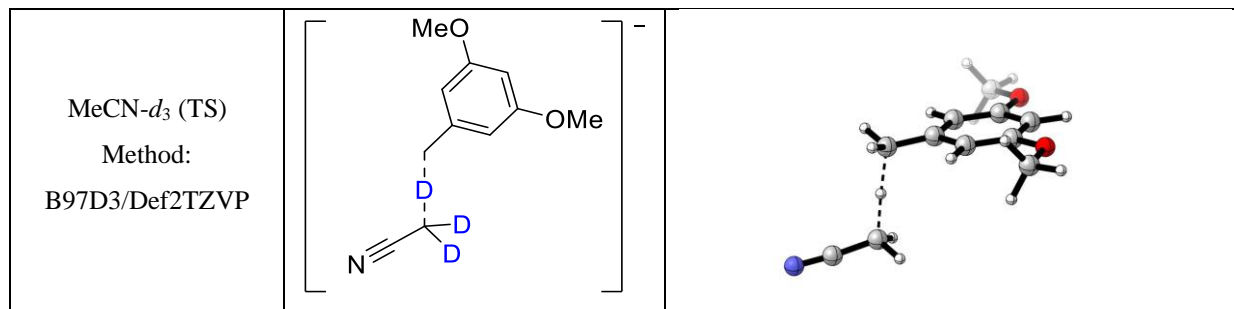
MeCN

**Optimized cartesian coordinates:**

C	0.00000000	0.00000000	-1.17778300
H	0.00000000	1.02765100	-1.55604300
H	0.88997200	-0.51382500	-1.55604300
H	-0.88997200	-0.51382500	-1.55604300
C	0.00000000	0.00000000	0.27869900
N	0.00000000	0.00000000	1.43751900

Thermodynamic details:

Electronic Energy (EE)	-132.72012	Hartree	
Zero-point Energy Correction	0.044237	Hartree	
Thermal Correction to Energy	0.047883	Hartree	
Thermal Correction to Enthalpy	0.048828	Hartree	
Thermal Correction to Free Energy	0.021229	Hartree	
EE + Zero-point Energy	-132.67588	Hartree	
EE + Thermal Energy Correction	-132.67224	Hartree	
EE + Thermal Enthalpy Correction	-132.67129	Hartree	
EE + Thermal Free Energy Correction	-132.69889	Hartree	
E (Thermal)	30.047	kcal/mol	
Heat Capacity (Cv)	10.484	cal/mol-kelvin	
Entropy (S)	58.087	cal/mol-kelvin	

MeCN-*d*₃ (TS)

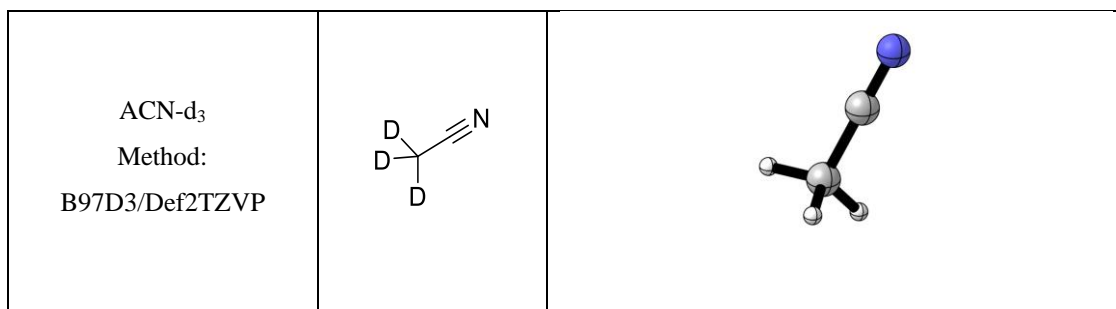
Optimized cartesian coordinates:

C	2.34153900	0.00037700	-0.38987100
C	1.69064500	1.19943300	-0.07303900
C	0.44154800	1.21421400	0.53988900
C	-0.22502300	-0.00028600	0.86751800
C	0.44198800	-1.21444400	0.53950900
C	1.69107700	-1.19901200	-0.07342000
H	3.31531000	0.00062800	-0.86673200
H	-0.05520400	2.14816100	0.78003700
H	-0.05441400	-2.14865500	0.77936000
O	2.39373000	2.34732400	-0.41411400
O	2.39457800	-2.34653800	-0.41486500
C	1.77432300	-3.59036000	-0.15064200
H	0.81743300	-3.69109200	-0.68459200
H	2.47009900	-4.35785000	-0.50486600
H	1.59007200	-3.73572600	0.92494700
C	1.77304200	3.59083700	-0.14944900
H	2.46854200	4.35869300	-0.50342100
H	0.81610500	3.69141800	-0.68334600
H	1.58875600	3.73576500	0.92619200
C	-1.56691100	-0.00061100	1.39239500
H(Iso=2)	-2.48962400	-0.00057700	0.26654600
H	-1.85984600	-0.90826300	1.92870200
H	-1.86017200	0.90675900	1.92899800
C	-3.34127000	-0.00053700	-0.89140900
H(Iso=2)	-3.04244500	-0.90006300	-1.43981400
H(Iso=2)	-3.04212800	0.89880100	-1.43994900
C	-4.71713400	-0.00027100	-0.54789600
N	-5.82741300	-0.00004700	-0.16596300

Thermodynamics Details:

Imaginary frequency: $\nu_{\text{imaginary}}: -747.38 \text{ cm}^{-1}$

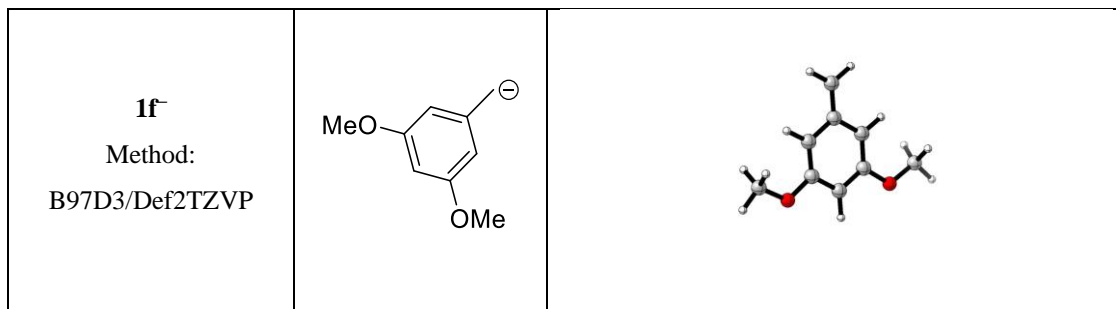
Electronic Energy (EE)	-632.60378	Hartree	
Zero-point Energy Correction		0.206216	Hartree
Thermal Correction to Energy	0.222385	Hartree	
Thermal Correction to Enthalpy	0.223329	Hartree	
Thermal Correction to Free Energy	0.159626	Hartree	
EE + Zero-point Energy	-632.39756	Hartree	
EE + Thermal Energy Correction	-632.38139	Hartree	
EE + Thermal Enthalpy Correction	-632.38045	Hartree	
EE + Thermal Free Energy Correction	-632.44415	Hartree	
E (Thermal)	139.549	kcal/mol	
Heat Capacity (Cv)	59.024	cal/mol-kelvin	
Entropy (S)	134.075	cal/mol-kelvin	

MeCN-*d*₃**Optimized cartesian coordinates:**

C	0.00000000	0.00000000	-1.17778300
H(Iso=2)	0.00000000	1.02765100	-1.55604300
H(Iso=2)	0.88997200	-0.51382500	-1.55604300
H(Iso=2)	-0.88997200	-0.51382500	-1.55604300
C	0.00000000	0.00000000	0.27869900
N	0.00000000	0.00000000	1.43751900

Thermodynamic Details:

Electronic Energy (EE)	-132.72012	Hartree	
Zero-point Energy Correction		0.034978	Hartree
Thermal Correction to Energy	0.038849	Hartree	
Thermal Correction to Enthalpy	0.039793	Hartree	
Thermal Correction to Free Energy	0.01129	Hartree	
EE + Zero-point Energy	-132.68514	Hartree	
EE + Thermal Energy Correction	-132.68127	Hartree	
EE + Thermal Enthalpy Correction	-132.68033	Hartree	
EE + Thermal Free Energy Correction	-132.70883	Hartree	
E (Thermal)	24.378	kcal/mol	
Heat Capacity (Cv)	11.898	cal/mol-kelvin	
Entropy (S)	59.989	cal/mol-kelvin	

Carbanion **1f**⁻

Optimized cartesian coordinates:

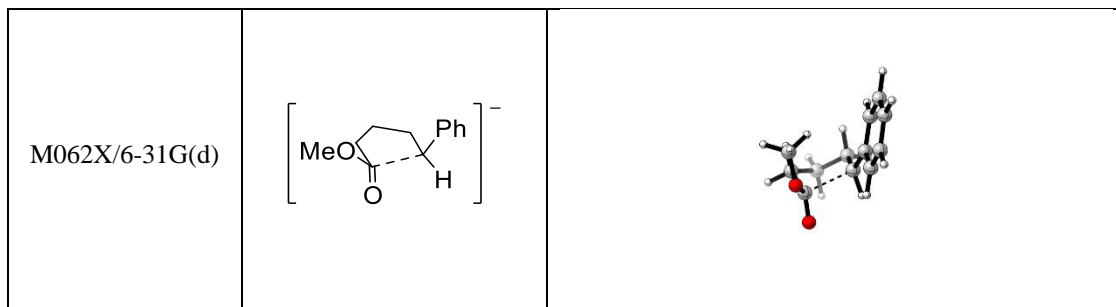
C	0.00000000	-1.27076800	0.00004300
C	-1.19611300	-0.53011800	0.00009500
C	-1.22295000	0.85308400	0.00005100
C	0.00000000	1.63104600	-0.00005200
C	1.22295000	0.85308500	-0.00010500
C	1.19611300	-0.53011700	-0.00005800
H	0.00000000	-2.35438800	0.00007800
H	-2.16284400	1.39641600	0.00009400
H	2.16284500	1.39641700	-0.00018300
O	-2.35355100	-1.31943400	0.00019500
O	2.35355200	-1.31943300	-0.00010600
C	3.59083700	-0.64661300	-0.00020800
H	3.71572100	-0.01055800	0.89153700
H	4.36466200	-1.42369300	-0.00022900
H	3.71560900	-0.01062100	-0.89201300
C	-3.59083800	-0.64661300	0.00024000
H	-4.36466300	-1.42369300	0.00031400
H	-3.71561500	-0.01055500	0.89199900
H	-3.71571700	-0.01062300	-0.89155300
C	-0.00000100	3.01972100	-0.00009600
H	0.93101300	3.58299300	-0.00017200
H	-0.93101400	3.58299300	-0.00005200

Thermodynamic Details:

Electronic Energy (EE)	-499.86681	Hartree	
Zero-point Energy Correction		0.172142	Hartree
Thermal Correction to Energy	0.183701	Hartree	
Thermal Correction to Enthalpy	0.184645	Hartree	
Thermal Correction to Free Energy	0.135297	Hartree	
EE + Zero-point Energy	-499.69466	Hartree	
EE + Thermal Energy Correction	-499.68311	Hartree	
EE + Thermal Enthalpy Correction	-499.68216	Hartree	
EE + Thermal Free Energy Correction	-499.73151	Hartree	
E (Thermal)	115.274	kcal/mol	
Heat Capacity (Cv)	44.035	cal/mol-kelvin	
Entropy (S)	103.86	cal/mol-kelvin	

7.3.2.3 Cyclization of phenylvaleric and phenylhexanoic acid esters

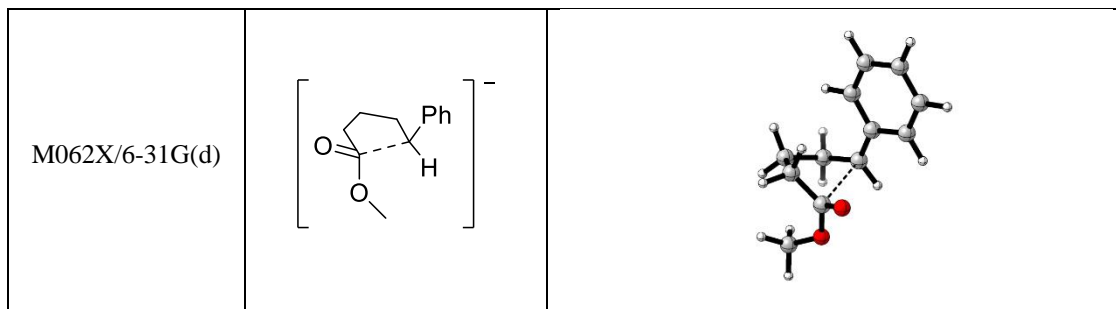
Cartesian coordinates (optimized Structures):

7a⁻ TS1**Optimized cartesian coordinates:**

C	-2.88622900	0.86983800	1.01368700
C	-1.59043200	1.25830300	0.71225500
C	-0.93105900	0.84195800	-0.49522200
C	-1.75367200	0.07529400	-1.39064800
C	-3.04202700	-0.29859300	-1.06999800
C	-3.63913300	0.07190000	0.14735100
H	-3.32757500	1.20456200	1.95333300
H	-1.05597500	1.89355900	1.41361600
H	-1.30917500	-0.25997700	-2.32493200
H	-3.60432200	-0.90587300	-1.77946100
H	-4.65505300	-0.22545500	0.39099600
C	0.41939100	1.08313600	-0.76083200
C	1.28239100	1.89824600	0.15250700
C	1.15027600	-1.29604700	-0.21524400
H	0.77444200	0.93305800	-1.78082600
C	2.77355300	1.63265100	-0.06585100
H	1.05564000	1.63396400	1.19900300
H	1.11019300	2.99370200	0.08661500
C	2.59364400	-0.90814600	-0.48277600
C	3.20479500	0.22271800	0.34495300
H	3.37434600	2.35914400	0.50068000
H	3.01921600	1.78715100	-1.12782400
H	3.17109800	-1.83114600	-0.30661900
H	2.66446300	-0.69626800	-1.55373400
H	4.29848500	0.14852400	0.26331500
H	2.95490700	0.06003100	1.40029000
O	0.83764200	-1.19854600	1.10969600
O	0.50704800	-1.98211600	-0.98776200
C	-0.41955900	-1.77033500	1.44943400
H	-0.66381300	-1.39316000	2.44399600
H	-1.19466400	-1.47689100	0.74016400
H	-0.34137200	-2.86516700	1.46821600

Thermodynamic Details:Imaginary frequency: $\nu_{\text{imaginary}}$: -198.50cm⁻¹

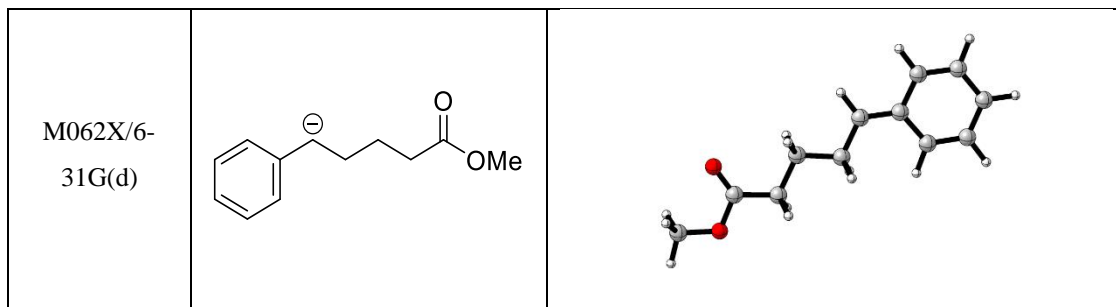
Electronic Energy (EE)	-616.46647	Hartree		
Zero-point Energy Correction			0.245712	Hartree
Thermal Correction to Energy	0.258049	Hartree		
Thermal Correction to Enthalpy	0.258993	Hartree		
Thermal Correction to Free Energy	0.206962	Hartree		
EE + Zero-point Energy	-616.22076	Hartree		
EE + Thermal Energy Correction	-616.20842	Hartree		
EE + Thermal Enthalpy Correction	-616.20748	Hartree		
EE + Thermal Free Energy Correction	-616.25951	Hartree		
E (Thermal)	161.928	kcal/mol		
Heat Capacity (Cv)	48.946	cal/mol-kelvin		
Entropy (S)	109.507	cal/mol-kelvin		

7a⁻ TS2**Optimized cartesian coordinates:**

C	3.81682900	-0.18072200	0.45050000
C	3.20578300	-1.21462100	-0.27894900
C	1.94309600	-1.07702100	-0.81503300
C	1.16986700	0.12422300	-0.66912900
C	1.81488200	1.15559300	0.09407600
C	3.08811200	0.99757000	0.62187200
H	4.81059700	-0.29844600	0.87265800
H	3.73785800	-2.15507200	-0.42352100
H	1.49423200	-1.90355900	-1.36248600
H	1.29892100	2.10278300	0.24102200
H	3.52667000	1.82285100	1.18414400
C	-0.12072000	0.24246900	-1.19175900
C	-1.56817600	-0.91589500	0.53348900
C	-0.94200100	1.48110800	-1.02414600
H	-0.48079800	-0.52798400	-1.86586800
C	-1.34904400	0.40139300	1.26392000
C	-1.44184800	1.69456700	0.44254500
H	-1.81604900	1.41366900	-1.68502800
H	-0.41432900	2.40408600	-1.32775100
H	-2.02553600	0.44468400	2.13256000
H	-0.33360800	0.29659100	1.65540700
H	-2.45925500	2.10772700	0.45432000
H	-0.81697500	2.44087400	0.94694200
O	-2.68871400	-1.04601500	-0.28708800
O	-1.00331700	-1.94176400	0.83431500
C	-3.75148400	-0.13185000	-0.20130000
H	-4.65247100	-0.67163600	-0.51056000
H	-3.90696900	0.23568700	0.82036700
H	-3.61781600	0.72909400	-0.86653200

Thermodynamic Details:Imaginary frequency: $\nu_{\text{imaginary}}: -101.82\text{cm}^{-1}$

Electronic Energy (EE)	-616.45352	Hartree
Zero-point Energy Correction	0.244866	Hartree
Thermal Correction to Energy	0.257593	Hartree
Thermal Correction to Enthalpy	0.258538	Hartree
Thermal Correction to Free Energy	0.205322	Hartree
EE + Zero-point Energy	-616.20866	Hartree
EE + Thermal Energy Correction	-616.19593	Hartree
EE + Thermal Enthalpy Correction	-616.19499	Hartree
EE + Thermal Free Energy Correction	-616.2482	Hartree
E (Thermal)	161.642	kcal/mol
Heat Capacity (Cv)	49.817	cal/mol-kelvin
Entropy (S)	112.001	cal/mol-kelvin

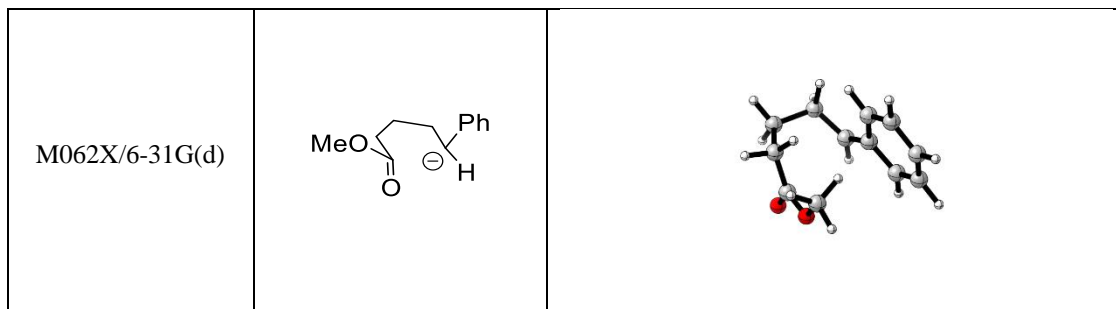
7a⁻ (Open)

Optimized cartesian coordinates:

C	-5.38506100	-0.49316400	-0.00022500
C	-5.01635400	0.86478600	-0.00015200
C	-3.69927200	1.26650700	-0.00001300
C	-2.59530800	0.33167300	0.00007200
C	-3.01012500	-1.05461500	0.00000700
C	-4.34215100	-1.42769800	-0.00014000
H	-6.42671300	-0.80015800	-0.00033700
H	-5.79478200	1.62998200	-0.00020800
H	-3.46160900	2.33043700	0.00003800
H	-2.24492800	-1.82847700	0.00007800
H	-4.58172700	-2.49291000	-0.00019000
C	-1.27201500	0.72775700	0.00018800
C	3.74500900	0.10845900	0.00007900
C	-0.13563500	-0.24464700	0.00026100
H	-1.02780600	1.78898700	0.00023400
C	2.38340700	-0.53474600	0.00040400
C	1.22467300	0.45383700	0.00010800
H	-0.16015700	-0.93061300	-0.87392500
H	-0.16003900	-0.93047000	0.87455200
O	4.73083000	-0.82669800	-0.00000400
O	3.99067100	1.28930300	-0.00012400
C	6.04700400	-0.29460400	-0.00040100
H	6.71933900	-1.15281700	-0.00040800
H	6.21575900	0.32251100	-0.88692900
H	6.21616800	0.32282400	0.88583400
H	1.30187800	1.10857200	0.87636600
H	1.30191200	1.10811900	-0.87648000
H	2.33290900	-1.19874300	0.87325600
H	2.33276300	-1.19935600	-0.87198200

Thermodynamics Details:

Electronic Energy (EE)	-616.46747	Hartree	
Zero-point Energy Correction		0.243781	Hartree
Thermal Correction to Energy	0.258257	Hartree	
Thermal Correction to Enthalpy	0.259201	Hartree	
Thermal Correction to Free Energy	0.19945	Hartree	
EE + Zero-point Energy	-616.22369	Hartree	
EE + Thermal Energy Correction	-616.20922	Hartree	
EE + Thermal Enthalpy Correction	-616.20827	Hartree	
EE + Thermal Free Energy Correction	-616.26802	Hartree	
E (Thermal)	162.059	kcal/mol	
Heat Capacity (Cv)	52.585	cal/mol-kelvin	
Entropy (S)	125.757	cal/mol-kelvin	

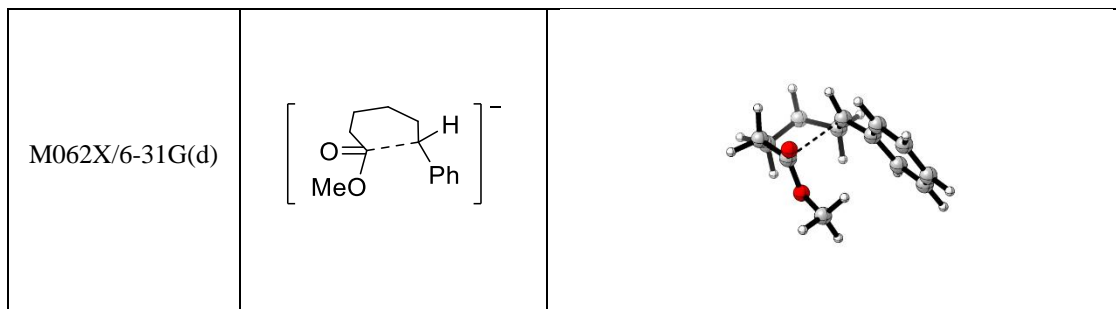
7a⁻ (closed, attack-conformer)

Optimized cartesian coordinates:

C	3.35831000	-0.22456700	0.31563200
C	2.80909300	-0.56874900	-0.93502300
C	1.61394400	-0.05086200	-1.37899100
C	0.81226700	0.86626100	-0.59393200
C	1.42985400	1.23138100	0.66559900
C	2.63946400	0.70007100	1.08137600
H	4.30190700	-0.63828100	0.65709300
H	3.33932400	-1.27489900	-1.57535600
H	1.21789600	-0.36319900	-2.34396500
H	0.92144900	1.93352600	1.32238200
H	3.03443900	1.01347200	2.04921400
C	-0.43224600	1.29452900	-1.02859800
C	-1.86082900	-1.04737700	-0.08163400
C	-1.37262000	2.12973900	-0.21426900
H	-0.79211800	0.92839800	-1.98802100
C	-1.89575800	-0.01607300	1.03615100
C	-2.46395800	1.31050800	0.52687200
H	-1.88549000	2.88519700	-0.83026800
H	-0.81300600	2.70186600	0.53838200
O	-0.92082400	-2.01904000	-0.05917900
O	-2.72618300	-1.12303600	-0.92339000
C	0.09406400	-2.03944600	0.93682700
H	0.68848600	-2.92916800	0.72224800
H	0.74024100	-1.16133700	0.88607700
H	-0.34413500	-2.13508700	1.93901500
H	-3.29105000	1.07586100	-0.15115000
H	-2.88153800	1.88630800	1.36529700
H	-0.90494600	0.13949300	1.47049000
H	-2.54490600	-0.43802500	1.81905200

Thermodynamics Details:

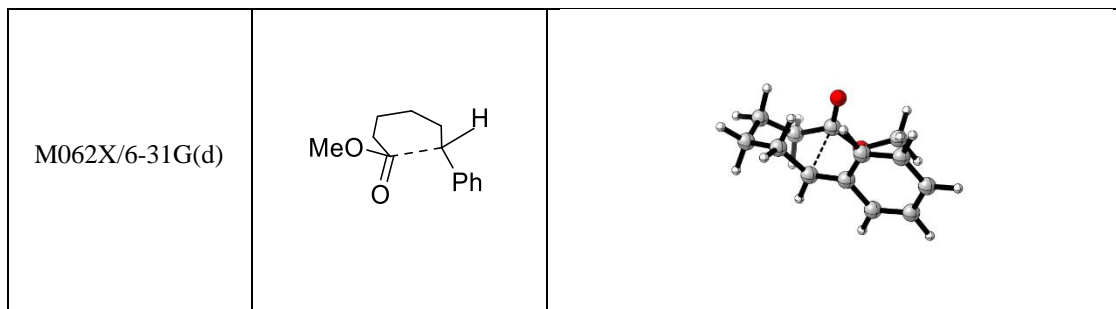
Electronic Energy (EE)	-616.47146	Hartree
Zero-point Energy Correction:	0.245823	Hartree
Thermal Correction to Energy:	0.259192	Hartree
Thermal Correction to Enthalpy:	0.260136	Hartree
Thermal Correction to Free Energy:	0.20586	Hartree
EE + Zero-point Energy:	-616.22564	Hartree
EE + Thermal Energy Correction:	-616.21227	Hartree
EE + Thermal Enthalpy Correction:	-616.21133	Hartree
EE + Thermal Free Energy Correction:	-616.2656	Hartree
E (Thermal):	162.645	kcal/mol
Heat Capacity (Cv):	51.627	cal/mol-kelvin
Entropy (S)	114.233	cal/mol-kelvin

9⁻ TS1**Optimized cartesian coordinates:**

C	-2.88622900	0.86983800	1.01368700
C	-1.59043200	1.25830300	0.71225500
C	-0.93105900	0.84195800	-0.49522200
C	-1.75367200	0.07529400	-1.39064800
C	-3.04202700	-0.29859300	-1.06999800
C	-3.63913300	0.07190000	0.14735100
H	-3.32757500	1.20456200	1.95333300
H	-1.05597500	1.89355900	1.41361600
H	-1.30917500	-0.25997700	-2.32493200
H	-3.60432200	-0.90587300	-1.77946100
H	-4.65505300	-0.22545500	0.39099600
C	0.41939100	1.08313600	-0.76083200
C	1.28239100	1.89824600	0.15250700
C	1.15027600	-1.29604700	-0.21524400
H	0.77444200	0.93305800	-1.78082600
C	2.77355300	1.63265100	-0.06585100
H	1.05564000	1.63396400	1.19900300
H	1.11019300	2.99370200	0.08661500
C	2.59364400	-0.90814600	-0.48277600
C	3.20479500	0.22271800	0.34495300
H	3.37434600	2.35914400	0.50068000
H	3.01921600	1.78715100	-1.12782400
H	3.17109800	-1.83114600	-0.30661900
H	2.66446300	-0.69626800	-1.55373400
H	4.29848500	0.14852400	0.26331500
H	2.95490700	0.06003100	1.40029000
O	0.83764200	-1.19854600	1.10969600
O	0.50704800	-1.98211600	-0.98776200
C	-0.41955900	-1.77033500	1.44943400
H	-0.66381300	-1.39316000	2.44399600
H	-1.19466400	-1.47689100	0.74016400
H	-0.34137200	-2.86516700	1.46821600

Thermodynamic Details:Imaginary frequency: $\nu_{\text{imaginary}}: -133.25 \text{ cm}^{-1}$

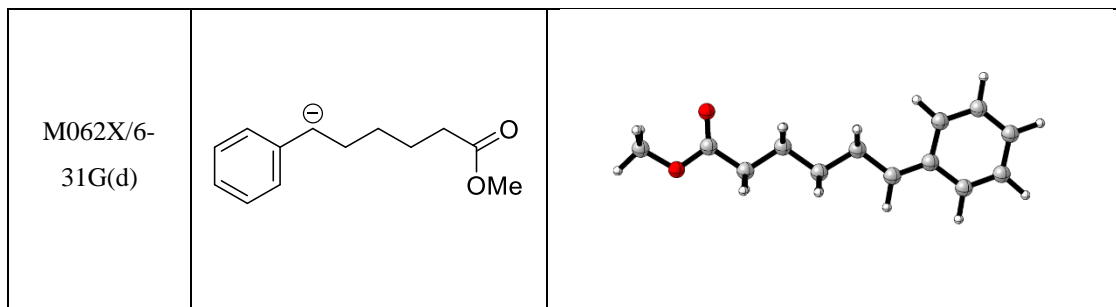
Electronic Energy (EE)	-655.76965	Hartree
Zero-point Energy Correction	0.274392	Hartree
Thermal Correction to Energy	0.288068	Hartree
Thermal Correction to Enthalpy	0.289012	Hartree
Thermal Correction to Free Energy	0.234628	Hartree
EE + Zero-point Energy	-655.49525	Hartree
EE + Thermal Energy Correction	-655.48158	Hartree
EE + Thermal Enthalpy Correction	-655.48063	Hartree
EE + Thermal Free Energy Correction	-655.53502	Hartree
E (Thermal)	180.765	kcal/mol
Heat Capacity (Cv)	54.165	cal/mol-kelvin
Entropy (S)	114.462	cal/mol-kelvin

9⁻ TS2**Optimized cartesian coordinates:**

C	2.77072600	-0.88760000	1.16696800
C	1.45551400	-1.19932100	0.86308000
C	0.87984400	-0.88953300	-0.41419600
C	1.79259000	-0.30942700	-1.35901900
C	3.10202000	-0.01381800	-1.03795100
C	3.62242000	-0.27801500	0.23853500
H	3.14807200	-1.12635100	2.16161100
H	0.83212700	-1.66625300	1.62003800
H	1.41229000	-0.07124400	-2.35137200
H	3.74085300	0.44208100	-1.79493400
H	4.65348600	-0.04368500	0.48694500
C	-0.47788100	-1.04895000	-0.71016200
C	-1.43569900	-1.81261600	0.15394000
C	-1.15280000	1.14159900	0.25642700
H	-0.76885000	-0.92604400	-1.75550300
C	-2.88861900	-1.52273600	-0.24250200
H	-1.30830600	-1.50889300	1.20533300
H	-1.27855400	-2.91045200	0.13577100
C	-2.48058800	1.01253400	-0.46962500
C	-3.34846000	-0.10417000	0.10857000
H	-3.56927600	-2.23634800	0.24378900
H	-2.99738200	-1.67914900	-1.32677000
H	-2.99666200	1.97814600	-0.33413700
H	-2.30487700	0.88842300	-1.54100100
H	-4.38386200	0.03537000	-0.23137200
H	-3.34613700	0.01394100	1.19896000
O	-0.29327000	1.92865000	-0.45361800
O	-1.02606300	0.95627100	1.45739100
C	0.86592000	2.31978200	0.26882300
H	1.35748000	1.46159500	0.73015200
H	1.53485000	2.77698700	-0.46242400
H	0.59948900	3.04613400	1.04740300

Thermodynamics Details:Imaginary frequency: $\nu_{\text{imaginary}}: -161.99 \text{ cm}^{-1}$

Electronic Energy (EE)	-655.77279	Hartree	
Zero-point Energy Correction		0.274765	Hartree
Thermal Correction to Energy	0.288225	Hartree	
Thermal Correction to Enthalpy	0.289169	Hartree	
Thermal Correction to Free Energy	0.235613	Hartree	
EE + Zero-point Energy	-655.49802	Hartree	
EE + Thermal Energy Correction	-655.48456	Hartree	
EE + Thermal Enthalpy Correction	-655.48362	Hartree	
EE + Thermal Free Energy Correction	-655.53718	Hartree	
E (Thermal)	180.864	kcal/mol	
Heat Capacity (Cv)	53.886	cal/mol-kelvin	
Entropy (S)	112.717	cal/mol-kelvin	

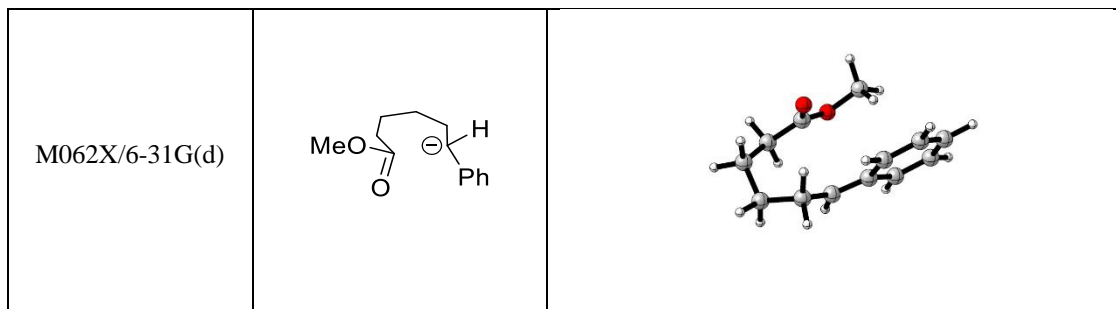
9⁻ Open form

Optimized cartesian coordinates:

C	4.87637500	1.49734900	-0.00072100
C	3.56712600	1.05202700	0.00062000
C	3.22837500	-0.35500300	0.00074400
C	4.38205500	-1.22805600	-0.00035000
C	5.67537500	-0.75458000	-0.00166700
C	5.96937500	0.62125900	-0.00195000
H	5.05695800	2.57411900	-0.00075600
H	2.76027500	1.78227000	0.00171400
H	4.20349400	-2.30362800	-0.00021400
H	6.49454200	-1.47614100	-0.00252200
H	6.99262500	0.98495800	-0.00299200
C	1.92847300	-0.82145400	0.00176500
C	0.73629900	0.08475200	0.00239400
C	-4.36543100	0.18263800	-0.00028800
H	1.74428100	-1.89526800	0.00202900
C	-0.57686900	-0.69771700	0.00099400
H	0.71901700	0.76943500	-0.87146900
H	0.71812800	0.76771000	0.87763300
C	-3.10653700	-0.64627800	-0.00019400
C	-1.82616900	0.18025400	0.00115900
H	-0.59404100	-1.36033100	0.87884000
H	-0.59308700	-1.35867900	-0.87810400
H	-3.14846800	-1.31114700	0.87215000
H	-3.14747200	-1.30976000	-0.87364300
H	-1.82261900	0.83936100	0.87757800
H	-1.82176400	0.84085700	-0.87412900
O	-5.47046500	-0.60277200	-0.00138700
O	-4.43510200	1.38647600	0.00045900
C	-6.70043600	0.10925000	-0.00151500
H	-6.77948800	0.74400700	-0.88789400
H	-7.48553200	-0.64674600	-0.00246000
H	-6.78037800	0.74270100	0.88571400

Thermodynamics Details:

Electronic Energy (EE)	-655.7593	Hartree
Zero-point Energy Correction	0.272647	Hartree
Thermal Correction to Energy	0.288487	Hartree
Thermal Correction to Enthalpy	0.289431	Hartree
Thermal Correction to Free Energy	0.225882	Hartree
EE + Zero-point Energy	-655.48666	Hartree
EE + Thermal Energy Correction	-655.47082	Hartree
EE + Thermal Enthalpy Correction	-655.46987	Hartree
EE + Thermal Free Energy Correction	-655.53342	Hartree
E (Thermal)	181.028	kcal/mol
Heat Capacity (Cv)	57.368	cal/mol-kelvin
Entropy (S)	133.75	cal/mol-kelvin

9⁻ (closed, attack-conformer)**Optimized cartesian coordinates:**

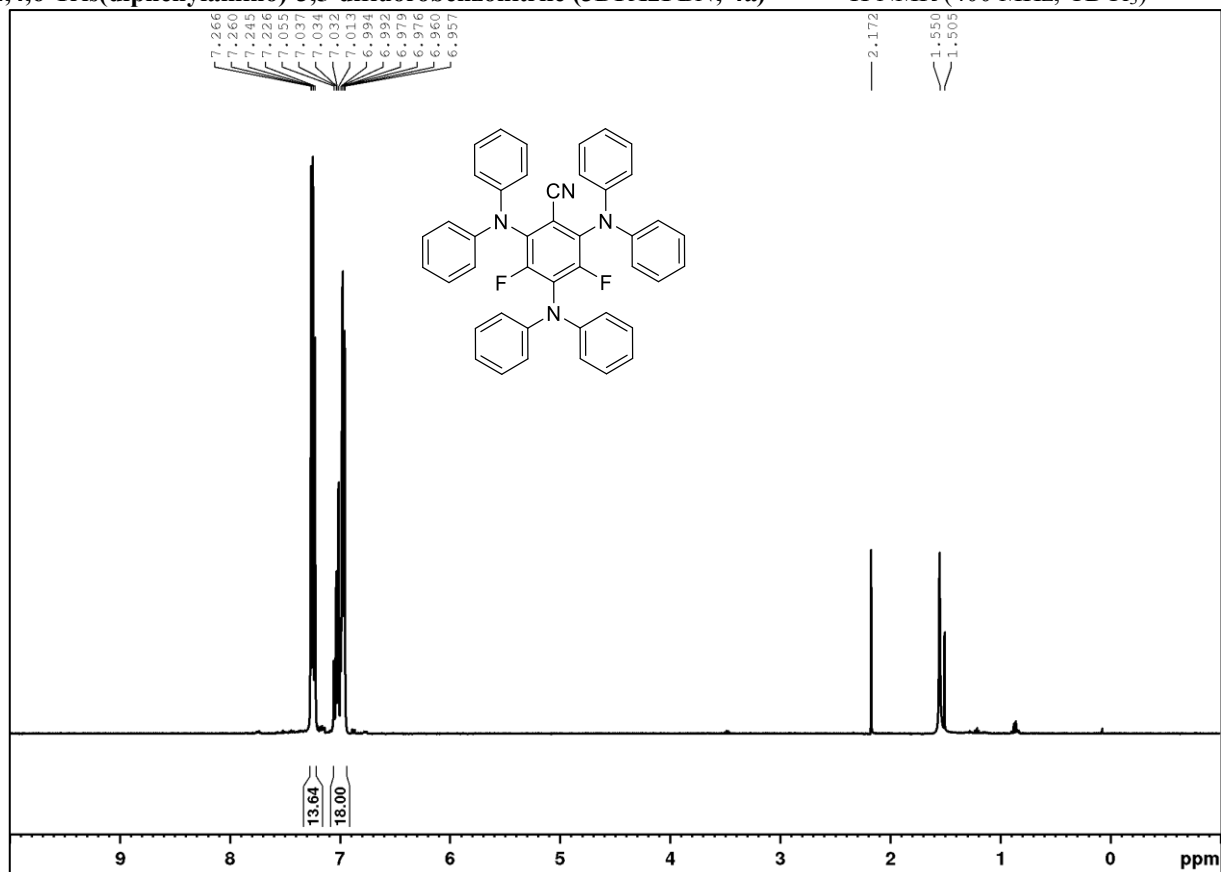
C	2.72829800	-0.77792500	1.22445900
C	1.43234200	-1.16045900	0.92729300
C	0.86505600	-0.99137600	-0.38953500
C	1.79114300	-0.46028500	-1.36239000
C	3.08040800	-0.09364800	-1.04062900
C	3.58522300	-0.22120800	0.26499300
H	3.08914000	-0.91748100	2.24444100
H	0.81460300	-1.58730800	1.71266400
H	1.43137800	-0.32607600	-2.38208100
H	3.71951000	0.31505100	-1.82487400
H	4.60308700	0.06625200	0.51077100
C	-0.45705800	-1.26340500	-0.70785600
C	-1.46504800	-1.84630700	0.23500000
C	-1.16475000	1.27799100	0.23667900
H	-0.75200000	-1.19389600	-1.75645600
C	-2.90341800	-1.49881000	-0.17664300
H	-1.30395500	-1.45437000	1.25198500
H	-1.40164500	-2.95062100	0.33274900
C	-2.44316700	1.02285500	-0.53654600
C	-3.32019400	-0.05133800	0.10728200
H	-3.61600300	-2.15858900	0.33981300
H	-3.02054700	-1.70133700	-1.25224100
H	-2.98498900	1.98280900	-0.54324100
H	-2.19052000	0.78648200	-1.57225200
H	-4.35520100	0.09169300	-0.23170900
H	-3.31017500	0.12090500	1.19031800
O	-0.26706000	1.94333600	-0.51453700
O	-1.03711700	1.10494600	1.43010000
C	0.93643200	2.29382800	0.16654000
H	1.35410500	1.43164800	0.68785300
H	1.62841500	2.62823800	-0.60615500
H	0.73661100	3.10086600	0.88202900

Thermodynamic Details:

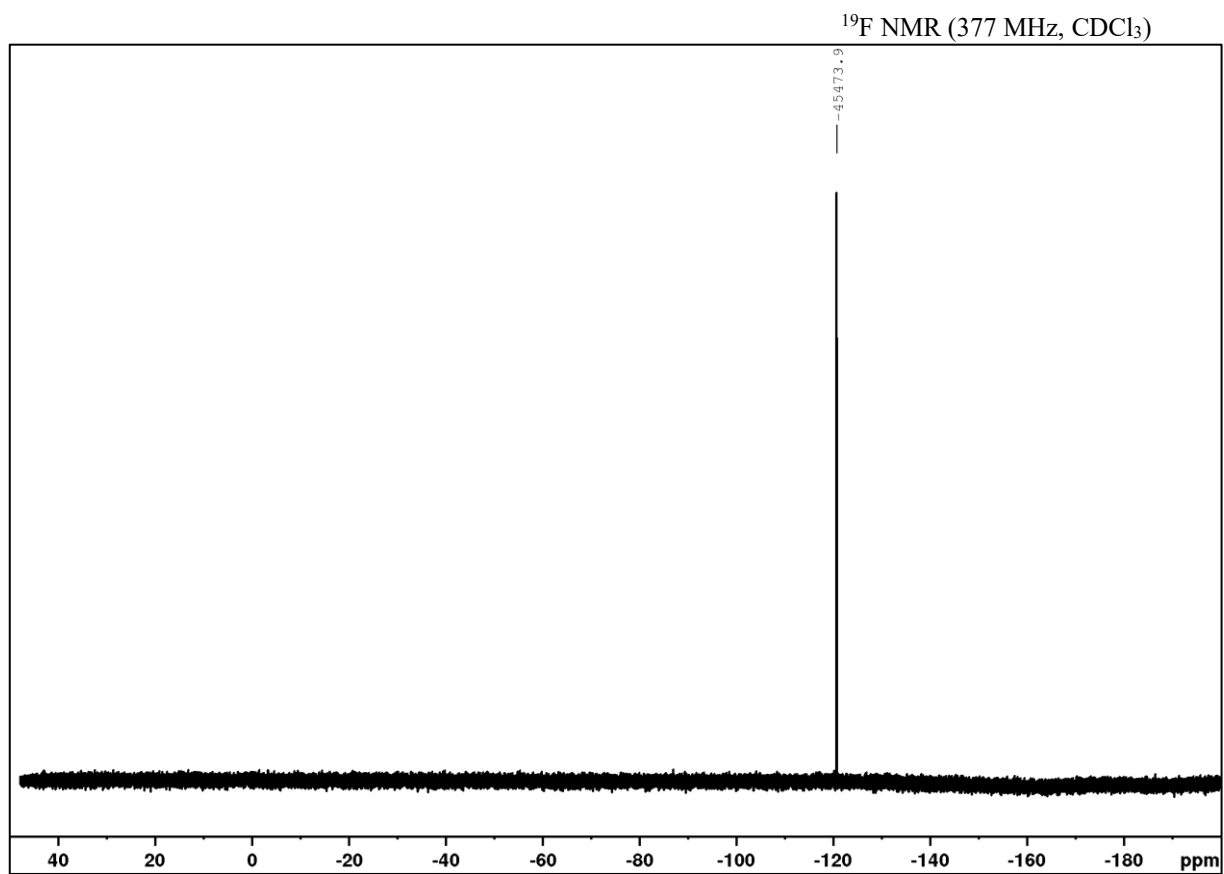
Electronic Energy (EE)	-655.77338	Hartree
Zero-point Energy Correction	0.274809	Hartree
Thermal Correction to Energy	0.289191	Hartree
Thermal Correction to Enthalpy	0.290135	Hartree
Thermal Correction to Free Energy	0.234504	Hartree
EE + Zero-point Energy	-655.49857	Hartree
EE + Thermal Energy Correction	-655.48419	Hartree
EE + Thermal Enthalpy Correction	-655.48325	Hartree
EE + Thermal Free Energy Correction	-655.53888	Hartree
E (Thermal):	181.47	kcal/mol
Heat Capacity (Cv):	56.173	cal/mol-kelvin
Entropy (S):	117.085	cal/mol-kelvin

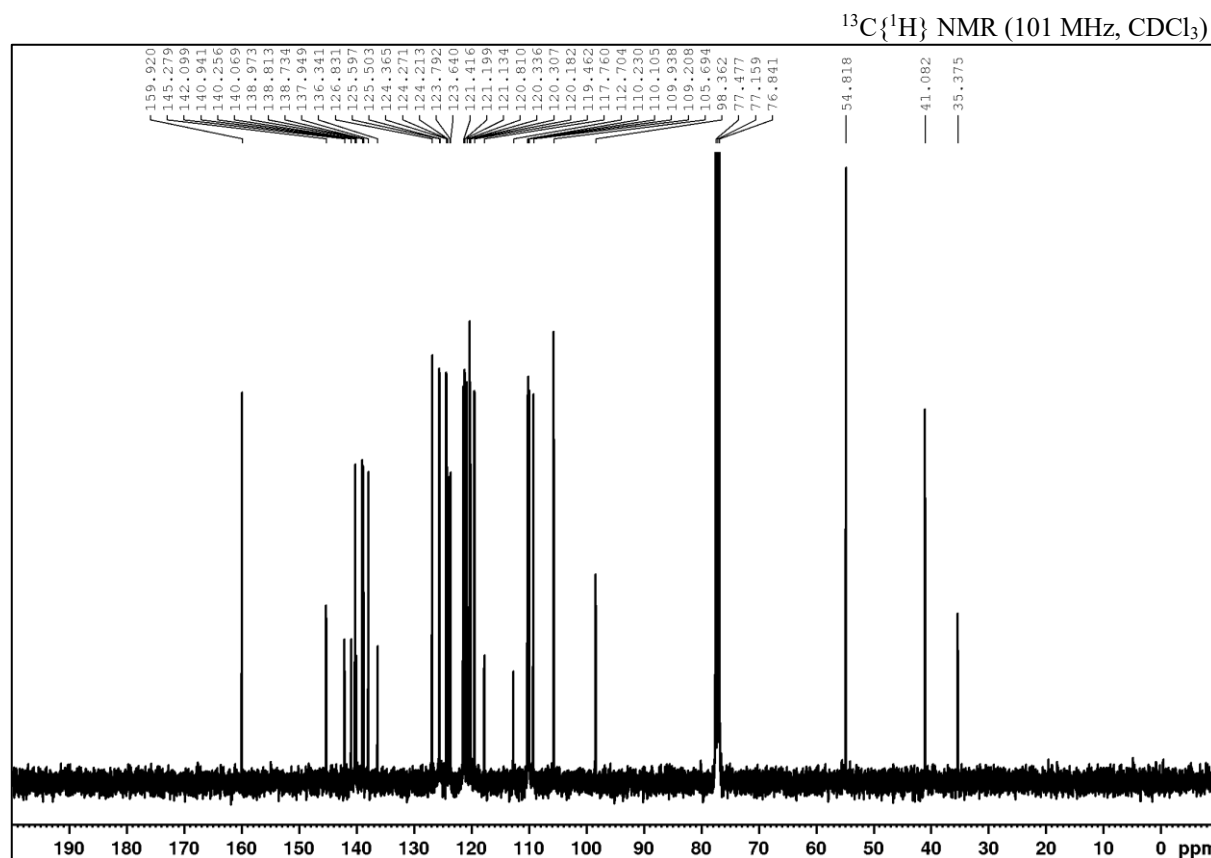
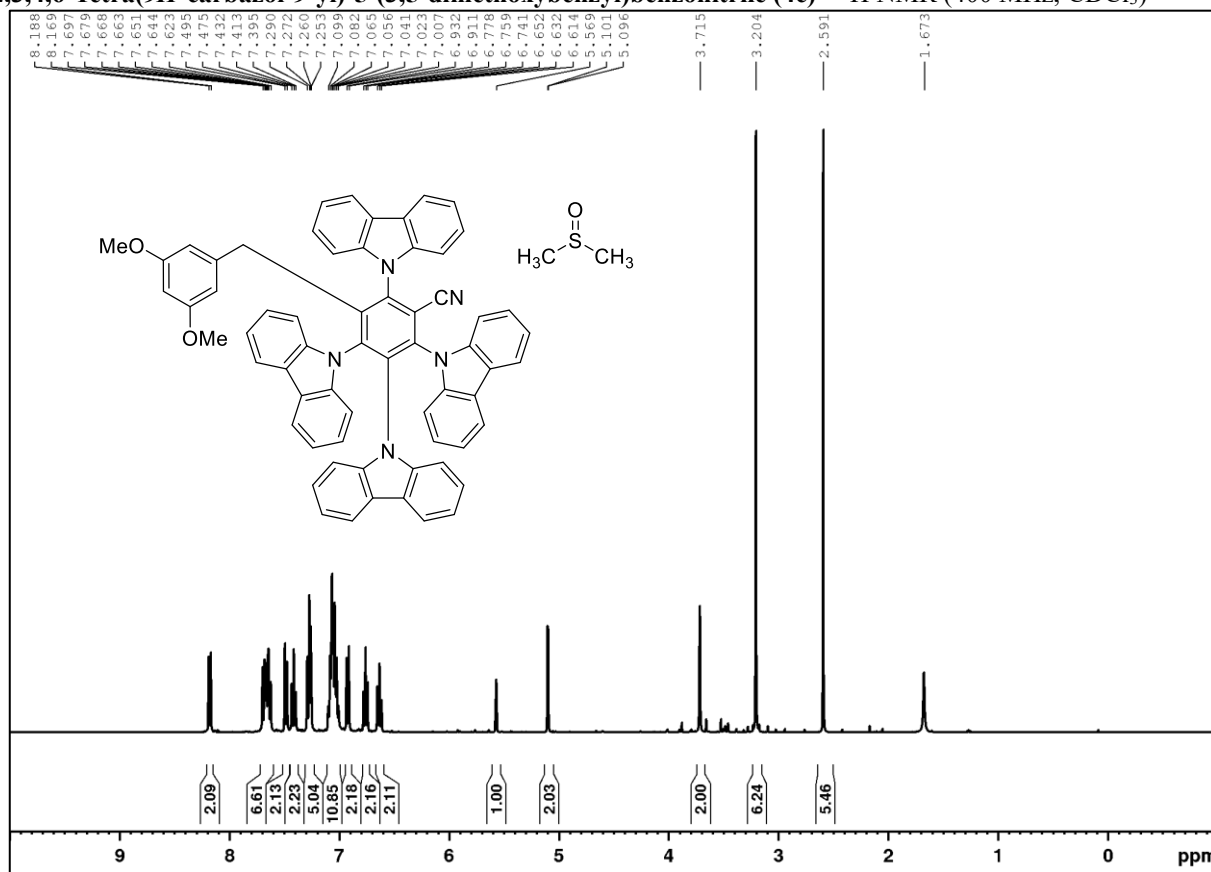
7.3.3 NMR spectra

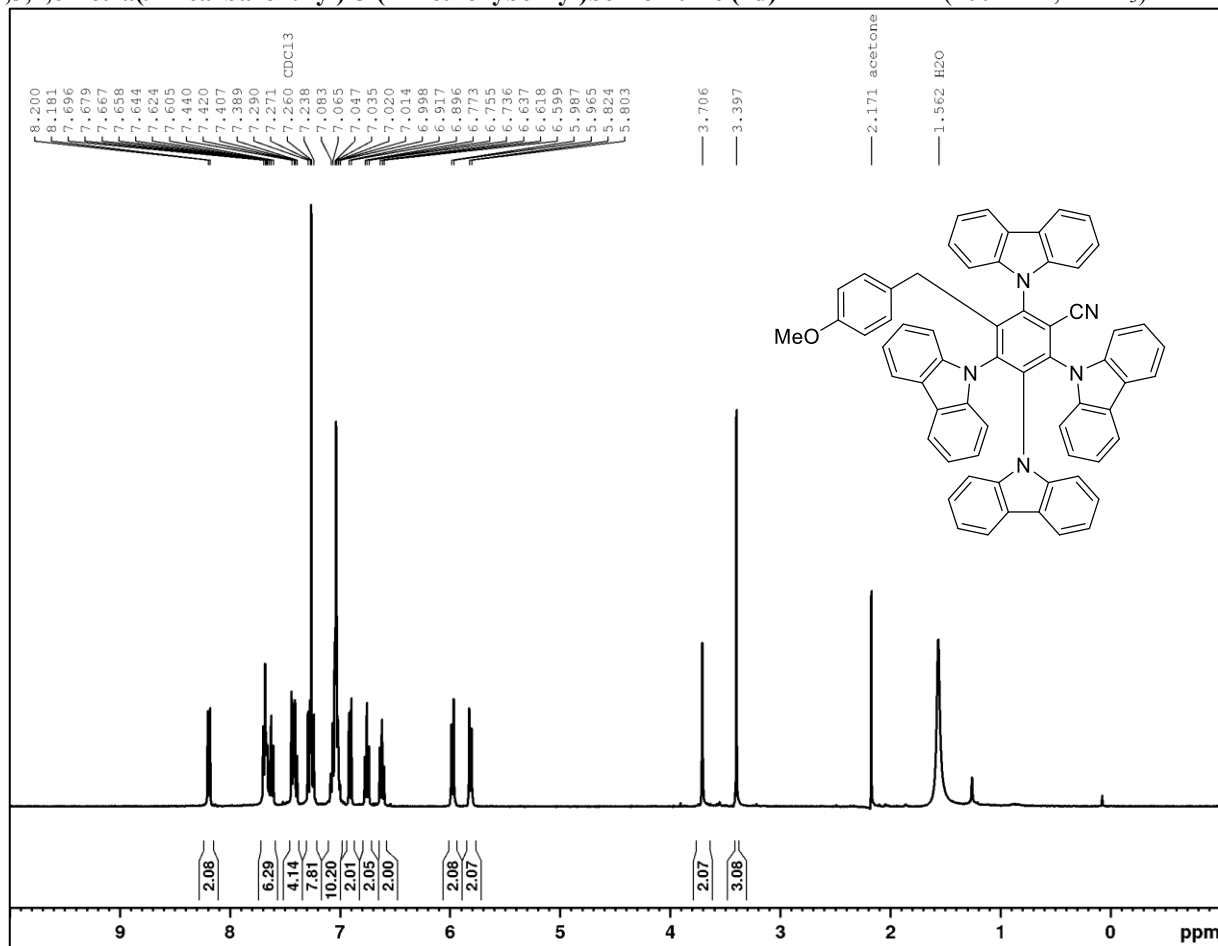
2,4,6-Tris(diphenylamino)-3,5-difluorobenzonitrile (3DPA2FBN; 4a)

 ^1H NMR (400 MHz, CDCl_3)

APPENDIX

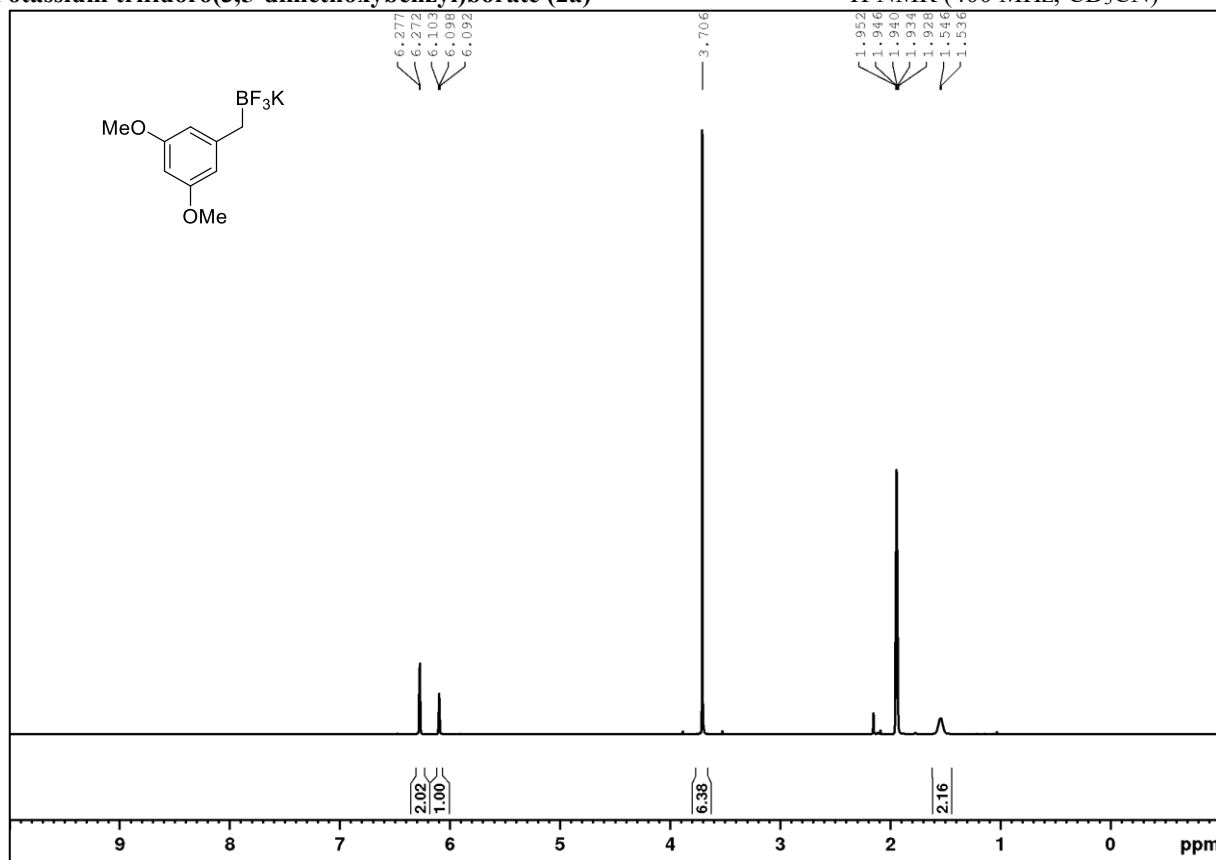


2,3,4,6-Tetra(9H-carbazol-9-yl)-5-(3,5-dimethoxybenzyl)benzonitrile (4c) ^1H NMR (400 MHz, CDCl_3)

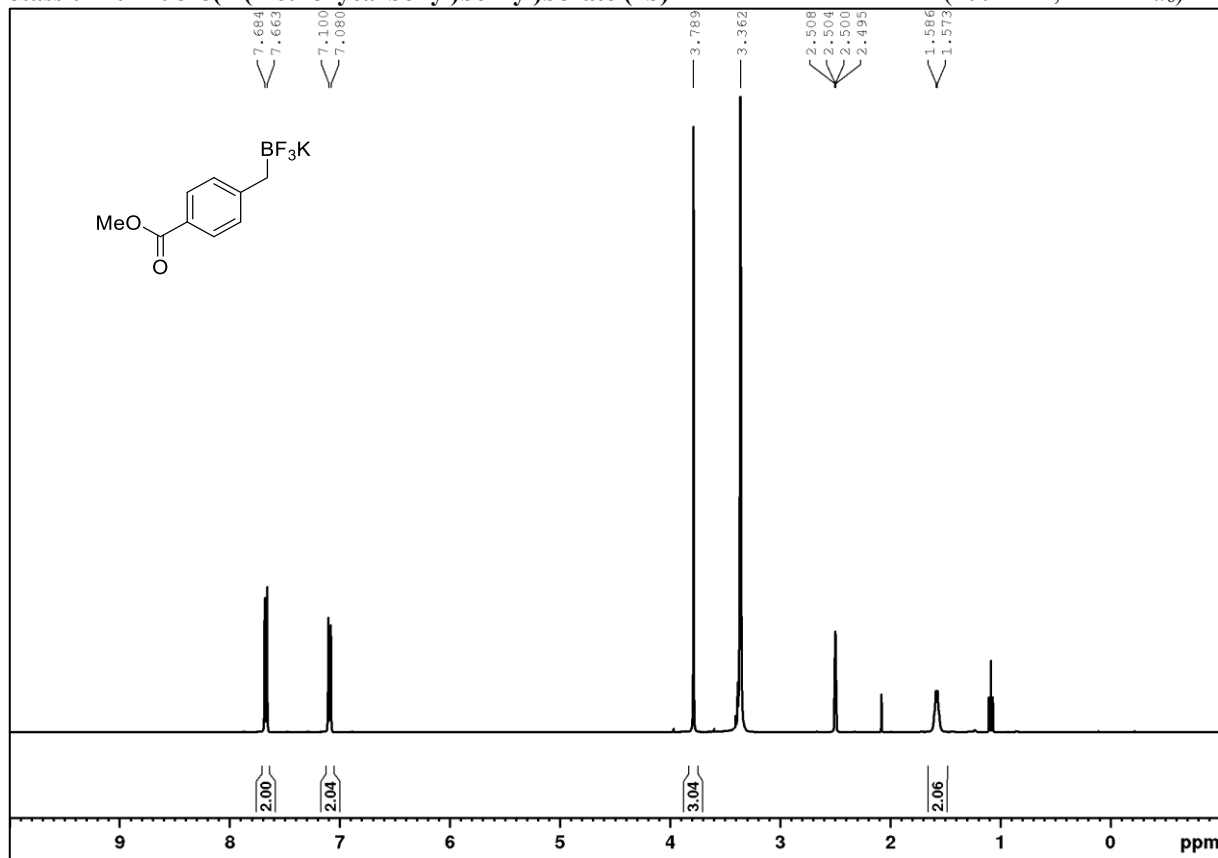
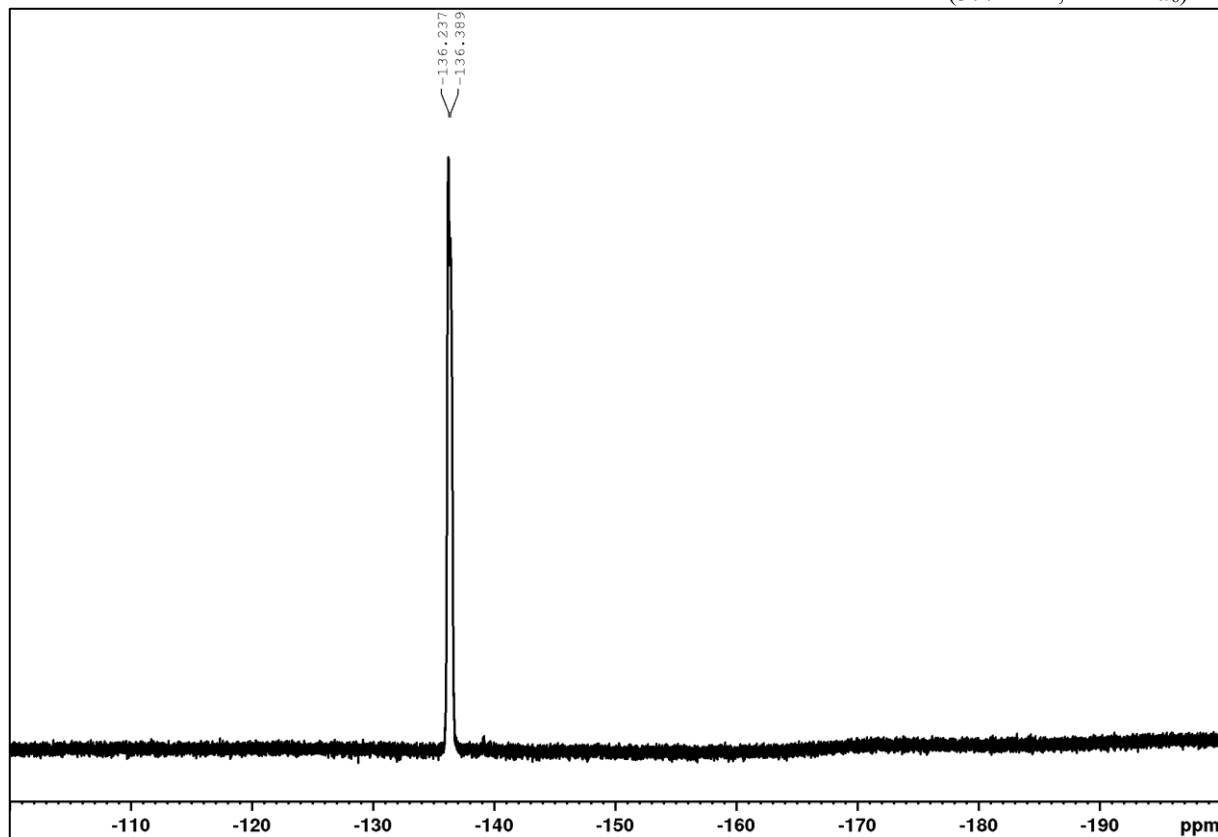
2,3,4,6-Tetra(9*H*-carbazol-9-yl)-5-(4-methoxybenzyl)benzonitrile (4d)¹H NMR (400 MHz, CDCl₃)

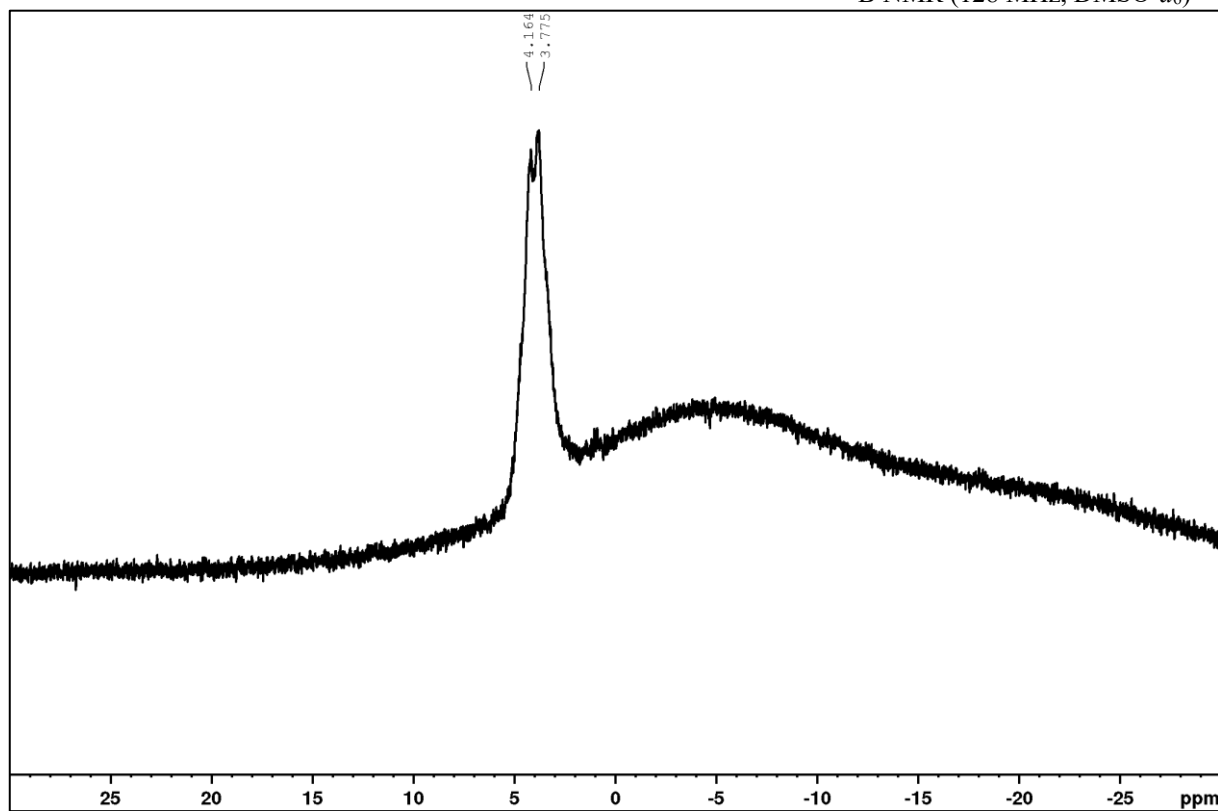
The signal for acetone was likely introduced by an insufficiently dried NMR tube. Due to low solubility, only poor signals could be obtained in the ¹³C.

Potassium trifluoro(3,5-dimethoxybenzyl)borate (2a)

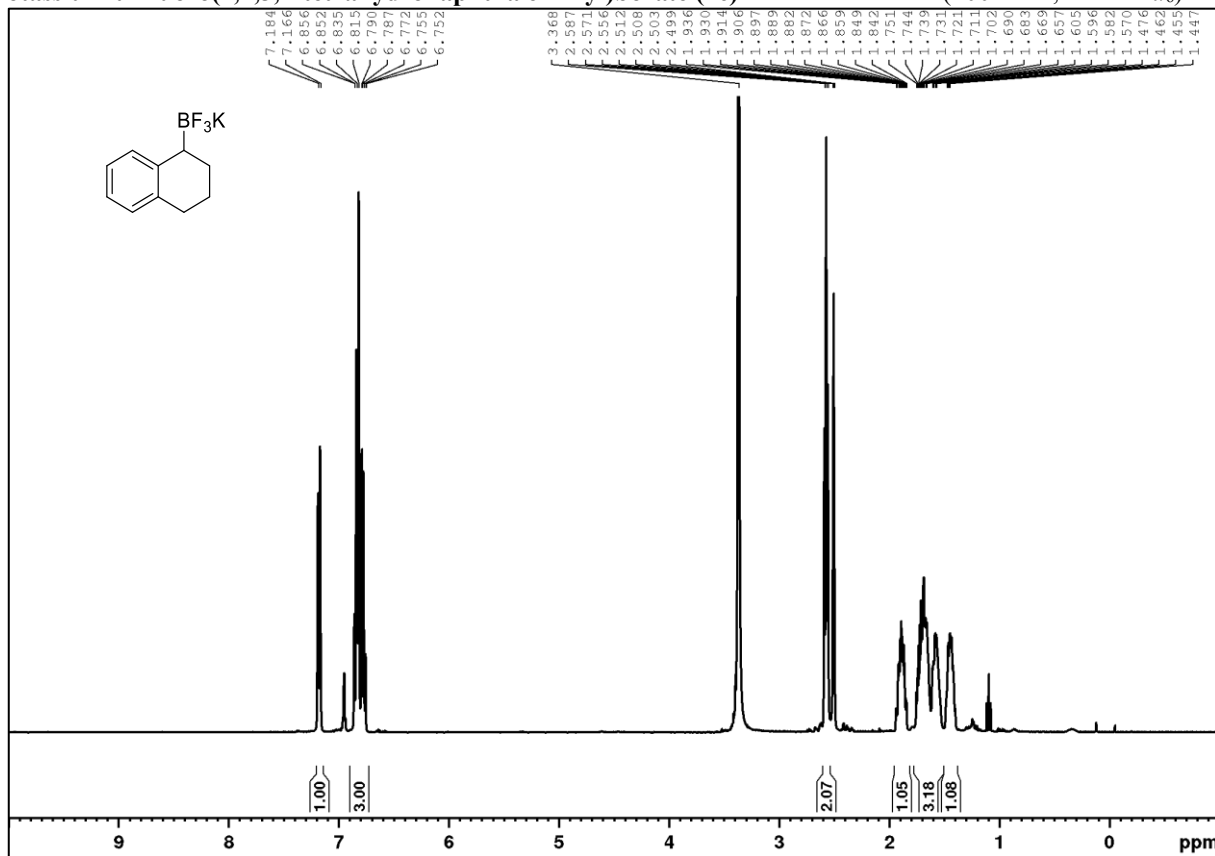
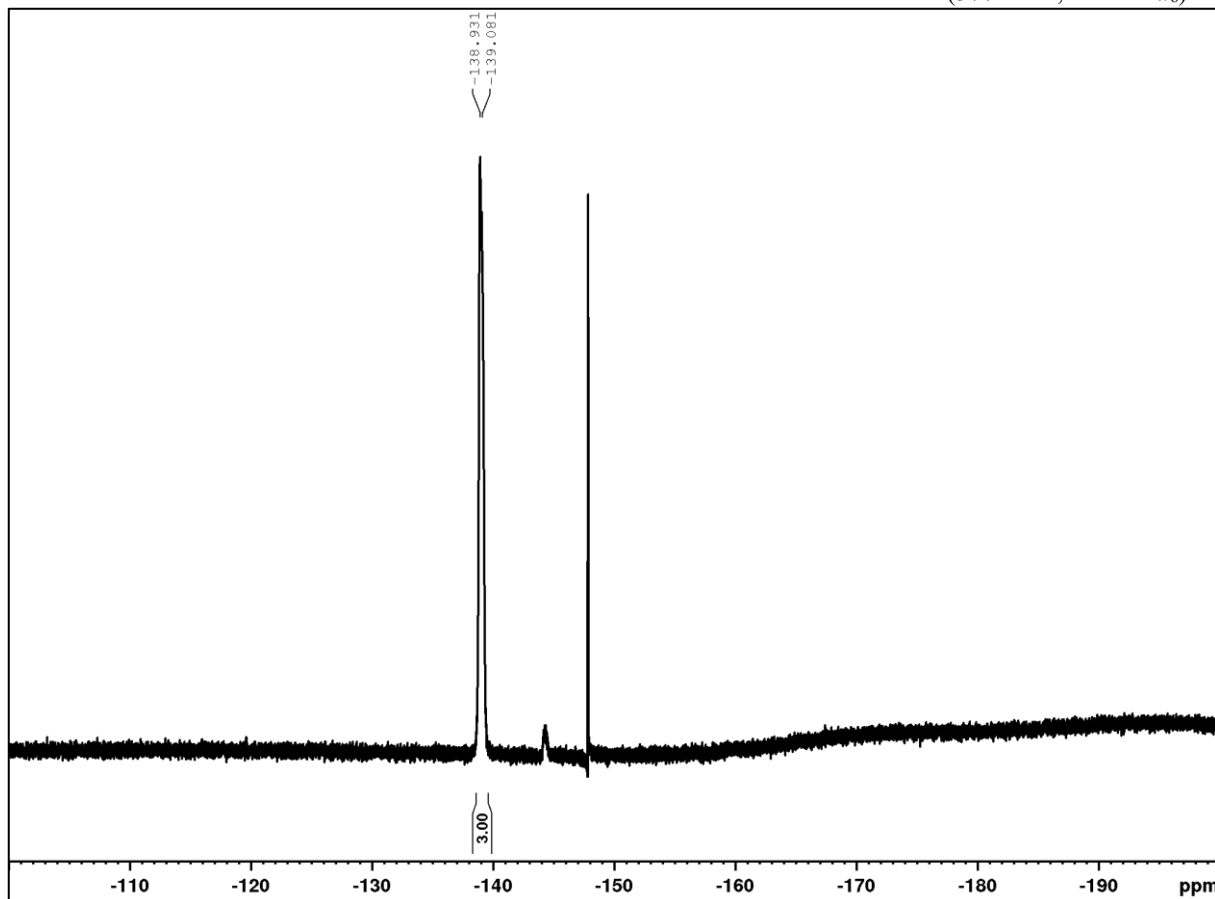
 ^1H NMR (400 MHz, CD_3CN)

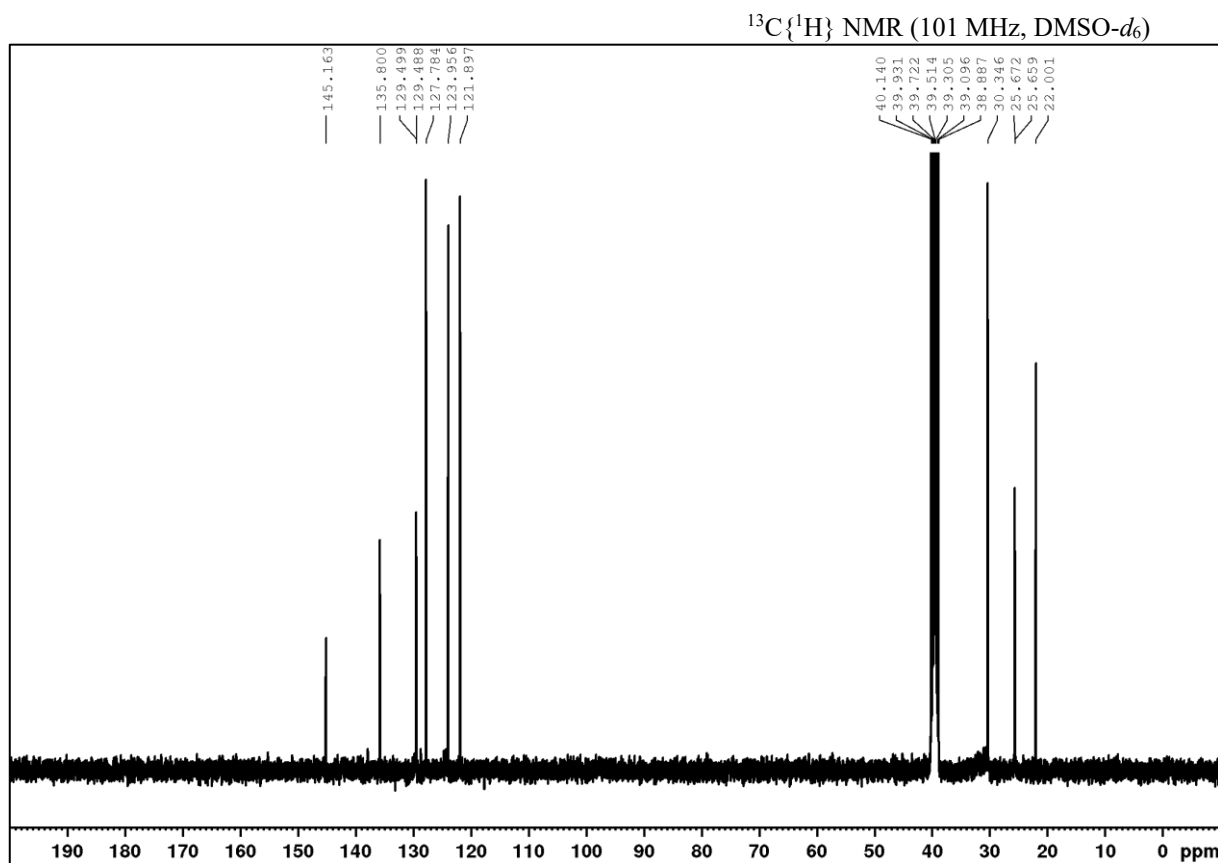
Potassium trifluoro(4-(methoxycarbonyl)benzyl)borate (2b)

 ^1H NMR (400 MHz, $\text{DMSO-}d_6$) ^{19}F NMR (377 MHz, $\text{DMSO-}d_6$)

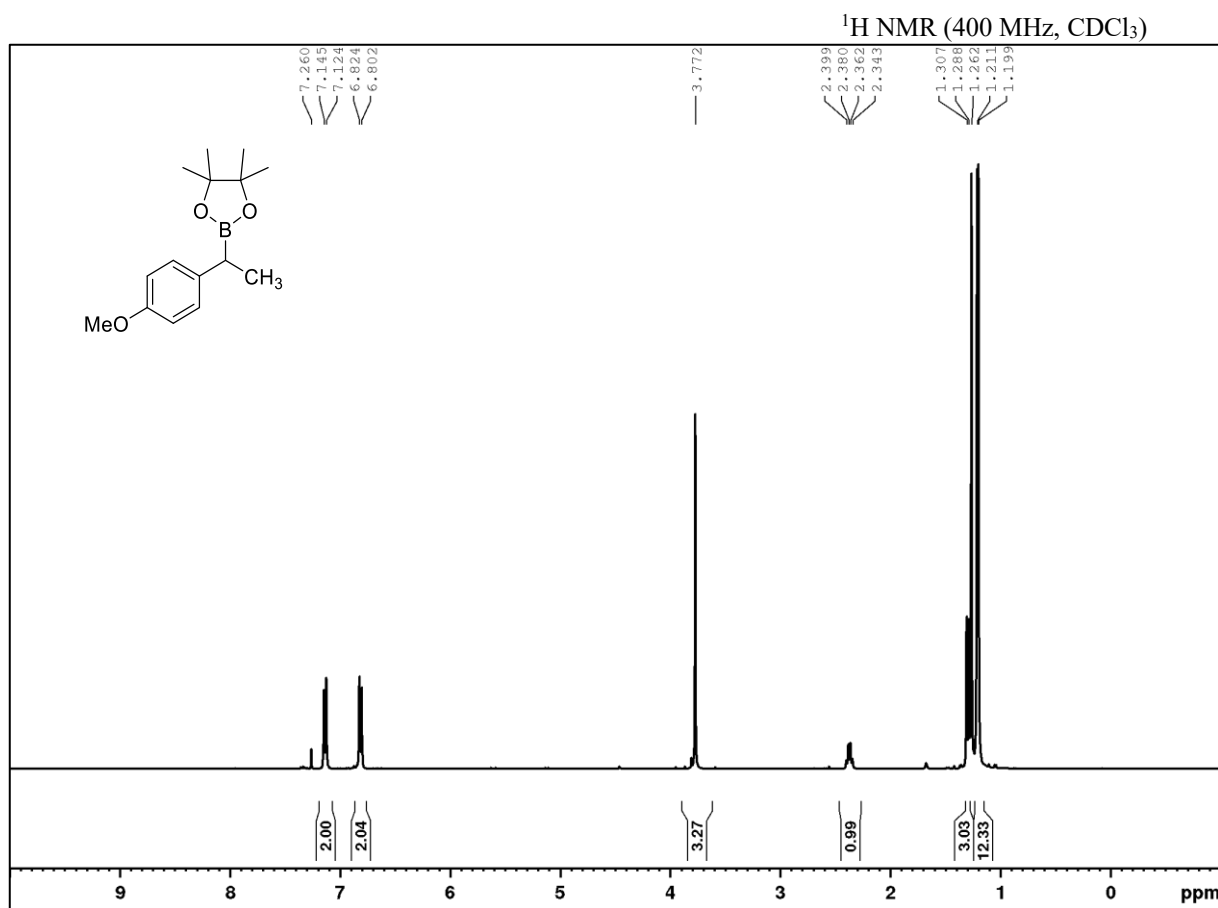
^{11}B NMR (128 MHz, DMSO- d_6)

Potassium trifluoro(1,2,3,4-tetrahydronaphthalen-1-yl)borate (2c)

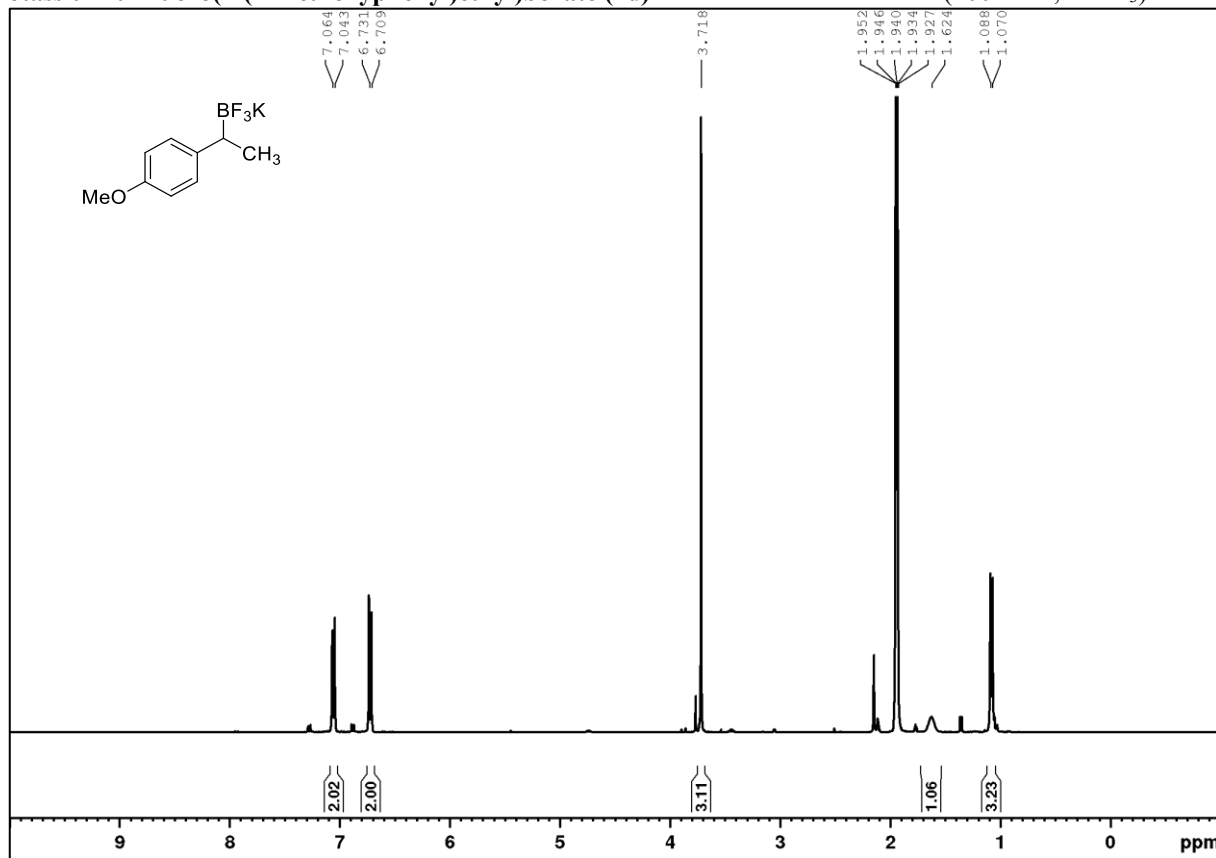
 ^1H NMR (400 MHz, $\text{DMSO-}d_6$) ^{19}F NMR (377 MHz, $\text{DMSO-}d_6$)



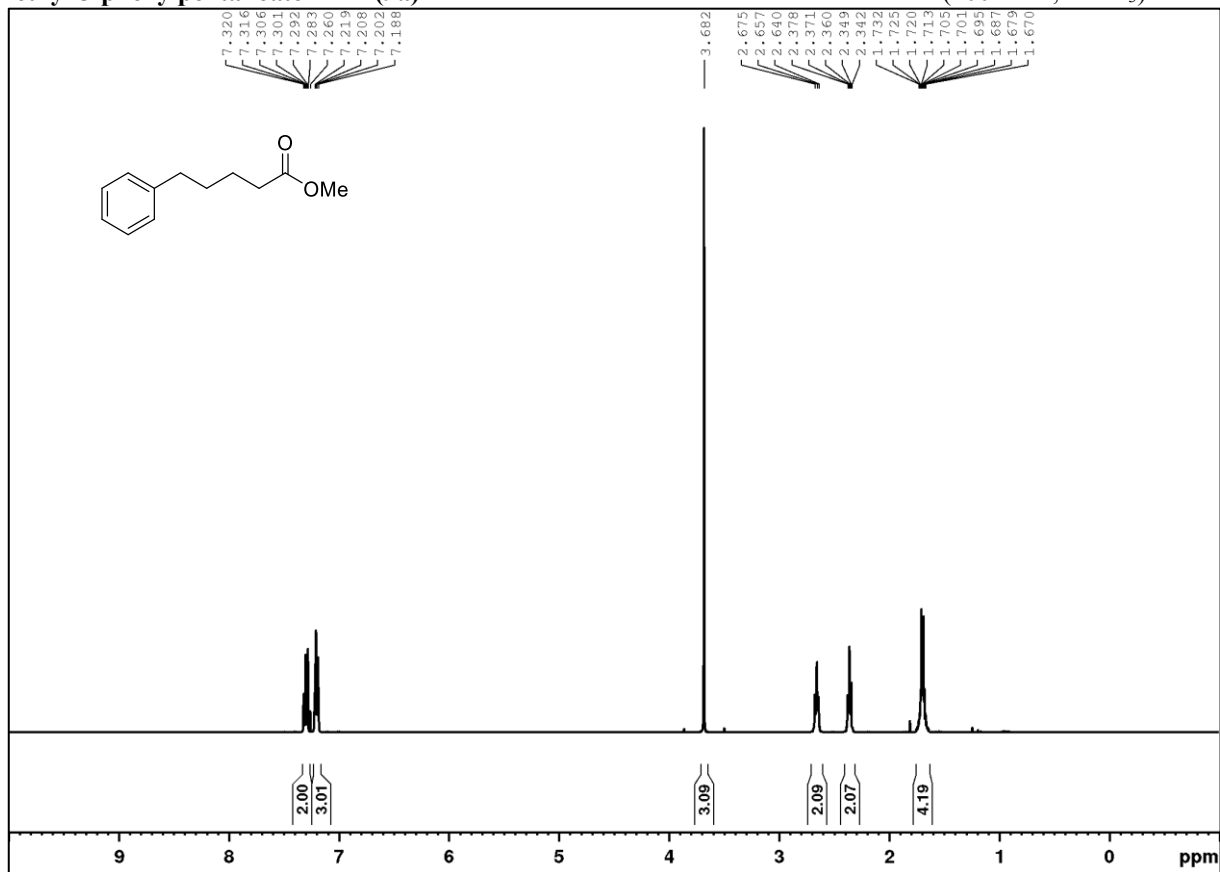
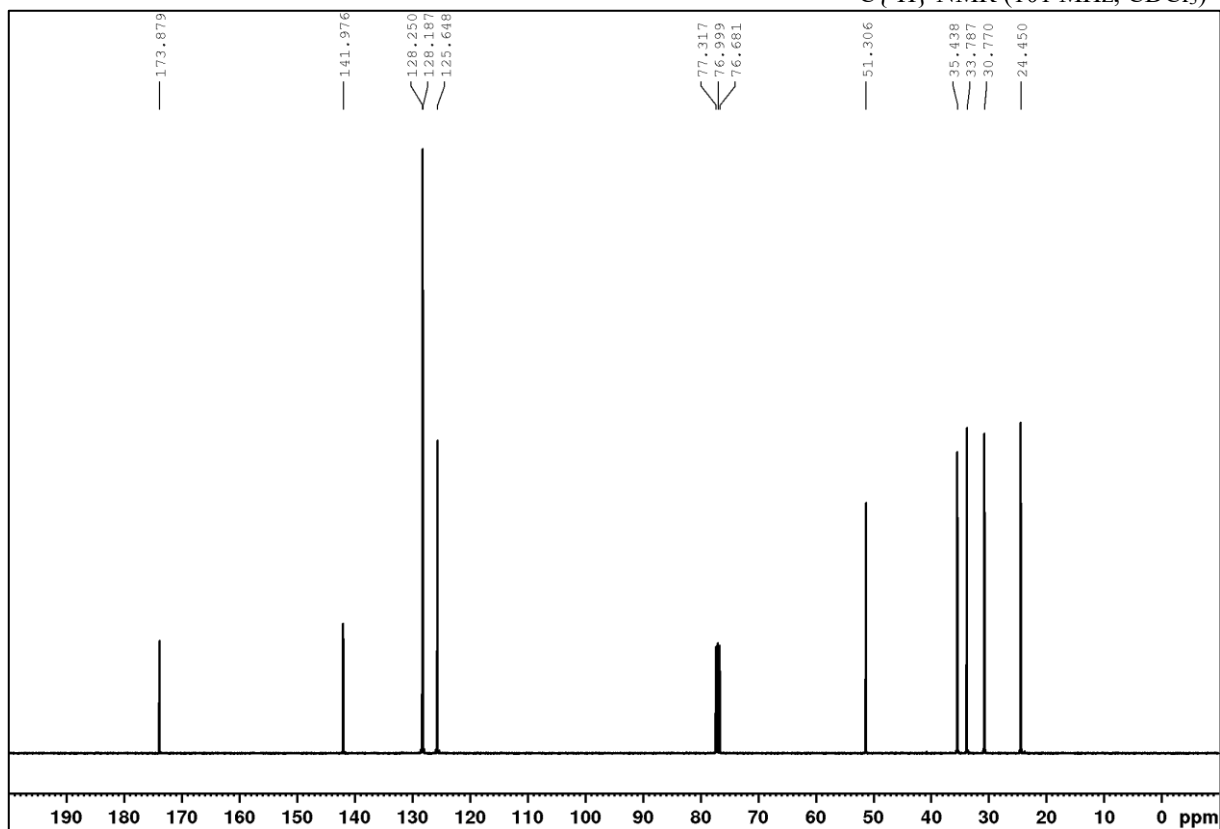
2-(1-(4-Methoxyphenyl)ethyl)-4,4,5,5-tetramethyl-1,3,2-dioxaborolane (17)



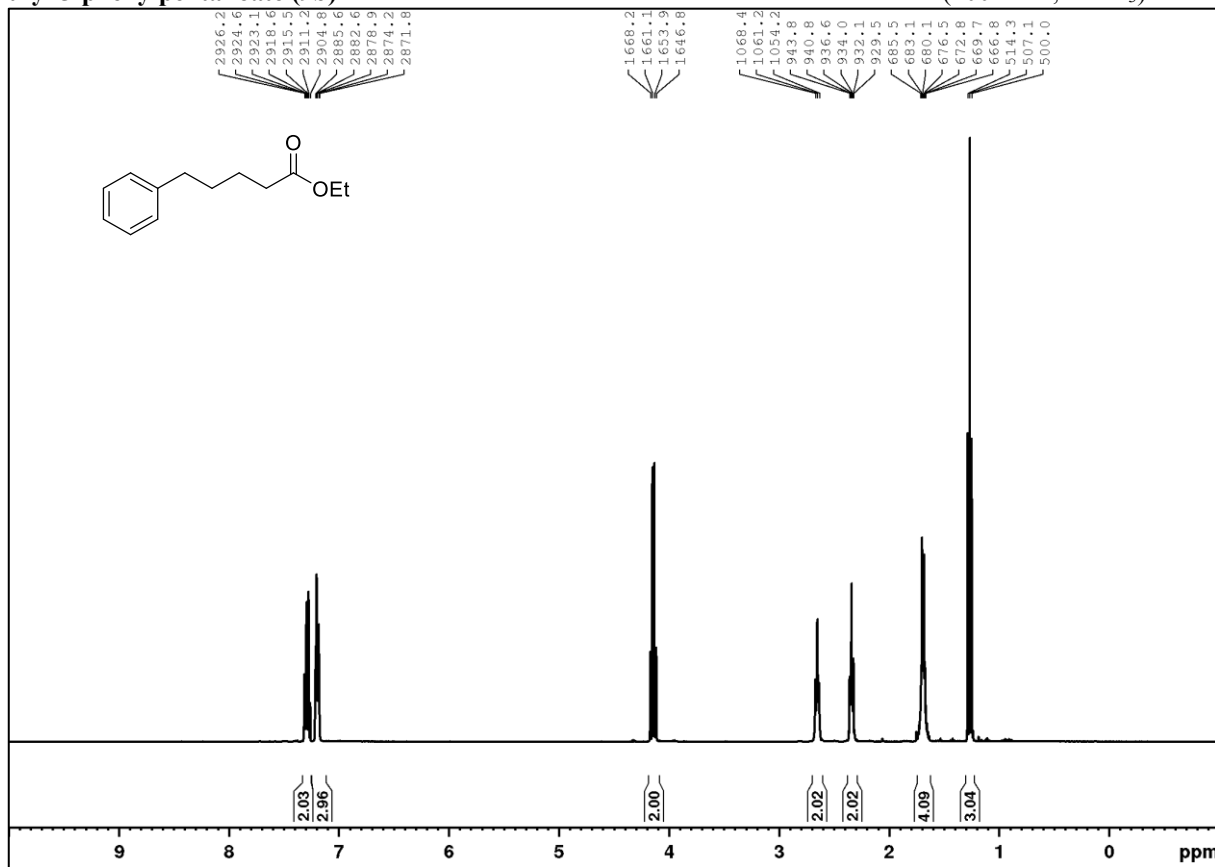
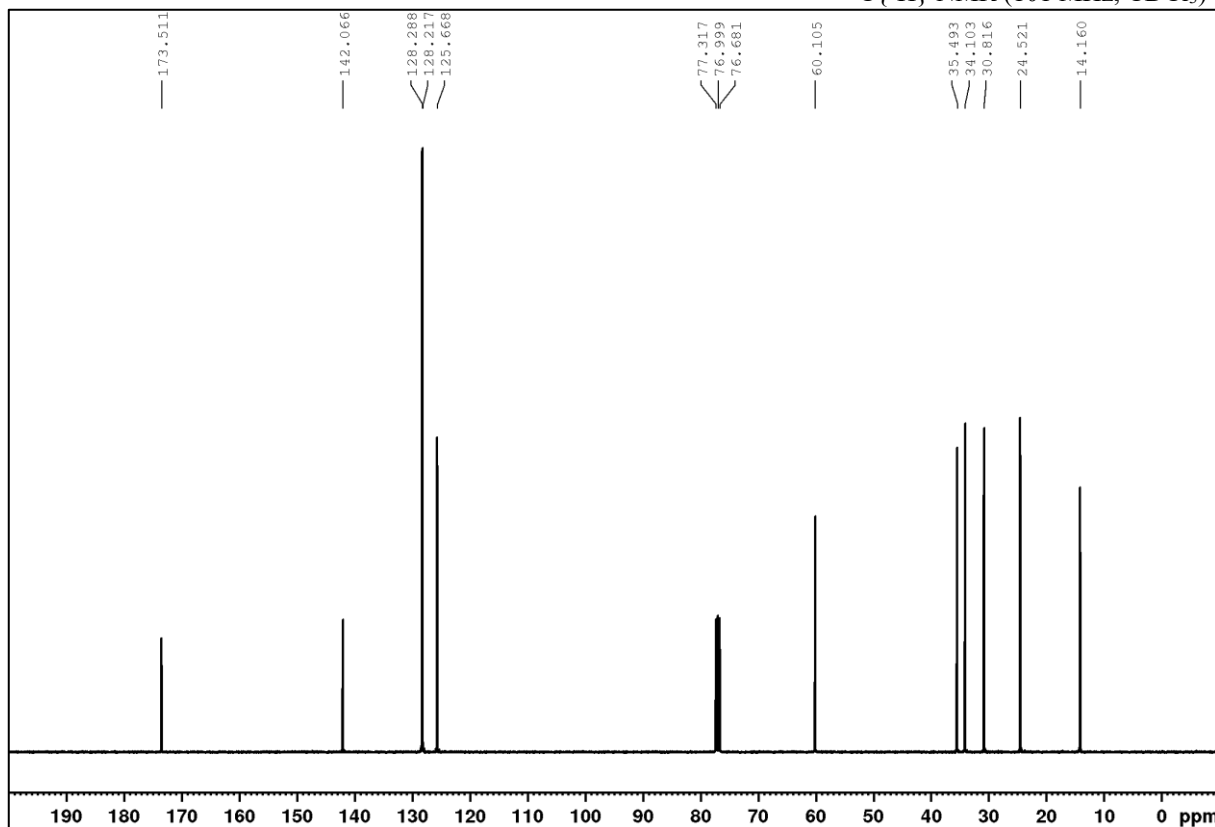
Potassium trifluoro(1-(4-methoxyphenyl)ethyl)borate (2d)

 ^1H NMR (400 MHz, CDCl_3)

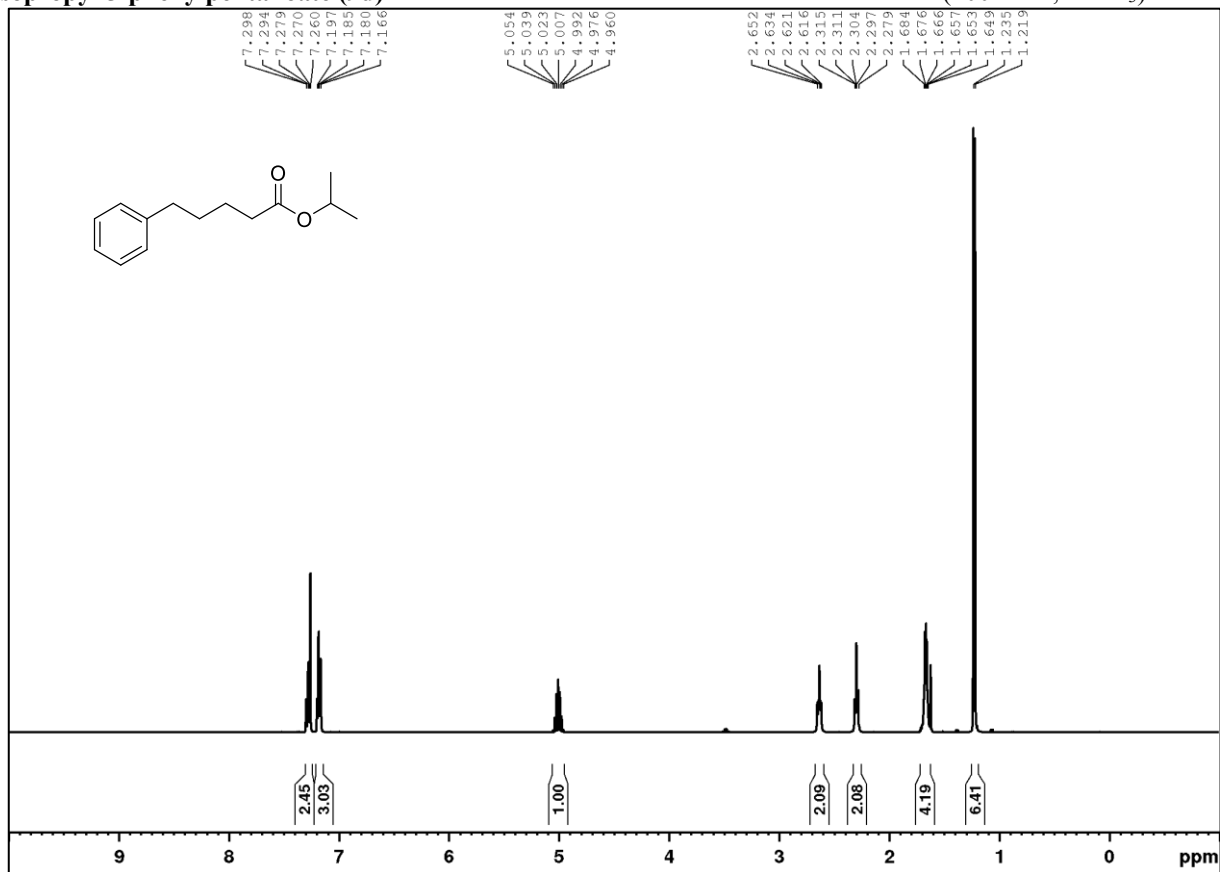
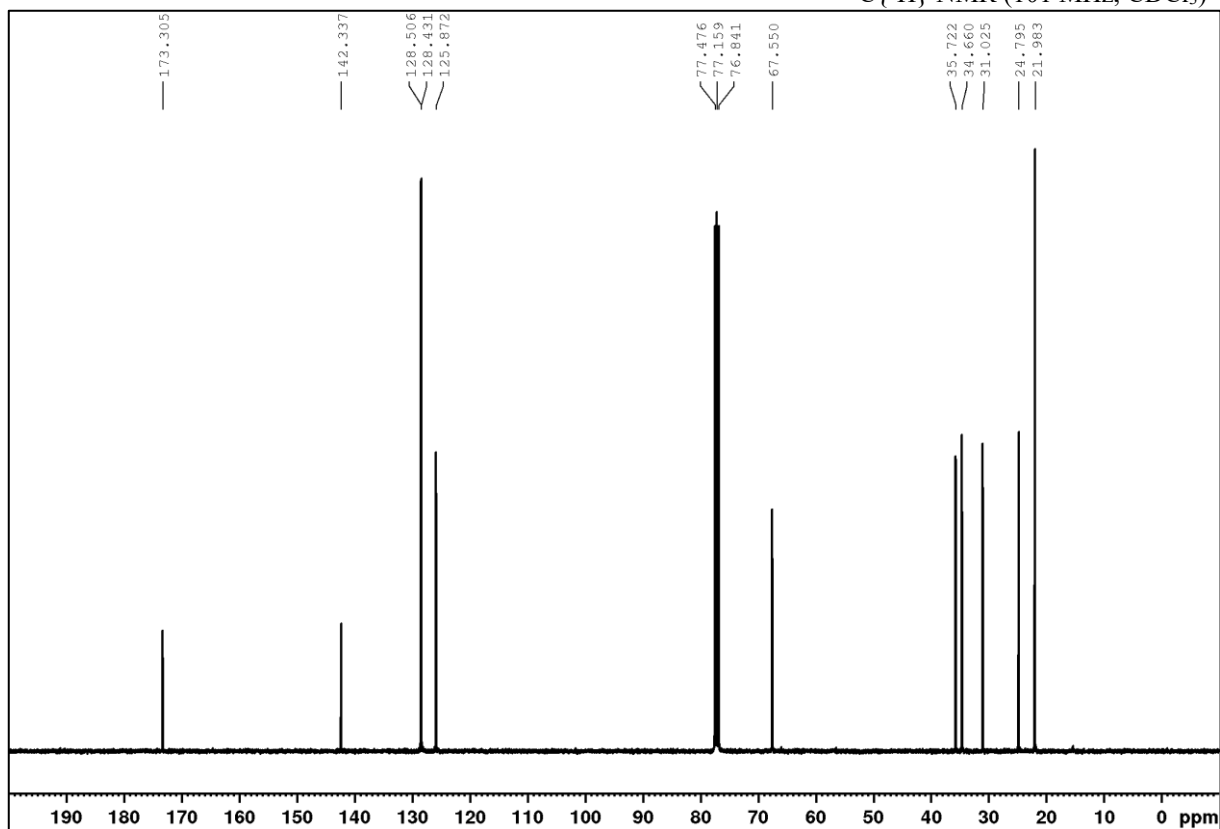
Methyl 5-phenylpentanoate (9a)

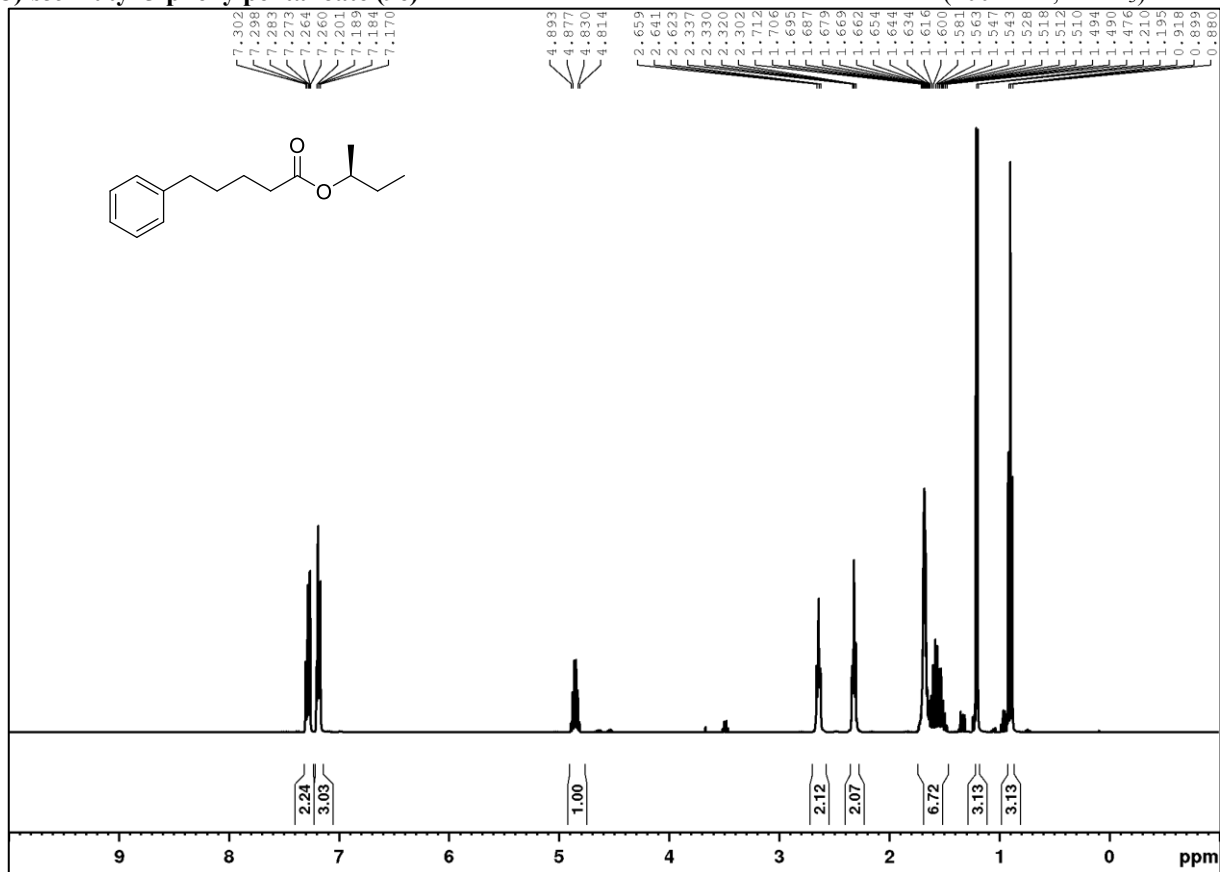
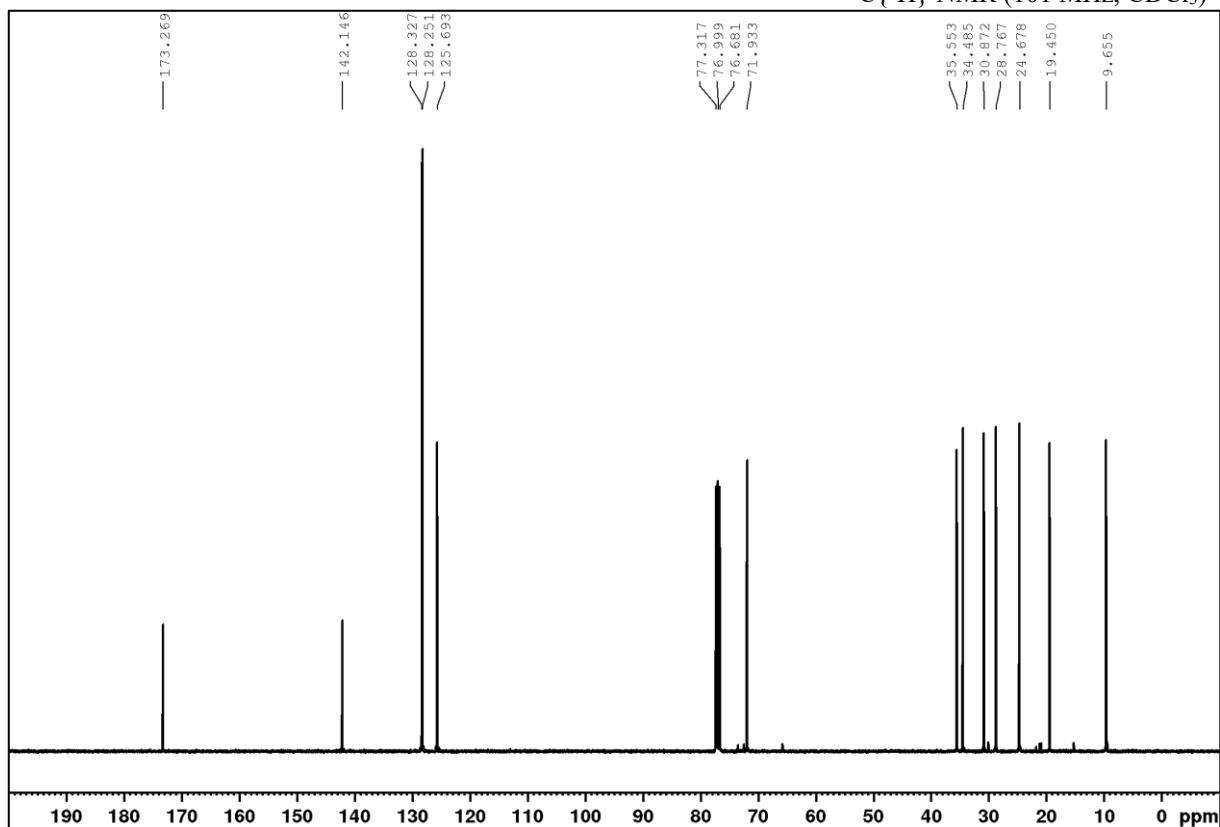
 ^1H NMR (400 MHz, CDCl_3) $^{13}\text{C}\{^1\text{H}\}$ NMR (101 MHz, CDCl_3)

Ethyl 5-phenylpentanoate (9b)

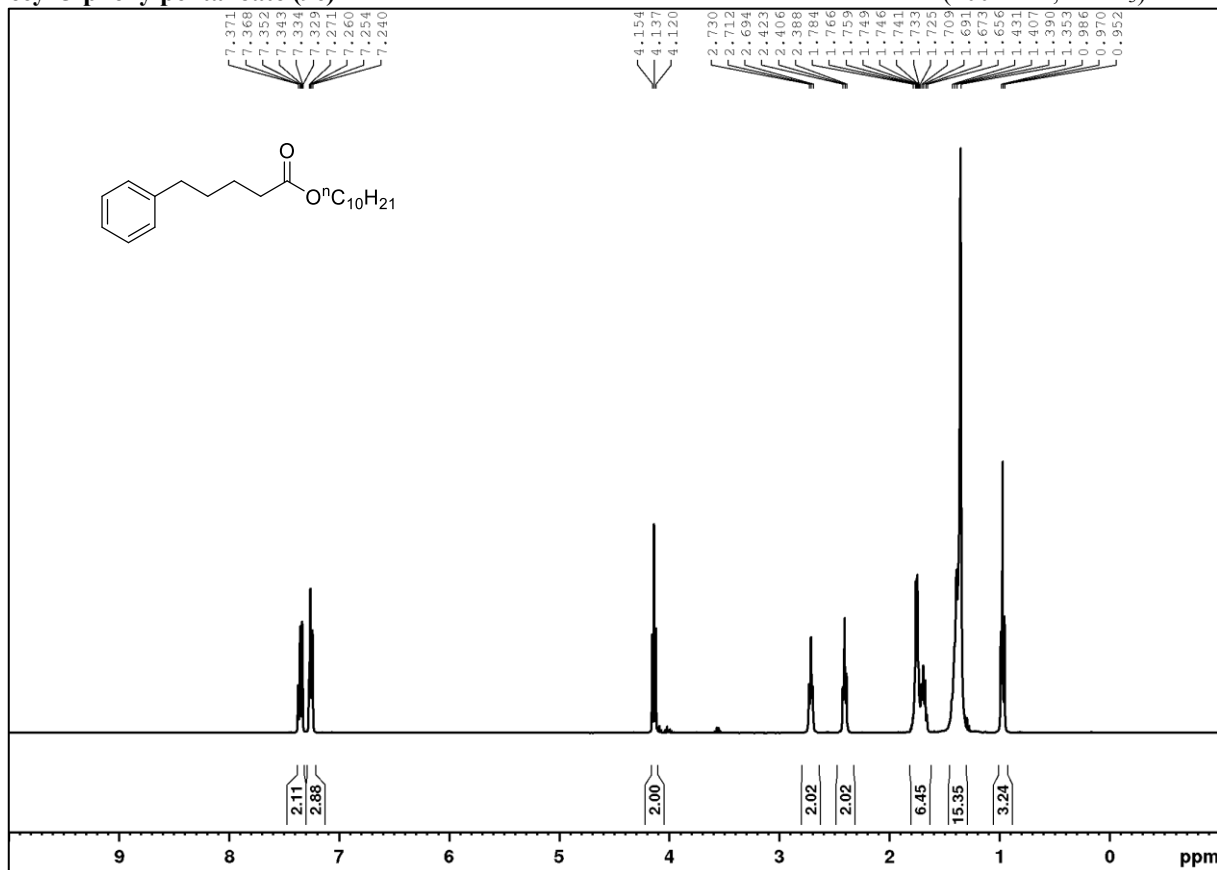
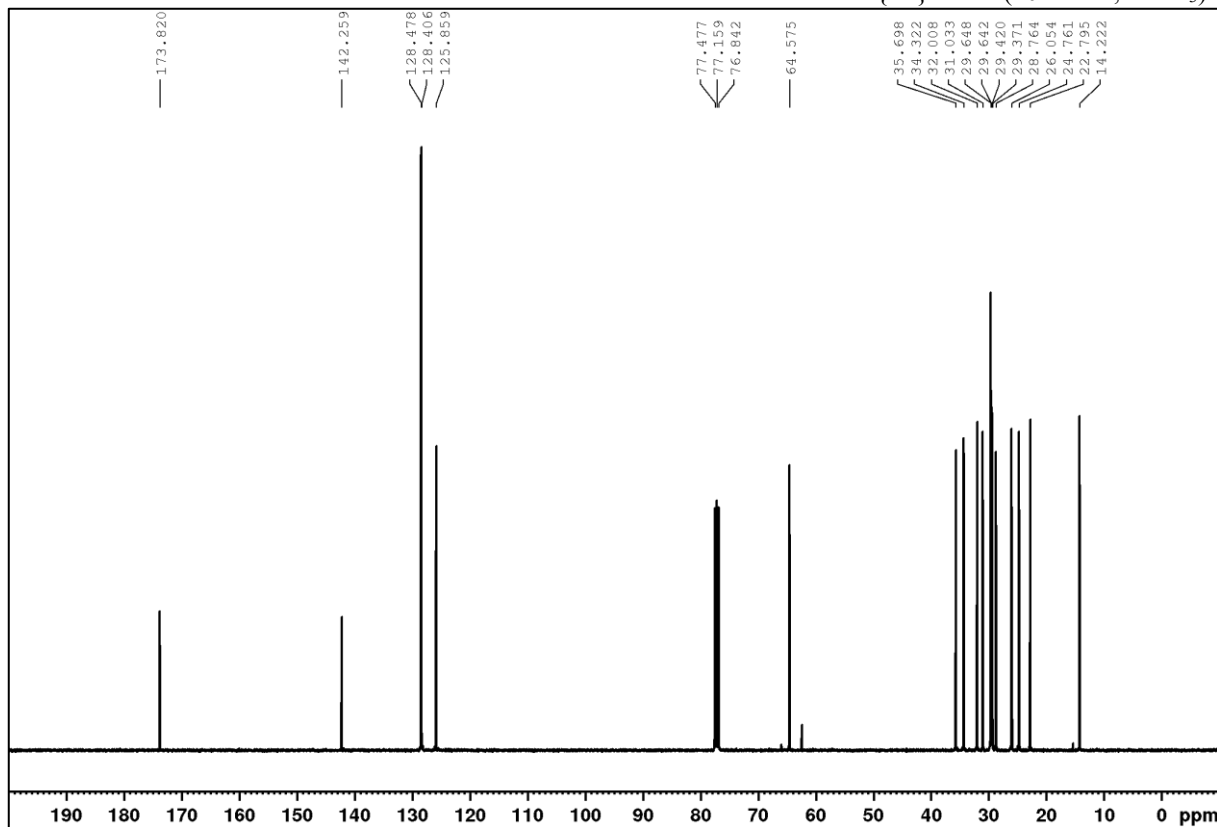
 ^1H NMR (400 MHz, CDCl_3) $^{13}\text{C}\{^1\text{H}\}$ NMR (101 MHz, CDCl_3)

Isopropyl 5-phenylpentanoate (9d)

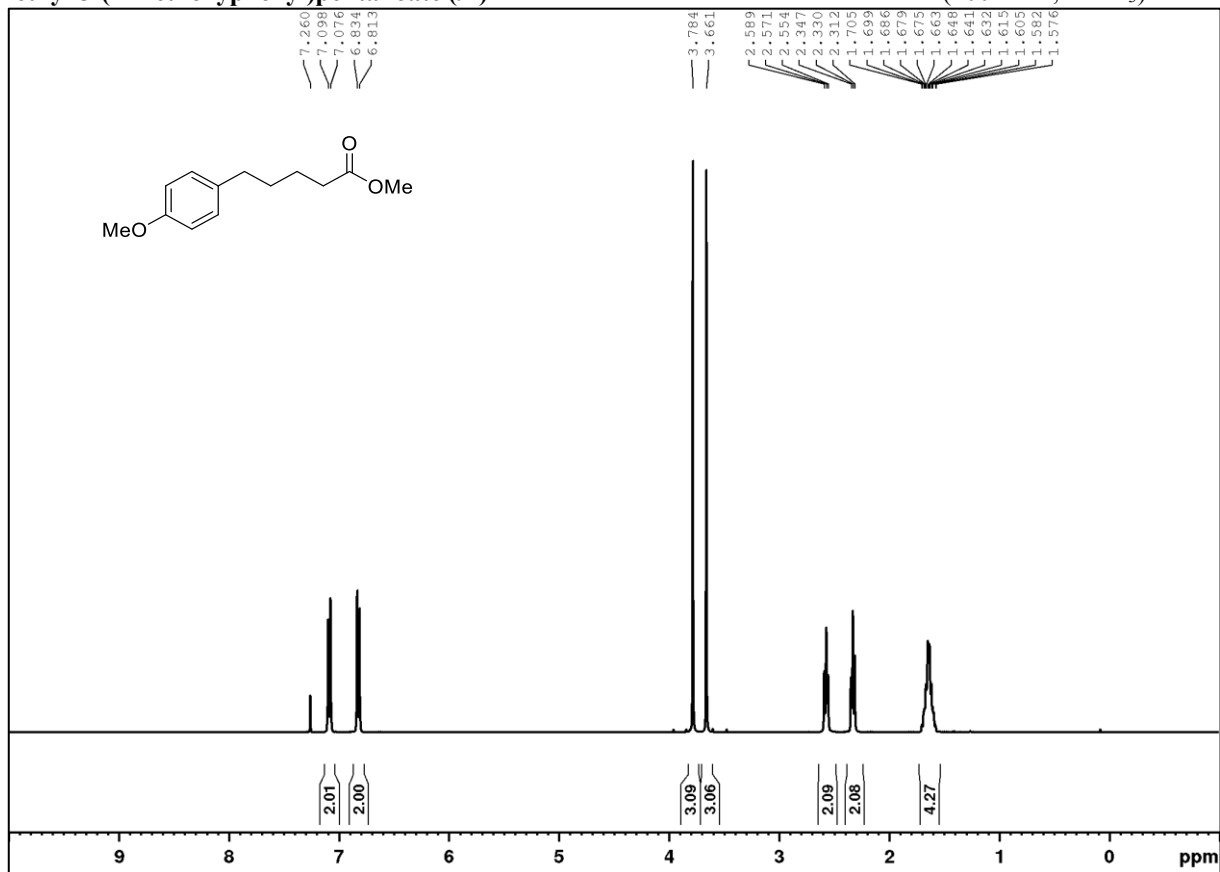
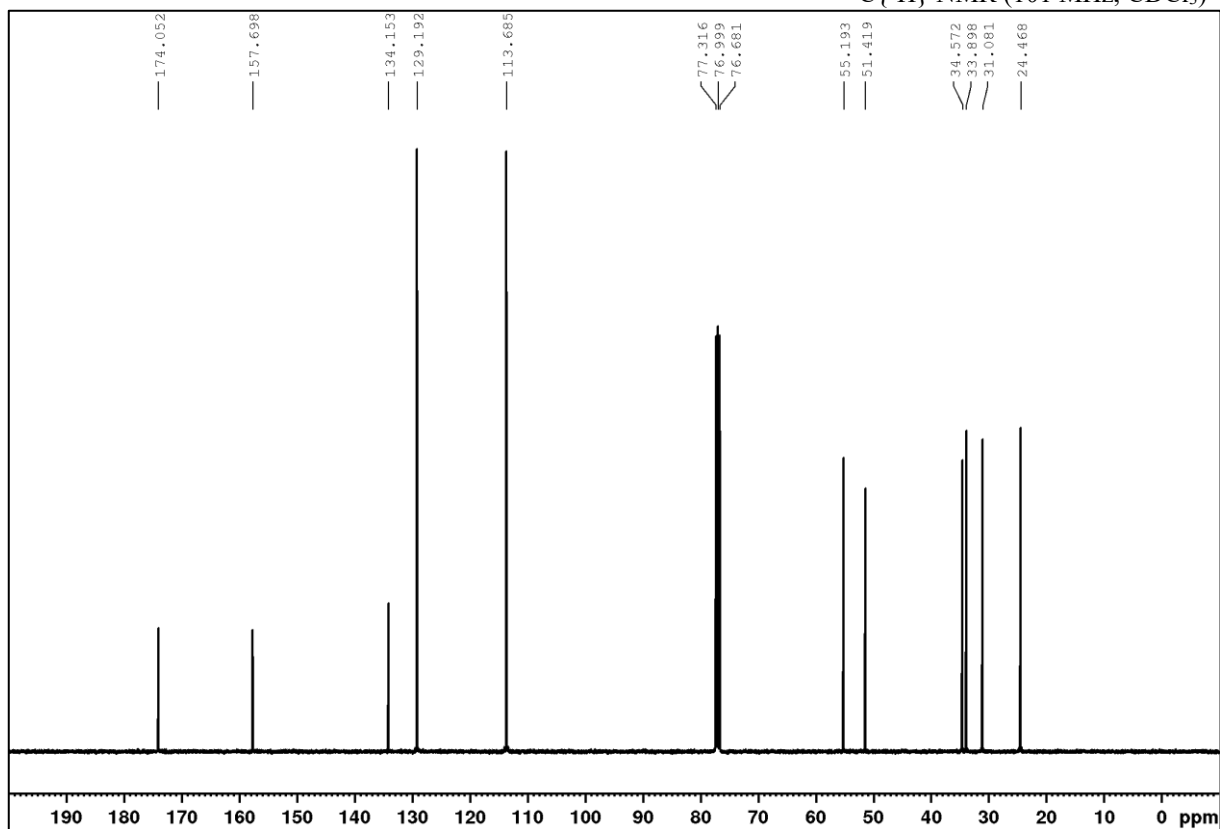
 ^1H NMR (400 MHz, CDCl_3) $^{13}\text{C}\{^1\text{H}\}$ NMR (101 MHz, CDCl_3)

(S)-sec-Butyl 5-phenylpentanoate (9e)**¹H NMR (400 MHz, CDCl₃)****¹³C{¹H} NMR (101 MHz, CDCl₃)**

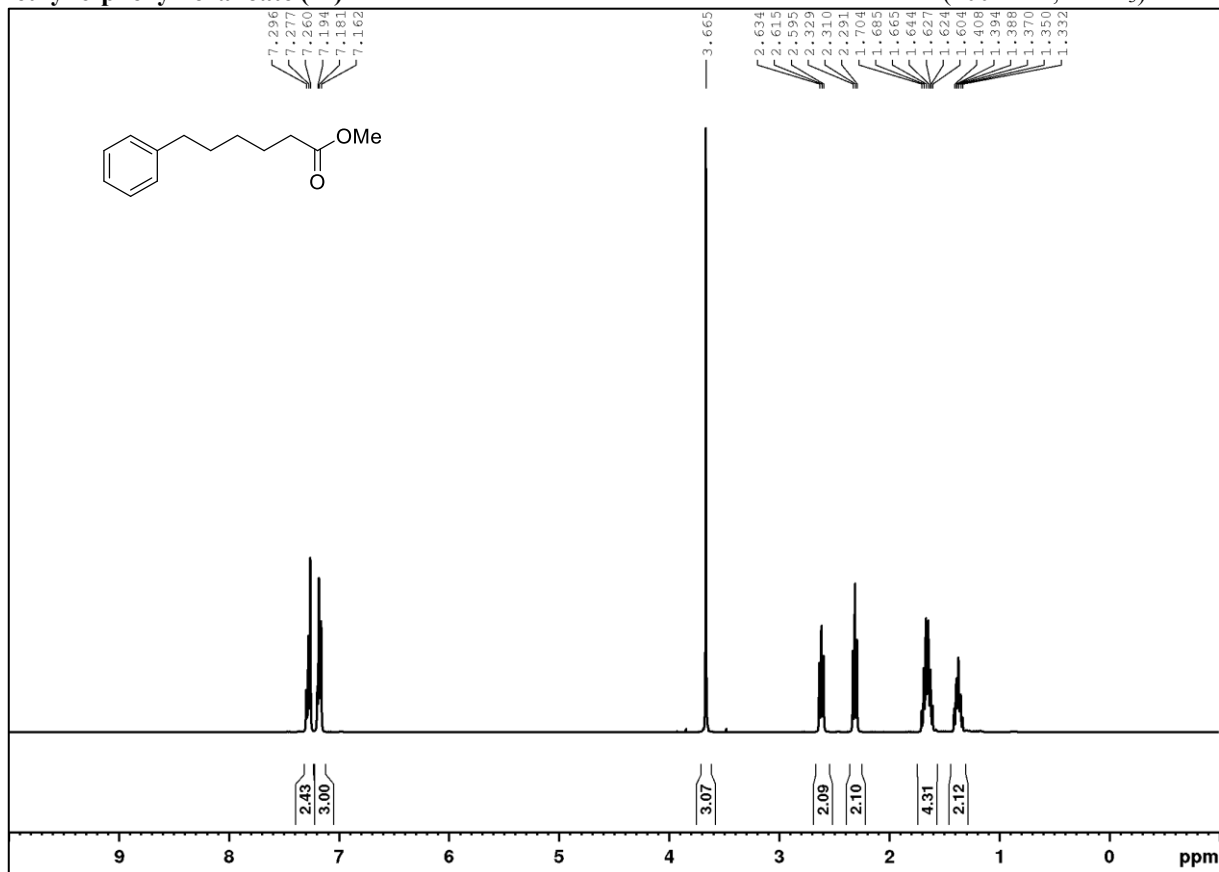
Decyl 5-phenylpentanoate (9c)

 ^1H NMR (400 MHz, CDCl_3) $^{13}\text{C}\{^1\text{H}\}$ NMR (101 MHz, CDCl_3)

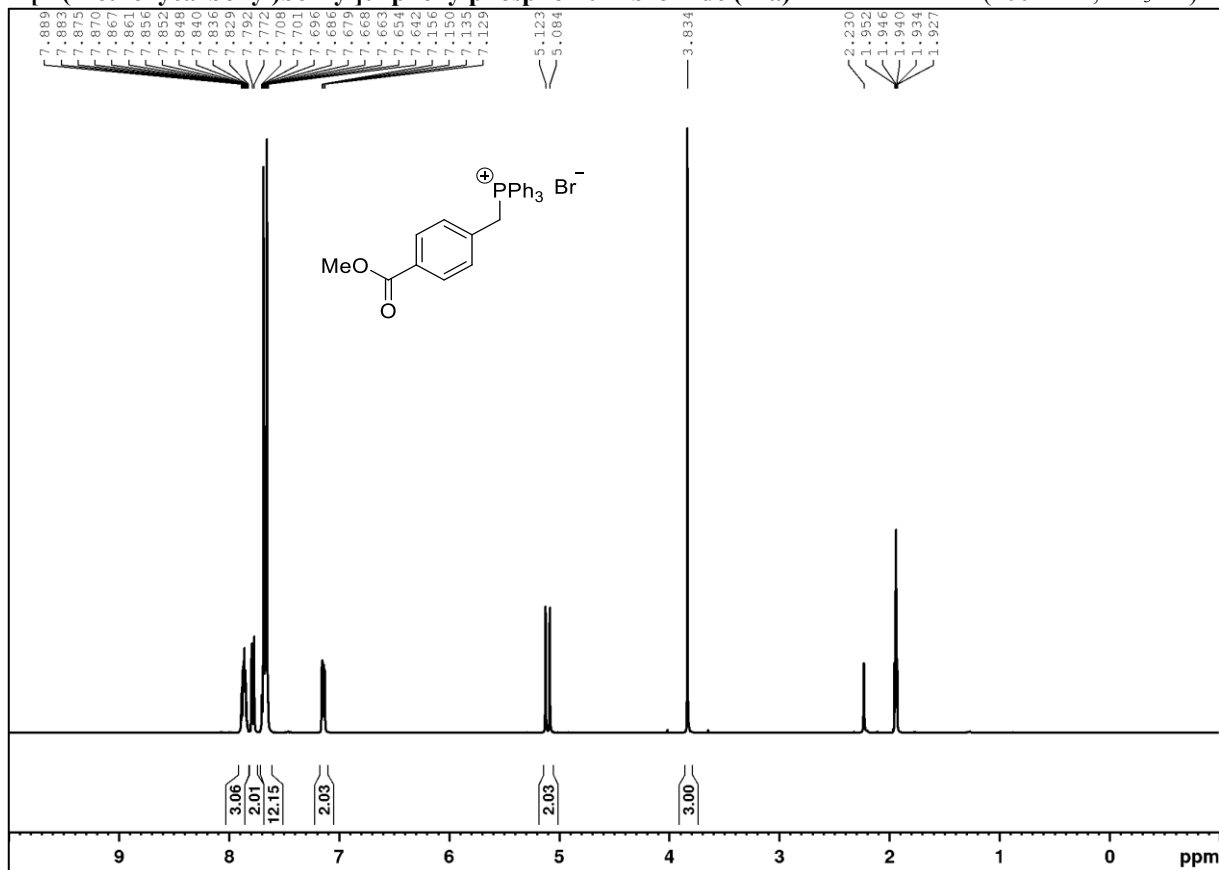
Methyl 5-(4-methoxyphenyl)pentanoate (9f)

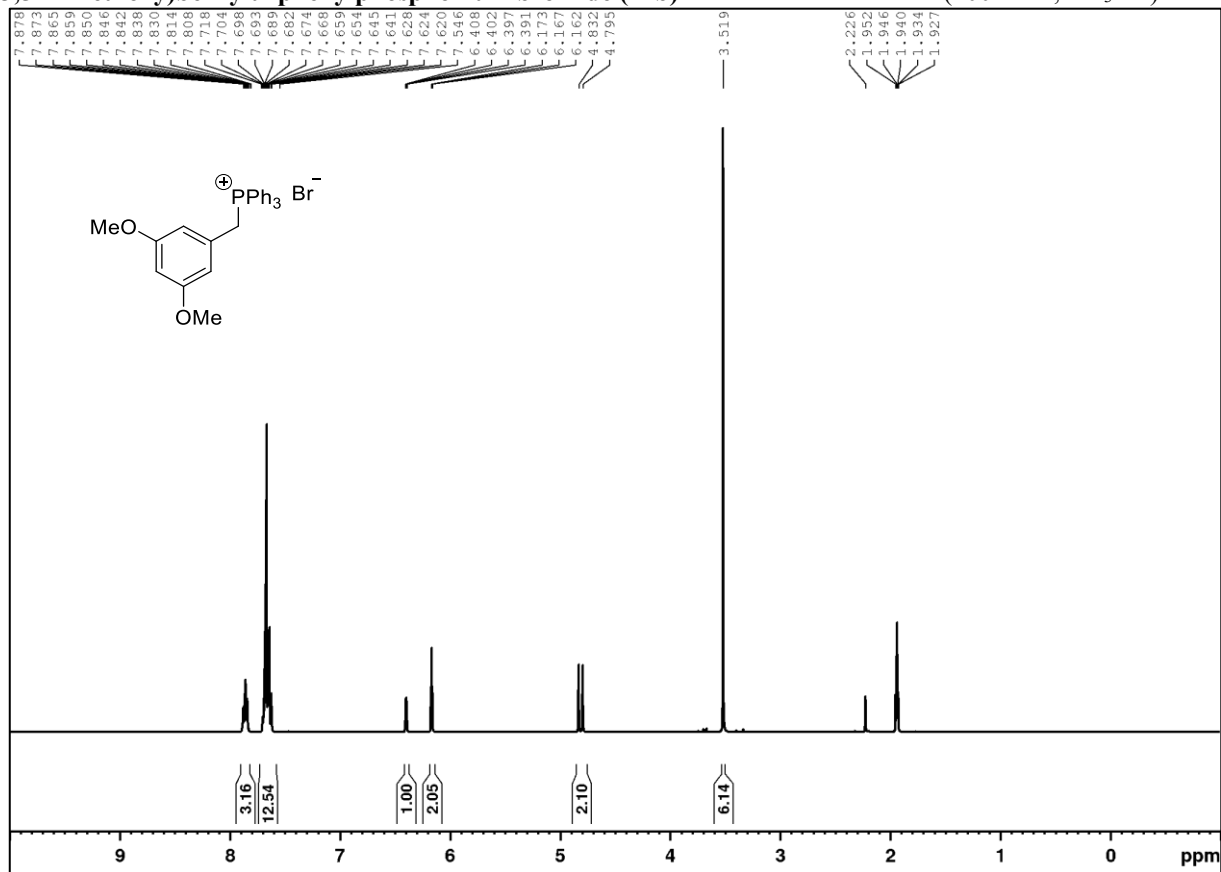
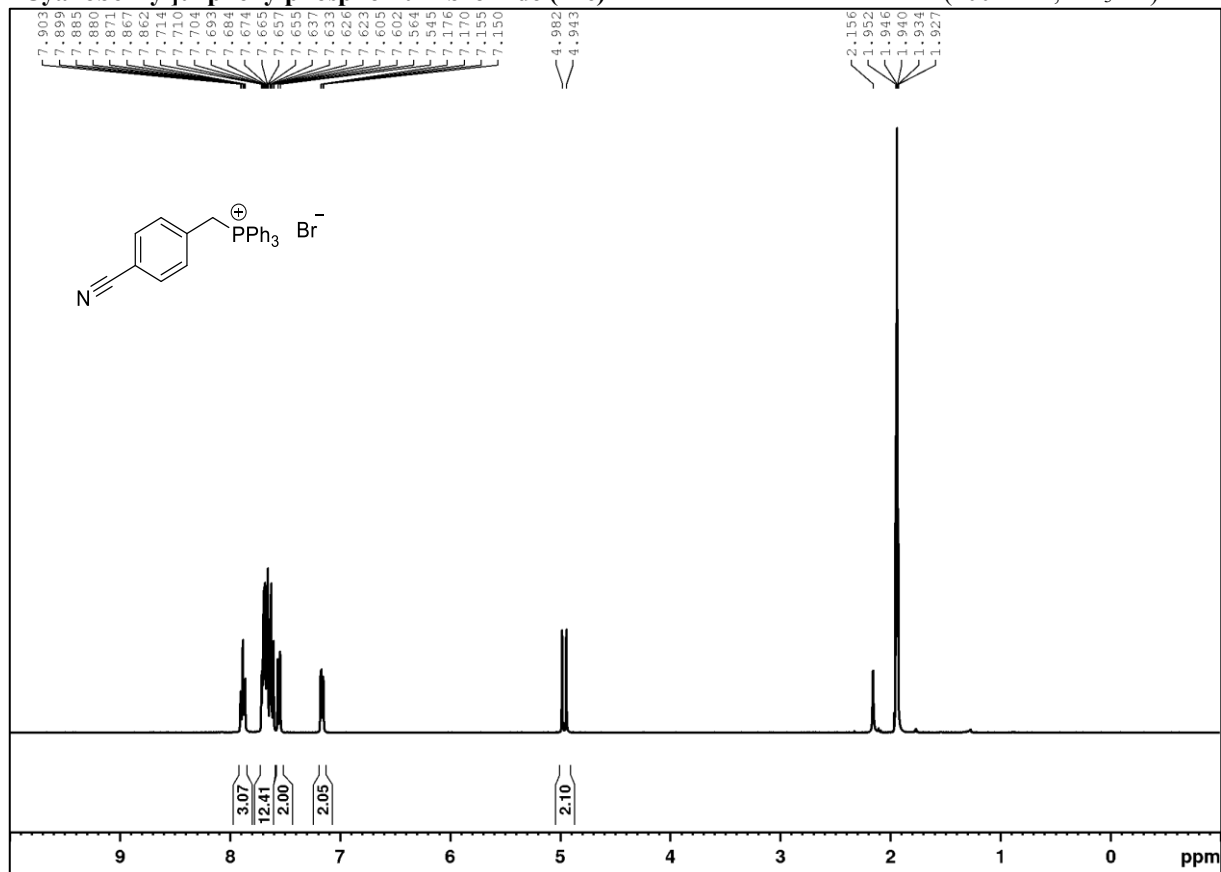
 ^1H NMR (400 MHz, CDCl_3) $^{13}\text{C}\{^1\text{H}\}$ NMR (101 MHz, CDCl_3)

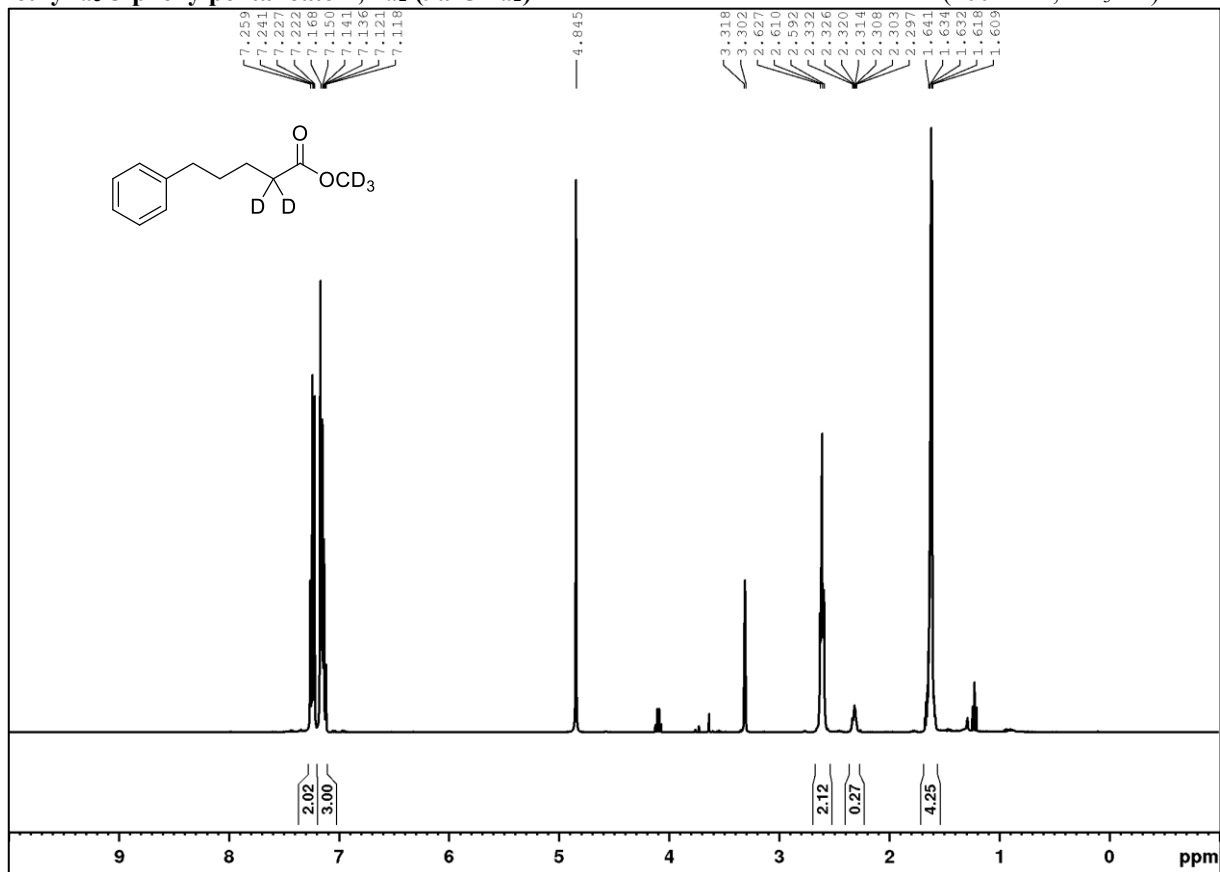
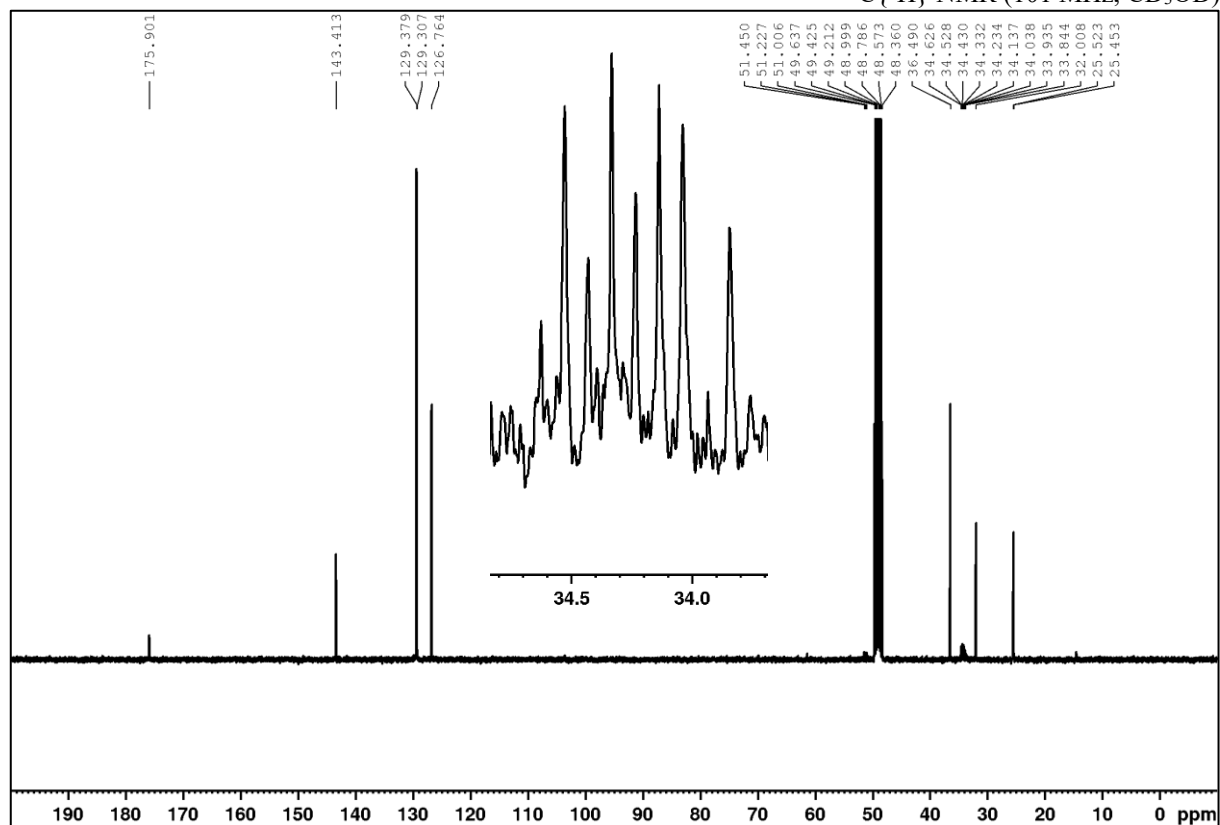
Methyl 6-phenylhexanoate (11)

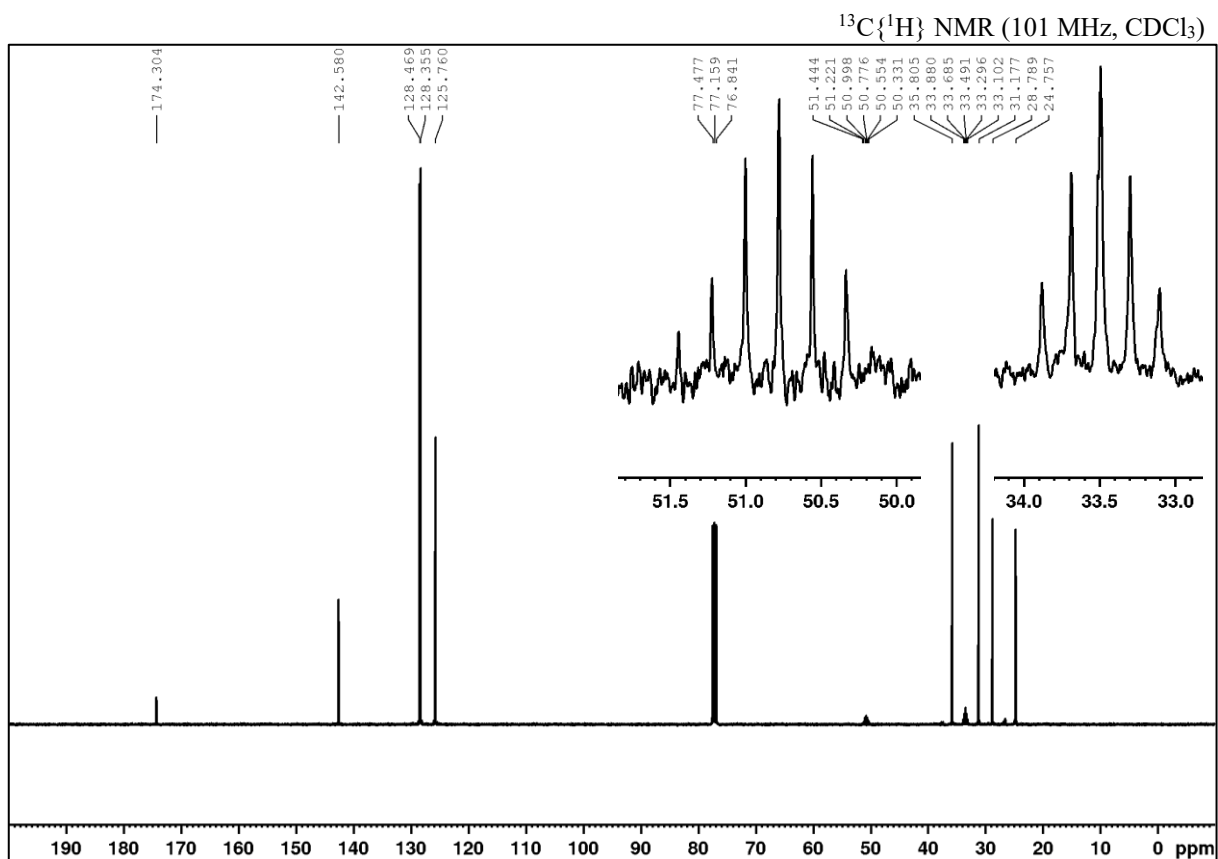
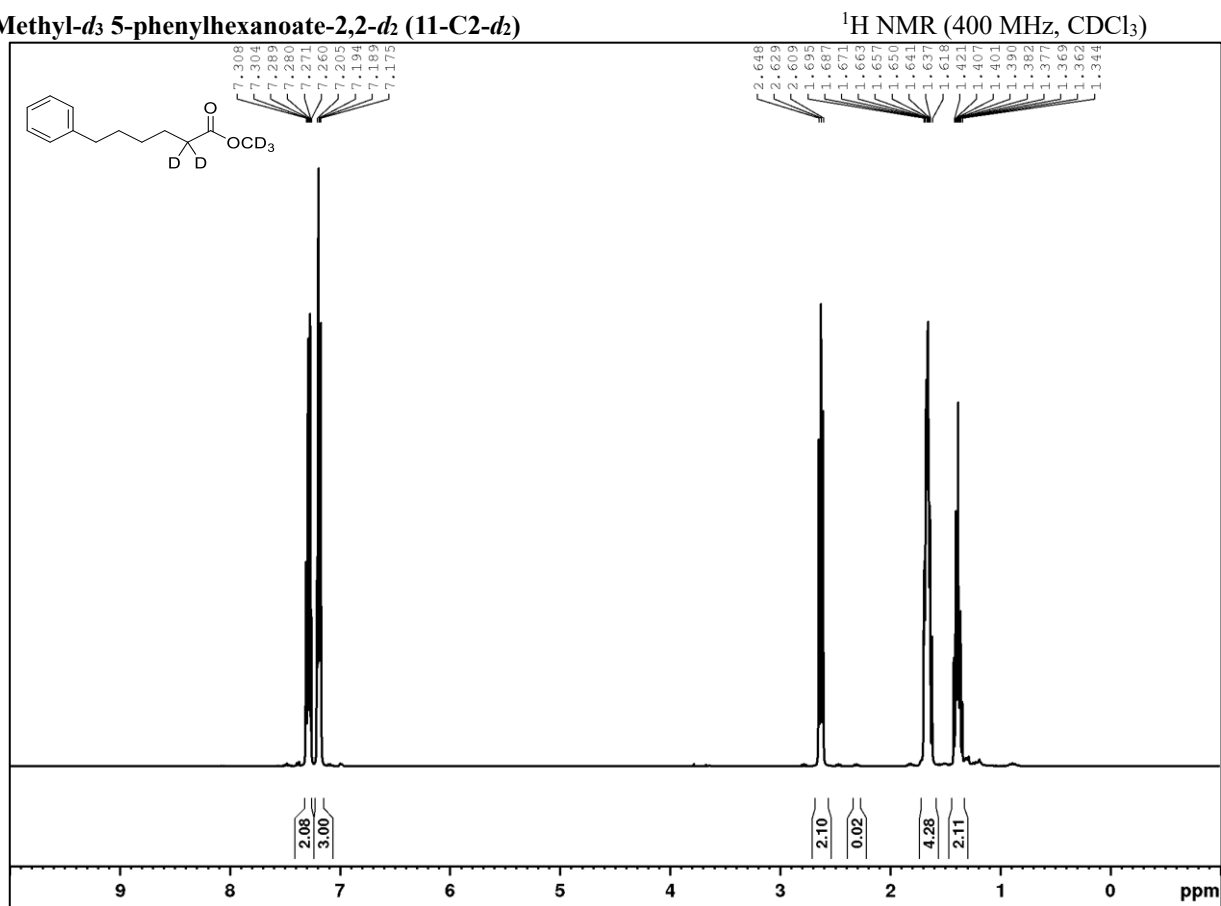
 $^1\text{H NMR}$ (400 MHz, CDCl_3)

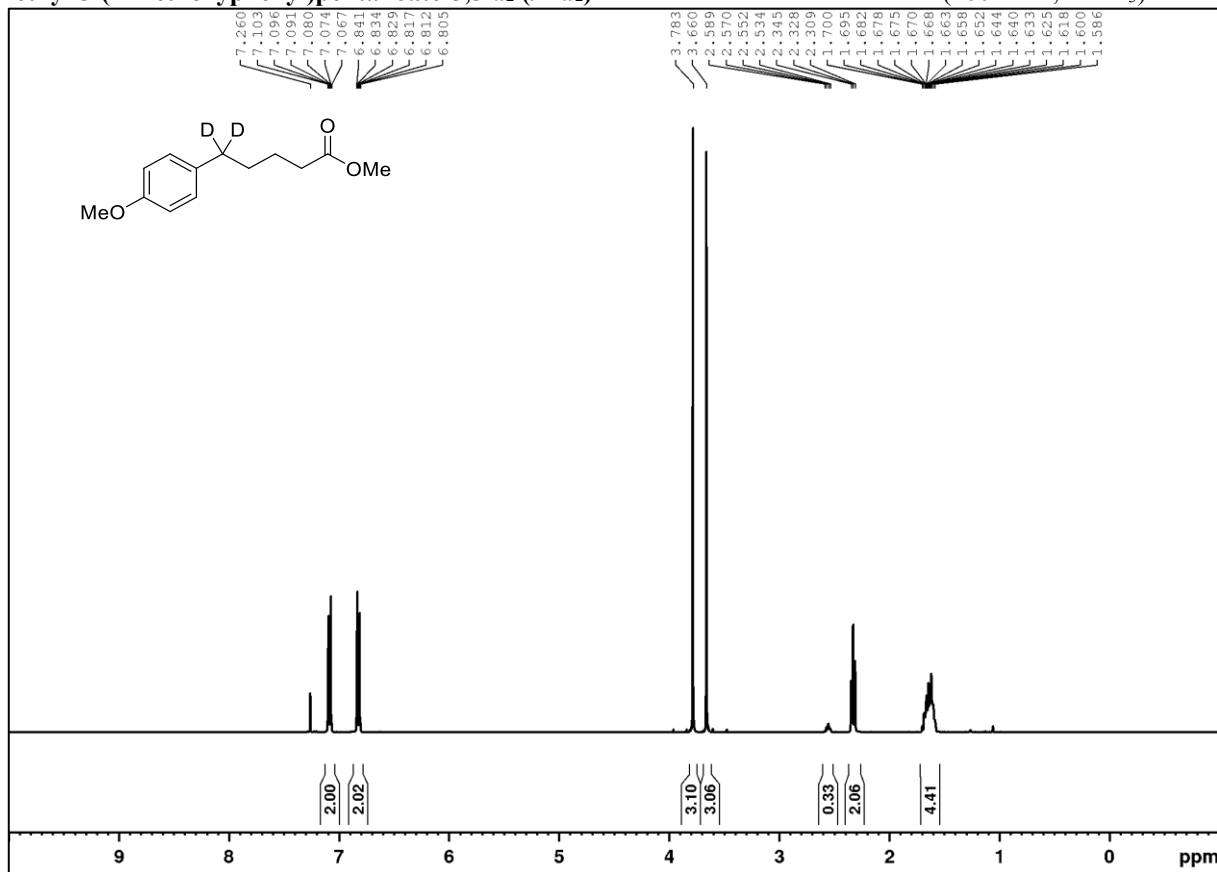
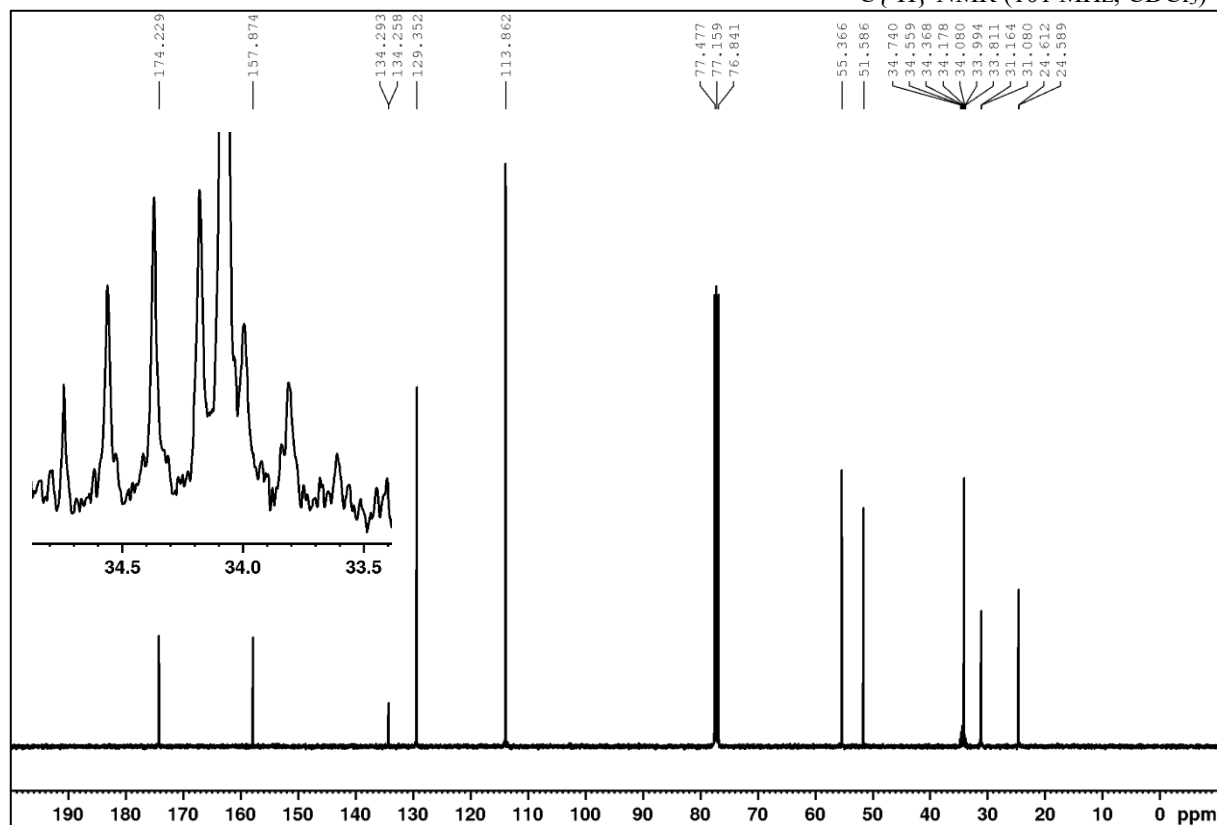
[4-(Methoxycarbonyl)benzyl]triphenylphosphonium bromide (14a)

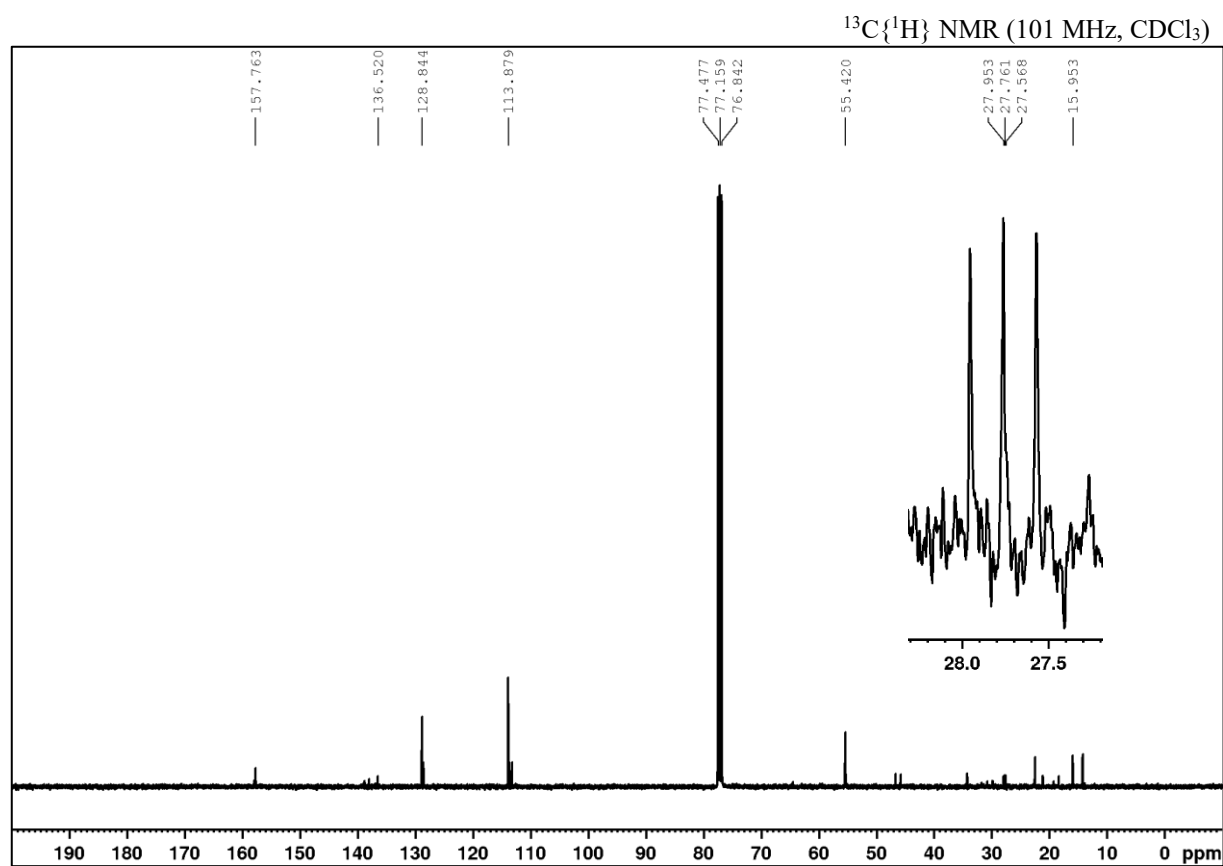
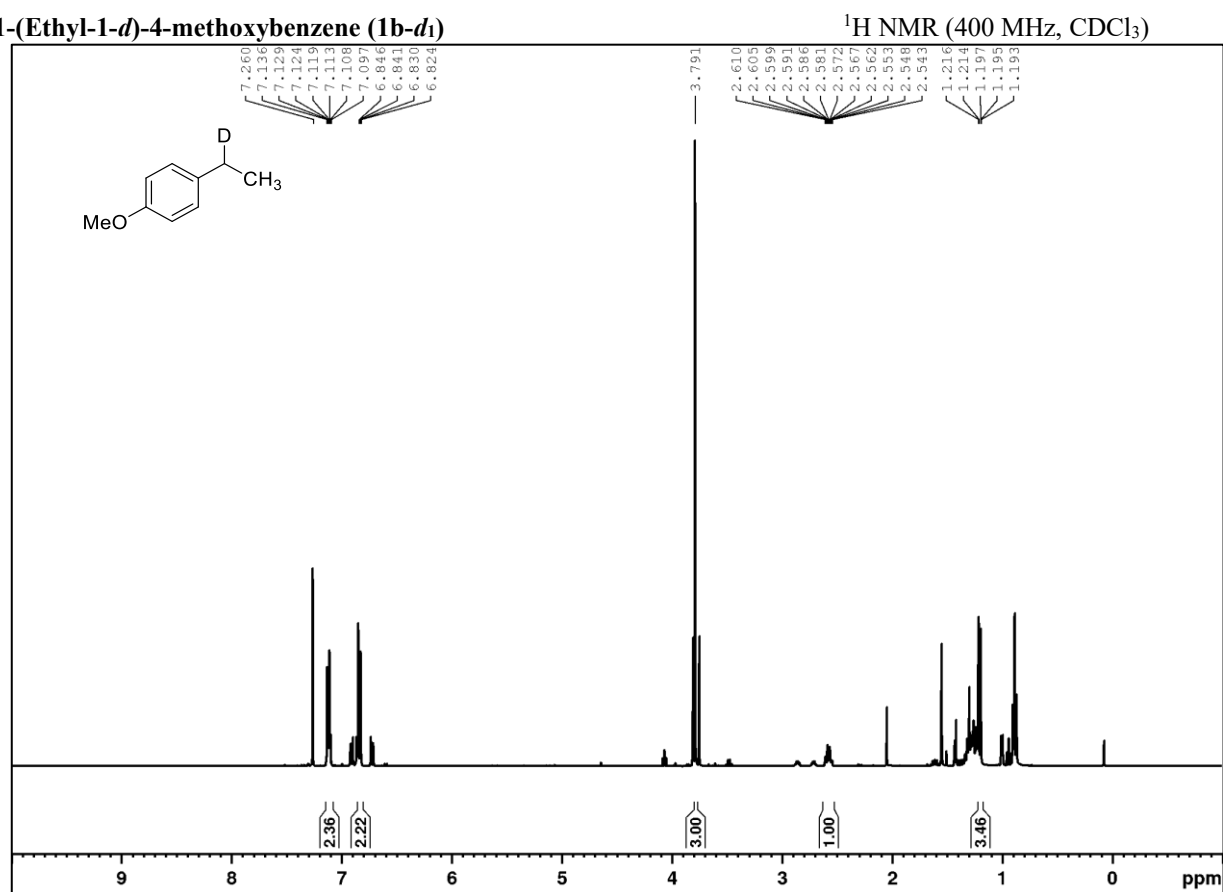
 $^1\text{H NMR}$ (400 MHz, CD_3CN)

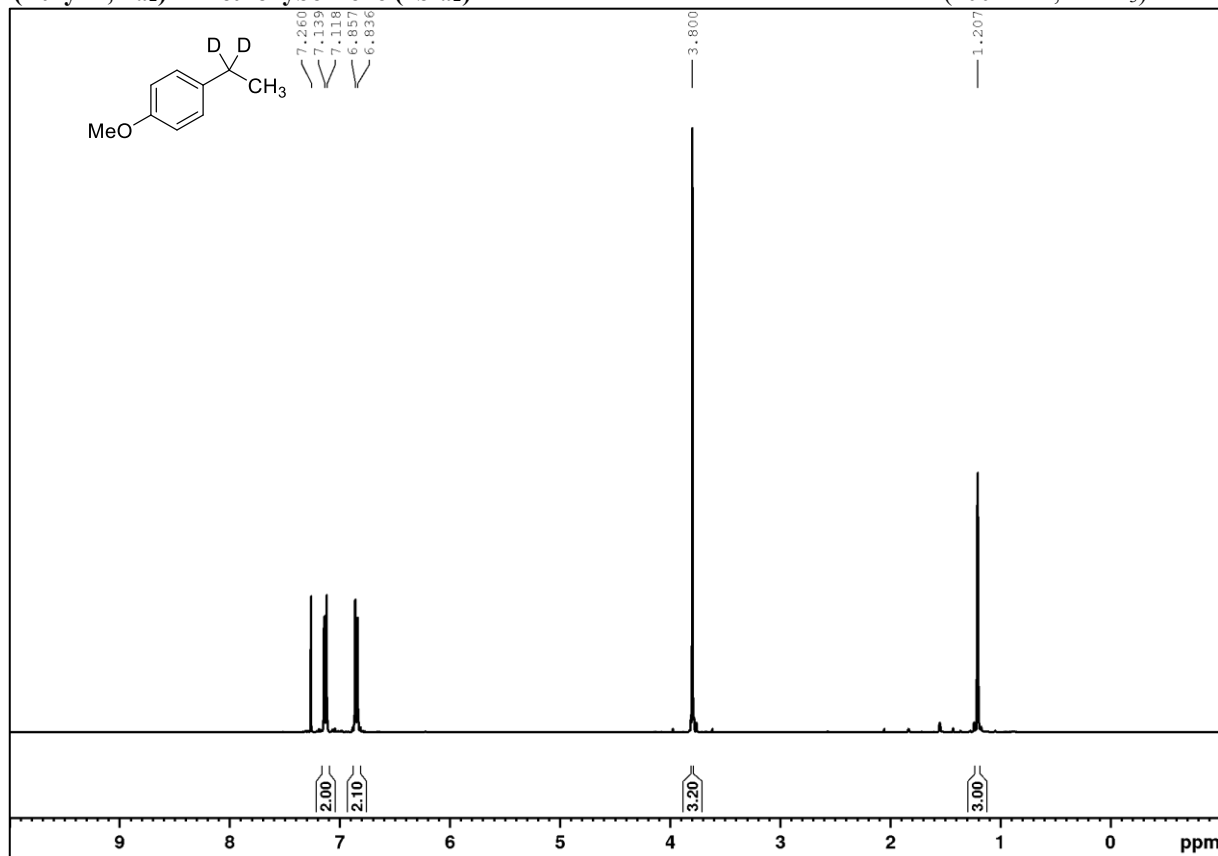
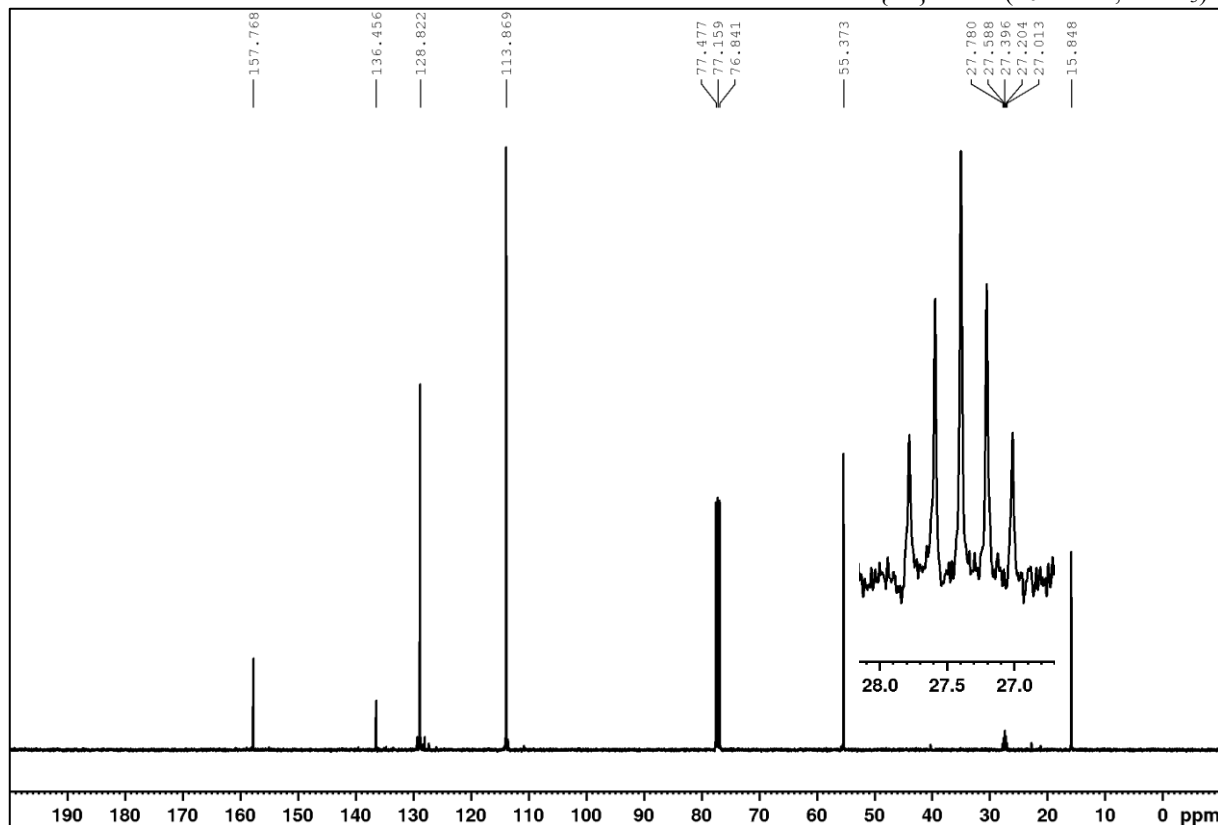
(3,5-Dimethoxy)benzyltriphenylphosphonium bromide (14b) $^1\text{H NMR}$ (400 MHz, CD_3CN)**[4-Cyanobenzyl]triphenylphosphonium bromide (14c)** $^1\text{H NMR}$ (400 MHz, CD_3CN)

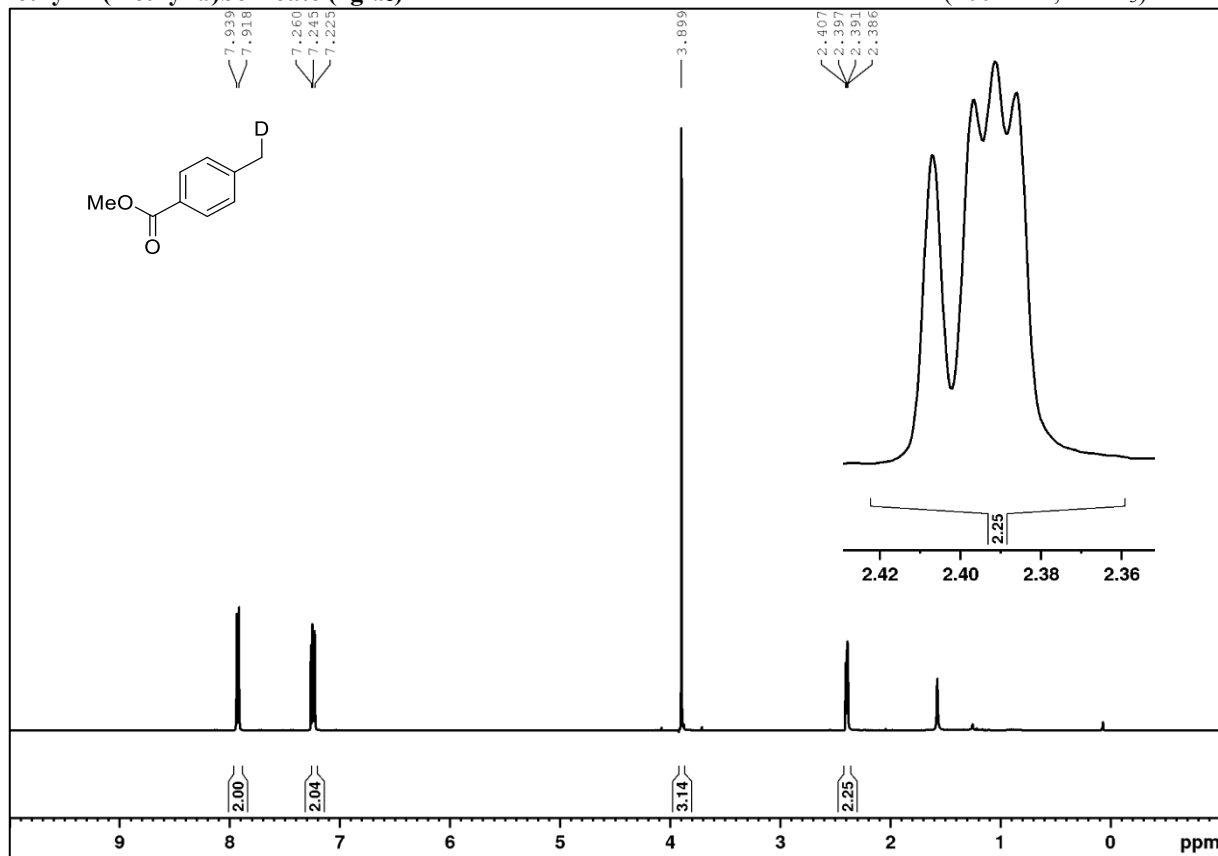
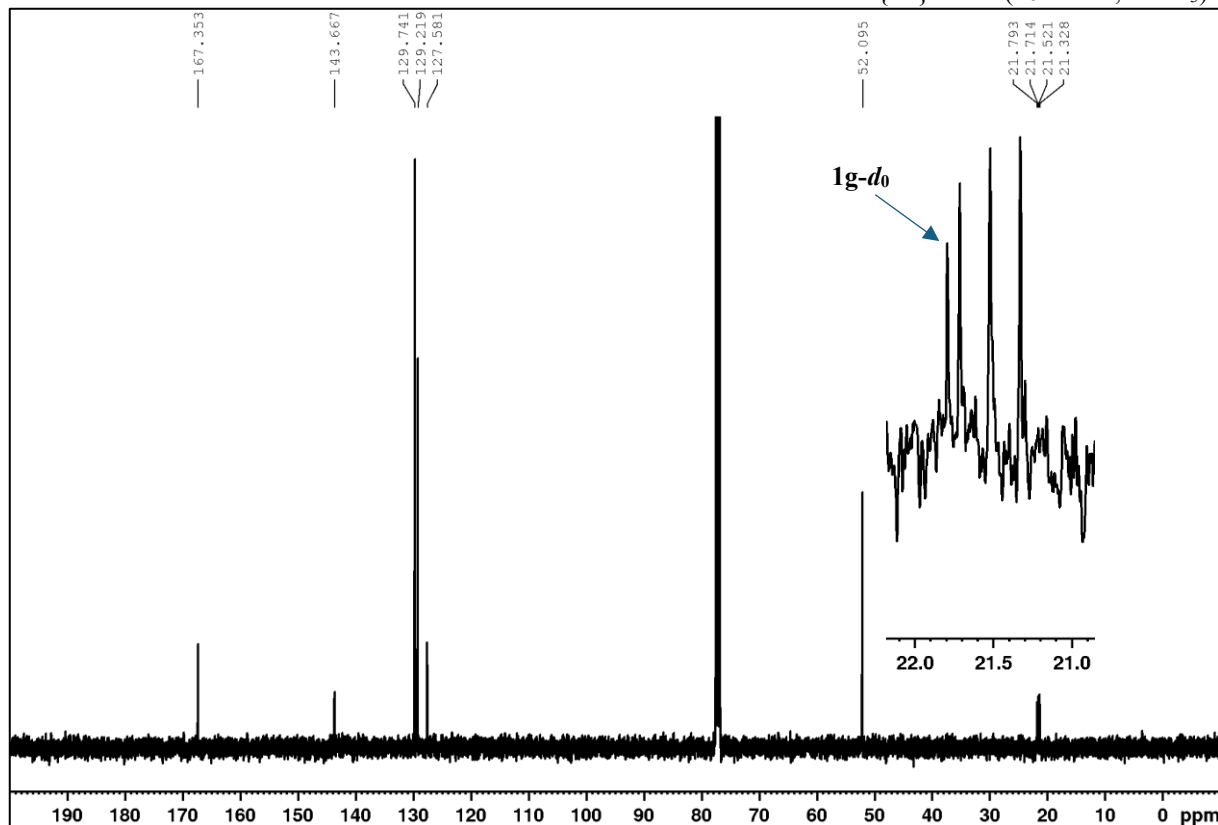
Methyl-*d*₃ 5-phenylpentanoate-2,2-*d*₂ (9a-C2-*d*₂)¹H NMR (400 MHz, CD₃OD)¹³C{¹H} NMR (101 MHz, CD₃OD)

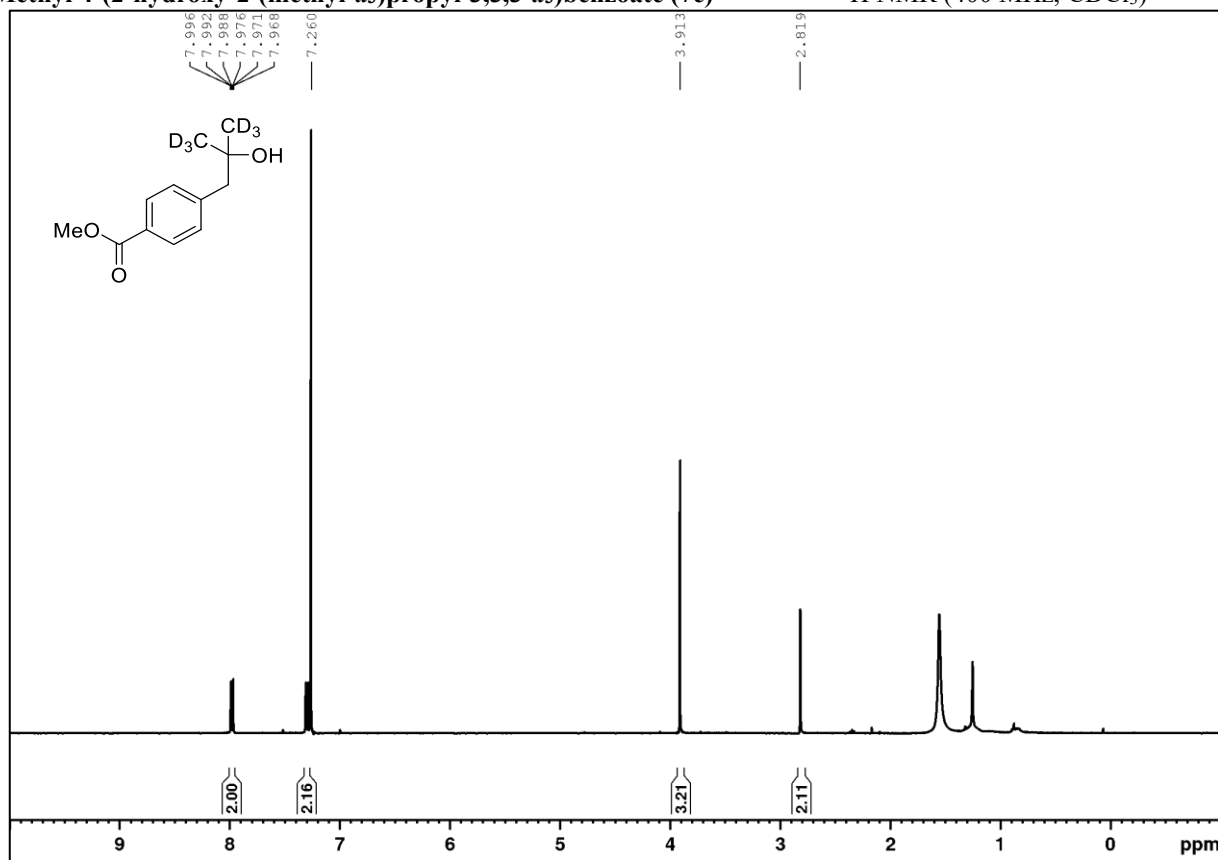
Methyl-*d*₃ 5-phenylhexanoate-2,2-*d*₂ (11-C2-*d*₂)

Methyl 5-(4-methoxyphenyl)pentanoate-5,5-*d*₂ (9f-*d*₂)¹H NMR (400 MHz, CDCl₃)¹³C{¹H} NMR (101 MHz, CDCl₃)

1-(Ethyl-1-*d*)-4-methoxybenzene (1b-*d*₁)

1-(Ethyl-1,1-*d*₂)-4-methoxybenzene (1b-*d*₂)¹H NMR (400 MHz, CDCl₃)¹³C{¹H} NMR (101 MHz, CDCl₃)

Methyl 4-(methyl-*d*)benzoate (**1g-d₁**) ^1H NMR (400 MHz, CDCl_3) $^{13}\text{C}\{^1\text{H}\}$ NMR (101 MHz, CDCl_3)

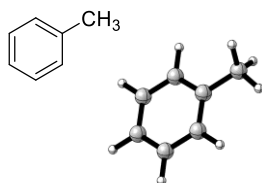
Methyl 4-(2-hydroxy-2-(methyl-*d*₃)propyl-3,3,3-*d*₃)benzoate (7c)¹H NMR (400 MHz, CDCl₃)

7.4 Appendix chapter 4

7.4.1 DFT calculations (optimized structures)

Toluene

Substrate



G: -271.38903891 Eh

H: -271.35376477 Eh

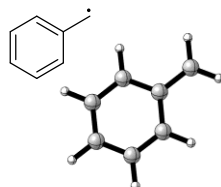
Charge: 0

Multiplicity: 1

Optimized cartesian coordinates:

C	3.38784481547119	-1.32301983790344	0.32765563708489	C	2.38305814715681	2.10917542460885	1.62228732574337
C	3.02359237360718	-0.28837550479583	1.18096150471360	H	3.35466150600551	0.37130611316951	-2.60949698147357
C	2.77343766662251	0.99600754601848	0.68732961085250	H	3.79328936102206	-1.90049284014914	-1.70869311945747
C	2.89843750132878	1.21388540287309	-0.68516001516021	H	1.48585575475855	1.84746424549715	2.19401486726823
C	3.26335612346781	0.17988408617984	-1.54396092869601	H	3.18083624692708	2.31278342522841	2.34579404795084
C	3.50933673783775	-1.09254458599621	-1.04079146405051	H	2.17923386774684	3.03451187590931	1.07721033201043
H	3.57731818602162	-2.31387333532258	0.73114733074215	H	2.70756398916160	2.20602108371251	-1.08748849410751
H	2.93041172286472	-0.47625209902995	2.24860334657928				

Benzyl radical



G: -270.75820463 Eh

H: -270.72187962 Eh

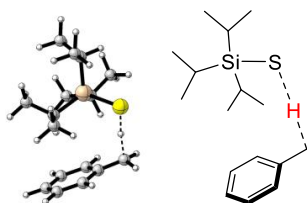
Charge: 0

Multiplicity: 2

Optimized cartesian coordinates

C	3.71310428901446	-1.31490218394319	-0.05490376270108	H	3.16573860356866	-1.08544666624680	2.00604768218542
C	3.20693983597211	-0.61847344793215	1.02537255384290	C	2.21647989968816	1.42785048959587	1.97335934503146
C	2.73247938823078	0.71462333042110	0.88014600163171	H	3.35197917441023	1.05432773173312	-2.46852479049912
C	2.80086210175170	1.29693244334582	-0.41581337016017	H	4.16830279823108	-1.27227562740349	-2.16517223878051
C	3.30949753883101	0.58923643648768	-1.48757803241513	H	2.16700400059385	0.97777050958905	2.95889357556623
C	3.76967459175946	-0.72055613021753	-1.31945609522200	H	1.85610777364212	2.44401726394142	1.85574861206009
H	4.06983924758549	-2.33229491591556	0.07942929922528	H	2.44482069672087	2.31481573654464	-0.55228895976507

HAT transition state toluene



G: -1314.28009906 Eh

H: -1314.20699697 Eh

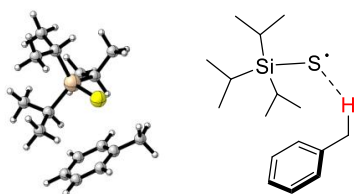
Charge: 0

Multiplicity: 2

Optimized cartesian coordinates:

C	3.71003528091204	-1.31520870242546	-0.05393963021528	C	-3.41028910901392	-1.65540615457127	0.91673391051570
C	3.16125575120387	-0.63237526465333	1.01783785658399	H	-2.95872130296487	-1.69045769531471	1.91348355315853
C	2.66584417929403	0.67957064720528	0.86233235581105	H	-4.49415974904324	-1.78770766523063	1.03033120571802
C	2.75908622333959	1.27867325447170	-0.41235403959020	H	-3.03662256730634	-2.51543327568864	0.34930841238259
C	3.31237261763523	0.59184379346421	-1.48012068803248	C	-1.92297479504327	2.79207837281302	-0.38519912685991
C	3.78376058701512	-0.71102853398669	-1.31001428294172	H	-2.04706466916386	2.89024641678331	0.69844671498492
H	4.08051080652014	-2.32686870385356	0.08370320581707	H	-1.61958667467456	3.76973055452108	-0.78187427954858
H	3.09342755402647	-1.11007710321132	1.99178789879193	H	-2.90322078906218	2.55824855115973	-0.81574295897690
C	2.02676752208954	1.35691709113606	1.96034282528548	C	-0.66780482646713	1.61537537860272	-2.25010493705043
H	3.37869218785871	1.070185911101054	-2.45308110695351	H	-1.56700866629866	1.26506261559412	-2.76987894657786
H	4.21077689894244	-1.25013009613915	-2.15021527394085	H	-0.41669235909208	2.59948189484911	-2.66844779576705
S	-0.78521602510736	0.44444291162933	2.25706342405348	H	0.15165809925828	0.93227312275343	-2.49835226981820
Si	-1.23704021315136	0.07137783600295	0.16840492606790	C	-0.65557158825312	-1.93012088954985	-1.83284772149495
C	-0.88424641365147	1.71748705467704	-0.73451951073145	H	0.10253249555697	-2.58664504529307	-2.27978308047687
H	0.07239878404849	2.03841182322882	-0.29357851554161	H	-1.54248156005688	-2.54513727240321	-1.64351865679924
H	0.66380363830374	0.89207303285453	2.01252601862576	H	-0.92545945402633	-1.17911713588000	-2.58171071561391
C	-3.10051944003661	-0.33944614703239	0.18829731017943	C	0.18271699407101	-2.43641828251480	0.48009482362920
H	-3.54336470388447	0.48083609302372	0.77485410162283	H	-0.71982060165620	-3.00487920968772	0.73149164482407
C	-0.12480952035602	-1.31826872611320	-0.52527546526204	H	0.91049354271228	-3.13992080699710	0.05397096617817
H	0.82594056123768	-0.81198290713884	-0.75733209854366	H	0.59039991790101	-2.04264620296831	1.41453054158309
C	-3.76282166513851	-0.32697639570136	-1.19877411181201	H	2.27865744858439	1.02756871700765	2.96761440616824
H	-4.84793515720047	-0.46244747738115	-1.09940302490426	H	1.83986824192659	2.42495350153489	1.85890140959937
H	-3.59897639906980	0.61260017441095	-1.73515433303304	H	2.39577119625261	2.29369582775319	-0.55032433450003
H	-3.39201627897139	-1.13962288275159	-1.83147560659465				

Reactant complex toluene



G: -1314.29079371 Eh

H: -1314.21445853 Eh

Charge: 0

Multiplicity: 2

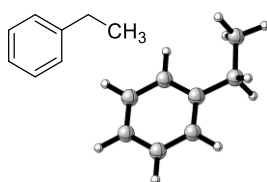
Optimized cartesian coordinates:

C	3.39092108540905	-1.32089673194552	0.32861311914585	H	3.35152702737798	0.36991039838097	-2.61139059689571
C	3.01573942239370	-0.28837287175066	1.18040120596520	H	3.80762579444574	-1.89818401218927	-1.70604480144465
C	2.76818180492921	0.99729646370877	0.68685784310065	S	-0.91413252339903	-0.14020459040103	2.34278782357870
C	2.89136114943918	1.21259491399870	-0.68727752260081	Si	-1.34866296727384	-0.11324517805652	0.23585492409179
C	3.26047169399301	0.17909030605022	-1.54553978393741	C	-0.87394675491637	1.61382551780468	-0.41507796413474
C	3.51559554907309	-1.09145865166262	-1.03994440679457	H	0.09746718991969	1.79090624459890	0.06945175322348
H	3.57953546004799	-2.31147906251955	0.73314831856528	H	1.48966758450219	1.84663243907360	2.19549084403910
H	2.91288272083897	-0.47596610268030	2.24692860509011	C	-3.21123677445260	-0.48583814835444	0.03922179759347
C	2.38729774949950	2.11011321270341	1.62361202737788	H	-3.69500804342101	0.22639489028224	0.72670310139968

C	-0.17256262022659	-1.42920649615740	-0.51837664654646	H	-1.55663362626291	1.49479420138355	-2.50228902888252
H	0.77156359830023	-0.87247852325287	-0.61847281078465	H	-0.33790778152734	2.73433974773780	-2.19656514984792
C	-3.77169408613767	-0.22222956308235	-1.36710481173211	H	0.13997125387156	1.03536792576836	-2.26641752232507
H	-4.85487510804381	-0.40080322584386	-1.38008499011399	C	-0.62389508493274	-1.87014514862619	-1.91768871740386
H	-3.60712791207446	0.80810205805049	-1.69595255751402	H	0.17314558724523	-2.46220880081607	-2.38795228743892
H	-3.32533682650650	-0.88697270373124	-2.11371897594183	H	-1.51389422590963	-2.50668571108667	-1.86636396473927
C	-3.56710191705912	-1.90082511950332	0.51422709422648	H	-0.84570776891307	-1.03175431428224	-2.58474144051656
H	-3.17140976817700	-2.10380318445368	1.51458667533192	C	0.09222597364241	-2.65450435736866	0.36345228137918
H	-4.65603986123325	-2.03460929583741	0.54654203107282	H	-0.82694836241323	-3.21478941642839	0.56569167003963
H	-3.16791989222808	-2.65920344046617	-0.16899356326746	H	0.79255608599163	-3.33255697307579	-0.14222691811508
C	-1.84740314205038	2.69018842414779	0.08430845089342	H	0.53057542293923	-2.37491395926311	1.32629310067459
H	-1.95581324752889	2.66197543382911	1.17482465389087	H	3.19019737002311	2.30417552014477	2.34408508186418
H	-1.49295405814897	3.69227035643781	-0.18938183451185	H	2.19041030763703	3.03917503256380	1.08112674076822
H	-2.84535746247341	2.56830789451058	-0.35276796134716	H	2.69681947412277	2.20385213954527	-1.09065284310097
C	-0.64910397140652	1.71549944490427	-1.92912049080723				

2a

Substrate 2a



G: -310.66138785 Eh

H: -310.62191776 Eh

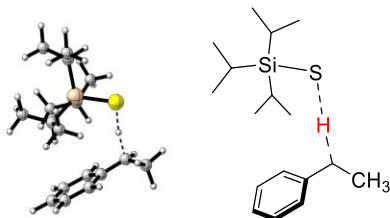
Charge: 0

Multiplicity: 1

Optimized cartesian coordinates:

C	3.54746406868165	-1.29050026529371	-0.26553538075926	H	3.09710460885453	1.20450905206139	-2.51421953468658
C	3.17842837049373	-0.61165757216360	0.89501548553773	H	3.80913332732501	-1.17509434784312	-2.39936196616907
C	2.77594890696199	0.72311335738409	0.84547092559511	H	1.29328863362768	1.76448382408941	1.96755796014730
C	2.75508880231854	1.36035991319515	-0.40072929692965	H	2.89572675726226	2.45641720309033	2.07510768118662
C	3.12078060691567	0.68743707519816	-1.55891799002333	H	2.44586359686725	2.40238428295390	-0.45821406264020
C	3.52014360623219	-0.64607994409720	-1.49589862327968	C	2.56565772684560	0.80159484452075	3.41316375383948
H	3.85882230033266	-2.32956253215633	-0.20277663599866	H	2.26832665481159	1.45990437988468	4.23488594877007
H	3.21014138314032	-1.13557353546177	1.84518681857874	H	1.96840906691923	-0.11288265009772	3.49072749693477
C	2.35499204833855	1.50043568619910	2.07425102655896	H	3.61692353407155	0.53305422853649	3.56280539333764

HAT transition state 2a



G: -1353.55808959 Eh

H: -1353.48162363 Eh

Charge: 0

Multiplicity: 2

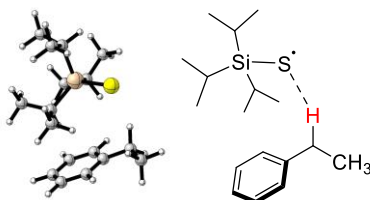
Optimized cartesian coordinates:

C	3.70440007517578	-1.29576733481958	-0.18769152985394	C	3.28307273066335	0.71307337183357	-1.45197523859644
C	3.17942935305140	-0.69847670310383	0.94798371811833	C	3.75317929221829	-0.59940207450700	-1.39463714633367
C	2.68583481074008	0.61972715223671	0.90597343002510	H	4.07502777342400	-2.31547555127297	-0.13546798396881
C	2.75826167484397	1.31360342989474	-0.31937331838020	H	3.13817619671437	-1.25988219086863	1.87549837627392

APPENDIX

C	2.0655500570352	1.25230789310711	2.05938333379291	H	-2.03772168991614	2.93834948030423	0.59005266922514
H	3.32929706863303	1.26756819431300	-2.38488511109753	H	-1.61258687088754	3.76605725427072	-0.92039601456094
H	4.15993928070679	-1.07337617710891	-2.28289136502844	H	-2.90252148163578	2.56077567759982	-0.90852814208141
S	-0.79407431686401	0.53599646109538	2.22726284441011	C	-0.67843875876941	1.55773457317295	-2.32007387216965
Si	-1.24208548380988	0.10055361119753	0.15233982872868	H	-1.58078380358186	1.19202635588737	-2.82370968174988
C	-0.88750053357966	1.71266286928240	-0.80800593812055	H	-0.42622404331531	2.52611745094510	-2.77300038744008
H	0.07306063080453	2.04229302107188	-0.38207029341621	H	0.13834165241255	0.86454944578338	-2.54822912289817
H	0.71192612041584	0.90123072703816	1.99447843812479	C	-0.65746054021889	-1.97269709387429	-1.77630695376079
C	-3.10606685456526	-0.31097639722376	0.18223476445367	H	0.10168015029645	-2.64519893467515	-2.19705152957514
H	-3.55034538116915	0.52312527526933	0.74789616966743	H	-1.54479326970247	-2.58038188859336	-1.56621281130089
C	-0.12833678793385	-1.31116283526533	-0.49242516088931	H	-0.92570143423415	-1.25032245300319	-2.55328526060912
H	0.82045890948869	-0.81057252039431	-0.74452811636775	C	0.18189615755505	-2.39001233725367	0.55384216613581
C	-3.76738375880939	-0.33335609519890	-1.20533994854675	H	-0.71928735713726	-2.95165276028092	0.82474131315307
H	-4.85141674086773	-0.47619732945931	-1.10401805791202	H	0.91383241415797	-3.10619102843097	0.15692151104197
H	-3.61105120315344	0.59665148597607	-1.76009602713211	H	0.58484403813892	-1.95989292888011	1.47447569185753
H	-3.38874024903583	-1.15540496444837	-1.82118248429812	H	1.93267275992408	2.33195516356796	1.95033094235748
C	-3.41497638961158	-1.60841443559240	0.94335744508773	H	2.39813452837522	2.33820822351108	-0.36759471334611
H	-2.96267336713367	-1.61779069624341	1.94030427444350	C	2.38548094852426	0.79647696960237	3.45892247519597
H	-4.49878305376313	-1.73828518311631	1.06062123283952	H	1.78300417138416	1.34627495099888	4.18663698065793
H	-3.04137201406245	-2.48235399318880	0.39752605612999	H	2.17927423696867	-0.26869229045936	3.59992704376869
C	-1.91909904160666	2.80359092457896	-0.49026059895735	H	3.44531398004354	0.96990458472415	3.68704053290204

Reactant complex 2a



G: -1353.56272452 Eh

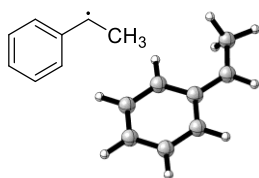
H: -1353.48364268 Eh

Charge: 0

Multiplicity: 2

Optimized cartesian coordinates:

C	3.54782882640275	-1.28995581318780	-0.26473883553245	H	-3.31221523507874	-1.75218707324821	1.76208603948014
C	3.19213953308648	-0.60633360734624	0.89662159328581	H	-4.67744987448170	-1.90726373441963	0.63790745458765
C	2.78923751329521	0.72889090124901	0.84760248724780	H	-3.09809342971663	-2.56648613206400	0.20695648819507
C	2.76872327259452	1.36513122317148	-0.40017845494057	C	-1.97641703966443	2.77966076741376	-0.38452236826722
C	3.12015854894952	0.68716203281729	-1.56034681052919	H	-2.17942831479624	2.88812209850337	0.68618971466219
C	3.50783624373025	-0.65031400772237	-1.49790273927677	H	-1.62591102606708	3.74917890691315	-0.76112602042843
H	3.85501101761878	-2.33022257036555	-0.20133874007707	H	-2.92588023658596	2.56124951796592	-0.88697408901408
H	3.22518938578195	-1.12845240226371	1.84746062167046	C	-0.60977957670071	1.55886350779609	-2.14497561324581
C	2.35786658011461	1.49907259625993	2.07473515921264	H	-1.47676005099069	1.22816469200168	-2.72776015944065
H	3.09371524668644	1.20343318522252	-2.51607332189946	H	-0.30043508920869	2.53202941004259	-2.54922553299699
H	3.78298926730387	-1.18408561045775	-2.40291175738879	H	0.20893379351265	0.85466871767007	-2.32356254880373
S	-1.20198771942364	0.40670974747760	2.33506381565750	C	-0.56937060513538	-2.00517247479238	-1.65398097817636
Si	-1.36999427170204	0.04602492266063	0.22401003815095	H	0.24751790810008	-2.64914393364395	-2.00471744594034
C	-0.93413919551027	1.68714704818027	-0.65006134054833	H	-1.45065231011668	-2.64241857207822	-1.52017083016826
H	-0.00209060188623	1.98657077399018	-0.14468619600804	H	-0.79097001645180	-1.29107623300185	-2.45317522982182
H	1.28901340629544	1.74617760123846	1.96789217526198	C	0.11532717003956	-2.38814509888683	0.73685985635299
C	-3.23894485389754	-0.39208309505283	0.04243165424390	H	-0.78754321755665	-2.95452980550329	0.99286371605177
H	-3.76293287864701	0.41176925617200	0.57924011661202	H	0.86474905709285	-3.10170437927060	0.36970462266666
C	-0.16835276711370	-1.32821581134812	-0.33378349094453	H	0.49210548235195	-1.94147552506809	1.66078434924807
H	0.77083296832915	-0.78211765574446	-0.51445710200845	H	2.88006743152330	2.46538633030926	2.07712654800541
C	-3.70805276526888	-0.36426619575245	-1.41949954663779	H	2.47081790999675	2.41060547404522	-0.45880297559352
H	-4.78976631573203	-0.55056733522828	-1.46009197079375	C	2.56463445198531	0.79936927980168	3.41305783400588
H	-3.52507807360332	0.60006300286200	-1.90138418664398	H	2.24871600435859	1.45264350851268	4.23153090134127
H	-3.22144388986764	-1.13892351772630	-2.01953107716544	H	1.97096084052294	-0.11817047932465	3.48187747190667
C	-3.59638650534253	-1.72804610372358	0.70595218259279	H	3.61733893930073	0.54200611333607	3.57290789731474

Radical 2a

G: -310.03723847 Eh

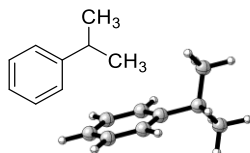
H: -309.99676631 Eh

Charge: 0

Multiplicity: 2

Optimized cartesian coordinates:

C	3.77723687743787	-1.26354677638206	-0.16940657175165	H	3.18172689466087	1.19872601329512	-2.43557371823930
C	3.33242381108650	-0.63212714111580	0.97849053301379	H	4.07905051347871	-1.11679055822025	-2.30164849164973
C	2.81492218510958	0.69013232514793	0.92981826708766	H	1.97156913079800	2.37398220091275	1.95242519965029
C	2.77586872567426	1.32878093567465	-0.33925691443188	H	2.38384267787160	2.34102087296181	-0.40205313338036
C	3.22308314553367	0.68744082422714	-1.47778195501847	C	2.35356763253227	0.77505967302327	3.45086567231282
C	3.72814408179146	-0.61467423952793	-1.40534843145629	H	1.94361067267133	1.47433820111618	4.18282725659867
H	4.16887914279067	-2.27525663829901	-0.10741580553206	H	1.75747367891298	-0.14690194588706	3.50035159379401
H	3.37877517463591	-1.15349906351928	1.92979475194795	H	3.36773862713870	0.50625272540644	3.77826171382899
C	2.35165247787560	1.36353259118610	2.08116053322555				

2b**Substrate 2b**

G: -349.93794805 Eh

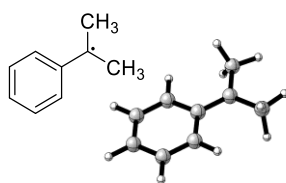
H: -349.89549105 Eh

Charge: 0

Multiplicity: 1

Optimized cartesian coordinates:

C	4.10448601204513	-0.89282278220611	-0.28116416107275	H	1.69741088229874	2.41512756929135	1.69468502729115
C	3.80157079992375	-0.12308438468997	0.83605648889947	H	1.40465289458069	1.85809944869722	-0.50065658452075
C	2.82620135908205	0.87730563503864	0.77619239326912	C	1.95865751898505	0.85751159823657	3.14355589406344
C	2.16583693513961	1.08358864238810	-0.43569875517411	H	1.65657783422128	1.48655955024173	3.98824179322685
C	2.46591357289632	0.31559390915725	-1.55794067905880	H	1.09399891134607	0.26704821601645	2.82475303031849
C	3.43707744662920	-0.67659541838882	-1.48434601569478	H	2.72611757393346	0.16276839607793	3.50243388918629
H	4.86496824479651	-1.66591646581350	-0.21338546162190	C	3.70032605323939	2.55163361509519	2.44452459891869
H	4.33260378004349	-0.30563260765781	1.76711648261035	H	4.08083171541699	3.17043868765328	1.62585311466804
C	2.49377173492558	1.71869083294193	1.99201831816413	H	3.42541124049836	3.20875586638112	3.27707583577793
H	1.93860938270362	0.49404881249094	-2.49098092917997	H	4.51758930883978	1.90578052303123	2.78491790117408
H	3.67343149845487	-1.27818701398274	-2.35719671124498				

Radical 2b

G: -349.31376769 Eh

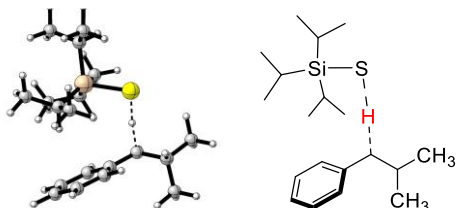
H: -349.27135215 Eh

Charge: 0

Multiplicity: 2

Optimized cartesian coordinates:

C	3.77230389149377	-1.26167714340567	-0.14284914386730	H	4.09683082440555	-1.16641702699108	-2.27613657917232
C	3.31784125984625	-0.60065911667605	0.98407726345405	H	2.39851016993927	2.33658851610010	-0.48907963169409
C	2.80394699001066	0.72250618326905	0.90873937717233	C	2.37126599412513	0.74680782578090	3.40920466071484
C	2.78140936202204	1.32751369896113	-0.37702834992476	H	1.97042202296515	1.40290201312326	4.18501919106906
C	3.23890636324167	0.65570808022000	-1.49653534270838	H	1.78491257489308	-0.18234712922082	3.42521650347486
C	3.73887305497345	-0.64377672975195	-1.39446380283067	H	3.39393998010382	0.47227399144088	3.70324883908840
H	4.15933391783965	-2.27281903689593	-0.04976171041139	C	1.80037961090898	2.80423443318540	1.95723050189662
H	3.35668104354165	-1.10679482847331	1.94304446986592	H	2.54929436642138	3.49978343811363	1.55386622840697
C	2.33479309680952	1.40868393619122	2.06534407064296	H	0.93235867648688	2.86022942700319	1.28567982437519
H	3.20735425743786	1.14781159893180	-2.46492469773165	H	1.48769624253423	3.18555131909426	2.93174640817935

2c**HAT transition state 2c**

G: -1432.10773530 Eh

H: -1432.02617819 Eh

Charge: 0

Multiplicity: 2

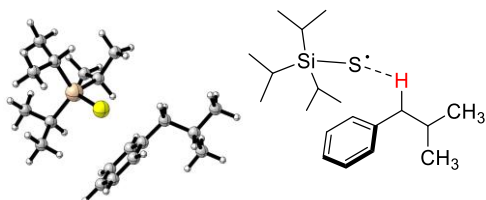
Optimized cartesian coordinates:

C	3.58633812423323	-1.48259060841991	0.01442955573347	H	-4.85614005282533	-0.36678950183166	-1.09900177550707
C	3.04645509608613	-0.78823559038129	1.08546624831933	H	-3.57709683629975	0.69998049714964	-1.68727366235264
C	2.63743135077569	0.55192548725323	0.94404557035395	H	-3.43046826218190	-1.05025095548508	-1.88280812463206
C	2.79371884573540	1.16015892990479	-0.31720537680668	C	-3.43902239218478	-1.71947234994756	0.82931753849442
C	3.33509945347555	0.46280910065048	-1.38604093896647	H	-2.98478423297149	-1.82360693794665	1.82022549437524
C	3.73086913408092	-0.86496807517940	-1.22771717483946	H	-4.52578119520950	-1.82701071627420	0.94212596816102
H	3.88775645759276	-2.51817516676244	0.14320853225704	H	-3.09251328098914	-2.55684070968499	0.21293579985474
H	2.92168138409594	-1.28955495170556	2.04058711376821	C	-1.84257730317477	2.74963175585686	-0.19198568003042
C	2.01825577297325	1.28490875953751	2.03722397776529	H	-1.95676455080399	2.77277500676755	0.89697872469782
H	3.45063070952300	0.95421069101206	-2.34787457131690	H	-1.51877378442886	3.74563292298914	-0.52120727933945
H	4.14906907071645	-1.41439037046240	-2.06581047374631	H	-2.83122075265496	2.56950716097641	-0.62923043511422
S	-0.73144659310585	0.18468607251543	2.26335409899094	C	-0.63527149279469	1.67530265613733	-2.14783805043937
Si	-1.21809806218099	-0.01998154426071	0.16104691856783	H	-1.54761062033540	1.38103737225494	-2.67934734690963
C	-0.83256901592884	1.67875416794819	-0.62628072339588	H	-0.36607082325280	2.67982486352896	-2.50135270514133
H	0.13626634745027	1.94732274133491	-0.17916984323503	H	0.16553707662860	0.99233371787441	-2.45123290475917
H	0.68600934764738	0.78371605373178	2.04913728282092	C	-0.71288408130848	-1.87933873996898	-1.99650300927446
C	-3.09407328448729	-0.37413554342733	0.17402087334558	H	0.02334228873396	-2.52132329034257	-2.49792030020656
H	-3.50504815321337	0.42391442897345	0.81190700534651	H	-1.61628248523815	-2.48176449046631	-1.84924605046662
C	-0.15923265479865	-1.38833966635554	-0.64786081987328	H	-0.96407437657739	-1.06565671984901	-2.68374365926638
H	0.80852846112193	-0.89797597144376	-0.84185307092762	C	0.11131497175751	-2.59330648008595	0.26376881612943
C	-3.76791691396591	-0.26220880643826	-1.20234927164382	H	-0.80795889617599	-3.15570060456232	0.46279177179457

APPENDIX

H	0.82100971002595	-3.27975113362383	-0.21718958931558	H	4.21630151849065	1.14789437899614	4.69990570941979
H	0.52571231241535	-2.29044688230716	1.22875222803912	H	4.52984112316191	0.67702631808405	3.01469686371620
H	1.81668032143993	2.33689582342603	1.80818288048089	H	4.15066528272009	2.36214931860312	3.40978516374194
H	2.49176628561076	2.19666687929863	-0.44584358618401	C	1.59809770093604	1.91416853976217	4.43059192774445
C	2.41954359530895	1.04187093020843	3.47958176590414	H	0.52527165591066	1.72998658323198	4.32307569485692
H	2.23036257494856	-0.01218189085841	3.72923778924804	H	1.87650875408616	1.71632301643266	5.47051746199288
C	3.92214034780830	1.31933108768163	3.65862531303458	H	1.78407302159697	2.97639173622935	4.23016833473514

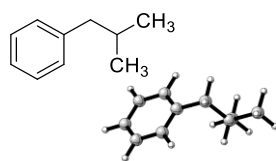
Reactant complex 2c



G: -1432.11465988 Eh
H: -1432.03055130 Eh
Charge: 0
Multiplicity: 2

Optimized cartesian coordinates:

C	2.76463955817292	-1.90023500804874	1.16720472406513	C	-1.56652964569690	2.19690462516045	0.68845315738021
C	2.34426838119815	-0.83197842025459	1.95824534799479	H	-1.60614360062704	1.80656597848336	1.71119331902641
C	2.43343232425273	0.48759940296355	1.49287983053384	H	-1.12947536393766	3.20327559520468	0.72932131605079
C	2.95690063302755	0.70415675798558	0.21763239680058	H	-2.59663687933736	2.30564456328081	0.32942870195662
C	3.37942088186117	-0.36096305354851	-0.57408631521854	C	-0.65704319106761	1.844444454444041	-1.65465860101354
C	3.28235825054150	-1.66770731892201	-0.10206458251284	H	-1.63110230686692	1.85203302095004	-2.15671417782393
H	2.67945395256171	-2.91468350733250	1.54589392383421	H	-0.29628746825285	2.88149286734878	-1.63342958539169
H	1.96570323870278	-1.01902732520369	2.95964056791314	H	0.03740615802541	1.26997509018090	-2.27660902257409
C	1.99116911175886	1.62809078470176	2.36810297104521	C	-1.01787274550405	-1.53835123619605	-2.77921099088079
H	3.78207610469826	-0.169744845819591	-1.56509985193760	H	-0.36812324074897	-2.01264105753091	-3.52624934568421
H	3.60359740141587	-2.49913993137196	-0.72257275182705	H	-1.96565465720401	-2.08822332176992	-2.78291557487448
S	-0.75138571260879	-1.19257742670522	1.90327371585708	H	-1.22308857962891	-0.51885609447634	-3.12012105999291
Si	-1.26968402001327	-0.54207980621230	-0.08043057142059	C	-0.12375771446034	-3.05137366474242	-0.97935924113137
C	-0.74153207667216	1.28516540917678	-0.22788928578247	H	-1.06893522428924	-3.59504089290252	-0.87035251183398
H	0.28476750383558	1.26349560667168	0.16713382107706	H	0.46886972707278	-3.56954901259530	-1.74526942551422
H	1.00370006378927	1.39228143883844	2.78711633604112	H	0.40594211620273	-3.12152031267788	-0.02638249159852
C	-3.18312342943522	-0.73332930390174	-0.08471398949540	H	1.87315255557234	2.53634112614670	1.76042905947870
H	-3.50549716362345	-0.23491337148435	0.84165559665479	H	3.03227388646805	1.72162058139275	-0.16017828462181
C	-0.35913683665965	-1.59255339739167	-1.39086039222552	C	2.96671214554991	1.93445335790991	3.52352684776033
H	0.62905413148771	-1.10899595014237	-1.46358233835934	H	3.07259691302139	1.01710660988701	4.12214165901971
C	-3.85843280900580	-0.00958944884274	-1.25973718083944	C	4.34716512158262	2.32719831109847	2.99811538420847
H	-4.94969129773533	-0.09039384225094	-1.16536254095750	H	5.03365761092911	2.54249529598143	3.82379064740587
H	-3.61190305733259	1.05531011623484	-1.29406819784070	H	4.78705778735756	1.53175833024776	2.38812396777423
H	-3.58231276966731	-0.45003091682161	-2.22281293908488	H	4.27739050869807	3.22886069262080	2.37601134776042
C	-3.63502676510991	-2.19833421816597	-0.01765952551905	C	2.38734977800712	3.03073550384040	4.41784365885934
H	-3.18291135942604	-2.72986167821700	0.82503743975553	H	1.40684368295318	2.74651182357246	4.81481022845630
H	-4.72640554262889	-2.25616431350486	0.08719851046261	H	3.04997857259081	3.23943451808474	5.26447637237655
H	-3.37026237843315	-2.73812878884662	-0.93389519005575	H	2.26440129541394	3.96296928378004	3.85263460016725

Substrate 2c

G: -389.21353649 Eh

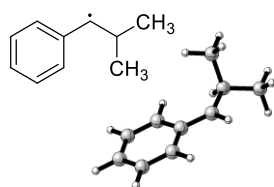
H: -389.16834094 Eh

Charge: 0

Multiplicity: 1

Optimized cartesian coordinates:

C	2.76012690902100	-1.89888351809006	1.16807295922618	H	1.85025055895614	2.52825654639235	1.76749795664988
C	2.32228199984229	-0.83782990210042	1.95262765278375	H	3.03892772280909	1.72581067441742	-0.13979354217946
C	2.41682703996543	0.48034148341347	1.49681364828535	C	2.96684239298122	1.93322888377819	3.51886226072408
C	2.95891116055414	0.70607562125211	0.23029420481445	H	3.08131811052305	1.01662471903110	4.11732118937694
C	3.39833981876520	-0.35285246346266	-0.55952159911986	C	4.34121137282794	2.32448243947491	2.97639924363675
C	3.30137358933535	-1.65957642578183	-0.09261293697408	H	5.03731251089419	2.54081629769030	3.79378029846898
H	2.67431348689530	-2.91661617586620	1.53867542776915	H	4.77242523764112	1.52751707192265	2.36262475136068
H	1.89482282464248	-1.03325689987000	2.93408617806437	H	4.26456552769706	3.22503452391142	2.35345842925488
C	1.97830792592652	1.62195507887828	2.37524472378766	C	2.40092217017378	3.03216484627684	4.41884818108814
H	3.81534430031906	-0.15599872152808	-1.54331018453978	H	1.42563989499516	2.75085292353029	4.83121645098273
H	3.64134243196354	-2.48742704188380	-0.70801597250939	H	3.07536755461793	3.24223297215966	5.25580208567133
H	0.99747844538879	1.39173215544711	2.81269622417062	H	2.27104801326422	3.96344691100694	3.85355036920665

Radical 2c

G: -388.58510972 Eh

H: -388.53921505 Eh

Charge: 0

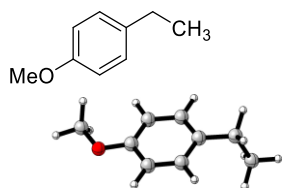
Multiplicity: 2

Optimized cartesian coordinates:

C	3.62865570333547	-1.45190628333155	-0.01946617960679	H	2.38959924761745	2.17476268553028	-0.55445914413606
C	3.28361889685867	-0.68471354497953	1.07836139145029	C	2.53746801429095	1.09133300930778	3.45495692457873
C	2.82320917914247	0.65176224854963	0.92155562410646	H	2.29032914792913	0.02465438935758	3.55717376352077
C	2.73775447769086	1.15540817245337	-0.40641582308974	C	3.96554357393661	1.29617787861310	3.99742028966679
C	3.08355035575547	0.37816829446347	-1.49384705509340	H	4.02891260585224	0.98713051865554	5.04724202669544
C	3.53303395434221	-0.93380847521096	-1.31322738681183	H	4.69580226258202	0.72045867343520	3.42045797214622
H	3.97870939635146	-2.46998037449612	0.12837930412585	H	4.24711690194351	2.35342402608207	3.93498611749983
H	3.36923688078682	-1.11075332722512	2.07310575266162	C	1.52861243585344	1.89151333398660	4.28469956340927
C	2.46190005736109	1.47369935934740	2.00994333387035	H	0.50651827693831	1.73429365670550	3.92562030376388
H	3.00600297587649	0.78993989154039	-2.49632687773854	H	1.57070397767381	1.59940395676902	5.33922956948689
H	3.80505902471418	-1.54334653909909	-2.16934124915309	H	1.74817348821252	2.96434229436501	4.22477240820216
H	2.14915970495479	2.49320183518043	1.78396285044487				

2e

Substrate 2e



G: -425.13871708 Eh

H: -425.09334334 Eh

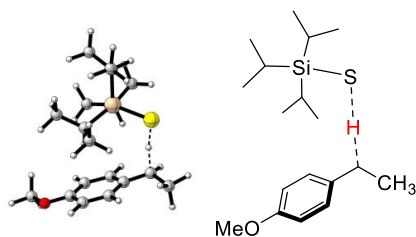
Charge: 0

Multiplicity: 1

Optimized cartesian coordinates:

C	3.20965683830274	-1.53290730214255	-0.33538506483382	H	1.40284338521858	1.91509396754573	2.01520519496326
C	2.67088831499158	-0.99092013610526	0.81924066865247	H	2.62682583709910	2.27131612606039	-0.06265933660382
C	2.44926474189281	0.38548758569590	0.94676920318485	C	3.01596929816922	1.20370490044653	3.26742075508549
C	2.79037566413627	1.19775365402086	-0.13059238555016	H	2.60731040790552	1.62330766815867	4.19296854806623
C	3.33495263486661	0.67517819125164	-1.30378817229929	H	3.52559628973910	0.26592491329360	3.51255765159468
C	3.54649809659955	-0.69954286281326	-1.40625858407283	H	3.76893427598697	1.89697435200721	2.87809588442638
H	3.37427265355400	-2.60145134751708	-0.43360727729432	O	4.06807229991170	-1.32660489448200	-2.50256057888975
H	2.41031031423609	-1.65284633369655	1.64270380271954	C	4.42245447603662	-0.51478742413527	-3.61501891098509
C	1.91129895513052	0.96711426436571	2.22905985909257	H	5.19802990892778	0.21617473366696	-3.34786305101329
H	3.57974093628775	1.34575301688257	-2.11938461441074	H	4.81502793947364	-1.19726507309972	-4.37083905050952
H	1.15494226378844	0.29235961820822	2.64950080619616	H	3.54878946774524	0.01323638238770	-4.02143334751900

HAT transition state 2e



G: -1468.03575054 Eh

H: -1467.95420525 Eh

Charge: 0

Multiplicity: 2

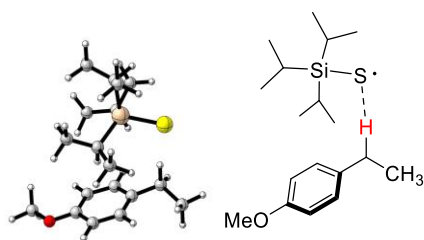
Optimized cartesian coordinates:

C	3.68424142566162	-1.33235557259861	-0.09406546132908	H	-3.56316496824312	0.53810867250095	0.69371818466712
C	3.16458773032282	-0.72606545361370	1.02924682337702	C	-0.11411590249484	-1.30218737905058	-0.45663503553750
C	2.67605176674937	0.59847063569015	0.99038735756423	H	0.84190009585964	-0.80162361159397	-0.67950397704869
C	2.76175172855968	1.27977017606392	-0.23830228389559	C	-3.72869468567655	-0.31478032258210	-1.26624995002326
C	3.27789056928942	0.68230037342903	-1.37750077821326	H	-4.81509720608313	-0.45839200204945	-1.19532136929483
C	3.73463883747722	-0.63935074084358	-1.31185862289361	H	-3.55755361391003	0.61678946857674	-1.81415602688414
H	4.05239483420628	-2.35303969741589	-0.06268902878362	H	-3.33279410873197	-1.13500701203978	-1.87362081050120
H	3.12100610025679	-1.28884679164453	1.95581399609702	C	-3.43850127884955	-1.59355551777707	0.88915625176611
C	2.04282645970118	1.22895021380218	2.13163004807969	H	-3.01164013512525	-1.60530710326405	1.89720110316124
H	3.32163793341793	1.24795049469394	-2.30093946380659	H	-4.52541847397837	-1.72041176802445	0.97845600292909
S	-0.83978334426254	0.54268020062885	2.24728530651766	H	-3.05365584420484	-2.46789708997971	0.35162175851294
Si	-1.24014647539191	0.11090249850103	0.16678409382880	C	-1.89293278836324	2.81559072088755	-0.49862416858376
C	-0.85581059949668	1.72191810500576	-0.78757473238734	H	-2.03955669899237	2.95011195882687	0.57829999686882
H	0.09253142117540	2.05003480123627	-0.33409074867061	H	-1.57295406644744	3.77760645939820	-0.92015635666203
H	0.67816668537680	0.89351323951240	2.04538766403057	H	-2.86567232377721	2.57518804761768	-0.94255666648230
C	-3.10540224234511	-0.29587227279312	0.13865271970941	C	-0.60496807904503	1.56704077820171	-2.29309696368411

APPENDIX

H	-1.49336473218238	1.20208754330305	-2.82148597402825	H	1.92276059578468	2.31062222508536	2.02782289132007
H	-0.33869263475424	2.53484125334677	-2.73983144590196	H	2.41163277046249	2.30722047677344	-0.29672590160187
H	0.21667137164044	0.87160882357669	-2.49695460193208	C	2.33040706065846	0.75986288671737	3.53453486208236
C	-0.60811290025114	-1.95938088668125	-1.75638466257102	H	1.71709215665953	1.30921947208525	4.25367380671851
H	0.16137169927137	-2.63181105564906	-2.15863589142656	H	2.10863975565914	-0.30399350681122	3.66331673831429
H	-1.50117838623975	-2.56669922028463	-1.57101061870643	H	3.38646099391557	0.91954085996893	3.78929263447055
H	-0.85681494485370	-1.23471882012019	-2.53787137992579	O	4.24612080849124	-1.33258453693833	-2.36188705379969
C	0.16578256170904	-2.38499314007999	0.59403912030590	C	4.28008246054822	-0.68553134408800	-3.63229638420397
H	-0.74384107534918	-2.94525672207024	0.83830641584800	H	4.92433182303337	0.20309607576125	-3.61022064338667
H	0.90752229377991	-3.10127397228736	0.21582583568587	H	4.69602506010685	-1.41689737320908	-4.32659823140661
H	0.54315520988255	-1.95744100687023	1.52671396901747	H	3.27115896939258	-0.40253917083117	-3.96013504730030

Reactant complex 2e



G: -1468.03864815 Eh

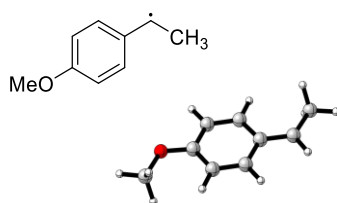
H: -1467.95455259 Eh

Charge: 0

Multiplicity: 2

Optimized cartesian coordinates:

C	3.67556997031381	-1.33302820296820	-0.20272749024836	C	-1.95841797713756	2.81253247096030	-0.46755153414188
C	3.19812771203766	-0.72969122484679	0.94659217523806	H	-2.22363151456449	2.94276001994429	0.58689914100877
C	2.73604811978151	0.59440103383602	0.93966939497045	H	-1.58716141708293	3.77456914341888	-0.84402326886003
C	2.80186083467033	1.29302076417486	-0.26789410992421	H	-2.87660493775846	2.58117965741879	-1.01997570042718
C	3.27462630373301	0.70575951146296	-1.43725654112858	C	-0.49771042867410	1.55238808218535	-2.11818741392975
C	3.70522189798297	-0.62295186792246	-1.40824668221755	H	-1.33372057756086	1.20862330850319	-2.73776387077538
H	4.02518157805878	-2.36073807863186	-0.19510875331352	H	-0.16509928807523	2.51506786631371	-2.52995697560988
H	3.16864760767901	-1.30843114260328	1.86440304621048	H	0.32687877226465	0.84159420946502	-2.23707985982777
C	2.10281200098974	1.22756051948851	2.14325781614736	C	-0.54276546131796	-2.00590636334118	-1.56508569388107
H	3.30186537261838	1.28837260069723	-2.35079451782110	H	0.27756335654220	-2.66575021123562	-1.87677996775214
S	-1.29093270523767	0.50692761565122	2.34808629233708	H	-1.43234854896082	-2.63282028607701	-1.43790978564189
Si	-1.39208880521795	0.09512080141588	0.24167939504059	H	-0.73922723983228	-1.31185543212347	-2.38847737247493
C	-0.90239118524109	1.71526577954138	-0.64683472130603	C	0.07844951063618	-2.32528758444431	0.85237224674958
H	-0.00239798684437	2.03195235133076	-0.09539750594417	H	-0.83111330724253	-2.88811294625540	1.09231743597226
H	1.01015430857766	1.00161241171833	2.11269444799095	H	0.84326899900313	-3.04453843923511	0.53042207098317
C	-3.24757857055893	-0.33267294182035	-0.02104356259396	H	0.41808510159355	-1.85207611859752	1.77796411351396
H	-3.78424300206277	0.49304822294778	0.46918071009310	H	2.16571221096266	2.31905629719494	2.05535040760067
C	-0.17496897051042	-1.29381219419893	-0.25346707957363	H	2.46240198635132	2.32584775626734	-0.30351698669190
H	0.77216444824127	-0.75892884796702	-0.42591935646556	C	2.62655627274644	0.77279227432900	3.50219008539371
C	-3.66732129946368	-0.35041615768862	-1.49828517997198	H	2.14190543250670	1.34005934543787	4.30193084682917
H	-4.75093399403767	-0.51381880576675	-1.57268952978351	H	2.41521075348050	-0.28502727368605	3.68435591526005
H	-3.44414817054795	0.59014194005845	-2.01020349783996	H	3.70906382763110	0.92295903397249	3.57724549056226
H	-3.17851205701498	-1.15779337488683	-2.05170510147996	O	4.17227552036292	-1.30913548108345	-2.48734256039029
C	-3.64960478106087	-1.64055459130319	0.6742223336420	C	4.17796161027296	-0.63789451638223	-3.74389579160332
H	-3.40493039754481	-1.62948786132689	1.74072057907692	H	4.84168077260240	0.23684497410171	-3.72730740119767
H	-4.72960759674485	-1.81050121918226	0.57294949284590	H	4.55387774753039	-1.36297208418230	-4.46727583546483
H	-3.14290385432877	-2.50215532517407	0.22496174393168	H	3.16529167400258	-0.32536386293609	-4.03218794383915

Radical 2e

G: -424.51348316 Eh

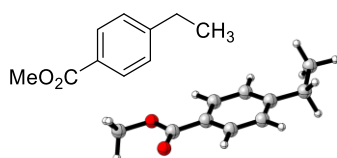
H: -424.46730210 Eh

Charge: 0

Multiplicity: 2

Optimized cartesian coordinates:

C	3.77278257757204	-1.28809016450591	-0.07438833446974	H	2.41436105036944	2.32266744197954	-0.32241128071483
C	3.30862464820923	-0.65926483540590	1.05925860714800	C	2.28797457194000	0.73144549115705	3.52573209696942
C	2.79918131271839	0.66935254732811	1.01649325001798	H	1.86379639447109	1.42480483880808	4.25558004785720
C	2.79609110268435	1.30723827050982	-0.25028814008188	H	1.68796687687654	-0.18921715164340	3.55575165911609
C	3.26124860249095	0.67977843441689	-1.39259034848014	H	3.29383601060079	0.45735583301985	3.87511529375510
C	3.75502117624248	-0.62848019824688	-1.31196034919450	O	4.23750378888407	-1.34435096023507	-2.36915459041586
H	4.16040671905565	-2.30163509671568	-0.03492019218947	C	4.24317790489365	-0.71315519333228	-3.64450789063069
H	3.33339108264203	-1.19237510060129	2.00477178807896	H	4.86886268180440	0.18970564047164	-3.64216056796834
C	2.31737980528396	1.33524707869083	2.16214400145551	H	4.66536603663799	-1.44314868377434	-4.33720635227635
H	3.23634884973228	1.21201211904420	-2.33673076883302	H	3.22601644513608	-0.45236672711242	-3.96715446785808
H	1.94644962175455	2.34922620614714	2.03641569871463				

2i**Substrate 2i**

G: -538.47850054 Eh

H: -538.42857252 Eh

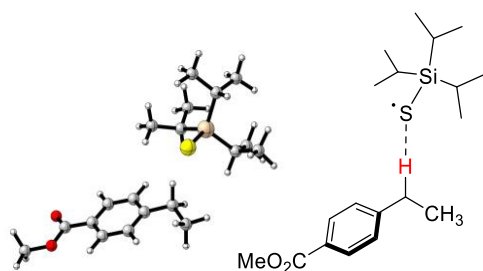
Charge: 0

Multiplicity: 1

Optimized cartesian coordinates:

C	3.64356037615759	-0.63437546984722	-0.95065498930405	H	2.87021566222717	2.69460422779799	0.84876074872451
C	2.90658198516688	-0.63430120774387	0.22840328008546	C	1.55830471033135	-0.73416343280975	2.85732585227609
C	2.61402032973534	0.55747356934218	0.89411765368909	H	1.02195641528777	-0.58277135563370	3.79864473683014
C	3.08515494308838	1.75608890363203	0.34211026085997	H	0.95390998872271	-1.40620443733983	2.23969996575144
C	3.81755467177228	1.76663362080371	-0.83174845879189	H	2.50168927261415	-1.24110501610869	3.08643805827083
C	4.10471327221040	0.56682184722876	-1.49126550153967	C	4.89670996694171	0.63192110485421	-2.74272725180743
H	3.86299366131795	-1.56984602701586	-1.45315327277023	O	5.31551470252565	1.65574903747814	-3.24110984795193
H	2.56249602962060	-1.58125950188349	0.63142924958645	O	5.10809547924268	-0.59277051987563	-3.28239341861025
C	1.80151989076992	0.60478458796592	2.16825642439338	C	5.87576242488291	-0.58999180077789	-4.50112277331305
H	4.18326376799838	2.69587614586672	-1.25713228697273	H	5.95246946758237	-1.63606437722233	-4.79949449153237
H	0.83551960627073	1.07828978398825	1.94048933077955	H	5.36775459564404	-0.00398888483519	-5.27235339688318
H	2.30428902791502	1.28798258789993	2.86551831083685	H	6.86792775197401	-0.16371638576439	-4.32725818260698

Reactant complex 2i



G: -1581.37614270 Eh

H: -1581.28565596 Eh

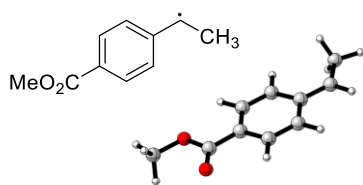
Charge: 0

Multiplicity: 2

Optimized cartesian coordinates:

C	3.64715015370377	-0.63759222851886	-0.9509939149564	H	-2.04024363998596	1.12936300242572	5.17053498333076
C	2.91015107353106	-0.64017748429451	0.22704878180326	H	-1.14505831364309	1.72036435297835	6.58252756386980
C	2.62266236317573	0.55121495782944	0.89725579613706	H	-2.45179340094275	2.69108214111347	5.89922927721026
C	3.09790414228375	1.75141931281270	0.34986032185916	C	0.01263134528679	3.95161524102214	5.40176444961872
C	3.82820681540994	1.76415634030544	-0.82463312919613	H	-0.72504423402484	4.74086674793222	5.58199318184893
C	4.11039012010616	0.56517039679261	-1.48803400301104	H	0.43368402307849	3.67326645931808	6.37653424293214
H	3.86429942246052	-1.57148820389759	-1.45731820596210	H	0.82495936469337	4.38147911271258	4.80686648630122
H	2.56033432294039	-1.58605561964365	0.62750680779260	C	-0.16966644785488	5.53954137697296	2.17318395328955
C	1.80552524113634	0.59679334270090	2.16099423686211	H	0.66876424184428	6.05106166832441	1.68334501578407
H	4.19566504230809	2.69348664990361	-1.24818679028504	H	-1.09006078594154	5.94980477570847	1.74397614467110
S	-1.68025513345327	1.09930078760647	2.08816199864307	H	-0.14706203966401	5.80908634110471	3.23355140633152
Si	-1.32900249131842	3.02067403051047	2.98062219827569	C	-0.12760874930647	3.72510301417509	0.42912255258117
C	-0.60813314094661	2.72074564044527	4.72269612575909	H	-1.10111400041973	3.99382522601711	0.00463537435322
H	0.21596699156623	2.01047761832812	4.54299348223539	H	0.63678093450144	4.30887969750168	-0.10031288750911
H	0.82611797751230	1.04523612481440	1.90510332358945	H	0.03745548839225	2.66690682426655	0.20967167763252
C	-3.10100686432417	3.76983901687091	3.04325645093080	H	2.27382493037101	1.31114608049540	2.85107442916400
H	-3.71904198576515	2.96775806087647	3.47306556454092	H	2.88488592654492	2.68830697015645	0.86022787490336
C	-0.07843367133650	4.02341651378769	1.93296677380445	C	1.56029205499114	-0.72991053592450	2.86822441524704
H	0.89970922126544	3.68492751830450	2.31619777484367	H	0.99530115610394	-0.56358461155155	3.79003663601489
C	-3.21008469554103	4.98804686994401	3.97261659412585	H	0.97106732062699	-1.41358067576170	2.24950620436504
H	-4.24990123189583	5.34073829652495	3.99276715500047	H	2.50338525966412	-1.22342529362605	3.12689830091219
H	-2.92538291045272	4.75552331300784	5.00227839673749	C	4.89911891674705	0.63258560481987	-2.74190450025735
H	-2.59052629424986	5.82247060078696	3.63002436475630	O	5.31742338325826	1.6577258877946	-3.23787855067565
C	-3.64939130877646	4.09442447914312	1.64734975758477	O	5.10699570896686	-0.59043308994691	-3.28512273734713
H	-3.59933431635740	3.23336914082141	0.97438247851696	C	5.86887881010689	-0.58577927737691	-4.50771609964399
H	-4.69765597610146	4.41233607094788	1.71812619101621	H	5.94266855562443	-1.63122352255611	-4.80884217167105
H	-3.09455855215924	4.91644485615497	1.18173245326221	H	5.35743929512287	0.00262307004429	-5.27480308437623
C	-1.62049393862659	2.02450982023224	5.64141855358815	H	6.86229192131561	-0.16099256725447	-4.33751712279838

Radical 2i



G: -537.85543685 Eh

H: -537.80467051 Eh

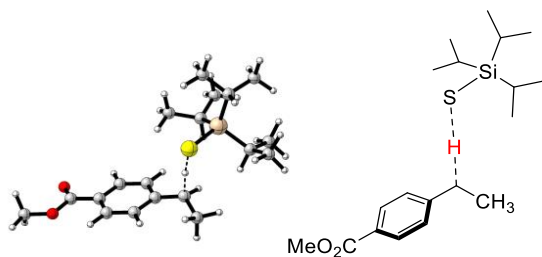
Charge: 0

Multiplicity: 2

Optimized cartesian coordinates:

C	3.47586137314385	-0.63637130949531	-0.79501256943916	C	1.58651401531741	-0.60827987439329	3.16727507384994
C	2.88286575271996	-0.64033235594162	0.44954287660178	H	1.14676064124154	-0.33881207991868	4.12969974550424
C	2.71407033104394	0.56434268617102	1.18689718238975	H	0.81512727813096	-1.12328887668264	2.57874416847556
C	3.18214451250898	1.76809978833491	0.58825360874269	H	2.37755104043088	-1.34710401145768	3.35668112699123
C	3.77213978537705	1.76573274664762	-0.65378922550121	C	4.56820363641542	0.62488920506829	-2.69610677424469
C	3.92888492084433	0.56439770077223	-1.36666960787608	O	4.96864902374981	1.64279473256735	-3.22457503000709
H	3.59571906465764	-1.56495855818381	-1.34195355126504	O	4.66445333923220	-0.59678764240188	-3.27897677728658
H	2.53980886589808	-1.57927350304736	0.87293237624899	C	5.27982123613795	-0.59541182986315	-4.58051412562618
C	2.11134758318865	0.59265234165626	2.45821802818126	H	5.27912573126189	-1.63671465819836	-4.90451954819671
H	4.12721024325479	2.68547532933544	-1.10775070059296	H	4.70664888915632	0.02578809893414	-5.27481035846717
H	2.02770110591414	1.55918026532767	2.94946332429874	H	6.30171905335437	-0.20985949955731	-4.52102276837820
H	3.06519430701980	2.70196335432617	1.13218206559686				

HAT transition state 2i



G: -1581.37189598 Eh

H: -1581.28480824 Eh

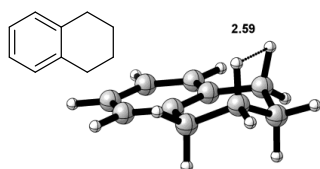
Charge: 0

Multiplicity: 2

Optimized cartesian coordinates:

C	3.33058202009007	-0.61266418866089	-0.86745366273698	C	-3.30045199136134	4.67327486576672	3.68812331969696
C	2.67960929942224	-0.60734073114941	0.35299501621062	H	-4.38607881325171	4.83056297725469	3.64189944110467
C	2.56219053183593	0.57849034254396	1.10390289665966	H	-3.04404489042696	4.47337895750300	4.73276770295350
C	3.11063885888605	1.76203716235647	0.56706240635395	H	-2.82434526825609	5.61643444775949	3.40164359072825
C	3.75819330306012	1.75880609748281	-0.65138297196713	C	-3.36490522851828	3.80359578426256	1.31783378649560
C	3.87803048579162	0.56953639979013	-1.38204301268982	H	-3.10216782724776	2.99082816807860	0.63320143137742
H	3.41949357454689	-1.53405423865653	-1.43180485634428	H	-4.45447692501618	3.93322582201703	1.28816372920672
H	2.25960633527274	-1.53199385278627	0.73514428758184	H	-2.91875460839475	4.72601243268079	0.92853013661206
C	1.86490583087234	0.62554139042446	2.37642822670823	C	-1.48841204313414	1.85817917160484	5.40240933982077
H	4.18637117486312	2.66731473584865	-1.06259624610557	H	-1.77232026917924	0.96298997688514	4.83885785924412
S	-0.97937855214366	1.14261608480206	1.80693338412723	H	-1.07247260285647	1.53675070211072	6.36604998432001
Si	-1.05107578971810	3.04463998342291	2.83800213042035	H	-2.402731114849540	2.42293415988543	5.61799232696948
C	-0.47417731810723	2.71228702060222	4.62925910525608	C	-0.06050878297066	3.95101095472260	5.43661364393229
H	0.43094016034107	2.09713951450589	4.49606054697044	H	-0.89903133283793	4.64034941604709	5.58597540697145
H	0.55857787580850	0.93015063245172	2.02909850079497	H	0.29652059453920	3.65650796240752	6.43223589198913
C	-2.89529452934601	3.52309198454433	2.75323830571473	H	0.74680281959774	4.50818648227306	4.95040944779350
H	-3.41328769904745	2.61566798128517	3.10211416685131	C	-0.16713543523405	5.75093977554944	2.34429056945973
C	0.14710680347159	4.28304319401833	2.00705721695748	H	0.63692299703605	6.40726530859338	1.98716120825530
H	1.12903115941199	4.04238236521517	2.45223143600284	H	-1.08833954720005	6.07123813775902	1.84530098135419

H	-0.29034856315116	5.93027661224557	3.41670808607767	H	1.13175782370842	-1.39542140902933	2.65614145413199
C	0.27105029343169	4.11531218339553	0.48616766442988	H	2.63493940208620	-1.02625147044357	3.52085008390728
H	-0.67333887166278	4.35647350649851	-0.01416756819730	C	4.59130227304881	0.62090341696270	-2.68028362443372
H	1.03723446300774	4.79348484064064	0.08687499667517	O	5.07780178812972	1.62493227306568	-3.15712166312300
H	0.53359372149683	3.09262478826388	0.20340660939340	O	4.64482214245067	-0.58922519461209	-3.28423873570652
H	2.07908425076692	1.53056697252778	2.95176524203560	C	5.32787636205427	-0.60116805119535	-4.55310427785959
H	3.01813059357461	2.68812193695369	1.12905810536210	H	5.28316761516687	-1.63458427275280	-4.89786513694964
C	1.66649021222616	-0.61567250345669	3.20619533300750	H	4.82829792964331	0.06549237876528	-5.26163497393790
H	1.08057785591909	-0.38735380068357	4.10042771658477	H	6.36554648599877	-0.27790758834829	-4.43120198644890

3b**Reactant complex 3b**

G: -388.03635104 Eh

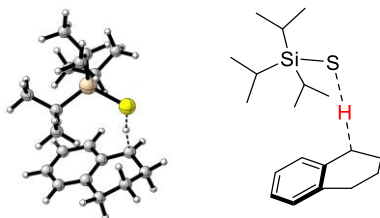
H: -387.99522205 Eh

Charge: 0

Multiplicity: 1

Optimized cartesian coordinates:

C	3.46612038868204	-1.37863269194440	-0.09015380324987	H	2.68540511579389	2.59171217036398	1.88863810114024
C	3.11072997670188	-0.62322235206071	1.03185335939811	H	2.40820123556494	2.29108180419774	-0.56271234635195
C	2.72471841970933	0.71292315863507	0.85848539962412	C	2.75958821694849	1.01030596587942	3.37611254858066
C	2.70683598810431	1.25267498498659	-0.43156084880065	H	3.84746549918575	1.12805748600914	3.47948579639557
C	3.06131689452929	0.49452186830877	-1.53841310476308	H	2.29656072502534	1.57492771489962	4.19383513173910
C	3.44465167105927	-0.83358301772992	-1.36620525175742	C	3.17684918453705	-1.25594090207302	2.40486465069843
H	3.76421960468461	-2.41627393629187	0.04802037199251	H	4.23266011958189	-1.32223065391516	2.70852992547846
C	2.30488073885078	1.57256550224837	2.03086783162427	H	2.81305334461547	-2.28933926254333	2.34666077471781
H	3.04105055135602	0.93600648084817	-2.53070288127013	C	2.40417977023085	-0.47247093600152	3.46446378303547
H	3.72387439618255	-1.44033902414076	-2.22285397568041	H	2.62803353488444	-0.87124162657179	4.46083192078109
H	1.20734551180410	1.65445852670788	2.02979014184376	H	1.32396011196771	-0.59563525981228	3.30360847482390

HAT transition state 3b

G: -1430.93450164 Eh

H: -1430.85677123 Eh

Charge: 0

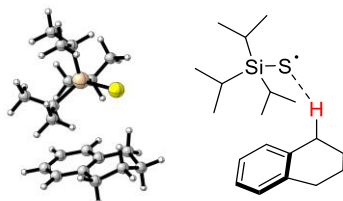
Multiplicity: 2

Optimized cartesian coordinates:

C	3.75553637578805	-1.33146418309637	-0.01542339666250	C	2.01818173786296	1.26498996693197	2.05942268257075
C	3.23296118078829	-0.68413396487279	1.10077394188525	H	3.21721772080431	1.02756748797525	-2.40249309064166
C	2.65889778348071	0.59941740759955	0.94025754417891	H	4.14948830255145	-1.26568944474235	-2.12894913587329
C	2.67757947501418	1.20200657025054	-0.33405225273648	S	-0.85420856383440	0.54963184582071	2.17360120842469
C	3.21279225372093	0.54723754055796	-1.42844257546451	Si	-1.29190436187332	0.12880332853654	0.09465178507101
C	3.74117237672243	-0.73599997841915	-1.27326231400020	C	-0.95103134004733	1.75657482064561	-0.84601037263725
H	4.18727873617334	-2.32291169099107	0.10468881175218	H	0.00191779369229	2.09291261351923	-0.40895215282201

H	0.66867813571079	0.91266144858949	1.97221671917966	H	0.09039401659029	0.94133168404199	-2.59267026156152
C	-3.15529087498528	-0.28962430201906	0.11981186766671	C	-0.71395720237581	-1.90657719484319	-1.87099622346657
H	-3.60072634762864	0.53725273273676	0.69508072951676	H	0.04368613775962	-2.56885779848765	-2.31018949339914
C	-0.17860925902215	-1.27282827781269	-0.57551037062664	H	-1.59931708790187	-2.51980161741168	-1.66888894272416
H	0.77147585267053	-0.77183048657490	-0.81879744784353	H	-0.98760496166030	-1.16815726701285	-2.63081675818949
C	-3.81927045870443	-0.29834907062855	-1.26663871198260	C	0.13297426498968	-2.37511820867588	0.44519611378450
H	-4.90411920883283	-0.43411648828856	-1.16407969070928	H	-0.76903460377738	-2.93321307595729	0.72037041914328
H	-3.65752822924372	0.63357428409008	-1.81661140590364	H	0.85236687229818	-3.09018572913510	0.02380060709662
H	-3.44789230433561	-1.11935107487434	-1.88810075556984	H	0.55623140194516	-1.96605100608390	1.36541438214497
C	-3.46122623380545	-1.59576555220936	0.86699033101716	H	1.88502688967735	2.34395096639085	1.94556807212319
H	-3.00715611629590	-1.61499638268220	1.86295231025623	H	2.26154725817770	2.19979002027044	-0.44839910907670
H	-4.54468029794547	-1.72864123704235	0.98454035101638	C	2.33946693952240	0.77718266741163	3.44988187436315
H	-3.08726761353294	-2.46302912277659	0.31076789339682	H	3.32294301682067	1.17718832876378	3.74593993006444
C	-1.99553792231577	2.83242409025261	-0.51835772844414	H	1.60835381089986	1.17338243790016	4.16429102992470
H	-2.12002048778546	2.95091875297676	0.56323936818945	C	3.34487323317998	-1.31471587044006	2.46827040075035
H	-1.69617796137982	3.80375332951116	-0.93330775783691	H	4.37279178981168	-1.14950804854701	2.82712552439055
H	-2.97467048831066	2.58638234303167	-0.94452780536407	H	3.22565101510138	-2.40140316120391	2.37971020857147
C	-0.73181995081208	1.62627587680369	-2.35880991112787	C	2.35997043144414	-0.75032903866070	3.49200386129871
H	-1.62881090991814	1.26231574668501	-2.87312082737082	H	2.62512146871510	-1.10071233533536	4.49568575602999
H	-0.48361190421691	2.60295374945561	-2.79586802441657	H	1.34741688862820	-1.11454875192414	3.28138784264352

Reactant complex 3b



G: -1430.93862421 Eh

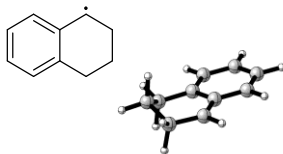
H: -1430.85893141 Eh

Charge: 0

Multiplicity: 2

Optimized cartesian coordinates:

C	3.45833802078900	-1.38049711366299	-0.09112712353472	C	-2.02000905419244	2.75822970726713	-0.2713055511774
C	3.10786688963754	-0.62382201307592	1.03125575175992	H	-2.23959811140665	2.80501010916819	0.80079616651563
C	2.72667962696791	0.71496807733639	0.85860847646108	H	-1.66201960567245	3.74733943343823	-0.58450584928735
C	2.72219070682307	1.25755663349344	-0.43113230074465	H	-2.96167820162827	2.57200059025717	-0.80064815161640
C	3.07191317275302	0.49749103134201	-1.53902152644862	C	-0.62570651815513	1.64313287845291	-2.07768439863708
C	3.43888324299493	-0.83567426235731	-1.36812004032243	H	-1.48488131181939	1.35705848019222	-2.69474220611832
H	3.74833215132598	-2.42035723477858	0.04710624226203	H	-0.30178358398071	2.63669659425084	-2.41521108653431
C	2.29704002466331	1.56741812663683	2.02931134121072	H	0.19007945536767	0.94383194965397	-2.28590471787391
H	3.06123351857598	0.94199005315484	-2.53022896793588	C	-0.57341603551732	-1.93152712622270	-1.77923140975365
H	3.71189860122055	-1.44450579558528	-2.22533842444474	H	0.26014820564391	-2.54058949758046	-2.15269957408896
S	-1.30018399276747	0.23545154623014	2.32727783036712	H	-1.45022063750379	-2.58588867895790	-1.71494358389869
Si	-1.42803128411403	-0.00192661276585	0.19513080372264	H	-0.78182333130322	-1.16422554195873	-2.53110100769690
C	-0.97493050679758	1.67986386814704	-0.58338780111835	C	0.02403046225041	-2.48283561398278	0.60057724895527
H	-0.05255790681957	1.95011955952736	-0.04439394310686	H	-0.88626549685163	-3.06939957145247	0.76945689028328
H	1.19486915787445	1.62466718111102	2.03681853680167	H	0.79508271055673	-3.16526943764323	0.21865011252687
C	-3.29153091586776	-0.43136877499416	-0.04703497152643	H	0.35129605182521	-2.10498141279118	1.57254812157241
H	-3.82998949827726	0.33641907891069	0.52728353559111	H	2.65121384146251	2.59568619974038	1.88434388890525
C	-0.21435554298947	-1.34930840709975	-0.40289406693123	H	2.43769048518274	2.29991755108236	-0.56294015357223
H	0.73250311525447	-0.79777634793211	-0.51239743394248	C	2.75900978907745	1.01345479598618	3.37463306043929
C	-3.73329468123979	-0.31504457024565	-1.51361622027381	H	3.84617253475895	1.14290704318944	3.47602446952966
H	-4.81318229810768	-0.50166379483102	-1.58721669207743	H	2.28902538623954	1.57574782549435	4.18949128512442
H	-3.54440716247725	0.67770183583428	-1.93079068526877	C	3.17557115953538	-1.25650047404676	2.40348785229392
H	-3.23153646854899	-1.05038014957345	-2.14984800129615	H	4.23366986610426	-1.32943749994959	2.69786816274490
C	-3.65740358288268	-1.80595964874942	0.52638737473478	H	2.80521630509607	-2.28759466715809	2.34460222072653
H	-3.37462182753689	-1.90163440350862	1.57874381889090	C	2.41456719667714	-0.47072379562069	3.46912542186863
H	-4.73931669301618	-1.97420950780823	0.44534045474651	H	2.64930138724333	-0.86659284492464	4.46403474291828
H	-3.16297372908444	-2.61168830484450	-0.02747225485162	H	1.33101830654350	-0.59577421134235	3.32464351513278

Radical 3b

G: -387.41303038 Eh

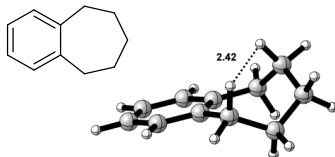
H: -387.37131685 Eh

Charge: 0

Multiplicity: 2

Optimized cartesian coordinates:

C	3.73776726214516	-1.35389680071434	-0.01792775397365	H	2.32989010229343	2.22611677778959	-0.43554050695318
C	3.32859014152122	-0.66470744573149	1.11229245434055	C	2.35190005080925	0.77178955886286	3.47427723544730
C	2.79889739637665	0.65598728971963	0.97668949146887	H	3.24287325052697	1.10592531609818	4.03460146635061
C	2.72962461396546	1.22089414320402	-0.32536334448769	H	1.49102103462496	1.14509398341066	4.04402995043686
C	3.15194595074574	0.51498417828961	-1.43368854467268	C	3.45181052355986	-1.25766005253188	2.49154634157489
C	3.65704697015360	-0.78137395639731	-1.28934836252848	H	4.42525647622756	-0.97027532438614	2.91975146016273
H	4.13347899312150	-2.36160638601813	0.09255696252063	H	3.44959941411517	-2.35208959478191	2.42929853748428
C	2.36096851607928	1.37126921850152	2.10704248409906	C	2.34037276972615	-0.75836560654421	3.41590830466436
H	3.08776349457178	0.96570141775612	-2.42008499135429	H	2.45859063028789	-1.17995711152066	4.42049747028930
H	3.98345225219129	-1.34184435434535	-2.16006381232132	H	1.37068079676373	-1.09693876962311	3.02823408272867
H	2.01973671019331	2.39585502896235	1.97774269472315				

3c**Substrate 3c**

G: -427.30124139 Eh

H: -427.25775319 Eh

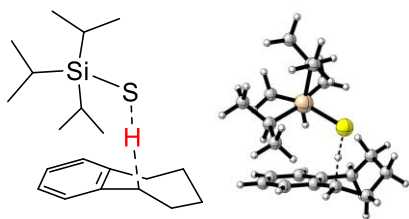
Charge: 0

Multiplicity: 1

Optimized cartesian coordinates:

C	-2.22159368938972	-2.89555574330983	-0.53817445387430	C	-0.84324814485303	0.71969800741770	1.40327823124663
C	-1.17745040069888	-2.91913646801800	0.37875028777921	H	-1.39653646294390	0.87874566184084	2.34148060029798
C	-0.77173957152894	-1.73297904608154	0.97454835166533	H	0.18519730948535	0.49156411374560	1.70533264683452
C	-1.38313457576201	-0.50609179240142	0.68897875362098	C	-3.39614636315743	1.80430434279919	0.47565022813049
C	-2.44395870683117	-0.48293391427358	-0.23692071733309	H	-4.29398125077677	2.39917886678465	0.26858565544135
C	-2.83980648872174	-1.68769811411401	-0.83044113561266	H	-3.59244935298894	1.27516945224299	1.41718452877565
H	-2.55664397084203	-3.80988422187195	-1.01941377325105	C	-0.85362281938106	2.01512722206837	0.58426682880503
H	-0.67824366471177	-3.85170868632236	0.62559467606036	H	-0.06910734587421	2.68653335936404	0.95397967993790
H	0.05123913970415	-1.74967099366845	1.68596622398346	H	-0.58588748215863	1.77703446232405	-0.45321424206686
H	-3.66303989839233	-1.67028325744508	-1.54156601805333	C	-2.19878802140254	2.74590736793708	0.63297375504183
C	-3.20231555974076	0.76901027872517	-0.63771932562020	H	-2.22380429059995	3.50497369677474	-0.16021638274696
H	-4.18271261128426	0.45008054337056	-1.00929391267282	H	-2.28849295346836	3.28628899598651	1.58472582004627
H	-2.70439661368105	1.24674134612472	-1.49540877643573				

HAT transition state 3c



G: -1470.19873587

H: -1470.11898801

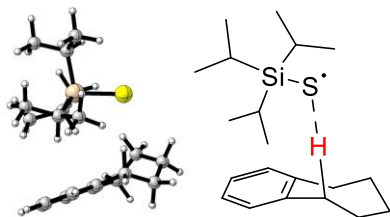
Charge: 0

Multiplicity: 2

Optimized cartesian coordinates:

C	-1.66250201940223	-3.09597931781947	-0.69956614146967	C	-1.84884292857108	-1.60565259490289	4.22847902552932
C	-0.82155372800592	-2.97123773855372	0.40431545422937	H	-3.35010290627409	-1.04552231345866	1.30814545380917
C	-0.45753087959424	-1.71050508487708	0.83885849261083	C	-5.33064802178849	-0.34125127748201	1.72327741410089
C	-0.91570532729188	-0.53633894366059	0.20196583824628	C	-4.40933714117848	-2.64561731717270	2.22781670295544
C	-1.76615966166916	-0.66859700543100	-0.92907439746423	H	-4.99861371561039	0.97027024022962	4.48537924496328
C	-2.11601650455405	-1.95195865482054	-1.34879059141502	C	-5.43008149225951	-0.90623070445233	5.42240551909793
H	-1.96627739283007	-4.07707449094925	-1.05238945698826	C	-3.72509560543643	0.78615745468463	6.19968978143181
H	-0.45315239649168	-3.85339277260996	0.91986549716878	H	-1.54488647168284	-2.12960464445076	3.30839290625104
H	0.19915363431578	-1.60562589873032	1.69937675787215	C	-2.38614526450123	-2.66599652284890	5.20400838744313
H	-2.77389316880004	-2.05644042562629	-2.20835618246738	C	-0.60250572347075	-0.93181191086338	4.81525705887380
C	-2.33513151898901	0.51280475770953	-1.68071878167281	H	-5.11615824901220	0.73127553758331	1.66159362773685
H	-3.13163039671350	0.13678146183890	-2.33182903021283	H	-5.71111022841441	-0.6675299891490	0.74621876007322
H	-1.57390136228539	0.93215432152937	-2.35564142108553	H	-6.14120777958233	-0.47574052696325	2.44915594573235
C	-0.51561416180061	0.73141543413556	0.79344788987606	H	-5.12858727754176	-2.85746520085732	3.02769874461467
H	-1.45800569322262	0.99492234967069	1.81413039823985	H	-4.85143966714426	-3.00501586812207	1.28905369387912
H	0.32535418302510	0.61654065407026	1.48222001057061	H	-3.51171580689534	-3.24495287298143	2.41309614115765
C	-2.88942508898143	1.62259731292507	-0.77539605864232	H	-6.18051463113615	-0.46777015454421	6.09355890724902
H	-3.70124316960119	2.14606493281450	-1.29420943835725	H	-5.96626851717553	-1.35118194214677	4.57884040735483
H	-3.33890727632938	1.16311396684426	0.11300220974129	H	-4.94092088514071	-1.71705356311253	5.97117139718936
C	-0.47521397198472	2.01816977869530	0.00114063255461	H	-3.03779712702657	1.58905804686481	5.91473053846358
H	0.12224495160684	2.75151179771136	0.55363160487908	H	-4.46181601910100	1.20295636803389	6.89893795688320
H	0.07844288834924	1.81236953568718	-0.92773269119225	H	-3.14833739382478	0.03225855692947	6.74805057439871
C	-1.83559412876698	2.64331607150839	-0.34452215799007	H	-1.62579591220284	-3.43594934425647	5.39024207962886
H	-1.67682585606971	3.37752745881908	-1.14490586100596	H	-2.63433712823770	-2.21819570478559	6.17255814705503
H	-2.21223599476991	3.19405744767882	0.52459211740930	H	-3.28304351197423	-3.16998899775688	4.83025852857579
S	-2.34352554703915	1.50202021914826	3.00273933328354	H	-0.84260752081623	-0.37614292255763	5.72897978856478
Si	-3.19695355082387	-0.39040439976789	3.62814929387454	H	0.15581758417098	-1.68308192147144	5.07461857270781
C	-4.08701014474823	-1.14798424405130	2.12034406149388	H	-0.15896987223468	-0.21498042932875	4.11778600129824
C	-4.42617510246895	0.16962440521599	4.97993032089443				

Reactant Complex 3c



G: -1470.20273502

H: -1470.12051340

Charge: 0

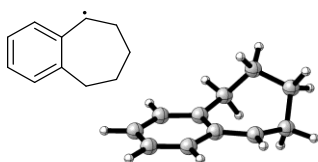
Multiplicity: 2

Optimized cartesian coordinates:

APPENDIX

C	-1.70590084565954	-3.20075589185695	-0.69546112277351	C	-1.84415308309907	-1.32984847933205	4.21577150017948
C	-0.77749836376262	-3.08895299190985	0.33328956497307	H	-3.38961626821842	-0.68120643461496	1.38606827667469
C	-0.38818733055409	-1.82674400954021	0.75848400693230	C	-5.42480698904572	-0.16142265793465	1.79499709319528
C	-0.90411722565503	-0.65467880045069	0.18981426278139	C	-4.34140589850395	-2.43389142228575	2.12383658770378
C	-1.83437328051280	-0.76804289236441	-0.86432384919482	H	-5.25198866063315	0.86769323060050	4.78394716224544
C	-2.21272037284002	-2.04900835452922	-1.27874784445858	C	-5.49299492851482	-1.16351668134964	5.42447874368960
H	-2.03141236161450	-4.17724396213816	-1.04244833272902	C	-3.94201299754222	0.54694968041500	6.45475744263440
H	-0.35737709564662	-3.97568441943202	0.79928896855245	H	-1.49090905432705	-1.68437792299999	3.23384188900015
H	0.34364084250496	-1.73567237962793	1.55861566656960	C	-2.23781958473444	-2.56678547991279	5.03933633692757
H	-2.94347768867724	-2.13900972033330	-2.08366535116680	C	-0.68493578574127	-0.58781488726883	4.89105938109157
C	-2.45604752406477	0.41318416681697	-1.58437255074075	H	-5.27644839083677	0.92402524426117	1.80794908151708
H	-3.37942918988993	0.05573601647145	-2.05422364485118	H	-5.76278817016468	-0.44289084644653	0.78906477330920
H	-1.80306435943555	0.71929989379579	-2.41614186430687	H	-6.24006020405229	-0.39707790977420	2.48946323775962
C	-0.44285175158395	0.65826224734359	0.77420441573398	H	-5.03878189967849	-2.77795979593132	2.89610615843279
H	-1.16419337676048	0.97899559707815	1.55689913040149	H	-4.75461453835657	-2.73251184395708	1.15166829458183
H	0.49545763026182	0.47834409437500	1.31084926101496	H	-3.39673343616386	-2.97258305716665	2.24865450109685
C	-2.77227532436540	1.63341131460940	-0.71202103310953	H	-6.23963694070661	-0.91677261378513	6.19116819270162
H	-3.58837133500299	2.20329822964581	-1.17249592315605	H	-6.03532960142937	-1.48902906167881	4.53236315677920
H	-3.15637545767942	1.29663664468845	0.25898664595751	H	-4.91356499158743	-2.01419272240916	5.79606898205991
C	-0.26927391157906	1.81187393898916	-0.21860332627271	H	-3.32658711543532	1.43686861485068	6.29292713735439
H	0.47107335452404	2.51846099647208	0.17442410855695	H	-4.70620412978035	0.79091806270089	7.20431686124478
H	0.15364357280332	1.41158102351681	-1.14965184858552	H	-3.30062322116054	-0.22857095978464	6.88813082569790
C	-1.57345781785842	2.56294067391559	-0.50400067908269	H	-1.38311188316717	-3.25017760957491	5.12602987789893
H	-1.43482072288824	3.19357388017703	-1.39215057181328	H	-2.53009553721955	-2.28675507083693	6.05742476368158
H	-1.79385356887772	3.23797326881109	0.33311592267532	H	-3.06541785084148	-3.12891589588697	4.59577847150659
S	-2.68182635103547	1.77963954118106	3.32002697467540	H	-0.98529814508490	-0.17107886624194	5.85920577180033
Si	-3.33239463252215	-0.22265399712595	3.74466615056831	H	0.15202900001525	-1.27521264879737	5.07299969629603
C	-4.13849213469114	-0.91210309993842	2.16030167614538	H	-0.32315339046857	0.24542694030559	4.28203785864476
C	-4.60455726354624	0.06116618333498	5.15878051867052				

Radical 3c



G: -426.67523491 Eh

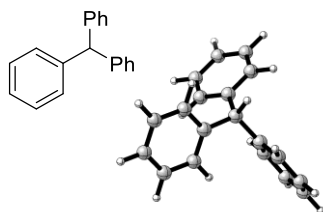
H: -426.63105786 Eh

Charge: 0

Multiplicity: 2

Optimized cartesian coordinates:

C	-2.31448106877636	-2.89486648528740	-0.42264882514651	H	-2.47083923522795	1.36555299582695	-1.53588104535121
C	-1.33437476976072	-2.90259521770710	0.57197540868736	C	-0.77370896954680	0.72008769157825	1.16723684943684
C	-0.87287799506612	-1.70928159874444	1.08669585861565	H	-0.05822059681441	0.5769909062271	1.97417418399866
C	-1.35447761265852	-0.45104708447108	0.62732946731664	C	-3.46997635722586	1.72899306496086	0.35863486294042
C	-2.38823273003035	-0.45649349946384	-0.36520918489628	H	-4.36570658372867	2.30424121332011	0.09593944687958
C	-2.83150760911311	-1.67655728991224	-0.86224008340044	H	-3.74603407679665	1.09622278404149	1.21074725732177
H	-2.68773573492403	-3.82624907238503	-0.83721942519829	C	-0.94260289136690	2.10062102339533	0.62308532369387
H	-0.93445269746893	-3.84331103155517	0.93964278634251	H	-0.22198375074819	2.77152962718034	1.10294375455509
H	-0.10213481143366	-1.71248112650883	1.85356272502793	H	-0.67994673627442	2.09409014770549	-0.44519051342306
H	-3.62329651822211	-1.67677477770908	-1.60835461374095	C	-2.35494491343737	2.69891091062872	0.77020540448946
C	-3.08516513787168	0.80907809261076	-0.81384404904695	H	-2.40199134267956	3.60600916896278	0.15304090122376
H	-3.98835075270842	0.51448659218645	-1.35915528492413	H	-2.51281818811917	3.01569432472401	1.80812367459826

6b**Substrate 6b**

G: -733.23136565 Eh

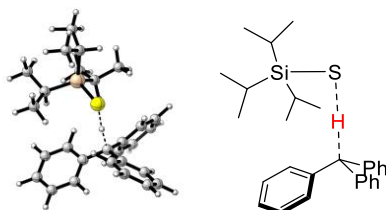
H: -733.17423835 Eh

Charge: 0

Multiplicity: 1

Optimized cartesian coordinates:

C	4.85872331486194	-0.92430842774806	0.44287999715938	C	3.57959080108368	1.49510442548561	5.49337997436014
C	4.12652370210167	-0.18131617527540	1.36636283375515	H	3.60118290449761	2.70640592192788	3.71436111321088
C	2.87536202503477	0.33327479815306	1.02891058397284	C	3.10667850424123	0.33502630939482	6.09663736709294
C	2.36964326267232	0.08589186825793	-0.25025417038925	H	1.90922544966416	-1.43636976598919	5.83708818729541
C	3.09656668367833	-0.65779933814838	-1.17150474968819	H	4.21618480343666	2.17723714196939	6.04992202583107
C	4.34736079074540	-1.16575335049210	-0.82724726889082	H	3.37017213223836	0.10618220430676	7.12519048596387
H	5.83162955770621	-1.31905590427565	0.72200308712836	C	2.11969918512016	2.67190602345951	1.63433696970000
H	4.52779630035841	-0.00371753102468	2.36013338235927	C	1.09818454560214	3.51314782572439	2.08468927909818
C	2.06218752767907	1.19197924538680	1.98812196858779	C	3.17551370432664	3.22710731372613	0.91294936395065
H	2.68617799444215	-0.84383360352224	-2.16007411058421	C	1.13021335355151	4.87668887822695	1.82122849274305
H	4.91645220998912	-1.74968585327622	-1.54481802725617	H	0.27452384491020	3.09011102953153	2.65629027858427
H	1.01271892318405	0.88458854205660	1.86627223897952	C	3.21170125874772	4.59525715669596	0.65107687869545
H	1.39791014702667	0.49128433971433	-0.52470751801152	H	3.97213355891740	2.58517325768904	0.54719586906906
C	2.41985469324023	0.93190205263438	3.44507937298195	C	2.19101096993962	5.42403233200298	1.10260820859300
C	1.94984899630672	-0.23203862091721	4.05933679747893	H	0.32513799989108	5.51447088574864	2.17527796067495
C	3.23657560175094	1.79321942227862	4.17655147911617	H	4.04145246650632	5.01169562976336	0.08681179005681
C	2.28744192269712	-0.52936095122490	5.37388131418969	H	2.21757994309931	6.48953036765508	0.89342934594325
H	1.31896992075104	-0.914355844989574	3.49329219824809				

HAT transition state 6b

G: -1776.13023535 Eh

H: -1776.03842838 Eh

Charge: 0

Multiplicity: 2

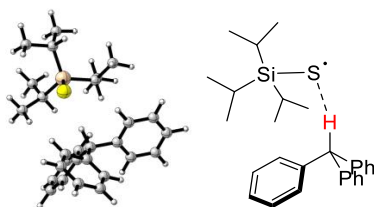
Optimized cartesian coordinates:

C	4.70492451728519	-1.43946547290042	0.73837356482507	Si	-1.36140174195963	0.16883248389719	0.04277151720978
C	4.01886179906325	-0.60156842924899	1.61070746448473	C	-1.06148454313982	1.93517809291409	-0.62393858966505
C	2.98214017749356	0.21829884640446	1.14602764805881	H	-0.01640680475936	2.15941610833463	-0.35439965108285
C	2.65813501906328	0.16823930062670	-0.21834973069536	H	0.99225446113610	0.66721155518007	1.91830260710851
C	3.33709686347036	-0.67235628788822	-1.08556308205961	C	-3.22636646878682	-0.15190027696837	0.34795129033893
C	4.36561346541034	-1.48437488614015	-0.60994138245875	H	-3.48046424757108	0.57447605155296	1.13532756747559
H	5.51236824065927	-2.05962028272756	1.11704097499565	C	-0.53343214456776	-1.11431847110184	-1.11496100507182
H	4.29841548623329	-0.56911572174720	2.65864304948721	H	0.33010234654563	-0.58408335215899	-1.54499795604634
C	2.21154602814253	1.12721974571012	2.04500790489034	C	-4.13739777083239	0.13684963245907	-0.85539623149167
H	3.05901495326878	-0.70277151973245	-2.13538370487568	H	-5.19049632427665	0.05535781947931	-0.55456785299393
H	4.89775039731912	-2.14602934173658	-1.28711069188056	H	-3.99129069810626	1.14212410427692	-1.26153182929781
S	-0.57267663209503	0.07757662011184	2.04976915422228	H	-3.97729710411600	-0.57755714143088	-1.66847967632352

APPENDIX

C	-3.50274405480734	-1.55604847123179	0.90531518322360	C	2.13734436374658	-0.28473811223395	4.11797580191910
H	-2.90755457712325	-1.76639759718266	1.79953799530878	C	2.94221991013644	1.97837500431834	4.31161151130513
H	-4.56297069165246	-1.66237976208677	1.17032101381453	C	2.35745381492167	-0.48007848543878	5.47354860124826
H	-3.27521447415427	-2.33016428452342	0.16348837186311	H	1.71955249311337	-1.08494908379921	3.51288574217064
C	-1.93290420006382	2.97032759879467	0.10089763227501	C	3.17128888215278	1.77647592259055	5.66828951636035
H	-1.86038744571543	2.86413925231231	1.18846701333566	H	3.17670017389070	2.93747866818537	3.86022302140441
H	-1.61838253133698	3.98917769804145	-0.15914862395201	C	2.87744157105922	0.55002940894922	6.25531993603775
H	-2.98849187219321	2.87012838383976	-0.17664365595951	H	2.11437518582114	-1.43757083695193	5.92505042754104
C	-1.17903040178435	2.08135742472636	-2.14815684402512	H	3.58155357566401	2.58351743360629	6.26858474969581
H	-2.19535533427175	1.87219839774161	-2.50094589047873	H	3.04830857065709	0.39702474654722	7.31700380030731
H	-0.93404870073919	3.10713799872824	-2.45349295305126	C	2.06596019852954	2.54561796871687	1.59093355060820
H	-0.49851088121561	1.40880422647284	-2.68161534679975	C	1.03254093998045	3.33019571957599	2.12384013146401
C	-1.42725962390618	-1.54006912277510	-2.29138891275002	C	2.94518290556843	3.13077780892133	0.67195141808138
H	-0.85514485234431	-2.15194398855696	-3.00109497460327	C	0.87737250292302	4.65370061523435	1.74072096645972
H	-2.26879193415748	-2.15032660255453	-1.94666407882863	H	0.33780515654091	2.87677594898195	2.82586991287399
H	-1.83658808247800	-0.68800513660671	-2.84388624846726	C	2.79089749556475	4.46051080191877	0.29371293236203
C	0.00880119279155	-2.34949804081038	-0.38502841950030	H	3.76246204682009	2.54399395703637	0.26434328535538
H	-0.79832394441554	-2.91114392433683	0.09924272444527	C	1.75485500076791	5.22508015447596	0.82039048767169
H	0.50759056004229	-3.02433252612706	-1.09371500726300	H	0.06132265348766	5.24034629631140	2.15282560219486
H	0.72803168267934	-2.07608869566178	0.39178550439281	H	3.48801971432086	4.90104304677243	-0.41338126354567
H	1.85608517432460	0.79820202409438	-0.59285427314020	H	1.63135548904716	6.26094822075179	0.51783524785643
C	2.42979707292774	0.94768476606628	3.51511205163450				

Reactant complex 6b



G: -1776.13016202 Eh

H: -1776.03759999 Eh

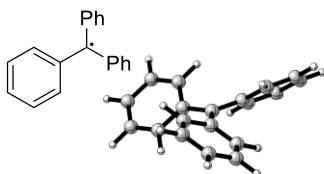
Charge: 0

Multiplicity: 2

Optimized cartesian coordinates:

C	4.60615007539011	-1.34497413661156	0.52267098938977	H	-4.95282039190077	-1.78715674345232	0.71447483650219
C	3.91231032571699	-0.56739120109624	1.44761439578876	H	-3.46448324064487	-2.42611907395635	0.01254475101793
C	2.93434854358377	0.33465075324564	1.02655943131722	C	-2.16249257268943	2.92348475785286	0.00475893373015
C	2.67204776066903	0.44041343301939	-0.34499302882856	H	-2.24680809616645	2.87202710585299	1.09562250431482
C	3.35874806948968	-0.33638988665504	-1.26711503417579	H	-1.78988653435519	3.92213137111057	-0.25700296449844
C	4.33108163308429	-1.23701761335447	-0.83517733645035	H	-3.17050532986750	2.82707031204076	-0.41569479790481
H	5.36575641014184	-2.03927049041684	0.87051158053781	C	-1.09463705575843	1.91315287716722	-2.06380077872853
H	4.13465399599195	-0.66262598382001	2.50574442948750	H	-2.04855687282616	1.71570297525996	-2.56566341696311
C	2.12189532351163	1.17648197067738	1.99795024064077	H	-0.76811054112264	2.91586613141016	-2.36846654895960
H	3.13635317315852	-0.23961505940349	-2.32636368746793	H	-0.36110730945553	1.19786778174168	-2.45130823062777
H	4.87060925999315	-1.84643659994236	-1.55438121237981	C	-1.21497054772895	-1.73653958901970	-2.03942254868111
S	-1.22194339923988	0.14918924853784	2.25815469511375	H	-0.49404535172215	-2.35740566920803	-2.58695863735531
Si	-1.63930968529302	0.10893232879452	0.15109039226264	H	-2.08330146503304	-2.36812780438127	-1.82281324575580
C	-1.22193730703053	1.84041215260714	-0.53552237556961	H	-1.54230443574416	-0.93903569171294	-2.71475926477099
H	-0.22416120272573	2.04823704925041	-0.11526157804253	C	-0.10487853307019	-2.35535346103826	0.14142096674267
H	1.07019604995914	0.81781950447598	1.90356050813708	H	-0.95138110834943	-2.93469236890588	5.62818422964581
C	-3.53242502519852	-0.24357206628886	0.14193241724995	H	0.53768183017233	-3.03789623148514	-0.42976534183172
H	-3.94537013841116	0.49325373345203	0.84627940427537	H	0.46362672405707	-1.99535829639230	1.00376013768951
C	-0.57389642646539	-1.19961810360743	-0.74960091721433	H	1.92550759374924	1.15187184475121	-0.68958862967359
H	0.32345219161001	-0.63595104461114	-1.04802778479882	C	2.49969951591985	0.95238527598269	3.45216806474632
C	-4.18902463636467	-0.0008034973833	-1.22454629642199	C	1.95302637981635	-0.12754181583326	4.14846291061396
H	-5.27532799823367	-0.13743501814072	-1.13889312188229	C	3.42387150800585	1.77337502315846	4.09986116261103
H	-4.01699726064801	1.01391214161454	-1.59657842400503	C	2.32546811079276	-0.38587555454508	5.46280744082878
H	-3.83107687927569	-0.70322316909084	-1.98226114587906	H	1.22466070917879	-0.76634851875530	3.65344222928696
C	-3.86498648573059	-1.64592609118119	0.66939980135367	C	3.80064002319381	1.51323141182378	5.41405229865919
H	-3.45782355458240	-1.81453892977680	1.67084469432372	H	3.84690635631046	2.62367169691340	3.57231423254438

C	3.25338679662702	0.43368656837023	6.10008000743829	H	0.13915431911133	2.91266359614707	2.52122507087112
H	1.88472778571594	-1.22563140798256	5.99252228696069	C	3.08154585363600	4.65593206126076	0.72138181138640
H	4.52021606361924	2.16235832147102	5.90512113500986	H	4.00887886272597	2.71454801115816	0.68722314270367
H	3.54191063879644	0.23616337858865	7.12847400906933	C	1.96543241684738	5.39799744866864	5.39799744866864
C	2.08088902208761	2.65187469444085	1.63953609202287	H	0.02865231938283	5.33743804024661	2.03537638475057
C	0.96742781472243	3.40726469939146	2.01746187607078	H	3.91298820339288	5.13923729960666	0.21598703757997
C	3.13827420307789	3.29067890011958	0.98928442955552	H	1.91761490612237	6.46093650304518	0.87525466250756
C	0.90689935597534	4.76805681618323	1.74415642243296				

Radical 6b

G: -732.62082919 Eh

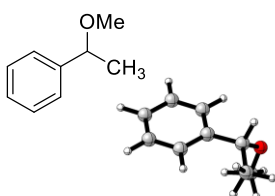
H: -732.56394671 Eh

Charge: 0

Multiplicity: 2

Optimized cartesian coordinates:

C	4.69755299805550	-1.55894451143441	0.67815643787244	C	2.89798243809184	1.76290723469896	5.86899414641076
C	4.24671800789685	-0.59637980044069	1.56800011584402	H	3.23511219018663	3.04667947820231	4.18396494156174
C	3.25428773030329	0.33390566678830	1.19322041490598	C	2.57180710352541	0.47985694928101	6.30609090137559
C	2.73599903750353	0.24437128301995	-0.11602740979577	H	2.04690049107742	-1.51745198083877	5.69531153143736
C	3.18466525586730	-0.72635652583982	-0.99804735628030	H	3.11291309856709	2.54461829237019	6.59230039550988
C	4.16954717925837	-1.63358240294761	-0.60998249740535	H	2.51786119385427	0.25952867768929	7.36808193874938
H	5.47461534793337	-2.25247817668388	0.98735032367565	C	2.38311058395356	2.65845861252313	1.63326770859744
H	4.67750704869766	-0.53544512341189	2.56299831379516	C	1.33946566865341	3.38130989436599	2.24871863112516
C	2.78323712807873	1.34829951940794	2.12397205725839	C	3.02422513483444	3.25185153291268	0.52538204646101
H	2.75628691401954	-0.78327171274796	-1.99488530322254	C	0.95687209604222	4.62711462110616	1.77643035777306
H	4.52168381312474	-2.39080731925839	-1.30411738794579	H	0.81529412620504	2.93715524811760	3.08968562836318
H	1.95545211610995	0.93445510189633	-0.42232994142217	C	2.64306333657382	4.50228726188657	0.06385772553243
C	2.71133035482410	1.05231236414513	3.54728205925356	H	3.84533807959812	2.72602422979894	0.04725709834794
C	2.38774857314490	-0.24053427140529	4.00991634595413	C	1.60603932280097	5.19856927980608	0.68298117686260
C	2.96267503778456	2.04858193740362	4.51401166472465	H	0.13855641189577	5.15476652218385	2.25844764623798
C	2.31520625085747	-0.51736048892472	5.36630727201023	H	3.16521733024835	4.94349080703019	-0.78060487761104
H	2.16842318424257	-1.01965002342783	3.28586777033776	H	1.30708861618917	6.17633294272701	0.31711595370547

7e**Substrate 7e**

G: -425.13006083 Eh

H: -425.08511788 Eh

Charge: 0

Multiplicity: 1

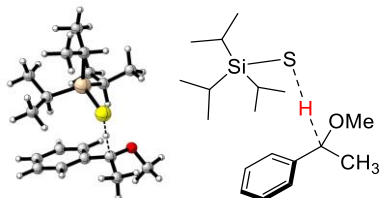
Optimized cartesian coordinates:

C	3.91776976572963	-1.07821009039483	-0.19934622381537	C	2.68007779669252	0.69987667814496	0.88623027730675
C	3.41811972281591	-0.48076107326763	0.95738138902428	C	2.45281507762636	1.27210619938699	-0.37023124694324

APPENDIX

C	2.95128120664421	0.68049017748257	-1.52286892206942	C	2.46442804492047	0.76665776045110	3.44598650755230
C	3.68716795112323	-0.50059310433765	-1.44135627816649	H	2.05950767104640	1.38184852003478	4.25477045600520
H	4.49123588320436	-1.99792604234755	-0.12446065086263	H	2.02837559162741	-0.23391786766263	3.52651581696633
H	3.61235393147822	-0.94876396379311	1.91732959421520	H	3.54626054637990	0.67679688459047	3.58562190014326
C	2.10204503978110	1.40005079923819	2.10817629476916	O	2.39704700656838	2.80579801436248	2.07606911206721
H	2.76466420638512	1.13930911672055	-2.48985904014636	C	3.77946838866522	3.11941653321254	2.19115939664626
H	4.07709899371227	-0.96570203603577	-2.34218981359272	H	4.38645112448637	2.57223917357207	1.45474221752954
H	1.00727666105454	1.38140638456267	2.01061563721412	H	3.86900477087525	4.19131724862673	1.99745427530240
H	1.88872755001091	2.19928083533924	-0.42949544021810	H	4.16669306917218	2.91236185211380	3.19927074107232

HAT transition state 7e



G: -1468.02872302 Eh

H: -1467.94692873 Eh

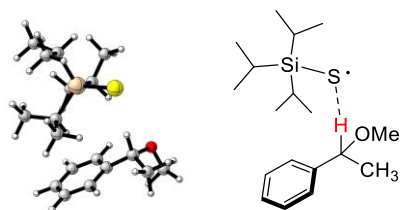
Charge: 0

Multiplicity: 2

Optimized cartesian coordinates:

C	3.62732635038837	-1.43734840884081	0.06025064061677	H	-3.06129654626953	-2.56683016384248	0.18549641383170
C	3.05950773345751	-0.73697810046529	1.11415665589896	C	-1.79822675159968	2.75865546332280	-0.09039149729278
C	2.66361199364154	0.60145609143391	0.95420627028084	H	-1.87481290839664	2.76764799412309	1.00182703563030
C	2.85264362144258	1.20983772918847	-0.29813770773504	H	-1.47104494247350	3.75530293579172	-0.41401589329314
C	3.42407880593272	0.50428976124383	-1.34773216443975	H	-2.80261742122906	2.59697348819527	-0.49890763174791
C	3.81056990600026	-0.82334981002198	-1.17717187874295	C	-0.65753480292094	1.70284615331259	-2.09682591218225
H	3.91979395825915	-2.47370441364245	0.20203416817550	H	-1.58305514527727	1.41657485893303	-2.60971314666851
H	2.90533618495164	-1.24118613496728	2.06251002738576	H	-0.39692630891757	2.71272223626089	-2.44163147784397
C	1.99612306260784	1.33218385694514	2.05084798306979	H	0.13567037324887	1.02577455230242	-2.43227180441743
H	3.56503033002914	0.99245904382377	-2.30790865497038	C	-0.70563954721563	-1.85243598459861	-1.98835886862890
H	4.24946119273990	-1.37633957326515	-2.00230522402869	H	0.02390568560562	-2.49109777012585	-2.50377985216541
S	-0.68887942011554	0.14833278806313	2.29842526352630	H	-1.60937433914929	-2.45390225753900	-1.83902516745869
Si	-1.19366588452167	-0.02031054574686	0.19836424301787	H	-0.96102509472803	-1.03071311409037	-2.66425125949685
C	-0.81186925904357	1.68537487087382	-0.57011940150691	C	0.14746021232110	-2.59290485547209	0.25177556550946
H	0.16825493041933	1.94515361960801	-0.14501251081329	H	-0.76679742903585	-3.16367564720525	0.45033940571207
H	0.75043937662594	0.79506105975926	2.04625377764312	H	0.85753348107825	-3.26828210531721	-0.24433608250834
C	-3.06918357918928	-0.38381849108878	0.21991197568687	H	0.56667403191183	-2.30093026718856	1.21804934228388
H	-3.47623263509605	0.39105462244400	0.88798129207794	H	2.54294130543235	2.24009939047505	-0.43646459878326
C	-0.13859094572385	-1.37665602641772	-0.63982964333528	C	2.39180145507253	1.03784419065468	3.47976050626031
H	0.82563464820852	-0.88014661174046	-0.83871766337089	H	1.76902993840407	1.62459841649715	4.16108506046475
C	-3.75781237766976	-0.22862081916347	-1.14478884177710	H	2.23031460931584	-0.01638333604454	3.71429049641023
H	-4.84294271169768	-0.35870585733190	-1.03667868238848	H	3.44857753561972	1.27023027149923	3.66061189160356
H	-3.58940137218490	0.75726188409182	-1.58827109777844	O	1.73050211467035	2.66922992878866	1.76239512662562
H	-3.41135818830007	-0.98004383779249	-1.86130781582851	C	2.71284392209396	3.60975378060323	2.20742042140922
C	-3.40074898683486	-1.75141944062201	0.83453223695095	H	3.70915750871534	3.35028756736029	1.82155644151458
H	-2.93133212501639	-1.88726363859178	1.81453774605660	H	2.40776513453582	4.57755923602213	1.80406593846876
H	-4.48548440032046	-1.86641433844498	0.95963834381856	H	2.75105556019695	3.67492438794996	3.30184739927291

Reactant complex 7e



G: -1468.03043804 Eh

H: -1467.94657950 Eh

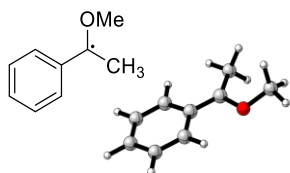
Charge: 0

Multiplicity: 2

Optimized cartesian coordinates:

C	3.69762123618153	-1.24569507510909	-0.25499133457196	H	-3.11085124299674	-2.67071529698857	0.03569543331854
C	3.26413850561699	-0.62759027607498	0.91536411738311	C	-2.34131565913541	2.76420290550729	-0.22304348434627
C	2.75729374664204	0.67359901408555	0.89079737442083	H	-2.66161439515445	2.84529424705465	0.81994037606057
C	2.71590960470578	1.34885155303679	-0.33357600278859	H	-2.04743797074325	3.76407035621787	-0.56741459443737
C	3.15638050264314	0.73632165363632	-1.50087540518467	H	-3.20984367127940	2.45816410126120	-0.81728613435120
C	3.64255924865861	-0.56850624242964	-1.46819305100657	C	-0.69190419428947	1.71952540118399	-1.84306182302243
H	4.08143512746374	-2.26141049891064	-0.21549674478613	H	-1.46988059213026	1.34929509588619	-2.51970804250239
H	3.30839996930400	-1.17779020130048	1.84986309916127	H	-0.41805972206813	2.72789595200610	-2.18218654053538
C	2.15641350145270	1.32957720578667	2.12509087704185	H	0.19176289625387	1.08477895091488	-1.95679274766860
H	3.11529652828157	1.27831275345231	-2.44190829228158	C	-0.42803614746744	-1.85191758440841	-1.55755696467675
H	3.98109086512717	-1.05051012912712	-2.38081448011507	H	0.47379587349926	-2.40704051265421	-1.84700863483640
S	-1.57235627988564	0.38920264719861	2.42896339358147	H	-1.25716065813301	-2.56824840842309	-1.53227424442373
Si	-1.59071947976490	0.03418840296741	0.30767808034247	H	-0.63596808506179	-1.12727943863839	-2.35112849264807
C	-1.17476972616765	1.78356434766819	-0.38699535699142	C	0.05603675659138	-2.27151200258023	0.87646675579177
H	-0.33377512116503	2.14355808875176	0.22417698866857	H	-0.80828484160443	-2.93253493008422	1.01195164052168
H	1.07303245712694	1.12900825923669	2.09032050129537	H	0.90629281962996	-2.89533339447328	0.57121824720872
C	-3.36621585804777	-0.50426049162024	-0.13881064483230	H	0.29229965523506	-1.82790935262588	1.84842448320103
H	-3.99010872066771	0.25404938036345	0.35885504428519	H	2.32728203413108	2.36285995569477	-0.35739308321926
C	-0.21778524998390	-1.19597341360067	-0.18404539348307	C	2.67047525287907	0.78264014277346	3.45293498649509
H	0.68332838509290	-0.56710369052794	-0.25093337293475	H	2.28490734803876	1.40299008567030	4.26731710653465
C	-3.71114425276018	-0.49323166872922	-1.63435683222049	H	2.30186855054801	-0.23473956640229	3.61251164741606
H	-4.76824237232877	-0.75458791396281	-1.77619247929379	H	3.76423096803446	0.76334681433527	3.50239340087492
H	-3.55519933034013	0.48837356255583	-2.09230211068459	O	2.23360384144595	2.75675092458686	2.04977856017753
H	-3.11901281705294	-1.22193475559684	-2.19639575153576	C	3.54869465003421	3.27985888806465	2.19668086972019
C	-3.70430902342334	-1.86667094055579	0.48578365500587	H	4.26314742746988	2.79023671877870	1.51809199814271
H	-3.51904672267134	-1.87702830457434	1.56568775516620	H	3.49028018739119	4.34190985100005	1.94460650296659
H	-4.76168974682047	-2.11336121868091	0.32464584176181	H	3.91380668462480	3.18305786050224	3.22901149807801

Radical 7e



G: -424.51170810 Eh

H: -424.46551442 Eh

Charge: 0

Multiplicity: 2

Optimized cartesian coordinates:

C	3.48628859925683	-1.57844482476505	-0.01094059382660	C	3.54952510238630	-1.07390524679014	-1.31212612726565
C	3.21383290514395	-0.74955250100066	1.06131602657074	H	3.65093464621160	-2.63776844506887	0.16686208791356
C	2.99375944131567	0.64343080421683	0.87584583545881	H	3.17025125580768	-1.18415867195447	2.05387822670270
C	3.06190577736999	1.13685316228085	-0.45871067286592	C	2.71731307879253	1.51970695218349	1.95367202171453
C	3.33289512244751	0.29117286284466	-1.51713460559315	H	3.37850139705182	0.69913850357985	-2.52348895797663

APPENDIX

H	3.76287869655341	-1.73159568828799	-2.14877085817481	O	2.42172142163178	2.80887747537189	1.58940563807524
H	2.89903019586603	2.19305788137261	-0.63609872109269	C	2.55972614031258	3.83675426981028	2.56676147441113
C	2.58128052143396	1.13913901856409	3.38677820772401	H	3.59125578501216	3.89532169905149	2.93900643536922
H	1.55509795751951	1.30263776680964	3.74658594217522	H	2.31010667876276	4.76826466366521	2.05511388486563
H	2.81877245773722	0.08726785301755	3.53711391834115	H	1.87411276407784	3.69959283297432	3.41197194111322
H	3.24765426530885	1.71859709212440	4.03799554636026				

7.4.2 Single-Crystal X-Ray Diffraction Analysis

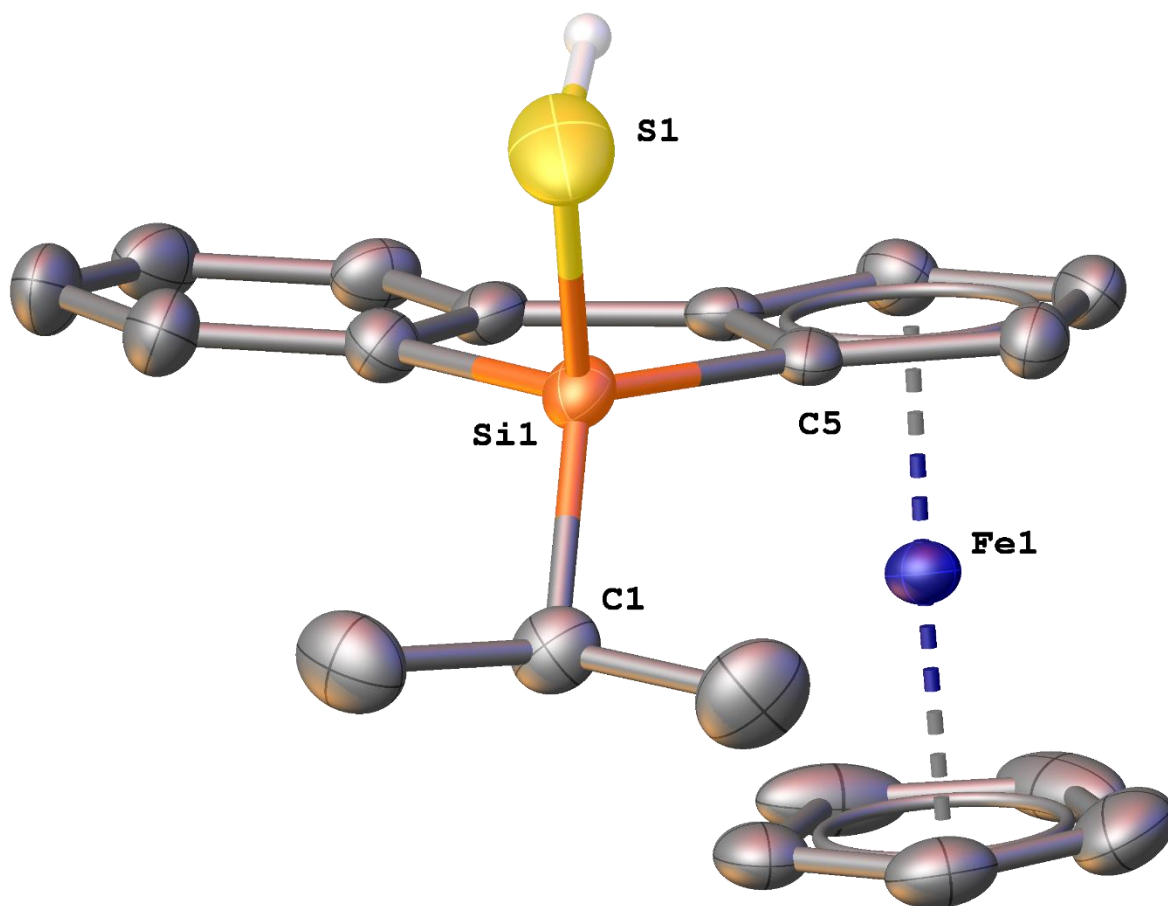
Compound **12a**: The asymmetric unit contains one molecule.

Compound **12b**: The asymmetric unit contains one molecule.

Compound	12a	12b
Data Set	AF246	AF250new_commented12b
(internal naming)		
CCDC Number	2354889	2354890
Formula	C ₁₉ H ₂₀ FeSSi	C ₂₂ H ₂₄ FeSSi
$\rho_{calc.} / \text{g}\cdot\text{cm}^{-3}$	1.403	1.413
μ / mm^{-1}	8.731	7.984
Formula Weight	364.35	404.41
Color	clear intense orange	clear intense orange
Shape	plate	irregular
Size/mm ³	0.38 x 0.22 x 0.1	0.3 x 0.2 x 0.17
T/K	12.98(10)	123.00(10)
Crystal System	orthorhombic	orthorhombic
Space Group	<i>P</i> 2 ₁ 2 ₁ 2 ₁	<i>P</i> 2 ₁ 2 ₁ 2 ₁
<i>a</i> /Å	7.5566(2)	8.348990(2)
<i>b</i> /Å	13.3052(3)	12.90523(2)
<i>c</i> /Å	17.1617(4)	17.6385(3)
α /°	90	90
β /°	90	90
γ /°	90	90
V/Å ³	1725.47(7)	1900.458(6)
Z	4	4
Z'	1	1
Wavelength/Å	1.54184	1.54184
Radiation Type	Cu K α	Cu K α
$2\theta_{min}$ /°	8.408	8.49
$2\theta_{max}$ /°	133.746	133.788
Measured Refl.	15492	1733445
Independent Refl.	3049	3366
R_{int}	0.0866	0.071224
Parameters	205	226
Restraints	0	910
Largest Peak	0.50	0.790
Deepest Hole	-0.79	-0.935
GooF	1.031	1.03254
wR_2 (all data)	0.1217	0.158447
wR_2	0.1175	0.155114
R_1 (all data)	0.0538	0.0603588
R_1	0.0475	0.057259

12a

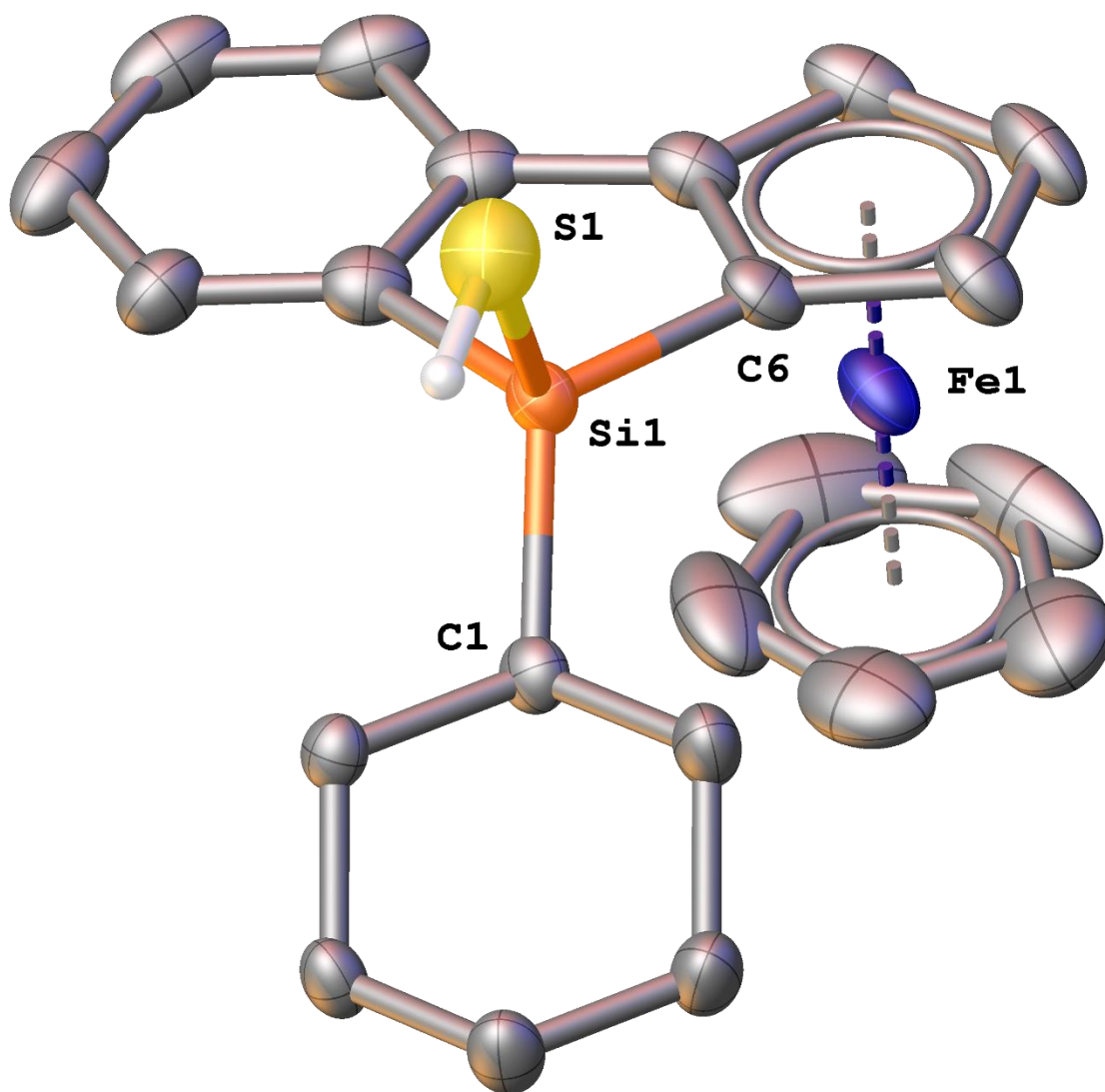
Hydrogen atoms except S–H are omitted for clarity.



Selected Bond Lengths in Å		Selected Bond Angles in °	
Si(1)–S(1)	2.122(2)	C(1)–Si(1)–S(1)	105.9(2)
Si(1)–C(1)	1.868(6)	C(1)–Si(1)–C(5)	118.4(3)
Si(1)–C(5)	1.857(6)	S(1)–Si(1)–C(5)	112.72(17)

12b

Hydrogen atoms except S–H are omitted for clarity.



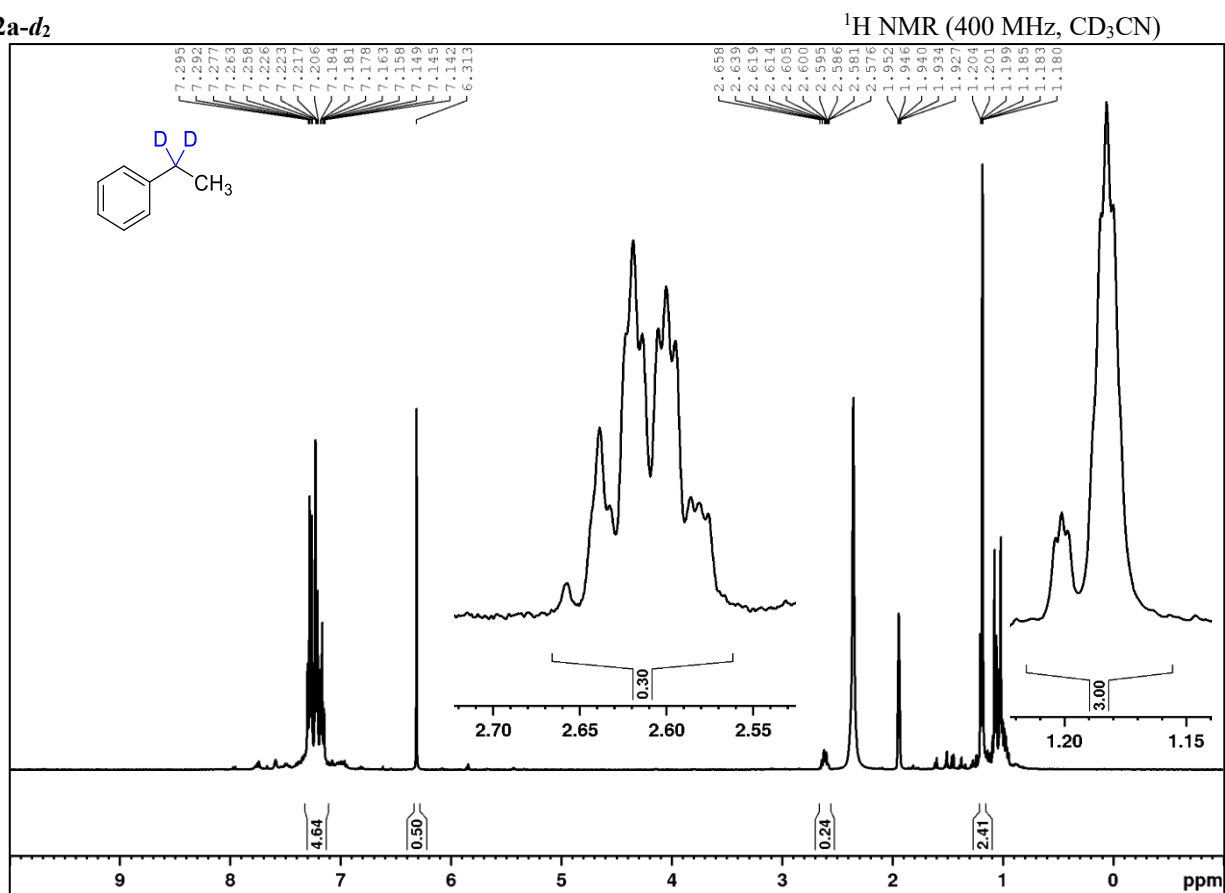
Selected Bond Lengths in Å		Selected Bond Angles in °	
Si(1)–S(1)	2.132(3)	C(1)–Si(1)–S(1)	109.2(2)
Si(1)–C(1)	1.865(7)	C(1)–Si(1)–C(6)	117.2(3)
Si(1)–C(6)	1.846(7)	S(1)–Si(1)–C(6)	111.4(2)

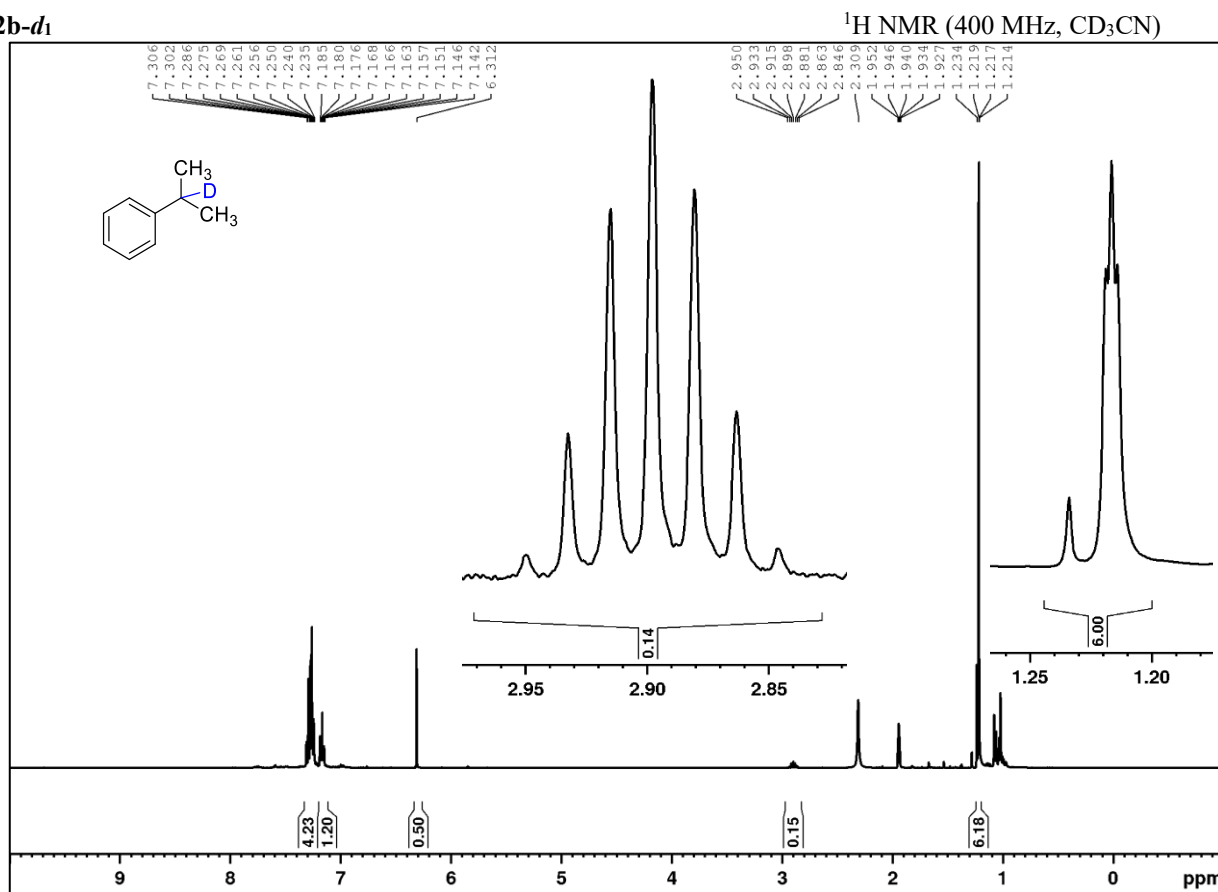
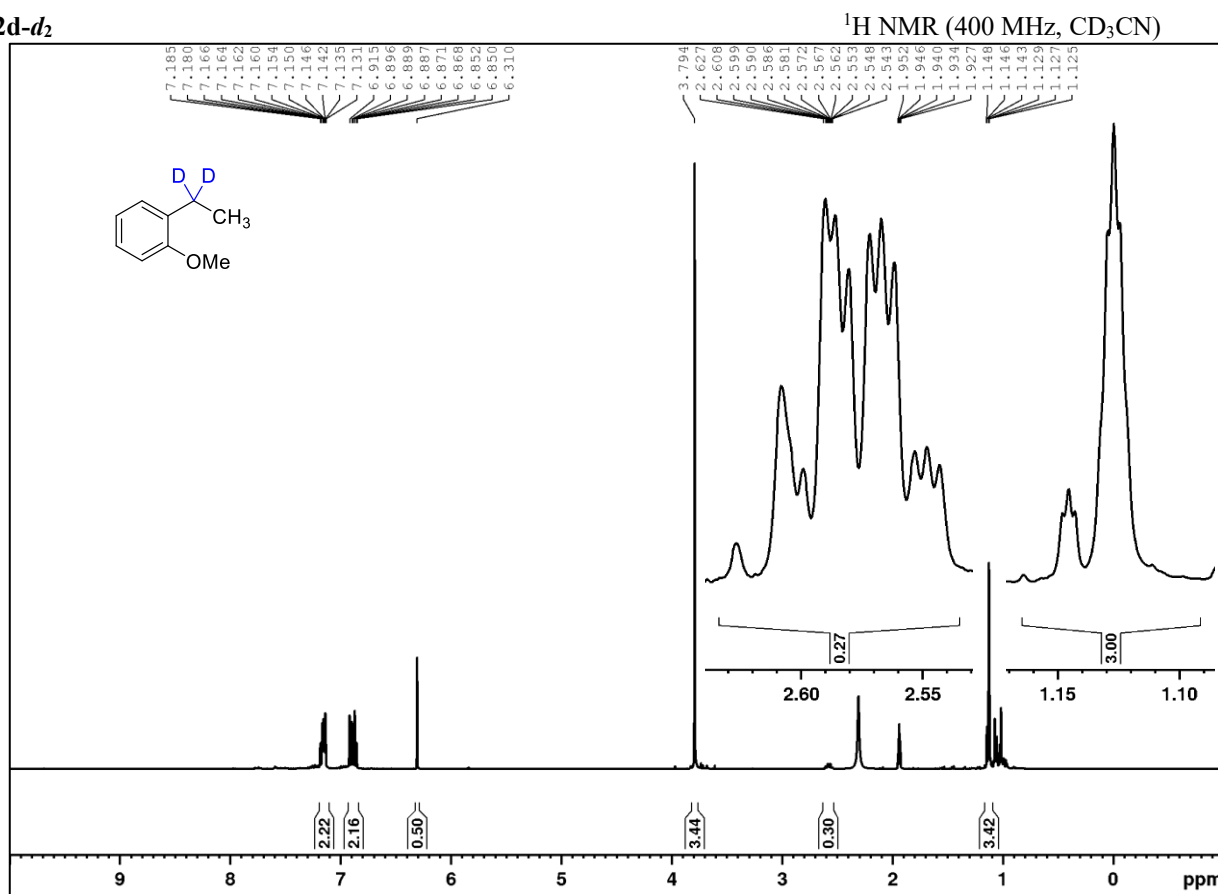
7.4.3 NMR spectra

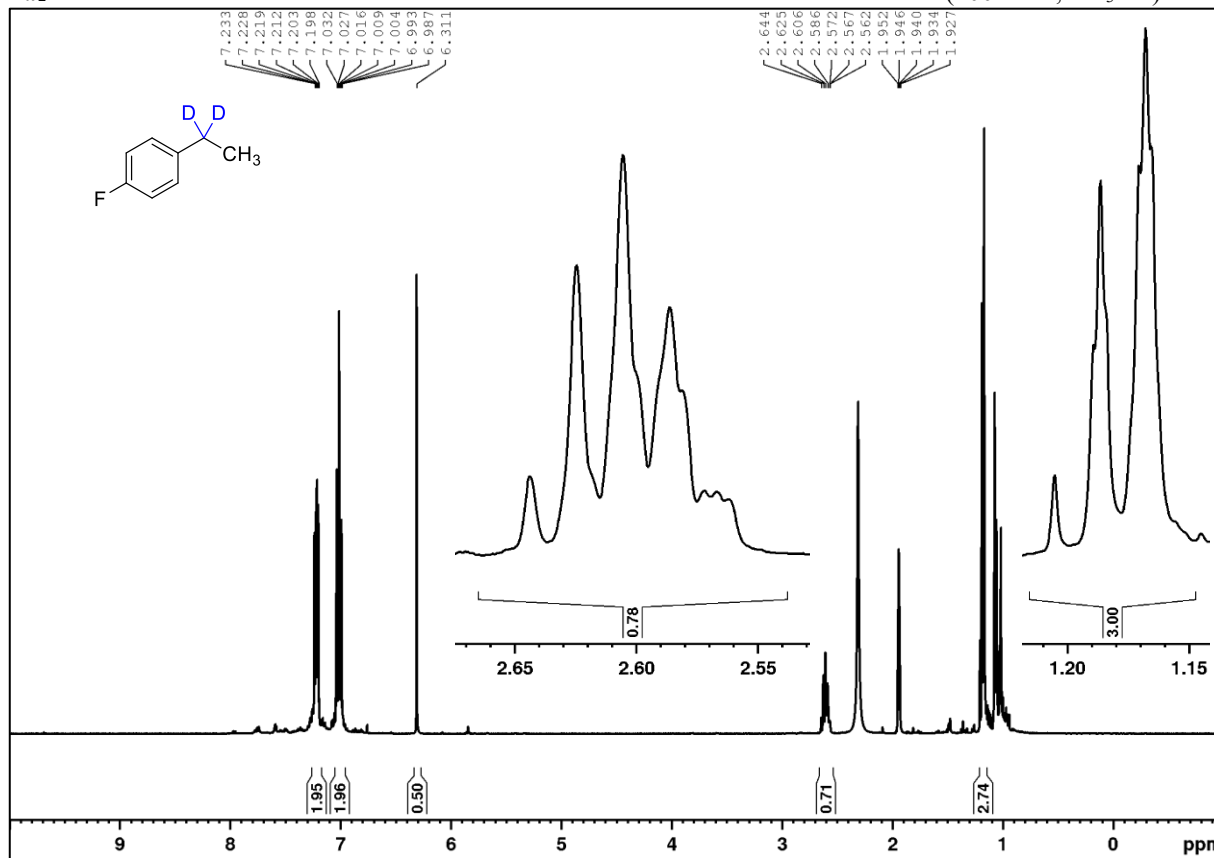
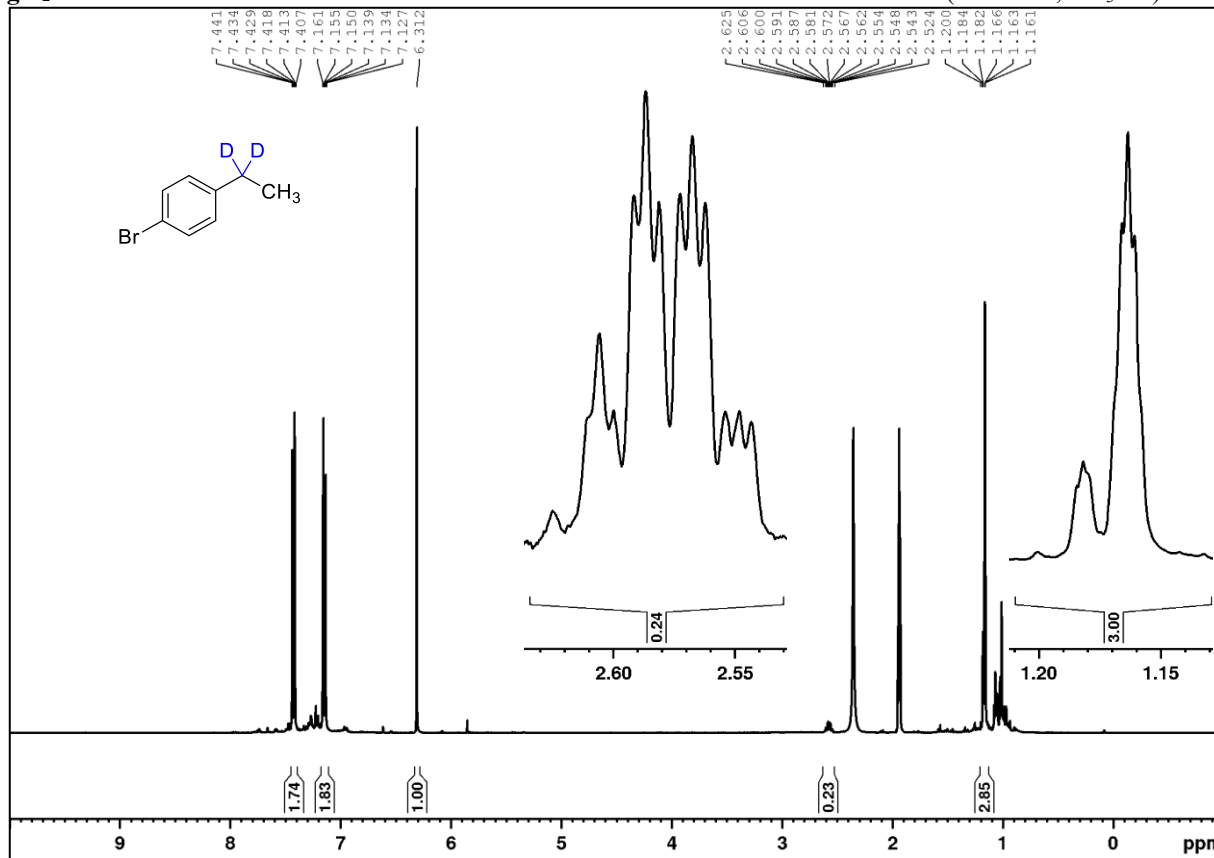
7.4.3.1 NMR spectra of crude reaction mixtures for determination of deuteration degrees

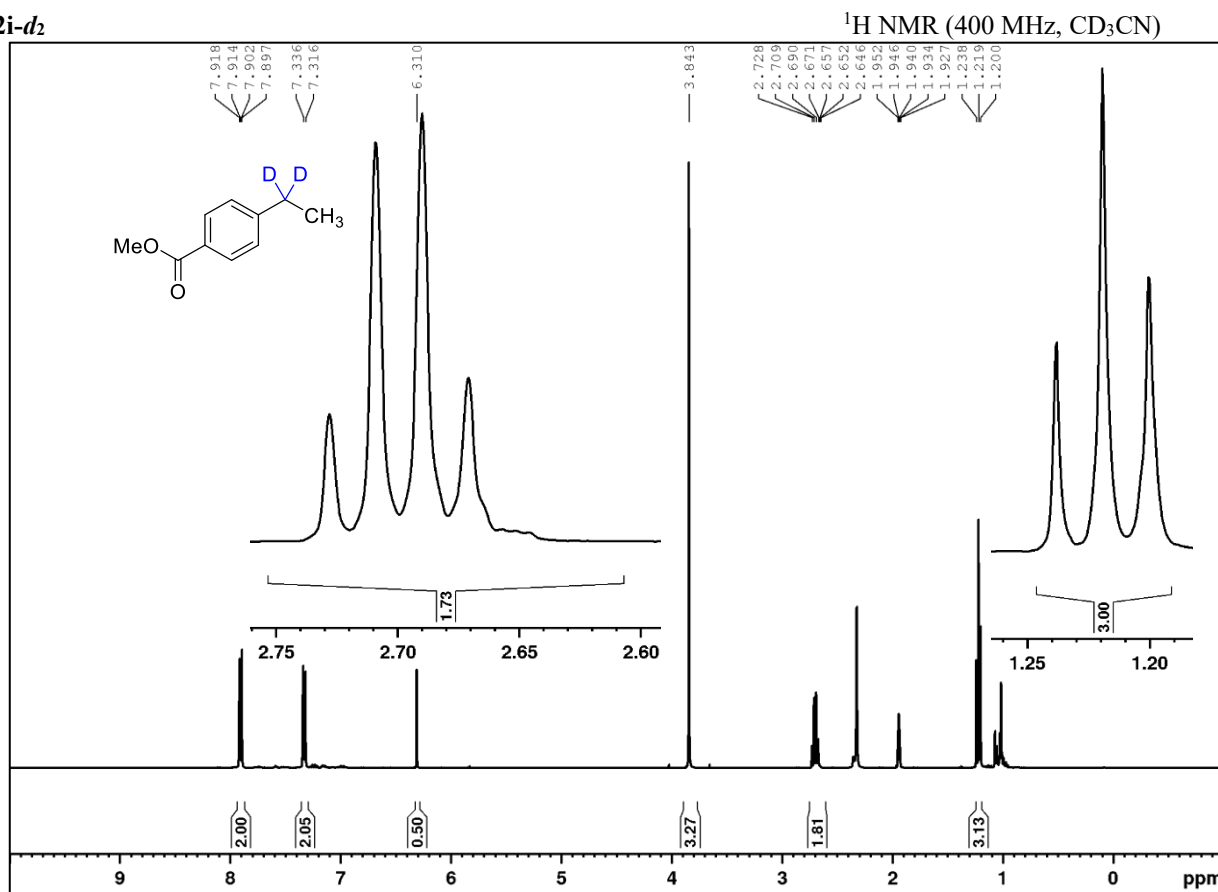
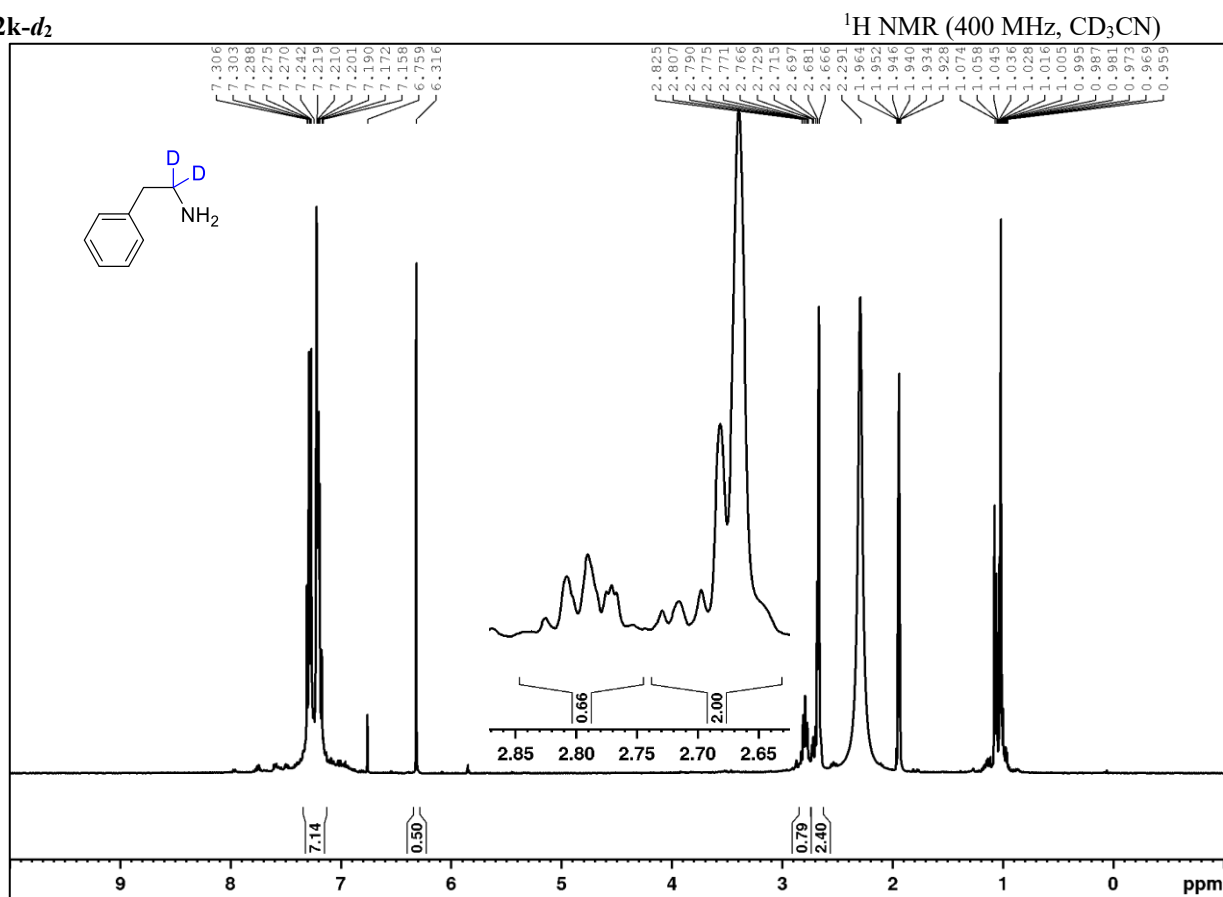
NMR spectra were recorded with 1,1,2,2-tetrachloroethane or the CD_3CN residual signal as standard for integration. The large spectra are calibrated with respect to the standard. Inserted individual peaks are added for the benzylic positions and neighboring positions influenced by the deuteration. These are calibrated on a well separated reference proton in the molecule for determination of the deuteration degrees.

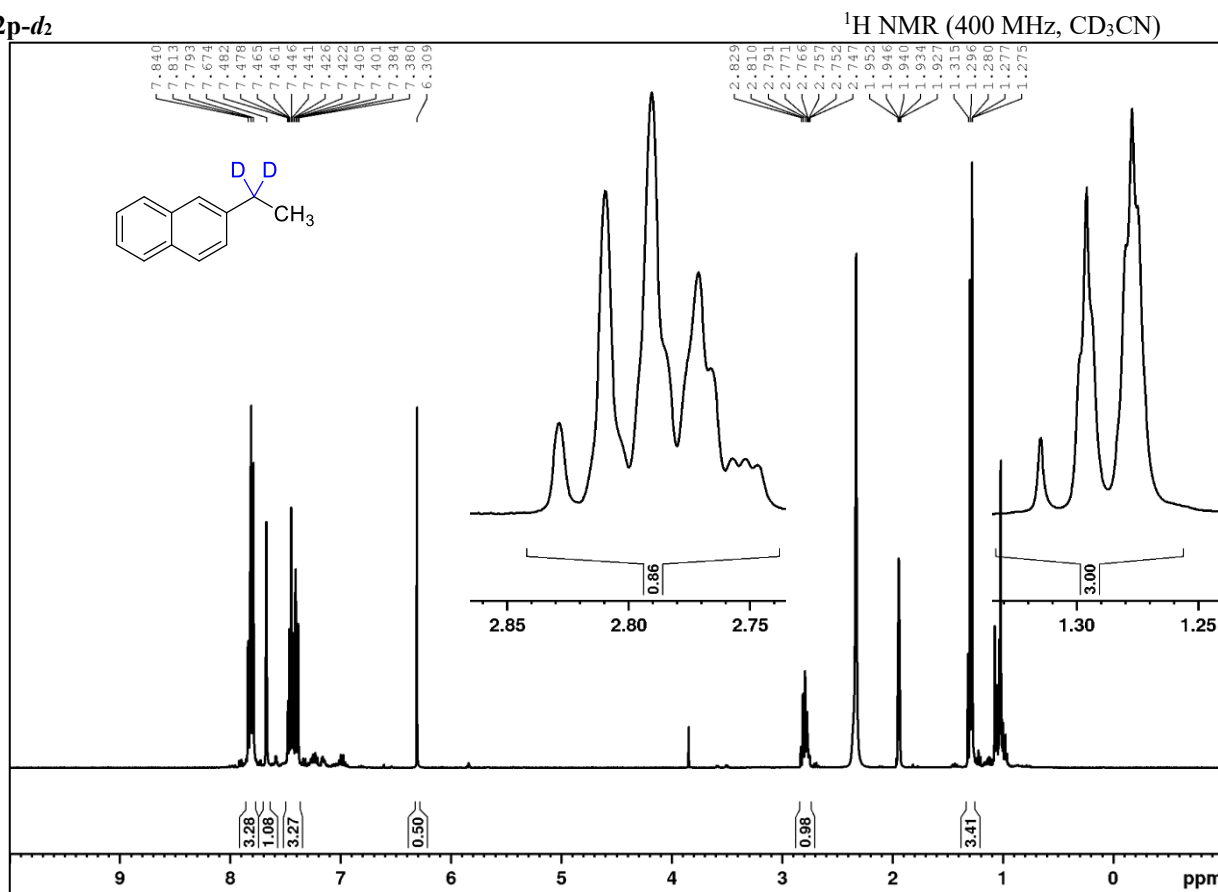
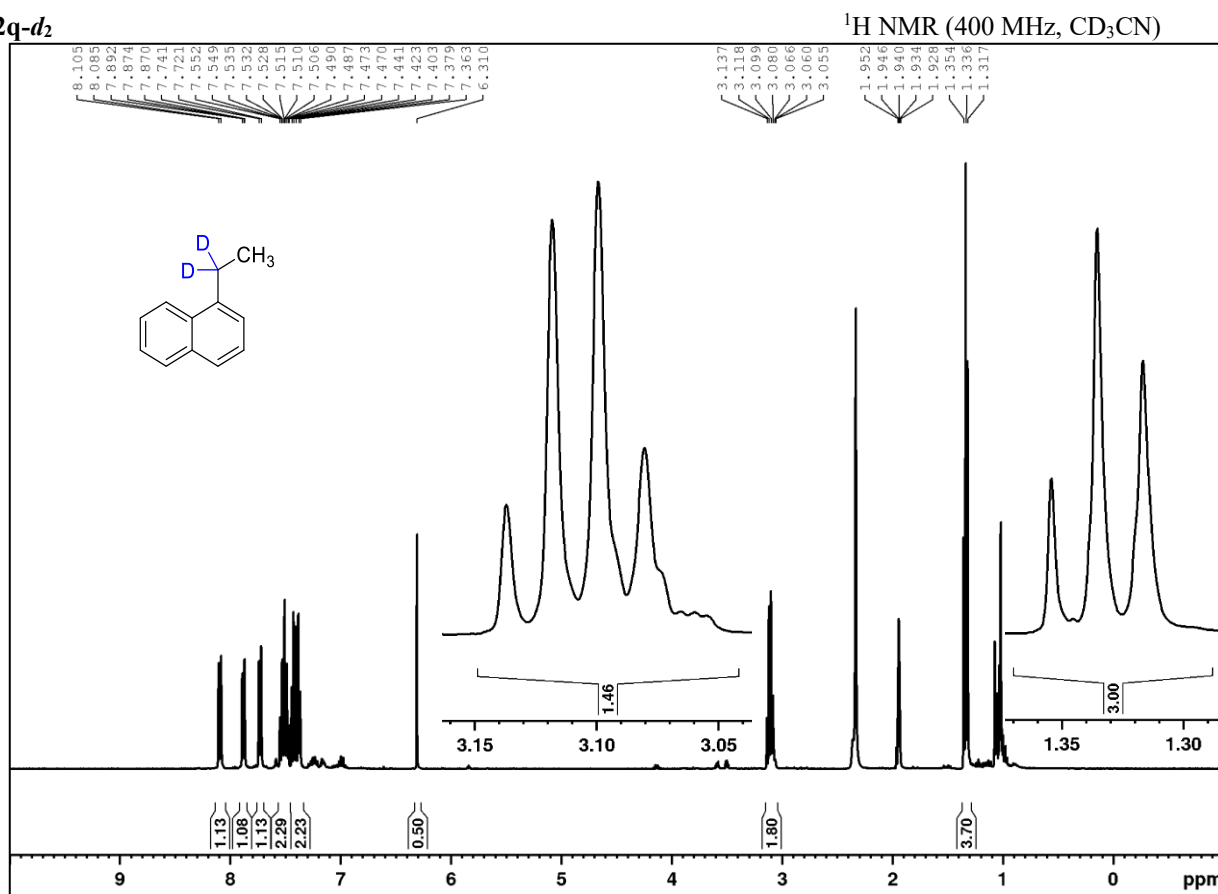
2a- d_2

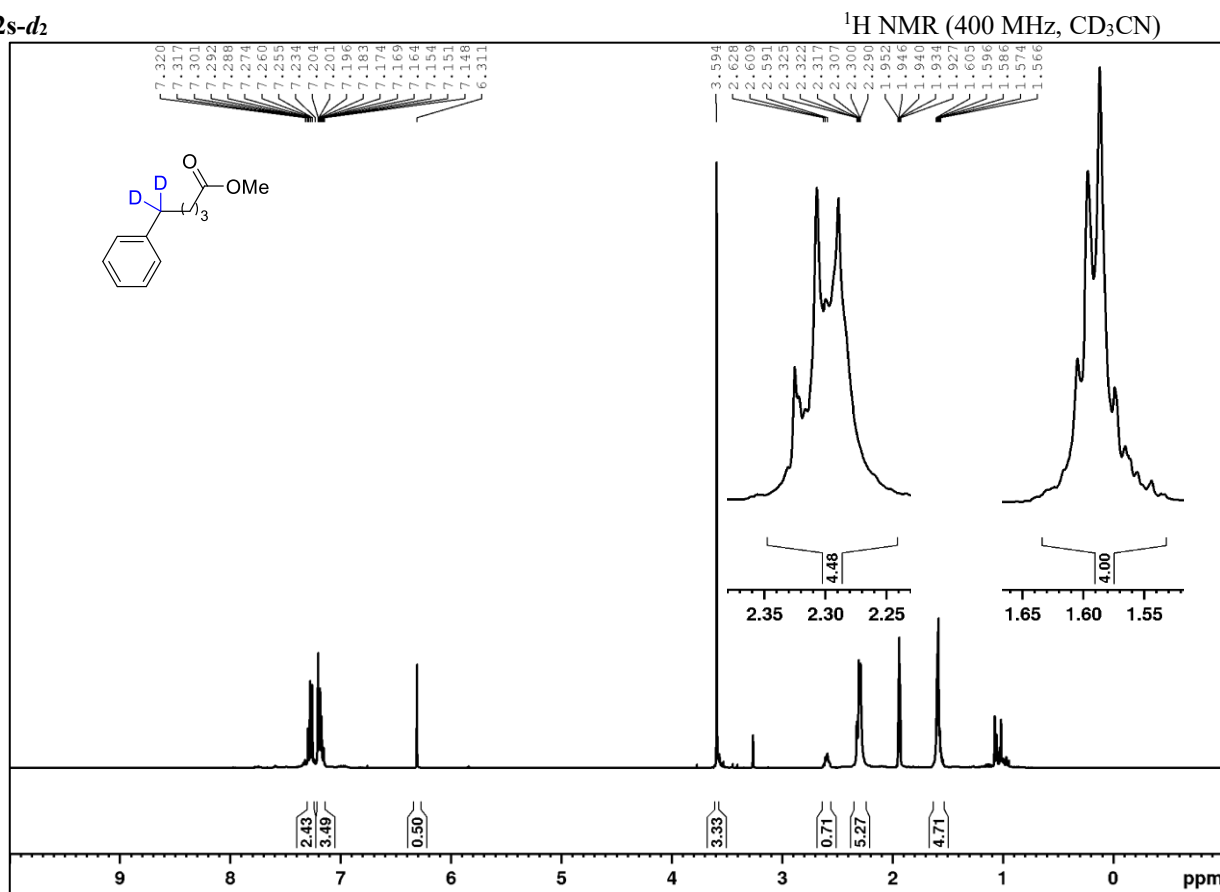
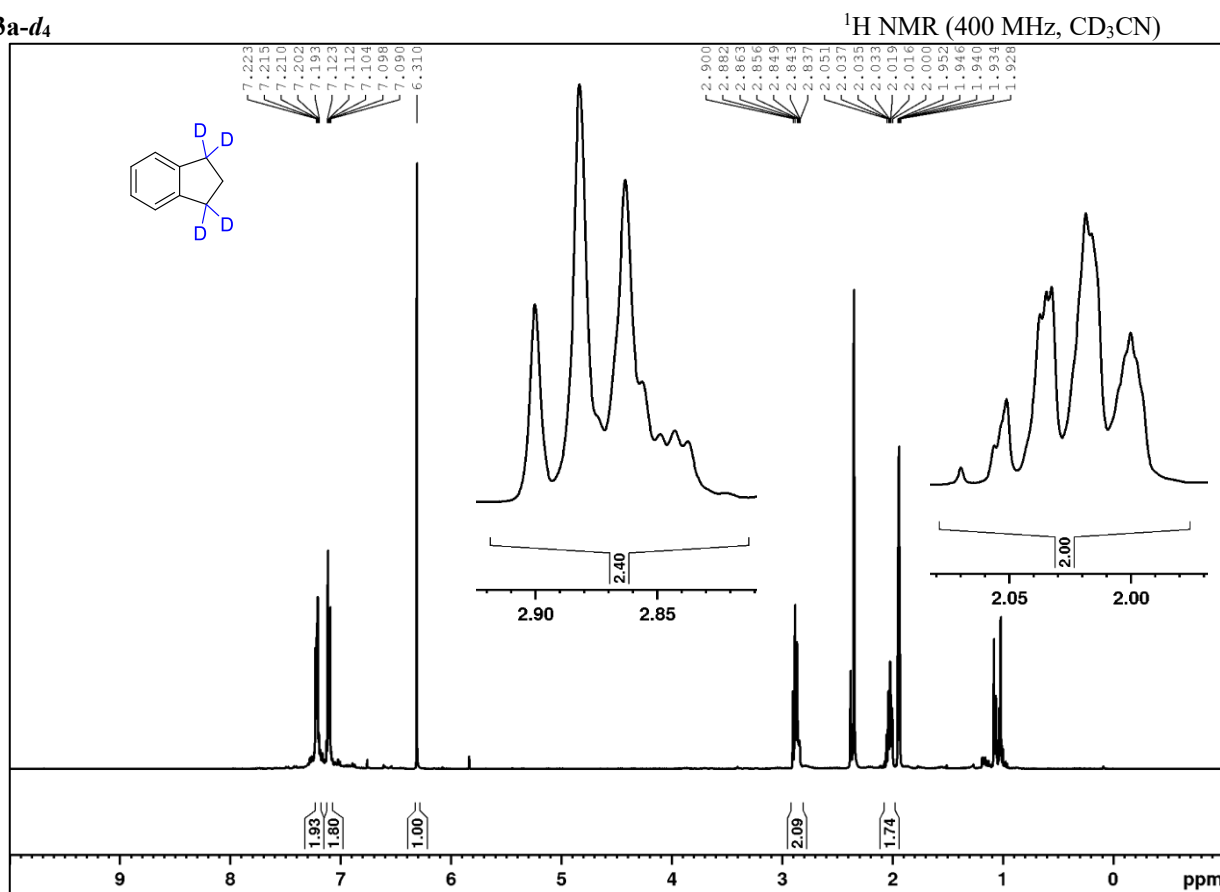


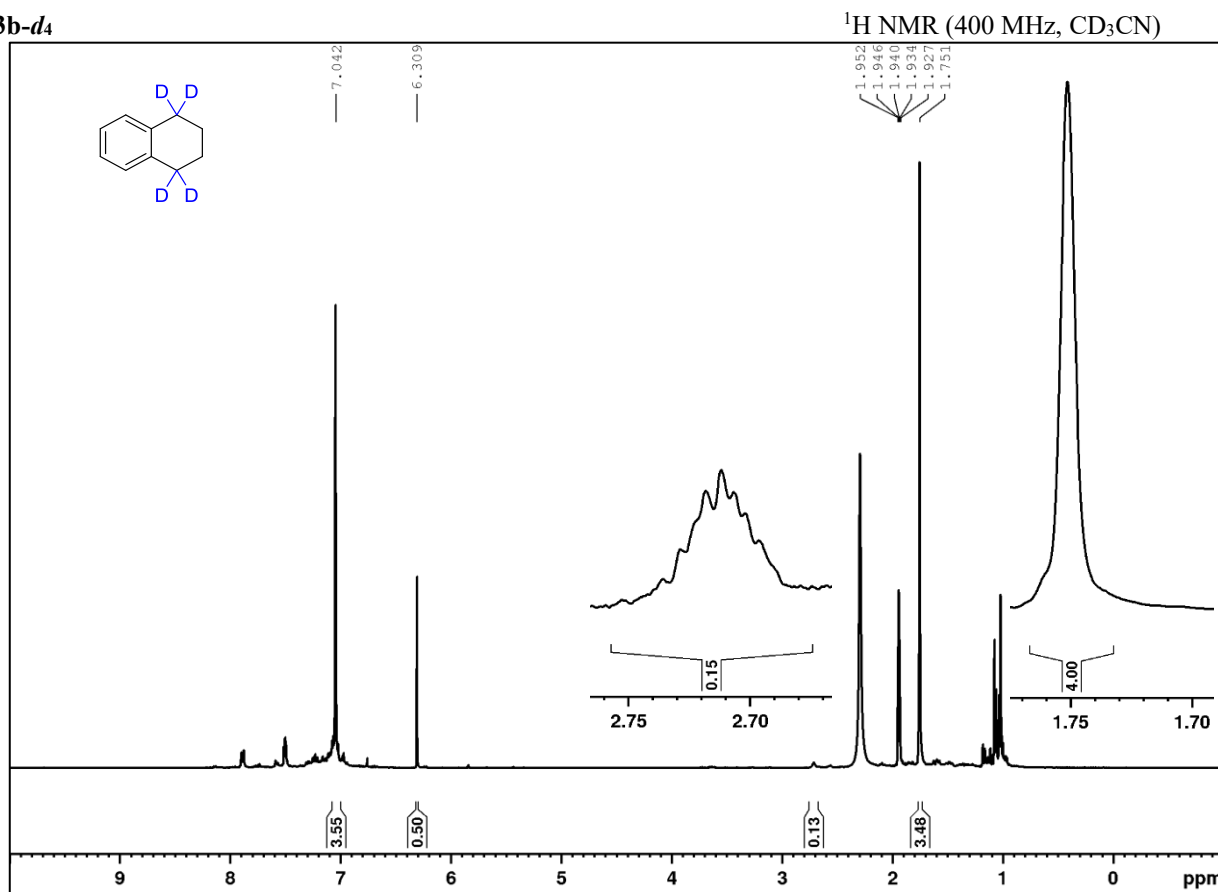
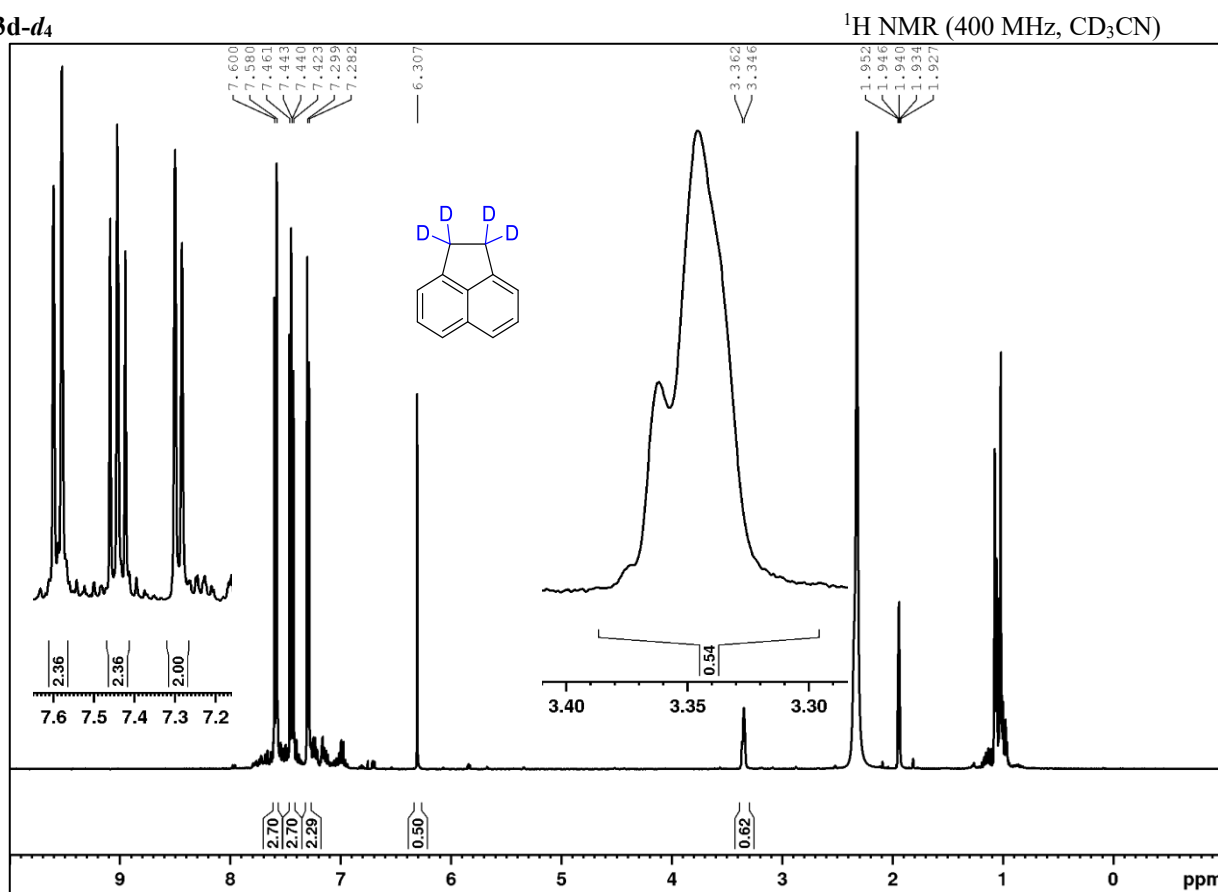
2b-d₁2d-d₂

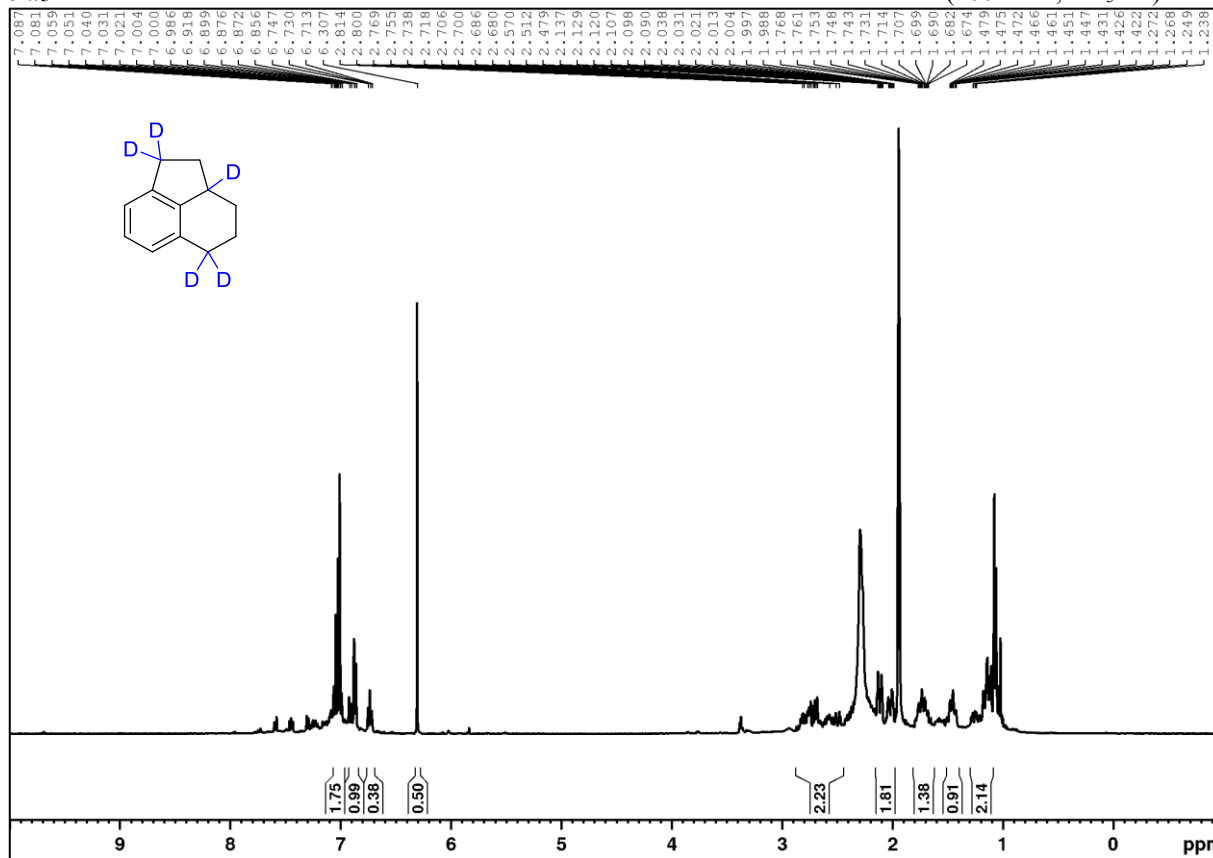
2f-d₂**¹H NMR (400 MHz, CD₃CN)****2g-d₂****¹H NMR (400 MHz, CD₃CN)**

2i-d₂**2k-d₂**

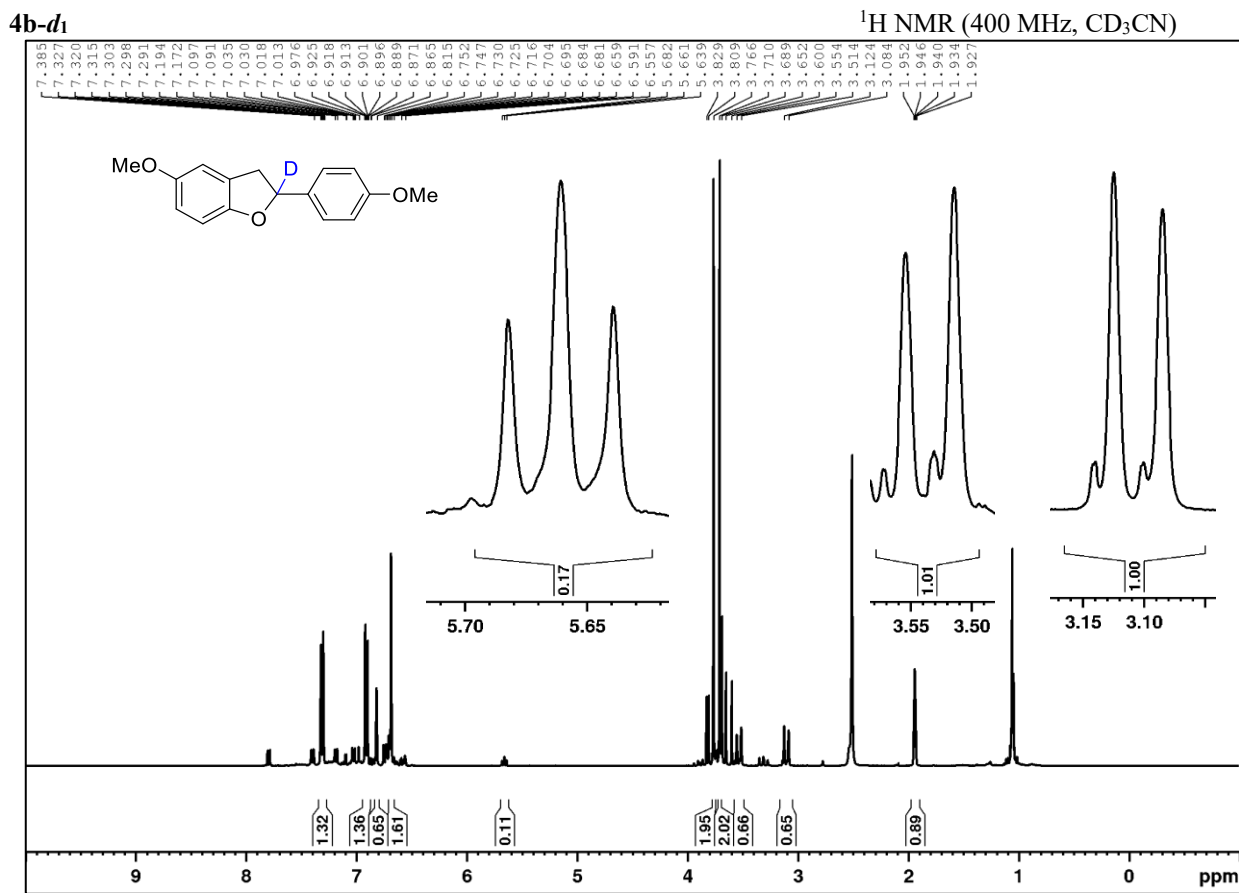
2p-d₂2q-d₂

2s-d₂**3a-d₄**

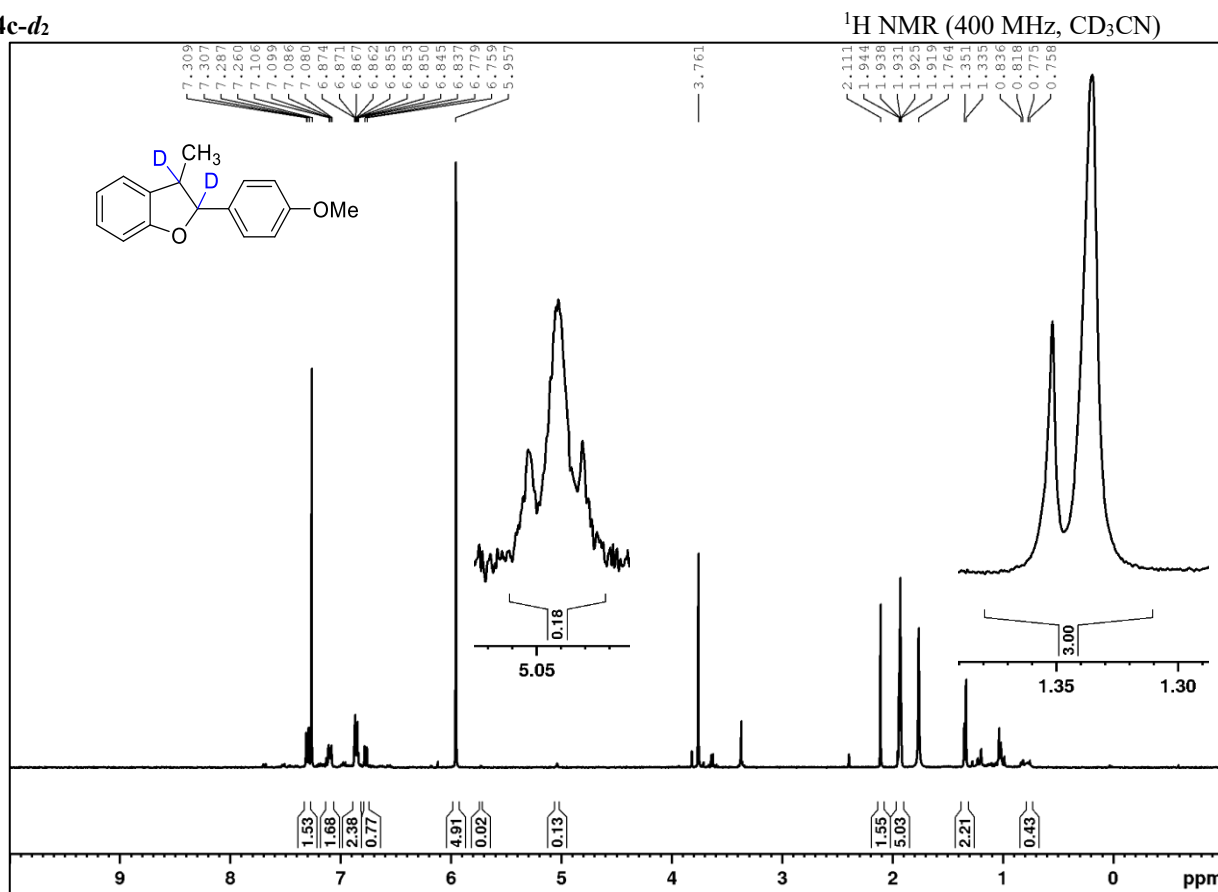
3b-d₄3d-d₄

3e-d₅**¹H NMR (400 MHz, CD₃CN)**

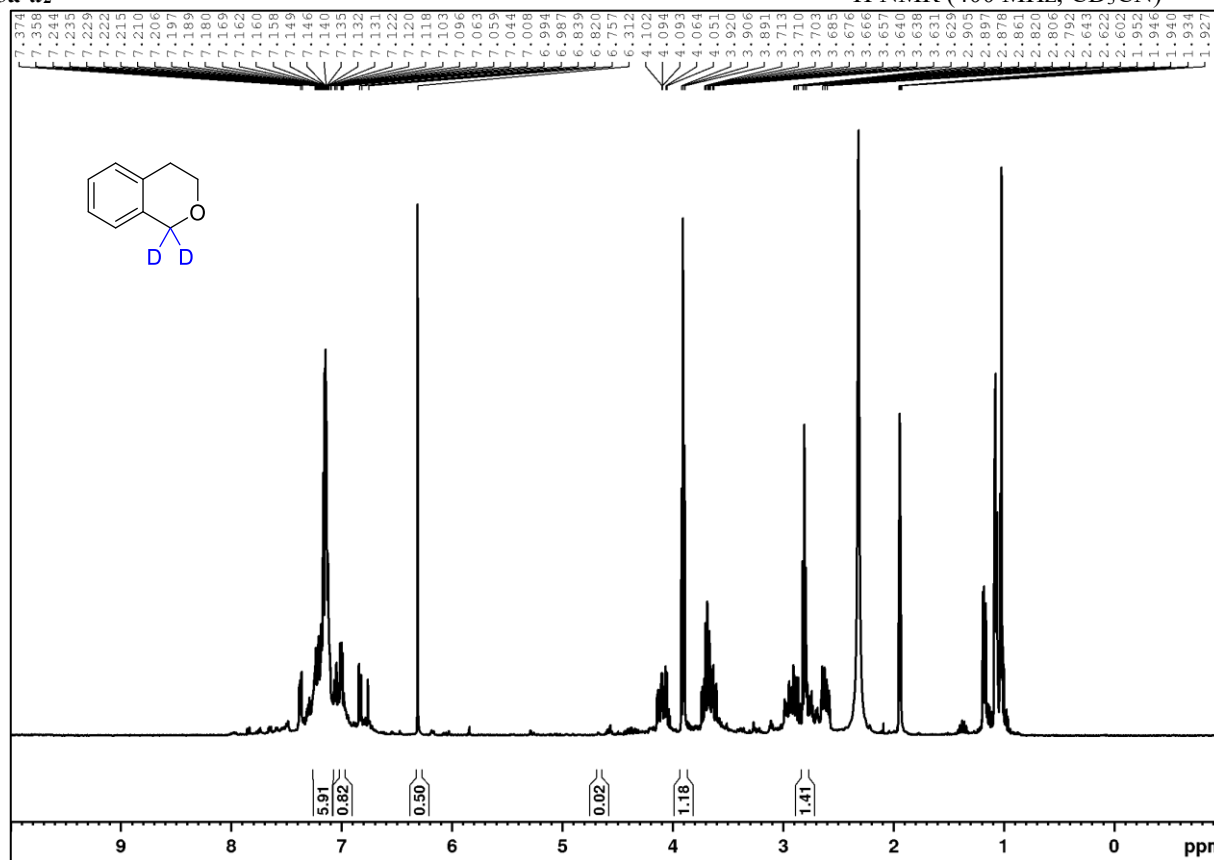
¹H and ¹³C NMR of the isolated compound can be found in section 7.4.3.2. Due to overlaps in the benzylic positions the deuteration was determined from the isolated compound.



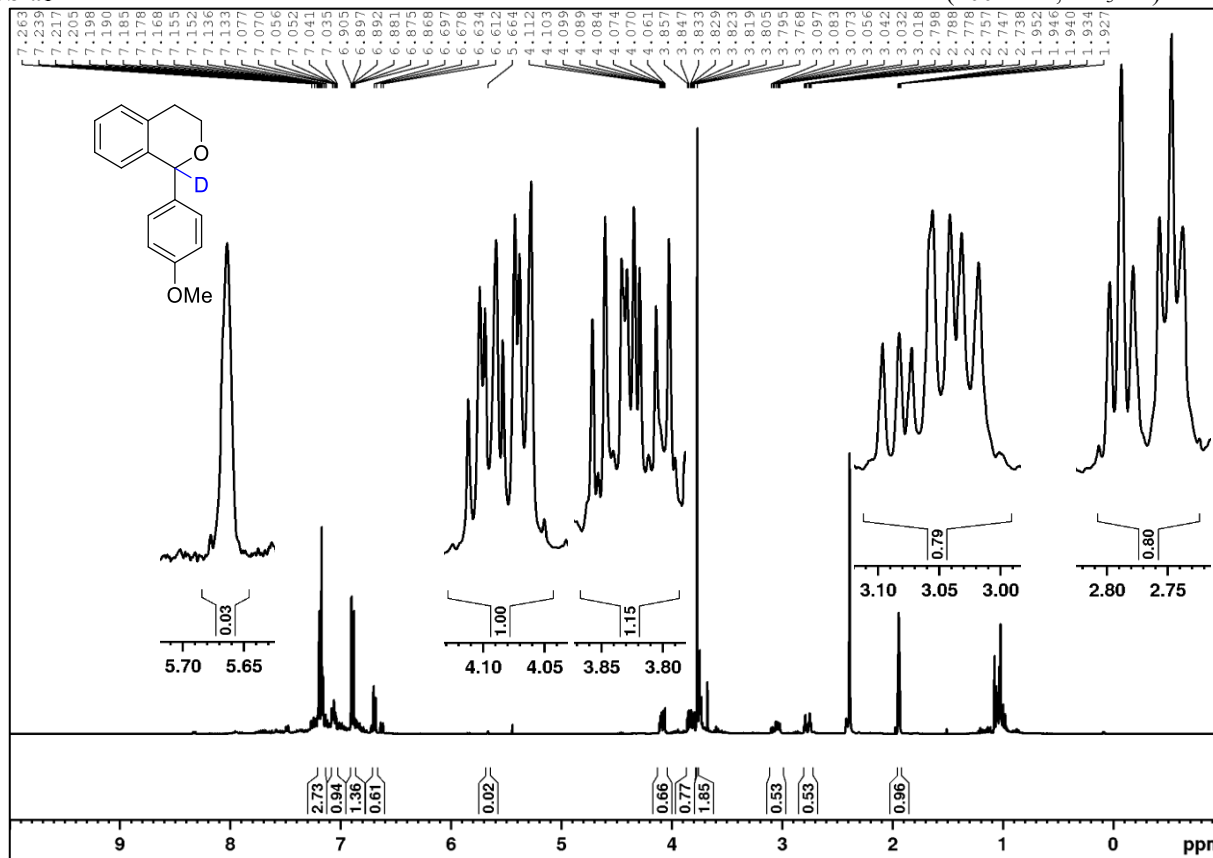
NMR spectra of the isolated compound can be found in section 7.4.3.2.

4c-d₂

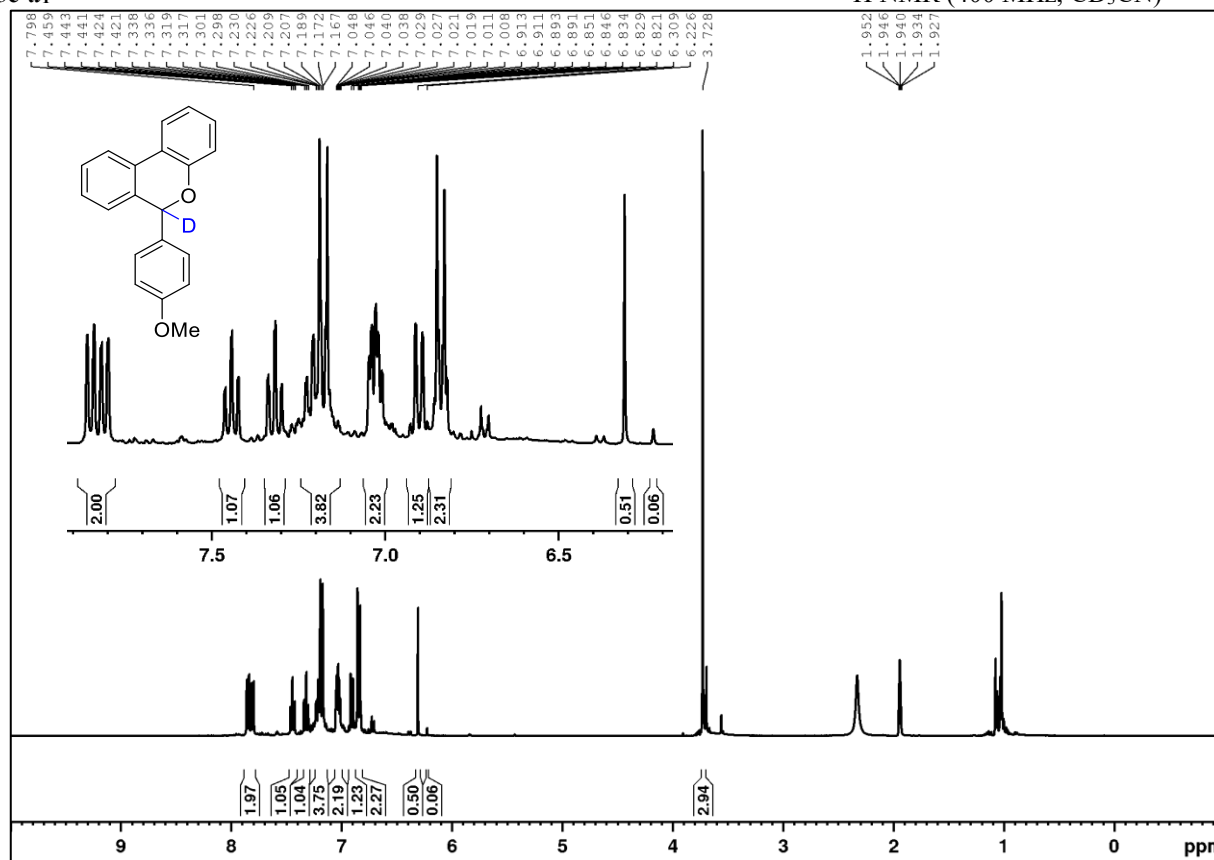
This ¹H NMR spectrum was part of the respective kinetics experiment in section 4.4.6. A 50 μ L aliquot was taken after 1 h of irradiation and diluted with 500 μ L CDCl₃. 1,1,2,2-tetrachloroethane was added as internal standard but the solvent residual signal of CD₃CN turned out to be more consistent as thus used as internal standard.

5a-d₂¹H NMR (400 MHz, CD₃CN)

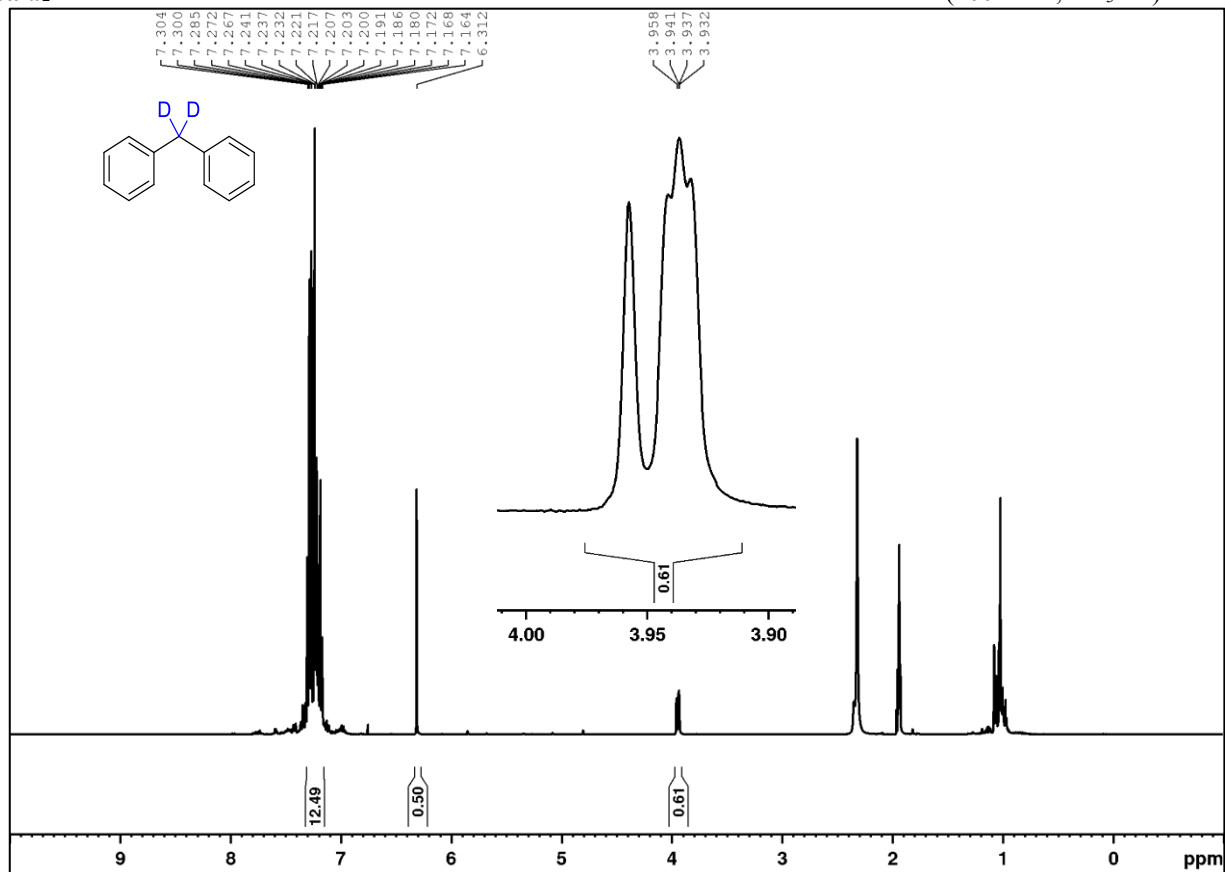
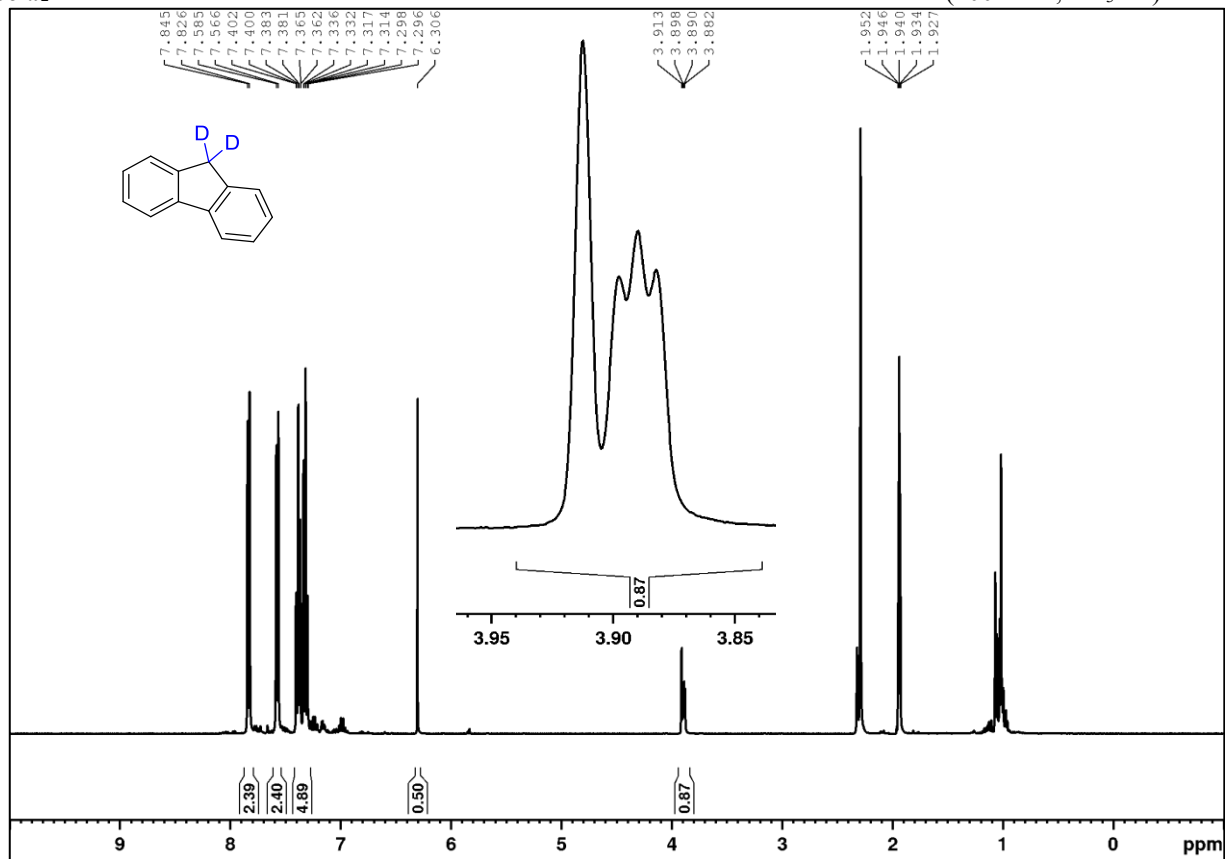
For spectra of the isolated compound see section 7.4.3.2.

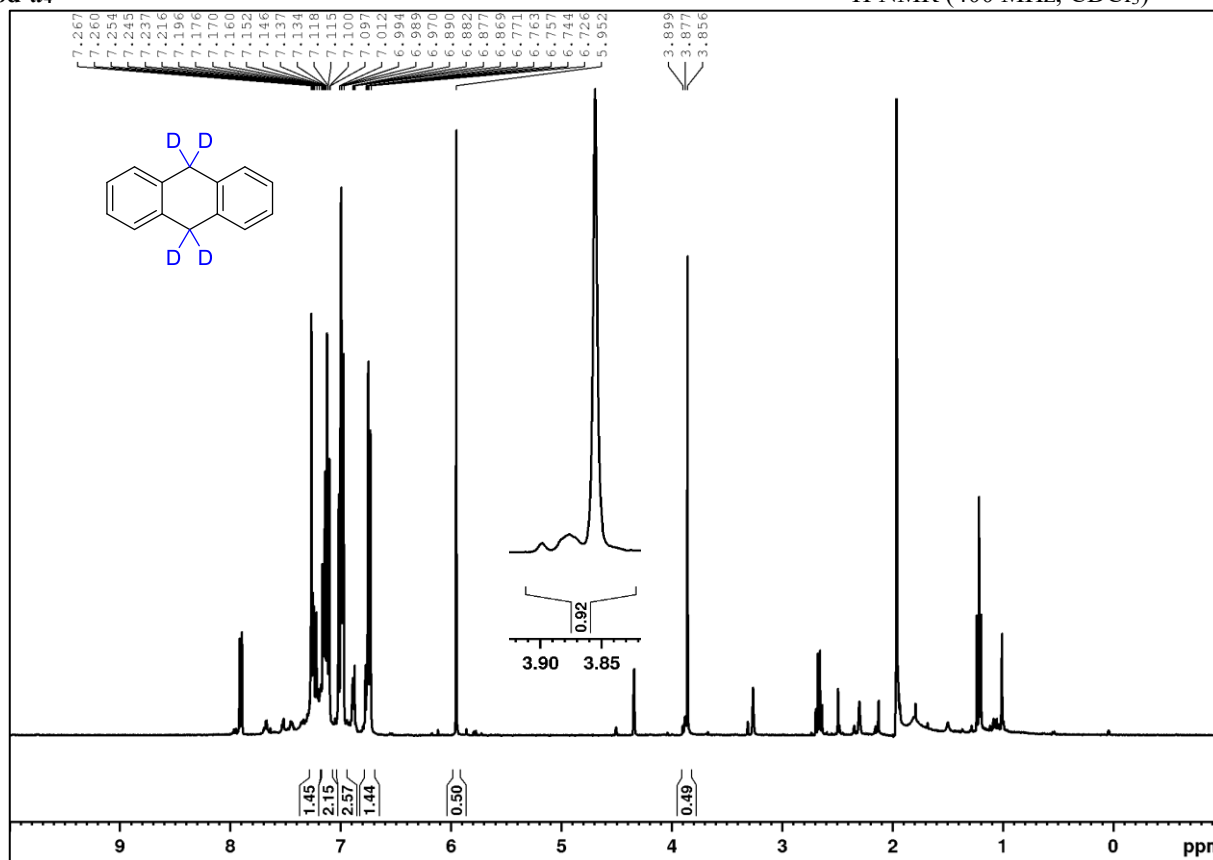
5b-d₁¹H NMR (400 MHz, CD₃CN)

The solvent residual signal was used as internal standard. For spectra of the isolated compound see section 7.4.3.2.

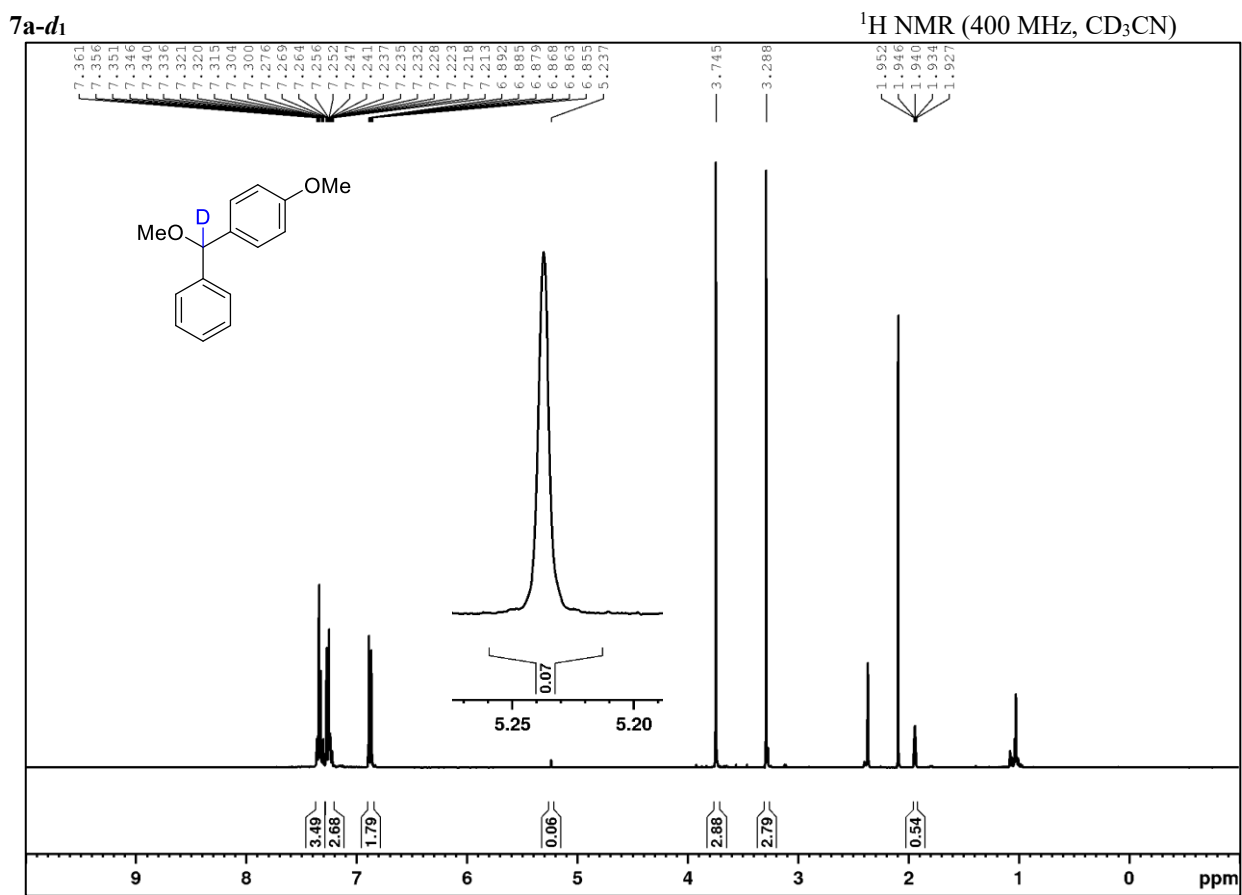
5c-d₁¹H NMR (400 MHz, CD₃CN)

For spectra of the isolated compound see section 7.4.3.2.

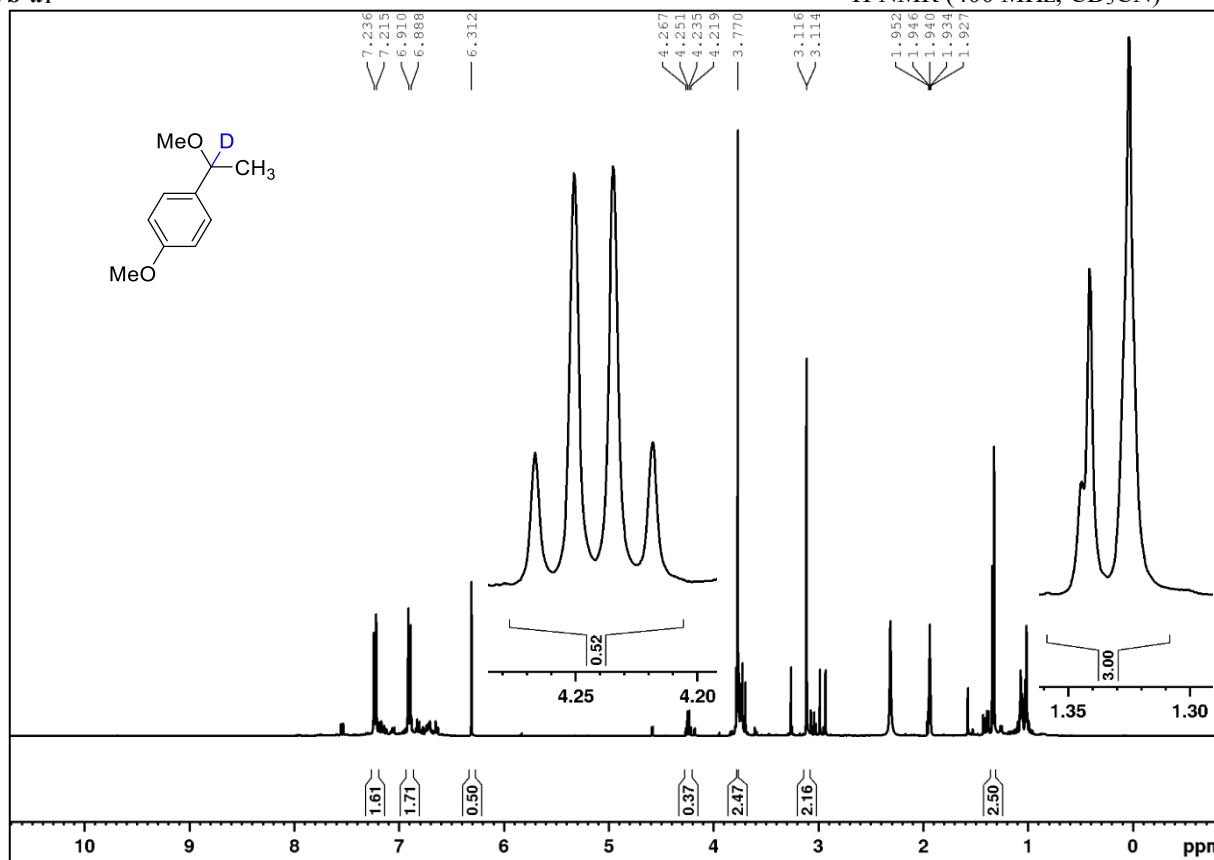
6a-d₂¹H NMR (400 MHz, CD₃CN)**6c-d₂**¹H NMR (400 MHz, CD₃CN)

6d-d₄¹H NMR (400 MHz, CDCl₃)

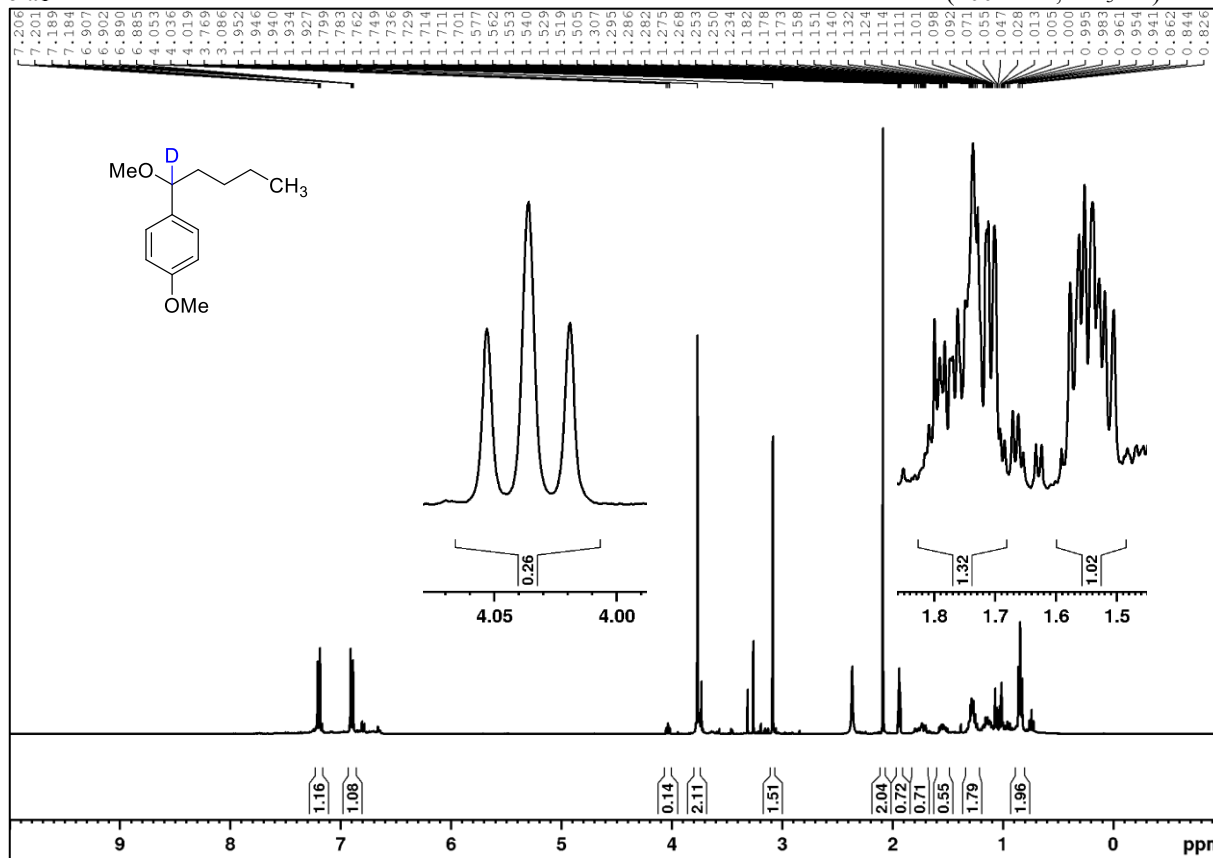
Due to low solubility of compound **6d** in CD₃CN the solvent was removed under reduced pressure and the crude product redissolved in CDCl₃ with 1,1,2,2-tetrachloroethane as internal standard.



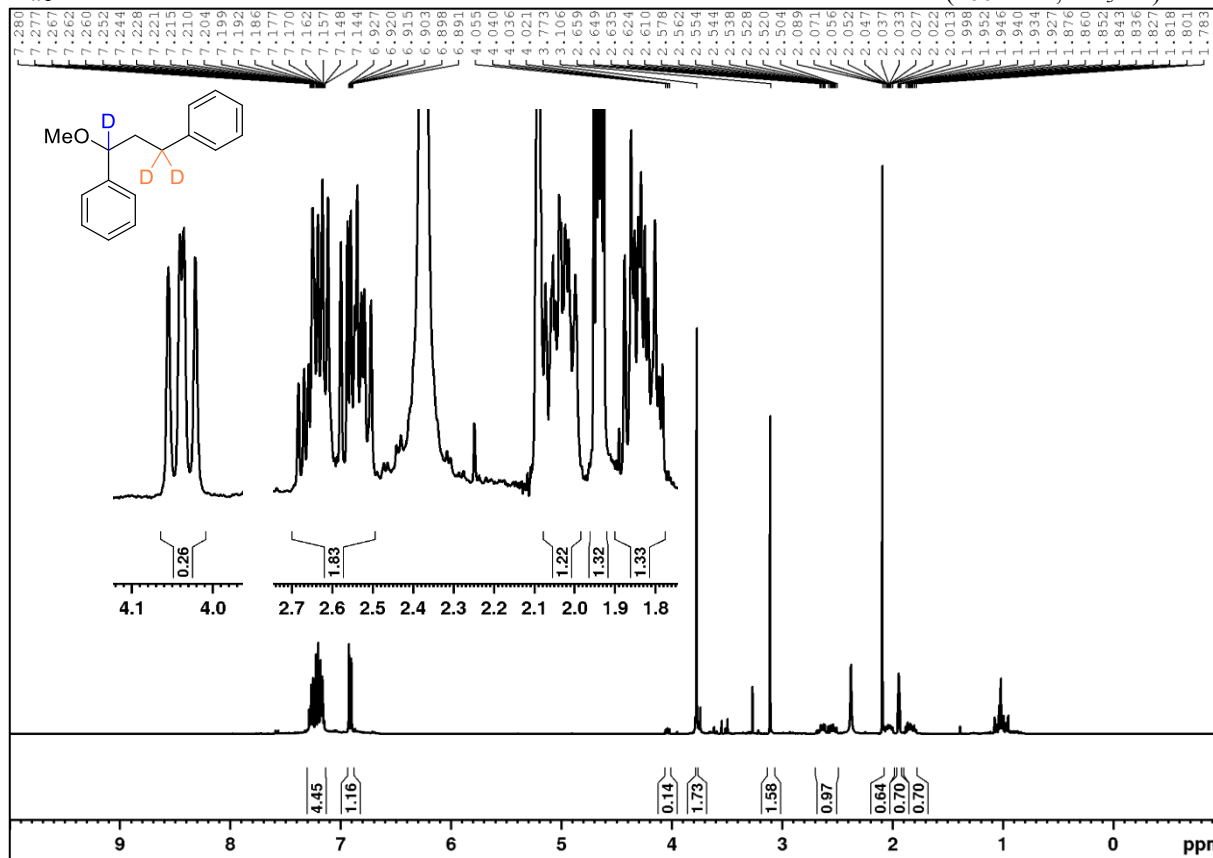
The solvent residual signal was used as internal standard. For spectra of the isolated compound see section 7.4.3.2.

7b-d₁¹H NMR (400 MHz, CD₃CN)

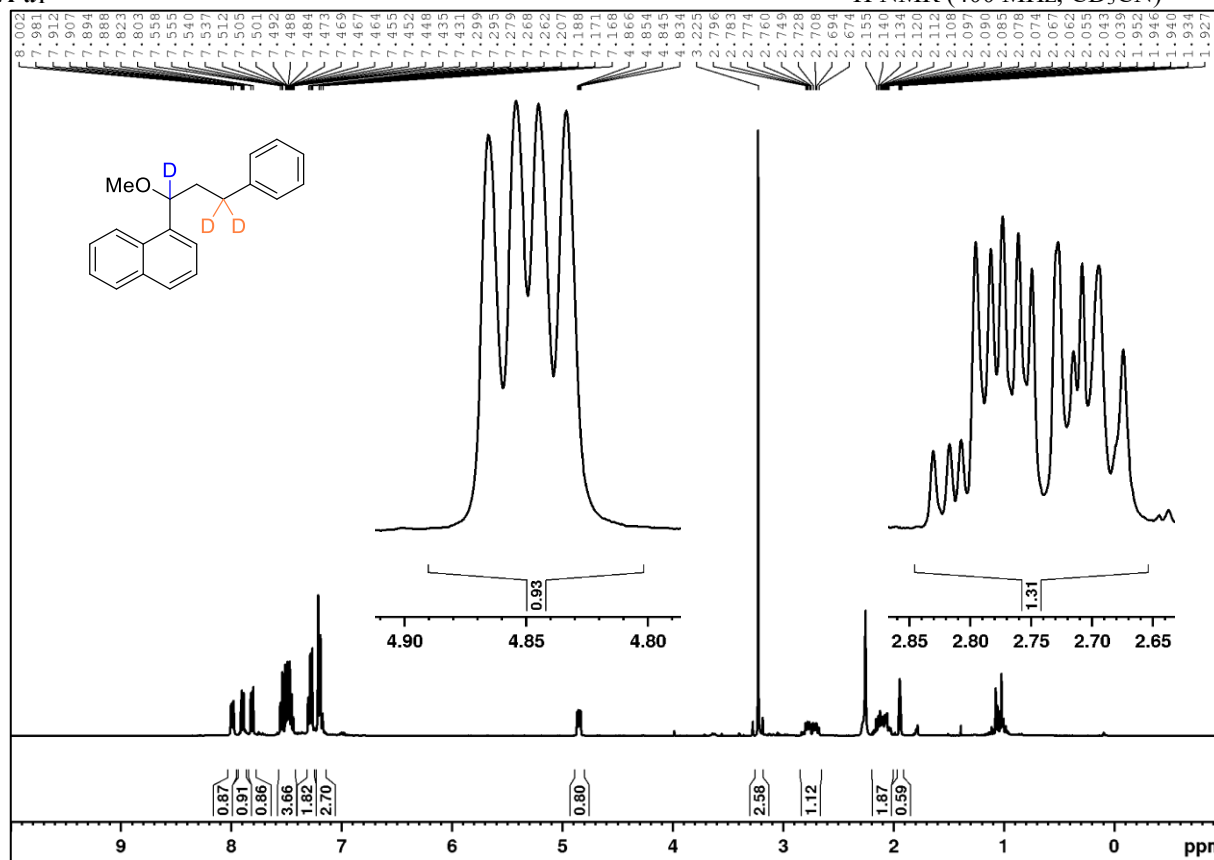
For spectra of the isolated compound see section 7.4.3.2.

7c-d₁¹H NMR (400 MHz, CD₃CN)

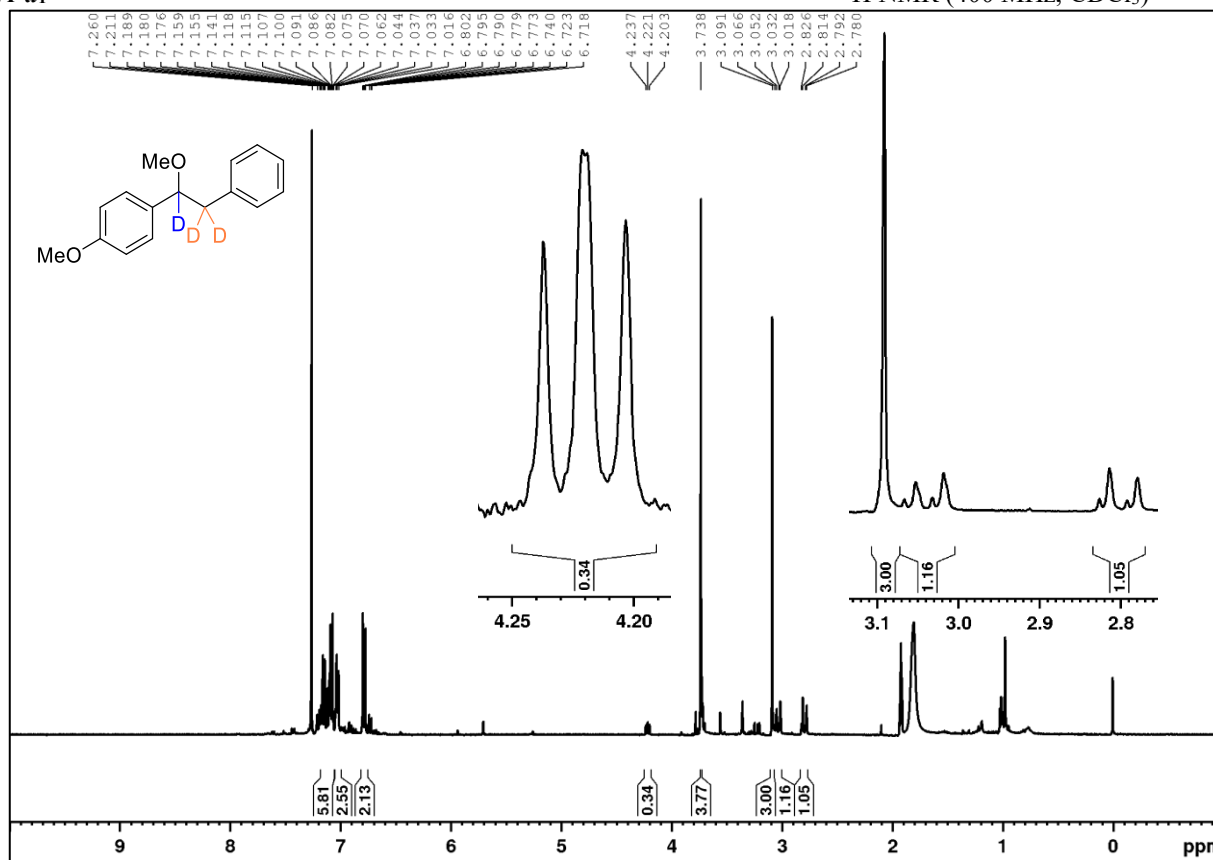
The solvent residual signal was used as internal standard.

7k-d₁¹H NMR (400 MHz, CD₃CN)

The solvent residual signal was used as internal standard. For spectra of the isolated compound see section 7.4.3.2.

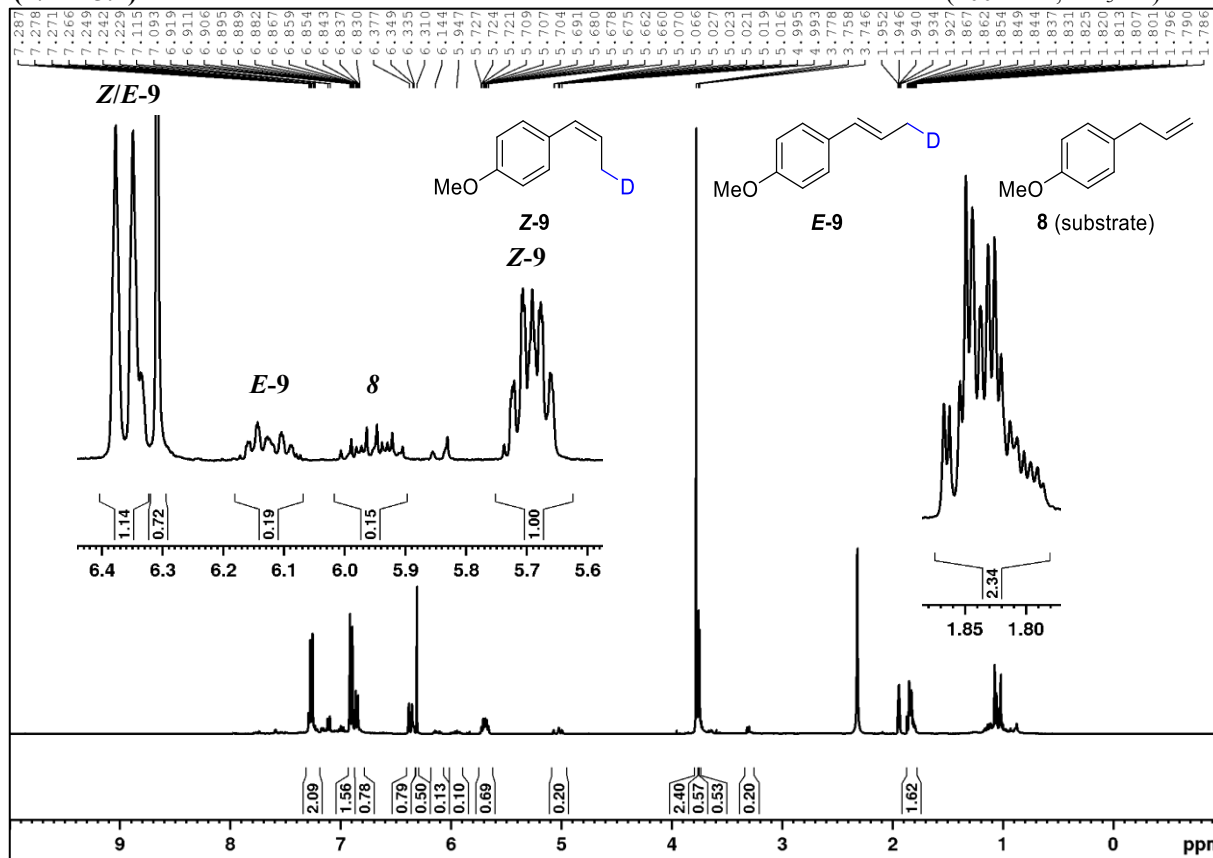
7i-d₁¹H NMR (400 MHz, CD₃CN)

The solvent residual signal was used as internal standard.

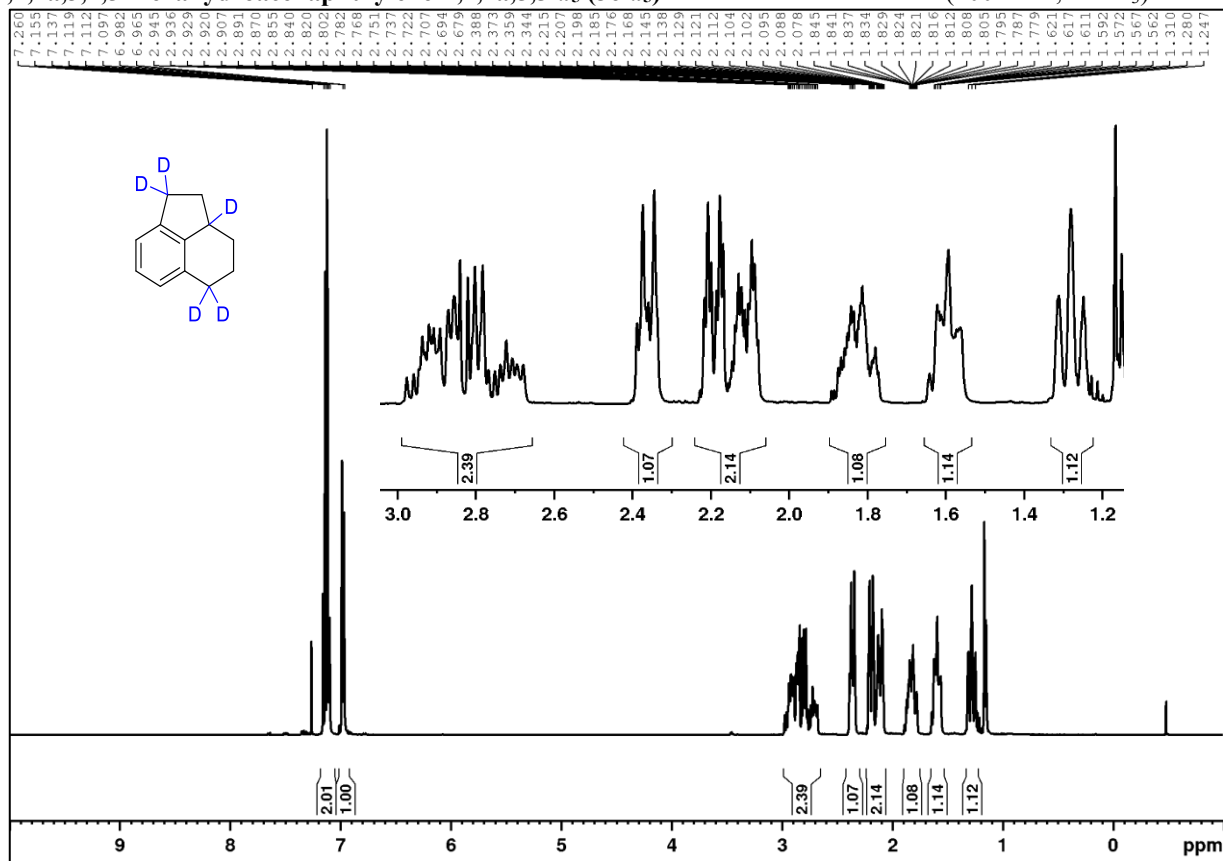
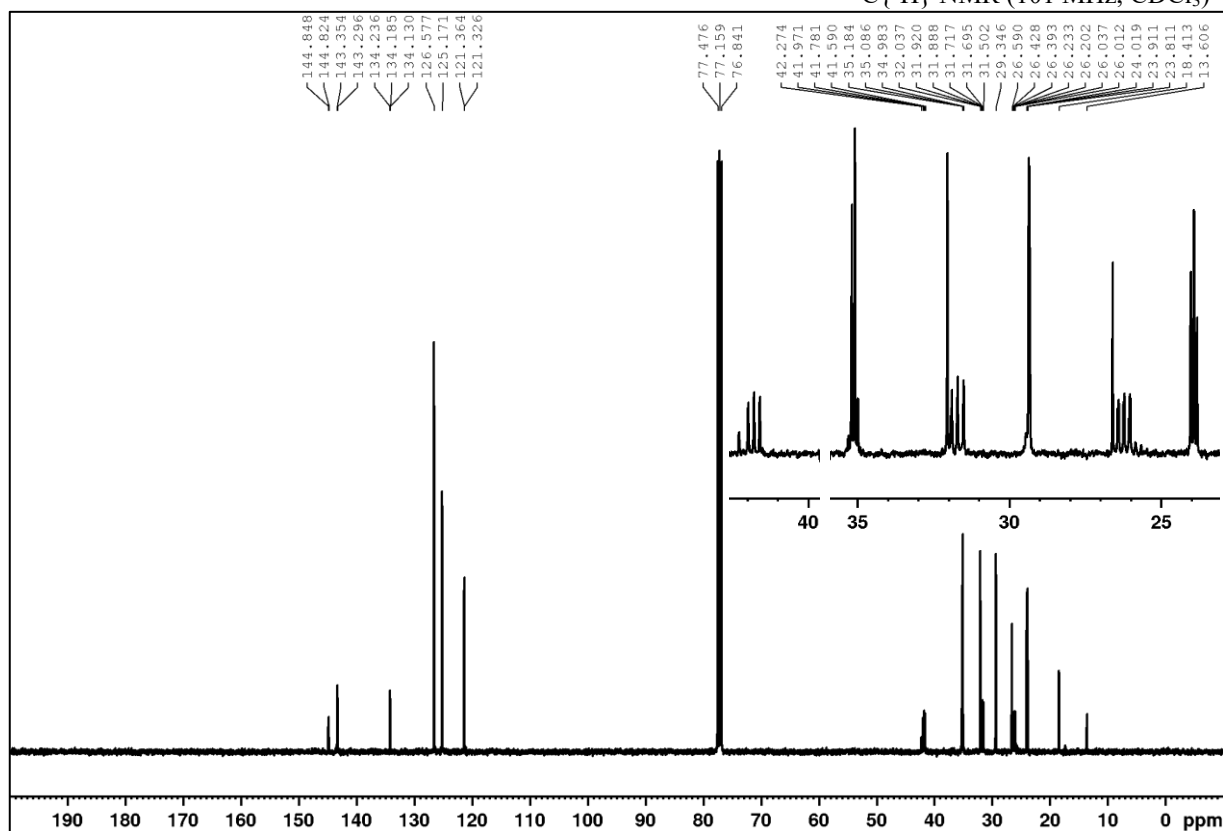
7f-d₁¹H NMR (400 MHz, CDCl₃)

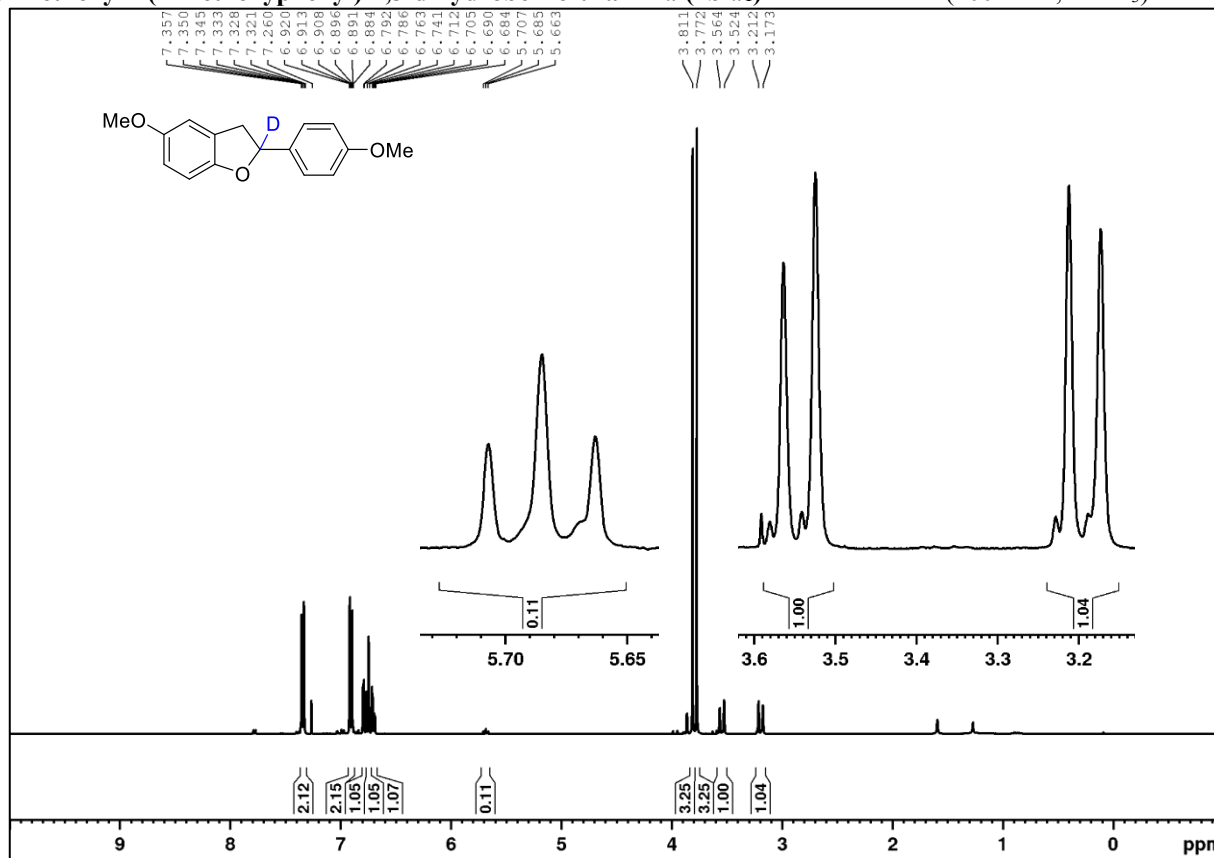
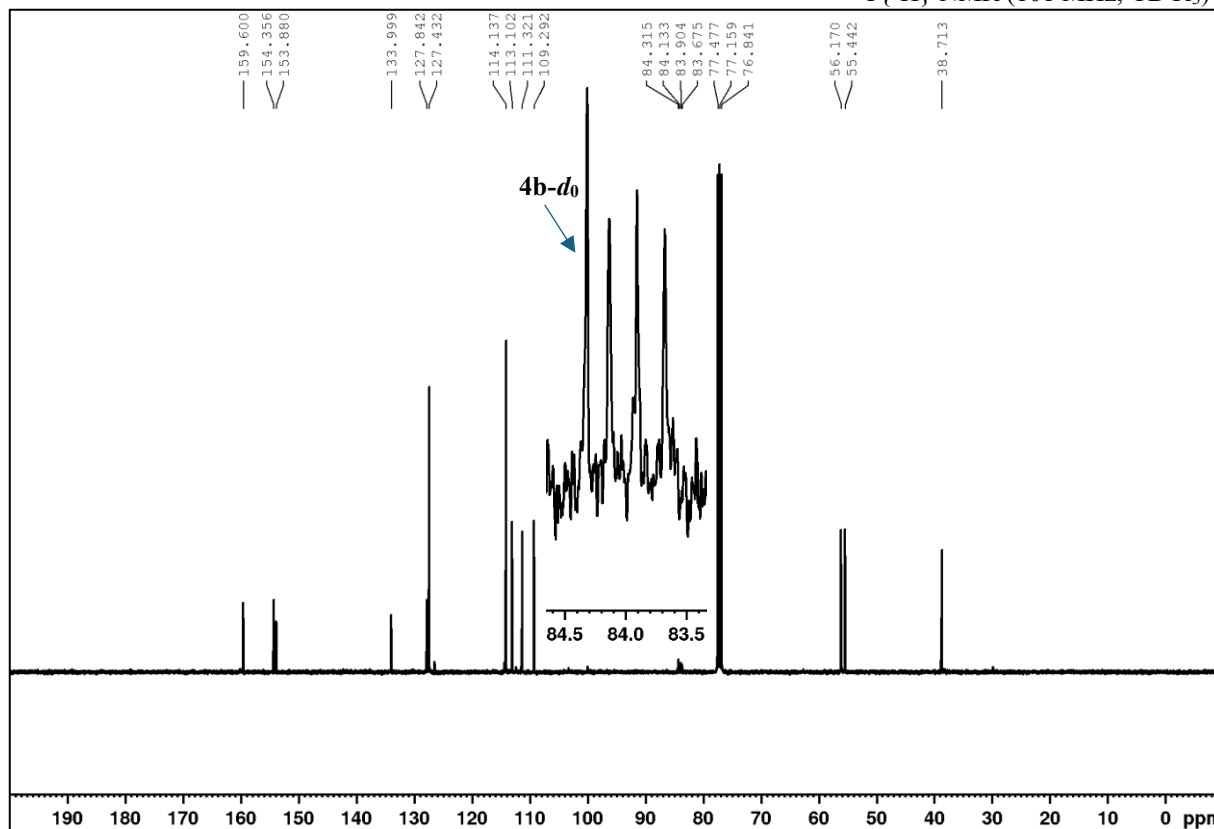
Crude product redissolved in CDCl₃ after evaporation of the solvent CH₃CN. The yield was not determined.

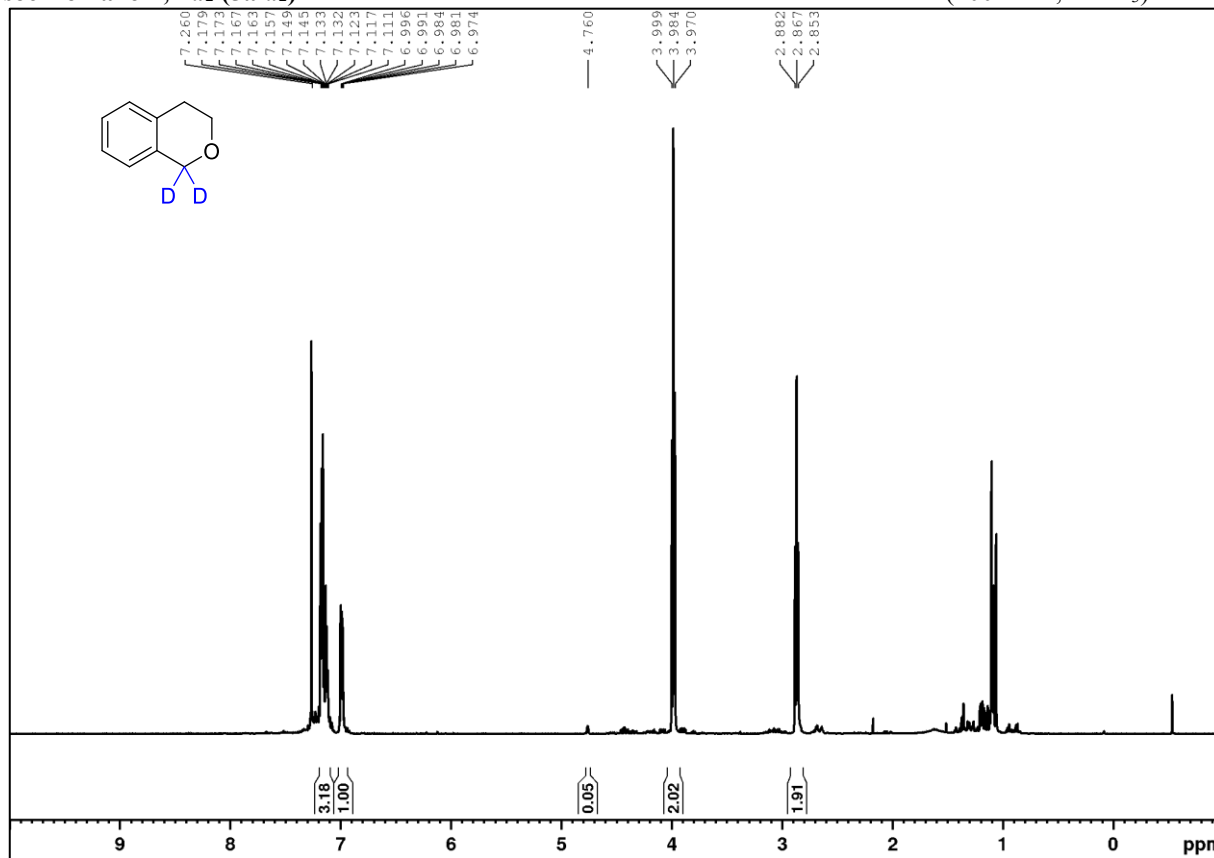
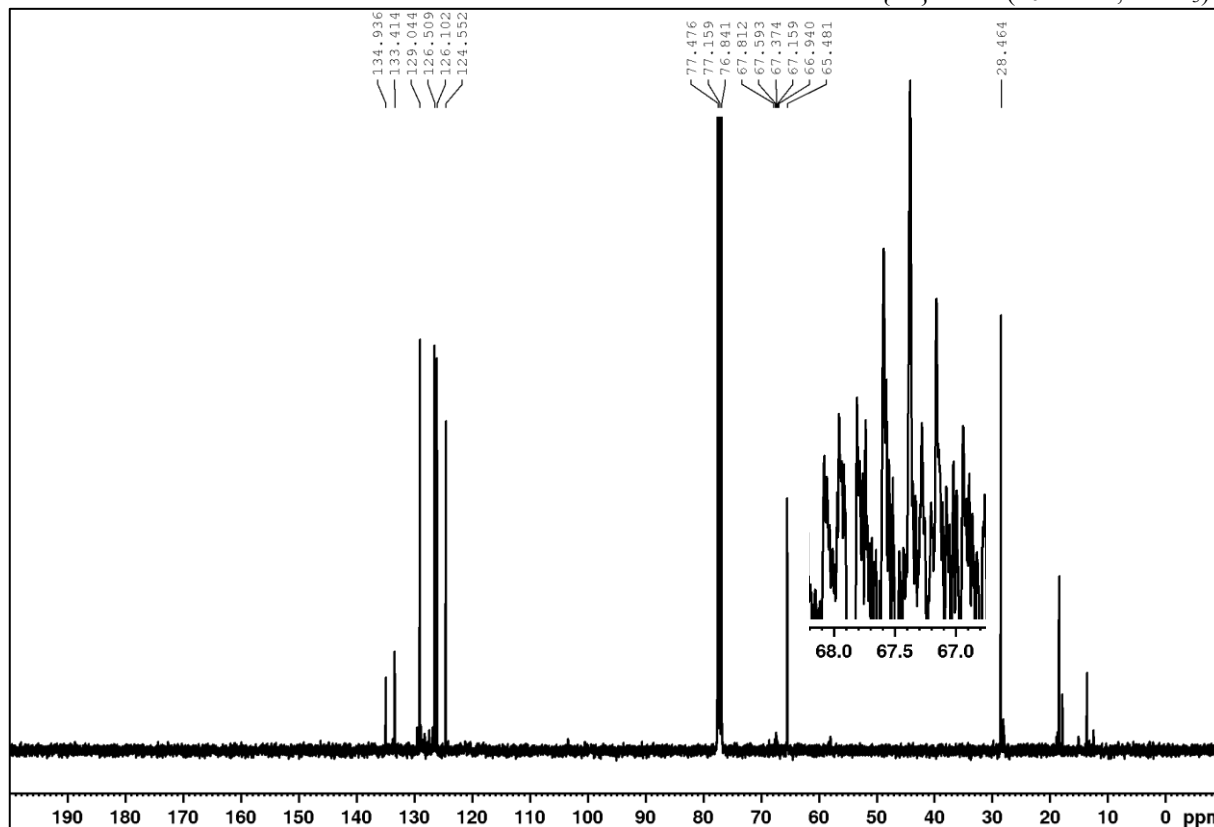
9 (Z/E = 5:1)

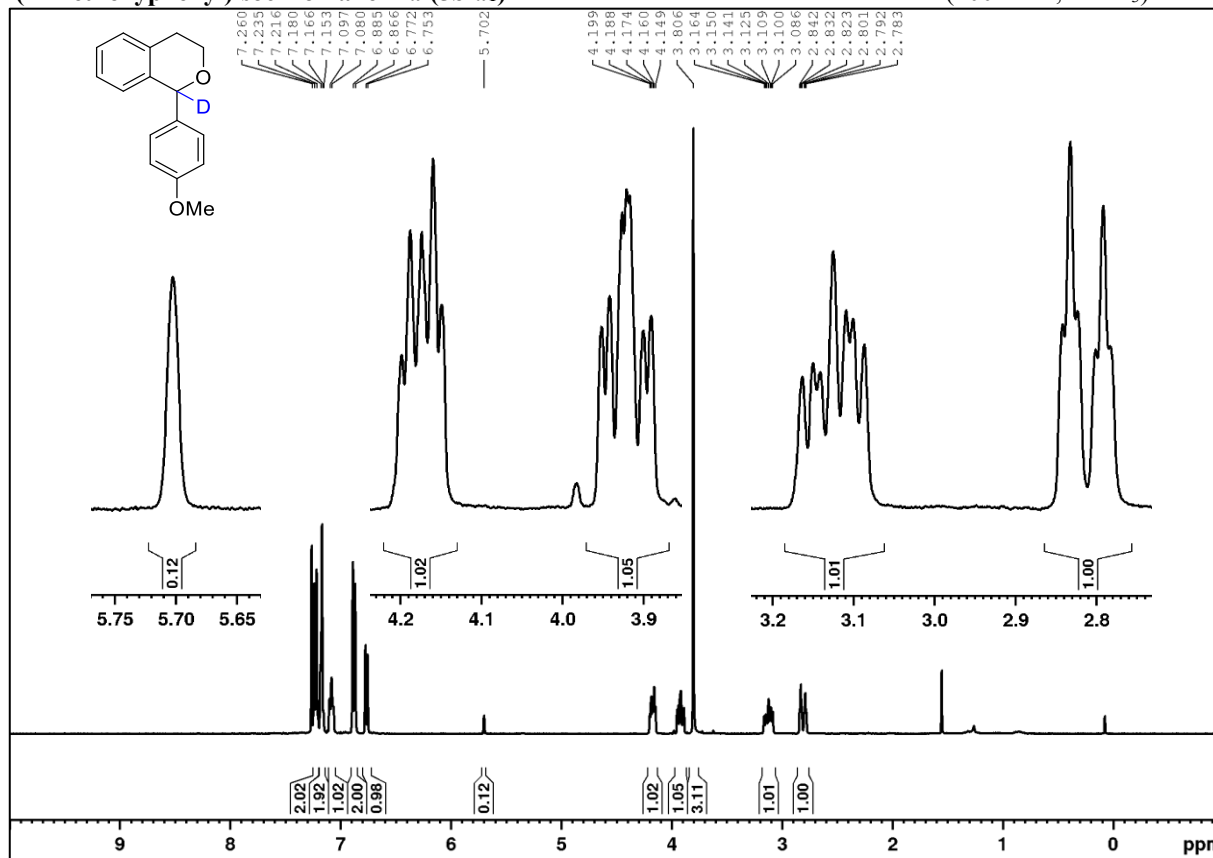
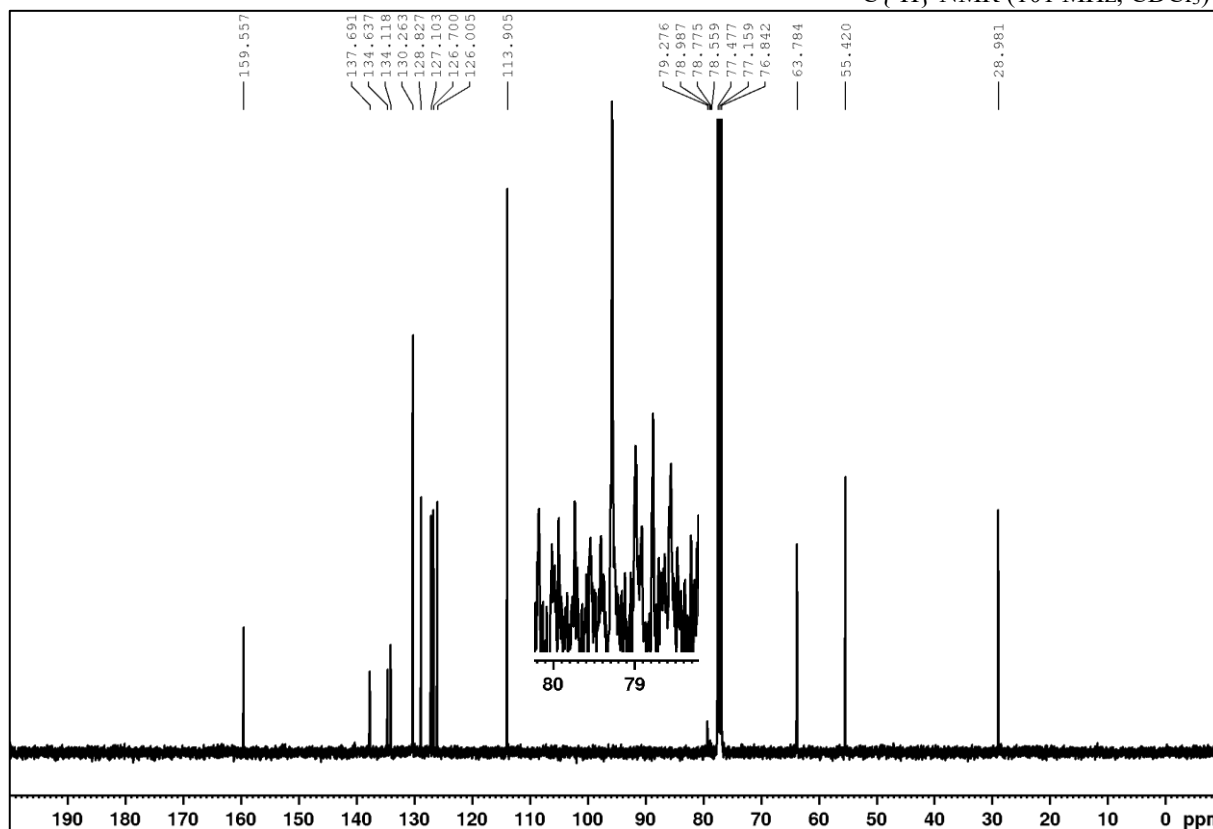
 ^1H NMR (400 MHz, CD_3CN)

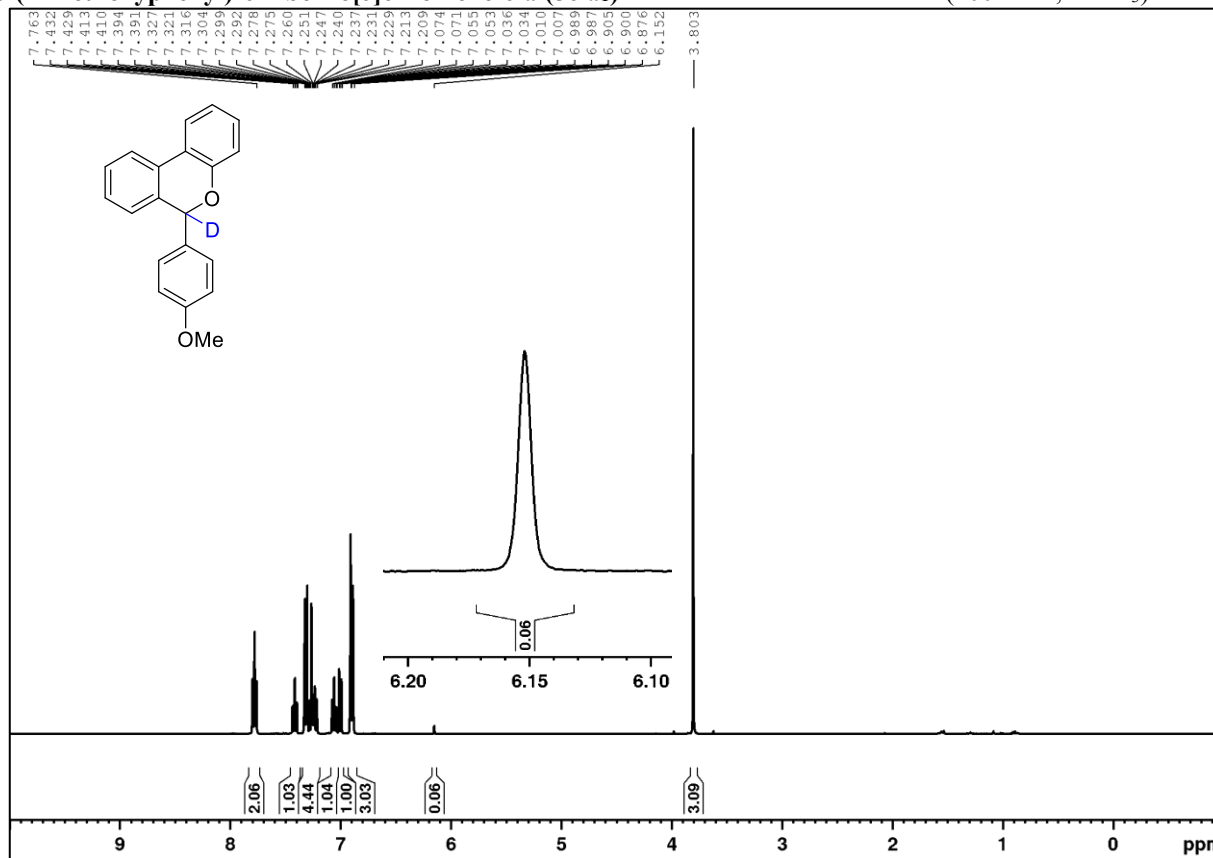
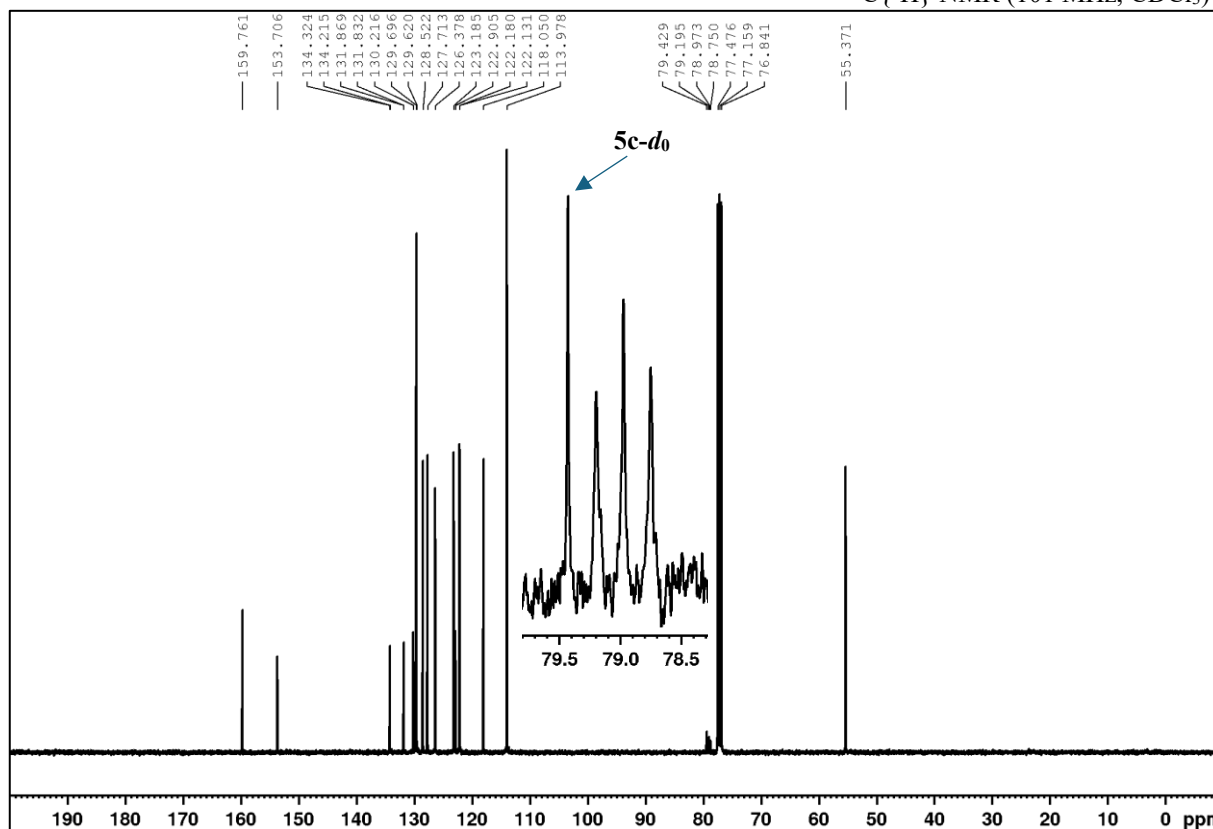
7.4.3.2 NMR spectra of isolated deuterated compounds

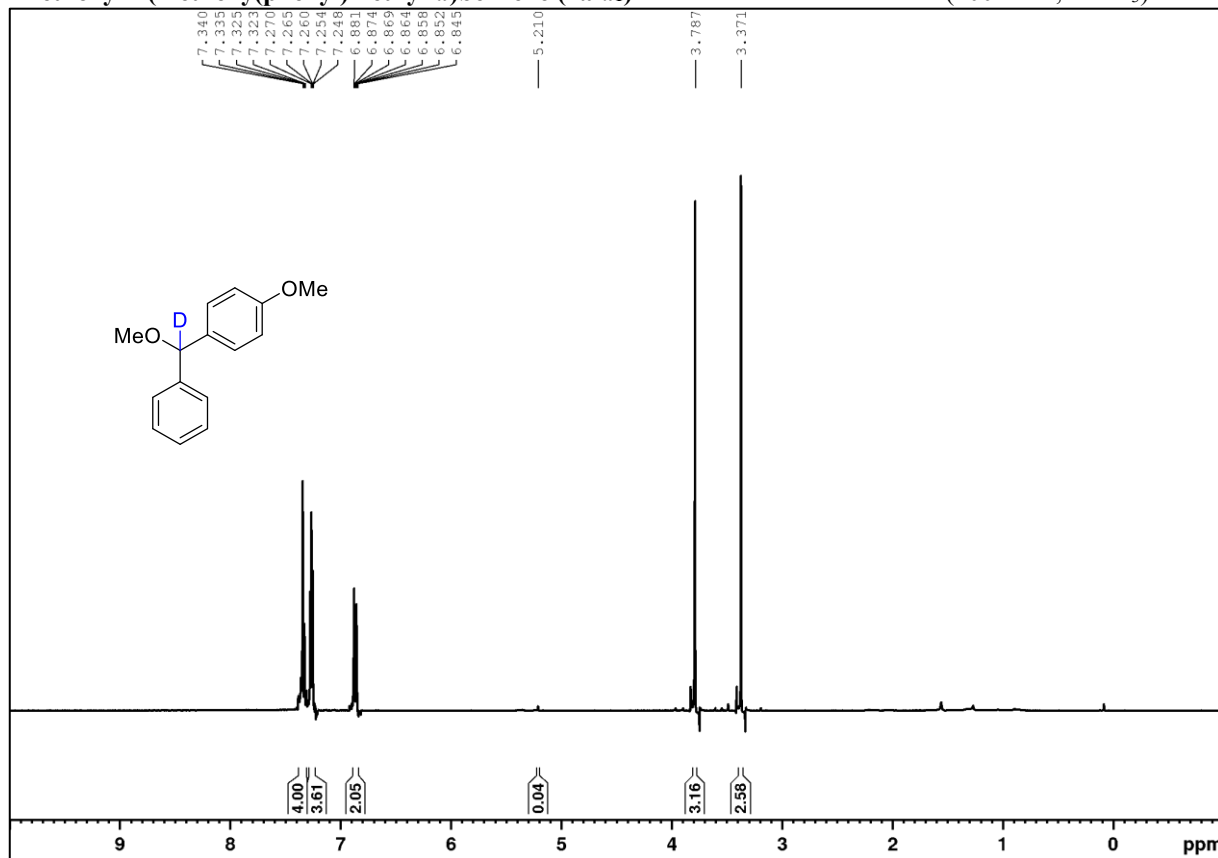
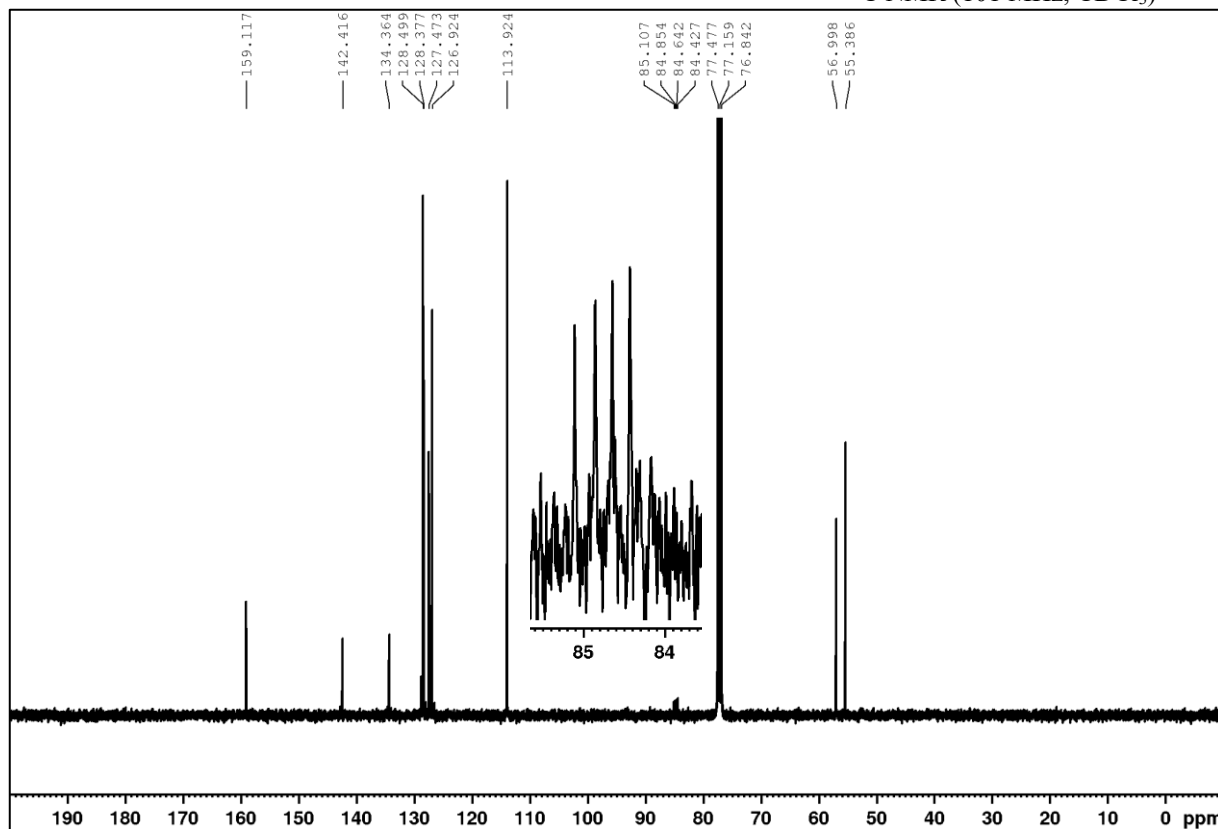
1,2,2a,3,4,5-Hexahydroacenaphthylene-1,1,2a,5,5-*d*₅ (3e-*d*₅)¹H NMR (400 MHz, CDCl₃)¹³C{¹H} NMR (101 MHz, CDCl₃)

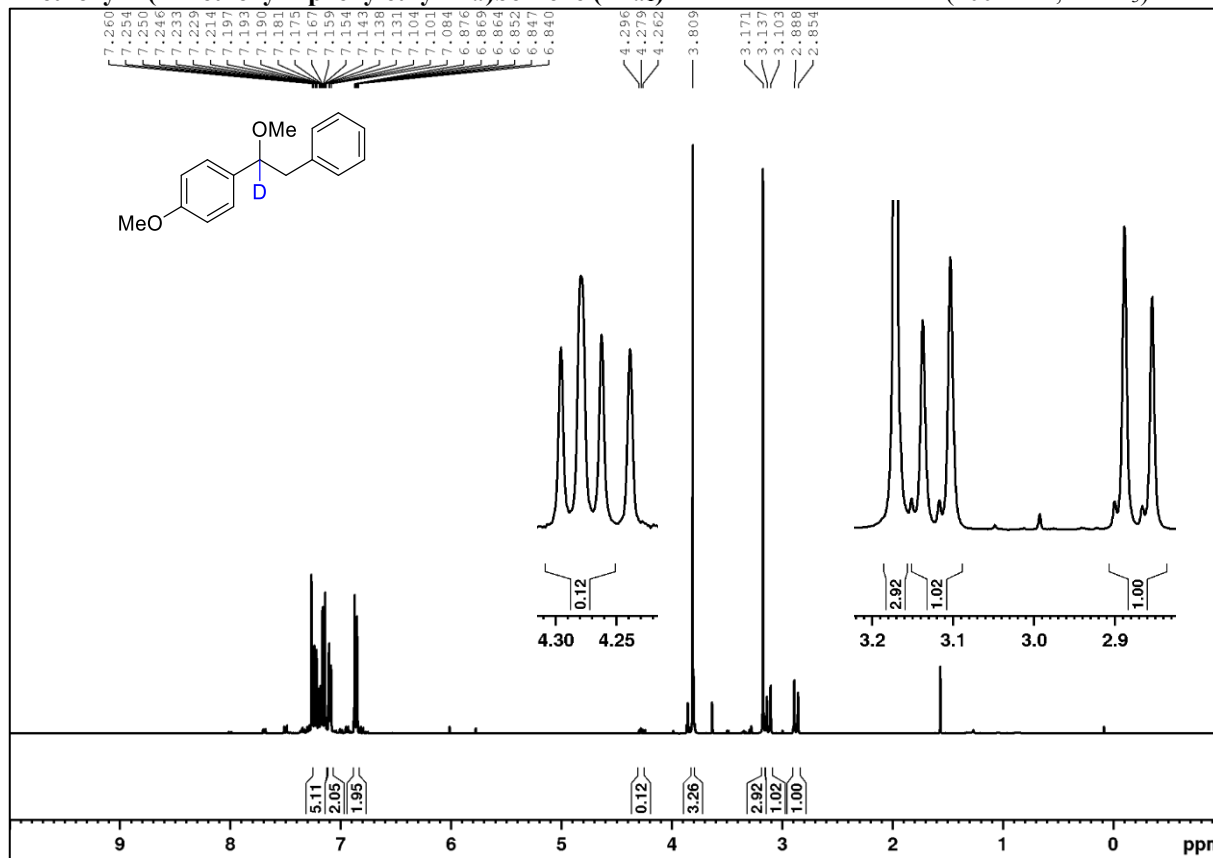
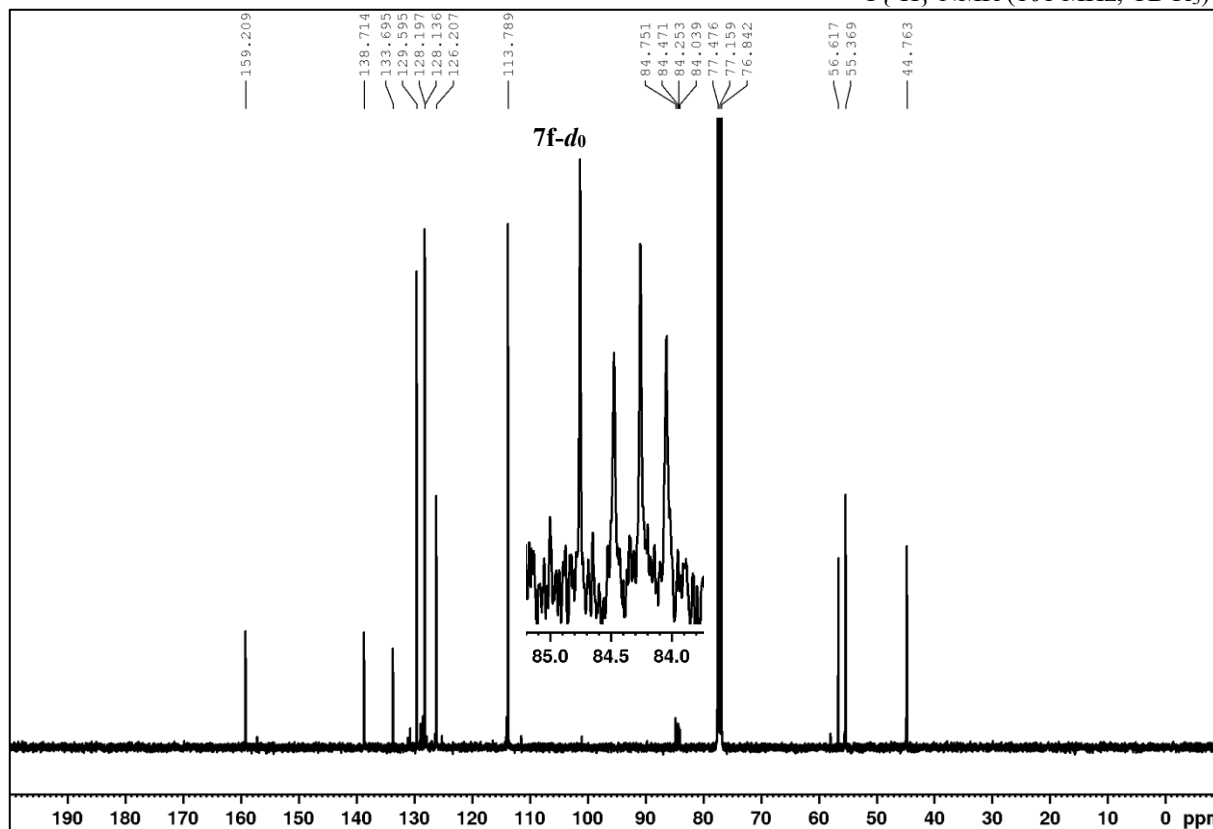
5-Methoxy-2-(4-methoxyphenyl)-2,3-dihydrobenzofuran-2-d (4b-d₁)¹H NMR (400 MHz, CDCl₃)¹³C{¹H} NMR (101 MHz, CDCl₃)

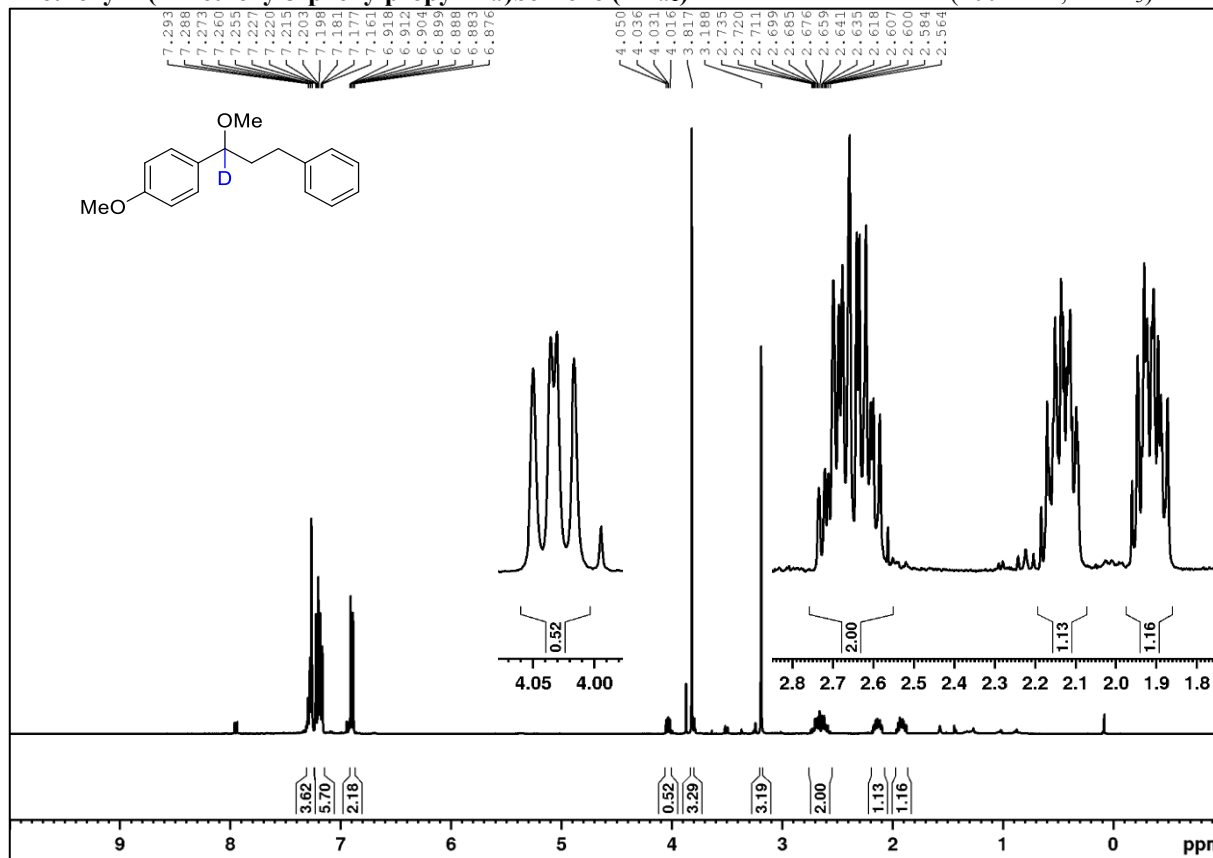
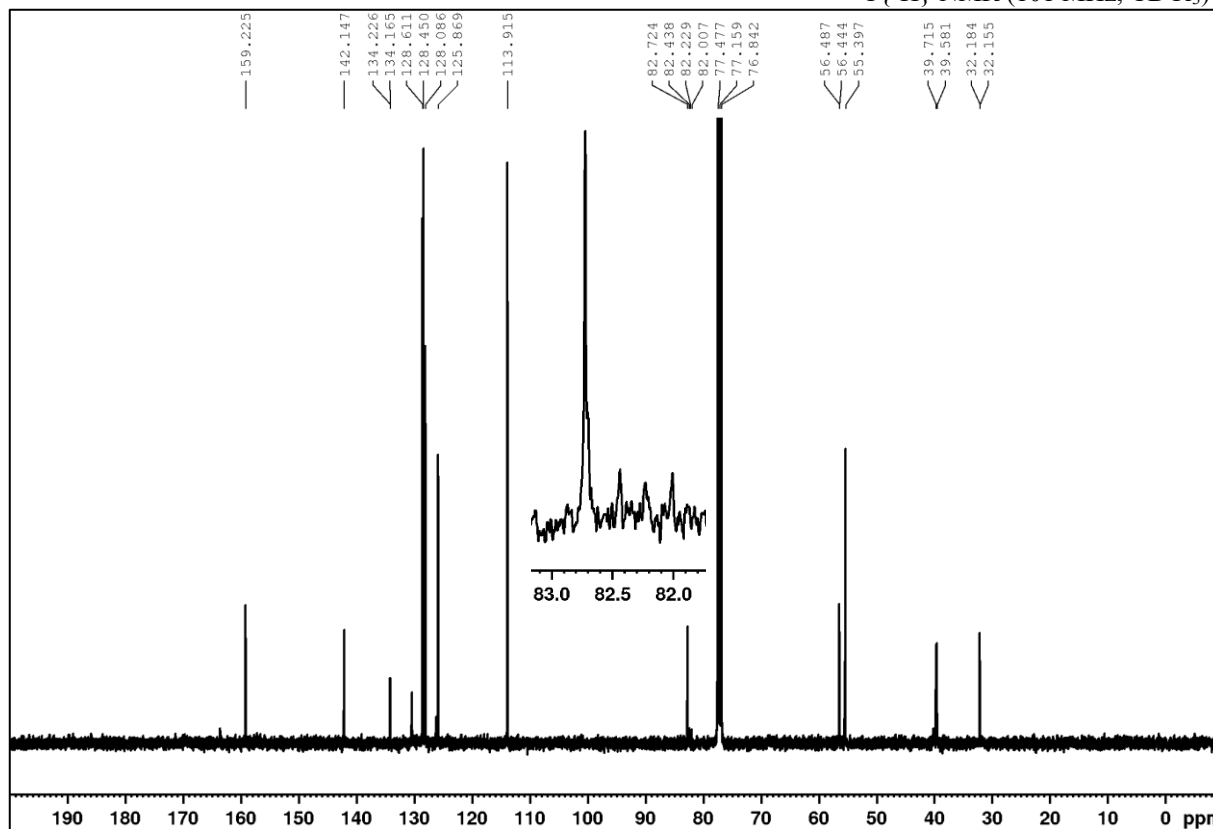
Isochromane-1,1-*d*₂ (5a-*d*₂)¹H NMR (400 MHz, CDCl₃)¹³C{¹H} NMR (101 MHz, CDCl₃)

1-(4-Methoxyphenyl)isochromane-1-d (5b-d₁)¹H NMR (400 MHz, CDCl₃)¹³C{¹H} NMR (101 MHz, CDCl₃)

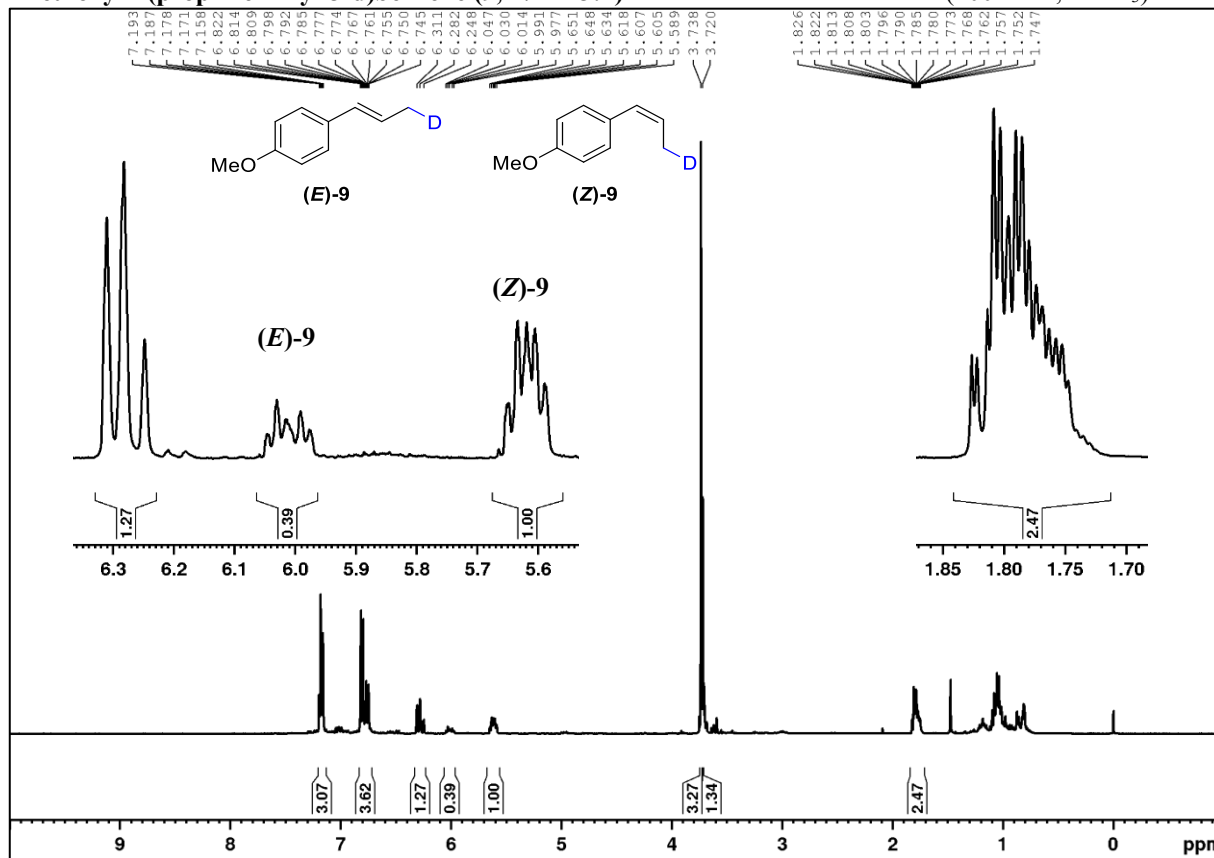
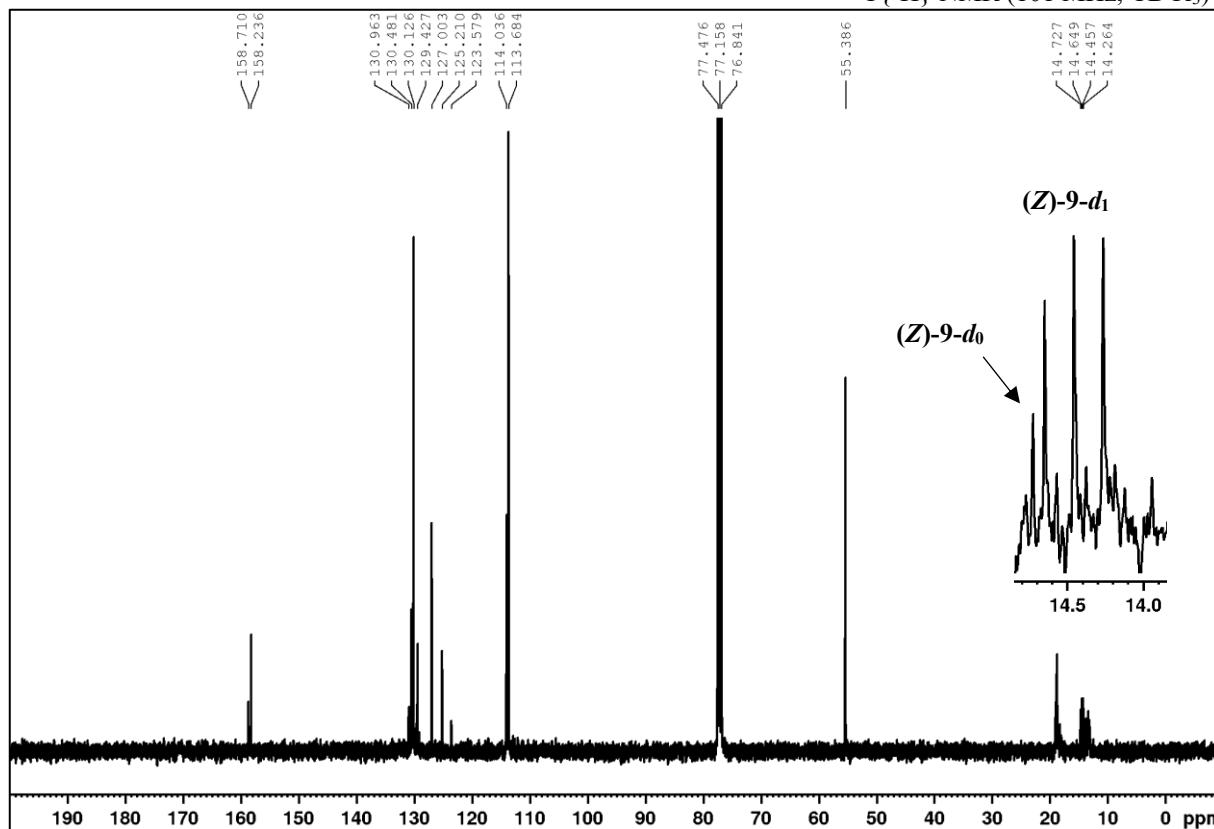
6-(4-Methoxyphenyl)-6H-benzo[c]chromene-6-d (**5c-d₁**)¹H NMR (400 MHz, CDCl₃)¹³C{¹H} NMR (101 MHz, CDCl₃)

1-Methoxy-4-(methoxy(phenyl)methyl-*d*)benzene (7a-*d*)¹H NMR (400 MHz, CDCl₃)¹³C NMR (101 MHz, CDCl₃)

1-Methoxy-4-(1-methoxy-2-phenylethyl-1-*d*)benzene (7f-*d*)¹H NMR (400 MHz, CDCl₃)¹³C{¹H} NMR (101 MHz, CDCl₃)

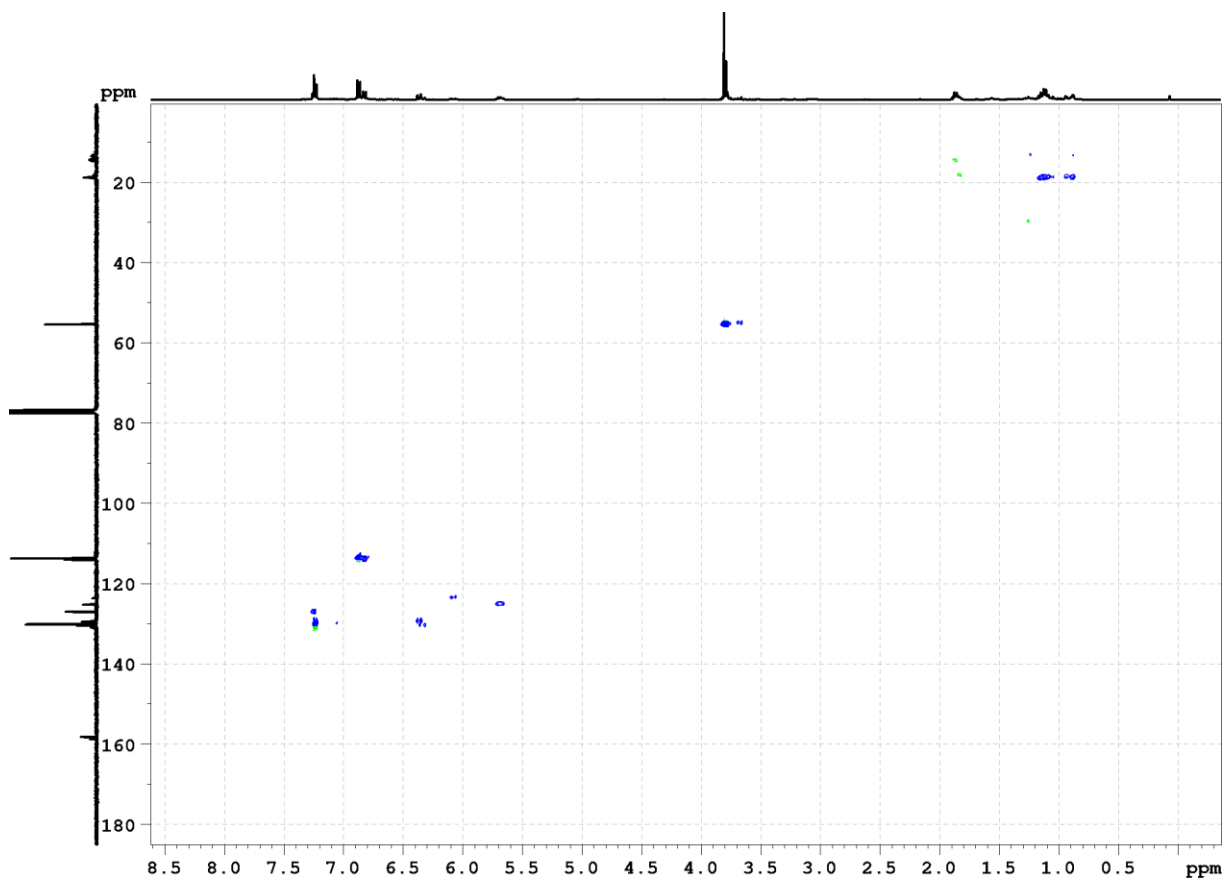
1-Methoxy-4-(1-methoxy-3-phenylpropyl-1-*d*)benzene (7k-*d*₁)¹H NMR (400 MHz, CDCl₃)¹³C{¹H} NMR (101 MHz, CDCl₃)

1-Methoxy-4-(prop-1-en-1-yl-3-d)benzene (9, Z/E = 3:1)

 ^1H NMR (400 MHz, CDCl_3) $^{13}\text{C}\{^1\text{H}\}$ NMR (101 MHz, CDCl_3)

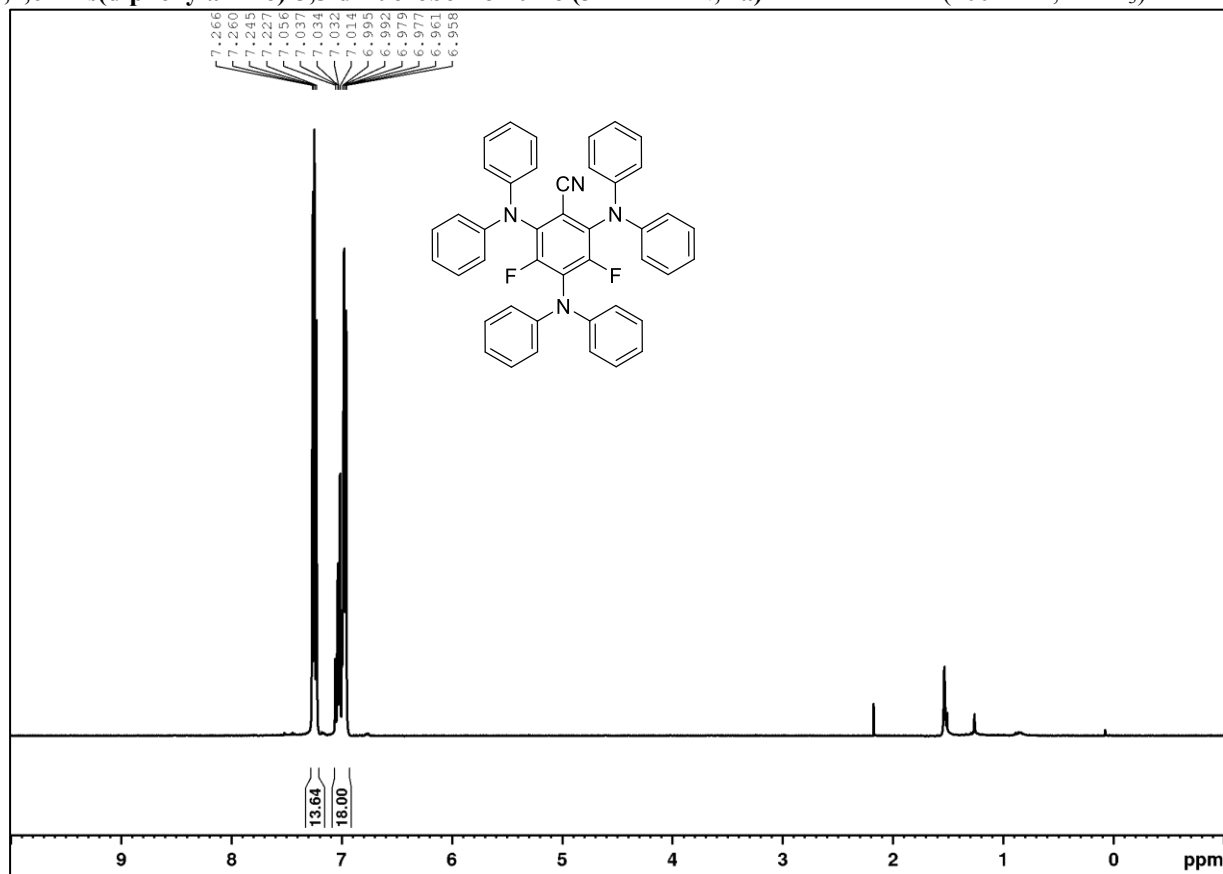
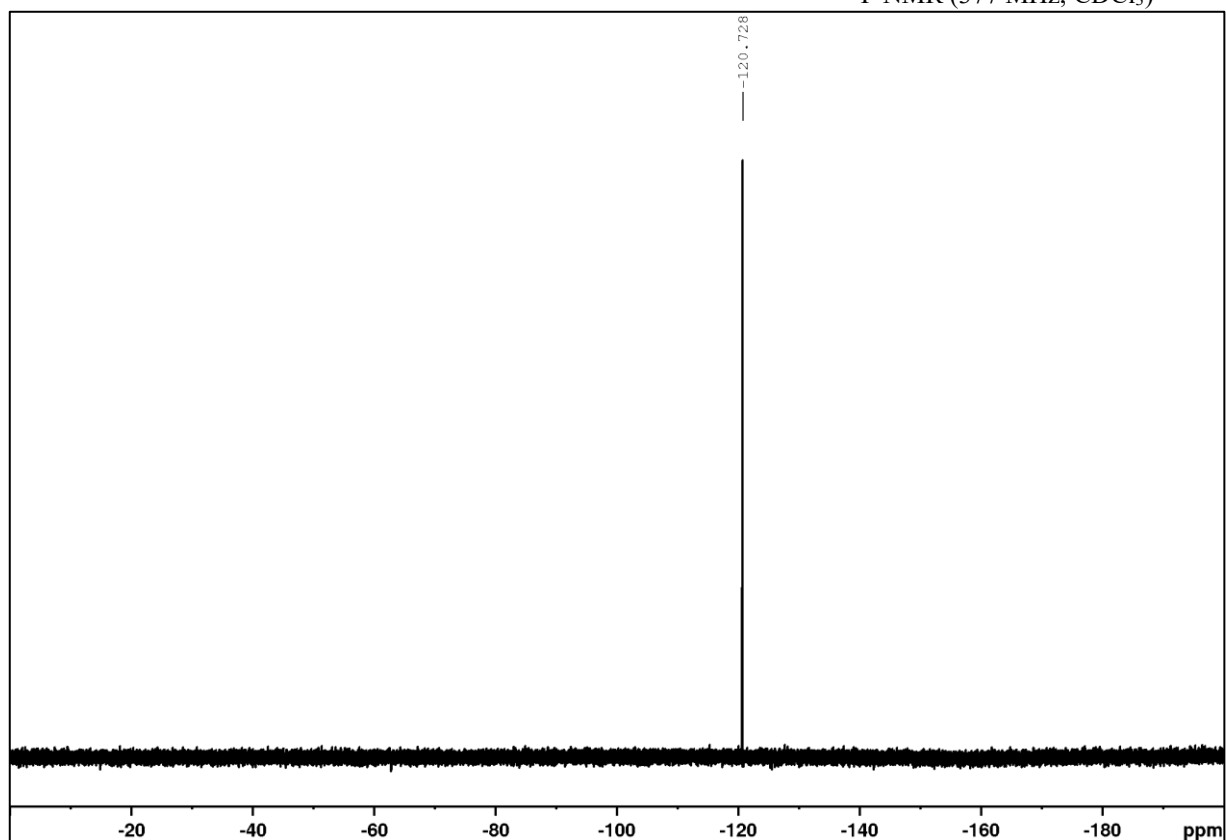
APPENDIX

(^1H , ^{13}C) HSQC (CDCl_3)

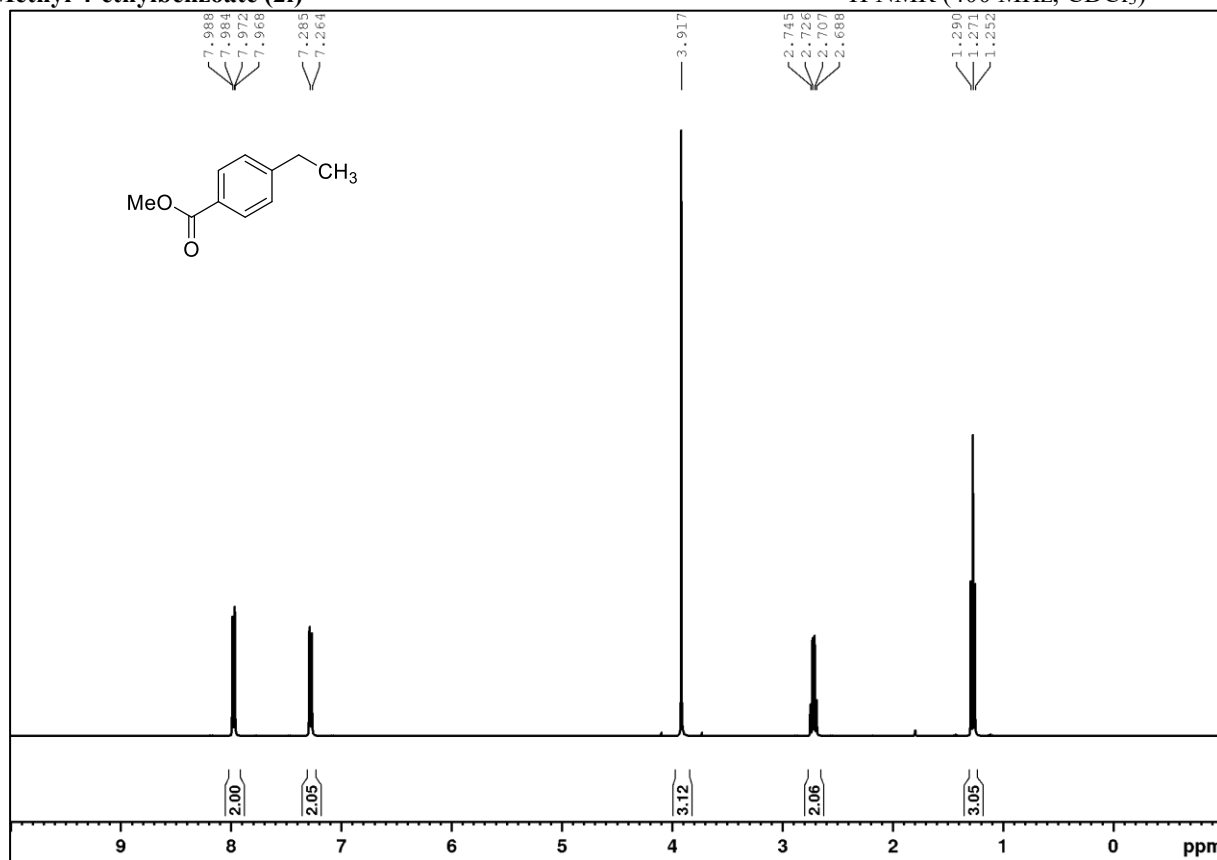
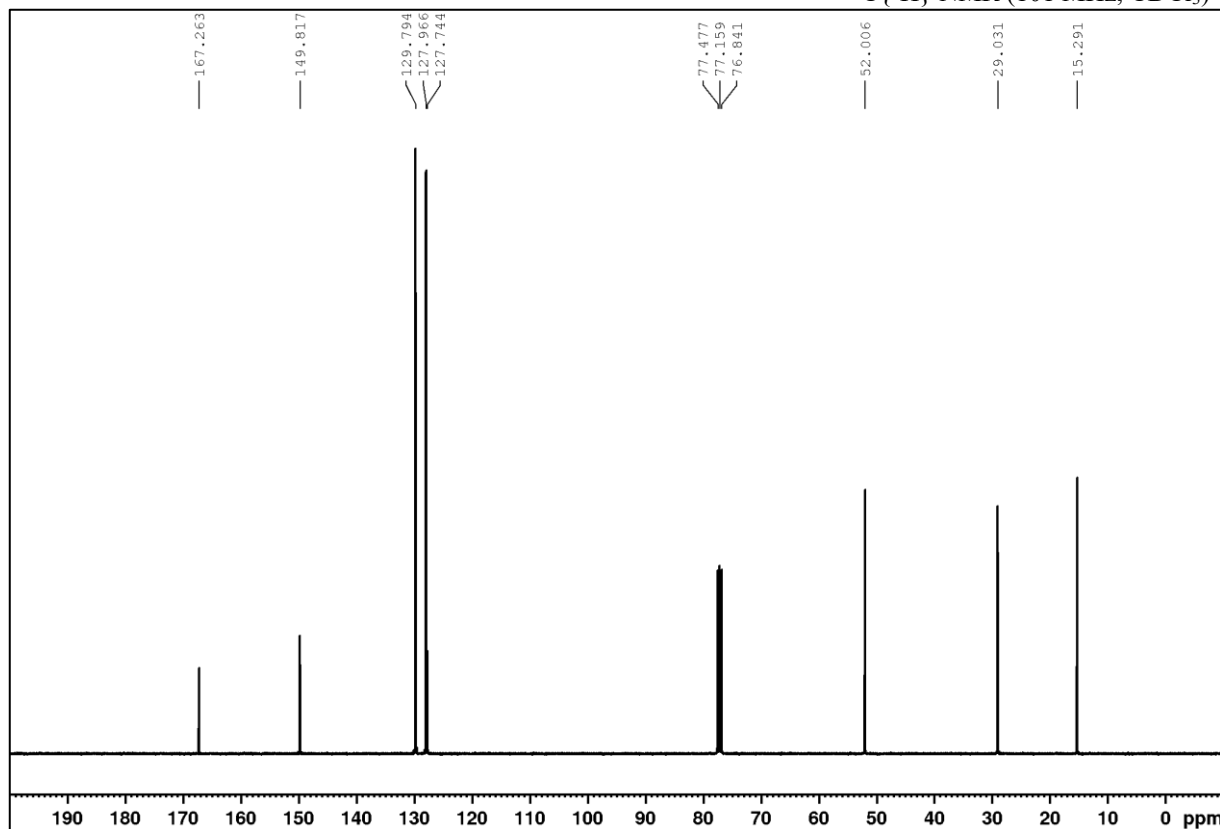


7.4.3.3 NMR spectra of other isolated compounds

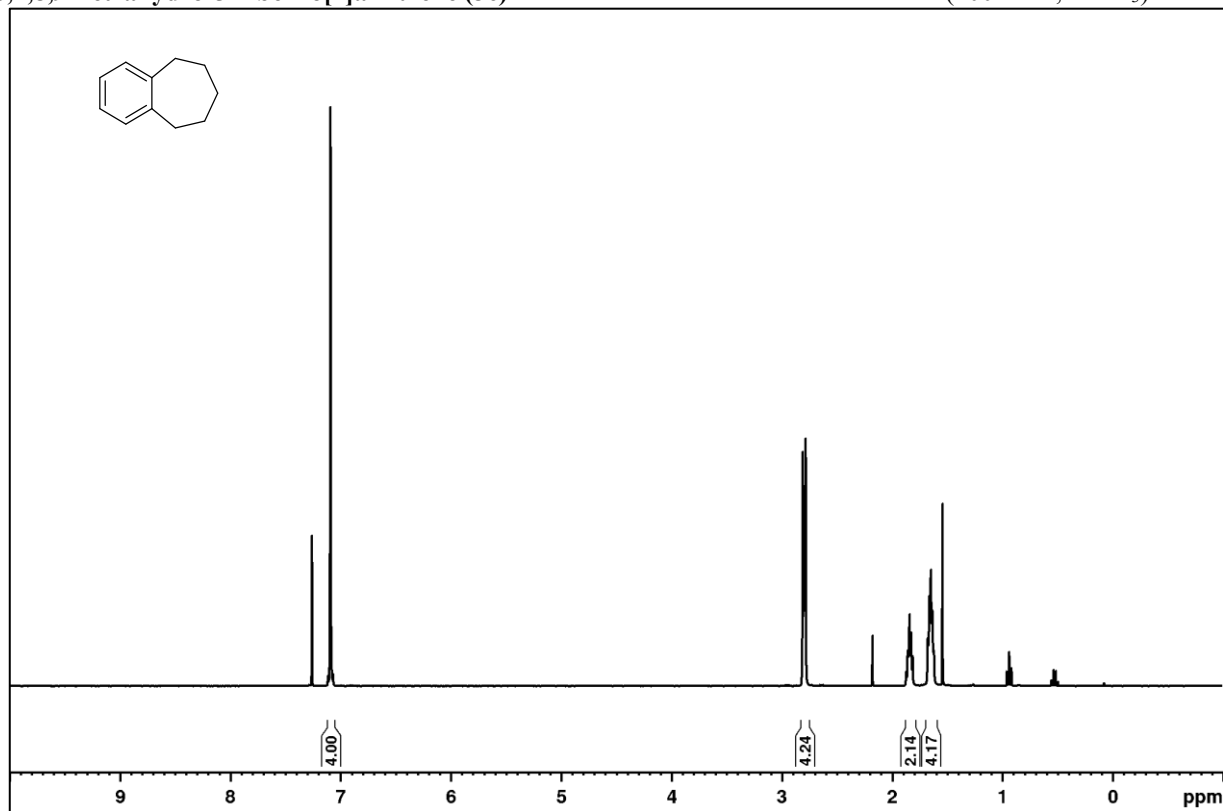
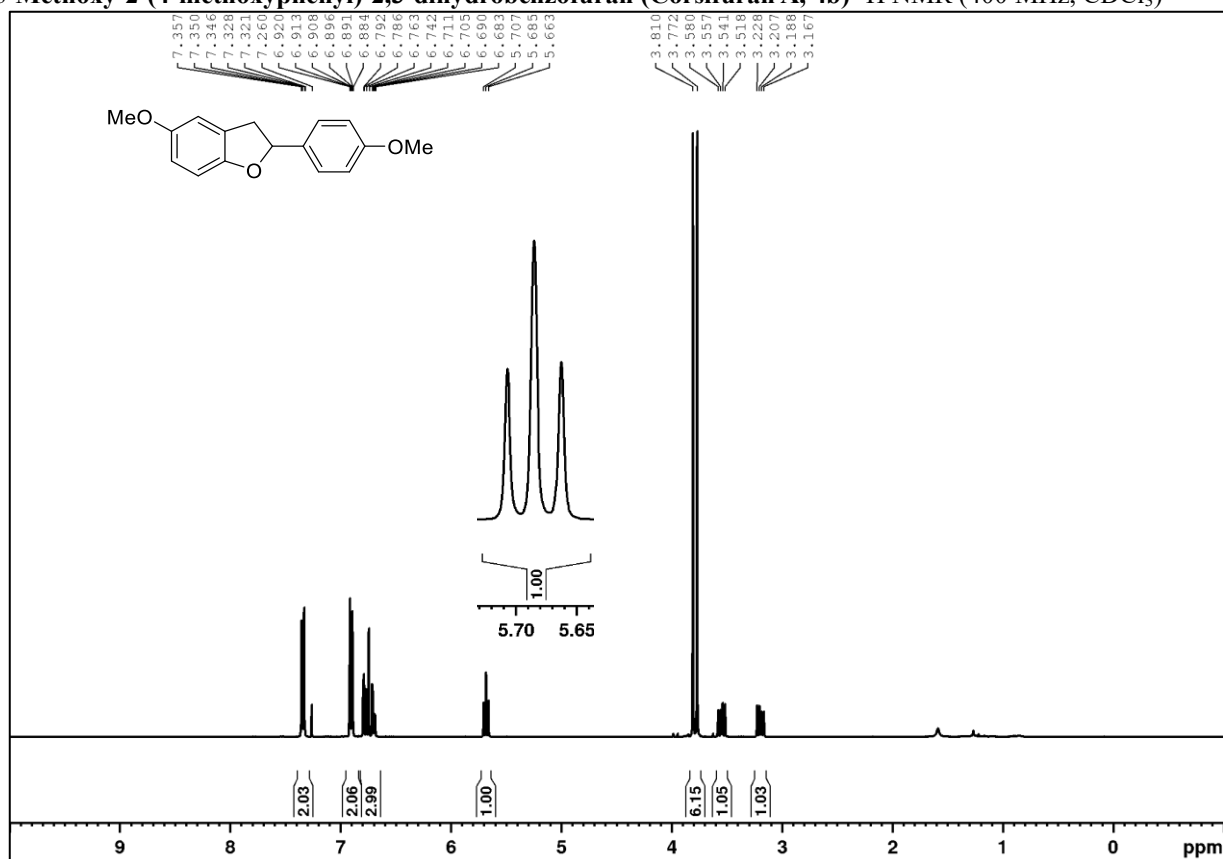
2,4,6-Tris(diphenylamino)-3,5-difluorobenzonitrile (3DPA2FBN, 1a)

 ^1H NMR (400 MHz, CDCl_3) ^{19}F NMR (377 MHz, CDCl_3)

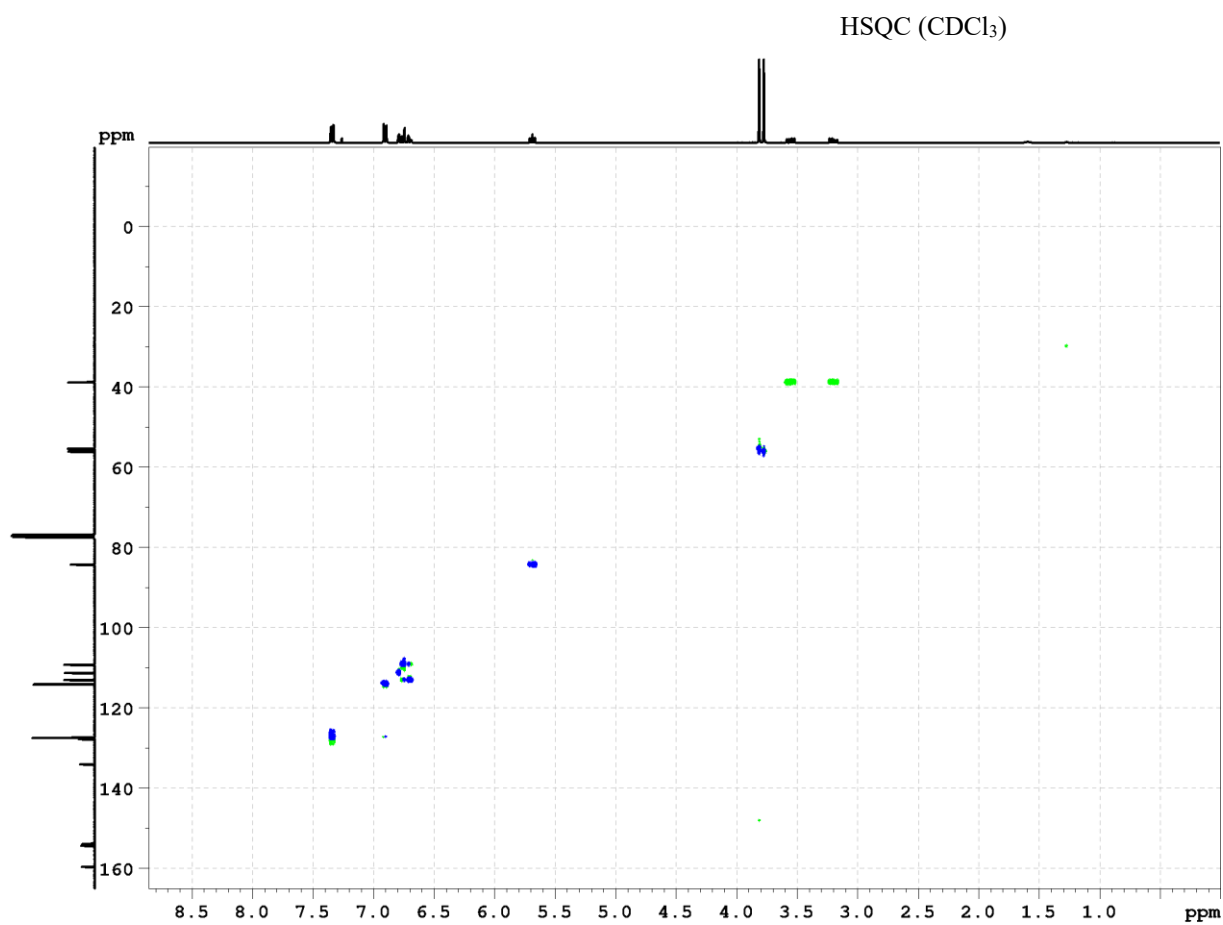
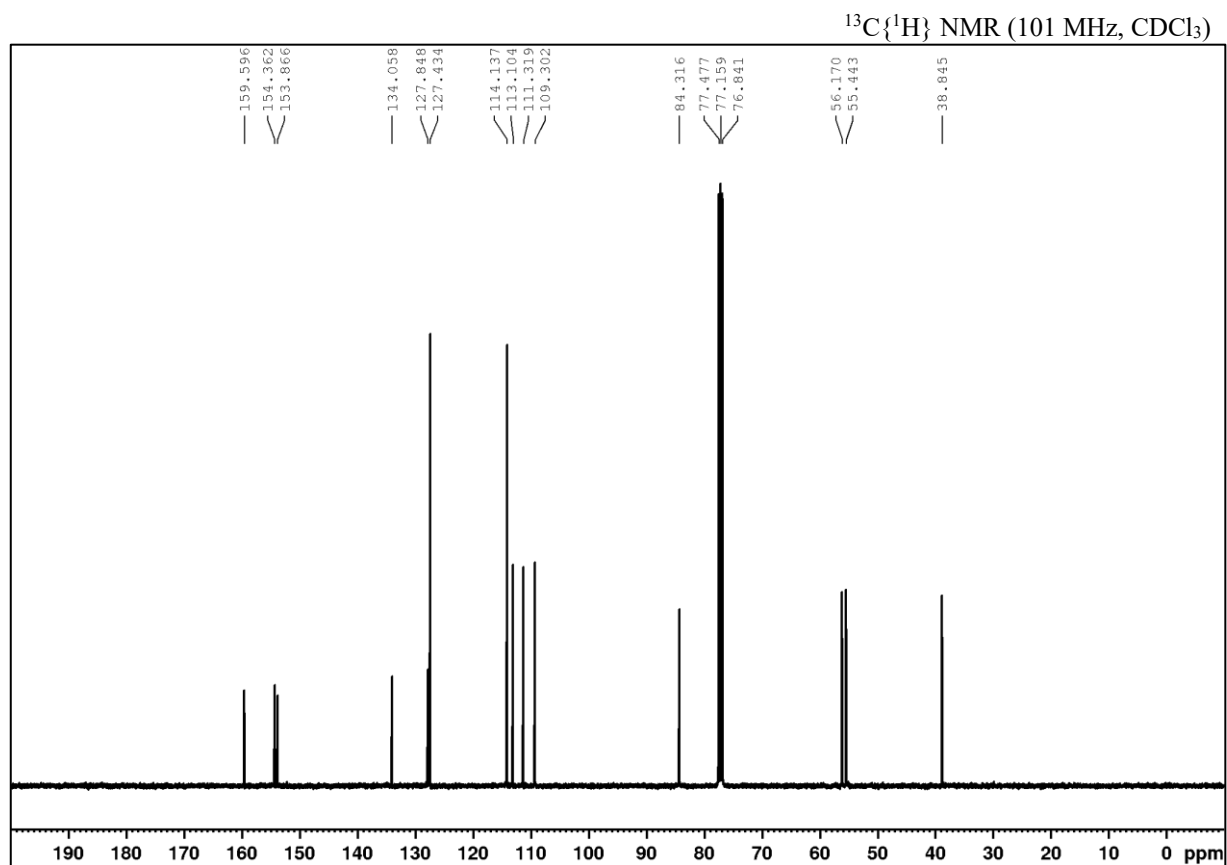
Methyl 4-ethylbenzoate (2i)

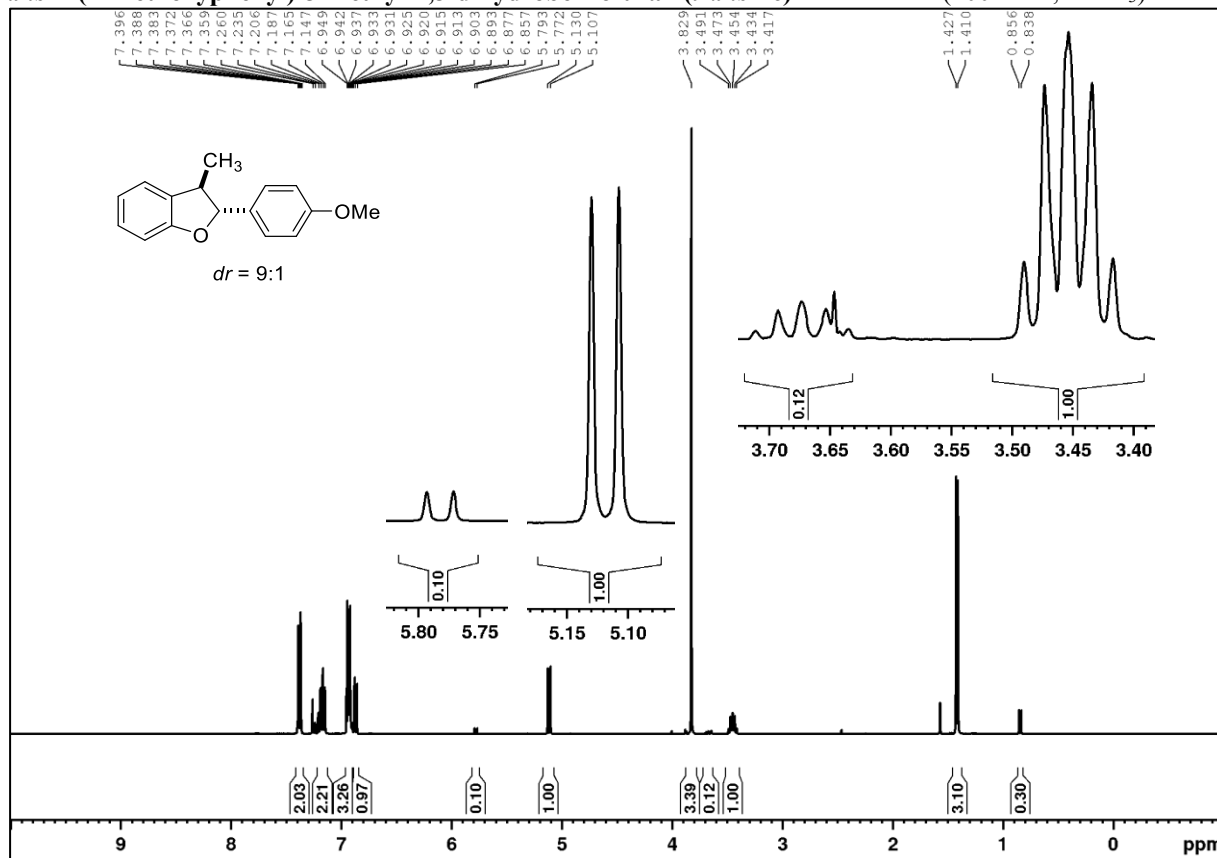
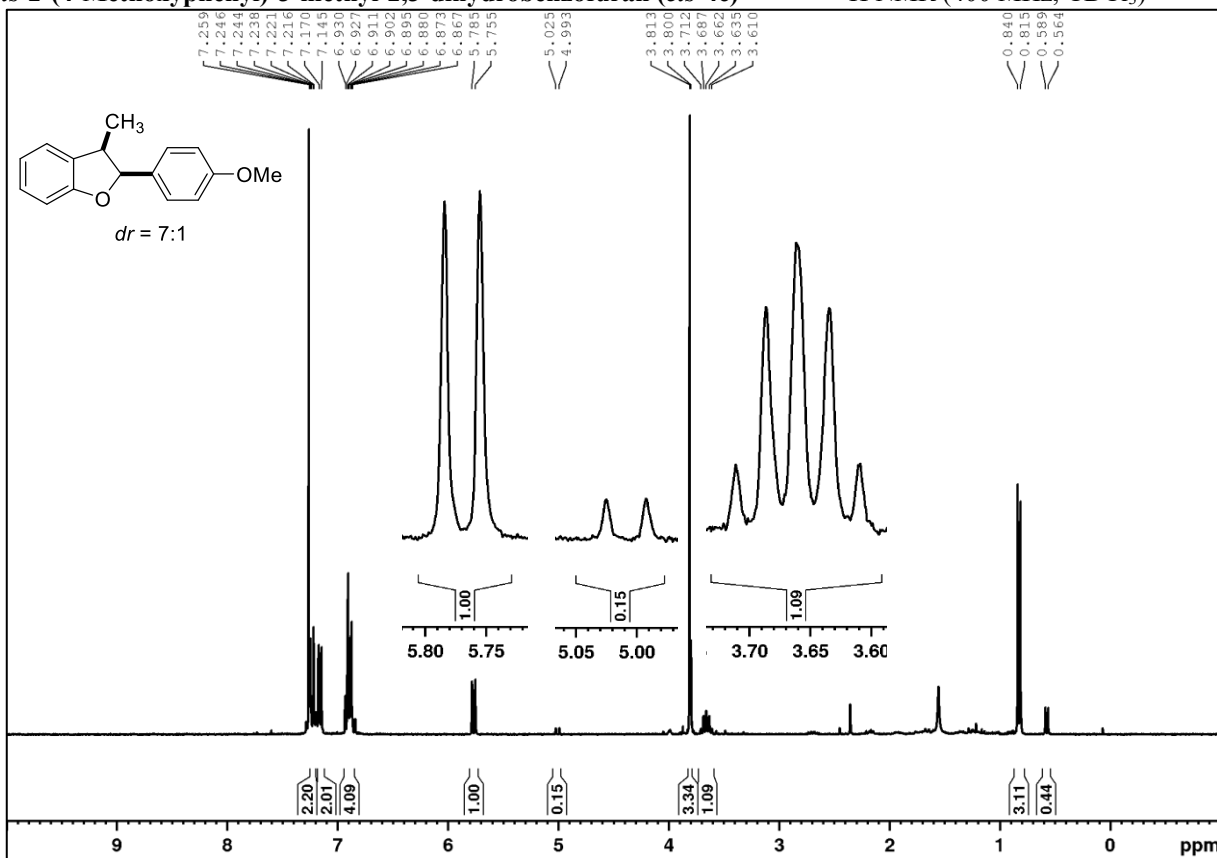
 ^1H NMR (400 MHz, CDCl_3) $^{13}\text{C}\{^1\text{H}\}$ NMR (101 MHz, CDCl_3)

6,7,8,9-Tetrahydro-5H-benzo[7]annulene (3c)

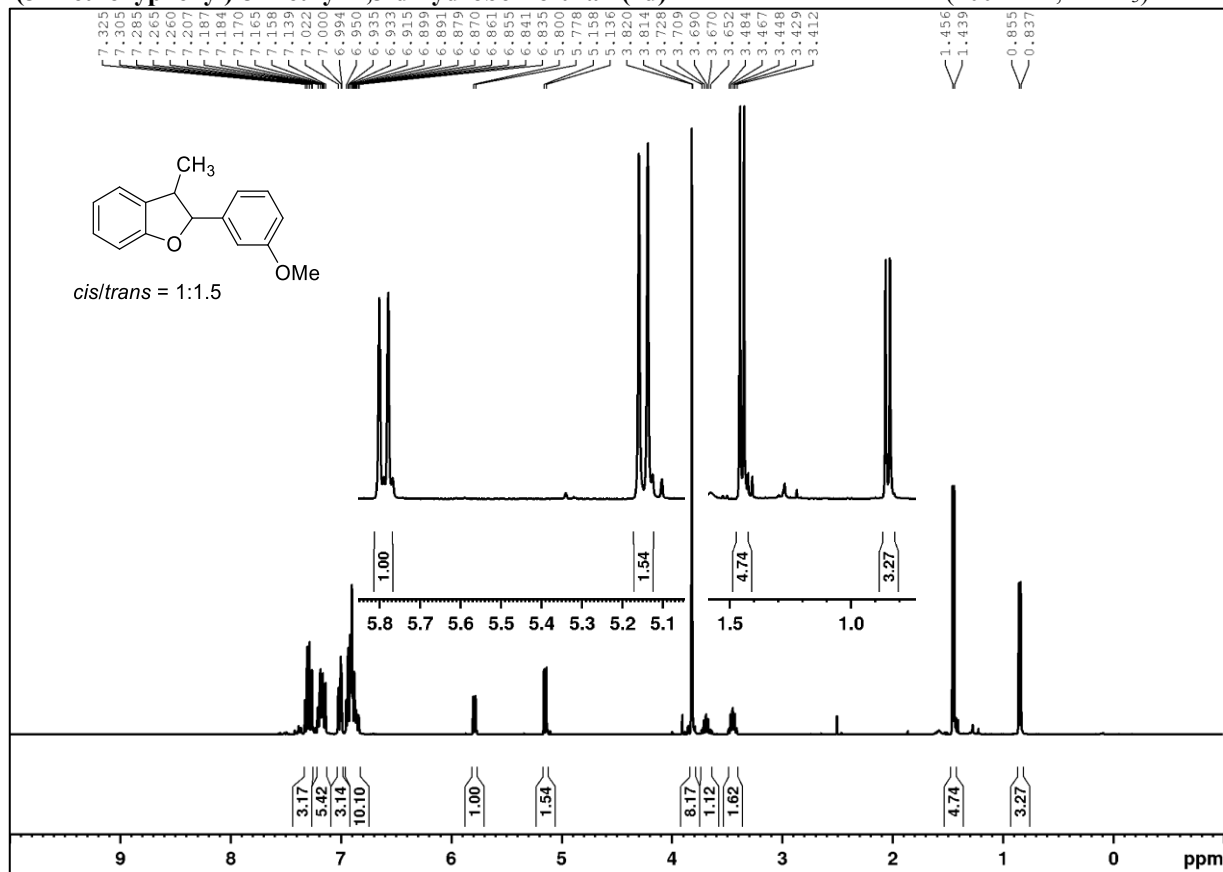
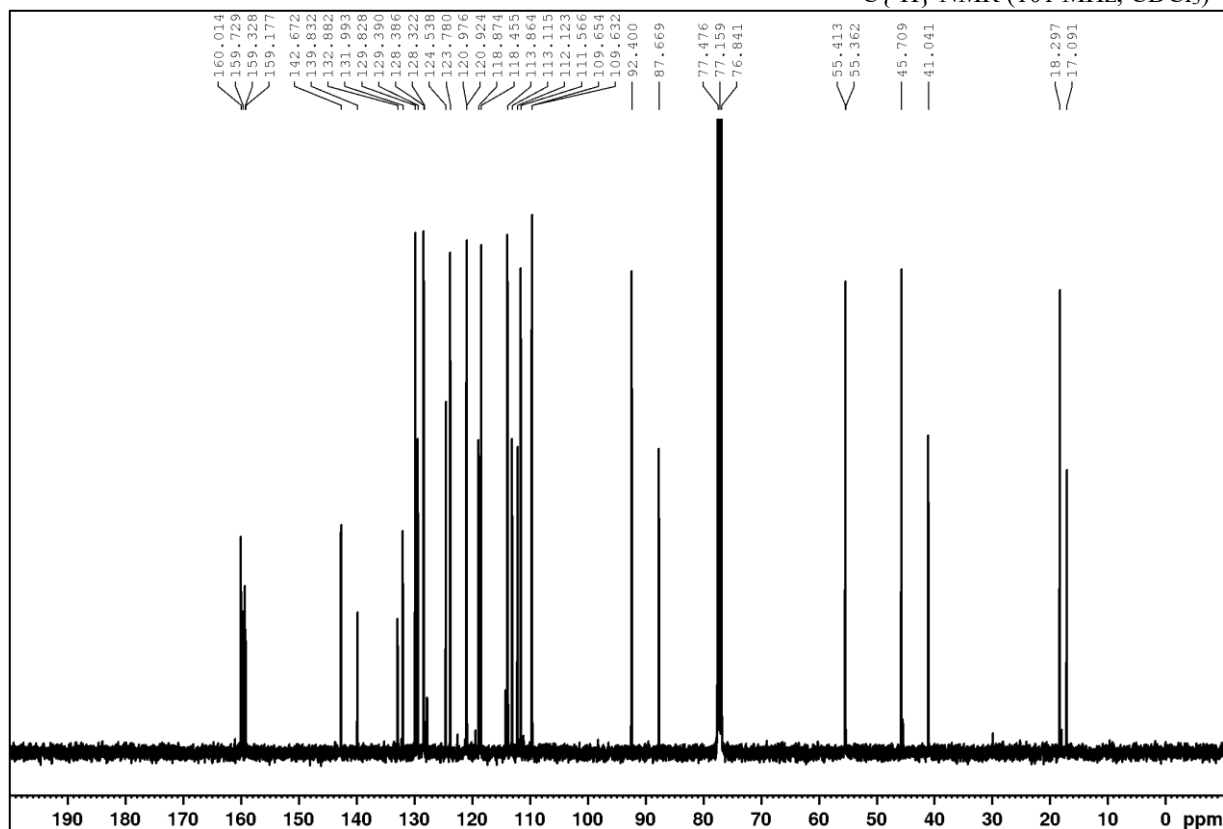
 ^1H NMR (400 MHz, CDCl_3)5-Methoxy-2-(4-methoxyphenyl)-2,3-dihydrobenzofuran (Corsifuran A, 4b) ^1H NMR (400 MHz, CDCl_3)

APPENDIX

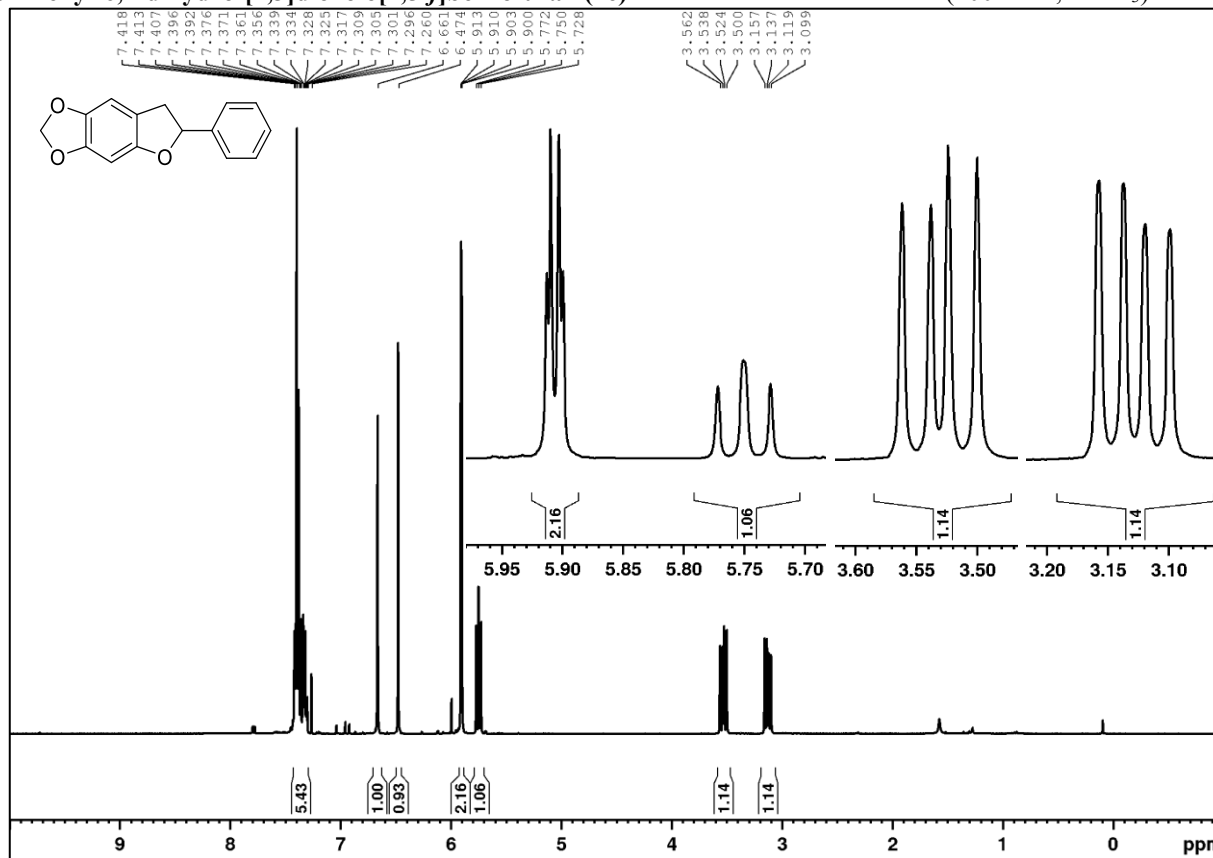
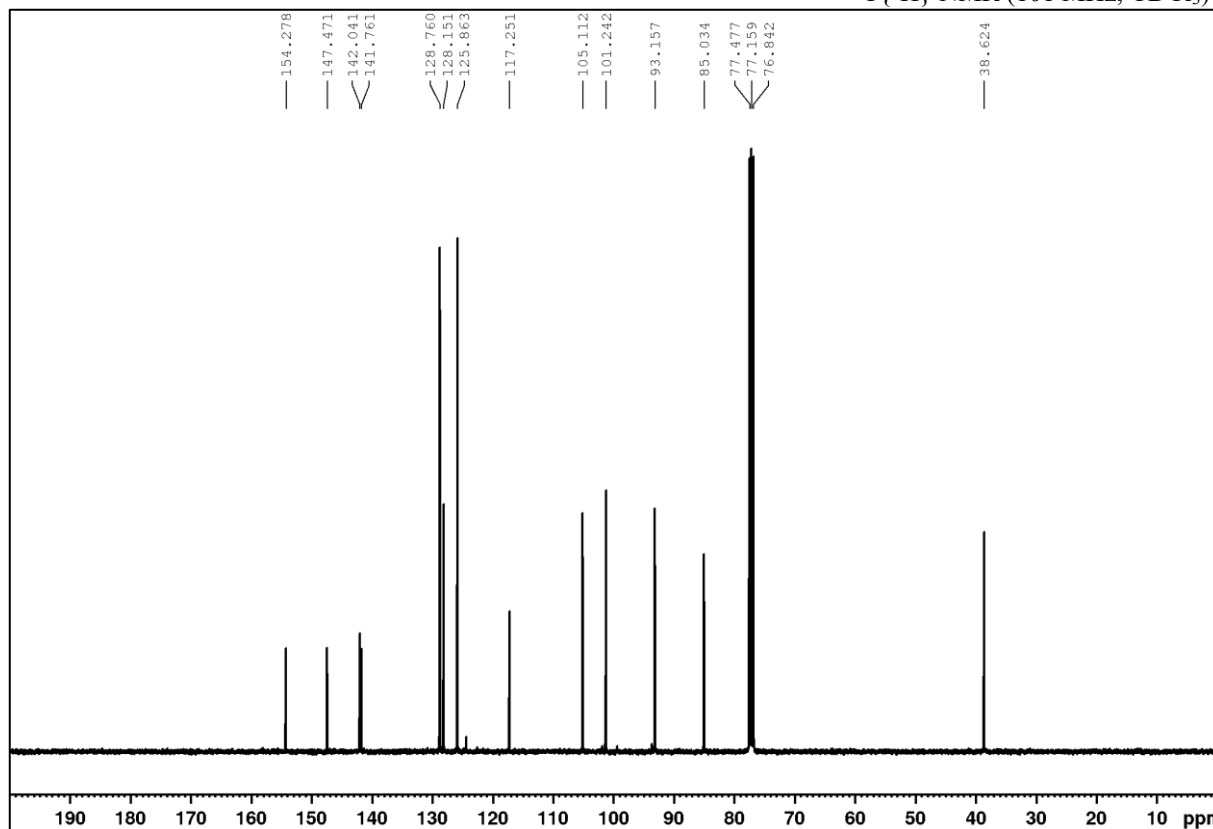


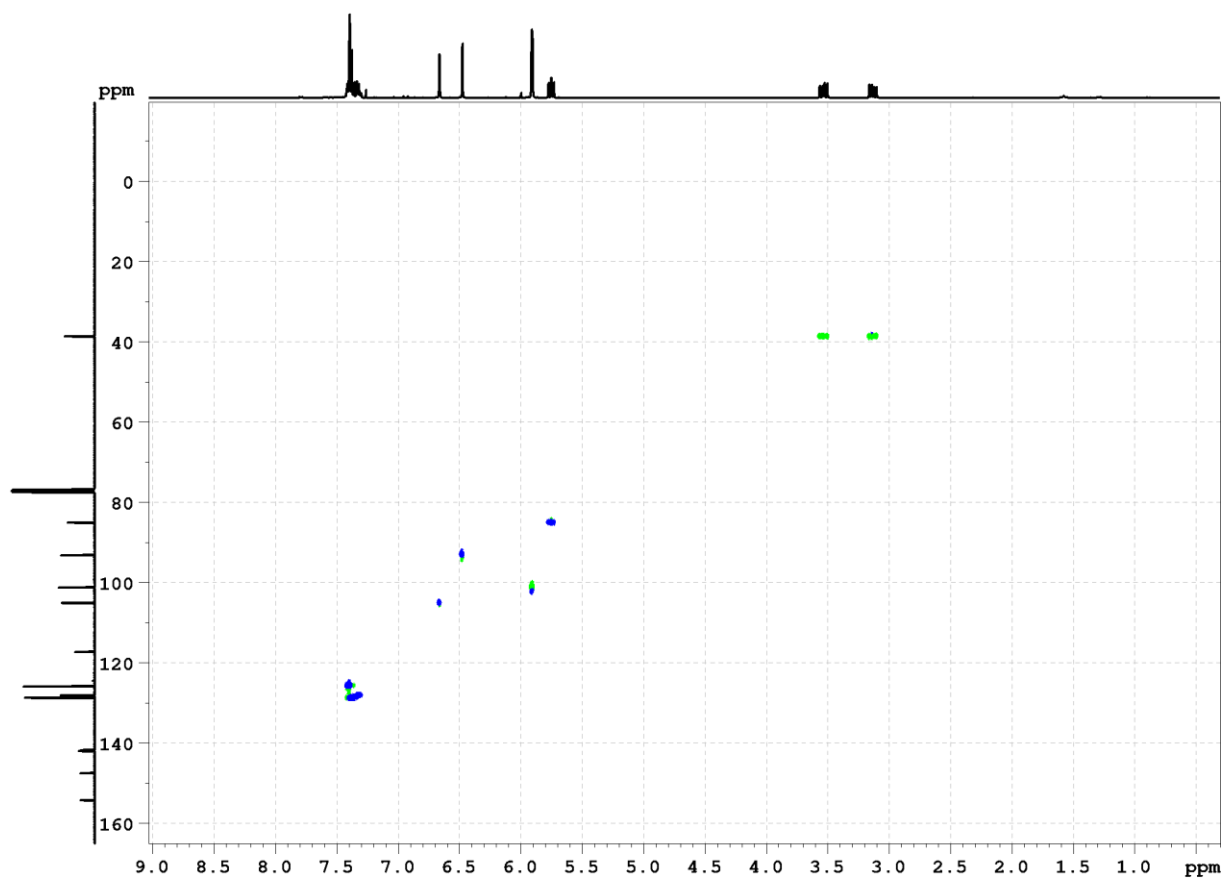
trans*-2-(4-Methoxyphenyl)-3-methyl-2,3-dihydrobenzofuran (*trans*-4c)** ¹H NMR (400 MHz, CDCl₃)cis*-2-(4-Methoxyphenyl)-3-methyl-2,3-dihydrobenzofuran (*cis*-4c)** ¹H NMR (400 MHz, CDCl₃)

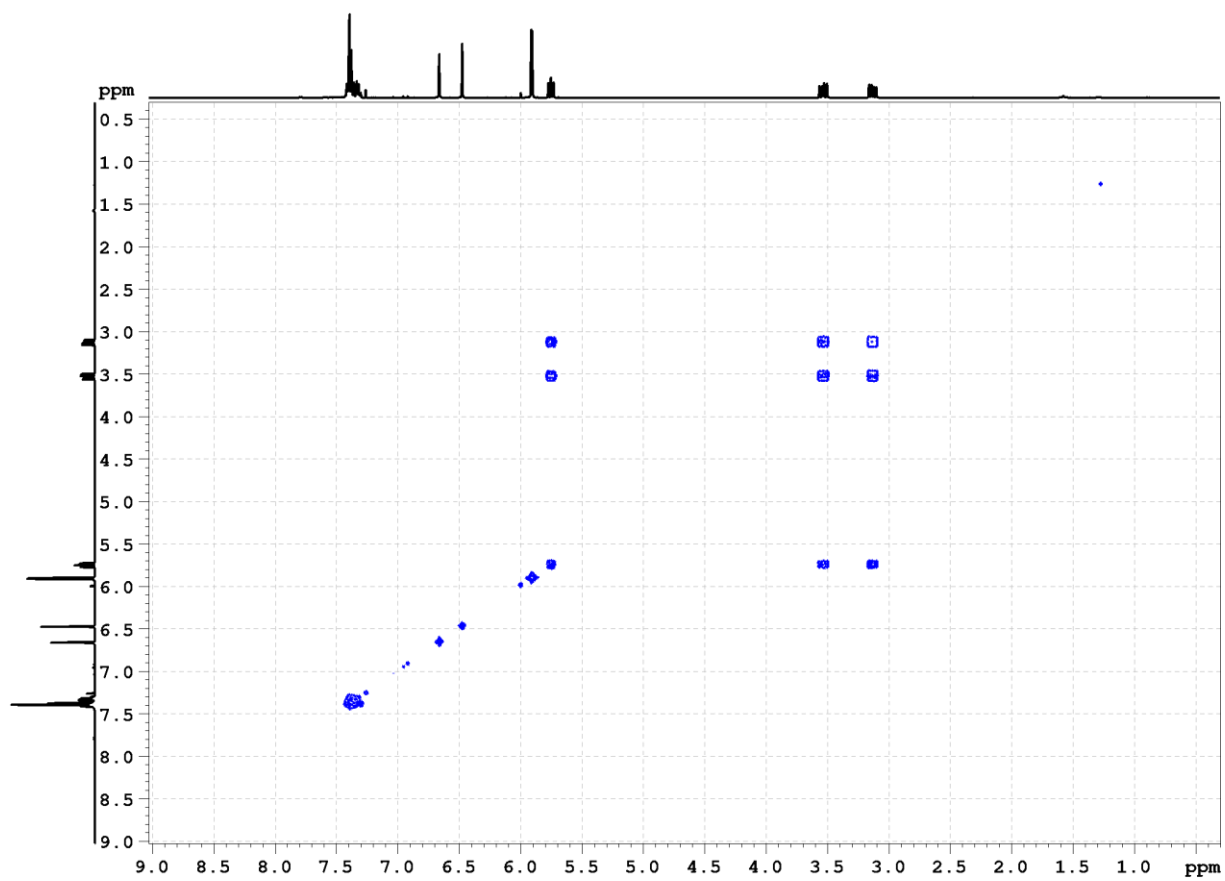
2-(3-Methoxyphenyl)-3-methyl-2,3-dihydrobenzofuran (4d)

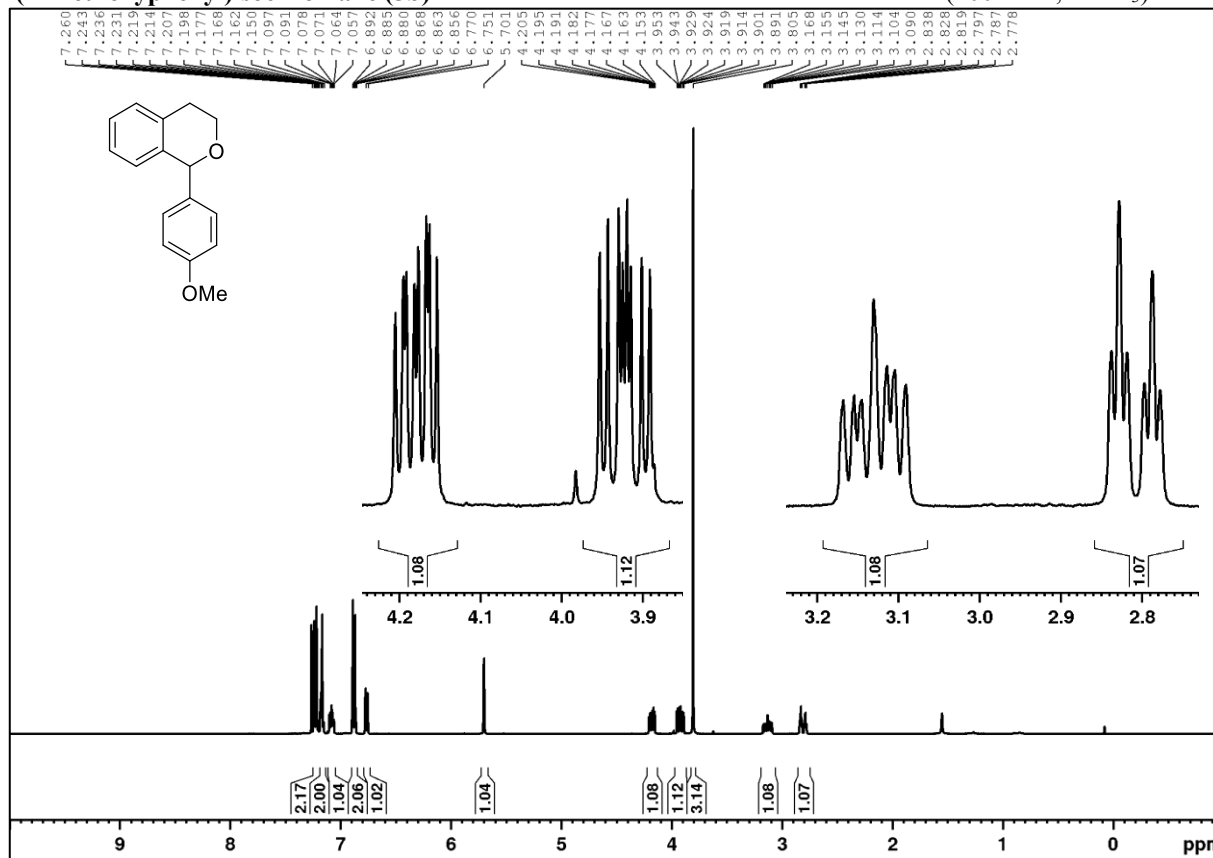
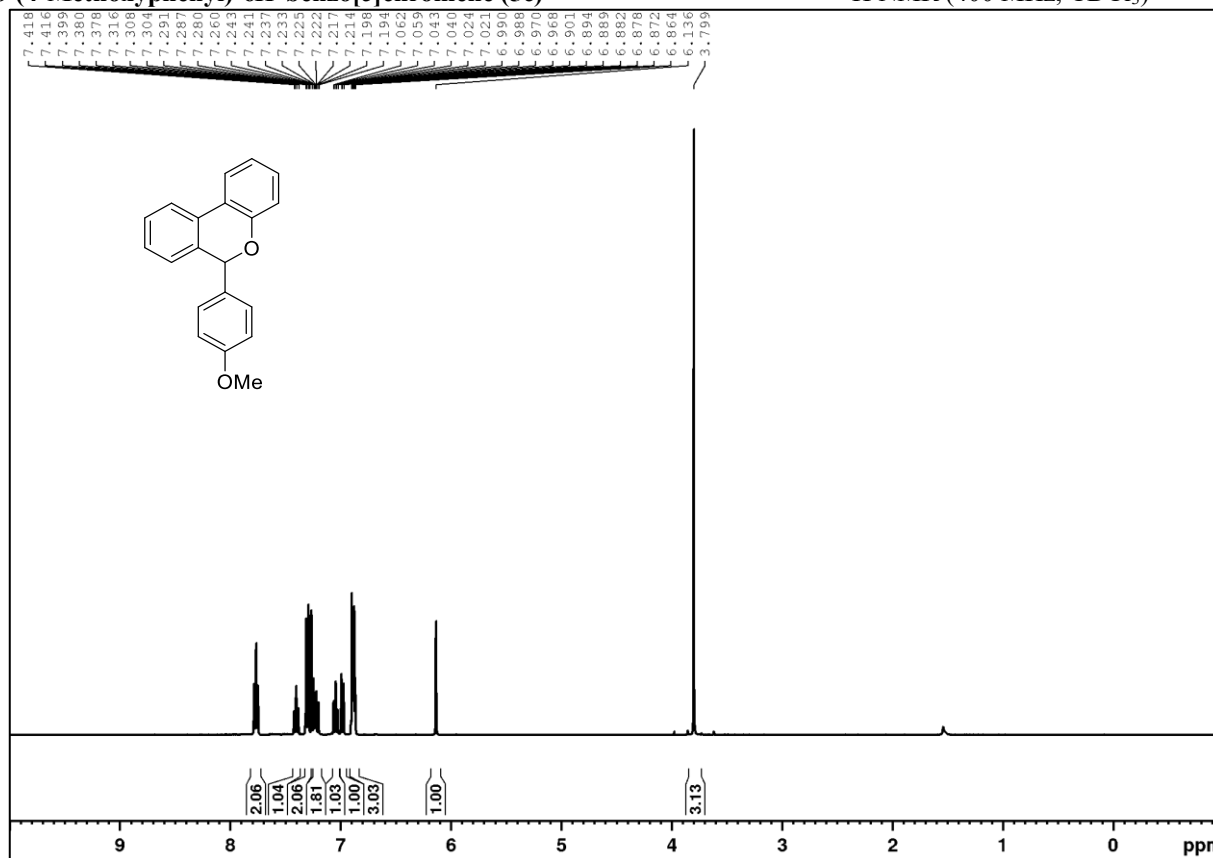
 ^1H NMR (400 MHz, CDCl_3) $^{13}\text{C}\{^1\text{H}\}$ NMR (101 MHz, CDCl_3)

6-Phenyl-6,7-dihydro-[1,3]dioxolo[4,5-f]benzofuran (4e)

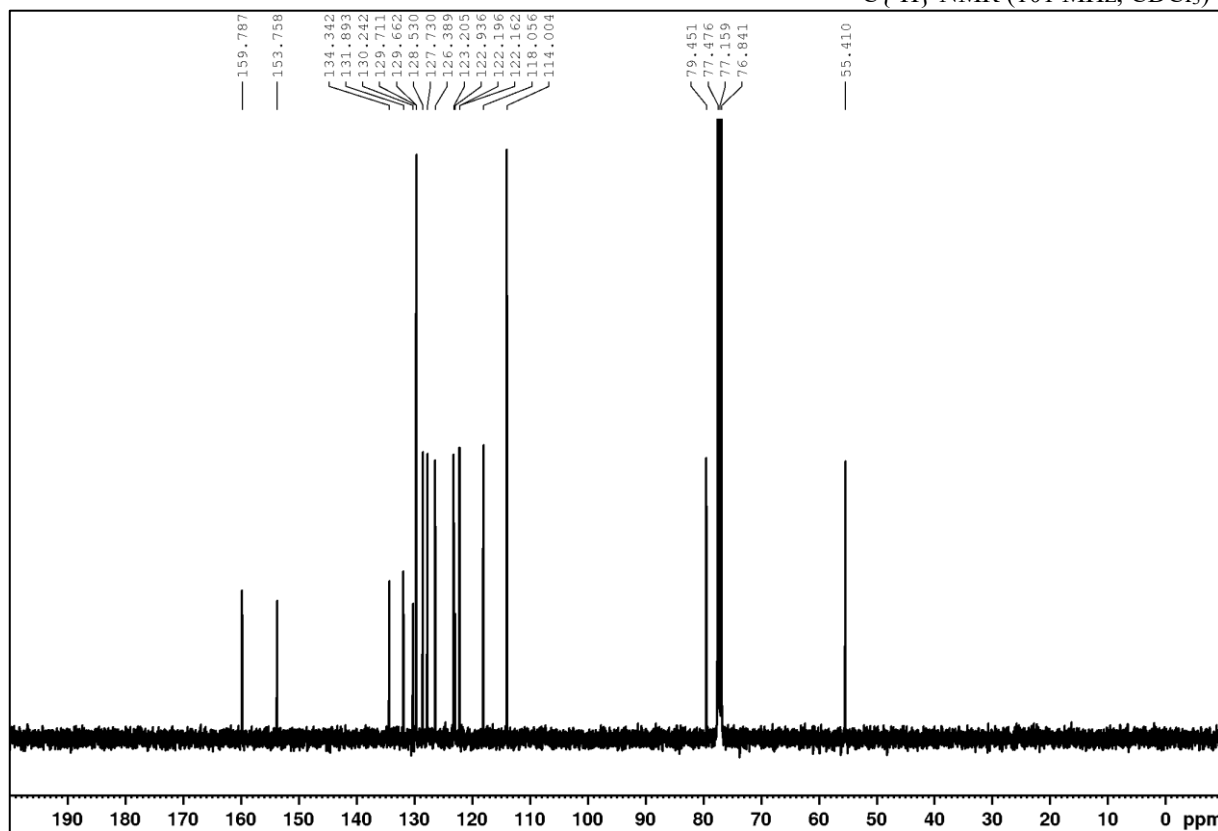
 ^1H NMR (400 MHz, CDCl_3) $^{13}\text{C}\{^1\text{H}\}$ NMR (101 MHz, CDCl_3)

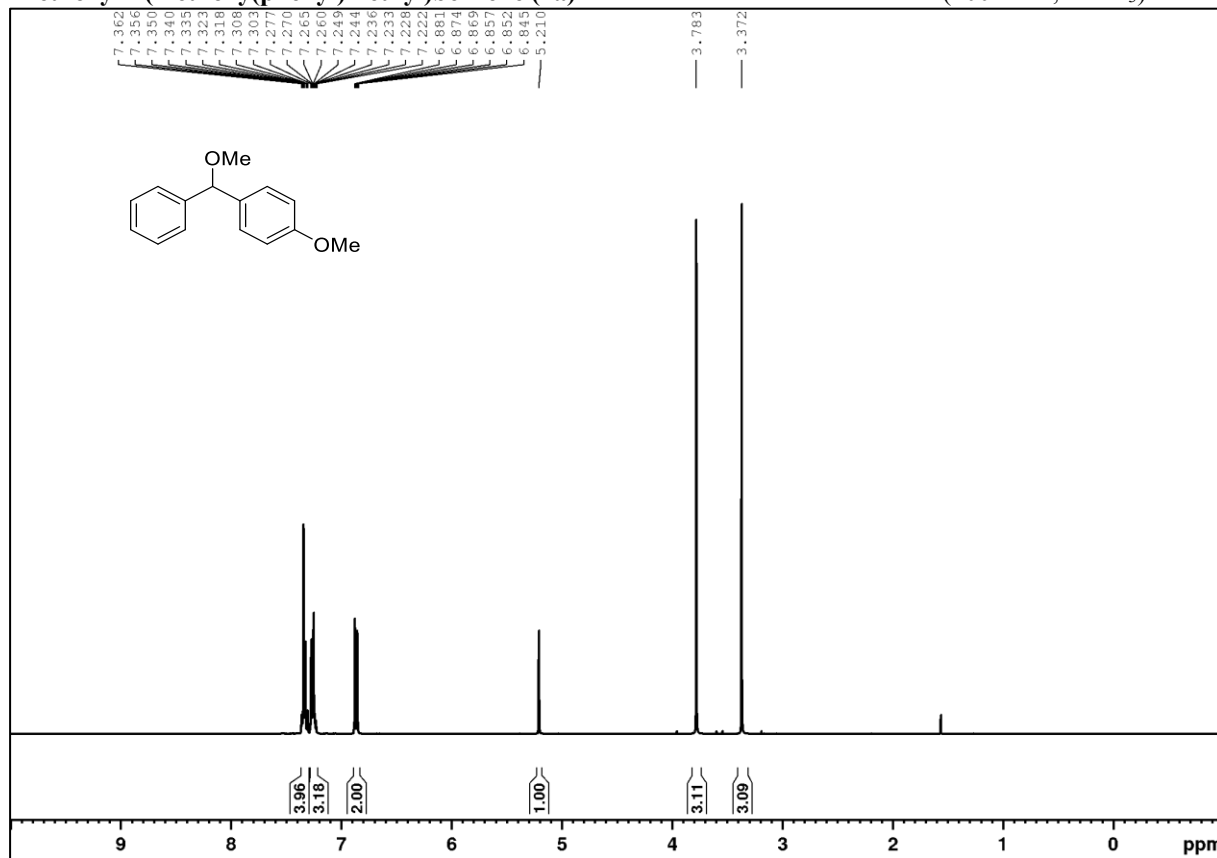
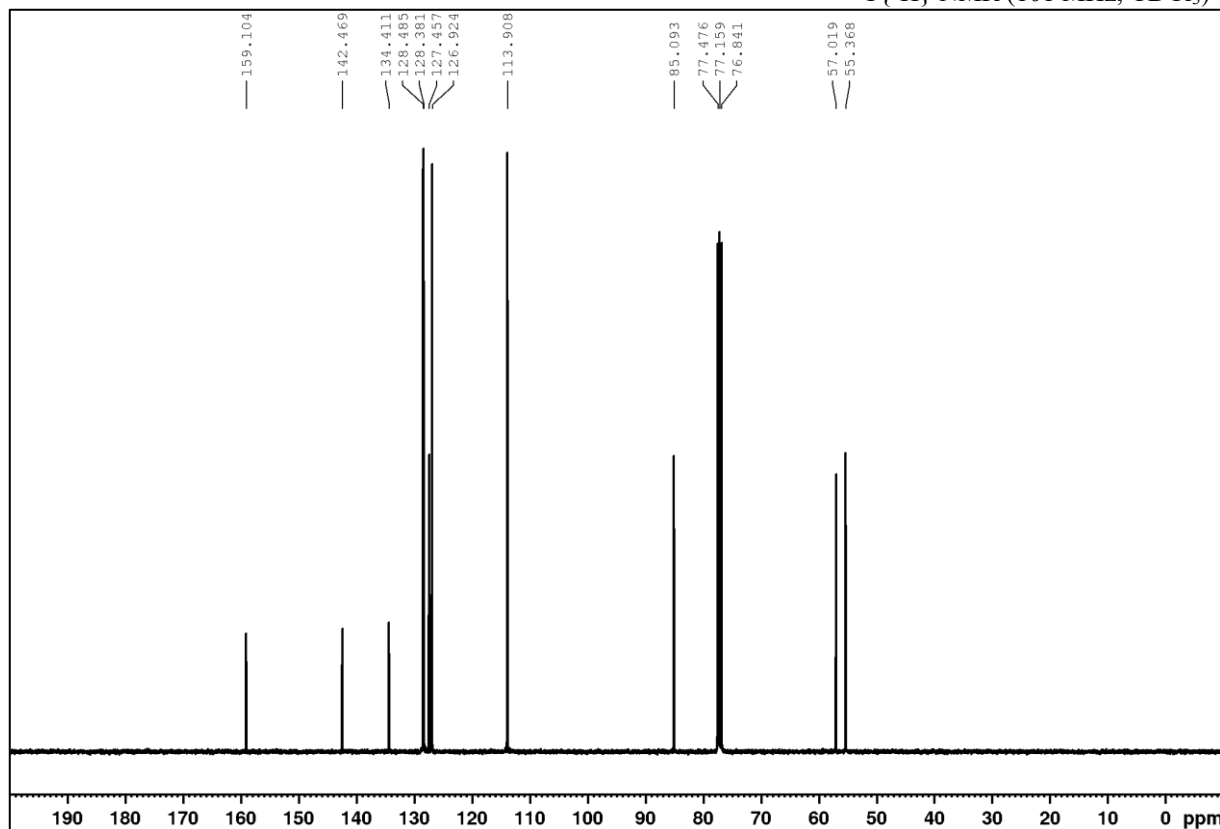
$(^1\text{H}, ^{13}\text{C})$ HSQC (CDCl_3)

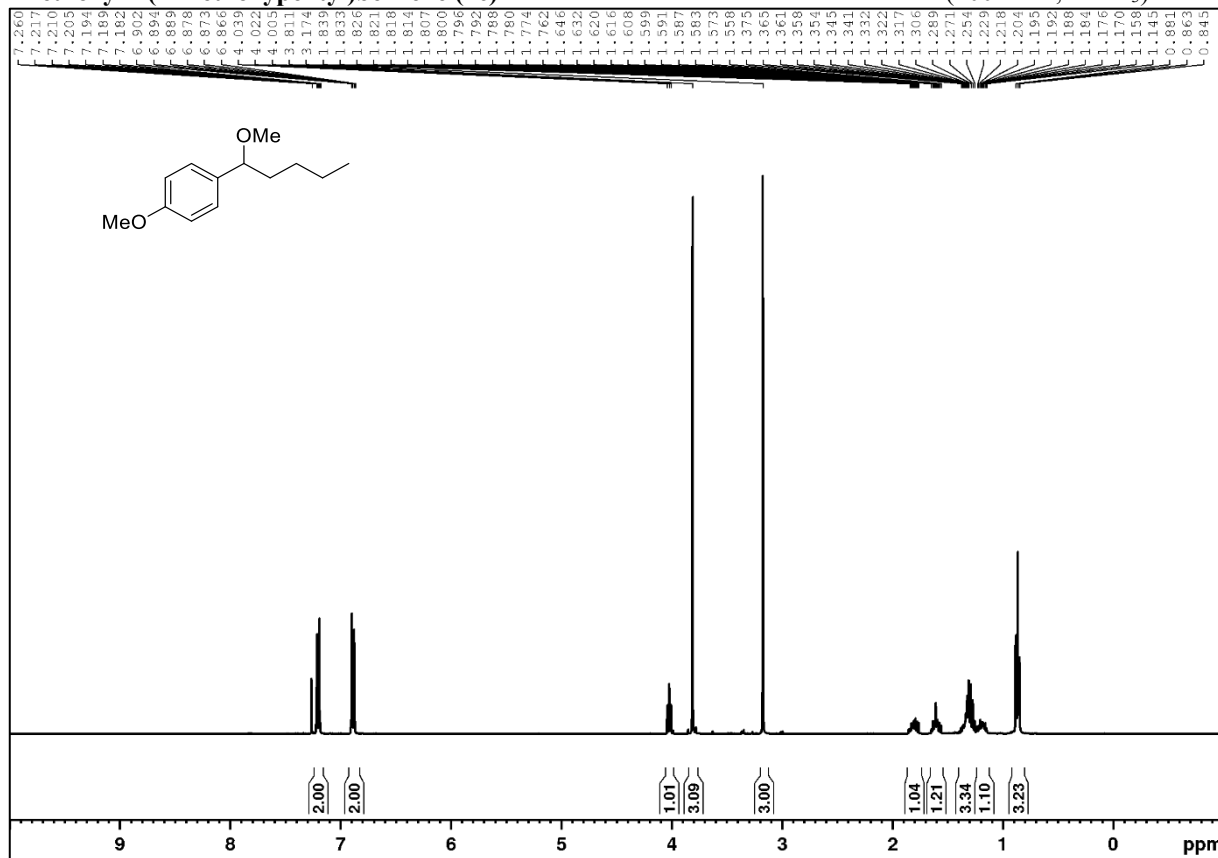
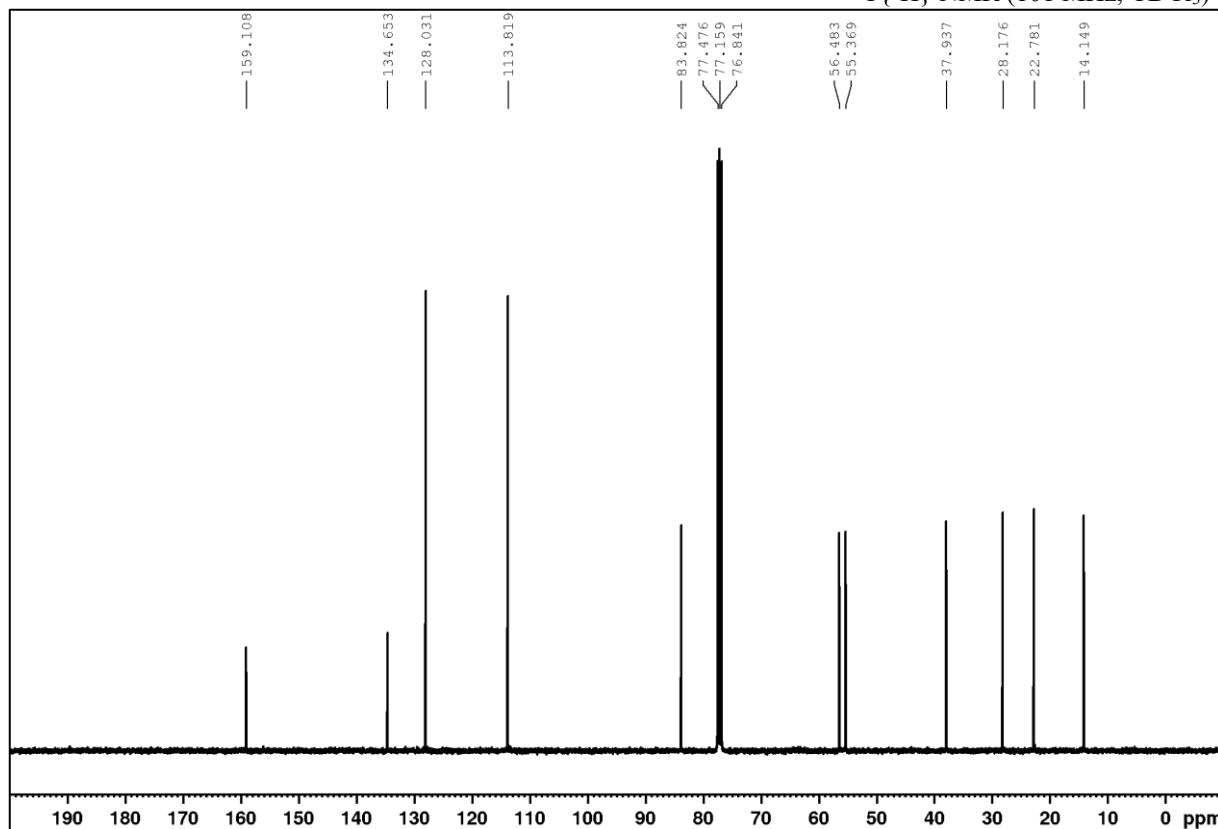
$(^1\text{H}-^1\text{H})\text{-COSY (CDCl}_3)$ 

1-(4-Methoxyphenyl)isochromane (5b)¹H NMR (400 MHz, CDCl₃)**6-(4-Methoxyphenyl)-6H-benzo[*c*]chromene (5c)**¹H NMR (400 MHz, CDCl₃)

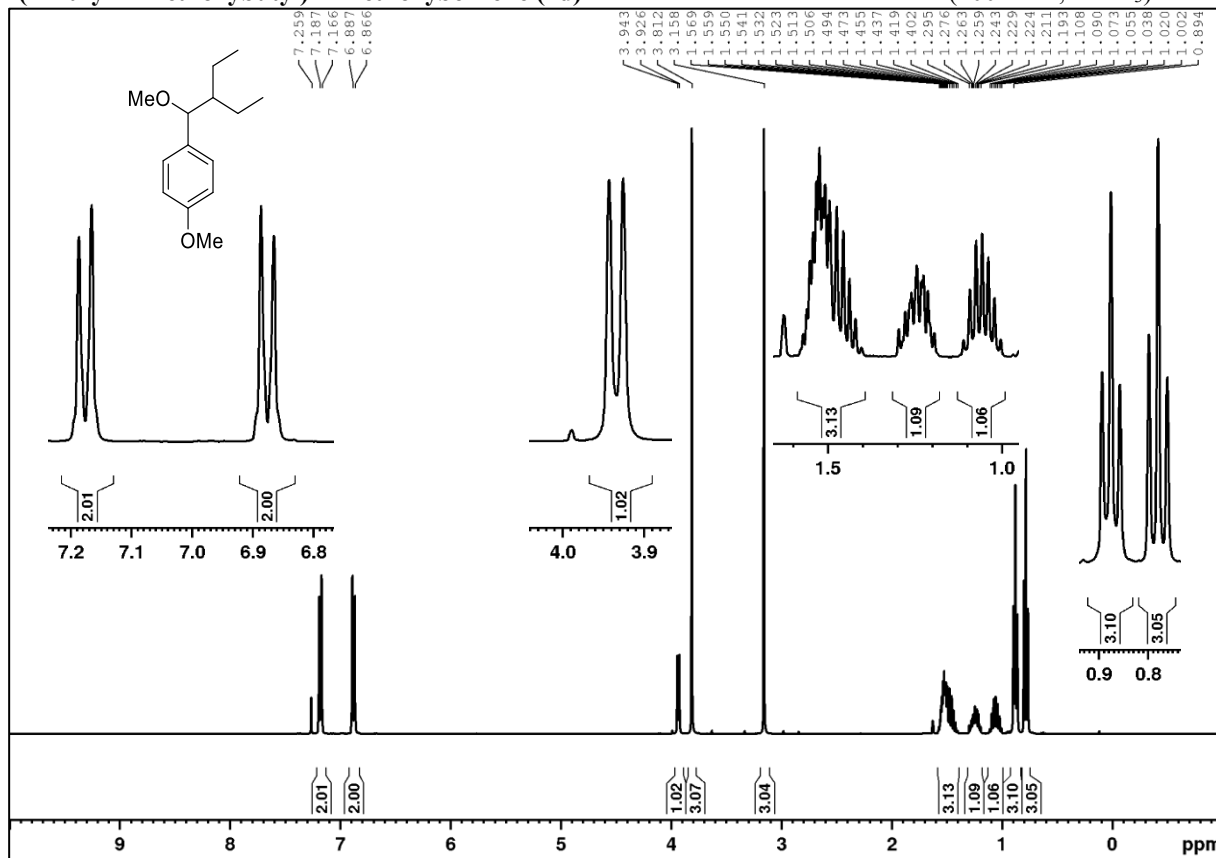
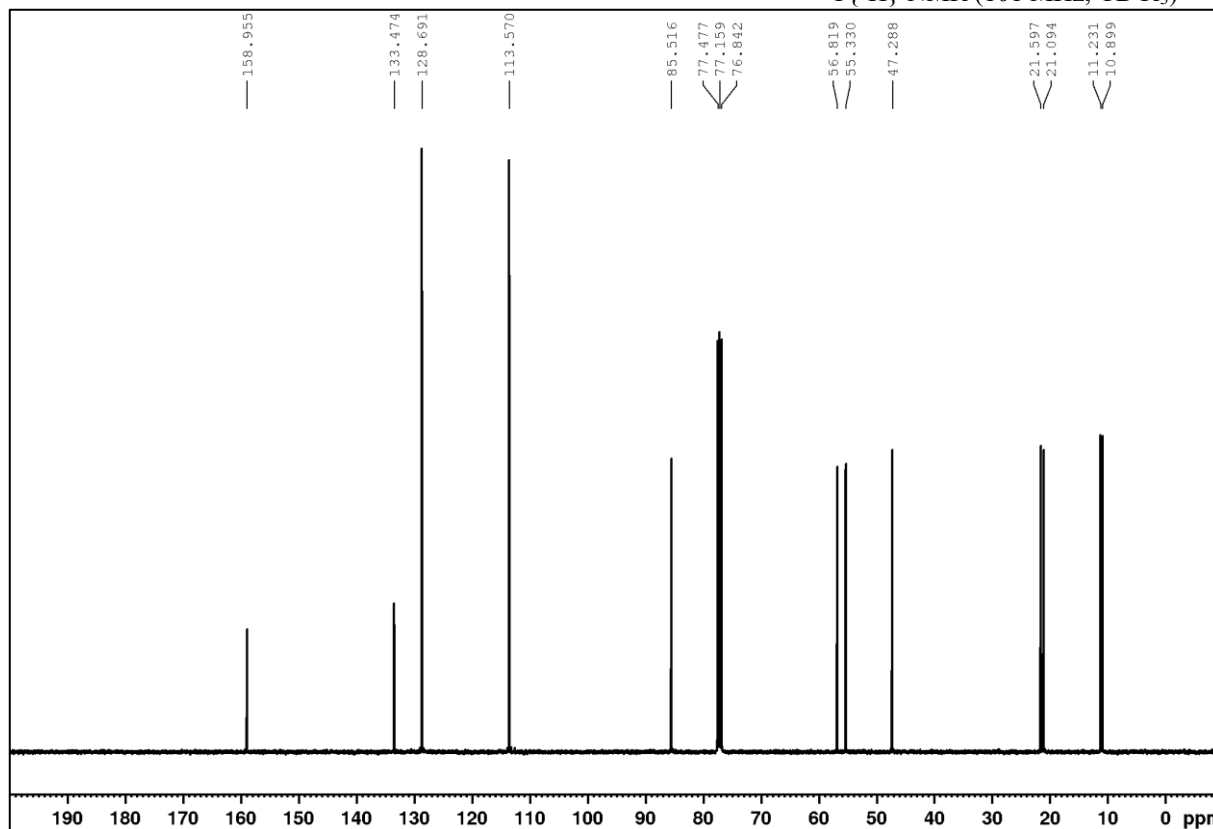
APPENDIX

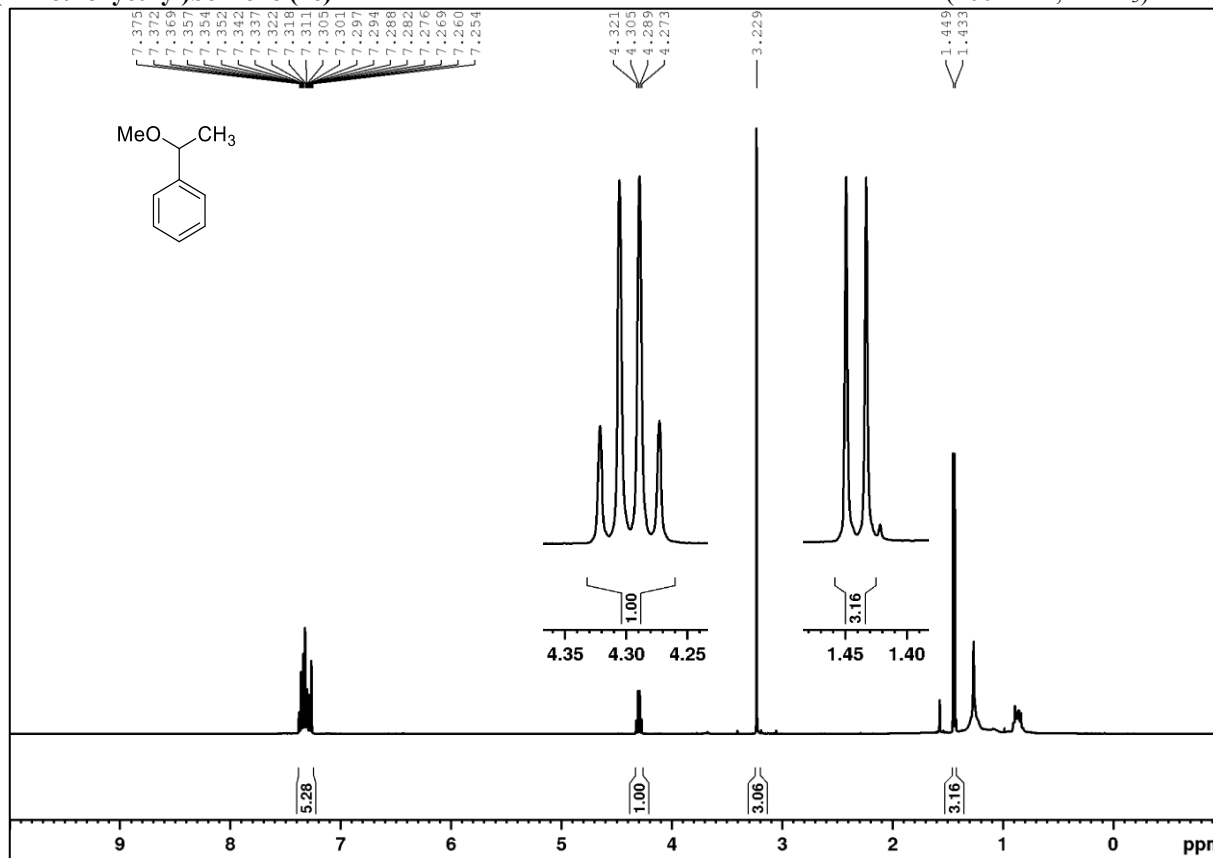
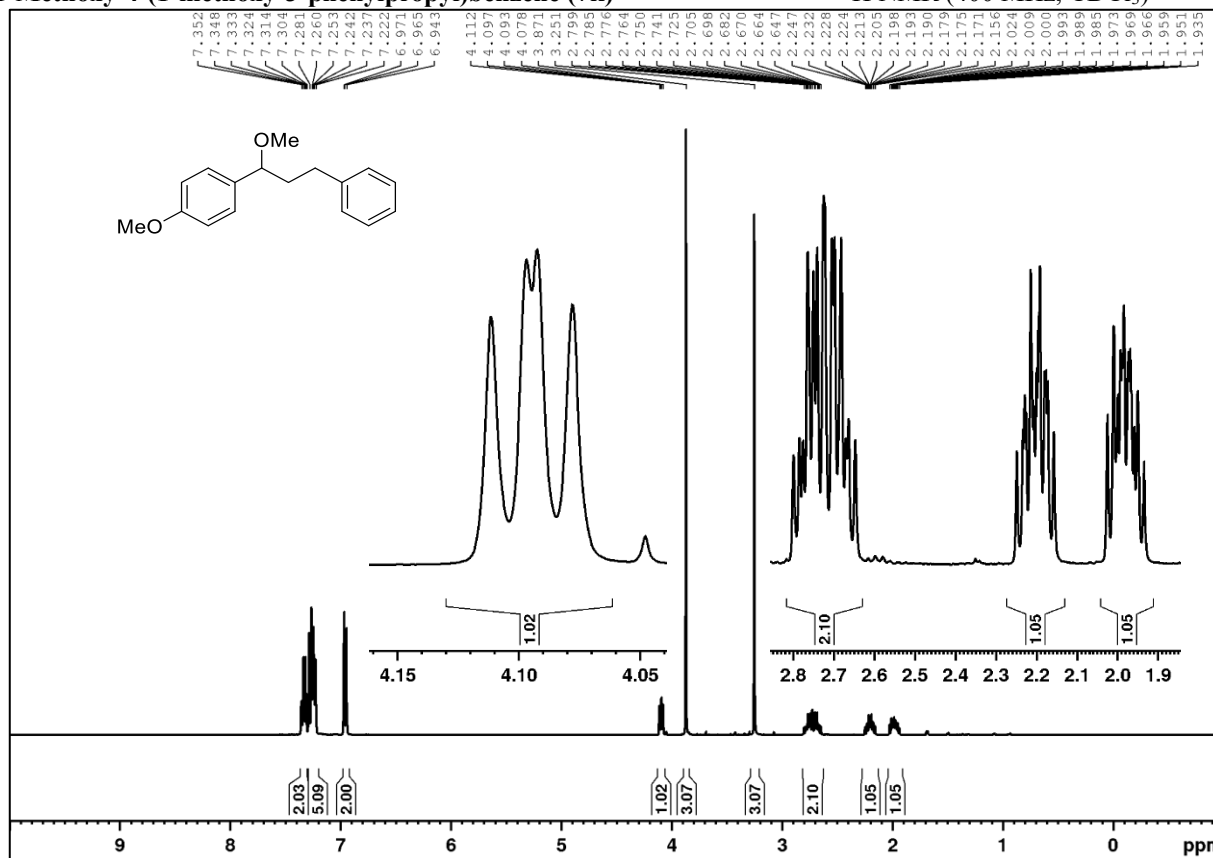
 $^{13}\text{C}\{^1\text{H}\}$ NMR (101 MHz, CDCl_3)

1-Methoxy-4-(methoxy(phenyl)methyl)benzene (7a) ^1H NMR (400 MHz, CDCl_3) $^{13}\text{C}\{^1\text{H}\}$ NMR (101 MHz, CDCl_3)

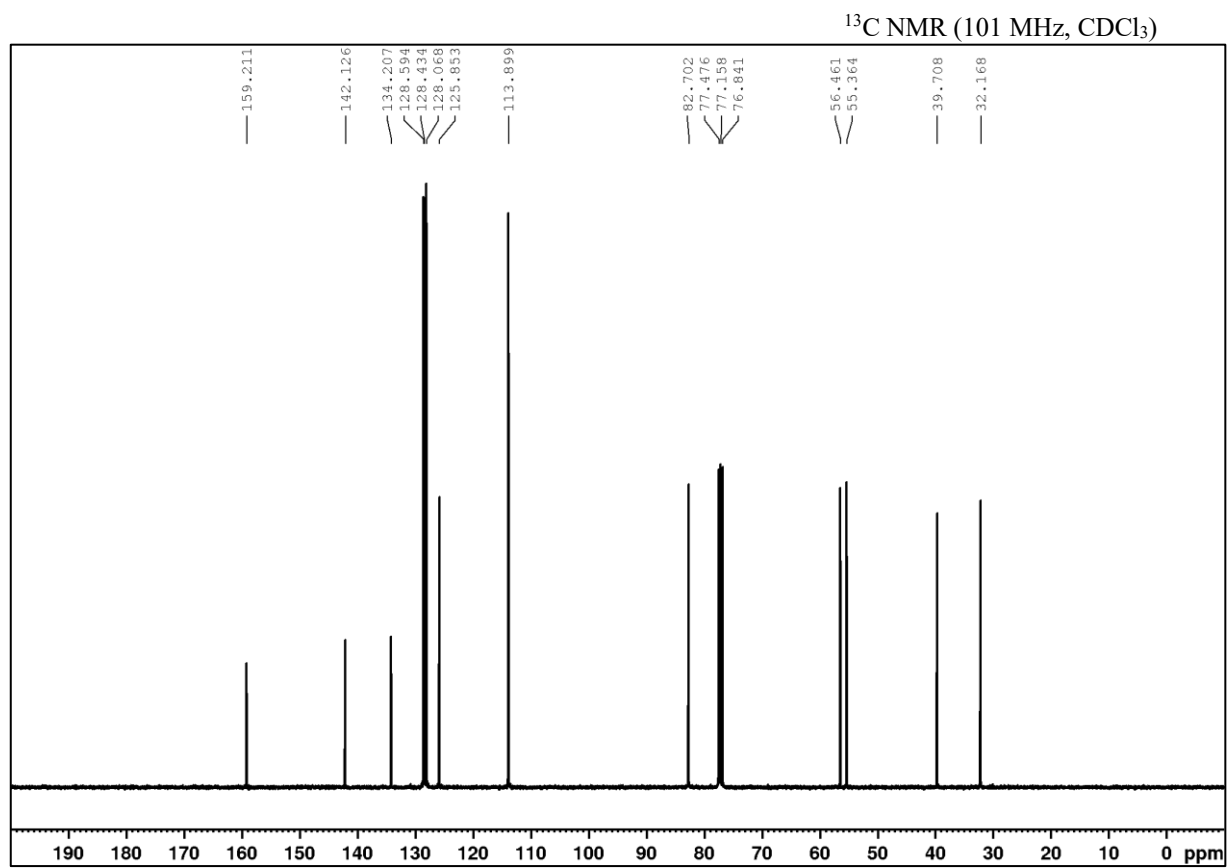
1-Methoxy-4-(1-methoxypropyl)benzene (7c) ^1H NMR (400 MHz, CDCl_3) $^{13}\text{C}\{^1\text{H}\}$ NMR (101 MHz, CDCl_3)

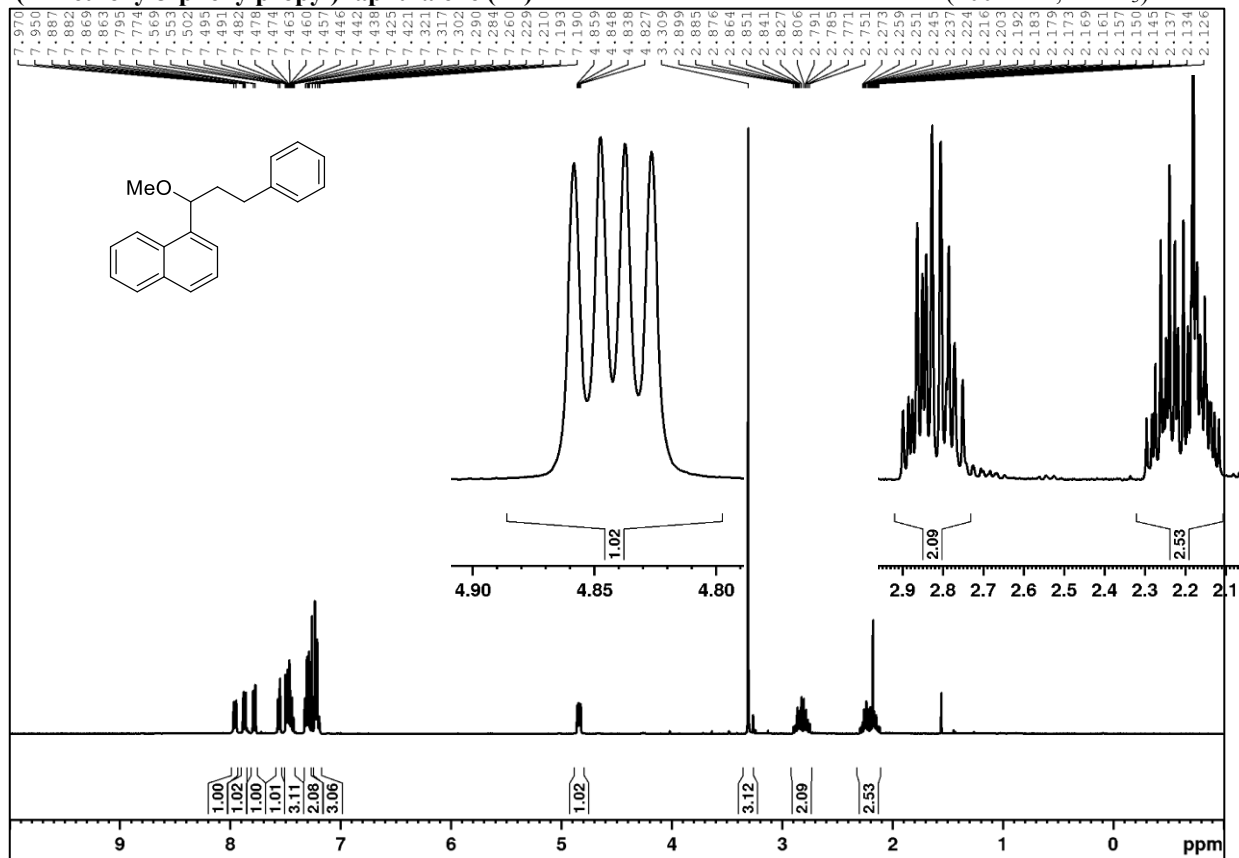
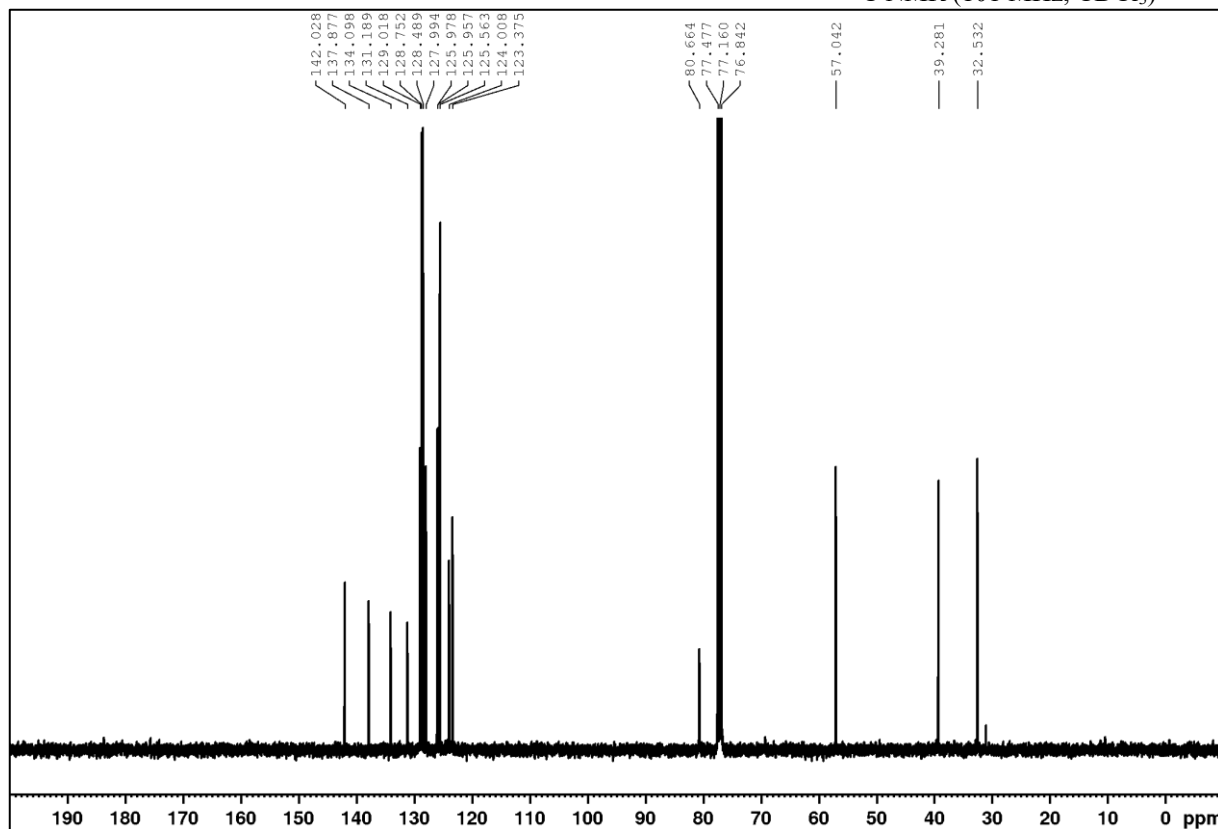
1-(2-Ethyl-1-methoxybutyl)-4-methoxybenzene (7d)

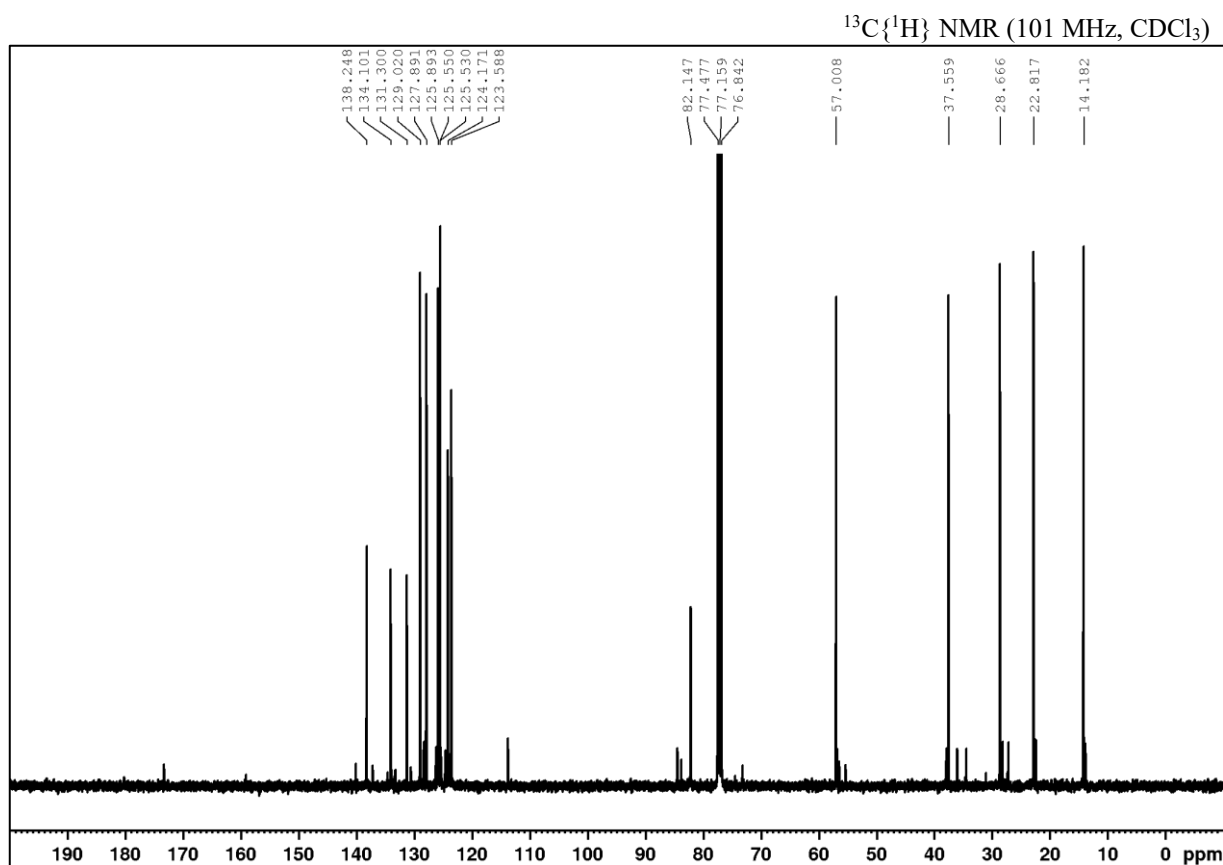
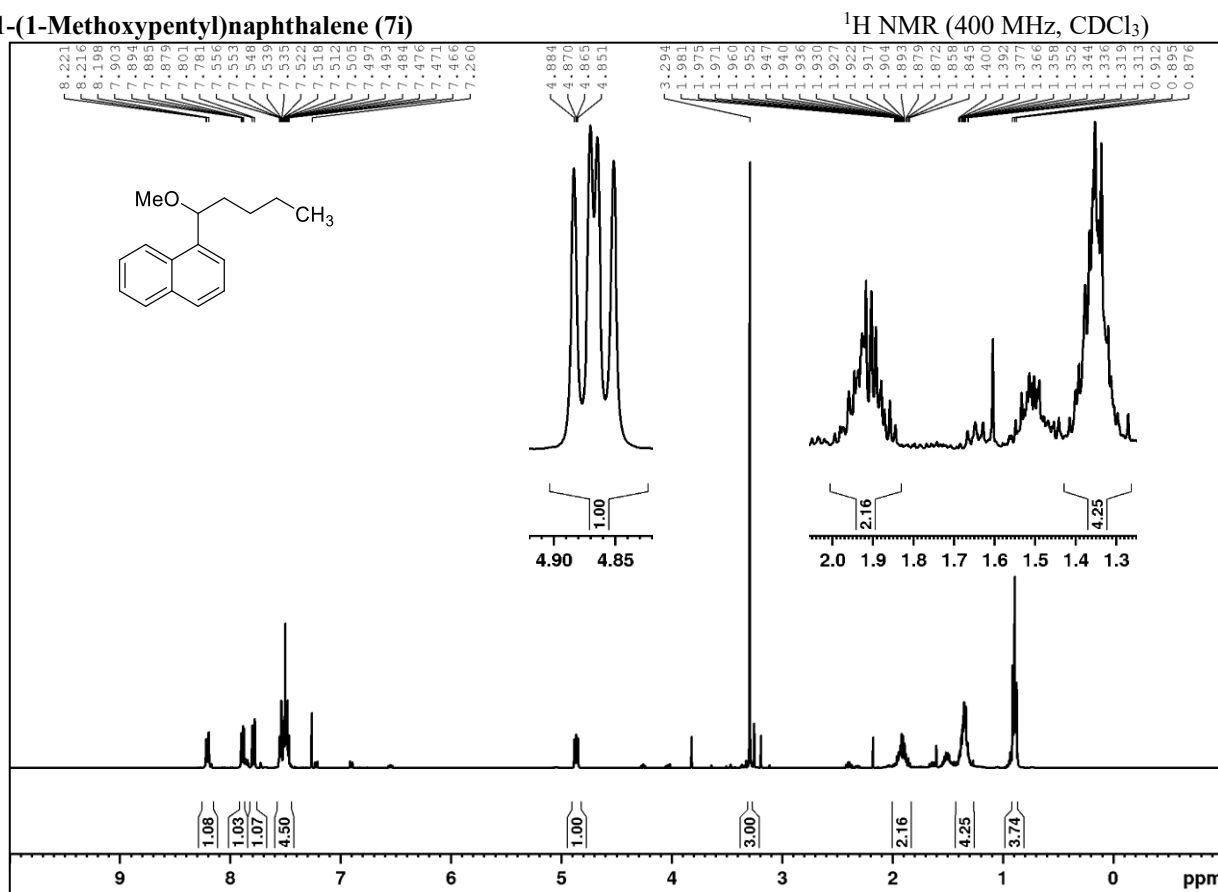
 ^1H NMR (400 MHz, CDCl_3) $^{13}\text{C}\{^1\text{H}\}$ NMR (101 MHz, CDCl_3)

(1-Methoxyethyl)benzene (7e) $^1\text{H NMR}$ (400 MHz, CDCl_3)**1-Methoxy-4-(1-methoxy-3-phenylpropyl)benzene (7k)** $^1\text{H NMR}$ (400 MHz, CDCl_3)

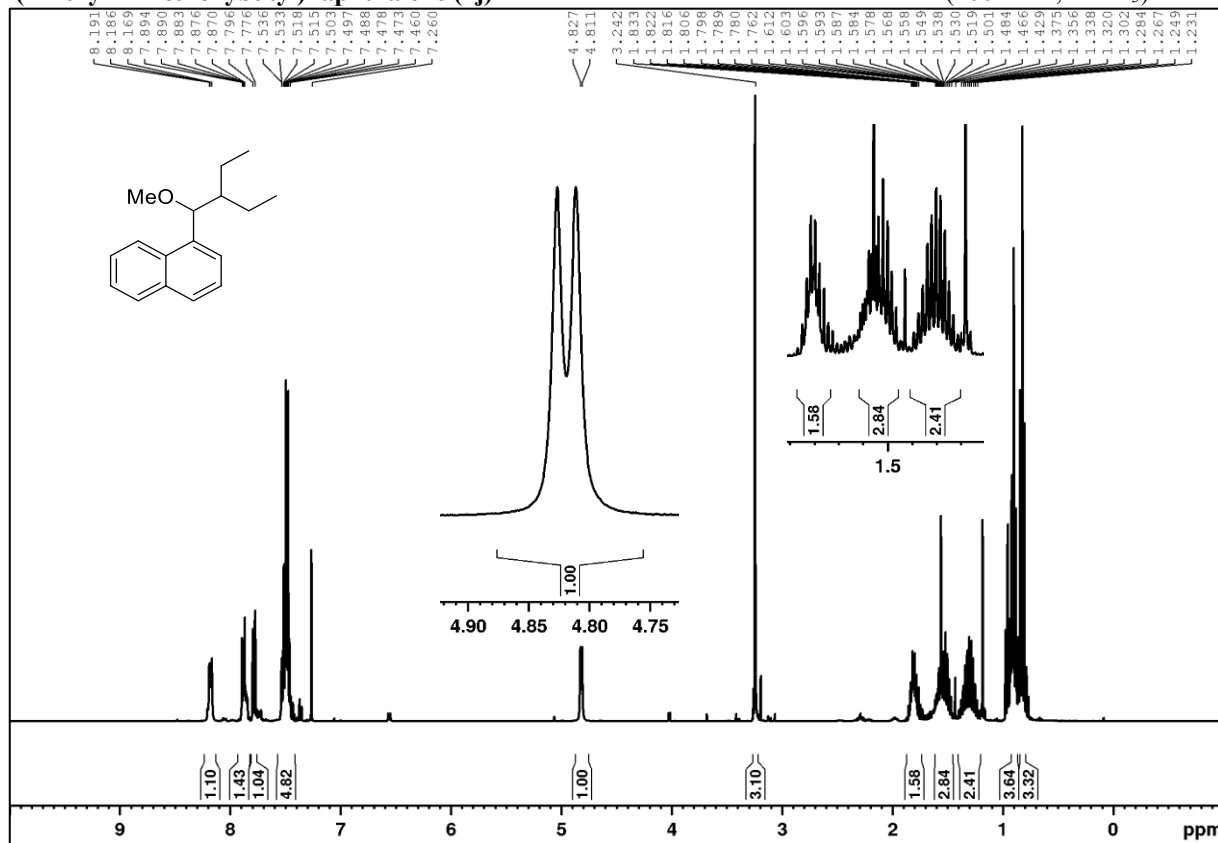
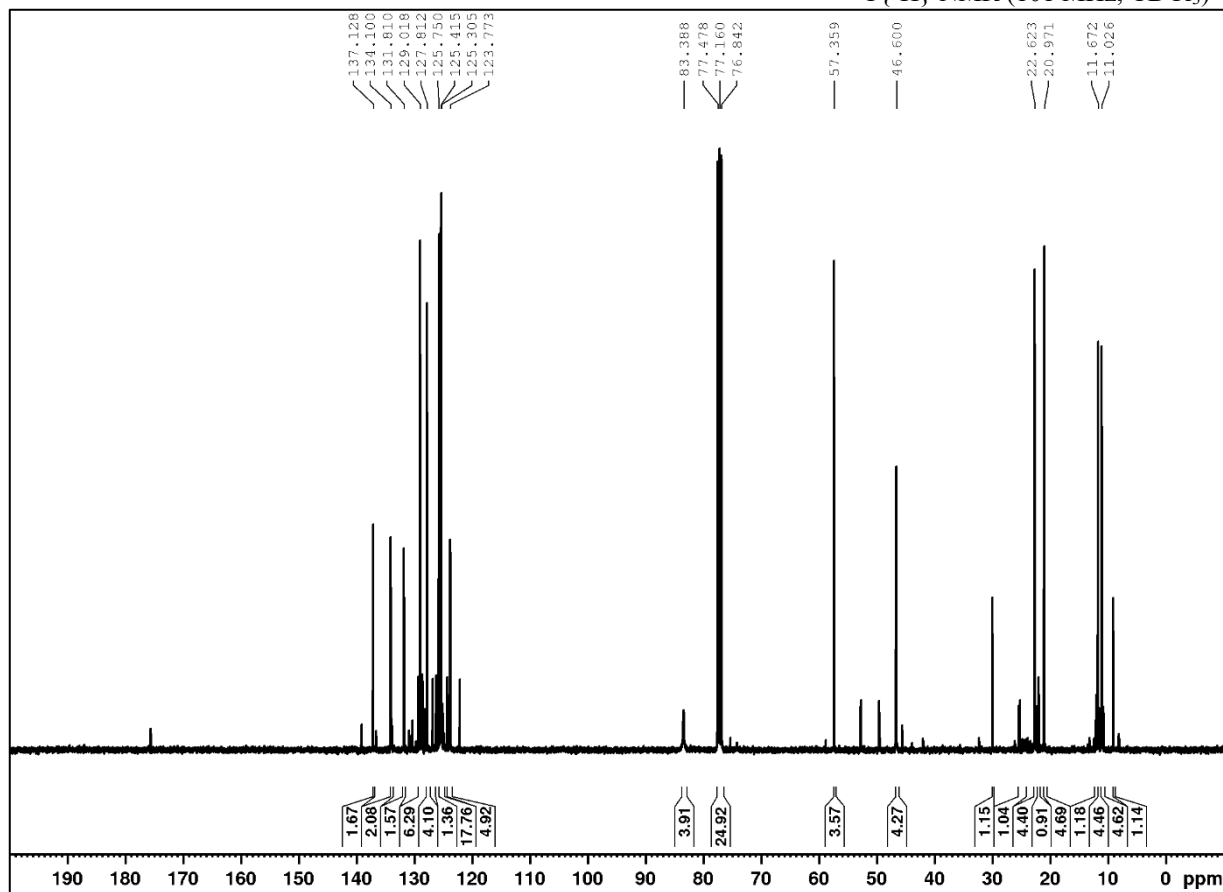
APPENDIX



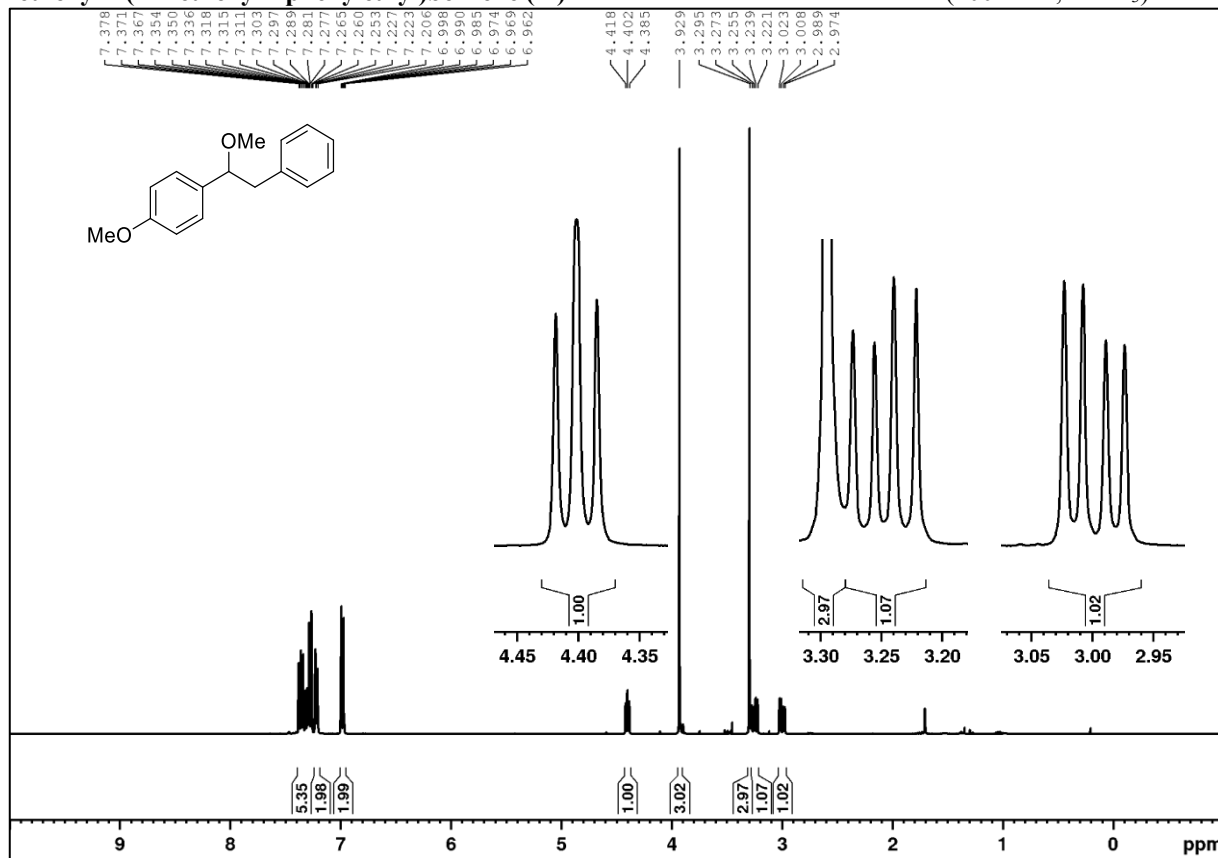
1-(1-Methoxy-3-phenylpropyl)naphthalene (7h) **^1H NMR (400 MHz, CDCl_3)** **^{13}C NMR (101 MHz, CDCl_3)**

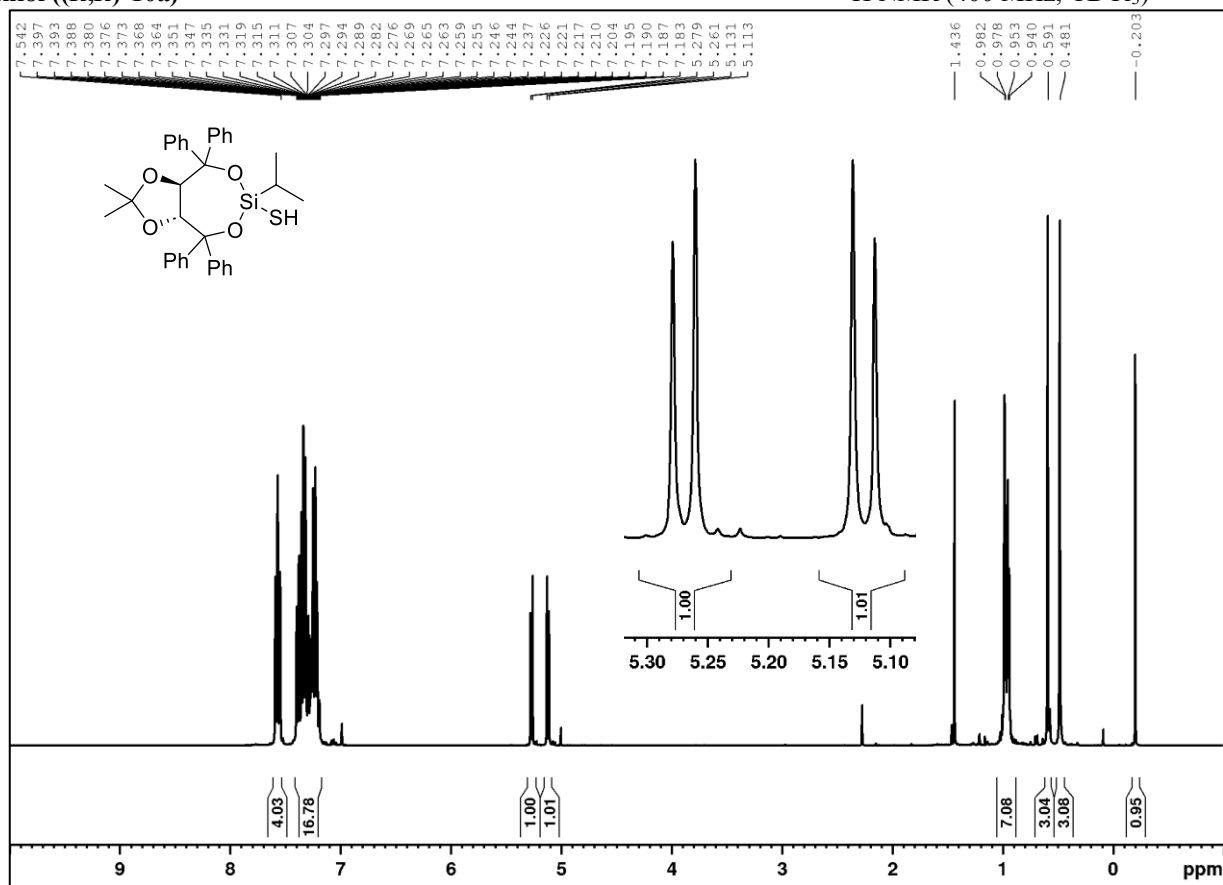
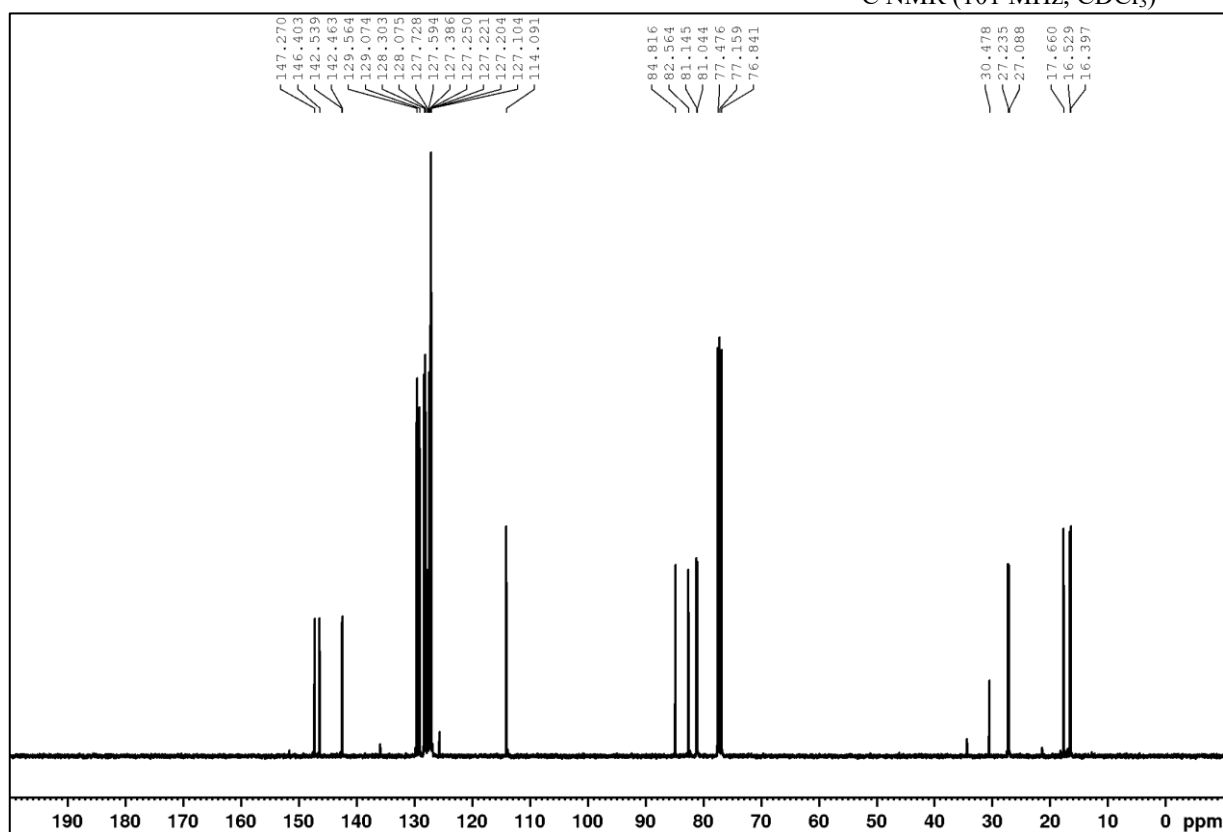
1-(1-Methoxypropyl)naphthalene (7i)

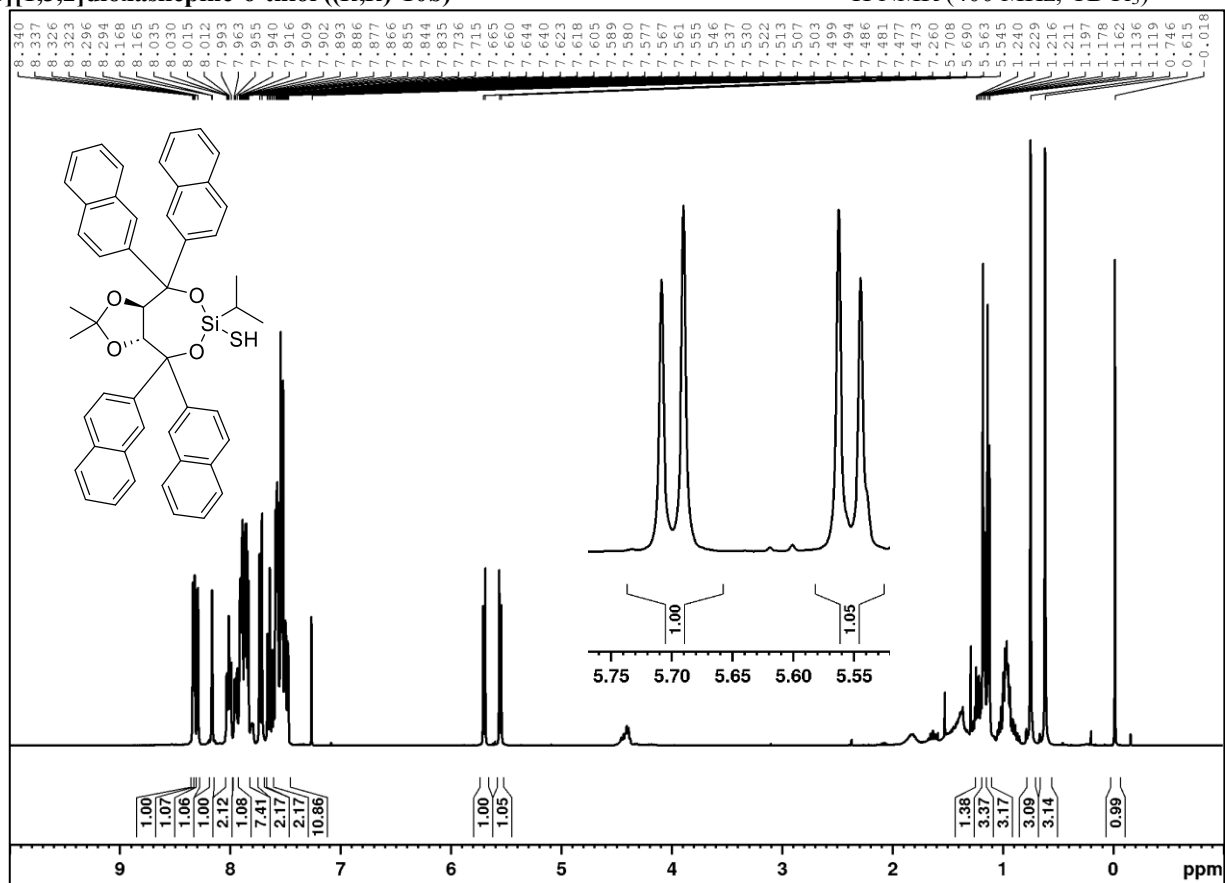
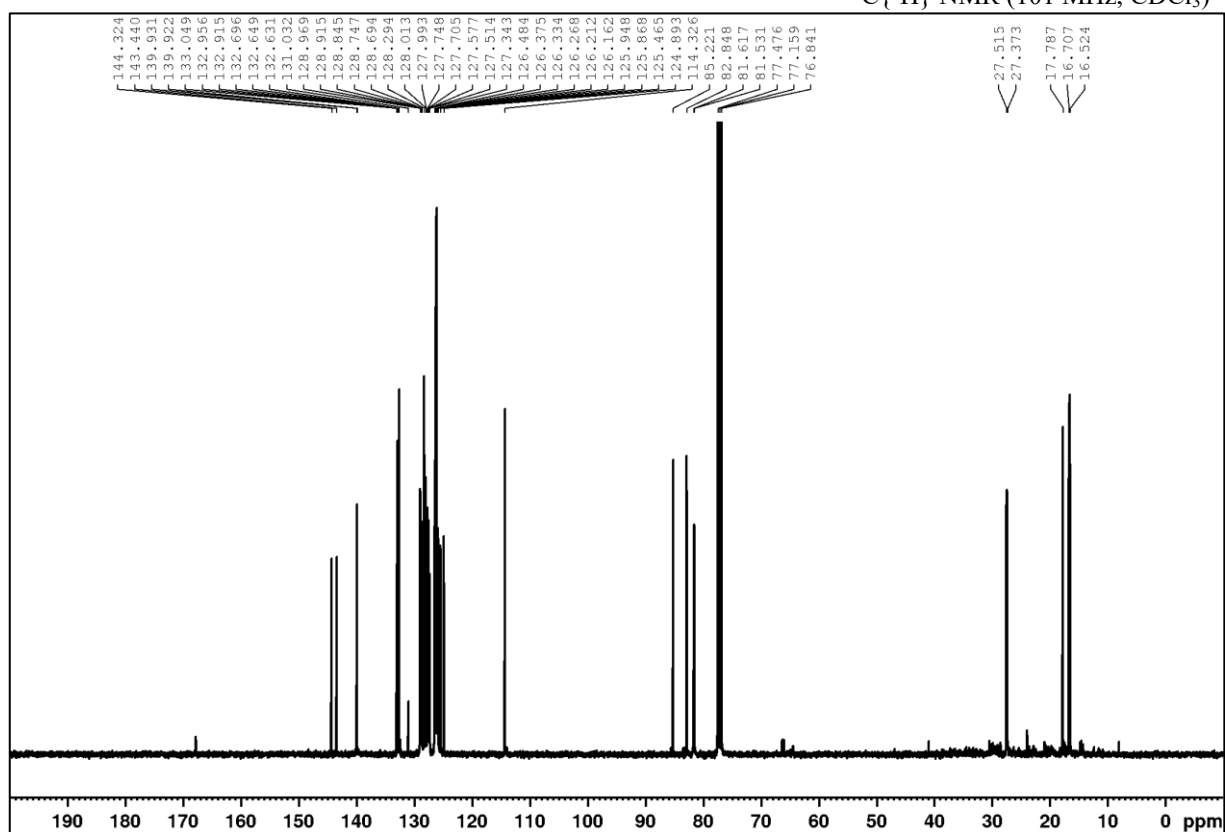
1-(2-Ethyl-1-methoxybutyl)naphthalene (7j)

 ^1H NMR (400 MHz, CDCl_3) $^{13}\text{C}\{^1\text{H}\}$ NMR (101 MHz, CDCl_3)

Methoxy-4-(1-methoxy-2-phenylethyl)benzene (7f)

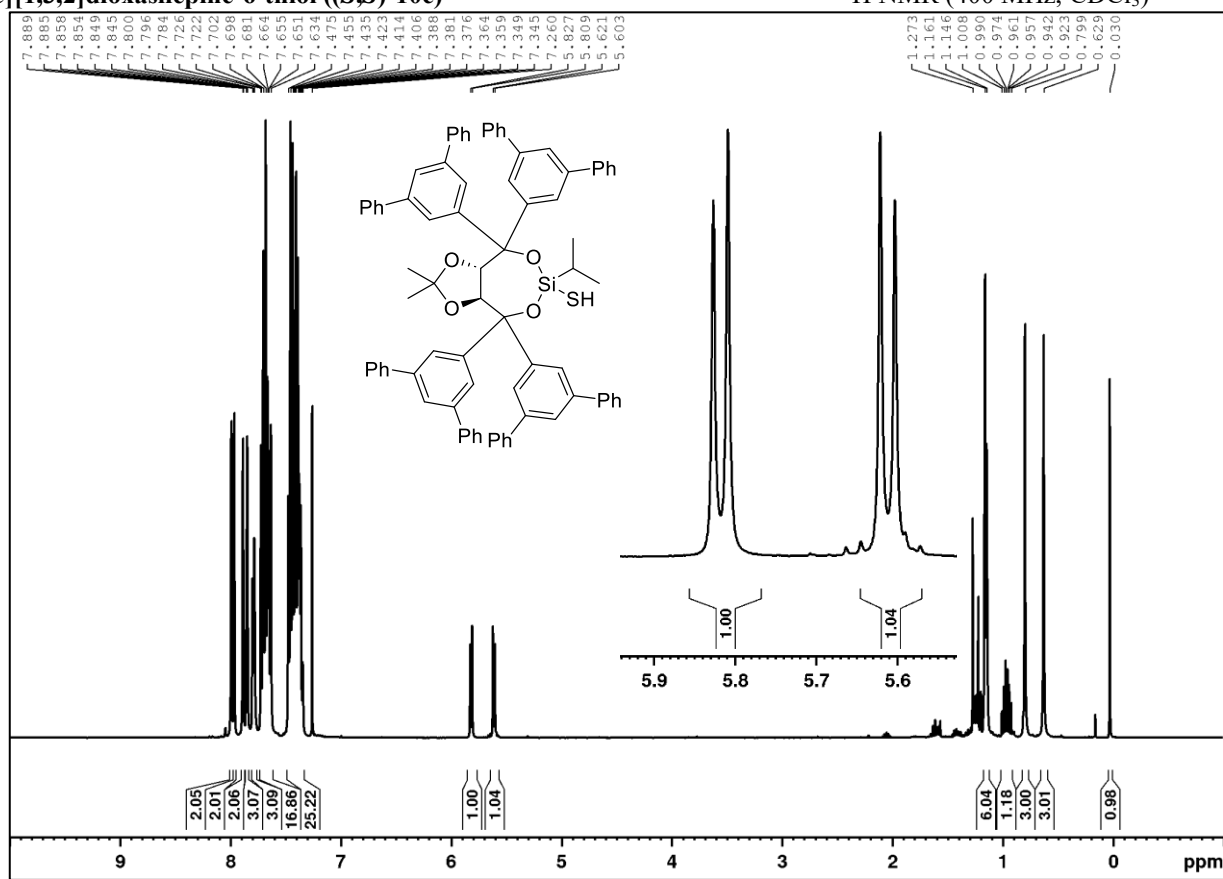
 ^1H NMR (400 MHz, CDCl_3)

(3*aR*,8*aR*)-6-isopropyl-2,2-dimethyl-4,4,8,8-tetraphenyltetrahydro-[1,3]dioxolo[4,5-*e*][1,3,2]dioxasilpine-6-thiol ((*R,R*)-10a)¹H NMR (400 MHz, CDCl₃)¹³C NMR (101 MHz, CDCl₃)

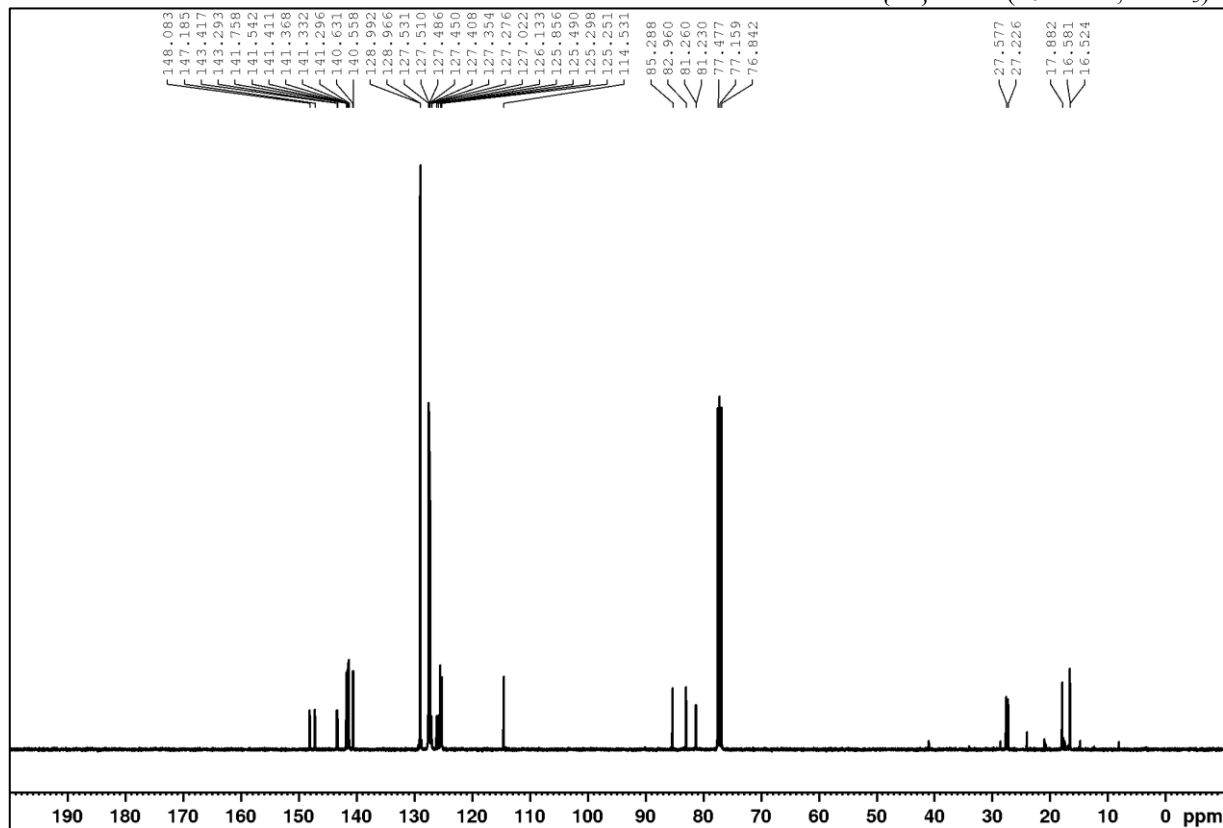
(3*aR*,8*aR*)-6-Isopropyl-2,2-dimethyl-4,4,8,8-tetra(naphthalen-2-yl)tetrahydro-[1,3]dioxolo[4,5-*e*][1,3,2]dioxasilpine-6-thiol ((*R,R*)-10b)¹H NMR (400 MHz, CDCl₃)¹³C{¹H} NMR (101 MHz, CDCl₃)

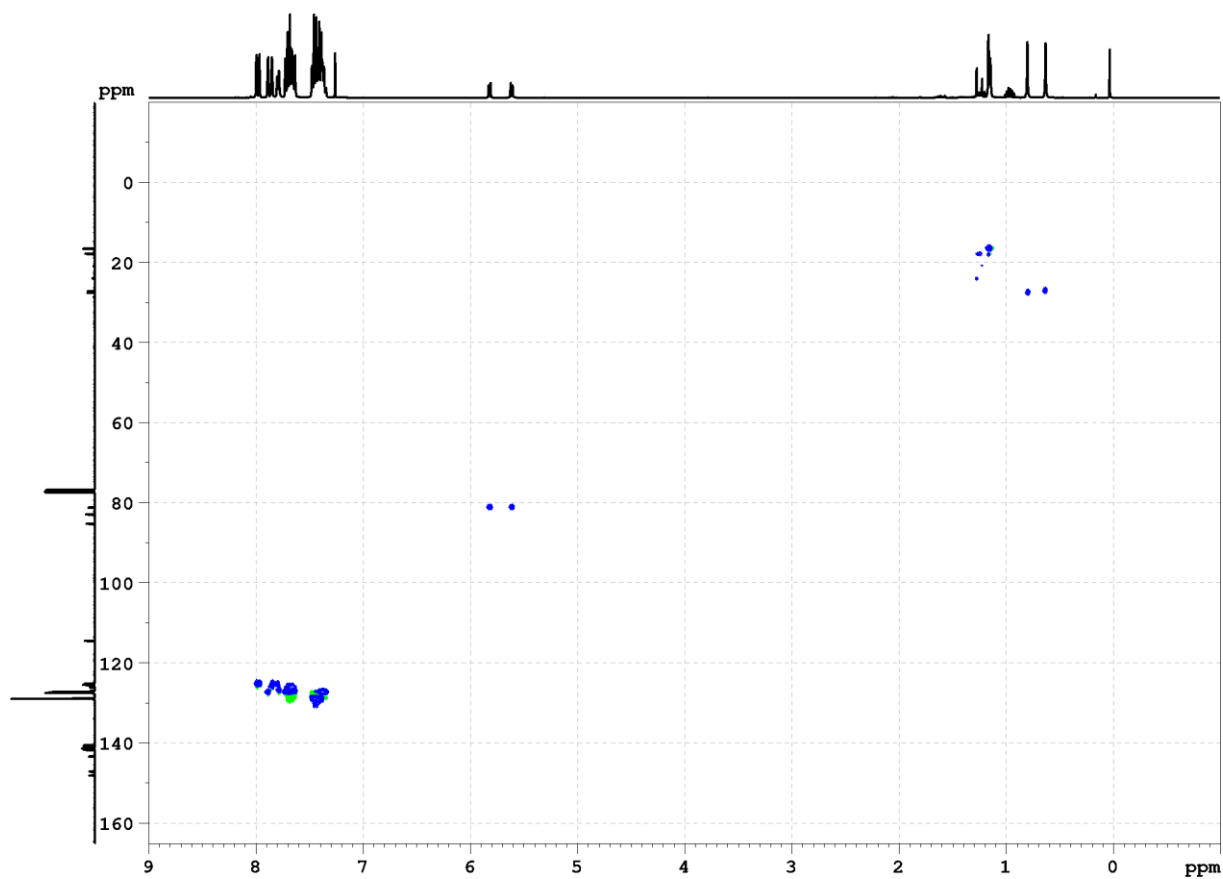
(3*aS*,8*aS*)-4,4,8,8-Tetra(1,1':3',1''-terphenyl)-5'-yl)-6-isopropyl-2,2-dimethyltetrahydro-[1,3]dioxolo[4,5-*e*][1,3,2]dioxasilepine-6-thiol ((*S,S*)-10c)

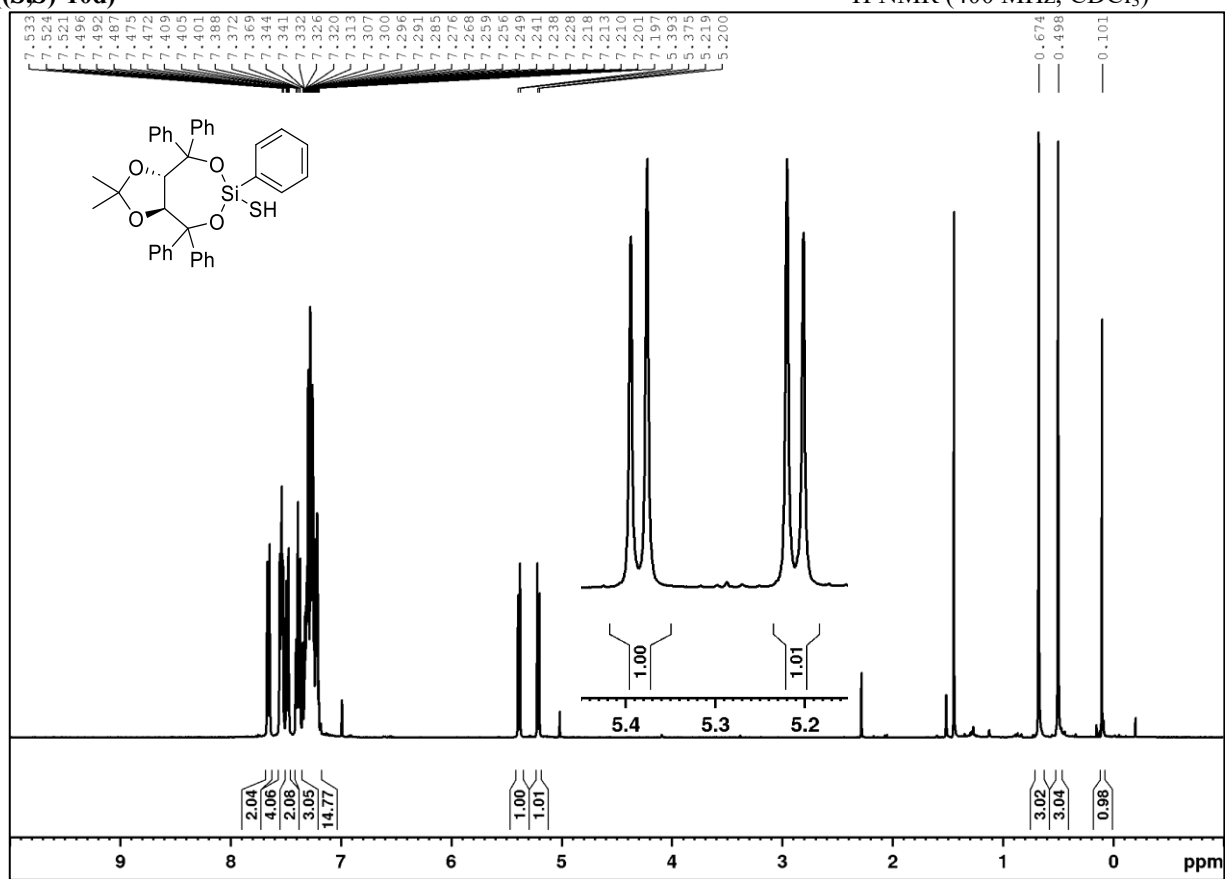
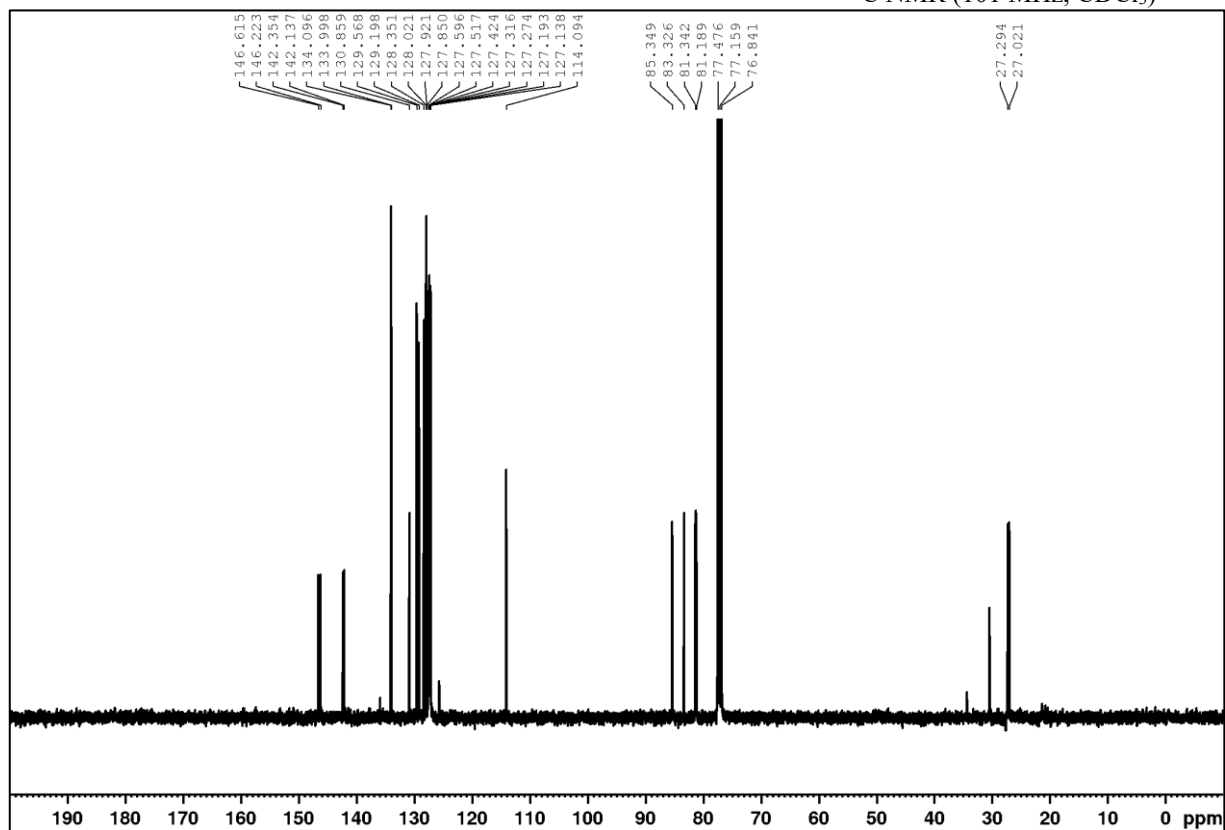
¹H NMR (400 MHz, CDCl₃)

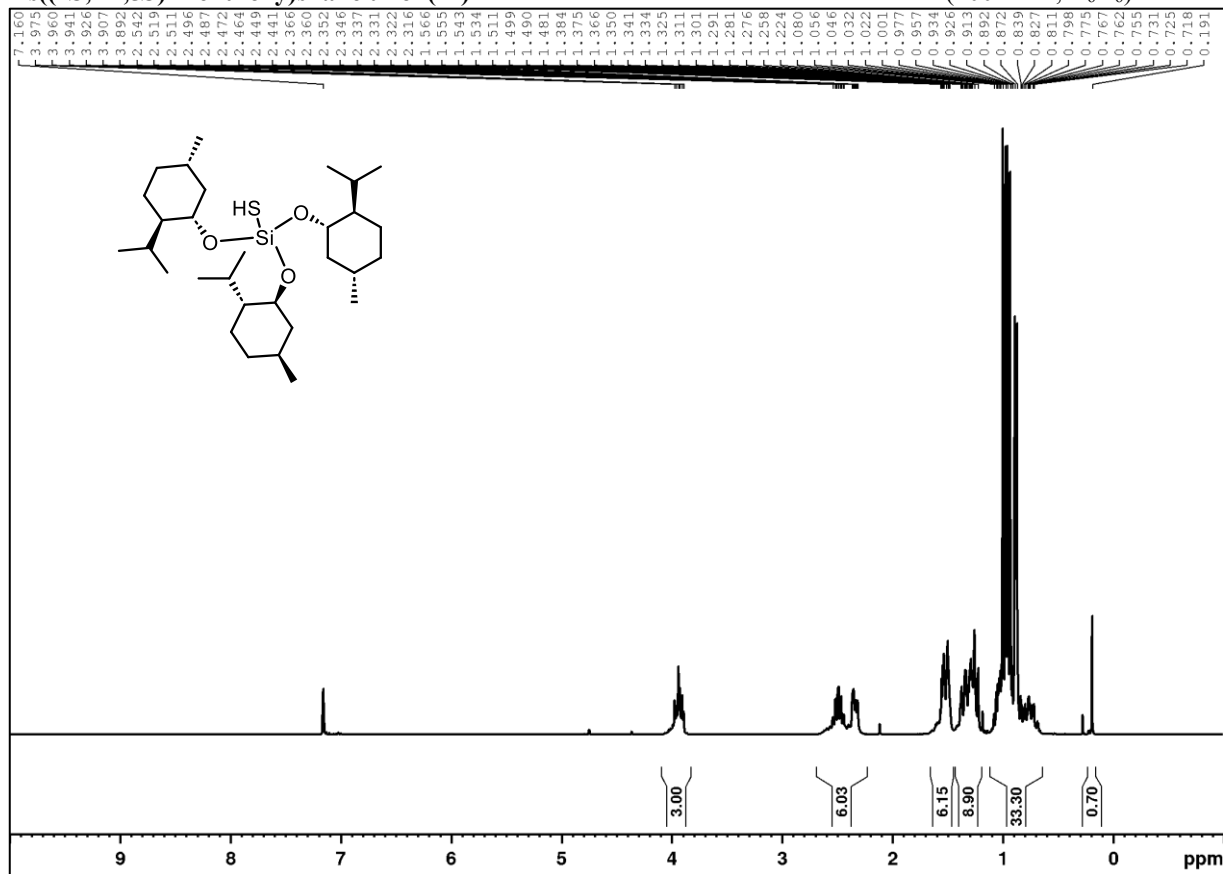
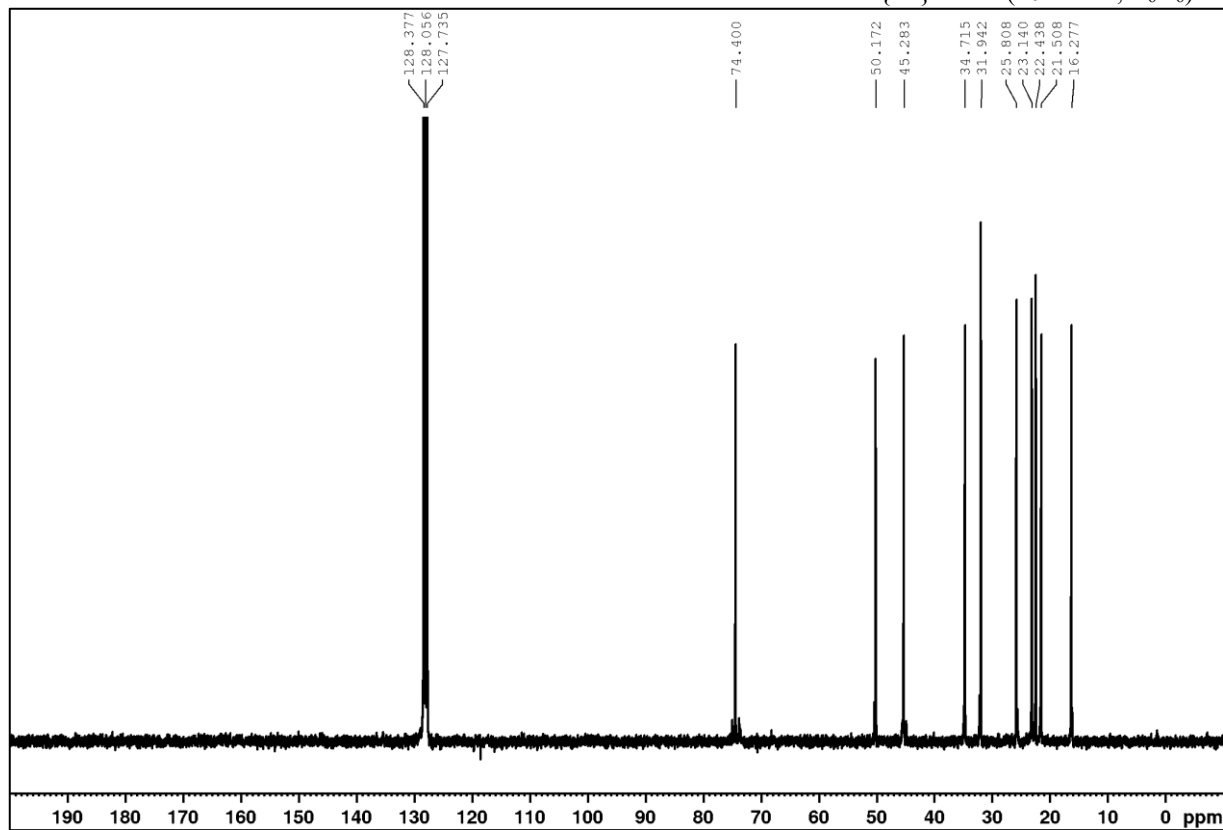


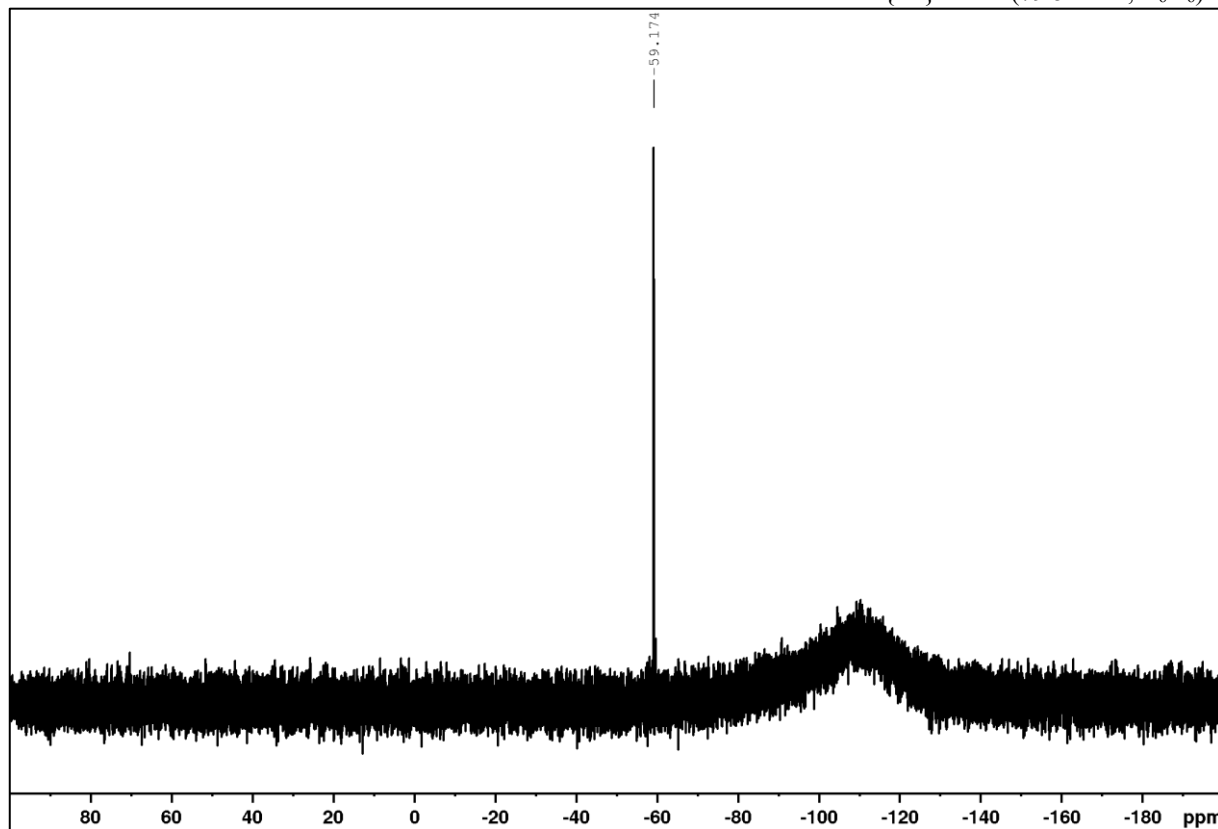
¹³C{¹H} NMR (101 MHz, CDCl₃)



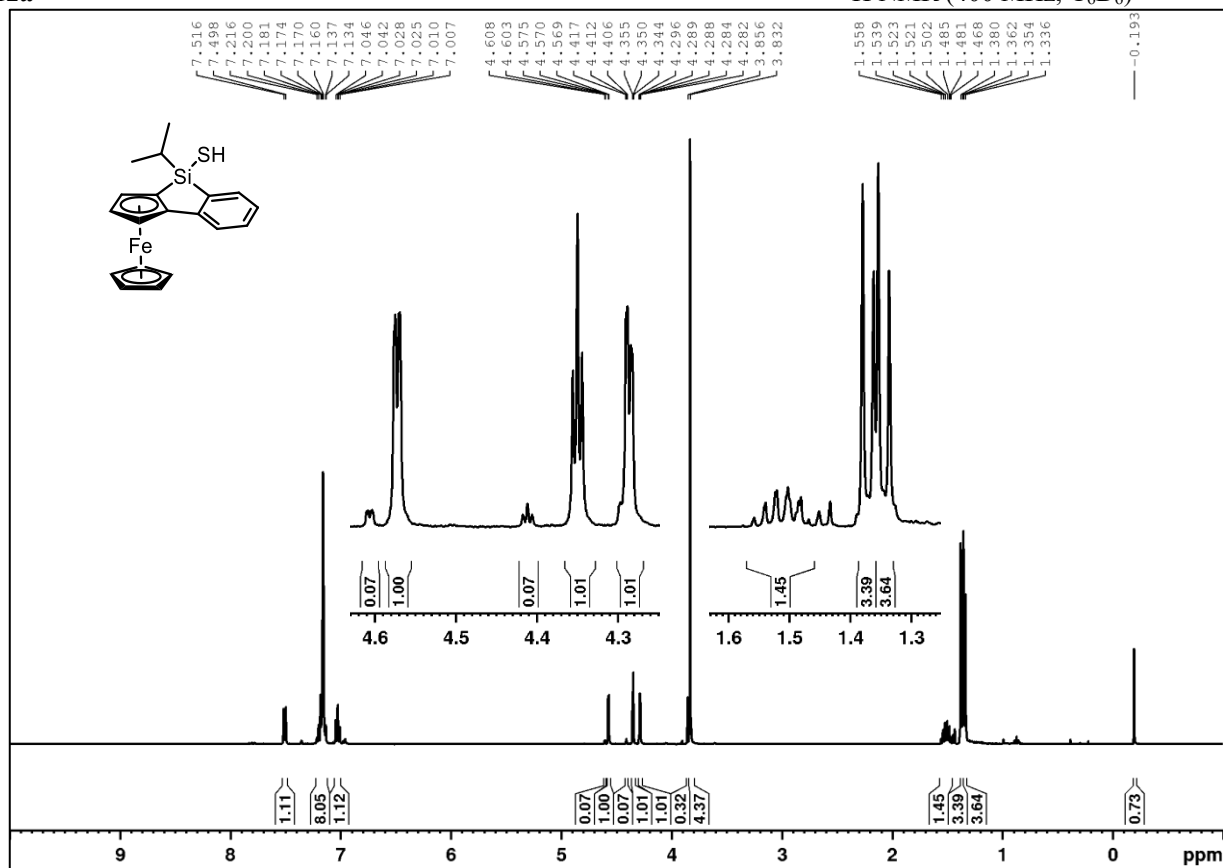
$(^1\text{H}, ^{13}\text{C})\text{-HSQC (CDCl}_3)$ 

(3a*S*,8a*S*)-2,2-Dimethyl-4,4,6,8,8-pentaphenyltetrahydro-[1,3]dioxolo[4,5-*e*][1,3,2]dioxasilepine-6-thiol
((*S,S*)-10d)¹H NMR (400 MHz, CDCl₃)¹³C NMR (101 MHz, CDCl₃)

Tris((1*S*,2*R*,5*S*)-menthoxy)silane thiol (11) ^1H NMR (400 MHz, C_6D_6) $^{13}\text{C}\{^1\text{H}\}$ NMR (101 MHz, C_6D_6)

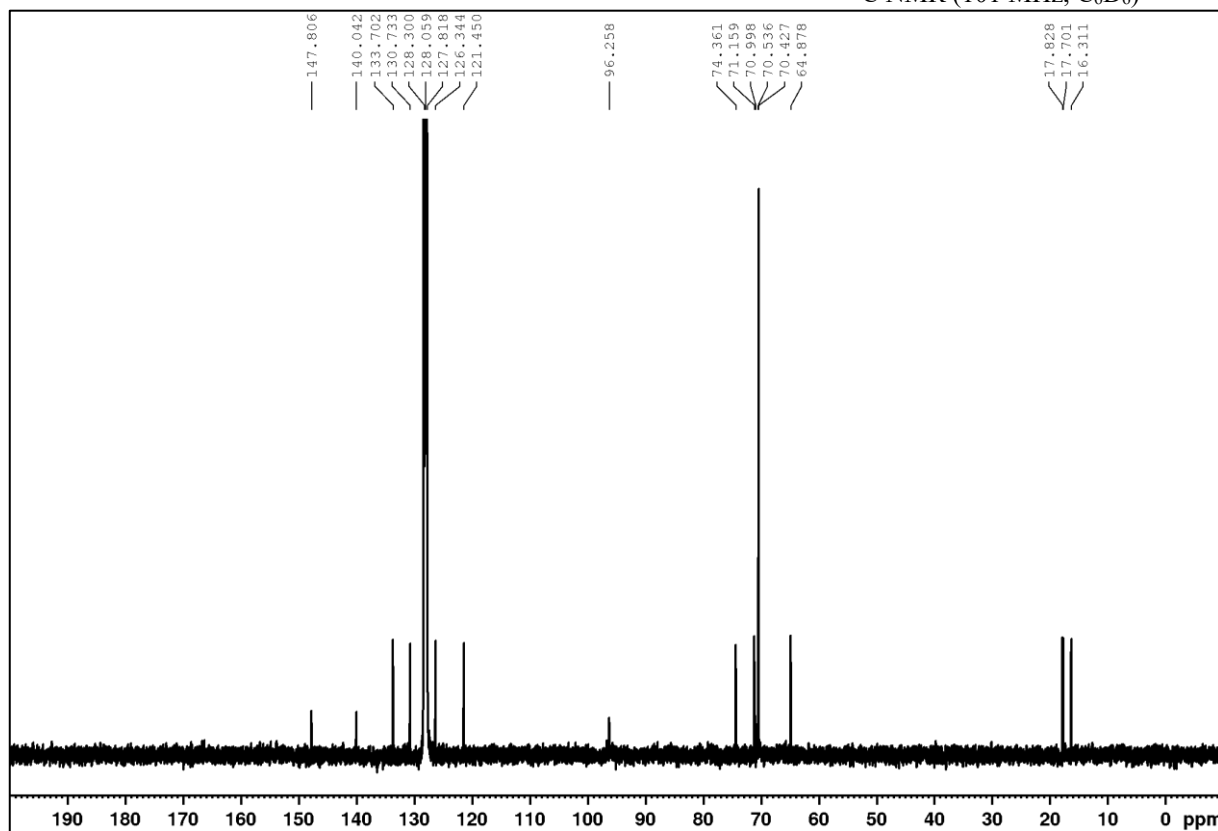
$^{29}\text{Si}\{^1\text{H}\}$ NMR (79.5 MHz, C_6D_6)

12a

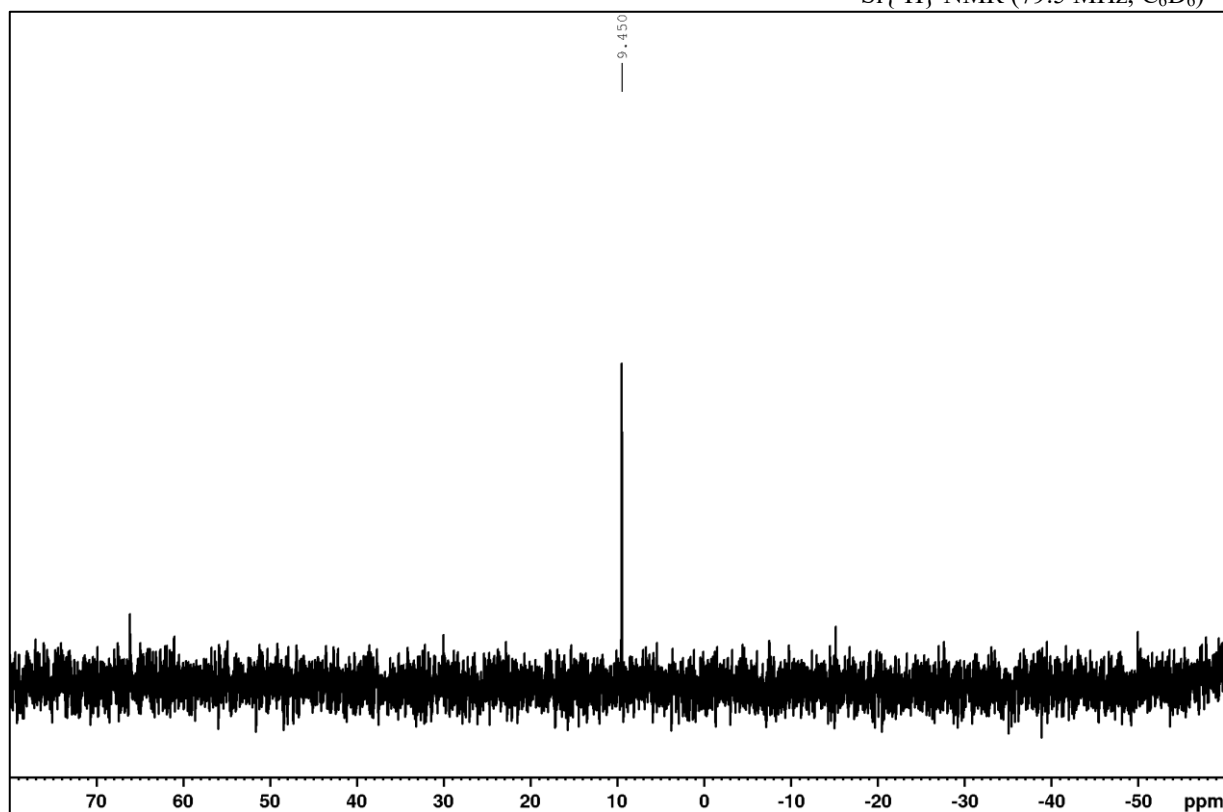
 ^1H NMR (400 MHz, C_6D_6)

APPENDIX

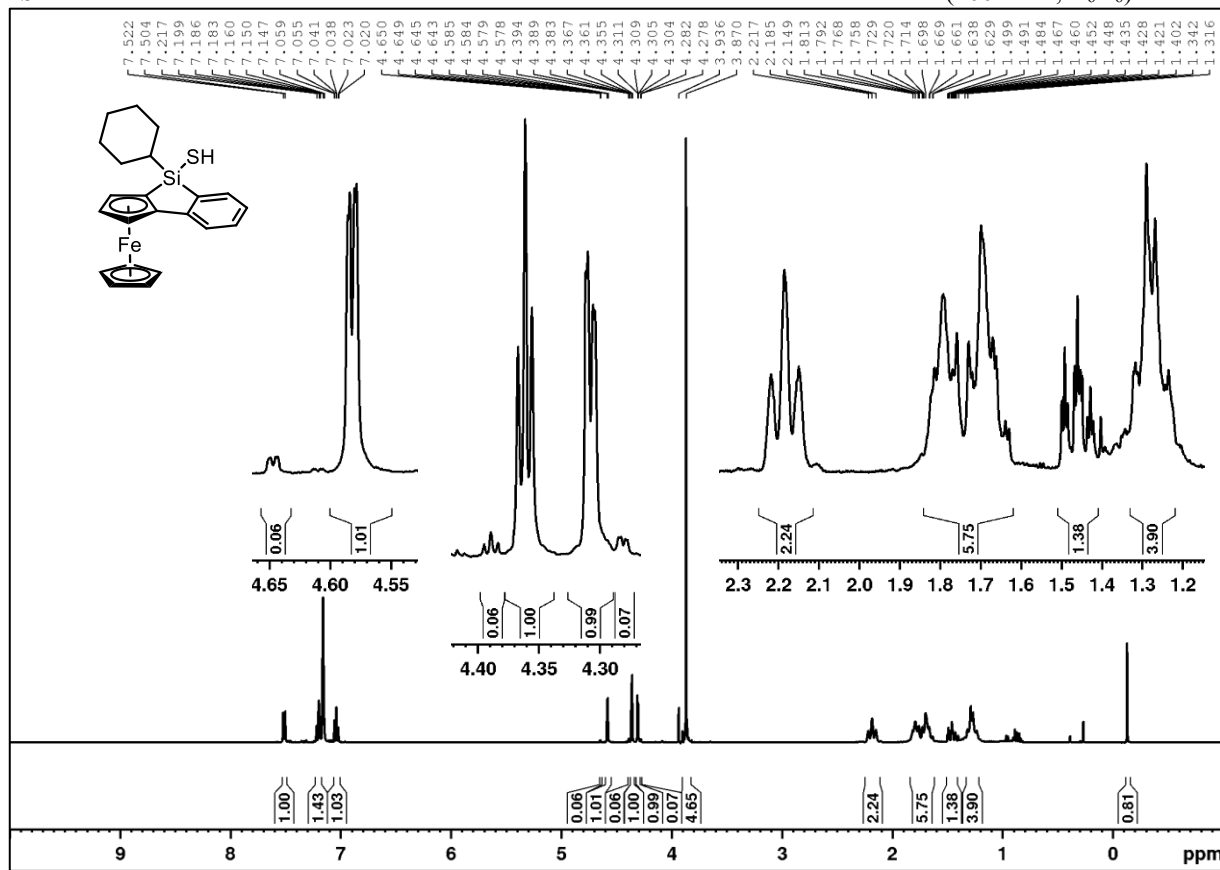
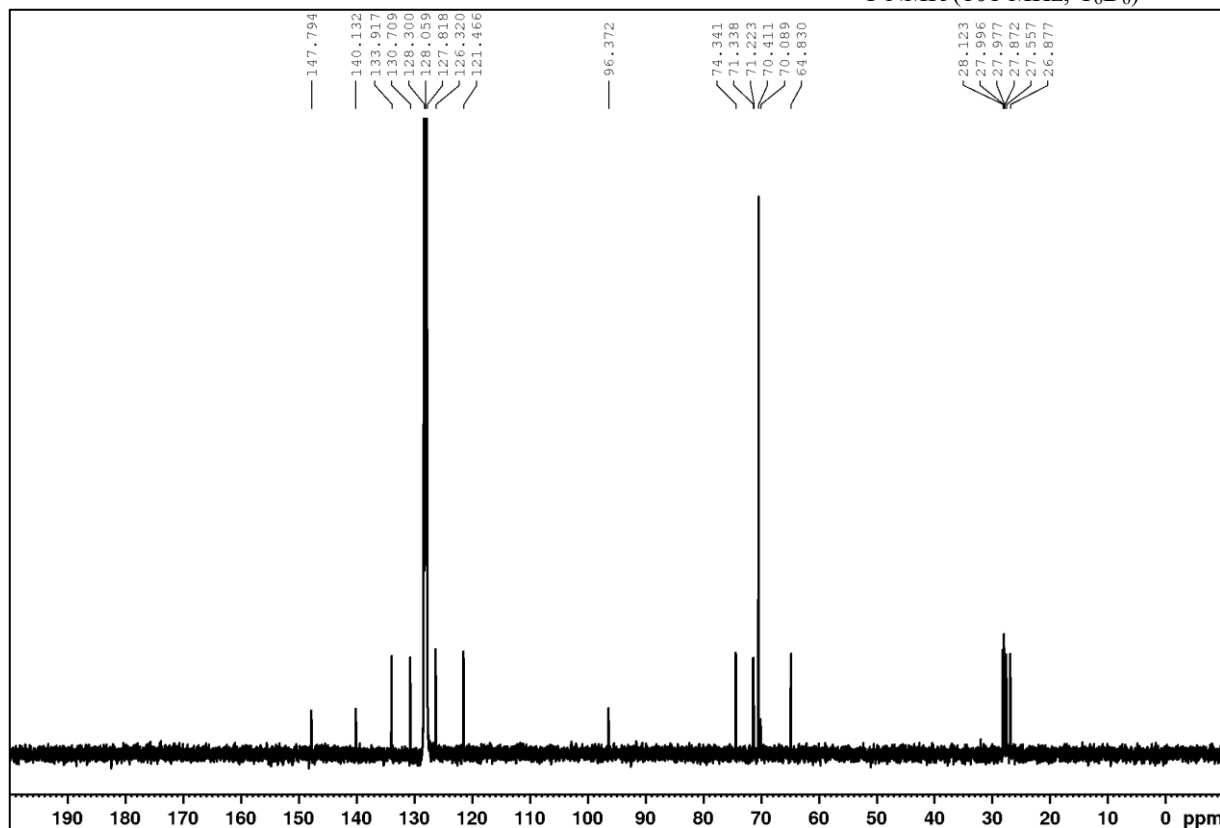
^{13}C NMR (101 MHz, C_6D_6)

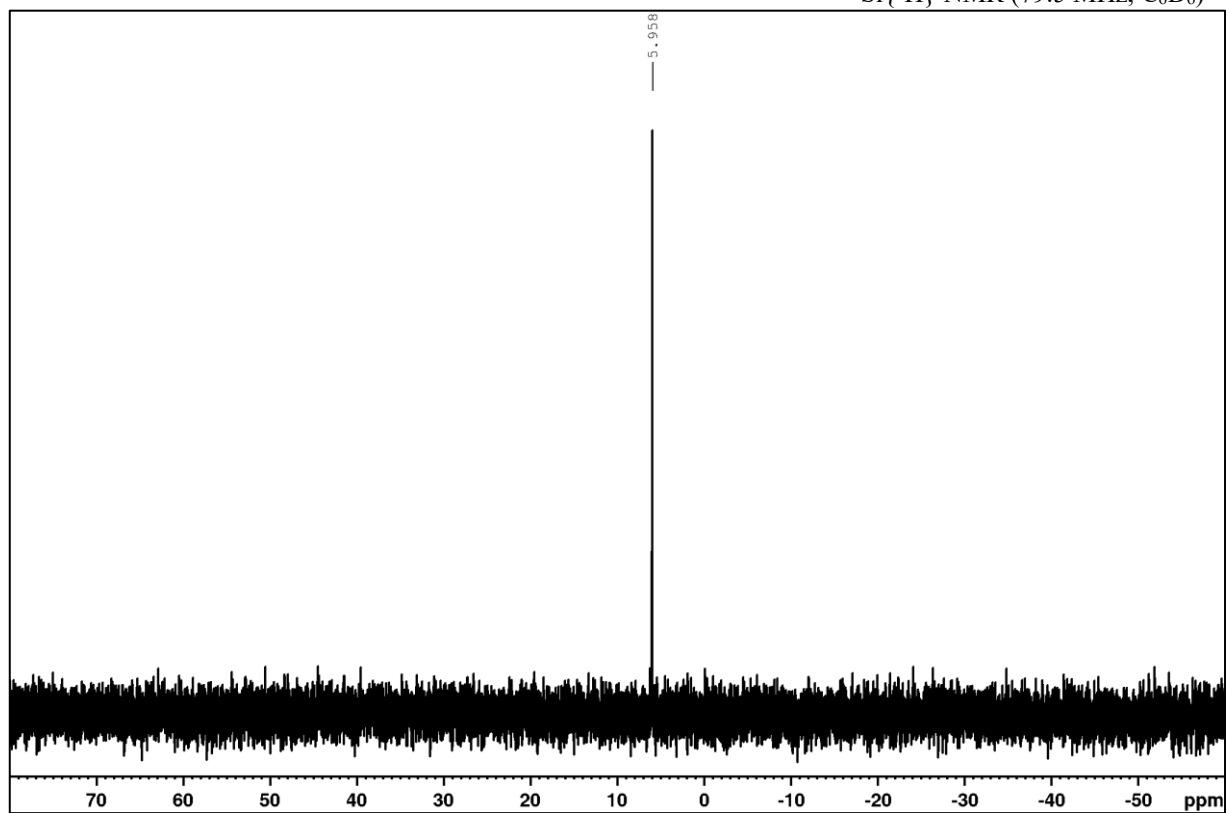


$^{29}\text{Si}\{^1\text{H}\}$ NMR (79.5 MHz, C_6D_6)

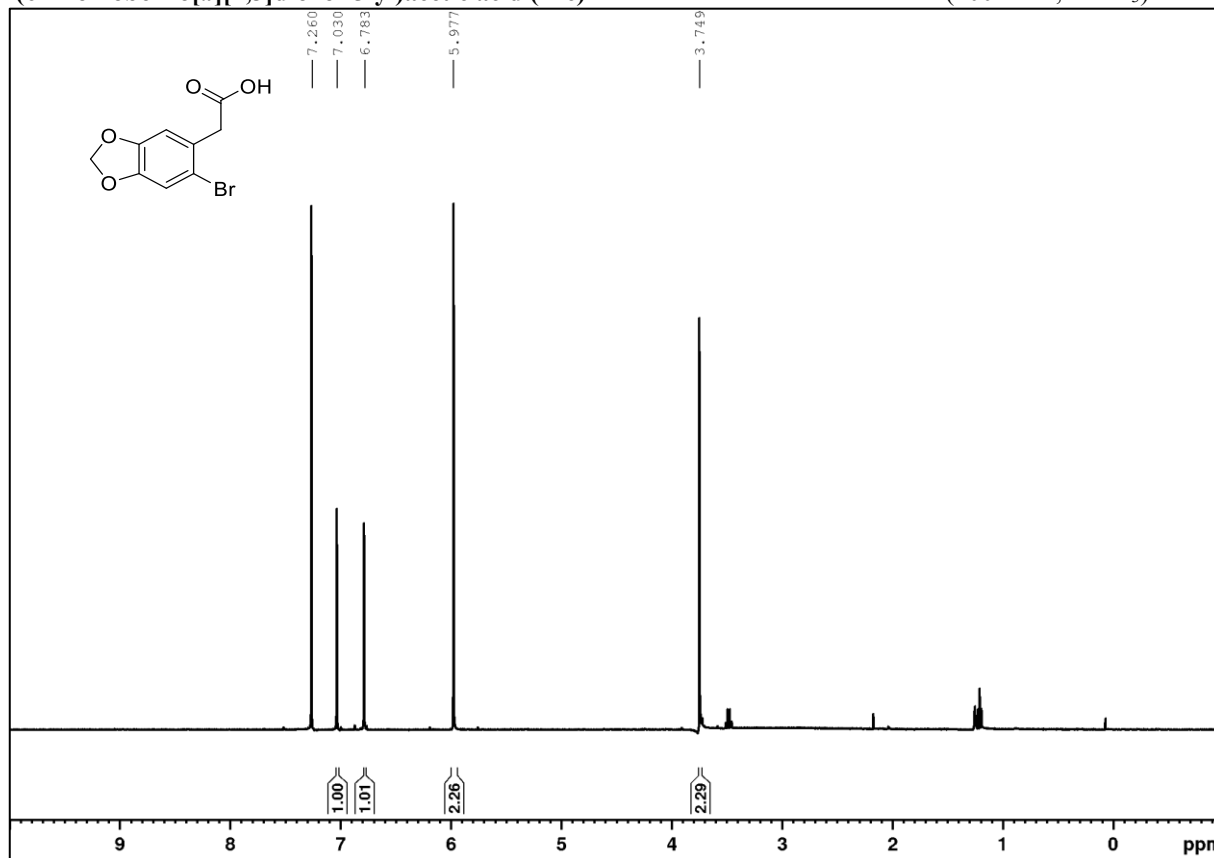


12b

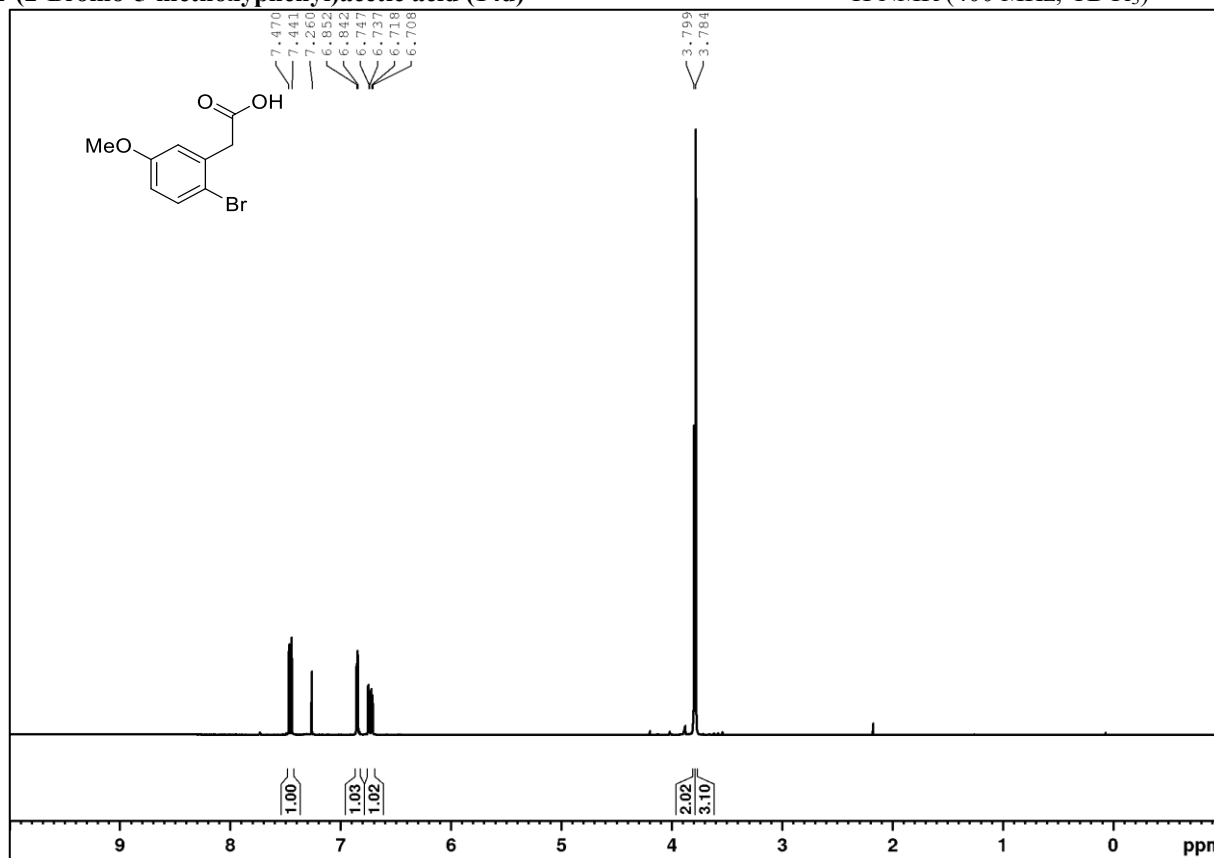
 ^1H NMR (400 MHz, C_6D_6) ^{13}C NMR (101 MHz, C_6D_6)

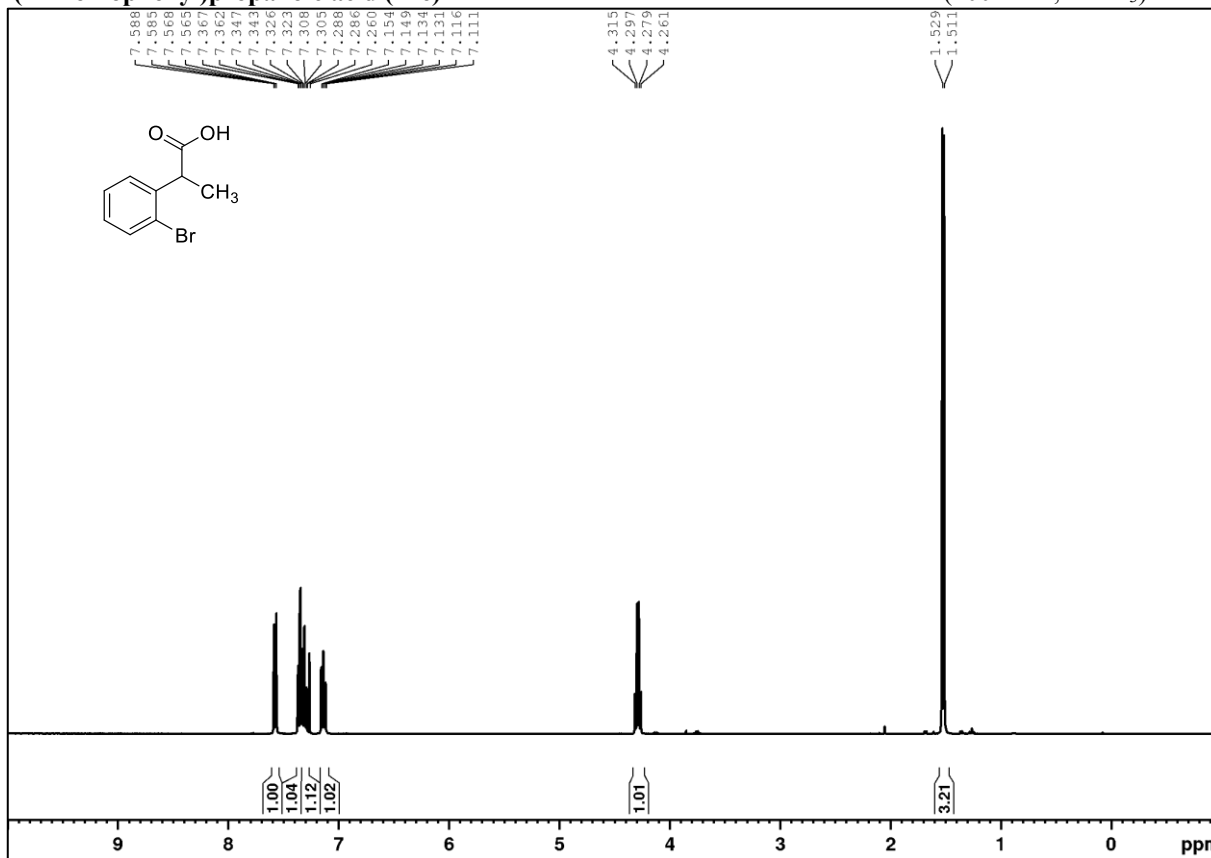
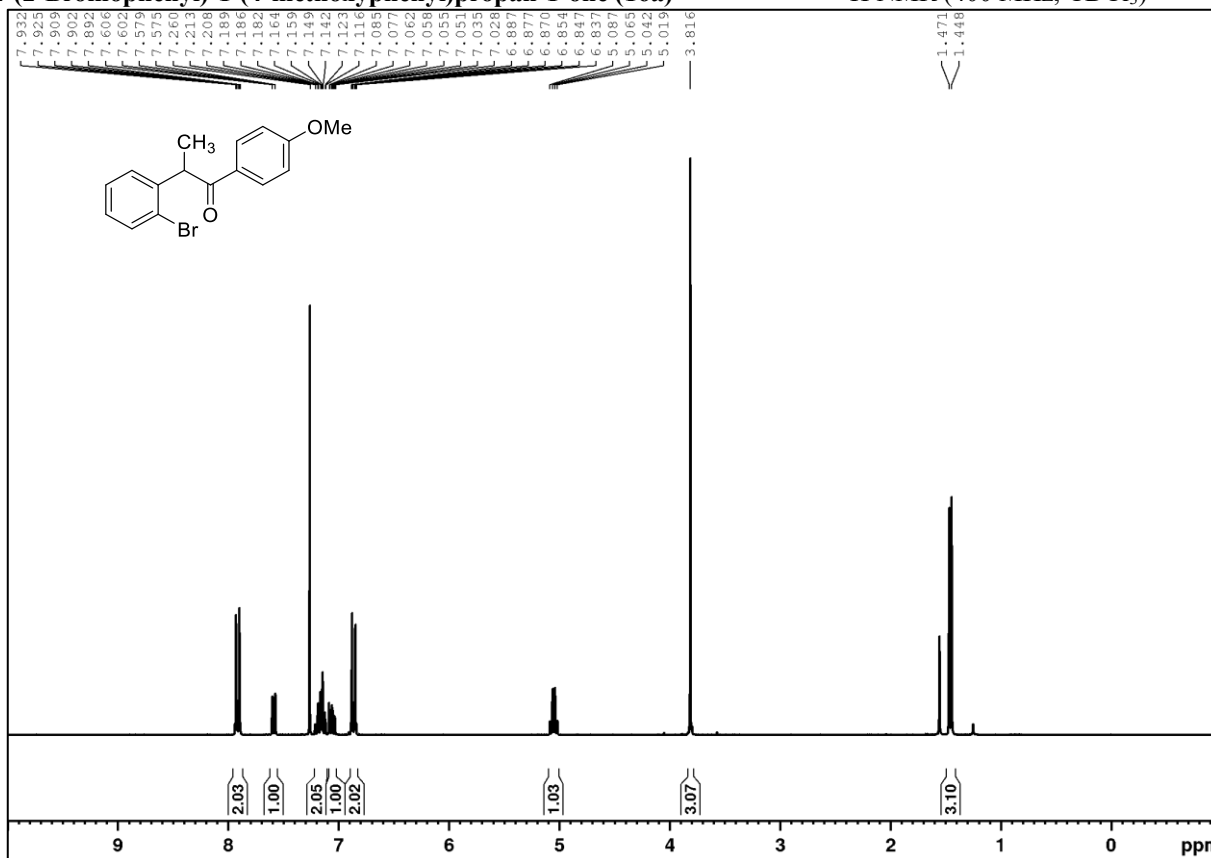
$^{29}\text{Si}\{^1\text{H}\}$ NMR (79.5 MHz, C_6D_6)

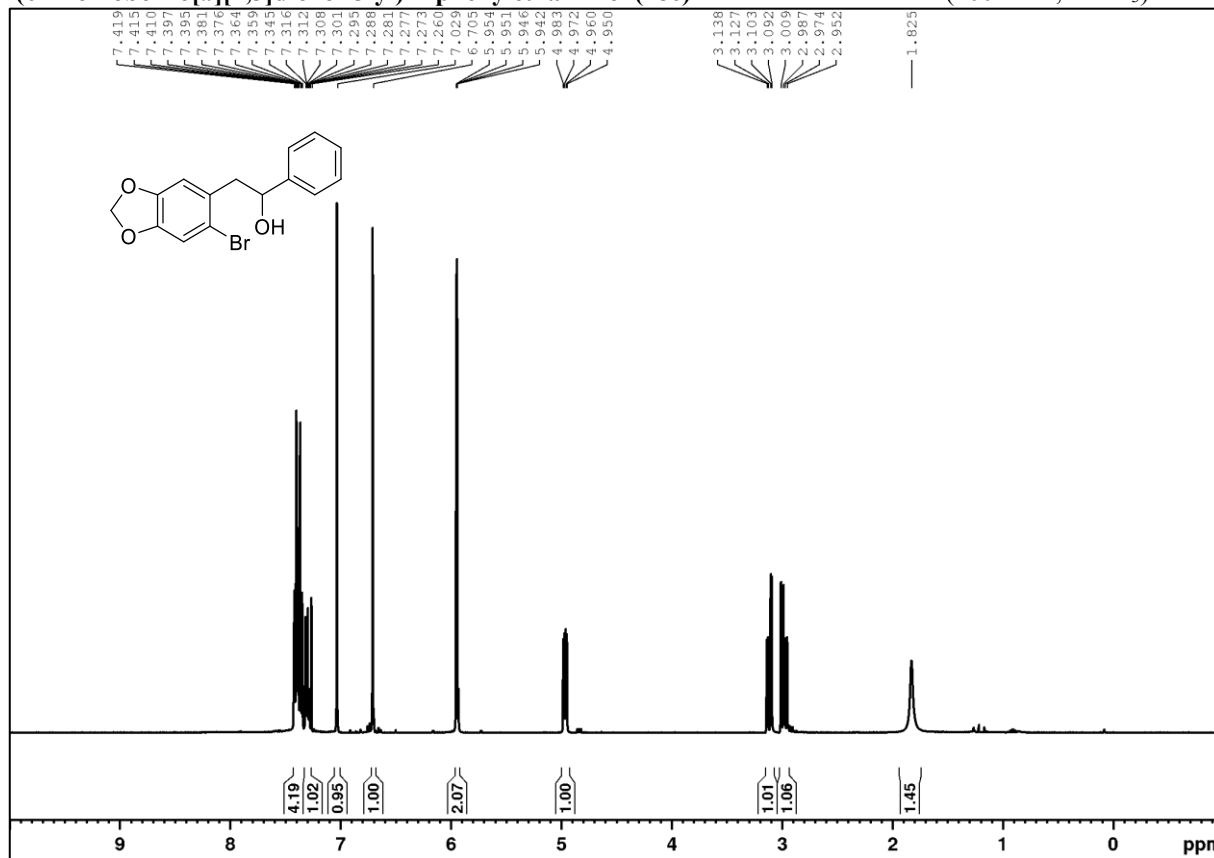
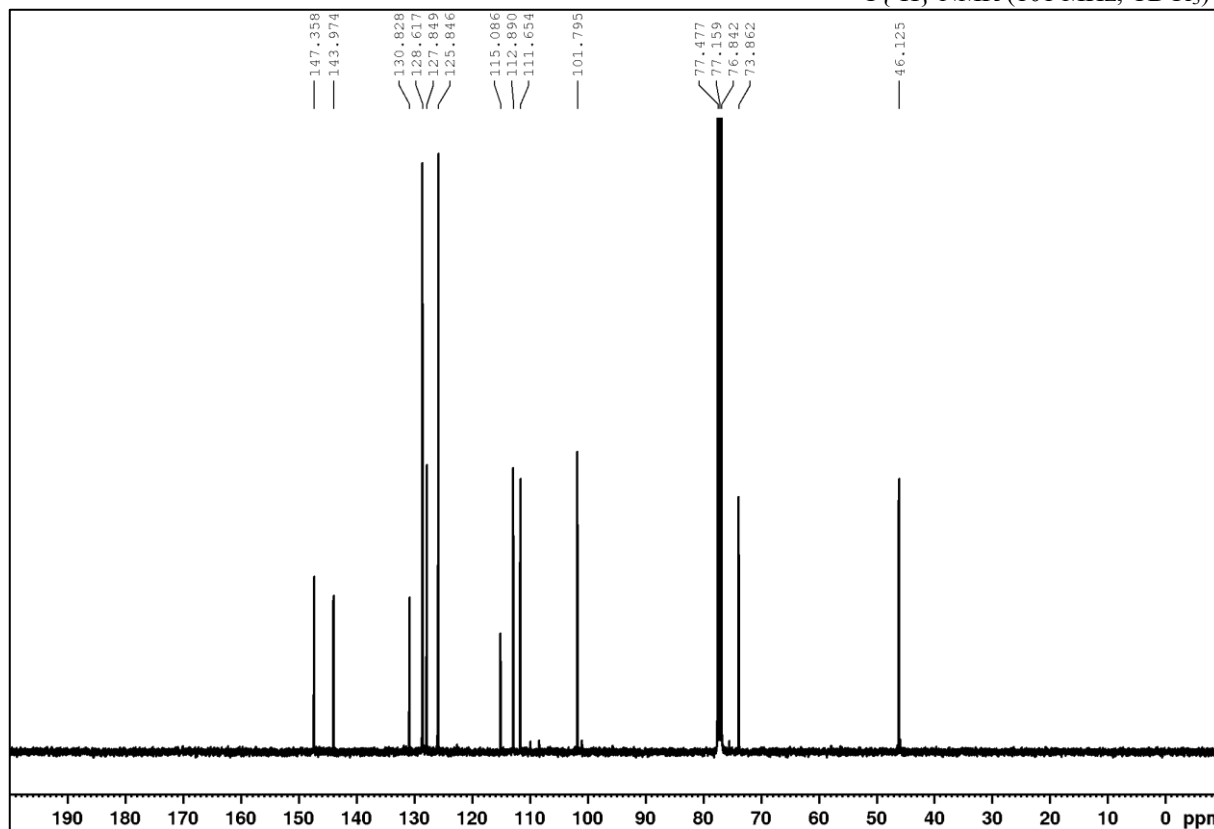
2-(6-Bromobenzo[d][1,3]dioxol-5-yl)acetic acid (14c)

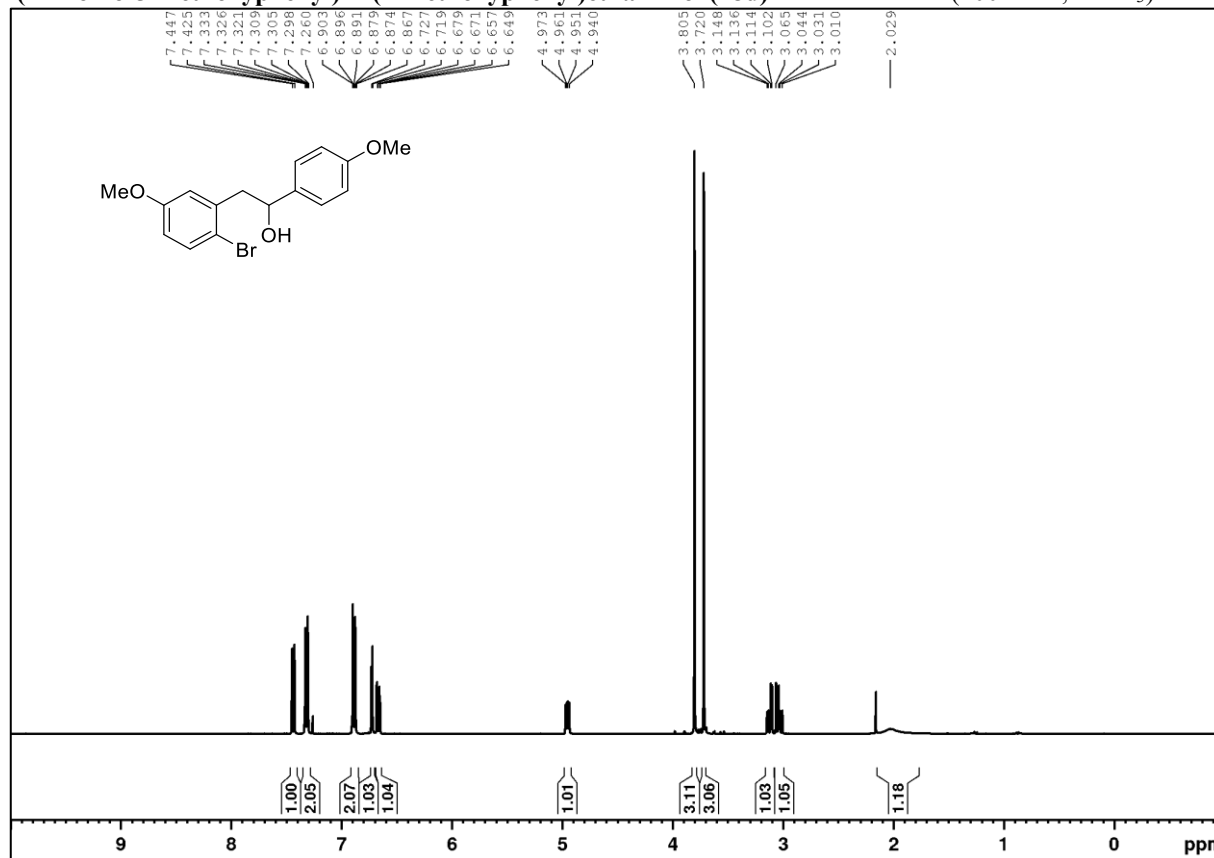
 ^1H NMR (400 MHz, CDCl_3)

2-(2-Bromo-5-methoxyphenyl)acetic acid (14d)

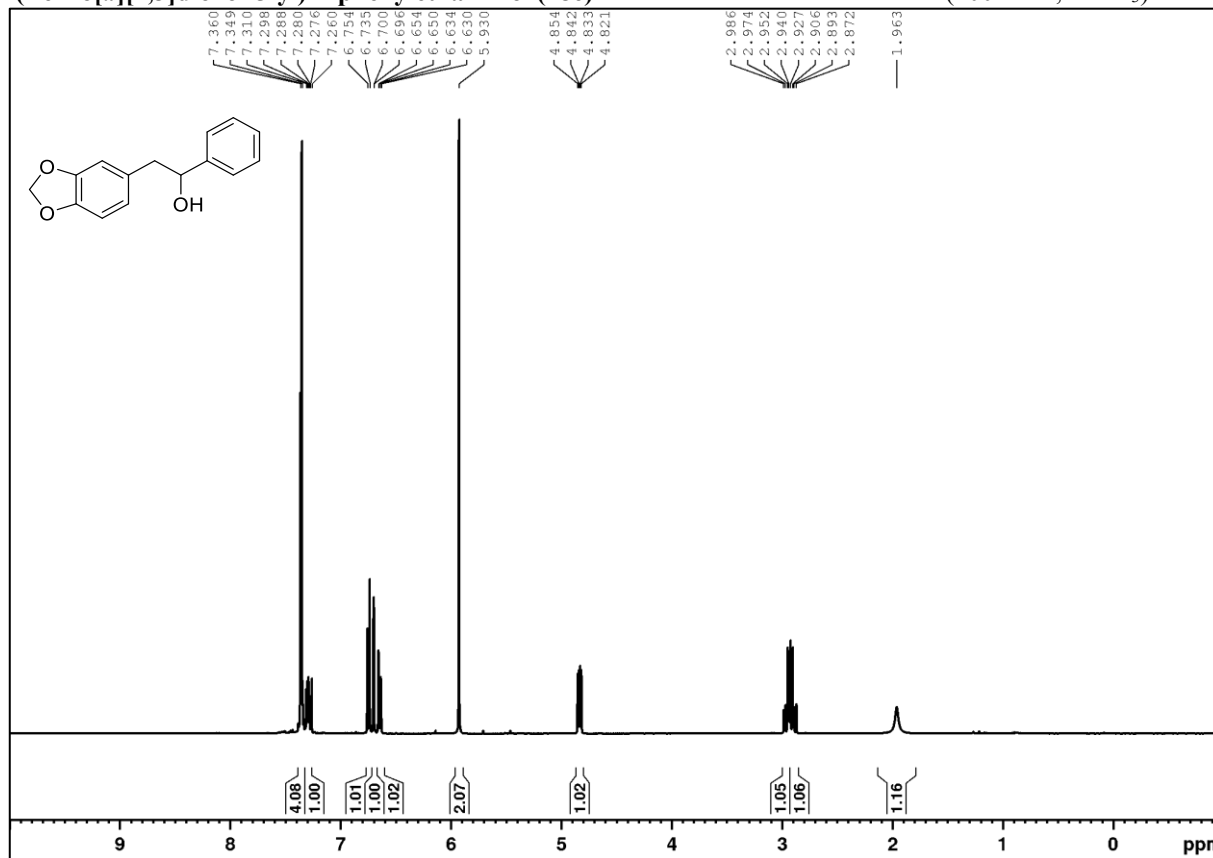
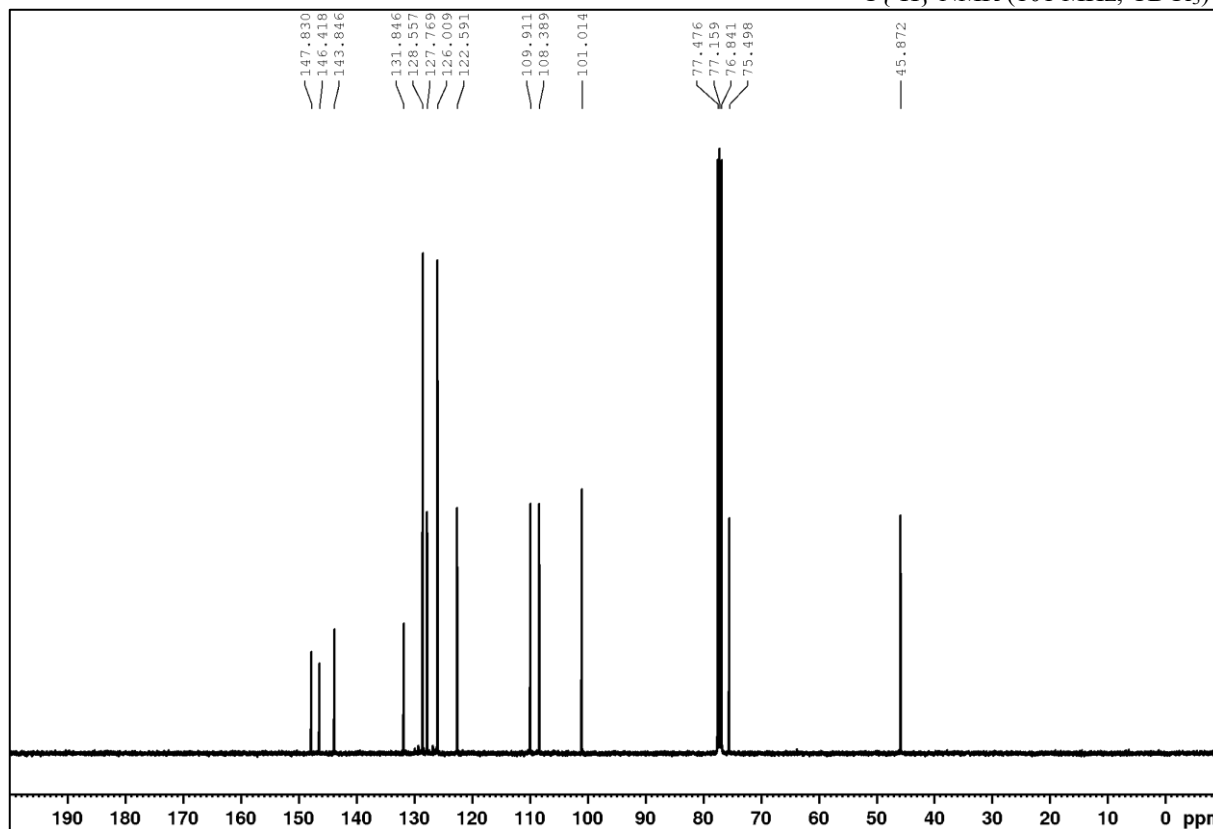
 ^1H NMR (400 MHz, CDCl_3)

2-(2-Bromophenyl)propanoic acid (14e)¹H NMR (400 MHz, CDCl₃)**2-(2-Bromophenyl)-1-(4-methoxyphenyl)propan-1-one (16a)**¹H NMR (400 MHz, CDCl₃)

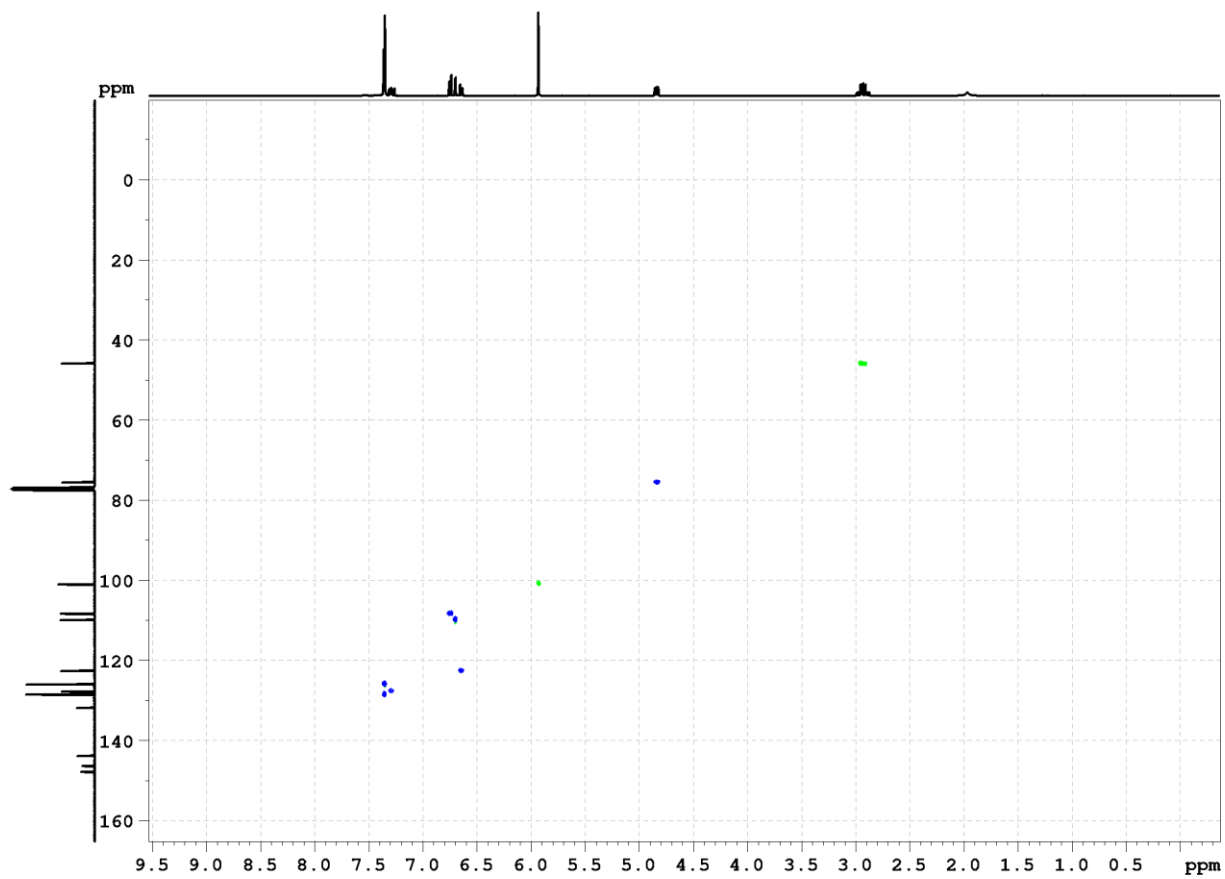
2-(6-Bromobenzo[*d*][1,3]dioxol-5-yl)-1-phenylethan-1-ol (18c) ^1H NMR (400 MHz, CDCl_3) $^{13}\text{C}\{^1\text{H}\}$ NMR (101 MHz, CDCl_3)

2-(2-Bromo-5-methoxyphenyl)-1-(4-methoxyphenyl)ethan-1-ol (18d) $^1\text{H NMR}$ (400 MHz, CDCl_3)

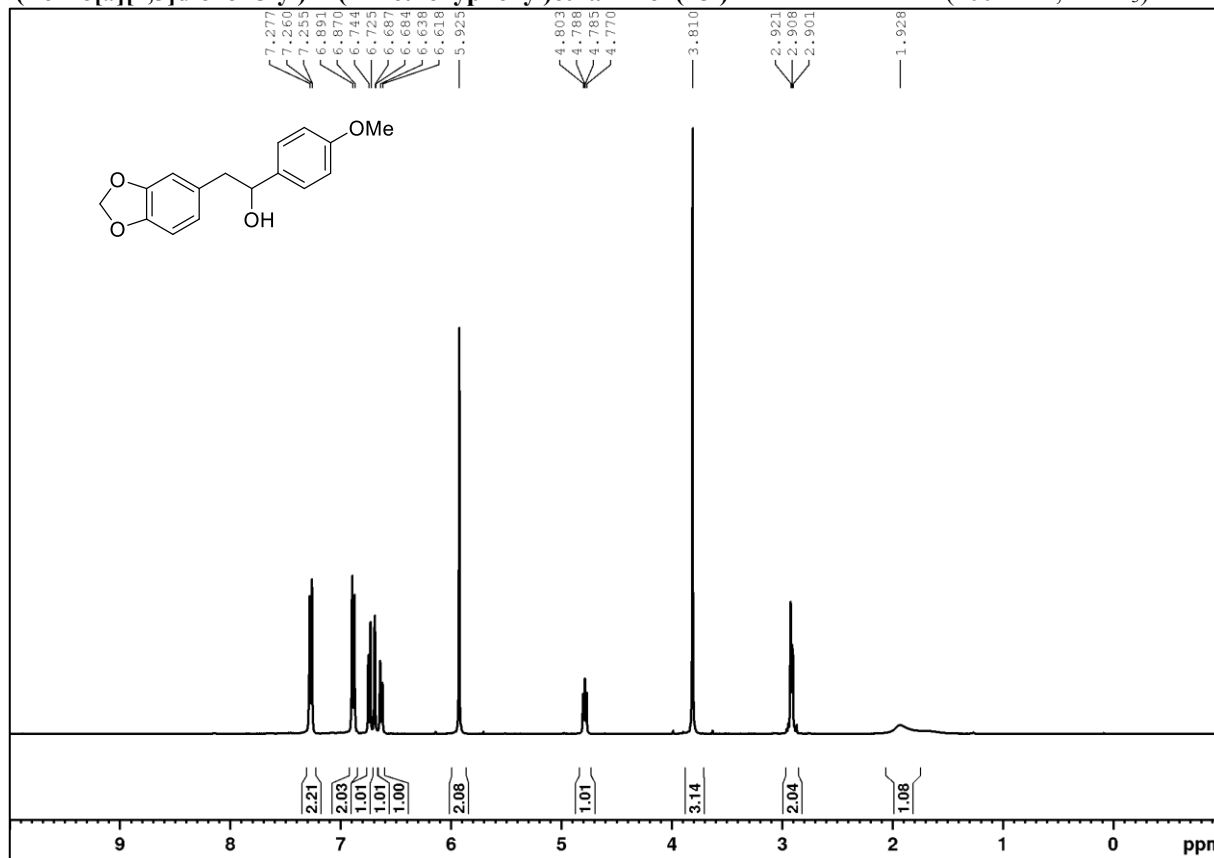
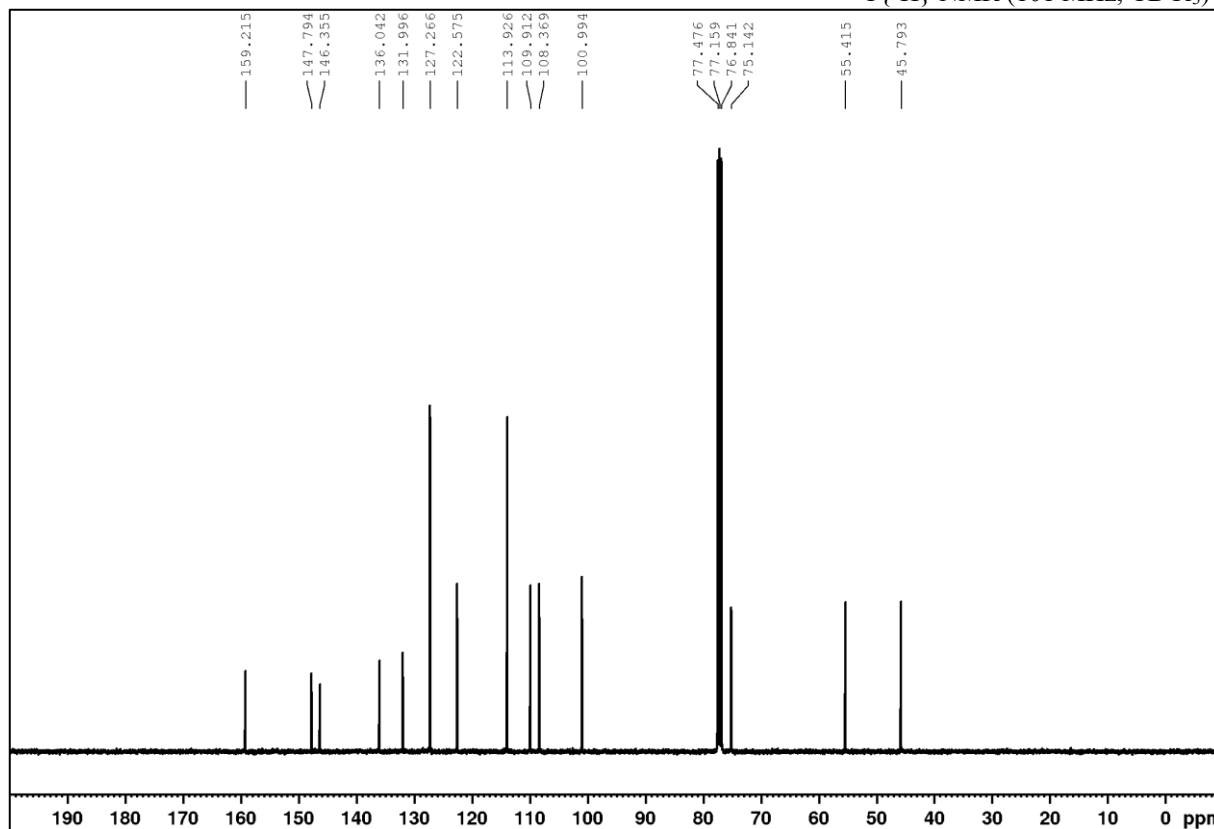
2-(Benzo[d][1,3]dioxol-5-yl)-1-phenylethan-1-ol (18c)

 ^1H NMR (400 MHz, CDCl_3) $^{13}\text{C}\{^1\text{H}\}$ NMR (101 MHz, CDCl_3)

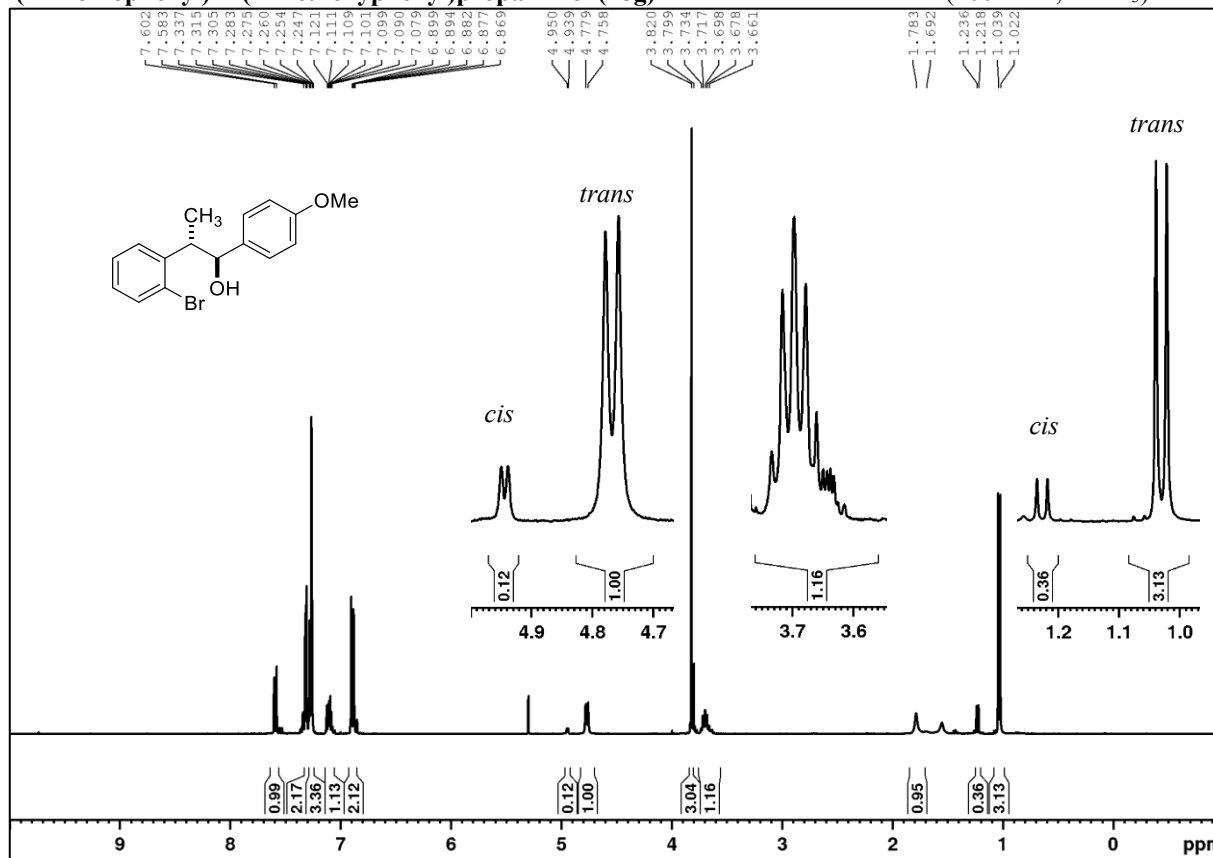
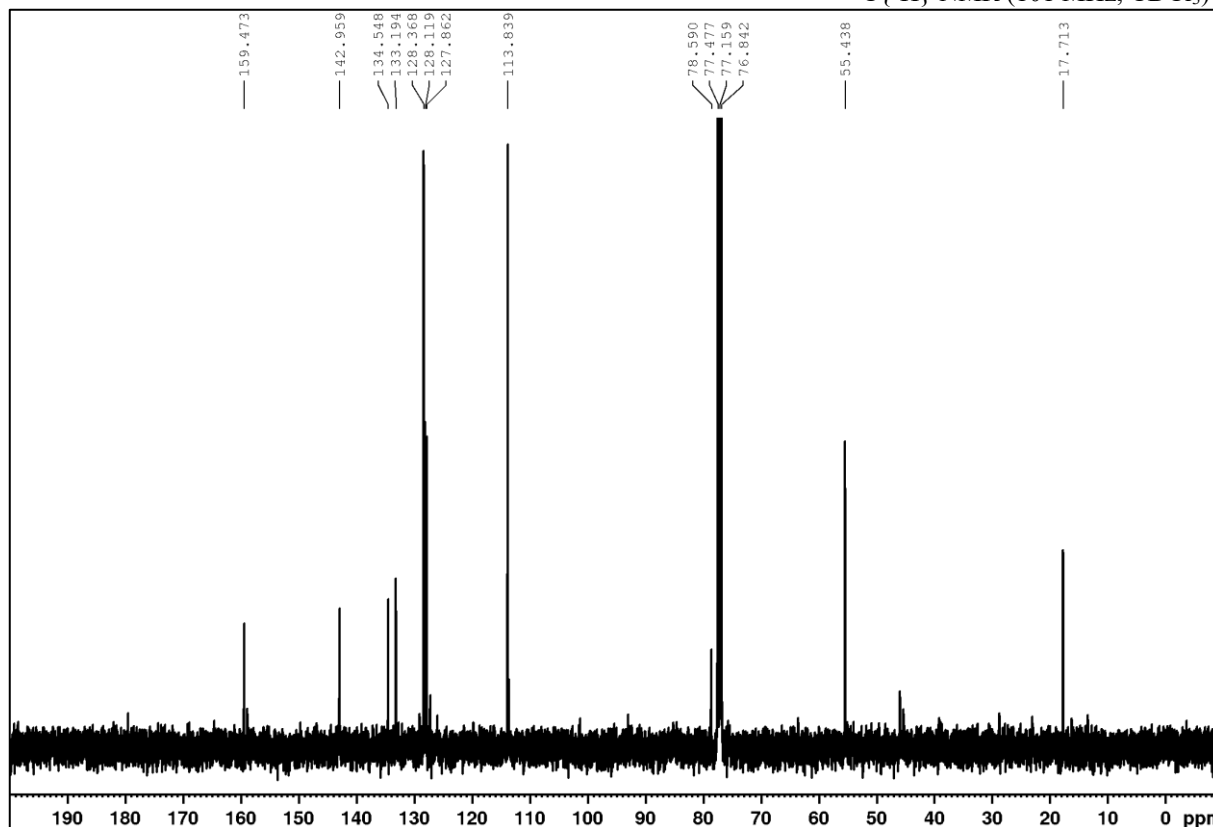
APPENDIX

 $(^1\text{H}, ^{13}\text{C})\text{-HSQC (CDCl}_3)$ 

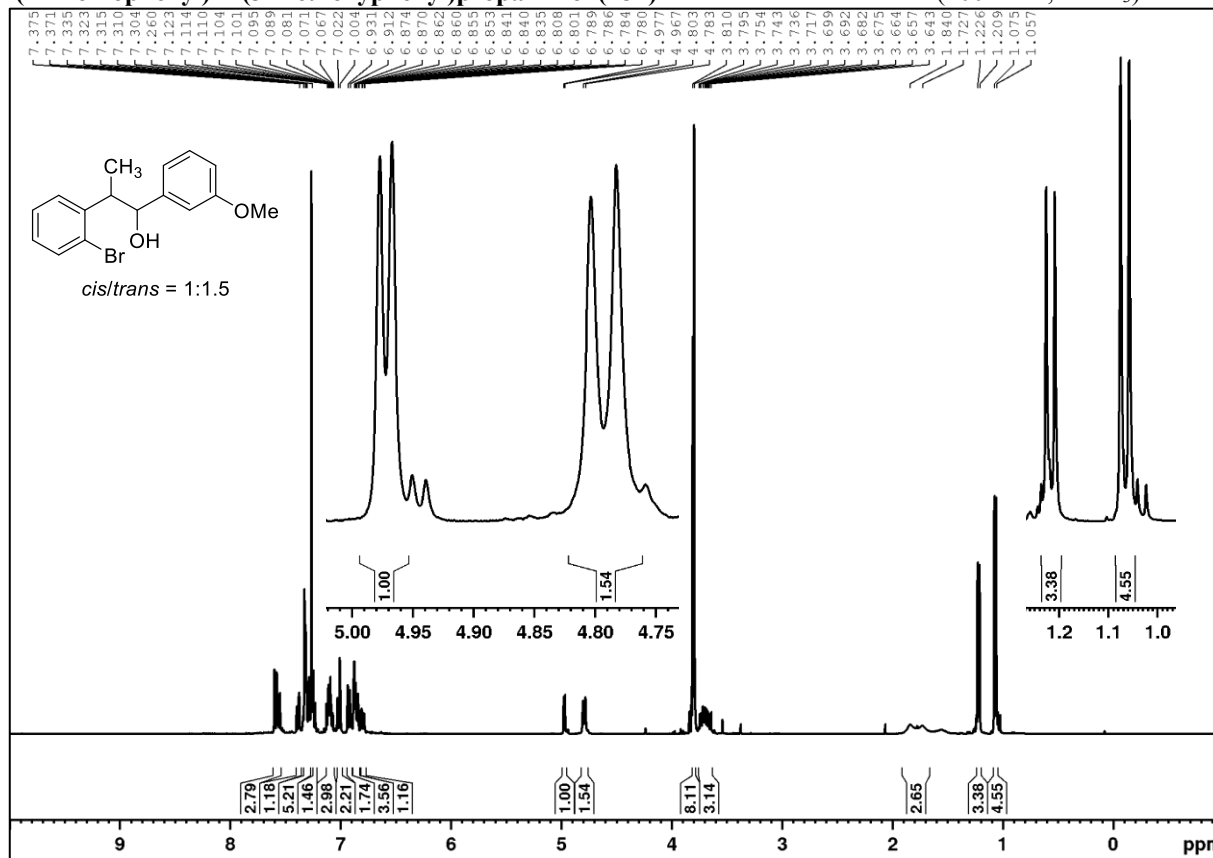
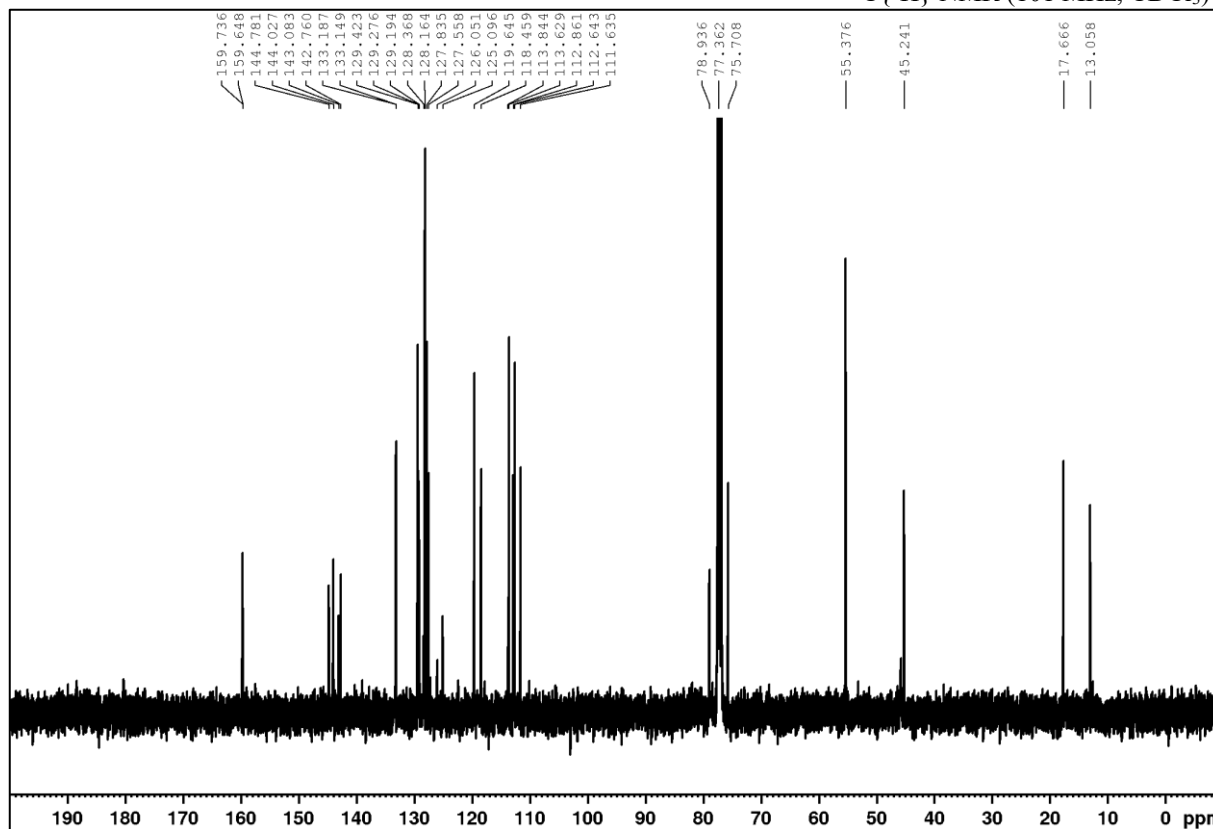
2-(Benzo[d][1,3]dioxol-5-yl)-1-(4-methoxyphenyl)ethan-1-ol (18f)

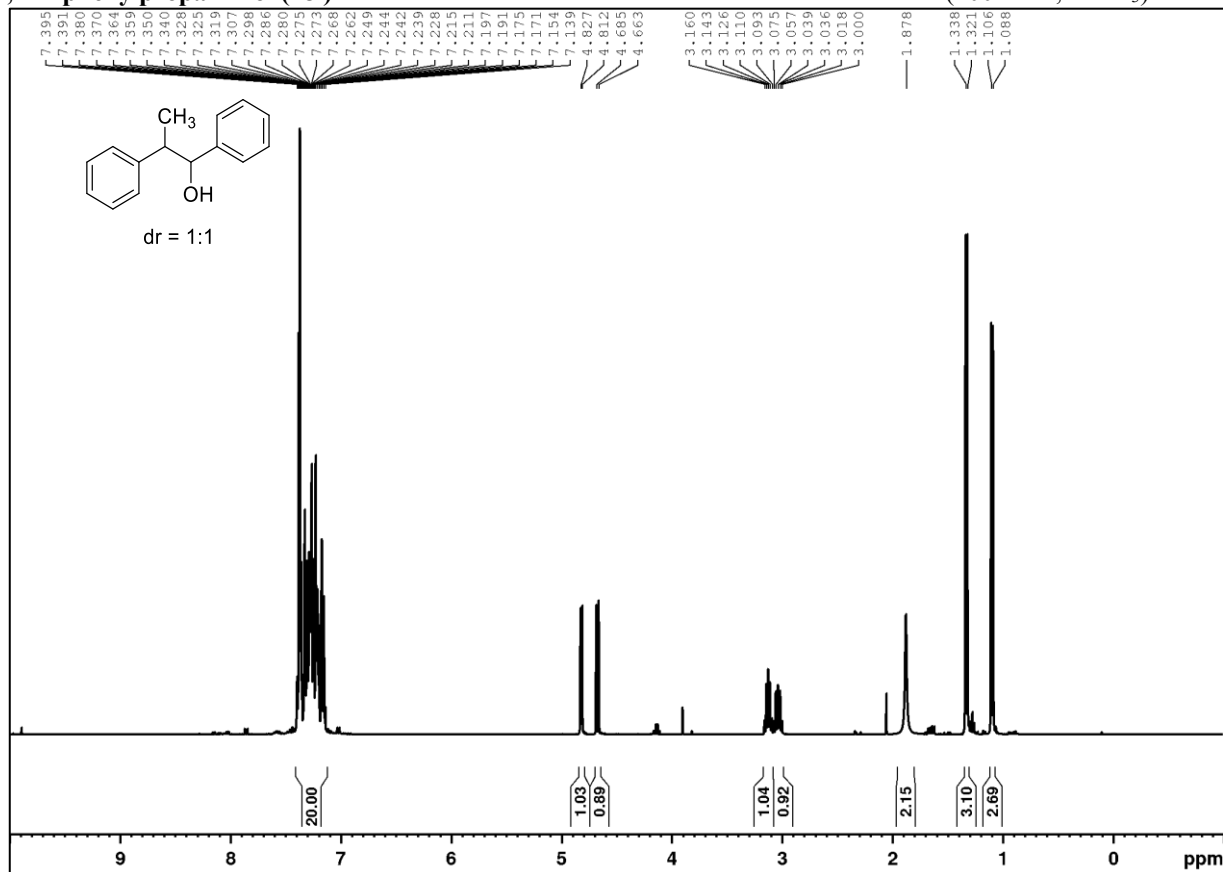
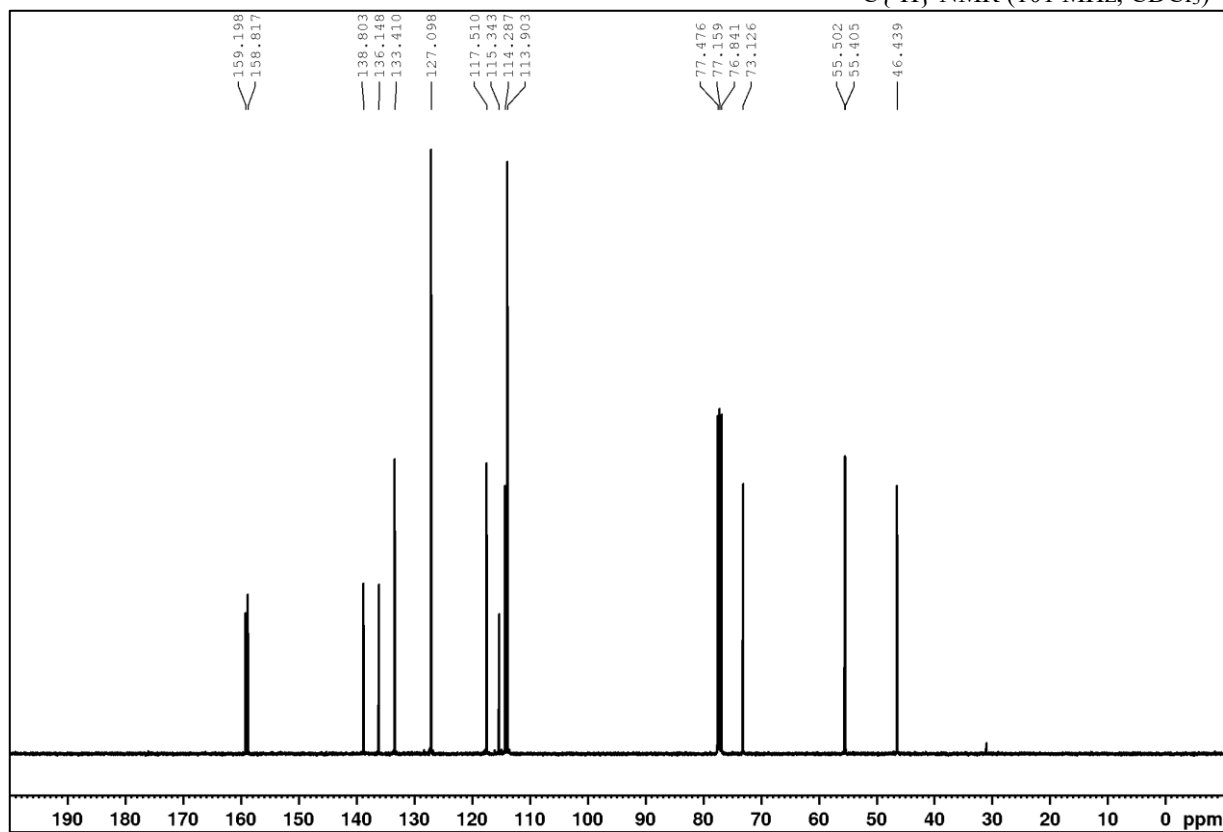
 ^1H NMR (400 MHz, CDCl_3) $^{13}\text{C}\{^1\text{H}\}$ NMR (101 MHz, CDCl_3)

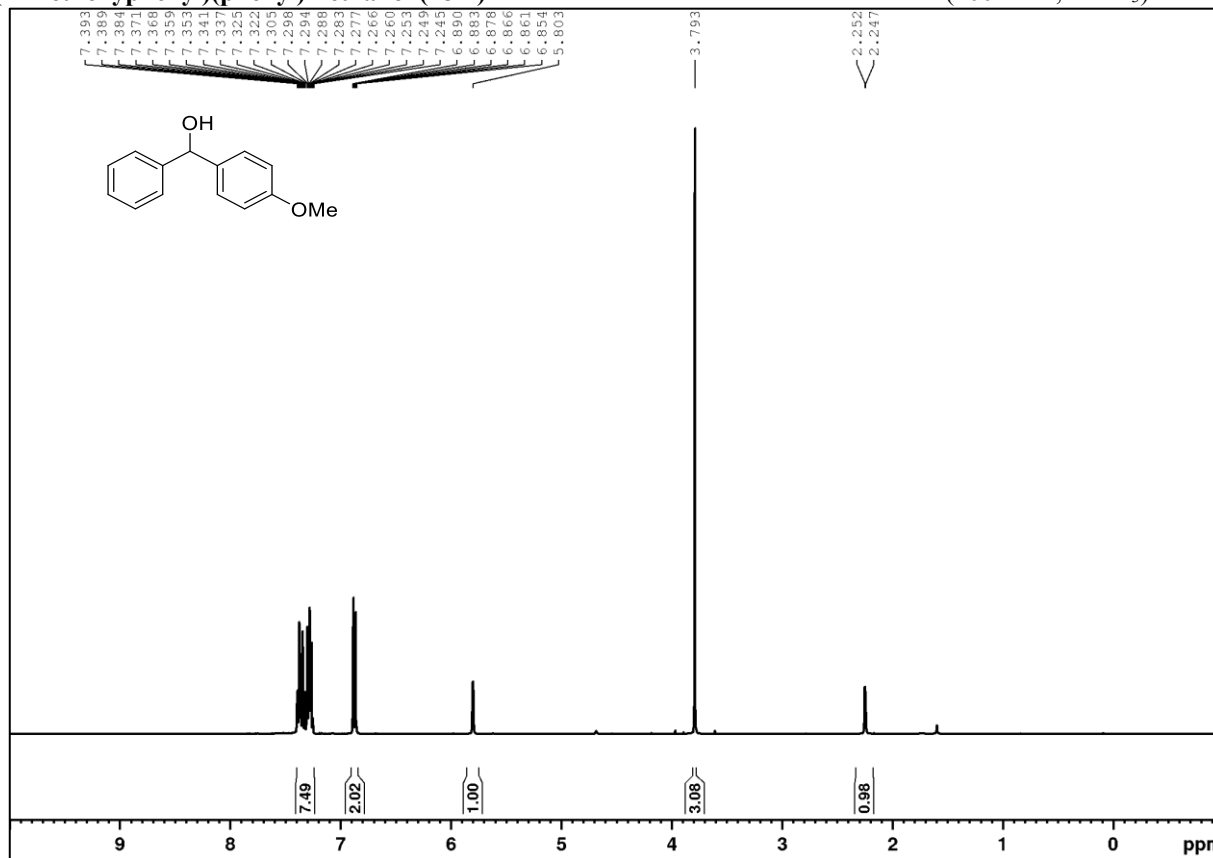
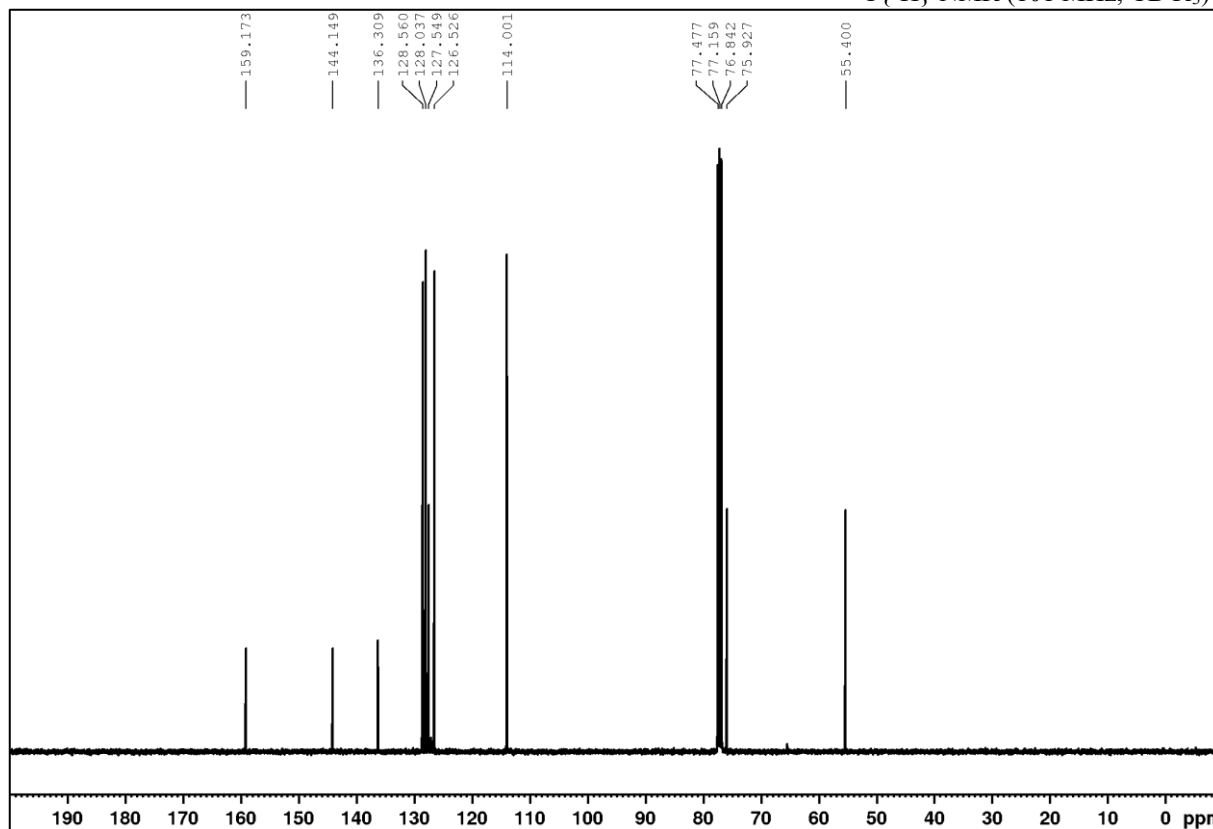
2-(2-Bromophenyl)-1-(4-methoxyphenyl)propan-1-ol (18g)

 ^1H NMR (400 MHz, CDCl_3) $^{13}\text{C}\{^1\text{H}\}$ NMR (101 MHz, CDCl_3)

2-(2-Bromophenyl)-1-(3-methoxyphenyl)propan-1-ol (18h)

H NMR (400 MHz, CDCl₃)¹³C{¹H} NMR (101 MHz, CDCl₃)

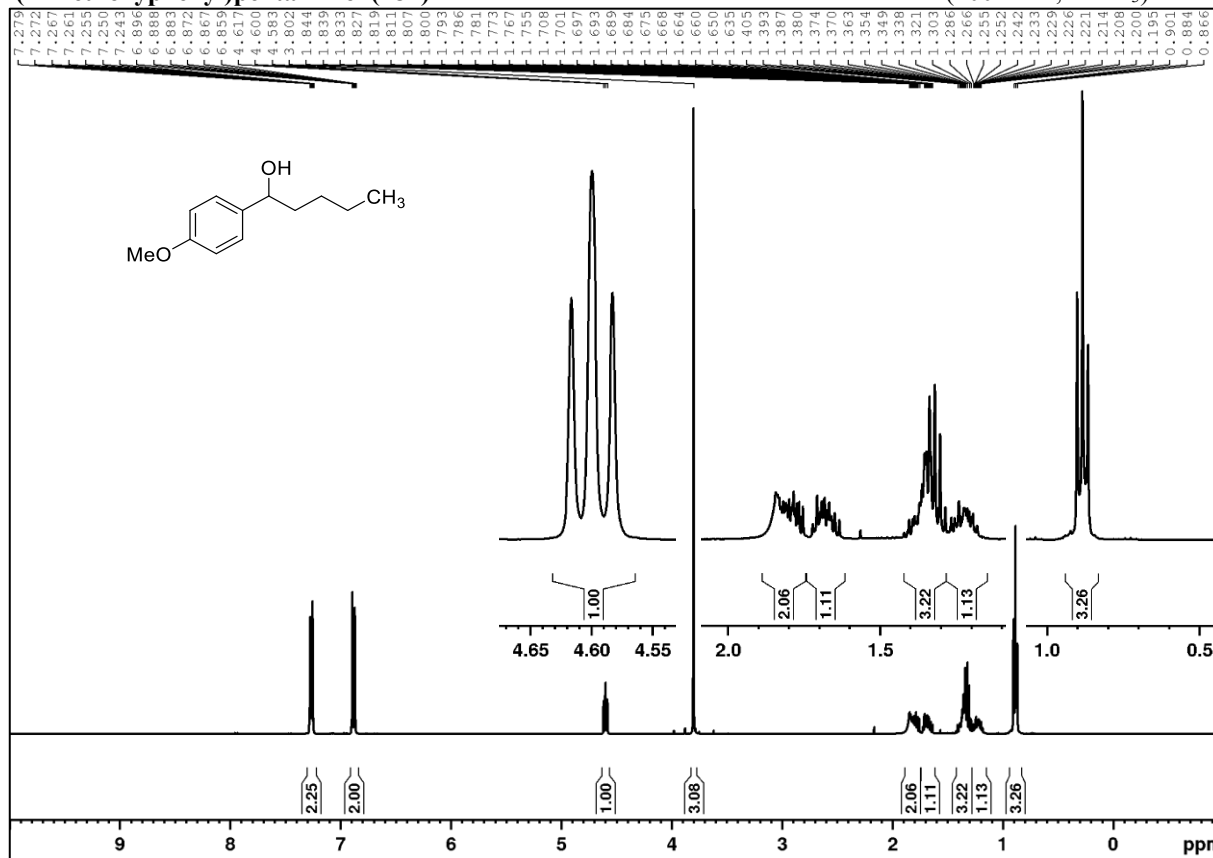
1,2-Diphenylpropan-1-ol (18i) ^1H NMR (400 MHz, CDCl_3) $^{13}\text{C}\{^1\text{H}\}$ NMR (101 MHz, CDCl_3)

(4-Methoxyphenyl)(phenyl)methanol (18m) ^1H NMR (400 MHz, CDCl_3) $^{13}\text{C}\{^1\text{H}\}$ NMR (101 MHz, CDCl_3)

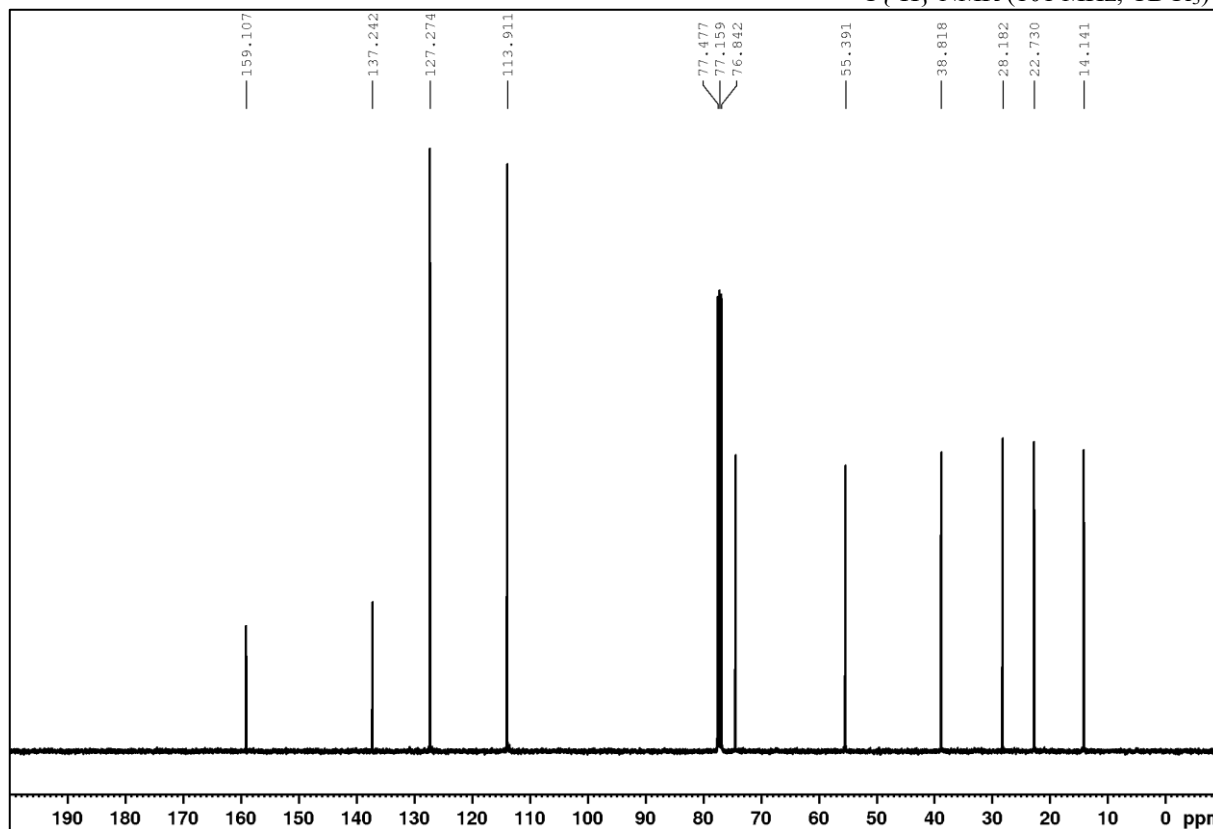
APPENDIX

1-(4-Methoxyphenyl)pentan-1-ol (18n)

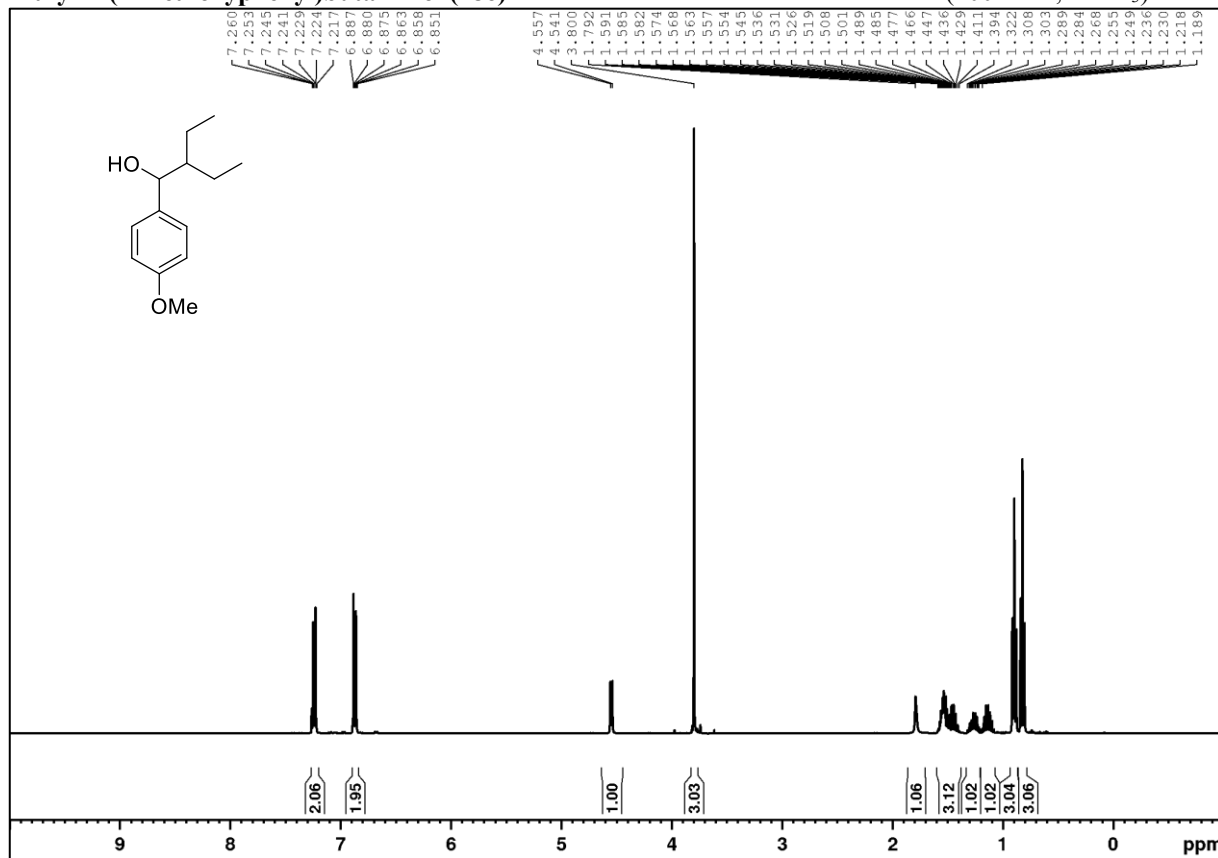
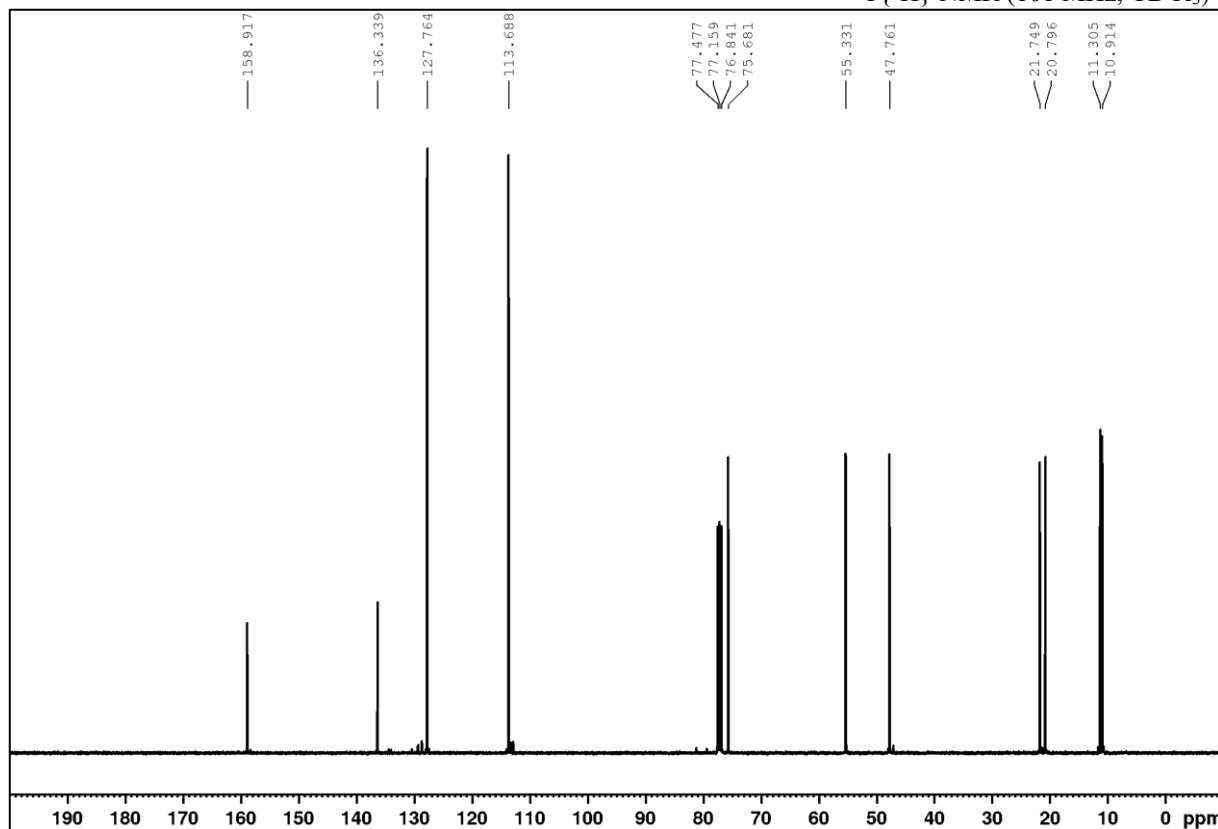
¹H NMR (400 MHz, CDCl₃)

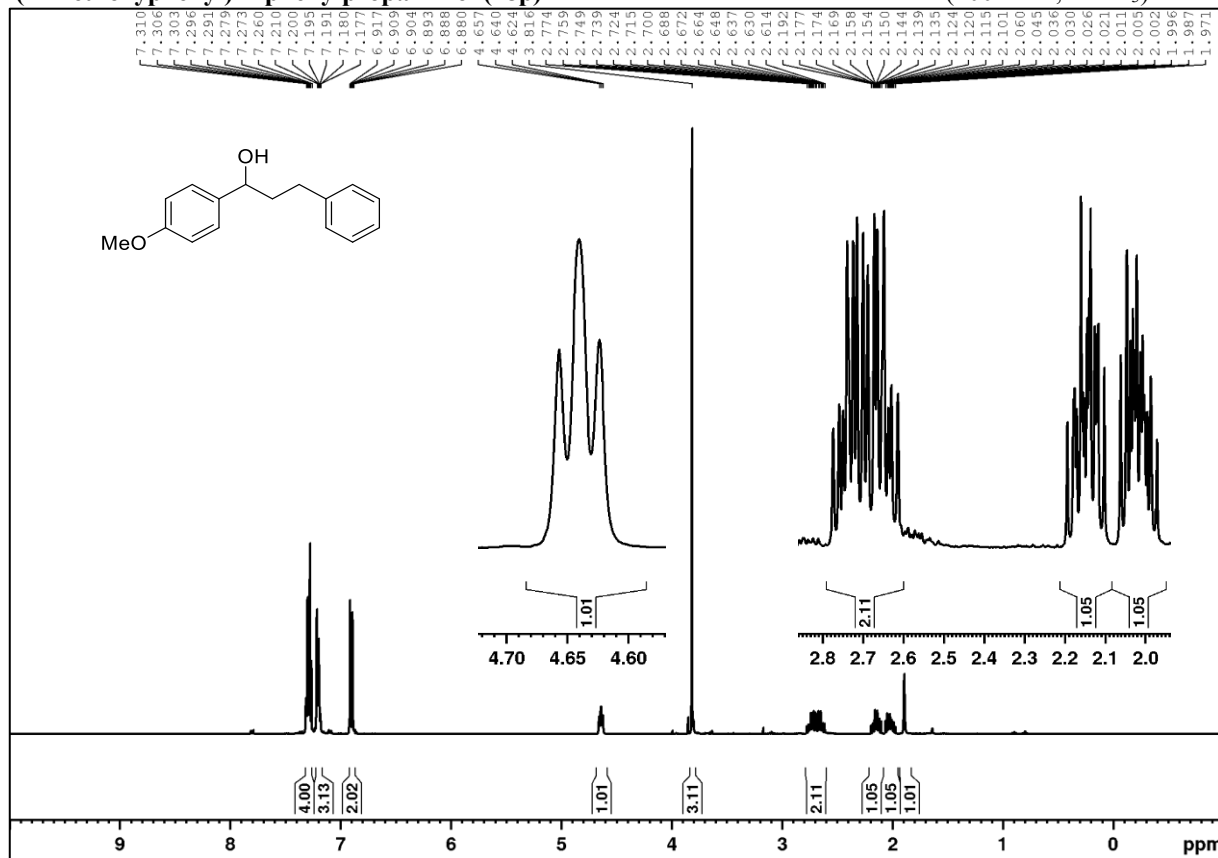
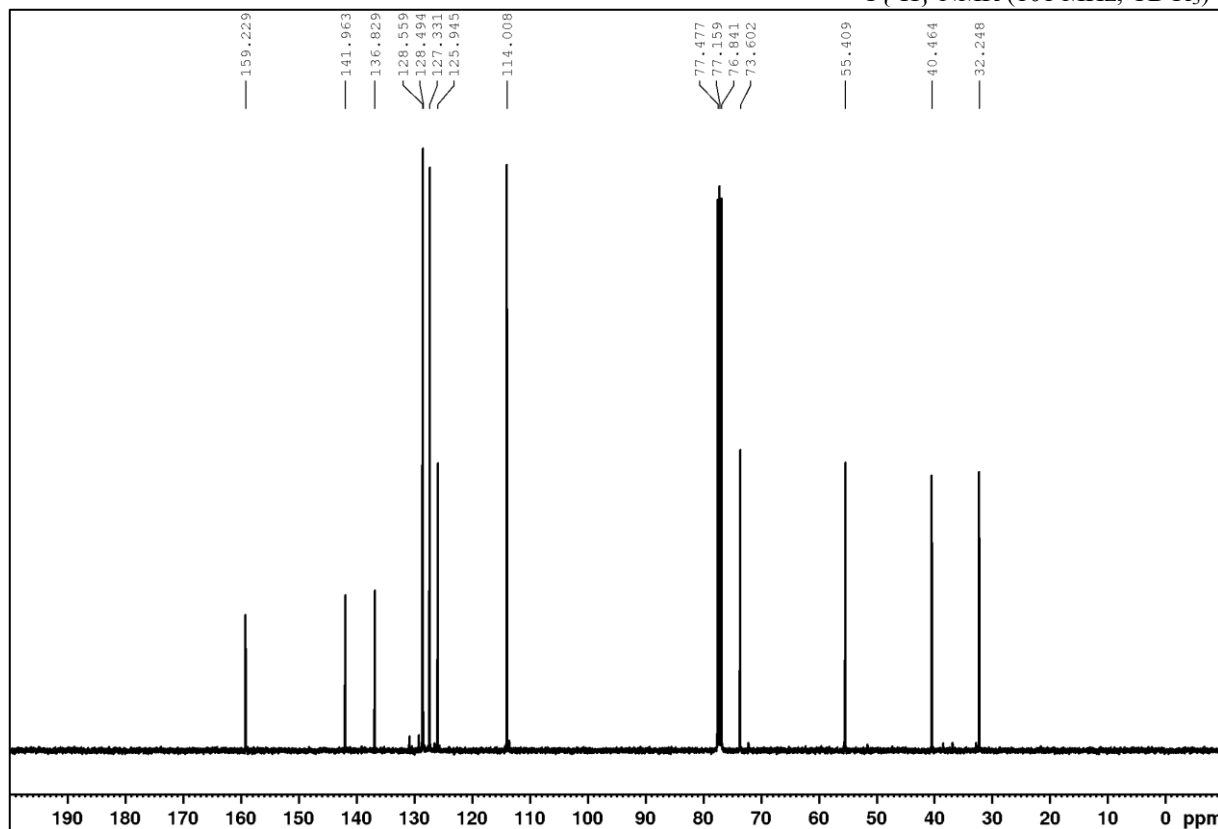


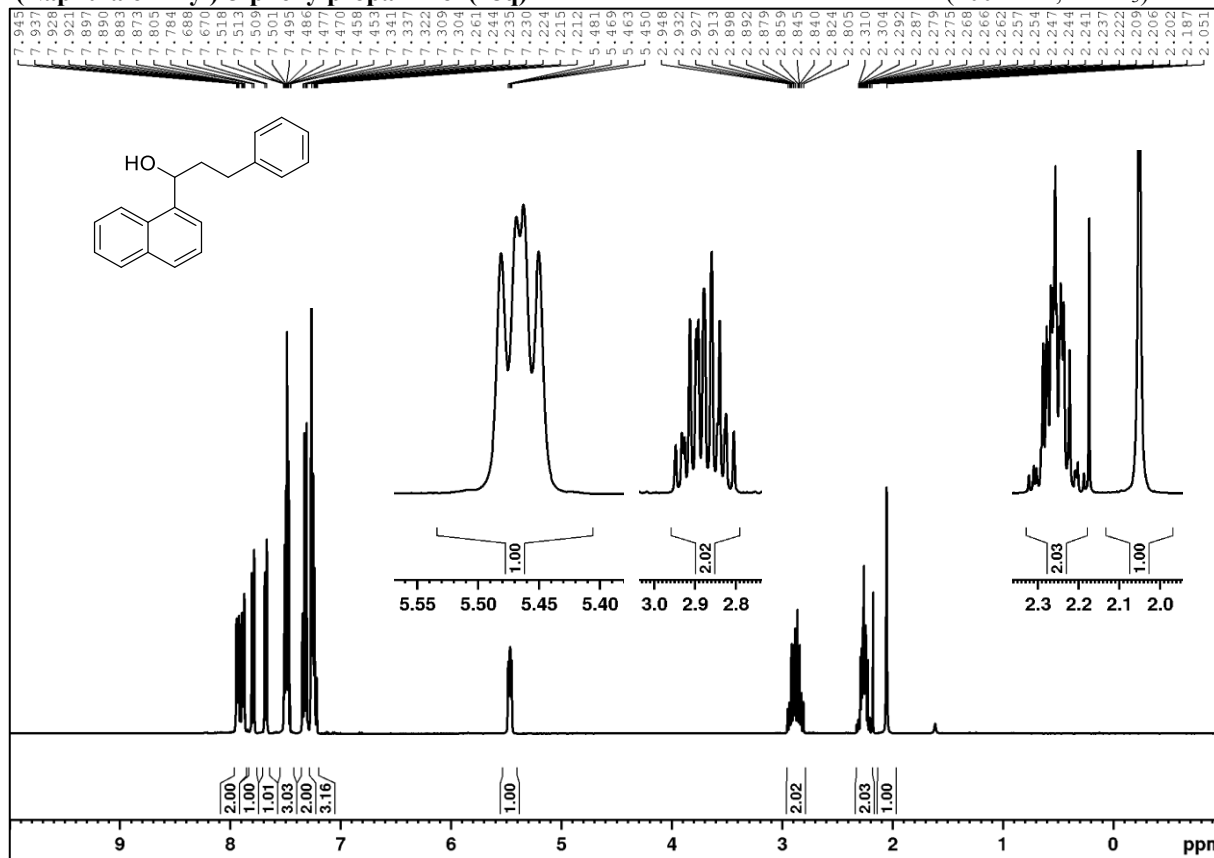
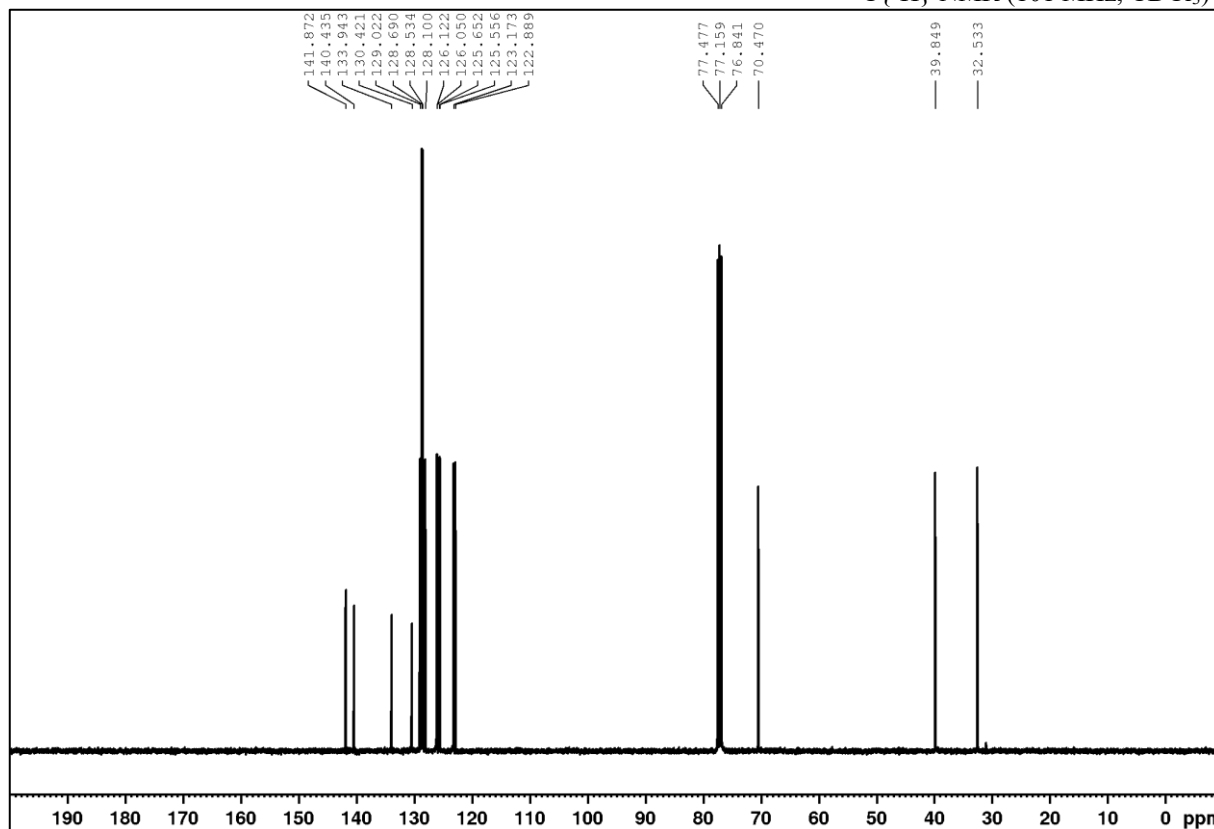
¹³C{¹H} NMR (101 MHz, CDCl₃)

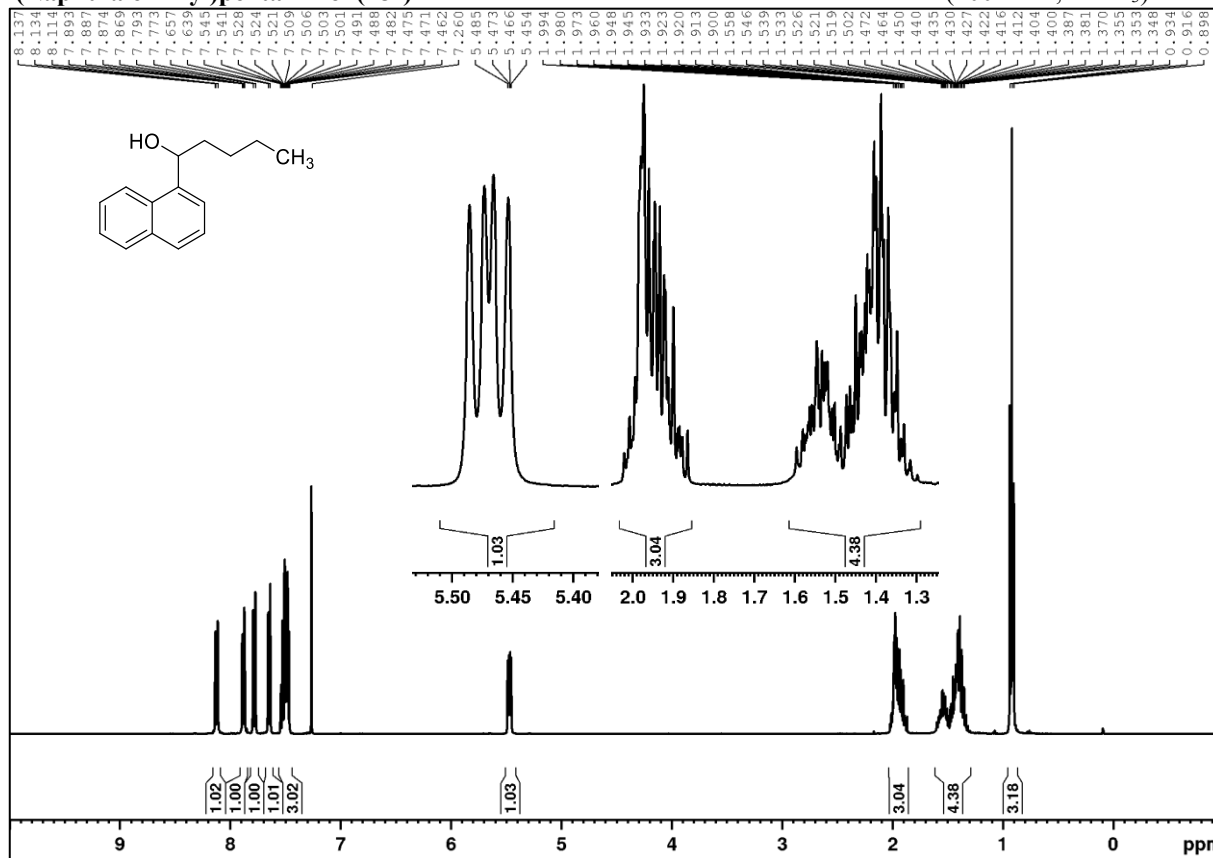
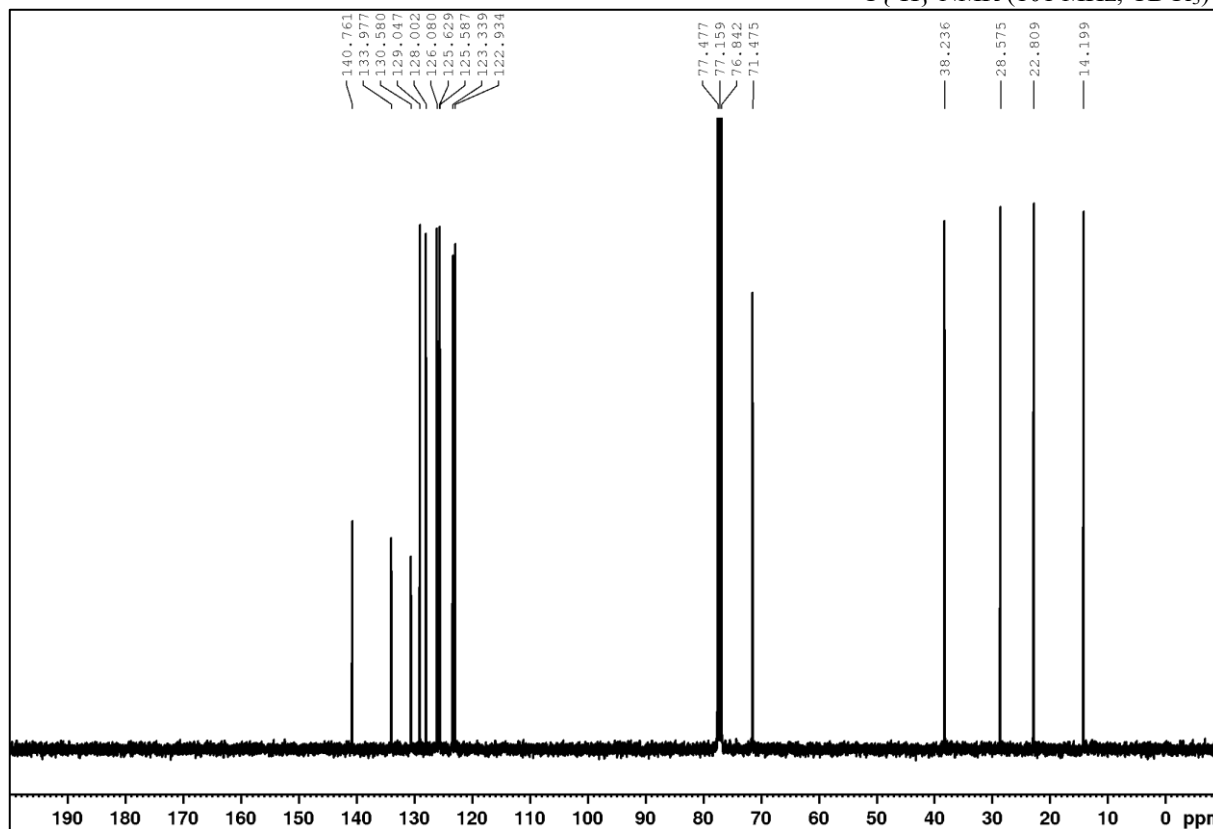


2-Ethyl-1-(4-methoxyphenyl)butan-1-ol (18o)

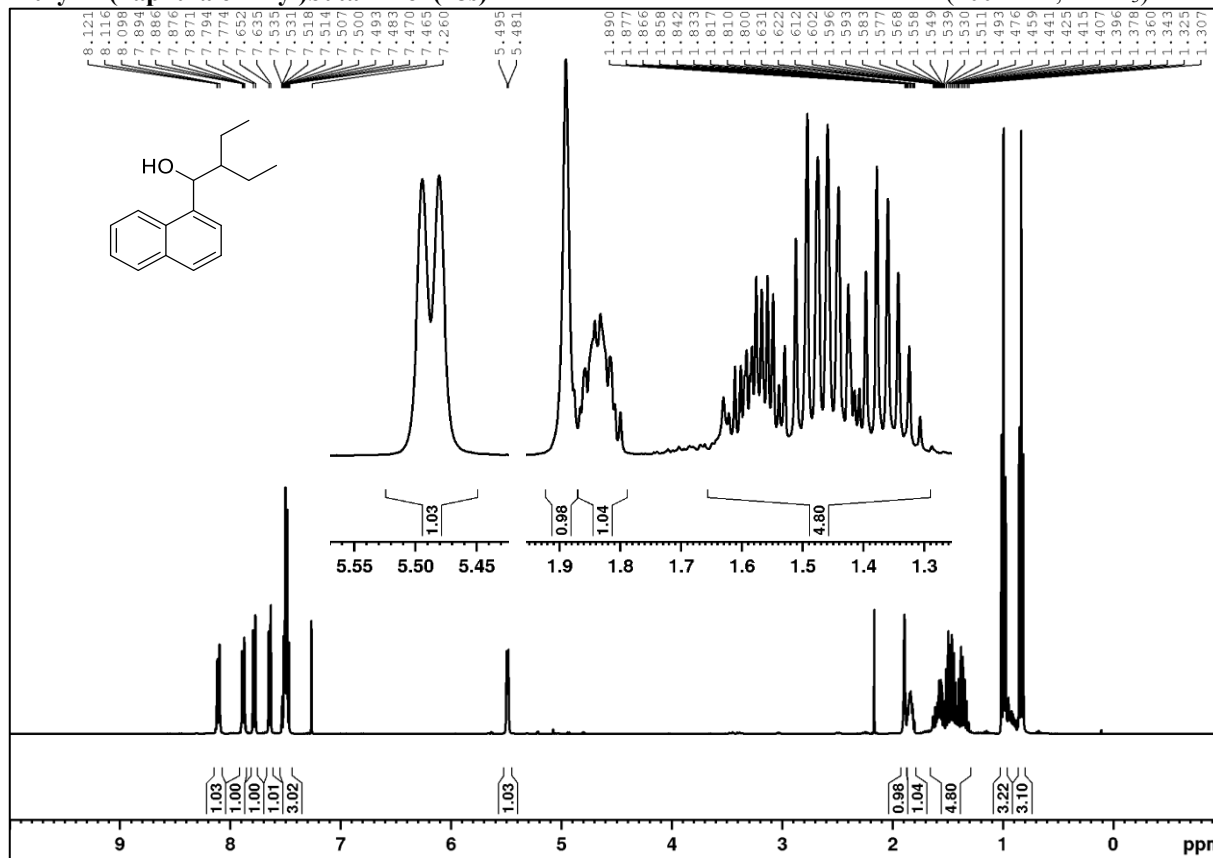
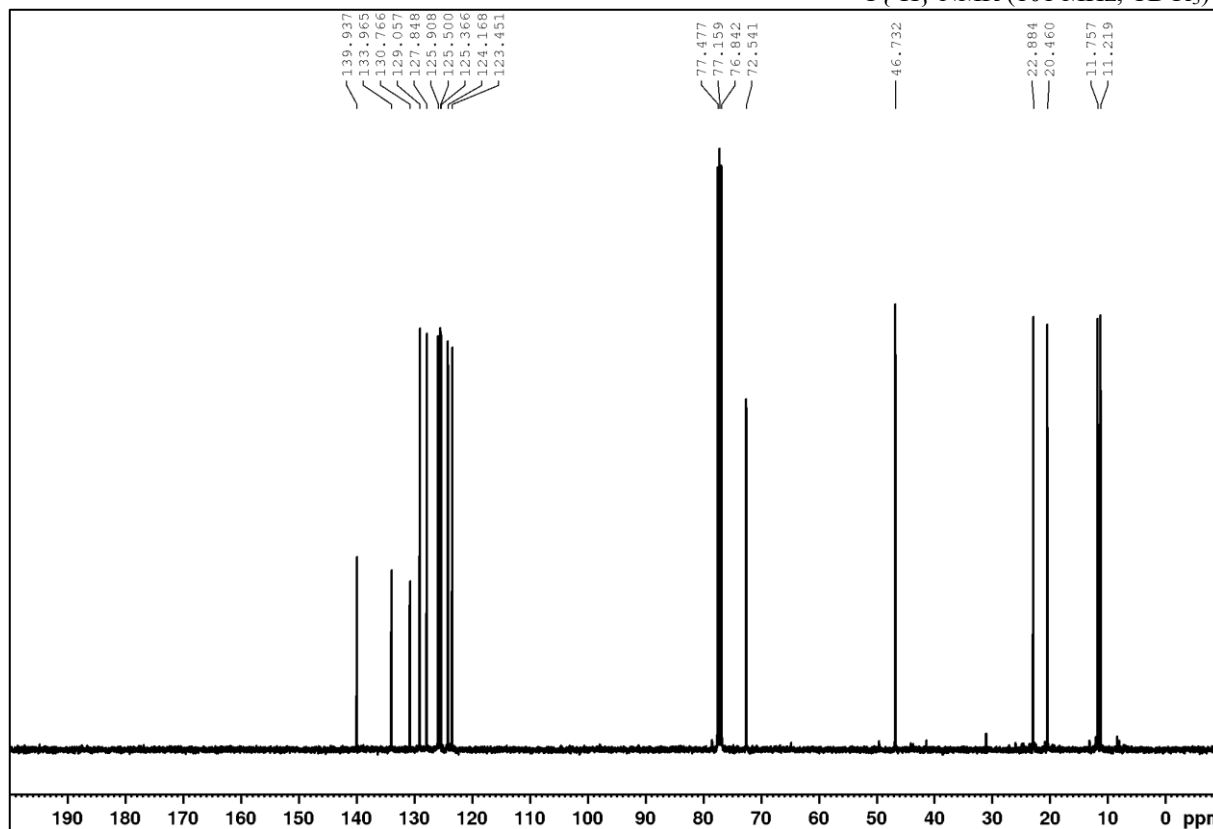
 ^1H NMR (400 MHz, CDCl_3) $^{13}\text{C}\{^1\text{H}\}$ NMR (101 MHz, CDCl_3)

1-(4-Methoxyphenyl)-2-phenylpropan-1-ol (18p) ^1H NMR (400 MHz, CDCl_3) $^{13}\text{C}\{^1\text{H}\}$ NMR (101 MHz, CDCl_3)

1-(Naphthalen-1-yl)-3-phenylpropan-1-ol (18q) ^1H NMR (400 MHz, CDCl_3) $^{13}\text{C}\{^1\text{H}\}$ NMR (101 MHz, CDCl_3)

1-(Naphthalen-1-yl)pentan-1-ol (18r)**¹H NMR (400 MHz, CDCl₃)****¹³C{¹H} NMR (101 MHz, CDCl₃)**

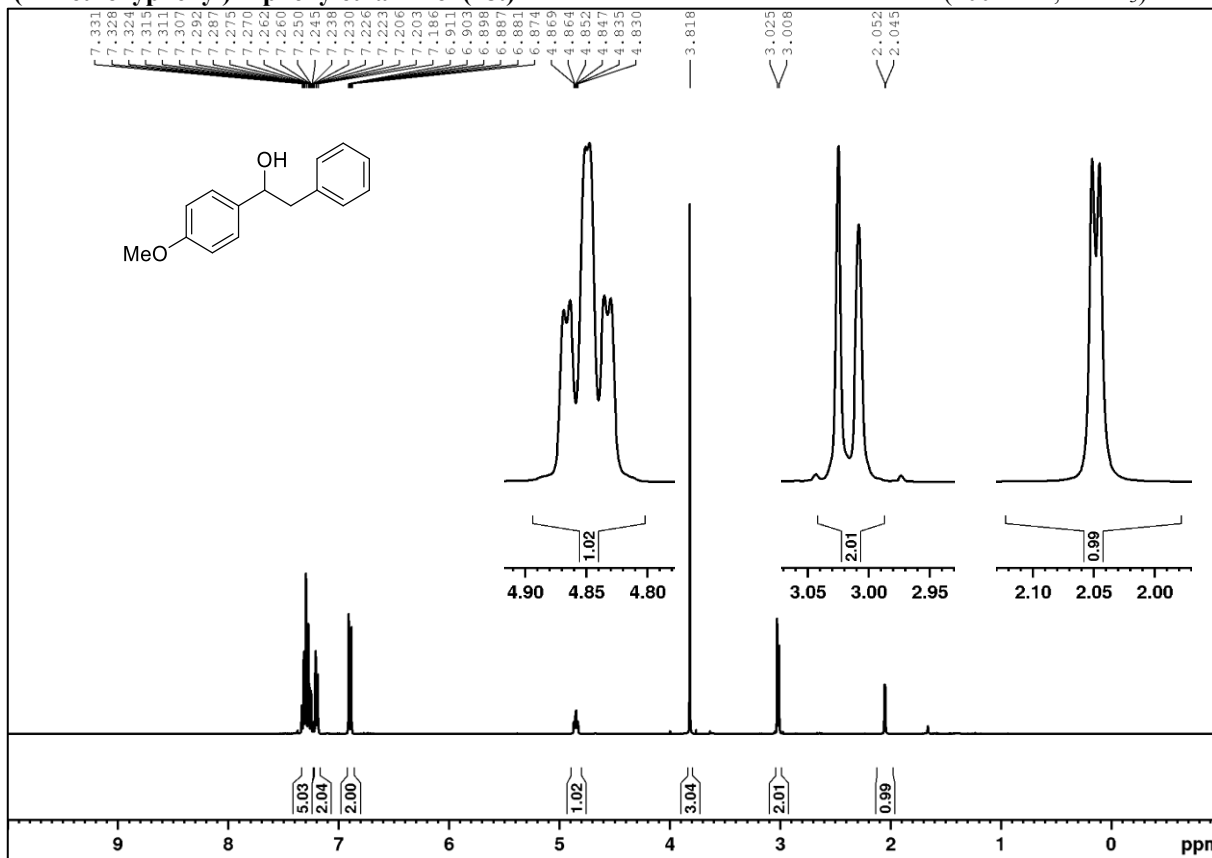
2-Ethyl-1-(naphthalen-1-yl)butan-1-ol (18s)

 ^1H NMR (400 MHz, CDCl_3) $^{13}\text{C}\{^1\text{H}\}$ NMR (101 MHz, CDCl_3)

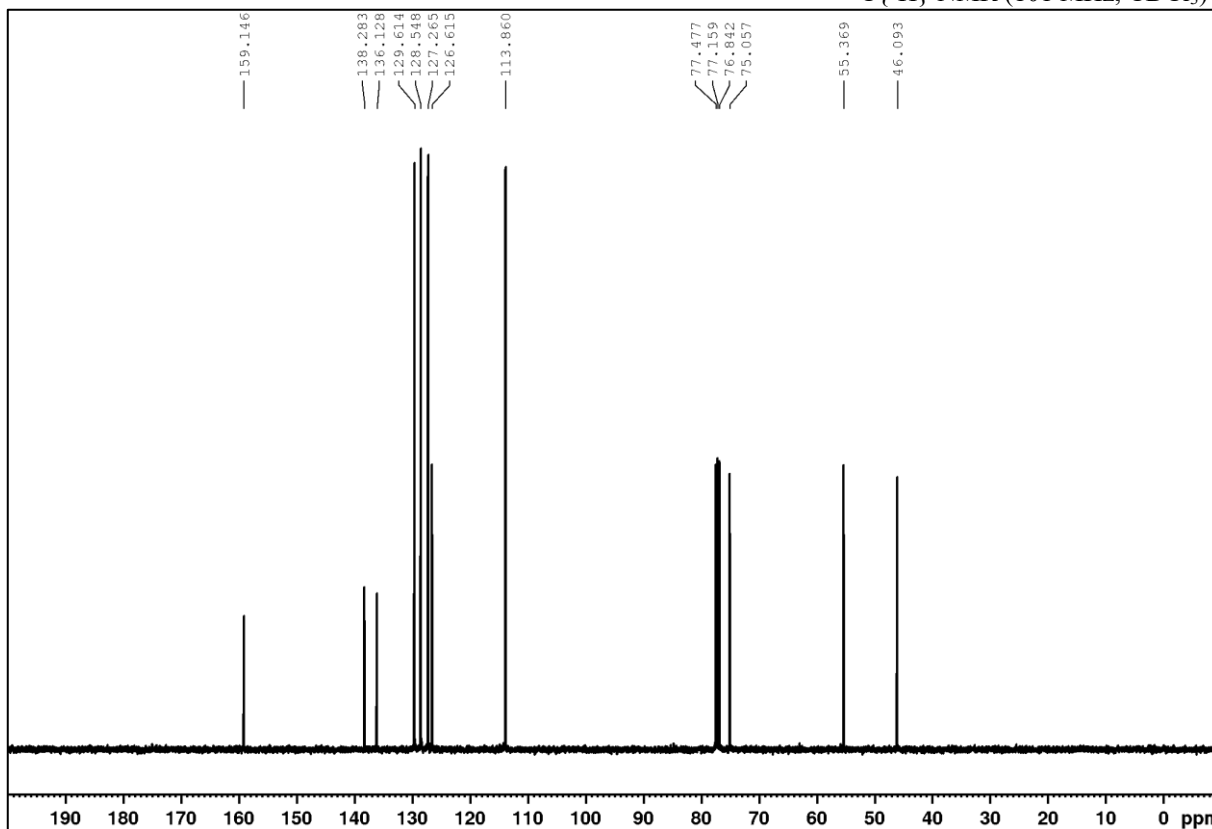
APPENDIX

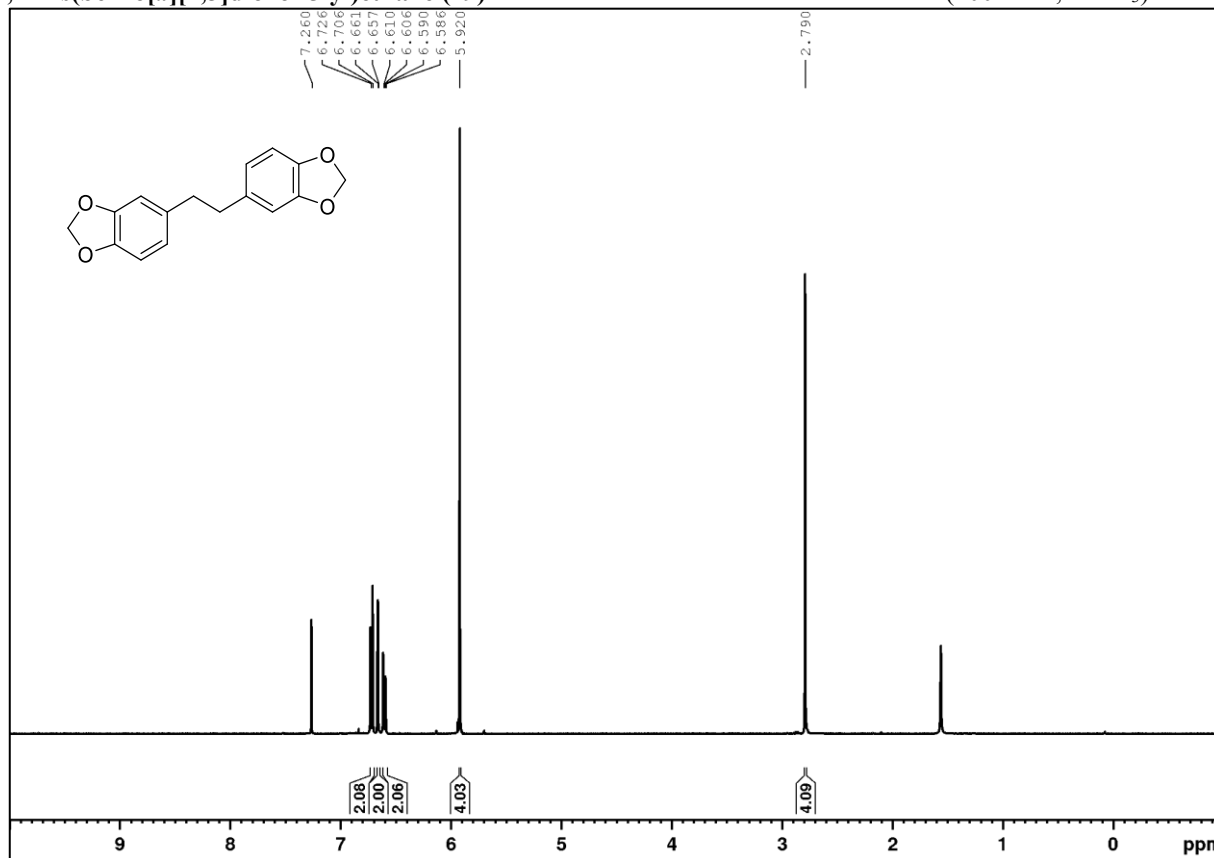
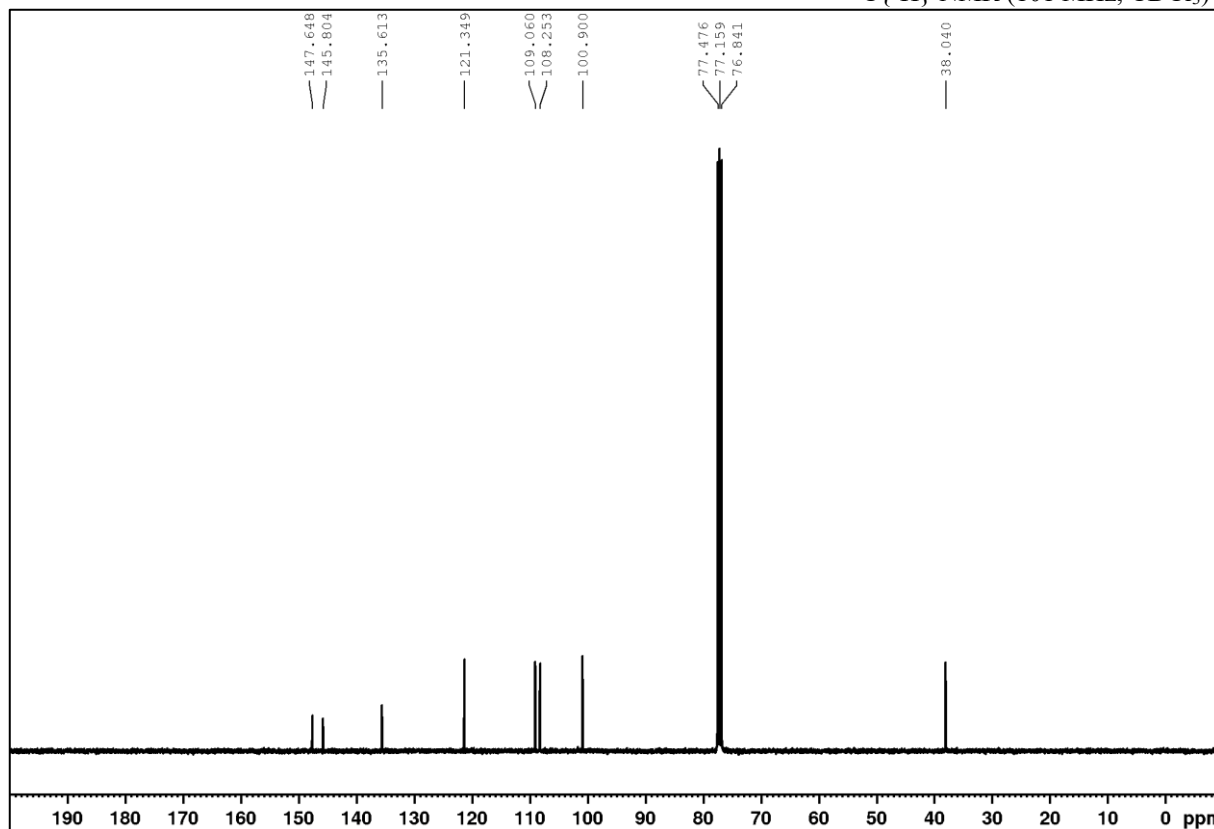
1-(4-Methoxyphenyl)-2-phenylethan-1-ol (18t)

^1H NMR (400 MHz, CDCl_3)

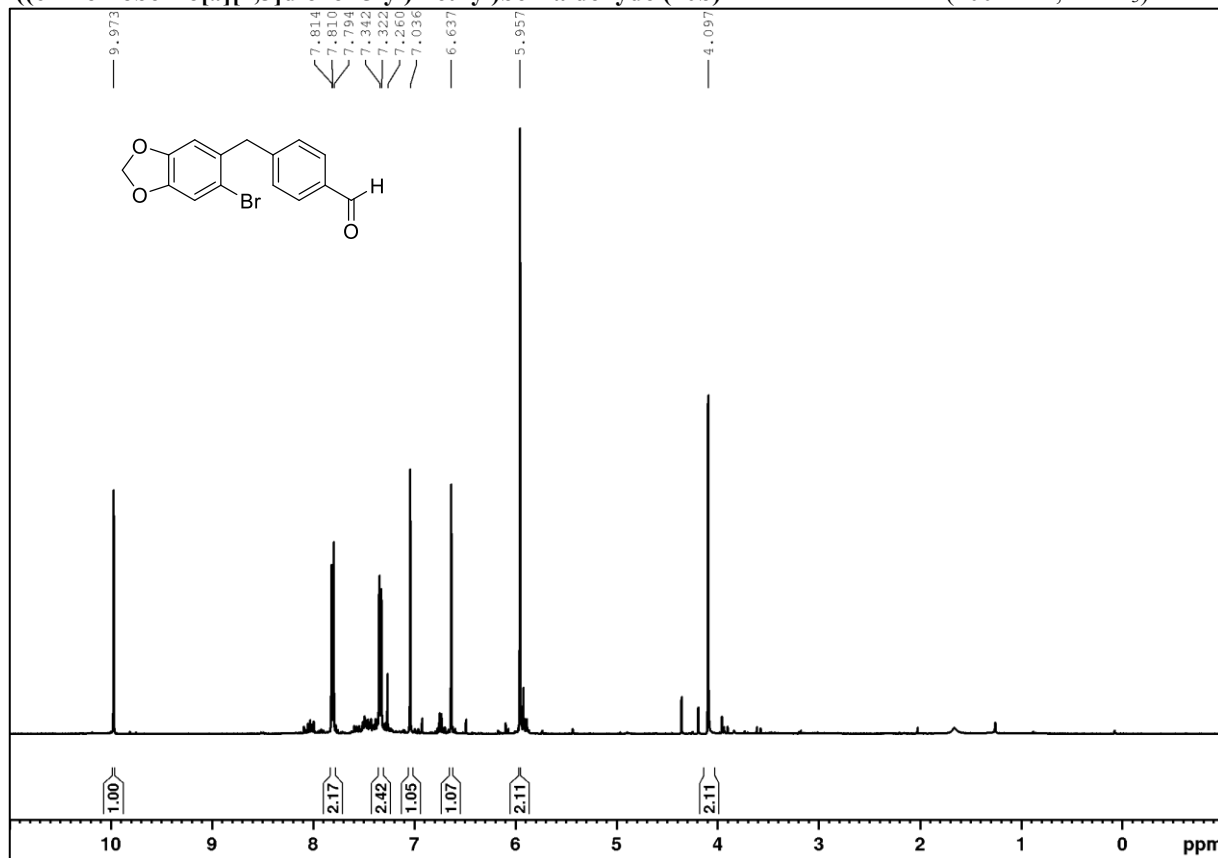
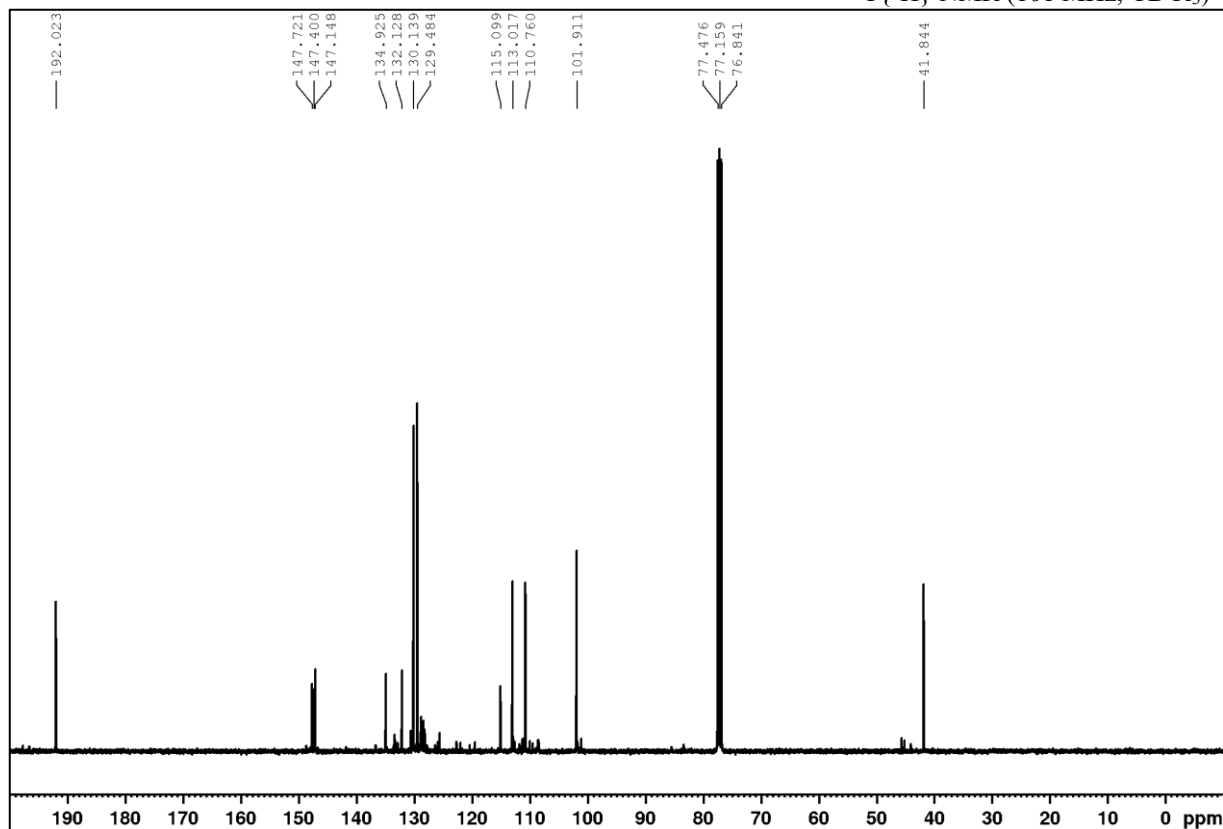


$^{13}\text{C}\{^1\text{H}\}$ NMR (101 MHz, CDCl_3)

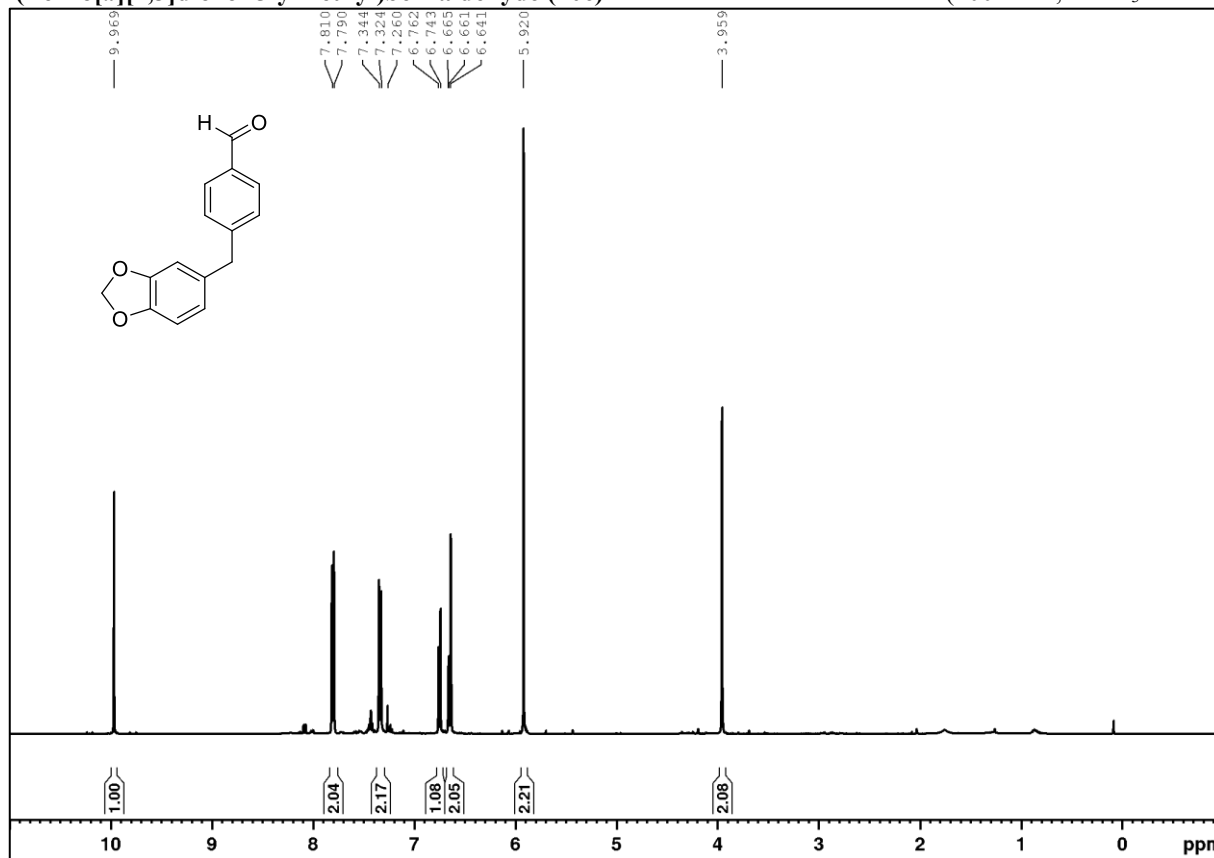
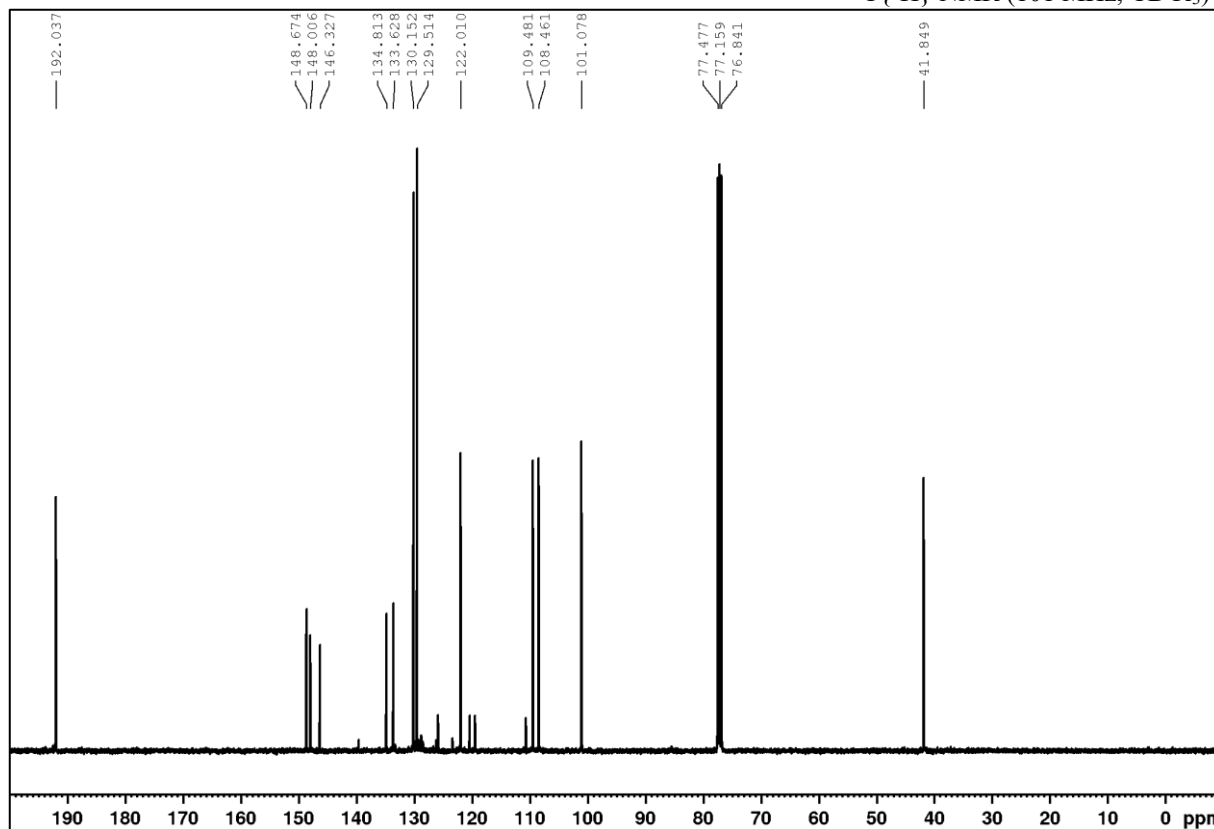


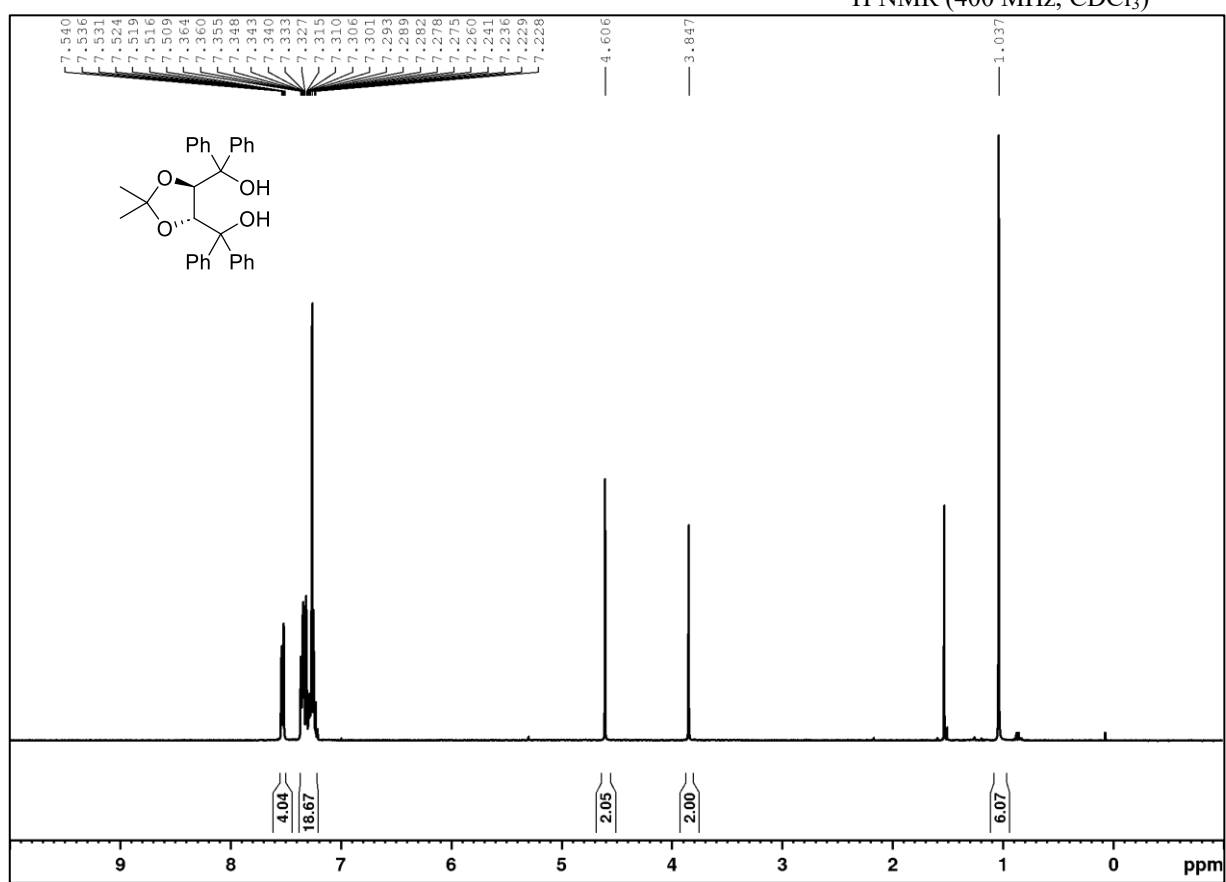
1,2-Bis(benzo[*d*][1,3]dioxol-5-yl)ethane (19)¹H NMR (400 MHz, CDCl₃)¹³C{¹H} NMR (101 MHz, CDCl₃)

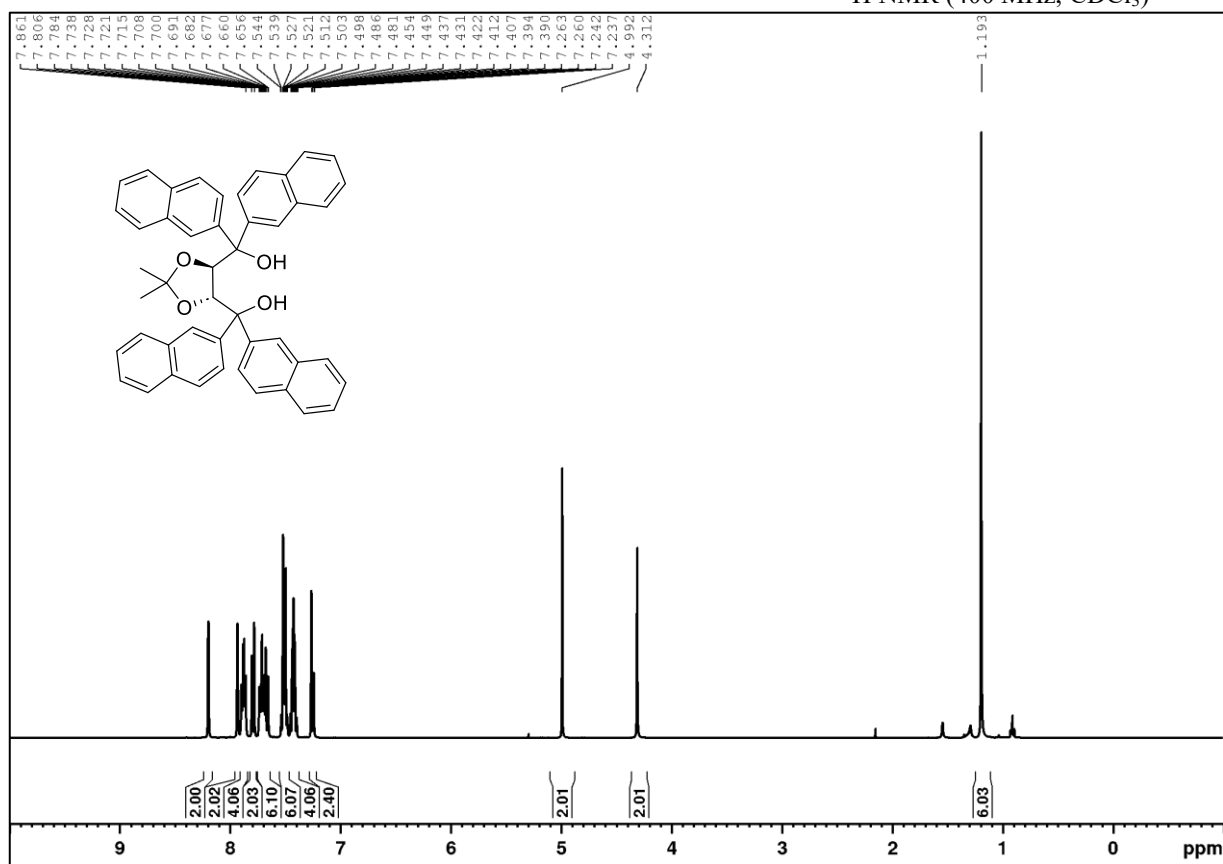
4-((6-Bromobenzo[d][1,3]dioxol-5-yl)methyl)benzaldehyde (20b)

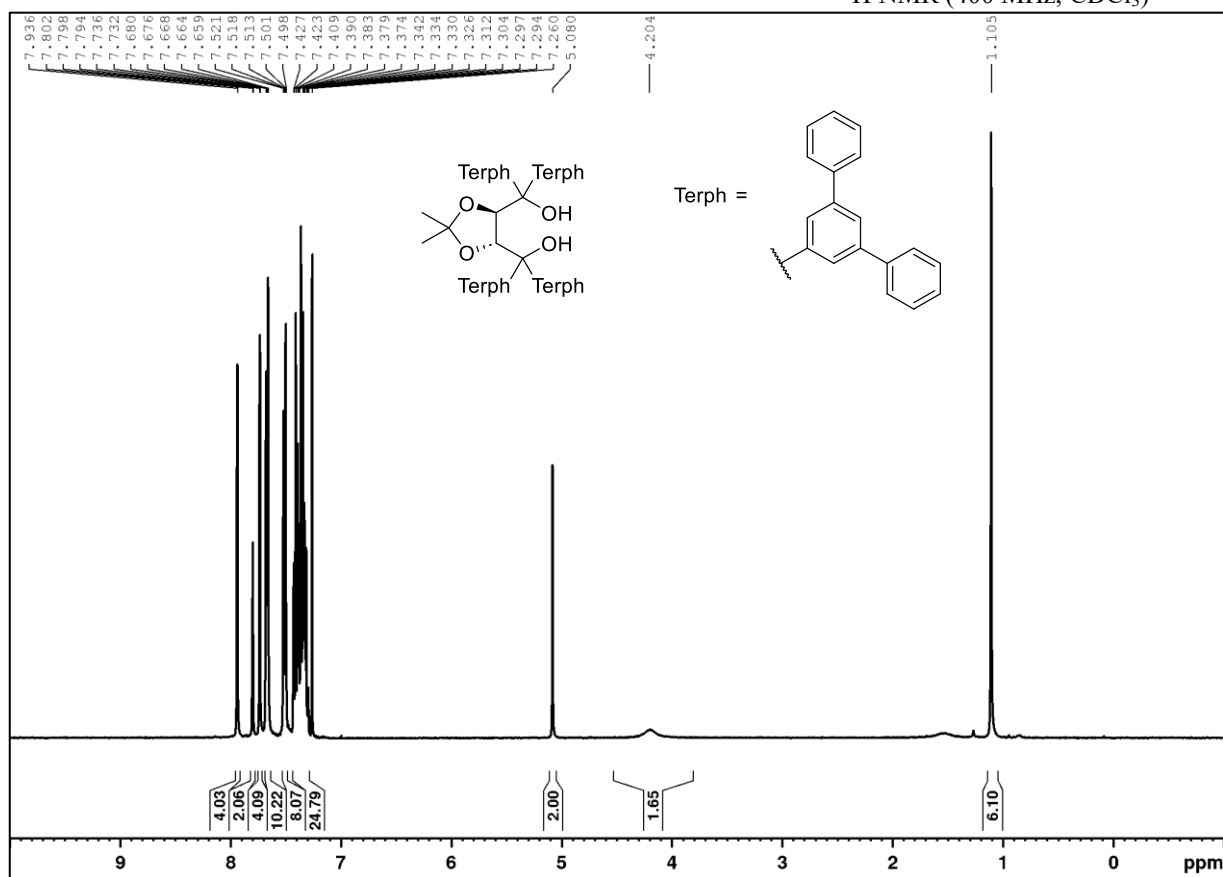
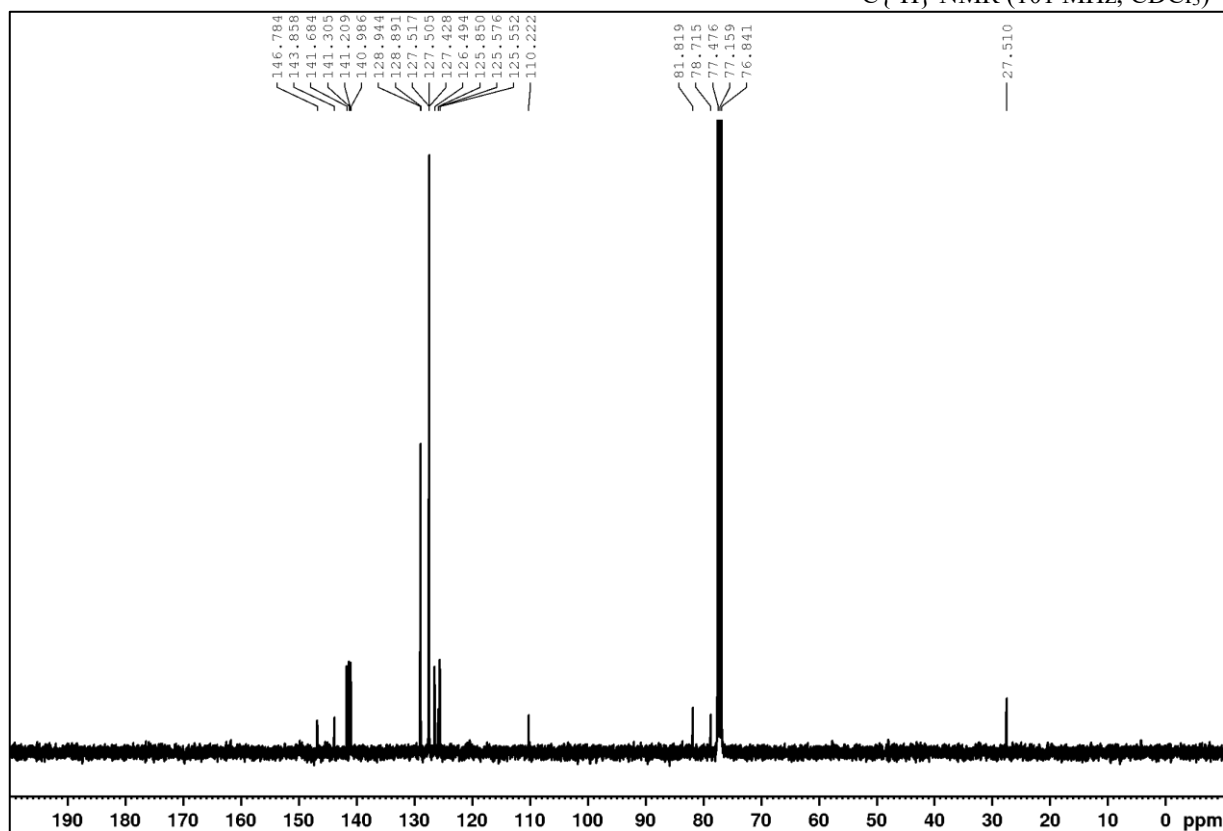
 ^1H NMR (400 MHz, CDCl_3) $^{13}\text{C}\{^1\text{H}\}$ NMR (101 MHz, CDCl_3)

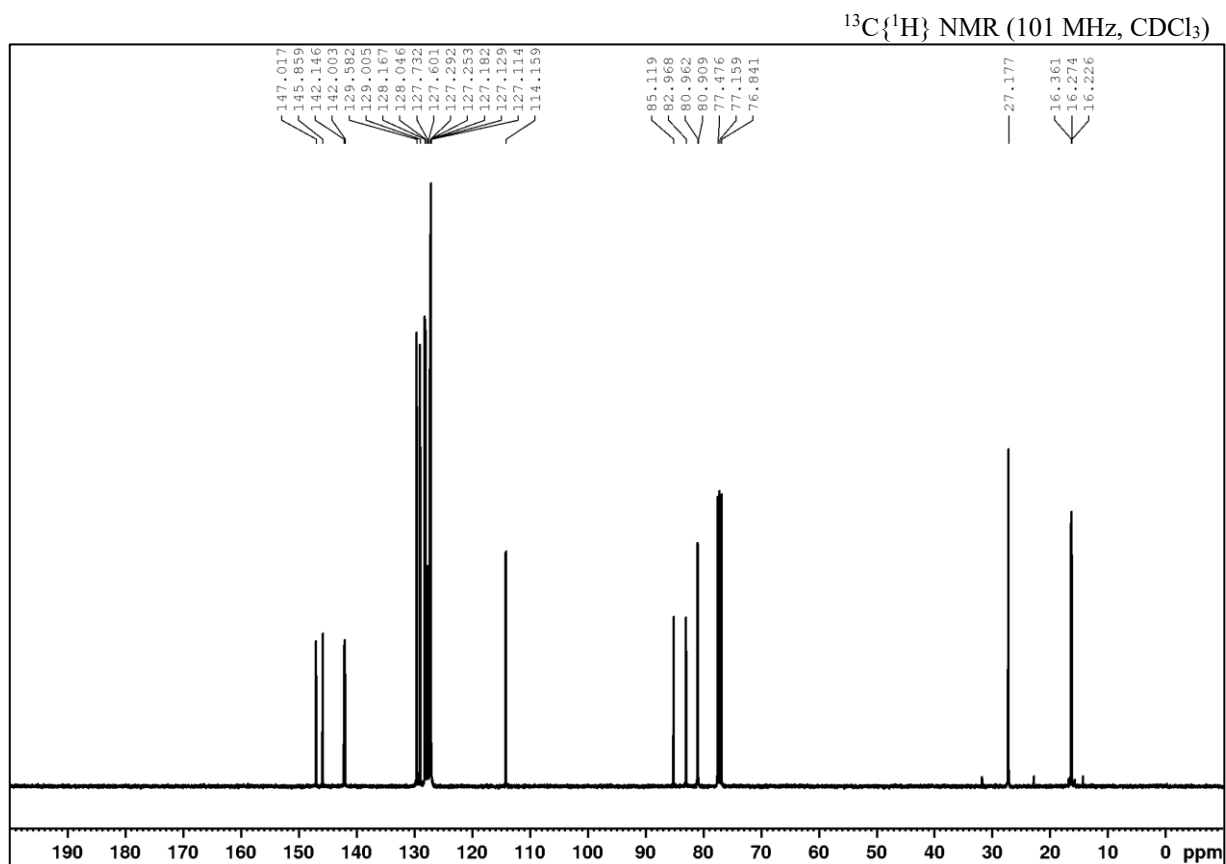
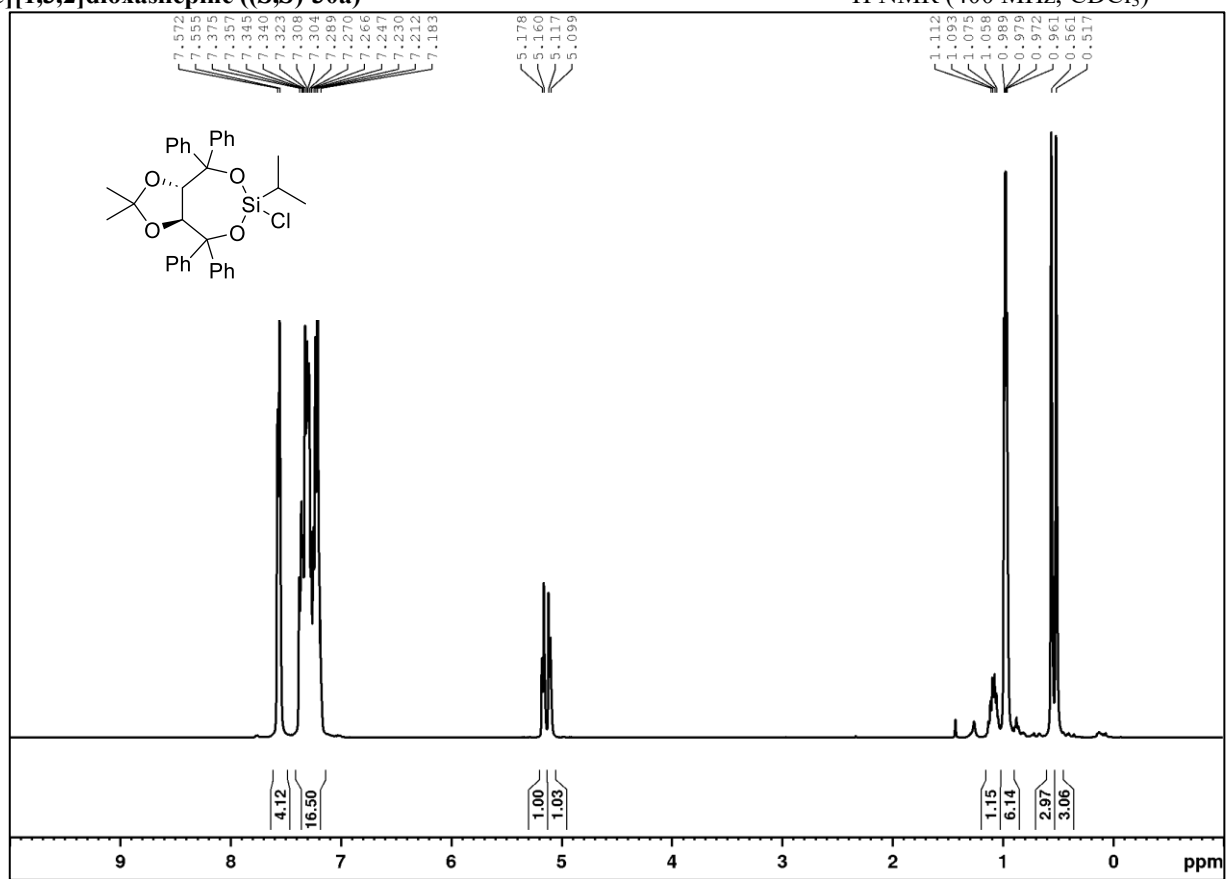
4-(Benzo[d][1,3]dioxol-5-ylmethyl)benzaldehyde (20c)

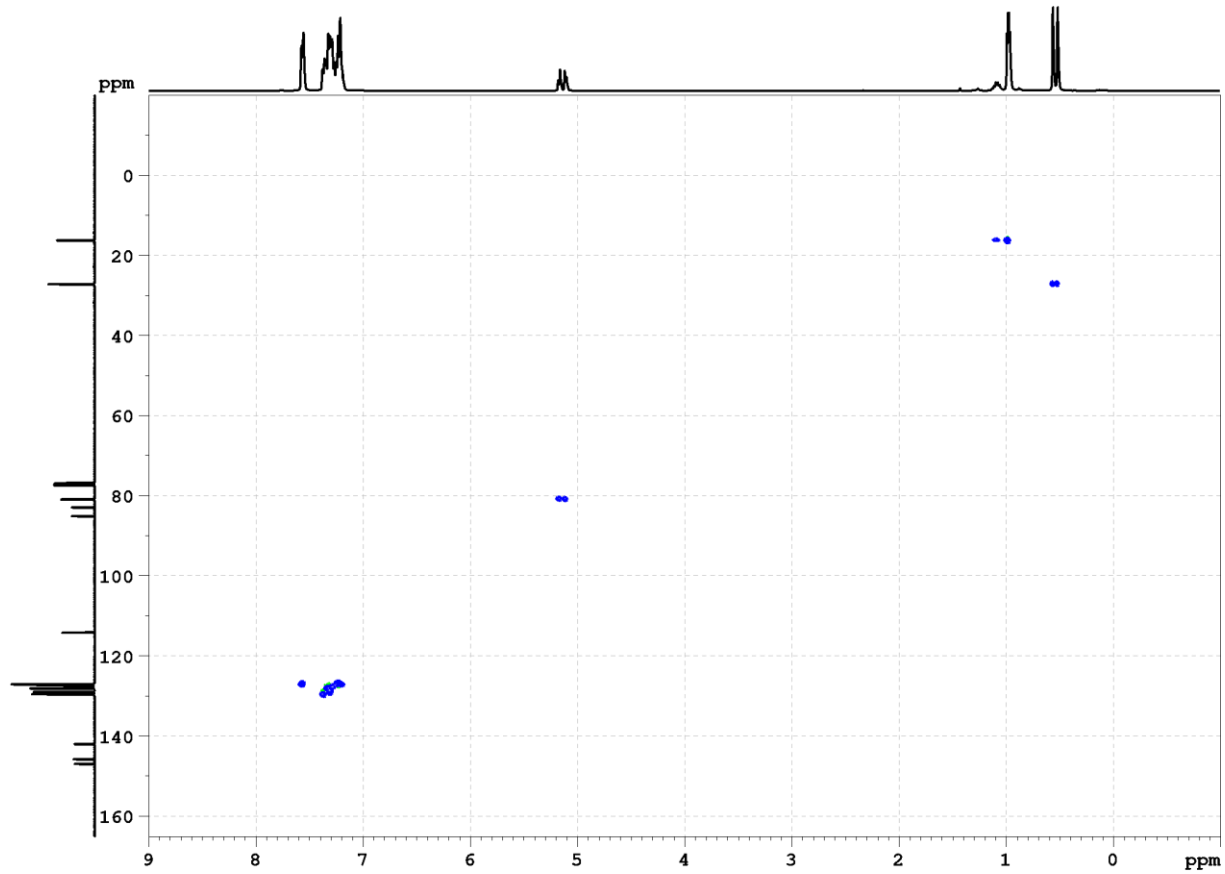
 ^1H NMR (400 MHz, CDCl_3) $^{13}\text{C}\{^1\text{H}\}$ NMR (101 MHz, CDCl_3)

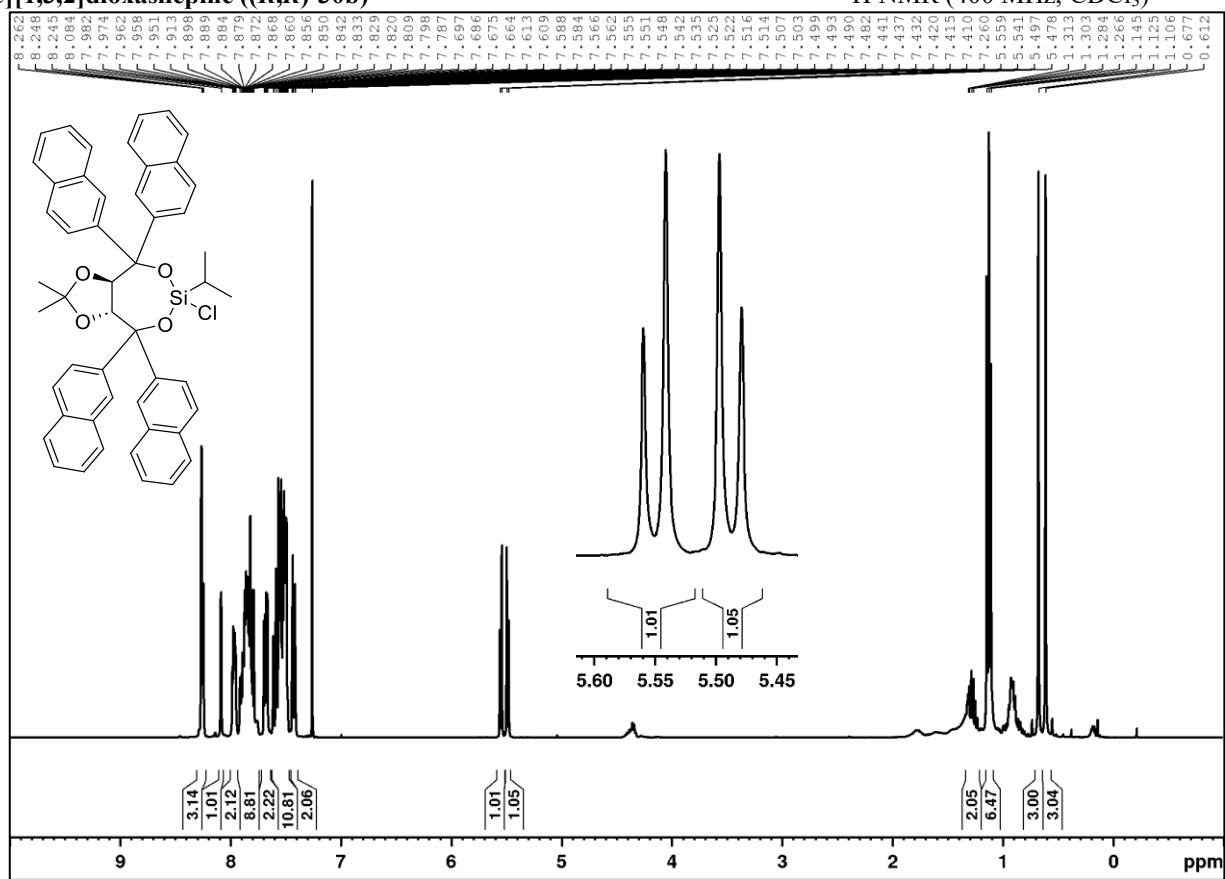
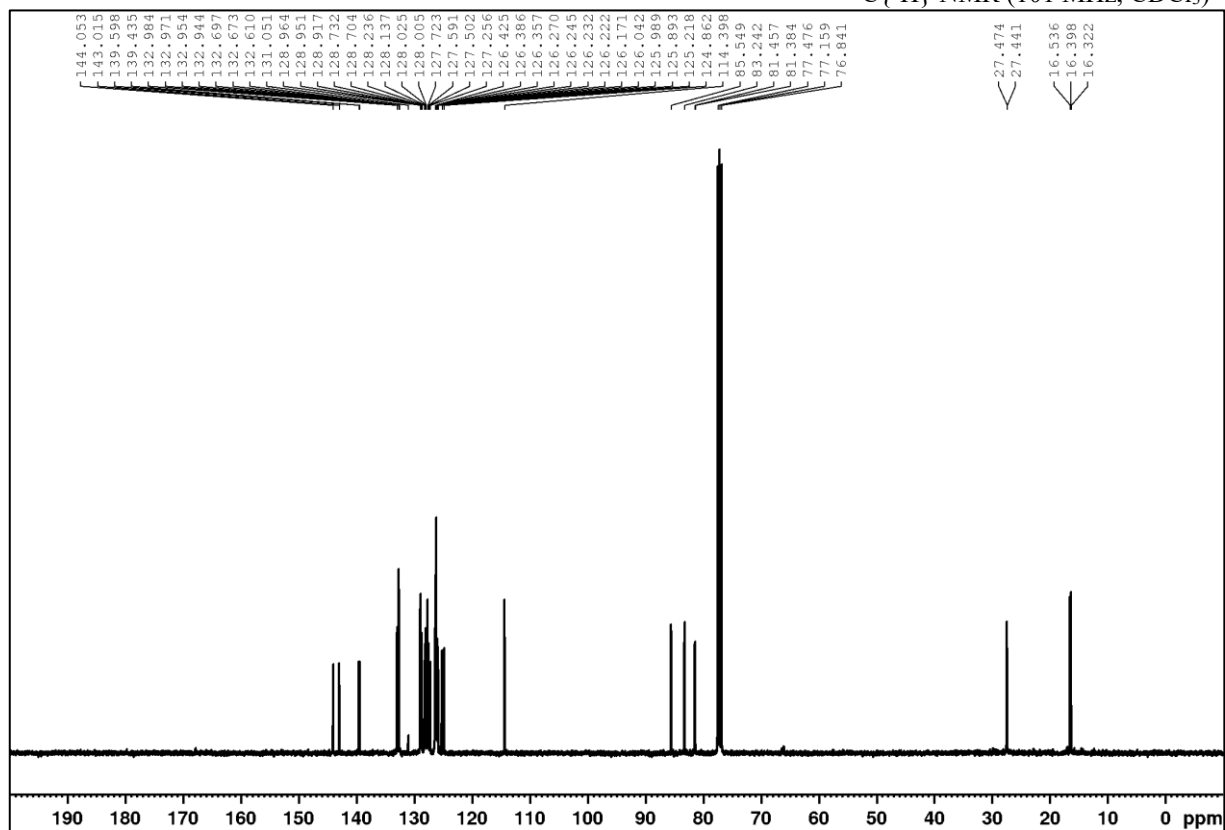
((4*R*,5*R*)-2,2-Dimethyl-1,3-dioxolane-4,5-diyl)bis(diphenylmethanol) ((*R,R*)-28a)¹H NMR (400 MHz, CDCl₃)

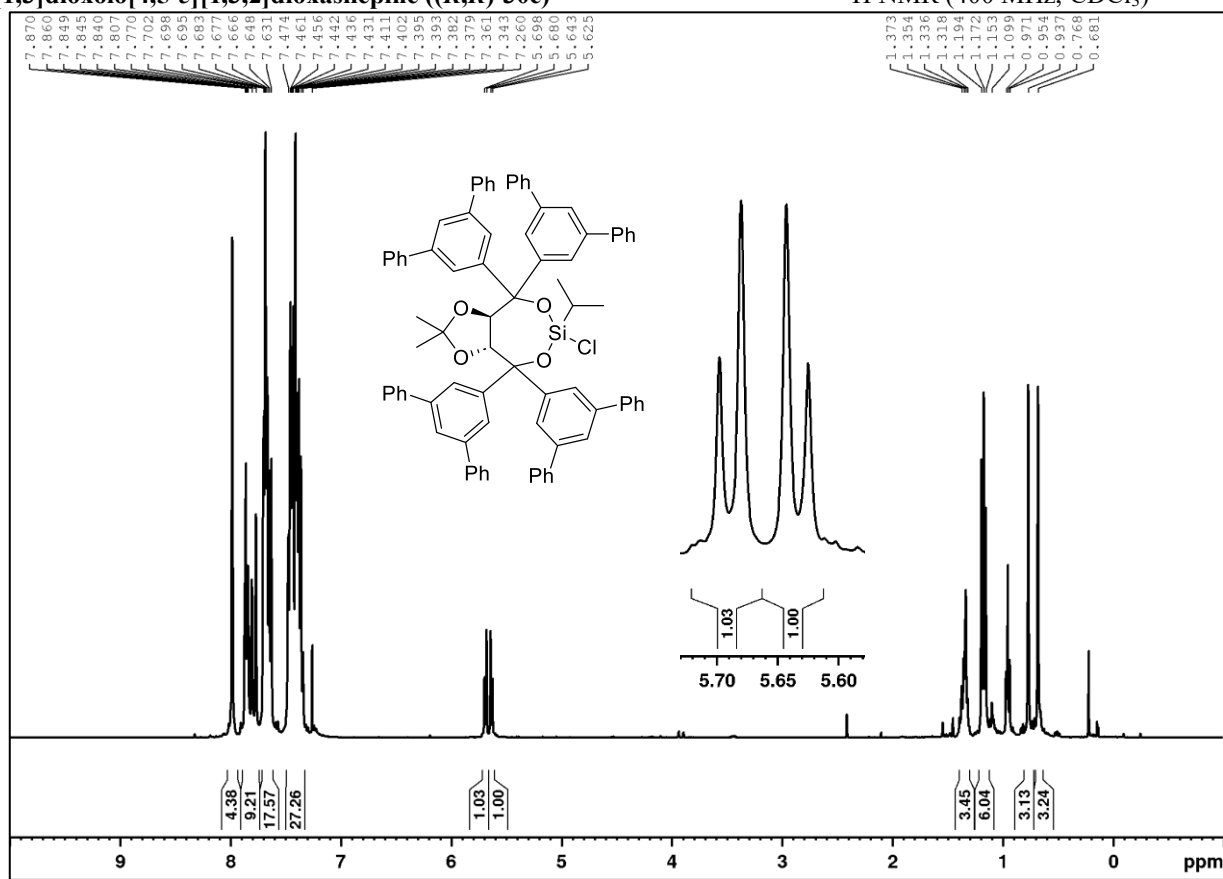
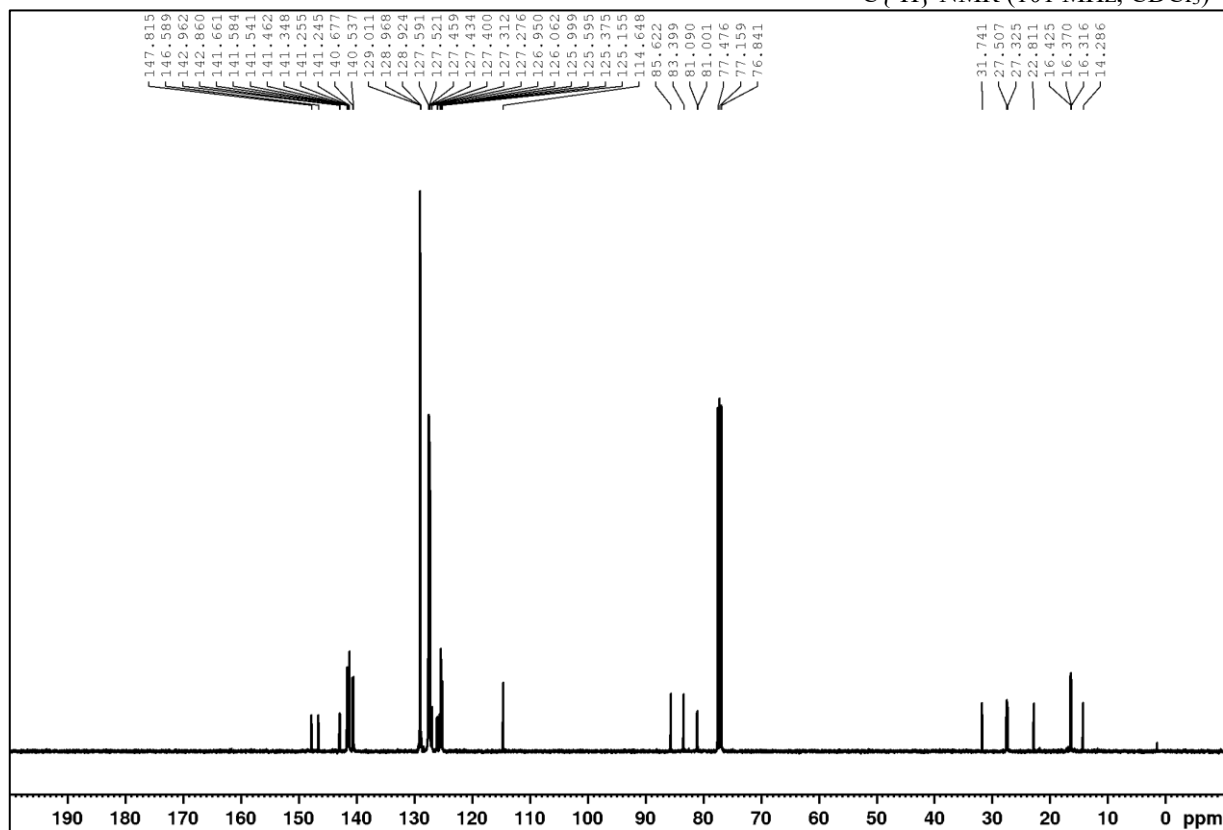
((4*R*,5*R*)-2,2-Dimethyl-1,3-dioxolane-4,5-diyl)bis(di(naphthalen-2-yl)methanol) ((*R,R*)-28b)¹H NMR (400 MHz, CDCl₃)

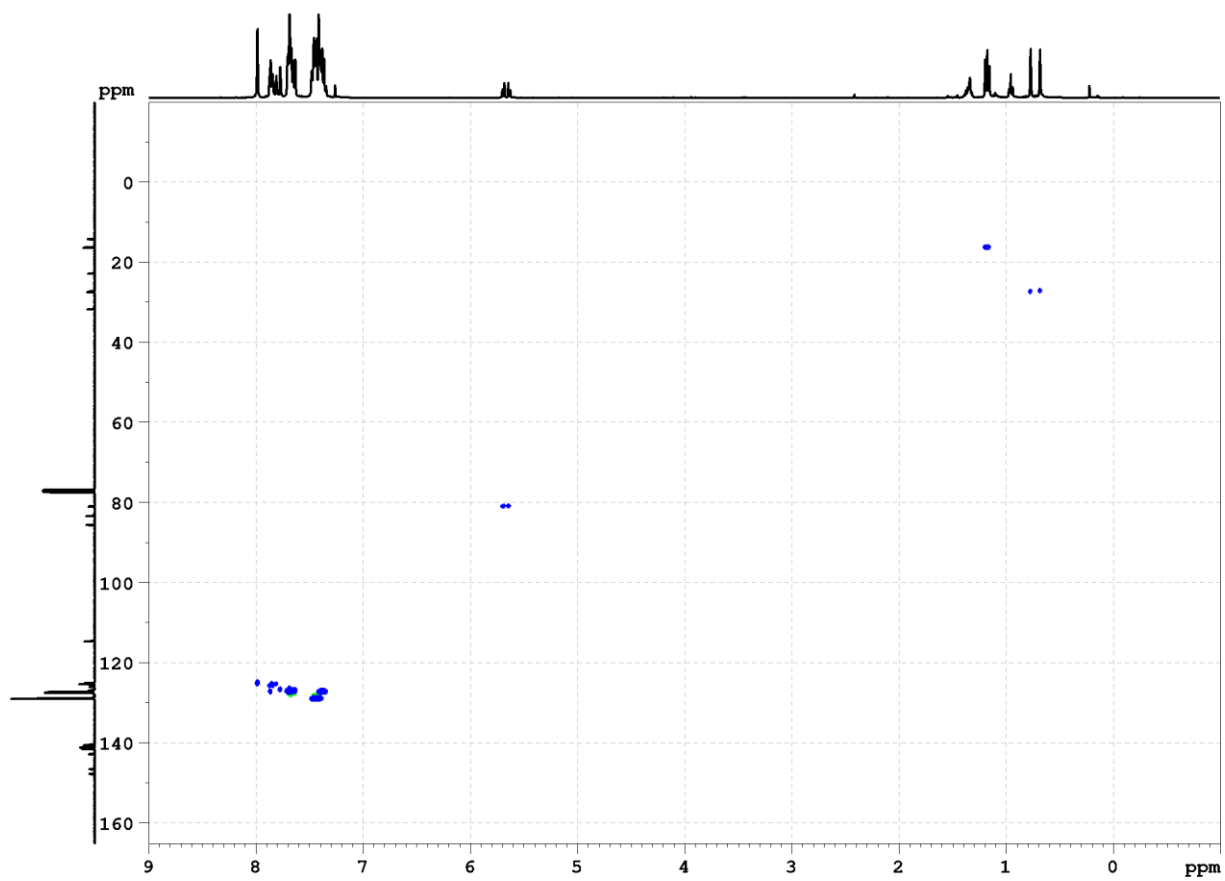
((4*R*,5*R*)-2,2-Dimethyl-1,3-dioxolane-4,5-diyl)bis(di([1,1':3',1''-terphenyl]-5'-yl)methanol) ((*R,R*)-28c)¹H NMR (400 MHz, CDCl₃)¹³C{¹H} NMR (101 MHz, CDCl₃)

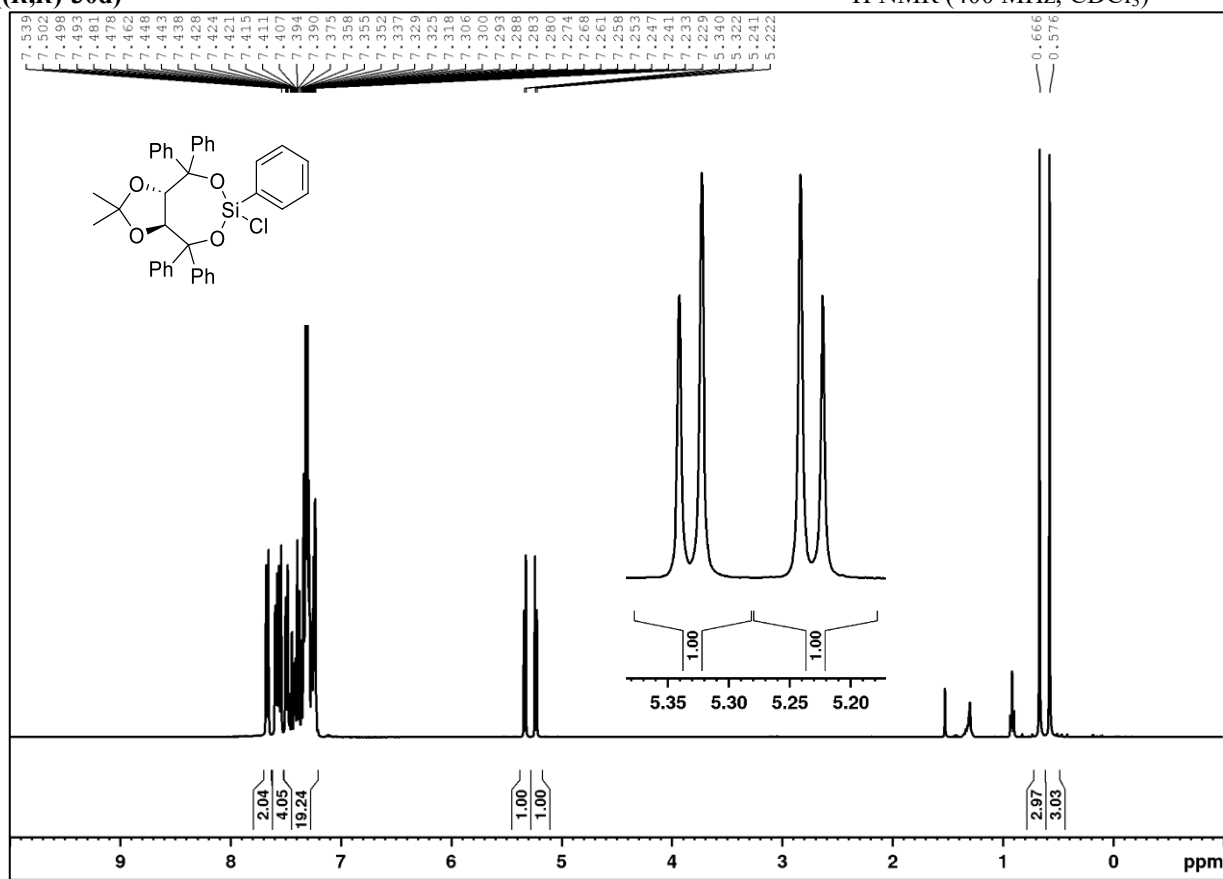
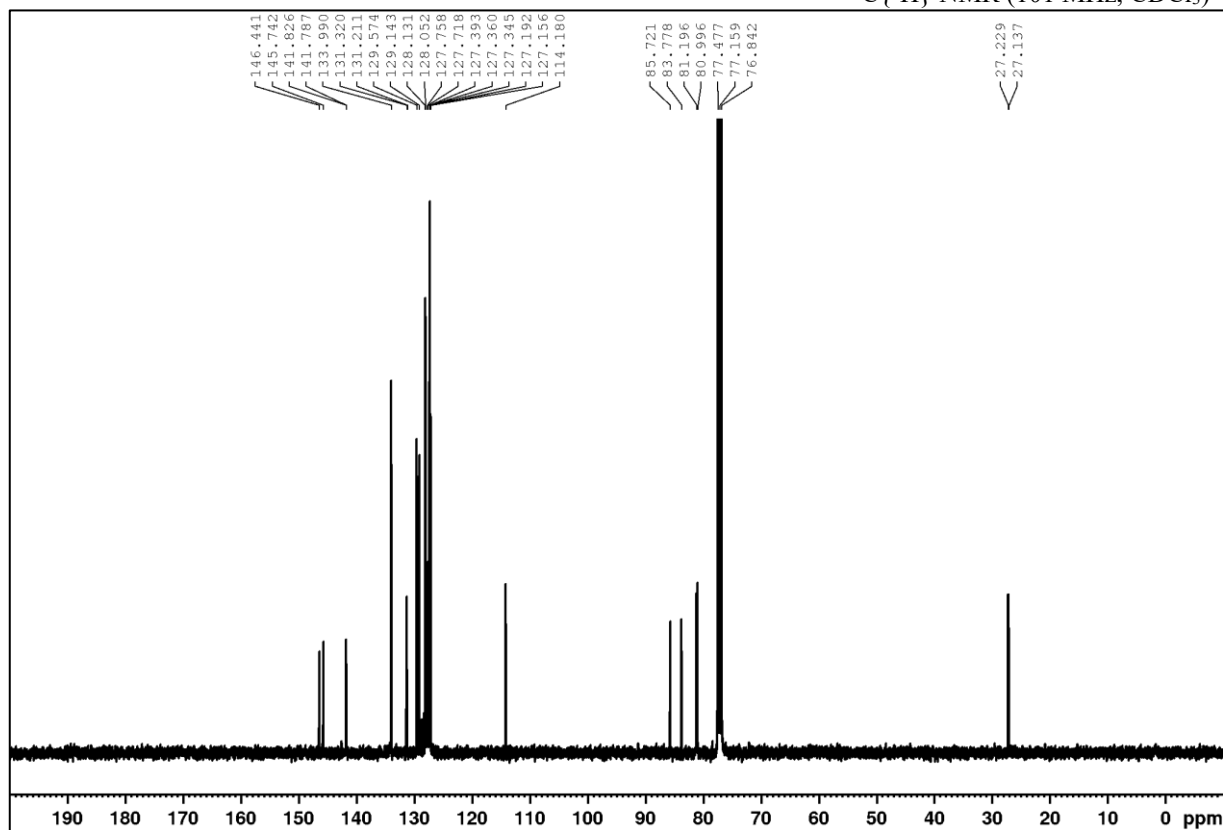
(3a*S*,8a*S*)-6-Chloro-6-isopropyl-2,2-dimethyl-4,4,8,8-tetraphenyltetrahydro-[1,3]dioxolo[4,5-*e*][1,3,2]dioxasilepine ((*S,S*)-30a)

$(^1\text{H}, ^{13}\text{C})\text{-HSQC (CDCl}_3)$ 

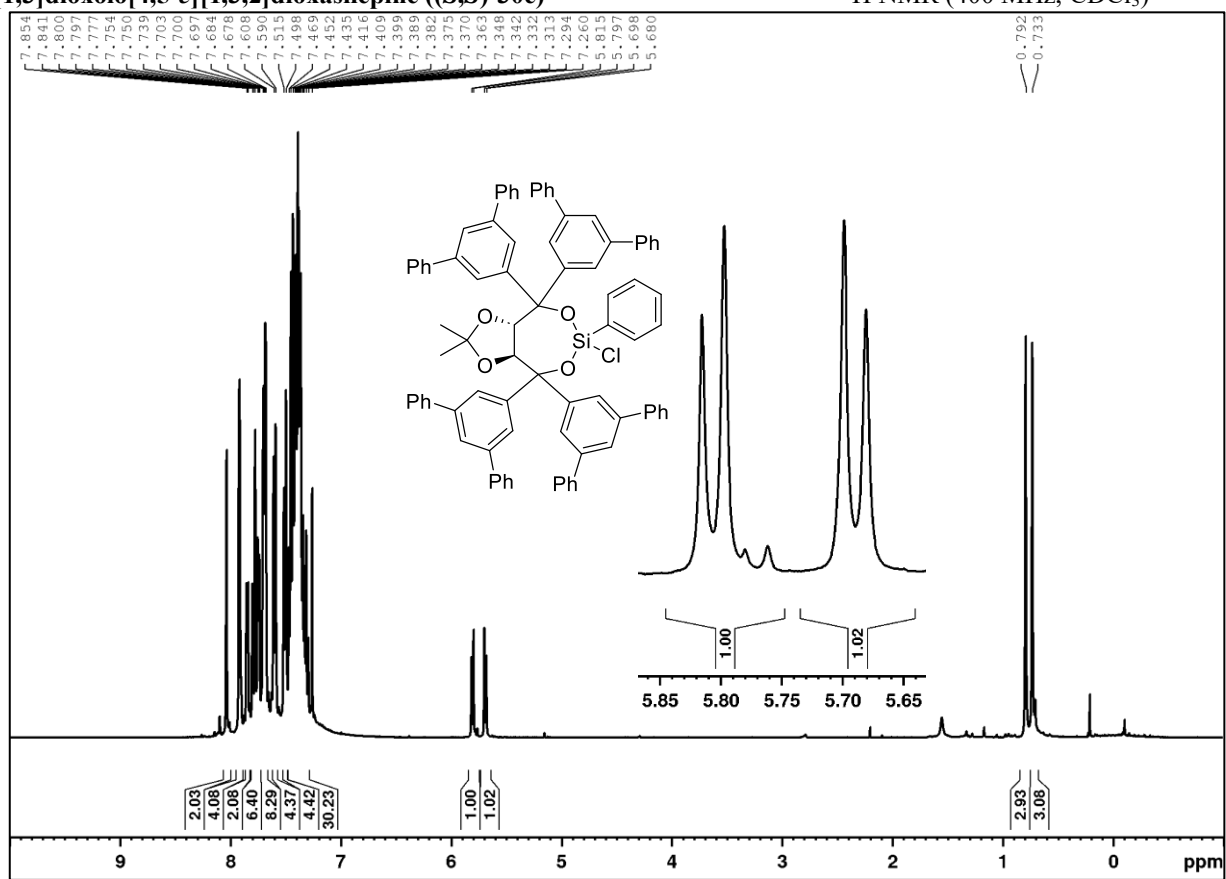
(3*aR*,8*aR*)-6-Chloro-6-isopropyl-2,2-dimethyl-4,4,8,8-tetra(naphthalen-2-yl)tetrahydro-[1,3]dioxolo[4,5-*e*][1,3,2]dioxasilpine ((*R,R*)-30b)¹H NMR (400 MHz, CDCl₃)¹³C{¹H} NMR (101 MHz, CDCl₃)

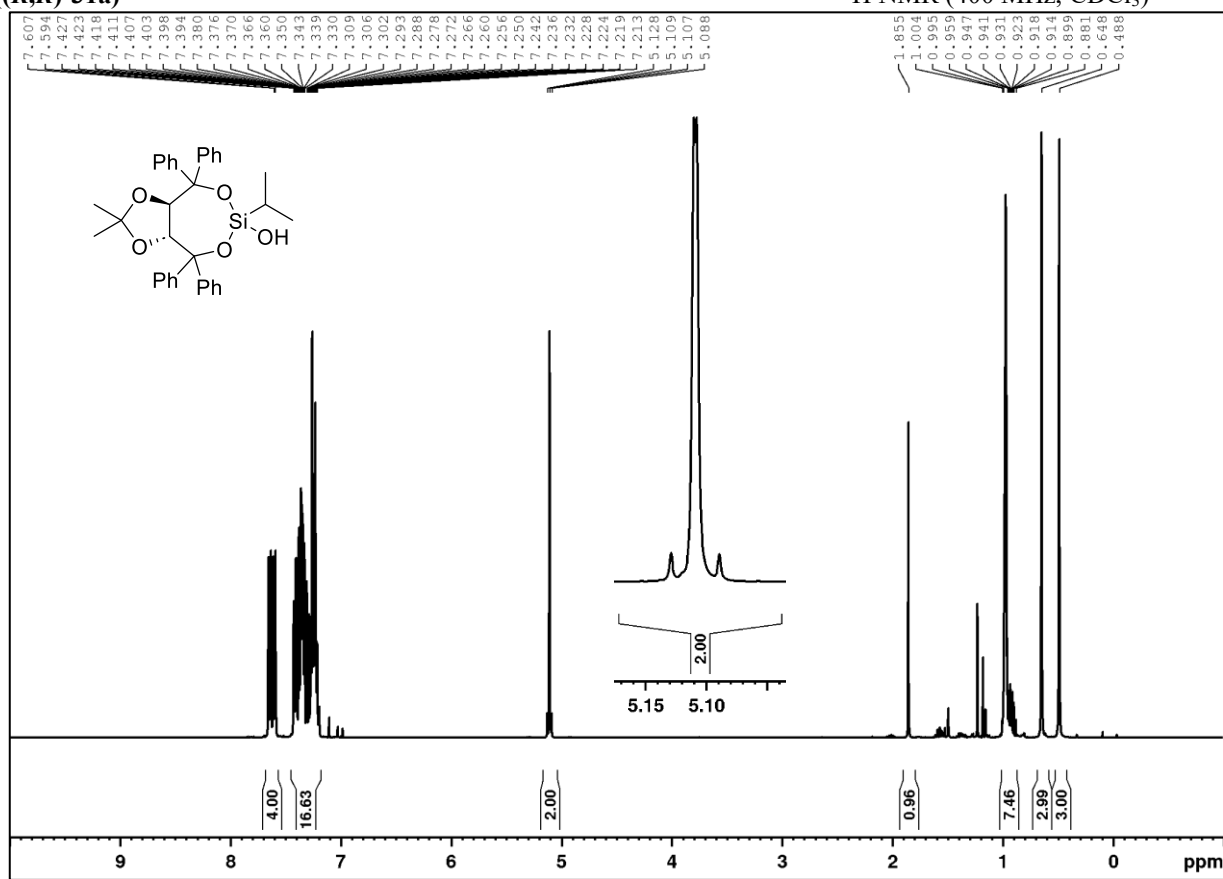
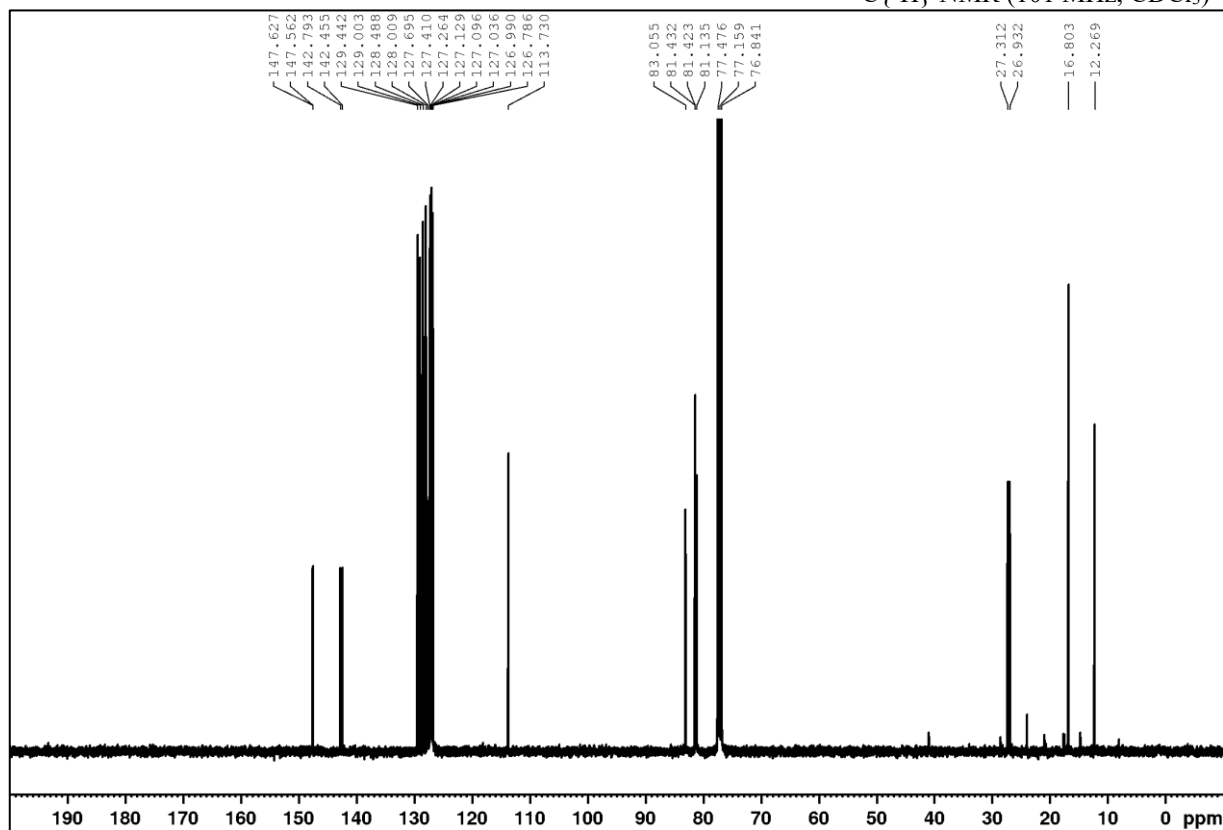
(3*aR*,8*aR*)-4,4,8-Tetra([1,1':3',1''-terphenyl]-5'-yl)-6-chloro-6-isopropyl-2,2-dimethyltetrahydro-[1,3]dioxolo[4,5-*e*][1,3,2]dioxasilepine ((*R,R*)-30c)¹H NMR (400 MHz, CDCl₃)¹³C{¹H} NMR (101 MHz, CDCl₃)

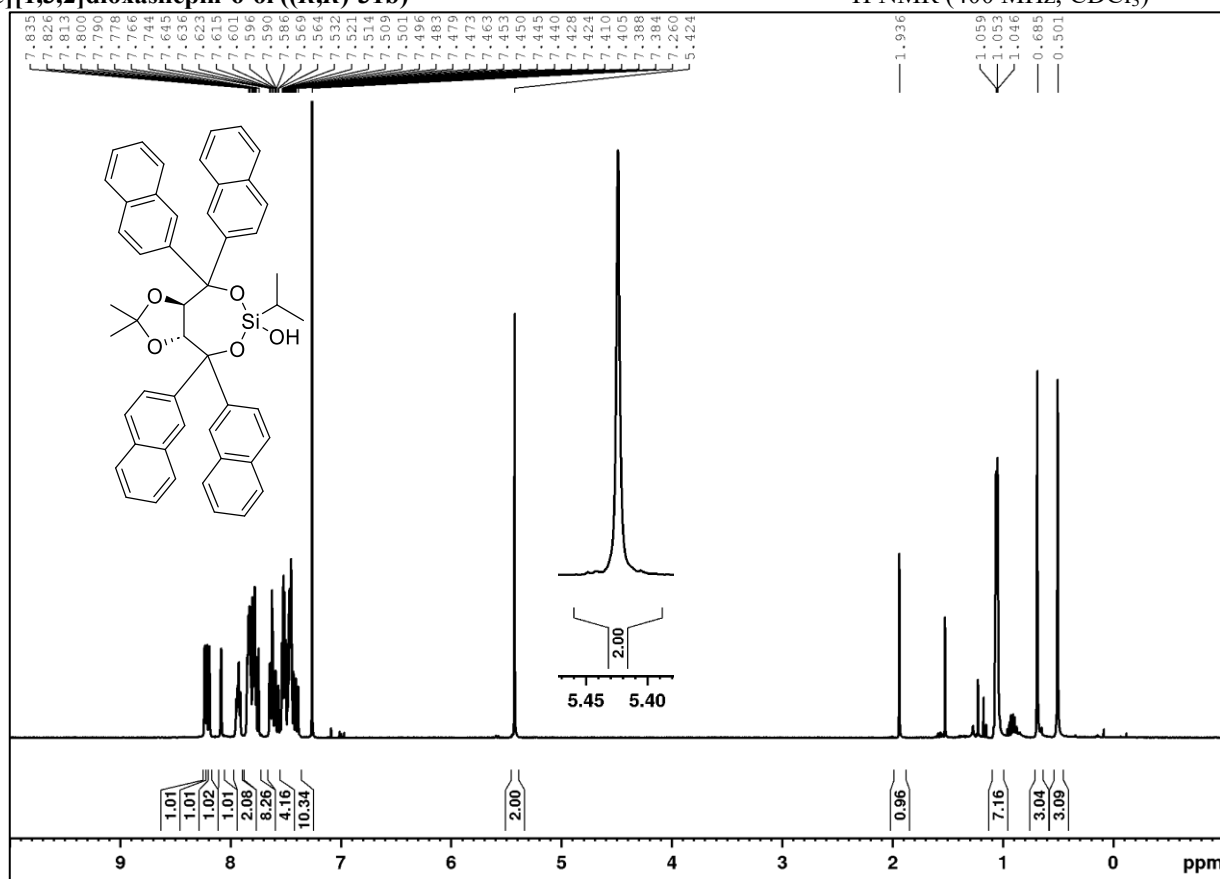
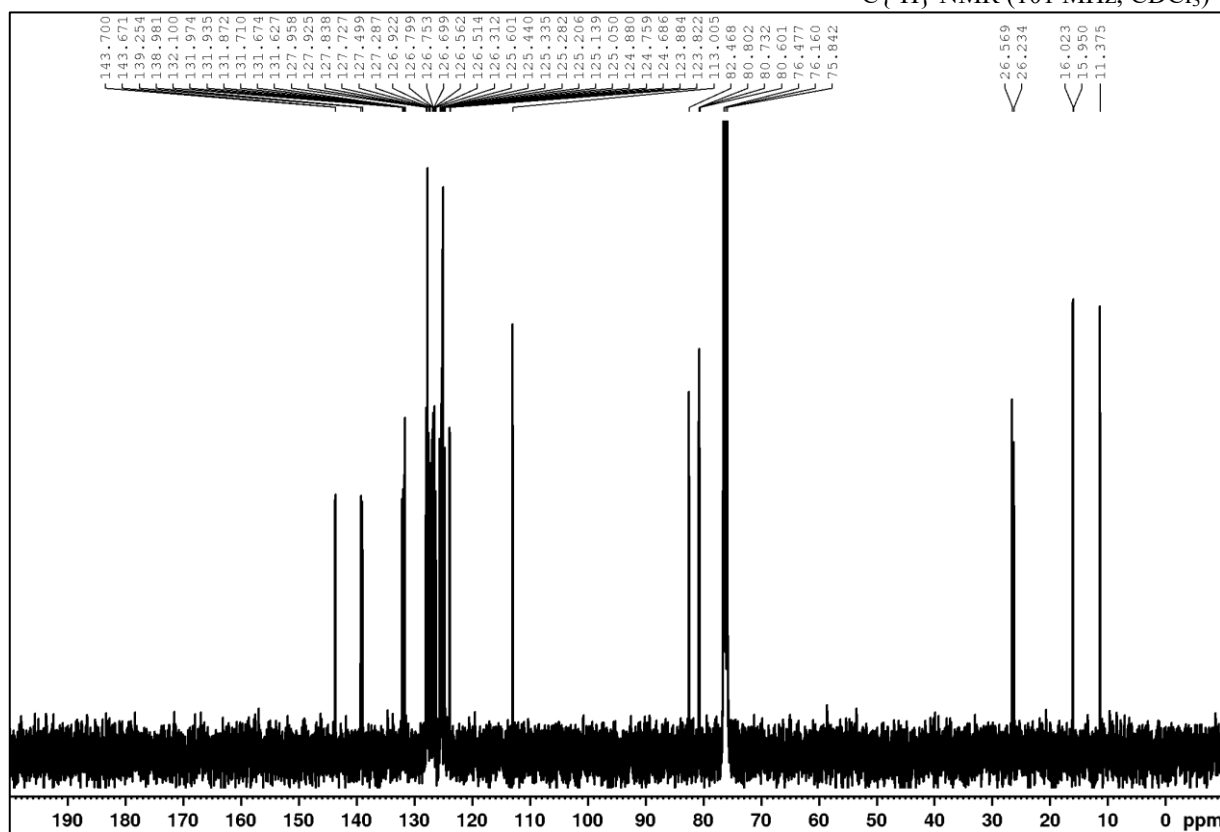
$(^1\text{H}, ^{13}\text{C})\text{-HSQC (CDCl}_3)$ 

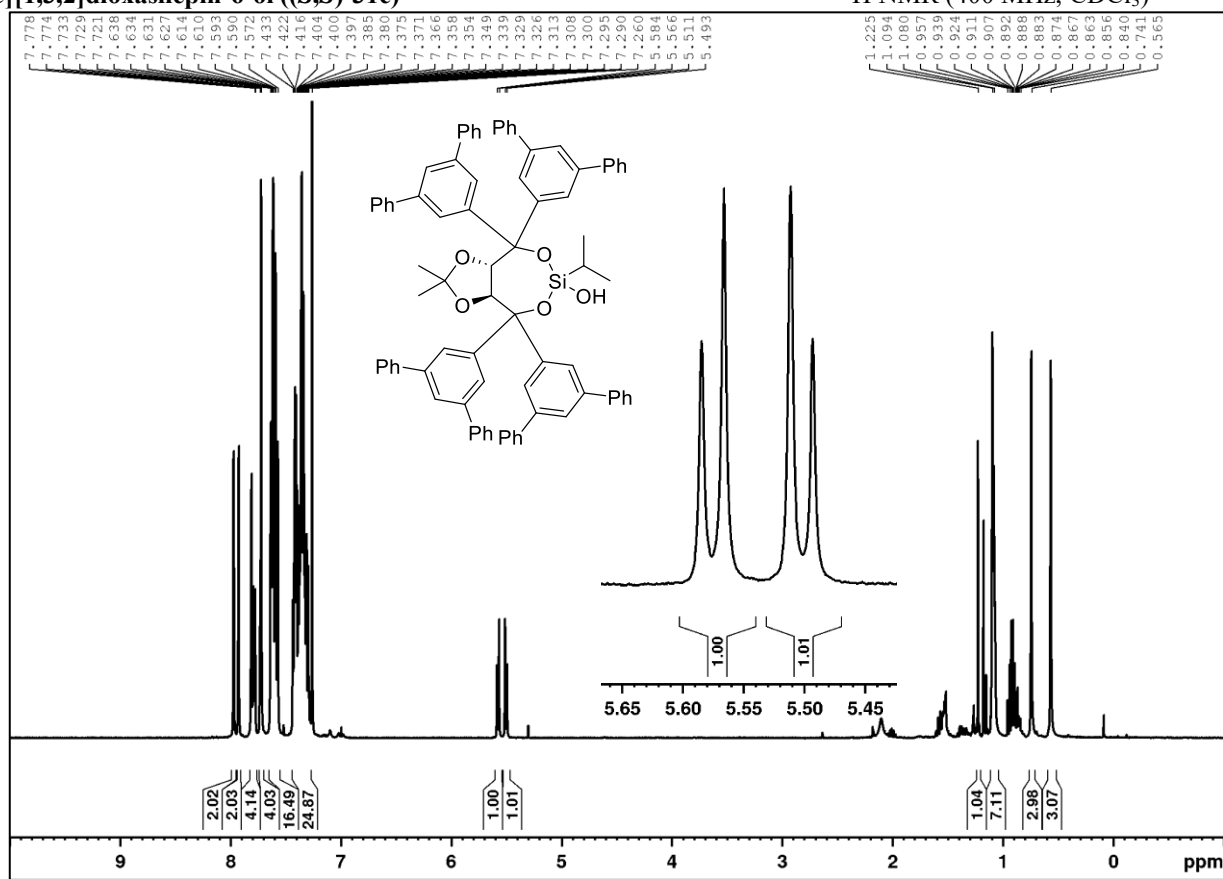
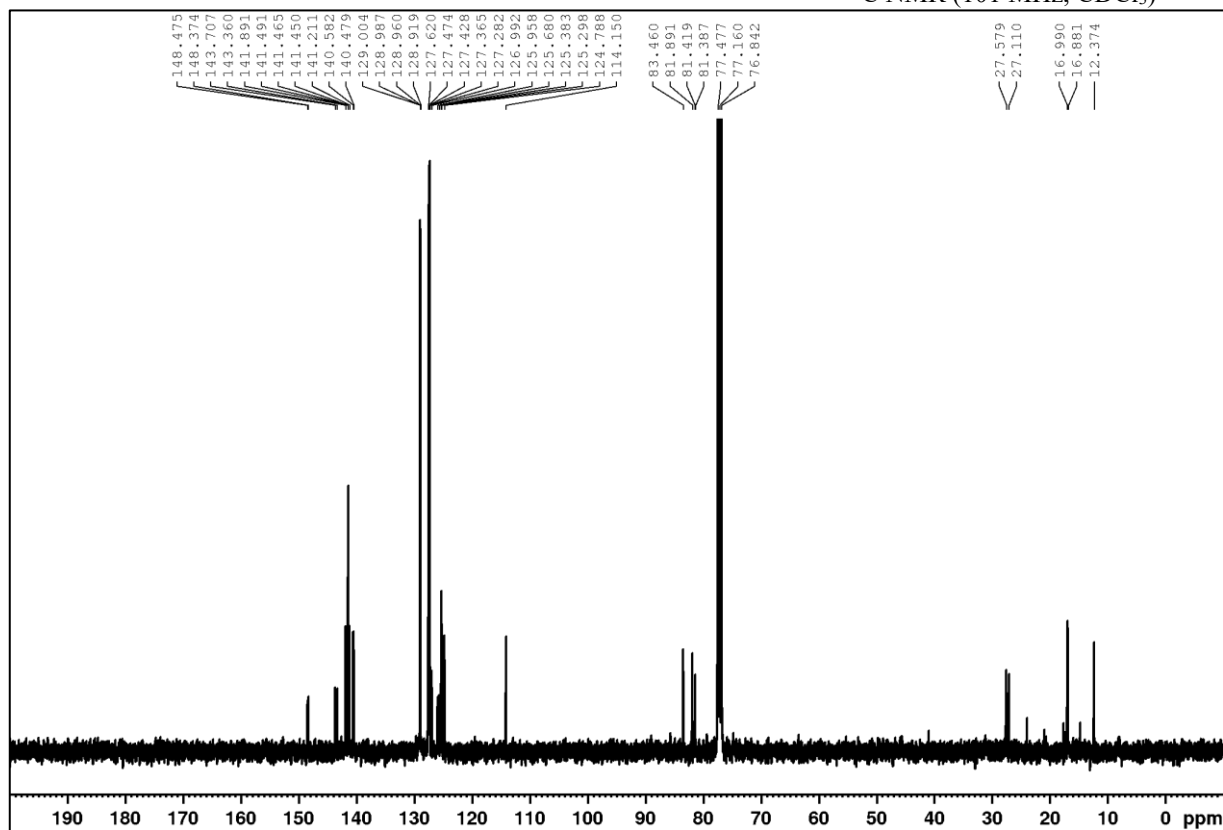
(3a*R*,8a*R*)-6-Chloro-2,2-dimethyl-4,4,6,8,8-pentaphenyltetrahydro-[1,3]dioxolo[4,5-*e*][1,3,2]dioxasilpine
(*R,R*)-30d¹H NMR (400 MHz, CDCl₃)¹³C{¹H} NMR (101 MHz, CDCl₃)

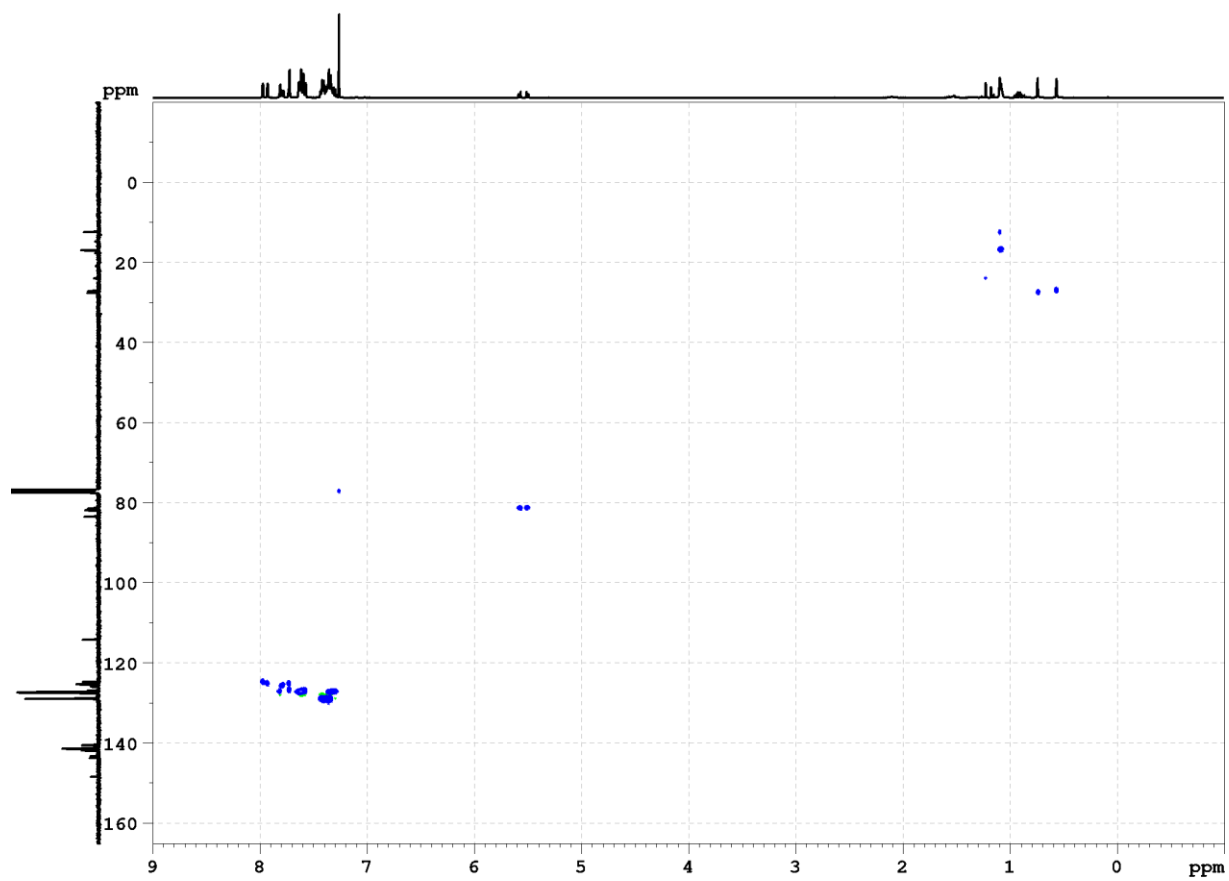
(3a*S*,8a*S*)-4,4,8,8-Tetra([1,1':3',1''-terphenyl]-5'-yl)-6-chloro-2,2-dimethyl-6-phenyltetrahydro-[1,3]dioxolo[4,5-*e*][1,3,2]dioxasilolepine ((*S,S*)-30e)
¹H NMR (400 MHz, CDCl₃)

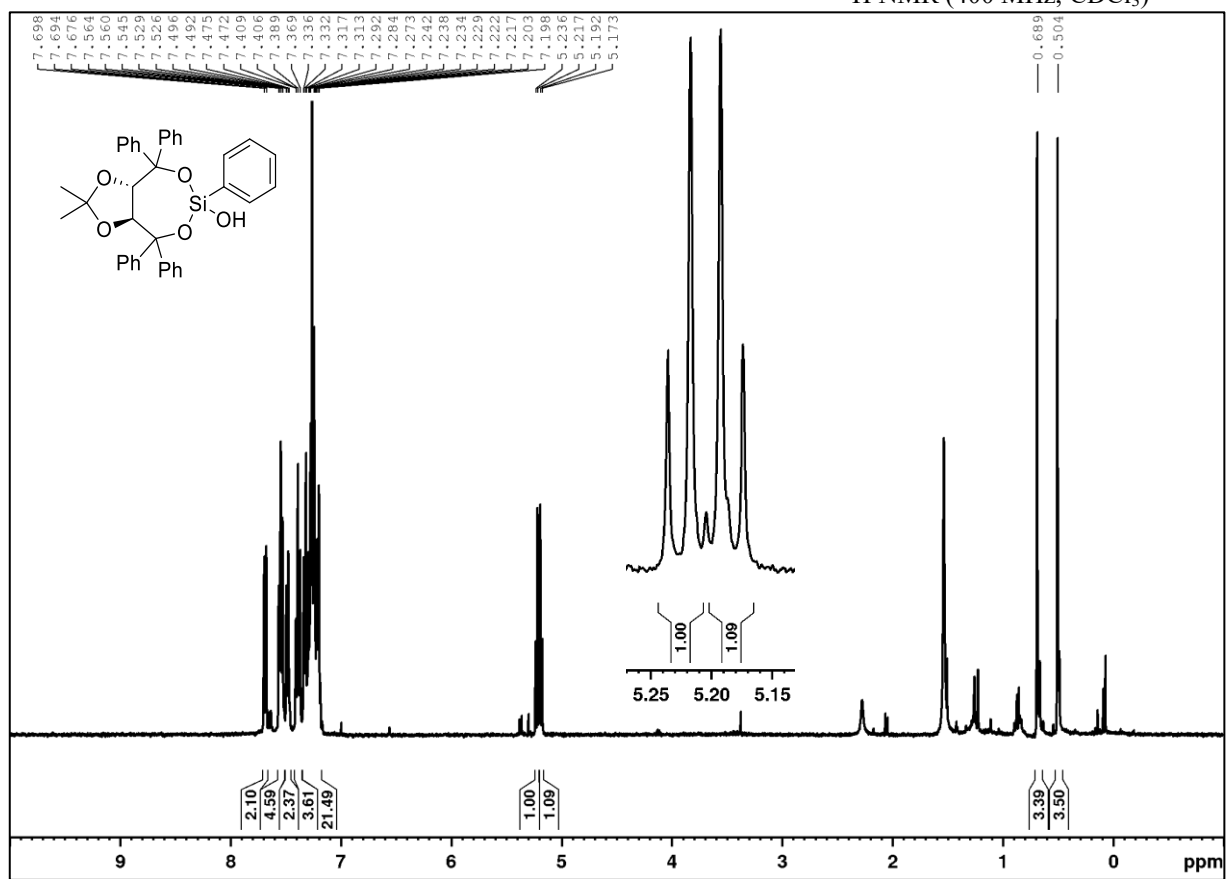


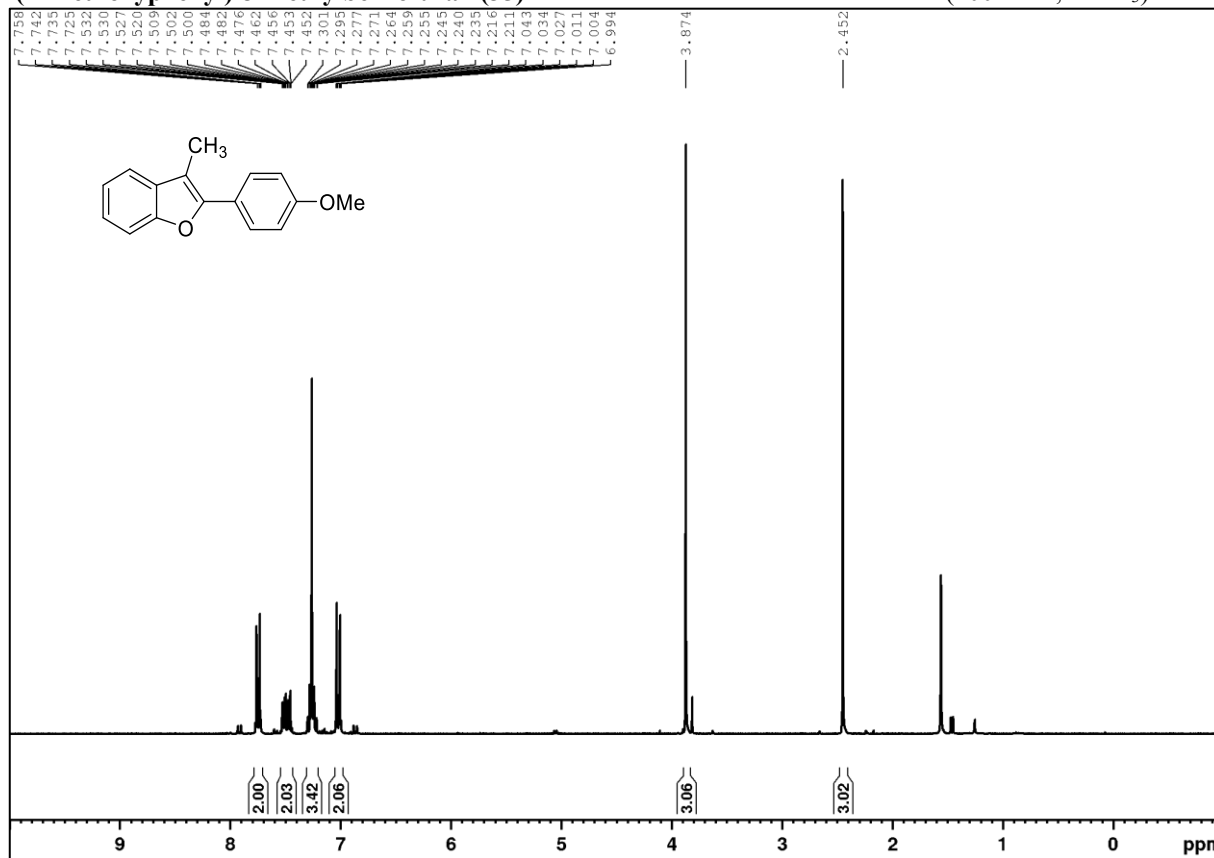
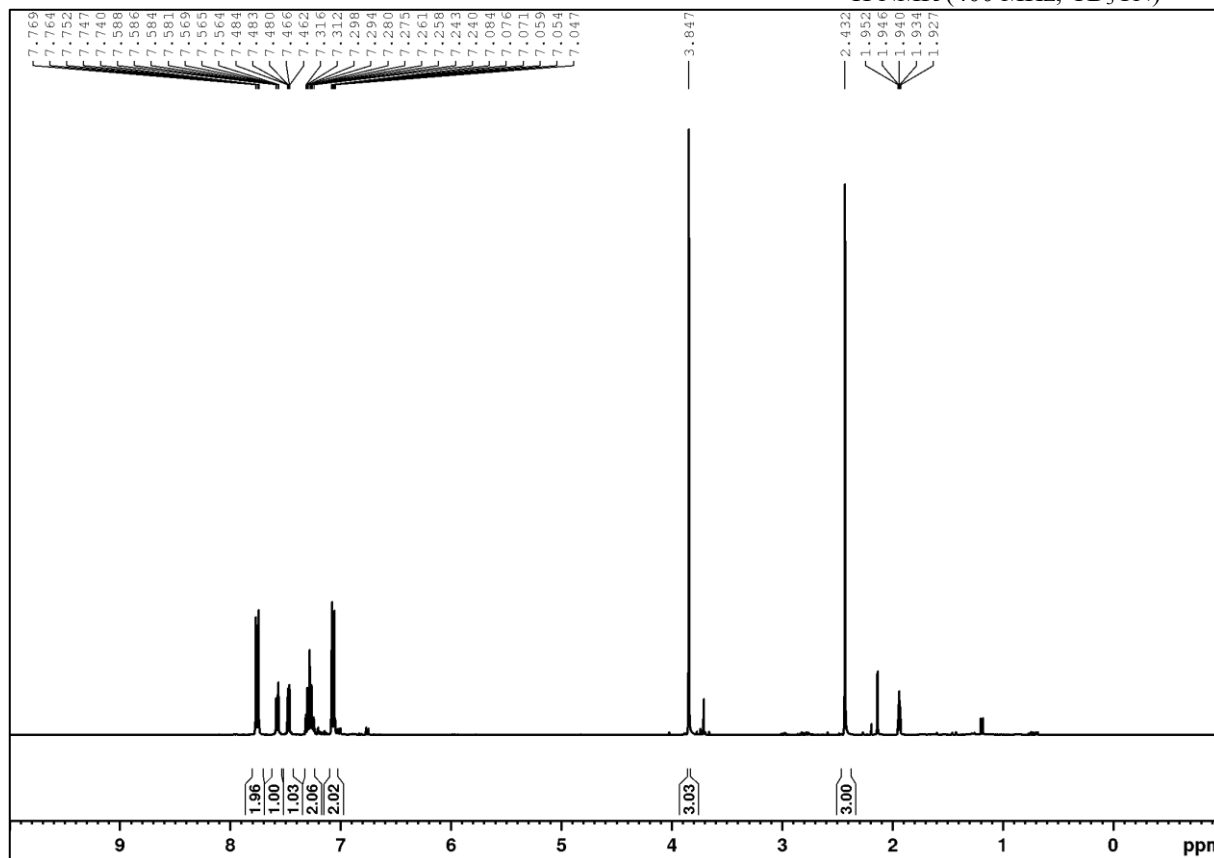
(3*aR*,8*aR*)-6-Isopropyl-2,2-dimethyl-4,4,8,8-tetraphenyltetrahydro-[1,3]dioxolo[4,5-*e*][1,3,2]dioxasilepin-6-ol
(*R,R*)-31a)¹H NMR (400 MHz, CDCl₃)¹³C{¹H} NMR (101 MHz, CDCl₃)

(3*aR*,8*aR*)-6-Isopropyl-2,2-dimethyl-4,4,8,8-tetra(naphthalen-2-yl)tetrahydro-[1,3]dioxolo[4,5-*e*][1,3,2]dioxasilepin-6-ol ((*R,R*)-31b)¹H NMR (400 MHz, CDCl₃)¹³C{¹H} NMR (101 MHz, CDCl₃)

(3a*S*,8a*S*)-4,4,8,8-Tetra([1,1':3',1''-terphenyl]-5'-yl)-6-isopropyl-2,2-dimethyltetrahydro-[1,3]dioxolo[4,5-*e*][1,3,2]dioxasilepin-6-ol ((*S,S*)-31c)¹H NMR (400 MHz, CDCl₃)¹³C NMR (101 MHz, CDCl₃)

$(^1\text{H}, ^{13}\text{C})\text{-HSQC (CDCl}_3)$ 

(3*a*S,8*a*S)-2,2-Dimethyl-4,4,6,8,8-pentaphenyltetrahydro-[1,3]dioxolo[4,5-*e*][1,3,2]dioxasilepin-6-ol ((*S,S*)-31d)
¹H NMR (400 MHz, CDCl₃)

2-(4-Methoxyphenyl)-3-methylbenzofuran (35)¹H NMR (400 MHz, CDCl₃)¹H NMR (400 MHz, CD₃CN)For comparison with the side product observed upon C-H activation of dihydrobenzofuran **4c**.

7.5 Curriculum Vitae

Personal Data

Name: Sascha Grotjahn
 Date of Birth: 30.12.1995
 Place of Birth: Eggenfelden
 Nationality: German

Education

05/2020 – 09/2024 **Ph. D. thesis** at the Institute of Organic Chemistry, University of Regensburg (Supervisor: Prof. Dr. Burkhard König)
 “Reactivity of Carbanions Generated via Reductive Radical-Polar Crossover and Regio-, Diastereo- and Enantioselectivity in their Generation”

10/2017 – 09/2019 **Master of Science** Advanced Synthesis and Catalysis, University of Regensburg
 Master thesis: “Synthesis of Fluorinated Cannabinoids via Photocatalytic Birch-Type Arylation” (Supervisor: Prof. Dr. Burkhard König, in collaboration with Prof. Dr. Jimmie Weaver, Oklahoma State University, USA)

10/2014 – 07/2019 **Bachelor of Science** in Chemistry, University of Regensburg
 Bachelor thesis: “Synthesis of Phenyl-substituted Cyclopentenones” (Supervisor: Prof. Dr. Oliver Reiser)

09/2006 – 06/2014 **Allgemeine Hochschulreife** at Karl-von-Closen Gymnasium Eggenfelden

Internships

01/2024 – 03/2024 King Abdullah University of Science and Technology, Thuwal, Saudi-Arabia
 Group of Prof. Dr. Magnus Rueping

03/2023 Radboud University Nijmegen, the Netherlands
 Group of Prof. Dr. Jana Roithová

08/2018 – 09/2018 Oklahoma State University, USA
 Group of Prof. Dr. Jimmie Weaver

Conferences

02/2022	BASF CaRLa Winter School, Heidelberg
10/2021	Exploratory Photochemistry: Light Creates Structure, Halle (Saale)
10/2019	Simpozij studenata kemičara (SiSK6), University of Zagreb, Croatia

Memberships

01/2017 – present	Gesellschaft Deutscher Chemiker
04/2021 – 09/2024	DFG – Graduate Research Training Group RTG 2620 “Ion Pair Effects in Molecular Reactivity”

Publications

1. **Sascha Grotjahn**, Burkhard König “Photosubstitution in Dicyanobenzene-based Photocatalysts” *Org. Lett.* **2021**, 23, 8, 3146–3150
2. Jon I. Day, **Sascha Grotjahn**; Sameera Senaweera, Burkhard König; Jimmie D. Weaver “Defluorodearomatization: A Photocatalytic Birch-Like Reduction That Enables C–C Bond Formation and Provides Access to Unnatural Cannabinoids” *J. Org. Chem.* **2021**, 86, 7928
3. **Sascha Grotjahn**, Christina Graf, Jan Zelenka, Aryaman Pattanaik, Lea Müller, Roger-Jan Kutta, Julia Rehbein, Jana Roithová, Ruth M. Gschwind, Patrick Nuernberger, Burkhard König “Reactivity of Superbasic Carbanions Generated via Reductive Radical-Polar Crossover in the Context of Photoredox Catalysis” *Angew. Chem., Int. Ed.* **2024**, e202400815
4. **Sascha Grotjahn**, Lea Müller, Aryaman Pattanaik, Alexander Falk, Giorgia Barison, Jonathan O. Bauer, Julia Rehbein, Ruth M. Gschwind and Burkhard König “Regio-, diastereo- and enantioselectivity in the photocatalytic generation of carbanions via hydrogen atom transfer and reductive radical-polar crossover” *Org. Chem. Front.*, **2024**, Advance Article
5. **Sascha Grotjahn**, Burkhard König (**2024**) “Common Ground and Divergence: OLED Emitters as Photocatalysts” manuscript submitted
6. Randall L. Davis, **Sascha Grotjahn**, Burkhard König, Daniel J. Buck, Jimmie D. Weaver (**2024**) “Novel fluorinated cannabinoid analogs modulate cytokine and chemokine expression in human microglial cells” manuscript submitted

8 Acknowledgements

First, I want to thank Prof. Dr. Burkhard König for supervision of my work and the many scientific discussions, ultimately leading to many successful projects. But also for the freedom to develop my own ideas and the freedom to investigate my projects not only with focus on a final publication, but also out of scientific curiosity. This freedom made working on the projects very enjoyable and I think that productive science must be based on encouraging curiosity and not on the pressure to produce as many publications as possible. Thank you for giving me the time and opportunity to finish my projects in the best possible way. Also, thank you for providing opportunities to conduct part of my research abroad to collect additional experience and conduct research that would not have been possible at University of Regensburg alone.

Special thanks go to all collaborators at University of Regensburg: Lea Müller, Aryaman Pattanaik, Christina Graf, Roger-Jan Kutta, Alexander Falk, and supervisors Prof. Dr. Patrick Nürnberger, Prof. Dr. Ruth Gschwind, Prof. Dr. Julia Rehbein, and PD Dr. Jonathan Bauer. The same thanks go to all international collaborators at KAUST and Radboud University: Amir Gizatullin, Tingting Yuan, Chen Zhu, Prof. Dr. Magnus Rueping, Jan Zelenka, and Prof. Dr. Jana Roithová. Your expertise was an integral part of making the projects as successful as they are.

Thank you to all members of the RTG 2620 – Ion Pairs in Molecular Reactivity, for providing insights into different fields of chemistry and for all the fruitful collaborations originating from the personal interaction. Consequently, I also thank the Deutsche Forschungsgemeinschaft for funding of all RTG activities and the research stay at Radboud University.

Thank you to all members and former members of the König group that helped making the time of my PhD studies so enjoyable. Special thanks go to Dominik Birnthal, Lea Müller, Jessica Stahl, Karsten Donabauer, and the permanent staff.

I thank Prof. Dr. Oliver Reiser and Prof. Dr. Patrick Nürnberger for examination of this thesis and PD Dr. Jonathan Bauer for serving as chairperson in my Ph.D. defense.

Apart from all colleagues I also want to thank my family. Especially my wife Sarah and my son Felix. It was not easy to write the thesis with so much distraction, but I am so grateful that I had the possibility stay at home during my son's first months. The time this prolonged the submission of this thesis was totally worth it.

Eidesstattliche Erklärung

Ich erkläre hiermit an Eides statt, dass ich die vorliegende Arbeit ohne unzulässige Hilfe Dritter und ohne Benutzung anderer als der angegebenen Hilfsmittel angefertigt habe; die aus anderen Quellen direkt oder indirekt übernommenen Daten und Konzepte sind unter Angabe des Literaturzitats gekennzeichnet.

Bei der Auswahl und Auswertung folgenden Materials haben mir die nachstehend aufgeführten Personen in der jeweils beschriebenen Weise unentgeltlich geholfen:

1. Lea Müller: Messung detaillierter NMR Kinetiken und gemeinsame Auswertung der entsprechenden Daten in Kapitel 4. Substrate für die Kinetiken wurden teilweise von Lea Müller synthetisiert, wie angegeben.
2. Christina Graf und Roger-Jan Kutta: Messung und Auswertung von Transienter Absorptionsspektroskopie in Kapitel 3. Der entsprechende Abschnitt und der experimentelle Teil wurden größtenteils von Christina Graf und Roger-Jan Kutta geschrieben und von mir überarbeitet und formatiert.
3. Aryaman Pattanaik: DFT Rechnungen in Kapitel 3 und 4.
4. Alexander Falk: Synthese von trimethoxysilanthiol und siliciumchiraler Verbindungen
5. Jan Zelenka: Gasphasenexperimente in Kapitel 3. Diese wurden für einen groben Überblick anfangs gemeinsam durchgeführt und detaillierte Messungen und Auswertungen wurden von J. Zelenka alleine durchgeführt. Der entsprechende experimentelle Teil wurde Größtenteils von Jan Zelenka geschrieben und von mir überarbeitet und formatiert.
6. Regina Hoheisel: CV-Messungen in Kapitel 2 und 3.
7. Folgende Personen haben im Rahmen von Bachelorarbeiten und Forschungspraktika unter meiner Aufsicht beigetragen: Daniel Kolb, Kathrin Strunk, Jonathan Schütte, Manuel Kobras, Lukas Welspillich, Thomas Tiefel, Miriam Berreiter, Nicola Bopp, Indrasish Dey und Giorgia Barison.

Weitere Personen waren an der inhaltlich-materiellen Herstellung der vorliegenden Arbeit nicht beteiligt. Insbesondere habe ich hierfür nicht die entgeltliche Hilfe eines Promotionsberaters oder anderer Personen in Anspruch genommen. Niemand hat von mir weder unmittelbar noch mittelbar geldwerte Leistungen für Arbeiten erhalten, die im Zusammenhang mit dem Inhalt der vorgelegten Dissertation stehen.

Die Arbeit wurde bisher weder im In- noch im Ausland in gleicher oder ähnlicher Form einer anderen Prüfungsbehörde vorgelegt. Ich versichere an Eides statt, dass ich nach bestem Wissen die reine Wahrheit gesagt und nichts verschwiegen habe.

.....
(Ort, Datum)

.....
(Unterschrift)